

# E

## Edge Crack, Bimaterial Systems

Meftah Hrairi<sup>1</sup> and Abdel-Fattah Rizk<sup>2</sup>

<sup>1</sup>Department of Mechanical Engineering,  
International Islamic University Malaysia,  
Kuala Lumpur, Malaysia

<sup>2</sup>Department of Engineering Mathematics and  
Physics, Alexandria University, Alexandria,  
Egypt

### Synonyms

Bonded dissimilar materials; Fracture mechanics; Stress intensity factor

### Overview

The multilayered structure components of dissimilar materials with different thermomechanical properties under thermal stresses are used in many engineering applications to protect the base metal from thermal and corrosion damage. For example, ceramic thermal barrier coating is used in jet engines, stainless steel cladding is used in pressure vessels and pipes, and a variety of bonded materials are used in microelectronic devices. The analytical solution as formulated in

edge crack, isotropic material, which is applicable to isotropic, homogeneous, linearly elastic plates, is further specialized here to the case of plates made of two bonded dissimilar materials. Indeed, the problem of thermoelastic edge cracking in two-layered bimaterial systems subjected to convective heating is considered. The medium is assumed to be insulated on one surface and exposed to sudden convective heating on another surface containing the edge crack. It is known that, when a bimaterial system's surface is heated, compressive stresses arise near the heating surface, forcing the crack surfaces to come together over a certain cusp-shaped contact length. It is also known that, for a cooled bimaterial system's surface, tensile stresses take place close to the cooling surface and tend to open the crack. So, the edge cracked heating surface problem is treated as an embedded crack with a smooth closure condition of the crack surfaces, with the crack contact length being an additional unknown variable. Superposition and uncoupled quasi-static thermoelasticity principles are adopted to formulate the problem. By using a Fourier integral transform technique, the mixed boundary value problem is reduced to a Cauchy type singular integral equation with an unknown function as the derivative of the crack surface displacement. The analysis is based upon the same simplifying conditions as in edge crack, isotropic material,

in addition to the fact that the bimaterial systems consist of two dissimilar linear isotropic homogeneous materials bonded along an ideal plane interface.

## Mathematical Formulation

Figure 1 illustrates the thermoelastic bimaterial systems for a mathematical formulation. It is composed of two layers of dissimilar materials with different thermoelastic properties. Layer 1, of thickness  $h_1$ , containing a crack of length  $l = (b - a)$  normal to the interface, is bonded to layer 2, of thickness  $h_2$ . The medium is initially assumed at homogenous temperature  $T_o$ . At  $t \geq 0$ , the plane  $x = 0$  is subjected to sudden convective heating with ambient temperature  $T_a$ , while the other boundary  $x = h_1 + h_2$  is assumed to be insulated.

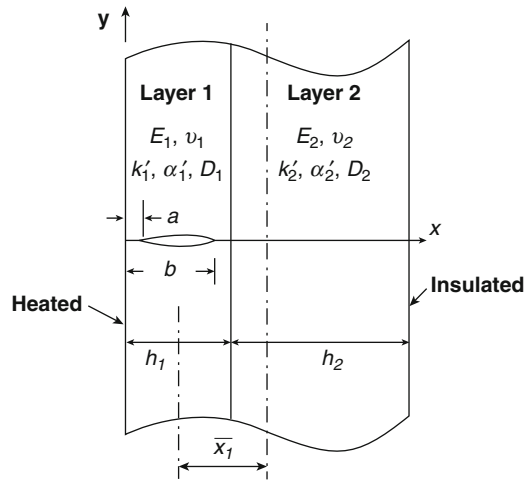
## Temperature Distribution

Let  $T_i(x, t)$  ( $i = 1, 2$ ) be the temperature of layer 1 and layer 2 at any instant time  $t$ . The governing differential equations and the initial and boundary conditions for the heat conduction problem are as follows:

$$\frac{\partial^2 \theta_i(x, t)}{\partial x^2} = \frac{1}{D_i} \frac{\partial \theta_i(x, t)}{\partial t} \quad (i = 1, 2) \quad (1)$$

$$\theta_i(x, 0) = 0 \quad (i = 1, 2) \quad (2)$$

$$k_1' \frac{\partial \theta_1(0, t)}{\partial x} = h[\theta_1(0, t) - \theta_o] \quad (3)$$



**Edge Crack, Bimaterial Systems, Fig. 1** Crack geometry in the bimaterial system under surface heating

$$\theta_1(h_1, t) = \theta_2(h_1, t) \quad (4)$$

$$k_1' \frac{\partial \theta_1(h_1, t)}{\partial x} = k_2' \frac{\partial \theta_2(h_1, t)}{\partial x} \quad (5)$$

$$\frac{\partial \theta_2(h_1 + h_2, t)}{\partial x} = 0 \quad (6)$$

where  $\theta_i(x, t) = T_i(x, t) - T_o$  ( $i = 1, 2$ ),  $\theta_o = T_a - T_o$ ,  $h$  is the coefficient of heat transfer and  $k_i'$ ,  $D_i$  ( $i = 1, 2$ ) are the coefficients of thermal conductivity and the thermal diffusivity, respectively. The solution of (1) subjected to the conditions from (2) to (6) can be obtained by applying the Laplace transform with the residue theorem [1], and the transient temperature distribution may be written in the form

$$\frac{\theta_1(x^*, \tau)}{\theta_o} = 1 - 2 \sum_{n=1}^{\infty} \frac{1}{\lambda_n} \frac{e^{-\tau \lambda_n^2} [\cos \lambda_n(x^* - 1) \cos(\delta R \lambda_n) + \eta \sin \lambda_n(x^* - 1) \sin(\delta R \lambda_n)]}{[(\lambda_n/Bi)(1 + \eta \delta R) \cos \lambda_n \cos(\delta R \lambda_n) - (\lambda_n/Bi)(\eta + \delta R) \sin \lambda_n \sin(\delta R \lambda_n)]} \frac{1}{+((1/Bi) + 1 + \eta \delta R) \sin \lambda_n \cos(\delta R \lambda_n) + ((\eta/Bi) + \delta R + \eta) \cos \lambda_n \sin(\delta R \lambda_n)}, 0 \leq x^* \leq 1 \quad (7)$$

$$\frac{\theta_2(x^*, \tau)}{\theta_o} = 1 - 2 \sum_{n=1}^{\infty} \frac{1}{\lambda_n} \frac{e^{-\tau \lambda_n^2} [\cos \delta \lambda_n (x^* - 1) \cos(\delta R \lambda_n) + \sin \delta \lambda_n (x^* - 1) \sin(\delta R \lambda_n)]}{[(\lambda_n / Bi)(1 + \eta \delta R) \cos \lambda_n \cos(\delta R \lambda_n) - (\lambda_n / Bi)(\eta + \delta R) \sin \lambda_n \sin(\delta R \lambda_n)]} \frac{1}{+((1/Bi) + 1 + \eta \delta R) \sin \lambda_n \cos(\delta R \lambda_n) + ((\eta/Bi) + \delta R + \eta) \cos \lambda_n \sin(\delta R \lambda_n)}, 1 \leq x^* \leq 1 + R \quad (8)$$

where  $x^* = x/h_1$ ,  $\tau = tD_1/h_1^2$  (Fourier number),  $\eta = (k_2/k_1)\sqrt{D_1/D_2}$ ,  $R = h_2/h_1$  (thickness ratio),  $\delta = \sqrt{D_1/D_2}$ ,  $Bi = hh_1/k_1'$  (Biot number), and  $\lambda_n$  are the roots of the transcendental equation

$$Bi [\cos \lambda_n \cos(\delta R \lambda_n) - \eta \sin \lambda_n \sin(\delta R \lambda_n)] = \lambda_n [\sin \lambda_n \cos(\delta R \lambda_n) + \eta \cos \lambda_n \sin(\delta R \lambda_n)] \quad (9)$$

where  $E_i, v_i, \alpha'_i$  ( $i = 1, 2$ ), are the Young's modulus, the Poisson's ratio, and the coefficient of linear thermal expansion respectively,  $\varepsilon_o(t)$  is the uniform strain that is given by

$$\varepsilon_o = \frac{\left(\frac{E_1}{1-v_1}\right) \alpha'_1 h_1 \bar{\theta}_1 + \left(\frac{E_2}{1-v_2}\right) \alpha'_2 h_2 \bar{\theta}_2}{\left(\frac{E_1}{1-v_1}\right) h_1 + \left(\frac{E_2}{1-v_2}\right) h_2} \quad (11)$$

where

$$\bar{\theta}_1 = \frac{1}{h_1} \int_0^{h_1} \theta_1(x, t) dx, \bar{\theta}_2 = \frac{1}{h_2} \int_{h_1}^{h_1+h_2} \theta_2(x, t) dx \quad (12)$$

### Thermal Stresses in the Uncracked Medium

The transient thermal stresses may be given by

$$\sigma_{iyy}^T(x, t) = \sigma_{izz}^T(x, t) = \frac{E_i}{1-v_i} \left[ \varepsilon_o(t) + \frac{x}{\rho(t)} - \alpha'_i \theta_i(x, t) \right], (i = 1, 2) \quad (10)$$

and the curvature  $1/\rho$  is given by

$$\frac{1}{\rho} = \frac{-(\bar{x}_1 + \frac{h_1}{2}) \left[ \left(\frac{E_1}{1-v_1}\right) \alpha'_1 h_1 \bar{\theta}_1 + \left(\frac{E_2}{1-v_2}\right) \alpha'_2 h_2 \bar{\theta}_2 \right] + \left(\frac{E_1}{1-v_1}\right) \alpha'_1 M_{t1} + \left(\frac{E_2}{1-v_2}\right) \alpha'_2 M_{t2}}{\left(\frac{E_1}{1-v_1}\right) I_1 + \left(\frac{E_2}{1-v_2}\right) I_2 + \left(\frac{E_1}{1-v_1}\right) \frac{(h_1+h_2)}{2} h_1 \bar{x}_1} \quad (13)$$

where  $I_1 = h_1^3/12$ ,  $I_2 = h_2^3/12$  are the moment of inertia about the centroidal axes of layer 1 and layer 2, respectively, and

where  $\bar{x}_1$  is the distance between the centroidal axis of layer 1 and the bending axis (isothermal plane,  $\theta_1 = \theta_2$ ) [2].

$$M_{t1} = \int_0^{h_1} \theta_1(x, t) x dx, M_{t2} = \int_{h_1}^{h_1+h_2} \theta_2(x, t) x dx$$

$$\bar{x}_1 = \frac{(h_1 + h_2)}{2} \frac{\left(\frac{E_2}{1-v_2}\right) h_2}{\left(\frac{E_1}{1-v_1}\right) h_1 + \left(\frac{E_2}{1-v_2}\right) h_2} \quad (14)$$

### The Crack Problem

The solution of the plane elasticity problem is required to solve the following governing differential equations for the displacements:

$$(\kappa_i - 1) \nabla^2 u_i + 2 \left( \frac{\partial^2 u_i}{\partial x^2} + \frac{\partial^2 v_i}{\partial x \partial y} \right) = 0, (i = 1, 2) \quad (15)$$

$$(\kappa_i - 1)\nabla^2 v_i + 2\left(\frac{\partial^2 u_i}{\partial x \partial y} + \frac{\partial^2 v_i}{\partial y^2}\right) = 0, (i = 1, 2) \quad (16)$$

where  $\kappa_i = (3 - 4\nu_i)$ , ( $i = 1, 2$ ), for plane strain, and  $u_i, v_i$ , ( $i = 1, 2$ ) are the  $x$  and  $y$  components of the displacement vectors, respectively. Since  $y = 0$  is a plane of symmetry, then the problem will be considered for  $0 < y < \infty$  which is subjected to the following conditions:

$$\sigma_{1xx}(0, y) = 0, \sigma_{1xy}(0, y) = 0 \quad (17)$$

$$\sigma_{1xx}(h_1, y) = \sigma_{2xx}(h_1, y), \sigma_{1xy}(h_1, y) = \sigma_{2xy}(h_1, y) \quad (18)$$

$$u_1(h_1, y) = u_2(h_1, y), v_1(h_1, y) = v_2(h_1, y) \quad (19)$$

$$\sigma_{2xx}(h_1 + h_2, y) = 0, \sigma_{2xy}(h_1 + h_2, y) = 0 \quad (20)$$

$$\begin{aligned} \sigma_{1xy}(x, 0) = 0, 0 < x < h_1, \text{ and } \sigma_{2xy}(x, 0) = 0 \\ v_2(x, 0) = 0, h_1 < x < h_1 + h_2 \end{aligned} \quad (21)$$

$$u_i(x, y) \rightarrow 0, v_i(x, y) \rightarrow 0, (i = 1, 2) \text{ as } y \rightarrow \infty \quad (22)$$

$$\begin{aligned} v_1(x, 0) = 0, 0 < x < a, b < x < h_1 \\ \sigma_{1yy}(x, 0) = -\sigma_{1yy}^T(x, t), a < x < b \end{aligned} \quad (23)$$

where  $\sigma_{1ij}(x, y)$ ,  $\sigma_{2ij}(x, y)$ , ( $i, j = x, y$ ) are the stresses in layer 1 and layer 2, respectively, and  $\sigma_{1yy}^T(x, t)$  is the thermal stress obtained from the uncracked problem. Differential equations (15) and (16) can be solved by expressing the displacement components  $u_i, v_i$ , ( $i = 1, 2$ ), in terms of the Fourier integral transform, i.e.,

$$\begin{aligned} u_i(x, y) = \frac{2}{\pi} \int_0^\infty A_i(x, \alpha) \cos \alpha y d\alpha \\ + \frac{1}{2\pi} \int_{-\infty}^\infty B_i(y, \beta) e^{ix\beta} d\beta, (i = 1, 2) \end{aligned} \quad (24)$$

$$\begin{aligned} v_i(x, y) = \frac{2}{\pi} \int_0^\infty F_i(x, \alpha) \sin \alpha y d\alpha \\ + \frac{1}{2\pi} \int_{-\infty}^\infty G_i(y, \beta) e^{ix\beta} d\beta, (i = 1, 2) \end{aligned} \quad (25)$$

where  $A_i, B_i, F_i, G_i$ , ( $i = 1, 2$ ), are the unknown functions to be determined. Substituting (24)–(25) into (15)–(16) and solving the resulting ordinary differential equations and using the stress-displacement relations with the conditions specified by (17)–(23) and defining a new unknown function  $\varphi(x) = \partial v_1(x, 0)/\partial x$ , the problem will be reduced to, after lengthy but straightforward manipulations, the following singular integral equation of the unknown function  $\varphi(x)$ :

$$\begin{aligned} \int_a^b \frac{\varphi(s)}{(s-x)} ds + \int_a^b k_1(x, s) \varphi(s) ds \\ = -\frac{\pi(\kappa_1 + 1)}{4\mu_1} \sigma_{1yy}^T(x, t), a < x < b \end{aligned} \quad (26)$$

where the kernel  $k_1(x, s)$  can be found in [3]. It can be seen that as long as the crack is away from the free surface ( $a > 0$ ) and the interface ( $b < h_1$ ), the kernel  $k_1(x, s)$  is bounded and the singular integral equation (26) has only a Cauchy singularity. In the limiting cases, for an edge crack ( $a = 0$ ) and crack terminating at the interface ( $b = h_1$ ), some terms in the kernel  $k_1(x, s)$  become unbounded and would contribute to the singular behavior of the solution. So, the kernel  $k_1(x, s)$  may be written in the form:

$$k_1(x, s) = k_1^b(x, s) + k_{1a}^s(x, s) + k_{1b}^s(x, s) \quad (27)$$

where  $k_1^b(x, s)$  is bounded in the interval  $[a, b]$ , including  $a = 0$  and  $b = h_1$ , and  $k_{1a}^s(x, s)$  and  $k_{1b}^s(x, s)$  are the singular terms as  $a = 0$  and  $b = h_1$ , respectively, and they are found to be



$$k_{1a}^s(x, s) = -\frac{1}{s+x} + \frac{6x}{(s+x)^2} - \frac{4x^2}{(s+x)^3} \quad (28)$$

$$k_{1b}^s(x, s) = \frac{c_{11}}{2h_1 - x - s} + \frac{c_{12}(h_1 - x)}{(2h_1 - x - s)^2} + \frac{c_{13}(h_1 - x)^2}{(2h_1 - x - s)^3} \quad (29)$$

where

$$c_{11} = \frac{3(m-1)}{2(m+\kappa_1)} - \frac{(m\kappa_2 - \kappa_1)}{2(m\kappa_2 + 1)}, \quad c_{12} = -6 \frac{m-1}{m+\kappa_1}$$

$$c_{13} = 4 \frac{m-1}{m+\kappa_1}, \quad m = \frac{\mu_1}{\mu_2} \quad (30)$$

Such kernels are called generalized Cauchy kernels.

### Singularities and Stress Intensity Factors

The singular behavior of the solution of the singular integral equation (26) at the irregular points  $a$  and  $b$  can be examined using the function theoretic method [4]. Let the unknown function  $\varphi(s)$  be expressed as

$$\varphi(s) = \frac{g(s)}{(s-a)^{\gamma_1}(b-s)^{\gamma_2}} \quad (31)$$

where  $g(s)$  is a bounded function in the closed interval  $[a, b]$  and nonzero at the end points  $a$  and  $b$  and  $\gamma_1, \gamma_2$  are the strength of the singularity at the end points which should satisfy  $0 < \text{Re}(\gamma_1, \gamma_2) < 1$ . Following [4], as long as we have an embedded crack in layer 1 ( $a > 0, b < h_1$ ), the singularities at the crack tips  $a$  and  $b$  are found to be  $\gamma_1 = 1/2$  and  $\gamma_2 = 1/2$ . While in the case of an edge crack ( $a = 0, b < h_1$ ), the singularity at the crack tip  $b$  is  $\gamma_2 = 1/2$ , and the singularity at the crack tip  $a = 0$  would satisfy the following characteristic equation

$$\cos \pi \gamma_1 - 2(\gamma_1 - 1)^2 + 1 = 0 \quad (32)$$

which has only one acceptable root given by  $\gamma_1 = 0$ . For the case of crack terminating at the interface ( $b = h_1$ ), the singularity  $\gamma_2$  at the tip  $b = h_1$  would depend on the material properties, and its characteristic equation will be given by [5]

$$\cos \pi \gamma_2 - \frac{1}{2} c_{13} \gamma_2 (\gamma_2 + 1) - c_{12} \gamma_2 - c_{11} = 0 \quad (33)$$

where  $c_{11}, c_{12}, c_{13}$  are given by (30).

Our interest is to calculate the stress intensity factors for mode I which are defined at the crack tips  $a$  and  $b$  as

$$K(a) = \lim_{x \rightarrow a^-} \sqrt{2(a-x)} \sigma_{1yy}(x, 0) \quad (34)$$

$$K(b) = \lim_{x \rightarrow b^+} \sqrt{2(x-b)} \sigma_{1yy}(x, 0) \quad (35)$$

in which  $\sigma_{1yy}(x, 0)$  is the stress outside the crack in layer 1. Note that (26) gives the stresses inside and outside the crack. Following [4] and using (26) and (31), the stress intensity factors for an embedded crack at  $a$  and  $b$  are given by

$$K(a) = \frac{4\mu_1}{\kappa_1 + 1} \left( \frac{2}{b-a} \right)^{1/2} g(a) \quad (36)$$

$$K(b) = -\frac{4\mu_1}{\kappa_1 + 1} \left( \frac{2}{b-a} \right)^{1/2} g(b) \quad (37)$$

and for an edge crack ( $a = 0, b < h_1$ ), the stress intensity factor at the crack tip  $b$  is given by

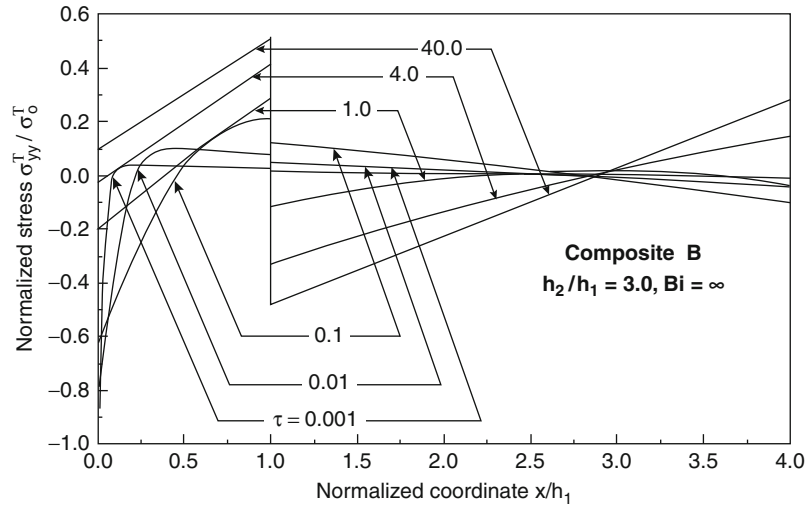
$$K(b) = -\frac{4\mu_1}{\kappa_1 + 1} \sqrt{2} g(b) \quad (38)$$

For the crack terminating at the interface ( $b = h_1$ ), the stress intensity factor at  $b$  is defined by

$$K(b = h_1) = \lim_{x \rightarrow h_1^+} \sqrt{2} (x - h_1)^{\gamma_2} \sigma_{2yy}(x, 0) \quad (39)$$

### Edge Crack, Bimaterial Systems,

**Fig. 2** Normalized thermal stresses at different Fourier number for Biot number  $Bi = \infty$



where  $\gamma_2$  is the singularity at crack tip  $b = h_1$  which can be obtained from (33) and  $\sigma_{2yy}(x, 0)$  is the stress in layer 2. Following [4] and using (26) and (31), the stress intensity factor at the crack tip can be evaluated from

$$K(b = h_1) = \frac{4\mu_2}{1 + \kappa_2} \sqrt{2} \frac{d_{21} + d_{22}\gamma_2}{(h_1 - a)^{\gamma_1} \sin \pi\gamma_2} g(h_1) \quad (40)$$

where

$$\begin{aligned} d_{21} &= \frac{m(\kappa_2 + 1)}{2(m + \kappa_1)} - \frac{3m(\kappa_2 + 1)}{2(m\kappa_2 + 1)} \\ d_{22} &= \frac{m(\kappa_2 + 1)}{(m\kappa_2 + 1)} - \frac{m(\kappa_2 + 1)}{(m + \kappa_1)}, \quad m = \frac{\mu_1}{\mu_2} \end{aligned} \quad (41)$$

and if  $a > 0$  ( $b = h_1$ ), the stress intensity factor at the crack tip  $a$  will be given by

$$K(a) = \frac{4\mu_1}{\kappa_1 + 1} \sqrt{2} \left( \frac{1}{h_1 - a} \right)^{\gamma_2} g(a) \quad (42)$$

In the formulation of the crack contact problem, we should include the crack contact length  $\varepsilon$  in the compressive zone as an additional unknown variable. The contact length would be

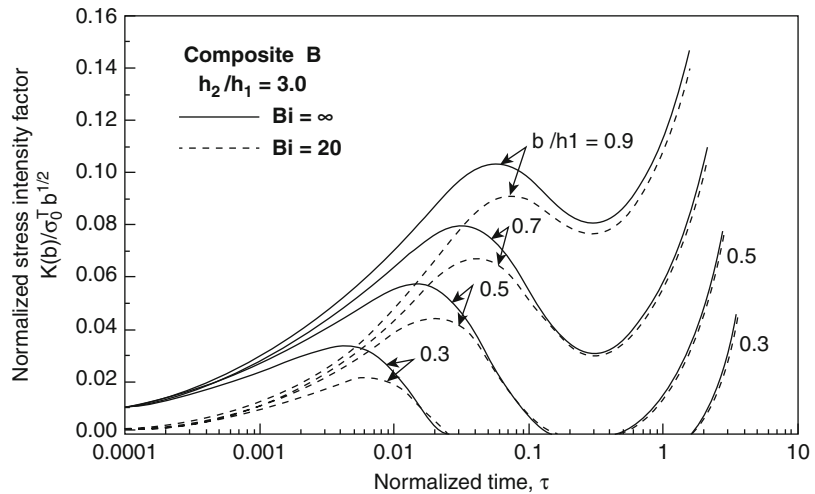
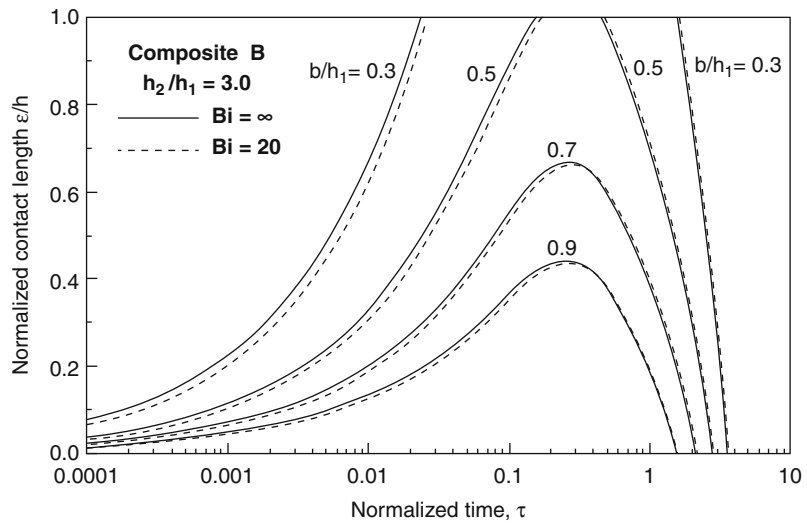
calculated by using the smooth closure condition of the crack surface at  $x = a$ , which is assured by the condition  $K(a) = 0$  [6]. So, the edge crack problem under thermal heating is solved as an embedded crack by fixing the crack length at  $x = b$  and then determining by iteration the location of the crack tip  $x = a$  at each time step such that the condition  $K(a) = 0$  is satisfied.

In a similar way as in edge crack, isotropic material, the numerical solution of the singular integral equation (26) is achieved by the expansion method developed in [7], and all the integrations appearing in the formulation are carried out numerically using the Jacobi-Gauss quadrature formula and the Laguerre-Gauss quadrature formula given in [8].

### Sample Results

The numerical results of the stress intensity factors for an edge crack could be calculated and presented as a function of time, crack length, heat transfer coefficient, and thickness ratio for different bimaterial systems.

As one example, consider the case of the plate shown in Fig. 1 made of a ceramic (layer 1) bonded to a ferritic steel (layer 2). The normalized transient thermal stresses are shown in Fig. 2.

**Edge Crack, Bimaterial Systems,****Fig. 3** Normalized stress intensity factors at different normalized crack lengths ( $b/h_1$ ), for Biot number ( $Bi = \infty, 20$ )**Edge Crack, Bimaterial Systems,****Fig. 4** Normalized crack contact length  $\varepsilon/b$  at different normalized crack lengths ( $b/h_1$ ), for Biot number ( $Bi = \infty, 20$ )

The variation of the normalized stress intensity factors for an edge crack problem ( $b/h_1 < 1$ ) defined by  $K(b)/\sigma_o^T \sqrt{b}$  and the variation of the normalized crack contact length  $\varepsilon/b$  versus Fourier number  $\tau = tD_1/h_1^2$  are presented in Figs. 3 and 4 [9].

**Cross-References**

► [Edge Crack, Isotropic Material](#)

**References**

1. Carslaw HS, Jaeger JC (1950) Conduction of heat in solids. Oxford University Press, Oxford
2. Burgreen D (1971) Elements of thermal stress analysis. C. P. Press, Jamaica
3. Rizk AA (2008) Stress intensity factor for an edge crack in two bonded dissimilar materials under convective cooling. Theor Appl Fracture Mech 49:251–267
4. Muskhelishvili NI (1953) Singular integral equations. Noordhoff, Groningen
5. Rizk AA, Erdogan F (1989) Cracking of coated materials under transient thermal stresses. J Therm Stresses 12:125–168

6. Bakioglu M, Erdogan F, Hesselman DPH (1976) Fracture mechanical analysis of self fatigue in surface compression strengthened glass plates. *J Mater Sci* 11:1826–1834
7. Kaya AC, Erdogan F (1987) On the solution of integral equations with strongly singular kernels. *Q Appl Math* 45:105–122
8. Stroud A, Secrest D (1966) Gaussian quadrature formulas. Prentice-Hall, New York
9. Rizk AA, Hrairi M (2009) Edge-cracked bimaterial systems under thermal heating. *Int J Solids Struct* 46:1648–1658

## Edge Crack, Composite Materials

Abdel-Fattah Rizk<sup>1</sup> and Meftah Hrairi<sup>2</sup>

<sup>1</sup>Department of Engineering Mathematics and Physics, Alexandria University, Alexandria, Egypt

<sup>2</sup>Department of Mechanical Engineering, International Islamic University Malaysia, Kuala Lumpur, Malaysia

## Synonyms

Fracture mechanics; Orthotropic materials; Stress intensity factor

## Overview

Composite structural elements are nowadays used in a variety of components for automotive, aerospace, marine, and architectural structures in addition to consumer products. Some of these composite materials are often subjected to the combined action of a mechanical loading and a thermal loading. Defects that may occur during the manufacturing stages of composites or while being in service decrease their strength and life. Consequently, an understanding of thermally induced stresses and the accurate evaluation of stress intensity factors in composite materials is essential for a comprehensive study of their response to an exposure to a temperature field including the prediction of failure and the calculation of crack growth rate in these structures.

The analytical solution as formulated in edge crack, isotropic material, which is applicable to isotropic, homogeneous, and linearly elastic plates, is further specialized here to the case of plates made of orthotropic material. In this entry, the analysis of the elastic homogeneous orthotropic semi-infinite plate with an edge crack perpendicular to the boundary under thermal shock is presented. The thermal stresses are created as a result of sudden cooling on the boundary by a ramp function temperature change. The formulation of the problem is carried out by using the superposition technique. First, the transient thermal stresses for the uncracked medium are obtained under appropriate initial and boundary conditions. Second, the isothermal cracked medium (the perturbation problem) is solved utilizing the thermal stresses obtained from the uncracked plate with opposite sign on the crack surfaces as the crack surface tractions. The Fourier transform technique is used to formulate the perturbation problem leading to a singular integral equation of the Cauchy type with an unknown function which is defined as the derivative of the crack surface displacement. The singular integral equation is solved numerically using the expansion method. The analysis is based upon the same simplifying conditions as in edge crack, isotropic material, and edge crack, bimaterial systems.

## Problem Formulation

Consider a homogenous orthotropic semi-infinite plate at uniform temperature  $T_\infty$  with a finite crack of length  $l = (b - a)$  perpendicular to the boundary  $y = 0$  as shown in Fig. 1a. It is assumed that the principal axes of the orthotropic material are aligned with the Cartesian coordinates  $(x, y, z)$ . At time  $t = 0$ , the boundary  $y = 0$  is suddenly cooled by a ramp function temperature change as shown in Fig. 1b in which the cooling rate is measured by  $t_o$ .

## Temperature Distribution

The most rapidly cooling rate occurs when  $t_o = 0$  which is corresponding to a unit step function

temperature change. The transient temperature distribution that is required to calculate the thermal stresses for the uncracked problem can be obtained by solving the diffusion equation

$$\frac{\partial^2 \theta}{\partial y^2} = \frac{1}{D_y} \frac{\partial \theta}{\partial t} \quad (1)$$

where  $\theta = T(y, t) - T_\infty$ ,  $T(y, t)$  is the temperature in the plate at any time  $t$  and  $D_y$  is the thermal diffusivity of the plate in  $y$ -direction. Equation (1) would be solved under the following initial and boundary conditions:

$$\theta(y, 0) = 0 \quad (2)$$

$$\theta(\infty, t) = 0 \quad (3)$$

$$\theta(0, t) = \frac{\theta_0}{t_0} t + \left( \theta_0 - \frac{\theta_0}{t_0} t \right) H(t - t_0) \quad (4)$$

where  $\theta_0 = T_o - T_\infty$  and  $H$  is the Heaviside unit step function. The solution of (1) under the initial and boundary conditions given by (2)–(4) can be obtained in a straightforward manner by applying the Laplace transform [1], and the transient temperature distribution will be given by

$$\frac{\theta(y, t)}{\theta_0} = \operatorname{erfc} \left[ \frac{y}{2\sqrt{D_y t}} \right] = 1 - \frac{2}{\pi} \int_0^\infty e^{-\left(\frac{w y}{\sqrt{t}}\right)^2} \sin \eta \frac{d\eta}{\eta} \quad (5)$$

for unit step function ( $t_o = 0$ ) and

$$\begin{aligned} \frac{\theta(y, t)}{\theta_0} &= \frac{t}{t_0} - \frac{2}{\pi} \int_0^\infty \left( \frac{y^2}{t_0 D_y} \right) \\ &\quad \times \left( 1 - e^{-\left(\frac{w y}{\sqrt{t}}\right)^2} \right) \sin \eta \frac{d\eta}{\eta^3}, \quad t \leq t_0 \\ \frac{\theta(y, t)}{\theta_0} &= 1 + \frac{2}{\pi} \int_0^\infty \left( \frac{y^2}{t_0 D_y} \right) e^{-\left(\frac{w y}{\sqrt{t}}\right)^2} \\ &\quad \times \left( 1 - e^{-\left(\frac{w y}{\sqrt{t}}\right)^2} \right) \sin \eta \frac{d\eta}{\eta^3}, \quad t > t_0 \end{aligned} \quad (6)$$

for ramp function ( $t_o > 0$ )

### Thermal Stresses for the Uncracked Problem

The transient thermal stresses for the uncracked medium can be obtained by assuming that the plate is unconstrained in  $y$  direction and fully constrained in  $x$  direction, so we may have

$$\sigma_{zz} = \sigma_{xz} = \sigma_{yz} = 0, \quad \varepsilon_{xx} = \varepsilon_{xy} = \varepsilon_{xz} = \varepsilon_{yz} = 0 \quad (7)$$

for generalized plane stress and

$$\varepsilon_{xx} = \varepsilon_{zz} = \varepsilon_{xy} = \varepsilon_{xz} = \varepsilon_{yz} = 0 \quad (8)$$

for plane strain. Since there are no stresses on the boundary  $y = 0$ , then

$$\sigma_{yy}(y, t) = 0, \quad 0 \leq y < \infty \quad (9)$$

By using (7)–(9) and the strain-stress relations that are given by

$$\begin{aligned} \varepsilon_{xx} - \alpha_x \theta &= \frac{1}{E_x} \sigma_{xx} - \frac{\nu_{yx}}{E_y} \sigma_{yy} - \frac{\nu_{zx}}{E_z} \sigma_{zz} \\ \varepsilon_{yy} - \alpha_y \theta &= -\frac{\nu_{xy}}{E_x} \sigma_{xx} + \frac{1}{E_y} \sigma_{yy} - \frac{\nu_{zy}}{E_z} \sigma_{zz} \\ \varepsilon_{zz} - \alpha_z \theta &= -\frac{\nu_{xz}}{E_x} \sigma_{xx} - \frac{\nu_{yz}}{E_y} \sigma_{yy} + \frac{1}{E_z} \sigma_{zz} \end{aligned} \quad (10)$$

where  $\alpha_i$ ,  $E_i$  ( $i = x, y, z$ ) are the coefficients of the thermal expansion and Young's modulus referred to the principal axes,  $\nu_{ij}$  ( $i, j = x, y, z$ ) are Poisson's ratio, and  $\nu_{ij}/E_i = \nu_{ji}/E_j$ , the thermal stresses can be expressed as

$$\sigma_{xx}^T(y, t) = -\bar{E} \bar{\alpha} \theta(y, t) \quad (11)$$

where

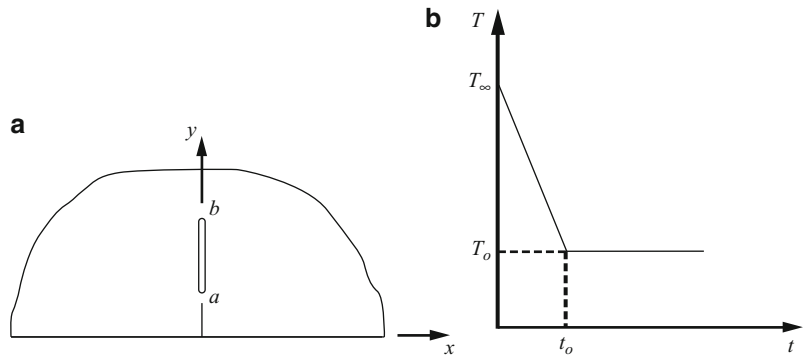
$$\bar{E} = E_x, \quad \bar{\alpha} = \alpha_x \quad (12)$$

for generalized plane stress and

$$\bar{E} = \frac{E_x}{1 - \nu_{xz} \nu_{zx}}, \quad \bar{\alpha} = (\alpha_x + \nu_{zx} \alpha_z) \quad (13)$$

for plane strain. By defining  $\sigma_o^T = -\bar{E} \bar{\alpha} \theta_o$ , the normalized thermal stresses can be written as

**Edge Crack, Composite Materials, Fig. 1** Crack geometry (a) and temperature change at the boundary (b)



$$\frac{\sigma_{xx}^T(y, t)}{\sigma_0^T} = \frac{\theta(y, t)}{\theta_0} \quad (14)$$

$$\begin{aligned} c_{11} &= \frac{1 - \nu_{xz}\nu_{zx}}{E_x}, \quad c_{22} = \frac{1 - \nu_{yz}\nu_{zy}}{E_y}, \\ c_{12} &= c_{21} = -\frac{\nu_{yx} + \nu_{zx}\nu_{yz}}{E_y} = -\frac{\nu_{xy} + \nu_{zy}\nu_{xz}}{E_x} \end{aligned} \quad (19)$$

### The Perturbation Problem

The perturbation problem for the cracked plate is formulated by using the thermal stresses for the uncracked plate (14), with opposite sign acting on the crack surfaces as the only external loads. Since  $y$  is an axis of symmetry, the problem will be considered for  $0 < x < \infty$ . Referring to Fig. 1a, the equations of equilibrium for displacements in plane elasticity are given by

$$\begin{aligned} \beta_1 \frac{\partial^2 u}{\partial x^2} + \frac{\partial^2 u}{\partial y^2} + \beta_3 \frac{\partial^2 v}{\partial x \partial y} &= 0 \\ \frac{\partial^2 v}{\partial x^2} + \beta_2 \frac{\partial^2 v}{\partial y^2} + \beta_3 \frac{\partial^2 u}{\partial x \partial y} &= 0 \end{aligned} \quad (15)$$

where  $u, v$  are the displacement components in  $x$  and  $y$  directions of the displacement vector and  $\beta_1, \beta_2, \beta_3$  are related to the engineering constants through the following relations

$$\beta_1 = \frac{b_{11}}{G_{xy}}, \quad \beta_2 = \frac{b_{22}}{G_{xy}}, \quad \beta_3 = 1 + \frac{b_{12}}{G_{xy}} \quad (16)$$

$$(b_{ij}) = B = C^{-1}, \quad C = (c_{ij}), \quad (i, j = 1, 2) \quad (17)$$

$$c_{11} = \frac{1}{E_x}, \quad c_{22} = \frac{1}{E_y}, \quad c_{12} = c_{21} = -\frac{\nu_{yx}}{E_y} = -\frac{\nu_{xy}}{E_x} \quad (18)$$

for generalized plane stress and

for plane strain.  $G_{xy}$  is the shear modulus in  $x - y$  plane. The differential equations (15) should be solved under the following homogenous boundary conditions

$$\sigma_{yy}(x, 0) = 0, \quad \sigma_{xy}(x, 0) = 0, \quad \sigma_{xy}(0, y) = 0 \quad (20)$$

and the mixed boundary condition

$$\begin{aligned} u(0, y) &= 0, \quad 0 < y < a, \quad b < y < \infty \\ \sigma_{xx}(0, y) &= -\sigma_{xx}^T(y, t), \quad a < y < b \end{aligned} \quad (21)$$

where  $\sigma_{xx}^T(y, t)$  are the thermal stresses obtained from the uncracked plate. The solution of (15) can be obtained by expressing the displacement components  $u, v$  in terms of the Fourier integral transform, i.e.,

$$\begin{aligned} u(x, y) &= \frac{2}{\pi} \int_0^\infty f_1(y, \alpha) \sin \alpha x d\alpha + \frac{1}{2\pi} \int_{-\infty}^\infty g_1(x, \beta) e^{i y \beta} d\beta \\ v(x, y) &= \frac{2}{\pi} \int_0^\infty f_2(y, \alpha) \cos \alpha x d\alpha + \frac{1}{2\pi} \int_{-\infty}^\infty g_2(x, \beta) e^{i y \beta} d\beta \end{aligned} \quad (22)$$

where  $f_1, f_2, g_1, g_2$  are unknown functions to be determined. Substituting (22) into (15) and solving ordinary differential equations, and

taking the advantage of  $u$  and  $v$  being bounded as  $x \rightarrow \infty$  and  $y \rightarrow \infty$ , the displacement components can be expressed as

$$\begin{aligned} u(x, y) &= \frac{2}{\pi} \int_0^\infty [C_1 e^{-\alpha s_1 y} + C_2 e^{-\alpha s_2 y}] \sin \alpha x d\alpha \\ &\quad + \frac{1}{2\pi} \int_{-\infty}^\infty \left[ D_1 e^{-\frac{|\beta|}{\beta_5} s_1 x} + D_2 e^{-\frac{|\beta|}{\beta_5} s_2 x} \right] e^{iy\beta} d\beta \\ v(x, y) &= \frac{2}{\pi} \int_0^\infty [-\beta_7 C_1 e^{-\alpha s_1 y} - \beta_8 C_2 e^{-\alpha s_2 y}] \cos \alpha x d\alpha \\ &\quad + \frac{1}{2\pi} \int_{-\infty}^\infty \frac{i\beta}{|\beta|} \left[ \beta_9 D_1 e^{-\frac{|\beta|}{\beta_5} s_1 x} + \beta_{10} D_2 e^{-\frac{|\beta|}{\beta_5} s_2 x} \right] e^{iy\beta} d\beta \end{aligned} \quad (23)$$

where  $C_1, C_2$  and  $D_1, D_2$  are unknown functions of the transform variables  $\alpha$  and  $\beta$ , respectively, and  $s_1, s_2$  are the positive roots of the characteristic equation

$$s^4 + \beta_4 s^2 + \beta_5^2 = 0 \quad (24)$$

$$s_1 = \sqrt{\frac{-\beta_4 + \beta_6}{2}}, \quad s_2 = \sqrt{\frac{-\beta_4 - \beta_6}{2}} \quad (25)$$

$$\beta_4 = \frac{\beta_3^2 - \beta_1 \beta_2 - 1}{\beta_2}, \quad \beta_5^2 = \frac{\beta_1}{\beta_2}, \quad \beta_6 = \sqrt{\beta_4^2 - 4\beta_5^2} \quad (26)$$

and

$$\begin{aligned} \beta_7 &= \frac{s_1 \beta_3}{1 - s_1^2 \beta_2}, \quad \beta_8 = \frac{s_2 \beta_3}{1 - s_2^2 \beta_2}, \\ \beta_9 &= -\frac{1}{\beta_3} \left( \frac{\beta_1 s_1}{\beta_5} - \frac{\beta_5}{s_1} \right), \quad \beta_{10} = -\frac{1}{\beta_3} \left( \frac{\beta_1 s_2}{\beta_5} - \frac{\beta_5}{s_2} \right) \end{aligned} \quad (27)$$

It is important to mention that the characteristic equation (24) may have real roots or complex roots. If the roots are real, the material is classified by material type I, and for complex roots, the material is classified by material type II. In the present work, we are interested in material type I, and a similar procedure may be obtained for material type II. In the case of material type I ( $s_1, s_2$  are real),  $\beta_6 < -\beta_4$  and  $\beta_4^2 - 4\beta_5^2 > 0$ ,  $\beta_6 > 0$ , then  $\beta_4 < 0$ . By using the following stress-displacement relations

$$\begin{aligned} \sigma_{xx} &= b_{11} \frac{\partial u}{\partial x} + b_{12} \frac{\partial v}{\partial y} \\ \sigma_{yy} &= b_{21} \frac{\partial u}{\partial x} + b_{22} \frac{\partial v}{\partial y} \\ \sigma_{xy} &= G_{xy} \left( \frac{\partial u}{\partial y} + \frac{\partial v}{\partial x} \right) \end{aligned} \quad (28)$$

the stresses  $\sigma_{xx}$ ,  $\sigma_{yy}$ , and  $\sigma_{xy}$  are given by

$$\begin{aligned} \sigma_{xx} &= \frac{2}{\pi} \int_0^\infty [(b_{11} + b_{12} \beta_7 s_1)(C_1 \alpha) e^{-\alpha s_1 y} \\ &\quad + (b_{11} + b_{12} \beta_8 s_2)(C_2 \alpha) e^{-\alpha s_2 y}] \cos \alpha x d\alpha \\ &\quad + \frac{1}{2\pi} \int_{-\infty}^\infty \left[ \left( -b_{12} \beta_9 - b_{11} \frac{s_1}{\beta_5} \right) (D_1 |\beta|) e^{-\frac{|\beta|}{\beta_5} s_1 x} \right. \\ &\quad \left. + \left( -b_{12} \beta_{10} - b_{11} \frac{s_2}{\beta_5} \right) (D_2 |\beta|) e^{-\frac{|\beta|}{\beta_5} s_2 x} \right] e^{iy\beta} d\beta \end{aligned} \quad (29)$$

$$\begin{aligned} \sigma_{yy} &= \frac{2}{\pi} \int_0^\infty [(b_{12} + b_{22} \beta_7 s_1)(C_1 \alpha) e^{-\alpha s_1 y} \\ &\quad + (b_{12} + b_{22} \beta_8 s_2)(C_2 \alpha) e^{-\alpha s_2 y}] \cos \alpha x d\alpha \\ &\quad + \frac{1}{2\pi} \int_{-\infty}^\infty \left[ \left( -b_{22} \beta_9 - b_{12} \frac{s_1}{\beta_5} \right) \right. \\ &\quad \times (D_1 |\beta|) e^{-\frac{|\beta|}{\beta_5} s_1 x} + \left( -b_{22} \beta_{10} - b_{12} \frac{s_2}{\beta_5} \right) \\ &\quad \times (D_2 |\beta|) e^{-\frac{|\beta|}{\beta_5} s_2 x} \left. \right] e^{iy\beta} d\beta \end{aligned} \quad (30)$$

$$\begin{aligned} \sigma_{xy} &= G_{xy} \left\{ \frac{2}{\pi} \int_0^\infty [(\beta_7 - s_1)(C_1 \alpha) e^{-\alpha s_1 y} \right. \\ &\quad + (\beta_8 - s_2)(C_2 \alpha) e^{-\alpha s_2 y}] \sin \alpha x d\alpha \\ &\quad + \frac{1}{2\pi} \int_{-\infty}^\infty \frac{i\beta}{|\beta|} \left[ \left( 1 - \beta_9 \frac{s_1}{\beta_5} \right) (D_1 |\beta|) e^{-\frac{|\beta|}{\beta_5} s_1 x} \right. \\ &\quad \left. + \left( 1 - \beta_{10} \frac{s_2}{\beta_5} \right) (D_2 |\beta|) e^{-\frac{|\beta|}{\beta_5} s_2 x} \right] e^{iy\beta} d\beta \right\} \end{aligned} \quad (31)$$

Defining new function

$$\phi(y) = \frac{\partial u(0, y)}{\partial y}, \quad 0 < y < \infty \quad (32)$$

and using the conditions (20) and (21) with the inversion of the Fourier transform, the unknown functions  $C_1, C_2, D_1, D_2$  can be obtained as

a function of  $\phi(y)$  and the problem will be reduced to the following singular integral equation

$$\int_a^b \frac{\phi(s)}{s-y} ds + \int_a^b k(y,s) \phi(s) ds = -\frac{\pi}{M} o_{xx}^T(y,t) \quad (33)$$

where

$$k(y,s) = \frac{2}{QM} \left[ \frac{q_{11}}{s\beta_{11} + s_1y} + \frac{q_{12}}{s\beta_{12} + s_1y} + \frac{q_{21}}{s\beta_{11} + s_2y} + \frac{q_{22}}{s\beta_{12} + s_2y} \right] \quad (34)$$

where  $\beta_{11} = \frac{\beta_s}{s_1}$ ,  $\beta_{12} = \frac{\beta_s}{s_2}$  and  $Q, M, q_{11}, q_{12}, q_{21}, q_{22}$  depend on the material constants and are given in Rizk, [2]. By examining (33), it is clear that the kernel  $k(y,s)$  is bounded as long as the crack is embedded. As the crack approaches the boundary  $y = 0$  ( $a = 0$ ), the kernel becomes unbounded ( $s \rightarrow 0$  and  $y \rightarrow 0$ ) which is known as the generalized Cauchy kernel.

### Singularities and Stress Intensity Factors

The singular behavior of the function  $\phi(y)$  around the crack tips can be examined by following the Muskhelishvili technique [3] using the function theoretic method. Let

$$\begin{aligned} \phi(s) &= \frac{f(s)}{(s-a)^{\gamma_1}(b-s)^{\gamma_2}} \\ &= \frac{e^{\pi i \gamma_2} f(s)}{(s-a)^{\gamma_1}(s-b)^{\gamma_2}} \end{aligned} \quad (35)$$

where  $f(s)$  is a continuous function in the interval  $a < s < b$ ,  $f(a) \neq 0$ ,  $f(b) \neq 0$  and  $\gamma_1, \gamma_2$  are the singularities at the crack tips  $a$  and  $b$ , respectively, which should satisfy  $0 < \text{Re}(\gamma_1, \gamma_2) < 1$ . Defining the sectionally holomorphic function of the complex variable  $z = y + ix$

$$F(z) = \frac{1}{\pi} \int_a^b \frac{\phi(s)}{s-z} ds \quad (36)$$

and performing the asymptotic analysis given by Muskhelishvili [3] near the crack end points,  $F(z)$  may be expressed as

$$\begin{aligned} F(z) &= \frac{f(a)}{(b-a)^{\gamma_2}} \frac{e^{\pi i \gamma_1}}{\sin \pi \gamma_1} \frac{1}{(z-a)^{\gamma_1}} \\ &\quad - \frac{f(b)}{(b-a)^{\gamma_1}} \frac{1}{\sin \pi \gamma_2} \frac{1}{(z-b)^{\gamma_2}} + F^*(z) \end{aligned} \quad (37)$$

where  $F^*(z)$  is bounded everywhere except possibly at the crack end points where it may have weaker singularities, i.e.,

$$|F^*(z)| < \frac{A_k}{(z-c_k)^{\gamma_k}}, \quad (k=1,2) \quad (38)$$

where  $A_k$  are positive constants,  $c_1 = a$ ,  $c_2 = b$  and  $\varepsilon_1 < \text{Re}(\gamma_1)$ ,  $\varepsilon_2 < \text{Re}(\gamma_2)$ . By using the Plemelj formula

$$F(y) = \frac{1}{2} [F^+(y) + F^-(y)], \quad a < y < b \quad (39)$$

Equation (37) becomes

$$\begin{aligned} \frac{1}{\pi} \int_a^b \frac{\phi(s)}{s-y} ds &= \frac{f(a) \cot \pi \gamma_1}{(b-a)^{\gamma_2}} \frac{1}{(y-a)^{\gamma_1}} \\ &\quad - \frac{f(b) \cot \pi \gamma_2}{(b-a)^{\gamma_1}} \frac{1}{(b-y)^{\gamma_2}} + F^*(y) \end{aligned} \quad (40)$$

Substituting (40) into (33) and multiplying by  $(y-a)^{\gamma_1}$  and letting  $y \rightarrow a$  and then multiplying by  $(y-b)^{\gamma_2}$  and letting  $y \rightarrow b$ , the characteristic equations for  $\gamma_1$  and  $\gamma_2$  are

$$\cot \pi \gamma_1 = 0 \quad (41)$$

$$\cot \pi \gamma_2 = 0 \quad (42)$$

with acceptable roots  $\gamma_1 = \frac{1}{2}$ ,  $\gamma_2 = \frac{1}{2}$  as for isotropic material. So the density function becomes

$$\phi(s) = \frac{f(s)}{\sqrt{(s-a)(b-s)}} \quad (43)$$



In the case of an edge crack ( $a \rightarrow 0$ ), the kernel  $k(y, s)$  would be singular and by applying the asymptotic analysis using the Muskhelishvili technique [3], we may have

$$\frac{1}{\pi} \int_0^b \frac{q_{ij} \phi(s)}{s \frac{\beta_s}{s_j} + s_i y} ds = \frac{q_{ij} \frac{s_j}{\beta_s} f(0)}{b^{\gamma_2} \left( \frac{s_i s_j}{\beta_s} y \right)^{\gamma_1} \sin \pi \gamma_1} + F_{ij}^*(y) \quad (44)$$

( $i, j = 1, 2$ )

where  $F_{ij}^*(y)$  has behavior similar to  $F^*(y)$ . Substituting (40) with  $a = 0$  and (44) into (33) and multiplying by  $y^{\gamma_1}$  and  $(b - y)^{\gamma_2}$  and letting  $y \rightarrow 0$  and  $y \rightarrow b$ , respectively, the characteristic equations for  $\gamma_1$  and  $\gamma_2$  become

$$\cos \pi \gamma_1 + \frac{2}{QM} \left[ \frac{q_{11}}{\beta_{11}} \left( \frac{\beta_{11}}{s_1} \right)^{\gamma_1} + \frac{q_{12}}{\beta_{12}} + \frac{q_{21}}{\beta_{11}} + \frac{q_{22}}{\beta_{12}} \left( \frac{\beta_{12}}{s_2} \right)^{\gamma_1} \right] = 0 \quad (45)$$

$$\cot \pi \gamma_2 = 0 \quad (46)$$

Note that  $s_1 s_2 = \beta_5$ . The only acceptable roots of (45) and (46) ( $0 < \text{Re}(\gamma_1, \gamma_2) < 1$ ) are  $\gamma_1 = 0$  and  $\gamma_2 = \frac{1}{2}$  as shown in [4], and the density function becomes

$$\phi(s) = \frac{f(s)}{\sqrt{(b - s)}} \quad (47)$$

The stress intensity factors in mode I at the irregular points  $a$  and  $b$  are defined by

$$K(a) = \lim_{y \rightarrow a^-} \sqrt{2(a - y)} \sigma_{xx}(0, y) \quad (48)$$

$$K(b) = \lim_{y \rightarrow b^+} \sqrt{2(y - b)} \sigma_{xx}(0, y) \quad (49)$$

where  $\sigma_{xx}(0, y)$  is the stress outside the crack. Observing that (33) gives the stresses inside and outside the crack, by substituting (33) into (48) and (49) and following Muskhelishvili [3], the stress intensity factors for an embedded crack at the irregular points  $a$  and  $b$  are given by

$$K(a) = M \frac{f(a)}{\sqrt{(b - a)/2}}, K(b) = -M \frac{f(b)}{\sqrt{(b - a)/2}} \quad (50)$$

For an edge crack ( $a = 0$ ), the stress intensity factor at the crack tip  $b$  will be given by

$$K(b) = -M \sqrt{2} f(b) \quad (51)$$

### Numerical Solution

The stress intensity factors given by (50) or (51) can be calculated by knowing the unknown function  $f(s)$  that can be determined numerically from the singular integral equation (33) using the expansion method developed by Kaya and Erdogan [5]. Normalizing the singular integral equation (33) using the following transfer variables

$$y = \frac{b - a}{2} r + \frac{b + a}{2}, \quad s = \frac{b - a}{2} \rho + \frac{b + a}{2} \quad (52)$$

Equation (33) will be reduced to

$$\begin{aligned} & \int_{-1}^{+1} \frac{F(\rho)}{(\rho - r)(1 + \rho)^{\gamma_1}(1 - \rho)^{\gamma_2}} d\rho \\ & + \int_{-1}^{+1} h(r, \rho) \frac{F(\rho)}{(1 + \rho)^{\gamma_1}(1 - \rho)^{\gamma_2}} d\rho \\ & = -\frac{\pi}{M} \sigma_{xx}^T(r, t), \quad -1 < r < 1 \end{aligned} \quad (53)$$

where

$$\begin{aligned} F(\rho) &= \left( \frac{2}{b - a} \right)^{\gamma_1 + \gamma_2} f(s) \\ h(r, \rho) &= \frac{b - a}{2} k(y, s) \end{aligned} \quad (54)$$

Multiplying (53) by  $M/\sigma_0^T$ , we may have

$$\begin{aligned} & \int_{-1}^{+1} \frac{F^*(\rho)}{(\rho - r)(1 + \rho)^{\gamma_1}(1 - \rho)^{\gamma_2}} d\rho \\ & + \int_{-1}^{+1} h(r, \rho) \frac{F^*(\rho)}{(1 + \rho)^{\gamma_1}(1 - \rho)^{\gamma_2}} d\rho \\ & = -\pi \frac{\sigma_{xx}^T(r, t)}{\sigma_0^T}, \quad -1 < r < 1 \end{aligned} \quad (55)$$

where  $F^*(\rho) = F(\rho)M/\sigma_0^T$ . Letting  $F^*(\rho)$  in the form of finite series as

$$F^*(\rho) = \sum_{n=0}^N a_n \rho^n, -1 < \rho < 1 \quad (56)$$

where  $a_n$  are  $(N+1)$  unknown coefficients to be determined. Substituting (56) into (55), we end up with a system of linear equations that are solved at certain collocation points which are chosen to be zeros of the Chebyshev polynomial. In the case of an embedded crack, only  $N$  collocation points, i.e.,

$$r_j = \cos \frac{\pi(2j-1)}{2N}, \quad j = 1, 2, \dots, N \quad (57)$$

which will give  $N$  equations in  $(N+1)$  coefficients in the form

$$\begin{aligned} \sum_{n=0}^N a_n \left[ \frac{\int_{-1}^{+1} \frac{\rho^n}{(\rho-r_j)(1+\rho)^{j+1}(1-\rho)^{j+2}} d\rho}{\int_{-1}^{+1} h(r_j, \rho) \frac{\rho^n}{(1+\rho)^{j+1}(1-\rho)^{j+2}} d\rho} \right] \\ = -\pi \frac{\sigma_{xx}^T(r_j, t)}{\sigma_0^T}, \quad j = 1, 2, \dots, N \end{aligned} \quad (58)$$

and for a unique solution, the following single-valuedness condition, which is obtained from (21) and (32), must be used, i.e.,

$$\int_a^b \phi(s) ds = 0 \quad (59)$$

which can be written as

$$\int_{-1}^{+1} a_n \frac{\rho^n}{(1+\rho)^{j+1}(1-\rho)^{j+2}} d\rho = 0 \quad (60)$$

Then the stress intensity factors at the crack tips  $a$  and  $b$  would be given by

**Edge Crack, Composite Materials, Table 1** The elastic constants of the orthotropic materials used in the numerical results (in GPa)

Material	$E_x$	$E_y$	$G_{xy}$	$\nu_{xy}$
A boron/epoxy	170.65	55.16	4.83	0.1114
B graphite/epoxy	294.0	6.4	4.9	0.23
C carbon/epoxy	142.0	10.3	7.2	0.27

$$\begin{aligned} K(a)/\sigma_0^T \sqrt{(b-a)/2} &= F^*(-1) \\ K(b)/\sigma_0^T \sqrt{(b-a)/2} &= -F^*(+1) \end{aligned} \quad (61)$$

In the case of an edge crack, the single-valuedness condition is no longer satisfied, and the number of the collocation points is  $(N+1)$  which will be

$$r_j = \cos \frac{\pi(2j-1)}{2(N+1)}, \quad j = 1, 2, \dots, N+1 \quad (62)$$

and the stress intensity factor at the crack tip  $b$  from (51) becomes

$$K(b)/\sigma_0^T \sqrt{b} = -F^*(+1) \quad (63)$$

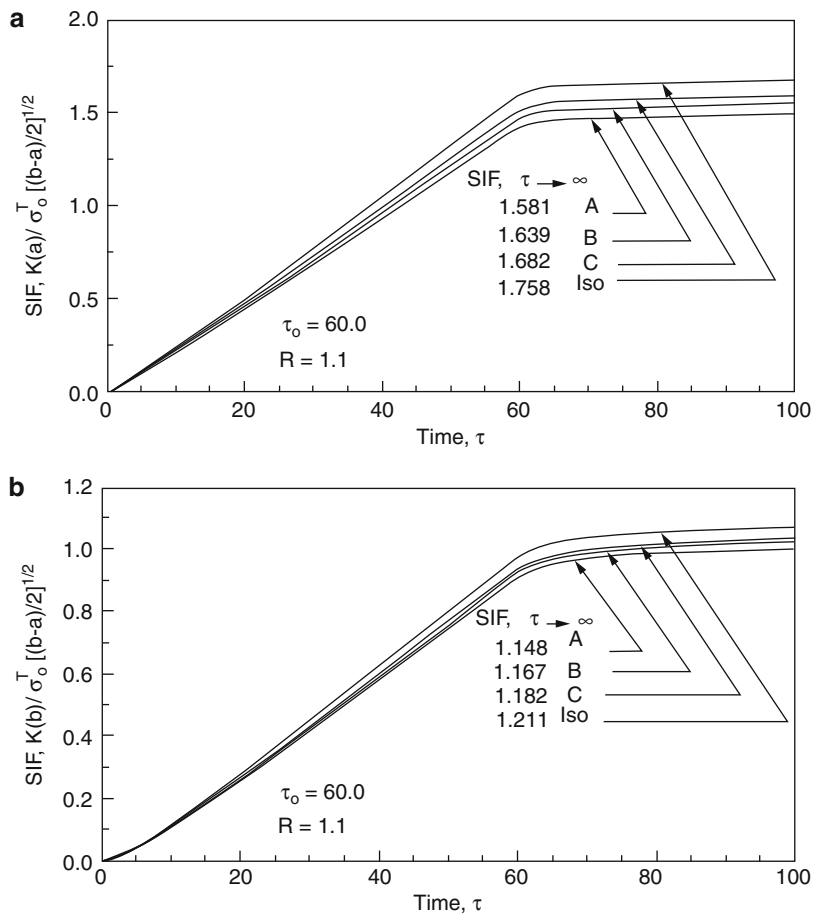
All numerical integrations in (58) are obtained by using Gauss quadrature formulas described in [6].

## Sample Results

Some results of the normalized stress intensity factors for an internal and edge crack are calculated from (61) and (63) for the generalized plane stress case only. The elastic properties of the orthotropic materials used in these calculations are given in Table 1, and they are chosen to be material type I. Figure 2 demonstrates the results for internal crack at crack tip  $y = a$

# Edge Crack, Composite Materials,

**Fig. 2** Normalized stress intensity factors for an internal crack,  $R = 1.1$ ,  $\tau_o = 60.0$



$(K(a)/\sigma_o^T \sqrt{(b-a)/2})$  and at the crack tip  $y = b$   $(K(b)/\sigma_o^T \sqrt{(b-a)/2})$  as a function of the normalized time  $(\tau = tD_y/[(b-a)/2]^2)$  and the normalized cooling rate  $(\tau_o = t_o D_y/[(b-a)/2]^2)$  and the location of the crack measured by  $R = (b+a)/(b-a)$ . Also, Fig. 3 shows the results for an edge crack ( $a = 0$ ) defined by  $K(b)/\sigma_o^T \sqrt{b}$  as function of the normalized time  $\tau$  and the normalized cooling rate  $\tau_o$ . The effect of the

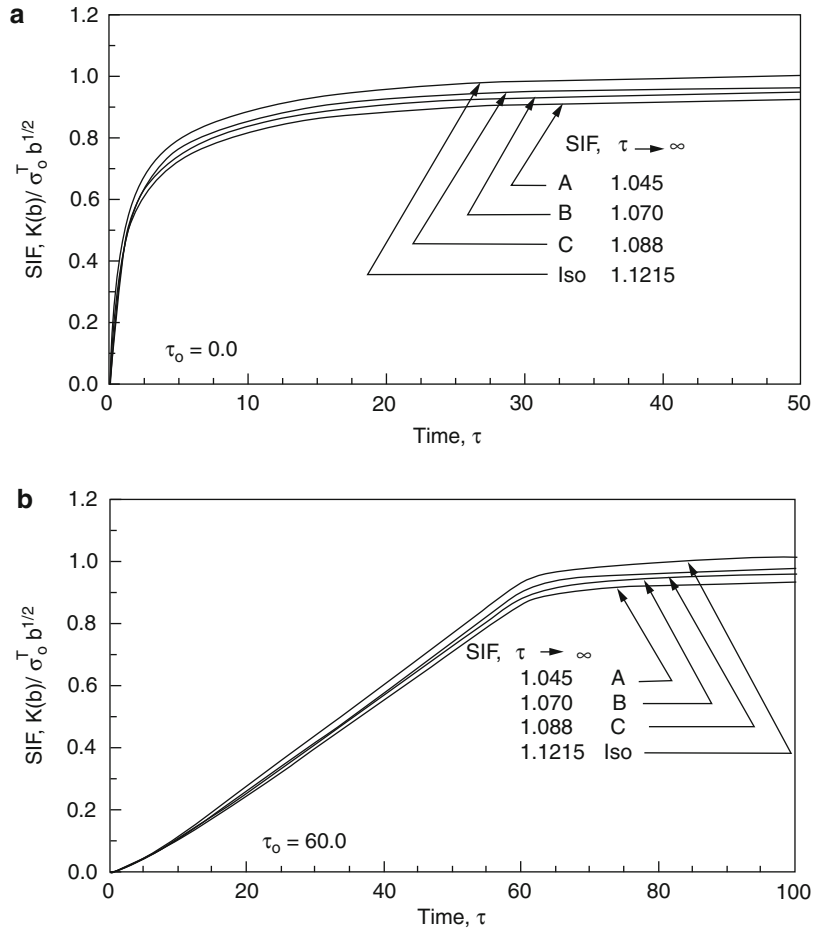
material properties for different orthotropic materials and isotropic materials is demonstrated in these figures.

## Cross-References

- [Edge Crack, Bimaterial Systems](#)
- [Edge Crack, Isotropic Material](#)

### Edge Crack, Composite Materials,

**Fig. 3** Normalized stress intensity factors for an edge crack ( $\tau_o = 0, 60$ )



### References

1. Carslaw HS, Jaeger JC (1950) Conduction of heat in solids. Oxford University Press, Oxford
2. Rizk AA (2006) Orthotropic semi-infinite medium with a crack under thermal shock. Theor Appl Fract Mech 46:217–231
3. Muskhelishvili NI (1953) Singular integral equations. Noordhoff, Groningen
4. Delale F, Erdogan F (1977) The problem of internal and edge cracks in orthotropic materials. J Appl Mech Trans ASME 44:237–242
5. Kaya AC, Erdogan F (1987) On the solution of integral equations with strongly singular kernels. Q Appl Math 45:105–122
6. Stroud A, Secrest D (1966) Gaussian quadrature formulas. Prentice-Hall, New York

### Edge Crack, Isotropic Material

Abdel-Fattah Rizk<sup>1</sup> and Meftah Hrairi<sup>2</sup>

<sup>1</sup>Department of Engineering Mathematics and Physics, Alexandria University, Alexandria, Egypt

<sup>2</sup>Department of Mechanical Engineering, International Islamic University Malaysia, Kuala Lumpur, Malaysia

### Synonyms

Fracture mechanics; Stress intensity factor

## Definition

Fracture mechanics only deals with cracked materials; it cannot help with situations involving uncracked materials. However, a majority of structures contain cracks which either are introduced during the manufacturing or are initiated early in the life of the structures. These types of cracks are frequently the source of service failures. Fracture mechanics is a systems approach to estimate the relationship between the stresses, the flaw geometry, and the material properties as it relates to the structural integrity of the component under consideration. The primary objectives are to prevent failures, promote effective design, and make efficient use of materials. The field of fracture mechanics matured in the last two decades of the twentieth century. Current research tends to result in incremental advances rather than major gains. The application of this technology to practical problems is so pervasive that fracture mechanics is now considered an established engineering discipline [1].

## Overview

The thermal loading of crack problems in an elastic plate has been of wide interest since it exists in many engineering applications such as aircraft, turbine engines, and power plants. The thermal shock may be due to sudden heating or cooling of the solid surface of the plate. In the case of an edge crack, the analysis of the problem under surface cooling is different than the analysis under surface heating. For a plate subjected to surface cooling, very high tensile stresses take place close to the cooled surface, which tend to open the crack surfaces. In the case of surface heating, compressive stresses are generated near the heated surface, forcing the crack surfaces to come into contact along a certain contact length. It is important to note that the solution for the temperature distribution as well as the solution for the transient thermal stresses is independent

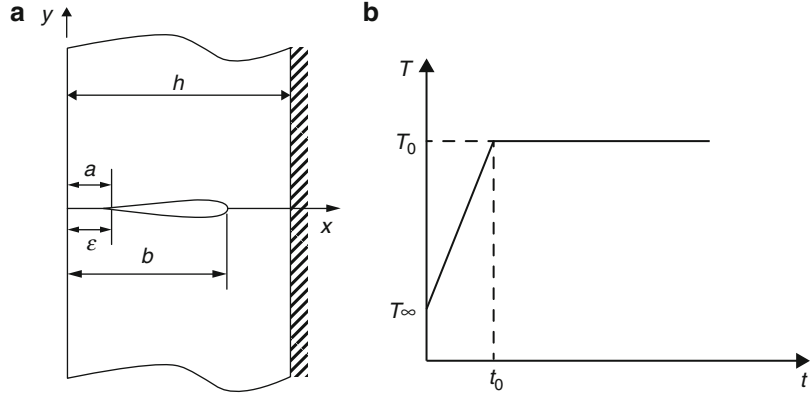
of whether the surface is heated or cooled. If the contact between the crack surfaces is not taken into account, the stress intensity factors will always yield negative values, but when the contact length is taken into account the resulting calculations produce positive stress intensity factors. So, the problem is considered to be an embedded crack problem with smooth closure conditions at the crack surfaces. In this entry, the problem of edge crack in an elastic plate under heating thermal shock is considered. The plate is assumed to be insulated on one face and heated on the other face containing the crack where a ramp heating function is assumed. The superposition technique is used to solve this problem. Governing equations describing temperature distribution, thermal stresses in the uncracked medium, displacements components of the crack problem as well as singularities and stress intensity factors are presented. The formulation presented here for isotropic and homogeneous materials may be generalized to include anisotropic and heterogeneous plates in addition to laminated plates.

## Basic Assumptions

Consider an elastic strip of thickness  $h$  with an edge crack as shown in Fig. 1. The elastic strip is assumed to be at an initial temperature  $T_\infty$ , and insulated at the boundary  $x = h$ . The boundary  $x = 0$ , which contains an edge crack, is subjected to sudden heating or cooling by changing the temperature to  $T_o$ . The analysis of edge crack problems under thermal loading is based upon the following simplifying conditions:

1. The plate is constructed of an isotropic, homogenous, and linearly elastic material.
2. The problem is quasi-static, i.e., inertia effects are neglected.
3. Thermoelastic coupling effects and the temperature dependence of the thermoelastic coefficients are negligible.

**Edge Crack, Isotropic Material, Fig. 1** Edge crack geometry heated on the surface  $x = 0$  with crack contact length and temperature boundary condition



4. Solution of the problem is obtained by using the superposition technique: the thermal stresses for the uncracked problem are evaluated, and then the mixed boundary value problem for the cracked strip is formulated with the crack surface tractions that are equal and opposite to the thermal stresses obtained from the uncracked problem.

### Mathematical Formulation of the Problem

Since the material is linear, the superposition technique is used, i.e., the total stress state in the medium is the sum of the two solutions. The first solution is obtained for the uncracked medium under transient thermal loading by using the transient temperature distribution that is obtained from the solution of the diffusion problem. The second solution is found for the isothermal cracked medium (mixed boundary value problem) by applying the stresses given by the first solution with opposite sign on the crack surfaces as the only external loads.

#### Temperature Distribution

The formulation of the crack problem makes use of the transient thermal stresses from the uncracked problem. The transient temperature distribution needed to obtain these stresses can be determined by solving the diffusion equation:

$$\frac{\partial^2 \theta(x, t)}{\partial x^2} = \frac{1}{D} \frac{\partial \theta(x, t)}{\partial t} \quad (1)$$

under the initial and boundary conditions:

$$\theta(x, 0) = 0 \quad (2)$$

$$\frac{\partial \theta(h, t)}{\partial x} = 0 \quad (3)$$

$$\theta(0, t) = \theta_o H(t) \quad (4)$$

where  $\theta(x, t)$  and  $\theta_o$  are defined:

$$\theta(x, t) = T(x, t) - T_\infty \quad (5)$$

$$\theta_o = T_o - T_\infty \quad (6)$$

And  $T(x, t)$ ,  $T_\infty$ , and  $T_o$  are the temperatures of the strip at any time  $t$ , the initial temperature and the sudden temperature change at the boundary, respectively.  $H(t)$  is the Heaviside function.

The solution of (1) subjected to the conditions (2)–(4) can be obtained by using Laplace transform [2] which takes the following form:

$$\frac{T(x^*, \tau) - T_o}{T_\infty - T_o} = 2 \sum_{n=1}^{\infty} \frac{e^{-\tau \lambda_n} \cos \lambda_n (x^* - 1)}{\lambda_n \sin \lambda_n} \quad (7)$$

where  $x^* = x/h$ ,  $\tau = tD/h^2$ , and  $D$  is the thermal diffusivity and

$$\lambda_n = \frac{\pi}{2} (2n - 1); \quad n = 1, 2, \dots \quad (8)$$

Now, by assuming a ramp function at the boundary  $x = 0$ , i.e.,

$$\theta(0, t) = \frac{\theta_0}{t_0}t + \left(\theta_0 - \frac{\theta_0}{t_0}t\right)H(t - t_0) \quad (9)$$

where  $t_0$  is the actual duration time of the heating ramp, the solution for the temperature distribution is also obtained by using Laplace transform and convolution theorem. By defining  $\tau_0 = t_0 D/h^2$ , the temperature distribution can be written in the form:

$$\begin{aligned} \frac{T(x^*, \tau) - T_0}{T_\infty - T_0} \\ = \left(1 - \frac{\tau}{\tau_0}\right) - 2 \sum_{n=1}^{\infty} \frac{(e^{-\tau \lambda_n^2} - 1) \cos \lambda_n (x^* - 1)}{\tau_0 \lambda_n^3 \sin \lambda_n}; \\ \tau \leq \tau_0 \end{aligned} \quad (10a)$$

$$\begin{aligned} \frac{T(x^*, \tau) - T_0}{T_\infty - T_0} \\ = 2 \sum_{n=1}^{\infty} \frac{e^{-\tau_0 \lambda_n^2} (e^{\tau_0 \lambda_n^2} - 1) \cos \lambda_n (x^* - 1)}{\tau_0 \lambda_n^3 \sin \lambda_n}; \tau > \tau_0 \end{aligned} \quad (10b)$$

### Thermal Stresses in the Uncracked Medium

Once the temperature distribution in the uncracked strip is known, the thermal stresses in the  $y$ -direction which satisfy the conditions of force and momentum equilibrium through the strip section can be determined by [3]

$$\sigma_{yy}^T(x, t) = \frac{\alpha E}{1 - \nu} \left[ -T(x, t) + \frac{4h - 6x}{h^2} \int_0^h T(x, t) dx + \frac{12x - 6h}{h^3} \int_0^h T(x, t) x dx \right] \quad (11)$$

where  $\alpha$  is the coefficient of thermal expansion,  $E$  modulus of elasticity, and  $\nu$  Poisson's ratio.

Substituting (7) into (11), the thermal stresses for unit step change become

$$\begin{aligned} \frac{\sigma_{yy}^T(x^*, \tau)(1 - \nu)}{\alpha E(T_\infty - T_0)} = -2 \sum_{n=1}^{\infty} \frac{e^{-\tau \lambda_n^2} \cos \lambda_n (x^* - 1)}{\lambda_n \sin \lambda_n} \\ + 2(4 - 6x^*) \sum_{n=1}^{\infty} \frac{e^{-\tau \lambda_n^2}}{\lambda_n^2} + 2(12x^* - 6) \sum_{n=1}^{\infty} \frac{e^{-\tau \lambda_n^2}}{\lambda_n^3 \sin \lambda_n} \end{aligned} \quad (12)$$

Also, substituting (10a), (10b) for a ramp function condition into (11), the thermal stresses can be written as follows:

$$\begin{aligned} \frac{\sigma_{yy}^T(x^*, \tau)(1 - \nu)}{\alpha E(T_\infty - T_0)} = - \left[ \left(1 - \frac{\tau}{\tau_0}\right) - 2 \sum_{n=1}^{\infty} \frac{(e^{-\tau \lambda_n^2} - 1) \cos \lambda_n (x^* - 1)}{\tau_0 \lambda_n^3 \sin \lambda_n} \right] \\ + (4 - 6x^*) \left[ \left(1 - \frac{\tau}{\tau_0}\right) - 2 \sum_{n=1}^{\infty} \frac{(e^{-\tau \lambda_n^2} - 1)}{\tau_0 \lambda_n^4} \right] \\ + (12x^* - 6) \left[ \frac{1}{2} \left(1 - \frac{\tau}{\tau_0}\right) - 2 \sum_{n=1}^{\infty} \frac{(e^{-\tau \lambda_n^2} - 1)}{\tau_0 \lambda_n^5 \sin \lambda_n} \right]; \tau \leq \tau_0 \end{aligned} \quad (13a)$$

$$\begin{aligned}
\frac{\sigma_{yy}^T(x^*, \tau)(1-\nu)}{\alpha E(T_\infty - T_0)} = & - \left[ 2 \sum_{n=1}^{\infty} \frac{e^{-\tau_o \lambda_n^2} (e^{\tau_o \lambda_n^2} - 1)}{\tau_o \lambda_n^3} \frac{\cos \lambda_n (x^* - 1)}{\sin \lambda_n} \right] \\
& + (4 - 6x^*) \left[ 2 \sum_{n=1}^{\infty} \frac{e^{-\tau \lambda_n^2} (e^{\tau_o \lambda_n^2} - 1)}{\tau_o \lambda_n^4} \right] \\
& + (12x^* - 6) \left[ 2 \sum_{n=1}^{\infty} \frac{e^{-\tau \lambda_n^2} (e^{\tau_o \lambda_n^2} - 1)}{\tau_o \lambda_n^5 \sin \lambda_n} \right]; \quad \tau > \tau_o
\end{aligned} \quad (13b)$$

### The Crack Problem

Once we have obtained the thermal stresses for the uncracked strip, the crack problem can be formulated by using these stresses with an opposite sign acting on the crack surface. The governing differential equations for the displacements in plane elasticity are given by

$$(\chi - 1)\nabla^2 u + 2\left(\frac{\partial^2 u}{\partial x^2} + \frac{\partial^2 v}{\partial x \partial y}\right) = 0 \quad (14)$$

$$(\chi - 1)\nabla^2 v + 2\left(\frac{\partial^2 u}{\partial x \partial y} + \frac{\partial^2 v}{\partial y^2}\right) = 0 \quad (15)$$

where  $u$ ,  $v$  are the  $x$ ,  $y$  components of the displacement vector,  $\chi = 3 - 4\nu$  for plane strain, and  $\chi = (3 - 4\nu)/(1 + \nu)$  for plane stress. By assuming  $y = 0$  is a plane of symmetry, the homogeneous boundary conditions are given by

$$\sigma_{xx}(0, y) = \sigma_{xx}(h, y) = 0; \quad 0 < y < \infty \quad (16)$$

$$\sigma_{xy}(0, y) = \sigma_{xy}(h, y) = 0; \quad 0 < y < \infty \quad (17)$$

and the mixed boundary conditions are

$$v(x, 0) = 0; \quad 0 < x < a, \quad b < x < h \quad (18)$$

$$\sigma_{xy}(x, 0) = -\sigma_{yy}^T; \quad a < x < b \quad (19)$$

where  $\sigma_{yy}^T$  is a known function of thermal stresses obtained from the uncracked problem. The density function is defined as

$$\phi(x) = \frac{\partial v(x, 0)}{\partial x} \quad (20)$$

The solutions of the differential (14) and (15) are obtained by expressing  $u$  and  $v$  in terms of the Fourier integral, i.e.,

$$\begin{aligned}
u(x, y) = & \frac{2}{\pi} \int_0^\infty f(x, \omega) \cos y \omega d\omega \\
& + \frac{1}{2\pi} \int_{-\infty}^\infty h(y, \beta) e^{i\omega\beta} d\beta
\end{aligned} \quad (21)$$

$$\begin{aligned}
v(x, y) = & \frac{2}{\pi} \int_0^\infty g(x, \omega) \sin y \omega d\omega \\
& + \frac{1}{2\pi} \int_{-\infty}^\infty q(y, \beta) e^{i\omega\beta} d\beta
\end{aligned} \quad (22)$$

where  $f$ ,  $h$ ,  $g$ , and  $q$  are unknown functions to be determined. By using stress displacement relations,  $\sigma_{xy}(x, 0) = 0$ , and the conditions specified by (16)–(20), the problem will be reduced, after a lengthy but straightforward method, to the following singular integral equation:

$$\begin{aligned}
\int_a^b \frac{\phi(s)}{s-x} ds + \int_a^b k(x, s) \phi(s) ds = \\
- \frac{\pi(\chi + 1)}{4\mu} \sigma_{yy}^T(x, t); \quad a < x < b
\end{aligned} \quad (23)$$

where  $k(x, s)$  is the Fredholm kernel of the singular integral equation which can be found in [4]. This kernel is bounded as long as the crack is an embedded crack ( $a > 0$ ,  $b < h$ ). In deriving (23)



we used  $\partial v / \partial x = 0$  outside the crack interval  $a < x < b$  rather than  $v = 0$ . Thus, the continuity of the displacement required that (23) must be solved under the following single valuedness condition:

$$\int_a^b \phi(x) dx = 0 \quad (24)$$

### Singularities and Stress Intensity Factors

The singular nature of the unknown function  $\phi(s)$  at the irregular points  $a$  and  $b$  may be determined by following the Muskhelishvili technique [5] using the function theoretic method. The solution can be put in the form

$$\phi(s) = \frac{g(s)}{(s-a)^{\gamma_1}(b-s)^{\gamma_2}} \quad (25)$$

where  $g(s)$  is Holder continuous in the interval  $a < s < b$ , and  $g(a) \neq 0$ ,  $g(b) \neq 0$ . Also, the singularity  $\gamma_1, \gamma_2$  at the end points should satisfy  $0 < \text{Re}(\gamma_1, \gamma_2) < 1$ . The singularities at the end points  $a, b$  are given by [5]

$$\gamma_1 = \gamma_2 = \frac{1}{2} \quad (26)$$

Our primary interest is to calculate the stress intensity factors which are defined as

$$K(a) = \lim_{x \rightarrow a} \sqrt{(2(a-x))} \sigma_{yy}(x, 0) \quad (27)$$

$$K(b) = \lim_{x \rightarrow b} \sqrt{(2(x-b))} \sigma_{yy}(x, 0) \quad (28)$$

where  $\sigma_{yy}(x, 0)$  is the stress outside the crack. Following [5], the stress intensity factors for an embedded crack can be written as

$$K(a) = \frac{4\mu}{\chi+1} \left( \frac{2}{b-a} \right)^{\frac{1}{2}} g(a) \quad (29)$$

$$K(b) = \frac{-4\mu}{\chi+1} \left( \frac{2}{b-a} \right)^{\frac{1}{2}} g(b) \quad (30)$$

The formulation of the crack contact problem should depend on the crack contact length  $\varepsilon$  in the compressive zone which is an additional unknown variable. The physical condition which accounts for this unknown is the smooth closure condition of the crack surfaces at  $x = a$  [6] i.e.,

$$K(a) = 0 \quad (31)$$

where  $K(a)$  is defined by (29). So, the calculation of the crack contact zone  $\varepsilon$  can be obtained from the solution of the embedded crack problem by fixing the crack length at  $x = b$  and then determining by iteration the location of the crack tip at  $x = a$  at each time step such that (31) is satisfied. In this manner, the crack contact zone  $\varepsilon$  and the stress intensity factors for edge crack stress at  $x = b$  for various crack lengths can be determined.

### Numerical Solution

To solve the singular integral equation (23), the following change in variables will be made:

$$s = \frac{b-a}{2} \rho + \frac{b+a}{2}, \quad x = \frac{b-a}{2} r + \frac{b+a}{2} \quad (32)$$

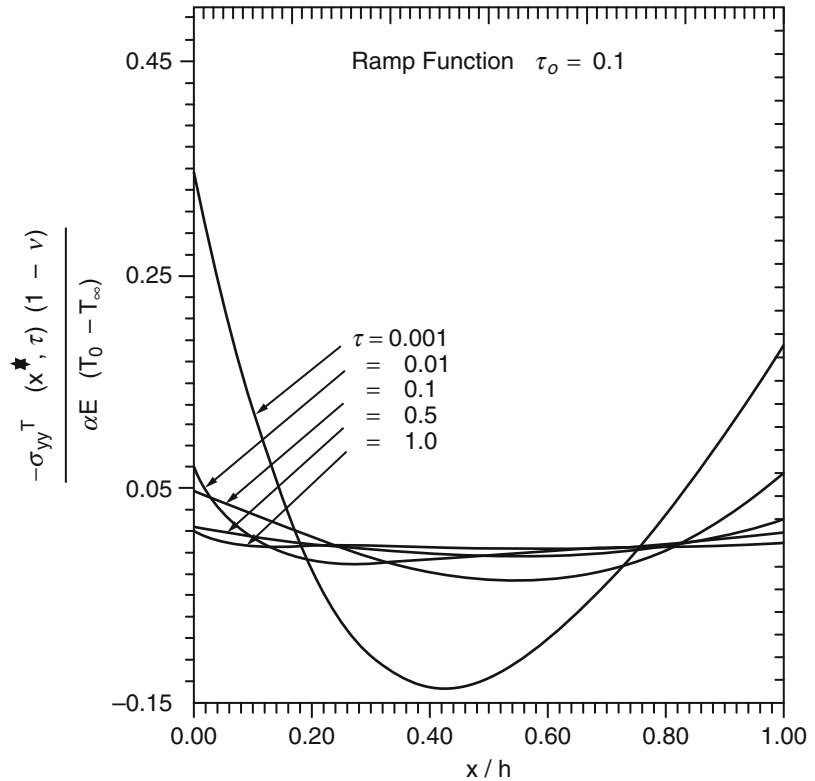
Then the singular integral equation can be reduced to

$$\begin{aligned} & \int_{-1}^1 \frac{\psi(\rho) d\rho}{(\rho-r)(1+\rho)^{\gamma_1}(1-\rho)^{\gamma_2}} \\ & + \int_{-1}^1 \bar{k}(r, \rho) \frac{\psi(\rho) d\rho}{(1+\rho)^{\gamma_1}(1-\rho)^{\gamma_2}} = \\ & - \pi \frac{\chi+1}{4\mu} \sigma_{yy}^T(r, t). \end{aligned} \quad (33)$$

where

$$\psi(\rho) = \left( \frac{2}{b-a} \right)^{\gamma_1+\gamma_2} g(s) \quad (34)$$

**Edge Crack, Isotropic Material, Fig. 2** Thermal stress distributions using heating ramp function  $\tau_o = 0.1$ , for different values of time,  $\tau$



$$\phi(s) = \frac{g(s)}{(s-a)^{\gamma_1}(b-s)^{\gamma_2}} = \frac{\psi(\rho)}{(1+\rho)^{\gamma_1}(1-\rho)^{\gamma_2}} \quad (35)$$

$$\bar{k}(r, \rho) = \frac{b-a}{2} k(r, \rho) \quad (36)$$

Subjected to the single valuedness condition

$$\int_{-1}^1 \frac{\psi(\rho)}{(1+\rho)^{\gamma_1}(1-\rho)^{\gamma_2}} d\rho = 0 \quad (37)$$

The numerical solution of (33) is obtained by using the expansion method developed in [7] which is easy to use and gives faster convergence to the solution when compared with other methods. Assume the solution is in the form of a finite series as

$$\psi(\rho) = \sum_{n=0}^N a_n \rho^n; -1 < \rho < 1 \quad (38)$$

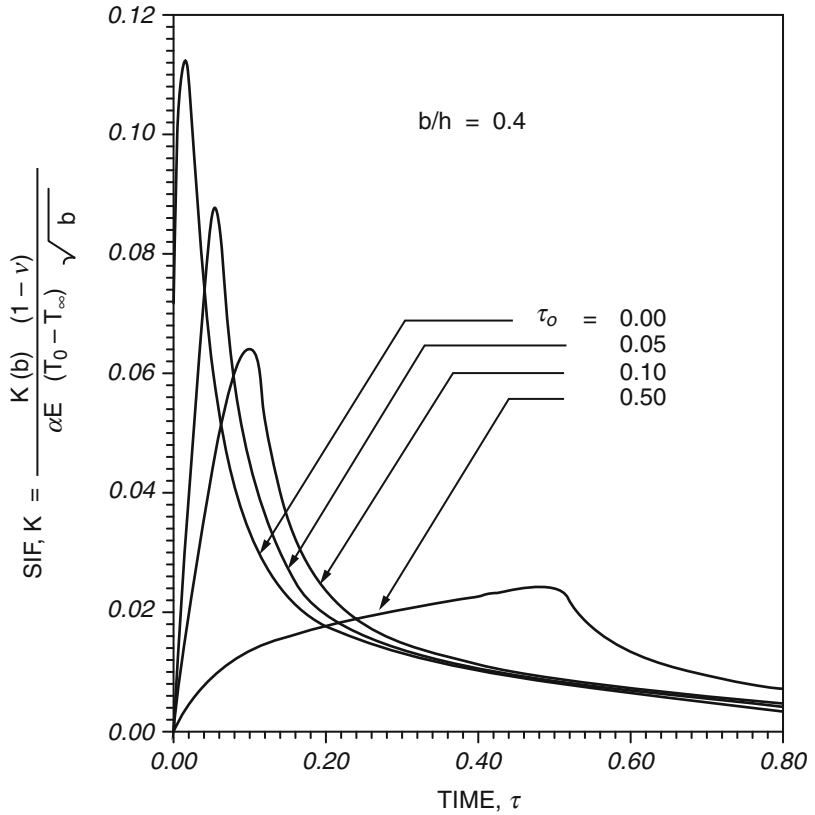
where  $a_n$  are the coefficients of the series to be determined. Substituting (38) into (33) and following [4], we obtain a system of linear equations that are solved at certain collocation points. The collocation points are chosen to be the zeros of Chebyshev polynomials of degree  $N$  in order to reduce the numerical errors. So, the collocation points are

$$r_j = \cos \frac{\pi(2j-1)}{2N}; j = 1, 2, \dots, N \quad (39)$$

These points will give us  $N$ -equations in  $(N+1)$  unknowns. So, (37) is an extra condition to obtain a unique solution. The numerical integration of (33) is obtained by using Gaussian integration procedure shown in [8].

### Edge Crack, Isotropic Material, Fig. 3

Stress intensity factor distributions at the crack location  $\frac{b}{h} = 0.4$  for different values of the heating rate  $\tau_o$



### Sample Results

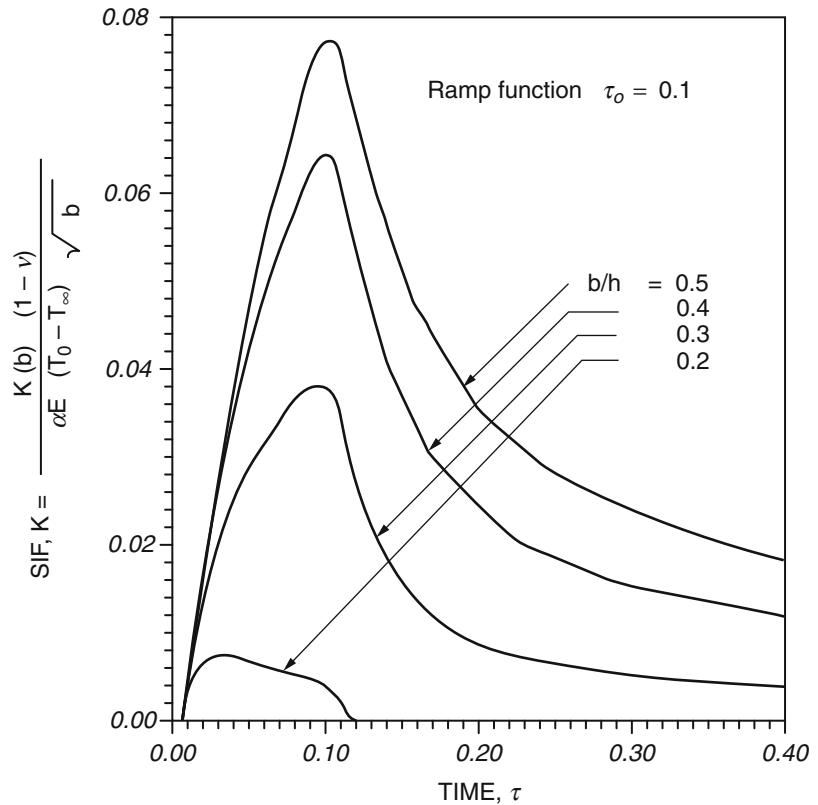
The results of thermal stresses, stress intensity factors, and crack contact length are obtained [8]. The latter two can be presented in function of time, crack length, heating rate, etc. Some of these results are shown for the edge-cracked plate under heating (Fig. 1). The normalized transient thermal stresses in the uncracked strip determined from (13) are shown in Fig. 2. Figures 3 and 4 show the normalized stress intensity factors defined by

$$K = \frac{(1-\nu)K(b)}{\alpha E (T_o - T_\infty) \sqrt{b}} \quad (40)$$

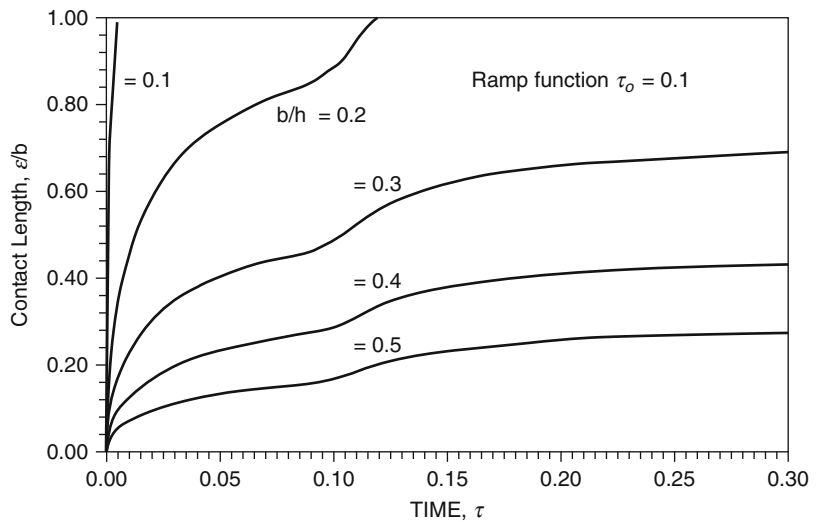
versus the normalized time (Fourier number,  $\tau$ ). It can be seen that the stress intensity factor

increases as a function of time to a maximum value and then decreases rapidly for all values of  $\frac{b}{h}$  and  $\tau_o$ . Also, it is observed from Fig. 4 that in the case of a heated surface, the stress intensity factor increases with increasing crack length. The opposite happens when the plate surface is cooled. This means that the thermal fracture with surface heating, especially with deep cracks, is more important than that for surface cooling. As the values of  $\tau$  increase, the stress intensity factors decrease and also delay the time at which the maximum stress intensity factor is reached (Fig. 3). Figure 5 shows the normalized crack lengths  $\frac{c}{b}$  versus normalized time  $\tau$ . It is clear that for short crack length,  $\frac{b}{h} = 0.1, 0.2$ , complete crack closure over the entire length of the crack will occur.

**Edge Crack, Isotropic Material, Fig. 4** Stress intensity factor distributions using heating rate  $\tau_o = 0.1$  for different values of the crack length  $\frac{b}{h}$



**Edge Crack, Isotropic Material, Fig. 5** Crack contact length using heating rate  $\tau_o = 0.1$  for different values of crack length  $\frac{b}{h}$



## References

1. Anderson TL (2005) Fracture mechanics: fundamentals and applications. CRC Press, Boca Raton
2. Carslaw HS, Jaeger JC (1950) Conduction of heat in solids. Oxford University Press, Oxford
3. Burgreen D (1971) Elements of thermal stress analysis. C. P. Press, Jamaica
4. Rizk AA (1994) Edge-cracked plate with one free and one constrained boundary subjected to sudden convective cooling. J Thermal Stresses 17: 453–469

5. Muskhelishvili NI (1953) Singular integral equations. Noordhoff, Groningen
6. Bakioglu M, Erdogan F, Hesselman DPH (1976) Fracture mechanical analysis of self fatigue in surface compression strengthened glass plates. *J Mater Sci* 11:1826–1834
7. Kaya AC, Erdogan F (1987) On the solution of integral equations with strongly singular kernels. *Q Appl Math* 45:105–122
8. Rizk AA (1993) A cracked plate under transient thermal stresses due to surface heating. *Eng Fract Mech* 45:687–696

## Edge Movability

► [Aerothermoelastic Behavior of Flat and Curved Panels](#)

## Effect of Creep on Cyclic Loading of Spherical Vessels Based on the Kinematic Hardening Models

Hossein Mahbadi<sup>1</sup> and Mohammad Reza Eslami<sup>2</sup>

<sup>1</sup>Mechanical Engineering Department, Islamic Azad University, Central Tehran Branch, Tehran, Iran

<sup>2</sup>Department of Mechanical Engineering, Amirkabir University of Technology, Tehran, Iran

### Definition

The definition of terms *primary stress* and secondary stress is given in the entry ► [Thermal Cyclic Loading of Beams Based on the Prager and Armstrong-Frederick Kinematic Hardening Models](#).

### Overview

In the entry ► [Thermal Cyclic Loading of Thick Spherical Vessels Based on the Prager and Armstrong-Frederick Kinematic Hardening Models](#), ratcheting, shakedown, or reversed

plasticity behavior of thick spherical vessels using the Prager and Armstrong–Frederick models were investigated. The results showed that the spherical symmetry has significant effect on some cases of cyclic loading in comparison to the cylindrical vessels. On the other hand, different results were obtained using the Armstrong–Frederick model for the same problems that were solved using the Prager model. In the present entry, the effect of creep on cyclic loading of thick spherical vessels under load- and strain-controlled cyclic loading is investigated. The vessel material is assumed to be isotropic and homogeneous and obeys a nonlinear strain hardening law in the plastic range. The secondary creep law is considered to obtain creep strains at elevated temperatures. The kinematic hardening theory based on the Prager [1] and Armstrong–Frederick [2] models with the von Mises associated flow rule is used to predict the ratcheting or shakedown behavior of thick cylindrical vessels. An incremental iterative method is used to analyze the structural behavior under cyclic loading conditions. Using the Prager and Armstrong–Frederick kinematic hardening models, the cyclic loading results of a vessel under various types of loads, including creep at the end of each load cycle, are compared with those in which creep is excluded.

### Mathematical Formulation

Consider a thick sphere of inside and outside radii  $a$  and  $b$  under pressures  $P_i$  and  $P_o$  at its inside and outside surfaces, respectively. The temperatures at inside and outside surfaces of the vessel are  $T_a$  and  $T_b$ , respectively. Accordingly, the temperature distribution  $T(r)$  through the vessel thickness is [3]

$$T(r) = T_a - (T_a - T_b) \frac{(1 - a/r)}{(1 - a/b)} \quad (1)$$

To normalize the equations, the following dimensionless quantities are defined:

$$\begin{aligned}
S_r &= \frac{\sigma_r}{\sigma_0}, S_\theta = \frac{\sigma_\theta}{\sigma_0}, S_\phi = \frac{\sigma_\phi}{\sigma_0}, e_r = \frac{\varepsilon_r}{\varepsilon_0} \\
e_\theta &= \frac{\varepsilon_\theta}{\varepsilon_0}, e_\phi = \frac{\varepsilon_\phi}{\varepsilon_0}, e_r^p = \frac{\varepsilon_r^p}{\varepsilon_0}, e_\theta^p = \frac{\varepsilon_\theta^p}{\varepsilon_0} \\
e_\phi^p &= \frac{\varepsilon_\phi^p}{\varepsilon_0}, e_r^c = \frac{\varepsilon_r^c}{\varepsilon_0}, e_\theta^c = \frac{\varepsilon_\theta^c}{\varepsilon_0}, e_\phi^c = \frac{\varepsilon_\phi^c}{\varepsilon_0} \\
e_r^{Res} &= \frac{\varepsilon_r^{Res}}{\varepsilon_0}, e_\theta^{Res} = \frac{\varepsilon_\theta^{Res}}{\varepsilon_0}, e_\phi^{Res} = \frac{\varepsilon_\phi^{Res}}{\varepsilon_0} \\
p_i &= \frac{P_i}{\sigma_0}, p_o = \frac{P_o}{\sigma_0}, \tau = \frac{E\alpha T}{(1-\nu)\sigma_0} \\
\rho &= \frac{r}{a}, \beta = \frac{b}{a}
\end{aligned} \quad (2)$$

where  $\sigma_r, \sigma_\theta$ , and  $\sigma_\phi$  are the radial, tangential, and axial stresses, respectively. Similarly,  $\varepsilon_r, \varepsilon_\theta, \varepsilon_\phi$  are the total strains;  $\varepsilon_r^p, \varepsilon_\theta^p, \varepsilon_\phi^p$  are the plastic strains;  $\varepsilon_r^c, \varepsilon_\theta^c, \varepsilon_\phi^c$  are the creep strains;  $\varepsilon_r^{Res}, \varepsilon_\theta^{Res}, \varepsilon_\phi^{Res}$  are the residual strains in the radial, tangential, and axial directions, respectively;  $\sigma_0$  is the yield stress; and  $\varepsilon_0$  is the yield strain. Poisson's ratio is denoted by  $\nu$ . The inclusion of the residual strains in the stress-strain relations is important, as the relations are capable to be used for the cyclic loading analysis.

The governing equations are as follows:

The equilibrium equation is

$$\frac{dS_r}{d\rho} = \frac{2(S_\theta - S_r)}{\rho} \quad (3)$$

The compatibility is

$$\frac{de_\theta}{d\rho} = \frac{e_r - e_\theta}{\rho} \quad (4)$$

The stress-strain relationship is

$$\begin{aligned}
e_r &= S_r - \nu(S_\theta + S_\phi) + (1-\nu)\tau + e_r^p + e_r^c + e_r^{Res} \\
e_\theta &= S_\theta - \nu(S_r + S_\phi) + (1-\nu)\tau + e_\theta^p + e_\theta^c + e_\theta^{Res}
\end{aligned} \quad (5)$$

The boundary conditions are

$$\begin{aligned}
S_r(1) &= -p_i \\
S_r(\beta) &= -p_o
\end{aligned} \quad (6)$$

From the spherical symmetry

$$\begin{aligned}
S_\theta &= S_\phi \\
e_\theta &= e_\phi
\end{aligned} \quad (7)$$

From the incompressibility condition

$$e_r^p + e_\theta^p + e_\phi^p = 0 \quad (8)$$

$$e_r^c + e_\theta^c + e_\phi^c = 0 \quad (9)$$

or

$$e_r^p = -2e_\theta^p \quad (10)$$

$$e_r^c = -2e_\theta^c \quad (11)$$

The same relations exist between the residual strains, provided the previous load cycles are spherically symmetric

$$e_r^{Res} = -2e_\theta^{Res} \quad (12)$$

Solving the governing equations, the radial and tangential stresses are

$$\begin{aligned}
S_r &= \frac{1}{1-\nu} \int_1^\rho \frac{e_r^p}{\rho} d\rho + \frac{1}{1-\nu} \int_1^\rho \frac{e_r^c}{\rho} d\rho \\
&\quad + \frac{1}{1-\nu} \int_1^\rho \frac{e_r^{Res}}{\rho} d\rho - \frac{2}{\rho^3} \int_1^\rho \tau \rho^2 d\rho + \frac{C_2}{\rho^3} + C_1 \\
S_\theta &= \frac{1}{1-\nu} \int_1^\rho \frac{e_r^p}{\rho} d\rho + \frac{e_r^p}{2(1-\nu)} \\
&\quad + \frac{1}{1-\nu} \int_1^\rho \frac{e_r^c}{\rho} d\rho + \frac{e_r^c}{2(1-\nu)} \\
&\quad + \frac{1}{1-\nu} \int_1^\rho \frac{e_r^{Res}}{\rho} d\rho + \frac{e_r^{Res}}{2(1-\nu)} \\
&\quad + \frac{1}{\rho^3} \int_1^\rho \tau \rho^2 d\rho - \tau - \frac{C_2}{2\rho^3} + C_1
\end{aligned} \quad (13)$$

where the constants of integration are given as

$$\begin{aligned}
C_1 &= -p_i - C_2 \\
C_2 &= \frac{\beta^3}{\beta^3 - 1} (p_i - p_o - \frac{1}{1 - \nu} \int_1^\beta \frac{e_r^p}{\rho} d\rho \\
&\quad - \frac{1}{1 - \nu} \int_1^\beta \frac{e_r^c}{\rho} d\rho - \frac{1}{1 - \nu} \int_1^\beta \frac{e_r^{Res}}{\rho} d\rho \\
&\quad - \frac{2}{\rho^3} \int_1^\beta \tau \rho^2 d\rho) \\
dA_r &= C'_1 de_r^p \\
dA_\theta &= C'_1 de_\theta^p \\
dA_\phi &= C'_1 de_\phi^p \\
dA_r &= C' de_r^p - \gamma' A_r |de_p| \\
dA_\theta &= C' de_\theta^p - \gamma' A_\theta |de_p| \\
dA_\phi &= C' de_\phi^p - \gamma' A_\phi |de_p|
\end{aligned} \tag{14}$$

## Flow Rule

According to the equations given in the entry ► [Thermal Cyclic Loading of Thick Spherical Vessels Based on the Prager and Armstrong-Frederick Kinematic Hardening Models](#), the normalized form of the yield criterion, effective stress, effective plastic strain, and flow rule is reduced to the following form due to the spherical symmetry of the problem:

$$|(s'_r - a'_r) - (s'_\theta - a'_\theta)| = \frac{2}{3} \tag{15}$$

$$\begin{aligned}
de_r^p &= \frac{3}{2} de_p (s'_r - a'_r) \\
de_\theta^p &= \frac{3}{2} de_p (s'_\theta - a'_\theta)
\end{aligned} \tag{16}$$

$$s_e = |s'_r - s'_\theta| \tag{17}$$

$$de_p = |de_r^p| = ds_e/H' \tag{18}$$

$$de_r^p = -2de_\theta^p = de_p \text{sgn}[(s'_r - a'_r) - (s'_\theta - a'_\theta)] \tag{19}$$

where  $H'$  is normalized plastic modulus according to the referenced entry and  $s'_r$ ,  $s'_\theta$ ,  $a'_r$ , and  $a'_\theta$  are the deviatoric stress and back stress components, respectively. According to the P (i.e., Prager) and AF (i.e., Armstrong-Frederick) kinematic hardening models, the back stress components are

## Creep Equations

Due to the timescale of loading and unloading, it is assumed that creep is activated only at the end of loading and unloading intervals. To evaluate the creep strains, the Norton power law is used to simulate the creep strains. The normalized flow rules of creep are based on the Levy-Mises equations in spherical coordinate systems and are defined as

$$\begin{aligned}
de_r^c &= s'_r d\lambda' \\
de_\theta^c &= s'_\theta d\lambda' \\
de_\phi^c &= -(de_r^c + de_\theta^c)
\end{aligned} \tag{22}$$

$$de_c = \sqrt{\frac{2}{3} (de_r^{c2} + de_\theta^{c2} + de_\phi^{c2})} \tag{23}$$

$$d\lambda' = \frac{b' s'^{n_1} e^{\frac{-Q'}{R\tau_c}}}{s_e} dt \tag{24}$$

For more description on flow rule, one may refer to the entry ► [Effect of Creep on Thermal Cyclic Loading of Thick Cylindrical Vessels Based on the Kinematic Hardening Models](#).

## Numerical Method

Since cyclic loading result of structures depends upon the history of loading, it must be solved incrementally due to the nonlinear nature of the

problem. Thus, a numerical incremental method needs to be used to solve (13), (16), (22), (18), (23), (17), and (20) or (21). Also, the yield condition is checked using (15). One may refer to the entry ► [Numerical Simulation of Cyclic Loading of Thermal Stresses](#) for solution method of mentioned equations.

## Results and Discussion

The same set of problems that are solved in the entry ► [Thermal Cyclic Loading of Thick Spherical Vessels Based on the Prager and Armstrong-Frederick Kinematic Hardening Models](#) are solved in this section. To study the effect of creep on cyclic response of thick spherical vessel, a secondary creep is assumed at the end of loading and unloading procedure of the vessel. The material properties of the vessel including a typical value for creep parameters are given in [Table 1](#).

In the first example, a vessel is subjected to the cyclic thermal load, where its inside temperature is cycled through  $T_i = 0$  to  $300^\circ\text{C}$ ,  $T_o = 0$  and experiences 10 h creep per half cycle. The average inside temperature cycle is  $T_{ave} = 150^\circ\text{C}$ , and the inside temperature which brings the inside surface of the vessel up to the yield is  $T_c = 144^\circ\text{C}$ . The normalized effective stress versus normalized effective mechanical strain (i.e.,  $s_e + e_p + e_c$ ) based on the P and AF models is drawn for inside radius of the vessel in [Figs. 1](#) and [2](#), respectively. Both figures show transient ratcheting to reversed plasticity behavior for thermal cyclic loading of the spherical vessel. According to the referenced entry in this section, when creep is excluded, the P model predicted reversed plasticity behavior which is different from the results obtained by the AF model.

In the second example, the vessel is subjected to the cyclic inside pressure between 0 and 300 MPa and experiences 100 h per half cycle interval. The critical pressure, where the inside surface yields, is  $P_c = 114$  MPa. The average pressure cycle is  $P_{av} = 150$  MPa. The vessel

**Effect of Creep on Cyclic Loading of Spherical Vessels Based on the Kinematic Hardening Models, Table 1** Vessel properties

Properties	Notation	Value	Unit
Modules of elasticity	$E$	173.2	GPa
Yield stress	$\sigma_0$	241	MPa
Thermal expansion	$\alpha$	10.8E-6	1/ $^\circ\text{C}$
Creep law coefficient	$b_1$	7.29E-10	1/h
Creep law power	$n_1$	3.5	–
Creep law power	$Q/R$	29,840	$^\circ\text{K}$
Outside to inside ratio	$b/a$	1.5	–
Ludwick curve parameter	$m$	2,631	MPa
Ludwick curve parameter	$n$	0.35	–
AF model parameter	$C$	55.3	GPa
AF model parameter	$\gamma$	280	–

behavior is predicted using the P and AF models, and the results of normalized effective stress versus normalized effective strain at inside surface of the vessel are shown in [Figs. 3](#) and [4](#), respectively. Due to the cycling of primary stresses, the case is load-controlled cyclic loading, and according to [Figs. 3](#) and [4](#), both models predict ratcheting for load-controlled cyclic loading.

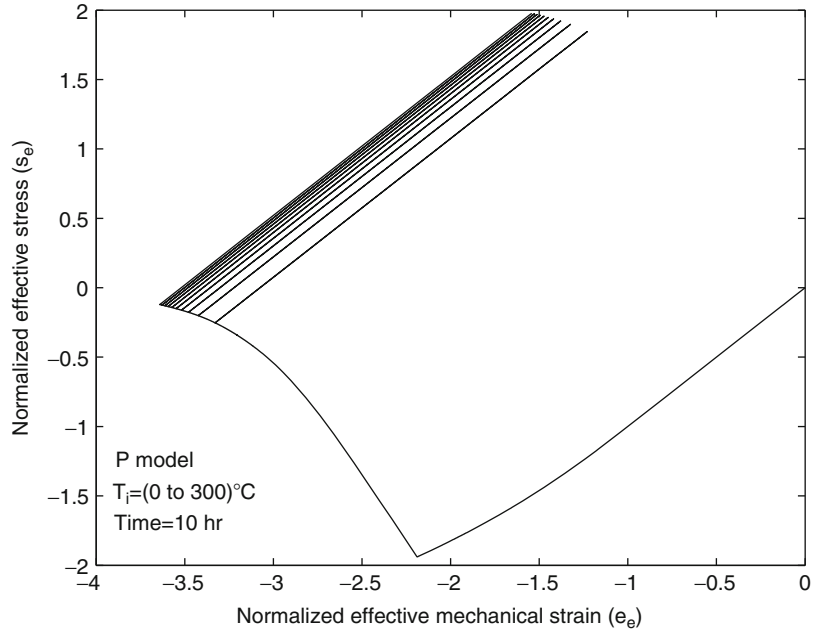
In the next example, a simultaneous constant inside pressure  $P_i = 40$  MPa and cyclic inside temperature  $T_i$  between 0 and  $300^\circ\text{C}$  are applied to the vessel, while the vessel experiences 10 h creep per half cycle interval. The critical temperature which brings inside surface of the vessel up to the yield, due to the constant pressure at inside surface of the vessel, is  $208^\circ\text{C}$ . The results for normalized effective stress versus normalized effective mechanical strain at inside surface of the vessel based on the P and AF models are shown in [Figs. 5](#) and [6](#), respectively. Due to the cycling of thermal load, the case is strain-controlled cyclic loading. As it can be seen from the figures, both models predict transient ratcheting to reversed plasticity behavior for strain-controlled cyclic loading of the vessel.

The last example considers a vessel subjected to thermal cyclic load at both inside and outside surfaces, while experiences 10 h creep per half



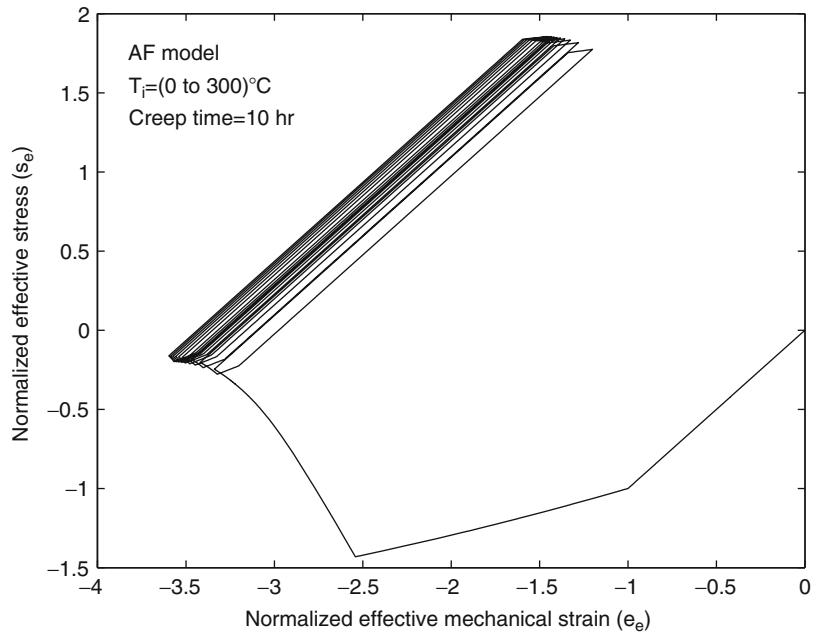
**Effect of Creep on Cyclic Loading of Spherical Vessels Based on the Kinematic Hardening Models, Fig. 1**

Inside temperature cyclic loading of thick sphere based on the P model



**Effect of Creep on Cyclic Loading of Spherical Vessels Based on the Kinematic Hardening Models, Fig. 2**

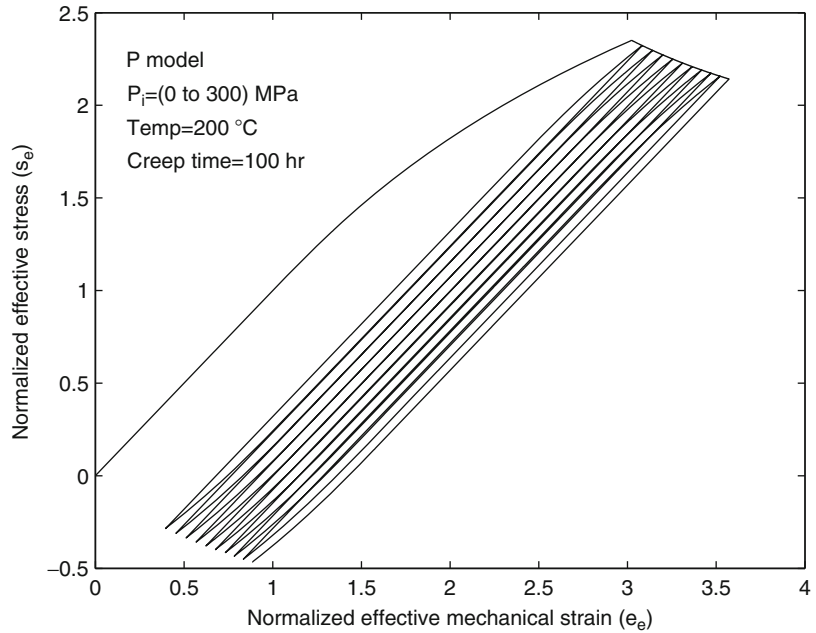
Inside temperature cyclic loading of thick sphere based on the AF model



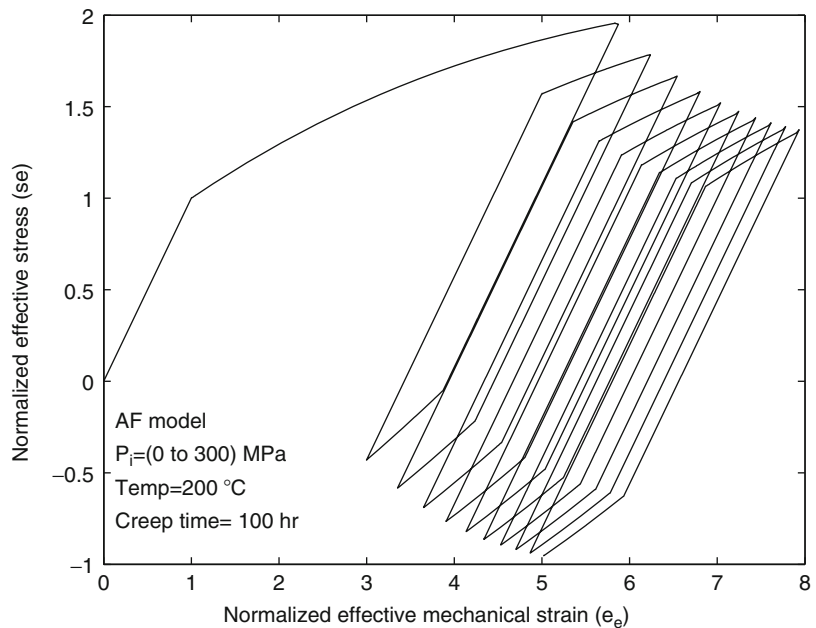
cycle interval. The inside temperature is cycled through ( $T_i = 0$  to  $250^\circ\text{C}$ ), and the outside temperature is cycled through  $T_o = 300$  to  $0^\circ\text{C}$ , and the normalized effective stress versus normalized

effective strain at inside surface of the vessel is shown in Figs. 7 and 8 for the P and AF models, respectively. Due to cycling of secondary stresses, the case is the strain-controlled cyclic

**Effect of Creep on Cyclic Loading of Spherical Vessels Based on the Kinematic Hardening Models, Fig. 3** Inside pressure cyclic loading of thick sphere based on the P model



**Effect of Creep on Cyclic Loading of Spherical Vessels Based on the Kinematic Hardening Models, Fig. 4** Inside pressure cyclic loading of thick sphere based on the AF model



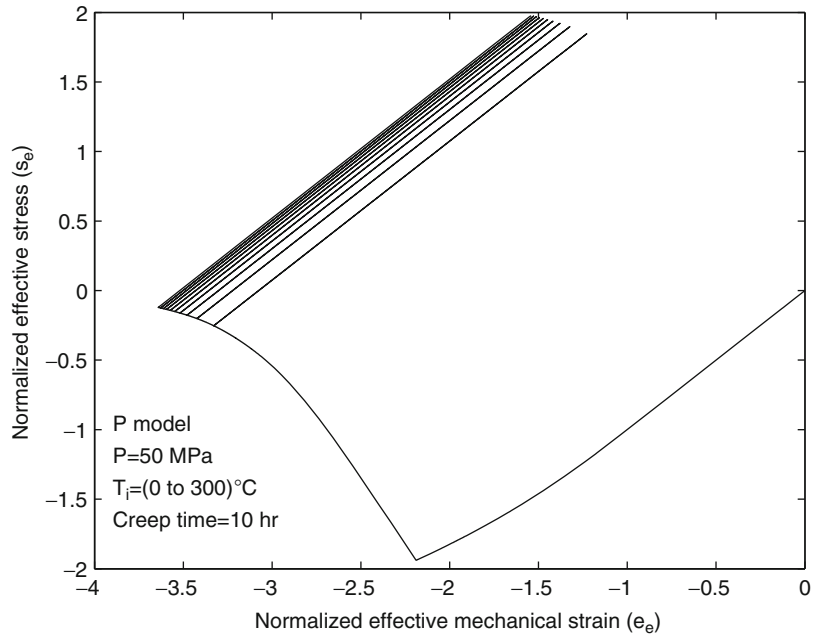
loading. Both models predict transient ratcheting to reversed plasticity behavior for this case of cyclic loading. It is interesting to compare the results to the entry ► [Effect of Creep on Thermal Cyclic Loading of Thick Cylindrical Vessels Based on the Kinematic Hardening Models](#),

where both models predicted ratcheting behavior for the same problem. The reason is predicted to be the symmetry of the vessel.

One may refer to [4] for more discussion on effect of creep on cyclic loading of thick spherical vessels. Also due to the experimental data

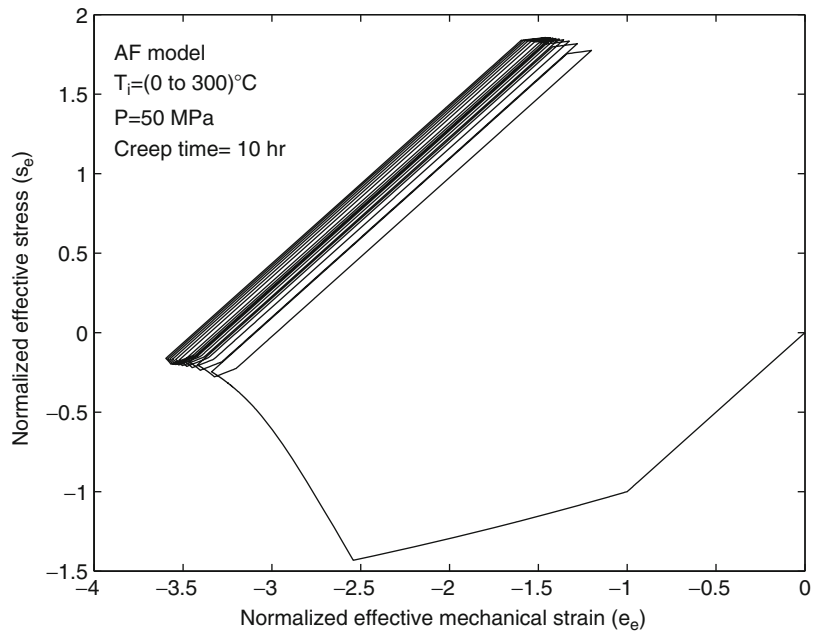
**Effect of Creep on Cyclic Loading of Spherical Vessels Based on the Kinematic Hardening Models, Fig. 5**

Inside temperature cyclic loading with constant inside pressure of thick sphere based on P model



**Effect of Creep on Cyclic Loading of Spherical Vessels Based on the Kinematic Hardening Models, Fig. 6**

Inside temperature cyclic loading with constant inside pressure of thick sphere based on AF model

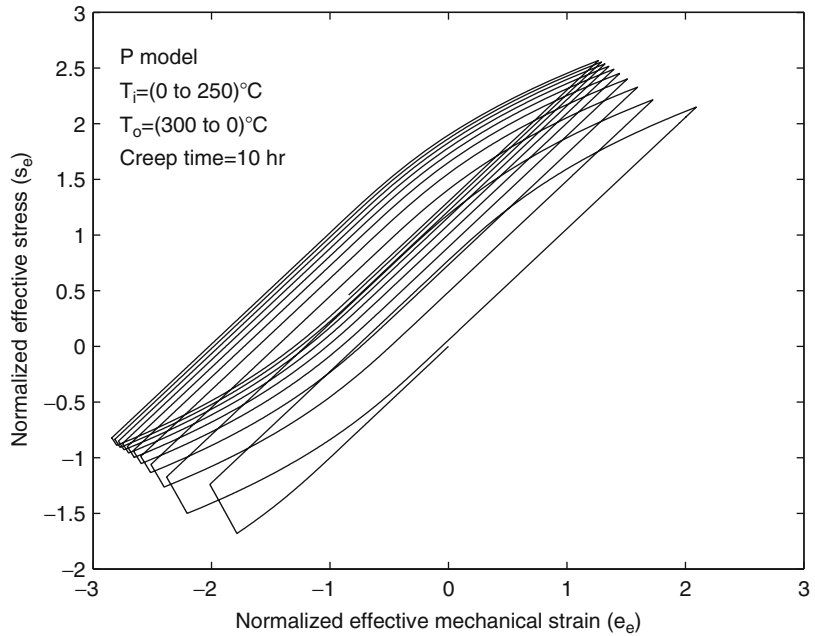


given by Hassan and Kyriakides [5, 6], more accurate results are expected using the AF model. One may refer to results shown in [7–9] for more information on cyclic loading of thermal stresses.

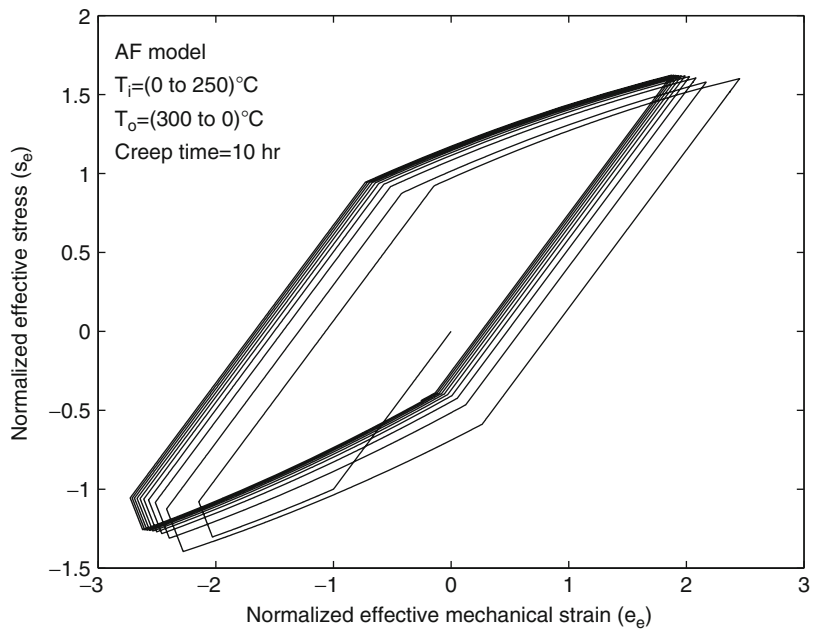
**Key Research Findings**

In this entry, effect of creep on cyclic behavior of thick spherical vessels is studied using both the Armstrong–Frederick and Prager kinematic

**Effect of Creep on Cyclic Loading of Spherical Vessels Based on the Kinematic Hardening Models, Fig. 7** Inside–outside temperature cyclic loading of thick sphere based on the P model



**Effect of Creep on Cyclic Loading of Spherical Vessels Based on the Kinematic Hardening Models, Fig. 8** Inside–outside temperature cyclic loading of thick sphere based on the AF model



hardening models. Results in this research show that when creep is considered, both of the models predict identical behavior for cyclic loading of thick spherical vessels. Ratcheting is obtained for

load-controlled cyclic loading of the vessel, and transient ratcheting to reversed plasticity behavior is obtained for strain-controlled cyclic loading. This is in contrast with the results

obtained in the entry ► [Thermal Cyclic Loading of Thick Spherical Vessels Based on the Prager and Armstrong-Frederick Kinematic Hardening Models](#). Another interesting conclusion is obtained in comparing the results of cycling of temperature at both inside and outside surfaces of the spherical vessels with those obtained for cylindrical vessels. Ratcheting behavior is obtained in this case of cyclic loading for cylindrical vessels both including and excluding creep. But, for the spherical vessel (including creep) considered in this entry, transient ratcheting to reversed plasticity behavior is obtained for the same problem. It seems that the effect of symmetry of the vessel is the main reason for this difference in cyclic response of spherical and cylindrical vessels.

## References

1. Prager W (1956) A new method of analyzing stresses and strains work-hardening plastic solids. *J Appl Mech* 23:493–496
2. Armstrong PJ, Frederick CO (1966) A mathematical representation of the multiaxial baushinger effect. CEGB report no RD/B/N 731
3. Hetnarski RB, Eslami MR (2009) Thermal stresses – advanced theory and applications. Springer, Dordrecht
4. Mahbadi H, Eslami MR (2011) Ratcheting of spherical vessels. In: APM1011, 39th summer school conference, advanced problems in mechanics, St. Petersburg, Russia
5. Hassan T, Kyriakides S (1992) Ratcheting in cyclic plasticity, part 1: uniaxial behavior. *Int J Plast* 8:91–116
6. Corona E, Hassan T, Kyriakides S (1996) On the performance of kinematic hardening rules in predicting a class of biaxial ratcheting histories. *Int J Plast* 12:117–145
7. Slavik D, Sehitoglu H (1986) Constitutive models suitable for thermal loading. *J Eng Mater Technol* 108:303–312
8. Yoshida F, Kabayashi M, Tsakimori K, Uno T, Fukuda Y, Igari T, Inoue T (1997) Inelastic analysis of material ratcheting of 316FR at varying temperature – results of benchmark project (B) by JSMS. In: Transaction of the 14th international conference on structural mechanics in reactor technology (SMiRT 14), Lyon, France, pp 221–228
9. Ng HW, Nadarajah C (1996) Biaxial ratcheting and cyclic plasticity for bree-type loading-part 1: finite element analysis. *ASME J Press Vessel Technol* 118:154–160

## Effect of Creep on Thermal Cyclic Loading of Beams Based on the Kinematic Hardening Models

Hossein Mahbadi<sup>1</sup> and Mohammad Reza Eslami<sup>2</sup>

<sup>1</sup>Mechanical Engineering Department, Islamic Azad University, Central Tehran Branch, Tehran, Iran

<sup>2</sup>Department of Mechanical Engineering, Amirkabir University of Technology, Tehran, Iran

## Definition

The definition of terms *ratcheting*, *shakedown*, and reversed plasticity are given in entry “► [Thermal Cyclic Loading of Beams Based on the Prager and Armstrong-Frederick Kinematic Hardening Models](#).”

## Overview

When creep is not considered, the isotropic hardening theory of plasticity predicts shakedown (elastic shakedown) for cyclic loading analysis of the beams under different types of thermal and mechanical loads and their combination [1, 2]. On the other hand, kinematic hardening theory of plasticity based on the Prager kinematic hardening model predicts reversed plasticity for all types of cyclic loadings of beams with maximum stress larger than twice the yield stress. Utilizing the Armstrong-Frederick model for kinematic hardening theory of plasticity results into ratcheting for cycling of mechanical loads and reversed plasticity for cycling of thermal loads. In this entry it is intended to investigate the effect of creep on cyclic loading of beams under mechanical and thermal loads. To this aim, it is assumed that the beam is loaded to flow into plastic region by mechanical and thermal loads, and then it is subjected to creep for a specified duration of time. After the creep, the beam is unloaded and again the beam is assumed under

secondary creep for a specified time due to existence of residual stresses. This procedure is repeated up to the last cycle of the load. To obtain the plastic strains at initial part of load cycle, both Prager [3] and Armstrong-Frederick [4] kinematic hardening models are used. For the creep analysis of the beam the secondary creep law is used to obtain the creep strains. An iterative method is proposed to analyze the beam under cyclic thermal and mechanical loads.

### Stress-strain Distribution

Consider a beam of isotropic material under axial load  $P$ , bending moment  $M$ , and transverse temperature distribution  $\theta(z)$  as shown in Fig. 1. The axial strain is

$$\varepsilon_x = \frac{\sigma_x}{E} + \alpha\theta + \varepsilon_x^p + \varepsilon_x^c + \varepsilon_x^{Res} \quad (1)$$

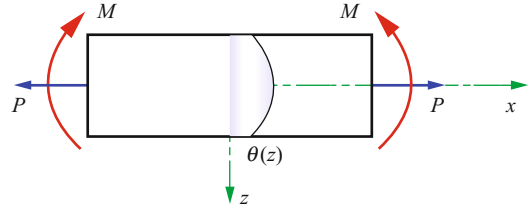
where  $\sigma_x$  is the axial stress,  $\varepsilon_x^p$  is the axial plastic strain,  $\varepsilon_x^c$  is the axial creep strain and  $\varepsilon_x^{Res}$  is the axial residual strain which is obtained from the previous load cycle,  $\theta(z)$  is temperature distribution across the beam height,  $E$  is the modulus of elasticity, and  $\alpha$  is the linear coefficient of thermal expansion. The dimensionless quantities are defined as

$$\begin{aligned} S &= \frac{\sigma_x}{\sigma_0}, \quad \tau = \frac{\alpha\theta}{\varepsilon_0}, \quad e_x = \frac{\varepsilon_x}{\varepsilon_0}, \quad e_x^p = \frac{\varepsilon_x^p}{\varepsilon_0}, \\ e_x^c &= \frac{\varepsilon_x^c}{\varepsilon_0}, \quad e_x^{Res} = \frac{\varepsilon_x^{Res}}{\varepsilon_0}, \quad \eta = \frac{y}{h} \end{aligned} \quad (2)$$

where  $2h$  is height of the beam cross section,  $\sigma_0$  is the initial yield stress, and  $\varepsilon_0$  is the initial yield strain. The dimensionless form of (1) is

$$e_x = S + \tau + e_x^p + e_x^c + e_x^{Res} \quad (3)$$

The compatibility equation and the boundary conditions are



**Effect of Creep on Thermal Cyclic Loading of Beams Based on the Kinematic Hardening Models, Fig. 1** Beam geometry and loading

$$\frac{\partial^2 e_x}{\partial \eta^2} = 0 \Rightarrow e_x = a + c\eta \quad (4)$$

$$\begin{aligned} \int_{-1}^1 S d\eta &= \frac{P}{\sigma_0 b h} = P^* \\ \int_{-1}^1 S \eta d\eta &= \frac{M}{\sigma_0 b^2 h} = M^* \end{aligned} \quad (5)$$

where  $b$  is the beam width. Substituting (4) in (1) and solving for  $S$  gives

$$S = a + c\eta - e_x^p - e_x^c - e_x^{Res} - \tau \quad (6)$$

Using the boundary conditions (5), the constants of integration  $a$  and  $c$  are obtained and are

$$\begin{aligned} a &= \frac{P^*}{2} + \frac{1}{2} \int_{-1}^1 e_x^p d\eta + \frac{1}{2} \int_{-1}^1 e_x^c d\eta \\ &\quad + \frac{1}{2} \int_{-1}^1 e_x^{Res} d\eta + \frac{1}{2} \int_{-1}^1 \tau d\eta \\ c &= \frac{3}{2} M^* + \frac{3}{2} \int_{-1}^1 e_x^p \eta d\eta + \frac{3}{2} \int_{-1}^1 e_x^c \eta d\eta \\ &\quad + \frac{3}{2} \int_{-1}^1 e_x^{Res} \eta d\eta + \frac{3}{2} \int_{-1}^1 \tau \eta d\eta \end{aligned} \quad (7)$$

Substituting the constants  $a$  and  $c$  in (4) gives

$$\begin{aligned} e_x &= \frac{P^*}{2} + \frac{3}{2} \eta M^* + \frac{1}{2} \int_{-1}^1 \tau d\eta + \frac{3}{2} \eta \int_{-1}^1 \tau \eta d\eta \\ &\quad + \frac{1}{2} \int_{-1}^1 e_x^p d\eta + \frac{3}{2} \eta \int_{-1}^1 e_x^p \eta d\eta + \frac{1}{2} \int_{-1}^1 e_x^c d\eta \\ &\quad + \frac{3}{2} \eta \int_{-1}^1 e_x^c \eta d\eta + \frac{1}{2} \int_{-1}^1 e_x^{Res} d\eta + \frac{3}{2} \eta \int_{-1}^1 e_x^{Res} \eta d\eta \end{aligned} \quad (8)$$

Calling the mechanical strain by  $e_x^M$ , it will be found that

$$\begin{aligned} e_x^M &= e_x - \tau \\ &= \frac{P^*}{2} + \frac{3}{2}\eta M^* - \tau + \frac{1}{2} \int_{-1}^1 \tau d\eta + \frac{3}{2}\eta \int_{-1}^1 \eta \tau d\eta \\ &\quad + \frac{1}{2} \int_{-1}^1 e_x^p d\eta + \frac{3}{2}\eta \int_{-1}^1 e_x^p \eta d\eta + \frac{1}{2} \int_{-1}^1 e_x^c d\eta \\ &\quad + \frac{3}{2}\eta \int_{-1}^1 e_x^c \eta d\eta + \frac{1}{2} \int_{-1}^1 e_x^{Res} d\eta + \frac{3}{2}\eta \int_{-1}^1 e_x^{Res} \eta d\eta \end{aligned} \quad (9)$$

### Flow Rule and Hardening Model

The normalized form of uniaxial yield criterion, flow rule, and Prager and Armstrong-Frederick kinematic hardening models to obtain the effective plastic strain and back stress for the uniaxial state of stress, according to the entry “► [Thermal Cyclic Loading of Beams Based on the Prager and Armstrong-Frederick Kinematic Hardening Models](#),” are

$$S - A = 1 \quad (10)$$

$$de_x^p = \frac{dS}{H'} = (S - A)de_p \quad (11)$$

$$dA = C'_1 de_x^p \quad (12)$$

$$dA = C' de_x^p - \gamma' A |de_x^p| \quad (13)$$

The definition of parameters used in the above equations is described in referenced entry.

### Creep Equations

In this entry, it is assumed that the creep occurs after loading or unloading procedure (i.e., not during the loading or unloading). That is, the time scale of loading and unloading in this entry is assumed to be short enough not to activate the creep. Thus, the creep process in these regions may be uncoupled from the plastic deformation.

The flow rule of creep is based on the Levy-Mises equations as

$$d\epsilon_{ij}^c = s_{ij} d\lambda \quad (14)$$

where  $d\lambda$  is a nonnegative quantity which may vary through the loading path and thus depends on the history of loading. It can be shown that the constant  $d\lambda$  in terms of the effective stress and increment of effective creep strains becomes

$$d\lambda = \frac{3}{2} \frac{d\epsilon_c}{\sigma_e} \quad (15)$$

The effective stress and effective creep strain, when the von Mises yield criteria is used, are defined as:

$$\begin{aligned} d\epsilon_c &= \sqrt{\frac{2}{3} d\epsilon_{ij}^c d\epsilon_{ij}^c} \\ \sigma_e &= \sqrt{\frac{3}{2} s_{ij} s_{ij}} \end{aligned} \quad (16)$$

where  $s_{ij}$  is deviatoric stress tensor. Due to the generality of the classical Norton creep law, in this entry the Norton creep law is employed to simulate the experimental creep strain versus time as follows:

$$\dot{\epsilon} = b \sigma^{n_1} e^{\frac{-Q}{R\tau_c}} \quad (17)$$

where  $b$  and  $n_1$  are material constant,  $R$  is the universal gas constant, and  $Q$  is the activation energy. For uniaxial state of stress, the effective creep strain and axial creep strain are identical. So, according to (17) the normalized axial increment of creep strain is

$$de_c = d\epsilon_x^c = b' \sigma^{n_1} e^{\frac{-Q'}{R\tau_c}} dt \quad (18)$$

Assuming  $T_0 = 0$  (i.e., the initial temperature), then  $b'$ ,  $Q'$ , and  $\tau_c$  in (18) are

$$\begin{aligned} b' &= bE\sigma_0^{n_1-1} \\ Q' &= E\alpha Q/\sigma_0 \\ \tau_c &= E\alpha \frac{273 + \theta}{\sigma_0} \end{aligned} \quad (19)$$

Applying the normalized form of creep flow rule 14,  $d\lambda'$  (i.e., the normalized form of  $d\lambda$ ) is found as follows:

$$d\lambda' = \frac{d\lambda}{E} = \frac{de^c_x}{S} \quad (20)$$

## Numerical Solution

Due to the nonlinearity of the problem and history dependency of the plastic and creep strains, the numerical method described in entry “► [Numerical Simulation of Cyclic Loading of Thermal Stresses](#)” is used to solve (6), (11), (18), (12), or (13). Also, the yield condition is checked using (10).

## Results and Discussion

In this section, effect of creep on load- and strain-controlled cyclic loading of beam structure is investigated. The problems in this section are solved using the P (i.e., Prager) and AF (i.e., Armstrong-Frederick) kinematic hardening models. The same set of problems are solved in entry “► [Thermal Cyclic Loading of Beams Based on the Prager and Armstrong-Frederick Kinematic Hardening Models](#).” The results obtained in this entry are compared with those obtained in the mentioned entry to show the effect of creep on ratcheting, shakedown, or reversed plasticity behavior of the beam structures. The geometry, elastic, plastic, and typical values for creep properties of the beam are given in Table 1. The Ludwick equation is considered to show the experimental stress–strain curve needed for the P model.

In the first example the beam is subjected to the cyclic thermal load with parabolic temperature distribution  $\theta(z) = \theta_0(z^2 - \frac{1}{3})$ , where  $\theta_0$  is thermal loading parameter and is cycled between 0 and 500 °C. The beam experiences 10 h creep per half cycle, and the thermal loading parameter which brings the beam up to the yield is 194 °C. The axial stress versus the mechanical strain at

**Effect of Creep on Thermal Cyclic Loading of Beams Based on the Kinematic Hardening Models, Table 1** Beam properties

Properties	Notation	Value	Unit
Modulus of elasticity	$E$	173.2	GPa
Yield stress	$\sigma_0$	241	MPa
Thermal expansion	$\alpha$	10.8E-6	1/°C
Creep law coefficient	$b_1$	7.29E-10	1/h
Creep law power	$n_1$	3.5	–
Creep law power	$Q/R$	29,840	°K
Beam height	$2h$	50	mm
Beam width	$b$	25	mm
Ludwick curve parameter	$m$	2,631	MPa
Ludwick curve parameter	$n$	0.35	–
AF model parameter	$C$	55.3	GPa
AF model parameter	$\gamma$	280	–

$z = 0$  and  $z = h/2$  surfaces of the beam are plotted in Figs. 2 and 3 for the P and AF models, respectively.

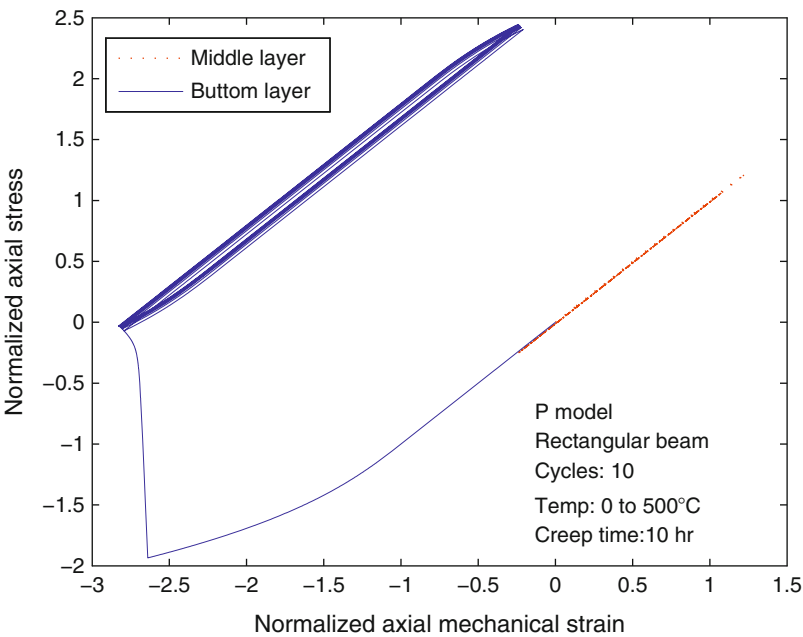
The figures show that both middle and bottom layers of the beam flow into yield. Both models predict ratcheting to reversed plasticity behavior at the bottom and middle layers.

In the second example the beam is subjected to the cyclic bending moment between  $-3,000$  to  $4,500$  kN · m and 1,000 h creep at uniform temperature 200 °C per half cycle. The bending moment which brings the top surface of the beam up to the yield is 2,524 kN · m. Results based on the P and AF models at  $z = h/2$  and  $z = 0$  are shown at Figs. 4 and 5, respectively. The case is load-controlled cyclic loading, and both figures show ratcheting for load-controlled cyclic loading of the beam. According to the entry “► [Thermal Cyclic Loading of Beams Based on the Prager and Armstrong-Frederick Kinematic Hardening Models](#),” when creep is not considered, the P model predicts reversed plasticity for the same case of cyclic loading.

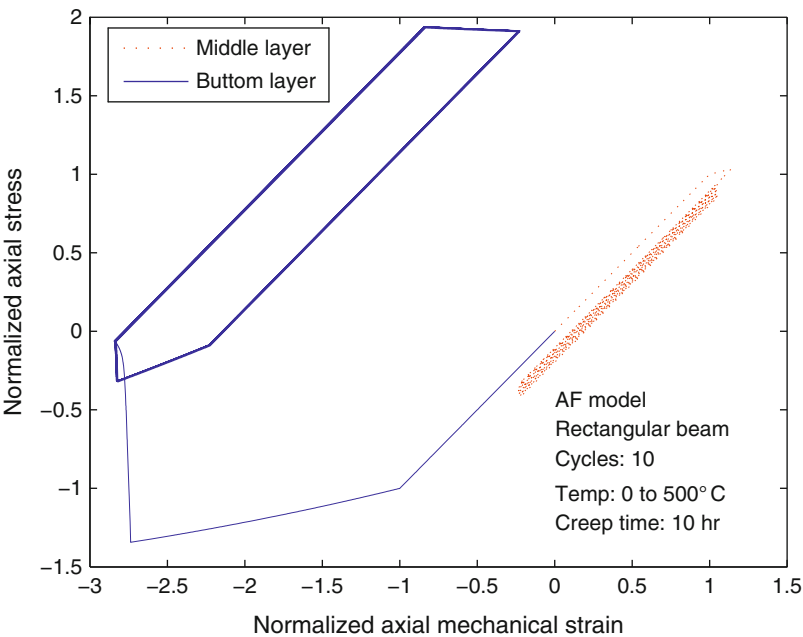
In the last example, the beam is subjected to the combined constant axial load and cycled thermal load. The constant axial load is 100 kN and thermal load parameter is cycled between 0 °C and 500 °C. The creep time per half cycle is 10 h and the temperature which brings the beam up to the yield is 259 °C. Figures 6 and 7 show the



**Effect of Creep on Thermal Cyclic Loading of Beams Based on the Kinematic Hardening Models, Fig. 2** Thermal cyclic loading of beam based on the P model



**Effect of Creep on Thermal Cyclic Loading of Beams Based on the Kinematic Hardening Models, Fig. 3** Thermal cyclic loading of beam based on the AF model

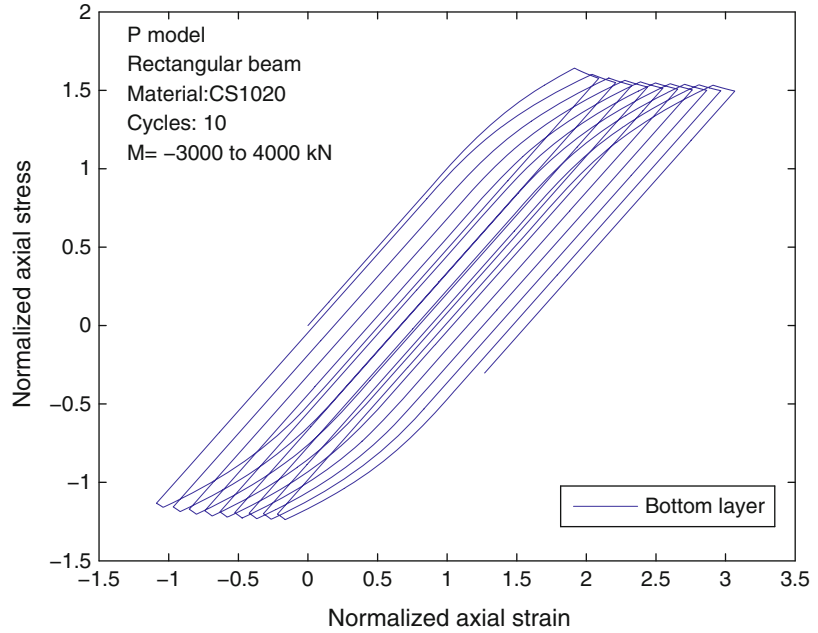


cyclic loading results for bottom and middle layers of the beam based on the P and AF models, respectively. As seen from the figures, both the P and AF models predict transient ratcheting to

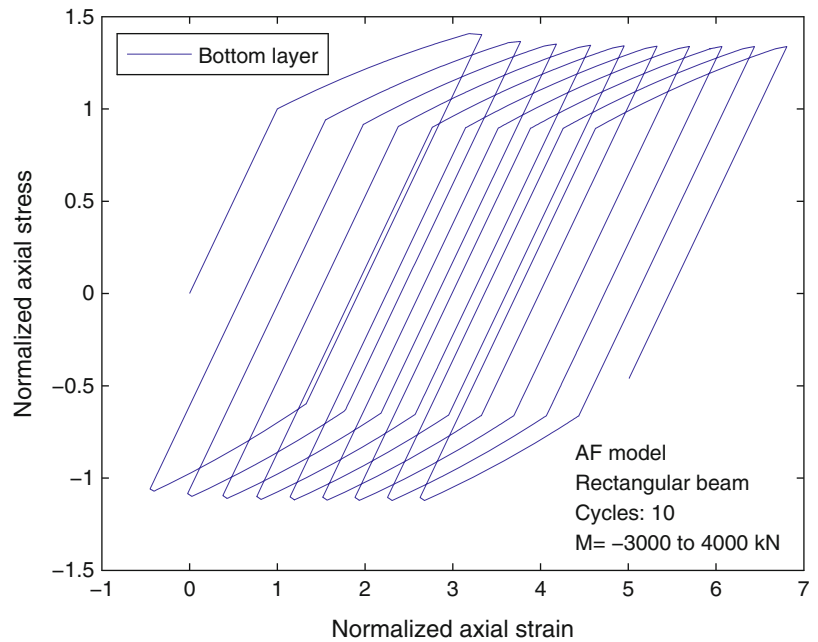
reversed plasticity behavior for bottom and middle layers of the beam.

Due to the experimental results given by [5], more accurate results are expected using the AF

**Effect of Creep on Thermal Cyclic Loading of Beams Based on the Kinematic Hardening Models, Fig. 4** Bending moment cyclic loading of the beam based on the P model



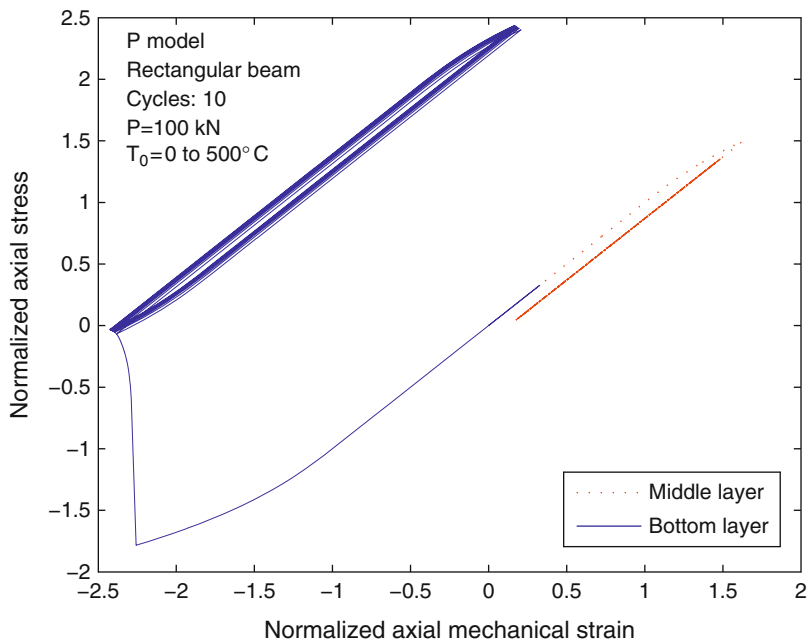
**Effect of Creep on Thermal Cyclic Loading of Beams Based on the Kinematic Hardening Models, Fig. 5** Bending moment cyclic loading of the beam based on the AF model



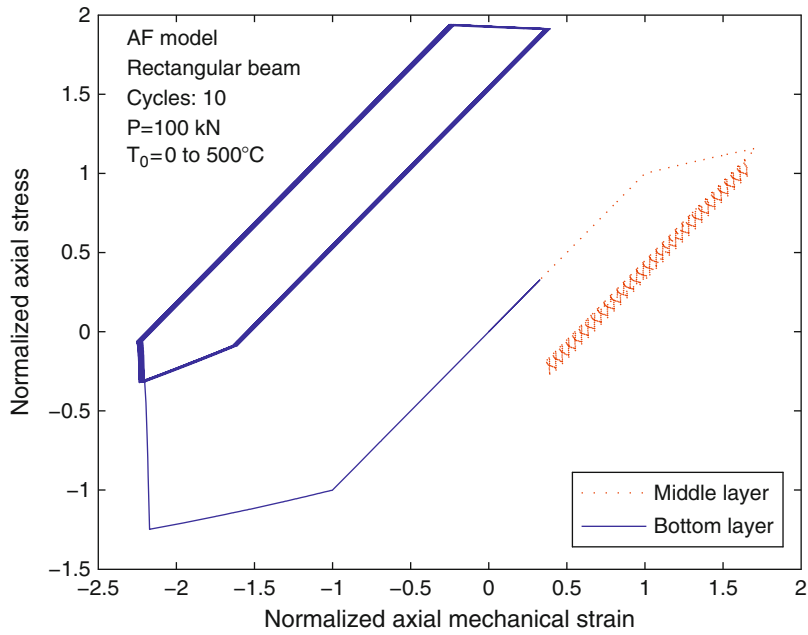
model rather than the P model. Also it is interesting to mention that when creep is considered, even the isotropic hardening theory of plasticity which is not proper for cyclic loading of

structures predicted identical behavior for load and strain-controlled cyclic loading of beam structures. Also for more problems in this area, the reader is referred to [6].

**Effect of Creep on Thermal Cyclic Loading of Beams Based on the Kinematic Hardening Models, Fig. 6** Constant axial load with cycled thermal load based on the P model



**Effect of Creep on Thermal Cyclic Loading of Beams Based on the Kinematic Hardening Models, Fig. 7** Constant axial load with cycled thermal load based on the AF model



**Key Research Findings**

In this entry effect of creep on cyclic loading results of the beam subjected to the load and strain-controlled cyclic loading is investigated using the P and AF models. According to

the results shown in entry “► [Thermal Cyclic Loading of Beams Based on the Prager and Armstrong-Frederick Kinematic Hardening Models](#),” when creep is not considered the Prager and Armstrong-Frederick kinematic hardening models predicted different results for cyclic

loading of beams under load- and strain-controlled cyclic loading. Based on the results obtained in this research when creep is considered, identical behavior is predicted for the load- and strain-controlled cyclic loading of beams. Both models predicted ratcheting for load-controlled cyclic loading of the beam and transient ratcheting to reversed plasticity for strain-controlled cyclic loading.

## References

1. Naderan-Tahan K, Eslami MR, Mahbadi H (2000) A cyclic loading analysis of structures of strain hardening material. In: 4th international conference of Iranian Society of Mechanical Engineers, Sharif University of Technology, Tehran
2. Mahbadi H, Eslami MR (2002) Load and deformation controlled cyclic loading of beams based on isotropic hardening model. *Trans Iran Soc Mech Eng* 3(1):28–46
3. Prager W (1956) A new method of analyzing stresses and strains work-hardening plastic solids. *J Appl Mech* 23:493–496
4. Armstrong PJ, Frederick CO (1966) A mathematical representation of the multiaxial Bauschinger effect. CEGB Report No. RD/B/N 731
5. Hassan T, Kyriakides S (1992) Ratcheting in cyclic plasticity, part 1: uniaxial behavior. *Int J Plast* 8:91–116
6. Mahbadi H, Gowhari AR, Eslami MR (2010) Elastic-plastic-creep cyclic loading of beams using the Prager kinematic hardening model. *IMEchE Int J Strain Anal* 39:127–136

## Effect of Creep on Thermal Cyclic Loading of Rotating Disks

Hossein Mahbadi<sup>1</sup> and Mohammad Reza Eslami<sup>2</sup>

<sup>1</sup>Mechanical Engineering Department,

Islamic Azad University, Central Tehran Branch, Tehran, Iran

<sup>2</sup>Department of Mechanical Engineering, Amirkabir University of Technology, Tehran, Iran

## Synonyms

Cyclic loading of secondary stresses; Strain-controlled cyclic loading

## Overview

In the entry “► [Thermal Cyclic Loading of Rotating Disks](#),” cyclic loading of rotating disk under cycled thermal and body forces based on the Prager and Armstrong-Frederick kinematic hardening model were investigated. According to the obtained results, depending on the types of loads, ratcheting, shakedown, or reversed plasticity is expected to occur using each of the mentioned models. Now in this entry, the effect of creep on cyclic response of rotating disks subjected to the cycled angular velocity, cycled temperature distribution, and combination of rotating disk and temperature distribution is obtained. The disk material is assumed to be isotropic and homogeneous and obeys a nonlinear strain-hardening law in the plastic range. The secondary creep law is considered to obtain creep strains at elevated temperatures. The kinematic hardening theory based on the Prager [1] and Armstrong-Frederick [2] models with von Mises associated flow rule is used to predict the ratcheting or shakedown behavior of rotating disks. An incremental iterative method is used to analyze the structural behavior under cyclic loading conditions. Using the Prager and Armstrong-Frederick kinematic hardening models, the cyclic loading results of a rotating disk under various types of loads, including creep at the end of each load cycle interval, are compared with those in which creep is excluded.

## Mathematical Formulation

A symmetric rotating disk with uniform thickness affected by the induced body force stresses due to the angular velocity  $w$  is considered. The inside radius of disk is  $a$ , outside radius is  $b$ , and the density of disk is assumed to be  $\rho'$ . A symmetric radial temperature distribution  $T(r)$  is considered as [3]

$$T(r) = \frac{1}{\ln b/a} \left( T_a \ln \frac{b}{r} + T_b \ln \frac{r}{a} \right) \quad (1)$$

The following dimensionless quantities are defined to normalize the equations of the disk:

$$\begin{aligned}
 S_r &= \frac{\sigma_r}{\sigma_0}, S_\theta = \frac{\sigma_\theta}{\sigma_0}, S_z = \frac{\sigma_z}{\sigma_0}, e_r = \frac{\varepsilon_r}{\varepsilon_0} \\
 e_\theta &= \frac{\varepsilon_\theta}{\varepsilon_0}, e_z = \frac{\varepsilon_z}{\varepsilon_0}, e_r^p = \frac{\varepsilon_r^p}{\varepsilon_0}, e_\theta^p = \frac{\varepsilon_\theta^p}{\varepsilon_0} \\
 e_z^p &= \frac{\varepsilon_z^p}{\varepsilon_0}, e_r^c = \frac{\varepsilon_r^c}{\varepsilon_0}, e_\theta^c = \frac{\varepsilon_\theta^c}{\varepsilon_0}, e_z^c = \frac{\varepsilon_z^c}{\varepsilon_0} \\
 e_r^{Res} &= \frac{\varepsilon_r^{Res}}{\varepsilon_0}, e_\theta^{Res} = \frac{\varepsilon_\theta^{Res}}{\varepsilon_0}, e_z^{Res} = \frac{\varepsilon_z^{Res}}{\varepsilon_0} \\
 \tau &= \frac{E\alpha T}{(1-\nu)\sigma_0}, \omega^2 = \frac{\rho' a^2 \omega^2}{\sigma_0}, \rho = \frac{r}{a}, \\
 \beta &= \frac{b}{a}
 \end{aligned} \quad (2)$$

where  $\sigma_r, \sigma_\theta$ , and  $\sigma_z$  are the radial, tangential, and axial stresses, respectively. Similarly,  $\varepsilon_r, \varepsilon_\theta, \varepsilon_z$  are the total strains,  $\varepsilon_r^p, \varepsilon_\theta^p, \varepsilon_z^p$  are the plastic strains,  $\varepsilon_r^c, \varepsilon_\theta^c, \varepsilon_z^c$  are the creep strains, and  $\varepsilon_r^{Res}, \varepsilon_\theta^{Res}, \varepsilon_z^{Res}$  are the residual strains in the radial, tangential, and axial directions, respectively;  $\sigma_0$  is the yield stress, and  $\varepsilon_0$  is the yield strain. The inclusion of the residual strains in the stress-strain relations is important, as the relations are capable to be used for the cyclic loading analysis.

The governing equations are:

Compatibility:

$$\frac{de_\theta}{d\rho} = \frac{e_r - e_\theta}{\rho} \quad (3)$$

Equilibrium:

$$\frac{dS_r}{d\rho} = \frac{S_\theta - S_r}{\rho} \quad (4)$$

Stress-strain relationship:

$$\begin{aligned}
 e_r &= S_r - \nu(S_\theta + S_z) + (1-\nu)\tau + e_r^p + e_r^c + e_r^{Res} \\
 e_\theta &= S_\theta - \nu(S_r + S_z) + (1-\nu)\tau + e_\theta^p + e_\theta^c + e_\theta^{Res} \\
 e_z &= S_z - \nu(S_\theta + S_r) + (1-\nu)\tau + e_z^p + e_z^c + e_z^{Res}
 \end{aligned} \quad (5)$$

From the incompressibility condition,

$$de_z^p = -(de_r^p + de_\theta^p) \quad (6)$$

$$de_z^c = -(de_r^c + de_\theta^c) \quad (7)$$

The plane stress assumption  $S_z = 0$  leads to

$$e_z = -\nu(S_r + S_\theta) + (1-\nu)\tau + e_z^p + e_z^c + e_z^{Res} \quad (8)$$

The boundary conditions are assumed as

$$\begin{aligned}
 S_r(1) &= 0 \\
 S_r(\beta) &= 0
 \end{aligned} \quad (9)$$

The solution of the governing equations subjected to the given boundary conditions are

$$\begin{aligned}
 S_r &= -\frac{1-\nu}{\rho^2} \int_1^\rho \rho \tau d\rho - \frac{1}{2\rho^2} \int_1^\rho \rho e_\theta^p d\rho \\
 &\quad - \frac{1}{2} \int_1^\rho \frac{e_\theta^p}{\rho} d\rho - \frac{1}{2\rho^2} \int_1^\rho \rho e_r^p d\rho + \frac{1}{2} \int_1^\rho \frac{e_r^p}{\rho} d\rho \\
 &\quad - \frac{1}{2\rho^2} \int_1^\rho \rho e_\theta^c d\rho - \frac{1}{2} \int_1^\rho \frac{e_\theta^c}{\rho} d\rho - \frac{1}{2\rho^2} \int_1^\rho \rho e_r^c d\rho \\
 &\quad + \frac{1}{2} \int_1^\rho \frac{e_r^c}{\rho} d\rho - \frac{(3+\nu)\rho^2 \omega^2}{8} + \frac{C_2}{\rho^2} + C_1 \\
 S_\theta &= \frac{1-\nu}{\rho^2} \int_1^\rho \rho \tau d\rho - (1-\nu)\tau - \frac{1}{2} \int_1^\rho \frac{e_\theta^p}{\rho} d\rho \\
 &\quad + \frac{1}{2\rho^2} \int_1^\rho \rho e_\theta^p d\rho - e_\theta^p + \frac{1}{2} \int_1^\rho \frac{e_r^p}{\rho} d\rho \\
 &\quad + \frac{1}{2\rho^2} \int_1^\rho \rho e_r^p d\rho - \frac{1}{2} \int_1^\rho \frac{e_\theta^c}{\rho} d\rho + \frac{1}{2\rho^2} \int_1^\rho \rho e_\theta^c d\rho \\
 &\quad - e_\theta^c + \frac{1}{2} \int_1^\rho \frac{e_r^c}{\rho} d\rho + \frac{1}{2\rho^2} \int_1^\rho \rho e_r^c d\rho \\
 &\quad - \frac{(3\nu+1)\rho^2 \omega^2}{8} - \frac{C_2}{\rho^2} + C_1
 \end{aligned} \quad (10)$$

where the constants of integration, using the boundary conditions (9), are

$$C_1 = -C_2 + \frac{(3+\nu)\omega^2}{8} \quad (11)$$

$$\begin{aligned}
C_2 = & -\frac{1-\nu}{\beta^2-1} \int_1^\beta \rho \tau d\rho - \frac{1}{2(\beta^2-1)} \int_1^\beta \rho e_\theta^p d\rho \\
& - \frac{\beta^2}{2(\beta^2-1)} \int_1^\beta \frac{e_\theta^p}{\rho} d\rho - \frac{1}{2(\beta^2-1)} \int_1^\beta \rho e_r^p d\rho \\
& + \frac{\beta^2}{2(\beta^2-1)} \int_1^\beta \frac{e_r^p}{\rho} d\rho - \frac{1}{2(\beta^2-1)} \int_1^\beta \rho e_\theta^c d\rho \\
& - \frac{\beta^2}{2(\beta^2-1)} \int_1^\beta \frac{e_\theta^c}{\rho} d\rho - \frac{1}{2(\beta^2-1)} \int_1^\beta \rho e_r^c d\rho \\
& + \frac{\beta^2}{2(\beta^2-1)} \int_1^\beta \frac{e_r^c}{\rho} d\rho - \frac{(3+\nu)\beta^2\omega^2}{8}
\end{aligned} \quad (12)$$

P (i.e., Prager) and AF (i.e., Armstrong-Frederick) kinematic hardening models are

$$\begin{aligned}
dA_r &= C'_1 de_r^p \\
dA_\theta &= C'_1 de_\theta^p \\
dA_z &= C'_1 de_z^p
\end{aligned} \quad (18)$$

$$\begin{aligned}
dA_r &= \frac{2}{3} C' de_r^p - \gamma' A_r |de_p| \\
dA_\theta &= \frac{2}{3} C' de_\theta^p - \gamma' A_\theta |de_p| \\
dA_z &= \frac{2}{3} C' de_z^p - \gamma' A_z |de_p|
\end{aligned} \quad (19)$$

The definition of parameters used in above equations is described in the referenced entry.

## Flow Rule and Hardening Model

According to the equations given in the entry “► [Thermal Cyclic Loading of Rotating Disks](#),” the normalized form of the yield criterion, effective stress, effective plastic strain, and flow rule are reduced to the following form:

$$\sqrt{\frac{3}{2} [(s'_r - a'_r)^2 + (s'_\theta - a'_\theta)^2 + (s'_z - a'_z)^2]} = 1 \quad (13)$$

$$\begin{aligned}
de_r^p &= \frac{3}{2} de_p (s'_r - a'_r) \\
de_\theta^p &= \frac{3}{2} de_p (s'_\theta - a'_\theta) \\
de_z^p &= -(de_r^p + de_\theta^p)
\end{aligned} \quad (14)$$

$$s_e = \sqrt{\frac{3}{2} (s'^2_r + s'^2_\theta + s'^2_z)} \quad (15)$$

$$de_p = \sqrt{\frac{2}{3} [(de_r^p)^2 + (de_\theta^p)^2 + (de_z^p)^2]} = ds_e / H' \quad (16)$$

$$e_e = s_e + e_p \quad (17)$$

In these equations, the normalized deviatoric stress and back stress components based on the

## Creep Equations

Due to the time scale of loading and unloading, it is assumed that creep is activated only at the end of loading and unloading intervals. To evaluate the creep strains, the Norton power law is used to simulate the creep strains. The normalized flow rule of creep is based on the Levy-Mises equations in cylindrical coordinate systems and is defined as

$$\begin{aligned}
de_r^c &= s_r d\lambda' \\
de_\theta^c &= s_\theta d\lambda' \\
de_z^c &= -(de_r^c + de_\theta^c)
\end{aligned} \quad (20)$$

$$de_c = \sqrt{\frac{2}{3} (de_r^{c2} + de_\theta^{c2} + de_z^{c2})} \quad (21)$$

$$d\lambda' = \frac{b' s_e^{n_1} e^{\frac{-Q'}{R\tau_c}}}{s_e} dt \quad (22)$$

For more description on flow rule, one may refer to the entry “► [Effect of Creep on Thermal Cyclic Loading of Thick Cylindrical Vessels Based on the Kinematic Hardening Models](#).”

## Numerical Method

Since cyclic loading result of structures is dependent to the history of loading, it must be solved incrementally due to the nonlinear nature of the problem. Thus, a numerical incremental method needs to be used to solve (10), (14), (20), (18) or (19), (16), (21), and (15). Also, the yield condition is checked using (13). It should be mentioned that all equations are written in normalized form for better convergence of numerical calculations, due to the large difference of order of magnitudes of stress and strain. One may refer to the entry “► Numerical Simulation of Cyclic Loading of Thermal Stresses” for solution method of mentioned equations.

## Results and Discussion

The response of a disk subjected to the combination of thermal and mechanical loads based on the P and AF models is studied in this section considering the creep effect at the end of loading and unloading intervals of the disk. The properties given in Table 1 include typical values for creep properties of the disk considered in this section and are used to simulate the cyclic loading behavior of the disk.

As a first problem, a disk subjected to the cyclic thermal load where its inside temperature is cycled through ( $T_i = 0$  to  $300^\circ\text{C}$ ,  $T_o = 0$ ) is considered, and results are shown for the P and AF models in Figs. 1 and 2, respectively. The temperature which brings the inside surface of the disk up to the yield is ( $T_c = 229^\circ\text{C}$ ), and the disk experiences 10 h creep per half cycle interval. These figures show normalized effective stress versus normalized effective mechanical strain at inside surface of the disk for strain-controlled cyclic loading of the disk. As it is seen from these figures, both models predict transient ratcheting to reversed plasticity behavior. According to results obtained in the entry “► Thermal Cyclic Loading of Rotating Disks,” when creep is not considered, different cyclic

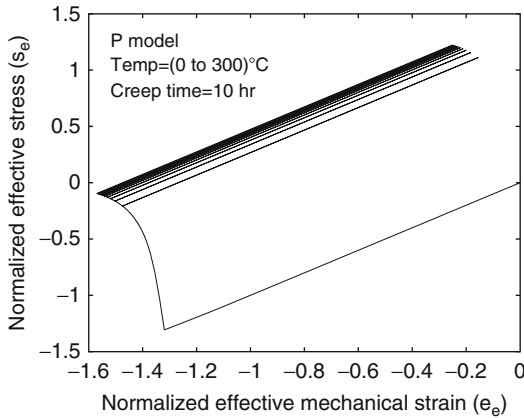
**Effect of Creep on Thermal Cyclic Loading of Rotating Disks, Table 1** Disk properties

Properties	Notation	Value	Unit
Modulus of elasticity	$E$	173.2	GPa
Yield stress	$\sigma_0$	241	MPa
Thermal expansion	$\alpha$	10.8E-6	1/ $^\circ\text{C}$
Creep law coefficient	$b_1$	7.29E-10	1/h
Creep law power	$n_1$	3.5	–
Creep law power	$Q/R$	29,840	$^\circ\text{K}$
Density	$\rho$	7,800	kg/m <sup>3</sup>
Outside to inside ratio	$b/a$	1.5	–
Ludwick curve parameter	$m$	2,631	MPa
Ludwick curve parameter	$n$	0.35	–
AF model parameter	$C$	55.3	GPa
AF model parameter	$\gamma$	280	–

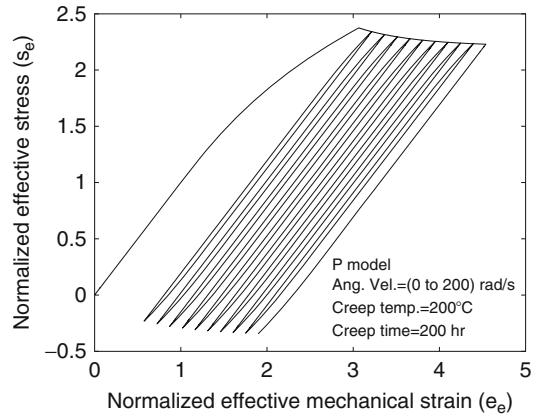
behaviors are predicted using each of the P and AF models.

In the second problem, the same disk is subjected to the cyclic angular velocity between 0 and 200 rad/s. The critical angular velocity which causes the yielding of the disk is  $\omega_c = 124$  rad/s, and the disk experiences 200 h creep per half cycle of load. The disk behavior is predicted using the P and AF models, and the results of normalized effective stress versus normalized effective strain at inside radius of the disk are shown in Figs. 3 and 4, respectively, for load-controlled cyclic loading of the disk. As it is seen from the figures, both of the P and AF models predicted ratcheting behavior for load-controlled cyclic loading of the disk. According to referenced entry in this section, each of the P and AF models predicted different behavior for load-controlled cyclic loading of the disk.

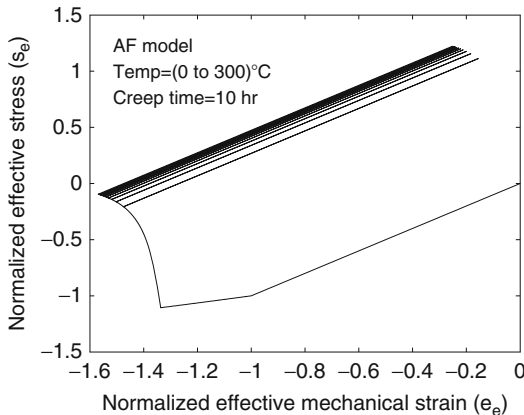
In the third problem, the disk is subjected to the simultaneous angular velocity, inside temperature, and outside temperature cyclic loading. The angular velocity is cycled between 0 and 200 rad/s, the inside temperature is cycled between 0 and  $200^\circ\text{C}$ , and the outside temperature is cycled between 0 and  $250^\circ\text{C}$ , as shown in Fig. 5. When the disk yields, the angular velocity is 116 rad/s, the inside temperature is  $116^\circ$ , and the outside temperature is  $145^\circ$ . The disk



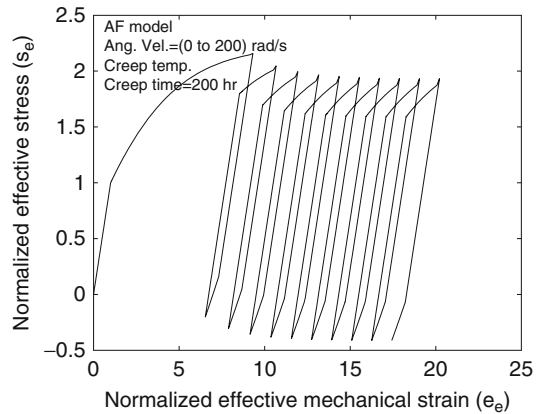
**Effect of Creep on Thermal Cyclic Loading of Rotating Disks, Fig. 1** Inside temperature cyclic loading of disk based on the P model



**Effect of Creep on Thermal Cyclic Loading of Rotating Disks, Fig. 3** Angular velocity cyclic loading of the disk based on the P model



**Effect of Creep on Thermal Cyclic Loading of Rotating Disks, Fig. 2** Inside temperature cyclic loading of disk based on the AF model



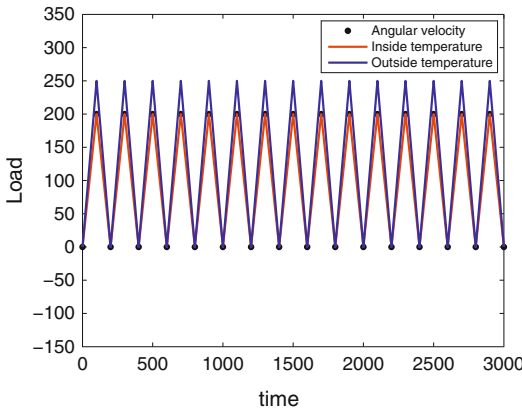
**Effect of Creep on Thermal Cyclic Loading of Rotating Disks, Fig. 4** Angular cyclic loading of the disk based on the AF model

experiences 200 h creep per half cycle interval. The normalized effective stress versus normalized effective mechanical strain is drawn in Figs. 6 and 7 for the P and AF models, respectively. Since both mechanical and thermal loads are cycled, the case is the combination of load-controlled and strain-controlled cyclic loading. As seen from the figures, both models predict ratcheting behavior. Although both of the primary and secondary stresses are developed in the disk, it seems the primary stresses are

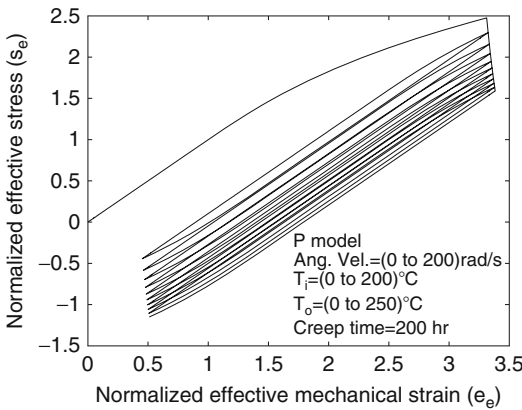
dominant, since ratcheting is achieved as the result of cyclic loading.

In the last example, the same disk is subjected to the combination of cycled angular velocity, inside temperature, and outside temperature, except that in this case the stress produced by thermal cyclic load is dominant to the mechanical cyclic load. The angular velocity is cycled between 0 and 120 rad/s, the inside temperature is cycled between 0 and 190°C, and the outside temperature is cycled between 0 and 550°C.



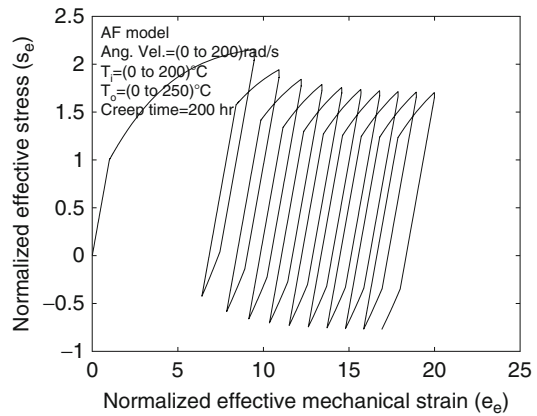


**Effect of Creep on Thermal Cyclic Loading of Rotating Disks, Fig. 5** Loading curve



**Effect of Creep on Thermal Cyclic Loading of Rotating Disks, Fig. 6** Combination of angular velocity, inside temperature, and outside temperature cyclic loading based on the P model

When the disk yields, the angular velocity is 59 rad/s, the inside temperature is 93 °C, and the outside temperature is 270 °C. The disk is subjected to 2,200 h creep per half cycle interval. The results for the P and AF models are shown in Figs. 8 and 9, respectively. As seen from the figures, both models predict transient ratcheting to reversed plasticity behavior as the result of cyclic loading. Although the case is the combination of load- and strain-controlled cyclic loading, since the secondary stresses are dominant to the primary stresses, the results predicted by



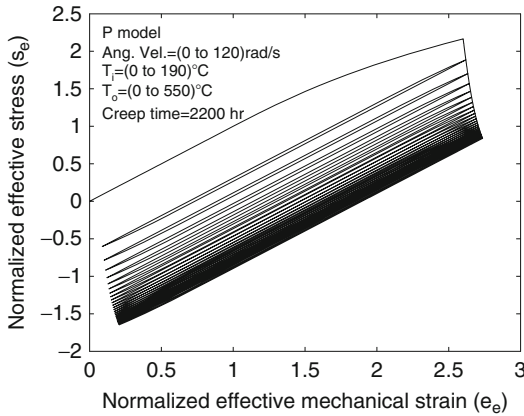
**Effect of Creep on Thermal Cyclic Loading of Rotating Disks, Fig. 7** Combination of angular velocity, inside temperature, and outside temperature cyclic loading based on the AF model

both models are transient ratcheting to reversed plasticity behavior.

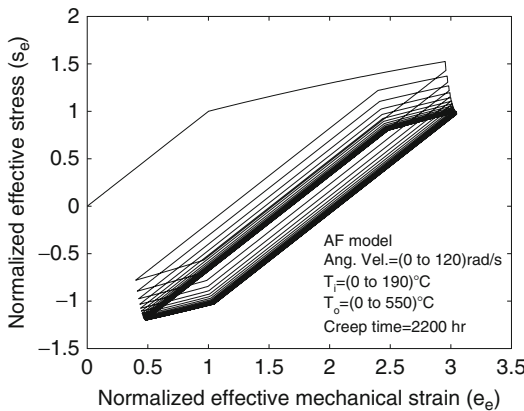
Different results are obtained by the P and AF models for a disk subjected to the cycled body force and thermal loads. Due to the experimental results of Hassan and Kyriakides [4, 5] for uniaxial and biaxial cyclic loading of the structures, the results obtained by the AF model is more compatible with the experimental data in comparison with the P model. To study more on this area, one may refer to Ref. [6, 7].

## Key Research Findings

Elastic–plastic–creep behavior of rotating disks under load- and strain-controlled cyclic lading is studied in this entry using the Prager and Armstrong-Frederick kinematic hardening models. When the disk is subjected to the load-controlled cyclic loading, both models predicted ratcheting behavior for cyclic loading of structures. Imposing the strain-controlled cyclic loading resulted to the transient ratcheting to reversed plasticity behavior. When the combination of load- and strain-controlled cyclic loadings are imposed to the disk, ratcheting is observed whenever primary stresses are dominant. On the other hand,



**Effect of Creep on Thermal Cyclic Loading of Rotating Disks, Fig. 8** Combination of angular velocity, inside temperature, and outside temperature cyclic loading based on the P model



**Effect of Creep on Thermal Cyclic Loading of Rotating Disks, Fig. 9** Combination of angular velocity, inside temperature, and outside temperature cyclic loading based on the AF model

transient ratcheting to reversed plasticity behavior is achieved whenever the secondary stresses are dominant. Comparison of the cyclic response of the disk in the presence of creep with those obtained in the entry “► [Thermal Cyclic Loading of Rotating Disks](#)” is interesting. When creep is excluded, different behaviors are observed for the cyclic response of the disk for the P and AF

models. When creep is considered, identical cyclic behaviors are predicted for the rotating disks under thermal loads.

## References

1. Prager W (1956) A new method of analyzing stresses and strains work-hardening plastic solids. *J Appl Mech* 23:493–496
2. Armstrong PJ, Frederick CO (1966) A mathematical representation of the multiaxial Bauschinger effect. CEBG report no. RD/B/N 731
3. Hetnarski RB, Eslami MR (2009) Thermal stresses – advanced theory and applications. Springer, Berlin
4. Hassan T, Kyriakides S (1992) Ratcheting in cyclic plasticity, part 1: uniaxial behavior. *Int J Plast* 8:91–116
5. Corona E, Hassan T, Kyriakides S (1996) On the performance of kinematic hardening rules in predicting a class of biaxial ratcheting histories. *Int J Plast* 12:117–145
6. Mahbadi H, Eslami MR (2008) Elastic–plastic–creep cyclic loading of rotating hollow disk. *Trans Iran J Mech Eng* 9:72–84
7. Mahbadi H, Eslami MR (2006) Analysis of rotating disks under cyclic thermal and mechanical loads. OPE2006 pressure vessel and piping conference, Chennai

## Effect of Creep on Thermal Cyclic Loading of Thick Cylindrical Vessels Based on the Kinematic Hardening Models

Hossein Mahbadi<sup>1</sup> and Mohammad Reza Eslami<sup>2</sup>

<sup>1</sup>Mechanical Engineering Department, Islamic Azad University, Central Tehran Branch, Tehran, Iran

<sup>2</sup>Department of Mechanical Engineering, Amirkabir University of Technology, Tehran, Iran

## Definition

The definition of terms *primary stress* and *secondary stress* is given in the entry

## ► Thermal Cyclic Loading of Thick Cylindrical Vessels Based on the Prager and Armstrong-Frederick Kinematic Hardening Models.

### Overview

According to the UK pressure vessel code BS PD 5500 [1] and the ASME boilers and pressure vessel code [2], the sum of primary and secondary stresses is responsible for ratcheting or shakedown behavior of the structures. Also, based on the ASME code, the cyclic loading load cases may be divided into the load- and strain-controlled categories. Accordingly, the cyclic loading of pressure on the inside surface of a vessel, which is categorized as load-controlled cyclic loading, produces primary stress cycling. The cyclic loading of temperature distribution producing thermal stresses is categorized as the strain-controlled cyclic loading and results into the secondary stress cycling. In this entry, the influence of creep on the cyclic loading behavior of thick cylindrical vessels under load- and strain-controlled cyclic loadings is investigated. The vessel material is assumed to be isotropic and homogeneous and obeys a nonlinear strain hardening law in the plastic range. The secondary creep law is considered to obtain creep strains at elevated temperatures. The kinematic hardening theory based on the Prager [3] and Armstrong-Frederick [4] models with the von Mises associated flow rule is used to predict the ratcheting or shakedown behavior of the thick cylindrical vessels. An incremental iterative method is proposed to analyze the structural behavior under cyclic loading conditions. Using the Prager and Armstrong-Frederick kinematic hardening models, the cyclic loading results of a vessel under various types of loads, including creep at the end of each load cycle, are compared with those in which creep is excluded.

### Mathematical Formulation

Consider a thick cylinder of inside radius  $a$  and outside radius  $b$  under internal pressure  $P_i$  and external pressure  $P_o$ . Assuming  $T_a$  and  $T_b$  to be the temperatures at inside and outside surfaces of the vessel, the radial temperature distribution  $T(r)$  is calculated from the heat conduction equation as [5]

$$T = \frac{1}{\ln b/a} \left( T_a \ln \frac{b}{r} + T_b \ln \frac{r}{a} \right) \quad (1)$$

To normalize the equations, the following dimensionless quantities are defined:

$$\begin{aligned} S_r &= \frac{\sigma_r}{\sigma_0}, S_\theta = \frac{\sigma_\theta}{\sigma_0}, S_z = \frac{\sigma_z}{\sigma_0}, e_r = \frac{\varepsilon_r}{\varepsilon_0} \\ e_\theta &= \frac{\varepsilon_\theta}{\varepsilon_0}, e_z = \frac{\varepsilon_z}{\varepsilon_0}, e_r^p = \frac{\varepsilon_r^p}{\varepsilon_0}, e_\theta^p = \frac{\varepsilon_\theta^p}{\varepsilon_0} \\ e_z^p &= \frac{\varepsilon_z^p}{\varepsilon_0}, e_r^c = \frac{\varepsilon_r^c}{\varepsilon_0}, e_\theta^c = \frac{\varepsilon_\theta^c}{\varepsilon_0}, e_z^c = \frac{\varepsilon_z^c}{\varepsilon_0} \\ e_r^{Res} &= \frac{\varepsilon_r^{Res}}{\varepsilon_0}, e_\theta^{Res} = \frac{\varepsilon_\theta^{Res}}{\varepsilon_0}, e_z^{Res} = \frac{\varepsilon_z^{Res}}{\varepsilon_0} \\ p_i &= \frac{P_i}{\sigma_0}, p_o = \frac{P_o}{\sigma_0}, \tau = \frac{E\alpha T}{(1-\nu)\sigma_0}, \rho = \frac{r}{a}, \\ \beta &= \frac{b}{a} \end{aligned} \quad (2)$$

where  $\sigma_r, \sigma_\theta$ , and  $\sigma_z$  are the radial, tangential, and axial stresses, respectively. Similarly,  $\varepsilon_r, \varepsilon_\theta, \varepsilon_z$  are the total strains;  $\varepsilon_r^p, \varepsilon_\theta^p, \varepsilon_z^p$  are the plastic strains;  $\varepsilon_r^c, \varepsilon_\theta^c, \varepsilon_z^c$  are the creep strains;  $\varepsilon_r^{Res}, \varepsilon_\theta^{Res}, \varepsilon_z^{Res}$  are the residual strains in the radial, tangential, and axial directions, respectively;  $\sigma_0$  is the yield stress; and  $\varepsilon_0$  is the yield strain. Poisson's ratio is denoted by  $\nu$ . The inclusion of the residual strains in the stress-strain relations is important, as the relations are capable to be used for the cyclic loading analysis.

The governing equations are as follows:

Compatibility and equilibrium equations are

$$\frac{de_\theta}{d\rho} = \frac{e_r - e_\theta}{\rho} \quad (3)$$

$$\frac{dS_r}{d\rho} = \frac{S_\theta - S_r}{\rho} \quad (4)$$

Stress-strain relationship is

$$\begin{aligned} e_r &= S_r - \nu(S_\theta + S_z) + (1 - \nu)\tau + e_r^p + e_r^c + e_r^{Res} \\ e_\theta &= S_\theta - \nu(S_r + S_z) + (1 - \nu)\tau + e_\theta^p + e_\theta^c + e_\theta^{Res} \\ e_z &= S_z - \nu(S_\theta + S_r) + (1 - \nu)\tau + e_z^p + e_z^c + e_z^{Res} \end{aligned} \quad (5)$$

From the incompressibility condition,

$$\begin{aligned} de_z^p &= -(de_r^p + de_\theta^p) \\ de_z^c &= -(de_r^c + de_\theta^c) \end{aligned} \quad (6)$$

The plane strain assumption leads to

$$S_z = \nu(S_r + S_\theta) - (1 - \nu)\tau - e_z^p - e_z^c - e_z^{Res} \quad (7)$$

The boundary conditions are assumed as

$$\begin{aligned} S_r(1) &= -p_i \\ S_r(\beta) &= -p_o \end{aligned} \quad (8)$$

To solve these equations with the given boundary conditions, first the compatibility equation is written in terms of the radial and tangential stresses using the plane strain stress-strain relationships and the incompressibility conditions. This equation together with the compatibility equation makes a system of differential equation, which results to the following solution for the radial and tangential stresses:

$$\begin{aligned} S_r &= -\frac{1}{2\rho^2(1-\nu^2)} \int_1^\rho e_\theta^p \rho d\rho \\ &\quad - \frac{1}{2(1-\nu^2)} \int_1^\rho \frac{e_\theta^p}{\rho} d\rho - \frac{1}{2\rho^2(1-\nu^2)} \int_1^\rho e_r^p \rho d\rho \\ &\quad + \frac{1}{2(1-\nu^2)} \int_1^\rho \frac{e_r^p}{\rho} d\rho - \frac{\nu}{\rho^2(1-\nu^2)} \int_1^\rho e_z^p \rho d\rho \\ &\quad - \frac{1}{2\rho^2(1-\nu^2)} \int_1^\rho e_\theta^c \rho d\rho - \frac{1}{2(1-\nu^2)} \int_1^\rho \frac{e_\theta^c}{\rho} d\rho \\ &\quad - \frac{1}{2\rho^2(1-\nu^2)} \int_1^\rho e_r^c \rho d\rho + \frac{1}{2(1-\nu^2)} \int_1^\rho \frac{e_r^c}{\rho} d\rho \\ &\quad - \frac{\nu}{\rho^2(1-\nu^2)} \int_1^\rho e_z^c \rho d\rho - \frac{1}{2\rho^2(1-\nu^2)} \int_1^\rho e_\theta^{Res} \rho d\rho \\ &\quad - \frac{1}{2(1-\nu^2)} \int_1^\rho \frac{e_\theta^{Res}}{\rho} d\rho - \frac{1}{2\rho^2(1-\nu^2)} \int_1^\rho e_r^{Res} \rho d\rho \\ &\quad + \frac{1}{2(1-\nu^2)} \int_1^\rho \frac{e_r^{Res}}{\rho} d\rho - \frac{\nu}{\rho^2(1-\nu^2)} \int_1^\rho e_z^{Res} \rho d\rho \\ &\quad - \frac{1}{\rho^2} \int_1^\rho \tau \rho d\rho + \frac{C_2}{\rho^2} + C_1 \\ S_\theta &= -\tau + \frac{1}{\rho^2} \int_1^\rho \tau \rho d\rho \\ &\quad + \frac{1}{2\rho^2(1-\nu^2)} \int_1^\rho e_\theta^p \rho d\rho - \frac{1}{2(1-\nu^2)} \int_1^\rho \frac{e_\theta^p}{\rho} d\rho \\ &\quad - \frac{1}{(1-\nu^2)} e_\theta^p + \frac{1}{2\rho^2(1-\nu^2)} \int_1^\rho e_r^p \rho d\rho \\ &\quad + \frac{1}{2(1-\nu^2)} \int_1^\rho \frac{e_r^p}{\rho} d\rho + \frac{\nu}{2(1-\nu^2)} \int_1^\rho \frac{e_z^p}{\rho} d\rho \\ &\quad - \frac{\nu}{(1-\nu^2)} e_z^p + \frac{1}{2\rho^2(1-\nu^2)} \int_1^\rho e_\theta^c \rho d\rho \\ &\quad - \frac{1}{2(1-\nu^2)} \int_1^\rho \frac{e_\theta^c}{\rho} d\rho - \frac{1}{(1-\nu^2)} e_\theta^c \\ &\quad + \frac{1}{2\rho^2(1-\nu^2)} \int_1^\rho e_r^c \rho d\rho + \frac{1}{2(1-\nu^2)} \int_1^\rho \frac{e_r^c}{\rho} d\rho \\ &\quad + \frac{\nu}{2(1-\nu^2)} \int_1^\rho \frac{e_z^{Res}}{\rho} d\rho - \frac{\nu}{(1-\nu^2)} e_z^c \\ &\quad + \frac{1}{2\rho^2(1-\nu^2)} \int_1^\rho e_\theta^{Res} \rho d\rho - \frac{1}{2(1-\nu^2)} \int_1^\rho \frac{e_\theta^{Res}}{\rho} d\rho \\ &\quad - \frac{1}{(1-\nu^2)} e_\theta^{Res} + \frac{1}{2\rho^2(1-\nu^2)} \int_1^\rho e_r^{Res} \rho d\rho \\ &\quad + \frac{1}{2(1-\nu^2)} \int_1^\rho \frac{e_r^{Res}}{\rho} d\rho + \frac{\nu}{2(1-\nu^2)} \int_1^\rho \frac{e_z^{Res}}{\rho} d\rho \\ &\quad - \frac{\nu}{(1-\nu^2)} e_z^{Res} - \frac{C_2}{\rho^2} + C_1 \end{aligned} \quad (9)$$

where the constants of integration, using the boundary conditions (17), are

$$\begin{aligned}
 C_1 &= -(p_i + C_2) \\
 C_2 &= \frac{\beta^2}{\beta^2 - 1} (p_o - p_i) \\
 &\quad - \frac{1}{2(1 - \nu^2)(\beta^2 - 1)} \int_1^\beta e_\theta^p \rho d\rho \\
 &\quad - \frac{\beta^2}{2(1 - \nu^2)(\beta^2 - 1)} \int_1^\beta \frac{e_\theta^p}{\rho} d\rho \\
 &\quad - \frac{1}{2(1 - \nu^2)(\beta^2 - 1)} \int_1^\beta e_r^p \rho d\rho \\
 &\quad + \frac{\beta}{2(1 - \nu^2)(\beta^2 - 1)} \int_1^\beta \frac{e_r^p}{\rho} d\rho \\
 &\quad - \frac{\nu}{(1 - \nu^2)(\beta^2 - 1)} \int_1^\beta e_z^p \rho d\rho \\
 &\quad - \frac{1}{2(1 - \nu^2)(\beta^2 - 1)} \int_1^\beta e_\theta^c \rho d\rho \\
 &\quad - \frac{\beta}{2(1 - \nu^2)(\beta^2 - 1)} \int_1^\beta \frac{e_\theta^c}{\rho} d\rho \\
 &\quad - \frac{1}{2(1 - \nu^2)(\beta^2 - 1)} \int_1^\beta e_r^c \rho d\rho \\
 &\quad + \frac{1}{2(1 - \nu^2)(\beta^2 - 1)} \int_1^\beta \frac{e_r^c}{\rho} d\rho \\
 &\quad - \frac{\nu}{(1 - \nu^2)(\beta^2 - 1)} \int_1^\beta e_z^c \rho d\rho \\
 &\quad - \frac{1}{2(1 - \nu^2)(\beta^2 - 1)} \int_1^\beta e_\theta^{Res} \rho d\rho \\
 &\quad - \frac{\beta}{2(1 - \nu^2)(\beta^2 - 1)} \int_1^\beta \frac{e_\theta^{Res}}{\rho} d\rho \\
 &\quad - \frac{1}{2(1 - \nu^2)(\beta^2 - 1)} \int_1^\beta e_r^{Res} \rho d\rho \\
 &\quad + \frac{1}{2(1 - \nu^2)(\beta^2 - 1)} \int_1^\beta \frac{e_r^{Res}}{\rho} d\rho \\
 &\quad - \frac{\nu}{(1 - \nu^2)(\beta^2 - 1)} \int_1^\beta e_z^{Res} \rho d\rho \\
 &\quad - \frac{1}{(\beta^2 - 1)} \int_1^\beta \tau \rho d\rho
 \end{aligned} \tag{10}$$

## Flow Rule

The normalized yield criterion, flow rule, effective plastic strain, effective stress, and hardening modulus according to the entry ► [Thermal Cyclic Loading of Thick Cylindrical Vessels Based on the Prager and Armstrong-Frederick Kinematic Hardening Models](#) are

$$\left[ \frac{3}{2} (s'_r - a'_r)^2 + (s'_\theta - a'_\theta)^2 + (s'_z - a'_z)^2 \right]^{\frac{1}{2}} = 1 \tag{11}$$

$$\begin{aligned}
 de_r^p &= \frac{3}{2} de_p (s'_r - a'_r) \\
 de_\theta^p &= \frac{3}{2} de_p (s'_\theta - a'_\theta) \\
 de_z^p &= -(de_\theta^p + de_r^p)
 \end{aligned} \tag{12}$$

$$de_p = \sqrt{\frac{2}{3} (de_r^p{}^2 + de_\theta^p{}^2 + de_z^p{}^2)} \tag{13}$$

$$s_e = \sqrt{\frac{3}{2} (s_r'^2 + s_\theta'^2 + s_z'^2)} \tag{14}$$

$$H' = \frac{H}{E} = \frac{ds_e}{de_p} \tag{15}$$

where  $s'_{ij} = s_{ij}/\sigma_0$  and  $a'_{ij} = a_{ij}/\sigma_0$  are normalized stress and back stress tensors, respectively. Also, the back stress components based on the P (i.e., Prager) and AF (i.e., Armstrong-Frederick) models are

$$\begin{aligned}
 dA_r &= C'_1 de_r^p \\
 dA_\theta &= C'_1 de_\theta^p \\
 dA_z &= C'_1 de_z^p
 \end{aligned} \tag{16}$$

$$\begin{aligned}
 dA_r &= \frac{2}{3} C' de_r^p - \gamma' A_r |de_p| \\
 dA_\theta &= \frac{2}{3} C' de_\theta^p - \gamma' A_\theta |de_p| \\
 dA_z &= \frac{2}{3} C' de_z^p - \gamma' A_z |de_p|
 \end{aligned} \tag{17}$$

The definition of parameters used in above equations is described in referenced entry.

### Creep Equations

To investigate the effect of creep on cyclic response of thick cylindrical vessels, it is assumed that creep occurs after loading and unloading procedure. That is, the timescale of loading and unloading in this entry is assumed to be short enough not to activate the creep during the loading and unloading procedure. Thus, the creep process at these regions may be uncoupled from the plastic deformation. The flow rule of creep is based on the Levy-Mises equations as

$$d\epsilon_{ij}^c = s_{ij}d\lambda \quad (18)$$

where  $s_{ij}$  is the deviatoric stress tensor and  $\lambda$  is a nonnegative quantity which may vary through the loading path and thus depends on the history of loading. It can be shown that the constant  $d\lambda$  in terms of the effective stress and increment of effective creep strains becomes

$$d\lambda = \frac{3}{2} \frac{d\epsilon_c}{\sigma_e} \quad (19)$$

The effective creep strain, when the von Mises yield criteria are used, is defined as

$$d\epsilon_c = \sqrt{\frac{2}{3} d\epsilon_{ij}^c d\epsilon_{ij}^c} \quad (20)$$

Due to the generality of the classical Norton creep law, in this entry, the Norton creep law is employed to simulate the experimental creep strain versus time as follows:

$$\dot{\epsilon}_c = b\sigma^{n_1} e^{\frac{-Q}{R\tau_c}} \quad (21)$$

where  $b$  and  $n_1$  are material constant,  $R$  is the universal gas constant, and  $Q$  is the activation energy. According to (21), the constant  $d\lambda$  is found as follows:

$$d\lambda = \frac{b\sigma^{n_1} e^{\frac{-Q}{R\tau_c}}}{\sigma_e} dt \quad (22)$$

The value of  $\sigma$  and  $\sigma_e$  is identical for the first half cycle of the load, but their values differ in subsequent portions of cyclic loading due to the change of coordinate system, as it is described in the entry ► [Numerical Simulation of Cyclic Loading of Thermal Stresses](#). Here,  $\sigma$  is the effective stress in main coordinate system, while  $\sigma_e$  is the effective stress in current coordinate system. The normalized form of flow rule (18) and effective creep strain (20) and  $d\lambda$  is

$$\begin{aligned} de_r^c &= s_r d\lambda' \\ de_\theta^c &= s_\theta d\lambda' \\ de_z^c &= -(de_r^c + de_\theta^c) \end{aligned} \quad (23)$$

$$de_c = \sqrt{\frac{2}{3} (de_r^{c2} + de_\theta^{c2} + de_z^{c2})} \quad (24)$$

$$d\lambda' = \frac{b's^{n_1} e^{\frac{-Q'}{R\tau_c}}}{s_e} dt \quad (25)$$

Assuming  $T_0 = 0$  (i.e., the initial temperature), then  $b'$ ,  $Q'$ , and  $\tau_c$  in (25) are

$$\begin{aligned} b' &= bE\sigma_0^{n_1-1} \\ Q' &= E\alpha Q/\sigma_0 \\ \tau_c &= E\alpha \frac{273 + \theta}{\sigma_0} \end{aligned} \quad (26)$$

### Numerical Method

Since cyclic loading result of structures depends upon the history of loading, it must be solved incrementally due to the nonlinear nature of the problem. Thus, a numerical incremental method needs to be used to solve (9), (12), (23), (13), (24), (14), and (16) or (17). Also, the yield condition is checked using (11). One may refer to the entry ► [Numerical Simulation of Cyclic Loading of Thermal Stresses](#) for solution method of the mentioned equations.

**Effect of Creep on Thermal Cyclic Loading of Thick Cylindrical Vessels Based on the Kinematic Hardening Models, Table 1** Vessel properties

Properties	Notation	Value	Unit
Modulus of elasticity	$E$	173.2	GPa
Yield stress	$\sigma_0$	241	MPa
Thermal expansion	$\alpha$	10.8E-6	1%/C
Creep law coefficient	$b_1$	7.29E-10	1/h
Creep law power	$n_1$	3.5	–
Creep law power	$Q/R$	29,840	°K
Outside to inside ratio	$b/a$	1.5	–
Ludwick curve parameter	$m$	2,631	MPa
Ludwick curve parameter	$n$	0.35	–
AF model parameter	$C$	55.3	GPa
AF model parameter	$\gamma$	280	–

## Results and Discussion

To investigate the effect of creep on cyclic response of thick cylindrical vessels, the same set of problems solved in ► [Thermal Cyclic Loading of Thick Cylindrical Vessels Based on the Prager and Armstrong-Frederick Kinematic Hardening Models](#) are solved considering creep at the end of loading and unloading intervals of the vessel. The material properties of the vessel including the typical values for creep parameters are given in [Table 1](#).

In the first example, a vessel is subjected to the cyclic thermal load, where its inside temperature is cycled through ( $T_i = 0 - 250^\circ\text{C}$ ,  $T_o = 0$ ) and experiences 1,000 h creep per half cycle interval. The average inside temperature cycle is  $T_{ave} = 125^\circ\text{C}$ , and the inside temperature which brings the inside surface of the vessel up to the yield is ( $T_c = 75.5^\circ\text{C}$ ). The normalized effective stress versus normalized effective mechanical strain (i.e.,  $s_e + e_p + e_c$ ) based on the P and AF models is drawn for inside radius of the vessel in [Figs. 1](#) and [2](#), respectively. Both figures show transient ratcheting to reversed plasticity behavior for thermal cyclic loading of the cylindrical vessel. According to the referenced entry in this section, when creep is excluded, the P model predicted reversed plasticity behavior which is different from the results obtained by the AF model.

In the second example, the vessel is subjected to the load-controlled cyclic loading. The vessel

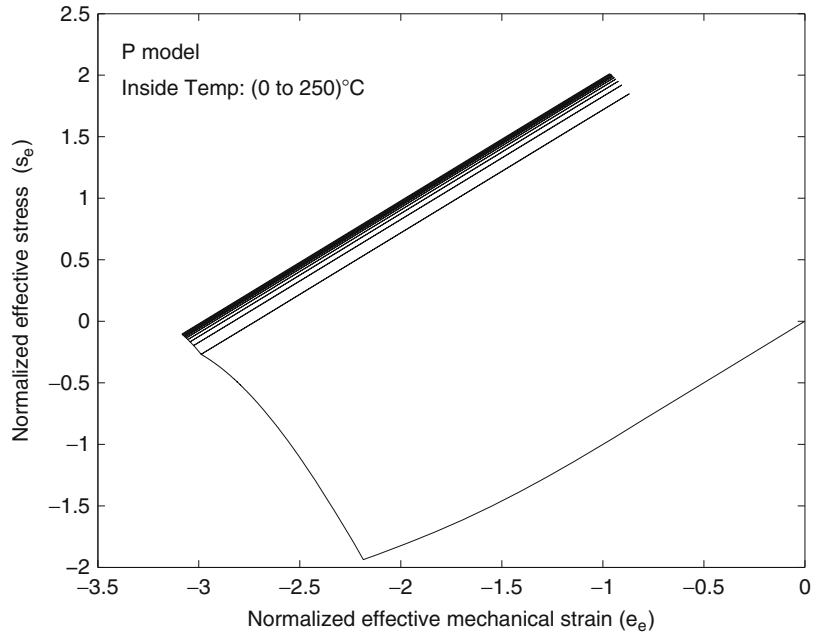
is subjected to the cyclic inside pressure between 0 and 240 MPa. The critical pressure, where the inside surface yields, is  $P_c = 77$  MPa. The average pressure cycle is  $P_{av} = 120$  MPa, and the vessel experiences 1,000 h at  $200^\circ\text{C}$  uniform temperature per half cycle interval. The vessel behavior is predicted using the P and AF models, and the results of normalized effective stress versus the normalized effective strain at inside surface of the vessel are shown in [Figs. 3](#) and [4](#), respectively. Due to the cycling of mechanical loads, the case is load-controlled cyclic loading. Both models predicted ratcheting for load-controlled cyclic loading of the vessel. According to the referenced entry in this section, when creep is excluded, the results predicted based on the P model differ from that of the AF model. It is interesting to note that when creep is included in cyclic loading simulation, both models predict identical behavior for load-controlled cyclic loading of the vessel.

In the next example, a simultaneous constant inside pressure  $P_i = 40$  MPa and cyclic inside temperature  $T_i$  between 0 and  $300^\circ\text{C}$  are applied to the vessel, while the vessel experiences 10h creep per half cycle. The critical temperature which brings inside surface of the vessel up to the yield, due to the constant pressure at inside surface of the vessel, is  $142.6^\circ\text{C}$ . The results for normalized effective stress versus normalized effective mechanical strain at inside surface of the vessel based on the P and AF models are shown in [Figs. 5](#) and [6](#), respectively. Due to the cycling of thermal load, the case is strain-controlled cyclic loading. As seen from the figures, both models predict transient ratcheting to reversed plasticity behavior for strain-controlled cyclic loading of the vessel.

The last example considers a vessel subjected to thermal cyclic load at both inside and outside surfaces, while experiences 1,000 h creep per half cycle. The inside temperature is cycled through ( $T_i = 0 - 230^\circ\text{C}$ ), and the outside temperature is cycled through  $T_o = 260$  to  $0^\circ\text{C}$ , and the normalized effective stress versus normalized effective strain at inside surface of the vessel is shown in [Figs. 7](#) and [8](#) for the P and AF models,

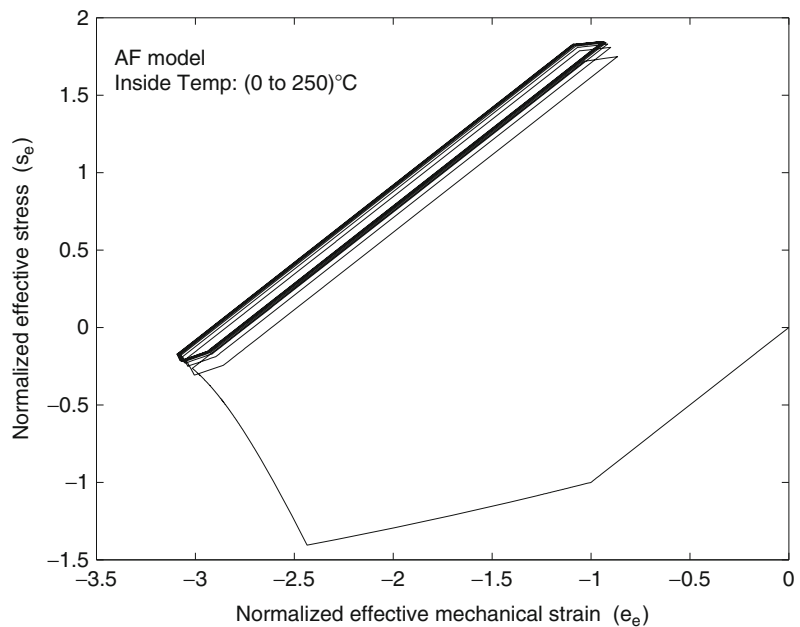
**Effect of Creep on Thermal Cyclic Loading of Thick Cylindrical Vessels Based on the Kinematic Hardening Models, Fig. 1**

Inside temperature cyclic loading of thick cylinder based on the P model



**Effect of Creep on Thermal Cyclic Loading of Thick Cylindrical Vessels Based on the Kinematic Hardening Models, Fig. 2**

Inside temperature cyclic loading of thick cylinder based on the AF model



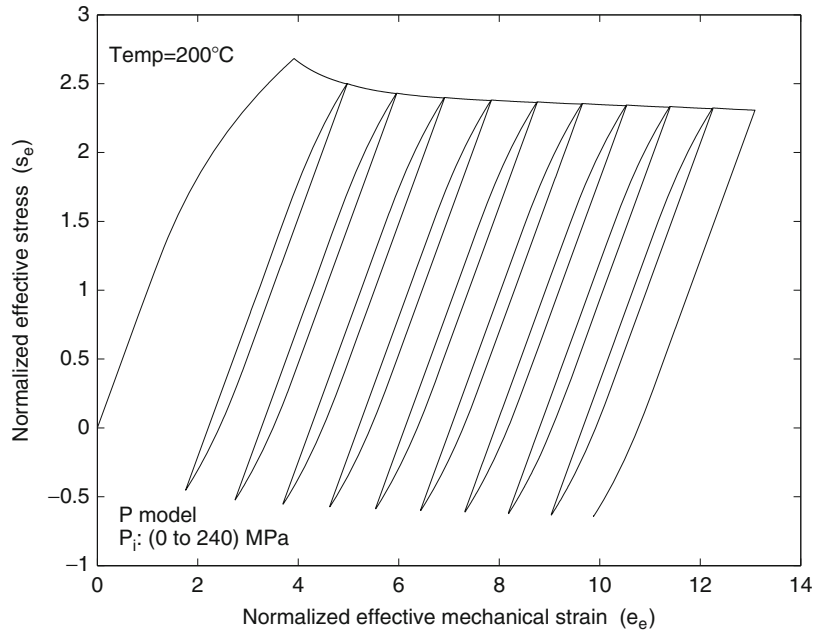
respectively. Due to cycling of secondary stresses, the case is the strain-controlled cyclic loading. As seen from the figures, both P and AF models predict ratcheting behavior. It is an interesting example showing that cycling of thermal loads results to ratcheting behavior. The same

problem for a spherical vessel is solved in entry [► Effect of Creep on Cyclic Loading of Spherical Vessels Based on the Kinematic Hardening Models](#), which the reader is referred to this entry to compare the results between spherical and cylindrical vessels.



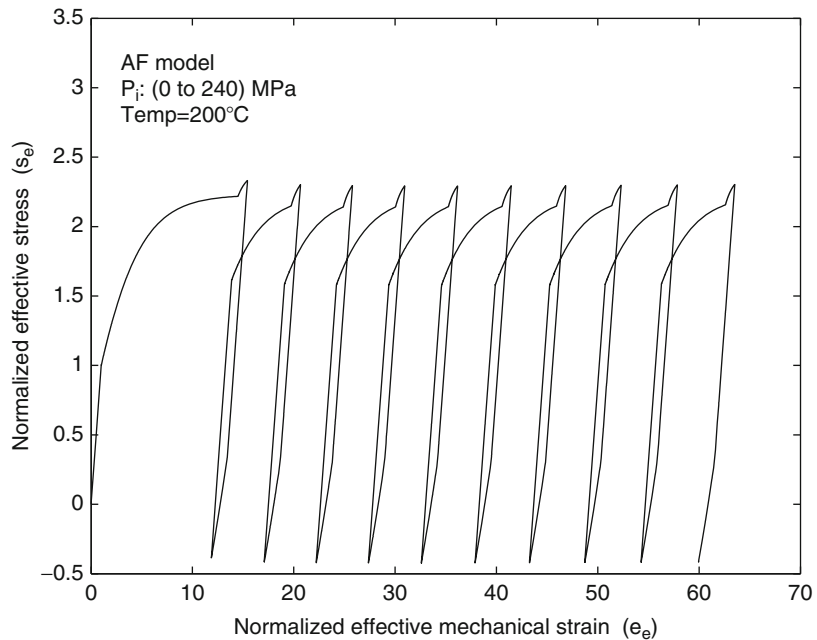
**Effect of Creep on Thermal Cyclic Loading of Thick Cylindrical Vessels Based on the Kinematic Hardening Models, Fig. 3**

Inside pressure cyclic loading of thick cylinder based on the P model



**Effect of Creep on Thermal Cyclic Loading of Thick Cylindrical Vessels Based on the Kinematic Hardening Models, Fig. 4**

Inside pressure cyclic loading of thick cylinder based on the AF model



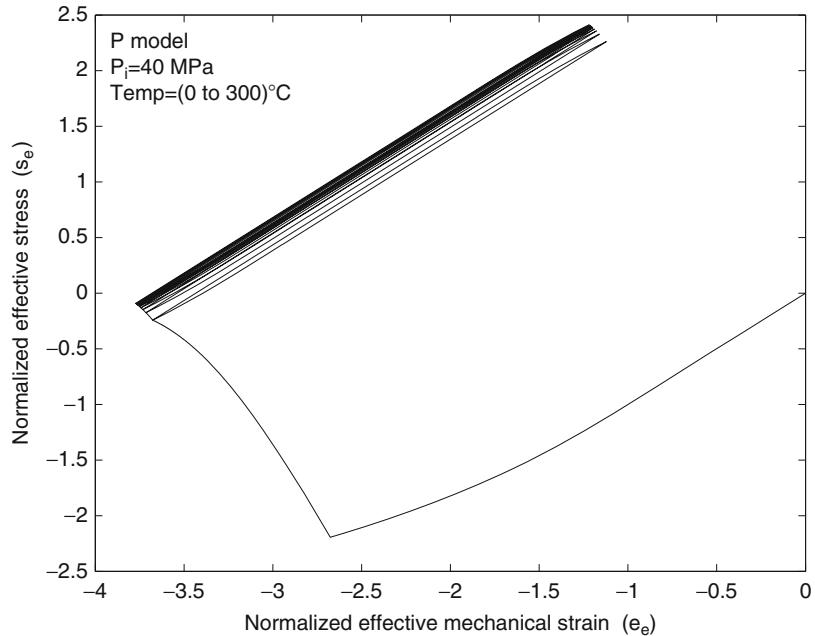
More problems on this field are solved in [6]. Due to the experimental data of Hassan and Kyriakides [7, 8] for uniaxial and biaxial cyclic loading of the structures, more accurate results are expected using the AF model.

**Key Research Findings**

In this entry, effect of creep on cyclic loading response of thick cylindrical vessel is investigated. To this aim, the stress and strain equations

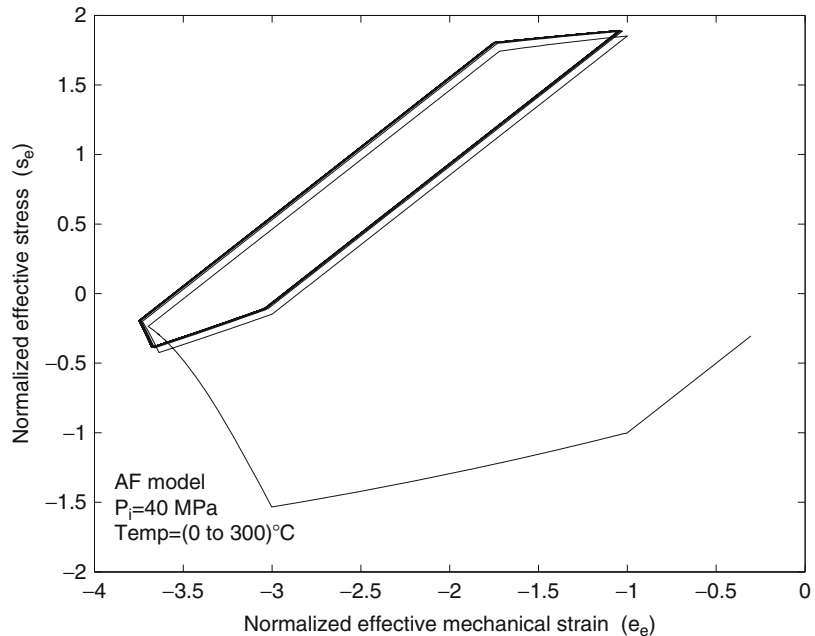
**Effect of Creep on Thermal Cyclic Loading of Thick Cylindrical Vessels Based on the Kinematic Hardening Models, Fig. 5**

Inside temperature cyclic loading with constant inside pressure of thick cylinder based on P model



**Effect of Creep on Thermal Cyclic Loading of Thick Cylindrical Vessels Based on the Kinematic Hardening Models, Fig. 6**

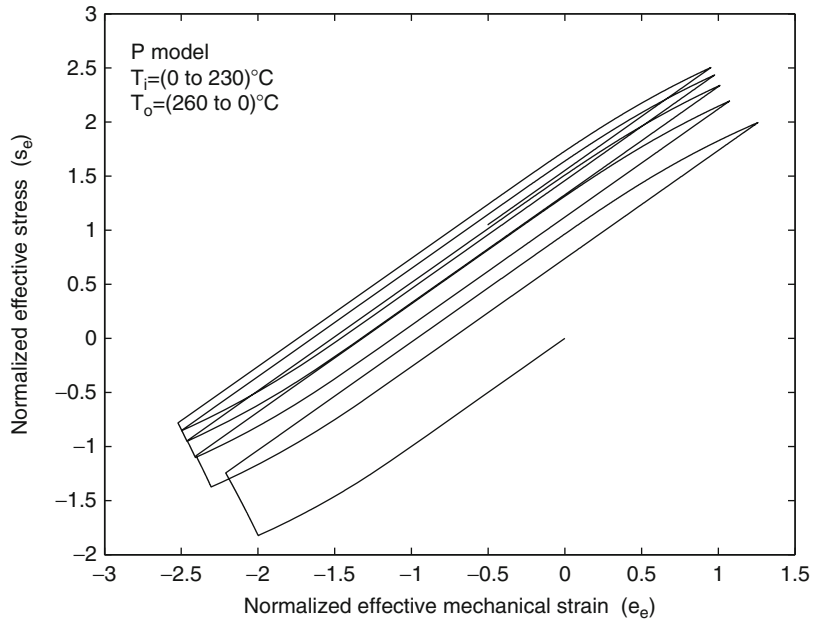
Inside temperature cyclic loading with constant inside pressure of thick cylinder based on AF model



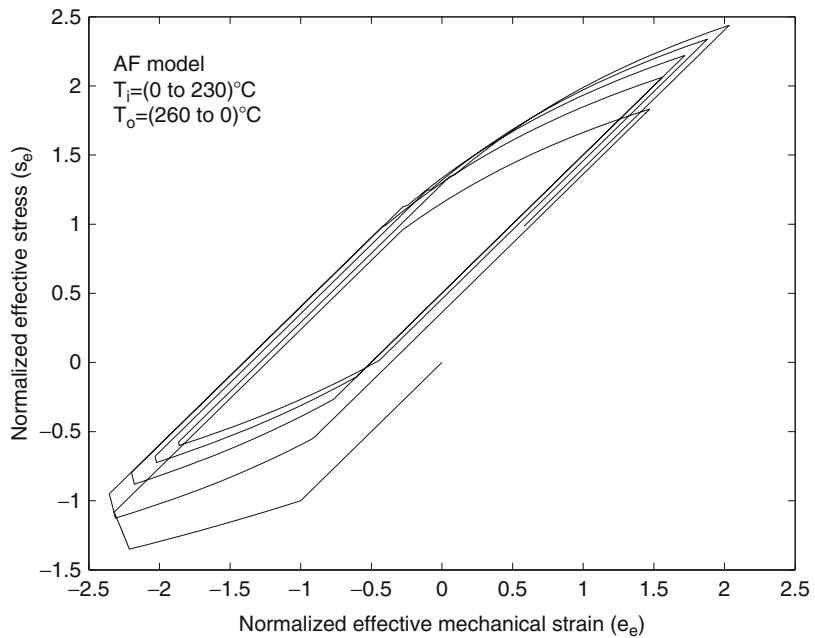
are adapted to evaluate the creep and plastic strains during the cyclic loading, where a numerical method is employed to solve these equations. The interesting research finding is that when creep is not considered, the Prager and Armstrong-Frederick kinematic hardening

models predict different cyclic response of thick cylindrical vessel. When creep deformation is considered, both kinematic hardening models predict identical behavior for cyclic loading of the vessel. When creep is considered, cycling of mechanical loads results into ratcheting, and

**Effect of Creep on Thermal Cyclic Loading of Thick Cylindrical Vessels Based on the Kinematic Hardening Models, Fig. 7** Inside-outside temperature cyclic loading of thick cylinder based on the Prager kinematic hardening model



**Effect of Creep on Thermal Cyclic Loading of Thick Cylindrical Vessels Based on the Kinematic Hardening Models, Fig. 8** Inside-outside temperature cyclic loading of thick cylinder based on the Armstrong-Frederick kinematic hardening model



cycling of thermal loads results into transient ratcheting to reversed plasticity behavior. Another interesting result is that, although the thermal loads develop secondary stresses through the thickness of the vessel, cycling of thermal loads at both inside and outside surfaces of the vessel results to ratcheting.

## References

1. BS PD 5500 (2009) Specification for unfired fusion welded pressure vessels. British Standards Institution, London
2. ASME Boiler and Pressure Vessel Code, Section VIII, Div. 2 (2007) American Society of Mechanical Engineers, New York

3. Prager W (1956) A new method of analyzing stresses and strains work-hardening plastic solids. *J Appl Mech* 23:493–496
4. Armstrong PJ, Frederick CO (1966) A mathematical representation of the multiaxial baushinger effect. CEGB Report No. RD/B/N 731
5. Hetnarski RB, Eslami MR (2009) Thermal stresses – advanced theory and applications. Springer, Dordrecht
6. Mahbadi H, Eslami MR (2011) Cyclic loading behaviour of thick cylindrical vessels under creep deformation. *Int J Strain Anal Eng Des* 46:727–739
7. Hassan T, Kyriakides S (1992) Ratcheting in cyclic plasticity, part 1: uniaxial behavior. *Int J Plast* 8:91–116
8. Corona E, Hassan T, Kyriakides S (1996) On the performance of kinematic hardening rules in predicting a class of biaxial ratcheting histories. *Int J Plast* 12:117–145

## Effect of Shear Stresses in Thermal Cylindrical Shells

Yoshihiro Ootao

Department of Mechanical Engineering,  
Graduate School of Engineering, Osaka  
Prefecture University, Nakaku, Sakai, Osaka,  
Japan

### Overview

The effect of transverse shear stresses is often neglected in the theory of thin cylindrical shells, while it is very important in thick cylindrical shells. In order to estimate the transverse shear stresses in thermal cylindrical shells, it is necessary to consider the transverse shear deformations. Thermal cylindrical shells may be isotropic, anisotropic, isotropic laminated, or anisotropic laminated. This entry considers the transient thermal stresses of a cross-ply laminated cylindrical shell as an example of anisotropic laminated cylindrical shells.

First, the transient heat conduction problem is presented. Next, the third-order and first-order

shear deformation theories are explained as thermoelastic problems. In order to compare these two theories, the classical shell theory is utilized. Lastly, a numerical result is shown in order to investigate the effect of shear stresses.

### Analysis

A cross-ply laminated cylindrical shell composed of  $n$  layers is considered [1]. The laminated cylindrical shell's inner and outer radii and length are represented by  $a$ ,  $b$ , and  $L$ , respectively.

### Heat Conduction Problem

The cross-ply laminated cylindrical shell is initially assumed to be at zero temperature and its inner and outer surfaces are suddenly heated by surrounding media that are at temperatures  $T_{af_a}(x)$  and  $T_{bf_b}(x)$  with relative heat transfer coefficients  $h_a$  and  $h_b$ , respectively. We assume that the end surfaces of the cross-ply laminated cylindrical shell are held at zero temperature. The temperature distribution is two-dimensional in the  $r - x$  plane, and the transient heat conduction equation for the  $i$ th layer takes the following form:

$$\frac{\partial T_i}{\partial t} = \kappa_{ri} \left( \frac{\partial^2 T_i}{\partial r^2} + \frac{1}{r} \frac{\partial T_i}{\partial r} \right) + \kappa_{xi} \frac{\partial^2 T_i}{\partial x^2}; \quad (1)$$

$$i = 1, 2, \dots, n$$

The initial and thermal boundary conditions are as follows:

$$t = 0; \quad T_i = 0; \quad i = 1, 2, \dots, n \quad (2)$$

$$r = a; \quad \frac{\partial T_1}{\partial r} - h_a T_1 = -h_a T_{af_a}(x) \quad (3)$$

$$r = r_i; \quad T_i = T_{i+1}, \quad \lambda_{ri} \frac{\partial T_i}{\partial r} = \lambda_{r,i+1} \frac{\partial T_{i+1}}{\partial r}; \quad (4)$$

$$i = 1, 2, \dots, n - 1$$

$$r = b; \quad \frac{\partial T_n}{\partial r} + h_b T_n = h_b T_{bf_b}(x) \quad (5)$$

Revised version of: Ootao Y, Tanigawa Y, Miyatake K (2009) Transient Thermal Stresses of a Cross-ply Laminated Cylindrical Shell Using a Higher-order Shear Deformation Theory. *Journal of Thermal Stresses* Vol 33-1: 55–74, reprinted by permission of © Taylor & Francis Group, LLC (<http://tandfonline.com>)

$$x = 0, L; T_i = 0; \quad i = 1, 2, \dots, n \quad (6)$$

In Eq. (1)–(6),  $T_i$  is the temperature change;  $t$  is the time;  $\kappa_{ki}$  is the thermal diffusivity; and  $\lambda_{ri}$  is the thermal conductivity, respectively. Introducing the finite sine transformation with respect to the variable  $x$  and the Laplace transformation with respect to the variable  $t$ , the solution of (1) can be obtained so as to satisfy the conditions of (2)–(6). This solution is shown as follows [1]:

$$T_i = \sum_{k=1}^{\infty} T_{ik}(r, t) \sin q_k x; \quad i = 1, 2, \dots, n \quad (7)$$

where

$$\begin{aligned} T_{ik}(r, t) = & \frac{2}{L} \left[ \frac{1}{F} \left\{ \bar{A}'_i I_0(\xi_i r) + \bar{B}'_i K_0(\xi_i r) \right\} \right. \\ & + \sum_{j=1}^i \frac{2 \exp(-\mu_j^2 t)}{\mu_j \Delta'(\mu_j)} \left\{ \bar{A}_i I_0(\beta_{ij} r) + \bar{B}_i K_0(\beta_{ij} r) \right\} \\ & \left. + \sum_{j=i+1}^{\infty} \frac{2 \exp(-\mu_j^2 t)}{\mu_j \Delta'(\mu_j)} \left\{ \bar{A}_i J_0(\gamma_{ij} r) + \bar{B}_i Y_0(\gamma_{ij} r) \right\} \right] \end{aligned} \quad (8)$$

In this equation,  $I_0(\cdot)$  and  $K_0(\cdot)$  are the zero-order modified Bessel functions of the first and second kind, and  $J_0(\cdot)$  and  $Y_0(\cdot)$  are the zero-order Bessel functions of the first and second kind, respectively. In addition,  $\Delta$  and  $F$  are the determinants of the  $2n \times 2n$  matrices  $[a_{kl}]$  and  $[e_{kl}]$ , respectively; the coefficients  $\bar{A}_i$  and  $\bar{B}_i$  are defined as the determinant of the matrix similar to the coefficient matrix  $[a_{kl}]$ , in which the  $2i$ th column or  $(2i-1)$ th column is replaced by the constant vector  $\{c_k\}$ , respectively. Similarly, the coefficients  $\bar{A}'_i$  and  $\bar{B}'_i$  are defined as the determinant of the matrix similar to the coefficient matrix  $[e_{kl}]$ , in which the  $2i$ th column or  $(2i-1)$ th column is replaced by the constant vector  $\{c_k\}$ , respectively. The nonzero elements of the coefficient matrices  $[a_{kl}]$ ,  $[e_{kl}]$  and the constant vector  $\{c_k\}$  are given as follows:

$$a_{11} = \begin{cases} h_a I_0(\beta_1 a) - \beta_1 I_1(\beta_1 a) \\ h_a J_0(\gamma_1 a) + \gamma_1 J_1(\gamma_1 a) \end{cases}$$

$$a_{12} = \begin{cases} h_a K_0(\beta_1 a) + \beta_1 K_1(\beta_1 a) \\ h_a Y_0(\gamma_1 a) + \gamma_1 Y_1(\gamma_1 a) \end{cases}$$

$$a_{2i,2i-1} = \begin{cases} I_0(\beta_i r_i) \\ J_0(\gamma_i r_i) \end{cases}, \quad a_{2i,2i} = \begin{cases} K_0(\beta_i r_i) \\ Y_0(\gamma_i r_i) \end{cases}$$

$$a_{2i,2i+1} = \begin{cases} -I_0(\beta_{i+1} r_i) \\ -J_0(\gamma_{i+1} r_i) \end{cases}, \quad a_{2i,2i+2} = \begin{cases} -K_0(\beta_{i+1} r_i) \\ -Y_0(\gamma_{i+1} r_i) \end{cases}$$

$$a_{2i+1,2i-1} = \begin{cases} \lambda_{ri} \beta_i I_1(\beta_i r_i) \\ -\lambda_{ri} \gamma_i J_1(\gamma_i r_i) \end{cases}$$

$$a_{2i+1,2i} = \begin{cases} -\lambda_{ri} \beta_i K_1(\beta_i r_i) \\ -\lambda_{ri} \gamma_i Y_1(\gamma_i r_i) \end{cases}$$

$$a_{2i+1,2i+1} = \begin{cases} -\lambda_{r,i+1} \beta_{i+1} I_1(\beta_{i+1} r_i) \\ \lambda_{r,i+1} \gamma_{i+1} J_1(\gamma_{i+1} r_i) \end{cases}$$

$$a_{2i+1,2i+2} = \begin{cases} \lambda_{r,i+1} \beta_{i+1} K_1(\beta_{i+1} r_i) \\ \lambda_{r,i+1} \gamma_{i+1} Y_1(\gamma_{i+1} r_i) \end{cases}; \quad i = 1, 2, \dots, n-1$$

$$a_{2n,2n-1} = \begin{cases} h_b I_0(\beta_n b) + \beta_n I_1(\beta_n b) \\ h_b J_0(\gamma_n b) - \gamma_n J_1(\gamma_n b) \end{cases}$$

$$a_{2n,2n} = \begin{cases} h_b K_0(\beta_n b) - \beta_n K_1(\beta_n b) \\ h_b Y_0(\gamma_n b) - \gamma_n Y_1(\gamma_n b) \end{cases} \quad (9)$$

$$e_{11} = h_a I_0(\xi_1 a) - \xi_1 I_1(\xi_1 a)$$

$$e_{12} = h_a K_0(\xi_1 a) + \xi_1 K_1(\xi_1 a)$$

$$e_{2i,2i-1} = I_0(\xi_i r_i), \quad e_{2i,2i} = K_0(\xi_i r_i)$$

$$e_{2i,2i+1} = -I_0(\xi_{i+1} r_i), \quad e_{2i,2i+2} = -K_0(\xi_{i+1} r_i)$$

$$e_{2i+1,2i-1} = \lambda_{ri} \xi_i I_1(\xi_i r_i), \quad e_{2i+1,2i} = -\lambda_{ri} \xi_i K_1(\xi_i r_i)$$

$$e_{2i+1,2i+1} = -\lambda_{r,i+1} \xi_{i+1} I_1(\xi_{i+1} r_i)$$

$$e_{2i+1,2i+2} = \lambda_{r,i+1} \xi_{i+1} K_1(\xi_{i+1} r_i); \quad i = 1, 2, \dots, n-1$$

$$e_{2n,2n-1} = h_b I_0(\xi_n b) + \xi_n I_1(\xi_n b)$$

$$e_{2n,2n} = h_b K_0(\xi_n b) - \xi_n K_1(\xi_n b) \quad (10)$$

$$c_1 = h_a T_a \hat{f}_a(q), \quad c_{2n} = h_b \bar{T}_b \hat{f}_b(q) \quad (11)$$

where the functions  $\hat{f}_a(q)$  and  $\hat{f}_b(q)$  represent the finite sine transformation of  $f_a(x)$  and  $f_b(x)$ , respectively. In (9), the upper parts of the elements  $a_{kl}$  correspond to the case of  $\mu_j^2 - \kappa_{xi} q_k^2 < 0$  and the lower part to the case of  $\mu_j^2 - \kappa_{xi} q_k^2 > 0$ . Furthermore, in (7) and (8),  $q_k$ ,  $\Delta'(\mu_j)$ ,  $\xi_i$ ,  $\beta_{ij}$ , and  $\gamma_{ij}$  are given by

$$\begin{aligned} q_k &= \frac{k\pi}{L}, \quad \Delta'(\mu_j) = \frac{d\Delta}{d\mu} \Big|_{\mu=\mu_j}, \quad \xi_i = \sqrt{\frac{\kappa_{xi}}{\kappa_{ri}}} q_k, \\ \beta_i^2 &= -\frac{\mu_j^2 - \kappa_{xi} q_k^2}{\kappa_{ri}} \quad \text{if } \mu_j^2 - \kappa_{xi} q_k^2 < 0 \\ \gamma_i^2 &= \frac{\mu_j^2 - \kappa_{xi} q_k^2}{\kappa_{ri}} \quad \text{if } \mu_j^2 - \kappa_{xi} q_k^2 > 0 \end{aligned} \quad (12)$$

and  $\mu_j$  represents the  $j$ th positive roots of the following transcendental equation:

$$\Delta(\mu) = 0 \quad (13)$$

The condition for the eigenvalue  $\mu_j$  is given by

$$\mu_1 < \mu_2 < \cdots < \mu_{j'} < \sqrt{\kappa_{xi}} q_k < \mu_{j'+1} < \cdots \quad (14)$$

### Thermoelastic Problem

The transient thermal stress of a cross-ply laminated cylindrical shell due to axisymmetric heat supply is analyzed using third-order shear deformation, first-order shear deformation, and classical theories [1].

### Third-Order Shear Deformation Theory (TSDT)

The displacement field is given by

$$u_i = u_0 + z\phi_x - \frac{4z^3}{3h^2} \left( \phi_x + \frac{dw}{dx} \right), \quad w_i = w \quad (15)$$

where  $u_0$  is the displacement in the  $x$  direction on the middle plane;  $w$  is the displacement in the  $z$  direction on the middle plane; and  $\phi_x$  is the rotation of the normal to the  $x$ -axis. The relationship between the coordinate  $z$  and the coordinate  $r$  is given as follows:

$$z = r - R \quad (16)$$

In (15) and (16),  $h$  and  $R$  are

$$h = b - a, \quad R = \frac{a+b}{2} \quad (17)$$

The displacement-strain relations are expressed as follows:

$$\varepsilon_{xxi} = \frac{du_i}{dx}, \quad \varepsilon_{\theta\theta i} = \frac{w}{R+z}, \quad \gamma_{xzi} = \frac{du_i}{dz} + \frac{dw}{dx} \quad (18)$$

The stress-strain relations are expressed as follows:

$$\begin{aligned} \sigma_{xxi} &= Q_{11i} \varepsilon_{xxi} + Q_{12i} \varepsilon_{\theta\theta i} - \beta_{xi} T_i \\ \sigma_{\theta\theta i} &= Q_{12i} \varepsilon_{xxi} + Q_{22i} \varepsilon_{\theta\theta i} - \beta_{\theta i} T_i \\ \sigma_{xzi} &= Q_{55i} \gamma_{xzi} \end{aligned} \quad (19)$$

where

$$\begin{aligned} \beta_{xi} &= Q_{11i} \alpha_{xi} + Q_{12i} \alpha_{\theta i} \\ \beta_{\theta i} &= Q_{12i} \alpha_{xi} + Q_{22i} \alpha_{\theta i} \end{aligned} \quad (20)$$

The resultant forces and moments are expressed as follows:

$$\begin{aligned} (N_{xx}, M_{xx}, P_{xx}) &= \int_{-h/2}^{h/2} \sigma_{xxi} \left( \frac{R+z}{R} \right) (1, z, z^3) dz \\ N_{\theta\theta} &= \int_{-h/2}^{h/2} \sigma_{\theta\theta i} dz \\ (Q_x, R_x) &= \int_{-h/2}^{h/2} \sigma_{xzi} \left( \frac{R+z}{R} \right) (1, z^2) dz \end{aligned} \quad (21)$$

The total potential energy of the cross-ply laminated cylindrical shell is given by where

$$\Pi = \int_0^{2\pi} \int_0^L \int_{-h/2}^{h/2} U(R+z) dz dx d\theta \quad (22)$$

where

$$U = \frac{1}{2} [\sigma_{xzi}(\varepsilon_{xzi} - \alpha_{zi}T_i) + \sigma_{\theta\theta i}(\varepsilon_{\theta\theta i} - \alpha_{\theta i}T_i) + \sigma_{xzi}\gamma_{xzi}] \quad (23)$$

Applying the principle of minimum total potential energy,  $\delta\Pi = 0$ , the equilibrium equations and the boundary conditions are obtained. The equilibrium equations are expressed as follows:

$$\frac{dN_{xx}}{dx} = 0 \quad (24)$$

$$\frac{dM_{xx}}{dx} - \frac{4}{3h^2} \frac{dP_{xx}}{dx} - Q_x + \frac{4}{h^2} R_x = 0 \quad (25)$$

$$\frac{N_{\theta\theta}}{R} - \frac{4}{3h^2} \frac{d^2P_{xx}}{dx^2} - \frac{dQ_x}{dx} + \frac{4}{h^2} \frac{dR_x}{dx} = 0 \quad (26)$$

We now consider the case of a simply supported cylindrical shell described by the following relations:

$$x = 0, L; \quad N_{xx} = 0, \quad M_{xx} - \frac{4}{3h^2} P_{xx} = 0, \quad w = 0 \quad (27)$$

Substituting (15), (18), and (19) into (21), the resultant forces and moments are

$$\begin{aligned} N_{xx} &= A_{11} \frac{du_o}{dx} + B_{11} \frac{d\phi_x}{dx} - C_{11} \frac{d^2w}{dx^2} + A_{12} \frac{w}{R} - N_{xx}^T \\ N_{\theta\theta} &= A_{12} \frac{du_o}{dx} + B_{12} \frac{d\phi_x}{dx} - C_{12} \frac{d^2w}{dx^2} + A_{22} \frac{w}{R} - N_{\theta\theta}^T \\ M_{xx} &= B'_{11} \frac{du_o}{dx} + D_{11} \frac{d\phi_x}{dx} - C'_{11} \frac{d^2w}{dx^2} + B'_{12} \frac{w}{R} - M_{xx}^T \\ P_{xx} &= B''_{11} \frac{du_o}{dx} + D'_{11} \frac{d\phi_x}{dx} - C''_{11} \frac{d^2w}{dx^2} + B''_{12} \frac{w}{R} - P_{xx}^T \\ (Q_x, R_x) &= (A_{55}, A'_{55}) \left( \phi_x + \frac{dw}{dx} \right) \end{aligned} \quad (28)$$

$$\begin{aligned} (A_{11}, A_{22}) &= \sum_{i=1}^n \int_{h_{i-1}}^{h_i} (Q_{11i}, Q_{22i}) \left( \frac{R+z}{R} \right) dz \\ (A_{12}, B'_{12}, B''_{12}, C_{12}) &= \sum_{i=1}^n \int_{h_{i-1}}^{h_i} Q_{12i} \left( 1, z, z^3, \frac{4z^3}{3h^2} \right) dz \\ B_{11} &= \sum_{i=1}^n \int_{h_{i-1}}^{h_i} Q_{11i} \left( 1 - \frac{4z^2}{3h^2} \right) \left( \frac{R+z}{R} \right) z dz \\ B_{12} &= \sum_{i=1}^n \int_{h_{i-1}}^{h_i} Q_{12i} \left( 1 - \frac{4z^2}{3h^2} \right) z dz \\ (B'_{11}, B''_{11}) &= \sum_{i=1}^n \int_{h_{i-1}}^{h_i} Q_{11i} \left( \frac{R+z}{R} \right) (z, z^3) dz \\ (C_{11}, C'_{11}, C''_{11}) &= \sum_{i=1}^n \int_{h_{i-1}}^{h_i} \bar{Q}_{11i} \frac{4}{3h^2} \left( \frac{R+z}{R} \right) (z^3, z^4, z^6) dz \\ (D_{11}, D'_{11}) &= \sum_{i=1}^n \int_{h_{i-1}}^{h_i} Q_{11i} \left( 1 - \frac{4z^2}{3h^2} \right) \left( \frac{R+z}{R} \right) (z^2, z^4) dz \\ (A_{55}, A'_{55}) &= \sum_{i=1}^n \int_{h_{i-1}}^{h_i} Q_{55i} \left( 1 - \frac{4z^2}{3h^2} \right) \left( \frac{R+z}{R} \right) (1, z^2) dz \end{aligned} \quad (29)$$

$$\begin{aligned} (N_{xx}^T, M_{xx}^T) &= \sum_{i=1}^n \int_{h_{i-1}}^{h_i} \beta_{xi} T_i \left( \frac{R+z}{R} \right) (1, z) dz \\ N_{\theta\theta}^T &= \sum_{i=1}^n \int_{h_{i-1}}^{h_i} \beta_{\theta i} T_i dz \\ P_{xx}^T &= \sum_{i=1}^n \int_{h_{i-1}}^{h_i} \beta_{xi} T_i \left( \frac{R+z}{R} \right) z^3 dz \end{aligned} \quad (30)$$

In (29) and (30),  $h_i$  is

$$h_i = a + \sum_{p=1}^i t_p - R \quad (31)$$

In (15)–(31),  $\sigma_{kli}$  is the stress component,  $\varepsilon_{kli}$  is the normal strain component,  $\gamma_{xzi}$  is the shear strain,  $\alpha_{ki}$  is the coefficient of linear thermal expansion,  $Q_{kli}$  is the elastic stiffness constant, and  $t_i$  is the thickness of the  $i$ th layer, respectively.

From (24) and the first expression of (27), the following equation is obtained

$$N_{xx} = 0 \quad (32)$$

Substitution of (28) into (32), (25), and (26) leads to the result

$$A_{11} \frac{du_o}{dx} + B_{11} \frac{d\phi_x}{dx} - C_{11} \frac{d^2w}{dx^2} + A_{12} \frac{w}{R} = N_{xx}^T \quad (33)$$

$$\begin{aligned} & \left( B'_{11} - \frac{4}{3h^2} B''_{11} \right) \frac{d^2u_0}{dx^2} + \left( D_{11} - \frac{4}{3h^2} D'_{11} \right) \frac{d^2\phi_x}{dx^2} \\ & - \left( C'_{11} - \frac{4}{3h^2} C''_{11} \right) \frac{d^3w}{dx^3} \\ & + \left( \frac{B'_{12}}{R} - \frac{4B''_{12}}{3Rh^2} - A_{55} + \frac{4}{h^2} A'_{55} \right) \frac{dw}{dx} \\ & - \left( A_{55} - \frac{4}{h^2} A'_{55} \right) \phi_x = \frac{dM_{xx}^T}{dx} - \frac{4}{3h^2} \frac{dP_{xx}^T}{dx} \end{aligned} \quad (34)$$

$$\begin{aligned} & \frac{A_{12}}{R} \frac{du_0}{dx} + \left( \frac{B_{12}}{R} - A_{55} + \frac{4}{h^2} A'_{55} \right) \frac{d\phi_x}{dx} \\ & - \left( \frac{C_{12}}{R} + \frac{4B''_{12}}{3Rh^2} + A_{55} - \frac{4}{h^2} A'_{55} \right) \frac{d^2w}{dx^2} + \frac{A_{22}}{R^2} w \\ & - \frac{4}{3h^2} \left( B'_{11} \frac{d^3u_0}{dx^3} + D'_{11} \frac{d^3\phi_x}{dx^3} - C'_{11} \frac{d^4w}{dx^4} \right) \\ & = \frac{N_{\theta\theta}^T}{R} - \frac{4}{3h^2} \frac{d^2P_{xx}^T}{dx^2} \end{aligned} \quad (35)$$

We assume the solutions of the displacement components and rotation in order to satisfy (27) in the following forms:

$$\begin{aligned} u_0 &= \sum_{k=1}^{\infty} U_k \cos q_k x \\ \phi_x &= \sum_{k=1}^{\infty} \Phi_k \cos q_k x \\ w &= \sum_{k=1}^{\infty} W_k \sin q_k x \end{aligned} \quad (36)$$

Substituting (7) and (8) into (30), we obtain  $N_{xx}^T$ ,  $N_{\theta\theta}^T$ ,  $M_{xx}^T$ , and  $P_{xx}^T$ :

$$\begin{aligned} & (N_{xx}^T, N_{\theta\theta}^T, M_{xx}^T, P_{xx}^T) \\ &= \sum_{k=1}^{\infty} (N_{xxk}^T, N_{\theta\theta k}^T, M_{xxk}^T, P_{xxk}^T) \sin q_k x \end{aligned} \quad (37)$$

For the sake of brevity, expressions for the constants  $N_{xxk}^T$ ,  $N_{\theta\theta k}^T$ ,  $M_{xxk}^T$ , and  $P_{xxk}^T$  in (37) are omitted here. Substituting (36) and (37) into (33)–(35), we obtain

$$-A_{11} q_k U_k - B_{11} q_k \Phi_k + \left( C_{11} q_k^2 + \frac{A_{12}}{R} \right) W_k = N_{xxk}^T \quad (38)$$

$$\begin{aligned} & - \left( B'_{11} - \frac{4B''_{11}}{3h^2} \right) q_k^2 U_k \\ & - \left[ \left( D_{11} - \frac{4D'_{11}}{3h^2} \right) q_k^2 + A_{55} - \frac{4A'_{55}}{h^2} \right] \Phi_k \\ & + \left[ \left( C'_{11} - \frac{4C''_{11}}{3h^2} \right) q_k^2 + \frac{B'_{12}}{R} - \frac{4B''_{12}}{3Rh^2} - A_{55} + \frac{4A'_{55}}{h^2} \right] q_k W_k \\ & = q_k \left( M_{xxk}^T - \frac{4P_{xxk}^T}{3h^2} \right) \end{aligned} \quad (39)$$

$$\begin{aligned} & - \left( \frac{A_{12}}{R} + \frac{4B''_{11}}{3h^2} q_k^2 \right) q_k U_k \\ & - \left( \frac{B_{12}}{R} - A_{55} + \frac{4A'_{55}}{h^2} + \frac{4D'_{11}}{3h^2} q_k^2 \right) q_k \Phi_k \\ & + \left[ \left( \frac{C_{12}}{R} + \frac{4B''_{12}}{3Rh^2} + A_{55} - \frac{4A'_{55}}{h^2} \right) q_k^2 \right. \\ & \left. + \frac{A_{22}}{R^2} + \frac{4C''_{11}}{3h^2} q_k^4 \right] W_k = \frac{N_{\theta\theta k}^T}{R} + \frac{4P_{xxk}^T}{3h^2} q_k^2 \end{aligned} \quad (40)$$

From (38)–(40), the constants  $U_k$ ,  $\Phi_k$ , and  $W_k$  can be obtained. The stress components can be evaluated by substituting (36) into (15) and (18), and then into (19).

### First-Order Shear Deformation Theory (FSDT)

The displacement field is given by

$$\begin{aligned} u_i &= u_0 + z\phi_x \\ w_i &= w \end{aligned} \quad (41)$$

The displacement–strain relations are expressed in (18). The stress–strain relations are expressed as follows:

$$\begin{aligned} \sigma_{xxi} &= Q_{11i} \varepsilon_{xxi} + Q_{12i} \varepsilon_{\theta\theta i} - \beta_{xi} T_i \\ \sigma_{\theta\theta i} &= Q_{12i} \varepsilon_{xxi} + Q_{22i} \varepsilon_{\theta\theta i} - \beta_{\theta i} T_i \\ \sigma_{xzi} &= k Q_{55i} \gamma_{xzi} \end{aligned} \quad (42)$$



where  $k$  is the shear correction coefficient. The equilibrium equations in dimensionless form are given by

$$\frac{dN_{xx}}{dx} = 0 \quad (43)$$

$$\frac{dM_{xx}}{dx} - Q_x = 0 \quad (44)$$

$$\frac{N_{\theta\theta}}{R} - \frac{dQ_x}{dx} = 0 \quad (45)$$

We now consider the case of a simply supported cylindrical shell given by the following relations:

$$x = 0, L; \quad N_{xx} = 0, \quad M_{xx} = 0, \quad w = 0 \quad (46)$$

The resultant forces and resultant moments are

$$\begin{aligned} N_{xx} &= A_{11} \frac{du_o}{dx} + B_{11} \frac{d\phi_x}{dx} + A_{12} \frac{w}{R} - N_{xx}^T \\ N_{\theta\theta} &= A_{12} \frac{du_o}{dx} + B_{12} \frac{d\phi_x}{dx} + A_{22} \frac{w}{R} - N_{\theta\theta}^T \\ M_{xx} &= B_{11} \frac{du_o}{dx} + D_{11} \frac{d\phi_x}{dx} + B_{12} \frac{w}{R} - M_{xx}^T \end{aligned} \quad (47)$$

From (43) and the first expression of (46), the following equation is obtained:

$$N_{xx} = 0 \quad (48)$$

Substitution of (47) into (48), (44), and (45) leads to the result

$$A_{11} \frac{du_o}{dx} + B_{11} \frac{d\phi_x}{dx} + A_{12} \frac{w}{R} = N_{xx}^T \quad (49)$$

$$\begin{aligned} B_{11} \frac{d^2 u_o}{dx^2} + D_{11} \frac{d^2 \phi_x}{dx^2} - A_{55} \phi_x \\ + \left( \frac{B_{12}}{R} - A_{55} \right) \frac{dw}{dx} = \frac{dM_{xx}^T}{dx} \end{aligned} \quad (50)$$

$$\begin{aligned} \frac{A_{12}}{R} \frac{du_o}{dx} + \left( \frac{B_{12}}{R} - A_{55} \right) \frac{d\phi_x}{dx} \\ - A_{55} \frac{d^2 w}{dx^2} + \frac{A_{22}}{R^2} w = \frac{N_{\theta\theta}^T}{R} \end{aligned} \quad (51)$$

In order to satisfy (46), we assume the solutions of the displacement components and rotation as (36). Substituting (36) and (37) into (49)–(51), we obtain

$$-A_{11} q_k U_k - B_{11} q_k \Phi_k + \frac{A_{12}}{R} W_k = N_{xxk}^T \quad (52)$$

$$\begin{aligned} -B_{11} q_k^2 U_k - (D_{11} q_k^2 + A_{55}) \Phi_k \\ + \left( \frac{B_{12}}{R} - A_{55} \right) q_k W_k = q_k M_{xxk}^T \end{aligned} \quad (53)$$

$$\begin{aligned} -\frac{A_{12}}{R} q_k U_k - \left( \frac{B_{12}}{R} - A_{55} \right) q_k \Phi_k \\ + \left( A_{55} q_k^2 + \frac{A_{22}}{R^2} \right) W_k = \frac{N_{\theta\theta k}^T}{R} \end{aligned} \quad (54)$$

From (52)–(54), the constants  $U_k$ ,  $\Phi_k$ , and  $W_k$  can be obtained. The stress components can be evaluated by substituting (36) into (41) and (18), and then into (42).

### Classical Shell Theory (CST)

The displacement field is given by

$$u_i = u_0 - z \frac{\partial w}{\partial x}, \quad w_i = w \quad (55)$$

The displacement–strain relations are expressed as follows:

$$\varepsilon_{xxi} = \frac{du_i}{dx}, \quad \varepsilon_{\theta\theta i} = \frac{w}{R} \quad (56)$$

The stress–strain relations are expressed as follows:

$$\begin{aligned} \sigma_{xxi} &= Q_{11i} \varepsilon_{xxi} + Q_{12i} \varepsilon_{\theta\theta i} - \beta_{xi} T_i \\ \sigma_{\theta\theta i} &= Q_{12i} \varepsilon_{xxi} + Q_{22i} \varepsilon_{\theta\theta i} - \beta_{\theta i} T_i \end{aligned} \quad (57)$$

The equilibrium equations are given by

$$\frac{dN_{xx}}{dx} = 0 \quad (58)$$

$$\frac{d^2 M_{xx}}{dx^2} - \frac{N_{\theta\theta}}{R} = 0 \quad (59)$$

We now consider the case of a simply supported cylindrical shell given by (46). The resultant forces and moments are

$$\begin{aligned} N_{xx} &= A_{11}^c \frac{du_o}{dx} - B_{11}^c \frac{d^2 w}{dx^2} + A_{12} \frac{w}{R} - N_{xx}^{cT} \\ N_{\theta\theta} &= A_{12} \frac{du_o}{dx} - B_{12}^c \frac{d^2 w}{dx^2} + A_{22}^c \frac{w}{R} - N_{\theta\theta}^T \quad (60) \\ M_{xx} &= B_{11}^c \frac{du_o}{dx} - D_{11}^c \frac{d^2 w}{dx^2} + B_{12}^c \frac{w}{R} - M_{xx}^{cT} \end{aligned}$$

where

$$\begin{aligned} (A_{11}^c, B_{11}^c, D_{11}^c) &= \sum_{i=1}^n \int_{h_{i-1}}^{h_i} Q_{11i}(1, z, z^2) dz \\ B_{12}^c &= \sum_{i=1}^n \int_{h_{i-1}}^{h_i} Q_{12i} z dz \quad (61) \\ A_{22}^c &= \sum_{i=1}^n \int_{h_{i-1}}^{h_i} Q_{22i} dz \\ (N_{xx}^{cT}, M_{xx}^{cT}) &= \sum_{i=1}^n \int_{h_{i-1}}^{h_i} \beta_{xi} T_i(1, z) dz \end{aligned}$$

From (58) and the first expression of (46), the following equation is given

$$N_{xx} = 0 \quad (62)$$

Substitution of (60) into (62) and (59) leads to the result

$$\begin{aligned} A_{11}^c \frac{du_o}{dx} - B_{11}^c \frac{d^2 w}{dx^2} + A_{12} \frac{w}{R} &= N_{xx}^{cT} \quad (63) \\ B_{11}^c \frac{d^3 u_o}{dx^3} - \frac{A_{12}}{R} \frac{du_o}{dx} - D_{11}^c \frac{d^4 w}{dx^4} \\ &+ \frac{2B_{12}^c}{R} \frac{d^2 w}{dx^2} - \frac{A_{22}^c}{R^2} w = \frac{d^2 M_{xx}^{cT}}{dx^2} - \frac{N_{\theta\theta}^T}{R} \quad (64) \end{aligned}$$

We assume the solutions of the displacement components in order to satisfy (46) in the following forms:

$$\begin{aligned} u_o &= \sum_{k=1}^{\infty} U_k \cos q_k x \\ w &= \sum_{k=1}^{\infty} W_k \sin q_k x \end{aligned} \quad (65)$$

Substituting (65) and (37) into (63) and (64), the constants  $U_k$  and  $W_k$  can be obtained as follows:

$$\begin{aligned} U_k &= \frac{1}{A_{11}^c q_k} \left[ \left( B_{11}^c q_k^2 + \frac{A_{12}}{R} \right) W_k - N_{xx}^{cT} \right] \\ W_k &= \left[ \left( B_{11}^c q_k^2 + \frac{A_{12}}{R} \right) N_{xx}^{cT} - \frac{A_{11}^c}{R} N_{\theta\theta}^T - A_{11}^c q_k^2 M_{xx}^{cT} \right] / \\ &\quad \left[ (B_{11}^{c2} - A_{11}^c D_{11}^c) q_k^4 - \frac{2}{R} (A_{11}^c B_{12}^c - A_{12} B_{11}^c) q_k^2 \right. \\ &\quad \left. + \frac{1}{R^2} (A_{12}^2 - A_{11}^c A_{22}^c) \right] \quad (66) \end{aligned}$$

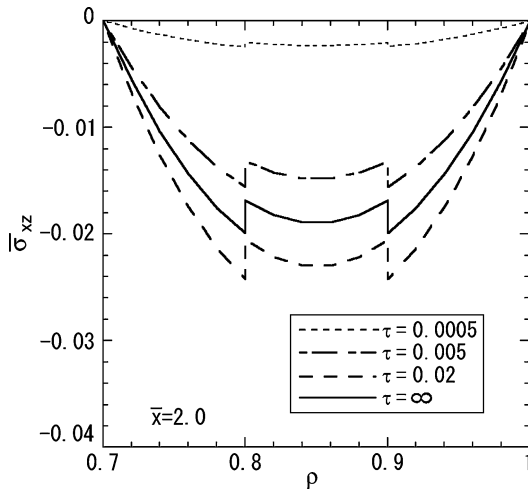
The stress components can be evaluated by substituting (65) into (55) and (56), and then into (57).

## Numerical Results

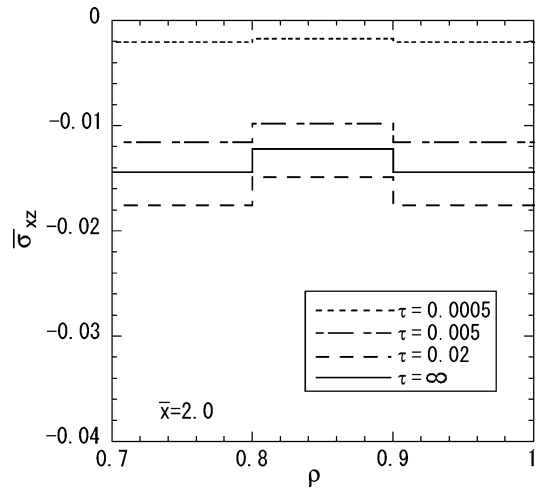
To illustrate the foregoing analysis, we consider the cross-ply laminated cylindrical shell composed of alumina fiber-reinforced aluminum composite, with the following properties [1]:

$$\begin{aligned} \kappa_L &= 41.1 \times 10^{-6} \text{ m}^2/\text{s}, \quad \kappa_T = 29.5 \times 10^{-6} \text{ m}^2/\text{s} \\ \alpha_L &= 7.6 \times 10^{-6} \text{ 1/K}, \quad \alpha_T = 14.0 \times 10^{-6} \text{ 1/K} \\ \lambda_L &= 105 \text{ W/mK}, \quad \lambda_T = 75 \text{ W/mK} \\ E_L &= 150 \text{ GPa}, \quad E_T = 110 \text{ GPa} \\ G_{LT} &= 35 \text{ GPa}, \quad G_{TT} = 41 \text{ GPa} \\ \nu_{LT} &= 0.33, \quad \nu_{TT} = 0.33, \quad \nu_{TL} = 0.242 \end{aligned} \quad (67)$$

where  $G$  and  $\nu$  are the shear modulus of elasticity and Poisson's ratio, respectively. We assume that each layer of cross-ply laminated cylindrical shell consists of the same orthotropic material. The numerical parameters of heat conduction and shape are as follows:



**Effect of Shear Stresses in Thermal Cylindrical Shells, Fig. 1** Variation of thermal stress  $\bar{\sigma}_{xz}$  ( $\bar{x}=2$ , TSDT)



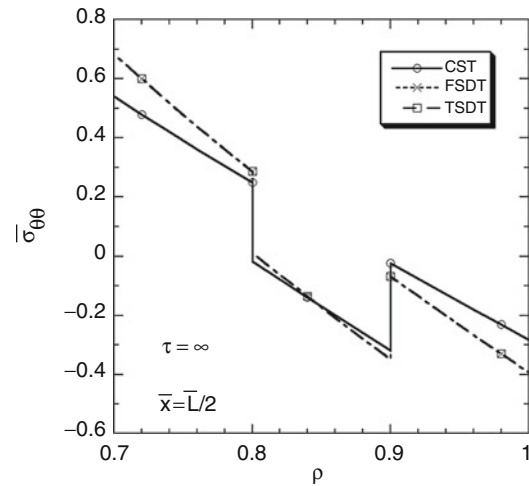
**Effect of Shear Stresses in Thermal Cylindrical Shells, Fig. 2** Variation of thermal stress  $\bar{\sigma}_{xz}$  ( $\bar{x}=2$ , FSDT)

$$h_a b = 10, \quad h_b b = 10, \quad a/b = 0.7, \quad L/b = 6.0$$

$$f_a(\theta) = f_b(\theta) = \left(1 - \frac{\bar{x}^2}{\bar{x}_0^2}\right) H(\bar{x}_0 - |\bar{x}'|)$$

$$\bar{x}' = x/b - \frac{L/b}{2}, \quad \bar{x}_0 = 1, \quad \frac{T_a}{T_0} = 0, \quad \frac{T_b}{T_0} = 1 \quad (68)$$

where  $H(x)$  is Heaviside's function. The cross-ply laminated cylindrical shell is partially heated from the outer surface. Figures 1 and 2 are the variations of shear stress  $\bar{\sigma}_{xz} = \sigma_{xz}/(\alpha_0 T_0 E_0)$  in the radial direction on the cross section ( $\bar{x} = x/b = 2$ ). The numerical results of the third-order shear deformation theory and the first-order shear deformation theory are shown in Figs. 1 and 2, respectively. In order to compare the numerical results obtained by the three different theories, Fig. 3 shows the variation of normal stress  $\bar{\sigma}_{\theta\theta} = \sigma_{\theta\theta}/(\alpha_0 T_0 E_0)$  in the radial direction on the cross section ( $x = L/2$ ) in the steady state. Figure 3 shows that the numerical results calculated by the shear deformation theories are larger than those found by the classical theory. In Figs. 2 and 3, the shear correction coefficient is taken to be  $5/6$ . In Figs. 1 and 2, the dimensionless values  $\tau = \kappa_0 t/b^2$  and  $\rho = r/b$  are introduced.



**Effect of Shear Stresses in Thermal Cylindrical Shells, Fig. 3** Variation of thermal stress  $\bar{\sigma}_{\theta\theta}$  ( $x = L/2$ ,  $\tau = \infty$ )

The typical values of material properties, such as  $\kappa_0$ ,  $\alpha_0$ , and  $E_0$ , used to normalize the numerical data are based on those of the fiber orientation.

## References

- Ootao Y, Tanigawa Y, Miyatake K (2010) Transient thermal stresses of a cross-ply laminated cylindrical shell using a higher-order shear deformation theory. *J Therm Stresses* 33: 55–74

## Effect of Thermal Stresses on Crack-Tip Toughness of Polycrystalline Ceramics

Serkan Nohut

Faculty of Engineering, Zirve University,  
Gaziantep, Turkey

### Synonyms

Alumina; Distinct element method; Internal residual stresses; Polycrystalline ceramics; Sintering

### Overview

Anisotropic thermal expansion coefficient of alumina grains is the main reason of occurrence of internal residual stresses during sintering in polycrystalline alumina ceramics. Investigation of the effect of internal residual stresses on the crack-tip toughness of alumina polycrystalline ceramics presents a matter of this entry. Crack-tip toughness has a significant role in the mechanical performance of alumina structures because it affects the stress value at which the crack starts to propagate, and it also determines the strength of alumina in the case of existence of small cracks. The relationship between the grain size, internal residual stresses, and the crack-tip toughness of polycrystalline ceramics (alumina) is the main subject of this entry. Application of the distinct element method (DEM) is discussed for the numerical prediction of effect of residual stresses on crack-tip toughness.

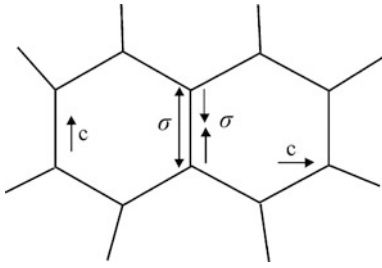
### Introduction

Polycrystalline ceramic materials generally exhibit both internal (bulk) and surface residual stresses [1, 2]. Internal residual stresses, which arise during sintering, occur primarily due to the inhomogeneous temperature distribution within the sample and the anisotropic thermal expansion

coefficient caused by randomly oriented crystals. Surface treatment such as mechanical grinding and polishing introduces residual stresses on the surface of the ceramics due to differential permanent deformation between the damaged and undamaged regions [3]. Such residual stresses affect the mechanical performance (e.g., strength, fracture toughness) of ceramic materials. Thereof, it is important to measure the residual stresses and to investigate the effect of these stresses on mechanical properties of ceramics. In this entry, the effect of internal residual stresses on the crack-tip toughness of alumina ceramics is discussed.

Surface residual stresses occur due to abrasive machining of the ceramic structures. During abrasive grinding, materials together with the flaws in the surface region are removed, while residual stresses are introduced into the newly formed surface region. The presence of a surface residual stress is normally thought to be a result of local plastic deformation. In polycrystalline alumina, diffusion-driven grain boundary sliding is possibly an important deformation mechanism [4]. The magnitude of surface residual stresses can be measured by using X-ray topography technique, photoelastic technique, indentation technique, X-ray diffraction technique, bending technique, and confocal Cr<sup>3+</sup> fluorescence microscopy [5].

Thermal stresses result from thermal expansion incompatibility in materials during the temperature change. Main reasons of thermal stresses are thermomechanical mismatch between two materials, nonuniform temperature distribution in a material, phase transformation and thermal expansion anisotropy in a single phase material. The first one appears due to thermal expansion mismatch between dissimilar materials (e.g., composites, multiphase structures, and layered composite structures). The second one occurs due to nonuniform heating/cooling of surface and interior part of the material. Thermal stresses due to phase transformation occur, for example, in pure zirconia or stabilized zirconia, and it results from volume changes during cooling due to cubic-to-tetragonal-to-monoclinic phase transformation. The main motivation of this entry is



**Effect of Thermal Stresses on Crack-Tip Toughness of Polycrystalline Ceramics, Fig. 1** Two-dimensional representation of tetragonal or hexagonal crystal structure

about the last type of thermal stress occurrence. The last one exists in single phase polycrystalline materials at the microscopic level where localized thermal stresses arise from thermal expansion mismatch among randomly oriented grains. Thermal stresses due to thermal anisotropy arise because of different thermal expansion coefficients in the radial and tangential directions in a cylindrical geometry during temperature change. For a material with crystal symmetry lower than cubic, the thermal expansion coefficient,  $\alpha$ , can differ along different crystal directions. For example, in Fig. 1, the two-dimensional representation of a tetragonal or hexagonal crystal structure is shown. Grains are randomly distributed, and they have random directions (i.e., random  $c$ -direction). In such a case, during cooling, stresses develop at grain boundaries. In brittle materials, some part of these stresses causes microcracks within or between individual grains, and the rest stay in the material as residual stresses (tension or compression stresses).

In polycrystalline alumina, which is a non-cubic and non-transforming material, internal residual stresses occur during sintering due to the thermal expansion anisotropy of constituent alumina crystals. These residual stresses are reported to be the main reason of the dependence of crack-tip toughness ( $K_{I0}$ ) on average grain size. In alumina, the average grain shape is hexagonal. The thermal expansion coefficient in the vertical direction ( $c$ -direction) of hexagonal grain is different from the horizontal direction ( $a$ -direction) of the grain [6]. This results in a different shrinkage rate in different directions

of grains. This difference causes some thermal stresses (so-called internal residual stresses) after shrinkage in alumina. In solid state sintering of ceramics, shrinkage is driven by the surface energy of the porous compacts. The grain boundary diffusion and volume diffusion are the main material transfer mechanisms which lead to shrinkage of compacts [7]. Often densification in alumina is attributed to a control by grain boundary diffusion where the dominant path for diffusion is usually along the grain boundary [8]. In this mechanism, it is assumed that the energy provided is available to drive the diffusional flux along the grain boundaries. However, Burton [9] stated that some energy is expended for materials to be added to (or removed from) a grain boundary when an interface reaction occurs. He and Ma [10] investigated the effect of grain size on the dominant densification mechanism by using alumina powders with average grain size of 0.9 and 7.0  $\mu\text{m}$ . They concluded that for small grain sizes, the interface reaction becomes the controlling process for sintering, and therefore, the transport path becomes shorter. As the grain size increases, the distance that materials have to travel along grain boundary increases, and the grain boundary diffusion becomes more important. Therefore, since the alumina with small grain size can have more time for the stress relaxation down to lower temperatures, when cooled from a stress-free processing temperature, smaller residual stresses are expected as compared to an alumina with larger grain size [11]. The effect of heating rates on densification rates can be determined by using the kinetic field diagrams. The kinetic field diagram is unique for a special type of green body. Therefore, when the grain size is changed, the kinetic field diagram has to be rebuilt. In general, the sintering rate (densification rate) increases with decreased particle size and with increased sintering temperature and time. Furthermore, the grain growth increases with decreasing grain size [12]. Saha et al. [13] suggested low heating rate for low anisotropy which means lower residual stresses considering the coefficient of thermal expansion anisotropy. More details about the thermodynamical background of the densification of dense powder compacts, coarsening of

grains and pores during the densification, are given by Lange [14].

As it is mentioned above, there is a strong relationship between the average grain size, internal residual stresses which occur due to anisotropic thermal expansion coefficient of alumina grains in different directions and the crack-tip toughness of polycrystalline alumina ceramics. Recently, there has been increasing attention given to crack-tip toughness (critical stress intensity factor) which determines the initiation of crack propagation and the strength of the ceramics in case of existence of small cracks. In the following, this relationship is described, and the effect of internal residual stresses on the crack-tip toughness of alumina is discussed according to experimental measurements. Afterward, a numerical model prepared by distinct element method (DEM) will be used in order to show the variation of crack-tip toughness with internal residual stresses.

## Failure of Advanced Ceramics

At low and ambient temperatures, failure of ceramics is always brittle and occurs without any significant plastic deformations. Brittle fracture occurs due to unavoidable presence of flaws that results either during cooling from the melt (volume cracks) or machining process of ceramic materials (surface cracks). These preexisting cracks cause a local stress concentration at the crack-tip which is several times higher than the applied stress, and the crack grows when the stress at crack-tip is equal to the theoretical strength. Size, position, and orientation of these cracks show variation from specimen to specimen. This variation causes a scattering of strength of ceramic materials. Therefore, strength is not a definite value for ceramics. Instead, stress intensity factor is used for the analysis of fracture of ceramic materials [15].

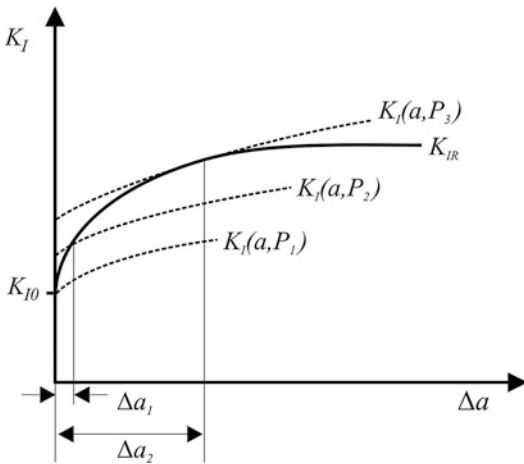
The stress intensity factor is commonly used as a measure of the driving force for crack propagation and is used in fracture mechanics to predict the stress state near the tip of a crack caused by a remote load or residual stresses. It is

a theoretical construct usually applied to a homogeneous, linear elastic material and is useful for providing a failure criterion for brittle materials. The stress intensity factor,  $K$ , is a function of loading, crack size, and structural geometry. The stress intensity factor is calculated by the following equation:

$$K_I = \sigma_A Y \sqrt{a} \quad (1)$$

where  $K_I$  is the stress intensity factor,  $a$  is the crack length,  $\sigma_A$  is the applied stress, and  $Y$  is the geometric function characterizing the influence of the body, crack size and shape, and type of loading. A Roman numeral subscript (I) indicates the mode-I fracture. Mode-I fracture is the condition in which the crack plane is normal to the direction of largest tensile loading. This is the most commonly encountered mode, and therefore, for the remainder of the material, we will consider  $K_I$ . In linear elastic fracture mechanics, the stress intensity factor increases with increasing the applied load until a critical value of  $K_I$  is reached, at which the crack is still in equilibrium and above which unstable crack propagation takes place. This critical value is called fracture toughness and termed  $K_{IC}$ . The unstable crack propagation occurs when  $K_I = K_{IC}$ . Fracture toughness is an indication of the amount of stress required to propagate a preexisting flaw. In the theory of fracture discussed until now, it was assumed that the unstable crack propagation occurs when the condition  $K_I = K_{IC}$  is satisfied. In many ceramics, a different behavior can be observed that the crack growth resistance increases with increasing crack extension due to so-called toughening mechanisms (e.g., crack bridging and phase transformation or microcracking zone) [16]. In other words, stable crack propagation occurs preceding the unstable failure.

The crack propagation behavior is no more characterized by a single value  $K_{IC}$  but with  $K_{IR}$  which increases from  $K_{I0}$  which is the onset value of crack growth (crack-tip toughness). In Fig. 2, an idealized R-curve behavior is represented. This figure also shows a series of stress intensity factor curves (shown with dashed lines) for



**Effect of Thermal Stresses on Crack-Tip Toughness of Polycrystalline Ceramics, Fig. 2**  $K_{IR}$  versus  $\Delta a$  curve for a material with a rising crack resistance

several levels of applied load ( $P_1 < P_2 < P_3$ ) which result in a stable crack growth of  $\Delta a_1$  and  $\Delta a_2$ .

Crack-tip toughness is an important parameter because it determines the crack propagation, and it is the strength of the ceramic materials which contains small cracks.

### Relationship Between Average Grain Size, Internal Residual Stresses, and Crack-Tip Toughness

There is a strong relationship between grain size, residual stresses, and the crack-tip toughness of alumina. An increase in residual stresses causes a decrease of crack-tip toughness. Increase of residual stresses is a result of increase of average grain size of alumina. This relationship is explained and discussed in this part regarding the experimental measurements.

Seidel and Rödel [17] measured  $K_{I0}$  of alumina as a function of average grain size by using crack profile measurements with scanning electron microscopy (SEM). Njiwa et al. [18] used crack opening displacement (COD) and strain gauge methods and observed a decreasing trend of  $K_{I0}$  with increasing average grain size. It was reported that an increase in the residual stresses

may increase the damage at the crack-tip stress field of a growing macrocrack in the form of a microcrack zone, deteriorate the local fracture resistance at the crack-tip, and lead to a decrease of  $K_{I0}$  with an increase in grain size [18].

In Fig. 3, the experimentally measured results are represented. The data points are approximated by a best line. Since strain gauge method overmeasures the  $K_{I0}$  due to poor quality of the amplifier, COD measurements are used as reference.

The relationship between the grain size, flaw size, and residual stresses was introduced by an expression for the first time by Krstic [19]. Krstic [19] reported that at small grain sizes (below approximately several microns), the residual stress plays a minor role in determining the strength level in the material. As the grain size increases, above approximately 10  $\mu\text{m}$ , the effect of residual stress becomes more important, and at very large sizes ( $>100 \mu\text{m}$ ), it dominates the fracture of the brittle materials.

Krell and Grigoryev [20] used X-ray diffraction data and computed a mean residual stress in  $c$ -direction of  $\langle \sigma_{\text{res},c} \rangle = 40\text{--}70 \text{ MPa}$  for an average grain size of 3  $\mu\text{m}$  and a level of  $\langle \sigma_{\text{res},c} \rangle = 20\text{--}30 \text{ MPa}$  for grain sizes below 1  $\mu\text{m}$ . Krell et al. [21] reported that the residual stresses take value of  $\langle \sigma_{\text{res},c} \rangle = 30\text{--}100 \text{ MPa}$  for grain sizes of 1–9  $\mu\text{m}$  and  $\langle \sigma_{\text{res},c} \rangle = 20\text{--}30 \text{ MPa}$  for grain sizes smaller than 1  $\mu\text{m}$ . By applying the technique of piezospectroscopy using the fluorescence from trace  $\text{Cr}^{3+}$  impurities, the residual stresses change  $\langle \sigma_{\text{res},c} \rangle = 130\text{--}270 \text{ MPa}$  for a grain size regime of 2–20  $\mu\text{m}$  [22].

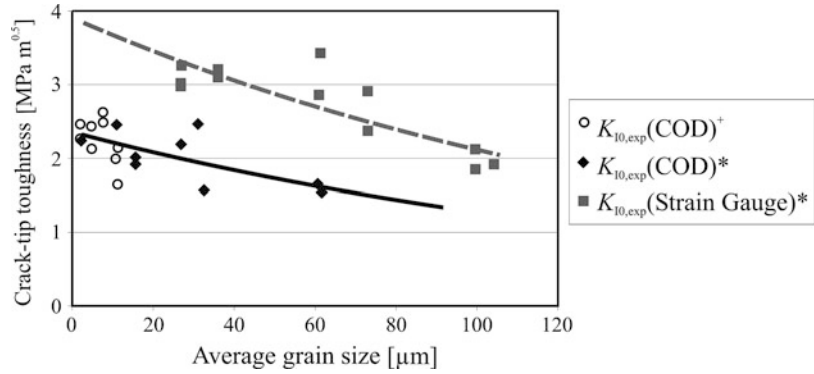
Figure 4 represents the residual stress measurements of Ma and Clarke [22] as a function of average grain size. The error bars in the graph show the maximum and minimum values. By using the experimental values, the residual stresses as a function of average grain size can be predicted with the help of Evans–Clarke model [11] as follows:

$$\frac{\langle \sigma \rangle (1 - \nu)}{\beta E \Delta \alpha} \cong \frac{Q/k}{\ln [12 \Omega D_0 \delta_b E / \sqrt{3} n k a^3 \dot{T}]} - T \quad (2)$$



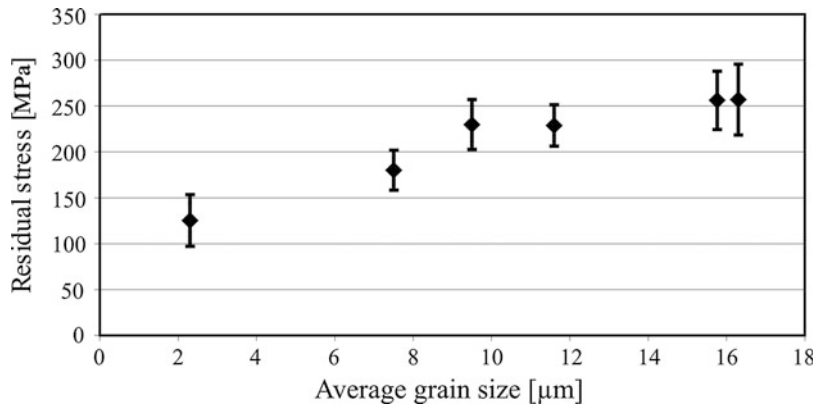
### Effect of Thermal Stresses on Crack-Tip Toughness of Polycrystalline Ceramics,

**Fig. 3** Experimentally measured dependence of crack-tip toughness on average grain size according to Seidel and Rödel<sup>+</sup> [17] and Njiwa et al. \* [18] (Reproduced with permission from [23])



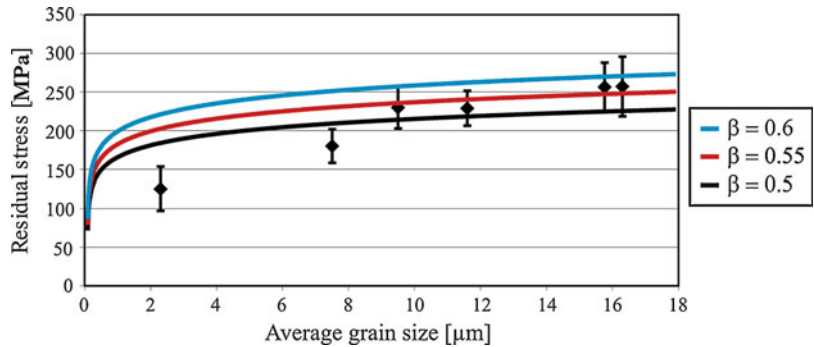
### Effect of Thermal Stresses on Crack-Tip Toughness of Polycrystalline Ceramics,

**Fig. 4** Measured residual stresses of alumina in *c*-direction as a function of grain size [22] (Reproduced with permission from [23])



### Effect of Thermal Stresses on Crack-Tip Toughness of Polycrystalline Ceramics,

**Fig. 5** Fitting of Evans–Clarke function for alumina with different  $\beta$  values (Reproduced with permission from [23])



where  $\langle \sigma \rangle$  is the average residual stress,  $\nu$  is the Poisson's ratio,  $\Delta\alpha$  is the deviation of the contraction coefficient from average,  $\beta$  is a coefficient that depends on the orientation of the adjacent grains and contains corrections to account for the effective elastic modulus,  $T$  is the temperature,  $\dot{T}$  is the cooling rate,  $Q$  is the activation energy for diffusion,  $k$  is the

Boltzmann constant,  $D_0\delta_b$  is the diffusion parameter,  $\Omega$  is the atomic volume,  $E$  is the elastic modulus, and  $a$  is the grain size. For  $\text{Al}_2\text{O}_3$ , with  $D_0\delta_b = 10^9 \text{ m}^3 \text{ s}^{-1}$ ,  $Q = 100 \text{ kcal/mole}$ ,  $\Omega = 10^{29} \text{ m}^3$ ,  $n = 30$ ,  $E = 420 \text{ GPa}$ ,  $\nu = 0.3$ , and  $\Delta\alpha = 7 \times 10^{-7} \text{ 1/K}$ , average residual stress as a function of grain size is given in Fig. 5 for different fitting parameter  $\beta$ .



For  $\beta$ , the Evans–Clarke function gives the best fitting of experimental measurements for the investigated alumina.

### Numerical DEM Model for the Investigation of Effect of Residual Stresses on Crack-Tip Toughness of Alumina

In this part, distinct element method (DEM) is used in order to simulate the effect of residual stresses (average grain size) on the crack-tip toughness of alumina polycrystalline ceramics [23]. It is a numerical mesh-free method which is used to simulate the motion and response of granular media and heterogeneous materials by modeling the dynamic behavior of assemblies of particles (e.g., circular discs, spheres, and blocks) [24]. In contrast with classical methods like finite element and boundary element methods that treat the medium as a continuum, the distinct element method treats the medium as a discontinuum. The emphasis of distinct element method is therefore in reproducing the mechanics of contacts and impacts between distinct blocks.

PFC<sup>2D</sup> (particle flow code in 2 dimensions) is a discontinuum code used in analysis, testing, and research in any field where the interaction of many discrete objects exhibiting large strain and/or fracturing is required. PFC<sup>2D</sup> particle flow model simulates the mechanical behavior of a system comprised of a collection of circular distinct particles. Circular particles displace independently from one another, and they interact at contacts which occur over a ravishingly small area. The particles are assumed to be rigid, and behavior of the contact is characterized by a soft contact [25]. The behavior of a heterogeneous bulk material can be modeled by the introduction of parallel bonds between the particles which break when the stresses acting on the bonds exceed the bond strength. In the DEM simulations, it is assumed that the heterogeneous materials consist of particles (grains in the material) and the bonds between the particles (grain boundaries in the material). In this way, the properties (e.g., Young's modulus and strength) of the

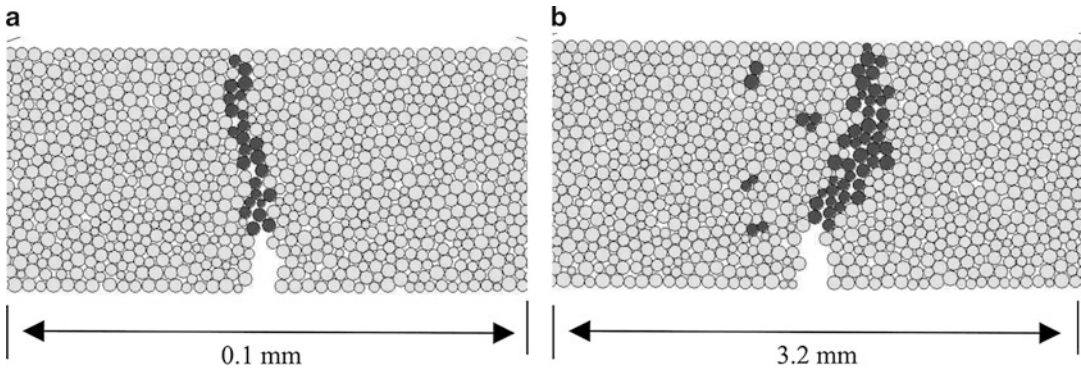
grains (particles) and the grains' boundaries (bonds) can be defined separately.

The single-edge-notched beam (SENB) test is simulated for the calculation of the fracture toughness. For every average grain size of a model material, the corresponding internal residual stress value is computed according to the Evans–Clarke model with  $\beta = 0.55$ . The residual stresses enter into the model as a standard deviation to the normally distributed normal and shear strength of the parallel bonds. As a result, the normal and shear strength of the parallel bonds between the grains in the model are distributed by a Gaussian distribution with a mean value of bond strength and a standard deviation of residual stress. Since tensile residual stress decreases the mean strength and compressive residual stress increases the mean strength, the required stress in order to break a parallel bond will be at some bonds higher and at some bonds lower than the mean strength value.

For each average grain size, seven different packing arrangements were produced since the particle arrangement may affect the behavior of the material. This difference between these seven packing arrangements was achieved during the model generation. The average value of seven simulations will be used as the main result, and the variability of these results will be given as error bars in the following.

In Fig. 6, the pictures of the failed specimens are given for  $G_{\text{avg}} = 2 \mu\text{m}$  and for  $G_{\text{avg}} = 80 \mu\text{m}$ . The residual stress values for  $G_{\text{avg}} = 2 \mu\text{m}$  and for  $G_{\text{avg}} = 80 \mu\text{m}$  are taken as 130 MPa and 430 MPa, respectively. The crack propagates between the particles with dark colors. A small region of the 4-point bending test specimen is given in order to show the crack path. In the longitudinal direction, there exist more particles. In Fig. 6a, the crack propagates almost straightly as a primary crack. In Fig. 6b, it is possible to observe crack redirecting and secondary cracks which are connected to primary crack. Moreover, there are some microcracks, which are not connected to primary crack and appeared in the region under the tension stresses.

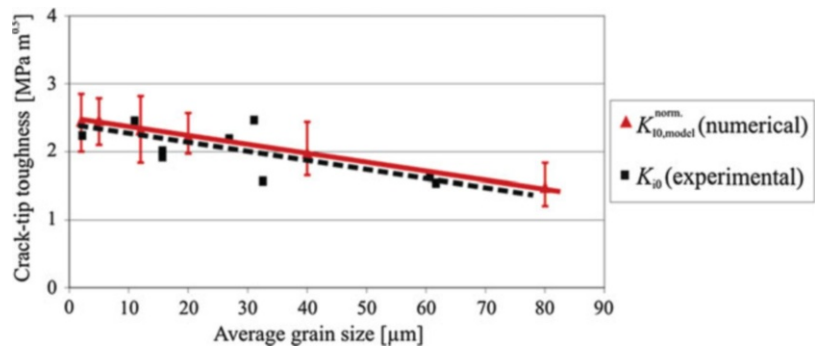
When the experimentally observed dependence of crack-tip toughness measured with



**Effect of Thermal Stresses on Crack-Tip Toughness of Polycrystalline Ceramics, Fig. 6** Representation of crack propagation in the specimens with average grain

size of (a)  $G_{\text{avg}} = 2 \mu\text{m}$  and (b)  $G_{\text{avg}} = 80 \mu\text{m}$  (Reproduced with permission from [23])

**Effect of Thermal Stresses on Crack-Tip Toughness of Polycrystalline Ceramics, Fig. 7** Comparison of the normalized  $K_{I0}$  values with experimentally measured ones (Reproduced with permission from [23])



COD method (see Fig. 3) is compared with the model results, it can be said that the DEM model gives almost the same values and creates the decreasing trend with increasing average grain size (see Fig. 7). Moreover, the experimentally measured values are inside the interval which can be shown using the error bars of the DEM model. This also shows the compatibility of experimental and numerical results.

## Conclusion

In this entry, the effect of thermal stresses, which occur during the sintering process due to the anisotropic thermal expansion coefficient of randomly oriented alumina crystals, on crack-tip toughness of alumina was discussed. An increase of average grain size of alumina results in an increase of internal residual stresses. If the

residual stresses increase, the crack-tip toughness of alumina decreases. As a result, a preexisting crack in an alumina component starts to propagate at a lower stress value. A numerical distinct element model was used for the prediction of crack-tip toughness as a function of grain size.

## References

1. Asokan T, Sudarshan TS (1994) Effect of residual stress on the surface flashover of alumina ceramics. *IEEE T Dielect El In* 1(1):97–105
2. Blendell JE, Coble RL (1982) Measurement of stress due to thermal expansion anisotropy in  $\text{Al}_2\text{O}_3$ . *J Am Ceram Soc* 65:174–178
3. Stokes RJ (1972) Effects of surface finishing on mechanical and other physical properties of ceramics. In: Schneider SJ, Rice RW (eds) *Science of ceramic machining and surface finishing*. National Bureau of standard special publication, Washington, DC, pp 343–352

4. Cannon RM, Rhodes WH, Heuer AH (1980) Plastic deformation of fine-grained alumina ( $\text{Al}_2\text{O}_3$ ): I, inter-face-controlled diffusional creep. *J Am Ceram Soc* 63:46–53
5. Tuan WH, Kuo JC (1999) Contribution of residual stress to the strength of abrasive ground alumina. *J Eur Ceram Soc* 19:1593–1597
6. Rahaman MN (2007) Sintering of ceramics. CRC Press, Boca Raton
7. Raether F, Horn PS (2009) Investigation of sintering mechanisms of alumina using kinetic field and master sintering diagrams. *J Eur Ceram Soc* 29(11): 2225–2234
8. Kingery WD, Bowen HK (1975) Introduction to ceramics. Wiley, New York
9. Burton B (1972) Interface reaction controlled diffusional creep: a consideration of grain boundary dislocation climb sources. *Mater Sci Eng* 10:9–13
10. He Z, Ma J (2005) Constitutive modeling of alumina sintering: grain-size effect on dominant densification mechanism. *Comp Mater Sci* 32(2):196–202
11. Evans AG, Clarke DR (1980) Residual stresses and microcracking induced by thermal contraction inhomogeneity. In: *Thermal Stress in Severe Environments*. Edited by D. P. H. Hasselman and R. A. Haller. Plenum, New York, pp 629–648
12. Kang SL (2005) Sintering: densification, grain growth and microstructure. Elsevier-Butterworth-Heinemann, Burlington
13. Saha BP, Johnson R, Ganesh I, Rao GVN, Bhattacharjee S, Mahajan YR (2001) Thermal anisotropy in sintered cordierite monolith. *Mater Chem Phys* 67:140–145
14. Lange FF (2008) Densification of powder compacts: an unfinished story. *J Eur Ceram Soc* 28(7):1509–1516
15. Munz D, Fett T (2001) Ceramics: mechanical properties, failure behaviour, materials selection. Springer, Berlin/New York
16. Llorca J, Steinbrech RW (1991) Fracture of alumina: an experimental and numerical study. *J Mater Sci* 26:6383–6390
17. Seidel J, Rödel J (1997) Measurement of crack tip toughness in alumina as a function of grain size. *J Am Ceram Soc* 80(2):433–438
18. Nijima ABK, Yousef SG, Fett T, Rödel J (2005) Influence of microcracking on crack-tip toughness of alumina. *Eng Fract Mech* 72(7):1011–1019
19. Krstic VD (2006) Effect of microstructure on fracture of brittle materials: unified approach. *Theor Appl Fract Mech* 45(3):212–226
20. Krell A, Grigoryev N (1990) Residual stresses and microporosity in oxide ceramics. *Sprechsaal* 123:1012–1015
21. Krell A, Terserak A, Schläfer D (1996) Grain size dependent residual microstresses in submicron  $\text{Al}_2\text{O}_3$  and  $\text{ZrO}_2$ . *J Eur Ceram Soc* 16(8):803–811
22. Ma Q, Clarke DR (1994) Piezospectroscopic determination of residual stresses in polycrystalline alumina. *J Am Ceram Soc* 76:1433–1440
23. Nohut S (2011) Prediction of crack-tip toughness of alumina for given residual stresses with parallel-bonded-particle model. *Comp Mater Sci* 50:1509–1519
24. Cundall PA (1971) A computer model for simulating progressive, large scale movements in blocky rock systems. In: *Proceedings of international symposium on rock mechanics*, Nancy II, pp 8
25. Potyondy DO, Cundall CA (2004) A bonded-particle model for rock. *Int J Rock Mech Min Sci* 41(8):1329–1364

### Further Reading

- Anne G, Hecht-Mijic S, Richter H, Vander Biest O, Vleugels J (2006) Strength and residual stresses of functionally graded  $\text{Al}_2\text{O}_3/\text{ZrO}_2$  discs prepared by electrophoretic deposition. *Scr Mater* 54(12):2053–2056
- Buresch FE (1985) Relations between the damage in and microstructure of ceramics. *Mater Sci Eng* 71:187–194
- Nohut S (2009) Reliability of advanced ceramics: macro- and mesoscale investigations. Cuvillier, Göttingen
- Paulik SW, Zimmerman MH, Faber KT (1996) Residual stress in ceramics with large thermal expansion. *J Mater Res* 11(11):2795–2803
- Swain MV, Hannink RHJ (1984) R-curve behavior in zirconia ceramics. In: Claussen N, Rühle M, Heuer AH (eds) *Advance in ceramics*, vol 12, Science and technology of zirconia II. American Ceramic Society, Columbus, pp 225–239
- Wachtman JB (1996) *Mechanical properties of ceramics*. Wiley-Interscience, New York, USA

## Effective Boundary Conditions

► [Generalized Boundary Conditions to Solving Thermal Stress Problems for Bodies with Thin Coatings](#)

## Effective Fracture Toughness in $\text{Al}_2\text{O}_3\text{-Al}_2\text{O}_3/\text{ZrO}_2$ -Laminates

Tanja Lube

Institut für Struktur- und Funktionskeramik,  
Montanuniversität Leoben, Leoben, Austria

### Overview

Ceramic laminates made from layers of different materials are proposed to improve fracture

toughness, strength, and reliability as compared to monolithic ceramics. Due to the strong bonding of materials with different thermal and elastic properties during the sintering, residual stresses arise in such structures. The residual stress state influences the mechanical performance of the entire structure significantly. Using, as an example, laminates made from  $\text{Al}_2\text{O}_3$  and  $\text{Al}_2\text{O}_3/\text{ZrO}_2$ -composites, the principal possibilities to tailor the residual stresses to meet different requirements are investigated by employing a weight function analysis. An optimal architecture (layer thickness ratio) which provides structures with a maximized toughness is introduced. The influence of variations of the material properties on the optimal architecture is studied. Finally, a strategy to exploit the residual stresses to design laminates with both a high toughness and a high strength is devised.

## Introduction

Due to their attractive properties (chemical and thermal stability, low density, high hardness and Young's modulus, specific physical behavior, etc.), modern ceramics are candidate materials for structural and functional applications. Their inherent brittleness and lack of deformation which lead to an unexpected and catastrophic failure limit their value under load-bearing conditions. The increasing of toughness or the creation of a defect tolerant failure mode is thus a principle goal in material development. Inspired by examples found in nature [1] and developed for other material classes (e.g., polymers or glasses [2]), layered ceramic structures have been developed. The involved layers consist of different materials. Such ceramic laminates may be categorized by the quality of the interface between the layers.

For multilayers with weak interfaces (in most cases, these interfaces are entities with a finite thickness, i.e., weak layers), strong ceramic sheets are coated with a material that will form a weak layer after sintering. Ideally, such systems

do not develop residual stresses due to thermal expansion mismatch. The beneficial effect of the weak layers can be exploited for cracks that grow normally to the interfaces of the laminate. During the fracture process, the crack propagates normally to the stress in the strong layer, then kinks into the weak layer where it continues to grow by forming a delamination crack between two adjacent layers of the thicker and stronger ceramic. The so-called graceful failure of these laminates is caused by repeating this cracking throughout the thickness of the laminate. The apparent toughness of the laminate can be increased by a factor of  $\sim 4$ , and the work required to break the sample raises by a factor of over 100, compared to a monolithic bar of the strong layer material [3].

Laminates with strong interfaces are designed to contain residual stresses within the different layers. These stresses arise due to a differential shrinkage during sintering [4], a thermal expansion mismatch, phase transformations [5–8], or a combination of those. Such laminates have been produced in different material systems, comprising systems of  $\text{Al}_2\text{O}_3 + \text{Al}_2\text{O}_3/\text{ZrO}_2$  composites [9–11],  $\text{Si}_3\text{N}_4 + \text{Si}_3\text{N}_4/\text{TiN}$  composites [12, 13],  $\text{Al}_2\text{O}_3/\text{t-ZrO}_2 + \text{Al}_2\text{O}_3/\text{m-ZrO}_2$  composites [14], and  $\text{B}_4\text{C} + \text{B}_4\text{C}/\text{SiC}$  composites [15].

The residual stresses exert substantial influence on the mechanical behavior of such laminates: they can, for instance, increase the fracture stress by shielding cracks from the applied load [16], they can decrease the scatter of strength [17], and they can lead to a threshold strength [18], act as crack stoppers [19], or improve the wear behavior [20, 21].

## Fracture Mechanics of Laminates with Residual Stresses

Failure of ceramics is generally caused by the extension of crack-like defects. It occurs if the stress intensity

$$K_{tip} = K_{appl}(a) = \sigma Y \sqrt{\pi a} \quad (1)$$

at the tip of a crack with length  $a$  under the action of an applied stress  $\sigma$  reaches or exceeds the fracture toughness  $K_c$  [22, 23]:

$$K_{tip} \geq K_c \quad (2)$$

The influence of residual stresses on the stress intensity factor of a crack propagating normally to the interfaces in a laminate can be assessed by considering that – in this case – the stress intensity at the crack tip is built up by two contributions: the stress intensity due to an externally applied load, (1), and the one caused by the residual stress,  $K_{res}$ :

$$K_{tip} = K_{appl}(a) + K_{res}(a) \quad (3)$$

Combining (2) and (3) and solving them with respect to  $K_{appl}(a)$  yields

$$K_{appl}(a) \geq K_c - K_{res}(a) = K_R(a) \quad (4)$$

If compressive residual stresses prevail, then  $K_{res} < 0$ , and thus,  $K_R(a) > K_c$ , i.e.,  $K_R(a)$  is greater than the fracture toughness of the material without the action of residual stresses. The residual stresses shield the crack tip from the applied load. This toughening effect is not caused by microstructural mechanisms acting as the crack extends, like in the case of crack face bridging [24] or transformation toughening [25], but is only caused by the existence of the residual stress. The crack length dependent  $K_R(a)$  is called the apparent R-curve of the laminate.

Knowledge of the apparent R-curve of a laminate provides insight into the mechanical behavior of laminates. The conditions for maximum shielding, the strength for certain crack sizes, the consequences for strength distributions, and the threshold strength can be predicted.

Of course, the apparent R-curve can be measured for any laminate. But in order to optimize the mechanical behavior of laminates, it is certainly favorable to know the R-curve a priori and to investigate how the architecture of a laminate (i.e., the layer thickness, the number of layers, etc.) and

the properties of the individual layers (elastic properties, thermal properties) affect it.

## Calculation of the Apparent R-curve: Weight Function Approach

Generally, the apparent R-curve for a certain laminate can be calculated by different methods. A key problem in all this calculations is the appropriate consideration of the elastic inhomogeneity of a periodic laminate and of the residual stress profile. Calculations on the basis of the configurational forces concept [26] and FE calculations [27] show, however, that the contribution of the elastic mismatch to the apparent R-curve is very small in cases relevant for ceramic laminates. This is the reason why qualitative calculations can be performed successfully using the weight function method.

This method allows to calculate the stress intensity factor for a crack of length  $a$  for an arbitrary stress distribution acting normal to the fracture path [28]. Applying this concept to a laminate layer with a residual stress  $\sigma_{res}$  results in

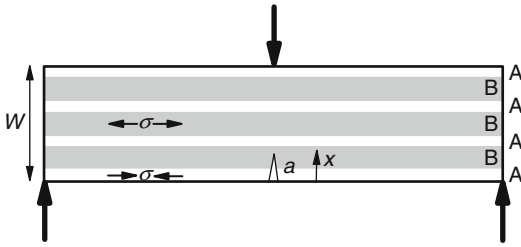
$$K_{res}(a) = \int_0^a h(x, a) \sigma_{res}(x) dx \quad (5)$$

where  $h(x, a)$  is the weight function and  $x$  is the distance along the crack (see Fig. 1).

A suitable weight function is the one for an edge crack in a bend bar since this loading situation is close to possible applications as well as a common experimental set up:

$$h(x, a) = \sqrt{\frac{2}{\pi a}} \frac{1}{\sqrt{1 - \frac{x}{a}}} \left[ 1 + \sum_{v=0}^2 \sum_{\mu=0}^4 \frac{A_{v\mu} \left(\frac{a}{W}\right)^\mu}{\left(1 - \frac{a}{W}\right)^{3/2}} \left(1 - \frac{x}{a}\right)^{v+1} \right] \quad (6)$$

where the coefficients  $A_{v\mu}$  are given in Table 1 and  $W$  is the total thickness of the bar.



**Effective Fracture Toughness in  $\text{Al}_2\text{O}_3\text{-Al}_2\text{O}_3/\text{ZrO}_2$ -Laminates, Fig. 1** Schematic of a laminate and the loading situation for which apparent R-curves were calculated

**Effective Fracture Toughness in  $\text{Al}_2\text{O}_3\text{-Al}_2\text{O}_3/\text{ZrO}_2$ -Laminates, Table 1** Coefficients  $A_{\nu\mu}$  for the weight function, (6) for a bend bar [38]

	$\mu = 0$	$\mu = 1$	$\mu = 2$	$\mu = 3$	$\mu = 4$
$\nu = 0$	0.50	2.45	0.07	1.32	-3.07
$\nu = 1$	0.54	-5.08	24.35	-32.72	18.12
$\nu = 2$	-0.19	2.56	-12.64	19.76	-10.99

## Residual Stresses in Laminates with Strong Interfaces

In order to apply (5) and (6) to estimate the apparent R-curve, the residual stress distribution in the laminate has to be known. For a symmetrical laminate, an analytical estimation of the stresses on a large distance from the surface is possible when assuming a plane strain condition with zero transversal stress [29]. For a symmetrical laminate, the equi-biaxial residual stresses in the layers are given by

$$\sigma_A = -E'_A \frac{\int_{T_0}^{T_{sf}} \Delta\alpha dT}{1 + \frac{N+1}{N-1} \frac{e}{\lambda}} \quad (7)$$

and

$$\sigma_B = -\sigma_A \frac{1}{\lambda} \frac{(N+1)}{(N-1)} \quad (8)$$

where  $E' = E/(1-\nu)$ ,  $E$  is Young's modulus,  $\nu$  is Poisson's ratio,  $N$  is the total (odd) number of layers,  $\lambda = t_B/t_A$  denotes the thicknesses ratio of the individual layers of different materials

**Effective Fracture Toughness in  $\text{Al}_2\text{O}_3\text{-Al}_2\text{O}_3/\text{ZrO}_2$ -Laminates, Table 2** Material properties used for the calculation of apparent R-curves

	$E$ (GPa)	$\nu$ (-)	$\alpha$ ( $10^{-6} \text{ K}^{-1}$ )	$K_{IC}$ ( $\text{MPa}\sqrt{\text{m}}$ )
$\text{Al}_2\text{O}_3$	391	0.241	8.64	3.8
AZ <sup>a</sup>	305	0.257	9.24	3.2
Y-TZP	205	0.32	11.3	6.2

<sup>a</sup>60 vol%  $\text{Al}_2\text{O}_3$  + 40 vol% Y-TZP

A and B, respectively,  $e = E_A/E_B$ , and  $\Delta\alpha = (\alpha_A - \alpha_B)$  is the thermal expansion mismatch. The stresses arise during the cooling from the sintering temperature in a temperature range between  $T_{sf}$  and  $T_0$ . For derivation of the latter equation, it has been assumed that all layers made of the outer material A have the same thickness; the same assumption holds for the layers made of the inner material B. As it follows from (7) and (8), the magnitude of the residual stresses can be tailored by choosing the materials (with the limitation that they have to form strong interfaces) and by adjusting the layer thickness ratio. A comparison with FEM calculation shows that the plane residual stresses reach a constant value at a distance of approximately 10–15 % of the width inside from the surface. The out-of-plane stress component declines substantially within one-layer thickness inside from the surface [26].

## Apparent R-Curves

Following the procedure outlined in the previous sections, the apparent R-curves can be calculated for symmetrical laminates made from  $\text{Al}_2\text{O}_3$  as A-layers and  $x \text{ Al}_2\text{O}_3/(1-x) \text{ Y-TZP}$  composites as B-layers. The material properties are summarized in Table 2. The Young's moduli and Poisson's ratios were measured using impulse excitation [30]; the technical thermal expansion coefficient between 20 °C and 1,200 °C was determined by conventional dilatometry [11], and fracture toughness was evaluated by

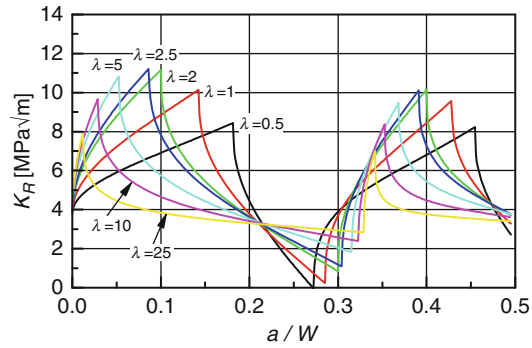


SEVNB [31]. Values for pure Y-TZP are taken from literature [32].

Laminates of such configuration have always compressive stresses in the outer layers. Such laminates are called ECS laminates [33] and are characterized by a negative characteristic stress  $\sigma_0 = \sigma_A - \sigma_B < 0$  [27]. The calculations refer to a loading situation schematically depicted in Fig. 1. If not otherwise stated, the laminate thickness is  $W = 3$  mm (called “reference” laminate according to a possible design condition). Laminates in this particular material system are easily fabricated by tape [34] or slip casting [5]. Usually they are sintered around 1,500 °C. It is assumed that any stresses arising due to differential sintering or differential shrinkage are relieved above  $T_{sf} \approx 1,200$  °C. This is supported by experimental evidence [35]. The reference temperature was  $T_0 = 20$  °C.

Apparent R-curves for a laminate with  $N = 7$ , A-layers made of Al<sub>2</sub>O<sub>3</sub> and B-layers made of the composite AZ (see Table 2), and a variety of  $\lambda$ -ratios are plotted in Fig. 2 as functions of the normalized crack length  $a/W$ . The values for the layer thicknesses and residual stresses are summarized in Table 3.  $\lambda < 1$  refers to A-layers with compressive stresses that are thinner than the B-layers with tensile stresses.

The apparent R-curves in Fig. 2 show an oscillating behavior. The apparent toughness increases in the compressive layers, reaches a local maximum at the first A/B interface, and decreases in the tensile layers. The possible increase in toughness in the first layer is proportional to the amplitude of the residual stress and the square root of the thickness of the layer. The residual stress itself is inversely proportional to the layer thickness (compare (6) and Table 3). This explains why the maximum shielding is achieved neither using very thin layers under high compressive stress nor with thick layers under low compressive stress but at an intermediate configuration. In the investigated case, the maximal toughness is achieved for the optimal layer thickness ratio  $\lambda_{opt} \approx 2.6$ . At this configuration, the toughness at the first interface is nearly three times the base toughness of the A-layer material.



**Effective Fracture Toughness in Al<sub>2</sub>O<sub>3</sub>-Al<sub>2</sub>O<sub>3</sub>/ZrO<sub>2</sub>-Laminates, Fig. 2** Apparent R-curves for  $W = 3$  mm,  $N = 7$ , and various ratios  $\lambda$ . A-layers are made of Al<sub>2</sub>O<sub>3</sub>; B-layers are made of AZ; see Table 2. The apparent R-curves are plotted for the first four layers

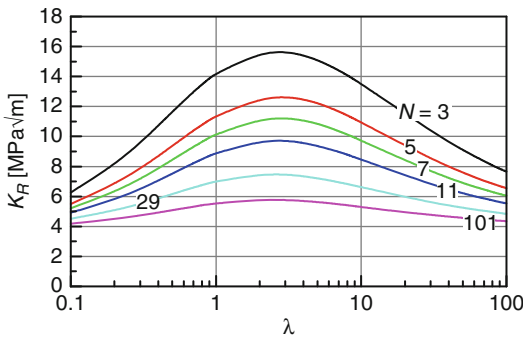
**Effective Fracture Toughness in Al<sub>2</sub>O<sub>3</sub>-Al<sub>2</sub>O<sub>3</sub>/ZrO<sub>2</sub>-Laminates, Table 3** Rounded values for layer thicknesses and residual stresses for the laminates investigated for Fig. 2.  $W = 3$  mm,  $N = 7$  for all laminates. A-layers are made of Al<sub>2</sub>O<sub>3</sub>; B-layers are made of AZ; see Table 2

$\lambda$	$t_A$ (mm)	$t_B$ (mm)	$\sigma_A$ (MPa)	$\sigma_B$ (MPa)
0.5	0.55	0.27	− 84	224
1	0.43	0.43	− 136	182
2	0.3	0.6	− 199	132
2.5	0.26	0.65	− 218	117
5	0.16	0.79	− 273	73
10	0.09	0.88	− 312	42
25	0.04	0.95	− 342	18

### Influences on Shielding

The relations for calculation of the apparent R-curves show that there are several possibilities to tune the apparent R-curve. The layer thickness ratio  $\lambda$  appears to be one parameter. The other parameter is the number of layers  $N$  at a given thickness  $W$ . To investigate the effect of such changes on  $\lambda_{opt}$ , the toughness at the first interface (i.e., at  $a = t_A$ ) was evaluated at various  $\lambda$ -ratios for changing boundary conditions for the same material combination as shown in Fig. 2.

In Fig. 3, the dependence of the maximum shielding at the first interface is plotted as a function of the layer thickness ratio  $\lambda$  for



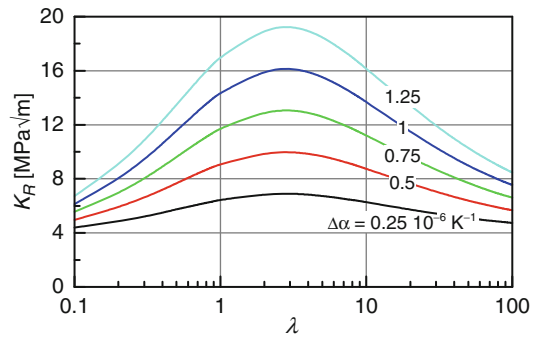
**Effective Fracture Toughness in  $\text{Al}_2\text{O}_3\text{-Al}_2\text{O}_3/\text{ZrO}_2$ -Laminates, Fig. 3** Maximum apparent toughness at the first interface for laminates with  $W = 3$  mm and different numbers of layers,  $N$ , as a function of the layer thickness ratio  $\lambda$ . A-layers are made of  $\text{Al}_2\text{O}_3$ ; B-layers are made of AZ; see Table 2

different layer numbers  $N$  for the reference laminate with  $W = 3$  mm.

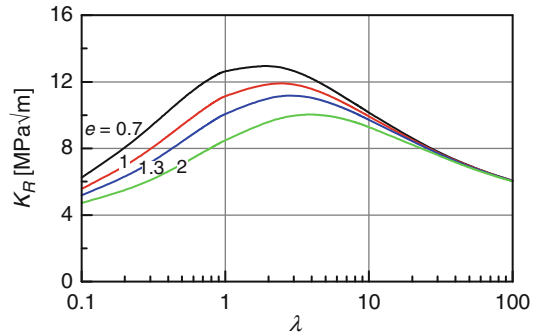
Figure 3 shows that the highest apparent toughness can be achieved with a small number of layers but that the optimal thickness ratio  $\lambda_{opt}$  is nearly not influenced by the number of layers (for the presented calculation results,  $2.4 \leq \lambda_{opt} \leq 2.63$ ). As compared to the reference laminate with seven layers, the baseline toughness can be increased by a factor of four with a tri-layered structure with the optimal layer thickness ratio.

More possibilities are offered by the choice of the layer materials and their relative elastic and thermal properties. In the investigated material system, the thermal expansion mismatch  $\Delta\alpha$  as well as the elastic modulus ratio  $e$  can be adjusted by choosing an appropriate mixing ratio of  $\text{Al}_2\text{O}_3$  and Y-TZP for the inner B-layers. According to Table 2,  $-3 \leq \Delta\alpha \leq 0$  and  $1 \leq e \leq 1.85$  is possible. Strictly, both quantities change simultaneously;  $\Delta\alpha$  decreases and  $e$  increases as the Y-TZP content in A + Z-composite is increased. However, by using different materials than those introduced here, also other combinations like varying  $\Delta\alpha$  at constant  $e$  and vice versa can be envisaged.

In Fig. 4, the maximum achievable shielding at the first interface for a 7-layer reference laminate is plotted as a function of  $\lambda$  for different



**Effective Fracture Toughness in  $\text{Al}_2\text{O}_3\text{-Al}_2\text{O}_3/\text{ZrO}_2$ -Laminates, Fig. 4** Maximum apparent toughness at the first interface for laminates with  $W = 3$  mm and different thermal expansion mismatch  $\Delta\alpha$ , as a function of the layer thickness ratio  $\lambda$

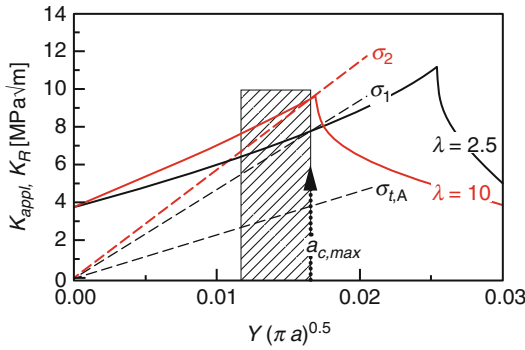


**Effective Fracture Toughness in  $\text{Al}_2\text{O}_3\text{-Al}_2\text{O}_3/\text{ZrO}_2$ -Laminates, Fig. 5** Maximum apparent toughness at the first interface for laminates with  $W = 3$  mm and different elastic mismatch values  $e$ , as a function of the layer thickness ratio  $\lambda$

values of the thermal mismatch  $\Delta\alpha$ . According to (6), the residual compressive stress  $\sigma_A$  increases as  $\Delta\alpha$  increases, and consequently, the maximum apparent toughness increases. For identical laminate architecture, it can be always achieved at the same  $\lambda_{opt} \approx 2.6$ .

Figure 5 shows a plot of the maximum shielding at the first interface for a 7-layer reference laminate for different values of the elastic mismatch  $e$ . In this case, a variation of the elastic properties also leads to a variation of the optimal architecture, i.e.,  $\lambda_{opt}$  slightly increases with increasing elastic mismatch. Stiffer inner layers,  $e < 1$ , lead to a higher apparent toughness than stiffer outer layers,  $e > 1$ .





**Effective Fracture Toughness in  $\text{Al}_2\text{O}_3\text{-Al}_2\text{O}_3/\text{ZrO}_2$ -Laminates, Fig. 6** Apparent R-curves of laminates with A-layers made of  $\text{Al}_2\text{O}_3$ ; B-layers are made of AZ (see Table 2) and  $W = 3$  mm,  $N = 7$ , and  $\lambda = 2.5$  and  $\lambda = 10$ . The dashed lines represent different applied stresses; the dashed area indicates the range of critical defect sizes

Even though the residual stresses are essential to provoke the desired apparent R-curve, they may also have detrimental consequences for the structural integrity of the laminates. High tensile stresses may lead to *tunnel cracks* in the tensile layers [32]. High compressive stresses may cause in-plane *edge cracks* at the surface of the compressive layers [36]. The occurrence of such cracks may be circumvented by restricting the layer thicknesses in order to limit the tensile or compressive stresses. Estimates on these limits are given in literature [27, 37].

### Fracture Behavior and Strength of Laminates

Up to this point, only the maximum toughness at the first interface has been investigated, and conditions for maximization of this peak value were given. In order to maximize the strength of a laminate, additional facts have to be considered. According to fracture mechanics, (1) and (2), the strength  $\sigma_f$  of a component is given by [23]

$$\sigma_f = \frac{K_c}{Y \sqrt{\pi a_c}} \quad (9)$$

where  $a_c$  is the critical crack length in the component. In a laminate,  $K_c$  of course has to be replaced by  $K_R(a)$ . This implies that, in order to

optimize the strength of a laminate, one not only has to know the apparent R-curve but also the range of typical critical crack lengths.

This is illustrated in Fig. 6 where the apparent R-curve of two laminates ( $\lambda = 2.5$  and  $\lambda = 10$ ) is plotted. The scale of the abscissa is chosen to represent  $K_{appl}(a)$ -curves, (1), as straight lines with different slopes for different applied stresses. In this plot, the strength  $\sigma_f$  for a given defect size  $a_c$  is the slope of the  $K_{appl}(a)$ -line which intersects the apparent R-curve at the abscissa value corresponding to  $a_c$ . If we consider a defect size distribution with a maximum critical crack length  $a_{c,max} \approx 80 \mu\text{m}$ , we can see that a laminate with  $\lambda = 2.5$  (which is close to the geometry with  $\lambda_{opt}$  and maximum peak toughness) will fail at  $\sigma_1 \approx 470$  MPa, while a laminate with  $\lambda = 10$  will fail at  $\sigma_2 \approx 575$  MPa. For comparison, a component made only from material A with the constant toughness  $K_A$  will fail at  $\sigma_{f,A} \approx 230$  MPa.

To maximize the strength of a laminated component, the apparent R-curve has to be tailored in such a way that the peak toughness is reached for the largest possible defects. This condition can be fulfilled if the outer layer  $t_A$  is just thick enough to contain the largest critical flaw.

### Summary

An investigation of the apparent toughness of symmetric ceramic laminates with residual stresses due to a thermal expansion mismatch using a weight function analysis has been discussed. It has been shown that the apparent toughness increases in layers with compressive residual stresses and decreases in layers with tensile residual stresses. The maximum toughening effect is always achieved at the first interface. The magnitude of the toughening can be tailored by variation of the laminate architecture, i.e., the number of layers and the layer thickness ratio, but also through adjusting the thermal or elastic mismatch by choosing suitable material combinations.

The maximum toughening appears in laminates with relatively thin compressive layers,

i.e., where the tensile layers are approx. 2.6 times thicker than the compressive layers. The magnitude increases as the number of layers decreases and as the thermal mismatch increases. The optimal layer thickness ratio can be shifted to different values by changing the elastic mismatch. More compliant compressive layers favor high apparent toughness at lower thickness ratios.

In order to design laminates with an optimized strength, it is necessary to take the defect size distribution in the material into account. Highest strength values can be expected for laminates where all defects are just contained within the first layer. This condition is not necessarily fulfilled at the architecture that maximizes the toughness.

The general trend for the optimization of laminates with external compressive stresses (ECS laminates) is to have layers with high compressive stresses. However, since the residual stresses may also lead to damage of the laminate by creating edge or tunnel cracks, this strategy can only be exploited to a certain extent.

## References

1. Laraia VJ, Heuer AH (1989) Novel composite microstructure and mechanical behavior of mollusk shell. *J Am Ceram Soc* 72:2177–2179
2. Doremus RH (1994) Glass science. Wiley-Interscience, New York
3. Clegg WJ, Kendall K, Alford NM, Button TW, Birchall JD (1990) A simple way to make tough ceramics. *Nature* 347:455–457
4. Cai PZ, Green DJ, Messing GL (1997) Constrained densification of alumina/zirconia hybrid laminates, II: viscoelastic stress computation. *J Am Ceram Soc* 80:1940–1948
5. Virkar AV, Huang JL, Cutler RA (1987) Strengthening of oxide ceramics by transformation-induced stresses. *J Am Ceram Soc* 70:164–170
6. Sánchez-Herencia AJ, Pascual C, He J, Lange FF (1999)  $\text{ZrO}_2/\text{ZrO}_2$  layered composites for crack bifurcation. *J Am Ceram Soc* 82:1512–1518
7. Pontin MG, Rao MP, Sánchez-Herencia AJ, Lange FF (2002) Laminar ceramics utilizing the zirconia tetragonal-to monoclinic phase transformation to obtain a threshold strength. *J Am Ceram Soc* 85:3041–3048
8. Bermejo R, Torres Y, Sanchez-Herencia AJ, Baudin C, Anglada M, Llanes L (2006) Residual stresses, strength and toughness of laminates with different layer thickness ratios. *Acta Mat* 54:4745–4757
9. Cai PZ, Green DJ, Messing GL (1998) Mechanical characterization of  $\text{Al}_2\text{O}_3/\text{ZrO}_2$  hybrid laminates. *J Eur Ceram Soc* 18:2025–2034
10. Moon RJ, Hoffman M, Hilden J, Bowman KJ, Trumble KP, Rödel J (2002) Weight function analysis on the R-curve behaviour of multilayered alumina/zirconia composites. *J Am Ceram Soc* 85:1505–1511
11. Lube T, Pascual Herrero J, Chalvet F, de Portu G (2007) Effective fracture toughness in  $\text{Al}_2\text{O}_3$  -  $\text{Al}_2\text{O}_3/\text{ZrO}_2$  laminates. *J Euro Ceram Soc* 27:1449–1453
12. Lugovy M, Slyunyayev V, Subbotin V, Orlovskaya N, Kübler J (2004) Crack arrest in  $\text{Si}_3\text{N}_4$ -based layered composites with residual stress. *Comp Sci Tech* 64:1947–1957
13. Blugan G, Dobedoe R, Lugovy M, Koebel S, Kuebler J (2006)  $\text{Si}_3\text{N}_4$ -TiN based micro-laminates with rising R-curve behaviour. *Comp B* 37:459–465
14. Bermejo R, Torres Y, Sánchez-Herencia AJ, Baudin C, Anglada M, Llanes L (2006) Fracture behaviour of an  $\text{Al}_2\text{O}_3$ - $\text{ZrO}_2$  multi-layered ceramic with residual stresses due to phase transformations. *Fatigue Fract Engng Mater Struct* 29:71–78
15. Orlovskaya N, Lugovy M, Subbotin V, Radchenko O, Adams J, Chheda M, Shih J, Sankar J, Yarmolenko S (2005) Robust design and manufacturing of ceramic laminates with controlled thermal residual stresses for enhanced toughness. *J Mat Sci* 40:5483–5490
16. Lakshminarayanan R, Shetty DK, Cutler RA (1996) Toughening of layered ceramic composites with residual surface compression. *J Am Ceram Soc* 79:79–87
17. Pascual Herrero J, Chalvet F, Lube T, de Portu G (2005) Strength distributions in ceramic laminates. *Mater Sci Forum* 492–493:581–586
18. Rao MP, Sánchez-Herencia AJ, Beltz GE, McMeeking RM, Lange FF (1999) Laminar ceramics that exhibit a threshold strength. *Science* 286:102–105
19. Bermejo R, Llanes L, Anglada M, Supancic P, Lube T (2005) Thermal shock behavior of an  $\text{Al}_2\text{O}_3/\text{ZrO}_2$  multilayered ceramic with residual stresses due to phase transformations. *Key Eng Mater* 290:191–198
20. Tarlazzi A, Roncari E, Pinasco P, Guicciardi S, Melandri C, de Portu G (2000) Tribological behaviour of  $\text{Al}_2\text{O}_3/\text{ZrO}_2$ - $\text{ZrO}_2$  laminated composites. *Wear* 244:29–40
21. Toschi F, Melandri C, Pinasco P, Roncari E, Guicciardi S, de Portu G (2003) Influence of residual stresses on the wear behaviour of alumina/alumina-zirconia laminated composites. *J Am Ceram Soc* 86:1547–1553

22. Anderson TL (2005) Fracture mechanics: fundamentals and applications. CRC Press, Orlando
23. Danzer R, Lube T, Supancic P, Damani R (2008) Fracture of ceramics. *Adv Eng Mater* 10:275–298
24. Mai Y-M, Lawn BR (1987) Crack-interface grain bridging as a fracture resistance mechanism in ceramics: II, theoretical fracture mechanics model. *J Am Ceram Soc* 70:289–294
25. McMeeking RM, Evans AG (1982) Mechanics of transformation-toughening in brittle materials. *J Am Ceram Soc* 65:242–246
26. Chen CR, Pascual J, Fischer FD, Kolednik O, Danzer R (2007) Prediction of fracture toughness of a ceramic multilayer composite - modelling and experiments. *Acta Mat* 55:409–421
27. Sestakova L, Bermejo R, Chlup Z, Danzer R (2011) Strategies for fracture toughness, strength and reliability optimisation of ceramic-ceramic laminates. *Int J Mater Res* 102:613–626
28. Bueckner HF (1970) A novel principle for the computation of stress intensity factors. *Z Angew Math Mech* 50:529–546
29. Oel HJ, Frechette VD (1967) Stress distribution in multiphase systems: I, composites with planar interfaces. *J Am Ceram Soc* 50:542–549
30. ASTM C 1259 (1998) Standard test method for dynamic Young's modulus, shear modulus and Poisson's ratio for advanced ceramics by impulse excitation of vibration. ASTM International, West Conshohocken
31. CEN/TS 14425-5 (2004) Fine ceramics (advanced ceramics, advanced technical ceramics) – determination of fracture toughness of monolithic ceramics at room temperature by the single-edge vee-notch beam (SEVNB) method. European Committee for Standardization, Brussels
32. Hillman C, Suo Z, Lange FF (1996) Cracking of laminates subjected to biaxial tensile stresses. *J Am Ceram Soc* 79:2127–2133
33. Bermejo R, Pascual Herrero J, Lube T, Danzer R (2008) Optimal strength and toughness of  $\text{Al}_2\text{O}_3$ - $\text{ZrO}_2$ -laminates designed with external or internal compressive layers. *J Eur Ceram Soc* 28:1575–1583
34. de Portu G, Miele L, Pezzotti G (2006) Laminated ceramic structures from oxide systems. *Comp B* 37:556–567
35. Pascual J, Chalvet F, Lube T, de Portu G (2007) Strain mismatch in ceramic multilayers: determination by strength measurements. *Key Eng Mater* 333:239–242
36. Ho S, Hillman C, Lange FF, Suo Z (1995) Surface cracking in layers under biaxial, residual compressive stress. *J Am Ceram Soc* 78:2353–2359
37. Gee IA, Dobedoe RS, Vann R, Lewis MH, Blugan G, Kübler J (2005) Enhanced fracture toughness by ceramic laminate design. *Adv Appl Ceram* 104:103–109
38. Fett T, Munz D (1997) Stress intensity factors and weight functions. Computational Mechanics, Southampton

## Effects of Elastic Foundation on Thermal Buckling of Circular/Annular Plates

Mohammad Reza Eslami and Yasser Kiani  
Department of Mechanical Engineering,  
Amirkabir University of Technology,  
Tehran, Iran

### Synonyms

Thermal buckling (instability) of in-contact plates

### Definition

Structures that are in contact with an elastic foundation generally buckle in higher temperatures when compared with their contact-less conditions. The elastic foundation has direct effect on buckled shape of the plate. In some cases, in-contact circular/annular plates buckle with higher number of nodal diameters. In such conditions, the number of critical points for design problems should also be taken into account. Therefore, both critical buckling temperature and buckled shape of the plate are studied herein. In what follows, temperature distribution through the plate is assumed to be symmetric and only through-the-thickness. Besides, contact conditions are considered to be complete, and the conventional Pasternak foundation is assumed, which acts in tension as well as compression. Both homogeneous and through-the-thickness nonhomogeneous plates are studied in the rest.

### Overview

Thermal stability analysis of in-contact circular/annular plates is limited in number. Laermann [1] studied the influence of a quasi-stationary temperature field on the stress state of a thin plate on an elastic half-space when loading and contact conditions are symmetric. Li and Yu [2] studied

the mode transition, buckling, and postbuckling of annular plates subjected to thermal loading. Many researches are available on stability analysis of in-contact plates subjected to mechanical loading. Xiao and Chang-jun [3] studied the symmetrical buckling and postbuckling analysis of annular plates based on a shooting method. For the case when circular plate is in contact with a Winkler elastic foundation and loading is of the uniform compression type, Wang [4] presented the exact solution for various boundary conditions. In this work, Wang examined the existence of asymmetrical deformations at the onset of symmetrical compression. Employing the third-order shear deformation theory of Reddy, Wang et al. [5] discussed the shear deformation effects on the symmetrical buckling load of the circular plate that are in contact with conventional Pasternak foundation. For other studies, one may refer to the works of Yu and Wang [6, 7], Gupta et al. [8, 9], Paliwal and Pathak [10], Raju and Rao [11, 12], and Kline and Peck [13].

## Theory

### Basic Equations

Consider an annular/circular plate with thickness  $h$ , inner radii  $b$ , and outer radii  $a$ , referred to the polar coordinates  $(r, \theta, z)$ , as shown in Fig. 1. The circular plate becomes a solid circular plate when  $b = 0$ . Displacement field components along  $(r, \theta, z)$  directions are indicated as  $(u, v, w)$ .

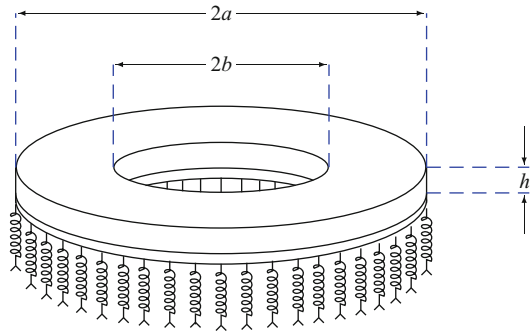
The Kirchhoff hypothesis is used in this study, which is accurate enough for thin circular-annular plates. According to this theory, displacement field on a generic point of the plate is written as function of displacement components of the mid-surface such that [14]

$$u(r, \theta, z) = u_0(r, \theta) - zw_{0,r}(r, \theta) \quad (1)$$

$$v(r, \theta, z) = v_0(r, \theta) - \frac{z}{r}w_{0,\theta}(r, \theta) \quad (2)$$

$$w(r, \theta, z) = w_0(r, \theta) \quad (3)$$

Here, a subscript zero exhibits the displacements on the mid-surface of the plate.



**Effects of Elastic Foundation on Thermal Buckling of Circular/Annular Plates, Fig. 1** The geometry of a circular or annular plate in contact with elastic foundation

The classical plate theory is developed based on the ignorance of transverse shear strains. Besides, normal strain along the thickness coordinate is vanished since the lateral displacement is a function of the in-plane coordinates only. Three remaining nonzero components of strain tensor considering the von Karman nonlinear assumptions are [14]

$$\varepsilon_{rr} = u_{,r} + \frac{1}{2}w_{,r}^2 \quad (4)$$

$$\varepsilon_{\theta\theta} = \frac{1}{r}v_{,\theta} + \frac{1}{r}u + \frac{1}{2r^2}w_{,\theta}^2 \quad (5)$$

$$\gamma_{r\theta} = \frac{1}{r}u_{,\theta} + v_{,r} - \frac{1}{r}v + \frac{1}{r}w_{,\theta}w_{,r} \quad (6)$$

Here,  $\varepsilon_{rr}$  and  $\varepsilon_{\theta\theta}$  are the normal strains and  $\gamma_{r\theta}$  is the shear strain, and a comma indicates partial derivative.

When temperature distribution through the plate and the initial reference temperature are indicated by  $T$  and  $T_0$ , respectively, the thermoelasticity theory of a continuum medium yields the following constitutive equation [15]:

$$\begin{bmatrix} \sigma_{rr} \\ \sigma_{\theta\theta} \\ \tau_{r\theta} \end{bmatrix} = \frac{E}{1-\nu^2} \begin{bmatrix} 1 & \nu & 0 \\ \nu & 1 & 0 \\ 0 & 0 & \frac{1-\nu}{2} \end{bmatrix} \begin{pmatrix} \begin{bmatrix} \varepsilon_{rr} \\ \varepsilon_{\theta\theta} \\ \gamma_{r\theta} \end{bmatrix} - (T - T_0) \begin{bmatrix} \alpha \\ \alpha \\ 0 \end{bmatrix} \end{pmatrix} \quad (7)$$

Based on the classical plate theory, the stress resultants are related to the stresses through the following equations [14]:

$$(N_{rr}, N_{\theta\theta}, N_{r\theta}) = \int_{-\frac{h}{2}}^{\frac{h}{2}} (\sigma_{rr}, \sigma_{\theta\theta}, \tau_{r\theta}) dz \quad (8)$$

$$(M_{rr}, M_{\theta\theta}, M_{r\theta}) = \int_{-\frac{h}{2}}^{\frac{h}{2}} z(\sigma_{rr}, \sigma_{\theta\theta}, \tau_{r\theta}) dz \quad (9)$$

Substituting (1–7) into (8), (9) gives the stress resultants in terms of the midplane displacement as

$$\begin{Bmatrix} N_{rr} \\ N_{\theta\theta} \\ N_{r\theta} \\ M_{rr} \\ M_{\theta\theta} \\ M_{r\theta} \end{Bmatrix} = \frac{1}{1-\nu^2} \times \begin{bmatrix} E_1 & \nu E_1 & 0 & E_2 & \nu E_2 & 0 \\ \nu E_1 & E_1 & 0 & \nu E_2 & E_2 & 0 \\ 0 & 0 & \frac{1-\nu}{2} E_1 & 0 & 0 & \frac{1-\nu}{2} E_2 \\ E_2 & \nu E_2 & 0 & E_3 & \nu E_3 & 0 \\ \nu E_2 & E_2 & 0 & \nu E_3 & E_3 & 0 \\ 0 & 0 & \frac{1-\nu}{2} E_2 & 0 & 0 & \frac{1-\nu}{2} E_3 \end{bmatrix} \begin{Bmatrix} u_{0,r} + \frac{1}{2} w_{0,r}^2 \\ \frac{1}{r} v_{0,\theta} + \frac{1}{r} u_0 + \frac{1}{2r^2} w_{0,\theta}^2 \\ \frac{1}{r} u_{0,\theta} + v_{0,r} - \frac{1}{r} v_0 + \frac{1}{r} w_{0,r} w_{0,\theta} \\ -w_{0,rr} \\ -\frac{1}{r^2} w_{0,\theta\theta} - \frac{1}{r} w_{0,r} \\ -\frac{2}{r} w_{0,r\theta} + \frac{2}{r^2} w_{0,\theta} \end{Bmatrix} - \begin{Bmatrix} N^T \\ N^T \\ 0 \\ M^T \\ M^T \\ 0 \end{Bmatrix} \quad (10)$$

where  $N^T$  and  $M^T$  are the thermal force and thermal moment resultants and  $E_1$ ,  $E_2$ , and  $E_3$  are constants to be calculated as

$$E_1 = \int_{-\frac{h}{2}}^{\frac{h}{2}} E dz = h e_1 \quad (11)$$

$$E_2 = \int_{-\frac{h}{2}}^{\frac{h}{2}} z E dz = h^2 e_2 \quad (12)$$

$$E_3 = \int_{-\frac{h}{2}}^{\frac{h}{2}} z^2 E dz = h^3 e_3 \quad (13)$$

$$N^T = \frac{1}{1-\nu} \int_{-\frac{h}{2}}^{\frac{h}{2}} E \alpha (T - T_0) dz \quad (14)$$

$$M^T = \frac{1}{1-\nu} \int_{-\frac{h}{2}}^{\frac{h}{2}} z E \alpha (T - T_0) dz \quad (15)$$

It is worth mentioning that the constant  $E_2$  (see (12)) indicates the stretching-bending coupling effect which is caused due to the separation of mid-surface and neutral surface. In functionally graded materials or composite materials with unsymmetrical midplane configuration, this constant has a nonzero value. For isotropic homogeneous plates, this constant is equal to zero, and the coupling between stretching and bending is vanished.

The equilibrium equations of an in-contact annular/circular FGM plate under thermal loadings may be derived on the basis of static version of virtual displacements method [14]. The total virtual potential energy of the plate  $\delta V$  is equal to the total virtual strain energy of the plate and elastic foundation. This function in an equilibrium position may be written as

$$\begin{aligned} \delta V = & \int_b^a \int_0^{2\pi} \int_{-\frac{h}{2}}^{\frac{h}{2}} (\sigma_{rr} \delta \varepsilon_{rr} + \sigma_{\theta\theta} \delta \varepsilon_{\theta\theta} + \tau_{r\theta} \delta \gamma_{r\theta}) r dz d\theta dr \\ & + \int_b^a \int_0^{2\pi} (K_w w_0 \delta w_0 + K_g (w_{0,r} \delta w_{0,r} \\ & + \frac{1}{r^2} w_{0,\theta} \delta w_{0,\theta})) r dr d\theta = 0 \end{aligned} \quad (16)$$

where in definition of the Pasternak elastic foundation energy, the constants  $K_w$  and  $K_g$  indicate the Winkler and the Pasternak stiffnesses, respectively. The equilibrium equations for an in-contact plate in polar coordinates are given as

$$\delta u_0 : N_{rr,r} + \frac{1}{r} N_{r\theta,\theta} + \frac{1}{r} (N_{rr} - N_{\theta\theta}) = 0 \quad (17)$$

$$\delta v_0 : N_{r\theta,r} + \frac{2}{r} N_{r\theta} + \frac{1}{r} N_{\theta\theta,\theta} = 0 \quad (18)$$

$$\begin{aligned}
\delta w_0 : & M_{rr,rr} + \frac{2}{r} M_{rr,r} + \frac{1}{r^2} M_{\theta\theta,\theta\theta} - \frac{1}{r} M_{\theta\theta,r} \\
& + \frac{2}{r} M_{r\theta,r\theta} + \frac{2}{r^2} M_{r\theta,\theta} + N_{rr} w_{0,rr} \\
& + N_{\theta\theta} \left( \frac{1}{r^2} w_{0,\theta\theta} + \frac{1}{r} w_{0,r} \right) \\
& + 2N_{r\theta} \left( \frac{1}{r} w_{0,r\theta} - \frac{1}{r^2} w_{0,\theta} \right) \\
& - K_w w_0 + K_g \left( w_{0,rr} + \frac{1}{r} w_{0,r} + \frac{1}{r^2} w_{0,\theta\theta} \right) = 0
\end{aligned} \quad (19)$$

In ► **Circular/Annular Plates, Thermal Buckling**, it is proved that for a through-the-thickness functionally graded material, bifurcation type of instability occurs when both inner and outer edges are clamped (for the case of a solid circular plate, the outer edge should be clamped). While for plates of circular/annular shape with arbitrary edge supports that are symmetrical with respect to their mid-surface, under uniform temperature rise loading, bifurcation exists. In this condition and in the prebuckling state, all three components of the displacement field ( $u_0, v_0, w_0$ ) are equal to zero. Therefore, the prebuckling force resultants are obtained based on (10) as

$$N_{rr}^0 = N_{\theta\theta}^0 = -N^T, \quad N_{r\theta}^0 = 0 \quad (20)$$

where a superscript 0 indicates the prebuckling state of the plate. The above forces are equal to those obtained in ► **Circular/Annular Plates, Thermal Buckling**, for plates without contact conditions. This characteristic is expected since the prebuckling response of the plate is deflection less. When thermal instability occurs, one may find the bifurcation point through the eigenvalue analysis of the stability equations.

### Stability Equations

The adjacent-equilibrium criterion may be used to obtain the stability equations of an annular or circular plate [16]. For this purpose, an equilibrium position which is governed by displacement components  $u_0^0, v_0^0$ , and  $w_0^0$  is considered. The displacement components of a neighboring state

of the stable equilibrium differ by  $u_0^1, v_0^1$  and  $w_0^1$  with respect to the equilibrium position. Here, the incremental displacements with superscript 1 are arbitrary perturbations. Thus, the total displacements of a neighboring state are

$$u_0 = u_0^0 + u_0^1, v_0 = v_0^0 + v_0^1, w_0 = w_0^0 + w_0^1 \quad (21)$$

In the present study, as stated previously, in prebuckling state  $u_0^0 = v_0^0 = w_0^0 = 0$ . However, (21) is presented in this form to yield a general approach. Similar to displacements, the stress resultants are divided into two terms representing the stable equilibrium and the neighboring state. The stress resultants with superscript 1 are linear functions of displacement with superscript 1 [16]. Following this procedure, using (17–19) and performing proper simplifications, the stability equations become

$$N_{rr,r}^1 + \frac{1}{r} N_{r\theta,\theta}^1 + \frac{1}{r} (N_{rr}^1 - N_{\theta\theta}^1) = 0 \quad (22)$$

$$N_{r\theta,r}^1 + \frac{2}{r} N_{r\theta}^1 + \frac{1}{r} N_{\theta\theta,\theta}^1 = 0 \quad (23)$$

$$\begin{aligned}
& M_{rr,rr}^1 + \frac{2}{r} M_{rr,r}^1 + \frac{1}{r^2} M_{\theta\theta,\theta\theta}^1 \\
& - \frac{1}{r} M_{\theta\theta,\theta}^1 + \frac{2}{r} M_{r\theta,r\theta}^1 + \frac{2}{r^2} M_{r\theta,\theta}^1 \\
& + N_{rr}^0 w_{0,rr}^1 + N_{\theta\theta}^0 \left( \frac{1}{r^2} w_{0,\theta\theta}^1 + \frac{1}{r} w_{0,r}^1 \right) \\
& + 2N_{r\theta}^0 \left( \frac{1}{r} w_{0,r\theta}^1 - \frac{1}{r^2} w_{0,\theta}^1 \right) \\
& - K_w w_0^1 + K_g \left( w_{0,rr}^1 + \frac{1}{r} w_{0,r}^1 + \frac{1}{r^2} w_{0,\theta\theta}^1 \right) = 0
\end{aligned} \quad (24)$$

To obtain the stability equations based on displacement field, (10) has to be substituted into the above equations. Upon substitution, second- and higher-order terms of incremental displacements may be omitted [16]. Resulting equations are three stability equations based on the classical plate theory for an FGM plate.



$$\begin{aligned}
& E_1 \left( u_{0,rr}^1 + \frac{1}{r} u_{0,r}^1 - \frac{1}{r^2} u_0^1 - \frac{1}{r^2} v_{0,\theta}^1 + \frac{1}{r} v_{0,r\theta}^1 \right) \\
& + \frac{(1-\nu)}{2} E_1 \left( \frac{1}{r^2} u_{0,\theta\theta}^1 - \frac{1}{r} v_{0,r\theta}^1 - \frac{1}{r^2} v_{0,\theta}^1 \right) \\
& - E_2 \left( w_{0,rrr}^1 - \frac{1}{r^2} w_{0,r}^1 + \frac{1}{r} w_{0,rr}^1 \right. \\
& \left. - \frac{2}{r^3} w_{0,\theta\theta}^1 + \frac{1}{r^2} w_{0,\theta\theta r}^1 \right) = 0
\end{aligned} \quad (25)$$

$$\begin{aligned}
& E_1 \left( \frac{1}{r^2} v_{0,\theta\theta}^1 + \frac{1}{r} u_{0,r\theta}^1 + \frac{1}{r^2} u_{0,\theta}^1 \right) \\
& + \frac{(1-\nu)}{2} E_1 \left( v_{0,rr}^1 + \frac{1}{r} v_{0,r}^1 - \frac{1}{r^2} v_0^1 + \frac{1}{r^2} u_{0,\theta}^1 - \frac{1}{r} u_{0,r\theta}^1 \right) \\
& - E_2 \left( \frac{1}{r} w_{0,rr\theta}^1 + \frac{1}{r^2} w_{0,r\theta}^1 + \frac{1}{r^3} w_{0,\theta\theta\theta}^1 \right) = 0
\end{aligned} \quad (26)$$

$$\begin{aligned}
& \frac{E_2}{1-\nu^2} \left( u_{0,rrr}^1 + \frac{2}{r} u_{0,rr}^1 - \frac{1}{r^2} u_{0,r}^1 + \frac{1}{r^3} u_0^1 + \frac{1}{r^3} u_{0,\theta\theta}^1 \right. \\
& \left. + \frac{1}{r^2} u_{0,r\theta\theta}^1 - \frac{1}{r^2} v_{0,r\theta}^1 + \frac{1}{r^3} v_{0,\theta}^1 + \frac{1}{r^3} v_{0,\theta\theta\theta}^1 + \frac{1}{r} v_{0,r\theta}^1 \right) \\
& - \frac{E_3}{1-\nu^2} \left( w_{0,rrrr}^1 + \frac{2}{r} w_{0,rrr}^1 - \frac{1}{r^2} w_{0,rr}^1 + \frac{1}{r^3} w_{0,r}^1 \right. \\
& \left. + \frac{2}{r^2} w_{0,rr\theta\theta}^1 - \frac{2}{r^3} w_{0,r\theta\theta}^1 + \frac{4}{r^4} w_{0,\theta\theta}^1 + \frac{1}{r^4} w_{0,\theta\theta\theta\theta}^1 \right) \\
& + N_{rr}^0 w_{0,rr}^1 + N_{\theta\theta}^0 \left( \frac{1}{r^2} w_{0,\theta\theta}^1 + \frac{1}{r} w_{0,r}^1 \right) \\
& + 2N_{r\theta}^0 \left( \frac{1}{r} w_{0,r\theta}^1 - \frac{1}{r^2} w_{0,\theta}^1 \right) \\
& - K_w w_0^1 + K_g \left( w_{0,rr}^1 + \frac{1}{r} w_{0,r}^1 + \frac{1}{r^2} w_{0,\theta\theta}^1 \right) = 0
\end{aligned} \quad (27)$$

Since the bifurcation point of the plate is the initiation of the out-of-plane deformation, it is reasonable to uncouple the above equations to reach an equation in terms of only the incremental out-of-plane displacement(s). This study is based on the classical plate theory, and the only out-of-plane component of displacement field is  $w_0^1$ . To uncouple the stability equations, (25) is differentiated with respect to  $r$ . Equation (26) is differentiated with respect to  $\theta$  and then divided by  $r$ . Two resulting equations are subtracted from Eq. (27). The following is the stability equation expressed in term of  $w_0^1$ :

$$\begin{aligned}
& D_k \left( w_{0,rrrr}^1 + \frac{2}{r} w_{0,rrr}^1 - \frac{1}{r^2} w_{0,rr}^1 + \frac{1}{r^3} w_{0,r}^1 \right. \\
& \left. + \frac{2}{r^2} w_{0,rr\theta\theta}^1 - \frac{2}{r^3} w_{0,r\theta\theta}^1 \right. \\
& \left. + \frac{4}{r^4} w_{0,\theta\theta}^1 + \frac{1}{r^4} w_{0,\theta\theta\theta\theta}^1 \right) \\
& - N_{rr}^0 w_{0,rr}^1 - N_{\theta\theta}^0 \left( \frac{1}{r^2} w_{0,\theta\theta}^1 + \frac{1}{r} w_{0,r}^1 \right) \\
& - 2N_{r\theta}^0 \left( \frac{1}{r} w_{0,r\theta}^1 - \frac{1}{r^2} w_{0,\theta}^1 \right) + K_w w_0^1 \\
& - K_g \left( w_{0,rr}^1 + \frac{1}{r} w_{0,r}^1 + \frac{1}{r^2} w_{0,\theta\theta}^1 \right) = 0
\end{aligned} \quad (28)$$

where  $D_k = \frac{E_1 E_3 - E_2^2}{E_1 (1-\nu^2)}$  is the equivalent flexural rigidity of an FGM plate.

It is worth mentioning that for symmetrically midplane circular and annular plates, with those certain conditions discussed, stretching and coupling behaviors are uncoupled. Therefore, for those classes of structures, there is no need to uncouple the in-plane and out-of-plane components of displacement field.

#### Solving the Stability Equation

In this section, an exact analytical solution for stability Equation (28) is presented. Substituting prebuckling forces from (20) to (28) gives

$$\begin{aligned}
& \left\{ \left( \frac{\partial^2}{\partial r^2} + \frac{1}{r} \frac{\partial}{\partial r} + \frac{1}{r^2} \frac{\partial^2}{\partial \theta^2} \right) \left( \frac{\partial^2}{\partial r^2} + \frac{1}{r} \frac{\partial}{\partial r} \right. \right. \\
& \left. \left. + \frac{1}{r^2} \frac{\partial^2}{\partial \theta^2} + \frac{N^T - K_g}{D_k} \right) + \frac{K_w}{D_k} \right\} w_0^1(r, \theta) = 0
\end{aligned} \quad (29)$$

For the sake of simplicity and generality, the following nondimensional parameters are introduced:

$$\begin{aligned}
& \bar{r} = \frac{r}{a}, \quad \beta = \frac{b}{a}, \quad \delta = \frac{h}{a}, \quad k_g = \frac{K_g a^2}{D_0} \\
& k_w = \frac{K_w a^4}{D_0}, \quad d = \frac{D_k}{D_0}, \quad n^T = \frac{N^T a^2}{D_0}
\end{aligned} \quad (30)$$

To consider the asymmetrical deformations of the plate at the presence of symmetrical loading, the buckled shape of the plate is assumed as [17]

$$w_0^1(a\bar{r}, \theta) = W_n(\bar{r}) \cos(n\theta) \quad (31)$$

where  $n$  is the number of nodal diameters. The value of  $n = 0$  indicates the symmetric buckled shape of the plate, and  $n > 0$  is associated with the asymmetric buckled shapes. Substituting (31) into (29), and with the aid of nondimensional parameters (30), the following ordinary differential equation is obtained:

$$\left( \frac{d^2}{d\bar{r}^2} + \frac{1}{\bar{r}} \frac{d}{d\bar{r}} - \frac{n^2}{\bar{r}^2} + k_1^2 \right) \left( \frac{d^2}{d\bar{r}^2} + \frac{1}{\bar{r}} \frac{d}{d\bar{r}} - \frac{n^2}{\bar{r}^2} + k_2^2 \right) W_n(\bar{r}) = 0 \quad (32)$$

The solution of this equation depends on  $k_1$  and  $k_2$  and should be classified as follows:

**Case 1.**  $n^T - k_g > 2\sqrt{k_w d}$ . In this case the exact solution of the stability equation (32) is found as

$$W_n(\bar{r}) = C_{1n}J_n(k_1\bar{r}) + C_{2n}Y_n(k_1\bar{r}) + C_{3n}J_n(k_2\bar{r}) + C_{4n}Y_n(k_2\bar{r}) \quad (33)$$

where

$$k_{1,2} = \sqrt{\frac{n^T - k_g \pm \sqrt{(n^T - k_g)^2 - 4dk_w}}{2d}} \quad (34)$$

**Case 2.**  $n^T - k_g = 2\sqrt{k_w d}$ . For this case, the stability equation has the following exact solution:

$$W_n(\bar{r}) = C_{1n}J_n(k_1\bar{r}) + C_{2n}Y_n(k_1\bar{r}) + C_{3n}\bar{r}J_{n+1}(k_1\bar{r}) + C_{4n}\bar{r}Y_{n+1}(k_1\bar{r}) \quad (35)$$

where

$$k_1 = \sqrt{\frac{n^T - k_g}{2d}} \quad (36)$$

**Case 3.**  $n^T - k_g < 2\sqrt{k_w d}$ . In such condition, the stability equation has the following explicit solution:

$$W_n(\bar{r}) = C_{1n} \left( \frac{J_n(k_1\bar{r}) + J_n(k_2\bar{r})}{2} \right) + C_{2n} \left( \frac{Y_n(k_1\bar{r}) + Y_n(k_2\bar{r})}{2} \right) + C_{3n} \left( \frac{J_n(k_1\bar{r}) - J_n(k_2\bar{r})}{2i} \right) + C_{4n} \left( \frac{Y_n(k_1\bar{r}) - Y_n(k_2\bar{r})}{2i} \right) \quad (37)$$

where

$$k_{1,2} = \sqrt{\frac{n^T - k_g \pm i\sqrt{4dk_w - (n^T - k_g)^2}}{2d}} \quad (38)$$

and  $i$  is the square root of  $-1$ .

**Annular Plate** The buckling criteria for the annular plate may be obtained when boundary conditions are imposed into the deflection equation of the plate. When plate is asymmetrical with respect to the midplane, both inner and outer edges are clamped, and therefore, following conditions have to be satisfied:

$$W_n(1) = \frac{dW_n}{d\bar{r}}(1) = W_n(\beta) = \frac{dW_n}{d\bar{r}}(\beta) = 0 \quad (39)$$

For the case when plate is symmetrical with respect to the midplane, the coefficient  $E_2$  is vanished from the stability equations. Therefore, the nondimensional constant  $d$  is equal to unity. When plate is subjected to uniform temperature rise loading, regardless to the edge support conditions, bifurcation occurs. Each edge may be clamped (C), simply supported (S), or roller (R). The mathematical expressions for this class of edge supports are

$$C : W_n(s) = \frac{dW_n}{d\bar{r}}(s) = 0 \quad (40)$$



$$S : W_n(s) = \frac{d^2 W_n}{d\bar{r}^2}(s) + \frac{\nu}{s} \frac{dW_n}{d\bar{r}}(s) = 0 \quad (41)$$

$$R : \frac{dW_n}{d\bar{r}}(s) = \frac{d^3 W_n}{d\bar{r}^3}(s) + \frac{1}{s} \frac{d^2 W_n}{d\bar{r}^2}(s) + \frac{n^2}{s^3} (3 - \nu) W_n(s) = 0 \quad (42)$$

where  $s$  may be equal to  $\beta$  for the inner edge or equal to unity for the outer edge. For each case of edge supports, imposing the associated mathematical expressions from (40–42) into the proper stability equation (33) or (35) or (37) results in four homogeneous algebraic equations in terms of  $C_{1n}$ ,  $C_{2n}$ ,  $C_{3n}$ , and  $C_{4n}$ . To gain a nontrivial solution, the determinant of the coefficients matrix has to be set equal to zero, which yields a nonlinear equation containing  $n$  and  $n^T$ . Now to find the nondimensional critical buckling loads of the plate  $n_{cr}^T$  for every positive integer number  $n$ , the associated determinant equation has to be solved. Finding the smallest positive root of the associated equation for each  $n$  and choosing the smallest among them yields the associated critical value of  $n^T$ , which is called  $n_{cr}^T$ . Note that since the buckling criteria equation is complicated, closed-form expression cannot be obtained. Nonetheless, following the mentioned procedure,  $n_{cr}^T$  is exactly obtained.

**Circular Plate** For the case of solid circular plate, the solution has to be bonded at the center point. Therefore, in (33) or (35) or (37), both constants  $C_{2n}$  and  $C_{4n}$  are equal to zero. The rest of the methodology is similar to the one established for the annular plate, except that only boundary conditions have to be considered for  $s = 1$ .

When the nondimensional critical load  $n_{cr}^T$  is extracted, critical buckling temperature is obtained similar to the procedure developed in ► [Circular/Annular Plates, Thermal Buckling](#).

## Key Research Findings

Among the extensive parametric studies reported in the open literature, it is obtained that:

- The clamped circular/annular FGM plates, when resting on the Winkler/Pasternak foundation, follow the bifurcation type of buckling. When at least one edge of an FGM plate is immovable simply supported or free, plate exhibits a nonlinear bending at the onset of thermal loading.
- An increase in the Winkler or Pasternak constants of elastic foundation results in higher critical buckling temperature for the plate.
- The Pasternak elastic foundations, when are stiff enough, have great effects on dictating the buckled shape of the plate. The number of nodal diameters depends upon the Winkler constant of elastic foundation. For the circular/annular plates with arbitrary combinations of clamped, simply supported, or roller edges, the shear constant of the elastic foundation has no influence on the number of nodal diameters.
- For circular plates with clamped or simply supported edge, when plate is untethered, symmetrical buckled shape exists. However, for a large range of the Winkler constant of elastic foundation when plate is in contact, it is found that number of nodal diameters fluctuates between zero and unity.
- For the annular/circular FGM plates, power law index of the composition rule has no effect on the number of nodal diameters. For the in-contact plates, however, number of nodal diameters is a function of power law index.

## Cross-References

- [Circular/Annular Plates, Thermal Buckling](#)

## References

1. Laermann KH (1982) The circular plate on elastic foundation under temperature loading. *J Therm Stress* 5:103–114
2. Li SR, Yu WS (2007) Thermal post-buckling and the critical buckling mode transition of heated elastic circular plates on elastic foundation. *Gongcheng Lixue/Eng Mech* 24:63–66
3. Xiao Y, Chang-jun C (1991) Buckling and post-buckling of annular plates on an elastic foundation. *Appl Math Mech* 12:785–797

4. Wang CY (2005) On the buckling of a circular plate on an elastic foundation. *J Appl Mech* 72:795–796
5. Wang CM, Xiang Y, Wang Q (2001) Axisymmetric buckling of Reddy circular plates on pasternak foundation. *J Eng Mech* 127:254–259
6. Yu LH, Wang CY (2010) Buckling mosaic of a circular plate on a partial elastic foundation. *Struct Eng Mech* 34:135–138
7. Yu LH, Wang CY (2009) Buckling mosaic of concentrically hinged or cracked circular plates on elastic foundation. *AIAA J* 47:2253–2255
8. Gupta US, Ansari AH, Sharma S (2006) Buckling and vibration of polar orthotropic circular plate resting on Winkler foundation. *J Sound Vib* 297:457–476
9. Gupta US, Lal R, Jain SK (1991) Buckling and vibrations of polar orthotropic circular plates of linearly varying thickness resting on an elastic foundation. *J Sound Vib* 147:423–434
10. Paliwal DN, Pathak RS (2003) Free vibrations and stability of orthotropic plates on a Pasternak foundation. *J Struct Eng (Madras)* 29:195–203
11. Rao GV, Raju KK (1986) A study of various effects on the stability of circular plates. *Comput Struct* 24:39–45
12. Raju KK, Rao GV (1984) Post-buckling of cylindrically orthotropic circular plates on elastic foundation with edges elastically restrained against rotation. *Comput Struct* 18:1183–1187
13. Kline LV, Peck CC (1967) Nature of roots occurring in buckling equations for circular plates on elastic foundations. *J Frankl Inst* 284:326–329
14. Reddy JN (2003) *Mechanics of laminated plates and shells: theory and analysis*. CRC Press, Boca Raton
15. Hetnarski RB, Eslami MR (2009) *Thermal stresses advanced theory and applications*. Springer, Berlin
16. Brush DO, Almorth BO (1975) *Buckling of bars plates and shells*. McGraw-Hill, New York
17. Wang CM, Wang CY, Reddy JN (2004) *Exact solutions for buckling of structural members*. CRC Press, Boca Raton

## Effects of Ring Supports on Thermo-Elastic Buckling of Circular Plate

Yasser Kiani and Mohammad Reza Eslami  
Department of Mechanical Engineering,  
Amirkabir University of Technology,  
Tehran, Iran

### Definition

When a circular plate is subjected to thermal loading and boundaries are immovable, buckling

phenomenon may occur. As one of the main conventional ideas to postpone the bifurcation point of the plate, intermediate ring supports are proposed. The case of a symmetrical ring support is examined, and plate is subjected to symmetrical thermal loading. Asymmetrical eigenvalue analysis of stability equations is developed to extract the critical buckling temperature and buckled shape of the plate.

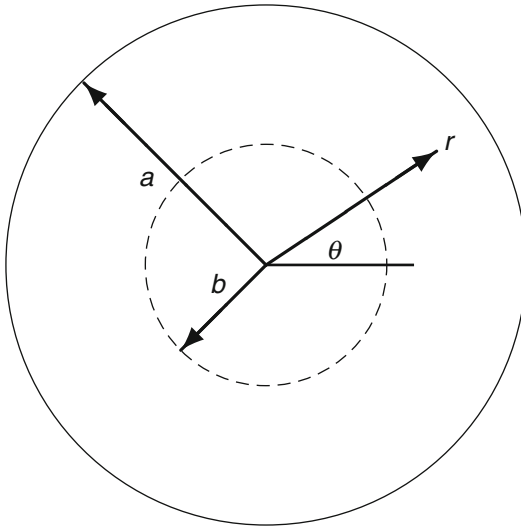
### Overview

The problem of buckling of circular plate with intermediate ring support is well reported in the literature. Most of these works deal with the case of uniformly compressed plate along outer radial edge. Various effects are discussed through these studies. There are a class of publications which are developed under the assumption of axisymmetrical deformations of the plate. In this case, one may refer to the exact solution of Wang et al. [1] which is developed based on Mindlin plate theory or the study of Laura et al. [2] which considers both annular and solid circular plates. Some of the newly reported studies consider the asymmetrical deformations of the plate under the symmetrical loading type. In some of these works, intermediate ring support is assumed to be elastic, and boundary conditions are considered in the general type of elastically restrained edge [3–6]. Wang et al. [7] modified the problem of the buckling of a plate over an intermediate elastic ring and concluded that there are differences between Mindlin and Kirchhoff theories in number of nodal diameters of the plate in buckling state in a very slight domain of ring position.

### Theory

#### Basic Equations

Consider a circular plate with thickness  $h$  and outer radii  $a$ , located on a centric intermediate ring support with radius  $b$  referred to the polar coordinates  $(r, \theta, z)$  as shown in Fig. 1. Plate is made from a homogeneous isotropic material with Young's modulus  $E$ , coefficient of thermal expansion  $\alpha$ , and Poisson's ratio  $\nu$ .



**Effects of Ring Supports on Thermo-Elastic Buckling of Circular Plate, Fig. 1** Schematic of a circular plate located over an intermediate ring support

Stability equation of the beam, in such a case, is represented in terms of only the out-of-plane component of the displacement field,  $w_0$  as (see ► [Circular/Annular Plates, Thermal Buckling](#)).

$$D \left( w_{0,rrrr} + \frac{2}{r} w_{0,rrr} - \frac{1}{r^2} w_{0,rr} + \frac{1}{r^3} w_{0,r} + \frac{2}{r^2} w_{0,rr\theta\theta} - \frac{2}{r^3} w_{0,r\theta\theta} + \frac{4}{r^4} w_{0,\theta\theta} + \frac{1}{r^4} w_{0,\theta\theta\theta\theta} \right) - N_{rr}^0 w_{0,rr} - N_{\theta\theta}^0 \left( \frac{1}{r^2} w_{0,\theta\theta} + \frac{1}{r} w_{0,r} \right) - 2N_{r\theta}^0 \left( \frac{1}{r} w_{0,r\theta} - \frac{1}{r^2} w_{0,\theta} \right) = 0 \quad (1)$$

where  $D = \frac{Eh^3}{12(1-\nu^2)}$  is the flexural rigidity of plate and terms with superscripts zero indicate the prebuckling state of the plate.

Here, the case of a uniformly distributed temperature across the whole domain of the plate is considered. In this case, when edges are immovable along radial direction, in-plane loads are generated. Since plate is isotropic and homogeneous, no thermal moments are produced under uniform temperature rise loading. As discussed in ► [Circular/Annular Plates, Thermal Buckling](#), in

such conditions, prebuckling state of the plate is totally without deformation. On the other hand, all, radial, circumferential, and transverse, components of displacement are equal to zero. Prebuckling force resultants of the plate are (see ► [Circular/Annular Plates, Thermal Buckling](#))

$$N_{rr}^0 = N_{\theta\theta}^0 = -\frac{1}{1-\nu} h E \alpha \Delta T, \quad N_{r\theta}^0 = 0 \quad (2)$$

When the prebuckling force resultants are inserted into (1), we may reach to

$$D \nabla^4 w_0 + \frac{1}{1-\nu} h E \alpha \Delta T \nabla^2 w_0 = 0 \quad (3)$$

For the sake of generality and simplicity, following nondimensional parameters are introduced:

$$\bar{r} = \frac{r}{a}, \beta = \frac{b}{a}, \delta = \frac{h}{a}, \mu^2 = \frac{12(1+\nu)\alpha\Delta T}{\delta^2} \quad (4)$$

Besides, for the case when a circular plate is located on an intermediate ring support with nondimensional radius  $\bar{r} = \beta$ , the circular plate may be divided into two new domains: the interior domain which consists of a circular plate with nondimensional radius  $\bar{r} = \beta$  and the exterior domain which is an annular plate with inner radii  $\bar{r} = \beta$  and outer radii  $\bar{r} = 1$ . To consider the asymmetrical shape of the plate in buckled state, buckling shape of the plate is written as

$$w_0(r, \theta) = W(\bar{r}) \cos(n\theta) \quad (5)$$

here  $-n$  is the number of nodal diameters.  $n = 0$  represents the symmetrical buckled state, and asymmetrical buckled states are indicated as  $n > 0$ . When (4) and (5) are inserted into the (3), the exact solution of the stability equation for the inner circular domain may be written in the following exact closed-form solution:

$$W_n^c(\bar{r}) = C_{1n} J_n(\mu \bar{r}) + C_{2n} Y_n(\mu \bar{r}) + C_{3n} \bar{r}^n + C_{4n} \left\{ \frac{Ln \bar{r}}{\bar{r}^{-n}} \right\} \quad (6)$$

And similarly, for the case when the solution of the annular plate is of interest, we may write

$$W_n^a(\bar{r}) = C_{5n}J_n(\mu\bar{r}) + C_{6n}Y_n(\mu\bar{r}) + C_{7n}\bar{r}^n + C_{8n}\left\{\frac{Ln\bar{r}}{\bar{r}^{-n}}\right\} \quad (7)$$

In each of the two above equations, the top form stands as the symmetrical case of buckling, and the bottom one is the asymmetrical buckling.

Where constants of the above equations are determined when the finiteness conditions, boundary condition of the inner ring and conditions of the outer edge are imposed into the above equations. These conditions are:

- Finiteness conditions at the center point of the circular plate which results in

$$C_{2n} = C_{4n} = 0 \quad (8)$$

- Deflection at the intermediate ring support according to the deflection solution of the circular plate should be vanished, which results in

$$C_{1n}J_n(\mu\beta) + C_{3n}\beta^n = 0 \quad (9)$$

- Deflection at the intermediate ring support according to the deflection solution of the annular plate should be vanished, which results in

$$C_{5n}J_n(\mu\beta) + C_{6n}Y_n(\mu\beta) + C_{7n}\beta^n + C_{8n}\left\{\frac{Ln\beta}{\beta^{-n}}\right\} = 0 \quad (10)$$

- Continuity of the slope at the position of the intermediate ring supports according to two distinct solutions, which gives us

$$C_{5n}\mu J_n'(\mu\beta) + C_{6n}\mu Y_n'(\mu\beta) + C_{7n}n\beta^{n-1} + C_{8n}\left\{\frac{\beta^{-1}}{-n\beta^{-n-1}}\right\} = C_{1n}\mu J_n'(\mu\beta) + C_{3n}n\beta^{n-1} \quad (11)$$

- Continuity of the moment at the position of the intermediate ring supports according to two distinct solutions. This condition simplifies to

continuity of the curvature with consideration of the continuity of the slope and vanishment of the deflection at ring position. The curvature continuity may be written as

$$\begin{aligned} & C_{5n}\mu^2 J_n''(\mu\beta) + C_{6n}\mu^2 Y_n''(\mu\beta) + C_{7n}n(n-1)\beta^{n-2} \\ & + C_{8n}\left\{\frac{-\beta^{-2}}{n(n+1)\beta^{-n-2}}\right\} \\ & = C_{1n}\mu^2 J_n''(\mu\beta) + C_{3n}n(n-1)\beta^{n-2} \end{aligned} \quad (12)$$

- At the outer edge,  $\bar{r} = 1$ , deflection should be vanished, that is,

$$C_{5n}J_n(\mu) + C_{6n}Y_n(\mu) + C_{7n} + C_{8n}\left\{\frac{0}{1}\right\} = 0 \quad (13)$$

- At the outer edge,  $\bar{r} = 1$ , depending on the type of boundary condition, slope (for clamped edge) or moment (for simply supported edge) should be vanished. These two conditions may be unified in the form  $W_n^{a''} + (v+c)W_n^{a'} = 0$ , where the case of  $c = 0$  represents the net zero radial moment (associated with simply supported edge) and the case  $c = \infty$  represents the zero slope condition (associated with clamped edge). This condition in mathematical form is written as

$$\begin{aligned} & C_{5n}(\mu^2 J_n''(\mu) + \mu(v+c)J_n'(\mu)) \\ & + C_{6n}(\mu^2 Y_n''(\mu) + \mu(v+c)Y_n'(\mu)) \\ & + C_{7n}n(n-1+v+c) \\ & + C_{8n}\left\{\frac{v+c-1}{n^2+n-n(v+c)}\right\} = 0 \end{aligned} \quad (14)$$

Recalling (9–14), a system of homogeneous equations is obtained. Treating this system as an eigenvalue problem results in a transcendental equation which itself contains both number of nodal diameters,  $n$ , and thermal parameter,  $\mu$ . For each value of number of nodal diameters, this equation has to be solved using a simple search root technique which results in the roots of the equation. For each  $n$ , the minimum positive root is assumed to be  $\mu_{cr}^n$ . Collecting the

minimum value among all the parameters  $\mu_{cr}^n$  results in the critical buckling temperature parameter, and the number of nodal diameters is then obtained accordingly.

## Key Research Findings

- In general, plates that are rest over an intermediate ring support buckle in higher temperatures when are compared with their contact-less conditions.
- For each type of boundary condition, there exists an optimum location for the position of the intermediate ring. The criterion for the position of the ring to be optimum is the maximum increase percentage of the critical buckling temperature with respect to the contact-less conditions. For the case of simply supported plates ( $\nu = 0.3$ ), the optimum position of the ring is  $\beta_{opt} = 0.463$  and for the case of clamped plates,  $\beta_{opt} = 0.265$
- It is worth mentioning that an intermediate ring support may increase the number of nodal diameters. Both simply supported and clamped plates when are without contact with intermediate ring buckle firstly in a symmetrical manner. When an intermediate ring is in contact with plate, and is located at center, plate buckles in an asymmetrical manner, where the number of nodal diameters is equal to unity. As the  $\beta$  increases, the asymmetrical buckled shape with unit number of nodal diameters persists until a prescribed radii. After that, symmetrical buckling occurs until ring is reached at  $\bar{r} = 1$ .

## Cross-References

- [Circular/Annular Plates, Thermal Buckling](#)

## References

1. Wang CM, Xiang Y, Kitipornchai S, Liew KM (1993) Axisymmetric buckling of circular mindlin plates with ring supports. *J Struct Eng* 119:782–793

2. Laura PAA, Gutierrez RH, Sanzi HC, Elvira G (2000) Buckling of circular, solid and annular plates with an intermediate circular support. *Ocean Eng* 27:749–755
3. Wang CY, Wang CM (2001) Buckling of circular plates with an internal ring support and elastically restrained edges. *Thin wall Struct* 39:821–825
4. Wang CY (2003) Buckling of a circular plate with internal elastic ring support. *Mech Base Des Struct Mach* 31:93–102
5. Rao LB, Rao CK (2010) Buckling analysis of circular plates with elastically restrained edges and resting on internal elastic ring support. *Mech Base Des Struct Mach* 38:440–452
6. Rao LB, Rao CK (2009) Buckling of circular plates with an internal elastic ring support and elastically restrained guided edge. *Mech Base Des Struct Mach* 37:60–72
7. Wang CM, Aung TM (2005) Buckling of circular mindlin plates with an internal ring support and elastically restrained edge. *J Eng Mech* 131:359–366

## Eigenstrains in Thermal Stresses

Masayuki Ishihara

Osaka Prefecture University, Naka-ku, Sakai, Japan

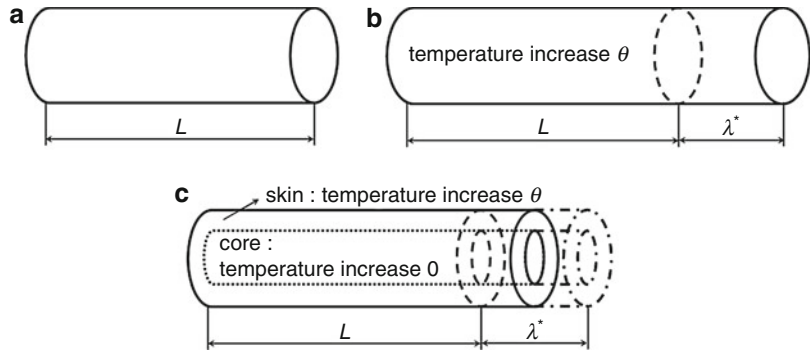
## Overview

Eigenstrains are the strains that do not induce stresses if they are distributed uniformly in a homogeneous body that is free from any external forces and surface constraints. Concrete examples of eigenstrains are free thermal expansions, hygroscopic expansions, piezoelectric deformations, phase transformations, plastic deformations, etc. With regard to thermal stresses, the most important form of eigenstrain is the free thermal expansion that occurs because of temperature changes in the body. In this entry, free thermal expansion in a body is considered as a form of eigenstrains.

First, the concept of eigenstrains is explained by considering the example of free thermal expansion and by generalizing this phenomenon. Next, the governing equations of the elastic field in a body having an arbitrary distribution of eigenstrains are presented, and the general solutions for the field are derived.

### Eigenstrains in Thermal Stresses, Fig. 1

Bar subjected to increase in temperature. (a) Original shape, (b) uniform temperature increase, (c) local temperature increase



For a body that has a subdomain with distributed eigenstrains, the subdomain is often referred to as an inclusion. This entry also discusses the problems of an infinite body with an ellipsoidal inclusion; these problems form the foundations of micromechanics.

where  $\beta$  denotes the coefficient of hygroscopic expansion. Further, if the bar exhibits piezoelectricity, the uniform electric field  $E_{\text{electric}}$  applied longitudinally or transversely will induce a strain described as

$$\varepsilon^* = dE_{\text{electric}} \quad (4)$$

### Eigenstrains

Eigenstrains are the strains that do not induce stresses if they are distributed uniformly in a homogeneous body that is free from any external forces and surface constraints. Consider a homogeneous bar, shown in Fig. 1a, that is free from any external forces and surface constraints.  $\alpha$ ,  $E$ , and  $L$  denote the coefficient of linear thermal expansion, the Young's modulus, and the length of the bar, respectively. When the bar is subjected to a uniform temperature increase  $\theta$ , it elongates freely, as shown in Fig. 1b, with strain and elongation described, respectively, as

$$\varepsilon^* = \alpha\theta \quad (1)$$

and

$$\lambda^* = \alpha\theta L \quad (2)$$

Other sources may induce such a strain. For instance, if the bar is hygroscopic, a uniform increase in moisture  $\Delta C$  will induce a strain described as

$$\varepsilon^* = \beta\Delta C \quad (3)$$

where  $d$  denotes the piezoelectric constant. Phase transformations and plastic deformations also induce normal and/or shear strains because they involve microstructural changes.

As mentioned above, the definition of eigenstrains assumes that the sources of the strains are distributed uniformly. In reality, however, such a situation is not often encountered, as the body under discussion usually contains localized sources of eigenstrains. In order to discuss the effect of the strains on the body in such a case, let us consider that the bar shown in Fig. 1a is subjected to a temperature increase  $\theta$  that is restricted to the skin with some thickness. For a body without the unheated core, the heated skin would have strain and elongation described by (1) and (2), respectively. On the other hand, for a body without the heated skin, the unheated core would not have strain and elongation. As the skin and the core are continuous, the magnitude of the resulting strain in the skin should stabilize at a value between zero and the value given by (1), as shown in Fig. 1c. In other words, the resulting strain in the skin,  $\varepsilon$ , is different from the eigenstrain  $\varepsilon^*$  itself, by the amount  $e$ , and is given by

$$\varepsilon = \varepsilon^* + e \quad (5)$$

The amount  $e$  is due to the reaction of the core on the skin, which is represented by the stress  $\sigma$ . If the bar is linearly elastic, the amount  $e$  is related to the stress  $\sigma$  through Hooke's law by the equation

$$\sigma = Ee \quad (6)$$

where  $E$  denotes Young's modulus. It should be noted that, following convention, the stress  $\sigma$  is assumed to be positive when the reaction is tensile and that, in the case shown in Fig. 1c,  $\sigma$  is actually negative. By substituting (6) into (5),

$$\varepsilon = \frac{\sigma}{E} + \varepsilon^* \quad (7)$$

from which the total strain  $\varepsilon$  can be interpreted to be the sum of the elastic strain  $\sigma/E$  and eigenstrain  $\varepsilon^*$ . Also, (7) can be rewritten as

$$\sigma = E(\varepsilon - \varepsilon^*) \quad (8)$$

from which we may infer that the stress  $\sigma$  is linearly related to the value of the total strain, less the eigenstrain  $\varepsilon^*$ .

Although equations (5) through (8) are derived only for the case of normal stress and strain, it can be extended to general three-dimensional cases as follows. Namely, the total strains  $\varepsilon_{ij}$  are different from the eigenstrains  $\varepsilon_{ij}^*$  by the amounts  $e_{ij}$  as

$$\varepsilon_{ij} = \varepsilon_{ij}^* + e_{ij} \quad (9)$$

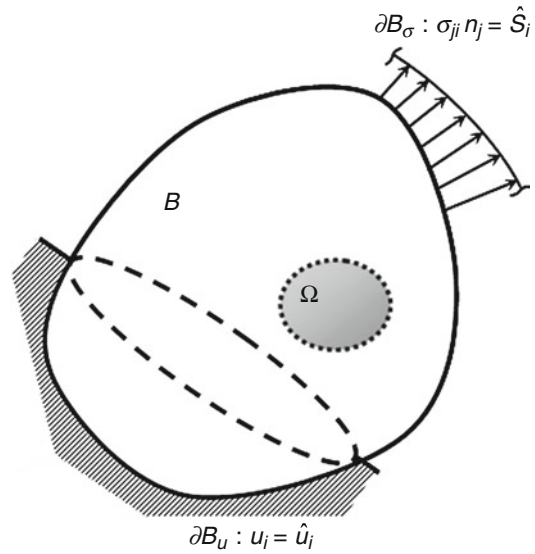
and, for a linearly elastic body, the amounts  $e_{ij}$  are referred to as elastic strains and are related to the stresses  $\sigma_{ij}$  through the elastic constants  $C_{ijkl}$  by the equation

$$\sigma_{ij} = C_{ijkl}e_{kl} \quad (10)$$

which gives us

$$\sigma_{ij} = C_{ijkl}(\varepsilon_{kl} - \varepsilon_{kl}^*) \quad (11)$$

Please note that all the components discussed in this entry are in the Cartesian coordinate system.



**Eigenstrains in Thermal Stresses, Fig. 2** Body with eigenstrains

## Elastic Fields Due to Eigenstrains

### Governing Equations

The governing equations of the elastic field in a body having an arbitrary distribution of eigenstrains are presented in this subsection.

Consider an elastic body  $B$  that contains a subdomain  $\Omega$  with an arbitrary distribution of eigenstrains, as shown in Fig. 2. From (9),

$$\left. \begin{aligned} e_{ij} &= \varepsilon_{ij} - \varepsilon_{ij}^* : \text{ in } \Omega, \\ e_{ij} &= \varepsilon_{ij} : \text{ in } B - \Omega \end{aligned} \right\} \quad (12)$$

Then, from (10), we can derive

$$\left. \begin{aligned} \sigma_{ij} &= C_{ijkl}e_{kl} = C_{ijkl}(\varepsilon_{kl} - \varepsilon_{kl}^*) : \text{ in } \Omega, \\ \sigma_{ij} &= C_{ijkl}e_{kl} = C_{ijkl}\varepsilon_{kl} : \text{ in } B - \Omega \end{aligned} \right\} \quad (13)$$

Moreover, as shown in Fig. 2, let body  $B$  be subject to surface tractions per unit area,  $\hat{s}_i$ , on  $\partial B_\sigma$ , a part of surface  $\partial B$ , and be constrained at prescribed displacements  $\hat{u}_i$  on the rest of  $\partial B$ , denoted as  $\partial B_u$ . Then, we obtain

$$\sigma_{ji}n_j = \hat{s}_i \text{ on } \partial B_\sigma; \quad u_i = \hat{u}_i \text{ on } \partial B_u \quad (14)$$



where  $n_j$  denotes the components of the unit vector normal to  $\partial B_\sigma$ . Since the total strains must be compatible [1], we get

$$\varepsilon_{ij} = \frac{1}{2}(u_{i,j} + u_{j,i}) \quad (15)$$

where  $u_i$  denote the displacements and infinitesimal strains are under consideration. Moreover, since the forces acting on the body must achieve equilibrium [1], we have

$$\sigma_{ji,j} + f_i = 0 \quad (16)$$

$$\sigma_{ij} = \sigma_{ji} \quad (17)$$

where  $f_i$  denote the components of body force per unit volume. It should be noted that, by considering (13), (15), and (17), the properties of elastic constants are obtained as

$$C_{ijkl} = C_{jikl} = C_{ijlk} \quad (18)$$

Thus, the elastic field of the body in question is obtained as the solution to (12) through to (18). Sometimes, the equilibrium equations in terms of displacements are used instead of (16), which are derived by substituting (15) into (13) and also considering (18), to get

$$\left. \begin{aligned} \sigma_{ij} &= C_{ijkl}(u_{k,l} - \varepsilon_{kl}^*) : \text{ in } \Omega, \\ \sigma_{ij} &= C_{ijkl}u_{k,l} : \text{ in } B - \Omega \end{aligned} \right\} \quad (19)$$

By substituting (19) into (16) and also considering (18), we get the results

$$\left. \begin{aligned} C_{ijkl}u_{k,lj} &= C_{ijkl}\varepsilon_{kl,j}^* - f_i : \text{ in } \Omega, \\ C_{ijkl}u_{k,lj} &= -f_i : \text{ in } B - \Omega \end{aligned} \right\} \quad (20)$$

also known as Navier's equations.

Next, the elastic strain energy of the body shown in Fig. 2, which needs to be obtained in some situations, is discussed. For the body, the elastic strain energy density  $U_0$  [1] is

$$U_0 = \frac{1}{2}\sigma_{ij}\varepsilon_{ij} \quad (21)$$

which is defined as the work done by external forces through elastic deformation, that is, the deformation with respect to the stress-free state in the presence of eigenstrains. By substituting (13) into (21), we have

$$U_0 = \frac{1}{2}C_{ijkl}\varepsilon_{ij}\varepsilon_{kl} = \frac{1}{2}C_{klij}\varepsilon_{kl}\varepsilon_{ij} \quad (22)$$

where the right-hand side is obtained by exchanging the dummy indices. It should be noted that, by differentiating (22) with  $\varepsilon_{ij}$  and  $\varepsilon_{kl}$ , the properties of elastic constants are obtained as

$$C_{ijkl} = C_{klij} \quad (23)$$

From (12) and (25), the elastic strain energy stored in body  $B$  is calculated as

$$\left. \begin{aligned} U &= \int_B U_0 dv = \int_B \frac{1}{2}\sigma_{ij}\varepsilon_{ij} dv \\ &= \int_\Omega \frac{1}{2}\sigma_{ij}(\varepsilon_{ij} - \varepsilon_{ij}^*) dv + \int_{B-\Omega} \frac{1}{2}\sigma_{ij}\varepsilon_{ij} dv \\ &= \int_B \frac{1}{2}\sigma_{ij}\varepsilon_{ij} dv - \int_\Omega \frac{1}{2}\sigma_{ij}\varepsilon_{ij}^* dv \end{aligned} \right\} \quad (24)$$

where  $dv$  denotes volume elements. By considering (15) and (17), the first term in the right side of (24) can be rewritten as

$$\left. \begin{aligned} \int_B \frac{1}{2}\sigma_{ij}\varepsilon_{ij} dv &= \int_B \frac{1}{2}\sigma_{ij} \cdot \frac{1}{2}(u_{i,j} + u_{j,i}) dv \\ &= \int_B \frac{1}{2}\sigma_{ij}u_{i,j} dv \end{aligned} \right\} \quad (25)$$

Moreover, by adding (16) to the integrand, the right-hand side of (25) becomes

$$\left. \begin{aligned} &\int_B \frac{1}{2}\sigma_{ij}u_{i,j} dv \\ &= \int_B \frac{1}{2}[\sigma_{ij}u_{i,j} + (\sigma_{ji,j} + f_i)u_i] dv \\ &= \int_B \frac{1}{2}(\sigma_{ji}u_i)_{,j} dV + \int_B \frac{1}{2}f_i u_i dv \end{aligned} \right\} \quad (26)$$



Then, by considering Gauss's divergence theorem and Cauchy's relation [1], the first term in the right-hand side of (26) can be rewritten as

$$\int_B \frac{1}{2} (\sigma_{ji} u_i)_{,j} dv = \int_{\partial B} \frac{1}{2} \sigma_{ji} u_i n_j da = \int_{\partial B} \frac{1}{2} s_i u_i da \quad (27)$$

where  $da$  denotes area elements,  $s_i$  the components of surface traction per unit area, and  $n_i$  the outward normal to surface  $\partial B$ . Thus, from (24) through to (27), one has

$$U = \int_{\partial B} \frac{1}{2} s_i u_i da + \int_B \frac{1}{2} f_i u_i dv - \int_{\Omega} \frac{1}{2} \sigma_{ij} \varepsilon_{ij}^* dv \quad (28)$$

When the body is free from surface tractions and body forces, (28) becomes

$$U = - \int_{\Omega} \frac{1}{2} \sigma_{ij} \varepsilon_{ij}^* dv \quad (29)$$

It is worth stating that, from (29), the elastic strain energy stored in the whole body  $B$  can be obtained from the field restricted to the subdomain denoted by  $\Omega$ , which shows the presence of eigenstrains.

### General Solutions

In this subsection, the general solutions of the elastic field in an infinite body with a periodic or an arbitrary distribution of eigenstrains that is free from any external forces and surface constraints are presented.

#### Periodic Distribution

Here, the case of a periodic distribution of eigenstrains is treated. The periodic distribution may seem unrealistic, since the distribution is generally considered to be arbitrary. The case treated here is, however, important in the sense that an arbitrary distribution can be decomposed into periodic distributions with various wavelengths (or wave numbers) by use of the Fourier transform.

Let us consider a periodic distribution of eigenstrains as

$$\varepsilon_{ij}^*(\mathbf{x}) = \bar{\varepsilon}_{ij}^*(\boldsymbol{\xi}) \exp(i\boldsymbol{\xi} \cdot \mathbf{x}) \quad (30)$$

where  $\mathbf{x}$  denotes the position in the body;  $\boldsymbol{\xi}$  denotes the wave number vector whose direction and magnitude are the normal to the wave surfaces and the wave number (related to wavelength  $\lambda$  as  $|\boldsymbol{\xi}| = 2\pi/\lambda$ ), respectively;  $\bar{\varepsilon}_{ij}^*(\boldsymbol{\xi})$  denotes the amplitude of the wave; and  $i = \sqrt{-1}$ . It should be noted that only the real part of (30) is actually observed, and the complex form is employed in order to simplify the following calculations. Further, the eigenstrains described by (30) are distributed throughout the infinite body. The displacements due to the eigenstrains may also be expressed as

$$u_i(\mathbf{x}) = \bar{u}_i(\boldsymbol{\xi}) \exp(i\boldsymbol{\xi} \cdot \mathbf{x}) \quad (31)$$

By substituting (31) into (20) in the absence of body forces, we get

$$C_{ijkl} \bar{u}_k \bar{\varepsilon}_{jl}^* = -i C_{ijkl} \bar{\varepsilon}_{kl}^* \bar{\varepsilon}_{ij}^* \quad (32)$$

By using notations

$$K_{ik} \equiv C_{ijkl} \bar{\varepsilon}_{jl}^*, \quad X_i \equiv -i C_{ijkl} \bar{\varepsilon}_{kl}^* \bar{\varepsilon}_{ij}^* \quad (33)$$

Equation (32) is rewritten as

$$\begin{bmatrix} K_{11} & K_{12} & K_{13} \\ K_{21} & K_{22} & K_{23} \\ K_{31} & K_{32} & K_{33} \end{bmatrix} \begin{Bmatrix} \bar{u}_1 \\ \bar{u}_2 \\ \bar{u}_3 \end{Bmatrix} = \begin{Bmatrix} X_1 \\ X_2 \\ X_3 \end{Bmatrix} \quad (34)$$

Equation (34) represents three equations in three unknowns  $\bar{u}_1$ ,  $\bar{u}_2$ , and  $\bar{u}_3$ , and can be solved easily as

$$\bar{u}_i(\boldsymbol{\xi}) = N_{ji}(\boldsymbol{\xi}) X_j / D(\boldsymbol{\xi}) \quad (35)$$

where  $N_{ij}(\boldsymbol{\xi})$  and  $D(\boldsymbol{\xi})$  denote the  $(i,j)$ -cofactor and the determinant of the coefficient matrix in (34). It should be noted that, from (18), (23), and (33),

$$K_{ij} = K_{ji}, \quad N_{ij} = N_{ji} \quad (36)$$

By substituting (35) into (31), the solutions for the displacements are obtained as

$$u_i(\mathbf{x}) = -iC_{jlmn}\bar{e}_{mn}^*(\xi)\xi_l N_{ji}(\xi)D^{-1}(\xi)\exp(i\xi \cdot \mathbf{x}) \quad (37)$$

The corresponding strains and stresses are obtained by substituting (37) into (15) and (19) which gives us

$$\varepsilon_{ij}(\mathbf{x}) = \frac{1}{2}C_{klmn}\bar{e}_{mn}^*(\xi)\xi_l [\xi_j N_{ki}(\xi) + \xi_i N_{kj}(\xi)] \times D^{-1}(\xi)\exp(i\xi \cdot \mathbf{x}) \quad (38)$$

and

$$\sigma_{ij}(\mathbf{x}) = C_{ijkl} [C_{pqmn}\bar{e}_{mn}^*(\xi)\xi_q \xi_l N_{pk}(\xi)D^{-1}(\xi) - \bar{e}_{kl}^*(\xi)] \exp(i\xi \cdot \mathbf{x}) \quad (39)$$

respectively.

#### Arbitrary Distribution

In this subsection, the case of an arbitrary distribution of eigenstrains is treated.

Let us consider an arbitrary distribution of eigenstrains expressed by the Fourier integral form [2] as

$$\bar{e}_{ij}^*(\mathbf{x}) = \int_{-\infty}^{\infty} \bar{e}_{ij}^*(\xi)\exp(i\xi \cdot \mathbf{x})d\xi \quad (40)$$

where

$$\bar{e}_{ij}^*(\xi) = (2\pi)^{-3} \int_{-\infty}^{\infty} \bar{e}_{ij}^*(\mathbf{x})\exp(-i\xi \cdot \mathbf{x})d\mathbf{x} \quad (41)$$

and

$$\left. \begin{aligned} \int_{-\infty}^{\infty} d\xi &\equiv \int_{-\infty}^{\infty} d\xi_1 \int_{-\infty}^{\infty} d\xi_2 \int_{-\infty}^{\infty} d\xi_3 \\ \int_{-\infty}^{\infty} d\mathbf{x} &\equiv \int_{-\infty}^{\infty} dx_1 \int_{-\infty}^{\infty} dx_2 \int_{-\infty}^{\infty} dx_3 \end{aligned} \right\} \quad (42)$$

By comparing (30) and (40), it is found that  $\bar{e}_{ij}^*(\xi)$  in (40) denote the densities in  $\xi$ -space of the

amplitude. From (40), the displacements due to the eigenstrains may be expressed as

$$u_i(\mathbf{x}) = \int_{-\infty}^{\infty} \bar{u}_i^*(\xi)\exp(i\xi \cdot \mathbf{x})d\xi \quad (43)$$

The solutions of displacements  $u_i(\mathbf{x})$ , strains  $\varepsilon_{ij}(\mathbf{x})$ , and stresses  $\sigma_{ij}(\mathbf{x})$  can be obtained in a similar manner, as shown in Subsubsection **Periodic Distribution**, and the results are as follows:

$$\left. \begin{aligned} u_i(\mathbf{x}) &= \\ -i \int_{-\infty}^{\infty} C_{jlmn}\bar{e}_{mn}^*(\xi)\xi_l N_{ji}(\xi)D^{-1}(\xi)\exp(i\xi \cdot \mathbf{x})d\xi \end{aligned} \right\} \quad (44)$$

$$\left. \begin{aligned} \varepsilon_{ij}(\mathbf{x}) &= \frac{1}{2} \int_{-\infty}^{\infty} C_{klmn}\bar{e}_{mn}^*(\xi) \\ &\times \xi_l [\xi_j N_{ki}(\xi) + \xi_i N_{kj}(\xi)]D^{-1}(\xi)\exp(i\xi \cdot \mathbf{x})d\xi \end{aligned} \right\} \quad (45)$$

and

$$\left. \begin{aligned} \sigma_{ij}(\mathbf{x}) &= C_{ijkl} \int_{-\infty}^{\infty} [C_{pqmn}\bar{e}_{mn}^*(\xi) \\ &\times \xi_q \xi_l N_{pk}(\xi)D^{-1}(\xi) - \bar{e}_{kl}^*(\xi)] \exp(i\xi \cdot \mathbf{x})d\xi \end{aligned} \right\} \quad (46)$$

Furthermore, by substituting (41) into (44), (45), and (46), we get

$$\left. \begin{aligned} u_i(\mathbf{x}) &= -i(2\pi)^{-3} \int_{-\infty}^{\infty} \int_{-\infty}^{\infty} C_{jlmn}\bar{e}_{mn}^*(\mathbf{x}')\xi_l N_{ji}(\xi) \\ &\times D^{-1}(\xi)\exp[i\xi \cdot (\mathbf{x} - \mathbf{x}')]d\xi d\mathbf{x}' \\ &= -(2\pi)^{-3} \frac{\partial}{\partial x_l} \int_{-\infty}^{\infty} \int_{-\infty}^{\infty} C_{jlmn}\bar{e}_{mn}^*(\mathbf{x}')N_{ji}(\xi) \\ &\times D^{-1}(\xi)\exp[i\xi \cdot (\mathbf{x} - \mathbf{x}')]d\xi d\mathbf{x}' \end{aligned} \right\} \quad (47)$$

$$\left. \begin{aligned} \varepsilon_{ij}(\mathbf{x}) &= (2\pi)^{-3} \int_{-\infty}^{\infty} \int_{-\infty}^{\infty} \frac{1}{2} C_{klmn}\bar{e}_{mn}^*(\mathbf{x}') \\ &\times \xi_l [\xi_j N_{ki}(\xi) + \xi_i N_{kj}(\xi)]D^{-1}(\xi) \\ &\times \exp[i\xi \cdot (\mathbf{x} - \mathbf{x}')]d\xi d\mathbf{x}' \end{aligned} \right\} \quad (48)$$

and

$$\left. \begin{aligned} \sigma_{ij}(\mathbf{x}) &= C_{ijkl}(2\pi)^{-3} \\ &\times \int_{-\infty}^{\infty} \int_{-\infty}^{\infty} [C_{pqmn}\varepsilon_{mn}^*(\mathbf{x}')\xi_q\xi_l N_{pk}(\xi)D^{-1}(\xi) \\ &\quad - \varepsilon_{kl}^*(\mathbf{x}')] \exp[i\xi \cdot (\mathbf{x} - \mathbf{x}')] d\xi d\mathbf{x}' \end{aligned} \right\} \quad (49)$$

### Green Functions

Here, the general solutions presented in Subsubsection [Arbitrary Distribution](#) are represented by the Green functions.

#### Definition and Interpretation

By inspecting the integrand in the right-hand side of (47),  $\varepsilon_{mn}^*(\mathbf{x}')$  or  $C_{jlmn}\varepsilon_{mn}^*(\mathbf{x}')$  can be viewed as the sources that induce the displacements  $u_i(\mathbf{x})$ , because, in the absence of eigenstrains, these factors vanish while other components of the equation do not. After obtaining these components, new functions  $G_{ij}(\mathbf{x} - \mathbf{x}')$  are defined as

$$\left. \begin{aligned} G_{ij}(\mathbf{x} - \mathbf{x}') &= (2\pi)^{-3} \int_{-\infty}^{\infty} N_{ji}(\xi)D^{-1}(\xi) \exp[i\xi \cdot (\mathbf{x} - \mathbf{x}')] d\xi \end{aligned} \right\} \quad (50)$$

By substituting (50) into (47), one has

$$u_i(\mathbf{x}) = - \int_{-\infty}^{\infty} C_{jlmn}\varepsilon_{mn}^*(\mathbf{x}') G_{ij,l}(\mathbf{x} - \mathbf{x}') d\mathbf{x}' \quad (51)$$

The corresponding strains and stresses are obtained by substituting (51) into (15) and (19) as

$$\left. \begin{aligned} \varepsilon_{ij}(\mathbf{x}) &= -\frac{1}{2} \int_{-\infty}^{\infty} C_{klmn}\varepsilon_{mn}^*(\mathbf{x}') \\ &\times [G_{ik,lj}(\mathbf{x} - \mathbf{x}') + G_{jk,li}(\mathbf{x} - \mathbf{x}')] d\mathbf{x}' \end{aligned} \right\} \quad (52)$$

and

$$\left. \begin{aligned} \sigma_{ij}(\mathbf{x}) &= -C_{ijkl} \left[ \int_{-\infty}^{\infty} C_{pqmn}\varepsilon_{mn}^*(\mathbf{x}') G_{kp,ql}(\mathbf{x} - \mathbf{x}') d\mathbf{x}' \right. \\ &\quad \left. + \varepsilon_{kl}^*(\mathbf{x}) \right] \end{aligned} \right\} \quad (53)$$

respectively.

Then, the physical interpretation of the functions  $G_{ij}(\mathbf{x} - \mathbf{x}')$  is examined. From (33) and (50) and the fact that  $N_{mk}(\xi)D^{-1}(\xi)$  denotes the  $(k, m)$ -component of the inverse of the coefficient matrix in (34), we get

$$\left. \begin{aligned} (2\pi)^3 C_{ijkl} G_{km,lj}(\mathbf{x} - \mathbf{x}') &= - \int_{-\infty}^{\infty} C_{ijkl} N_{mk}(\xi) D^{-1}(\xi) \xi_l \xi_j \exp[i\xi \cdot (\mathbf{x} - \mathbf{x}')] d\xi \\ &= - \int_{-\infty}^{\infty} K_{ik} [N_{mk}(\xi) D^{-1}(\xi)] \exp[i\xi \cdot (\mathbf{x} - \mathbf{x}')] d\xi \\ &= -\delta_{im} \int_{-\infty}^{\infty} \exp[i\xi \cdot (\mathbf{x} - \mathbf{x}')] d\xi \end{aligned} \right\} \quad (54)$$

From (54) and the identity for the three-dimensional delta function [3]

$$\left. \begin{aligned} \delta(\mathbf{x} - \mathbf{x}') &= \delta(x_1 - x'_1) \delta(x_2 - x'_2) \delta(x_3 - x'_3) \\ &= (2\pi)^{-3} \int_{-\infty}^{\infty} \exp[i\xi \cdot (\mathbf{x} - \mathbf{x}')] d\xi \end{aligned} \right\} \quad (55)$$

we obtain

$$C_{ijkl} G_{km,lj}(\mathbf{x} - \mathbf{x}') = -\delta_{im} \delta(\mathbf{x} - \mathbf{x}') \quad (56)$$

Meanwhile, from (20), we arrive at Navier's equation in the absence of eigenstrains as

$$C_{ijkl} u_{k,lj} = -f_i \quad (57)$$

By comparing (56) and (57) for an arbitrary choice of  $m$ , it is found that  $G_{km,lj}(\mathbf{x} - \mathbf{x}')$  and  $\delta_{im} \delta(\mathbf{x} - \mathbf{x}')$  correspond to  $u_{k,lj}$  and  $f_i$ , respectively. In other words, function  $G_{km}(\mathbf{x} - \mathbf{x}')$  can be interpreted as the displacement due to

the body force  $\delta_{im}\delta(\mathbf{x} - \mathbf{x}')$ . Here, since  $\delta_{im}\delta(\mathbf{x} - \mathbf{x}') = \delta(\mathbf{x} - \mathbf{x}')$  for  $i = m$  and  $\delta_{im}\delta(\mathbf{x} - \mathbf{x}') = 0$  for  $i \neq m$ , function  $\delta_{im}\delta(\mathbf{x} - \mathbf{x}')$  can be interpreted as the  $x_i$ -component of the unit body force acting in  $x_m$  direction at  $\mathbf{x}'$ . Therefore, function  $G_{km}(\mathbf{x} - \mathbf{x}')$  can be interpreted as the  $x_k$ -component of the displacement at  $\mathbf{x}$  due to the unit body force acting in the  $x_m$  direction at  $\mathbf{x}'$ . Functions that can be interpreted as above are referred to as Green functions or fundamental solutions. Thus, as shown in (51), the displacements (and the corresponding strains and stresses) can be obtained by superposing the “sources”  $C_{jlmn}\varepsilon_{mn}^*(\mathbf{x}')$  multiplied by (the derivatives of) the Green functions at various points of application,  $\mathbf{x}'$ .

### Examples

Here, examples of Green functions and the solutions using them are presented.

Let us consider an isotropic infinite body with an arbitrary distribution of eigenstrains that is free from any external forces and surface constraints. For the body, the elastic constants are expressed by the Lamé constants  $\lambda$  and  $\mu$  as [4]

$$C_{ijkl} = \lambda\delta_{ij}\delta_{kl} + \mu(\delta_{ik}\delta_{jl} + \delta_{il}\delta_{jk}) \quad (58)$$

It should be noted that the Lamé constants  $\lambda$  and  $\mu$  are related to the Young's modulus  $E$  and the Poisson's ratio  $\nu$  by

$$\lambda = \frac{\nu E}{(1 + \nu)(1 - 2\nu)}, \quad \mu = \frac{E}{2(1 + \nu)} \quad (59)$$

By substituting (58) into (33), the  $(i, j)$ -cofactor and the determinant of the coefficient matrix in (34) are obtained as

$$\left. \begin{aligned} D(\boldsymbol{\xi}) &= \mu^2(\lambda + 2\mu)\xi^6, \\ N_{ij}(\boldsymbol{\xi}) &= \mu\xi^2[(\lambda + 2\mu)\delta_{ij}\xi^2 - (\lambda + \mu)\xi_i\xi_j] \end{aligned} \right\} \quad (60)$$

where  $\xi = |\boldsymbol{\xi}| = \xi_k\xi_k$ . By substituting (60) into (50), we get

$$G_{ij}(\mathbf{x}) = (2\pi)^{-3} \int_{-\infty}^{\infty} \frac{(\lambda + 2\mu)\delta_{ij}\xi^2 - (\lambda + \mu)\xi_i\xi_j}{\mu(\lambda + 2\mu)\xi^4} \times \exp(i\boldsymbol{\xi} \cdot \mathbf{x}) d\boldsymbol{\xi} \quad (61)$$

By performing the integrations of (65), Lord Kelvin first showed in 1882 that

$$\left. \begin{aligned} G_{ij}(\mathbf{x}) &= \frac{1}{8\pi\mu x} \left[ 2\delta_{ij} - \frac{\lambda + \mu}{\lambda + 2\mu} \left( \delta_{ij} - \frac{x_i x_j}{x^2} \right) \right] \\ &= \frac{1}{4\pi\mu} \frac{\delta_{ij}}{|\mathbf{x}|} - \frac{1}{16\pi\mu(1 - \nu)} \frac{\partial^2 |\mathbf{x}|}{\partial x_i \partial x_j} \end{aligned} \right\} \quad (62)$$

where  $x = |\mathbf{x}| = x_k x_k$ . The derivation of (62) from (61) and the discussions on the Green functions for anisotropic bodies are found in the literature [5].

Next, let us consider that a uniform temperature increase  $\theta_0$  occurs in a sphere of radius  $a$ , with its center at the origin of the coordinate system. In this case, eigenstrains in the sphere are expressed from (1) by

$$\left. \begin{aligned} \varepsilon_{ij}^* &= \alpha\theta_0\delta_{ij} : \text{ in } \Omega, \\ \varepsilon_{ij}^* &= 0 : \text{ in } B - \Omega \end{aligned} \right\} \quad (63)$$

where  $B$  and  $\Omega$  denote the infinite body and the subdomain occupied by the sphere, respectively. By substituting (58), (59), (62), and (63) into (51), we have

$$\left. \begin{aligned} u_i(\mathbf{x}) &= -C_{klmn}\varepsilon_{mn}^* \frac{\partial}{\partial x_l} \int_{\Omega} G_{ik}(\mathbf{x} - \mathbf{x}') d\mathbf{x}' \\ &= -\alpha\theta_0(3\lambda + 2\mu)\delta_{kl} \\ &\quad \times \frac{\partial}{\partial x_l} \int_{\Omega} \left[ \frac{1}{4\pi\mu} \frac{\delta_{ik}}{|\mathbf{x} - \mathbf{x}'|} - \frac{1}{16\pi\mu(1 - \nu)} \frac{\partial^2 |\mathbf{x} - \mathbf{x}'|}{\partial x_i \partial x_k} \right] d\mathbf{x}' \\ &= -\alpha\theta_0 \frac{1 + \nu}{8\pi(1 - \nu)(1 - 2\nu)} \\ &\quad \times \left[ 4(1 - \nu) \frac{\partial\phi(\mathbf{x})}{\partial x_i} - \frac{\partial^3 \psi(\mathbf{x})}{\partial x_i \partial x_k \partial x_k} \right] \end{aligned} \right\} \quad (64)$$

where the functions

$$\phi(\mathbf{x}) = \int_{\Omega} \frac{d\mathbf{x}'}{|\mathbf{x} - \mathbf{x}'|}, \quad \psi(\mathbf{x}) = \int_{\Omega} |\mathbf{x} - \mathbf{x}'| d\mathbf{x}' \quad (65)$$

denote the potential at  $\mathbf{x}$  and the moment around  $\mathbf{x}$ , respectively, due to the uniform distribution in  $\Omega$ . By inspecting (65), one has

$$\frac{\partial^2 \psi(\mathbf{x})}{\partial x_k \partial x_k} = 2\phi(\mathbf{x}) \quad (66) \quad \text{and}$$

Therefore, (64) becomes

$$u_i(\mathbf{x}) = -\alpha\theta_0 \frac{1+v}{4\pi(1-v)} \frac{\partial \phi(\mathbf{x})}{\partial x_i} \quad (67)$$

Since  $\phi(\mathbf{x})$  denotes the potential at  $\mathbf{x}$  due to the uniform distribution in  $\Omega$ , it follows that [3]

$$\left. \begin{aligned} \phi(\mathbf{x}) &= 2\pi \left( a^2 - \frac{x^2}{3} \right) : \text{ in } \Omega, \\ \phi(\mathbf{x}) &= \frac{4\pi a^3}{3x} : \text{ in } B - \Omega \end{aligned} \right\} \quad (68)$$

By substituting (68) into (67), we get

$$\left. \begin{aligned} u_i(\mathbf{x}) &= \alpha\theta_0 \frac{1+v}{3(1-v)} x_i : \text{ in } \Omega, \\ u_i(\mathbf{x}) &= \alpha\theta_0 \frac{1+v}{3(1-v)} \frac{a^3 x_i}{x^3} : \text{ in } B - \Omega \end{aligned} \right\} \quad (69)$$

which gives the radial displacements

$$\left. \begin{aligned} \mathbf{u}(\mathbf{x}) &= \alpha\theta_0 \frac{1+v}{3(1-v)} \mathbf{x} : \text{ in } \Omega, \\ \mathbf{u}(\mathbf{x}) &= \alpha\theta_0 \frac{1+v}{3(1-v)} \frac{a^3 \mathbf{x}}{x^3} : \text{ in } B - \Omega \end{aligned} \right\} \quad (70)$$

Equation (70) is equivalent to the result that is obtained by solving the axisymmetrical form of Navier's equation and is often found in textbooks on thermal stresses [6, 7]. Furthermore, by substituting (58), (59), and (69) into (15) and (19),

the solutions of strains and stresses are obtained, respectively, as

$$\left. \begin{aligned} \varepsilon_{ij}(\mathbf{x}) &= \alpha\theta_0 \frac{1+v}{3(1-v)} \delta_{ij} : \text{ in } \Omega, \\ \varepsilon_{ij}(\mathbf{x}) &= \alpha\theta_0 \frac{1+v}{3(1-v)} \frac{a^3}{x^3} \left( \delta_{ij} - \frac{3x_i x_j}{x^2} \right) : \text{ in } B - \Omega \end{aligned} \right\} \quad (71)$$

$$\left. \begin{aligned} \sigma_{ij}(\mathbf{x}) &= -\frac{2\alpha\theta_0 E}{3(1-v)} \delta_{ij} : \text{ in } \Omega, \\ \sigma_{ij}(\mathbf{x}) &= \alpha\theta_0 \frac{E}{3(1-v)} \frac{a^3}{x^3} \left( \delta_{ij} - \frac{3x_i x_j}{x^2} \right) : \text{ in } B - \Omega \end{aligned} \right\} \quad (72)$$

from which we conclude that the strains and stresses in  $\Omega$  are uniform.

## Inclusions

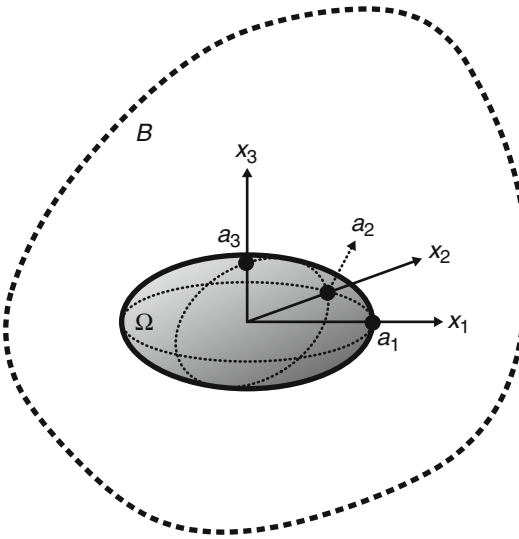
In this section, problems regarding inclusions are discussed, since they are an important topic in relation to eigenstrains.

### Terminology

When a body with uniform elastic constants has a subdomain where eigenstrains are distributed, the subdomain is referred to as an *inclusion*. Furthermore, when a body without eigenstrains has a subdomain with elastic constants that are different from those in the rest of the domain, the subdomain is referred to as an *inhomogeneity*; lastly, when a body with a subdomain as described above also has eigenstrains, then that subdomain is referred to as an *inhomogeneous inclusion*. In this section, an emphasis is placed on the concept of an infinite body with an ellipsoidal inclusion where eigenstrains are distributed uniformly.

### Ellipsoidal Inclusions

Consider an infinite elastic body  $B$  which contains an ellipsoidal subdomain



**Eigenstrains in Thermal Stresses, Fig. 3** Ellipsoidal inclusion

$$\Omega : \frac{x_1^2}{a_1^2} + \frac{x_2^2}{a_2^2} + \frac{x_3^2}{a_3^2} \leq 1 \quad (73)$$

with uniform eigenstrains  $\varepsilon_{ij}^*$ , as shown in Fig. 3. The body is assumed to be free from any external forces and surface constraints. The special case where  $B$  is an isotropic body,  $\Omega$  is a sphere, and eigenstrains are isotropic was treated in Subsubsection Examples, where it was found that the strains and stresses in  $\Omega$  were uniform as shown in (71) and (72); this special case has been proven to also hold true for the general case treated in this subsection. In other words, when  $\Omega$  is ellipsoidal and  $\varepsilon_{ij}^*$  is uniform in  $\Omega$ , it has been proven that the strains and stresses are also uniform in  $\Omega$  as governed by the equations

$$\varepsilon_{ij} = S_{ijkl} \varepsilon_{kl}^* : \text{ in } \Omega \quad (74)$$

and

$$\left. \begin{aligned} \sigma_{ij} &= C_{ijkl} (S_{klmn} \varepsilon_{mn}^* - \varepsilon_{kl}^*) \\ &= C_{ijkl} (S_{klmn} - I_{klmn}) \varepsilon_{mn}^* : \text{ in } \Omega \end{aligned} \right\} \quad (75)$$

where  $S_{ijkl}$  is referred to as Eshelby's tensor and  $I_{klmn}$  denotes the unit tensor of the fourth rank. It should be noted that

$$S_{ijkl} = S_{jikl} = S_{ijlk} \quad (76)$$

For the case of an isotropic body, the explicit forms of Eshelby's tensors for various shapes of ellipsoids are already available and summarized in the literature [5]. For example, the nonzero components of the Eshelby's tensor for a sphere ( $a_1 = a_2 = a_3 = a$ ) are obtained from

$$\left. \begin{aligned} S_{1111} &= S_{2222} = S_{3333} = \frac{7-5\nu}{15(1-\nu)} \\ S_{1122} &= S_{2233} = S_{3311} \\ &= S_{3322} = S_{2211} = S_{1133} = \frac{5\nu-1}{15(1-\nu)} \\ S_{1212} &= S_{2323} = S_{3131} = \frac{4-5\nu}{15(1-\nu)} \end{aligned} \right\} \quad (77)$$

and (76). When eigenstrains are given by (63), we can substitute (63) and (77) into (74) to obtain

$$\left. \begin{aligned} \varepsilon_{ij} &= S_{ij11} \varepsilon_{11}^* + S_{ij22} \varepsilon_{22}^* + S_{ij33} \varepsilon_{33}^* \\ &= \left[ \frac{7-5\nu}{15(1-\nu)} + 2 \times \frac{5\nu-1}{15(1-\nu)} \right] \alpha \theta_0 \delta_{ij} \\ &= \frac{1+\nu}{3(1-\nu)} \alpha \theta_0 \delta_{ij} : \text{ in } \Omega \end{aligned} \right\} \quad (78)$$

which is, of course, identical to the first of the set of equations in (71).

The solutions of the fields outside  $\Omega$  have also been found in the literature [5]. As is illustrated by (71) and (72), although the strains and stresses outside  $\Omega$  are not uniform, the elastic strain energy stored in the whole body,  $B$ , can be obtained easily. As can be seen from (29), the elastic strain energy can be obtained from the field, only within the inclusion  $\Omega$ . Since the strains and stresses are uniform in  $\Omega$  as mentioned in (74) and (75), the integration in (29) is replaced by the multiplication of the inclusion's volume. Thus, one has

$$U = -\frac{1}{2} C_{ijkl} (S_{klmn} - I_{klmn}) \varepsilon_{mn}^* \varepsilon_{ij}^* \cdot \frac{4\pi a_1 a_2 a_3}{3} \quad (79)$$

The discussions in this subsection form the foundations of micromechanics and are also useful in solving the problems of thermal stresses, by treating the free thermal expansion due to thermal loads as a form of eigenstrains.

## References

1. Timoshenko SP, Goodier JN (1970) Theory of elasticity, 3rd edn. McGraw-Hill, New York
2. Sneddon IA (1972) The use of integral transforms. McGraw-Hill, New York
3. Courant R, Hilbert D (1989) Methods of mathematical physics, vol 2. Wiley-VCH, Berlin
4. Fung YC (1993) First course in continuum mechanics, 3rd edn. Prentice Hall, New Jersey
5. Mura T (1987) Micromechanics of defects in solids, 2nd edn. Springer, Berlin, revised edition
6. Boley BA, Weiner JH (1997) Theory of thermal stresses. Dover, New York
7. Noda N, Hetnarski RB, Tanigawa Y (2003) Thermal stresses, 2nd edn. Taylor & Francis, New York

## Eigenstress Profile

- [Residual Stress Profile in Ceramic Laminates](#)

## Eigenstress Profile in Ceramic Laminates

- [Residual Stress Profile in Ceramic Laminates](#)

## Eigenvalue

- [Thermoelastic Damping in Resonators](#)

## Elastic and Thermal Field Coupling

- [Thermomechanical Coupling in Multilayered Plates and Shells](#)

## Elastic Cylindrical Shells

- [Saint-Venant's Problem for Cosserat Elastic Shells](#)

## Elastic Modulus (E)

- [Thermal Shock Resistance \(TSR\) and Thermal Fatigue Resistance \(TFR\) of Refractory Materials. Evaluation Method Based on the Dynamic Elastic Modulus](#)

## Elastic Plates on Winkler Foundation

- [Plates on Elastic Foundation](#)

## Elastic T-Stresses for a Closed Crack with and Without Kink

X. F. Li

School of Civil Engineering, Central South University, Changsha, People's Republic of China

## Overview

Crack-tip stress field plays a significant role in describing crack growth. The stress intensity factor only reflects the intensity of singular stress field. In addition, elastic T-stress as a secondary factor is used to describe the main contribution of nonsingular stress field. Propagation of a fault usually occurs in geomechanics and kink or wing can generate under confining pressure. The effect of elastic T-stresses on crack initiation angle is analyzed for a closed crack. For a cracked medium under compression, two T-stresses, parallel to and perpendicular to the crack plane, exist near the crack tip, and play a significant role in determining crack growth direction.

## Introduction

For elastic media without defects and inclusions, stress fields in the elastic media are always finite. For those with defects such as crack or rigid line inclusions, which mean a mathematical cut or rigid body without thickness, the stress fields near the crack or inclusion tips always exhibit singular behaviors. The determination of singular elastic fields is a fundamental task within the framework of linear elasticity fracture mechanics. Hitherto, there have been a lot of analytical and numerical approaches to obtain singular elastic fields induced by crack. Since the angular distribution of singular stress field is unified and independent of applied loads, two physical quantities are significant. One is the singularity index, and usually singular stress field near the crack tip is governed by power singularity or by oscillation singularity. The other is the singular intensity factor, often denoted as  $K$ . For power singularity,  $\sigma_{ij} \sim Kr^\lambda f_{ij}(\theta)$ ,  $f_{ij}(\theta)$  being the angular distribution functions and  $r$  being the distance from the crack tip,  $\lambda = -1/2$  is the most frequently encountered, and this case occurs for a crack embedded in a homogeneous elastic medium. In addition,  $\lambda \neq -1/2$  also occurs for certain cases, e.g., a mode III crack terminating at and perpendicular to an interface of two dissimilar elastic media. Another interesting case is a crack lying in the interface between two perfectly bonded dissimilar elastic media. For this case, the induced stress field has a oscillation singularity,  $\sigma_{ij} \sim Kr^{-1/2+\varepsilon} f_{ij}(\theta)$ ,  $\varepsilon$  being the material parameter. This theoretical solution has surprising unphysical explanations. For example, such a solution gives rise to the crack faces overlapping. In addition to the leading term, the  $K$ -field, of the stress field, the secondary effect obviously results from the contribution of the constant-term stress. From a mathematical viewpoint, for a homogeneous cracked elastic medium we expand the remaining part of  $\sigma_{ij} - Kr^{-1/2} f_{ij}(\theta)$  as Taylor series in  $r$ , and the T-stress corresponds to the constant term [1]. From a physical viewpoint, for a straight crack embedded in an elastic medium, the constant term

is not equal to zero, even for uniaxial tension perpendicular to the crack direction. In general, the constant term, named T-stress, in connection with the singular stress field at a crack tip can much enrich the crack tip information. Now the stress intensity factors together with the T-stress at a crack tip has been widely accepted as a bi-parameter fracture criterion in predicting crack propagation in brittle materials and in predicting shape and size of small scale yielding around the crack tip in elastic-plastic materials [2].

According to the classical statement, for a crack embedded in a two-dimensional elastic medium, the crack-tip field can be expressed in terms of the leading singular terms and secondary constant terms as follows:

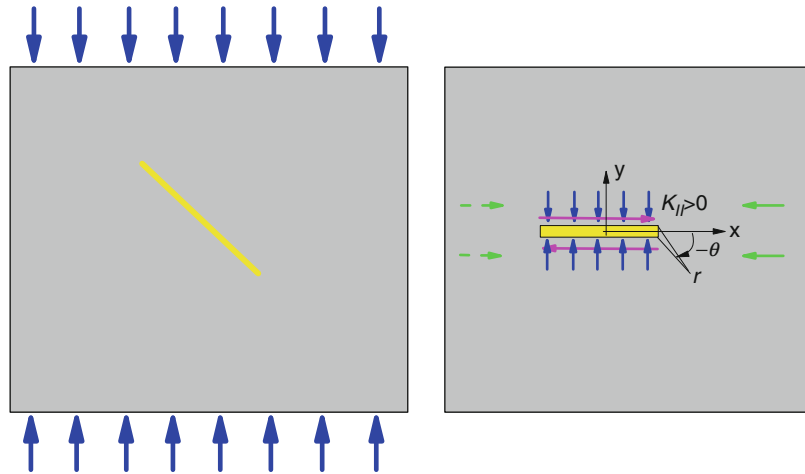
$$\begin{aligned} \begin{Bmatrix} \sigma_{xx} \\ \sigma_{yy} \\ \sigma_{xy} \end{Bmatrix} &= \frac{K_I}{\sqrt{2\pi r}} \cos \frac{\theta}{2} \begin{Bmatrix} 1 - \sin \frac{\theta}{2} \sin \frac{3\theta}{2} \\ 1 + \sin \frac{\theta}{2} \sin \frac{3\theta}{2} \\ \sin \frac{\theta}{2} \cos \frac{3\theta}{2} \end{Bmatrix} \\ &+ \frac{K_{II}}{\sqrt{2\pi r}} \begin{Bmatrix} -\sin \frac{\theta}{2} (2 + \cos \frac{\theta}{2} \cos \frac{3\theta}{2}) \\ \sin \frac{\theta}{2} \cos \frac{\theta}{2} \cos \frac{3\theta}{2} \\ \cos \frac{\theta}{2} (1 - \sin \frac{\theta}{2} \sin \frac{3\theta}{2}) \end{Bmatrix} \\ &+ \begin{Bmatrix} T_x \\ 0 \\ 0 \end{Bmatrix} + O(r^{1/2}) \end{aligned} \quad (1)$$

for  $r/2a \ll 1$ ,  $K_I, K_{II}$  denote the mode-I and mode-II stress intensity factors,  $T_x$  is a T-stress, defined as the first term of the nonsingular terms in the normal stress component and describing the contribution of transverse stress parallel to the crack plane [3], and  $O(r^{1/2})$  stands for higher-order terms with respect to  $r$ , which are negligibly small as compared with the singular and constant terms in a close vicinity of the crack tip. In the above expressions,  $r$  and  $\theta$  are local polar coordinates with the origin located at the crack tip (Fig. 1).

Since the introduction of the T-stress originally by Willaims [3], there have been a large number of the researches on the T-stress. These researches focus on the influence of the T-stress



**Elastic T-Stresses for a Closed Crack with and Without Kink, Fig. 1** A crack embedded in an elastic plate in compression



on crack initiation together with crack growth path including crack kink angle, crack yield zone, and so on. In addition, the determination of the T-stress for static and dynamic cases is also of interest, in particular for various crack configurations. In analytic approaches, some representative methods are available. For example, in addition to standard Williams' expansion method, some other methods for determining the T-stress have been proposed, including Eshelby's path-independent integral technique, higher-order weight function method, stress difference method, finite element method, and boundary element method. In addition, complex potential method and singular integral equation method are also powerful analytic techniques for determining the T-stress. A lot of T-stress solutions have been collected in the monograph [4].

## Two T-Stress Terms at a Closed Crack Tip

Crack growth strongly depends on an asymptotic stress field in a close vicinity of the crack tip. For a tensile opening crack, the asymptotic crack-tip stress field is well known, as shown in (1). In nature, a large amount of evidence shows that crack may kink or wing can be created in compression [5, 6]. However, for such a closed crack in compression, the above-mentioned asymptotic crack-tip stress field seems not to be proper. The reason is that once a crack is closed, the mode-I

stress intensity factor vanishes. Instead of the  $K_I$ -term, another constant term must be added. Consequently, neglecting friction between two crack surfaces, we assume that an elastic plate with a crack is in compression subjected to applied mixed-mode loads, which causes the crack to be in a state of compression-shear. In other words, at the crack surfaces, we can write

$$\sigma_{yy} = \sigma_0, \quad \sigma_{xy} = \tau_0 \quad (2)$$

where  $\sigma_0 < 0$ . It is easily found that in place of (1), the crack-tip stress field should be

$$\begin{aligned} \begin{Bmatrix} \sigma_{xx} \\ \sigma_{yy} \\ \sigma_{xy} \end{Bmatrix} &= \frac{K_{II}}{\sqrt{2\pi r}} \begin{Bmatrix} -\sin \frac{\theta}{2} (2 + \cos \frac{\theta}{2} \cos \frac{3\theta}{2}) \\ \sin \frac{\theta}{2} \cos \frac{\theta}{2} \cos \frac{3\theta}{2} \\ \cos \frac{\theta}{2} (1 - \sin \frac{\theta}{2} \sin \frac{3\theta}{2}) \end{Bmatrix} \\ &+ \begin{Bmatrix} T_x \\ T_y \\ 0 \end{Bmatrix} \end{aligned} \quad (3)$$

or

$$\sigma_{rr} = \frac{K_{II}}{\sqrt{2\pi r}} C_{02}(\theta) + T_x \cos^2 \theta + T_y \sin^2 \theta \quad (4)$$

$$\sigma_{\theta\theta} = \frac{K_{II}}{\sqrt{2\pi r}} C_{12}(\theta) + T_x \sin^2 \theta + T_y \cos^2 \theta \quad (5)$$

$$\sigma_{r\theta} = \frac{K_{II}}{\sqrt{2\pi r}} C_{02}(\theta) - (T_x - T_y) \sin \theta \cos \theta \quad (6)$$

with

$$\begin{aligned} C_{02}(\theta) &= \frac{1}{2}(3\cos\theta - 1)\sin\frac{\theta}{2} \\ C_{12}(\theta) &= -\frac{3}{2}(1 + \cos\theta)\sin\frac{\theta}{2} \end{aligned} \quad (7)$$

where  $r, \theta$  stand for polar coordinates with origin located at the crack tip. In addition to the classical component  $T_x$ , a new component  $T_y$  also changes the distribution of stress field around the crack tip. The latter  $T_y$  was always neglected in previous analyses.

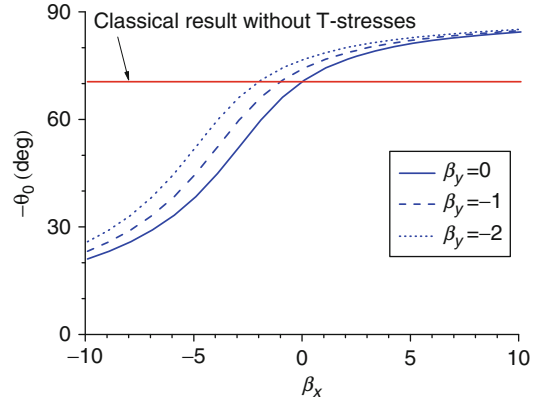
In studying crack growth, the favorable direction for a crack to advance, named the kink angle, can be determined by many fracture criteria. The simplest fracture criterion is the most tensile stress (MTS) criterion, denoted as the  $\sigma_\theta$ -criterion [7]. Generally speaking, the  $\sigma_\theta$ -criterion can provide quite accurate results for tensile fracture in a variety of brittle materials [8]. The conventional MTS criterion does not contain the contribution of the T-stress. Here, we further extend this criterion to include the effect of the T-stress. Keeping (5) in mind and with the help of

$$\left. \frac{d\sigma_{\theta\theta}}{d\theta} \right|_{\theta=\theta_0} = 0, \quad \left. \frac{d^2\sigma_{\theta\theta}}{d\theta^2} \right|_{\theta=\theta_0} < 0 \quad (8)$$

the kink angle is found to satisfy the following equation:

$$(3\cos\theta - 1)K_{II} - \frac{16}{3}\sqrt{2\pi r_c}(T_x - T_y)\sin\frac{\theta}{2}\cos\theta = 0 \quad (9)$$

where  $r_c$  is a critical distance from the crack tip. Solving (9), an explicit expression for the crack kink angle is obtainable. We omit the procedure and the final result is



**Elastic T-Stresses for a Closed Crack with and Without Kink, Fig. 2** Kink angle as a function of  $\beta_x$

$$-\theta_0 = \begin{cases} 2\sin^{-1}\left[\eta + 2\sqrt{\frac{1}{6} + \eta^2}\cos\omega_1\right], & \text{for } T_x < T_y \\ \cos^{-1}(1/3) = 70.5^\circ, & \text{for } T_x = T_y \\ 2\sin^{-1}\left[\eta + 2\sqrt{\frac{1}{6} + \eta^2}\cos\omega_2\right], & \text{for } T_x > T_y \end{cases} \quad (10)$$

with

$$\omega_j = \frac{1}{3} \left[ \cos^{-1} \frac{\eta(\eta^2 - \frac{1}{4})}{(\frac{1}{6} + \eta^2)^{\frac{3}{2}}} + 2(j-2)\pi \right] \quad (11)$$

$$\eta = -\frac{3}{16\alpha(\beta_x - \beta_y)} \quad (12)$$

$$\beta_x = \frac{T_x\sqrt{\pi a}}{K_{II}}, \beta_y = \frac{T_y\sqrt{\pi a}}{K_{II}}, \alpha = \sqrt{\frac{2r_c}{a}} \quad (13)$$

for  $K_{II} > 0$ . Note that if  $K_{II} < 0$ , the kink angle  $-\theta_0$  should be  $\theta_0$  instead of (10).

To examine the influence of  $T_y$  on the crack kink angle, the above-obtained results are presented graphically in the subsequent figures. Figure 2 gives the crack kink angle  $\theta_0$  as a function of  $\beta_x$  with  $\beta_y = 0, -1, -2$ . As seen from Fig. 2, the kink angle progressively rises as the  $\beta_x$  increases. This is to say that a tensile horizontal T-stress  $T_x$  causes the kink angle to become larger, and a compressive horizontal T-stress  $T_x$  causes the kink angle to become smaller. On the

other hand, from Fig. 2 one can see that a decrease in  $\beta_y$  causes the kink angle  $\theta$  to increase for a fixed  $\beta_x$ . Therefore, it can be concluded that in addition to the leading singular stress field, the secondary  $T$ -stresses strongly affects the crack kink angle. Moreover, the kink angle may be either a smaller angle or a larger angle, depending on the magnitude of the  $T$ -stresses. Such theoretical predictions are supported by existing observations on the crack kink angle. For example, wing cracks have been observed in various angles ranging from lower than  $20^\circ$  to nearly  $90^\circ$  in sandstone, granite, granodiorite, limestone, shale, ice, PMMA, etc.

Furthermore, we compare the results of fracture toughness when considering two  $T$ -stresses and neglecting one or both. To drive the flaw to propagate along the favorable kink angle determined above, another necessary condition must be met. The maximum circumferential tensile stress at a critical distance  $r_c$  must be equal to or exceed its critical value  $\sigma_c$ :

$$-\frac{3K_{IIc}}{2\sqrt{2\pi r_c}}\sin\theta_0\cos\frac{\theta_0}{2} + T_x\sin^2\theta_0 + T_y\cos^2\theta_0 = \sigma_c \quad (14)$$

where we have designated  $K_{IIc}$  in magnitude as the *apparent* mode-II fracture toughness when the flaw starts to advance under compressive loading. From the above,  $K_{IIc}$  is clearly dependent on the  $T$ -stresses, rather than a constant. This may be the reason why most experimental measurements of  $K_{IIc}$  are not a constant for a cracked plate under compressive loading for different crack orientation angles, since in this case the effects of  $T_x$  and  $T_y$  on  $K_{IIc}$  are remarkable, and cannot be neglected.

On the other hand, for a pure tensile opening crack, a critical circumferential stress value  $\sigma_c$  is characterized by the usual mode-I fracture toughness  $K_{IC}$  being a material constant, i.e.,

$$\sigma_c = \frac{K_{IC}}{\sqrt{2\pi r_c}} \quad (15)$$

Bearing in mind that the kink angle obeys equation (9), after some manipulations

one can derive the relationship between  $K_{IIc}$  and  $K_{IC}$  below:

$$\frac{K_{IIc}}{K_{IC}} = -\frac{4\cos\theta_0}{3\sin\theta_0\cos^3\frac{\theta_0}{2}}\left(1 - \frac{T_y}{\sigma_c}\right) \quad (16)$$

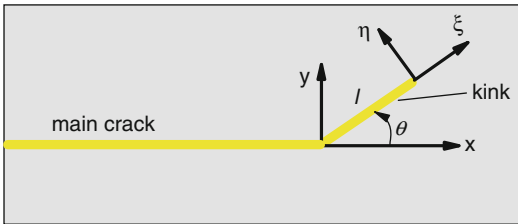
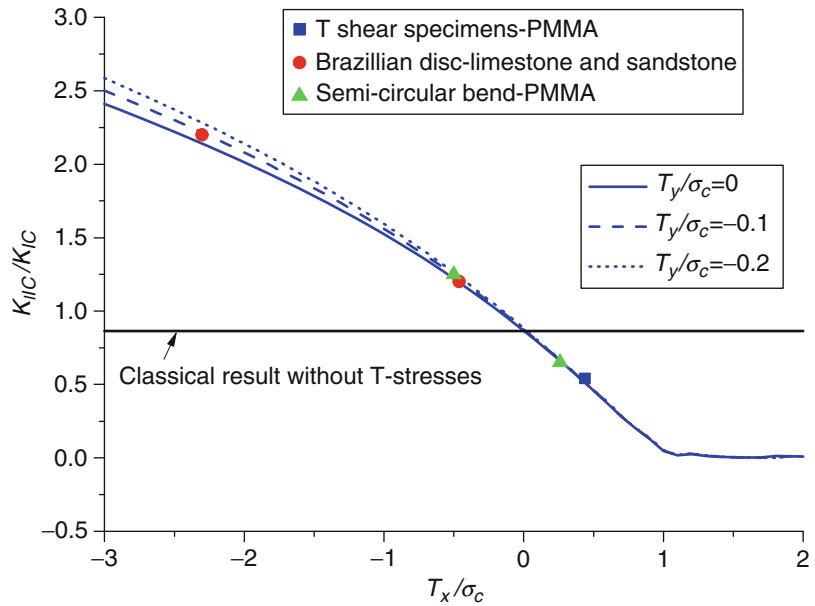
Since  $\theta_0$  is a function of both  $T_y$  and  $T_x$ , not only  $T_y$  but also  $T_x$  affects  $K_{IIc}$ . The variation of  $K_{IIc}/K_{IC}$  against  $T_x/\sigma_c$  for various values of  $T_y/\sigma_c$  is plotted in Fig. 3. The effect of  $T_y$  on fracture toughness is consistent with the experimental observation of Bing and Sun [9], who found that the fracture toughness cannot be characterized by the singular field relative to  $K_{II}$  alone. Relevant experimental observations indicate that measurement results of  $K_{IIc}/K_{IC}$  for tested materials such as limestone, mudstone, soft sandstone, and PMMA are not close to a unified unchanging constant. In the presence of friction, some discussion can be found in [10].

## T-Stresses at a Kink Tip

In the previous, the  $T$ -stress at a closed tip has been analyzed. During crack growth, of much significance is crack kinking by a small change in angle [11–13]. Here, consider a crack with a kink of arbitrary length and arbitrary angle embedded in an infinite isotropic elastic medium, as shown in Fig. 4. For a usual situation, the length of the main crack  $2a$  is always much larger than that of the kink  $l$  inclined in  $\theta$  to the main crack. Of interest is the case where the kink angle lies in a range from  $0$  to  $\pi/2$ . Here two coordinate systems are used. One denoted as  $(x, y)$  is established such that the main crack lies at the negative  $x$ -axis and the origin is located at the right crack tip, and the other denoted as  $(\xi, \eta)$  is chosen such that the kink lies at the negative  $\xi$ -axis and the origin is at the right kink tip. Thus, the main crack occupies the region  $-2a < x < 0$ ,  $y = 0$ , and a kink occupies the region  $-l < \xi < 0$ ,  $\eta = 0$ . Although the stress intensity factors and  $T$ -stress near a kink tip can be determined by many approaches such as the singular integral equation method, these methods only provide numerical results, rather than

### Elastic T-Stresses for a Closed Crack with and Without Kink,

**Fig. 3** Apparent fracture toughness versus  $T_x/\sigma_c$



**Elastic T-Stresses for a Closed Crack with and Without Kink, Fig. 4** Schematic of a main crack with a kink

analytical closed-form solution. In what follows, approximate closed-form solution is given by asymptotic analysis. To this end, an infinitesimal kink  $l \ll a$  with a small kink angle is assumed [14].

Here, we still consider a closed crack, but with an open kink. The closure of the main crack is due to far-field compressive loading, which possibly causes the closed crack to advance. The entire elastic field around the kink tip  $\sigma_{ij}^k$  after the crack kinks can be obtained by superposition of  $\sigma_{ij}^m$  and  $\sigma_{ij}^p$ , i.e.,

$$\sigma_{ij}^k = \sigma_{ij}^m + \sigma_{ij}^p \quad (17)$$

where  $\sigma_{ij}^m$  stands for the elastic field around the main crack tip before the crack kinks, and  $\sigma_{ij}^p$

represents perturbed elastic field induced by the kink, where the kink surfaces are loaded by the negative values of  $\sigma_{ij}^m$ .

At the beginning of kinking propagation, the length of the kink is so small as compared with that of the main crack that the main crack is assumed to be semi-infinite. Then, for a kink with a small angle, following the treatment of Cotterell and Rice [15], the stress intensity factors at the tip of an infinitesimal kink can be obtained by the following integral:

$$\begin{pmatrix} K_I^k \\ K_{II}^k \end{pmatrix} = \sqrt{\frac{2}{\pi}} \int_0^l \begin{pmatrix} \sigma_{\theta\theta} \\ \sigma_{r\theta} \end{pmatrix} \frac{dr}{\sqrt{l-r}} \quad (18)$$

Next, with the aid of the Green's function for a semi-infinite crack subjected to a pair of concentrated forces at the crack surfaces, we apply the above formulae to the kink exerted by distributed stresses where the distributed stresses correspond to those induced by a semi-infinite crack. Using the Westergaard stress functions for a semi-infinite crack lying at  $x < 0, y = 0$ , opened by a pair of concentrated tensile and shear forces,  $P$  and  $Q$ , at an arbitrary position  $b$  at the crack surface from the crack tip

$$\begin{pmatrix} Z_I(z) \\ Z_{II}(z) \end{pmatrix} = \begin{pmatrix} P \\ Q \end{pmatrix} \frac{1}{\pi(z+b)} \sqrt{\frac{b}{z}} \quad (19)$$

where  $z = x + iy$ , we get the induced elastic field expressed in terms of  $Z_I$  and  $Z_{II}$ , i.e.,

$$\sigma_{xx} = \operatorname{Re} [Z_I(z) + yZ'_{II}(z)] - \operatorname{Im} [yZ'_I(z) - 2Z_{II}(z)] \quad (20)$$

$$\sigma_{yy} = \operatorname{Re} [Z_I(z) - yZ'_{II}(z)] + \operatorname{Im} [yZ'_I(z)] \quad (21)$$

$$\sigma_{xy} = -\operatorname{Re} [yZ'_I(z) - Z_{II}(z)] - \operatorname{Im} [yZ'_{II}(z)] \quad (22)$$

where the prime denotes differentiation with respect to  $z$ . Consequently, for distributed loading in the coordinate system  $(\xi, \eta)$ , from (19) the corresponding Westergaard functions can be calculated by the following integral:

$$\begin{pmatrix} Z_I(\zeta) \\ Z_{II}(\zeta) \end{pmatrix} = -\frac{1}{\pi} \int_0^l \begin{pmatrix} \sigma_{\theta\theta} \\ \sigma_{r\theta} \end{pmatrix} \frac{1}{\zeta + l - r} \sqrt{\frac{l-r}{\zeta}} dr \quad (23)$$

where  $\zeta = \xi + i\eta$ ,  $r$  stands for distance from the main crack tip, and  $l - r$  corresponding to  $b$  in (19) denotes a distance from the kink tip.

For a closed main crack, we get asymptotic distribution of stress field at the main crack tip, which is identical to (4)–(6) with a substitution of  $K_{II}$  with  $K_{II}^m$ ,  $K_{II}^m$  denoting the mode-II stress intensity factors relative to the main crack,  $T_x^m, T_y^m$  being the two T-stresses at the closed main crack tip, parallel to and perpendicular to the crack plane.

Putting these results into (23), one can easily get

$$\begin{aligned} Z_I(\zeta) &= \frac{C_{12}(\theta)K_{II}^m}{\sqrt{2\pi}} \left[ \frac{1}{\sqrt{\zeta}} - \frac{1}{\sqrt{(\zeta+l)}} \right] \\ &+ \frac{2}{\pi} \left[ \sqrt{\frac{l}{\zeta}} - \tan^{-1} \sqrt{\frac{l}{\zeta}} \right] (T_x^m \sin^2 \theta + T_y^m \cos^2 \theta) \end{aligned} \quad (24)$$

$$\begin{aligned} Z_{II}(\zeta) &= \frac{C_{02}(\theta)K_{II}^m}{\sqrt{2\pi}} \left[ \frac{1}{\sqrt{\zeta}} - \frac{1}{\sqrt{(\zeta+l)}} \right] \\ &- \frac{2}{\pi} \left[ \sqrt{\frac{l}{\zeta}} - \tan^{-1} \sqrt{\frac{l}{\zeta}} \right] (T_x^m - T_y^m) \sin \theta \cos \theta \end{aligned} \quad (25)$$

Since the stress intensity factors and the T-stress are dependent upon the elastic field ahead of the intimate vicinity of the prolongation of a crack or kink tip, consequently, from the relations (20), (21), and (22) the perturbed elastic field along the prolongation of the kink is  $\sigma_{\xi\xi}^p = \sigma_{\eta\eta}^p = Z_I(\xi)$ ,  $\sigma_{\xi\eta}^p = Z_{II}(\xi)$ .

On the other hand, owing to the assumption of an infinitesimal length of the kink at an angle  $\theta$  to the crack plane, the elastic stress field around the kink tip can be directly written by those around the main crack tip prior to crack kinking, which has the same as (4)–(6) only with a substitution  $r = \xi + l$ .

Therefore, based on (15), the entire elastic field around the kink tip posterior to crack kinking,  $\sigma_{ij}^k$ , can be given by sum of  $\sigma_{ij}^m$  and  $\sigma_{ij}^p$ . That is, we have

$$\begin{aligned} \sigma_{\xi\xi}^k &= \frac{C_{12}(\theta)K_{II}^m}{\sqrt{2\pi\xi}} + \frac{K_{II}^m}{\sqrt{2\pi(\xi+l)}} (1 + 3\cos\theta) \sin \frac{\theta}{2} \\ &+ (T_x^m - T_y^m) \cos 2\theta \\ &+ (T_x^m \sin^2 \theta + T_y^m \cos^2 \theta) \left( 1 + \frac{2}{\pi} \sqrt{\frac{l}{\xi}} - \frac{2}{\pi} \tan^{-1} \sqrt{\frac{l}{\xi}} \right) \end{aligned} \quad (26)$$

$$\begin{aligned} \sigma_{\eta\eta}^k &= \frac{C_{12}(\theta)K_{II}^m}{\sqrt{2\pi\xi}} + (T_x^m \sin^2 \theta + T_y^m \cos^2 \theta) \\ &\left( 1 + \frac{2}{\pi} \sqrt{\frac{l}{\xi}} - \frac{2}{\pi} \tan^{-1} \sqrt{\frac{l}{\xi}} \right) \end{aligned} \quad (27)$$

$$\begin{aligned} \sigma_{\xi\eta}^k &= \frac{C_{02}(\theta)K_{II}^m}{\sqrt{2\pi\xi}} - (T_x^m - T_y^m) \sin \theta \\ &\cos \theta \left( 1 - \frac{2}{\pi} \sqrt{\frac{l}{\xi}} - \frac{2}{\pi} \tan^{-1} \sqrt{\frac{l}{\xi}} \right) \end{aligned} \quad (28)$$

As a check, if imposing  $l = 0$ , one can find that the above asymptotic stress field reduce to those for a main crack, i.e., (4)–(6).

With the above elastic field ahead of the kink tip, stress intensity factors are readily found to be

$$K_I^k = C_{12}(\theta)K_{II}^m + 2\left(T_x^m \sin^2 \theta + T_y^m \cos^2 \theta\right)\sqrt{\frac{2l}{\pi}} \quad (29)$$

$$K_{II}^k = C_{02}(\theta)K_{II}^m - 2\left(T_x^m - T_y^m\right)\sqrt{\frac{2l}{\pi}}\sin\theta \cos\theta \quad (30)$$

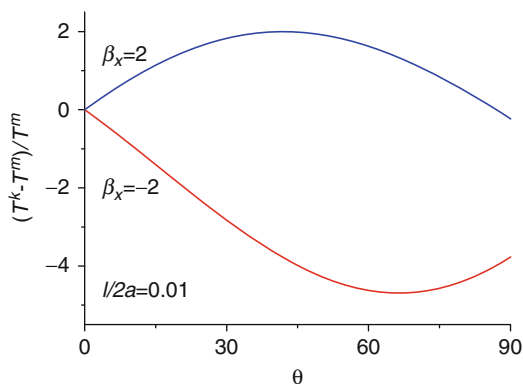
This means that the stress intensity factors at the kink tip depend upon not only the stress intensity factors at the main crack tip but also the T-stress at the main crack. Moreover, the length of the kink has a pronounced influence on the stress intensity factors at the kink tip when the T-stress is taken into account.

On the other hand, from the obtained asymptotic stress field ahead of the kink tip, the T-stress parallel to the kink plane at the kink tip is expressed in terms of the stress intensity factors of mode-I and II and the T-stress at the main crack tip as follows:

$$T^k = \frac{K_{II}^m}{\sqrt{2\pi l}}(1 + 3 \cos\theta)\sin\frac{\theta}{2} + \left(T_x^m - T_y^m\right)\cos 2\theta \quad (31)$$

which indicates that in addition to the T-stress at the main crack tip, the stress intensity factors of mode-I and II strongly affect the T-stress at the kink tip. Also, the T-stress is related to the angle and length of the kink. It is interesting to note that although the main crack is closed due to compressive loading, the kink is open, and so there is one the T-stress term, parallel to the kink plane. Of course, for an open main crack or a closed kink, similar analyses can be made and omitted.

Figure 5 show the relative variation of the difference between the T-stresses for a closed main crack and an opening kink with respect to the T-stress for the main crack where  $T^m = T_x^m - T_y^m$ . If  $\beta_x > 0$ , the T-stress from the



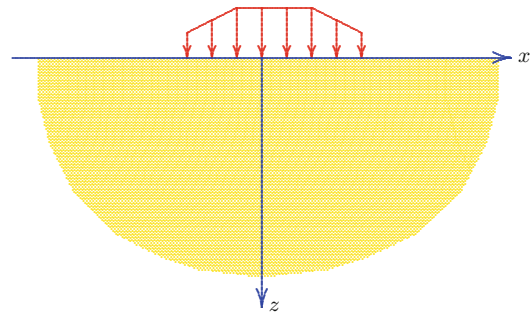
**Elastic T-Stresses for a Closed Crack with and Without Kink, Fig. 5**  $(T^k - T^m)/T^m$  against kink angle

main crack to the kink increases, and if  $\beta_x < 0$ , the T-stress decreases. Note that the above-derived results are valid for small angles, and so for large angles, nothing can be concluded from the above.

## References

1. Haefele PM, James DL (1995) The constant stress term. *Eng Fract Mech* 50:869–882
2. Larsson SG, Carlsson AJ (1973) Influence of non-singular stress terms and specimen geometry on small scale yielding at crack tips in elastic-plastic materials. *J Mech Phys Solids* 21:263–277
3. Williams ML (1957) On the stress distribution at the base of stationary crack. *J Appl Mech* 24:109–114
4. Fett T (1998) A compendium of T-stress solutions. Forschungszentrum Karlsruhe GmbH, Karlsruhe
5. Schulson EM, Fortt AL, Iliescu D, Renshaw CE (2006) On the role of frictional sliding in the compressive fracture of ice and granite: terminal vs. post-terminal failure. *Acta Mater* 54:3923–3932
6. Mutlu O, Pollard DD (2008) On the patterns of wing cracks along an outcrop scale flaw: a numerical modeling approach using complementarity. *J Geophys Res* 113:B06403
7. Erdogan F, Sih GC (1963) On the crack extension in plates under plane loading and transverse shear. *J Basic Eng* 85:519–527
8. Williams JG, Ewing PD (1972) Fracture under complex stress—the angled crack problem. *Int J Fract* 8:441–446
9. Bing QD, Sun CT (2007) Effect of compressive transverse normal stress on mode II fracture toughness in polymeric composites. *Int J Fract* 145:89–97

10. Li XF, Liu GL, Lee KY (2009) Effects of T-stresses on fracture initiation for a closed crack in compression with frictional crack faces. *Int J Fract* 160:19–30
11. He MY, Hutchinson JW (1991) Kinking of a crack out of an interface: role of in-plane stress. *J Am Ceram Soc* 74:767–771
12. Gao H, Chiu C (1992) Slightly curved or kinked cracks in anisotropic elastic solids. *Int J Solids Struct* 29:947–972
13. Leblond J-B, Frelat J (2000) Crack kinking from an initially closed crack. *Int J Solids Struct* 37:1595–1614
14. Li XF, Xu LR (2007) T-stresses across static crack kinking. *J Appl Mech* 74:181–190
15. Cotterell B, Rice JR (1980) Slightly curved or kinked cracks. *Int J Fract* 16:155–169



**Elastostatics of a Half Space, Fig. 1** Half space with surface load

## Elastodynamics

### ► Thermoelastic Dynamic Instability (TEDI)

## Elastostatics of a Half Space

Arnold Verruijt  
Faculty of Civil Engineering and Geosciences,  
Delft University of Technology, Delft,  
The Netherlands

### Overview

The theory of elasticity is the simplest consistent part of continuum mechanics and is a special case of the theory of thermal stresses. Many solutions of problems from the theory of elasticity can be found in the classical textbooks of Love [8], Landau and Lifschitz [7], Green and Zerna [4], Sokolnikoff [13], and Timoshenko and Goodier [14] and in more modern books. Some of these solutions are presented here, with their derivations. They can be used to verify and validate the solutions of thermal stress problems, by considering the special case of an isothermal state.

All the problems presented refer to an elastic half space, with various types of vertical loads on the free surface, such as a point load, a line load, a strip load, and a disk load. The solutions are

obtained by using integral transform methods, such as Fourier transforms or Hankel transforms.

### Introduction

Problems to be considered are the determination of the stresses and the deformations of an elastic half space under the influence of loads applied on the upper surface (see Fig. 1) in particular vertical loads. The material is supposed to be homogeneous and isotropic and linear elastic, so that its mechanical properties can be fully characterized by an elastic modulus  $E$  and Poisson's ratio  $\nu$  or some other combination of two elastic constants, for instance, the Lamé constants  $\lambda$  and  $\mu$ . The strains are assumed to be small compared to 1.

### Basic Equations

The basic equations of the theory of elasticity are the conditions on the stresses, the strains, and the displacements in a linear elastic continuum. These are the conditions of equilibrium, the constitutive relations, and the compatibility conditions.

The stresses and displacements are described in a Cartesian coordinate system  $x$ ,  $y$ ,  $z$ . The components of the displacement vector in the three coordinate directions are denoted by  $u_x$ ,  $u_y$ , and  $u_z$ . If it is assumed that the

displacement gradients are small compared to 1, then the expressions for the strains are

$$\begin{aligned}\varepsilon_{xx} &= \frac{\partial u_x}{\partial x}, & \varepsilon_{xy} &= \frac{1}{2} \left( \frac{\partial u_x}{\partial y} + \frac{\partial u_y}{\partial x} \right) \\ \varepsilon_{yy} &= \frac{\partial u_y}{\partial y}, & \varepsilon_{yz} &= \frac{1}{2} \left( \frac{\partial u_y}{\partial z} + \frac{\partial u_z}{\partial y} \right) \\ \varepsilon_{zz} &= \frac{\partial u_z}{\partial z}, & \varepsilon_{zx} &= \frac{1}{2} \left( \frac{\partial u_z}{\partial x} + \frac{\partial u_x}{\partial z} \right)\end{aligned}\quad (1)$$

The three normal strains  $\varepsilon_{xx}$ ,  $\varepsilon_{yy}$ , and  $\varepsilon_{zz}$  express the relative elongation of line elements in the three coordinate directions ( $\Delta l/l$ ), and the three shear strains  $\varepsilon_{xy}$ ,  $\varepsilon_{yz}$ , and  $\varepsilon_{zx}$  express the deformation of right angles. The volume strain  $e = \Delta V/V$  is the sum of the normal strains in the three coordinate directions:

$$e = \varepsilon_{xx} + \varepsilon_{yy} + \varepsilon_{zz} \quad (2)$$

The stresses can be expressed into the strains by the generalized form of Hooke's law. For an isotropic material, this is

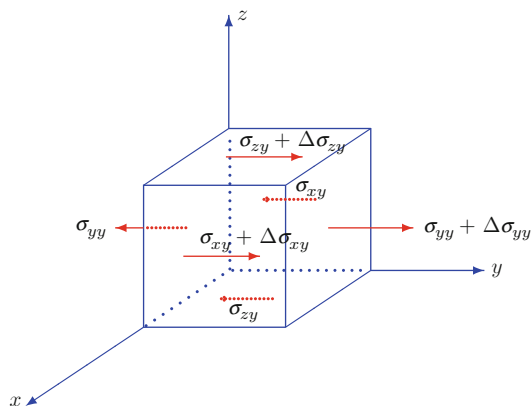
$$\begin{aligned}\sigma_{xx} &= \lambda e + 2\mu \varepsilon_{xx} & \sigma_{xy} &= 2\mu \varepsilon_{xy} \\ \sigma_{yy} &= \lambda e + 2\mu \varepsilon_{yy} & \sigma_{yz} &= 2\mu \varepsilon_{yz} \\ \sigma_{zz} &= \lambda e + 2\mu \varepsilon_{zz} & \sigma_{zx} &= 2\mu \varepsilon_{zx}\end{aligned}\quad (3)$$

Here  $\lambda$  and  $\mu$  are the Lamé constants. These constants are related to the modulus of elasticity  $E$  (Young's modulus) and Poisson's ratio  $\nu$  by

$$\lambda = \frac{\nu E}{(1 + \nu)(1 - 2\nu)}, \quad \mu = \frac{E}{2(1 + \nu)} \quad (4)$$

For the stresses in Equation (3), the sign convention is that a stress component is positive when acting in positive coordinate direction on a plane with an outward normal in positive direction. This is the usual sign convention in continuum mechanics, which implies that tensile stresses are positive.

The stresses must satisfy the equations of equilibrium. In the absence of body forces, these are



**Elastostatics of a Half Space, Fig. 2** Equilibrium of an element

$$\begin{aligned}\frac{\partial \sigma_{xx}}{\partial x} + \frac{\partial \sigma_{yx}}{\partial y} + \frac{\partial \sigma_{zx}}{\partial z} &= 0, & \sigma_{xy} &= \sigma_{yx} \\ \frac{\partial \sigma_{xy}}{\partial x} + \frac{\partial \sigma_{yy}}{\partial y} + \frac{\partial \sigma_{zy}}{\partial z} &= 0, & \sigma_{yz} &= \sigma_{zy} \\ \frac{\partial \sigma_{xz}}{\partial x} + \frac{\partial \sigma_{yz}}{\partial y} + \frac{\partial \sigma_{zz}}{\partial z} &= 0, & \sigma_{zx} &= \sigma_{xz}\end{aligned}\quad (5)$$

The second of these equations is illustrated in Fig. 2.

The stresses, strains, and displacements in an isotropic linear elastic body must satisfy all the equations given above and in addition must satisfy the conditions on the boundary, which may specify the surface stress or the surface displacement or a combination. For general methods of analysis, the reader is referred to textbooks on the theory of elasticity, e.g., by Timoshenko and Goodier [14], Sokolnikoff [13], Sadd [10], and Hetnarski and Ignaczak [5]. In the next sections, some elementary solutions will be presented.

For the purpose of future reference, it is convenient to express the equations of equilibrium in terms of the displacements. If it is assumed that the parameters  $\lambda$  and  $\mu$  are constants (which means that the material is homogeneous), one obtains from (1), (3), and (5),



$$\begin{aligned}
 (\lambda + \mu) \frac{\partial e}{\partial x} + \mu \nabla^2 u_x &= 0 \\
 (\lambda + \mu) \frac{\partial e}{\partial y} + \mu \nabla^2 u_y &= 0 \\
 (\lambda + \mu) \frac{\partial e}{\partial z} + \mu \nabla^2 u_z &= 0
 \end{aligned} \quad (6)$$

These are called the Navier equations. They are three equations with three unknowns. Their solution usually also involves the stresses, however, because the boundary conditions may be expressed in terms of the stresses.

### Boussinesq Problems

An important class of problems is formed by the problems for a half space ( $z > 0$ ), bounded by the plane  $z = 0$ , loaded by vertical normal stresses on the surface only. This is called the class of Boussinesq problems, after the French scientist who published several solutions of such problems in 1885.

This type of problem can be solved conveniently by introducing a specially chosen displacement function  $\phi$  ([4], p. 171), from which the displacements can be derived by the following formulas:

$$u_x = (1 - 2\nu) \frac{\partial \phi}{\partial x} + z \frac{\partial^2 \phi}{\partial x \partial z} \quad (7)$$

$$u_y = (1 - 2\nu) \frac{\partial \phi}{\partial y} + z \frac{\partial^2 \phi}{\partial y \partial z} \quad (8)$$

$$u_z = -2(1 - \nu) \frac{\partial \phi}{\partial z} + z \frac{\partial^2 \phi}{\partial z^2} \quad (9)$$

Substitution of these expressions into (6) shows that all three equations of equilibrium are identically satisfied, provided that the function  $\phi$  satisfies the Laplace equation

$$\nabla^2 \phi = 0 \quad (10)$$

The advantage of the introduction of the function  $\phi$  is that there now is only a single unknown function, which must satisfy a

relatively simple differential equation, (10), for which many particular solutions and several general solution methods are available. That the solutions are useful appears when the stresses are expressed in the function  $\phi$ . With (1), (3), and (10), one obtains for the normal stresses

$$\frac{\sigma_{xx}}{2\mu} = (1 - 2\nu) \frac{\partial^2 \phi}{\partial x^2} + z \frac{\partial^3 \phi}{\partial x^2 \partial z} - 2\nu \frac{\partial^2 \phi}{\partial z^2} \quad (11)$$

$$\frac{\sigma_{yy}}{2\mu} = (1 - 2\nu) \frac{\partial^2 \phi}{\partial y^2} + z \frac{\partial^3 \phi}{\partial y^2 \partial z} - 2\nu \frac{\partial^2 \phi}{\partial z^2} \quad (12)$$

$$\frac{\sigma_{zz}}{2\mu} = -\frac{\partial^2 \phi}{\partial z^2} + z \frac{\partial^3 \phi}{\partial z^3} \quad (13)$$

For the shear stresses, the following expressions are obtained:

$$\frac{\sigma_{xy}}{2\mu} = (1 - 2\nu) \frac{\partial^2 \phi}{\partial x \partial y} + z \frac{\partial^3 \phi}{\partial x \partial y \partial z} \quad (14)$$

$$\frac{\sigma_{yz}}{2\mu} = z \frac{\partial^3 \phi}{\partial y \partial z^2} \quad (15)$$

$$\frac{\sigma_{zx}}{2\mu} = z \frac{\partial^3 \phi}{\partial x \partial z^2} \quad (16)$$

From the last two equations, it can be seen that on the surface  $z = 0$ , the shear stresses are always zero:

$$z = 0 : \sigma_{zx} = \sigma_{zy} = 0 \quad (17)$$

This means that the function  $\phi$  can only be used for problems for which the plane  $z = 0$  is free from shear stresses. This is an essential restriction. On the other hand, this restriction appears to lead to a relatively simple mathematical problem, namely, the solution of the Laplace equation (10). On the boundary  $z = 0$ , the stress  $\sigma_{zz}$  may be prescribed or the displacement  $u_z$ . On the surface  $z = 0$ , the expression for the vertical displacement reduces to

$$z = 0 : u_z = -2(1 - \nu) \frac{\partial \phi}{\partial z} \quad (18)$$

and the expression for the vertical normal stress reduces to

$$z = 0 : \sigma_{zz} = -2\mu \frac{\partial^2 \phi}{\partial z^2} \quad (19)$$

Thus, if the displacement or the stress on the surface is given, this means that either the first or the second derivative of the displacement function  $\phi$  is known. In the next sections a number of solutions will be presented.

The displacement components in a system of cylindrical coordinates are the radial displacement  $u_r$ , the tangential displacement  $u_\theta$ , and the vertical displacement  $u_z$ . These can be expressed as follows [4]:

$$u_r = (1 - 2\nu) \frac{\partial \phi}{\partial r} + z \frac{\partial^2 \phi}{\partial r \partial z} \quad (20)$$

$$u_\theta = (1 - 2\nu) \frac{1}{r} \frac{\partial \phi}{\partial \theta} + \frac{z}{r} \frac{\partial^2 \phi}{\partial \theta \partial z} \quad (21)$$

$$u_z = -2(1 - \nu) \frac{\partial \phi}{\partial z} + z \frac{\partial^2 \phi}{\partial z^2} \quad (22)$$

The stress components are

$$\frac{\sigma_{rr}}{2\mu} = (1 - 2\nu) \frac{\partial^2 \phi}{\partial r^2} + z \frac{\partial^3 \phi}{\partial r^2 \partial z} - 2\nu \frac{\partial^2 \phi}{\partial z^2} \quad (23)$$

$$\frac{\sigma_{\theta\theta}}{2\mu} = -(1 - 2\nu) \frac{\partial^2 \phi}{\partial r^2} + \frac{z}{r} \frac{\partial^2 \phi}{\partial r \partial z} - \frac{\partial^2 \phi}{\partial z^2} \quad (24)$$

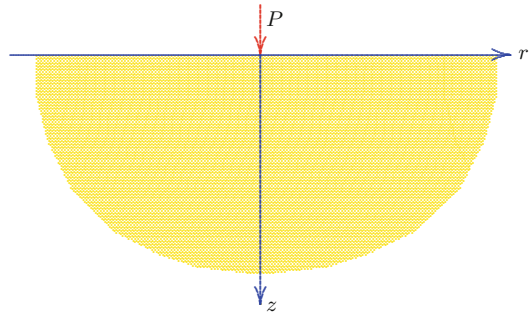
$$\frac{\sigma_{zz}}{2\mu} = -\frac{\partial^2 \phi}{\partial z^2} + z \frac{\partial^3 \phi}{\partial z^3} \quad (25)$$

It may be useful to also give an expression for the isotropic stress, defined as

$$\sigma_0 = \frac{1}{3}(\sigma_{xx} + \sigma_{yy} + \sigma_{zz}) \quad (26)$$

Using the expressions given above, it is found that

$$\sigma_0 = -\frac{2}{3}(1 + \nu) \frac{\partial^2 \phi}{\partial z^2} \quad (27)$$



**Elastostatics of a Half Space, Fig. 3** Boussinesq's problem: point load on half space

### Point Load

A classical case, the solution of which was first given by Boussinesq, is the problem of a concentrated point force on the half space  $z > 0$  (see Fig. 3).

The solution is assumed to be given by the function

$$\phi = -\frac{P}{4\pi\mu} \ln(z + R) \quad (28)$$

where

$$R = \sqrt{x^2 + y^2 + z^2} \quad (29)$$

It can easily be verified that this function indeed satisfies the differential equation (10). That it satisfies the correct boundary conditions is not immediately obvious but may be verified by considering the stress field.

Differentiation of  $\phi$  with respect to  $z$  gives

$$\frac{\partial \phi}{\partial z} = -\frac{P}{4\pi\mu} \frac{1}{R} \quad (30)$$

$$\frac{\partial^2 \phi}{\partial z^2} = \frac{P}{4\pi\mu} \frac{z}{R^3} \quad (31)$$

$$\frac{\partial^3 \phi}{\partial z^3} = \frac{P}{4\pi\mu} \left( \frac{1}{R^3} - 3 \frac{z^2}{R^5} \right) \quad (32)$$

The vertical normal stress  $\sigma_{zz}$  is now found to be, with (13),

$$\sigma_{zz} = -\frac{3P}{2\pi} \frac{z^3}{R^5} \quad (33)$$

On the surface  $z = 0$ , this stress is zero everywhere, except in the origin, where the stress is infinitely large. That the solution is correct can be verified by integration of the vertical stress over the surface are, which will show that the resultant force is indeed equal to  $P$ .

The vertical displacement is, with (8),

$$u_z = \frac{P}{4\pi\mu R} \left[ 2(1-\nu) + \frac{z^2}{R^2} \right] \quad (34)$$

On the surface  $z = 0$ , the displacement is, expressed in terms of  $E$  and  $\nu$ ,

$$z = 0 : u_z = \frac{P(1-\nu)}{2\pi\mu r} = \frac{P(1-\nu^2)}{\pi E r} \quad (35)$$

where  $r = \sqrt{x^2 + y^2}$ . In the origin the displacement is singular, as might be expected in this case of a concentrated force. All the other stresses and displacements can easily be derived from the solution (28).

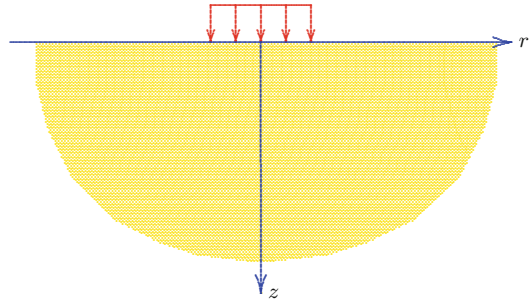
### Uniform Load on a Circular Area

Starting from the elementary solution (28), many other interesting solutions can be obtained by superposition ([13,14]; Sadd 1950; [5]). As an example, the displacement of the center of a circular area carrying a uniform load is presented (see Fig. 4).

The starting point of the considerations is the observation that a load of magnitude  $p dA$  at a distance  $r$  from the origin results in a vertical displacement at the origin of

$$\frac{p dA (1-\nu^2)}{\pi E r}$$

as follows immediately from the formula (35).



**Elastostatics of a Half Space, Fig. 4** Uniform load on circular area

The displacement due to a uniform load over a circular area with radius  $a$  can be obtained by integration over that area. Because  $dA = r dr d\theta$ , one obtains, after integration over  $\theta$  from  $\theta = 0$  to  $\theta = 2\pi$  and integration over  $r$  from  $r = 0$  to  $r = a$ ,

$$r = 0, z = 0 : u_z = \frac{2pa(1-\nu^2)}{E} \quad (36)$$

This is a well-known and useful formula. If the formula is expressed in the total load  $P = \pi a^2 p$ , it reads

$$r = 0, z = 0 : u_z = \frac{2P(1-\nu^2)}{\pi a E} \quad (37)$$

This shows that the displacement of a foundation plate can be reduced by making it larger, as one would expect intuitively.

### Fourier Transforms

A large class of solutions can be found by the use of Fourier transforms [11]. Some examples are presented here, for the case of plane strain deformations of an elastic half plane ( $u_y = 0$ ). An elegant and powerful alternative for the method of Fourier transforms is the complex variable method [9], which can also be applied to more general geometries, using conformal transformations. This method will not be considered here.

A solution using Fourier transforms may be of the form

$$\phi = \int_0^\infty \{f(\alpha) \cos(\alpha x) + g(\alpha) \sin(\alpha x)\} \exp(-\alpha z) d\alpha \quad (38)$$

where  $f(\alpha)$  and  $g(\alpha)$  are as yet unknown functions of the variable  $\alpha$ .

That (38) is indeed a solution follows immediately by substitution of the elementary solutions  $\cos(\alpha x) \exp(-\alpha z)$  and  $\sin(\alpha x) \exp(-\alpha z)$  into the differential equation (10). For  $z \rightarrow \infty$  the solution will always approach zero, which suggests that this solution can perhaps be used for cases in which the stresses can be expected to vanish for  $z \rightarrow \infty$ .

With (13), one now obtains

$$z = 0 : \frac{\sigma_{zz}}{2\mu} = - \int_0^\infty \alpha^2 \{f(\alpha) \cos(\alpha x) + g(\alpha) \sin(\alpha x)\} d\alpha \quad (39)$$

Suppose that the boundary condition is

$$z = 0, -\infty < x < \infty : \sigma_{zz} = q(x) \quad (40)$$

in which  $q(x)$  is a given function. Then the condition is that

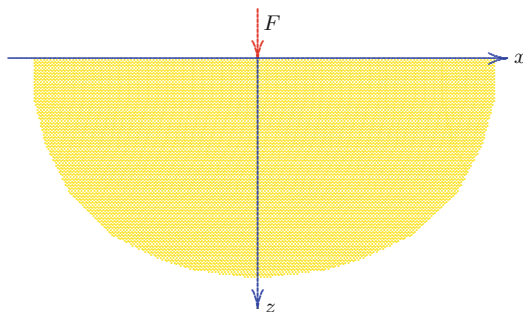
$$\int_0^\infty \{A(\alpha) \cos(\alpha x) + B(\alpha) \sin(\alpha x)\} d\alpha = q(x) \quad (41)$$

where

$$A(\alpha) = -2\mu\alpha^2 f(\alpha) \quad (42)$$

$$B(\alpha) = -2\mu\alpha^2 g(\alpha) \quad (43)$$

The problem of determining the functions  $A(\alpha)$  and  $B(\alpha)$  from (41) is exactly the standard problem from the theory of Fourier transforms. The solution is given by the inversion theorem, which will not be derived here (see the literature on Fourier analysis (e.g., [11])). The final result is



**Elastostatics of a Half Space, Fig. 5** Flamant's problem: line load on half space

$$A(\alpha) = \frac{1}{\pi} \int_{-\infty}^{\infty} q(t) \cos(\alpha t) dt \quad (44)$$

$$B(\alpha) = \frac{1}{\pi} \int_{-\infty}^{\infty} q(t) \sin(\alpha t) dt \quad (45)$$

The problem has now been solved, at least in principle, for an arbitrary surface load  $q(x)$ . In a specific case, with a given surface load  $q(x)$ , the integrals (44) and (45) must be evaluated, and then the results must be substituted into the general solution (38). Depending on the load function, this may be a difficult mathematical problem. In the next section a simple example is given, in which all integrals can be evaluated analytically.

## Line Load

As a first example, the case of a line load on a half space will be considered (Flamant's problem) (see Fig. 5). In this case the load function is

$$q(x) = \begin{cases} -F/(2\varepsilon), & |x| < \varepsilon \\ 0, & |x| > \varepsilon \end{cases} \quad (46)$$

where it will later be assumed that  $\varepsilon \rightarrow 0$ . From (44) and (45) it follows that

$$A(\alpha) = -\frac{F}{\pi\varepsilon} \frac{\sin(\alpha\varepsilon)}{\alpha} \\ B(\alpha) = 0$$

If  $\varepsilon \rightarrow 0$  this reduces to

$$A(\alpha) = -F/\pi \quad (47)$$

$$B(\alpha) = 0 \quad (48)$$

With (42) and (43), one obtains

$$f(\alpha) = \frac{F}{2\pi\mu\alpha^2} \quad (49)$$

$$g(\alpha) = 0 \quad (50)$$

The solution of the problem therefore is

$$\phi = \frac{F}{2\pi\mu} \int_0^\infty \frac{\cos(\alpha x) \exp(-\alpha z)}{\alpha^2} d\alpha \quad (51)$$

Although this integral does not converge, due to the behavior of the factor  $\alpha^2$  in the denominator near  $\alpha \rightarrow 0$ , the result may well be useful, because the relevant quantities are derived expressions, such as the stresses, which require differentiation. It is found that the expressions for the stresses are

$$\sigma_{xx} = -\frac{2F}{\pi} \frac{x^2 z}{(x^2 + z^2)^2} \quad (52)$$

$$\sigma_{zz} = -\frac{2F}{\pi} \frac{z^3}{(x^2 + z^2)^2} \quad (53)$$

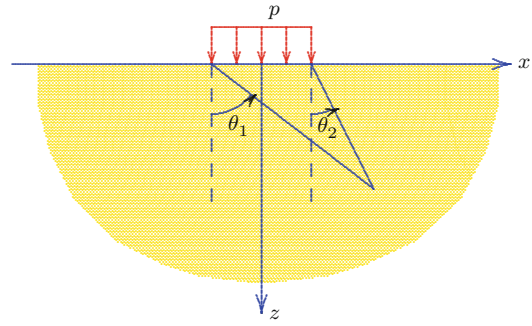
$$\sigma_{xz} = -\frac{2F}{\pi} \frac{xz^2}{(x^2 + z^2)^2} \quad (54)$$

These are usually called the Flamant formulas. Their form is somewhat simpler when using polar coordinates  $x = r \cos \theta$  and  $z = r \sin \theta$ ,

$$\sigma_{xx} = -\frac{2F}{\pi r} \sin \theta \cos^2 \theta \quad (55)$$

$$\sigma_{zz} = -\frac{2F}{\pi r} \sin^3 \theta \quad (56)$$

$$\sigma_{xz} = -\frac{2F}{\pi r} \sin^2 \theta \cos \theta \quad (57)$$



**Elastostatics of a Half Space, Fig. 6** Strip load on half space

When the stress components are also transformed into polar coordinates, the formulas are even simpler:

$$\sigma_{rr} = -\frac{2F}{\pi r} \sin \theta = -\frac{2Fz}{\pi r^2} \quad (58)$$

$$\sigma_{\theta\theta} = 0 \quad (59)$$

$$\sigma_{r\theta} = 0 \quad (60)$$

It appears that the only nonvanishing stress is the radial stress and that it decreases inversely proportional to the distance from the origin and with the sine of the angle with the horizontal axis.

### Strip Load

Another classical example is the case of a strip load on a half space (see Fig. 6). The width of the strip is denoted by  $2a$ . In this case the boundary condition is

$$q(x) = \begin{cases} -p, & |x| < a \\ 0, & |x| > a \end{cases} \quad (61)$$

The stress function  $\phi$  is found to be

$$\phi = \frac{p}{\pi\mu} \int_0^\infty \frac{\sin(\alpha a) \cos(\alpha x) \exp(-\alpha z)}{\alpha^3} d\alpha \quad (62)$$

or

$$\phi = \frac{p}{2\pi\mu} \int_0^\infty \frac{\{\sin[\alpha(x+a)] - \sin[\alpha(x-a)]\} \exp(-\alpha z)}{\alpha^3} d\alpha$$

$$\sigma_{xx} = -\frac{p}{\pi} \left\{ \arctan\left(\frac{x+a}{z}\right) - \arctan\left(\frac{x-a}{z}\right) - \frac{(x+a)z}{(x+a)^2 + z^2} + \frac{(x-a)z}{(x-a)^2 + z^2} \right\} \quad (63)$$

Again, this integral does not converge, but its second and third derivatives, which are needed to determine the stresses, do converge.

The vertical normal stress  $\sigma_{zz}$  can be obtained using (13). The result is

$$\sigma_{zz} = -\frac{2p}{\pi} \int_0^\infty \frac{(1+\alpha z) \sin(\alpha a) \cos(\alpha x) \exp(-\alpha z)}{\alpha} d\alpha \quad (64)$$

The integral can be found using tables of Laplace or Fourier transforms (see, e.g., [3]). This gives

$$\sigma_{zz} = -\frac{p}{\pi} \left\{ \arctan\left(\frac{x+a}{z}\right) - \arctan\left(\frac{x-a}{z}\right) + \frac{(x+a)z}{(x+a)^2 + z^2} - \frac{(x-a)z}{(x-a)^2 + z^2} \right\} \quad (65)$$

This is a well-known formula (see, e.g., [11]). It can also be written in the form

$$\sigma_{zz} = -\frac{p}{\pi} \{\theta_1 - \theta_2 + \sin \theta_1 \cos \theta_1 - \sin \theta_2 \cos \theta_2\} \quad (66)$$

where the angles  $\theta_1$  and  $\theta_2$  are indicated in Fig. 6.

The horizontal normal stress  $\sigma_{xx}$  can be obtained using (11). The result is

$$\sigma_{xx} = -\frac{2p}{\pi} \int_0^\infty \frac{(1-\alpha z) \sin(\alpha a) \cos(\alpha x) \exp(-\alpha z)}{\alpha} d\alpha \quad (67)$$

The integral can be found to give (see [11])

which can also be written in the form

$$\sigma_{xx} = -\frac{p}{\pi} \{\theta_1 - \theta_2 - \sin \theta_1 \cos \theta_1 + \sin \theta_2 \cos \theta_2\} \quad (69)$$

## Axially Symmetric Problems

Problems for an elastic half space loaded by a radially symmetric normal stress on the surface  $z = 0$  can conveniently be solved by the Hankel transform method (Sneddon 1961). The problem can be formulated in terms of the displacement function  $\phi$  introduced in (8). This function must satisfy the Laplace equation (10). In axially symmetric coordinates, this equation is

$$\frac{\partial^2 \phi}{\partial r^2} + \frac{1}{r} \frac{\partial \phi}{\partial r} + \frac{\partial^2 \phi}{\partial z^2} = 0 \quad (70)$$

The Hankel transform of the function  $\phi$  is defined as

$$\Phi(\xi, z) = \int_0^\infty r \phi(r, z) J_0(r\xi) dr \quad (71)$$

where  $J_0(x)$  is the Bessel function of the first kind and order zero. The inverse transformation is (Sneddon 1961)

$$\phi(r, z) = \int_0^\infty \xi \Phi(\xi, z) J_0(\xi r) d\xi \quad (72)$$

The advantage of the Hankel transformation is that the operator

$$\frac{\partial^2}{\partial r^2} + \frac{1}{r} \frac{\partial}{\partial r}$$

is transformed into multiplication by  $-\xi^2$ . This means that the differential equation (70) becomes, after application of the Hankel transform,

$$\frac{d^2 \Phi}{dz^2} - \xi^2 \Phi = 0 \quad (73)$$

which is an ordinary differential equation. The general solution of this equation is

$$\Phi = A \exp(\xi z) + B \exp(-\xi z) \quad (74)$$

where the integration constants  $A$  and  $B$  may depend upon the transformation parameter  $\xi$ . In the half space  $z > 0$ , the constant  $A$  can be assumed to vanish.

If the boundary condition is

$$z = 0 : \sigma_{zz} = q(r) \quad (75)$$

then we obtain, with (19) and (74),

$$-2\mu B \xi^2 = \int_0^\infty r q(r) J_0(\xi r) dr \quad (76)$$

from which the value of  $B$  can be determined. In the next two sections, some examples will be given.

## Uniform Load on a Circular Area

A well-known classical problem is the problem of a uniform load over a circular area. This problem was already considered above, where the displacement of the origin was derived from a particular solution (see (36)). Here the complete solution will be derived by a straightforward analysis.

In this case the load function  $q(r)$  is

$$q(r) = \begin{cases} -p, & r < a \\ 0, & r > a \end{cases} \quad (77)$$

Substitution of this function into the general expression (76) gives

$$B = \frac{p}{2\mu \xi^2} \int_0^a r J_0(\xi r) dr \quad (78)$$

This is a well-known integral ([1], 11.3.20). The result is

$$B = \frac{pa}{2\mu \xi^3} J_1(\xi a) \quad (79)$$

where  $J_1(x)$  is the Bessel function of the first kind and order one.

The displacement function  $\phi$  now is

$$\phi = \frac{pa}{2\mu} \int_0^\infty \frac{J_1(\xi a) \exp(-\xi z) J_0(\xi r)}{\xi^2} d\xi \quad (80)$$

Although this integral itself cannot be evaluated, because of the logarithmic singularity in the origin, certain useful results can still be derived from it, because the physical quantities such as the displacements and the stresses must be derived from it by differentiation, and after differentiation the integrals may well converge, as indeed they do.

The vertical displacement of the surface can be obtained from formula (18). With (80) this gives

$$\begin{aligned} z = 0 : u_z &= \frac{pa(1-\nu)}{\mu} \int_0^\infty \frac{J_1(\xi a) J_0(\xi r)}{\xi} d\xi \quad (81) \end{aligned}$$

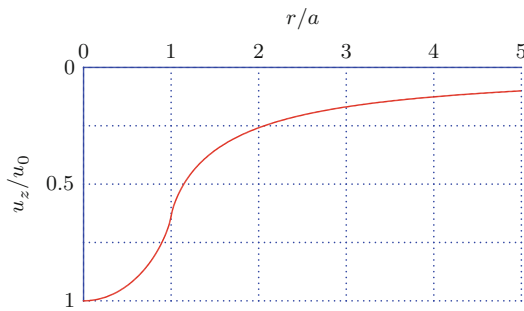
This integral can be expressed in terms of complete elliptic integrals:

$$z = 0 : u_z = \frac{2pa(1-\nu)}{\pi\mu} \begin{cases} E(r^2/a^2), & r < a \\ F(r^2/a^2), & r > a \end{cases} \quad (82)$$

where

$$F(x) = \sqrt{x} [E(1/x) - (1 - 1/x) K(1/x)] \quad (83)$$

and where  $K(x)$  and  $E(x)$  are complete elliptic integrals of the first and second kind, respectively (see [1]). For  $x = 0$ , both  $K(x)$  and  $E(x)$  are



**Elastostatics of a Half Space, Fig. 7** Displacements of the surface

equal to  $\pi/2$ . The result (82) is also given by Timoshenko and Goodier [14].

Figure 7 shows the displacements of the surface in this case in graphical form. The displacement of the origin is of special interest. This is found to be

$$r = 0, z = 0 : u_z = u_0 = \frac{pa(1 - \nu)}{\mu} \quad (84)$$

which agrees with expression (36) found before.

The vertical normal stress  $\sigma_{zz}$  is, with (25) and (80),

$$\frac{\sigma_{zz}}{p} = - \int_0^\infty a(1 + \xi z) J_1(\xi a) \exp(-\xi z) J_0(\xi r) d\xi \quad (85)$$

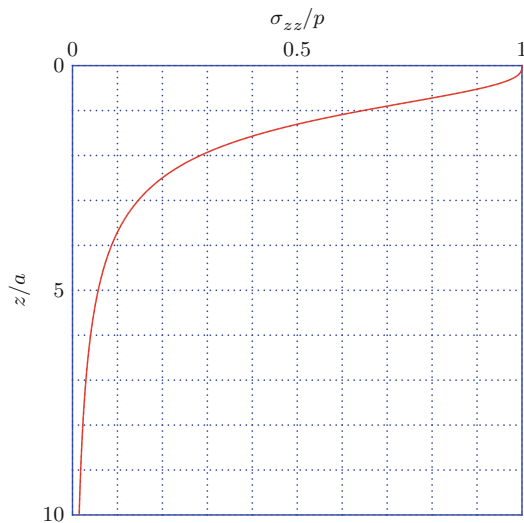
For  $r = 0$ , which is along the vertical axis, this integral reduces to

$$r = 0 : \frac{\sigma_{zz}}{p} = - \int_0^\infty a(1 + \xi z) J_1(\xi a) \exp(-\xi z) d\xi \quad (86)$$

which can easily be evaluated using a table of Laplace transforms [2]. The result is

$$r = 0 : \frac{\sigma_{zz}}{p} = -1 + \frac{z^3}{(a^2 + z^2)^3} \quad (87)$$

This is a well-known formula (see, e.g., [14], p. 405).



**Elastostatics of a Half Space, Fig. 8** Vertical stress  $\sigma_{zz}$  for  $r = 0$

The vertical stress along the central axis of the load is shown graphically in Fig. 8. Just under the load, the vertical stress is  $-p$ , of course, and this stress gradually diminishes when the general expression (85) cannot easily be expressed into closed form. In order to perform a numerical integration, it is convenient to introduce dimensionless coordinates  $x = a\xi$ ,  $\rho = r/a$ , and  $\zeta = z/a$ . The integral then becomes

$$\frac{\sigma_{zz}}{p} = - \int_0^\infty (1 + \zeta x) J_0(\rho x) J_1(x) \exp(-\zeta x) dx \quad (88)$$

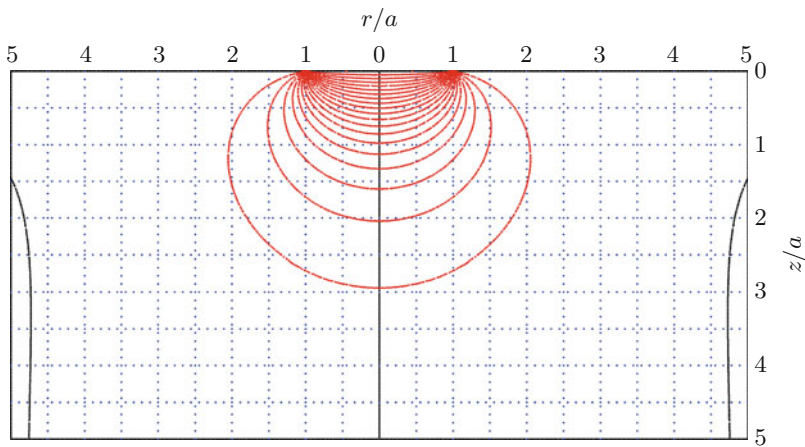
The maximum value of the integral occurs at the origin, for  $\rho = \zeta = 0$ , and this maximum value is found to be 1.

Using expression (23), it is found that the horizontal radial stress can be evaluated by the integral

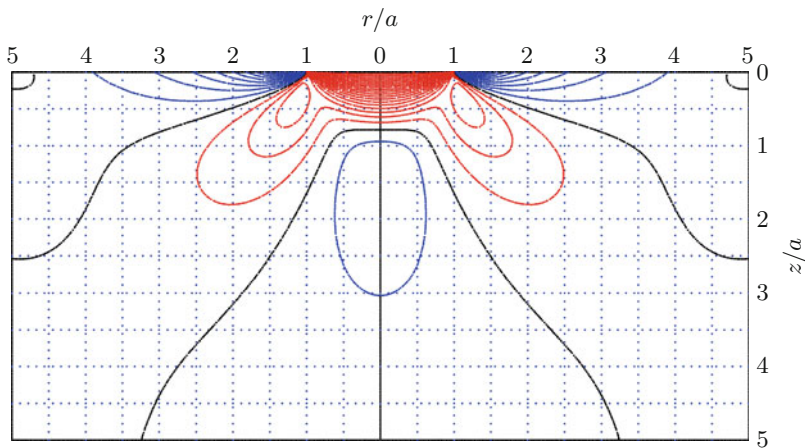
$$\frac{\sigma_{rr}}{p} = - \int_0^\infty \left\{ (1 - \zeta x) J_0(\rho x) - (1 - 2\nu - \zeta x) \frac{J_1(\rho x)}{\rho x} \right\} J_1(x) \exp(-\zeta x) dx \quad (89)$$



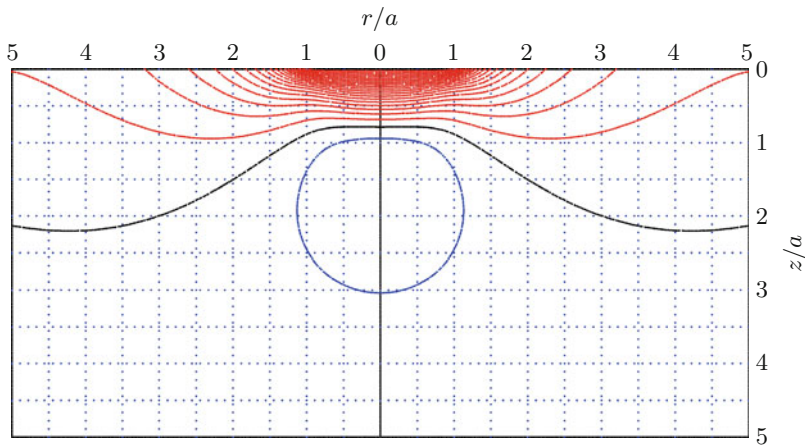
**Elastostatics of a Half Space, Fig. 9** Disk load, isotropic stress,  $\nu=0$



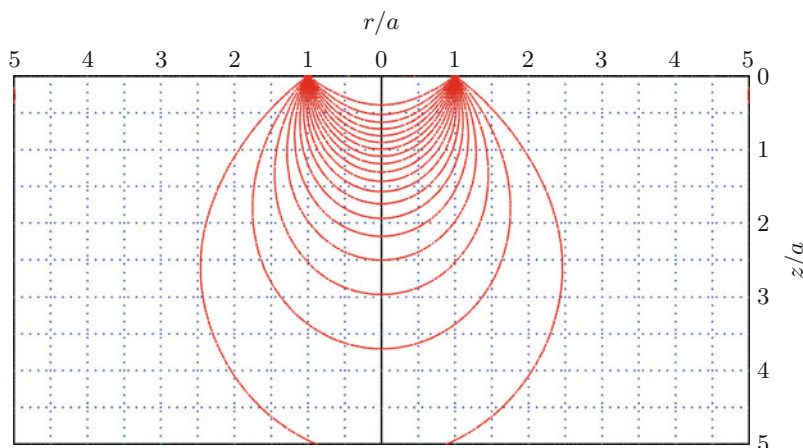
**Elastostatics of a Half Space, Fig. 10** Disk load, radial stress



**Elastostatics of a Half Space, Fig. 11** Disk load, tangential stress



**Elastostatics of a Half Space, Fig. 12** Disk load, vertical stress



The maximum value of the integral occurs at the origin, for  $\rho = \zeta = 0$ , and this maximum value is found to be  $\frac{1}{2} + \nu$ .

Using expression (24), it is found that the horizontal tangential stress can be evaluated by the integral

$$\frac{\sigma_{\theta\theta}}{p} = - \int_0^\infty \left\{ 2\nu J_0(\rho x) + (1 - 2\nu - \zeta x) \frac{J_1(\rho x)}{\rho x} \right\} J_1(x) \exp(-\zeta x) dx \quad (90)$$

The maximum value of the integral occurs at the origin, for  $\rho = \zeta = 0$ , and this maximum value is found to be  $\frac{1}{2} + \nu$ .

Using expression (27), it is found that the isotropic stress can be evaluated by the integral

$$\frac{\sigma_0}{p} = -\frac{2}{3}(1 + \nu) \int_0^\infty J_0(\rho x) J_1(x) \times \exp(-\zeta x) dx \quad (91)$$

The maximum value of the integral occurs at the origin, for  $\rho = \zeta = 0$ , and this maximum value is found to be 1, so that the maximum value of the isotropic stress is  $\frac{2}{3}(1 + \nu)$ . It can be verified from the above equations that  $\sigma_0 = \frac{1}{3}(\sigma_{rr} + \sigma_{\theta\theta} + \sigma_{zz})$ , as required.

Contours of the various stress components can be constructed by a computer program evaluating the various integrals. Examples for  $\nu = 0$  are shown in Figs. 9–12.

## Further Solutions

For many other problems, solutions can be found in the literature. Interesting examples are the solution of problems with mixed boundary conditions, such as the problem for a rigid plate pressed into an elastic half space, and problems for cracks in an elastic plane. Solutions for such problems are given by Sneddon [12] and Kassir and Sih [6]. Some results are also given by Verruijt [15].

## References

1. Abramowitz M, Stegun IA (1964) Handbook of mathematical functions. National Bureau of Standards, Washington
2. Churchill RV (1972) Operational mathematics, 3rd edn. McGraw-Hill, New York
3. Erdélyi A, Magnus W, Oberhettinger F, Tricomi FG (1954) Tables of integral transforms, vol 2. McGraw-Hill, New York
4. Green AE, Zerna W (1954) Theoretical elasticity. Clarendon, Oxford
5. Hetnarski RB, Ignaczak J (2011) The mathematical theory of elasticity, 2nd edn. CRC Press, Boca Raton
6. Kassir MK, Sih GC (1975) Three-dimensional crack problems. Noordhoff, Leyden
7. Landau LD, Lifschitz EM (1965) Elastizitätstheorie. Akademie, Berlin
8. Love AEH (1927) A treatise on the mathematical theory of elasticity, 4th edn. Cambridge University Press, Cambridge
9. Muskhelishvili NI (1953) Some basic problems of the mathematical theory of elasticity (Translated from the Russian by Radok JRM). Noordhoff, Groningen

10. Sadd MH (2005) Elasticity, theory, applications and numbers. Elsevier, Amsterdam
11. Sneddon IN (1951) Fourier transforms. McGraw-Hill, New York
12. Sneddon IN (1966) Mixed boundary value problems in potential theory. North-Holland, Amsterdam
13. Sokolnikoff IS (1956) Mathematical theory of elasticity. McGraw-Hill, New York
14. Timoshenko SP, Goodier JN (1970) Theory of elasticity, 3rd edn. McGraw-Hill, New York
15. Verruijt A (2010) An introduction to soil dynamics. Springer, Dordrecht

---

## Electric Boundary Conditions

- [Fracture of Piezoelectric Materials](#)

---

## Electric Current

- [Heat Conduction Problem for a Strip with a Notch](#)
- [Thermal Stresses Under Electric Current](#)

---

## Electric Field-Electric Potential Relations

- [Constitutive and Geometrical Equations for the Thermomechanical Analysis of Shells](#)

---

## Electrically Conducting Cracks

- [Fracture of Piezoelectric Materials](#)

---

## Electrically Insulating Cracks

- [Fracture of Piezoelectric Materials](#)
- [Strip Dielectric Breakdown Model in Piezoelectric Fracture Mechanics](#)

---

## Electrically Permeable or Impermeable Interface Cracks

- [Contact Zone Model for an Interface Crack in a Piezoelectric Bimaterial Under Thermoelectromechanical Loadings](#)

---

## Electroactive Materials

- [Fracture of Electrostrictive Materials](#)

---

## Electroconductive Composites Subjected to Magnetoelastic and Thermomechanical Loadings: Nonlinear Response and Stability

Davresh Hasanyan<sup>1</sup>, Zhanming Qin<sup>2</sup>, Jiefang Li<sup>1</sup> and Dwight Viehland<sup>1</sup>

<sup>1</sup>Department of Material Science and Engineering, Virginia Polytechnic Institute and State University, Blacksburg, VA, USA

<sup>2</sup>State Key Lab for Strength and Vibration of Mechanical Structures, Xi'an Jiaotong University, Xi'an, People's Republic of China

## Overview

Materials in which magnetic-elastic, thermal-elastic, and thermomagnetic coupling occur simultaneously in the same phase and allow coupling between the two others are known as magnetothermoelasticity. The phenomenon of coupling between the thermomechanical behavior of materials and the electromagnetic behavior of materials has been reported since the nineteenth century. By the middle of the twentieth century, electroelastic (piezoelectric) and magnetoelastic (piezomagnetic) materials were finding their first applications in hydrophones. In the last two decades, the concept of electromagneticelastic composite materials has arisen especially due to developments

in microelectromechanical systems (MEMS), nanostructures, sensors, and actuators. Such composites can exhibit field coupling that is not present in any of the monolithic constituent materials. With applications in ultrasonic imaging devices, sensors, actuators, transducers, and many other emerging components, there is a strong need for theories that can predict the coupled response of these so-called smart materials and composites, as well as structures composed of them (see [10–12, 31, 33, 35–37, 42, 52, 53]).

Magnetoelasticity is outlined in classical works of [1–5, 7, 10–12, 15, 21, 22, 27, 28, 32–39, 41, 47–51]. The application of magneto-active plate structures was examined by [31, 42, 46–52].

The advanced materials and micro/nano device technologies together with information technologies can be effectively integrated if the nonlinear interactions between the multiple fields can be understood and optimized for a given mission. This requires valid theoretical developments that can adequately represent the phenomenon associated with multiple functionalities and efficient methods to optimize the multi-parameter problem.

The equations of motion of electrically conducting plates in a magnetic field approached in a linear/nonlinear context have been derived by many authors [2–6, 8, 9, 16–20, 29, 35, 40, 43, 45, 54]. In [2–6, 16–20], these equations were obtained on the basis of the hypothesis of magnetoelasticity of thin plates. Linear equations of magnetoelastic perfectly electrically conducting thin plates were obtained in [2, 3, 5, 23–25] on the basis of the Kirchhoff hypothesis. By using Kirchhoff hypotheses in [4, 17], two-dimensional linear magnetoelasticity equations were obtained for perfectly conducting plates. Refs. [16–20] are devoted to formulating the nonlinear equation of a conducting plate in a magnetic field. Refs. [18, 19, 43] investigated the nonlinear behavior of a plate in a magnetic field. A model of the equations of generalized magnetothermoelasticity in a perfectly conducting medium is given [13, 14].

The interest in problems of vibration and instability of current carrying thin walled structures grew out from the study of similar

instabilities in plasma physics. Superconductors can carry very high currents and find use in plasma confinement of thermonuclear power generation and in magnetic levitation of high speed transportation systems. Such a work was reported in [8, 26, 33], where it was concluded that a flexible rod carrying current is inherently unstable. The theory of magnetothermoelasticity is concerned with the interacting effects of an externally applied magnetic field on the elastic and thermoelastic deformations of a solid body. This theory is being developed because of the possibilities of their extensive practical applications in aerospace engineering, geophysics, optics, acoustics as well as in other areas. A comprehensive review of the earlier contributions to the subject can be found in [33, 38, 39, 42].

Following paragraphs devoted to the foundation of a geometrically nonlinear dynamic theory of thermoelastic thin plates that are electrically conducting and immersed in a magnetic field of arbitrary spatial orientation is addressed. The plate model is developed within the Kirchhoff hypothesis. It is assumed that elastic, electrical, and thermal properties of the plate are orthotropic, which implies that in the Ohm's and Ampere's laws, as well in the Maxwell's equations, the terms of the order of magnitude of relativistic correction are negligibly small, and as a result are discarded. These terms concern the electrical free charges appearing in the Ohm's law, the electrical terms in the Maxwell's stress tensor, and the displacement current in Ampere's law. The involved equations reveal that the external magnetic field components appear in the terms associated with the body forces (referred to as *ponderomotive* forces). As a result, these terms intervene in the equations of motion of flat plates. Another complexity concerns the fact that the components of the induced magnetic field depend on both transverse plate deflection and tangential displacement quantities. This implies that even for a symmetric and geometrically linear plate, the magnetoelastic effects induce a coupling between the bending and the stretching motions (see e.g. Ref. 5). Finally, the governing equations

of plates and shells have to be obtained by taking into consideration and fulfilling the boundary conditions at the intersection surfaces between the outer and inner electromagnetic and thermal fields. These involve the conditions that should be prescribed at the bounding surfaces of the plate, where a discontinuity of the electromagnetic and thermal quantities of the outer (surrounding) and inner (i.e., within the plate) electromagnetic quantities is experienced.

### Basic Assumption

Consider an orthotropic electrically conducting elastic plate. We assume that the plate is of uniform thickness and that the constituent layers can be of different materials. The points of the non-deformed plate are referred to the 3-D Cartesian coordinate system  $x_i$  ( $i = 1, 2, 3$ ), where  $(x_1, x_2)$  are the in-plane coordinates associated with the points of undeformed mid-plane of the plate, while  $x_3$  ( $|x_3| \leq h$ ) is the thickness coordinate. The plate occupies  $\Omega_{pl} = \{-l_1 \leq x_1 \leq l_1; -l_2 \leq x_2 \leq l_2; -h \leq x_3 \leq h\}$  and vibrates in the vacuum ( $(x_1, x_2, x_3) \in \mathbb{R}_3/\Omega_{pl}$ ,  $\mathbb{R}_3$  - is three-dimensional Euclidean space). The bottom and top planes of the  $j$ th constituent layer are defined by the interfaces  $z_j$  and  $z_{j+1}$ , respectively, whose thickness is  $h_j = z_{j+1} - z_j$ . The plate is immersed in an external magnetic field  $\mathbf{H}_0^{ex}$ . It is assumed that the initial magnetic field  $\mathbf{H}_0$  ( $(\mathbf{H}_0)_1, (\mathbf{H}_0)_2, (\mathbf{H}_0)_3$ ) is known. Note that the magnetic field  $\mathbf{H}_0$  can be generated either by the electrical current  $J_0$ , or by the external enclosed magnetic field  $\mathbf{H}_0^{ex}$ .

### Field Equations

We consider an electrically conducting elastic plate subjected to thermomechanical loads and immersed in a 3-D time-dependent magnetic field  $\mathbf{H}$ . The material of the plate is assumed to be homogeneous and anisotropic. In the modeling of the plate, the geometric nonlinearities are incorporated. While the elastic, thermal, and the electromagnetic fields can be determined from

the elastic, thermal, and Maxwell's equations, the interaction of these three fields will generate new phenomena. As it will be subsequently shown, the electromagnetic field influences the thermoelastic field by entering the elastic stress equations of motion as the magnetic body forces (referred to as Lorentz's ponderomotive force), whereas the elastic and thermal fields in its turn influence the electromagnetic field by modifying Ohm's law.

In order to be reasonably self-contained, in what follows, we summarize the dynamic electromagnetic as well as the equations of motion of a 3-D elastic medium. Expressed in Gauss's system of units, in the absence of electrical free charges, the relevant equations are (see [7, 10–12, 21, 28, 36, 37, 41, 42]):

$$\text{curl } \mathbf{E} = -\frac{\partial \mathbf{B}}{\partial t} \Rightarrow \text{Faraday's Law} \quad (1)$$

$$\text{curl } \mathbf{H} = \mathbf{J} \Rightarrow \text{Ampere's Law} \quad (2)$$

$$\mathbf{J} = \hat{\sigma}(\mathbf{E} + \frac{\partial \mathbf{V}}{\partial t} \times \mathbf{B}) \text{ Ohm's Law} \quad (3)$$

Equations of motion of a geometrically nonlinear 3-D elastic body in Lagrangian description:

$$[S_{jr} (\delta_{ir} + V_{i,r})]_{,j} + f_i = \rho_0 \ddot{V}_i \quad (4)$$

The modified Fourier's law of heat conduction (see [7, 10–12, 21, 28, 36, 37, 41, 42]):

$$k_{ij}\theta_{,ij} - T_0\beta_{ij}\dot{e}_{ij} - c_e\dot{\theta} + W^t = 0 \quad (5)$$

Equation (4) include the electromagnetic effects in terms of Lorentz's ponderomotive forces and magnetization effects. In Eq. (4),  $\delta_{ij}$  is the Kronecker delta,  $S_{ij} (\equiv S_{ji})$  are the components of the second Piola-Kirchhoff stress tensor and  $\mathbf{V}$  ( $V_1, V_2, V_3$ ) is the displacement vector of components  $V_i$  of the points of the 3-D elastic medium, while in Eq. (5),  $W^t$  represents the intensity of heat source, which is  $W^t = \hat{\sigma}^{-1} \vec{J} \cdot \vec{J}$  when the Joule's heat effect will



be considered. Note that  $\hat{\sigma} = \begin{pmatrix} \sigma_{11} & \sigma_{12} & 0 \\ \sigma_{12} & \sigma_{22} & 0 \\ 0 & 0 & \sigma_{33} \end{pmatrix}$

is the matrix of electrical conductivity, where  $\sigma_{11} = \sigma_1 \cos^2 \vartheta + \sigma_2 \sin^2 \vartheta$ ,  $\sigma_{22} = \sigma_2 \cos^2 \vartheta + \sigma_1 \sin^2 \vartheta$ ,  $\sigma_{12} = (\sigma_2 - \sigma_1) \sin \vartheta \cos \vartheta$ ,  $\sigma_{33} = \sigma_3$ ;  $\sigma_i$  ( $i = 1, 2, 3$ ) is the electric conductivity in  $x_i$  ( $i = 1, 2, 3$ ) direction;  $\vartheta$  is the ply angle;  $\theta = T - T_0$  ( $T_0$  is the reference temperature, over which the perturbed temperature is  $T$ );  $k_{ij}$  and  $\beta_{ij}$  are the thermal coefficients.

In Eq. (4),  $f_i$  are the components of effective ponderomotive force vector  $f$  per unit volume. The expression of  $f_i$  resulting as superposition of Lorentz and magnetization effects is (see [7, 10–12, 21, 28, 36, 37, 41, 42, 48, 49, 53]):

$$f = f^L + f^M \quad (6)$$

where

$$f^L = \mathbf{J} \times \mathbf{B} \text{ and } f^M = \mathbf{M} \cdot \nabla \mathbf{H} \quad (7)$$

For anisotropic, linear ferromagnetic materials, the constitutive equations are:

$$\mathbf{B} = \hat{\mu} \mathbf{H}$$

$$\mathbf{J} = \hat{\sigma}(\mathbf{E} + \dot{\mathbf{V}} \times \mathbf{B})$$

$$\mathbf{M} = \hat{\chi} \mathbf{H}$$

$$S_{ij} = C_{ijkl} e_{kl} + T_0 \beta_{ij} \theta = C_{ijkl} (e_{kl} - T_0 \alpha_{kl} \theta) \quad (8a-d)$$

In these equations,  $\hat{\mu}$  is the matrix of magnetic permeability and  $\hat{\chi} (\equiv \hat{\mu} - 1)$  is the matrix of magnetic susceptibility;  $C_{ijkl}$  are the elastic coefficients,  $\alpha_{kl}$  is thermal coefficient. In Ohm's law (8b), the effects of temperature are disregarded;

Equations (4), (5), and (8) describe the interaction between the elastic, thermal, and electromagnetic fields. In these equations,  $\mathbf{E}$  and  $\mathbf{H}$  are the electric and magnetic field vectors,

respectively,  $\mathbf{J}$  is the current-density vector,  $\mathbf{B}$  is the magnetic induction vector,  $c$  is the speed of electromagnetic waves in the corresponding medium;  $\rho_0$  is the mass per unit volume of the elastic solid in the undeformed state. In the above equations, as well as in the next ones, the Einstein summation convention over a repeated index is implied, where Latin indices range from 1 to 3, while Greek indices range from 1 to 2. In addition, partial differentiation is denoted by a comma,  $(\cdot)_{,i} \equiv \partial(\cdot)/\partial x_i$ , whereas the overdots denote time derivatives.

To the previously displayed equations, we have to add the following one

$$\text{div} \mathbf{B} = 0 \quad (9)$$

For the elastic plate modeled within the Kirchhoff hypothesis its material being considered to be anisotropic, the pertinent constitutive equations correlating Piola-Kirchhoff stress  $\hat{S}$  with the Lagrangian strain tensor  $\hat{e}$  are given by:

$$\hat{S} = \hat{Q}(\hat{e} - \hat{\alpha} \theta) \quad (10a-c)$$

where

$$\hat{S} = \begin{pmatrix} S_{11} \\ S_{22} \\ S_{12} \end{pmatrix}; \hat{Q} = \begin{bmatrix} Q_{11} & Q_{12} & Q_{16} \\ Q_{12} & Q_{22} & Q_{26} \\ Q_{16} & Q_{26} & Q_{66} \end{bmatrix};$$

$$\hat{\alpha} = \begin{pmatrix} \alpha_{11} \\ \alpha_{22} \\ \alpha_{12} \end{pmatrix}; \hat{e} = \begin{pmatrix} e_{11} \\ e_{22} \\ e_{12} \end{pmatrix}$$

Within the Lagrangian description and consistent with von Kármán's assumption, the 3-D strain components  $e_{\alpha\beta}$  expressed in terms of the 3-D displacement components  $V_\alpha$  and  $V_3$  are (see [1–10, 30, 44]):

$$2e_{\alpha\beta} = V_{\alpha,\beta} + V_{\beta,\alpha} + V_{3,\alpha} V_{3,\beta} \quad (11)$$

The previously displayed equations are associated with the inner domain occupied by

the plate. For the domain outside the plate, (considered to coincide with the vacuum), the equations governing the electromagnetic field are given by:

$$\text{curl } \mathbf{H}_e = 0, \text{ div } \mathbf{H}_e = 0, \text{ curl } E_e = -\frac{1}{c_e} \frac{\partial \mathbf{H}_e}{\partial t} \quad (12a-c)$$

In these equations, the index “e” identifies quantities associated with the outer plate domain (i.e., of the vacuum).

For simple media  $c \cong c_e$ . Finally, toward establishing the governing equations of electro-magnetic conducting plates, it should be recalled (see, e.g., [6]) that in a magnetic field, the forces that are induced act on the external surfaces of the conducting body as well. These forces are related to the Maxwell’s stress tensor and are defined by:

$$T_{ij} = B_i H_j - \frac{1}{2} \mathbf{H}^2 \delta_{ij}, \quad i, j = 1, 2, 3 \quad (13)$$

where  $H_i$  are the components of the magnetic field  $\mathbf{H}$ .

At the external surfaces of the plate that separate two media with different electromagnetic properties, the field vectors experience discontinuities that are specified by a number of boundary conditions. Restricting ourselves to the conditions that will be required in the next developments, these conditions are:

$$\begin{aligned} \mathbf{n} \times [\mathbf{E} - \mathbf{E}_e] &= 0 \\ \mathbf{n} \times [\mathbf{H} - \mathbf{H}_e] &= \mathbf{J}_s \\ \mathbf{n} \cdot [\mathbf{B} - \mathbf{B}_e] &= 0 \end{aligned} \quad (14a-c)$$

where  $\mathbf{n}$  is the unit vector of the external normal to the plate surface;  $\mathbf{J}_s$  is electric current vector at the surface of the body. These conditions stipulate that the tangential components of  $\mathbf{E}$  and the normal components of  $\mathbf{B}$  are continuous at the medium interfaces.

In the same context, the additional boundary conditions that should be fulfilled on the

bounding surfaces  $x_3 = \pm h$  of the plate are expressed as (see Refs. 5, 8–10):

$$n_i [S_{ij} + S_{jr} V_{i,r} + T_{ij}] = F_j + n_i (T_{ij})_e \quad (15)$$

where  $n_i$  are the components of the unit vector  $\mathbf{n}$ , while  $F_j$  are the components of the surface load vector  $\mathbf{F}$  of mechanical origin. Boundary conditions (14) supplement the ones provided by Eqs. (13). The boundary conditions for the thermal field can be represented in the form [19, 42, 43]:

$$n_i k_{ij} \theta_{,j} + \alpha_s [\theta - \theta_s] = 0 \quad (16)$$

where  $\alpha_s$  is the thermal coefficient and  $\theta_s$  gives temperature on a surface of the plate.

The above displayed equations reveal the complexity of the electromagnetically conducting thermoelastic 3-D bodies, in general, and of their 2-D counterpart, in particular. This is compounded by the fact that in some equations, such as in Eqs. (4), (5), and (8), there are nonlinear terms that considerably complicate the investigation of the problem. At this point, one should distinguish between the structural nonlinearities involved in Eqs. (4) and (9), the ones of purely electromagnetic origin involved in Eqs. (5) and (11), and those of mixed nature, involved in the Ohm’s law, Eq. (3). In the following treatment, only the geometrical nonlinearities will be retained. With regard to the nonlinearities of electromagnetic and mixed origin, appearing in the previously indicated equations, these will be linearized within the *small disturbance concept*.

## Reduction of 3-D Magnetoelastic Equations to the 2-D Plate Counterpart

The plate under consideration is referred to an orthogonal 3-D Cartesian coordinate system,  $x_\alpha$ , in which, the coordinates  $x_\alpha$ , ( $\alpha = 1, 2$ ) coincide with the in-plane coordinates, while  $x_3$  is the thickness-wise coordinate ( $-h \leq x_3 \leq h$ )

with  $x_3 = 0$  defining the mid-plane of the plate (see [19, 43]).

Although the dynamic equations of electro-magnetically conducting plates in the presence of external magnetic fields can be obtained via a variational procedure, in this chapter, the method carried out in Ref. 3, based on the integration through the plate thickness of the 3-D equations of motion of electromagnetically conducting media, will be applied.

### Kinematical Equation

By virtue of the Kirchhoff hypothesis, the following 3-D displacement field is postulated

$$V_\alpha = v_\alpha - x_3 v_{3,\alpha}, \quad V_3 = v_3 \quad (17)$$

where  $v_\alpha \equiv v_\alpha(x_1, x_2, t)$  and  $v_3(x_1, x_2, t)$  denote the 2-D displacement quantities. Consistent with (14), the 3-D Lagrangian strain components, Eqs. (9), yield  $2e_{\alpha\beta} = \varepsilon_{\alpha\beta} + x_3 \kappa_{\alpha\beta}$ , where  $\varepsilon_{\alpha\beta}$  and  $\kappa_{\alpha\beta}$  denote the 2-D strain measures. As a result of the adoption of von-Kármán approximation, the 2-D strain measures assume the form:

$$2\varepsilon_{\alpha\beta} = v_{\alpha,\beta} + v_{\beta,\alpha} + v_{3,\alpha} v_{3,\beta}, \quad \kappa_{\alpha\beta} = -v_{3,\alpha\beta} \quad (18a, b)$$

where  $\varepsilon_{\alpha\beta} \equiv \varepsilon_{\alpha\beta}(x_1, x_2, t)$  and  $\kappa_{\alpha\beta} \equiv \kappa_{\alpha\beta}(x_1, x_2, t)$  denote the membrane and bending strains measures, respectively.

### Equations of Motion

Restricting in equations of motion (4), the geometric nonlinearities to those involving the transverse displacement  $v_3$  and its gradients, only, these equations become:

$$S_{11,1} + S_{12,2} + S_{13,3} + f_1 - (\rho_0 \ddot{v}_1 - \rho_0 x_3 \ddot{v}_{3,1}) = 0 \quad (19I)$$

$$S_{21,1} + S_{22,2} + S_{23,3} + f_2 - (\rho_0 \ddot{v}_2 - \rho_0 x_3 \ddot{v}_{3,2}) = 0 \quad (19II)$$

$$\begin{aligned} & (S_{13} + S_{11} v_{3,1} + S_{12} v_{3,2})_{,1} \\ & + (S_{23} + S_{21} v_{3,1} + S_{22} v_{3,2})_{,2} \\ & + (S_{33} + S_{31} v_{3,1} + S_{32} v_{3,2})_{,3} \\ & + f_3 - \rho_0 \ddot{v}_3 = 0. \end{aligned} \quad (19III)$$

Appropriate integration of Eqs. (19)I, II, III through the wall thickness, in the sense of  $\int_{-h}^h (I; II; III) dx_3 = 0$  and  $\int_{-h}^h (I; II) x_3 dx_3 = 0$ , where I, II, and III, correspond to the first, second, and third equations of (19), having in view the proper definition of 2-D stress resultants  $N_{\alpha\beta}$ ,  $Q_{\alpha 3}$  and stress-couples  $M_{\alpha\beta}$ , and carrying out the exact elimination of transverse shear stress resultants  $Q_{\alpha 3}$  among the last three equations of motion reduced to the 2-D form yields:

$$N_{11,1} + N_{12,2} + S_{13}^+ - S_{13}^- + \int_{-h}^h f_1 dx_3 = 2\rho_0 h \ddot{v}_1 \quad (20a)$$

$$N_{21,1} + N_{22,2} + S_{23}^+ - S_{23}^- + \int_{-h}^h f_2 dx_3 = 2\rho_0 h \ddot{v}_2 \quad (20b)$$

$$\begin{aligned} & M_{11,11} + 2M_{12,12} + M_{22,22} + N_{11} v_{3,11} \\ & + N_{22} v_{3,22} + 2N_{12} v_{3,12} + (N_{11,1} + N_{12,2}) v_{3,1} \\ & + [N_{22,2} + N_{12,1}] v_{3,2} + (S_{33}^+ - S_{33}^-) \\ & + (S_{31}^+ - S_{31}^-) v_{3,1} + (S_{32}^+ - S_{32}^-) v_{3,2} + h[S_{31}^+ + S_{31}^-]_{,1} \\ & + h[S_{32}^+ + S_{32}^-]_{,2} + \frac{\partial}{\partial x_1} \int_{-h}^+ f_1 x_3 dx_3 \\ & + \frac{\partial}{\partial x_2} \int_{-h}^+ f_2 x_3 dx_3 + \int_{-h}^+ f_3 dx_3 = 2\rho_0 \ddot{v}_3 \end{aligned} \quad (20c)$$

In these equations,  $S_{3i}^+ \equiv S_{3i}|_{+h}$ ,  $S_{3i}^- \equiv S_{3i}|_{-h}$ . Moreover, in the derivation of



the 2-D equations of motion, the rotatory inertia terms have been discarded. Note that in

$$\text{Eqs. (20a–20c), } \int_{-h}^h (\cdot) dx_3 = \sum_{k=1}^N \int_{z_k}^{z_{k+1}} (\cdot) dz_k,$$

where  $N$  is the number of the constituent layers.

For the sake of completion, the expressions of transverse shear stress resultants are also displayed:

$$\begin{aligned} Q_{13} &= M_{11,1} + M_{12,2} + h(S_{31}^+ + S_{31}^-) \\ &\quad + \int_{-h}^{+h} f_{1x_3} dx_3 = 0 \\ Q_{23} &= M_{21,1} + M_{22,2} + h(S_{32}^+ + S_{32}^-) \\ &\quad + \int_{-h}^{+h} f_{2x_3} dx_3 = 0 \end{aligned} \quad (21d-e)$$

At this point, it should be remarked that as a result of the inclusion of geometric nonlinearities, by virtue of the previously displayed equations and of elastic constitutive equations:

$$\begin{Bmatrix} \hat{N} \\ \hat{M} \end{Bmatrix} = \begin{pmatrix} \hat{A} & \hat{B} \\ \hat{B} & \hat{D} \end{pmatrix} \begin{Bmatrix} \hat{\varepsilon} \\ \hat{\kappa} \end{Bmatrix} - \begin{Bmatrix} \hat{N}^t \\ \hat{M}^t \end{Bmatrix} \quad (22)$$

where  $\hat{\varepsilon} = (\varepsilon_{11} \ \varepsilon_{22} \ \varepsilon_{12})^T$ ;  $\hat{\kappa} = (\kappa_{11} \ \kappa_{22} \ \kappa_{12})^T$  ( $(\cdot)^T$  is the transpose operator of the matrix  $(\cdot)$ ); the elements of matrices  $\hat{A}$ ,  $\hat{D}$ ,  $\hat{B}$ ,  $\hat{N}^t$  and  $\hat{M}^t$  are given in a form:

$$\begin{aligned} (A_{ij}, B_{ij}, D_{ij}) &= \int_{-h}^h Q_{ij}(1, x_3, x_3^2) dx_3; \\ (N_i^t, M_i^t) & \\ &= \int_{-h}^h \sum_{j=1}^3 Q_{ij} \alpha_{ij}(1, x_3) \theta dx_3 \end{aligned} \quad (23)$$

In the case of single-layer, from formulas (23) we get:

$$\begin{aligned} \hat{A} &= 2h\hat{Q}; \quad \hat{D} = h^3\hat{Q}/3 \\ \hat{N}^t &= \hat{Q}\hat{\alpha}\theta_0 2h; \quad \hat{M}^t = \hat{Q}\hat{\alpha}\theta_1 h^3/3; \quad \hat{B} = 0 \end{aligned} \quad (24)$$

In Eq. (24), it is assumed that the thermal field experiences a linear variation through the plate thickness given by  $\theta = \theta_0 + \frac{x_3}{h}\theta_1$ .

### Equations of Electrodynamics

From Eq. (6) considered in conjunction with Eqs. (3) and (7), it clearly appears that the components of the Lorentz force vector are nonlinear. As it was previously mentioned, within the present plate model only geometrical nonlinearities will be retained. Consequently, due to the implementation of the small disturbance linearization concept, the equations will become linear from the electromagnetic point of view. To this end, the electromagnetic field quantities are represented as:

$$\mathbf{E} = \mathbf{E}_0 + \mathbf{e}, \quad \mathbf{H} = \mathbf{H}_0 + \mathbf{h}, \quad \mathbf{B} = \mathbf{B}_0 + \mathbf{b} \quad (25)$$

In these equations:  $\mathbf{e}(\equiv \mathbf{e}(x_1, x_2, x_3, t))$ ,  $\mathbf{h}(\equiv \mathbf{h}(x_1, x_2, x_3, t))$  and  $\mathbf{b}(\mathbf{b} \equiv (x_1, x_2, x_3, t))$  are small disturbance of the primary electromagnetic field quantities,  $\mathbf{E}_0$ ,  $\mathbf{H}_0$ , and  $\mathbf{B}_0$ , respectively. As a result, the squares of disturbance quantities are second order terms that are negligibly small when compared with the undisturbed primary electromagnetic field quantities.

Such a procedure of linearization will be considered next. For the problem at hand,  $\mathbf{E}_0$  is a zero quantity, and only the induced electric field vector is different of zero, implying that for this case Eq. (25a) should be replaced by  $\mathbf{E} = \mathbf{0} + \mathbf{e}$ .

The Maxwell's equations for perturbed electromagnetic fields will be

$$\operatorname{curl} \mathbf{e} = -\frac{\partial \mathbf{b}}{\partial t} \quad (26)$$

$$\operatorname{curl} \mathbf{h} = \mathbf{j} \quad (27)$$

$$\mathbf{j} = \hat{\sigma} (\mathbf{e} + \frac{\partial \mathbf{V}}{\partial t} \times \mathbf{B}_0) \quad (28)$$

We assume that the plate is thin, and as a result, the reduction of the 3-D equations to their 2-D counterparts is achievable via the adoption of the Kirchhoff hypothesis. In addition, using Ambartsumyan's theory [2], the components  $e$  ( $x_1, x_2, x_3, t$ ) and  $h$  ( $x_1, x_2, x_3, t$ ) follow the rule:

$$\begin{aligned} e_1 &\equiv e_1(x_1, x_2, t) = \varphi(x_1, x_2, t) \\ e_2 &\equiv e_2(x_1, x_2, t) = \psi(x_1, x_2, t) \\ h_3 &\equiv h_3(x_1, x_2, t) = f(x_1, x_2, t) \end{aligned} \quad (29a-c)$$

In other words, in accordance with Ambartsumyan's model based on the asymptotic analysis of magnetoelastic field equations, the tangential components of  $\mathbf{e}$  (i.e.,  $e_1$  and  $e_2$ ), and the transversal components of the  $\mathbf{h}$  (i.e.,  $h_3$ ), are uniform across the plate thickness, and of course, constitute unknown quantities. These functions being determined, the remaining components, i.e.,  $e_3$  and  $h_1$  and  $h_2$ , can be obtained by using the relevant equations of electrodynamics.

In the next section, it will be assumed that magnetic permeability of a plate is zero, i.e.,  $\hat{\chi} = 0$ . We will assume also that undisturbed magnetic field within the plate is represented in the form  $\mathbf{B}_0 = \mathbf{B}_0^{(0)} + x_3 \mathbf{B}_0^{(1)}$ , where  $\mathbf{B}_0^{(0)}$  and  $\mathbf{B}_0^{(1)}$  are constant vectors. The boundary conditions (14) for the components of a perturbed magnetic field on a surface  $x_3 = \pm h$  can be represented as:

$$h_i = h_i^{(e)}, \quad (i = 1, 2, 3) \quad (30a-c)$$

Integrating Eqs. (26)–(28), using boundary conditions (30a–c) and assumptions (29a–c) for

the other components of electromagnetic field ( $h_1, h_2$  and  $e_3$ ), we get:

$$\begin{aligned} \begin{pmatrix} h_1 \\ -h_2 \end{pmatrix} &= \frac{1}{2} \begin{pmatrix} h_1^+ + h_1^- \\ h_2^+ + h_2^- \end{pmatrix} + x_3 \begin{pmatrix} \partial f / \partial x_1 \\ -\partial f / \partial x_2 \end{pmatrix} \\ &\quad + \hat{\sigma}^* [x_3 \hat{E}_0 + \frac{1}{2} (x_3^2 - h^2) \hat{E}_1 + x_3^3 \hat{E}_2] \end{aligned} \quad (31)$$

$$\begin{aligned} e_3(x_1, x_2, x_3, t) &= \frac{1}{\sigma_{33}} \left( \frac{\partial h_2}{\partial x_1} - \frac{\partial h_1}{\partial x_2} \right) \\ &\quad - (M_3^{(0)} + x_3 M_3^{(1)} + x_3^2 M_3^{(2)}) \end{aligned} \quad (33)$$

where

$$\begin{aligned} \hat{\sigma}^* &= \begin{pmatrix} \sigma_{12} & \sigma_{22} \\ \sigma_{11} & \sigma_{12} \end{pmatrix}, \hat{E}_0 = \begin{pmatrix} \varphi + M_1^{(0)} \\ \psi + M_2^{(0)} \end{pmatrix} \\ \hat{E}_1 &= \begin{pmatrix} M_1^{(1)} \\ M_2^{(1)} \end{pmatrix}, \hat{E}_2 = \begin{pmatrix} M_1^{(2)} \\ M_2^{(2)} \end{pmatrix} \end{aligned}$$

Note that while  $\hat{E}_1$  and  $\hat{E}_2$  are dependent upon only on the displacements of the plate,  $\hat{E}_0$  is dependent on functions  $\varphi$  and  $\psi$ , as well.

Equations for the unknown functions  $\varphi, \psi$  and  $f$ , after some transformation can take the form:

$$\begin{aligned} \frac{h_2^+ - h_2^-}{2h} &= \frac{\partial f}{\partial x_2} - [a_{11}\varphi + a_{12}\psi + a_{11}M_1^{(0)} \\ &\quad + a_{12}M_2^{(0)} + b_{11}M_1^{(1)} + b_{12}M_2^{(1)} + c_{11}M_1^{(2)} \\ &\quad + c_{12}M_2^{(2)}] \end{aligned} \quad (34)$$

$$\begin{aligned} \frac{h_1^+ - h_1^-}{2h} &= \frac{\partial f}{\partial x_1} + [a_{12}\phi + a_{22}\psi + a_{12}M_1^{(0)} \\ &\quad + a_{22}M_2^{(0)} + b_{12}M_1^{(1)} + b_{22}M_2^{(1)} + c_{12}M_1^{(2)} \\ &\quad + c_{22}M_2^{(2)}] \end{aligned} \quad (35)$$

$$\frac{\partial \psi}{\partial x_1} - \frac{\partial \phi}{\partial x_2} = -\frac{\partial f}{\partial t} \quad (36)$$

In Eqs. (31)–(36), the following notations are adopted:

$$(\hat{a}, \hat{b}, \hat{c}) \equiv \frac{1}{2h} \int_{-h}^h (1, x_3, x_3^2) \hat{\sigma} dx_3 \quad (37)$$

$$\begin{aligned} M^{(0)} &\equiv \frac{\partial v^{(0)}}{\partial t} \times B_0^{(0)}, & M^{(1)} &\equiv \frac{\partial v^{(0)}}{\partial t} \times B_0^{(1)} \\ &+ \frac{\partial v^{(1)}}{\partial t} \times B_0^{(0)}, & M^{(2)} &\equiv \frac{\partial v^{(1)}}{\partial t} \times B_0^{(1)} \end{aligned} \quad (38)$$

$$h_i^{\pm} \equiv h_i^{(e)}(x_1, x_2, \pm h, t) \quad (39)$$

Consistent with the Kirchhoff hypothesis, the components of the vectors  $\mathbf{v}^{(0)}$  and  $\mathbf{v}^{(1)}$  in Eq. (38) are given as:

$$\begin{aligned} v_i^{(0)} &= \partial v_i / \partial t, \quad (i = 1, 2, 3) \\ v_1^{(1)} &= -\partial^2 v_3 / \partial x_1 \partial t \\ v_2^{(1)} &= -\partial^2 v_3 / \partial x_2 \partial t \\ v_3^{(1)} &= 0 \end{aligned}$$

From Eq. (28), in conjunction with Eqs. (34)–(39), we get for a perturbed component of electrical current  $\mathbf{j}$ :

$$\begin{aligned} j_1(x_1, x_2, x_3, t) &= \sigma_{11} \varphi + \sigma_{12} \psi + \sigma_{11} M_1^{(0)} + \sigma_{12} M_2^{(0)} \\ &+ x_3 (\sigma_{11} M_1^{(1)} + \sigma_{12} M_2^{(1)}) + x_3^2 (\sigma_{11} M_1^{(2)} + \sigma_{12} M_2^{(2)}) \end{aligned} \quad (40)$$

$$\begin{aligned} j_2(x_1, x_2, x_3, t) &= \sigma_{12} \varphi + \sigma_{22} \psi + \sigma_{12} M_1^{(0)} + \sigma_{22} M_2^{(0)} \\ &+ x_3 (\sigma_{12} M_1^{(1)} + \sigma_{22} M_2^{(1)}) + x_3^2 (\sigma_{12} M_1^{(2)} + \sigma_{22} M_2^{(2)}) \end{aligned} \quad (41)$$

$$j_3 = \frac{\partial h_2}{\partial x_1} - \frac{\partial h_1}{\partial x_2} \quad (42)$$

In matrix form, Eqs. (40)–(41) can be expressed as:

$$\hat{j}_{pl} = \begin{pmatrix} j_1 \\ j_2 \end{pmatrix} = \hat{\sigma} [\hat{E}_0 + x_3 \hat{E}_1 + x_3^2 \hat{E}_2] \quad (40, 41)$$

### Thermal Equation

If we assume that the thermal field  $\theta$  experiences a linear variation through the plate thickness:

$$\theta = \theta_0(x_1, x_2, t) + \frac{x_3}{h} \theta_1(x_1, x_2, t) \quad (43)$$

Consistent with the results in Ref. 17,  $\theta_0$  and  $\theta_1$  fulfill the following equations:

$$L\theta_0 - (\alpha_+ \theta_0 + \alpha_- \theta_1) = -2hQ - (\alpha_+ t_+^c + \alpha_- t_-^c) \quad (44)$$

$$L\theta_1 - 3(\alpha_0 \theta_1 + \alpha_- \theta_0) = -2hQ - 3(\alpha_+ t_-^c + \alpha_- t_+^c) \quad (45)$$

where

$$\begin{aligned} L &= \Lambda_{11} \partial_{11}^2 + 2\Lambda_{12} \partial_{12}^2 + \Lambda_{22} \partial_{22}^2 - C \partial_t, \\ \partial_{ij} &= \partial / \partial x_i \partial x_j, \quad \partial_t = \partial / \partial t \end{aligned}$$

$$\Lambda_{ij} = \int_{-h}^h k_{ij} dx_3, \quad C = \int_{-h}^h c_v dx_3, \quad \alpha_{\pm} = \alpha_3^+ \pm \alpha_3^-,$$

$$\alpha_0 = 4\Gamma + \alpha_+, \quad \Gamma = \frac{1}{2h} \int_{-h}^h k_{33} dx_3,$$

$$t_{\pm}^c = 0.5(t_c^+ \pm t_c^-)$$

### Expressions for Electromagnetic Forces

When the magnetization of the material is zero, the body forces in (20)–(21) is expressed in the form:

$$\begin{aligned} \int_{-h}^h \mathbf{f} dx_3 &= 2h \left[ \frac{1}{2h} \int_{-h}^h \mathbf{j} dx_3 \times \mathbf{B}_0^{(0)} \right. \\ &\quad \left. + \frac{1}{2h} \int_{-h}^h \mathbf{j} x_3 dx_3 \times \mathbf{B}_0^{(1)} \right] \\ \int_{-h}^h \mathbf{f} x_3 dx_3 &= 2h \left[ \frac{1}{2h} \int_{-h}^h \mathbf{j} x_3 dx_3 \times \mathbf{B}_0^{(0)} \right. \\ &\quad \left. + \frac{1}{2h} \int_{-h}^h \mathbf{j} x_3^2 dx_3 \times \mathbf{B}_0^{(1)} \right] \end{aligned} \quad (47)$$

where

$$\mathbf{j} = \begin{pmatrix} \hat{j}_{pl} \\ \hat{j}_3 \end{pmatrix}^T$$

From the surface conditions (14)–(15):

$$S_{i3}^+ \pm S_{i3}^- = 0, \quad (i = 1, 2, 3) \quad (48)$$

Toward evaluating expressions (46)–(47), the following results are summarized:

$$\begin{aligned} \frac{1}{2h} \int_{-h}^h \hat{j}_{pl} dx_3 &= \hat{a} \hat{E}_0 + \hat{b} \hat{E}_1 + \hat{c} \hat{E}_2 \\ \frac{1}{2h} \int_{-h}^h \hat{j}_{pl} x_3 dx_3 &= \hat{b} \hat{E}_0 + \hat{c} \hat{E}_1 + \hat{d} \hat{E}_2 \\ \frac{1}{2h} \int_{-h}^h \hat{j}_{pl} x_3^2 dx_3 &= \hat{c} \hat{E}_0 + \hat{d} \hat{E}_1 + \hat{e} \hat{E}_2 \\ \frac{1}{2h} \int_{-h}^h \hat{j}_3 dx_3 &= - \left[ \frac{\partial \hat{h}_1^*}{\partial x_2} + \frac{\partial (-\hat{h}_2^*)}{\partial x_1} \right] \\ \frac{1}{2h} \int_{-h}^h x_3 \hat{j}_3 dx_3 &= - \left[ \frac{\partial \hat{h}_1^{**}}{\partial x_2} + \frac{\partial (-\hat{h}_2^{**})}{\partial x_1} \right] \\ \frac{1}{2h} \int_{-h}^h \hat{j}_3 x_3^2 dx_3 &= - \left[ \frac{\partial \hat{h}_1^{***}}{\partial x_2} + \frac{\partial (-\hat{h}_2^{***})}{\partial x_1} \right] \end{aligned} \quad (49a-f)$$

where

$$\begin{aligned} \begin{pmatrix} \hat{h}_1^* \\ -\hat{h}_2^* \end{pmatrix} &= \frac{1}{2h} \begin{pmatrix} \int_{-h}^h h_1 dx_3 \\ - \int_{-h}^h h_2 dx_3 \end{pmatrix} = \frac{1}{2} \begin{pmatrix} h_1^+ + h_1^- \\ -(h_1^+ + h_1^-) \end{pmatrix} \\ &+ \hat{a}^* \hat{E}_0 + \hat{b}^* \hat{E}_1 + \hat{c}^* \hat{E}_2; \\ \begin{pmatrix} \hat{h}_1^{**} \\ -\hat{h}_2^{**} \end{pmatrix} &= \frac{1}{2h} \begin{pmatrix} \int_{-h}^h h_1 x_3 dx_3 \\ - \int_{-h}^h h_2 x_3 dx_3 \end{pmatrix} = \frac{h^2}{3} \begin{pmatrix} \partial f / \partial x_1 \\ -\partial f / \partial x_2 \end{pmatrix} \\ &+ \hat{a}^{**} \hat{E}_0 + \hat{b}^{**} \hat{E}_1 + \hat{c}^{**} \hat{E}_2; \\ \begin{pmatrix} \hat{h}_1^{***} \\ -\hat{h}_2^{***} \end{pmatrix} &= \frac{1}{2h} \begin{pmatrix} \int_{-h}^h h_1 x_3^2 dx_3 \\ - \int_{-h}^h h_2 x_3^2 dx_3 \end{pmatrix} \\ &= \frac{h^2}{3} \begin{pmatrix} h_1^+ + h_1^- \\ -(h_1^+ + h_1^-) \end{pmatrix} \\ &+ \hat{a}^{***} \hat{E}_0 + \hat{b}^{***} \hat{E}_1 + \hat{c}^{***} \hat{E}_2 \\ (\hat{a}, \hat{b}, \hat{c}, \hat{d}, \hat{e}) &= \frac{1}{2h} \int_{-h}^h (1, x_3, x_3^2, x_3^3, x_3^4) \hat{\sigma} dx_3 \\ (\hat{a}^*, \hat{b}^*, \hat{c}^*) &= \frac{1}{2h} \int_{-h}^h \left( x_3, \frac{x_3^2 - h^2}{2}, \frac{x_3^3}{3} \right) \hat{\sigma}^* dx_3 \\ (\hat{a}^{**}, \hat{b}^{**}, \hat{c}^{**}) &= \frac{1}{2h} \int_{-h}^h x_3 \left( x_3, \frac{x_3^2 - h^2}{2}, \frac{x_3^3}{3} \right) \hat{\sigma}^* dx_3 \\ (\hat{a}^{***}, \hat{b}^{***}, \hat{c}^{***}) &= \frac{1}{2h} \int_{-h}^h x_3^2 \left( x_3, \frac{x_3^2 - h^2}{2}, \frac{x_3^3}{3} \right) \hat{\sigma}^* dx_3 \end{aligned} \quad (50a-g)$$

Equations of motion of anisotropic elastic plates Eqs. (20–23), the thermal equations (44)–(45) and the equations of electrodynamics Eqs. (34–36) constitute the full system of equations governing the motion of multilayered, anisotropic, electroconductive elastic thin plates in a combined thermal and magnetic fields.

Developed theory enables one to investigate the interacting effects among the magnetic, the thermal, and the elastic fields in orthotropic thin plates. In the same context, the problem of the free vibration, stability and wave propagation as influenced by the electroconductivity of the constituent materials, by the magnetic and thermal fields can be addressed.

## References

1. Alblas JB (1974) Electra-magneto-elasticity. In: Zeman JL, Ziegler F (eds) Topics in applied continuum mechanics. Springer, Vienna, pp 71–114
2. Ambartsumyan SA, Bagdasaryan GE (1996) Electroconductive plates and shells in a magnetic field [in Russian]. Nauka, Moscow, p 288
3. Ambartsumyan SA, Belubekyan MV (1991) Some problems of electromagnetoelasticity of plates, [in Russian]. YSU, Yerevan, p143
4. Bagdasaryan GE (1983) Equations of magnetoelastic vibrations of thin perfectly conducting plates. Sov Appl Mech 19(N12):1120–1124
5. Bagdasaryan GE (1999) Vibrations and stability of magneto elastic systems [in Russian]. Editorial Board of Yerevan State University, Yerevan, p 435
6. Bagdasaryan GE, Danoyan ZN (1985) The basic equations and relations of nonlinear magnetoelastic vibration of thin electroconducting plates [in Russian]. Proc Nat Acad Sci Armen, Mech 38(2):17–29
7. Brown WF Jr (1966) Magneto elastic interactions, vol 9, Tracts in natural philosophy. Springer, Berlin
8. Chattopadhyay S, Moon FC (1975) Magnetoelastic buckling and vibration of a rod carrying electric current. J Appl Mech 42:809–814
9. Dolbin NI, Morozov AI (1966) Elastic bending vibrations of a rod carrying electric current. Zhurnal Prikl Mech I Tech Fiziki (in translation) N3:97–103
10. Eringen AC (1980) Mechanics of continua, 2nd enlarged edn. Krieger, New York
11. Eringen AC, Maugin GA (1990) Electrodynamics of continua I. Springer, Foundations and solid media, p 436
12. Eringen AC, Maugin GA (1989) Electrodynamics of continua. Springer, New York
13. Ezzat MA, El-Karamany AS (2002) Magnetothermoelasticity with thermal relaxation in a conducting medium with variable electrical and thermal conductivity. J Therm Stress 25:859–875
14. Ezzat MA, Youssef HM (2005) Generalized magneto-thermoelasticity in a perfectly conducting medium. Int J Solids Struct 42:6319–6334
15. Green AE, Naghdi PM (1983) On electromagnetic effects in the theory of shells and plates. Phil Trans R Soc Lond A 309:559–610
16. Hasanyan DJ (2009) Mathematical modeling and analysis of magneto thermo-elastic plate. J Therm Stress 32(1–2):65
17. Hasanyan DJ, Khachatryan GM, Philiposyan GT (2001) Mathematical modeling and investigation of nonlinear vibration of perfectly conductive plates in an inclined magnetic field. Thin-Walled Struct 39(1):111–112
18. Hasanyan DJ, Librescu L, Ambur DR (2006) Buckling and postbuckling of magnetoelastic flat plates carrying an electric current. Int J Solids Struct 43(16):4971–4996
19. Hasanyan DJ, Librescu L, Qin Z, Ambur DR (2005) Magneto-thermo-elasticity of geometrically nonlinear laminated composite plates, Part I: foundation of the theory. J Sound Vib 287(1–2): 153–175
20. Hasanyan D, Librescu L, Qin Z, Young R (2007) Thermoelastic cracked plates carrying nonstationary electrical current. J Therm Stress 28:729–745
21. Hutter K, Pao YH (1974) A dynamic theory for magnetizable elastic solids with thermal and electrical conduction. J Elast 4:89–119
22. Hutter K, Van De Ven AAF (1978) Field matter interactions in thermoelastic solids, vol 88, Lecture notes in physics. Springer, Berlin
23. Kaliski S (1962) Magnetoelastic vibration of perfectly conducting plates and bars assuming the principle of plane sections. Proc Vib Probl 3(N4):225–234
24. Kaliski S (1966) Cherenkov generation of thermal waves for the wave equations of thermo-electromagnetoelasticity. Arch Mech Stosow 6:18–25
25. Kaliski S, Nowacki W (1969) Thermal excitations in coupled fields. In: Nowacki WK (ed) Progress in thermoelasticity. P. W. N, Warsaw, pp 83–101
26. Kazarian KB (1985) Magnetoelastic stability of a current-carrying rod in an external magnetic field. Eng Trans 33(N3):277–283
27. Kiral E, Eringen AC (1990) Constitutive equations of nonlinear electromagnetic-elastic crystals. Springer, New York, p 236
28. Landau LD, Lifshitz EM (1984) Electrodynamics of continuous media. Pergamon, Oxford, p 460
29. Li J (2003) Uniqueness and reciprocity theorems for linear thermo-electro-magneto-elasticity. Q J Mech Appl Math 56(1):35–43
30. Librescu L (1975) Elastostatics and kinetics of anisotropic and heterogeneous shell-type structures. Noordhoff International, Leyden, p 560
31. De Lorentz HG, Tiersten HF (1975) On the interaction of the electromagnetic field with heat conducting deformable semiconductors. J Math Phys 16:938–957
32. Maugin GA, Pouget J, Drouot R, Collet B (1992) Nonlinear electromechanical couplings. Wiley, New York, p 394
33. Maugin GA (1988) Continuum mechanics of electromagnetic solids. North-Holland, New York, p 598

34. Maugin GA, Eringen AC (1977) On the equations of the electrodynamics of deformable bodies of finite extent. *J Met* 16:101–147
35. Moon FC (1978) Problems in magneto-solid mechanics. In: Nemat-Nasser S (ed) *Mechanics today*, vol 4. Pergamon, Oxford
36. Nowacki W (1986) *Thermoelasticity*, 2nd edn. P.W.N. Warsaw/Pergamon, Oxford
37. Nowinski JL (1978) Theory of thermoelasticity with applications. Sijthoff & Noordhoff, Alphen aan den Rijn, p 836
38. Paria G (1968) Magneto-elasticity and magneto-thermo-elasticity. In: Kuerti G (ed) *Advances in applied mechanics*, vol 10. Academic, New York, pp 73–112
39. Parkus H (1972) Magneto-Thermoelasticity Lecture notes, CISM, Udine. Springer, Vienna.
40. Paul HS, Narasimhan R (1987) The vibration of a thermoelastic plate in a large static magnetic field. *Indian J Pure Appl Math* 18(5):451–460
41. Podstrigach YS, Burak YI, Kondrat WF (1977) Magneto-thermoelasticity of electroconducting bodies. Naukovo Dumka, Kiev, p 247 (in Russian)
42. Parton VZ, Krudiyavtsev BA (1988) *Electromagnetoelasticity piezoelectrics and electrically conductive solids*. Taylor & Francis, New York
43. Qin Z, Hasanyan DJ, Librescu L, Ambur DR (2005) Magneto-thermo-elasticity of geometrically nonlinear laminated composite plates, Part II: vibration and wave propagation. *J Sound Vib* 287(1–2):177–201
44. Reddy JN (1996) *Mechanics of laminated composite plates*. CRC Press, Theory and analysis, p 782
45. Rudnicki M (2002) Eigenvalue solutions for free motion of electroconductive plate in magnetic field. *Int J Eng Sci* 40:93–107
46. Tauchert TR (1992) Piezothermoelastic behavior of a laminated plate. *J Therm Stress* 15:25–37
47. Tiersten HF (1969) *Linear piezoelectric plate vibrations*. Plenum, New York
48. Tiersten HF (1971) On the nonlinear equations of thermoelectroelasticity. *Int J Eng Sci* 9:587–604
49. Tiersten HF (1964) Coupled magnetomechanical equations for magnetically saturated insulators. *J Math Phys* 5:1298–1318
50. Toupin RA (1956) The elastic dielectric. *J Rat Mech Anal* 5:849–915
51. Truesdell CA, Toupin RA (1960) The classical field theories. In: Flügge S (ed) *Handbuch der Physik*, Bd. III/1. Springer, Berlin, pp 226–790
52. Uchino K (1997) *Piezoelectric actuators and ultrasonic motors*. Kluwer, Hingham
53. Verma PDS, Singh M (1984) Finite deformation theory for soft ferromagnetic elastic solids. *Int J Non-Linear Mech* 19(N4):273–286
54. Wilson AJ (1963) The propagation of magneto-thermo-elastic plane waves. *Proc Camb Phil Soc* 59:483–488

---

## Electroconductivity

- [Dynamic Stability of Electroconductive Cylindrical Shells in Magnetic Field](#)
- [Vibrations of Electroconductive Cylindrical Shells in a Magnetic Field](#)

---

## Electromagnetism

- [Green's Functions of Magneto-Electro-Elastic Plate Under Thermal Loading](#)

---

## Electromagneto Coupled and Generalized Thermoelasticity

Magdy A. Ezzat

Department of Mathematics, Faculty of Education, Alexandria University, Alexandria, Egypt

Department of Mathematics, Faculty of Science and Letter in Al Bukayriyyah, Al-Qassim University, Al-Qassim, Saudi Arabia

## Definition

The theories of magnetoelasticity and magnetothermoelasticity are concerned with the interacting effects of an externally applied magnetic field on the elastic and thermoelastic deformations of a solid body. If an electrically conducting elastic solid is subjected to a mechanical load while immersed in a varying magnetic field, the laws of Hooke and Maxwell will still determine the elastic field and the electromagnetic field respectively.

## Overview

In the last one or two decades, the subject matter of magnetoelastic interactions has rapidly

developed. The corresponding theories in turn have stimulated extensive studies, especially concerning their applications to various physical situations. Although most of the ideas and mathematical formalisms for continuum physics were already available in the late nineteenth century, magnetoelasticity and the allied wave propagation problems have been a development of the twentieth century and, more particularly, of the post war years. The relevant concepts and methods draw not only on classical linear elasticity and classical magnetostatics, but also on nonlinear continuum mechanics (large deformations, strong initial fields), statistical mechanics of matter in electromagnetic fields, and notions of quantum mechanics. Furthermore, most of the physical effects thus described were placed in evidence only very recently [1].

The increasing wide use in sensing and actuation has attracted much attention toward theories about materials exhibiting couplings between elastic, electric, magnetic, and thermal fields. The foundations of magnetoelasticity were presented by Knopoff [2] and Chadwick [3] and developed by Kaliski and Petykiewicz [4]. Paria [5] discussed the propagation of plane magnetothermoelastic waves in an isotropic unbounded medium under the influence of a uniform thermal field and with a magnetic field acting transversely to the direction of the propagation. Wilson [6] extended Paria's results by introducing a component of the magnetic field parallel to the direction of the propagation. In the cited papers, it was assumed that the interactions between the two fields take place by means of the Lorentz forces appearing in the equations of motion and by means of a term entering Ohm's law and describing the electric field produced by the velocity of a material particle moving in a magnetic field. Usually, in these investigations, the heat equation under consideration is taken as the uncoupled or the coupled [7]. Sherief and Ezzat studied a thermal-shock problem in generalized magnetothermoelasticity with thermal relaxation time [8]. Ezzat and El-Karamany studied some problems in magnetothermoelasticity in a conducting medium with variable electrical and

thermal conductivities [9]. Ezzat et al. [10] have established the model of two-dimensional equations of generalized magnetothermoelasticity.

## Basic Methodology

### Modeling Linear Coupled Magnetothermoelasticity

The first set of equations constitutes the Maxwell's equations of electrodynamics of slowly moving bodies:

$$\text{curl } \mathbf{h} = \mathbf{J} + \frac{\partial \mathbf{D}}{\partial t} \quad (1)$$

$$\text{curl } \mathbf{E} = -\frac{\partial \mathbf{B}}{\partial t} \quad (2)$$

$$\text{div } \mathbf{h} = 0, \text{ div } \mathbf{E} = \rho_e \quad (3)$$

$$\mathbf{B} = \mu_o(\mathbf{H} + \mathbf{h}), \mathbf{D} = \epsilon_o \mathbf{E} \quad (4)$$

where  $\mathbf{h}$  and  $\mathbf{E}$  denote perturbations of the magnetic and electric fields, respectively,  $\mathbf{J}$  is the electric current density,  $\rho_e$  is the charge density,  $\mu_o$  and  $\epsilon_o$  are the magnetic and electric permeabilities, respectively,  $\mathbf{B}$  and  $\mathbf{D}$  are the magnetic and electric induction vectors, respectively, and  $\mathbf{H}$  is the initial constant magnetic field.

The second group of equations is the equations of motion:

$$\rho \frac{\partial^2 u_i}{\partial t^2} = \sigma_{ij,j} + T_{ij,j} + F_i \quad (5)$$

where  $\sigma_{ij}$  is given by the constitutive equation

$$\sigma_{ij} = \lambda e_{kk} \delta_{ij} + 2\mu e_{ij} - \gamma(T - T_o) \delta_{ij} \quad (6)$$

and  $T_{ij}$  the Maxwell electromagnetic stress tensor related to the quantity  $\mathbf{h}$  in the following manner:

$$T_{ij} = \mu_o [H_i h_j + H_j h_i - \delta_{ij} (h_k H_k)] \quad (7)$$

so that the quantity  $T_{ij,j} = (\mathbf{J} \wedge \mathbf{B})_i$  is the  $i$ -component of the Lorentz force. The above



equations should be supplemented by the relations between strain and displacements

$$e_{ij} = \frac{1}{2} (u_{i,j} + u_{j,i}) \quad (8)$$

and Ohm's law for moving media

$$\mathbf{J} = \sigma_o \left[ \mathbf{E} + \mu_o \frac{\partial \mathbf{u}}{\partial t} \wedge (\mathbf{H} + \mathbf{h}) \right]$$

where  $\sigma_o$  is the electric conductivity. We may linearize the above equation by neglecting small quantities of the second-order giving

$$\mathbf{J} = \sigma_o \left[ \mathbf{E} + \mu_o \frac{\partial \mathbf{u}}{\partial t} \wedge \mathbf{H} \right] \quad (9)$$

and for a perfect conducting medium ( $\sigma_o \rightarrow \infty$ ), the electric field is defined as:

$$\mathbf{E} = -\mu_o \frac{\partial \mathbf{u}}{\partial t} \wedge \mathbf{H} \quad (10)$$

The last field equation is the equation of energy balance, namely,

$$\rho c_\varepsilon \dot{T} + \gamma T_o \dot{e} = -\text{div } \mathbf{q} \quad (11)$$

where  $\mathbf{e} = \text{div } \mathbf{u}$  is the cubical dilatation and  $\mathbf{q} = -k\nabla T$  is the Fourier law of heat conduction.

The heat equation for the coupled thermoelasticity is:

$$kT_{,ii} = \rho c_\varepsilon \dot{T} + \gamma T_o \dot{e} \quad (12)$$

where  $k$  is the thermal conductivity.

In the above equations, a comma denotes material derivatives and the summation convention that are used. The previous equations constitute a complete system of coupled magnetothermoelasticity for an isotropic electrically conducting medium.

## Modeling Linear Generalized Magnetothermoelasticity

In the literature concerning thermal effects in continuum mechanics, several parabolic and hyperbolic theories for describing the heat conduction are developed. A review of these theories is presented in the articles by Chandrasekharaiah [11] and Hetnarski and Ignaczak [12, 13].

Two generalizations to the coupled theory were introduced. The first is due to Lord and Shulman [14], who obtained a wave-type heat equation by postulating a new law of heat conduction to replace the classical Fourier's law. This law contains the heat flux vector as well as its time's derivative. The generalized Fourier's law is:

$$\mathbf{q} + \tau_o \dot{\mathbf{q}} = -k\nabla T$$

where  $\tau_o$  is the relaxation time.

The heat equation of this theory is of the wave-type, it automatically ensures finite speeds of propagation for heat and elastic waves, so that

$$kT_{,ii} = \rho c_\varepsilon (\dot{T} + \tau_o \ddot{T}) + \gamma T_o (\dot{e} + \tau_o \ddot{e}) \quad (13)$$

and the remaining governing equations for this theory, namely, the equations of motion and constitutive relations, remain the same as those for the coupled and the uncoupled theories.

The second generalization to the coupled theory of elasticity is what is known as the theory of thermoelasticity with two relaxation times or the theory or the temperature-rate-dependent thermoelasticity theory developed by Green and Lindsay [15]. This theory contains two constants that act as relaxation times and modifies all the equations of the coupled theory, not the heat equation only. The classical Fourier's law of heat conduction is not violated if the medium under consideration has a center of symmetry.

In this theory, the constitutive equation takes the form:

$$\sigma_{ij} = \lambda e_{kk} \delta_{ij} + 2\mu e_{ij} - \gamma (T - T_o + v\dot{T}) \delta_{ij} \quad (14)$$



The equation of motion for an electrically conducting solid in the presence of a constant magnetic field takes the form:

$$\sigma_{ij,j} = \rho \ddot{u}_i + (\mathbf{J} \wedge \mathbf{B})_i \quad (15)$$

The energy equation is:

$$kT_{,ii} = \rho c_e (\dot{T} + \tau \ddot{T}) + \gamma T_o \dot{e} \quad (16)$$

where  $\tau$  and  $v$  are two relaxation times.

### Generalized Magnetothermoelasticity

We consider a thermoelastic perfect conducting medium permeated by an initial magnetic field. This produces an induced magnetic field  $\mathbf{h}$  and induced electric field  $\mathbf{E}$ , which satisfy the linearized equations of electromagnetism and are valid for slowly moving media [16]:

$$\text{curl } \mathbf{h} = \mathbf{J} + \varepsilon_o \frac{\partial \mathbf{E}}{\partial t} \quad (17)$$

$$\text{curl } \mathbf{E} = -\mu_o \frac{\partial \mathbf{h}}{\partial t} \quad (18)$$

$$\mathbf{E} = -\mu_o (\mathbf{u} \times \mathbf{H}) \quad (19)$$

$$\text{div } \mathbf{h} = 0, \quad \mathbf{B} = \mu_o \mathbf{H} \quad (20)$$

The above equations are supplemented by the displacement equations of the theory of elasticity, taking into account the Lorentz force:

$$\rho \frac{\partial^2 u_i}{\partial t^2} = \sigma_{ij,j} + \mu_o (\mathbf{J} \wedge \mathbf{H})_i \quad (21)$$

The constitutive equation is:

$$\sigma_{ij} = \lambda e_{kk} \delta_{ij} + 2\mu e_{ij} - \gamma (T - T_o + v \dot{T}) \delta_{ij} \quad (22)$$

The generalized equation of heat conduction which is proposed by Ezzat and El-Karamany [17] takes the form:

$$kT_{,ii} = \rho c_e (\dot{T} + \tau_o \ddot{T}) + \gamma T_o (\dot{e} + n_o \tau_o \ddot{e}) \quad (23)$$

where  $n_o$  is a nondimensional constant. Equation (23) becomes that for LS-theory when  $v = 0$ ,  $n_o = 1$ ,  $\alpha = 1$ ,  $\tau_o > 0$  and becomes that of GL-theory when  $n_o = 0$ ,  $\alpha = 1$ ,  $v = \tau_o$ .

Now, we shall consider a homogeneous isotropic thermoelastic conducting solid occupying half-space  $x \geq 0$ , which is initially quiescent and where all the state functions depend only on the state functions  $x$  and the time  $t$ .

The displacement vector has components:

$$u_x = u(x, t), \quad u_y = u_z = 0 \quad (24)$$

The strain component takes the form:

$$e = e_{xx} = \frac{\partial u}{\partial x} \quad (25)$$

The constitutive equation yields:

$$\sigma = \sigma_{xx} = (2\mu + \lambda)e - \gamma(\Theta + v \dot{\Theta}) \quad (26)$$

The heat equation becomes:

$$k \frac{\partial^2 \Theta}{\partial x^2} = \rho c_e (\dot{\Theta} + \tau_o \ddot{\Theta}) + \gamma T_o (\dot{e} + n_o \tau_o \ddot{e}) \quad (27)$$

$$\Theta = T - T_o \quad (28)$$

A constant magnetic field with components  $(0, H_o, 0)$  is permeating the medium. The induced magnetic field  $\mathbf{h}$  will have one component in the  $y$ -direction, while the induced electric field  $\mathbf{E}$  will have one component in  $z$ -direction. Then, (17)–(19) yield:

$$\mathbf{J} = \left( \frac{\partial h}{\partial x} - \varepsilon_o \frac{\partial E}{\partial t} \right) \quad (29)$$

$$\mathbf{h} = -H_o \mathbf{e} \quad (30)$$

$$E = -\mu_0 H_0 \frac{\partial u}{\partial t} \quad (31)$$

$$\bar{f}(s) = \int_0^t e^{-st} f(t) dt = L\{f(t)\}$$

By substituting for  $h$  and  $E$  from equations (25) and (29)–(31), equation (24) becomes, on using (25), we get:

$$\frac{\partial^2 \sigma}{\partial x^2} + \mu_o H_o^2 \frac{\partial^2 e}{\partial x^2} = \rho \alpha \ddot{e} \quad (32)$$

where  $\alpha_o = \sqrt{\frac{\mu_o H_o^2}{\rho}}$  is the Alfven velocity,  $c$  is the speed of light, and  $\alpha = 1 + \frac{\alpha_o^2}{c^2}$ .

Let us introduce the following nondimensional variables:

$$\begin{aligned} x^* &= c_o \eta_o x, & u^* &= c_o \eta_o u, & t^* &= c_o^2 \eta_o t \\ \tau^* &= c_o^2 \eta_o \tau, & v^* &= c_o^2 \eta_o v, & \Theta^* &= \frac{\gamma \Theta}{\rho c_o^2} \\ c_o^2 &= \frac{\lambda + 2\mu}{\rho}, & \eta_o &= \frac{\rho c_E}{K}, & \varepsilon &= \frac{\delta_o \gamma}{\rho c_E} \\ \sigma^* &= \frac{\sigma}{\rho c_o^2}, & h^* &= \frac{h}{H_o}, & E^* &= \frac{E}{\mu_o H_o c_o} \end{aligned}$$

In terms of these nondimensional variables, we have (dropping the asterisks for convenience):

$$h = -e \quad (33)$$

$$E = -\frac{\partial u}{\partial t} \quad (34)$$

$$\frac{\partial^2 \sigma}{\partial x^2} + \beta \frac{\partial^2 e}{\partial x^2} = \alpha \ddot{e} \quad (35)$$

$$\begin{aligned} \frac{\partial^2 \Theta}{\partial x^2} &= \left( \frac{\partial \Theta}{\partial t} + \tau_o \frac{\partial^2 \Theta}{\partial t^2} \right) \\ &+ \varepsilon \left( \frac{\partial e}{\partial t} + n_o \tau_o \frac{\partial^2 e}{\partial t^2} \right) \end{aligned} \quad (36)$$

$$\sigma = e - \left( \Theta + v \frac{\partial \Theta}{\partial t} \right) \quad (37)$$

where  $\beta = \frac{\alpha_o^2}{c^2}$ .

Taking the Laplace transforms defined by the relation

of both sides of equations (33)–(37), we obtain:

$$\bar{h} = -\bar{e} \quad (38)$$

$$\bar{E} = -s \bar{u} \quad (39)$$

$$\frac{d^2 \bar{\Theta}}{dx^2} = s(1 + \tau_o s) \bar{\Theta} + \varepsilon s(1 + n_o \tau_o s) \bar{e} \quad (40)$$

$$\bar{\sigma} = \bar{e} - (1 + v s) \bar{\Theta} \quad (41)$$

$$\frac{d^2 \bar{\sigma}}{dx^2} + \beta \frac{d^2 \bar{e}}{dx^2} = \alpha s^2 \bar{e} \quad (42)$$

where all the initial state functions are equal to zero.

Eliminating  $\bar{e}$  from (40)–(42), we obtain:

$$\frac{d^2 \bar{\Theta}}{dx^2} = L_1 \bar{\Theta} + L_2 \bar{\sigma} \quad (43)$$

where

$$\begin{aligned} L_1 &= s(1 + \tau_o s) + \varepsilon s(1 + n_o \tau_o s)(1 + v s) \\ L_2 &= \varepsilon s(1 + n_o \tau_o s) \end{aligned}$$

and

$$\frac{d^2 \bar{\sigma}}{dx^2} = M_1 \bar{\Theta} + M_2 \bar{\sigma} \quad (44)$$

where

$$M_1 = \frac{(1 + v s)(\alpha s^2 - \beta L_1)}{1 + \beta}$$

$$M_2 = \frac{\alpha s^2 - \beta(1 + v s)L_2}{1 + \beta}$$

It should be noted that the corresponding expressions for different theories can be obtained from the previous equations as:

1. Thermoelasticity (Biot Theory) when  $\tau_o = v = n_o = 0, \alpha = 1$
2. Magnetothermoelasticity when  $\tau_o = v = n_o = 0, \alpha > 1$
3. Generalized thermoelasticity with one relaxation time (LS-Theory) when  $v = 0, n_o = 1, \alpha = 1, \tau_o > 0$
4. Generalized magnetothermoelasticity with one relaxation time (Sherief and Ezzat) when  $v = 0, n_o = 1, \alpha > 1, \tau_o > 0$
5. Generalized thermoelasticity with two relaxation times (GL-Theory) when  $n_o = 0, \alpha = 1, v = \tau_o$
6. Generalized magnetothermoelasticity with two relaxation times (El-Karamany and Ezzat) when  $n_o = 0, v = \tau_o, \alpha > 1$

### Thermal-Shock Problem in Magnetothermoelasticity

The problem considered is that of producing combined elastic and electromagnetic waves in an elastic perfect conducting half-space by means of thermal shock acting on the boundary of the half-space. It is assumed that the elastic half-space is adjacent to a vacuum.

1. Thermal boundary condition:

A thermal shock is applied to the boundary plane  $x = 0$  in the form:

$$\Theta(0, t) = \Theta_o H(t), \text{ or } \bar{\Theta}(0, s) = \bar{\Theta}_o = \frac{\Theta_o}{s} \quad (45)$$

where  $H(\cdot)$  is the Heaviside unit step function.

2. Mechanical boundary condition:

The bounding plane  $x = 0$  is taken to be traction-free, i.e.,

$$\sigma(0, t) + T_{11}(0, t) - T_{11}^o(0, t) = 0 \quad (46)$$

where  $T_{11}^o$  is the Maxwell stress tensor in a vacuum.

Since the transverse components of the vectors  $\mathbf{E}$  and  $\mathbf{h}$  are continuous across the bonding plane, i.e.,  $E(0, t) = E^o(0, t)$  and  $h(0, t) = h^o(0, t)$ ,  $t > 0$  where  $E^o$  and  $h^o$  are the components of the induced electric and magnetic fields in free space and the relative permeability is very nearly unity, it follows that  $T_{11}(0, t) = T_{11}^o(0, t)$  and (46) reduces to:

$$\sigma(0, t) = 0, \text{ or } \bar{\sigma}(0, s) = \bar{\sigma}_o = 0 \quad (47)$$

The state space approach developed earlier by Ezzat was adopted

State space approach which is a standard approach in modern control theory and developed earlier by Ezzat [18] is adopted to get the exact solution in the Laplace transform domain in the following forms:

$$\bar{\Theta}(x, s) = \frac{\Theta_o \left[ (k_1 - L_1) e^{-\sqrt{k_2}x} - (k_2 - L_1) e^{-\sqrt{k_1}x} \right]}{s (k_1 - k_2)} \quad (48)$$

$$\bar{\sigma}(x, s) = \frac{\Theta_o M_1 \left( e^{-\sqrt{k_1}x} - e^{-\sqrt{k_2}x} \right)}{s (k_1 - k_2)} \quad (49)$$

From (38), the strain takes the form:

$$\bar{e} = \Theta_o s (k_1 - k_2) \left( \frac{[(1 + vs)(k_1 - L_1) - M_1] e^{-\sqrt{k_2}x}}{-[(1 + vs)(k_2 - L_1) - M_1] e^{-\sqrt{k_1}x}} \right) \quad (50)$$

From (24), the displacement takes the form:

$$\bar{u}(x, s) = \frac{\Theta_o \left( C e^{-\sqrt{k_1}x} - D e^{-\sqrt{k_2}x} \right)}{s k_1 - k_2} \quad (51)$$

where

$$C = \frac{(1 + vs)(k_2 - L_1) - n M_1}{\sqrt{k_1}}, \quad D = \frac{(1 + vs)(k_1 - L_1) - n M_1}{\sqrt{k_2}}$$

Those complete the solution in the Laplace transform domain.

## Results

In order to invert the Laplace transform in the above equations, we adopt a numerical inversion method based on a Fourier series expansion proposed [19].

The copper material was chosen for purposes of numerical evaluations, and the constants of the problem were taken as follows (Table 1):

The computations were carried out for  $t = 0.1$ . The results of the thermal stress are shown in Fig. 1. In this Figure, the solid lines represent the solution obtained using the coupled theory (C-Theory) and dashed lines represent the solution obtained using the Lord-Shoulman theory (LS-Theory) while dotted lines represent the solution obtained using the Green-Lindsay theory (GL-Theory).

The important phenomenon observed in a semispace problem, where the medium is of infinite extent, is that the solution of any of the considered functions for the generalized theory vanishes identically outside a bounded region of space. This clearly demonstrates the difference between the coupled and the generalized theories of thermoelasticity. In the first and older theory, the waves propagate with infinite speeds, so the value of any of the functions is not identically zero (though it may be very small) for any large

value of  $x$ . In the generalized theory, the response to the thermal and mechanical effects does not reach infinity instantaneously but remains in a bounded region of space that expands with passing of time.

Figure 1 shows that the speed of the wave propagation of the temperature in generalized theories is finite and coincides with the physical behavior of the elastic material.

### Electromagneto Coupled and Generalized Thermoelasticity, Table 1 Values of the constants [20]

$$\kappa = 386 \text{ N/Ks}$$

$$\alpha_T = 1.78(10)^{-5} \text{ K}^{-1}$$

$$C_E = 383.1 \text{ m}^2/\text{K}$$

$$\eta_o = 8886.73 \text{ s/m}^2$$

$$\mu = 3.86(10)^{10} \text{ N/m}^2$$

$$\lambda = 7.76(10)^{10} \text{ N/m}^2$$

$$\rho = 8954 \text{ kg/m}^3$$

$$\tau_o = 0.02 \text{ s}$$

$$T_o = 293 \text{ K}$$

$$c_o = 4158 \text{ m/s}$$

$$\varepsilon_o = (10)^{-9}/(36\pi) \text{ C}^2/\text{Nm}^2$$

$$\mu_o = 1.256(10)^{-6} \text{ N s}^2/\text{C}^2$$

$$\varepsilon = 0.0168$$

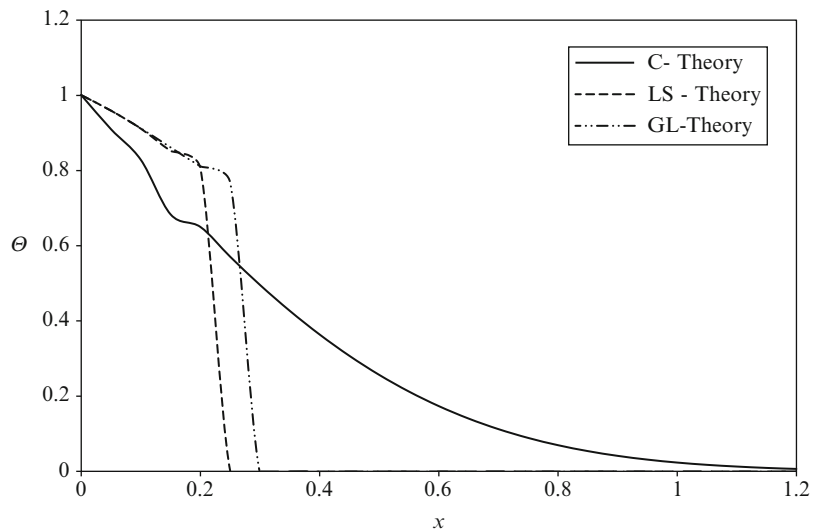
$$\Theta_o = 1$$

$$B_o = \mu_o$$

$$H_o = 1 \text{ T}$$

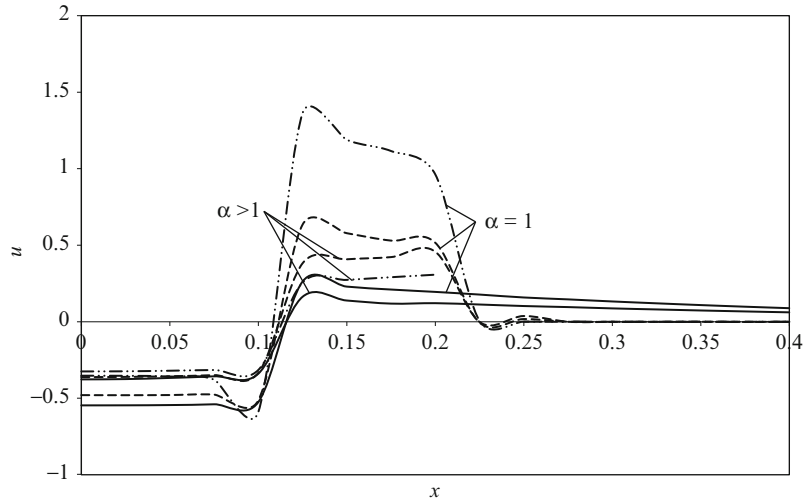
### Electromagneto Coupled and Generalized Thermoelasticity,

**Fig. 1** Temperature distribution for a semi space problem under different theories



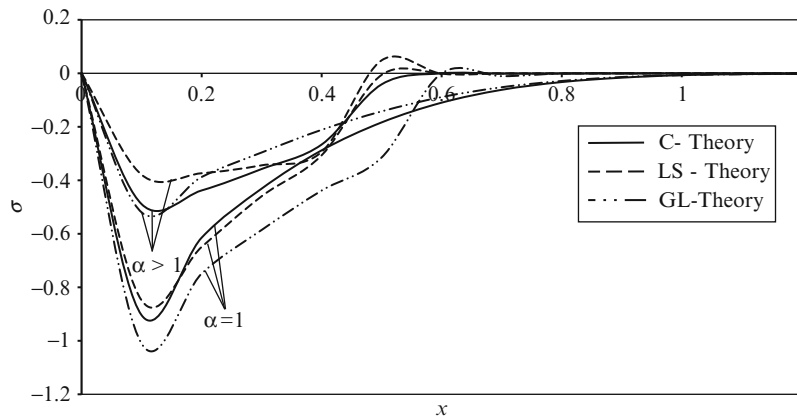
### Electromagneto Coupled and Generalized Thermoelasticity,

**Fig. 2** Displacement distribution for a semi-space problem under different theories



### Electromagneto Coupled and Generalized Thermoelasticity,

**Fig. 3** Thermal stress distribution for a semi space problem under different theories



Figures 2 and 3 show the variation of the displacement and thermal stress with distance. We observe that for  $\alpha = 1.0$ , the results coincide with all the previous results of applications that are taken in the context of thermoelasticity theory. For magnetothermoelasticity ( $\alpha > 0$ ), we notice that the magnetic field acts to decrease the magnitude of the thermal stress component. This is mainly due to the fact that the magnetic field corresponds to term signifying positive force that tends to accelerate the charge carriers.

### Cross Reference

► [State-Space Approach to Generalized Thermoelasticity](#)

### References

1. Maugin GA (1981) Wave motion in magnetizable deformable solids(Review). *Int J Eng Sci* 19:321–388
2. Knopoff L (1955) The intersection between elastic waves motion and a magnetic field in electrical conductors. *J Geophys Res* 60:441–456
3. Chadwick P (1960) Thermoelasticity, the dynamic theory, progress in solid mechanics, vol 1. North-Holland, Amsterdam, pp 236–328
4. Kaliski S, Petykiewicz J (1959) Equation of motion coupled with the field of temperature in a magnetic field involving mechanical and electrical relaxation for anisotropic bodies. *Proc Vibr Probl* 4:3–11
5. Paria G (1967) Magneto-elasticity and magneto-thermoelasticity. *Adv Appl Mech* 10:73
6. Wilson AJ (1963) Proceedings. *Math Proc Camb Phil Soc* 59:483–488
7. Biot M (1956) Thermoelasticity and irreversible thermodynamics. *J Appl Phys* 27:240–253

8. Sherief HH, Ezzat MA (1996) A thermal-shock problem in magneto-thermoelasticity with thermal relaxation. *Int J Solids Struct* 30:4449–4459
9. Ezzat MA, El-Karamany AS (2002) Magnetothermoelasticity with thermal relaxation in a conducting medium with variable electrical and thermal conductivity. *J Therm Stress* 25:859–875
10. Ezzat MA, Othman MA, Smaan AA (2001) State space approach to two-dimensional electromagneto-thermoelastic problem with two relaxation times. *Int J Eng Sci* 39:1383–1404
11. Chandrasekharaiah DS (1998) Hyperbolic thermoelasticity: a review of recent literature. *Appl Mech Rev* 51:705–729
12. Hetnarski RB, Ignaczak J (1999) Generalized thermoelasticity. *J Therm Stress* 22:451–470
13. Hetnarski RB, Ignaczak J (2000) Nonclassical dynamical thermoelasticity. *Int J Solids Struct* 37:215–224
14. Lord H, Shulman Y (1967) A generalized dynamical theory of thermoelasticity. *J Mech Phys Solids* 15:299–309
15. Green A, Lindsay K (1972) A generalized dynamical theory of thermoelasticity. *J Elast* 2:1–7
16. Ezzat MA (1997) State space approach to generalized magneto-thermoelasticity with two relaxation times in a medium of perfect conductivity. *Int J Eng Sci* 35:741–752
17. El-Karamany AS, Ezzat MA (2002) On the boundary integral formulation of thermo- viscoelasticity theory. *Int J Eng Sci* 40:1943–1956
18. Ezzat MA (2008) State space approach to solids and fluids. *Can J Phys Rev* 86:1241–1250
19. Honig G, Hirdes U (1984) A method for the numerical inversion of the Laplace transform. *J Comp Appl Math* 10:113–132
20. Sherief HH, Ezzat MA (1998) A problem in generalized in magneto-thermoelasticity for an infinitely long annular cylinder. *J Eng Math* 34: 387–402

---

## Electromechanically Coupled Materials

- [Fracture of Electrostrictive Materials](#)
- [Piezothermoelasticity with Finite Wave Speeds](#)

---

## Electrostatic Traction

- [Fracture of Piezoelectric Materials](#)

---

## Electrostriction

- [Fracture of Electrostrictive Materials](#)

---

## Electro-Thermo-Mechanical System: Thermoelastic Damping in Resonators

Zhili Hao

Department of Mechanical and Aerospace Engineering, Old Dominion University, Norfolk, VA, USA

## Synonyms

[Quality factor related to thermoelastic damping \( \$Q\_{TED}\$ \)](#); [Thermoelastic damping \(TED\)](#); [Thermoelastic dissipation](#); [Thermoelastic loss](#)

## Definition

Thermoelastic damping (TED) refers to the process in which part of the vibration energy of a mechanical resonator is dissipated into thermal energy, through irreversible heat conduction accompanying elastic vibrations in the resonator. The mechanical quality factor ( $Q$ ) related to thermoelastic damping in a resonator is commonly denoted by  $Q_{TED}$ .

## Overview

The laws of thermodynamics predict that a variation of strain in a solid is accompanied by a variation of temperature, which causes an irreversible flow of heat in the solid [1, 2]. This irreversible heat conduction gives rise to an increase in entropy and consequently to dissipation of vibration energy. This process of

energy dissipation is commonly referred to as *thermoelastic damping*. Although the earliest study on thermoelastic damping in beam resonators was conducted by Zener [3, 4] in the 1930s, thermoelastic damping had not received much attention until its significance in micromechanical resonators was recognized in the early 2000s [5, 6].

Generally speaking, micromechanical resonators are comprised of a micromechanical structure and integrated transducers that convert the motion of the micromechanical structure into an electrical signal and vice versa. Owing to its small size, it is feasible to package a micromechanical resonator in vacuum, and thereby, air damping is eliminated. Consequently, thermoelastic damping, anchor loss, and surface loss come to the fore and determine the mechanical quality factor ( $Q$ ) of a micromechanical resonator operating in vacuum [7]:

$$\frac{1}{Q} = \frac{1}{Q_{\text{TED}}} + \frac{1}{Q_{\text{anchor}}} + \frac{1}{Q_{\text{surface}}} \quad (1)$$

Since the  $Q$  plays a critical role in determining the ultimate performance of a micromechanical resonator, it becomes one of the most important parameters of a resonator. As compared to anchor loss and surface loss, thermoelastic damping is an inherent loss mechanism in a resonator and thus imposes an upper limit of the achievable  $Q$  for a resonator.

To predict thermoelastic damping in a resonator and further improve the quality factor related to thermoelastic damping,  $Q_{\text{TED}}$ , various studies on thermoelastic damping in resonators have been conducted and significant results have been obtained. Currently, theoretical solutions to thermoelastic damping in resonators with relatively simple structures, including beams [5, 8], rings [9], and disks (or circular thin plates) [8], have been derived. Meanwhile, numerical models of thermoelastic damping in resonators with complex structural geometries have been developed [10–13]. Some design guidelines for improving the  $Q_{\text{TED}}$  of a resonator have also been established.

## Basic Methodology

From experimental observations, thermoelastic coupling at the micro/nano-scale is very weak, so thermoelastic damping behavior in a micromechanical resonator can be captured using the governing equations of linear thermoelasticity.

### Governing Equations of Linear Thermoelasticity

Consider a resonator that is made from an isotropic material and is initially at a uniform temperature,  $T_0$ . In the absence of internal heat source and body force, the governing equations of linear thermoelasticity for this resonator are written as [1]:

$$(\lambda + 2\mu) \cdot \nabla(\nabla \cdot \vec{u}) - \mu \cdot \nabla \times \nabla \times \vec{u} - \beta_T \cdot \nabla \theta = \rho \cdot \frac{\partial^2 \vec{u}}{\partial t^2} \quad (2a)$$

$$\kappa \cdot \nabla^2 \theta - C_P \cdot \rho \cdot \frac{\partial \theta}{\partial t} = \beta_T \cdot T_0 \cdot \frac{\partial}{\partial t} (\nabla \cdot \vec{u}) \quad (2b)$$

where  $\kappa$ ,  $\rho$ , and  $C_P$  are the thermal conductivity, density, and specific heat of the material used, respectively. While  $\lambda$  and  $\mu$  are Lamé coefficients,  $\beta_T$  is a coefficient related to thermal expansion effect of the material used. In terms of the material properties, these coefficients can be expressed in three-dimensional (3D) cases and two-dimensional (2D) cases, respectively, as below [8]:

$$\lambda = \frac{\nu \cdot E}{(1 + \nu) \cdot (1 - 2\nu)}, \quad \mu = \frac{E}{2(1 + \nu)}, \quad \beta_T = \frac{\alpha_T \cdot E}{1 - 2\nu} \quad (3a)$$

$$\lambda = \frac{\nu \cdot E}{1 - \nu^2}, \quad \mu = \frac{E}{2(1 + \nu)}, \quad \beta_T = \frac{\alpha_T \cdot E}{1 - \nu} \quad (2D) \quad (3b)$$

where  $E$ ,  $\nu$ , and  $\alpha_T$  are Young's modulus, Poisson's ratio, and linear thermal expansion coefficient of the material used, respectively.

**Electro-Thermo-Mechanical System: Thermoelastic Damping in Resonators, Table 1** Physical properties of some commonly used materials for micromechanical resonators [10, 11]

Materials	Single crystal silicon	Polysilicon	Silicon <100>	Silicon <110>	Si <sub>0.35</sub> Ge <sub>0.65</sub>	Polydiamond
Poisson's ratio	—	0.22	0.28	0.064	0.23	0.12
Elastic modulus (GPa)	$c_{11} = 166$ $c_{12} = 65$ $c_{44} = 80$	157	130	169	155	1,120
Density (kg/m <sup>3</sup> )	2,330	2,330	2,330	2,330	4,810	3,440
Thermal conductivity (W/m·K)	90	90	90	90	59	1,400
Specific heat (J/kg·K)	700	700	700	700	377	565
Linear thermal expansion coefficient (1/K)	$2.6 \times 10^{-6}$	$2.6 \times 10^{-6}$	$2.6 \times 10^{-6}$	$2.6 \times 10^{-6}$	$2.6 \times 10^{-6}$	$1.0 \times 10^{-6}$

For a resonator that is made from an anisotropic material and is initially at a uniform temperature,  $T_0$ , its governing equations of linear thermoelasticity in tensor form are given by [10]:

$$\frac{1}{2} c_{ijkl} (u_{k,lj} + u_{l,kj}) - c_{ijkl} \alpha_{kl} \theta_{,j} = \rho \frac{\partial^2 u_i}{\partial t^2} \quad (4a)$$

$$k_{ij} \theta_{,jj} - \rho C_P \frac{\partial \theta}{\partial t} = T_0 \beta_{ij} \frac{\partial \varepsilon_{ij}}{\partial t} \quad (4b)$$

where  $i, j, k, l = 1, 2, 3$ ;  $c_{ijkl}$  is the fourth-order tensor of the elastic stiffness;  $\beta_{ij} = c_{ijkl} \alpha_{kl}$  is the thermoelastic coupling tensor, where  $\alpha_{kl}$  is the thermal expansion tensor;  $\kappa_{ij}$  is the thermal conductivity tensor; and  $\partial \varepsilon_{ij} / \partial t$  is the rate of the elastic strain  $\varepsilon_{ij}$ .

The physical properties of some commonly used materials for micromechanical resonators are listed in Table 1. In the two sets of the thermoelastic-coupled governing equations,  $\vec{u}$  (or  $u_i$ ) and  $\theta = T - T_0$  denote the elastic displacement and the temperature variation from the initial temperature, respectively. While the last term on the left side of the elastic equation, (2a) or (4a), represents the stress caused by the temperature variation in a resonator, the term on the right side of the heat conduction equation, (2b) or (4b), represents the internal heat source resulting from the elastic dilatation,  $\nabla \cdot \vec{u}$  (or  $\varepsilon_{ii}$ ), in the resonator. These two terms are the factors coupling the elastic vibrations and the temperature variation together in a resonator.

### Fundamental Assumption

To simplify the calculation of thermoelastic damping while with enough accuracy, a well-accepted assumption [3, 5] is that thermoelastic coupling is very weak and has negligible influence on the uncoupled elastic vibration modes of a resonator, so the elastic and thermal problems are essentially decoupled. In other words, the elastic strain causes a temperature variation in the resonator, but the temperature variation does not affect the uncoupled elastic vibration modes. Since thermoelastic damping has been theoretically and experimentally proven to be very small, this assumption is sound and practical. Following this assumption, the uncoupled elastic vibration modes can be obtained from the elastic equation, giving rise to the elastic displacement. Then, substituting the elastic displacement into the heat conduction equation yields the temperature variation. Upon knowing the two variables, the elastic displacement,  $\vec{u}$  (or  $u_i$ ), and the temperature variation,  $\theta$ , in the coupled governing equations, two methods can be utilized to calculate thermoelastic damping.

### Two Methods for Calculating Thermoelastic Damping

Two methods have been developed to solve the governing equations of linear thermoelasticity for thermoelastic damping. One is complex-frequency method [5], in which thermoelastic damping is formulated in the elastic wave field; the other is thermal-energy method [8], in which



**Electro-Thermo-Mechanical System: Thermoelastic Damping in Resonators, Table 2** Nature of the two variables in the governing equations of linear thermoelasticity in complex-frequency method and thermal-energy method

	Elastic displacement $\vec{u} = \vec{u}_0 \cdot e^{i\omega t}$	Temperature variation $\theta = \theta_0 \cdot e^{i\omega t}$
Complex-frequency method	$\vec{u}_0$ : real $\omega$ : complex	$\theta_0$ : real $\omega$ : complex
Thermal-energy method	$\vec{u}_0$ : real $\omega$ : real	$\theta_0$ : complex $\omega$ : real

thermoelastic damping is interpreted in the thermal field.

#### Complex-Frequency Method

In complex-frequency method, the two variables in the governing equations are assumed to be time harmonic with real amplitudes and the same complex resonant frequency. The nature of these two variables in complex-frequency method is listed in Table 2, together with their nature in thermal-energy method. The effect of thermoelastic damping on the elastic vibrations of a resonator is taken into account by expressing the resonant frequency as a complex value [5]:

$$\omega = (\omega_r + \omega_i \cdot i) \text{ with } \omega_r, \omega_i \geq 0, \text{ and } i = \sqrt{-1} \quad (5)$$

where  $\omega_r$  is the real value yielding the new resonant frequency of the resonator in the presence of thermoelastic coupling, while  $\omega_i$  is the imaginary value representing thermoelastic damping.

Based on the fundamental assumption, the elastic displacement is first obtained from the uncoupled elastic equation, which is equivalent to neglecting the thermal term in the equation. Then, the elastic displacement is substituted into the heat conduction equation to obtain the temperature variation. Substituting the obtained temperature variation into the coupled elastic equation gives rise to a complex Young's modulus. Since the resonant frequency of a resonator is proportional to the square root of Young's

modulus,  $\omega \propto \sqrt{E}$ , incorporating the complex Young's modulus into the equation for the resonant frequency yields an explicit expression for the complex frequency. Finally, in terms of the derived complex frequency, the quality factor related to thermoelastic damping,  $Q_{\text{TED}}$ , is calculated as [5]:

$$Q_{\text{TED}}^{-1} = 2 \cdot \left| \frac{\text{Im}(\omega)}{\text{Re}(\omega)} \right| \quad (6)$$

#### Thermal-Energy Method

In thermal-energy method, thermoelastic damping is interpreted as the generation of thermal energy per cycle of vibration: the very essence of thermoelastic damping. Thus, one may calculate thermoelastic damping by seeking this generation of thermal energy. As listed in Table 2, the elastic displacement and the temperature variation are both treated as time-harmonic variables with the same real resonant frequency, but the elastic displacement holds a real amplitude, while the temperature variation must hold a complex amplitude, due to thermoelastic coupling.

Here, we derive the expression for the generated thermal energy in one cycle of vibration for resonators made from isotropic materials. During heat conduction, entropy of an infinitesimal volume,  $dv$ , in a resonator varies at a rate of:

$$\frac{ds}{dt} = \frac{\kappa \cdot \nabla^2 T}{T} \cdot dv \quad (7)$$

where  $s$  denotes the entropy of the volume and the temperature is represented by  $T = T_0 + \theta$ , where the relation  $\theta \ll T_0$  exists, because the temperature variation due to thermoelastic coupling is very small. By using Taylor series expansion and neglecting the higher-order expansion terms, (7) is rewritten as:

$$\frac{ds}{dt} = \left( 1 - \frac{\theta}{T_0} \right) \frac{\kappa \cdot \nabla^2 \theta}{T_0} \cdot dv \quad (8)$$

Then, substituting (2b) into the above equation leads to the following relation:

$$\frac{ds}{dt} = \left(1 - \frac{\theta}{T_0}\right) \frac{\rho C_P}{T_0} \left[ \frac{\partial \theta}{\partial t} + \frac{\beta_T T_0}{\rho C_P} \cdot \frac{\partial}{\partial t} (\nabla \cdot \vec{u}) \right] \cdot dv \quad (9)$$

Based on the definition of entropy, the thermal energy generated in irreversible heat conduction is written as:

$$dQ = T_0 \cdot ds \quad (10)$$

where the relation  $\theta \ll T_0$  is used again. Substituting (9) into (10) and integrating the later equation over one time period of vibration,  $t_0$ , and across the whole volume of the resonator lead to the expression for the generation of thermal energy per cycle of vibration [8]:

$$\Delta Q = \rho C_P \int_0^{t_0} \int_V \left(1 - \frac{\theta}{T_0}\right) \cdot \left[ \frac{\partial \theta}{\partial t} + \frac{\beta_T T_0}{\rho C_P} \frac{\partial}{\partial t} (\nabla \cdot \vec{u}) \right] \cdot dv \cdot dt \quad (11)$$

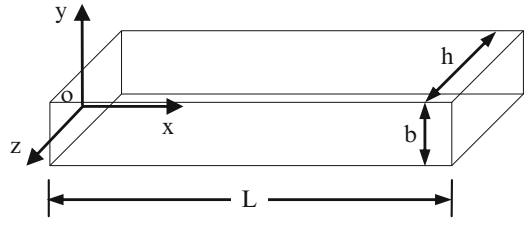
Since the elastic displacement is real and the temperature variation is complex, (11) is simplified as:

$$\Delta Q = -\beta_T \int_0^{t_0} \int_V \theta \cdot \frac{\partial}{\partial t} (\nabla \cdot \vec{u}) \cdot dv \cdot dt \quad (12)$$

The imaginary part of the temperature variation is out of phase with the elastic displacement and contributes to thermoelastic damping. Since the derivative of the elastic displacement ( $\sim e^{i\omega t}$ ) with respect to time is a pure imaginary value, the real part of the above expression,  $\text{Re}(\Delta Q)$ , is equal to the generation of thermal energy per cycle of vibration, or thermoelastic damping. Therefore, according to the definition of the mechanical quality factor, the  $Q$  related to thermoelastic damping is calculated as

$$Q_{\text{TED}} = 2\pi \cdot \frac{W}{\text{Re}(\Delta Q)} \quad (13)$$

where  $W$  denotes the stored maximum vibration energy in the resonator. Similar derivation can be conducted to derive the expression for the



**Electro-Thermo-Mechanical System: Thermoelastic Damping in Resonators, Fig. 1** Schematic of a beam resonator and its associated coordinates

generated thermal energy in one cycle of vibration for resonators made from anisotropic materials.

### Thermoelastic Damping in Beam Resonators

Due to their geometric simplicity, beam resonators are the most commonly studied micromechanical resonators. The two methods described above have been applied to derive a theoretical solution to their thermoelastic damping.

#### Uncoupled Elastic Vibrations

Figure 1 shows the schematic of a beam resonator. The length, width, and thickness of the beam are denoted by  $L$ ,  $b$ , and  $h$ , respectively. For simplicity, we assume that the ratio of the beam length to the beam width is larger than 20 ( $L/b > 20$ ), so that the Euler-Bernoulli beam theory is used for the vibration analysis. The governing equation for its flexural-mode vibrations along the  $y$ -axis is written as:

$$\frac{\partial^2 Y}{\partial t^2} = -\frac{EI}{\rho A} \cdot \frac{\partial^4 Y}{\partial x^4} \quad (14)$$

where  $I = b^3 h / 12$  and  $A = b \cdot h$  are the elastic moment of inertia and the cross-section area of the beam, respectively.

The beam resonator undergoes time-harmonic vibrations,  $Y = Y_0(x) \cdot e^{i\omega t}$ , with the uncoupled resonant frequency,  $\omega_0$ , given by [7]:

$$\omega_0 = \frac{\pi^2 \beta^2}{L^2} \sqrt{\frac{EI}{\rho A}} \quad (15)$$

where  $\beta$  denotes the mode constant. The uncoupled flexural-mode vibration shape is written as:

$$Y_0 = \frac{U_0}{2} \cdot \left\{ \cosh\left(\beta\pi \frac{x}{L}\right) - \cos\left(\beta\pi \frac{x}{L}\right) + \gamma \left[ \sinh\left(\beta\pi \frac{x}{L}\right) - \sin\left(\beta\pi \frac{x}{L}\right) \right] \right\} \quad (16)$$

where  $\gamma$  denotes the mode shape factor. The stored maximum vibration energy in the beam resonator is calculated as [7]:

$$W = \frac{1}{8} \rho A L \omega_0^2 U_0^2 \quad (17)$$

According to the generalized Hooke's law, the total elastic strain along each axis due to the elastic stress and the temperature variation takes the following form:

$$\varepsilon_{xx} = \frac{1}{E} \sigma_{xx} + \alpha_T \theta \quad (18a)$$

$$\varepsilon_{yy} = \varepsilon_{zz} = -\frac{\nu}{E} \sigma_{xx} + \alpha_T \theta \quad (18b)$$

Therefore, the elastic dilatation due to the uncoupled elastic vibrations and the temperature variation is written as:

$$\begin{aligned} \nabla \cdot \vec{u} &= \varepsilon_{xx} + \varepsilon_{yy} + \varepsilon_{zz} \\ &= (2\nu - 1)y \frac{d^2 Y_0}{dx^2} e^{i\omega t} + 2(1 + \nu) \alpha_T \theta \end{aligned} \quad (19)$$

Compared with its first term, the second term of the elastic dilatation in (19) has negligible effect on heat conduction [8] and thus will be omitted in the following heat conduction analysis.

## Heat Conduction

Due to the high ratio of the beam length to the beam width ( $L/b > 20$ ), the temperature gradient along the beam length ( $x$ -axis) is much smaller than that across the beam width ( $y$ -axis). Therefore, heat conduction in the beam is assumed to occur only along the  $y$ -axis. The heat conduction equation, (2b), can be simplified as:

$$\chi \cdot \frac{\partial^2 \theta}{\partial y^2} - \frac{\partial \theta}{\partial t} = \frac{\beta_T T_0}{\rho C_P} \cdot \frac{\partial}{\partial t} (\nabla \cdot \vec{u}) \quad (20)$$

With the aid of (19), (20) can be rewritten as:

$$\frac{\partial^2 \theta_0}{\partial y^2} - \frac{\omega}{i\chi} \theta_0 = \frac{\omega}{i\chi} \frac{\Delta_E}{\alpha_T} \cdot y \cdot \frac{d^2 Y_0}{dx^2} \quad (21)$$

where  $\Delta_E = E \cdot \alpha_T^2 \cdot T_0 / \rho \cdot C_P$  is the *thermal relaxation strength* that is related to the material properties and the initial temperature of the resonator. The solution to (21) can be written as below:

$$\theta_0 = B_1 \sin(ky) + B_2 \cos(ky) + \frac{\Delta_E}{\alpha_T} \cdot y \cdot \frac{d^2 Y_0}{dx^2} \quad (22)$$

where  $B_1$  and  $B_2$  are two constants and

$$\begin{aligned} k &= \sqrt{\frac{\omega}{i\chi}} = (1 - i) \cdot \frac{\xi}{b}, \text{ with} \\ \xi &= b \cdot \sqrt{\frac{\omega}{2\chi}} \text{ and } i = \sqrt{-1} \end{aligned} \quad (23)$$

Applying the adiabatic condition (note: for a resonator operating in vacuum, the adiabatic condition reflects the reality) at the boundaries of  $y = \pm b/2$  to (22) leads to the explicit expression for the temperature variation across the beam width:

$$\theta_0 = \frac{\Delta_E}{\alpha_T} \cdot \frac{d^2 Y_0}{dx^2} \cdot b \cdot \left[ \frac{y}{b} - \frac{\sin(ky)}{kb \cdot \cos(kb/2)} \right] \quad (24)$$

## Theoretical Solution to Thermoelastic Damping

### Complex-Frequency Method

In terms of the elastic vibration displacement, the elastic strain experienced by a beam resonator undergoing flexural-mode vibrations is written as:

$$\varepsilon_{xx} = -y \frac{\partial^2 Y}{\partial x^2} \quad (25a)$$

$$\varepsilon_{yy} = \varepsilon_{zz} = v y \frac{\partial^2 Y}{\partial x^2} + (1 + \nu) \alpha_T \theta \quad (25b)$$

If we follow the standard derivation procedure for isothermal beams with no thermoelastic coupling but with the modified thermoelastic strain, (25a) and (25b), the governing equation for flexural-mode vibrations in a beam then takes the following format:

$$\rho A \frac{\partial^2 Y}{\partial t^2} + \frac{\partial^2}{\partial x^2} \left( EI \frac{\partial^2 Y}{\partial x^2} + E \alpha_T I_T \right) = 0 \quad (26)$$

where  $I_T$  is the thermal moment of inertia contributed by the temperature vibration across the beam width:

$$I_T = \int_A y \theta dy dz \quad (27)$$

Since the solution to the temperature variation, (24), is obtained, we can substitute it into the integral  $I_T$ , (27), for the thermal moment of inertia. Finally, the coupled elastic vibration equation for the beam is written as:

$$\omega^2 Y_0 = \frac{EI}{\rho A} \{1 + \Delta_E (1 + f(\omega))\} \frac{\partial^4 Y_0}{\partial x^4} \quad (28)$$

where the complex function,  $f(\omega)$ , is given by:

$$\begin{aligned} f(\omega) &= \frac{24}{k^3 b^3} \left[ \frac{kb}{2} - \tan\left(\frac{kb}{2}\right) \right] \\ &= \frac{6}{\xi^3} \frac{\sinh(\xi) - \sin(\xi)}{\cosh(\xi) + \cos(\xi)} \\ &\quad + \frac{6}{\xi^3} \cdot \left[ \xi - \frac{\sinh(\xi) + \sin(\xi)}{\cosh(\xi) + \cos(\xi)} \right] i \end{aligned} \quad (29)$$

where  $\xi = b\sqrt{\omega/(2\chi)}$ .

Equation (28) is identical to the governing equation, (14), with no thermoelastic damping in the format, except that the isothermal value of Young's modulus  $E$  is replaced by a frequency-dependent modulus:

$$E_\omega = E \{1 + \Delta_E (1 + f(\omega))\} \quad (30)$$

By substituting (30) into the original expression for the resonant frequency, (15), the complex frequency is given by:

$$\omega = \frac{\pi^2 \beta^2}{L^2} \sqrt{\frac{E_\omega I}{\rho A}} = \omega_0 \sqrt{1 + \Delta_E [1 + f(\omega)]} \quad (31)$$

By using Taylor series expansion, neglecting the higher-order terms, and replacing  $f(\omega)$  into the square root by  $f(\omega_0)$ , (31) then becomes:

$$\omega = \omega_0 \left\{ 1 + \frac{\Delta_E}{2} [1 + f(\omega_0)] \right\} \quad (32)$$

The real and imaginary parts of (32) can be easily extracted, giving rise to the resonant frequency and the damping, with the thermoelastic correction of order  $\Delta_E$ :

$$\text{Re}(\omega) = \omega_0 \left\{ 1 + \frac{\Delta_E}{2} \left[ 1 - \frac{6}{\xi^3} \cdot \frac{\sinh(\xi) - \sin(\xi)}{\cosh(\xi) + \cos(\xi)} \right] \right\} \quad (33a)$$

$$\text{Im}(\omega) = \omega_0 \frac{\Delta_E}{2} \left[ \frac{6}{\xi^3} \cdot \frac{\sinh(\xi) + \sin(\xi)}{\cosh(\xi) + \cos(\xi)} - \frac{6}{\xi^2} \right] \quad (33b)$$

Using the definition of the quality factor in the elastic wave field, (6), the theoretical solution to thermoelastic damping in a beam resonator, which is to the first order of  $\Delta_E$ , is obtained [5]:

$$Q_{\text{TED}}^{-1} = \frac{E \alpha_T^2 T_0}{\rho C_P} \left[ \frac{6}{\xi^2} - \frac{6}{\xi^3} \cdot \frac{\sinh(\xi) + \sin(\xi)}{\cosh(\xi) + \cos(\xi)} \right] \quad (34)$$

### Thermal-Energy Method

Because of the complex expression for  $k$  in (23), the amplitude of the temperature variation in (24) is complex. While its real part is in phase with the elastic vibration displacement, the imaginary part of the temperature variation is out of phase with the elastic displacement and causes thermoelastic damping. In (24), the first term is the particular solution corresponding to the elastic vibration displacement, and the second term is the general solution resulting from heat conduction. The temperature variation from the elastic vibration displacement holds a real value and therefore does not contribute to thermoelastic damping. In contrast, the temperature variation from the general solution is complex, indicating that part of its heat conduction is irreversible and causes thermoelastic damping.

The elastic dilatation, (19), and the temperature variation, (24), are substituted into (12), giving rise to the following expression for generated thermal energy in one cycle of vibration:

$$\Delta Q = \frac{E^2 \alpha_T^2 T_0}{\rho C_P} \pi i L \left( \frac{\beta \pi}{L} \right)^4 \frac{U_0^2}{4} [1 - f(\omega)] \quad (35)$$

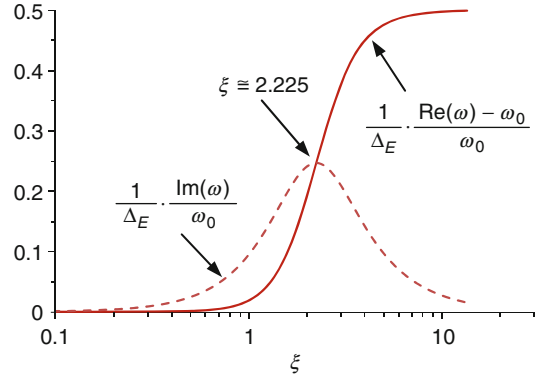
Corresponding to the imaginary part of the temperature variation, the real part of (35) is equal to the generation of thermal energy per cycle of vibration:

$$\begin{aligned} \text{Re}(\Delta Q) = & \frac{E^2 \alpha_T^2 T_0}{\rho C_P} \pi L \left( \frac{\beta \pi}{L} \right)^4 \frac{U_0^2}{4} \\ & \frac{6}{\xi^3} \cdot \left[ \xi - \frac{\sinh(\xi) + \sin(\xi)}{\cosh(\xi) + \cos(\xi)} \right] \end{aligned} \quad (36)$$

The combination of (13), (17), and (36) leads to the explicit expression for the  $Q_{\text{TED}}$  of a beam resonator undergoing flexural-mode vibrations [8]:

$$Q_{\text{TED}}^{-1} = \frac{E \alpha_T^2 T_0}{\rho C_P} \left[ \frac{6}{\xi^2} - \frac{6}{\xi^3} \cdot \frac{\sinh(\xi) + \sin(\xi)}{\cosh(\xi) + \cos(\xi)} \right] \quad (37)$$

This solution is exactly the same as the result, (34), obtained using complex-frequency method.

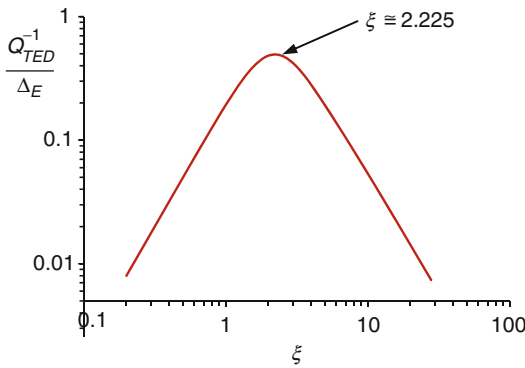


**Electro-Thermo-Mechanical System: Thermoelastic Damping in Resonators, Fig. 2** Universal behavior of the normalized frequency shift and the normalized attenuation of flexural-mode vibrations in a beam resonator versus the dimensionless variable,  $\xi$  [5]

### Physical Implications

Figure 2 shows the universal behavior of the normalized frequency shift,  $[\text{Re}(\omega) - \omega_0]/\omega_0 \Delta_E$ , and of the normalized attenuation,  $\text{Im}(\omega_0)/\omega_0 \Delta_E$ , in a beam resonator as functions of the dimensionless variable,  $\xi$ . Thermoelastic coupling leads to an upward shift of the uncoupled resonant frequency of a beam resonator. However, since the thermal relaxation strength is extremely small (in the order of  $\sim 10^{-4}$ ), this frequency shift is simply neglected in the design of beam resonators. The maximum attenuation of flexural-mode vibrations in a beam resonator occurs at  $\xi \cong 2.225$ .

Figure 3 shows that thermoelastic damping in a beam resonator exhibits a Lorentzian behavior, where maximum damping occurs at the Debye peak of  $\xi \cong 2.225$ . Accordingly, the  $Q_{\text{TED}}$  of a beam resonator reaches its lowest value at the Debye peak. The existence of the Debye peak can be qualitatively understood in the following way: If the frequency of elastic vibrations in a resonator is very small, then the vibrations are isothermal and very little energy is dissipated. If the vibration frequency is very high, then the resonator has no time to relax, and the vibrations are adiabatic, meaning that very little energy is dissipated. It is only when the vibration frequency is on the order of the resonator's effective relaxation rate [3–5] that maximum energy dissipation occurs.



**Electro-Thermo-Mechanical System: Thermoelastic Damping in Resonators, Fig. 3** Relation of the  $Q_{TED}^{-1}$  of a beam resonator to the dimensionless variable,  $\xi$  [5]

### Numerical Simulation of Thermoelastic Damping

For those micromechanical resonators with complex structural geometries, numerical simulation is necessary to calculate their thermoelastic damping. In this regard, commercial finite element analysis (FEA) software, such as ANSYS and COMSOL, has been utilized to calculate thermoelastic damping in resonators with different structural geometries, and self-written numerical algorithms have also been developed for resonators with structures of regular shapes.

Using COMSOL, Duwel et al. [11] solved the two coupled governing equations for thermoelastic damping in beam and block resonators, without the fundamental assumption and with the fundamental assumption, respectively. The numerical model of thermoelastic damping with the fundamental assumption is essentially based on complex-frequency method. This numerical model is capable of identifying the thermal modes contributing most to damping and thus provides some insights on simple structural modification for improving the  $Q_{TED}$  of a beam resonator.

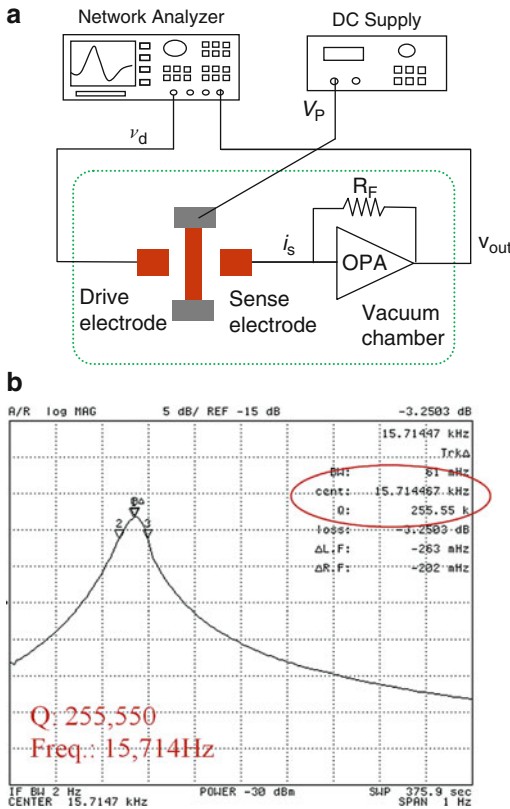
Built upon thermal-energy method, Hao et al. [10] solved the two coupled governing equations in ANSYS for some typical micromechanical resonators, including block and disk resonators, as well as tuning-fork gyroscopes. The numerical model built in ANSYS consists of two sequential simulations: uncoupled elastic vibration and

transient heat conduction. In the numerical implementation of thermal-energy method, the temperature variation is not treated as a time-harmonic variable and holds purely a real value, which is different from the theoretical implementation of thermal-energy method for calculating thermoelastic damping in a beam resonator. As compared with the numerical model of thermoelastic damping based on complex-frequency method, the numerical model based on thermal-energy method does not involve any complex values and proves to be highly computationally efficient. Moreover, the simulation results from this numerical model are capable of illustrating the distribution of thermoelastic damping in a resonator.

Yi [12] developed numerical algorithms for calculating thermoelastic damping in ring resonators and investigated how geometrical design parameters affect their thermoelastic damping. In the numerical algorithms, a perturbation analysis is applied to derive a linear vibration equation, which contains the complex resonant frequency of the elastic vibrations. Therefore, the numerical algorithms are essentially based on complex-frequency method. Later on, the numerical algorithms [13] were expanded to study thermoelastic damping in ring, disk, and elliptical plate resonators.

### Experimental Techniques

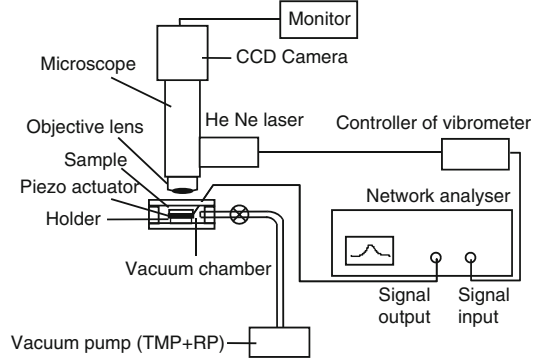
Figure 4a shows the schematic of an experimental technique for measuring the mechanical quality factor ( $Q$ ) of micromechanical resonators with integrated transducers in vacuum [14]. A resonator die is mounted on a printed circuit board (PCB), which contains an amplification circuit. Bonding wires are bonded between the transducers (drive electrode and sense electrode) and the PCB for electrical connection. Then, the PCB with a wire-bonded resonator is put into a vacuum chamber. To excite and detect elastic vibrations of the resonator, a two-port configuration is employed: A DC polarization voltage,  $V_p$ , is applied to the micromechanical structure and an AC drive voltage signal,  $v_d$ , is applied to the



**Electro-Thermo-Mechanical System: Thermoelastic Damping in Resonators, Fig. 4** (a) Schematic of an experimental technique for measuring the  $Q$  of a micromechanical resonator with integrated transducers in vacuum and (b) measured frequency response – the output of a network analyzer [14]

drive electrode, while the sense current signal,  $i_s$ , is detected from the sense electrode and is further amplified to be a voltage output,  $v_{out}$ . As shown in Fig. 4b, the output of the network analyzer is the frequency response of a resonator, showing the measured resonant frequency and  $Q$  [14].

Figure 5 shows the schematic of an experimental technique for measuring the  $Q$  of a resonator without integrated transducers in vacuum [6]. A piezoelectric actuator is employed to excite the elastic vibrations in the resonator. The vibrations are measured by a laser vibrometer, which is based on the Doppler shift in the reflected light. The network analyzer outputs the measured frequency response of the resonator.



**Electro-Thermo-Mechanical System: Thermoelastic Damping in Resonators, Fig. 5** Schematic of an experimental technique for measuring the  $Q$  of a micro-mechanical resonator without integrated transducers [6]

As expressed in (1), this measured  $Q$ ,  $Q_{measured}$ , is the sum of thermoelastic damping, anchor loss, and surface loss. Currently, no experimental techniques can separately measure the three loss mechanisms in a resonator. Thus, it is very challenging to compare the  $Q_{measured}$  with the calculated  $Q_{TED}$ . A common solution to this problem is to design a resonator with thermoelastic damping being the sole dominant loss, according to the gained insights on anchor loss and surface loss, and then simply treat the  $Q_{measured}$  as the measured  $Q_{TED}$ .

## Thermoelastic Damping in Other Resonators

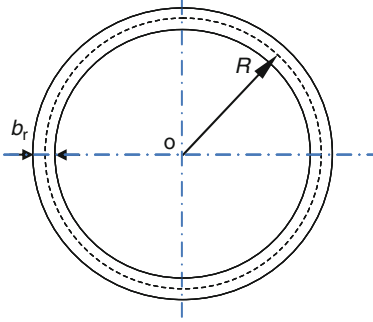
Besides beam resonators, other typical micromechanical resonators include ring gyroscopes, tuning-fork gyroscopes, block resonators, and disk resonators.

### Gyroscopes Operating in Flexural Modes

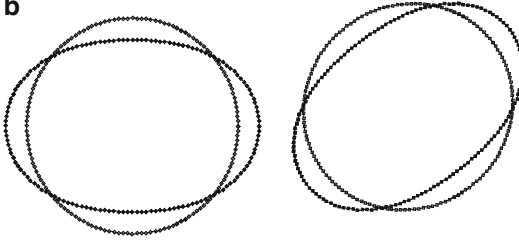
Rings and tuning-fork structures are commonly employed in microgyroscopes. Strictly speaking, these ring and tuning-fork gyroscopes are micromechanical resonators in that they vibrate in two flexural modes during operation. Owing to their symmetric structures and operation flexural modes symmetric to their anchors, both ring and tuning-fork gyroscopes show that their anchor



a



b



**Electro-Thermo-Mechanical System: Thermoelastic Damping in Resonators, Fig. 6** (a) Schematic of a ring structure and its associated coordinates and (b) two flexural modes in operation

loss is mostly negligible, as compared to thermoelastic damping. Thus, thermoelastic damping in these gyroscopes determines their achievable  $Q$  and has been investigated.

Figure 6a shows the schematic of a ring structure in a ring gyroscope and its associated coordinates. The resonant frequency of in-plane flexural-mode vibrations of mode order,  $n$ , of a ring is given by:

$$\omega_n = \frac{1}{\sqrt{12}} \cdot \frac{b_r}{R^2} \cdot \frac{n(n^2 - 1)}{\sqrt{n^2 + 1}} \cdot \sqrt{\frac{E}{\rho}} \quad (38)$$

where  $b_r$  and  $R$  denote the ring width and radius of the neutral plane of the ring, respectively. The ring operates in the two in-plane flexural modes of mode order of  $n = 2$ , as shown in Fig. 6b.

Wong et al. [9] derived a theoretical solution to thermoelastic damping in a ring using complex-frequency method. The solution is identical to that for a beam resonator, with the dimensionless variable,  $\xi$ , being calculated using the ring width and the resonant frequency of the two flexural modes in operation:

$$\xi = b_r \cdot \sqrt{\frac{\omega_2}{2\chi}} \quad (39)$$

Thus, thermoelastic damping in a ring gyroscope also demonstrates a Lorentzian behavior, and care must be taken to avoid the Debye peak during the ring gyroscope design.

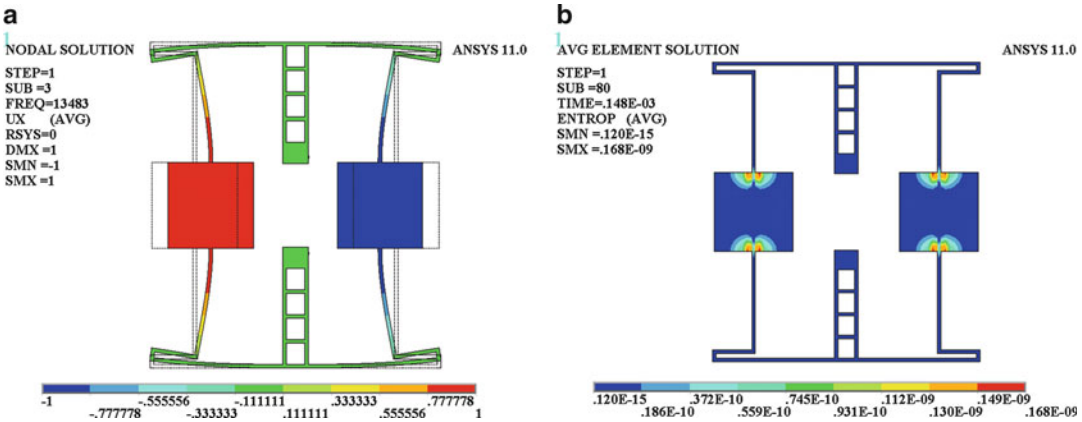
A tuning-fork structure employed in a gyroscope is typically comprised of a set of beams and two proof masses. Due to their structural complexity, no theoretical solution is available for calculating thermoelastic damping in a tuning-fork gyroscope. A numerical model based on thermal-energy method has been developed to calculate the  $Q_{TED}$  of a tuning-fork gyroscope [10]. Figure 7a illustrates one of the flexural modes in operation of a tuning-fork gyroscope, and Fig. 7b shows the distribution of thermoelastic damping across the tuning-fork structure. The calculated  $Q_{TED}$  of this tuning-fork gyroscope is 87,635, very close to the measured  $Q$  of 81,000 [15]. This indicates that thermoelastic damping is the sole dominant loss in this gyroscope.

### Resonators Operating in Bulk Modes

Block and disk (circular thin-plate) resonators operating in bulk mode have been developed for wireless communications, where high frequencies are required (typically above 10 MHz). In these bulk-mode resonators, anchor loss is the sole dominant loss, and thermoelastic damping is completely negligible.

Figure 8a shows a SEM (scanning electron microscope) picture of a block resonator [16]. This block resonator operates in one of its longitudinal bulk modes, as shown in Fig. 8b. The rectangular block is the main body of the block resonator, determining the resonant frequency, while the two support beams are located at the resonant node of the rectangular block to minimize anchor loss. Figure 8c illustrates the distribution of thermoelastic damping across the block resonator [10]. It is interesting to note that thermoelastic damping occurs mainly in the support region, rather than the main body of the whole mechanical structure. The calculated  $Q_{TED}$  of this block resonator is  $1.5 \times 10^6$ , well





**Electro-Thermo-Mechanical System: Thermoelastic Damping in Resonators, Fig. 7** (a) One of the flexural modes in operation of a tuning-fork gyroscope and (b)

accompanying distribution of thermoelastic damping across the tuning-fork structure [10]

above the measured  $Q$  of 180,000 [16]. This indicates that anchor loss is the sole dominant loss in this block resonator.

Figure 9 shows a disk resonator operating in its elliptic bulk mode (second-order contour mode). The main body of the disk resonator is the disk, determining its frequency, while a support beam is located at the edge of the disk, which coincides with a resonant node of the elliptic bulk mode to minimize anchor loss. As shown in Fig. 9c, thermoelastic damping also occurs mainly in the support region of this disk resonator. The calculated  $Q_{TED}$  of this resonator is  $7 \times 10^6$ , well above the measured  $Q$  of 39,300 [17].

Without considering the support beam, Hao [8] conducted a theoretical analysis of thermoelastic damping in a disk resonator. This analysis has found that thermoelastic damping in a bulk-mode disk resonator also exhibits a Lorentzian behavior. However, the minimum  $Q_{TED}$  (or the Debye peak of thermoelastic damping) of a disk resonator operating in bulk mode occurs at the resonant frequency as high as a few tens of GHz or alternately at the radius of  $<1 \mu\text{m}$ , which falls out of the range of current engineering practice. When the resonant frequency is below 1 GHz, the  $Q_{TED}$  of a disk resonator is well above  $1 \times 10^6$  [8].

## Key Research Findings

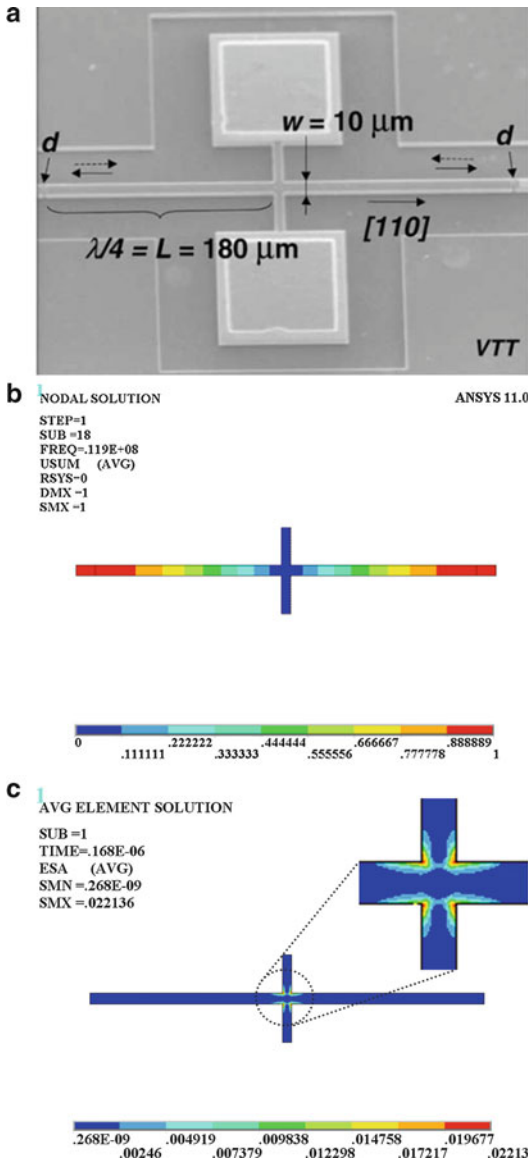
### Key Factors Affecting the $Q_{TED}$ of Resonators

From the design perspective, the  $Q_{TED}$  of a resonator is of great concern, rather than thermoelastic damping itself. Therefore, how the  $Q_{TED}$  of a resonator is affected by different factors is described here.

#### Operation Modes: Bulk Mode Versus Flexural Mode

Whether the vibration mode in operation of a resonator is bulk mode or flexural mode affects the  $Q_{TED}$  of the resonator in a much more significant manner than any other design parameters of a resonator. This is because the Debye peak of thermoelastic damping in a bulk-mode resonator happens at extremely high frequencies or at the nanometer scale, which falls out of the range of current engineering practice, while this Debye peak occurs at relatively low frequencies for flexural-mode resonators, which are well under current engineering practice.

Generally speaking, thermoelastic damping in a bulk-mode resonator, such as block and disk resonators, is not a concern at all, while anchor loss is the sole dominant loss, determining the overall  $Q$  of the resonator. Conversely, thermoelastic damping is the dominant loss in



**Electro-Thermo-Mechanical System: Thermoelastic Damping in Resonators, Fig. 8** (a) A SEM picture [16], (b) longitudinal bulk-mode vibrations [10], and (c) accompanying distribution of thermoelastic damping [10] for a block resonator with two support beams and made from single crystal silicon

a flexural-mode resonator in most cases, including ring gyroscopes, tuning-fork gyroscopes, and beam resonators. Thus, care must be taken to avoid the Debye peak during the resonator design so that its overall  $Q$  can be improved.

### Environmental Temperature and Residual Stress

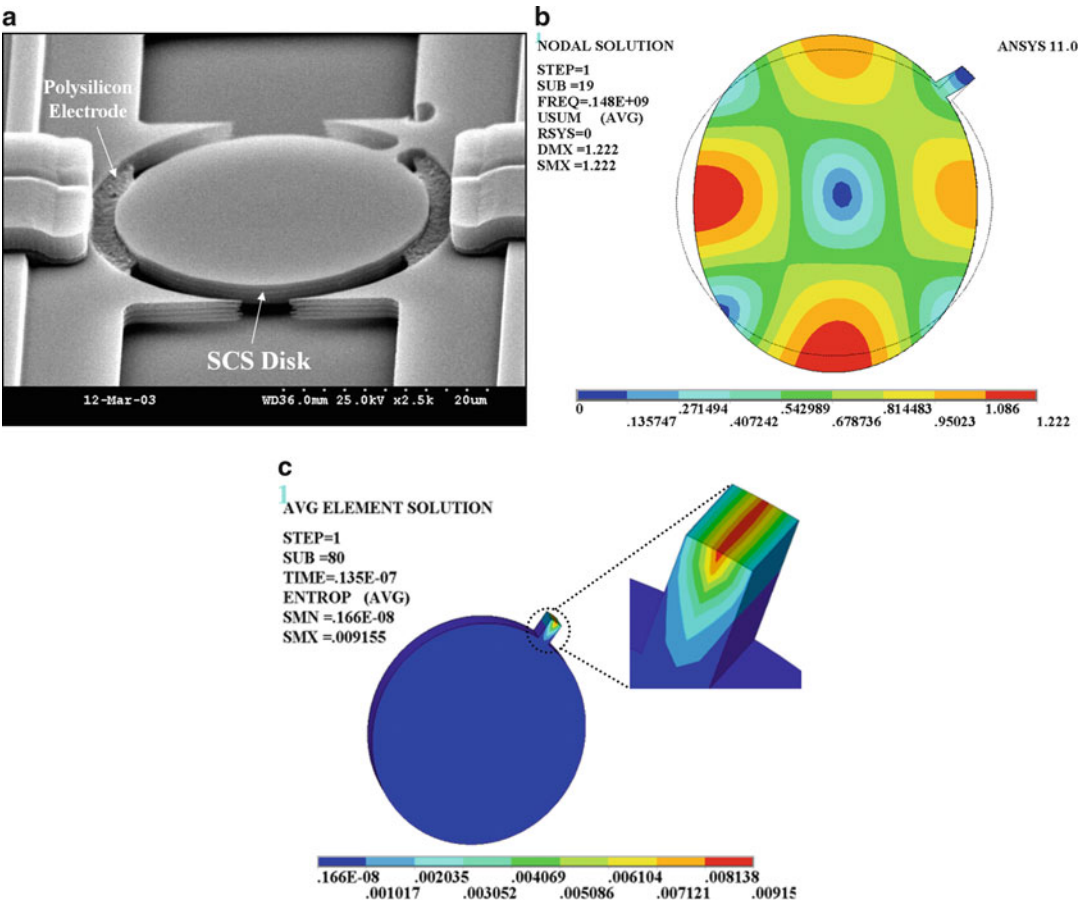
In addition to the design parameters of a resonator, a few other factors also affect the  $Q_{\text{TED}}$  of a resonator. Obviously, according to (34), the temperature of the working environment of a resonator affects the  $Q_{\text{TED}}$ . As the environmental temperature goes up, the  $Q_{\text{TED}}$  of a resonator decreases. Residual stress is unavoidable for those resonators built upon deposited thin films. Therefore, the effect of residual stress (or initial stress) on the  $Q_{\text{TED}}$  is also studied. Based on complex-frequency method, Kumar and Haque [18] investigated the effect of residual stress on the  $Q_{\text{TED}}$  of a beam resonator, finding that the  $Q_{\text{TED}}$  of a beam resonator goes up with the axial tensile stress and goes down with the axial compressive stress. Although the effect of residual stress on the  $Q_{\text{TED}}$  of other resonators with complex structural geometries has not been investigated, it can be deduced that residual stress will vary the original  $Q_{\text{TED}}$  of the same resonator with no residual stress.

### Design Strategies for Improving the $Q_{\text{TED}}$ of Resonators

Accumulated from the analytical and experimental studies, a few design strategies have been obtained for improving the  $Q_{\text{TED}}$  of micromechanical resonators. Note that these strategies are applicable solely to those flexural-mode resonators. Since thermoelastic damping in bulk-mode resonators proves not to be a concern, there is no need to reduce this damping.

For a resonator with a symmetric structure and operating in a flexural mode that is symmetric to its anchor, thermoelastic damping is the sole dominant loss in this resonator. One strategy for improving its  $Q$  is to add slots to the flexural structure of a resonator, as suggested by Candler et al. [19]. Based on their numerical model of thermoelastic damping, slots of certain dimensions are added to the flexural structure at the desirable locations, as shown in Fig. 10, so that the heat flow across the beams are disrupted, thermoelastic damping is reduced, and its  $Q_{\text{TED}}$  is improved.

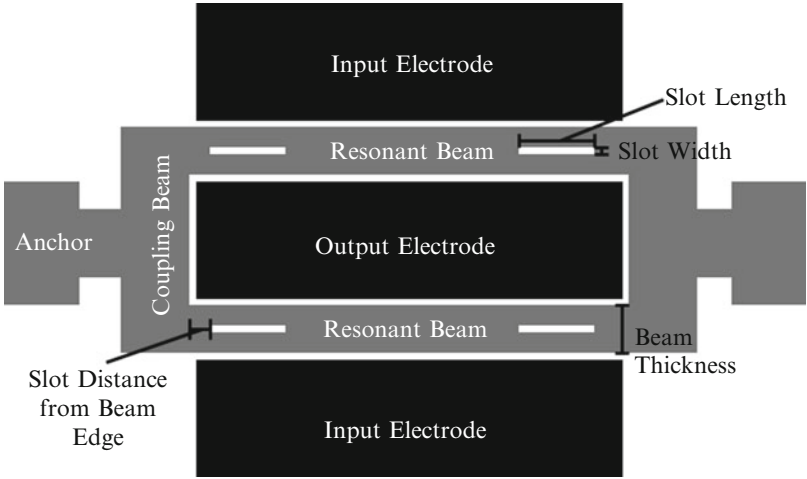
Since the  $Q_{\text{TED}}$  is closely associated with the beam width and resonant frequency of a flexural-mode resonator, an intuitive design strategy for

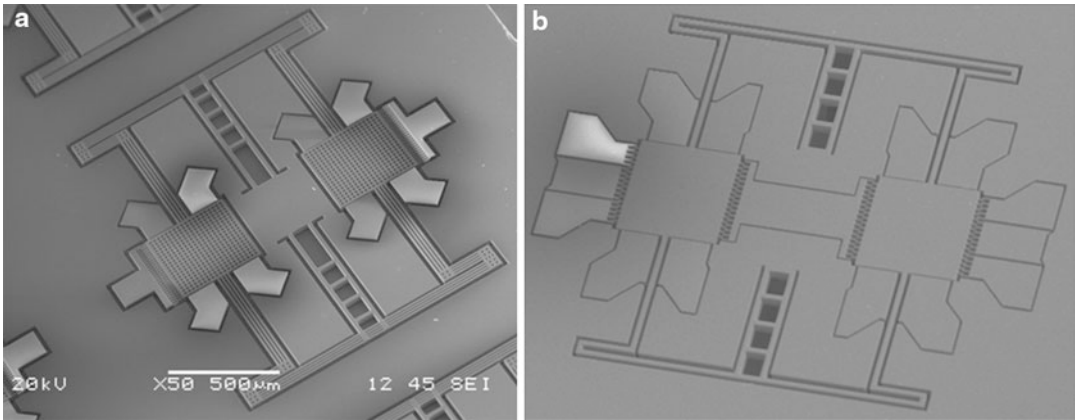


**Electro-Thermo-Mechanical System: Thermoelastic Damping in Resonators, Fig. 9** (a) A SEM picture [17], (b) elliptic bulk-mode elastic vibrations [10], and

(c) accompanying distribution of thermoelastic damping [10] for a disk resonator with a side-support beam and made from single crystal silicon

**Electro-Thermo-Mechanical System: Thermoelastic Damping in Resonators, Fig. 10** Schematic of a flexural-mode resonator with slots being added for improving its  $Q_{TED}$  [19]





**Electro-Thermo-Mechanical System: Thermoelastic Damping in Resonators, Fig. 11** (a) Multiple-beam tuning-fork gyroscope with  $Q_{\text{measured}} = 255,550$  [14] and (b) single-beam tuning-fork gyroscope with  $Q_{\text{measured}} = 81,000$  [15]

improving the  $Q_{\text{TED}}$  is to reduce the beam width and/or reduce the resonant frequency. By reducing the resonant frequency to  $\sim 2$  kHz, Prikhodko et al. [20] demonstrated a tuning-fork gyroscope with its overall  $Q$  of above  $1 \times 10^6$ . To maintain a relatively high resonant frequency while achieve a high  $Q$ , Wang et al. [14] incorporated multiple slim beams into a tuning-fork gyroscope, as shown in Fig. 11a. This multiple-beam tuning-fork gyroscope demonstrated a  $Q$  of 255,550 at a frequency of  $\sim 16$  kHz (Fig. 4b), much higher than 81,000 measured from a single-beam tuning-fork gyroscope [15], as shown in Fig. 11b.

Based on their work on the effect of residual stress on thermal damping in a beam resonator, Kumar and Haque [16] suggest that tensile residual stress be added to a beam resonator for improving the  $Q_{\text{TED}}$  of the original beam resonator.

## References

- Nowacki W (1975) Dynamic problems of thermoelasticity. Noordhoff International, Leyden
- Landau LD, Lifshitz EM (1959) Theory of elasticity. Pergamon, London
- Zener C (1937) Internal friction in solids I: theory of internal friction in reeds. Phys Rev 52:230–235
- Zener C (1938) Internal friction in solids II. General theory of thermoelastic internal friction. Phys Rev 53:90–99
- Lifshitz R, Roukes ML (2000) Thermoelastic damping in micro- and nanomechanical systems. Phys Rev B 61:5600–5609
- Yang J, Ono T, Esashi M (2002) Energy dissipation in submicrometer thick single-crystal silicon cantilevers. J Microelectromech Syst 11(6):775–783
- Hao Z, Erbil A, Ayazi F (2003) An analytical model for support loss in micromachined block resonators with in-plane flexural vibrations. Sens Actuat A Phys 109:156–164
- Hao Z (2008) Thermoelastic damping in the contour-mode vibrations of micro- and nanoelectromechanical circular thin-plate resonators. J Sound Vib 313(1–2):77–96
- Wong SJ, Fox CHJ, McWilliam S (2006) Thermoelastic damping of the in-plane vibration of thin silicon rings. J Sound Vib 293(1–2):266–285
- Hao Z, Yang Xu Y, Durgam SK (2009) A thermal-energy method for calculating thermoelastic damping in micromechanical resonators. J Sound Vib 322(4–5):870–882
- Duwel A, Candler RN, Kenny TW, Varghese M (2006) Engineering MEMS resonators with low thermoelastic damping. J Microelectromech Syst 15(6):1437–1445
- Yi YB (2008) Geometric effects on thermoelastic damping in MEMS resonators. J Sound Vib 309:588–599
- Yi YB (2010) Finite element analysis of thermoelastic damping in contour-mode vibrations of micro- and nanoscale ring, disk, and elliptical plate resonators. ASME J Vib Acoust 132(4):1–7, Art. 041015
- Wang R, Cheng P, Xie F, Young D, Hao Z (2011) A multiple-beam tuning-fork gyroscope with high quality factors. Sens Actuat A Phys 166:22–33
- Zaman MF, Sharma A, Hao Z, Ayazi A (2008) A mode-matched silicon-yaw tuning-fork gyroscope with subdegree-per-hour allan deviation bias instability. J MEMS 17(6):1526–1536

16. Mattila T, Kiihamaki J, Lamminmaki T, Jaakkola O, Rantakari P, Oja A, Seppa H, Kattelus H, Tittonen I (2002) A 12MHz micromechanical bulk acoustic mode oscillator. *Sens Actuat A Phys* 101:1–9
17. Pourkamali S, Hao Z, Ayazi F (2004) VHF single crystal silicon elliptic bulk-mode capacitive disk resonators part II: implementation and characterization. *J Microelectromech Syst* 13(6):1054–1062
18. Kumar A, Haque MA (2010) Stress-dependent thermal relaxation effects in micro-mechanical resonators. *Acta Mech* 212:83–91
19. Candler RN, Duwel A, Varghese M, Chandorkar SA, Hopcroft MA, Park WT, Kim B, Yama G, Partridge A, Lutz M, Kenny TW (2006) Impact of geometry on thermoelastic dissipation in micromechanical resonant beams. *J Microelectromech Syst* 15(4):927–934
20. Prikhodko IP, Zotov SA, Trusov AA, Shkel AM (2011) Sub-degree-per-hour silicon MEMS rate sensor with 1 million q-factor. *Transducers 2011 conference, Beijing, 3–9 June 2011*, pp 2809–2812

## Elliptic Hole

► [Green's Function of Thermoelastic Mixed Boundary Value Problem for Elliptic Hole](#)

## Elliptic Inclusion in an Anisotropic Body

Ching-Kong Chao

Department of Mechanical Engineering, National Taiwan University of Science and Technology, Taipei, Taiwan, Republic of China

### Overview

The thermoelastic problem for an isotropic medium containing a circular or ovaloid hole by the method of Muskhelishvili [1] was first studied by Florence and Goodier [2, 3]. Since then, a number of the hole or crack problems have received considerable interest such as Sturla and Barber [4] for anisotropic material with a plane crack by applying a Green's function formulation, Hwu [5] for anisotropic body with an elliptic hole based upon Stroh formalism [6, 7], and Tam and Wang [8] for anisotropic materials

with a hole or a rigid inclusion based upon Lekhnitskii complex potential approach [9]. As to thermoelastic inclusion problems, the thermal stresses induced by circular inclusions subjected to arbitrary thermal loadings were recently solved by Chao and Shen [10] based on Laurent series expansion and the method of analytical continuation.

In this entry, an elliptic inclusion embedded in an anisotropic body under remote uniform heat flow is solved by using the Lekhnitskii formulation for anisotropic elasticity which is extended to include the thermal effect combined with the method of analytical continuation [1]. A transformation function is applied to remedy the discontinuity problem which occurs when the transformation is required to be single valued and conformal in the entire domain including the matrix and inclusion. Moreover, the concept of superposition is applied to formulate the general solutions which allow us to remove the unwelcome terms of complex potentials in the matrix which may result in unbounded stresses at infinity. Both the temperature and stress functions either in the matrix or in the inclusion are expressed in compact matrix notation.

### Formulations

For two-dimensional anisotropic thermoelasticity, both the stresses and temperature can be represented in terms of three stress functions  $\phi_1(z_1)$ ,  $\phi_2(z_2)$ ,  $\phi_3(z_3)$ , and a temperature function  $g'(z_t)$ , with the arguments  $z_a = x_1 + s_\alpha x_2$ ,  $\alpha = 1, 2, 3, t$ . The elasticity eigenvalues  $s_\alpha (\alpha = 1, 2, 3)$  derived by Lekhnitskii [9] satisfy the sixth-order characteristic equation

$$l_2(s)l_4(s) - l_3^2(s) = 0 \quad (1)$$

with

$$l_2(s) = a_{44} - 2a_{45}s + a_{55}s^2$$

$$l_3(s) = -a_{24} + (a_{25} + a_{46})s - (a_{14} + a_{56})s^2 + a_{15}s^3$$

$$l_4(s) = a_{22} - 2a_{26}s + (2a_{12} + a_{66})s^2 - 2a_{16}s^3 + a_{11}s^4 \quad (2)$$

where  $a_{ij}(i, j = 1, 2, \dots, 6)$  denote the compliance tensor of an anisotropic material. The heat eigenvalue  $s_i$  is the root of the thermal characteristic equation with positive imaginary part

$$k_{22}s^2 + 2k_{12}s + k_{11} = 0 \quad (3)$$

where  $k_{ij}(i, j = 1, 2)$  are the heat conductivity coefficients. The temperature  $T$ , resultant heat flow  $Q$ , heat flux  $q_i$ , displacement  $u_i$ , resultant force  $p_i$ , and stresses  $\sigma_{ij}$  for uncoupled steady-state anisotropic thermoelasticity can be written as

$$T = 2\text{Re}[g'(z_t)] \quad (4)$$

$$Q = 2\text{Re}\left[i(k_{11}k_{22} - k_{12}^2)^{1/2}g'(z_t)\right] \quad (5)$$

$$q_i = -2\text{Re}[(k_{i1} + s_i k_{i2})g''(z_t)] \quad (6)$$

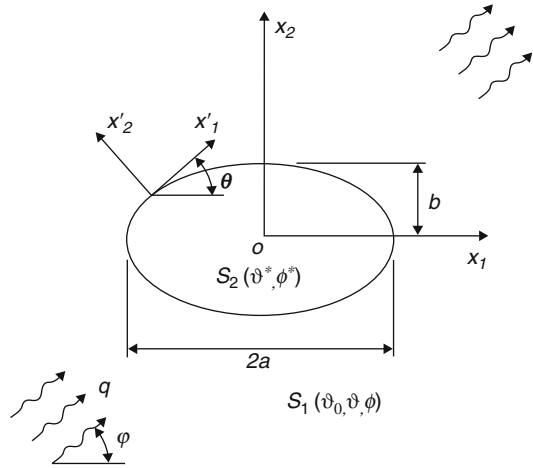
$$u_i = 2\text{Re}\left[\sum_{j=1}^3 A_{ij}\phi_j(z_j) + c_i g(z_t)\right] \quad (7)$$

$$p_i = -2\text{Re}\left[\sum_{j=1}^3 L_{ij}\phi_j(z_j) + d_i g(z_t)\right] \quad (8)$$

$$\sigma_{2i} = 2\text{Re}\left[\sum_{j=1}^3 L_{ij}\phi'_j(z_j) + d_i g'(z_t)\right] \quad (9)$$

$$\sigma_{1i} = -2\text{Re}\left[\sum_{j=1}^3 L_{ij}s_j\phi'_j(z_j) + s_i d_i g'(z_t)\right] \quad (10)$$

with  $Q = \int q_1 dx_2 - q_2 dx_1$ . Here,  $(\cdot)$  is designated as the derivative with respect to the associated arguments and  $\text{Re}$  denotes the real part of a complex function. Hereafter, boldfaced symbols represent vectors or matrices. The matrices  $L$ ,  $A$  and the vectors  $c$ ,  $d$  in (7)–(10) have been derived by Lekhnitskii [9] and Chao and Chang [11], respectively.



**Elliptic Inclusion in an Anisotropic Body,**  
Fig. 1 Elliptic inclusion under a remote uniform heat flow

Consider the thermoelastic problem of an anisotropic solid containing an elliptic inclusion (see Fig. 1). The materials are assumed to be perfectly bonded along the common boundary. In the present problem, the regions occupied by the matrix and the inclusion are denoted by  $S_1$  and  $S_2$ , respectively, while the starred and nonstarred quantities will be referred to the inclusion and the matrix, respectively. Now, we introduce the transformation function

$$z_\alpha = \frac{1}{2} \left\{ (a - ibs_\alpha)\zeta_\alpha + (a + ibs_\alpha)\frac{1}{\zeta_\alpha} \right\} \quad (11)$$

which will transform the region outside the elliptic inclusion of the  $z_\alpha$ -plane onto the exterior of a unit circle in the transformed  $\zeta_\alpha$ -plane and the region inside the elliptic inclusion onto the annular region between the unit circle and a circle of radius  $\sqrt{m_\alpha}$  which is defined as [12]

$$\sqrt{\frac{a + ibs_\alpha}{a - ibs_\alpha}} = \sqrt{m_\alpha} e^{i\theta_\alpha} \quad (12)$$

where  $\theta_\alpha$  is the argument corresponding to the modulus  $\sqrt{m_\alpha}$ . It has been shown that  $\sqrt{m_\alpha} < 1$  if the imaginary part of  $s_\alpha$  is set to be positive. Note that the transformation is single valued outside the elliptic inclusion. However, it becomes



double valued and nonconformal inside the elliptic inclusion. To remedy this discontinuity, the following restriction should be satisfied [12]:

$$f(\sqrt{m_\alpha}\sigma e^{-i\theta\alpha}) = f(\sqrt{m_\alpha}e^{i\theta\alpha}/\sigma) \quad (13)$$

where  $\sigma = e^{i\psi}$  denotes the points located on the unit circle.

## Temperature Field

Consider a uniform heat flux  $q$  directed at an angle  $\varphi$  with respect to the positive  $x_1$ -axis is disturbed by the presence of an elliptic inclusion (see Fig. 1). By applying the conformal mapping technique described above, the general solutions of the thermal field for the inclusion problem can be written as

$$\left. \begin{aligned} T &= [g'_0(\zeta) + g'(\zeta)] + [\overline{g'_0(\zeta)} + \overline{g'(\zeta)}] \\ Q &= i\beta[g'_0(\zeta) + g'(\zeta)] - i\beta[\overline{g'_0(\zeta)} + \overline{g'(\zeta)}] \end{aligned} \right\}, \zeta \in S_1 \quad (14)$$

$$\left. \begin{aligned} T^* &= g'^*(\zeta) + \overline{g'^*(\zeta)} \\ Q^* &= i\beta^*g'^*(\zeta) - i\beta^*\overline{g'^*(\zeta)} \end{aligned} \right\}, \zeta \in S_2 \quad (15)$$

where  $\beta = (k_{11}k_{22} - k_{12}^2)^{1/2}$  and the overbar denotes the conjugate of a complex function.  $g'_0(\zeta)$  represents the temperature function associated with the unperturbed field which is related to the solution of homogeneous media;  $g'(\zeta)$  (or  $g'^*(\zeta)$ ) is the temperature function corresponding to the perturbed field of matrix (or inclusion) which is holomorphic in region  $S_1$  (or  $S_2$ ) except some singular points. Since the inclusion and the matrix are assumed to be perfectly bonded along the interface, both the temperature and resultant heat flow must be continuous. That is,

$$T = T^*, Q = Q^*, \quad \text{along the interface } \zeta = \sigma = e^{i\psi} \quad (16)$$

By using the continuity conditions given in (16) and applying the method of analytical continuation, the temperature function can be obtained as

$$g'(\zeta) = \left( -hm_{2t} + \frac{\beta - \beta^*}{\beta + \beta^*} \overline{hm_{1t}} + \frac{2\beta^*}{\beta + \beta^*} \Gamma_1^* e_1 \right) \zeta^{-1} \quad (17)$$

$$g'^*(\zeta) = e_1 \zeta + \Gamma_1^* e_1 \zeta^{-1} \quad (18)$$

where

$$\Gamma_k^* = \left( \frac{a + ib s_t^*}{a - ib s_t^*} \right)^k \quad (19)$$

and

$$\left. \begin{aligned} h &= \frac{q(\cos \varphi + \overline{s_t} \sin \varphi)}{i\beta(s_t - \overline{s_t})} \\ m_{1t} &= (a - ib s_t)/2, m_{2t} = (a + ib s_t)/2 \end{aligned} \right\} \quad (20)$$

## Thermal Stresses

Due to the linear property, the principle of superposition can be used, and the solution can be represented as the sum of a homogeneous media subjected to a remote uniform heat flow and a corrective solution for which the temperature functions are  $g'(\zeta)$  in the matrix and  $g'^*(\zeta)$  in the inclusion. The general solutions for the inclusion problem are now be written as

$$\left. \begin{aligned} u &= A\phi(\zeta) + \overline{A\phi(\zeta)} + c g(\zeta) + \overline{c g(\zeta)} \\ p &= -L\phi(\zeta) - \overline{L\phi(\zeta)} - d g(\zeta) - \overline{d g(\zeta)} \end{aligned} \right\}, \zeta \in S_1 \quad (21)$$

$$\left. \begin{aligned} u^* &= A^* \phi^*(\zeta) + \overline{A^* \phi^*(\zeta)} + c^* g^*(\zeta) \\ &\quad + \overline{c^* g^*(\zeta)} - c g_0(\zeta) - \overline{c g_0(\zeta)} \\ p^* &= -L^* \phi^*(\zeta) - \overline{L^* \phi^*(\zeta)} - d^* g^*(\zeta) \\ &\quad - \overline{d^* g^*(\zeta)} + d g_0(\zeta) + \overline{d g_0(\zeta)} \end{aligned} \right\}, \zeta \in S_2 \quad (22)$$

After integrating the temperature functions with respect to  $z_t$ , we obtain

$$\begin{aligned} g(\zeta) &= \gamma_1 \log \zeta + \gamma_2 \zeta^{-2} \\ g^*(\zeta) &= \frac{1}{2} e_1 m_{1t} \zeta^2 + \frac{1}{2} \Gamma_1^* e_1 m_{2t} \zeta^{-2} \\ g_0(\zeta) &= \frac{1}{2} h m_{1t}^2 \zeta^2 + \frac{1}{2} h m_{2t}^2 \zeta^{-2} \end{aligned}$$

where

$$\begin{aligned} \gamma_1 &= \left( -h m_{2t} + \frac{\beta - \beta^*}{\beta + \beta^*} \overline{h m_{1t}} + \frac{2\beta^*}{\beta + \beta^*} \Gamma_1^* e_1 \right) m_{1t} \\ \gamma_2 &= \frac{1}{2} \gamma_1 \frac{m_{2t}}{m_{1t}}. \end{aligned} \quad (23)$$

For the condition that both the stresses and displacements are single valued either in the matrix or in the inclusion, the stress functions  $\phi(\zeta)$  and  $\phi^*(\zeta)$  must take the form

$$\phi(\zeta) = f(\zeta) + \delta \log \zeta \quad (24)$$

$$\phi^*(\zeta) = \sum_{-\infty}^{\infty} \lambda_k \zeta^k \quad (25)$$

where

$$\begin{aligned} \lambda_{-k} &= G_k^* \lambda_k, \\ G_k^* &= \left\langle \left\langle \left( \frac{a + i b s_a^*}{a - i b s_a^*} \right)^k \right\rangle \right\rangle, \quad (\alpha = 1, 2, 3) \end{aligned} \quad (26)$$

The angular bracket stands for the diagonal matrix, i.e.,  $\langle \langle f_a \rangle \rangle = \text{diag}\{f_1, f_2, f_3\}$  and  $f(\zeta)$ ,  $\delta$ ,  $\lambda_k$  are all  $3 \times 1$  matrices. The coefficient  $\delta$  in (24) is given by

$$\begin{aligned} \delta &= A^{-1} (\overline{B}^{-1} - B^{-1})^{-1} (\gamma_1 d - \overline{\gamma_1 d}) \\ &\quad + L^{-1} (\overline{B} - B)^{-1} (\gamma_1 c - \overline{\gamma_1 c}) \end{aligned} \quad (27)$$

where  $B = AL^{-1}$ .

Now, the remaining unknown function  $f(\zeta)$  in (24) and unknown constant  $\lambda_k$  in (25) will be inclusion and the matrix are assumed to be

perfectly bonded along the interface, the displacements and surface tractions at the interface should be continuous. That is,

$$u = u^*, \quad p = p^*, \quad \text{along the interface} \quad \zeta = \sigma = e^{i\psi} \quad (28)$$

By using the continuity conditions (28) and applying the method of analytical continuation, we obtain

$$\begin{aligned} \lambda_2 &= [I - S \overline{G}_2^* S G_2^*]^{-1} \left\{ S \overline{G}_2^* \left[ \overline{n} \left( \gamma_2 + \frac{1}{2} h m_{2t}^2 \right) \right. \right. \\ &\quad \left. \left. + r \frac{-1}{2} \Gamma_1^* e_1 m_{2t} + v \frac{-1}{2} \overline{e_1 m_{1t}} + w \frac{-1}{2} \overline{h m_{1t}^2} \right] \right. \\ &\quad \left. - \left[ n \left( \overline{\gamma_2} + \frac{1}{2} \overline{h m_{2t}^2} \right) + r \frac{1}{2} \overline{\Gamma_1^* e_1 m_{2t}} \right. \right. \\ &\quad \left. \left. + v \frac{1}{2} e_1 m_{1t} + w \frac{1}{2} h m_{1t}^2 \right] \right\} \end{aligned} \quad (29)$$

$$\lambda_k = 0, \quad \text{for } k \neq -2, 2 \quad (30)$$

and

$$\begin{aligned} f(\zeta) &= \left\{ H G_2^* \lambda_2 - \left[ a \left( \gamma_2 + \frac{h}{2} m_{2t}^2 \right) \right. \right. \\ &\quad \left. \left. + b \frac{1}{2} \Gamma_1^* e_1 m_{2t} + k \frac{1}{2} \overline{e_1 m_{1t}} + m \frac{1}{2} \overline{h m_{1t}^2} \right] \right\} \zeta^{-2} \end{aligned} \quad (31)$$

where  $I$  is a  $3 \times 3$  identity matrix, and the coefficients given in (29) and (31) are

$$\begin{aligned} H_{ij} &= \sum_{k=1}^6 M_{ik}^{-1} \overline{M}_{k(j+3)} \\ a_i &= \sum_{k=1}^6 M_{ik}^{-1} R_{k1}, \quad b_i = \sum_{k=1}^6 M_{ik}^{-1} R_{k3} \\ k_i &= \sum_{k=1}^6 M_{ik}^{-1} R_{k4}, \quad m_i = \sum_{k=1}^6 M_{ik}^{-1} R_{k2} \end{aligned} \quad (32)$$



and

$$\begin{aligned} S_{ij} &= \sum_{k=1}^6 \bar{M}_{(i+3)k}^{-1} M_{k(j+3)} \\ n_i &= \sum_{k=1}^6 \bar{M}_{(i+3)k}^{-1} \bar{R}_{k1} \\ r_i &= \sum_{k=1}^6 \bar{M}_{(i+3)k}^{-1} \bar{R}_{k3} \\ v_i &= \sum_{k=1}^6 \bar{M}_{(i+3)k}^{-1} \bar{R}_{k4} \\ w_i &= \sum_{k=1}^6 \bar{M}_{(i+3)k}^{-1} \bar{R}_{k2} \end{aligned} \quad (33)$$

with  $M$  and  $R$  being the  $6 \times 6$  matrix and  $6 \times 4$  matrix. Having the results of  $\lambda_k$ ,  $f(\zeta)$ , the stress functions  $\phi(\zeta)$ ,  $\phi^*(\zeta)$  can now be obtained from (24) and (25), respectively, and the whole field solutions in (4)–(10) are determined accordingly with the understanding that a replacement of  $\zeta_1$ ,  $\zeta_2$ ,  $\zeta_3$ , or  $\zeta_t$  should be made for each component function. The stresses in the inclusion can be directly obtained by differentiating the function (25) with respect to  $z_\alpha$  as

$$\begin{aligned} \frac{d\phi^*}{dz_\alpha} &= (2\lambda_2\zeta - 2\lambda_{-2}\zeta^{-3}) / (m_{1\alpha} - m_{2\alpha}\zeta^{-2}) \\ &= 2(\lambda_2\zeta + G_1^*\lambda_2\zeta^{-1}) / m_{1\alpha} \\ &= 2\lambda_2\zeta / m_{1\alpha}^2 \end{aligned} \quad (34)$$

Similarly, the derivative of the temperature function (30) can be expressed as

$$\frac{dg^*}{dz_t} = e_1 z_t / m_{it} \quad (35)$$

Upon substitution of (34) and (35) into (9) and (10), it is interesting to see that the stresses in the inclusion are always linear functions of the coordinates  $z_\alpha = x_1 + s_\alpha x_2$  and  $z_t = x_1 + s_t x_2$ , which is basically different from the result of uniform stresses existing in the inclusion of the corresponding isothermal elastic problem.

## Holes and Cracks

When the inclusion is an insulated and traction-free hole, the boundary condition of  $p = 0$  in (21) leads to

$$L\phi(\zeta) + \overline{L\phi(\zeta)} = -dg(\zeta) - \overline{dg(\zeta)} \quad (36)$$

The temperature function  $g(\zeta)$  can be directly obtained from integration of (17) by letting  $\beta^* = 0$  as

$$\begin{aligned} g(\zeta) &= \frac{1}{2} (-hm_{2t} + \overline{hm_{1t}}) m_{2t} \zeta^{-2} \\ &\quad - (hm_{2t} + \overline{hm_{1t}}) m_{1t} \log \zeta \end{aligned} \quad (37)$$

Based upon the solutions of (24) and (37) and applying the method of analytic continuation, the traction-free condition (36) yields

$$Lf(\zeta) + \frac{1}{2} d(-hm_{2t} + \overline{hm_{1t}}) m_{2t} \zeta^{-2} = 0 \quad (38)$$

Solving for (38) results in

$$f(\zeta) = \frac{1}{2} L^{-1} d(hm_{2t} - \overline{hm_{1t}}) m_{2t} \zeta^{-2} \quad (39)$$

The final expression of the stress function becomes

$$\begin{aligned} \phi(\zeta) &= \frac{1}{2} L^{-1} d(hm_{2t} - \overline{hm_{1t}}) m_{2t} \zeta^{-2} \\ &\quad + \delta \log \zeta \end{aligned} \quad (40)$$

which is identical to the result given by Tam and Wang [8].

If one lets the minor semiaxis  $b$  of the ellipse approach zero, an elliptic hole can be made into a crack of length  $2a$ . The solutions for the uniform heat flux obstructed by a plane crack in a general anisotropic body can be obtained by letting  $b = 0$  in (37) and (40) as

$$g(\zeta) = \frac{a^2}{8} (-h + \bar{h}) \zeta^{-2} + \frac{a^2}{4} (\bar{h} - h) \log \zeta \quad (41)$$

and

$$\phi(\zeta) = \frac{a^2}{8} L^{-1} d(h - \bar{h}) \zeta^{-2} + \delta \log \zeta \quad (42)$$

Substituting (41) and (42) into (9) and letting  $x_2 = 0$ ,  $|x_1| > a$ , the stresses  $\sigma_2 = \{\sigma_{2i}\}$  ahead of the crack tip along the  $x_1$ -axis are obtained as

$$\sigma_2 = \frac{2}{\sqrt{x_1^2 - a^2}} \operatorname{Re} \left[ L\delta + \frac{a^2(h - \bar{h})}{4} d \right] \quad (43)$$

With the usual definition, the stress intensity factors are given by

$$\begin{aligned} \left\{ \begin{array}{c} K_{II} \\ K_I \\ K_{III} \end{array} \right\} &= \lim_{x_1 \rightarrow a} \sqrt{2\pi(x_1 - a)} \sigma_2 \\ &= 2\sqrt{\frac{\pi}{a}} \operatorname{Re} \left\{ L\delta + \frac{a^2(h - \bar{h})}{4} d \right\} \end{aligned} \quad (44)$$

which are identical to the results given by Hwu [5].

## Conclusions

In this entry, a general solution is given for the thermal stress field due to the obstruction of a uniform heat flow by an elliptic inclusion in a generally anisotropic body. Note that the complex functions  $cg_0(\zeta) + \overline{cg_0(\zeta)}$  and  $dg_0(\zeta) + \overline{dg_0(\zeta)}$  associated with the solutions of the homogeneous problem due to a uniform heat flow will not produce stress which permits us to subtract these complex functions from (7) to (8) without difficulty. Keeping in mind that the arguments of each complex function in (21) and (22) are written in terms without referring to the associated eigenvalues  $s$ , while a replacement of  $\zeta_1$ ,  $\zeta_2$ ,  $\zeta_3$ , or  $\zeta_t$  must be made for each function to calculate field quantities from (4) to (10) once the solutions of  $\phi(\zeta)$  and  $\phi^*(\zeta)$  are obtained.

**Acknowledgment** This study was financially supported by the National Science Council, Republic of China, through grant no. NSC 86-2212-E011-006.

## References

1. Muskhelishvili NI (1953) Some basic problems of mathematical theory of elasticity. Noordhoff, Groningen
2. Florence AL, Goodier JN (1959) Thermal stress at spherical cavities and circular holes in uniform heat flow. *J Appl Mech* 26:293–294
3. Florence AL, Goodier JN (1960) Thermal stress due to disturbance of uniform heat flow by an insulated ovaloid hole. *J Appl Mech* 27:635–639
4. Sturla FA, Barber JR (1988) Thermal stress due to a plane crack in general anisotropic material. *J Appl Mech* 55:372–376
5. Hwu C (1990) Thermal stresses in an anisotropic plate disturbed by an insulated elliptic hole or crack. *J Appl Mech* 57:916–922
6. Stroh AN (1958) Dislocations and cracks in anisotropic elasticity. *Philos Mag* 7:625–646
7. Hwu C, Ting TCT (1989) Two-dimensional problems of the anisotropic elastic solid with an elliptic inclusion. *QJ Mech Appl Math* 42:553–572
8. Tam JQ, Wang YM (1993) Thermal stresses in anisotropic bodies with a hole or a rigid inclusion. *J Therm Stresses* 16:455–471
9. Lekhnitskii SG (1963) Theory of elasticity of an anisotropic elastic body. Holden-Day, San Francisco
10. Chao CK, Shen MH (1997) On bonded circular inclusions in plane thermoelasticity. *J Appl Mech* 64:1000–1004
11. Chao CK, Chang RC (1994) Thermoelastic problem of dissimilar anisotropic solids with a rigid line inclusion. *J Appl Mech* 61:978–980
12. Hwu C, Yen WJ (1993) On the anisotropic elastic inclusions in plane elastostatics. *J Appl Mech* 60:626–632

---

## Elliptical Hole

► [Green's Function for Thermal and Mechanical Mixed Boundary Value Problem for an Elliptical Hole](#)

---

## Elliptical Rigid Inclusion

► [Solution of an Elliptical Rigid Inclusion with Debondings](#)

## Ellipticity

► [Ellipticity Condition and Acceleration Waves in Nonlinear Thermoelastic Solids](#)

## Ellipticity Condition and Acceleration Waves in Nonlinear Thermoelastic Solids

Victor A. Eremeyev  
Otto–von–Guericke University Magdeburg,  
Magdeburg, Germany  
South Scientific Center of RASci and South  
Federal University, Rostov on Don, Russia

## Synonyms

[Acceleration waves](#); [Ellipticity](#); [Nonlinear thermoelasticity](#)

## Definition

By the term “ellipticity”, we mean the property of partial differential equations describing deformations of nonlinear elastic solids. Elliptic operator is a generalization of the well-known Laplace operator. The ellipticity is defined by the condition that the coefficients of the highest-order (second-order) derivatives constitute a positive definite quadratic form. In the nonlinear mechanics of solids, ellipticity plays a role of so-called constitutive restriction. Ellipticity is closely related with the condition of propagation of acceleration waves in nonlinear solids. Acceleration wave is a propagating nonmaterial surface across which the acceleration (but not the velocity) is discontinuous. Acceleration waves are similar, but not the same, to sound waves in prestressed solids.

## Overview

Ellipticity of equilibrium equations of the nonlinear elasticity belongs to the class of so-called constitutive restrictions, see [1–3]. From the physical point of view, the ellipticity is a natural property of statics of elastic media. The violation of ellipticity means that there exist discontinuous solutions of equilibrium equations. On the other hand, in some cases we should not avoid the violation of ellipticity because discontinuous solutions can model such physical phenomena as slip surfaces, shear bands, phase transition interfaces, etc.

The investigations of acceleration waves in nonlinear elastic and thermoelastic media are presented in [1, 2]. Existence of acceleration waves in any direction is equivalent to the fact that all eigenvalues of an algebraic spectral problem for the acoustic tensor are positive for any direction of wave propagation. In the nonlinear elasticity, the condition of existence of acceleration waves coincides with the strong ellipticity of equilibrium equations of nonlinear elastic solids.

In what follows, we use the tensor notations of [3, 4].

## One-Dimensional Case

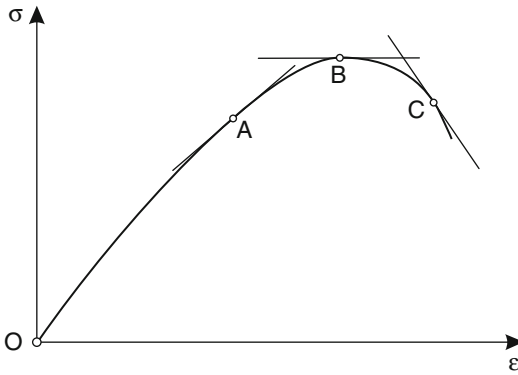
For the sake of simplicity, let us first consider deformation of the one-dimensional (1D) continuum, namely, tension of a nonlinear elastic rod. Let  $X$  denote the position (coordinate) of a rod point in the reference (undeformed) configuration, while  $x(X, t)$  denotes the position of the same point of in the actual (deformed) configuration at instant  $t$ . Hence, the deformation of the rod is represented by the mapping

$$x = x(X, t) \equiv X + u(x, t)$$

where  $u$  is the displacement.

Lagrangian equilibrium equation is given by

$$\sigma' + f(X, u, u') = 0 \quad (1)$$



**Ellipticity Condition and Acceleration Waves in Nonlinear Thermoelastic Solids, Fig. 1** Nominal stress versus strain

where  $\sigma = \sigma(X, u')$  is the nominal stress, the prime denotes the derivative with respect to the Lagrangian coordinate  $X$ ,  $(\dots)' = \frac{d}{dX}(\dots)$ , and  $f$  is the density of external forces.

For the hyper-elastic solids, we assume existence of the strain energy density  $W$  such that  $\sigma = \frac{\partial W}{\partial \varepsilon}$ , where  $\varepsilon = u'$  is the strain. Possible dependence  $\sigma$  on  $\varepsilon$  is presented in Fig. 1.

We transform (4) in the form

$$Q(X, u')u'' + \frac{\partial}{\partial X}\sigma(X, u') + f(X, u, u') = 0 \quad (2)$$

where  $Q = \frac{\partial}{\partial u'}\sigma(X, u') \equiv \frac{\partial^2 W}{\partial \varepsilon^2}$  is the tangent modulus.

We call (2) *strong elliptic* at point  $(X, \varepsilon)$  if the tangent modulus is positive

$$Q(X, \varepsilon) > 0 \quad (3)$$

The condition of strong ellipticity (3) is local as it is defined independently at each point of the rod. For example, the 1D equilibrium equation is elliptic at the point A in Fig. 1 while at the points B and C it is not the case. Obviously, the points B and C correspond to the fading branch of stress–strain curve which can be considered as an unstable state of the rod under static loading. Thus, the loss of ellipticity relates with the material instability.

Let us now consider an acceleration wave in the nonlinear elastic rod. The motion equation of the rod has the form

$$\sigma' + f(X, u, u') = \rho \ddot{u} \quad (4)$$

where the overdot denotes the material derivative with respect to  $t$  and  $\rho$  is the 1D mass density. By its definition, in the 1D case the acceleration wave is a moving point  $X = S(t)$  at which the acceleration undergoes jump, while the displacement and its first derivatives are continuous

$$\begin{aligned} \llbracket u \rrbracket &= 0, \quad \llbracket \dot{u} \rrbracket = 0, \quad \llbracket u' \rrbracket = 0, \quad \llbracket \ddot{u} \rrbracket \neq 0, \\ \llbracket \dot{u}' \rrbracket &\neq 0, \quad \llbracket u'' \rrbracket \neq 0 \quad \text{at } X = S(t) \end{aligned} \quad (5)$$

Here a jump for quantities at  $X = S(t)$  is denoted by the double square brackets, for example,

$$\llbracket u \rrbracket = \lim_{X \rightarrow S(t)+0} u(X) - \lim_{X \rightarrow S(t)-0} u(X) \equiv u^+ - u^-$$

From (5) it follows that  $\llbracket \sigma \rrbracket = 0$ .

For any continuous and piecewise continuously differentiable at  $X = S(t)$  function  $f(X, t)$ , the following relation holds true:

$$V \llbracket f' \rrbracket + \llbracket \dot{f} \rrbracket = 0 \quad (6)$$

where  $V = \dot{S}(t)$  is the velocity of the moving point  $X = S(t)$  playing a role of acceleration wave in the 1D case.

Applying the compatibility condition (6) to the velocity and strain we obtain

$$\llbracket \ddot{u} \rrbracket = a, \quad \llbracket \dot{\varepsilon} \rrbracket = -\frac{a}{V}, \quad \llbracket \varepsilon' \rrbracket = \frac{a}{V^2} \quad (7)$$

where  $a$  is the jump of the acceleration. So the acceleration wave transmits the jump of acceleration. This is a reason why it has such name.

Assuming  $f$  to be a continuous function, from (4) we derive

$$\llbracket \sigma' \rrbracket = \rho \llbracket \ddot{u} \rrbracket \quad (8)$$

With the identity  $[\![\sigma']\!] = Q [\![\varepsilon']\!]$ , we transform (8) into the form

$$Q [\![\varepsilon']\!] = \rho [\![\ddot{u}]\!] \quad (9)$$

Substituting (7) into (9) we obtain

$$Qa = \rho V^2 a \quad (10)$$

Equation (10) always has the trivial solution  $a = 0$ . We are not interested in this solution because it does not correspond to any wave. Nontrivial solution of (10) relates with the propagating acceleration wave with the velocity  $V$ . Since  $V$  is assumed to be a real number, the condition of existence of nontrivial solution of (10) consists of the inequality  $Q > 0$  which coincides with the strong ellipticity condition defined above.

The considered above 1D case can be straightforward extended for three-dimensional case.

### Three-Dimensional Case

Deformation of nonlinear thermoelastic solids is described by the mapping

$$\mathbf{x} \equiv \mathbf{x}(\mathbf{X}, t) = \mathbf{X} + \mathbf{u}(\mathbf{X}, t) \quad (11)$$

The vector  $\mathbf{x}$  describes the position of a material point in the actual configuration at instant  $t$ , while  $\mathbf{X}$  describes the position of the material point in the reference configuration.  $\mathbf{u}$  is the displacement vector. Additionally to (11) at any point of the solid, the temperature field is defined

$$\theta = \theta(\mathbf{X}, t)$$

Lagrangian motion and thermoconductivity equations are

$$\text{Div } \mathbf{T}_\kappa + \rho \mathbf{f} = \rho \ddot{\mathbf{u}}, \quad \rho \theta \dot{\eta} = -\text{Div } \mathbf{q} + \rho h \quad (12)$$

Here  $\mathbf{T}_\kappa$  is the first Piola-Kirchhoff stress tensor,  $\text{Div}$  the divergence operator in Lagrangian coordinates,  $\rho$  the mass density in the reference configuration,  $\mathbf{f}$  the vector of mass forces,  $\eta$  the specific entropy,  $\mathbf{q}$  the heat flux in the reference configuration, and  $h$  the density of external heat source.

The constitutive equations of a nonlinear thermoelastic medium are given by

$$\begin{aligned} \psi &= \psi(\mathbf{F}, \theta; \mathbf{X}), \quad \mathbf{T}_\kappa = \rho \psi_{,\mathbf{F}}, \\ \eta &= -\psi_{,\theta}, \\ \mathbf{q} &= \mathbf{q}(\mathbf{F}, \theta, \text{Grad } \theta) \end{aligned} \quad (13)$$

where  $\mathbf{F} = \text{Grad } \mathbf{x}$  is the deformation gradient, and we use the following notations:

$$\psi_{,\mathbf{F}} = \frac{\partial \psi}{\partial \mathbf{F}}, \quad \psi_{,\theta} = \frac{\partial \psi}{\partial \theta}, \quad \dots$$

In what follows, we use the referential *Fourier law* for  $\mathbf{q}$

$$\mathbf{q} = -\mathbf{k}(\theta) \cdot \text{Grad } \theta \quad (14)$$

where  $\mathbf{k}$  is the positive definite thermoconductivity tensor.

We assume  $\psi$  to be a twice continuously differentiable function and vector function  $\mathbf{q}$  to be continuously differentiable.

In the case of thermodynamic equilibrium, we have equations

$$\text{Div } \mathbf{T}_\kappa + \rho \mathbf{f} = 0, \quad -\text{Div } \mathbf{q} + \rho h = 0 \quad (15)$$

Using the theory of partial differential equations (PDEs), see [5], we formulate the strong ellipticity conditions of (15) as follows, see also [1, 3],

$$\begin{aligned} (\mathbf{N} \otimes \mathbf{a}) \cdot \cdot \mathbf{T}_{\kappa, \mathbf{F}} \cdot \cdot (\mathbf{N} \otimes \mathbf{a}) &> 0, \quad \mathbf{N} \cdot \mathbf{k}(\theta) \cdot \mathbf{N} > 0, \\ \forall \mathbf{a} \neq \mathbf{0}, \quad \forall |\mathbf{N}| &= 1 \end{aligned} \quad (16)$$

where  $\otimes$  is the tensor product and  $\cdot \cdot$  the double dot product, see [4]. Inequality (16)<sub>1</sub> can be written in terms of  $\psi$

$$(\mathbf{N} \otimes \mathbf{a}) \cdot \cdot \psi_{,\mathbf{FF}} \cdot \cdot (\mathbf{N} \otimes \mathbf{a}) > 0, \quad \forall \mathbf{a} \neq \mathbf{0}, \quad \forall |\mathbf{N}| = 1 \quad (17)$$

or in an equivalent form as follows:

$$\frac{d^2}{d\tau^2} \psi(\mathbf{F} + \tau \mathbf{a} \otimes \mathbf{N})|_{\tau=0} > 0, \quad \forall \mathbf{a} \neq \mathbf{0}, \quad \forall |\mathbf{N}| = 1 \quad (18)$$

Introducing the acoustic tensor  $\mathbf{Q}$  by the formula

$$\mathbf{Q}(\mathbf{N}) = \psi_{,F_{kl}F_{mn}} N_l N_n \mathbf{i}_k \otimes \mathbf{i}_m, \quad k, l, m, n = 1, 2, 3$$

where  $N_k$  and  $F_{mn}$  are the components of  $\mathbf{N}$  and  $\mathbf{F}$  in the Cartesian base  $\mathbf{i}_k$ , we represent the strong ellipticity conditions as a requirement of positive definiteness of the acoustic tensor

$$\mathbf{a} \cdot \mathbf{Q}(\mathbf{N}) \cdot \mathbf{a} > 0, \quad \forall \mathbf{a} \neq \mathbf{0}, \quad \forall |\mathbf{N}| = 1 \quad (19)$$

Inequality (19) is a three-dimensional analogue of (3).

The weak form of (19) and of other equivalent forms (16), (17), (18) is called the *Hadamard inequality*, that is, the inequality, see [1–3],

$$\mathbf{a} \cdot \mathbf{Q}(\mathbf{N}) \cdot \mathbf{a} \geq 0, \quad \forall \mathbf{a}, \quad \forall |\mathbf{N}| = 1 \quad (20)$$

For example, in the 1D case the state corresponding the point *B* in Fig. 1 satisfies (20).

Let us note that in the theory of PDEs there are different definitions of ellipticity, see [5]. In particular, the *ordinary ellipticity* or the *ellipticity in Petrovsky's sense* consists of the inequality

$$\det \mathbf{Q}(\mathbf{N}) \neq 0, \quad \forall |\mathbf{N}| = 1 \quad (21)$$

For the 1D case, the equilibrium equation is elliptic in Petrovsky's sense at points *A* and *C* but not at *B*.

Extensive discussion of the strong ellipticity and the Hadamard inequality in the nonlinear elasticity is presented in [1–3].

In what follows, let us consider the relation between the ellipticity and the conditions of the acceleration wave propagation in the thermoelastic medium. Acceleration wave is a traveling smooth surface  $S(t)$  on which the following balance equations must be valid:

$$[\![\mathbf{F}]\!] = \mathbf{0}, \quad [\![\dot{\mathbf{u}}]\!] = \mathbf{0} \quad (22)$$

In the nonlinear thermoelastic medium, there are two types of acceleration waves:

- The *homothermal* acceleration wave corresponds the case when *the temperature field and its first derivatives are continuous at  $S(t)$* :

$$[\![\theta]\!] = 0, \quad [\![\text{Grad } \theta]\!] = \mathbf{0}, \quad [\![\dot{\theta}]\!] = 0 \quad (23)$$

- The *homentropic* (or *homocaloric*) acceleration wave corresponds the case when *the entropy field and its first derivatives are continuous at  $S(t)$* :

$$[\![\eta]\!] = 0, \quad [\![\text{Grad } \eta]\!] = \mathbf{0}, \quad [\![\dot{\eta}]\!] = 0 \quad (24)$$

In the 3D continuum, a generalization of (6) is given by the *Maxwell theorem*:

*For a continuously differentiable field  $\mathbf{Y}$  such that  $[\![\mathbf{Y}]\!] = \mathbf{0}$  the following relations hold*

$$[\![\dot{\mathbf{Y}}]\!] = -V\boldsymbol{\phi}, \quad [\![\text{Grad } \mathbf{Y}]\!] = \boldsymbol{\phi} \otimes \mathbf{N} \quad (25)$$

where  $\boldsymbol{\phi}$  is the tensor amplitude of the jump of the first gradient of  $\mathbf{Y}$  and  $\mathbf{N}$  is the unit normal to  $S(t)$ ; the tensor amplitude is a tensor of the order equal to the order of  $\mathbf{Y}$ .

For the homothermal acceleration wave, straightforward application of Maxwell's theorem to the continuous fields of  $\dot{\mathbf{u}}$ ,  $\mathbf{T}_\kappa$ ,  $\mathbf{q}$

and to Grad  $\theta$  results in the system of equations at  $S(t)$ :

$$\begin{aligned}\llbracket \ddot{\mathbf{u}} \rrbracket &= -V\mathbf{a}, & \llbracket \text{Grad } \dot{\mathbf{u}} \rrbracket &= \mathbf{a} \otimes \mathbf{N}, \\ V\llbracket \text{Div } \mathbf{T}_\kappa \rrbracket &= -\llbracket \dot{\mathbf{T}}_\kappa \rrbracket \cdot \mathbf{N} \\ \llbracket \text{Grad Grad } \theta \rrbracket &= g\mathbf{N} \otimes \mathbf{N}, & \llbracket \text{Grad } \dot{\theta} \rrbracket &= -Vg\mathbf{N}, \\ V\llbracket \text{Div } \mathbf{q} \rrbracket &= -\llbracket \dot{\mathbf{q}} \rrbracket \cdot \mathbf{N}\end{aligned}$$

where  $\mathbf{a}$  and  $g$  are the amplitudes of the jumps in the acceleration and in the second gradient of the temperature, respectively.

Using transformations of similar ones in the previous section, we obtain the condition of propagation of the homothermal wave in the form

$$\mathbb{Q}_\theta(\mathbf{N}) \cdot \boldsymbol{\zeta} = V^2 \boldsymbol{\zeta} \quad (26)$$

where  $\boldsymbol{\zeta} = (\mathbf{a}, g) \in \mathbb{R}^4$ ,  $\mathbb{Q}_\theta$  is given by

$$\mathbb{Q}_\theta(\mathbf{N}) \equiv \begin{bmatrix} \mathbf{Q}(\mathbf{N}) & \mathbf{0} \\ -\rho_0 \theta \mathbf{N} \cdot \boldsymbol{\psi}_{,\theta\mathbf{F}} & \mathbf{N} \cdot \mathbf{k}(\theta) \cdot \mathbf{N} \end{bmatrix}$$

$\mathbb{Q}(\mathbf{N})_\theta$  is the *homothermal acoustic tensor* in the nonlinear thermoelastic continuum. The spectral problem (26) is a generalization of (10). A homothermal acceleration wave exists only if (26) has nontrivial solutions and the eigenvalues for the problem (26) are real and positive. Thus, we should impose the additional restriction on  $\mathbb{Q}_\theta(\mathbf{N})$

$$\boldsymbol{\zeta} \cdot \mathbb{Q}_\theta(\mathbf{N}) \cdot \boldsymbol{\zeta} > 0, \quad \forall \boldsymbol{\zeta} \neq \mathbf{0}, \quad \forall |\mathbf{N}| = 1 \quad (27)$$

Obviously, the inequality (27) coincides with the strong ellipticity condition (16).

Thus, *the condition for existence of a homothermal acceleration wave for all directions of propagations in a non-linear thermoelastic continuum is equivalent to the condition of strong ellipticity of the equilibrium equations of the continuum.*

The homocaloric wave is a less interesting case because in a heat-conductive medium any acceleration wave is homothermal one. In heat nonconductive media, a homocaloric acoustic tensor differs from  $\mathbb{Q}_\theta$ , in general, see [2].

## References

1. Truesdell C, Noll W (1965) The nonlinear field theories of mechanics. In: Flügge S (ed) Handbuch der physik, vol III/3. Springer, Berlin, pp 1–602
2. Truesdell C (1984) Rational thermodynamics, 2nd edn. Springer, New York
3. Lurie AI (1990) Nonlinear elasticity. North-Holland, Amsterdam
4. Lebedev LP, Cloud MJ, Eremeyev VA (2010) Tensor analysis with applications in mechanics. World Scientific, New Jersey
5. Agranovich M (1997) Elliptic boundary problems. In: Agranovich M, Egorov Y, Shubin M (eds) Partial differential equations IX: elliptic boundary problems, vol 79, Encyclopaedia of mathematical sciences. Springer, Berlin, pp 1–144

## Energetics

Tomasz Sobota, Sławomir Grądział and  
Wiesław Zima

Institute of Thermal Power Engineering, Faculty  
of Mechanical Engineering, Cracow University  
of Technology, Cracow, Poland

## Overview

The word *energy* refers to different things. In general, it is the potential to create change and the ability to act, transform, or set in motion. Other meanings refer to energy as a natural resource and as the technology related with exploiting and using the resource, both industrially and economically [1].

Energy is an abstract physical quantity that cannot be measured in a pure state, but only its variations in material systems can be observed. These variations are equivalent to the work required to change one system from its initial state to a subsequent one. Energy cannot be created or destroyed; it can only be transformed from one to another form. Obviously there are forms of energy that can be transformed or used more easily than others, and, in the end, all forms of energy will become heat energy, one of the most disordered forms of energy.



Another definition of the word *energy* refers to the natural resources necessary to produce energy as engineers and physicists understand it. This understanding of energy is very important and affects us all. Its role in the global economy is essential.

In this entry, some of the most important sources of energy used by humanity will be presented. Description of the uses of clean, renewable sources of energy (solar, wind, water, and geothermal), and energy from fossil fuels will be presented.

Modern life is unimaginable without electricity. It lights houses, buildings, and streets; provides domestic and industrial heat; and powers most equipment used in homes, offices, and machinery in factories. Improving access to electricity worldwide is critical to alleviating poverty.

Electricity is the most convenient and versatile form of energy. Demand for it, therefore, has been growing at a rate faster than other forms of energy. Power industry too has noted a remarkable rate of growth both in terms of its volume and technological sophistication over the last few decades. Electricity plays a crucial role in both industrial and agricultural sectors, and the consumption of electricity in the country is an indicator of productivity and growth. In view of this, power development has been given high priority in development program [2, 3].

## Sources of Energy

Energy can take on many forms, so that there are many possible sources from which work and heat can be generated. Energy resources can be generally divided into *renewable* and *nonrenewable*.

Renewable energy resources are not used up or exhausted through use. The resources of renewable energy are limitless because they can be recovered or regenerated. Some of these sources of energy are the Sun, the wind, and water. Biomass and geothermal energy can also be considered as renewable energy resources depending on the form of utilization.

*Solar energy.* The Sun delivers the Earth great quantities of energy, which can be used for heating

(solar collector heating systems) as well as for producing electricity (photovoltaic, solar trough, solar power towers, or solar dish/engine systems).

*Wind energy.* Solar radiation forms regions of high and low pressure that creates flows of air in the atmosphere. Wind is one of the most encouraging renewable energy resources because of its relative safety and cleanliness. The most important disadvantages are lack of ability to foresee precisely the strength and blowing period of winds and undesirable impact groups of large towers on the local landscape. Electricity is produced in wind-driven wind turbines.

*Water energy.* Is used for electrical energy production in hydropower plants. The main drawback is that the construction of reservoirs, canals, and dams modifies the ecosystems where they are located and is the most expensive but, on the other hand, the most efficient. About 20 % of the world's electricity is generated by the hydroelectric power plants.

*Tidal energy.* Belongs to the newer forms of electrical energy production

*Geothermal energy.* Is created by the heat in the crust and mantle of the Earth. The advantage is constant energy output but requires building of power plants in regions where water is very close to these heated sections.

Nonrenewable energy resources are natural gas, oil, and coal called as fossil fuels. The current energy supply depends mainly on fossil energy. A large amount of fossil fuels has already been used up in the twentieth century. Because of the increasing exploitation of the fossil reservoirs, future extraction will be more and more difficult and therefore much more expensive than today. If fossil fuel use continues unchecked, all available reserves of petroleum and natural gas will be exploited within the twenty-first century. Only coal reserves will be available for a longer period of time. However, even if major fossil fuel reserves should be discovered, this would not change the fact that fossil fuel reserves are limited. The time span of their availability can be extended only by some years or decades at best.

Coal plays a vital role in electricity generation worldwide. Coal-fired power plants currently fuel 41 % of global electricity. In some countries, coal



fuels a higher percentage of electricity. The importance of coal to electricity generation worldwide is set to continue, with coal fueling 44 % of global electricity in 2030.

The Earth's uranium reserves for operating nuclear power stations are limited as well. The estimated global reserves are less than 20 million t, of which 12.52 million t is only speculative. If the total world primary energy demand in 2000, about  $1.1 \cdot 10^{14}$  kWh, had been provided by nuclear power, the reasonably assured, economically exploitable reserves would have lasted only about 2 years. Breeder reactors can increase this time by a factor of about 60 [3, 4].

## Power Plant

Generally, a power plant is an assembly of systems or subsystems to generate electricity (coal mills, power boiler, TurboGen set, air preheaters, feedwater heaters, environment protection units like particle removing, flue gas desulfurization, and nitrogen removing). The power plant itself must be useful economically and environmental friendly to the society. The system conversion efficiency's supreme goal is to develop and design [2].

The power plants can be classified as:

1. Conventional
  - (a) Steam engines power plants
  - (b) Steam turbine power plants
  - (c) Diesel power plants
  - (d) Gas turbine power plants
  - (e) Hydroelectric power plants
  - (f) Nuclear power plants
2. Nonconventional
  - (a) Thermoelectric generator
  - (b) Thermionic generator
  - (c) Fuel cell power plants
  - (d) Photovoltaic power system
  - (e) MHD power plants
  - (f) Biogas and biomass energy power system
  - (g) Geothermal energy
  - (h) Wind energy power system
  - (i) Ocean thermal energy conversion (OTEC)
  - (j) Wave and tidal wave

Power plants convert a primary source of energy to electrical energy. The primary sources

are *fossil fuels*, such as coal, oil, and natural gas; *nuclear fuels* (fissile elements: uranium, plutonium, and thorium); and *renewable energy*, such as solar, wind, geothermal, hydro, and energy from the oceans (tides, waves, or the difference in temperature between surface and bottom, so-called ocean temperature energy conversion (OTEC)).

In the production of electricity in the world, the key role plays coal-fired steam power plants, nuclear, and hydroelectric power plants. From nuclear and hydroelectric power plants comes almost 40 % of world electricity generation.

Systems that convert these primary sources into electricity are in turn generally classified as follows:

1. The Rankine cycle, primarily using water and steam as a working fluid but also organic fluids (ammonia, hydrocarbon, and Freon). It is widely used as the conversion system for fossil and nuclear fuels, solar energy, geothermal energy, and OTEC.
2. The Brayton cycle using, as a working fluid, hot air-fossil fuel combustion products or a gas such as helium that is heated by nuclear fuel.
3. The combined cycle, a combination of Rankine and Brayton cycles in series.
4. Wind or water turbines, using wind, hydropower, ocean tides, and ocean waves.
5. Direct energy conversion devices, which transform some primary sources to electricity directly, such as photovoltaic cells for solar energy [5–7].

The processes taking place in power systems are sufficiently complicated that idealizations are typically employed to develop thermodynamic models. Depending on the degree of simplification, such models may provide only qualitative information about the performance of the equivalent real-world systems. However, such information is useful in determining how changes in major operating parameters might affect actual performance [8].

## The Rankine Cycle

The Rankine cycle is a versatile one that can use a wide range of heat sources. In its most common

form, it uses water and steam as a working fluid. It can be created to generate large quantities of electric power, exceeding 1,000 MW in a single power plant. It has the highest conversion efficiency (ratio of electrical energy generated to heat energy added) of all large applied conversion systems. The thermodynamically ideal counterparts of this cycle are composed of four internally reversible processes in series: two isentropic processes (pumping feedwater to the power boiler evaporator and steam expansion in turbine) interchanged with two constant pressure processes (evaporation of water and steam superheating, and condensation of exhaust steam from turbine) [5, 6, 9–11].

High-pressure, superheated steam is routed to a steam turbine, where it expands through the turbine becoming a two-phase mixture of steam and water, usually 89–92 % steam by mass, where the pressure and temperature are typically 8 kPa and 38 °C but vary according to the available cooling conditions in the condenser. The exhaust steam from the turbine is cooled in a condenser at constant pressure and temperature, condensing to a saturated liquid. The condensate is then pumped through a feedwater system, where it is heated in stages by feedwater heaters (closed and open). After this regenerative heating process, the temperature of boiler feedwater is about 0.6–0.75 the boiling temperature at the maximum pressure in the cycle. Next, the heat is added to feedwater in a power boiler, converting it to superheated steam.

The thermal energy of the stem is converted to mechanical work by the turbine, which in turn drives an electric generator to produce electricity. Modern power plant turbines are made of multiple sections, usually in tandem (on one axis). The first section, a high-pressure impulse turbine, receives inlet steam and exhausts to a reheater in the power boiler. The reheated steam, at about 20–25 % of the pressure and about the same temperature as live steam, enters an intermediate-pressure reaction turbine, from which it leaves to low-pressure reaction turbine.

The process of condensation allows to generate the net power by a power plant. To increase the cycle efficiency, the condenser operates at the

lowest temperature and therefore the lowest possible pressure. This is done by using the lowest temperature coolant available, usually water from large supply (open cooling system) or using closed cooling system with cooling towers. The most common condenser is the shell and tube heat exchanger. Another type of steam condenser, so-called the direct contact or open, is used in special applications.

## **Increase the Efficiency of the Rankine Cycle**

The basic idea behind all the modifications to increase the thermal efficiency of a power cycle is the same: increase the average temperature at which heat is transferred to the working fluid in the boiler, or decrease the average temperature at which heat is rejected from the working fluid in the condenser. The side effect of lowering the condenser pressure is increase in the moisture content of the steam at the final stages of the turbine.

Superheating the steam to high temperatures causes both the network and heat input increase. The overall effect is an increase in thermal efficiency since the average temperature at which heat is added increases. Superheating to higher temperatures decreases the moisture content of the steam at the turbine exit, which is desirable. The temperature is limited by metallurgical considerations. Presently the highest steam temperature allowed at the turbine inlet is about 620 °C [2, 7, 12, 13].

Increasing the boiler pressure for a fixed steam temperature at the turbine inlet causes the side effect: the moisture content of steam at the turbine exit increases. This side effect can be corrected by reheating the steam. The steam expands in the turbine in two stages and is reheated in between. Reheating is a practical solution to the excessive moisture problem in turbines, and it is commonly used in modern steam power plants.

The last method to increase the Rankine cycle efficiency is to heat up (to regenerate) the feedwater before it enters the boiler. A practical

**Energetics,****Table 1** Technical data of some modern coal-fired ultracritical power plants [12]

Power plant/country	Installed net capacity MW <sub>e</sub>	Steam conditions MPa/°C/°C/°C	Design net efficiency %
Nordjyllandsværket 3/Denmark	384	29/582/580/580	44.9
Niederaussem K/Germany	965	27/580/600	37
Genesee 3/Canada	450	25/570/570	39.6
Isogo Unit 1/Japan	568	25/600/610	40.6

regeneration process in steam power plants is accomplished by bleeding steam from the turbine. This steam, which could have produced more work by expanding further in the turbine, is used to heat the feedwater instead.

In a modern pulverized coal combustion power plant, coal is burnt as it is blown into a boiler, and the released heat raises the steam temperature that supplies a steam turbine generator. In the boilers, the burners can be mounted on the walls of the furnace chamber (at the front, rear, or side) firing perpendicular to the water walls or can be mounted at the corners of the furnace chamber, and fire is directed tangentially. For low-volatile coals such as anthracites, the burners point vertically downward to give a longer residence time for combustion before the product gases leave the furnace. Welded tubing that forms the wall of the boiler combustion chamber recovers heat for water evaporation in subcritical boilers. In a supercritical boiler, the water changes directly into vapor, when the critical temperature is passed, without a liquid/vapor boundary. In both subcritical and supercritical boilers of the two-pass type, superheat and reheat heat transfer surfaces are mounted above the furnace and in a subsequent convection section of the boiler, in which there is also an economizer to extract more heat. The last stage of heat recovery is just after the boiler and heats the combustion air, providing a means both of drying the coal to assist its combustion and recycling energy to the boiler. In opposite to the two-pass boiler designs, the tower type has the superheater and reheater mounted above the furnace chamber. In tower boilers, the economizer may be mounted either above the superheater and reheater sections or above the air heater. The commonly used turbine

arrangement is the tandem compound system, which has all turbine sections (high, intermediate, and low pressure) mounted in line, driving a single electricity generator. In all modern power generation units, the steam is reheated in the boiler before entering the intermediate-pressure turbine. The flue gases that leave power boiler flow through the selective catalytic reduction (SCR) or for nitrogen oxides control, electrostatic precipitator or bag filters for dust removal, and flue gas desulfurization system for sulfur oxides control.

The latter is necessary for supercritical boilers, whose higher steam conditions allow the highest efficiencies. Some steam is always extracted from the turbine to heat the boiler feedwater, as this raises cycle efficiency [2, 7, 12, 13] (Table 1).

## Nuclear Power Plants

Nuclear power is the use of sustained nuclear fission to generate heat and electricity. Nuclear power plants provide about 6 % of the world's energy and 16 % of the world's electricity. In 2011, the IAEA reported 436 nuclear power reactors in operation in the world with 372,000 MW<sub>e</sub> total net installed capacity, operating in 31 countries. Sixteen countries depend on nuclear power for at least a quarter of their electricity. France gets around three quarters of its power from nuclear energy, while Belgium, Bulgaria, Czech Republic, Hungary, Slovakia, South Korea, Sweden, Switzerland, Slovenia, and Ukraine get one third or more. Japan and Finland normally get more than a quarter of their power from nuclear energy, while in the USA, one fifth is from nuclear. Among countries which do not host

nuclear power plants, Italy gets about 10 % of its power from nuclear and Denmark about 8 % [5, 14].

Nuclear power systems use the controlled release of energy from splitting the atoms of elements such as uranium and plutonium as a heat source for the generation of electricity or for direct thermal heat. In a nuclear power reactor, the energy released from continuous fission of the atoms (chain reaction) in the fuel as heat is used for steam generation. The steam is used to drive a turbine coupled to a generator which produces electricity.

The common components of most types of energetics nuclear reactors are as follows:

1. Fuel – usually pellets of uranium oxide ( $\text{UO}_2$ ) arranged in tubes to form fuel rods, and the rods are from fuel benches placed in the reactor core.
2. Moderator, usually water, heavy water, or graphite, which slows down the neutrons released from fission for sustenance and continuation of chain reaction.
3. Control rods, made with neutron-absorbing material such as cadmium, hafnium, or boron, to control the rate of reaction or to stop.
4. Coolant to remove heat from reactor core and transfer it to steam generators. As a coolant, liquid (water or heavy water) or gas (helium, carbon dioxide) can be used. In light water reactors, the moderator functions also as coolant.
5. Pressure vessel or pressure tubes – containing the reactor core and moderator and coolant.
6. Steam generator is a part of the cooling system where the heat from the reactor is used to make steam for the turbine.
7. Containment – the concrete structure around the reactor core designed to protect it from outside intrusion and to protect the surrounding from the effects of radiation in case of any major accidents inside [5, 14, 15].

Four generations of nuclear power reactors are distinguished. Generation I reactors were developed in the 1950s–1960s. They mostly used natural uranium fuel and used graphite as moderator. Generation II reactors are commonly used nowadays. They typically use enriched uranium fuel

and are mostly cooled and moderated by water. Generation III advanced reactors are developments of the second generation with enhanced safety. The generation IV reactors are still at the design stage. These reactors will have closed fuel cycles and burn actinides forming part of spent fuel.

## Division of Power Boilers

One of the conditions of safe boiler operation is ensuring sufficient cooling of the evaporator pipes, i.e., ensuring the appropriate flow of medium in the pipes. The flow can be induced by the following:

- Using the natural circulation of the medium in a closed circulation outline created as a result of the difference in density of water and a steam-water mixture.
- Using the operation of additional circulation pumps, but if the contribution of the pump uplift pressure is low as compared to the natural uplift pressure, it is called a supported circulation; when the contribution of the pump uplift pressure prevails, it is called a forced circulation.
- Using the operation of the main supply water pumps to pump the medium through the heaters, evaporator, and steam superheater one-cycle flow.

With regard to the aforementioned kinds of water circulation, power boilers can be divided as follows:

1. Drum boilers
  - (a) With a natural circulation
  - (b) With an supported circulation
  - (c) With a forced circulation
2. Drumless boilers
  - (a) With water separator
  - (b) One-cycle flow

## Boilers with Natural Circulation

The phenomenon of natural medium circulation occurs in a closed circulation outline that is generally formed from systems of downpipes and

riser pipes, connected on the top with a drum and with collective chambers at the bottom. Water density in the downpipes (unheated section) is higher than the density of steam-water mixture in the riser pipes (heated section). The difference in density resulting from the formation of steam in the riser pipes under the influence of heat supplied from the combustion chamber generates a natural uplift pressure, forcing the movement of the fluid. The movement comes along with a loss of pressure as a result of frictional resistance in the pipes and localized resistance, caused by the changes in the flow direction and fittings installed in the circulation outline. The water flow intensity in the circulation contour is much higher than the quantity of steam it generates. The ratio between the two values is known as the circulation multiplicity of the water cycle circulation:

$$k = \frac{G_w}{D} \quad (1)$$

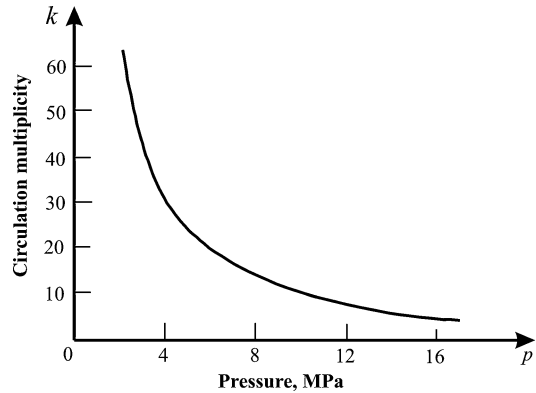
where  $G_w$  is the water stream in the outlines, kg/s, and  $D$  is the quantity of steam generated in the outline, kg/s.

The circulation multiplicity of a circuit can be identified separately for each circulation outline or as a mean for the entire boiler. The reverse of the circulation multiplication factor is the dryness rate of the steam leaving the circulation outline:

$$x = \frac{1}{k} \quad (2)$$

An increase in the combustion chamber thermal load causes an increase in the steam dryness rate  $x$  and simultaneously an increase in speed. The higher the dryness rate  $x$ , the lower the steam-water mixture density, and cooling of the evaporator pipes deteriorates. Therefore, as the thermal load increases, dangerous film boiling may occur. That is why steam dryness  $x$  at the riser pipe outlets must not exceed 0.2 for boilers with a natural circulation. Hence, the multiplication factor of the circulation  $k$  must not be lower than 5.

Figure 1 presents the relationship between the circulation multiplication factor for boilers with a natural circulation in the function of pressure in the evaporator [16, 17].



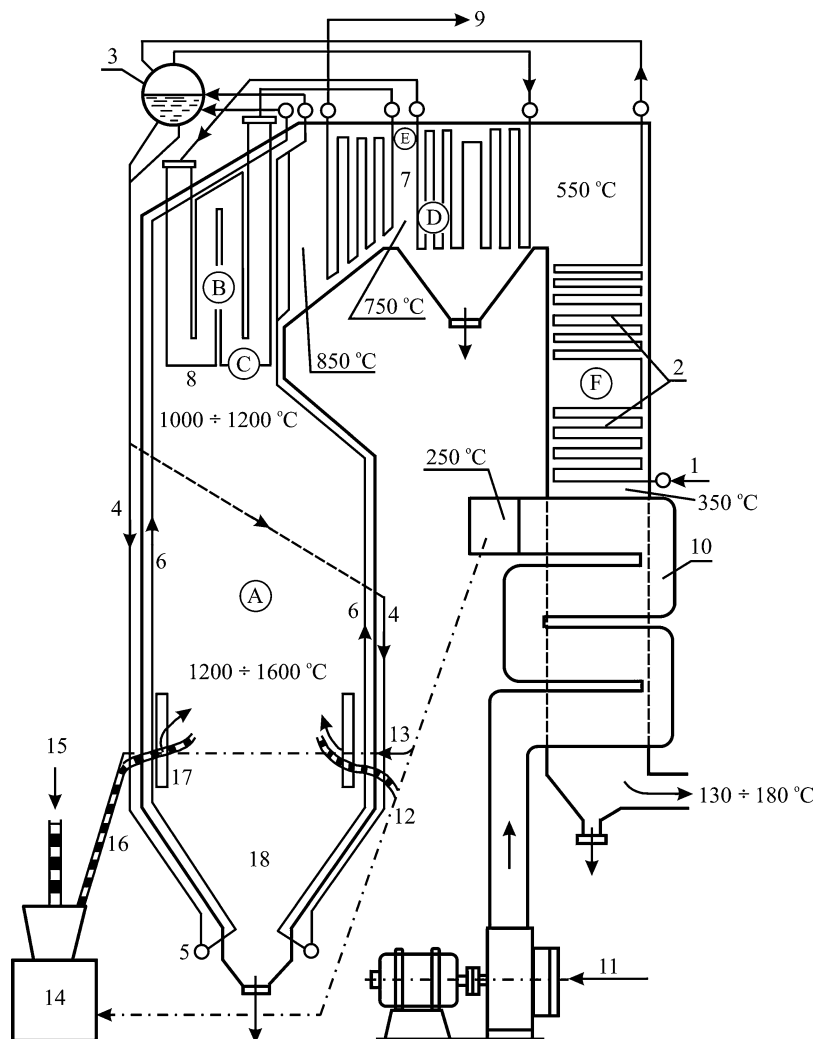
**Energetics, Fig. 1** Circulation multiplicity  $k$  of water circulation in a boiler with a natural circulation in the function of pressure  $p$

Figure 2 presents a diagram of a pulverized coal two-pass boiler with a natural water circulation [16]. The combustion chamber (A) where heating surfaces (screens), absorbing heat by radiation, are located is the first pass of the boiler. Next, there is a bulkhead chamber (B) where heating surfaces also absorb heat by means of radiation. The combustion chamber is usually closed with a narrowing at the top, aimed at mixing exhaust gas leaving the combustion chamber. In this place, the rear water wall forms a festoon (C). In the boiler bridge (D), convection surfaces are installed. The top of the boiler is closed with a ceiling (E). The other pass of the boiler is formed by a pass (F) with further heating surfaces installed: other steam superheaters as well as air and economizers.

The supply water pump pumps water (1) through the economizer (2) to the drum (3). Next the water is supplied to collective chambers (5) with unheated downpipes (4). The rear pipe screens of the combustion chamber wall are fixed in the collective chambers. The upper ends of the pipe screen (6) come to the upper collective chambers connected with transfer pipes to the drum (3). Water flowing from the bottom, from the collector (5) to the pipe screen (6) heated by flames and exhaust pipes in the combustion chamber, takes over the heat, and the first steam bubbles are formed. The steam-water mixture in the pipes has a lower density than water in the

**Energetics,**

**Fig. 2** Diagram of a two-pass boiler with a natural water circulation *A* furnace chamber, *B* bulkhead chamber, *C* festoon, *D* boiler bridge, *E* ceiling, *F* second pass; 1 supply water, 2 economizer, 3 drum, 4 downpipes, 5 collective chambers, 6 pipe screen, 8 superheater, 9 superheater, 10 supply to the turbine, 11 air heater, 12 air supply to the fan, 13 primary air, 14 secondary air, 15 mills, 16 coal supply, 17 dust-air mixture supply, 18 burners, 19 slag hopper



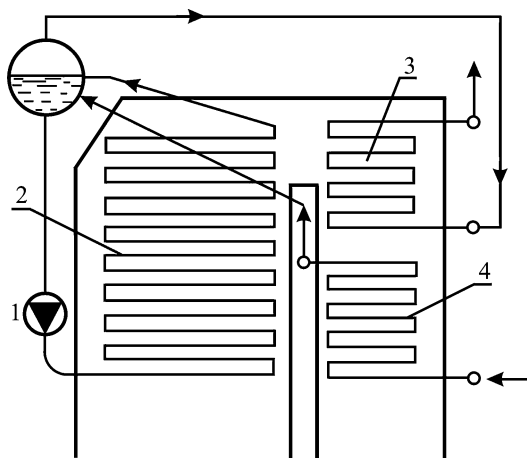
downpipes without steam bubbles. As a result of the difference in density between the downpipes and the pipe screen, water circulates automatically. Riser pipes, downpipes, collective chambers, and the drum form the evaporator where saturated steam is formed. The created saturated steam circulates from the drum to the superheaters, consisting of chambers and coils made of pipes (7) and (8) and is taken to the turbine with a pipeline (9) after superheating.

The air heater (10), through which the air fan pumps the air (11), is located behind the economizer (2). A part of the air (12) is supplied to the coal mills as primary air. The other part of the air is supplied as secondary air (13) with powder

(16) to the powdered-coal burners (17). Slag and ash formed as a result of incineration fall into the slag hopper (18) from which they are removed from the boiler.

### Boilers with a Supported Circulation

Boilers with natural water circulation can be constructed only for the evaporator pressure  $p < 17$  MPa. At high-pressure values, e.g., 20 MPa, in order to ensure sufficient cooling of the pipes by the flow of steam-water mixture and to prevent film boiling, supported circulation will be used in the evaporator by activating the circulation



**Energetics, Fig. 3** Diagram of La Monta forced circulation drum boiler: 1 circulation pump, 2 evaporator, 3 steam superheater, 4 water superheater

pump. A large stream of mass pumped through the pump tears off the steam film created at the wall. A 1,650 Mg/h steam efficiency and 500 MW power boiler installed in Poland (Kozienice Power Plant) are an example of such a boiler.

### Boilers with a Forced Circulation

La Monta boiler (Fig. 3) is a typical example of a drum boiler with a forced water circulation [16]. The circulation pump (1) forces water circulation in the evaporator coils (2). Forced water circulation allows for more possibilities of shaping the heating surface of the evaporator that usually consists of a large number of parallel coils located on the furnace chamber walls in this type of boiler. Within the critical pressure range, even for minor pressure changes, changes in the water density are so high that the operating conditions of circulation pumps are very difficult, and hence a cycle with a circulation pump can be used for pressures lower than 21 MPa.

### Drumless Boilers

At higher pressure than in boilers with a natural circulation, the flow of medium is insufficient to ensure a failure-free evaporator operation.

An auxiliary pump to deal with this deficiency can be used, but a thick-wall element, i.e., the drum, remains and limits both the start-up speed and transformation of the power unit load into thermal stress inside the boiler. As a result, drumless boilers were created. The boilers are designed for subcritical and supercritical pressure. In the case of supercritical pressure, there is no evaporator (evaporation heat is 0). The group of drumless boilers covers once-through boilers without water separators, the Benson and Ramzin system, and boilers with water separators.

Once-through boilers operate based on a single flow of water through the boiler steam-water system. The circulation multiplication factor for this kind of boilers is  $k = 1$ . The most common constructions of once-through boilers include: Benson, Sulzer, and Ramzin (Fig. 4) [16].

The Benson boiler used to be the most common type of once-through boilers. Its typical features include a vertical arrangement of radiant evaporator pipes in the form of screens divided into sections through which the water flows in sequence, starting from the lower chamber to the upper chamber (Fig. 4a). Water is supplied from the upper chamber to the lower chamber of the next section with downpipes (7). From the last section of pipes, the steam enters a transient zone (5) in the area of lower flue gas temperatures, where complete evaporation and salt separation occurs.

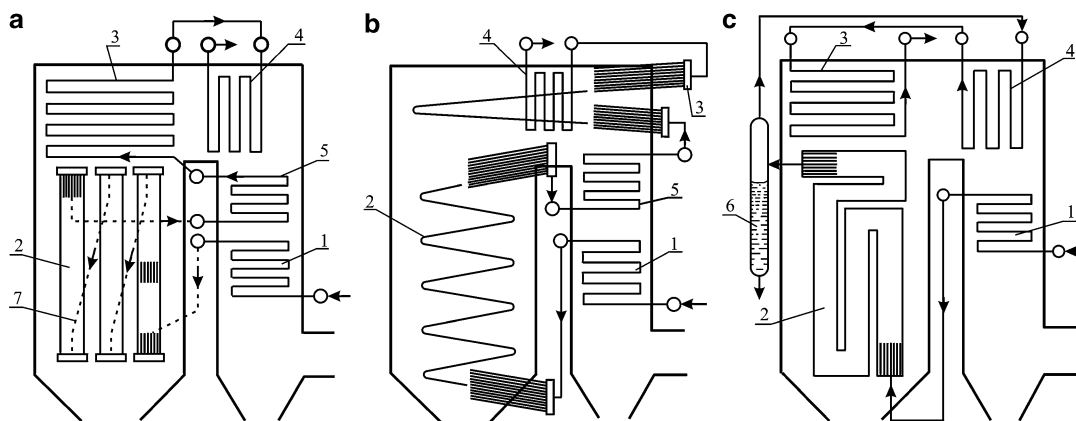
Ramzin boilers come with pipes that run at a slight angle to the horizontal plane, arranged in a helical manner along the combustion chamber circumference (Fig. 4b). The final evaporation stage takes place in the transient zone (5).

The flow in a Sulzer boiler is completed with no intermediate chambers, with a line of parallel pipes in a meandering arrangement. In this kind of boiler, there is no transient zone – there is only a water separator between the evaporator and the superheater (Fig. 4c).

### Fluid Bed Boilers

Fluidization occurs when gas flows through bulk material with an appropriate grain size





**Energetics, Fig. 4** Diagrams of once-through boilers: (a) Benson, (b) Sulzer, (c) Ramzin; 1 economizer, 2 evaporator screens, 3, 4 steam superheater, 5 transient zone, 6 water separator, 7 downpipes

distribution in the boiler furnace vertically upward, at a speed exceeding the critical fluidization speed above which the bulk material grains are lifted. The prerequisite for fluidization is for the resisting force of the particles flowing through the gas to compensate for the particle force of gravity reduced by the uplift pressure. Coal combustion in fluid bed power boiler furnaces occurs under conditions of intense mixing of bulk material in the stream of fluidizing gas (air). It ensures very good conditions for heat, mass, and momentum exchange, which contributes to equalizing the temperature along the furnace chamber height and maintaining at an optimum level for the process of dry flue gas desulfurization (840–860 °C). A lower combustion temperature limited by the ash softening point and air staging efficiently reduce NO<sub>x</sub> emission [17].

A fluid bed boiler, with regard to the speed of the flowing medium and pressure in the furnace chamber, can be divided into the following types:

- AFBC – atmospheric fluidized bed combustion boilers
- PFBC – pressurized fluidized bed combustion boilers
- CFBC – circulating fluidized bed combustion boilers
- PCFBC – pressurized circulating fluidized bed combustion boilers

High-capacity units are built in modern power plants, combined with observing environmental

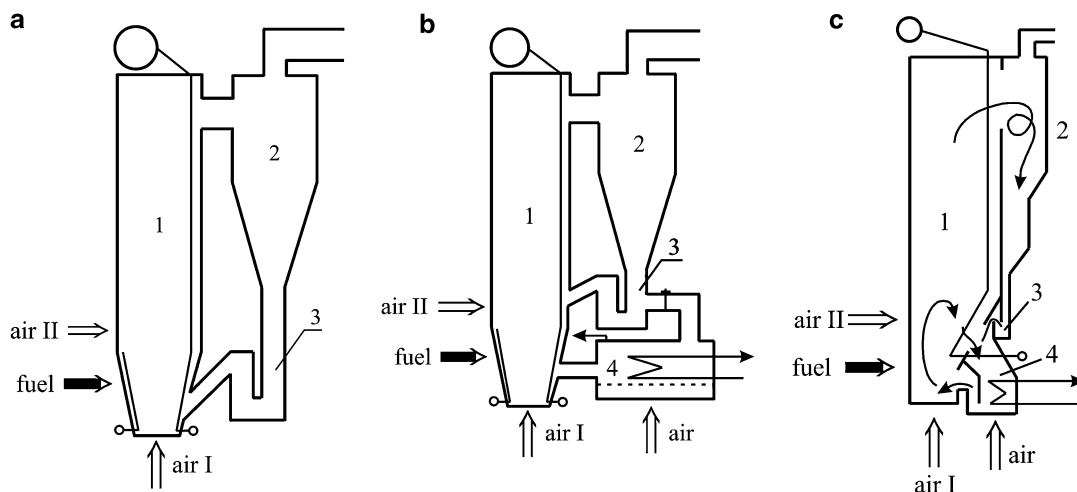
protection requirements including reducing fuel consumption, quality of the produced ash, and pollution emission. Using a fluid bed boiler helps reduce toxic components emitted from coal combustion. So far, CFB boilers have found the widest application in power engineering. For almost 30 years, the boilers have been successfully used in global power engineering. The fluid bed technology has become a challenge to conventional steam boilers as well as to powder boilers for supercritical steam parameters in electrical energy production. The fluid bed combustion technology is aiming at increasing the dimensions of a boiler unit, with a good example of the largest CFB boiler in the world in Łagisza Power Plant already put into service.

CFB boilers vary as to the circulation organization – it applies first of all to the separator construction and location, ash return system, and arrangement of heating surfaces. Figure 5 presents a diagram of CFB boilers.

In the simplest solution offered by Ahlstrom Pyropower (Fig. 5a), bulk material is removed from the separator (hot or cooled cyclone) with downpipes through the water trap to the furnace chamber. The heat exchange surfaces are integrated with the furnace chamber and convection pass.

In the Lurgi arrangement (Fig. 5b), a part of the bed material may flow through some additional surfaces of the external heat exchanger





**Energetics, Fig. 5** Diagrams of CFB boilers: (a) Ahlstrom Power, (b) Lurgi, (c) compact; 1 furnace chamber, 2 separator, 3 trap closure, 4 heat exchanger

(e.g., included in the superheating system), which reduces the quantity of heating surfaces in the boiler itself and facilitates load control.

A similar solution is applied in a compact boiler (Fig. 5c) with an internal separator, but the heat exchanger is directly integrated with the furnace chamber, which allows for more boiler control possibilities.

## Supercritical Steam Boilers

An increase in the price of fuel and regulations aimed at natural environment protection forced companies generating electrical energy and suppliers of technologies for power plants to improve the efficiency of using the chemical energy of fossil fuels. It is developed in a number of ways. One of them is constructing high-efficiency power units with the main component being a once-through steam boiler with supercritical or ultrasupercritical steam parameters [17–21]. The capacity of power units can be increased by using high parameters of the steam, high-capacity turbines, lower pressure in the condenser, and a double or triple interstage steam superheating. The previous solutions used a fresh steam temperature of 560–610 °C and 26–30 MPa pressure.

In 1954, the first once-through boiler was activated, with steam supercritical parameters, in the Benson technology ( $t = 605\text{ °C}$ ,  $p = 30\text{ MPa}$ ) [18]. At present, over two hundred units with supercritical steam parameters operate globally. The installed power in the largest one is 1,300 MW and fresh steam parameters:  $t = 600\text{ °C}$ ,  $p = 35\text{ MPa}$ .

Steam boilers with supercritical parameters are designed as Benson-type once-through boilers. They can be constructed as single-pass or double-pass (tower) boilers. The furnace chamber walls can be made with a vertical or spiral arrangement of the pipes. A spiral arrangement of the pipes on the furnace chamber walls makes each pipe pass through four walls, which significantly reduces the differences in the pipe lengths and the quantity of absorbed heat. This arrangement ensures adjusting the medium temperatures at the wall outlets even with great differences in the quantity of heat absorbed by each wall.

The first unit in the world with supercritical steam parameters, 460 MW, with a CFB boiler was installed in the Łagisza Power Plant in Poland [17]. The main parameters of the boiler are as follows: steam mass capacity 1,345 Mg/h, fresh steam pressure  $p = 27.5\text{ MPa}$ , fresh steam

temperature 560 °C, pressure of secondary superheated steam 5.48 MPa, and temperature of secondary superheated steam 580 °C.

## Solar Power Plants

Solar radiation is electromagnetic radiation with a wide wavelength range (0.2–2.5  $\mu\text{m}$ ). The intensity of the solar radiation reaching the external layer of the atmosphere is known as the solar constant and amounts to 1,367  $\text{W/m}^2$ . As a result of reflection, absorption by gaseous atmospheric components ( $\text{O}_3$ ,  $\text{H}_2\text{O}$ , and  $\text{CO}_2$ ), and scattering by particles of dust, ice crystals, and water drops in the atmosphere, the stream of energy directly reaching the Earth's surface is less than 1,000  $\text{W/m}^2$ . There are two types of radiation: directly reaching the Earth (unscattered) and scattered. The total power of solar radiation incident on a plane tangent to the Earth's surface is the sum of both components. The solar radiation intensity in any given area of the Earth depends on the Sun's altitude above the horizon (geographical width) and the season.

The solar energy resources are enormous but hard to manage. It is mainly due to the low intensity of solar radiation close to the Earth and its varied concentration, which requires constructing mirrors of large area (absorbers) following the apparent movement of the Sun.

Nowadays, two methods are used to generate electrical energy with solar radiation energy:

- Heliothermal (indirect)
- Helioelectrical (direct)

The heliothermal method, based on the photothermal conversion phenomenon, is by far the most popular method. Photothermal conversion consists of transforming the solar radiation energy into thermal energy. The conversion is possible due to using concentrating solar power (CSP) technologies. The technologies use mirrors to focus solar radiation energy and transform the energy into heat to generate turbine-powering steam. The turbine, in turn, powers the electrical energy generator.

There are two dominant concepts in the construction of heliothermal power plants: the

central receiver system (CRS) and distributed solar system (DSS).

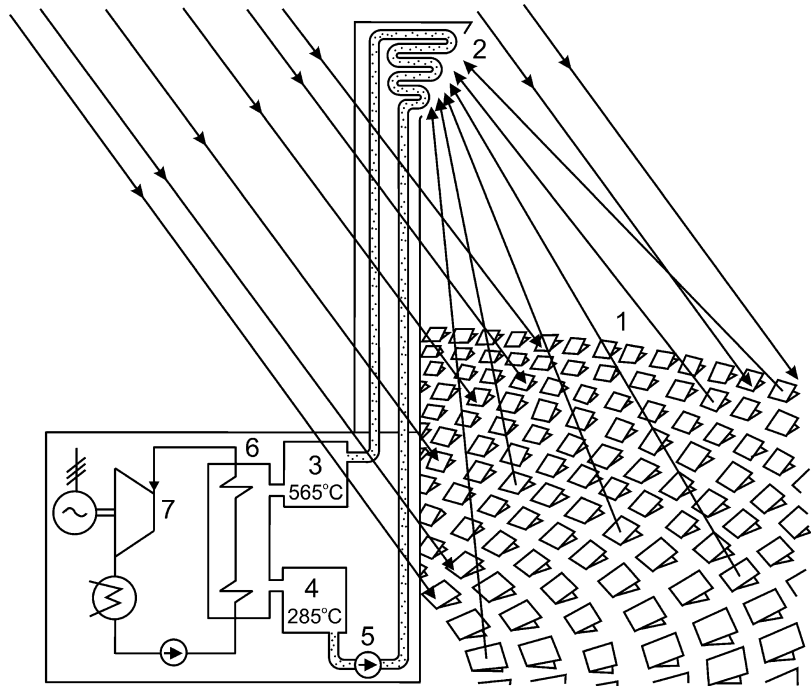
The central receiver system means reflecting solar rays from a large surface with flat mirrors, heliostats, and directing them toward a tower absorber located centrally on a 70–165-m-high tower. The heliostats come with relevant drives and are able to follow the apparent movement of the Sun due to computerized control systems.

In a water-cooled once-through absorber, the generated water steam drives the turbine. If liquid metal coolants (salt, alkaline metal salts), air, or helium are used, circulating in the primary circulation, they give away the heat in the steam generator forming the water-steam cycle of the power plant (Fig. 6). The cooling medium reaches a temperature of ca. 550 °C. Heat accumulated in the coolant (3) allows for the power plant operation with reduced power at night and on cloudy days. With regard to the high cost of construction and operation of solar power plants with tower absorbers, there are only a few power plants of this type operating globally, reaching the capacity of ca. 20 % [16]. For instance, the Heliostat Solar Power Plant in Seville (Spain) comes with a 165-m-tall tower and 1,255 mirror heliostats, of area 120  $\text{m}^2$  each. The power of this solar power plant is 20 MW.

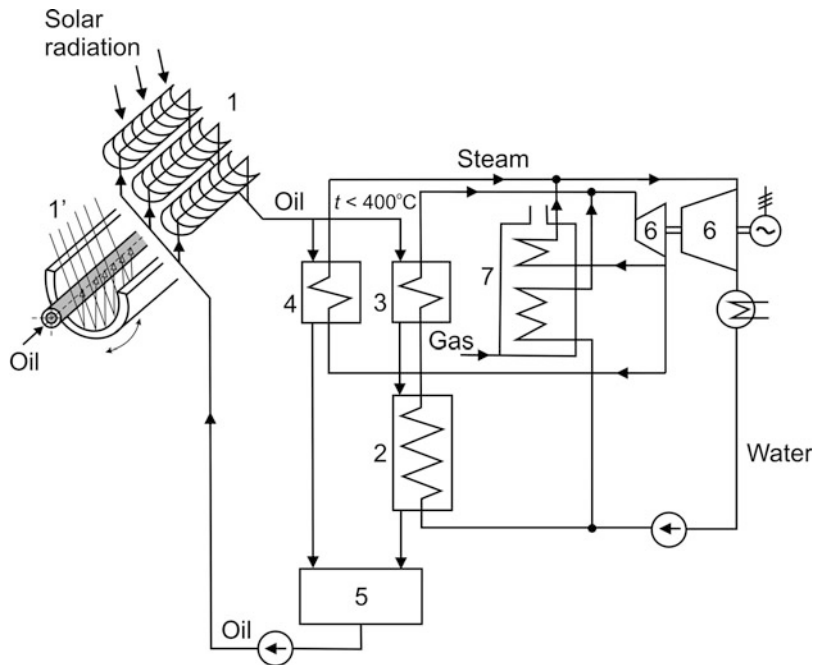
A decentralized system (DSS) most commonly uses parabolic trough solar concentrators (linear focal points) forming solar farms where solar radiation is converted into heat. Solar radiation is focused onto absorption pipes with the flowing working medium, located before parabolic concentrators (Fig. 7). Considering breaks in solar radiation, the presented system also uses additional burning (gas or liquid fuel). Synthetic oils, alkaline metal salts, or water can be the heat media in the primary cycles. If water is used, single-outlet systems with evaporation in the collector pipes can be constructed [22]. Absorption pipes are plated with one layer of black chromium and placed inside vacuum glass pipes to prevent heat loss. The medium flowing through a number of concentrators reaches a temperature up to 400 °C, lower than the temperature in the tower absorber. Oil gives away the heat in the steam generator (Fig. 7) forming the water-steam

**Energetics,**

**Fig. 6** Schematic diagram of a tower heliothermal power plant with a liquid metal coolant / heliostat field, 2 absorber, 3 and 4 cooling medium tanks, 5 circulation pump, 6 steam generator, 7 steam turbine

**Energetics,**

**Fig. 7** Schematic diagram of solar “farm” power plant / system of trough concentrators, 1' fragment of pipe concentrator, 2 evaporator, 3 and 4 primary and secondary steam superheater, 5 compensating tank, 6 steam turbine, 7 steam boiler



circulation, and the generated steam powers the turbine. For instance, the power plant in the Mojave Desert, South California (9 units with the total power of 354 MW), constructed between 1986 and

1991, consists of 400,000 concentrators with a total area of over 4 km<sup>2</sup>. The length of each linear concentrator is 6 m. The average efficiency of the power plant is 14 % and peak efficiency 22.5 % [16].

Considering the current solar technologies based on solar radiation concentration, used for electrical power generation, solar parabolic trough systems are the most advanced and most commonly applied systems. They allow for high power generation at low cost.

Since the aforementioned CRS and DSS systems operate based on the conventional Rankine steam cycle, they can be also designed to use fossil fuels (mainly gas) as auxiliary fuel. It will allow for electrical power generation when the Sun is not shining.

Another solution for a decentralized system is parabolic dish solar concentrators, also known as distributed-point-focus systems where the receiver is mounted above the center of each dish.

The dishes focus solar radiation on the receiver (engine/generator) using the Stirling thermodynamic cycle to generate electrical energy directly without steam formation. The receiver contains liquid that is heated to 1,000 °C. Parabolic dishes follow the Sun continuously and hence reach a high degree of solar radiation concentration and great efficiency, transforming over 30 % of solar radiation energy into electrical energy. A single parabolic dish – Stirling engine – can generate 3–25 kW of power. Installation of a number of such dishes allows for the power plant to generate a power of several dozen MW.

This technology, however, is not suitable for storing heat energy. Parabolic-shaped dish reflectors ensure electrical energy generation only when the Sun is shining.

The helioelectric method means direct transformation of solar radiation energy into electric energy with photovoltaic cells. Since the transformation occurs with no participation of heat, it is of relatively high efficiency – ca. 13–15 % [16]. Photovoltaic cells are mainly made of mono- or polycrystalline silicon. Cells with  $p$  and  $n$  layer made of the same material are called monocrystalline cells  $p$ – $n$ . Cells composed of a great number of crystals of the same material are called polycrystalline cells (with lower efficiency). A typical solar cell has an active area of ca. 100 cm<sup>2</sup> (10 × 10 cm). The bottom side of the element is fully metalized and makes one of the electrodes. The applied mesh (e.g., with

a vacuum method) forms the other electrode covering ca. 7 % of the photovoltaic cell and has antireflective layers (e.g., of titanium dioxide). At a solar radiation intensity of 1,000 W/m<sup>2</sup>, it provides voltage  $U_0 = 0.6$  V at an open circuit. A photovoltaic module usually consists of 18, 36 or more silicon elements connected in series and placed between two toughened glass plates, 3–5 mm thick.

For instance, the Solar Photovoltaic Power Plant in North America (Nevada) consists of 70,000 photovoltaic modules. The power of this solar power plant is 14.2 MW.

## References

1. Curley R (2008) Energy and movement in Britannica illustrated science library. In: Levy M (ed) Encyclopaedia Britannica. Encyclopaedia Britannica Inc., Chicago
2. Raja AK, Srivastva AP, Dwivedi M (2006) Power plant engineering. New Age International (P) Ltd, New Delhi
3. Quaschnig V (2005) Understanding renewable energy systems. Earthscan, London
4. BP statistical review of World energy. June 2011 <http://www.bp.com/sectionbodycopy.do?categoryId=7500&contentId=7068481>. Accessed 10 May 2012
5. Dorf RC (ed) (2000) Engineering handbook. CRC, Boca Raton
6. Çengel YA, Boles MA (2001) Thermodynamics: an engineering approach. McGraw Hill, New York
7. Stultz SC, Kitto JB (1992) Steam. Its generation and use. The Babcock & Wilcox Company, Barberton
8. Kreith F (ed) (2000) The CRC handbook of thermal engineering. CRC, Boca Raton
9. Drbal FL (1966) Power plant engineering. Springer, New York
10. Flynn D (2003) Thermal power plant simulation and control. The Institution of Electrical Engineers, Stevenage
11. Miller BC (2005) Coal energy systems. Elsevier, Burlington
12. Tanaka N (2007) Fossil fuel-fired power generation. Case studies of recently constructed coal- and gas-fired power plants. International Energy Agency, Paris
13. Leyzerovich AS (2008) Steam turbines for modern fossil-fuel power plants. The Fairmont Press, Lilburn
14. Kok KD (ed) (2009) Nuclear engineering handbook. CRC, Boca Raton
15. World Nuclear Association, <http://www.world-nuclear.org/how/npreactors.html>. Accessed 12 May 2012

16. Pawlik M, Strzelczyk F (2009) Power plants. WNT, Warsaw (in Polish)
17. Taler J (ed) (2011) Thermal and flow processes in large steam boilers. Modeling and monitoring. PWN, Warsaw (in Polish)
18. Franke J, Kral R (2001) Benson boiler. Best choice. Siemens Power Journal pp 1–4
19. Franke J, Cossmann R, Huschauer H (1993) Benson steam generator with vertically-tubed furnace. Large-scale test under operating conditions demonstrates safe design. VGB Kraftwerkstechnik 73(4):353–359
20. Franke J, Köhler W, Wittchow E (1995) Evaporator designs for Benson Boilers. State of the art and latest development trends. VGB Kraftwerkstechnik 73(4):307–315
21. Sobota T (2010) Supercritical steam pressure power boilers. In: Kosman G, Rusin A, Taler J, Pawlik M (eds) Issues of design and operation of power boilers and steam turbines for supercritical coal units (in Polish), Gliwice, Publishing House of Silesian University pp 16–28
22. Chmielniak T (2008) Energy technologies. WNT, Warsaw (in Polish)

## Energy

Janusz Badur and Michał Karcz  
Energy Conversion Department, Institute of  
Fluid Flow Machinery, Polish Academy of  
Sciences, Gdańsk, Poland

## Overview

Energy is an abstract notion that helps to understanding the nature and contributes to the creation of the civilization. The energy notion has a huge meaning not only due to practical reason – it is essential for economy and philosophy too. Therefore, the description of the development of the physical concept of energy must be preceded by the metaphysical foundations given by Aristotle. Evolution of the kinetic energy of the rigid body motion concept starting from the *vis viva* notion is presented. Further, the main problems connected with the internal energy concept in the form of “energy storage” and the transformations of different forms of energy are discussed. Balance of energy is finally presented as a sum of internal, kinetic, potential, and radiation energies

in the system that are compensated by the total energy flux, which consists of working, heating, chemical, electric, magnetic, and radiation energy fluxes at the system boundaries. The law of energy conservation can be considered as the most important one which is superior over any other laws of nature.

## Metaphysical Foundations of Energy Concept

In philosophy, and especially in its fundamental part, that is, metaphysics, there is no place for the concepts and methods of reasoning developed by physics and chemistry. Philosophy assumes that most of the physical and chemical concepts are not known in nature *in spe* – these are employed by science only as a kind of “mental keys” for the description and understanding of the universe. Only the concept of “energy” is accepted by the philosophers in its metaphysical sense. They consider energy as a fundamental feature of the nature which serves as a basis for other – the already known and yet not known features of the nature. Without energy in the metaphysics, there is no creation of matter, no creation of weightless fields, and no any formation and decay of all of the driving potentials of nature. In the metaphysics by Aristotle, the energy has only two forms of realization. One of them is a basic, perfect, and inaccessible potential of nature that may create a form of active and visible world during the act of creation. The second form of energy of motion is permanently involved in a process of creation and annihilation of beings. It “pours” from the unavailable source to the real world and vice versa – our reality “dies,” thus becoming a perfect potential of nature again. The basic method of the physical world creation from the perfect potential is realized by an “energy action” (as mathematically defined by Maupertuis in 1744), which takes place on a quantized way, thus creating quantized real beings.

As far as the metaphysical knowledge can be assimilated by an illumination only, this part of philosophy is no longer being developed [1].

However, in an implicit manner, by the creation of the paradigms of thinking, metaphysics is still present in the process of human cognition. For example, the thesis of quantized energy action has its hidden implications in the modern *quantum mechanics*, and the thesis of the existence of “eternal light” is the prototype of the “dark energy” concept in cosmology. Metaphysical energy division into potential and active parts is an analogue of the potential energy (gravitational field) and the kinetic energy of body motion.

In summary, the metaphysics of Aristotle and his successors brought the fundamental paradigms of thought to the energy science. One is an inherent relationship between the energy and the so-called peripatetic motion, because the active energy is an integral measure of the amount of motion. The opposite to this peripatetic motion is immobility of the nature’s source which can be measured only by the perfect potential. The paradigm of the peripatetic motion is still present in our reasoning concerning the principles of the energy conversion and the transformation of its forms. Peripatetic motion is a sort of quantum motion that constitutes every other motion, thus being the basis of all chemical processes, nuclear physics, mechanics, and thermodynamics. It means that the energy as an integral measure of peripatetic motion is identical in its elementary quality; therefore, energies of mechanical, heat, electrical, and magnetic motions can be added without the necessity of using of any energy conversion factors (equivalents). In other words, in Aristotle’s metaphysics, all known energy equivalents as heat-mechanical (Rumford, Carnot, Joule), electro-chemical (Faraday), electro-mechanical (Thomson), mechanical-heat (Clausius) are equal one. This concept of homogeneous energy was adopted from the Greek philosophy by Rankine, who assumed a quantized energy transfer by the “vortex atom” [2].

## Disputes over *vis viva*

In the Middle Ages, the metaphysics and natural philosophy of Aristotle were discarded and the concept of peripatetic motion was limited only to

the mechanical motion (Jean Buridan, c.1292-c.1360). The laws governing the mechanical motion were not known. There was a need to define a “topological charge” which ensures the continuation of arrows motion during a flight and which would define the amount of available motion. There were two candidates:  $mv$  that is, the product of mass and velocity (momentum) and other product  $mv^2$  called by philosophers *vis viva* (Leibniz 1667). But even after Newton’s discovery (1677), who found that the real cause of the mechanical motion is *vis impressa* (in a geometric version) and that the momentum of the universe is constant, there were disputes over the primary force that governs the mechanical motion, that is, *vis viva* or *vis impressa*. Such disputes were continued also after the works of Wallis (1699) and Euler (1729) who gave the analytical form of Newton’s law  $m\vec{a} = \vec{f}$ . The historical studies by Duhem, and then also by Truesdell (1980), showed, however, that when the peripatetic motion other than mechanical motion was considered, then natural philosophers used the more general notion of *vis viva*. This dichotomy of thinking had continued through the eighteenth century. For example, Johann Bernoulli (1741), when defining the law of motion of the liquid in the pipes, employed the momentum balance (balance *vis impressa*), and apparently, Daniel Bernoulli (1739) used as a law of motion an integral form of balance of *vis viva*.

## Internal Energy

It can be noticed that all of these proposals and hypotheses refer to the perfect phenomena of nature, which are not yet affected by human activity. Industrial Revolution of eighteenth century, however, resulted in application of a tremendous amount of machineries and heat engines. There was a reasonable demand for the governing laws of practical meaning – it was especially important from the economical point of view. The machines operate periodically; thus, the mechanical motion in the single cycle is a self-compensating quantity. Therefore, in the process of analyzing the operating principles,



the main role played the technical concepts such as *heating* and *working*, which allowed to define usefulness of the heat engine in every single cycle. The working and heating processes, if continue for some time, may be defined by an abstract, integral in time quantities, that is, *work* and *heat*. By the fact that it was possible to measure the effects of both processes, which were accumulated in the form of work or heat “storages” located in the working medium, a new complex and abstract concept could be introduced – the concept of energy storage or energy stored in the working medium. Initially, the work storage (work supply) and heat storage (heat supply) were treated independently. Depending on whether the law of conservation of energy was formulated in units of work (Clausius 1850) or in units of heat (Thomson 1854), the substantial work or heat storages could be specified. Only Rankine (1850), writing the law of conservation of energy in an analytical manner postulated by Mayer and Joule’s, concluded that there is only one universal energy storage – the *internal energy*, which possesses a single substantial carrier that is common to all forms of energy transfer. Rankine also stated that all energy equivalents are thus redundant. This was, in relation to the statements of Clausius and Thomson, an extremely radical step which broke the fundamental paradigms on separateness of energy forms.

In terms of Clausius, the substance subjected to the process of working can accumulate and store work without any losses and then, after moving the substance (working body) in another place, can release it at any time – but only in the same mechanical form. Then, under an irreversible operation, the working process can be transformed into the heating process in an amount determined by the mechanical equivalent of heat  $A_{\text{Clausius}}$ . It should be underlined that the concept of accumulation of work in the medium in the form of “work supply” had some origins in consideration on simple machines, where mechanical energy is transformed in the same type of energy. This led to the law of energy balance that was limited only to the mechanical phenomena (Lazar Carnot, 1803 – integral in time and

space). Quite early appeared the mechanical case of internal energy per unit mass of the substance. It was Green’s internal energy (1839) for three-dimensional elastic deformation of a solid body and Petit’s internal energy (1818) for a three-dimensional rapid compression of gas. Whittaker (1910) noted, however, that Green’s internal energy not exactly refers to solid [3]. It was Kirchhoff (1850) who used it first to derive the simplified equations of motion of a thin plate.

In terms of Thomson, the internal energy was expressed in units of heat and was defined by him as a “heat supply” that is ready to be transferred outside without any losses. Thomson’s version of the internal energy conversion principle assumes that the working medium possesses the ability of accumulation of the heating process effects only as a heat. The body which is warmed in one place can transfer the energy outside in another place and time, but only during the heating process. Under irreversible processes, the heating may evolve into working, which can be calculated using the thermal equivalent of work  $J_{\text{Joule}}$ . Both Clausius and Thomson emphasized the ideality of internal energy storage, which means that nothing is lost from the “work supply” (Clausius) or “heat supply” (Thomson). The medium at first adopts and later releases the same amount of stored work or heat.

The modern definition of internal energy was finally given by Rankine (1850). His revealing hypothesis on the internal energy conversion assumes that the matter of the working medium does not store either heat or work. The working medium during heating process does not increase its heat supply but increases its internal energy, and similarly, the working medium during working process does not increase its work supply but also increases its internal energy. Thus, the conversion of energy of mechanical motion into the thermal motion possesses an intermediate step in the form of the internal energy changes. This transformation occurs during charging or emptying of internal “storage.” In other words, the thermal energy transferred to the medium in the heating process leads to the increase of the medium’s internal energy, and the internal

energy can “leave” the medium, for example, converting itself into work (working process).

Such internal transformation is possible due to the motion of atoms, electrons, molecules, etc. In the working medium, there is only one universal type of reversible energy storage. Rankine’s model of internal energy conversion that bases on the anticipated concept of “vortex atom” does not differ much from the contemporary models of the atom, the nucleus, and electrons. The external energy fluxes related to heating and working processes inside the Rankine vortex atom transform into a hidden Aristotelian active energy or hidden generalized *vis viva*:  $m\vec{v} \cdot \vec{v} + \vec{\omega} \cdot \vec{I}\vec{\omega}$ , which consists of translational and rotational *vis viva*. The conversion of energy, which is received by an external observer as a replacement of heating by working process, also takes place inside the Rankine vortex atom in a reversible manner as a change of  $\vec{\omega} \cdot \vec{I}\vec{\omega}$  into  $m\vec{v} \cdot \vec{v}$ . In the frame of Rankine vortex atom (1851), temperature and entropy (called by Rankine *a thermodynamic function*) have a clear geometric presentation. They are introduced as parameters of state, that is, the parameters associated with reversible energy storage. It is fundamentally different concept than one presented by Clausius (1865), who needed 14 years to come with the concept of entropy embedded in the chaotic motion of millions of moving gas molecules.

Rankine’s internal energy concept was creatively extended by Gibbs (1876), who was probably one researcher, except Truesdell, able to properly interpret the work of Rankine. Gibbs perceived that Rankine’s model of vortex atom is so comprehensive that it can also describe the chemical, magnetic, and electric energy storages. Therefore, instead of many different storages, Gibbs introduced a universal internal energy, which is responsible for the implicit transformation of energy. Rankine’s internal energy paradigm, supplemented further by Gibbs, is still in use in the thermodynamics of continuum, and perhaps also in the whole physics and chemistry. Idea of internal energy describes the mechanism of reversible accumulation of energy, which is transferred to the mass unit of the medium during different processes such like mechanical

working, heating, electrical, magnetic and chemical working, etc. Internal energy is a primary quantity which cannot be measured directly.

## Kinetic Energy

Rankine’s concept of internal energy can be treated to some extent as an analytical representation of Aristotle’s division of entelechy of motion into the potential and active parts. It is also mentioned by Rankine (1855) during development of the “kinetic energy” concept:  $\frac{1}{2}m\vec{v} \cdot \vec{v}$ . He treated all perceptible physical world of matter as a manifestation of an active motion. This motion can be divided into balanced internal motion, measured quantitatively by the internal energy, and an external energy of motion, which is only a qualitative component of *vis viva*, called the “kinetic energy.” Because both the internal and kinetic energies are of the same nature, these can be calculated using the same units without employing Joule’s equivalent of energy. Rankine was in some opposition to Joule, whose goal was to find the equivalent as a ratio of internal energy to the kinetic energy ( $J_{\text{Joule}} = \mathcal{U}/K$ ). Joule’s approach was also innovative, but only in relation to the concept of Sadi Carnot who was preferring the equivalent of work in the form  $J_{\text{Carnot}} = \mathcal{W}_{\text{cycle}}/Q_{\text{cycle}}$ .

## Thermodynamical Parameters of State

Together with the concept of the internal energy, a new notion has been introduced by Rankine – the thermodynamical parameters of state, which allow to estimate the change of internal energy. Two kinds of parameters were attributed to the every form on energy – primary one, which is intensive mass dependent and a secondary one, which is dual, extensive mass independent. The first parameter was named a *metaphoric* function, and the second was called a *metamorphic* function (Rankine 1855). The first examples of the parameters of state for gas were the specific volume and the specific entropy (intensive parameters) and complementary to



them, thermodynamic pressure and temperature (extensive parameters). More parameters appear when the solid body is considered, namely, tensor of deformation density and tensor of specific entropy and complementary to them, tensor of stresses (pressure) and tensor of temperature.

The parameters of state in the Rankine proposal were a practical way for calculating the amount and the change of the internal energy. The primary intensive parameters of state do not reflect individualism of the internal motion; they are anthropocentric, convenient for measurements averages over the internal motion. Unfortunately, the internal energy conversion so clearly imagined by “vortex atom,” when analyzed in terms of parameters of the state, is no longer a simple representation. It is hard to imagine graphically an exemplary conversion as for the case when the internal energy remains constant, but the specific volume decreases at the expense of the specific entropy increase. The internal energy concept expressed by primary parameters of state was finally formulated by Gibbs (1873), who defined the relationship between primary and dual parameters of state:

$$\text{dual parameter of state} = \frac{\partial(\text{specific internal energy})}{\partial(\text{primary parameter of state})} \quad (1)$$

This equation is one of the most fortunate in the thermodynamics foundations. It allows to relate the set of equations describing the arbitrary process with the law of energy conservation. The equations which describe the physical processes, such as heat conduction in the solid body, may be erroneously formulated in the sense that they can lead to the violation of the law of energy conservation. Therefore, in order to transform the governing equations, such as Schrödinger equation, into the energetic relationship, it is necessary to know Gibb’s constitutive relation (1) and the well-defined partial energy fluxes for working and heating processes of all kind.

Gibbs realized that for the internal energy changes occurring due to changes of the primary parameters of state, it is important to determine

the total internal changes expressed by changes of both primary and dual parameters of state:

$$\begin{aligned} d(\text{specific internal energy}) \\ = \sum \left( \begin{array}{c} \text{dual} \\ \text{parameter of state} \end{array} \right) d \\ \times \left( \begin{array}{c} \text{primary} \\ \text{parameter of state} \end{array} \right) \end{aligned} \quad (2)$$

which have exemplary form

$$\text{for fluids:} \quad d\epsilon = pdv + \theta d\eta + \mu dc + \dots \quad (3)$$

$$\begin{aligned} \text{for solids:} \\ d\epsilon = p_{ij}dv_{ij} + \theta_{ij}d\eta_{ij} + \mu_{ij}dc_{ij} + \dots \end{aligned} \quad (4)$$

Here, increment  $d$  means the substantial differentiation in time ( $d/dt$ ). For the solid bodies, which accumulate not only volumetric but also shape changes, exist tensors of specific deformations, specific entropy, specific concentration, etc.

## Potential Energy

The concept of the energetic potential  $\Phi$  was introduced by Laplace in 1797 for the description of the gravitational force (*vis viva mollata* later *vis latente*) acting between two massive bodies (action at distance). Laplace assumed that each of the massive bodies coming from the nature’s source of potential possess the spatial memory of this source, which is described by involved energy of the source  $\Phi$ . In other words, Laplace’s concept described the action of the anticipated gravitational field by the potential, later called the potential energy. This concept had a huge advantage over Newton’s gravity model – in this concept, there is no need for adjustments in the form of additional postulate of the existence of “eternal light.” Recall that Newton’s model had a serious drawback. His concept did not describe the permanence of the firmament (*stellae fixae*), and to explain why the stars do not fall one another, Newton postulated additional unknown, that is, the pressure of

light – “eternal light,” which repelled the stars from each other. Today, the role of the eternal light in cosmology meets the “dark energy” notion, also postulated *ex nihilo* [7]. Under earthly conditions, the Laplace potential is described accurately enough by the distance of the body from the Earth’s surface enlarged by Earth’s radius (position vector). Now extending the Gibbs-Rankine’s concept of state parameters also for the potential energy  $\Phi$ , it can be concluded that the position vector  $\vec{x}$  plays a role of the primary state parameter and the gravitational acceleration  $\vec{b}$  is a dual state parameter:  $\vec{b} = -\partial\Phi/\partial\vec{x}$ .

## Energy of Radiation

There exists also an additional internal energy – energy of radiation – which is not associated with the substance of the working medium and which is localized in space. In 1865, Maxwell proposed that this non-substantial energy of electromagnetic field  $\varepsilon_{em}$  can be expressed by the primary state parameters as electric field  $\vec{E}$  and magnetic field  $\vec{H}$ . Maxwell identified also the dual state parameters of radiation energy, that is, the electric displacement vector  $\vec{D} = \partial e_{em}/\partial\vec{E}$  and the magnetic displacement vector  $\vec{B} = \partial e_{em}/\partial\vec{H}$ . This concept allows later to formulate the energetically consistent theory of radiative heat transfer by Planck (1905).

## Mathematical Denotation of the Fundamental Concepts

It is necessary to assign the mathematical objects to the verbal concepts of energy. Since in literature exist dozens of different signs for the same quantities, it is reasonable to employ the system of denotations as proposed in the papers of pioneers, mostly Rankine, Gibbs, Duhem, and Natanson (Kestin 1980). The method of description bases here on the foundations of rational thermodynamics given by Truesdell [4] and Kestin [5, 6].

Let us mark the finite volume by the sign  $d\mathcal{V}$ , and the volume of thermodynamic system  $\mathcal{B}$  by letter  $\mathcal{V}$ . The system  $\mathcal{B}$  interacts with the external environment by the processes acting at the system boundary  $\partial\mathcal{V}$ . The internal, kinetic, and potential energy can be denoted by  $\mathcal{U}, \mathcal{K}, \Phi$  respectively, and the energy of radiation by  $\varepsilon_{em}$ . All these quantities are expressed in the energy unit – joule ( $1 \text{ J} = 0.62415 \cdot 10^{19} \text{ eV}$ ). These integrals for the system amounts of the energy reflect in a good manner the anthropocentric character of our knowledge, and they are commonly employed in the science and technique. Beside the integral quantities, there are some quantities related to the unit of mass, as:

Internal energy

$$\mathcal{U} = \iiint_{\mathcal{V}} \rho \varepsilon d\mathcal{V} = \iiint_{V_0} \rho_0 \varepsilon d\mathcal{V} \quad (5)$$

Kinetic energy

$$\mathcal{K} = \iiint_{\mathcal{V}} \frac{1}{2} \rho \vec{v} \cdot \vec{v} d\mathcal{V} = \iiint_{V_0} \frac{1}{2} \rho_0 \vec{v} \cdot \vec{v} d\mathcal{V} \quad (6)$$

Potential energy

$$\Phi = \iiint_{\mathcal{V}} \rho \Phi d\mathcal{V} = \iiint_{V_0} \rho_0 \Phi d\mathcal{V} \quad (7)$$

Two volumes of system can be distinguished – the referential volume  $\mathcal{V}_0$  non-deformed, used in Lagrange’s description, and the actual volume  $\mathcal{V}$  related to Euler’s description.

Let us denote by  $\rho_0$  and  $\rho$  the mass density in its initial state and actual state, respectively. Following Gibbs, the specific internal energy (J/kg) related to the unit mass can be denoted by  $\varepsilon$ . The quantities  $\rho\varepsilon$  and  $\rho_0\varepsilon$  are volumetric energy densities related to actual and initial volumes, respectively. Fourth kind of energy that undergoes balancing is an energy of radiation:

$$\mathcal{E}_{em} = \iiint_{\infty} e_{em} d\mathcal{V} \quad (8)$$

where  $e_{em}$  (J/m<sup>3</sup>) is a volumetric density of energy of electromagnetic field postulated by

Maxwell (1874). It means that the field quantity cannot be related to the mass of substance, only to the volume where the radiation is acting. Let us, according to Rankine, assume that the energy fluxes are additive. It allows to formulate the total energy flux as the sum of particular processes:

$$\mathcal{F}_{energy} = \mathcal{F}_{working} + \mathcal{F}_{heating} + \mathcal{F}_{chem} + \mathcal{F}_{elec} + \mathcal{F}_{mag} + \dots \quad (9)$$

where respectively appear working, heating, chemical, electric, and magnetic energy fluxes. This mathematical set can be treated as universal one – there is a place for new, yet unknown processes. There is a lack of radiative flux, described by Poynting's vector (1899), because it is directly related to the system substantial boundary. The substantial boundary  $\partial V$  is oriented outside by the normal unit vector  $\vec{n}$  that allows to write the energy flux as a normal component of the total energy vector:

$$\mathcal{F}_{energy} = \iint_{\partial V} (\vec{\mathcal{F}}_{work} + \vec{\mathcal{F}}_{heat} + \vec{\mathcal{F}}_{chem} + \vec{\mathcal{F}}_{elec} + \vec{\mathcal{F}}_{mag} + \dots) \cdot \vec{n} dA \quad (10)$$

Two first energy fluxes are very well known in literature:  $\vec{\mathcal{F}}_{work}$  is a mechanical energy flux of Umov (1874) and Volterra (1899) and  $\vec{\mathcal{F}}_{heat}$  is a heat energy flux of Rankine (1850) and Stokes (1851).

The essence of the proper definition for the various fluxes is to find the proper relationship for the energy flux with the fluxes of momentum, angular momentum, mass, entropy, electricity, etc. If the internal energy  $\varepsilon$  is expressed by the primary parameters of the state and there are no spatial and time gradients of the parameters of state, then fluxes of the mechanical energy and heat can be expressed by a relatively simple combination of the momentum flux tensor  $\vec{t}$  and entropy flux vector  $\vec{h}$  [4–6]:

$$\vec{\mathcal{F}}_{work} = \vec{t}\vec{v} \quad \vec{\mathcal{F}}_{heat} = \theta\vec{h} \quad (11)$$

where  $\vec{v}$  is the velocity vector of the substance and  $\theta$  is the absolute temperature. In the case of the field energy, there exists the pointing radiation energy flux defined as  $\vec{\mathcal{F}}_{em} = \vec{E} \times \vec{H}$ .

The universal law of energy conservation can be now anticipated. This universal law states that the change of the system of the energy storage occurs at the expense of processes (fluxes) or mathematically:

$$\begin{aligned} & \frac{d}{dt}(\mathcal{U} + \mathcal{K} + \Phi + \mathcal{E}_{em}) \\ &= \iint_{\partial V} \vec{\mathcal{F}}_{energy} \cdot \vec{n} dA + \iint_{\infty} \vec{\mathcal{F}}_{em} \cdot \vec{n} dA + \mathcal{S}_e \end{aligned} \quad (12)$$

Here, the energy source  $\mathcal{S}_e$  is a measure of non-conservation of the energy. For the phenomenon occurring between time  $t_{in}$  and  $t_{out}$  (time scale associated with human activity), this energy balance equation can be integrated.

Due to the reversibility of the total energy storage, the integral on LHS of (12) depends only on the initial and final state of the storage. As far as the occurring processes are summed exactly, (12) finally transforms into

$$\begin{aligned} & (\mathcal{U} + \mathcal{K} + \Phi + \mathcal{E}_{em})|_{t_{out}} \\ & - (\mathcal{U} + \mathcal{K} + \Phi + \mathcal{E}_{em})|_{t_{in}} \\ &= \int_{t_{in}}^{t_{out}} (\mathcal{F}_{energy} + \mathcal{F}_{em}) d\tau \end{aligned} \quad (13)$$

It is a formulation known as an integral in time and space form of the primary energy conservation law (12).

Special integral form can be obtained for the phenomenon occurring periodically. In this case, the summary energy changes in a single cycle are equal zero, and the balance can be simplified to the closed integrals of fluxes, which compensate each other. If considered phenomenon consists of heating and working only, then their line integrals are called the cycle heat and cycle work, and (13) can be written as

$$\mathcal{F}_{work}^{cycle} + \mathcal{F}_{heat}^{cycle} = 0 \quad (14)$$

which can be read as follows. After single, complete cycle of transformations, the internal, kinetic, and potential energies stored in the working medium take on their initial value, and the cycle work is equal the cycle heat:

$$\begin{aligned}
 \mathcal{F}_{work}^{cycle} &= \oint \left( \iint_{\partial V} \vec{\mathcal{F}}_{work} \cdot \vec{n} dA \right) d\tau \\
 &= \oint \left( \iint_{\partial V} \vec{T} \cdot \vec{n} dA \right) d\tau \\
 \mathcal{F}_{heat}^{cycle} &= \oint \left( \iint_{\partial V} \vec{\mathcal{F}}_{heat} \cdot \vec{n} dA \right) d\tau \\
 &= \oint \left( \iint_{\partial V} \theta \vec{h} \cdot \vec{n} dA \right) d\tau
 \end{aligned} \tag{15}$$

Here, in (13) and (14), it has been assumed that  $\mathcal{S}_e = 0$  but strictly speaking, only the law of energy conservation, known as the first law of thermodynamics, should decide about the existence of the internal energy source  $\mathcal{S}_e$ .

## The Law of Energy Conservation

One of the most fascinating steps of civilization is related to the energy conservation law – its anticipation, development, and the rational explanation. Until today, there is no any empirical evidence of the conservation of energy; nevertheless, in the opinion of researchers, it is the most unquestionable and inviolable law of nature. Its philosophical origins come from Greek's metaphysics who assumed that even more general law of the conservation of peripatetic motion is valid in the nature. This law can be split then into many special laws of conservation, which cannot necessarily be a scalar one, as in the case of energy. Leonardo da Vinci (1499) disagreed with this concept. He compared the nature and the man himself to the great machine, and hence, da Vinci proposed to split the law of the conservation of peripatetic motion into two special laws: (a) there is no possibility of existence of the eternal engine in the nature (*perpetuum mobile* of the first kind) and (b) there is no possibility of

any mechanical perpetual motion in the nature (*perpetuum mobile* of the second kind). This concept had enormous impact on the scientific investigations in the nineteenth century. It became the prototype for the *first and second laws of thermodynamics*. Kuhn noticed that there were at least 12 researchers who contributed to the final formulation of the law of energy conservation and its mathematical representation [7]. In fact, more than 12 researchers should be considered [8]. For example, already Sadi Carnot in 1824 postulated the law (14) in the form  $2.7 \mathcal{F}_{work}^{cycle} + \mathcal{F}_{heat}^{cycle} = 0$  which did not require a prior knowledge of the concept of “internal energy.” On the other hand, Mayer (1842) and Joule (1847) formulated the law of indestructibility of energy and assumed that the system is not affected by any processes, that is,  $\mathcal{F}_{energy} = 0$  and the law of conservation of energy has a simple form that consists of three parts:

$$\mathcal{U} + \mathcal{K} + \Phi = const \tag{16}$$

In the case of a large system, such like the universe, this balance leads to  $E_{Universe} = \mathcal{U} + \mathcal{K} + \Phi = const = nE_{Sun}$ . It was formulated by Mayer (1851) in the form of, energy of the universe is constant and approximately equals the numbers of stars in the firmament, multiplied by the energy of the sun.

The universal conversion law for all energy fluxes was verbally formulated by Grove (1841) and mathematically written by Helmholtz (1847). The principle of energy conversion stated that the substance has the ability to receive the energy by one process, is able to store it without any losses, and is able to release energy by another process. The final theory of energy conversion was developed by Rankine (1855), and now, it is an inviolable foundation of the mathematical description of all the natural phenomena.

Today, there is an agreement that the key hypothesis of energy conservation given by Mayer and Joule's saying that energy is indestructible can be used even in the smallest subatomic scale. In practice, the source of energy in total energy balance (12) must always be equal to zero, regardless the volume of the considered system:

$$\mathcal{S}_e = \iiint_V \rho s_e dV = 0 \quad (17)$$

It means that in the nature, there are no any processes which can create a new amount of energy. Researchers are convinced that the energy is indestructible despite of the fact that energy is only a scalar, coarse, and abstract invariant of processes occurring in nature.

## Cross-References

► [Energy and First Law of Thermodynamics](#)

## References

1. Heller M (2005) *Filozofia Przyrody – Zarys Historyczny*. Wydawnictwo Znak, Kraków
2. Rankine WJ (1880) *Miscellaneous scientific papers*. Charles Griffin, London
3. Whittaker E (1910) *A history of the theories of Aether and electricity*. Longman, Green and Co, London
4. Truesdell CA (1980) *The tragicomical history of thermodynamics*. Springer, New York
5. Kestin J (1966) *A course of thermodynamics*, vol I. Blaisdell Toronto, Waltham
6. Kestin J (1968) *A course of thermodynamics*, vol II. Blaisdell Toronto, Waltham
7. Kuhn T (1959) Energy consideration as an example of simultaneous discovery. In: Clagett M (ed) *Critical problems in the history of science*. University of Wisconsin Press, Madison, pp 321–356
8. Badur J (2009) *Rozwój pojęcia energii*. IFFM Publishers, Gdańsk

## Energy and First Law of Thermodynamics

Bernhard J. Peters

Faculté des Sciences, de la Technologie et de la Communication, Université du Luxembourg,  
Luxembourg, Luxembourg

## Synonyms

[Conservation of energy](#); [Energy](#); [First law of thermodynamics](#); [Thermodynamic system](#)

## Overview

Energy belongs to the fundamental concepts of thermodynamics and plays an important role in numerous engineering applications. The classical concept of thermodynamics distinguishes between work and heat as different appearances of energy. It may be stored within or transferred between systems. Work and heat may also be converted interchangeably, however, with some restrictions applicable. Therefore, the concept of energy, e.g., work and heat, is extended by the first law of thermodynamics that is commonly referred to as conservation of energy. Consequently, energy cannot be created or destroyed. Thus, the first law of thermodynamics describes the interaction of a thermodynamic system with its surroundings in terms of transfer of heat and work and relates it to the inner thermodynamic state of the system itself.

## Energy

Energy is one of the fundamental concepts of thermodynamics and dealt with in a large number of engineering applications [1]. Some basic ideas about energy include that energy may be stored within systems, is transformable from one form to another, or may be transferred between systems.

## Work

Work  $W$  is commonly referred to as the result of a force  $\vec{F}$  moving along a certain path between  $s_1$  and  $s_2$ :

$$W = \int_{s_1}^{s_2} \vec{F} \cdot d\vec{s} \quad (1)$$

where the integral is defined as the scalar product of the force vector  $\vec{F}$  and the displacement vector  $d\vec{s}$  and thus, yields work as a scalar quantity [2]. Consequently, a definition of positive and negative work may be as follows:

Work is positive if it is added to a system.

In order to evaluate the integral of (1), the variation of the force with displacement has to

be taken into account. Thus, the work depends on the path it takes during a process and is not only dependent on the initial and final states of the system. Therefore, work is **not** a property. Many thermodynamic applications are concerned with the time rate of work called power  $P = dW/dt = \dot{W}$ :

$$P = \frac{d}{dt} \int_{s_1}^{s_2} \vec{F} \cdot d\vec{s} = \int_{v_1}^{v_2} \vec{F} \cdot d\vec{v} \quad (2)$$

where the velocity as  $d\vec{v} = \frac{d\vec{s}}{dt}$  has been introduced.

Similar to (1), work of a spring during compression or expansion is defined. If the characteristic of a spring is of the following linear form  $\vec{F} = c \vec{s}$ , the integral as the work of a spring  $W_{spring}$  may be readily evaluated as

$$W_{spring} = \int_{s_1}^{s_2} c \vec{s} \cdot d\vec{s} = \frac{1}{2} c (s_2^2 - s_1^2) \quad (3)$$

Electrical work writes as follows:

$$W_{electrical} = \int_{t_1}^{t_2} UI dt \quad (4)$$

where  $U$  and  $I$  stand for tension and current, respectively.

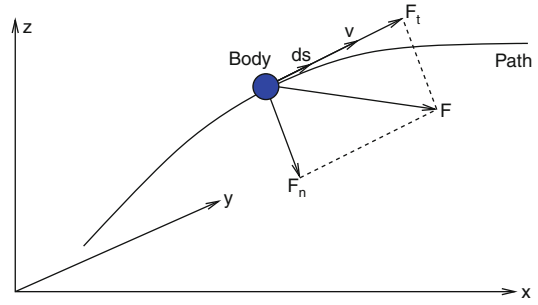
### Work and Kinetic Energy

A body moving along a path as sketched in Fig. 1 is acted on by a resultant force  $\vec{F}$ , which may vary in time and space. It is decomposed into a component  $\vec{F}_n$  normal to the path and a component  $\vec{F}_t$  along the path. The latter influences the velocity of the body according to Newton's second law as follows:

$$\vec{F}_t = m \frac{d\vec{v}}{dt} \quad (5)$$

where  $m$  and  $\vec{v}$  denote the mass of the body and velocity, respectively. The velocity of the body in general is a function of time and space  $\vec{v} = f(t, \vec{s})$ . Thus, applying the chain rule gives

$$\vec{F}_t = m \frac{d\vec{v}}{ds} \frac{d\vec{s}}{dt} = m \vec{v} \frac{d\vec{v}}{ds} \quad (6)$$



**Energy and First Law of Thermodynamics, Fig. 1** Moving body

where  $\vec{v} = d\vec{s}/dt$  is introduced. Carrying out an integration from position  $s_1$  to  $s_2$  yields

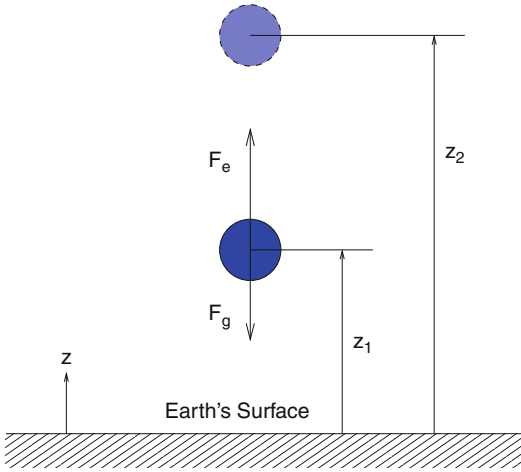
$$\int_{s_1}^{s_2} \vec{F}_t \cdot d\vec{s} = \int_{v_1}^{v_2} m \vec{v} d\vec{v} = \frac{1}{2} m (v_2^2 - v_1^2) \quad (7)$$

The scalar quantity  $\frac{1}{2} m v^2$  represents the kinetic energy of the body and the left-hand side denotes the work of the force  $\vec{F}_s$  according to (1), as the body moves along its path from  $s_1$  to  $s_2$ . It is also a scalar quantity, so that the work on the body equals the change in its kinetic energy. When a resultant force accelerates a body, the work done on the body may be regarded as a transfer of energy to the body, where it is stored as kinetic energy. Thus, kinetic energy is an extensive property of a body.

### Work and Potential Energy

Newton's second law may also be employed to a body that moves under the influence of a gravitational force, e.g., gravity of the earth, as shown in Fig. 2.

In the present case, two forces due to gravity  $\vec{F}_g = m \vec{g}$  and an external force  $\vec{F}_e$  act on the body. Thus, the sum of all forces acting on a body causes a change in velocity when the body moves vertically from an elevation  $z_1$  to an elevation  $z_2$  relative to the surface of the earth. The total work done on the body is the sum of the work of the individual forces and yields with (1).



**Energy and First Law of Thermodynamics, Fig. 2** Moving body with gravitational forces

$$\begin{aligned} \frac{1}{2} m (v_2^2 - v_1^2) &= \int_{s_1}^{s_2} \vec{F}_e \cdot d\vec{s} - \int_{s_1}^{s_2} \vec{F}_g \cdot d\vec{s} \\ &= \int_{s_1}^{s_2} \vec{F}_e \cdot d\vec{s} - \int_{s_1}^{s_2} m \vec{g} \cdot d\vec{s} \end{aligned} \quad (8)$$

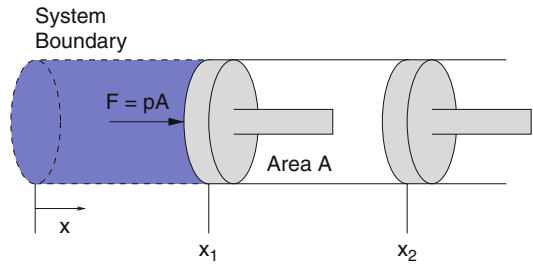
The first integral on the right-hand side represents the work done by the external force, and the second integral is evaluated as follows:

$$\int_{s_1}^{s_2} m \vec{g} \cdot d\vec{s} = m g (z_2 - z_1) \quad (9)$$

The quantity  $mgz$  denotes the potential gravitational energy and is an extensive property. By incorporating this expression into (8) and rearranging, it gives

$$\frac{1}{2} m (v_2^2 - v_1^2) + m g (z_2 - z_1) = \int_{s_1}^{s_2} \vec{F}_e \cdot d\vec{s} \quad (10)$$

that the total work of all forces excluding gravitational force acting on a body accounts for the sum of the changes of kinetic and potential energy. This expresses that work transferred to a body is stored as potential energy and/or kinetic energy or that work extracted from a body reduces its potential energy and/or kinetic energy. If in a special case the only force acting



**Energy and First Law of Thermodynamics, Fig. 3** Work done by an expanding gas

on a body is gravity, then the right-hand side of (10) vanishes and the equation reduces to

$$\frac{1}{2} m (v_2^2 - v_1^2) + m g (z_2 - z_1) = 0 \quad (11)$$

or

$$\frac{1}{2} m v_2^2 + m g z_2 = \frac{1}{2} m v_1^2 + m g z_1 = \text{const} \quad (12)$$

stating that the sum of potential and kinetic energy remains constant and is conserved. This principle illustrates also that energy may be transformed from one form to another in particular and exchanged between potential and kinetic energy.

#### Work Due to Compression and Expansion

The work done by an expanding gas in a closed system of a piston and a cylinder as depicted in Fig. 3 is due to the gas pressure that exerts a normal force  $\vec{F} = p A \vec{n}$  on the piston where  $A$  is the area of the piston,  $\vec{n}$  the unit normal of the piston surface, and  $p$  the averaged uniform pressure on the piston. If the piston is displaced by a distance  $d\vec{x}$ , the work done by the system is

$$\delta W = -\vec{F} \cdot d\vec{x} = -p A dx \quad (13)$$

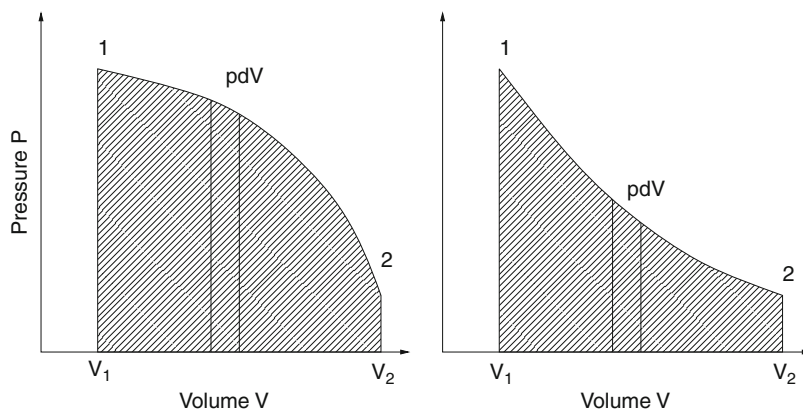
Since the product  $A dx$  equals the change in volume  $dV$  normal to the piston surface, the work writes as follows:

$$\delta W = -p dV \quad (14)$$



## Energy and First Law of Thermodynamics,

**Fig. 4** Pressure-volume diagram



Thus, for a change from volume  $V_1$  to volume  $V_2$ , integration yields the total work as

$$W = \int_{V_1}^{V_2} \delta W = - \int_{V_1}^{V_2} p dV \quad (15)$$

During expansion, the volume increases so that the work is negative. For compression,  $dV$  is positive and so is work. Although this concept was derived for a piston-cylinder assembly, it is applicable to systems with arbitrary shapes.

In order to evaluate the integral  $\int_{V_1}^{V_2} p dV$ , the pressure has to be known for each position of the piston between  $x_1$  and  $x_2$ . This relationship may be difficult to obtain such as in an internal combustion engine of an automobile during the expansion stroke. Representative pressure-volume diagrams are depicted in Fig. 4 where the hatched area under the p-V curve represents the work between state 1 and 2. Obviously, when proceeding from state 1 to state 2, the work is very dependent on the path followed. Although states 1 and 2 are identical in both diagrams of Fig. 4, the areas under the p-V curve are very different. Thus, work is a path function, and its differential is an inexact differential indicated with the symbol  $\delta$ .

## Heat

In the preceding section, several work modes were introduced that transfer energy macroscopically to or from a system. Microscopically, energy may be transferred between a system and its surroundings through its molecules that form

the system boundary. Thus, if the molecules of the system and the surrounding are at different levels of activity, e.g., molecular velocities, the faster molecules will transfer energy to the slower molecules by collisions between them. A force occurs only during a very short time span during the collisions and is responsible for the transfer of energy. Temperature is associated with molecular activity, and the microscopic transfer of energy is macroscopically referred to as heat. Hence, heat represents energy that is transferred between systems of different temperature, e.g., molecular activity, and occurs only in the direction of temperature decrease. As a convention, heat  $Q$  transferred into a system is taken as positive, and heat  $Q$  extracted from a system is taken as negative:

$Q > 0$  : heat transfer **into** the system

$Q < 0$  : heat transfer **from** the system

The amount of heat transferred depends not just only on the end states but also on the details of the process that takes place between these states. Therefore, heat is **not** a property and its differential is written as  $\delta Q$ . Its integration yields the amount of heat transfer as

$$Q = \int_{s_1}^{s_2} \delta Q \neq Q_2 - Q_1 \quad (16)$$

There exist three different modes of heat transfer: conduction, convection, and radiation.



Conduction

Heat transfer by conduction takes place in solids, liquids, and gases due to temperature differences; however, it is usually associated with solids. It is macroscopically quantified by Fourier’s law:

$$\dot{Q} = -\lambda A \frac{dT}{dx} \tag{17}$$

where  $\lambda$ ,  $A$ , and  $dT/dx$  stand for thermal conductivity, area, and temperature gradient, respectively. Fourier’s law expresses that the rate of heat transferred is proportional to the temperature difference across an area and the conductivity of the material.

Convection

Convection describes heat transfer between a solid surface and an adjacent liquid or gas moving past this surface. The transfer of heat from the surface to the fluid is described by Newton’s empirical cooling law:

$$\dot{Q} = \alpha A (T_s - T_f) \tag{18}$$

where  $\alpha$ ,  $A$ ,  $T_s$ , and  $T_f$  denote the heat transfer coefficient, surface area, surface temperature, and fluid temperature. The heat transfer coefficient is an empirical parameter that depends on the geometry, the fluid properties, and the pattern of the flow near the surface. Furthermore, convection may be due to relatively slow buoyancy-induced fluid motions, referred to as free or natural convection, or forced convection by fans or pumps. Typical values for the heat transfer coefficient in free and forced convection are listed in Table 1.

Radiation

Energy transferred through radiation is a result of electromagnetic waves or photons. Unlike conduction, this mode of heat transfer does not require a medium and may even take place in a vacuum. Solid surfaces, liquid, and gases emit, transmit, and adsorb thermal radiation to a varying extent. The rate at which thermal radiation is emitted from a surface of area  $A$  is described by the Stefan-Boltzmann law:

$$\dot{Q} = \varepsilon \sigma T^4 A \tag{19}$$

with  $\varepsilon$ ,  $\sigma$ ,  $T$ , and  $A$  being the emissivity indicating how effectively a surface radiates, Stefan-Boltzmann

**Energy and First Law of Thermodynamics, Table 1** Heat transfer coefficients

Application	$\alpha$ [ $W/m^2K$ ]
Free convection	
Gases	2–25
Liquids	50–1,000
Forced convection	
Gases	25–250
Liquids	50–20,000

constant ( $\sigma = 5.67 \times 10^{-8} W/m^2K^4$ ), temperature, and radiating surface, respectively.

First Law of Thermodynamics

In the previous section, systems were analyzed by the concepts of potential and kinetic energy which affect velocity and position. However, systems of engineering interest interact typically in more complex modes with their surroundings that change also other properties such as temperature. Therefore, in thermodynamics, the concept of energy has to be extended to include a variety of interactions with surroundings such as transfer of heat and work [3, 4]. These extensions are based on experimental evidence.

Closed System

The first law of thermodynamics is, therefore, a more universal expression for the conservation of energy. It may be stated in words as follows:

change in the  
amount of energy  
contained within  
the system  
during some  
time interval

=

net amount of  
energy transfer  
into the system  
by heat transfer  
during some  
time interval

+

net amount of  
energy extracted  
from the  
system by work  
during some  
time interval

This statement requires that the energy of a closed system increases or decreases by an amount equal to the net amount of energy transferred across its boundaries. Thus, the change of energy  $E$  is equal to the amount added by heating  $Q_{1\rightarrow 2}$  plus the amount extracted by doing work  $W_{1\rightarrow 2}$  on the environment during a process between the two states 1 and 2:

$$E_2 - E_1 = Q_{1\rightarrow 2} + W_{1\rightarrow 2} \quad (20)$$

where  $E$  denotes the total energy of the system including kinetic energy, potential energy, and other forms of energy such as electrical, magnetic, or chemical energy. The change of energy  $E_2 - E_1$  depends only on the states 1 and 2, whereas both heat transfer  $Q_{1\rightarrow 2}$  and work transfer  $W_{1\rightarrow 2}$  depend on the states 1 and 2 and the path that links the two states. In engineering thermodynamics, the total energy is considered to consist of macroscopic contributions. Thus, the total energy includes kinetic energy, potential energy, and the remaining part referred to as internal energy  $U$ .

$$E = \frac{1}{2} m v^2 + m g z + U \quad (21)$$

Like total energy, internal energy is an extensive property of the system. On a microscopic level, internal energy may be interpreted to incorporate the kinetic energy due to translation, rotation, and vibration of the molecules, the chemical bonds between the atoms, intermolecular forces, electron orbital states, nuclear spin, and binding forces in the nucleus.

Incorporating the contributions of the total energy into (20), the first law of thermodynamics takes the following form:

$$\begin{aligned} U_2 - U_1 + \frac{1}{2} m (v_2^2 - v_1^2) + m g (z_2 - z_1) \\ = Q_{1\rightarrow 2} + W_{1\rightarrow 2} \end{aligned} \quad (22)$$

or expressed in specific quantities:

$$\begin{aligned} u_2 - u_1 + \frac{1}{2} (v_2^2 - v_1^2) + g (z_2 - z_1) \\ = q_{1\rightarrow 2} + w_{1\rightarrow 2} \end{aligned} \quad (23)$$

For negligible kinetic and potential energies, the law reduces to

$$U_2 - U_1 = Q_{1\rightarrow 2} + W_{1\rightarrow 2} \quad (24)$$

or in differential form as

$$\underbrace{\overbrace{dU}^{\text{Internal energy change}}}_{\text{Property}} = \underbrace{\overbrace{\delta Q}_{\text{Heat transfer}} + \overbrace{\delta W}_{\text{Work transfer}}}_{\text{Interaction of nonproperties}} \quad (25)$$

where  $dU$  is a small change in the internal energy of the system,  $\delta Q$  is a small amount of heat transferred to the system, and  $\delta W$  is a small amount of work done by the system:

The increase in the internal energy of a system is equal to the amount of energy added by heating the system, plus the amount lost as a result of the work done by the system on its surroundings.

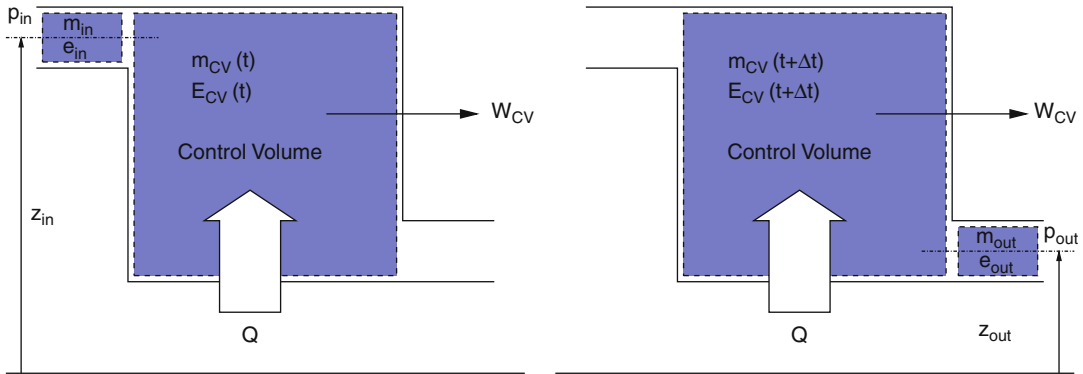
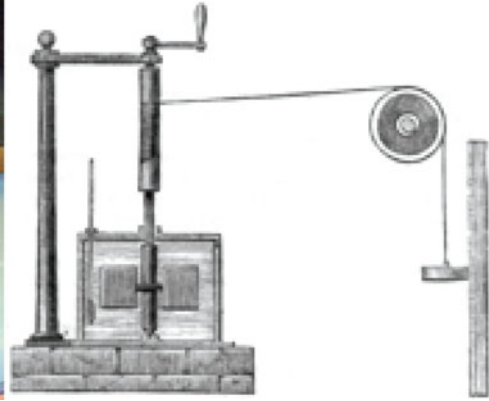
Thus, the concept of heat and work allows for an exact evaluation of the change of internal energy; however, conversely, the change of internal energy cannot be traced back to the quantity of heat into or out of the system nor the work performed on or by the system as illustrated by Joule's most memorable experiment as depicted in Fig. 5.

He carried out a series of experiments between 1843 and 1850, in which he heated a pool of water by an array of paddle wheels driven by a falling weight. After several repetitions, a temperature rise in the liquid occurred and was subsequently measured. As a result, a unit of heat was always equal to the same number of units of work independent on, however, the work was done on the liquid nor whatever liquid, i.e., water, mercury, and whale oil was used. Thus, Joule had shown that heat and work were equivalent in a sense that work could be converted into an equivalent amount of heat. Conversely, only some of the heat can be converted to work, but not all.

Only in cases where no heat transfer occurs, e.g., adiabatic systems, the change in internal energy equals the work transfer as formulated

### Energy and First Law of Thermodynamics,

**Fig. 5** Joule's experiment [5]



**Energy and First Law of Thermodynamics, Fig. 6** Open system

by Rudolf Clausius in 1850 as a first explicit statement of the first law of thermodynamics:

There is a state function  $E$ , called energy, whose differential equals the work exchanged with the surroundings during an adiabatic process.

### Open Systems

As in the case of a closed system of the previous section, energy transfer across the boundary of a system was considered by means of work and heat transfer. In addition, energy that accompanies mass as it leaves or enters a system is taken into account for an open system as depicted in Fig. 6.

Figure 6 shows a system that contains a fixed quantity of matter  $m(t) = m_{CV}(t) + m_{in}$  in the control volume and inlet region at time  $t$  and a different quantity of matter

$m(t + \Delta t) = m_{CV}(t + \Delta t) + m_{out}$  in the control volume and the outlet region at time  $t + \Delta t$ . Thus, the open system is represented by a flow of a closed system through a specified region at time  $t$  and  $t + \Delta t$ . Similarly, the energy of the system at time  $t$  is

$$\begin{aligned} E(t) &= E_{CV}(t) + E_{in} \\ &= E_{CV}(t) + m_{in} \left( u_{in} + g z_{in} + \frac{v_{in}^2}{2} \right) \end{aligned} \quad (26)$$

where  $E_{CV}(t)$  is the internal, kinetic, and potential energy of the mass in the control volume at time  $t$ . The second term on the right-hand side is the energy associated with the mass entering the control volume from the inlet region. During a time

interval, the mass  $m_{in}$  initially in the inlet region crosses the boundary of the control volume, and a mass  $m_{out}$  initially contained within the control volume leaves it into the outlet region. Thus, both mass and energy in the control volume may have changed over the time interval. Similarly, the masses  $m_{in}$  and  $m_{out}$  may not be the same, nor are their energies necessarily equal. Therefore, the energy of the system at  $t + \Delta t$  is

$$E(t + \Delta t) = E_{CV}(t + \Delta t) + E_{out} = E_{CV}(t + \Delta t) + m_{out} \left( u_{out} + gz_{out} + \frac{v_{out}^2}{2} \right) \quad (27)$$

During the time interval, a transfer of work and heat may take place, so that the change in energy according to the first law for a closed system writes as follows:

$$E(t + \Delta t) - E(t) = Q + W \quad (28)$$

which by introducing (26) and (27) yields

$$\left[ E_{CV}(t + \Delta t) + m_{out} \left( u_{out} + gz_{out} + \frac{v_{out}^2}{2} \right) \right] - \left[ E_{CV}(t) + m_{in} \left( u_{in} + gz_{in} + \frac{v_{in}^2}{2} \right) \right] = Q + W \quad (29)$$

and after rearranging gives

$$E_{CV}(t + \Delta t) - E_{CV}(t) = Q + W + m_{in} \left( u_{in} + gz_{in} + \frac{v_{in}^2}{2} \right) - m_{out} \left( u_{out} + gz_{out} + \frac{v_{out}^2}{2} \right) \quad (30)$$

Dividing the last expression by  $\Delta t$  and applying a limiting procedure as  $\Delta t$  approaches zero, the boundaries of the system and the control volume coincide, so that with the following expressions

$$\lim_{\Delta t \rightarrow 0} \frac{E_{CV}(t + \Delta t) - E_{CV}(t)}{\Delta t} = \frac{dE_{CV}}{dt} \quad (31)$$

$$\lim_{\Delta t \rightarrow 0} \frac{Q}{\Delta t} = \dot{Q} \quad (32)$$

$$\lim_{\Delta t \rightarrow 0} \frac{W}{\Delta t} = \dot{W} \quad (33)$$

$$\lim_{\Delta t \rightarrow 0} \frac{m_{in} \left( u_{in} + gz_{in} + \frac{v_{in}^2}{2} \right)}{\Delta t} = \dot{m}_{in} \left( u_{in} + gz_{in} + \frac{v_{in}^2}{2} \right) \quad (34)$$

$$\lim_{\Delta t \rightarrow 0} \frac{m_{out} \left( u_{out} + gz_{out} + \frac{v_{out}^2}{2} \right)}{\Delta t} = \dot{m}_{out} \left( u_{out} + gz_{out} + \frac{v_{out}^2}{2} \right) \quad (35)$$

the following form of the first law for an open system is obtained:

$$\frac{dE_{CV}}{dt} = \dot{Q} + \dot{W} + \dot{m}_{in} \left( u_{in} + gz_{in} + \frac{v_{in}^2}{2} \right) - \dot{m}_{out} \left( u_{out} + gz_{out} + \frac{v_{out}^2}{2} \right) \quad (36)$$

where  $dE_{CV}/dt$ ,  $\dot{m}_{in}$ , and  $\dot{m}_{out}$  are the rate of change of energy contained in the control volume and the mass flow rates at the inlet and outlet, respectively. Furthermore, the last expression introduces a further mode of energy transfer by the energy  $u + gz + v^2/2$  that accompanies the mass entering and exiting the control volume. For vanishing fluxes over the boundary, the form of the first law for a closed system is obtained.

The work term in the previous expressions includes energy transfer by work across all boundaries of the control volume and, thus, is the net rate of energy transfer. In particular, the contribution of mass crossing the boundaries at the inlet and outlet is incorporated. Therefore, the work may be decomposed into the contributions of the inlet  $\dot{W}_{in}$  and outlet  $\dot{W}_{out}$  and that of the control volume  $\dot{W}_{CV}$ . The pressure associated with the flowing matter generates at the inlet and outlet area a force that moves with the

velocity and, thus, represents an equivalent energy transfer.

$$\dot{W} = \dot{W}_{CV} - \dot{W}_{out} + \dot{W}_{in} = \dot{W}_{CV} - (p_{out}A_{out})v_{out} + (p_{in}A_{in})v_{in} \quad (37)$$

Substituting (37) in (36) and collecting the appropriate terms yields the following form:

$$\frac{dE_{CV}}{dt} = \dot{Q}_{CV} + \dot{W}_{CV} + \dot{m}_{in} \left( u_{in} + \frac{p_{in}}{\rho_{in}} + g z_{in} + \frac{v_{in}^2}{2} \right) - \dot{m}_{out} \left( u_{out} + \frac{p_{out}}{\rho_{out}} + g z_{out} + \frac{v_{out}^2}{2} \right) \quad (38)$$

where the terms  $\dot{m}_{in} p_{in} / \rho_{in}$  and  $\dot{m}_{out} p_{out} / \rho_{out}$  account for the work performed by the pressure at the inlet and outlet, respectively, and are commonly labeled flow work. The sum  $u + p / \rho$  is referred to as enthalpy  $h$ . Furthermore, practical applications may include several inlets and outlets that are taken into account by summations of the appropriate locations. Accordingly, the energy balance takes the following form:

$$\frac{dE_{CV}}{dt} = \dot{Q}_{CV} + \dot{W}_{CV} + \sum \dot{m}_{in} \left( h_{in} + g z_{in} + \frac{v_{in}^2}{2} \right) - \sum \dot{m}_{out} \left( h_{out} + g z_{out} + \frac{v_{out}^2}{2} \right) \quad (39)$$

Equation (39) is the most general form of the first law for open systems. However, quite often depending on the application, simplifications may be employed such as the steady-state form, for which  $dE_{CV}/dt = 0$  and  $\dot{m}_{in} = \dot{m}_{out}$ .

#### Steady-State Form

$$\dot{Q}_{CV} + \sum \dot{m} \left( h_{in} + g z_{in} + \frac{v_{in}^2}{2} \right) = -\dot{W}_{CV} + \sum \dot{m} \left( h_{out} + g z_{out} + \frac{v_{out}^2}{2} \right) \quad (40)$$

or dividing by the mass flow rate.

#### Steady-State Form in Specific Quantities

$$q_{CV} + \sum \left( h_{in} + g z_{in} + \frac{v_{in}^2}{2} \right) = -w_{CV} + \sum \left( h_{out} + g z_{out} + \frac{v_{out}^2}{2} \right) \quad (41)$$

where  $q_{CV} = \dot{Q}_{CV} / \dot{m}$  and  $w_{CV} = \dot{W}_{CV} / \dot{m}$  are rates of energy transfer per unit mass flowing through the control volume. In a large number of applications, there is only one inlet and outlet present and kinetic and potential energy is negligible, so that the following simple form evolves:

$$\dot{Q}_{CV} + \dot{W}_{CV} = \dot{m}(h_{out} - h_{in}) \quad (42)$$

For a liquid with a constant density and neglecting heat transfer and changes in internal energy, the form used for a pump or a turbine is obtained.

#### Hydraulic Form

$$\dot{W}_{CV} = \dot{m} \left[ \frac{p_{out} - p_{in}}{\rho} + \frac{v_{out}^2 - v_{in}^2}{2} + g(z_{out} - z_{in}) \right] \quad (43)$$

#### Specific Heats

Considering a simple system, only two variables such as temperature  $T$  and specific volume  $v$  are necessary to establish the state of a system. Consequently, the internal energy  $u$  is perceived as a function of temperature and specific volume; that is,

$$u = u(T, v) \quad (44)$$

Hence, the total differential in terms of partial derivatives is expressed as

$$du = \left. \frac{\partial u}{\partial T} \right|_v + \left. \frac{\partial u}{\partial v} \right|_T \quad (45)$$

The right-hand side of (45) consists of properties, and therefore, the partial derivative is also

a property and is referred to as the constant-volume specific heat  $c_v$ :

$$c_v = \left. \frac{\partial u}{\partial T} \right|_v \quad (46)$$

Likewise, the total differential of the enthalpy dependent on two variables temperature  $T$  and pressure  $p$

$$h = h(T, p) \quad (47)$$

evaluates as

$$dh = \left. \frac{\partial h}{\partial T} \right|_p + \left. \frac{\partial h}{\partial p} \right|_T \quad (48)$$

where

$$c_p = \left. \frac{\partial h}{\partial T} \right|_p \quad (49)$$

is the constant-pressure specific heat. In general,  $c_v$  depends on specific volume  $v$  and temperature  $T$ , whereas  $c_p$  is a function of temperature  $T$  and pressure  $p$ . Specific heat data are available for common solids, liquids, and gases in a form of tables, charts, or computer software.

The values of internal energy and enthalpy are not obtained by direct measurement. They are related to a reference state or value to which an in principle arbitrary reference state of internal energy or enthalpy is assigned. For water, the reference state is saturated liquid at 0.01 °C. Thus, as long as calculations involve only difference of a property as expressed by the first law, the use of these values relative to an arbitrary reference value at an arbitrary reference state is unambiguous because for then, the reference value cancels. Of course, if the reference changes, the values assigned to a particular property change also, but the differences remain the same.

Experimental evidence supports the assumption that liquids and solids may be treated as incompressible substances because the specific

volume or density vary to a small extent only and that the internal energy is mainly dependent on temperature. Thus, the specific heat  $c_v$  is also a function of temperature alone and, therefore, is expressed as an ordinary derivative:

$$c_v(T) = \frac{du}{dT} \quad (50)$$

Although the specific volume is constant, enthalpy depends on both temperature and pressure:

$$h(T, p) = u(T) + pv \quad (51)$$

By differentiating (51) with respect to temperature at constant pressure yields

$$\underbrace{\left. \frac{\partial h}{\partial T} \right|_p}_{c_p} = \underbrace{\frac{du}{dT}}_{c_v} \quad (52)$$

so that for incompressible substance, distinguishing between  $c_v$  and  $c_p$  vanishes ( $c_v = c_p = c$ ). Hence, the changes in internal energy and enthalpy between two states are given by

$$u_2 - u_1 = \int_{T_1}^{T_2} c(T) dT \quad (53)$$

$$\begin{aligned} h_2 - h_1 &= u_2 - u_1 + v(p_2 - p_1) \\ &= \int_{T_1}^{T_2} c(T) dT + v(p_2 - p_1) \end{aligned} \quad (54)$$

Over a limited temperature, the specific heat  $c$  varies to a small extent only, so that it may be treated as constant and (53) and (54) become

$$u_2 - u_1 = c(T_2 - T_1) \quad (55)$$

$$h_2 - h_1 = c(T_2 - T_1) + v(p_2 - p_1) \quad (56)$$

**Energy and First Law of Thermodynamics, Table 2** Table of specific heat capacities at 25 °C unless otherwise noted. <sup>a</sup>Assuming an altitude of 194 m above mean sea level (the worldwide median altitude of human habitation), an indoor temperature of 23 °C, a dew point of 9 °C (40.85 % relative humidity), and 760 mmHg sea level-corrected barometric pressure (molar water vapor content = 1.16 %) [5]

Substance	Phase	$c_p$ J/g K	$c_{p,m}$ J/mol K	$c_{v,m}$ J/mol K
Aluminum	Solid	0.897	24.2	
Ammonia	Liquid	4.700	80.08	
Antimony	Solid	0.207	25.2	
Arsenic	Solid	0.328	24.6	
Beryllium	Solid	1.82	16.4	
Bismuth	Solid	0.123	25.7	
Cadmium	Solid	0.231		
Chromium	Solid	0.449		
Copper	Solid	0.385	24.47	
Diamond	Solid	0.5091	6.115	
Glass	Solid	0.84		
Gold	Solid	0.129	25.42	
Granite	Solid	0.790		
Graphite	Solid	0.710	8.53	
Iron	Solid	0.450	25.1	
Lead	Solid	0.129	26.4	
Lithium	Solid	3.58	24.8	
Magnesium	Solid	1.02	24.9	
Paraffin wax	Solid	2.5	900	
Polyethylene (rotomolding grade)	Solid	2.3027		
Silica (fused)	Solid	0.703	42.2	
Silver	Solid	0.233	24.9	
Sodium	Solid	1.23		
Tin	Solid	0.227		
Tungsten	Solid	0.134	24.8	
Uranium	Solid	0.116	27.7	
Water at −10 °C (ice)	Solid	2.05	38.09	
Zinc	Solid	0.387	25.2	

Table 2 provides specific heat capacities for a selection of different materials.

## References

1. Moran MJ, Shapiro HN (2000) Fundamentals of engineering thermodynamics. Wiley, New York
2. Cengel YA, Boles MA (2001) Thermodynamics: an engineering approach. McGraw-Hill, Boston
3. Bejan A (2006) Advanced engineering thermodynamics. Wiley, Hoboken
4. Sonntag A, Borgnakke C (2007) Engineering thermodynamics. Wiley
5. Wikipedia

## Energy Method, Anisotropic and Heterogeneous Plates

Theodore R. Tauchert  
Department of Mechanical Engineering,  
University of Kentucky, Lexington, KY, USA

## Overview

As an alternative to the direct approach (illustrated in ► [Plates, Anisotropic and Heterogeneous](#)) for deriving the equations governing the

thermoelastic response of a plate, an approach based upon energy considerations may be used. Generalizing the procedure employed in ► [energy method, homogeneous isotropic plates](#), the *principle of minimum potential energy*, in conjunction with the calculus of variations, is employed to obtain the equilibrium equations and natural boundary conditions for an anisotropic, heterogeneous plate. Application of the Rayleigh-Ritz technique is then discussed for the problem of coupled stretching-bending of a rectangular plate subject to a stationary temperature field in combination with a transverse load and edge loads.

### Energy Formulation

The *principle of minimum potential energy* is used here to obtain the equations governing the coupled in-plane stretching and transverse bending of a thin, heterogeneous, anisotropic plate subject to a stationary temperature field, a transverse load, edge forces and edge moments. The principle may be stated as follows [1]:

Of all displacement fields which satisfy the prescribed constraint conditions, the correct state is that which makes the total potential energy of the structure a minimum.

The total potential energy  $\Pi$  for an elastic structure is equal to the sum of the strain energy  $U$  and the potential  $V$  of the applied forces. For an anisotropic, linearly-elastic plate of volume  $\mathcal{V}$ , the thermoelastic strain energy can be written in terms of the stress components  $\sigma_{ij}$ , normal strains  $\epsilon_{ij}$ , shear strains  $\gamma_{ij}$  and temperature  $T$  as [2]

$$U = \frac{1}{2} \int_{\mathcal{V}} [\sigma_{xx}\epsilon_{xx} + \sigma_{yy}\epsilon_{yy} + \sigma_{zz}\epsilon_{zz} + \sigma_{xy}\gamma_{xy} + \sigma_{yz}\gamma_{yz} + \sigma_{zx}\gamma_{zx} - (\sigma_{xx} + \sigma_{yy} + \sigma_{zz})\alpha T] d\mathcal{V} \quad (1)$$

Substituting the stress and strain expressions as presented in ► [plates, anisotropic](#)

and [heterogeneous](#) into (1), and integrating with respect to the thickness coordinate  $z$ , yields [3]

$$U = \int_0^b \int_0^a \left[ \frac{A_{11}}{2} \left( \frac{\partial u^0}{\partial x} \right)^2 + A_{12} \left( \frac{\partial u^0}{\partial x} \right) \left( \frac{\partial v^0}{\partial y} \right) + \frac{A_{22}}{2} \left( \frac{\partial v^0}{\partial y} \right)^2 + A_{16} \left( \frac{\partial u^0}{\partial x} \right) \left( \frac{\partial^0 u}{\partial y} + \frac{\partial v^0}{\partial x} \right) + A_{26} \left( \frac{\partial v^0}{\partial y} \right) \left( \frac{\partial u^0}{\partial y} + \frac{\partial v^0}{\partial x} \right) + \frac{A_{66}}{2} \left( \frac{\partial u^0}{\partial y} + \frac{\partial v^0}{\partial x} \right)^2 - B_{11} \left( \frac{\partial u^0}{\partial x} \right) \left( \frac{\partial^2 w}{\partial x^2} \right) - B_{12} \left( \frac{\partial u^0}{\partial x} \frac{\partial^2 w}{\partial y^2} + \frac{\partial v^0}{\partial y} \frac{\partial^2 w}{\partial x^2} \right) - B_{22} \left( \frac{\partial v^0}{\partial y} \right) \left( \frac{\partial^2 w}{\partial y^2} \right) - B_{16} \left( \frac{\partial u^0}{\partial y} \frac{\partial^2 w}{\partial x^2} + \frac{\partial v^0}{\partial x} \frac{\partial^2 w}{\partial x^2} + 2 \frac{\partial u^0}{\partial x} \frac{\partial^2 w}{\partial x \partial y} \right) - B_{26} \left( \frac{\partial u^0}{\partial y} \frac{\partial^2 w}{\partial y^2} + \frac{\partial v^0}{\partial x} \frac{\partial^2 w}{\partial y^2} + 2 \frac{\partial v^0}{\partial y} \frac{\partial^2 w}{\partial x \partial y} \right) - 2B_{66} \left( \frac{\partial u^0}{\partial y} + \frac{\partial v^0}{\partial x} \right) \left( \frac{\partial^2 w}{\partial x \partial y} \right) + \frac{D_{11}}{2} \left( \frac{\partial^2 w}{\partial x^2} \right)^2 + D_{12} \left( \frac{\partial^2 w}{\partial x^2} \right) \left( \frac{\partial^2 w}{\partial y^2} \right) + \frac{D_{22}}{2} \left( \frac{\partial^2 w}{\partial y^2} \right)^2 + 2D_{16} \left( \frac{\partial^2 w}{\partial x^2} \right) \left( \frac{\partial^2 w}{\partial x \partial y} \right) + 2D_{26} \left( \frac{\partial^2 w}{\partial y^2} \right) \left( \frac{\partial^2 w}{\partial x \partial y} \right) + 2D_{66} \left( \frac{\partial^2 w}{\partial x \partial y} \right)^2 - N_x^T \left( \frac{\partial u^0}{\partial x} \right) - N_{xy}^T \left( \frac{\partial u^0}{\partial y} + \frac{\partial v^0}{\partial x} \right) - N_y^T \left( \frac{\partial v^0}{\partial y} \right) + M_x^T \left( \frac{\partial^2 w}{\partial x^2} \right) + 2M_{xy}^T \left( \frac{\partial^2 w}{\partial x \partial y} \right) + M_y^T \left( \frac{\partial^2 w}{\partial y^2} \right) \right] dx dy \quad (2)$$

where  $u^0$ ,  $v^0$ ,  $w$  are the displacement components in the  $x$ ,  $y$ ,  $z$  directions of the middle surface of a rectangular plate ( $0 \leq x \leq a$ ,  $0 \leq y \leq b$ ). Furthermore,  $A_{ij}$ ,  $B_{ij}$ ,  $D_{ij}$  are the extensional, coupling and bending stiffnesses, defined by [3]



$$(A_{ij}, B_{ij}, D_{ij}) = \int_{-h/2}^{h/2} (1, z, z^2) \bar{Q}_{ij} dz \quad (3)$$

and the thermal forces and thermal moments are defined, respectively, by the matrices

$$\begin{Bmatrix} N_x^T \\ N_y^T \\ N_{xy}^T \end{Bmatrix} = \int_{-h/2}^{h/2} \begin{bmatrix} \bar{Q}_{11} & \bar{Q}_{12} & \bar{Q}_{16} \\ \bar{Q}_{12} & \bar{Q}_{22} & \bar{Q}_{26} \\ \bar{Q}_{16} & \bar{Q}_{26} & \bar{Q}_{66} \end{bmatrix} \begin{Bmatrix} \alpha_x \\ \alpha_y \\ 2\alpha_{xy} \end{Bmatrix} T dz \quad (4)$$

$$\begin{Bmatrix} M_x^T \\ M_y^T \\ M_{xy}^T \end{Bmatrix} = \int_{-h/2}^{h/2} \begin{bmatrix} \bar{Q}_{11} & \bar{Q}_{12} & \bar{Q}_{16} \\ \bar{Q}_{12} & \bar{Q}_{22} & \bar{Q}_{26} \\ \bar{Q}_{16} & \bar{Q}_{26} & \bar{Q}_{66} \end{bmatrix} \begin{Bmatrix} \alpha_x \\ \alpha_y \\ 2\alpha_{xy} \end{Bmatrix} Tz dz \quad (5)$$

in which  $\bar{Q}_{ij}$  are the transformed reduced stiffness coefficients [3].

If the plate is subject to a transverse load  $q(x, y)$ , together with prescribed in-plane edge forces  $\bar{N}_x, \bar{N}_y, \bar{N}_{xy}$ , transverse edge loads  $\bar{Q}_x, \bar{Q}_y$  and edge moments  $\bar{M}_x, \bar{M}_y, \bar{M}_{xy}$ , then the potential of the external loading is [3]

$$\begin{aligned} V = & - \int_0^b \int_0^a q w dx dy - \int_0^b \left[ \bar{N}_x u^0 + \bar{N}_{xy} v^0 + \bar{Q}_x w \right. \\ & \left. - \bar{M}_x \frac{\partial w}{\partial x} - \bar{M}_{xy} \frac{\partial w}{\partial y} \right]_0^a dy \\ & - \int_0^a \left[ \bar{N}_y v^0 + \bar{N}_{xy} u^0 + \bar{Q}_y w - \bar{M}_y \frac{\partial w}{\partial y} - \bar{M}_{xy} \frac{\partial w}{\partial x} \right]_0^b dx \end{aligned} \quad (6)$$

Application of the principle of minimum potential energy requires minimization of the functional  $\Pi = U + V$ . For this we employ the calculus of variations. For those not familiar with this branch of mathematics, a brief introduction to the subject is given in [1],

Appendix C; for a more rigorous treatment one may refer to [4]. According to the calculus, a necessary condition for  $\Pi$  to have a minimum is that the first variation  $\delta \Pi$  vanish identically. Thus, taking the variation of  $\Pi$  and performing integration by parts, it can be shown that [3]

$$\begin{aligned} \delta \Pi = & \int_0^b \int_0^a \left[ - \left( A_{11} \frac{\partial^2 u^0}{\partial x^2} + 2A_{16} \frac{\partial^2 u^0}{\partial x \partial y} \right. \right. \\ & + A_{66} \frac{\partial^2 u^0}{\partial y^2} + A_{16} \frac{\partial^2 v^0}{\partial x^2} + (A_{12} + A_{66}) \frac{\partial^2 v^0}{\partial x \partial y} \\ & + A_{26} \frac{\partial^2 v^0}{\partial y^2} - B_{11} \frac{\partial^3 w}{\partial x^3} - 3B_{16} \frac{\partial^3 w}{\partial x^2 \partial y} \\ & - (B_{12} + 2B_{66}) \frac{\partial^3 w}{\partial x \partial y^2} - B_{26} \frac{\partial^3 w}{\partial y^3} \\ & \left. \left. - \frac{\partial N_x^T}{\partial x} - \frac{\partial N_{xy}^T}{\partial y} \right) \delta u^0 \right. \\ & - \left( A_{16} \frac{\partial^2 u^0}{\partial x^2} + (A_{12} + A_{66}) \frac{\partial^2 u^0}{\partial x \partial y} \right. \\ & + A_{26} \frac{\partial^2 u^0}{\partial y^2} + A_{66} \frac{\partial^2 v^0}{\partial x^2} + 2A_{26} \frac{\partial^2 v^0}{\partial x \partial y} \\ & + A_{22} \frac{\partial^2 v^0}{\partial y^2} - B_{16} \frac{\partial^3 w}{\partial x^3} - (B_{12} + 2B_{66}) \frac{\partial^3 w}{\partial x^2 \partial y} \\ & - 3B_{26} \frac{\partial^3 w}{\partial x \partial y^2} - B_{22} \frac{\partial^3 w}{\partial y^3} - \frac{\partial N_y^T}{\partial y} - \frac{\partial N_{xy}^T}{\partial x} \left. \right) \delta v^0 \\ & + (D_{11} \frac{\partial^4 w}{\partial x^4} + 4D_{16} \frac{\partial^4 w}{\partial x^3 \partial y} \\ & + 2(D_{12} + 2D_{66}) \frac{\partial^4 w}{\partial x^2 \partial y^2} + 4D_{26} \frac{\partial^4 w}{\partial x \partial y^3} \\ & + D_{22} \frac{\partial^4 w}{\partial y^4} - B_{11} \frac{\partial^3 u^0}{\partial x^3} - 3B_{16} \frac{\partial^3 u^0}{\partial x^2 \partial y} \\ & - (B_{12} + 2B_{66}) \frac{\partial^3 u^0}{\partial x \partial y^2} - B_{26} \frac{\partial^3 u^0}{\partial y^3} \\ & - B_{16} \frac{\partial^3 v^0}{\partial x^3} - (B_{12} + 2B_{66}) \frac{\partial^3 v^0}{\partial x^2 \partial y} \\ & - 3B_{26} \frac{\partial^3 v^0}{\partial x \partial y^2} - B_{22} \frac{\partial^3 v^0}{\partial y^3} + \frac{\partial^2 M_x^T}{\partial x^2} \\ & \left. \left. + 2 \frac{\partial^2 M_{xy}^T}{\partial x \partial y} + \frac{\partial^2 M_y^T}{\partial y^2} - q \right) \delta w \right] dx dy \end{aligned}$$

$$\begin{aligned}
& + \int_0^b \left\{ [(N_x - \bar{N}_x) \delta u^0]_{x=0}^{x=a} + [(N_{xy} - \bar{N}_{xy}) \delta v^0]_{x=0}^{x=a} \right. \\
& + \left[ \left( \frac{\partial M_x}{\partial x} + 2 \frac{\partial M_{xy}}{\partial y} - \bar{K}_x \right) \delta w \right]_{x=0}^{x=a} \\
& - \left[ (M_x + \bar{M}_x) \delta \left( \frac{\partial w}{\partial x} \right) \right]_{x=0}^{x=a} \Big\} dy \\
& + \int_0^a \left\{ [(N_{xy} - \bar{N}_{xy}) \delta u^0]_{y=0}^{y=b} + [(N_y - \bar{N}_y) \delta v^0]_{y=0}^{y=b} \right. \\
& + \left[ \left( \frac{\partial M_y}{\partial y} + 2 \frac{\partial M_{xy}}{\partial x} - \bar{K}_y \right) \delta w \right]_{y=0}^{y=b} \\
& - \left[ (M_y + \bar{M}_y) \delta \left( \frac{\partial w}{\partial y} \right) \right]_{y=0}^{y=b} \Big\} dx \\
& - \left[ (2M_{xy} - \bar{R}_{xy}) \delta w \right]_{x=0, y=0}^{x=a, y=b} \\
& + \left[ (2M_{xy} - \bar{R}_{xy}) \delta w \right]_{x=0, y=0}^{x=a, y=0} = 0
\end{aligned} \quad (7)$$

where use has been made of the relations for the resultant in-plane forces per unit length  $N_x, N_y, N_{xy}$ , the bending moments per unit length  $M_x, M_y$ , and the twisting moment per unit length  $M_{xy}$ , namely (see ► [Plates, Anisotropic and Heterogeneous](#))

$$\begin{aligned}
\begin{Bmatrix} N_x \\ N_y \\ N_{xy} \end{Bmatrix} &= \begin{bmatrix} A_{11} & A_{12} & A_{16} \\ A_{12} & A_{22} & A_{26} \\ A_{16} & A_{26} & A_{66} \end{bmatrix} \begin{Bmatrix} \frac{\partial u^0}{\partial x} \\ \frac{\partial v^0}{\partial y} \\ \frac{\partial u^0}{\partial y} + \frac{\partial v^0}{\partial x} \end{Bmatrix} \\
&+ \begin{bmatrix} B_{11} & B_{12} & B_{16} \\ B_{12} & B_{22} & B_{26} \\ B_{16} & B_{26} & B_{66} \end{bmatrix} \begin{Bmatrix} -\frac{\partial^2 w}{\partial x^2} \\ -\frac{\partial^2 w}{\partial y^2} \\ -2\frac{\partial^2 w}{\partial x \partial y} \end{Bmatrix} - \begin{Bmatrix} N_x^T \\ N_y^T \\ N_{xy}^T \end{Bmatrix}
\end{aligned} \quad (8)$$

$$\begin{aligned}
\begin{Bmatrix} M_x \\ M_y \\ M_{xy} \end{Bmatrix} &= \begin{bmatrix} B_{11} & B_{12} & B_{16} \\ B_{12} & B_{22} & B_{26} \\ B_{16} & B_{26} & B_{66} \end{bmatrix} \begin{Bmatrix} \frac{\partial u^0}{\partial x} \\ \frac{\partial v^0}{\partial y} \\ \frac{\partial u^0}{\partial y} + \frac{\partial v^0}{\partial x} \end{Bmatrix} \\
&+ \begin{bmatrix} D_{11} & D_{12} & D_{16} \\ D_{12} & D_{22} & D_{26} \\ D_{16} & D_{26} & D_{66} \end{bmatrix} \begin{Bmatrix} -\frac{\partial^2 w}{\partial x^2} \\ -\frac{\partial^2 w}{\partial y^2} \\ -2\frac{\partial^2 w}{\partial x \partial y} \end{Bmatrix} - \begin{Bmatrix} M_x^T \\ M_y^T \\ M_{xy}^T \end{Bmatrix}
\end{aligned} \quad (9)$$

Also appearing in (7) are the prescribed *Kirchhoff forces*  $\bar{K}_x = \frac{\partial M_{xy}}{\partial y} + \bar{Q}_x$  and  $\bar{K}_y = \frac{\partial M_{xy}}{\partial x} + \bar{Q}_y$  which take into account both the twisting moments and shear forces, and the quantity  $\bar{R}_{xy} = 2\bar{M}_{xy}$  which represents an applied resultant concentrated force at the corner of the plate ([5], p.85). Requiring that (7) be satisfied for arbitrary variations  $\delta u^0, \delta v^0$  and  $\delta w$  and their derivatives, it follows that the displacement equations of equilibrium are identical to those given in ► [plates, anisotropic and heterogeneous](#), namely

$$\begin{aligned}
& A_{11} \frac{\partial^2 u^0}{\partial x^2} + 2A_{16} \frac{\partial^2 u^0}{\partial x \partial y} + A_{66} \frac{\partial^2 u^0}{\partial y^2} + A_{16} \frac{\partial^2 v^0}{\partial x^2} \\
& + (A_{12} + A_{66}) \frac{\partial^2 v^0}{\partial x \partial y} + A_{26} \frac{\partial^2 v^0}{\partial y^2} \\
& - B_{11} \frac{\partial^3 w}{\partial x^3} - 3B_{16} \frac{\partial^3 w}{\partial x^2 \partial y} - (B_{12} + 2B_{66}) \frac{\partial^3 w}{\partial x \partial y^2} \\
& - B_{26} \frac{\partial^3 w}{\partial y^3} - \frac{\partial N_x^T}{\partial x} - \frac{\partial N_{xy}^T}{\partial y} = 0
\end{aligned} \quad (10)$$

$$\begin{aligned}
& A_{16} \frac{\partial^2 u^0}{\partial x^2} + (A_{12} + A_{66}) \frac{\partial^2 u^0}{\partial x \partial y} + A_{26} \frac{\partial^2 u^0}{\partial y^2} \\
& + A_{66} \frac{\partial^2 v^0}{\partial x^2} + 2A_{26} \frac{\partial^2 v^0}{\partial x \partial y} + A_{22} \frac{\partial^2 v^0}{\partial y^2} \\
& - B_{16} \frac{\partial^3 w}{\partial x^3} - (B_{12} + 2B_{66}) \frac{\partial^3 w}{\partial x^2 \partial y} - 3B_{26} \frac{\partial^3 w}{\partial x \partial y^2} \\
& - B_{22} \frac{\partial^3 w}{\partial y^3} - \frac{\partial N_y^T}{\partial y} - \frac{\partial N_{xy}^T}{\partial x} = 0
\end{aligned} \quad (11)$$

$$\begin{aligned}
& D_{11} \frac{\partial^4 w}{\partial x^4} + 4D_{16} \frac{\partial^4 w}{\partial x^3 \partial y} + 2(D_{12} + 2D_{66}) \\
& \frac{\partial^4 w}{\partial x^2 \partial y^2} + 4D_{26} \frac{\partial^4 w}{\partial x \partial y^3} + D_{22} \frac{\partial^4 w}{\partial y^4} \\
& - B_{11} \frac{\partial^3 u^0}{\partial x^3} - 3B_{16} \frac{\partial^3 u^0}{\partial x^2 \partial y} \\
& - (B_{12} + 2B_{66}) \frac{\partial^3 u^0}{\partial x \partial y^2} - B_{26} \frac{\partial^3 u^0}{\partial y^3} \\
& - B_{16} \frac{\partial^3 v^0}{\partial x^3} - (B_{12} + 2B_{66}) \frac{\partial^3 v^0}{\partial x^2 \partial y} \\
& - 3B_{26} \frac{\partial^3 v^0}{\partial x \partial y^2} - B_{22} \frac{\partial^3 v^0}{\partial y^3} \\
& + \frac{\partial^2 M_x^T}{\partial x^2} + 2 \frac{\partial^2 M_{xy}^T}{\partial x \partial y} + \frac{\partial^2 M_y^T}{\partial y^2} = q
\end{aligned} \quad (12)$$

plus boundary conditions that are in agreement with those presented in ► [plates, classical theory](#) and in [3].

The existence of coupling (terms containing  $B_{ij}$ ) between the in-plane displacements  $u^0$  and  $v^0$  and the transverse displacement  $w$  is apparent in (10–12).

## Rayleigh–Ritz Method

For an approximate solution via the Rayleigh–Ritz method (see for example [3]), the displacements can be expressed in the finite series form

$$\begin{aligned} u^0(x, y) &= \sum_m \sum_n A_{mn} \psi_{mn}(x, y) \\ v^0(x, y) &= \sum_m \sum_n B_{mn} \chi_{mn}(x, y) \\ w(x, y) &= \sum_m \sum_n C_{mn} \phi_{mn}(x, y) \end{aligned} \quad (13)$$

where the functions  $\psi_{mn}$ ,  $\chi_{mn}$  and  $\phi_{mn}$  are chosen such that (13) satisfy all kinematic boundary conditions. Introducing this assumed solution into the total potential energy expression  $\Pi = U + V$ , and imposing the condition  $\delta\Pi = 0$ , yields

$$\frac{\partial\Pi}{\partial A_{mn}} = 0, \quad \frac{\partial\Pi}{\partial B_{mn}} = 0, \quad \frac{\partial\Pi}{\partial C_{mn}} = 0 \quad (14)$$

which can be solved to obtain the Ritz coefficients  $A_{mn}$ ,  $B_{mn}$  and  $C_{mn}$ .

## Cross-References

- [Energy Method, Homogeneous Isotropic Plates](#)
- [Plates, Anisotropic and Heterogeneous](#)

## References

1. Tauchert TR (1974) Energy principles in structural mechanics. McGraw-Hill, New York; (1980) reprinted by Indo American Books, Delhi

2. Boley BA, Weiner JH (1980) Theory of thermal stresses. Wiley, New York
3. Tauchert TR (1986) Thermal stresses in plates – statical problems. In: Hetnarski RB (ed) Thermal stresses I. Elsevier, Amsterdam, pp 23–141
4. Courant R, Hilbert D (1953) Methods of mathematical physics, vol 1. Interscience, New York
5. Timoshenko S, Woinowsky-Krieger S (1959) Theory of plates and shells, 2nd edn. McGraw-Hill, New York

## Energy Method, Homogeneous Isotropic Plates

Theodore R. Tauchert

Department of Mechanical Engineering,  
University of Kentucky, Lexington, KY, USA

## Overview

As an alternative to the direct “vectorial” approach normally used in deriving the equations governing deformations of structures, a scalar approach based upon energy considerations may be used. Here the *principle of minimum potential energy*, in conjunction with the calculus of variations, is employed to obtain the plate equilibrium equations and natural boundary conditions, consistent with ► [plates, classical theory](#). The energy formulation also serves as a basis for various approximate methods of analysis, including the Rayleigh–Ritz and finite element methods. Application of the Rayleigh–Ritz technique is illustrated here for the problem of flexure of a rectangular plate subject to a thermal moment. Corresponding thermoelastic plate analyses based upon finite element procedures, while not included here, may be found in [1, 2] and in numerous other publications.

## Energy Formulation

The *principle of minimum potential energy* is used here to obtain the equations governing the in-plane stretching and transverse bending of a thin, homogeneous, isotropic plate subject to

a stationary temperature field  $T(x, y, z)$ . The principle may be stated as follows [3]:

Of all displacement fields which satisfy the prescribed constraint conditions, the correct state is that which makes the total potential energy of the structure a minimum.

The total potential energy  $\Pi$  for an elastic structure is equal to the sum of the strain energy  $U$  and the potential  $V$  of the applied forces. For an isotropic, linearly elastic plate of volume  $\mathcal{V}$ , the thermoelastic strain energy can be written in terms of the stress components  $\sigma_{ij}$ , normal strains  $\varepsilon_{ij}$ , shear strains  $\gamma_{ij}$ , and temperature  $T$  as [4]

$$U = \frac{1}{2} \int_{\mathcal{V}} [\sigma_{xx}\varepsilon_{xx} + \sigma_{yy}\varepsilon_{yy} + \sigma_{zz}\varepsilon_{zz} + \sigma_{xy}\gamma_{xy} + \sigma_{yz}\gamma_{yz} + \sigma_{zx}\gamma_{zx} - (\sigma_{xx} + \sigma_{yy} + \sigma_{zz})\alpha T] d\mathcal{V} \quad (1)$$

Substituting the stress and strain expressions as presented in ► [plates, classical theory](#) into (1), and integrating with respect to the thickness coordinate  $z$ , yields [2]

$$U = \iint_{\mathcal{A}} \left\{ \frac{A}{2} \left( \frac{\partial u^0}{\partial x} + \frac{\partial v^0}{\partial y} \right)^2 + \frac{(1-\nu)A}{4} \left[ \left( \frac{\partial u^0}{\partial y} + \frac{\partial v^0}{\partial x} \right)^2 - 4 \frac{\partial u^0}{\partial x} \frac{\partial v^0}{\partial y} \right] + \frac{D}{2} \left( \frac{\partial^2 w}{\partial x^2} + \frac{\partial^2 w}{\partial y^2} \right)^2 + (1-\nu)D \left[ \left( \frac{\partial^2 w}{\partial x \partial y} \right)^2 - \frac{\partial^2 w}{\partial x^2} \frac{\partial^2 w}{\partial y^2} \right] - N^T \left( \frac{\partial u^0}{\partial x} + \frac{\partial v^0}{\partial y} \right) + M^T \left( \frac{\partial^2 w}{\partial x^2} + \frac{\partial^2 w}{\partial y^2} \right) \right\} dx dy \quad (2)$$

where  $u^0, v^0, w$  are the displacement components in the  $x, y, z$  directions of the plate middle surface;  $\mathcal{A}$  is the area of the middle surface;  $A = Eh/(1-\nu^2)$  and  $D = Eh^3/12(1-\nu^2)$  represent extensional and bending stiffnesses of plate of depth  $h$ , respectively; and  $M^T$  and  $N^T$  are the thermal moment and thermal force, respectively, given by

$$M^T = \frac{E\alpha}{1-\nu} \int_{-h/2}^{h/2} T(x, y, z) z dz, \quad (3)$$

$$N^T = \frac{E\alpha}{1-\nu} \int_{-h/2}^{h/2} T(x, y, z) dz$$

The potential  $V$  of a transverse load  $q(x, y)$  is

$$V = - \iint_{\mathcal{A}} qw dx dy \quad (4)$$

If the edges of the plate are subject to applied forces or couples, their potentials must also be included in  $V$ .

Thus, for a rectangular plate ( $0 \leq x \leq a$ ,  $0 \leq y \leq b$ ) subject to a temperature variation  $T(x, y, z)$  and a transverse load  $q(x, y)$ , but no applied edge loads, the total potential energy becomes [2, 5]

$$\begin{aligned} \Pi = & \iint_0^b \int_0^a \left\{ \frac{A}{2} \left( \frac{\partial u^0}{\partial x} + \frac{\partial v^0}{\partial y} \right)^2 + \frac{(1-\nu)A}{4} \left[ \left( \frac{\partial u^0}{\partial y} + \frac{\partial v^0}{\partial x} \right)^2 - 4 \frac{\partial u^0}{\partial x} \frac{\partial v^0}{\partial y} \right] + \frac{D}{2} \left( \frac{\partial^2 w}{\partial x^2} + \frac{\partial^2 w}{\partial y^2} \right)^2 + (1-\nu)D \left[ \left( \frac{\partial^2 w}{\partial x \partial y} \right)^2 - \frac{\partial^2 w}{\partial x^2} \frac{\partial^2 w}{\partial y^2} \right] - N^T \left( \frac{\partial u^0}{\partial x} + \frac{\partial v^0}{\partial y} \right) + M^T \left( \frac{\partial^2 w}{\partial x^2} + \frac{\partial^2 w}{\partial y^2} \right) - qw \right\} dx dy \quad (5) \end{aligned}$$

Application of the principle of minimum potential energy requires minimization of the functional  $\Pi$  in (5). For this, we employ the calculus of variations. For those not familiar with this branch of mathematics, a brief introduction to the subject is given in [3, Appendix C]; for a more rigorous treatment one may refer to [6]. According to the calculus, a necessary condition for  $\Pi$  to have a minimum is that the first variation  $\delta \Pi$  vanish identically. Thus, taking the variation of  $\Pi$  and performing integration by parts, it can be shown that [2]

$$\begin{aligned}
\delta \Pi = & \int_0^b \int_0^a \left\{ - \left[ A \left( \frac{\partial^2 u^0}{\partial x^2} + \nu \frac{\partial^2 v^0}{\partial x \partial y} \right) + \frac{(1-\nu)A}{2} \right. \right. \\
& \times \left( \frac{\partial^2 u^0}{\partial y^2} + \frac{\partial^2 v^0}{\partial x \partial y} \right) - \frac{\partial N^T}{\partial x} \left. \right] \delta u^0 \\
& - \left[ \frac{(1-\nu)A}{2} \left( \frac{\partial^2 u^0}{\partial x \partial y} + \frac{\partial^2 v^0}{\partial x^2} \right) \right. \\
& + A \left( \nu \frac{\partial^2 u^0}{\partial x \partial y} + \frac{\partial^2 v^0}{\partial y^2} \right) - \frac{\partial N^T}{\partial y} \left. \right] \delta v^0 \\
& + \left[ D \left( \frac{\partial^4 w}{\partial x^4} + 2 \frac{\partial^4 w}{\partial x^2 \partial y^2} + \frac{\partial^4 w}{\partial y^4} \right) \right. \\
& + \left. \frac{\partial^2 M^T}{\partial x^2} + \frac{\partial^2 M^T}{\partial y^2} - q \right] \delta w \left. \right\} dx dy \\
& + \int_0^b \left\{ \left[ N_x \delta u^0 \right]_{x=0}^{x=a} + \left[ N_{xy} \delta v^0 \right]_{x=0}^{x=a} \right. \\
& + \left[ \left( \frac{\partial M_x}{\partial x} + 2 \frac{\partial M_{xy}}{\partial y} \right) \delta w \right]_{x=0}^{x=a} \\
& - \left[ M_x \delta \left( \frac{\partial w}{\partial x} \right) \right]_{x=0}^{x=a} \left. \right\} dy + \int_0^a \left\{ \left[ N_{xy} \delta u^0 \right]_{y=0}^{y=b} \right. \\
& + \left[ N_y \delta v^0 \right]_{y=0}^{y=b} + \left[ \left( \frac{\partial M_y}{\partial y} + 2 \frac{\partial M_{xy}}{\partial x} \right) \delta w \right]_{y=0}^{y=b} \\
& - \left[ M_y \delta \left( \frac{\partial w}{\partial y} \right) \right]_{y=0}^{y=b} \left. \right\} dx - \left[ 2 M_{xy} \delta w \right]_{x=0, y=b}^{x=a, y=b} \\
& + \left[ 2 M_{xy} \delta w \right]_{x=0, y=0}^{x=a, y=0} = 0
\end{aligned}$$

where use has been made of the relations for the resultant in-plane forces per unit length  $N_x, N_y$ , and  $N_{xy}$ , the bending moments per unit length  $M_x$  and  $M_y$ , and the twisting moment  $M_{xy}$ , namely (see ► [Plates, Classical Theory](#))

$$\begin{aligned}
N_x &= A \left( \frac{\partial u^0}{\partial x} + \nu \frac{\partial v^0}{\partial y} \right) - N^T \\
N_y &= A \left( \nu \frac{\partial u^0}{\partial x} + \frac{\partial v^0}{\partial y} \right) - N^T \\
N_{xy} &= \frac{(1-\nu)A}{2} \left( \frac{\partial u^0}{\partial y} + \frac{\partial v^0}{\partial x} \right)
\end{aligned} \quad (7)$$

and

$$\begin{aligned}
M_x &= -D \left( \frac{\partial^2 w}{\partial x^2} + \nu \frac{\partial^2 w}{\partial y^2} \right) - M^T \\
M_y &= -D \left( \nu \frac{\partial^2 w}{\partial x^2} + \frac{\partial^2 w}{\partial y^2} \right) - M^T \\
M_{xy} &= -(1-\nu)D \frac{\partial^2 w}{\partial x \partial y}
\end{aligned} \quad (8)$$

In order that (6) be satisfied for arbitrary variations  $\delta u^0, \delta v^0, \delta w, \delta(\partial w/\partial x)$  and  $\delta(\partial w/\partial y)$ , all terms within square brackets must be identically zero. Therefore, throughout the plate

$$\begin{aligned}
A \left( \frac{\partial^2 u^0}{\partial x^2} + \nu \frac{\partial^2 v^0}{\partial x \partial y} \right) + \frac{(1-\nu)A}{2} \left( \frac{\partial^2 u^0}{\partial y^2} + \frac{\partial^2 v^0}{\partial x \partial y} \right) &= \frac{\partial N^T}{\partial x} \\
\frac{(1-\nu)A}{2} \left( \frac{\partial^2 u^0}{\partial x \partial y} + \frac{\partial^2 v^0}{\partial x^2} \right) + A \left( \nu \frac{\partial^2 u^0}{\partial x \partial y} + \frac{\partial^2 v^0}{\partial y^2} \right) &= \frac{\partial N^T}{\partial y} \\
D \left( \frac{\partial^4 w}{\partial x^4} + 2 \frac{\partial^4 w}{\partial x^2 \partial y^2} + \frac{\partial^4 w}{\partial y^4} \right) &= q - \frac{\partial^2 M^T}{\partial x^2} - \frac{\partial^2 M^T}{\partial y^2}
\end{aligned} \quad (9)$$

while on the edges  $x = 0, a$

$$\begin{aligned}
u^0 &\text{ prescribed, or } N_x = 0 \\
v^0 &\text{ prescribed, or } N_{xy} = 0 \\
w &\text{ prescribed, or } \frac{\partial M_x}{\partial x} + 2 \frac{\partial M_{xy}}{\partial y} = 0 \\
\frac{\partial w}{\partial x} &\text{ prescribed, or } M_x = 0
\end{aligned} \quad (10)$$

(6) and on the edges  $y = 0, b$

$$\begin{aligned}
u^0 &\text{ prescribed, or } N_{xy} = 0 \\
v^0 &\text{ prescribed, or } N_y = 0 \\
w &\text{ prescribed, or } \frac{\partial M_y}{\partial y} + 2 \frac{\partial M_{xy}}{\partial x} = 0 \\
\frac{\partial w}{\partial y} &\text{ prescribed, or } M_y = 0
\end{aligned} \quad (11)$$

whereas at the corners  $(0, 0), (a, 0), (0, b)$  and  $(a, b)$

$$w \text{ prescribed, or } 2M_{xy} = 0 \quad (12)$$

Equations (9) are identical to the governing differential equations obtained using equilibrium

conditions in ► [plates, classical theory](#). Furthermore, the edge and corner conditions (10–12) represent special cases of the boundary conditions presented there.

## Rayleigh-Ritz Method

A variety of methods based upon the principle of minimum potential energy are available for deriving approximate solutions in situations where exact solutions are difficult or impossible to obtain. One such procedure is the Rayleigh-Ritz method, applied here to the problem of plate bending. Accordingly, the displacement field is approximated by functions which contain a finite number of independent coefficients. The assumed functions are chosen to satisfy the kinematic boundary conditions (those involving translations and rotations), but they need not satisfy the static boundary conditions (ones involving forces and moments). The unknown coefficients in the assumed solution are determined by invoking the principle of minimum potential energy. In particular, for the problem of flexure, we represent the transverse displacement  $w$  in the series form

$$w(x, y) = \sum_{m=1}^M \sum_{n=1}^N C_{mn} \phi_{mn}(x, y) \quad (13)$$

where the functions  $\phi_{mn}(x, y)$  satisfy those boundary conditions which involve  $w$ ,  $\partial w / \partial x$  and  $\partial w / \partial y$ . The assumed solution (13) is substituted into the expression for the potential energy  $\Pi$ ; in the case of plate bending  $\Pi$  is given by (see (5))

$$\begin{aligned} \Pi = \int_0^b \int_0^a & \left\{ \frac{D}{2} \left( \frac{\partial^2 w}{\partial x^2} + \frac{\partial^2 w}{\partial y^2} \right)^2 \right. \\ & + (1 - \nu) D \left[ \left( \frac{\partial^2 w}{\partial x \partial y} \right)^2 - \frac{\partial^2 w}{\partial x^2} \frac{\partial^2 w}{\partial y^2} \right] \\ & \left. + M^T \left( \frac{\partial^2 w}{\partial x^2} + \frac{\partial^2 w}{\partial y^2} \right) - q w \right\} dx dy \quad (14) \end{aligned}$$

Application of the principle of minimum potential energy,  $\delta \Pi = 0$ , yields the  $M + N$  simultaneous algebraic equations

$$\frac{\partial \Pi}{\partial C_{mn}} = 0 \quad (m = 1, 2, \dots, M; n = 1, 2, \dots, N) \quad (15)$$

Equations (15) can be solved to obtain the Ritz coefficients  $C_{mn}$ .

General discussions of the choice of approximating functions  $\phi_{mn}(x, y)$  and the convergence of the sequence (13) are given in [6, 7].

As an example of the Ritz technique, consider the thermal deflection of a square plate, simply supported on  $x = 0, a$ , clamped on  $y = 0, a$ , and subject to a uniform thermal moment  $M^T$ . An admissible representation for  $w$  is

$$w = \sum_{m=1}^M \sum_{n=1}^N C_{mn} \sin \frac{m\pi x}{a} \left( 1 - \cos \frac{2n\pi y}{a} \right) \quad (16)$$

The expression (16) satisfies the kinematic boundary conditions of the problem, although it fails to satisfy the static boundary condition  $M_x = 0$  on  $x = 0, a$ . If a single term ( $C_{11}$ ) is retained in (16), the Ritz method yields an approximate deflected shape in which the maximum deflection (occurring at  $x = y = a/2$ ) is equal to  $0.0191a^2 M^T / D$ ; two-term ( $C_{11}, C_{31}$ ) and three-term ( $C_{11}, C_{31}, C_{51}$ ) approximations give the values  $0.0144a^2 M^T / D$  and  $0.0157a^2 M^T / D$ , respectively. The exact value of the displacement, calculated according to the formulation given in ► [rectangular plates, statical problems](#), is  $0.0158a^2 M^T / D$ .

## References

1. Huebner KH (1975) The finite element method for engineers. Wiley, New York
2. Tauchert TR (1986) Thermal stresses in plates – statical problems. In: Hetnarski RB (ed) Thermal stresses I. Elsevier, Amsterdam, pp 23–141
3. Tauchert TR (1974) Energy principles in structural mechanics. McGraw-Hill, New York; (1980) reprinted by Indo American Books, Delhi

4. Boley BA, Weiner JH (1980) Theory of thermal stresses. Wiley, New York
5. Washizu K (1968) Variational methods in elasticity and plasticity. Pergamon, Oxford
6. Courant R, Hilbert D (1953) Methods of mathematical physics, vol 1. Interscience, New York
7. Kantorovich LV, Krylov VI (1958) Approximate methods of higher analysis, 4th edn. Interscience, New York

## Energy Potentials

### ► Thermoelastic Stresses, Variational Methods

## Enhanced Thermal Shock Resistance of Ceramics

Fan Song  
State Key Laboratory of Nonlinear Mechanics  
(LNM), Institute of Mechanics, Chinese  
Academy of Sciences, Beijing, People's  
Republic of China

## Overview

Enhancing the thermal shock resistance of ceramic materials is one of the important objects that researchers have been studying the mechanisms of the thermal shock failure of materials. According to the theories of heat transfer and thermal stresses, the traditional routes enhancing the thermal shock resistance of materials focus mainly on increasing the inherent strength and/or the fracture toughness of the materials themselves. However, the realization of these routes is a very difficult task in practice. In terms of the previous studies on thermal shock failure, Lanin and Fedik [1] already gave a very comprehensive review that had involved the existing mechanisms and methods of enhancing the thermal shock resistance of ceramic materials.

In this section, a heuristic method to make ceramics insensitive to thermal shock will be mainly introduced. This method, which is

recently proposed by Song et al. [2] and is radically different from existing methods, brings a novel concept for increasing the thermal shock resistance of ceramic materials.

## Basic Principle

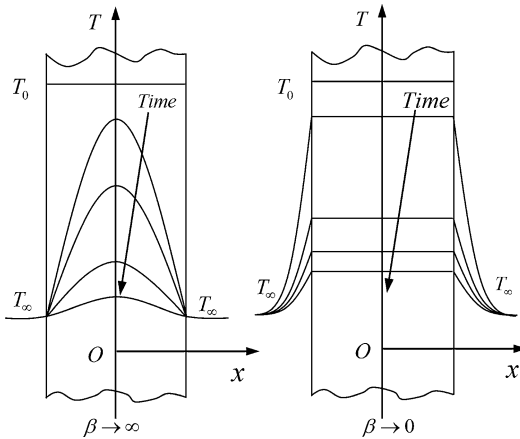
The primary failure mechanism for ceramics in thermal shock is considered to be crack initiation when the stresses imposed by a thermal gradient exceed the strength of the materials [3–5]. Both existing theories and experiments prove that initial cracks occur on the surface of ceramics during cooling, whereas initial cracks occur in the interior of ceramics during heating. According to the theories of heat transfer and thermal stresses, a dimensionless number referred to as Biot's modulus is associated intimately with the thermal gradient generated in the materials during heat transfer and is written by:

$$\beta = \frac{\delta h}{k} = \frac{\delta/k}{1/h} \quad (1)$$

where  $\delta$  is the characteristic dimension of materials,  $h$  is the surface convective heat transfer coefficient, and  $k$  is the thermal conductivity of materials. In addition,  $\delta/k$  stands for the conductive heat transfer resistance of the interior of materials and  $1/h$  is the convective heat transfer resistance of the surfaces of materials. When Biot's modulus limits infinite, i.e.,  $\delta/k \gg 1/h$ , the maximum thermal gradient occurs in the interior of materials during heat transfer, whereas Biot's modulus limits zero, i.e.,  $1/h \gg \delta/k$ , there is no thermal gradient in the materials, as shown in Fig. 1.

This is an indication that if the surface thermal resistance of ceramics,  $1/h$ , can be sufficiently increased so as to make Biot's modulus small enough, the thermal gradient in the interior of the ceramics will also be small enough. So, the thermal stresses generated in the ceramics can be too small to result in the failure of the ceramics in thermal shock. For example, because the convective heat transfer coefficient of water quench,  $h$ , is of the order of magnitude of  $10^4 \text{ W} \cdot (\text{m}^2 \cdot \text{K})^{-1}$ ,





**Enhanced Thermal Shock Resistance of Ceramics, Fig. 1** Schematic illustrations showing the evolution of the temperature profile on the surface of a solid and in the interior of a solid when Biot's modulus  $\beta$  limits infinite and zero, respectively

the heated ceramics will be subject to the thermal shock failure in water quench, whereas as the convective heat transfer coefficient of air,  $h$ , is of the order of magnitude of  $1 \text{ W} \cdot (\text{m}^2 \cdot \text{K})^{-1}$ , the heated ceramics will not be subject to the thermal shock failure in air. Therefore, the problem enhancing the thermal shock resistance of ceramics can be translated into another one, i.e., how to adhere a layer with sufficient low  $h$  on the surfaces of ceramics, and the adhesive layer can be efficiently retained in the course of thermal shock of the ceramics, such as an air layer.

## Case Study

### Materials and Experiments

The ceramic studied herein is a refractory ceramic,  $\text{ZrB}_2$ -20 %  $\text{SiC}_p$ -5 %  $\text{AlN}$  (ZSA). Its flexural strength at room temperature is  $738.6 \pm 45.4 \text{ MPa}$  and the melting point in common atmospheric pressure about  $3,210^\circ\text{C}$ . Specimens were first cut into  $3 \times 4 \times 36 \text{ mm}$  bars at the ambient temperature of about  $20^\circ\text{C}$ , and then heated at a rate of  $10^\circ\text{C}/\text{min}$  up to a preset temperature and held at this temperature for 20 min. After that, the heated specimens were placed into water at the ambient temperature for quenching and

maintained for 10 min. The strength was then measured using three-point bending at the ambient temperature. The experimental results indicate that the quenched specimens exhibit a mean strength identical to that of unquenched one as long as the temperature is smaller than  $400^\circ\text{C}$ . But above this value, the strength suddenly decreased to  $105.4 \pm 47.2 \text{ MPa}$ , which was less than 15 % of their intrinsic strength, as shown in Fig. 2a [2]. Experimental observations proved that there are cracks produced on the surfaces of the ceramics when the quenching temperature was greater than  $400^\circ\text{C}$ , and the higher the temperature is, the more the number of the surface crack is, as shown in Fig. 2b [2].

### Surface Roughening

For the sake of creating an air layer to adhere on the surfaces of the ceramics, the surfaces of the specimens were made by high temperature plasma etching techniques and chemically corroded by the mixed solution of  $\text{HNO}_3$  and  $\text{HF}$ . As a result, the surfaces become rough with nano-scale circular rod fins, as shown in Fig. 3a and b [2]. These nano-fins stand up almost vertically and are randomly distributed on the surfaces of the ceramics. The average diameter, thickness, and numerical density of the nano-fins were measured to be  $d = 81.52 \pm 15.29 \text{ nm}$ ,  $L = 375.18 \pm 32.06 \text{ nm}$ , and  $n = 71 \pm 12 \mu\text{m}^{-2}$ , respectively. The areal fractions of the nano-fins and the void space were calculated to be  $f_M = n\pi d^2/4 \approx 0.37$  and  $f_V = 1 - f_M \approx 0.63$ , respectively, on the rough surface of the ceramic.

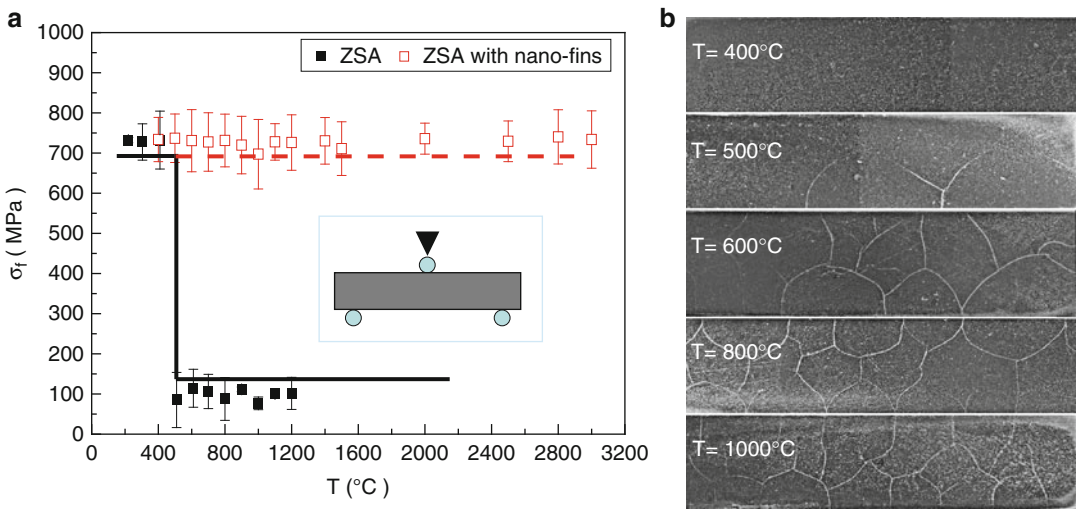
Obviously, the rough surface made of the nano-fins displayed a typical hydrophobic structure [6, 7]. The contact angles of water droplets on the surfaces with and without the nano-fins were measured to be  $\theta_r = 121.6 \pm 2.2^\circ$  and  $\theta_E = 70.6 \pm 1.8^\circ$ , respectively, as shown in Fig. 3a and b inset.

Using the Cassie-Baxter model [8],

$$\cos \theta_{CB} = -1 + f_M(\cos \theta_E + 1) \quad (2)$$

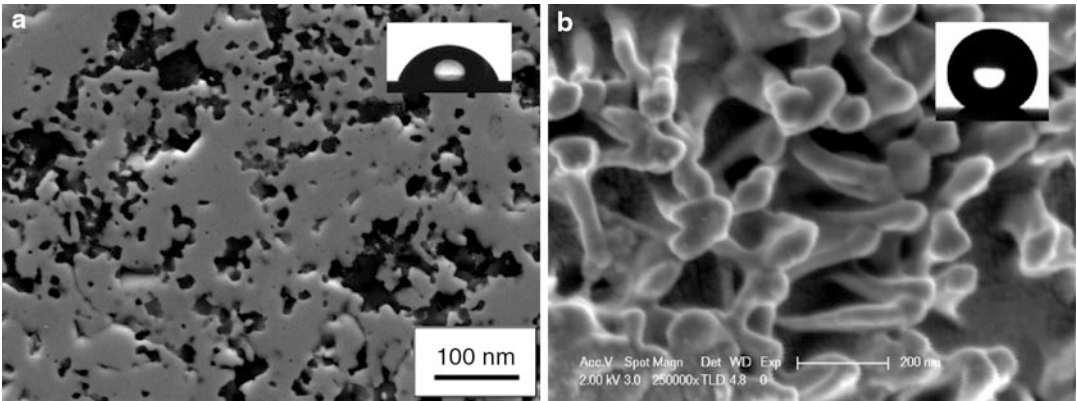
The average water contact angles of the surfaces with the nano-fins were readily computed to be about  $120.5^\circ$ , which was in good agreement





**Enhanced Thermal Shock Resistance of Ceramics, Fig. 2** (a) Experimental results showing the changes of the flexural strength of the ZSAs without and with nano-fins along with the different temperatures of thermal

shock; (b) Microscope images showing the surface cracks of the ZSAs without nano-fins quenched in room temperature water, the initial temperature of the ZSAs are 400, 500, 600, 800, and 1,000 °C, respectively, after Song et al. [2]



**Enhanced Thermal Shock Resistance of Ceramics, Fig. 3** SEM images showing different surface structures. (a) the surface structure of the ZSA without nano-fins, which displays the water contact angles of  $70.6 \pm 1.8^\circ$

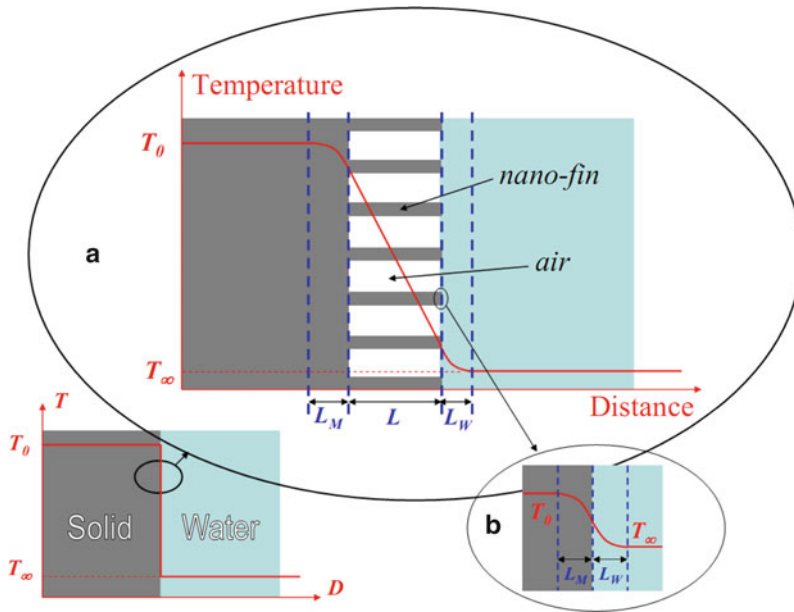
showing in inset; (b) the surface structure of the ZSA with nano-fins, which displays the water contact angles of  $121.6 \pm 2.2^\circ$  showing in inset, after Song et al. [2]

with the experimental results. This demonstrated that there was a thin air layer created by the nano-fins on the actual surfaces of the ceramics when the ceramics quenched into water, the average thickness of which was approximately equal to that of the nano-fins, according to Cassie-Baxter model [6–8], as shown in Fig. 4 inset A. Therefore, the nano-fins not only decreased the surface energy of the ceramics but also yielded a strong

water-repellent force so as to make water unable to contact directly the actual surface of the ceramics during quenching [9].

**Resistance Analysis**

As the flexural strength of the ceramics with the nano-fins after thermal shock was tested again, their flexural strength was retained up to the melting point, as shown in Fig. 1. This result



**Enhanced Thermal Shock Resistance of Ceramics, Fig. 4** Schematic illustrations showing the temperature distribution at the interface between the solid with nano-fins and water during quenching.  $T_0$  and  $T_\infty$  are the initial temperature of the solid and the temperature of water, respectively. Inset A, the interfacial structure composing of the solid, the nano-fins, the entrapped air and water,

where  $L_M$ ,  $L$  and  $L_W$  stand for the lengths of the regions of internal conduction, the interface and the surface convection resistance, respectively. Inset B, the evolution of the temperature profile at the contact interface between the top of a nano-fin and water, which is the same as the interface between the surface of the solid without the nano-fins and water

was an indication that these nano-fins effectively enhanced the heat transfer resistance of the interface between the ceramics and the quenching medium so that the thermal gradient and stresses produced on the surface of the ceramics were largely decreased during thermal shock. In fact, no cracks were observed on the surfaces of the nano-fins after thermal shock.

When the heated ceramic with the nano-fins was quenched into water, the total resistance at the interface can be expressed as:

$$R_t = R_M + R + R_W \quad (3)$$

Equation (3) has contributions from the three regions: the internal region of the ceramic with a characteristic thickness of  $L_M$ ; the surface region of the void space with a characteristic thickness of  $L$ ; and the contact region of water with a characteristic thickness of  $L_W$ , as shown

in Fig. 3 inset A. From the theory of heat transfer,  $R_M = L_M/k_M \approx 1.4 \times 10^{-5} \text{ m}^2\text{KW}^{-1}$ , where  $k_M \approx 60 \text{ W}\cdot(\text{m}\cdot\text{K})^{-1}$  is the thermal conductivity of the ceramic [10] and  $L_M \approx 0.82 \text{ mm}$  is the characteristic dimension of the tested ceramic which is roughly equal to the ratio of the volume and the surface area of material;  $R_W = 1/(f_M h_W) \approx 2.7 \times 10^{-4} \text{ m}^2\text{KW}^{-1}$ , where  $h_W$  is the forced convection coefficient of water and is taken as on the order of magnitude of  $1.0 \times 10^4 \text{ W}\cdot(\text{m}^2\cdot\text{K})^{-1}$  (uncertainties of the convection coefficient of  $\pm 25\%$  were quite common in practice [11, 12]); and  $R \approx f_M (L/k_M) + f_V (1/h_A) \approx 0.63 \text{ m}^2\text{KW}^{-1}$ , where  $h_A$  is the natural convection coefficient of the entrapped air in the void space created by the nano-fins on the surface of the ceramic, which is of the order of magnitude of  $1.0 \text{ W}\cdot(\text{m}^2\cdot\text{K})^{-1}$  [11, 12]. Therefore, the total resistance at the interface was obtained as  $R_t \approx 0.63 \text{ m}^2\text{KW}^{-1}$ , which is an indication that

the total resistance was predominately determined by that of the entrapped air in the void space created by the nano-fins. Moreover, the radiation resistance in the void space was not considered here because it is very small in comparison with the convection resistance yielded by the entrapped air in the void space.

In particular, when the heated ceramic without the nano-fins was quenched into water, the total resistance at the interface was  $r_t = L_M/k_M + 1/h_W \approx 1.14 \times 10^{-4} \text{ m}^2\text{K/W}$ . Therefore, the resistance of the ceramic with the nano-fins was  $R_i/r_t \approx 5.53 \times 10^3$  times greater than that of the ceramic without the nano-fins. Additionally, the Biot's modulus of the ceramic with the nano-fins is  $R_M/(R + R_W) \approx 2.2 \times 10^{-5}$ , which is much less than 0.1 and implies that the temperature of the interior of the ceramic during quenching was uniformly descendent [11, 12], while a steep temperature difference occurred at the interface composed of the nano-fins, as shown in Fig. 4 inset A. Therefore, the strong thermal gradient and stresses produced by the steep temperature difference only acted on the nano-fins rather than the actual surface of the tested ceramic. Because each of the nano-fins was able to expand freely along the direction of their length, there were no strong thermal stresses produced in the interior of the nano-fins, i.e., the nano-fins did not fail during thermal shock. There are the stress concentrations in the immediate vicinity of nano-fins during quenching, but the level of the stress concentrations in comparison with the intrinsic strength of the material is too low to result in the nano-fins and material itself failure.

In conclusion, the main role of nano-fins is to confine all the temperature gradient within the air/nano-fin layer so that the temperature profile remains almost flat within the ceramics during the whole quenching. And since thermal stresses are proportional to temperature gradient rather than temperature, they remain small within ceramics during the whole quenching. Therefore, the high resistance produced by the entrapped air in the nano-fins is such that the ceramics never exhibited the catastrophic reduction of strength and failure by thermal shock until their melting points.

## Future Study

Above case study is just an example, but it brings a heuristic idea: Using other methods besides the traditional methods can also enhance the thermal shock resistance of ceramics. However, still many questions remain that need to be solved in the future. For example, how to control the diameter, thickness, and numerical density of the nano-fins so as to increase the efficiency of thermal resistance, etc. We notice that this study is only employed in the cold quench of heated ceramics. Whether can we find some methods that applied to other types of thermal shock of ceramics or not?

## References

1. Lanin A, Fedik I (2008) Thermal stress resistance of materials. Springer, Berlin/Heidelberg
2. Song F, Meng SH, Xu XH, Shao YF (2010) Enhanced thermal shock resistance of ceramics through biomimetically inspired nanofins. *Phys Rev Lett* 104(12):125–502
3. Fahrenholtz WG, Hilmas GE, Talmy IG, Zaykoski JA (2007) Refractory diborides of zirconium and hafnium. *J Am Ceram Soc* 90(5): 1347–1364
4. Kingery WD (1955) Factors affecting thermal stress resistance of ceramic materials. *J Am Ceram Soc* 38(1):3–15
5. Hasselman DPH (1963) Elastic energy at fracture and surface energy as design criteria for thermal shock. *J Am Ceram Soc* 46(11):535–540
6. Blossey R (2003) Self-cleaning surfaces – virtual realities. *Nat Mater* 2(5):301–306
7. Lafuma A, Quere D (2003) Superhydrophobic states. *Nat Mater* 2(7):457–460
8. Cassie ABD, Baxter S (1944) Wettability of porous surfaces. *Trans Faraday Soc* 40:546–550
9. Gao XF, Jiang L (2004) Water-repellent legs of water striders. *Nature* 432(7013):36
10. Chamberlain AL, Fahrenholtz WG, Hilmas GE, Ellerby DT (2004) High-strength zirconium diboride-based ceramics. *J Am Ceram Soc* 87(6): 1170–1172
11. Holman JP (2002) Heat transfer. McGraw-Hill Education (Asia) Co./China Machine Press, Singapore
12. Incropera FP, DeWitt DP, Bergman TL, Lavine AS (2007) Fundamentals of heat and mass transfer, 6th edn. Wiley, New York

## Entropy and Thermodynamic Temperature

Gerard A. Maugin

Institut Jean Le Rond d'Alembert, Unité mixte de recherche 7190, Université Pierre et Marie Curie, Paris, France

### Overview

*Entropy and thermodynamic temperature* form the fundamental pair of conjugate state variables in thermodynamics. This entry concerns both the “extensive” member of this pair, entropy – its definition in relation to heat and temperature, its introduction as a state function via the Carnot-Clausius theorem, its definite role in the statement of the second law of thermodynamics, and finally its balance for open thermodynamic systems – and the naturally “intensive” member of this pair, thermodynamic temperature. Although entropy finds its sound physical definition in probabilistic notions within the framework of statistical mechanics, here, only the phenomenological approach is reported in view of engineering applications in the thermodynamics of continua. Similarly, while a more comfortable definition of thermodynamic temperature may be based on considerations of statistical mechanics, this entry reports the more engineering-like definition based on the phenomenological considerations of the pioneers, Carnot and Clausius. These considerations are related to the efficiency of heat engines.

### Definition of Entropy

*Entropy*, a term coined by Rudolf Clausius (1822–1888) in 1865, is classically defined as a measure of how much the decay process from hot to cold (as witnessed in Carnot's experiments) has progressed. It was later to acquire a statistical thermodynamics definition whereby entropy is governed by probabilities, and it allows for a decrease in disorder even in a closed system. It served to explain why some

processes permitted by the conservation of energy occur spontaneously while their time reversals do not, although theoretically permitted by the conservation laws. Entropy never decreases in isolated thermodynamic systems (see [2–4]). Its increases correspond to irreversible changes in the system when some energy is expended as waste heat, heat representing the most degraded form of energy. Accordingly, it points to an “arrow of time” for all physical processes, forbidding the existence of any “perpetuum mobile.” It is a non-conserved state function telling that there exists a natural tendency toward the dissipation of useful energy. In Clausius' words, it represents the “transformation contents” of a thermodynamic system during a change of state or, in other words, a measure of energy dispersal at a specific temperature. It can also be said that entropy is a measure of the effectiveness or usefulness of a given quantity of energy [e.g., energy at high temperature (hence lower entropy) tends to be more useful than the same amount of energy at a lower temperature (i.e., higher entropy)].

As a state function entropy depends only on the current state of the system and not on how that state was achieved.

### Definition of Thermodynamic Temperature

Thermodynamic temperature is the *absolute* measure of temperature – given in units called “degrees K” or *kelvins* [4]. It is one of the main parameters of the science of thermodynamics. In statistical physics, temperature arises from the kinetic energy of the vibrational motions of the particles building up matter. In such a framework, thermodynamic temperature is an *absolute* scale because it vanishes at the zero point – i.e., absolute zero – the temperature at which the above mentioned particles have minimal motion and cannot become “colder.” This scale is monotonously increasing from zero up and, therefore, is always positive. “Hotter” relates to higher temperatures and “colder” to lower temperatures. For our purpose, however, a more engineering-like

approach considering the historical development that first analyzed the efficiency of heat engines is enlightening. This will refer to the original work of Sadi Carnot (1796–1832). A heat engine is a device that converts heat into mechanical work, and temperature controls the flow of heat between two systems.

The notion of efficiency is defined thus. The heat engine works between a high (hot) temperature  $T_H$  and a low (cold) temperature  $T_C$ . The work per cycle,  $W_{cycle}$ , done by the heat engine is equal to the difference between the heat energy  $q_H$  put in the system at high temperature and the heat energy  $q_C$  ejected at the low temperature in this cycle. The efficiency of the engine is then defined by

$$Eff = \frac{W_{cycle}}{q_H} = \frac{q_H - q_C}{q_H} = 1 - \frac{q_C}{q_H} \quad (1)$$

Carnot's theorem and the fact that any cycle can be composed of any number of smaller cycles result in that the ratio  $q_C/q_H$  is a function of the respective temperatures at which they occur. This function is a monotonic function  $f(T)$  which by convention can be put equal to  $T$  itself. Thus, (1) yields

$$Eff = 1 - \frac{T_C}{T_H} \quad (2)$$

Then efficiency is one or 100 % for  $T_C = 0$ . Otherwise, it is always less than 1. Because of (1) and (2), we can write

$$\frac{q_H}{T_H} - \frac{q_C}{T_C} = 0 \quad (3)$$

The generalization of this result is none other than the Carnot-Clausius theorem which relates entropy, heat, and temperature [4].

## Relation of Entropy to Heat and Temperature

Entropy is a well-defined quantity at thermodynamic equilibrium (thermostatics) only.

Inspired by the works of Carnot, Clausius has shown that the line integral  $\oint \delta Q/T$  – involving a heat increment  $\delta Q$  at temperature  $T$  – for *reversible* processes is independent of the path. Accordingly, the differential  $dS = \delta Q/T = \delta q_{rev}/T$  defines a state function  $S$  which is called the *entropy*. Indeed, we have (theorem of Carnot-Clausius)

$$\int_{state\ 1}^{state\ 2=state\ 1} \delta Q/T = \int_{state\ 1}^{state\ 2} dS = S(state\ 2) - S(state\ 1) = 0 \quad (4)$$

Clausius also found that at each stage of a cycle, work and heat are not equal, but their difference must be a state function (now called the *internal energy*  $U$ ) that vanishes once the cycle is completed. In terms of differentials, if pressure  $p$  is the only external parameter associated with volume  $V$ , we will have the fundamental relation:  $dU = TdS - pdV$ . This of course shows that entropy and temperature form a conjugate pair of thermodynamic variables. But, in fact, this relation is always true, even if irreversibilities appear in the considered system.

When states at the beginning and end of a cycle differ with a loss of efficiency in the thermal machine, the result (4) is invalidated. As a consequence of Carnot's works on the efficiency of thermal machines, Clausius found that for such an evolution,

$$S(state\ 2) > S(state\ 1) \quad (5)$$

so that entropy can only grow if  $T_2 < T_1$ . As a matter of fact, the entropy change between two thermodynamic states, state 1 and state 2, is generally made of two parts: one part,  $\Delta_{int}S$  relating to a lack of thermal insulation and to mass exchanges (this may also be referred to as entropy change due to interactions with the “surroundings” of the system) and the other part,  $\Delta_iS$  due to the processes taking place inside the system. That is, instead of (5), we should write

$$S(state\ 2) - S(state\ 1) = \Delta_{int}S + \Delta_iS \quad (6)$$

with

$$\Delta_{int}S = 0 \quad (7)$$

when the system is thermally insulated (this corresponds to an *adiabatic path* for the state change) and [5–6]

$$\begin{aligned} \Delta_i S &= 0 \text{ for reversible changes} \\ \Delta_i S &> 0 \text{ for irreversible changes} \\ \Delta_i S &< 0 \text{ for impossible changes} \end{aligned} \quad (8)$$

This is the essence of the second law of thermodynamics. For pure adiabatic processes, the  $\Delta_i S$  in (8) can be replaced by  $\Delta S$  in virtue of (7).

The above-sketched out arguments have been mathematically formalized by C. Caratheodory (1873–1950) early in the twentieth century (see Chapter 2 in Maugin [1]). Following Caratheodory, we can also say that the reciprocal of temperature plays the role of an integrating factor for heat. Accordingly, we can write

$$T = \frac{dq_{rev}}{dS} \quad (9)$$

For a system in which entropy  $S$  is a function  $S(E)$  of its energy, then

$$\frac{1}{T} = \frac{dS}{dE} \quad (10)$$

In continuum thermodynamics where  $\theta$  is commonly used to denote the absolute temperature and  $e = \bar{e}(\eta, \cdot)$  is the internal energy per unit mass while  $\eta$  denotes the entropy per unit mass (thus, an intensive quantity), (9) is written as

$$\theta = \frac{\partial \bar{e}}{\partial \eta} > 0 \quad (11)$$

so that the function  $\bar{e}(\eta, \cdot)$  must be an ever-increasing function of entropy if the *absolute* notion of the thermodynamic temperature is to be respected.

The conjugation relation between entropy and thermodynamic temperature shows in the change

of thermodynamic potential from internal energy  $e$  to Helmholtz free energy  $\psi$  as we have, per unit mass,

$$\psi = e - \eta\theta \quad \text{or} \quad \eta\theta = e + (-\psi) \quad (12)$$

The last of these is a standard Legendre transformation with [7]

$$\theta = \frac{\partial \bar{e}(\eta, \cdot)}{\partial \eta}, \quad \eta = \frac{\partial(-\psi)}{\partial \theta} = -\frac{\partial \bar{\psi}}{\partial \theta}, \quad \psi = \bar{\psi}(\eta, \cdot) \quad (13)$$

where the dot in the functional dependence stands for any other thermodynamic variable such as strain in thermoelasticity. The transformation (12) transforms the convexity of  $e$  with respect of  $\eta$  into the concavity of  $\psi$  with respect to  $\theta$ , from which there follows the non-negativity of the heat capacity (per unit mass and *kelvin*)

$$C = -\frac{\partial^2 \psi}{\partial \theta^2} \geq 0 \quad (14)$$

Important note: The above shows that thermodynamic temperature, just like entropy, is a well-defined physical quantity only at equilibrium. For systems evolving far outside equilibrium, one has to make some strong assumptions about the possible existence of such notions (see [5–7]).

## Balance of Entropy for Open Systems

For an *open* thermodynamic system, we can write the balance of entropy  $S$  in the following general form (a differential rewriting of (6)) [5–6]:

$$\frac{dS}{dt} = \sum_{k=1}^K \frac{dM_k}{dt} \hat{S}_k + \frac{1}{T} \frac{dQ}{dt} + \left( \frac{dS}{dt} \right)_i \quad (15)$$

where the three terms in the right-hand side stand for the net rate of entropy flow due to the flows of mass into and out of the system (here,  $\hat{S}$  is the entropy per unit mass), the rate of entropy flow due to the flow of heat across the boundary of the system, and the rate of entropy generated inside the system.



Equation (15) can be compared to the local equation (per unit actual volume) of *entropy balance* in a continuum without exchange of mass ( $dM_k/dt = 0, \forall k$ ) which can be written as [8–9]

$$\rho \frac{d}{dt}(S^t/\rho) = -\nabla \cdot \mathbf{s} + \rho \hat{\eta} + \rho \tilde{\eta} \quad (16)$$

where  $\rho$  is the mass density at time  $t$ ,  $S^t$  is the entropy per unit volume (hence,  $S^t/\rho$  is intensive) at time  $t$ ,  $\mathbf{s}$  is the (in)flux of entropy,  $\hat{\eta}$  is the entropy source per unit mass, and  $\tilde{\eta}$  is the entropy generated per unit mass at material point  $\mathbf{X}$  in the body. The first two terms in the right-hand side of this equation play the role of the term  $\dot{Q}/T$  of (15), while the last term plays the role of  $\dot{S}_i$ . In standard continuum thermodynamics (cf. [8–9]),

$$\mathbf{s} = \mathbf{q}/\theta, \quad \hat{\eta} = h/\theta \quad (17)$$

where  $\mathbf{q}$  is the (in)flux of heat and  $h$  is the energy source per unit mass in the body. The fact that

$$\tilde{\eta} \geq 0 \quad (18)$$

reflects the second law of thermodynamics (dissipation is positive). It is the aim of irreversible thermodynamics to relate the entropy production  $\tilde{\eta}$  to the various irreversible phenomena which may occur inside the system (see [5, 9] for this aspect).

## References

1. Maugin GA (1999) The thermomechanics of nonlinear irreversible processes. World Scientific, Singapore
2. Zemansky MW (1951; first edition). Heat and thermodynamics, London (last revised edition with co-author R. Dittman, McGrawHill, New York, 1997)
3. Guggenheim EA (1957) Thermodynamics. North-Holland, Amsterdam
4. Kestin J (1966) A course in thermodynamics. Blaisdell, Waltham
5. de Groot SR, Mazur P (1962) Non-equilibrium thermodynamics. North-Holland, Amsterdam, Dover edition, New York, 1984
6. Haase R (1969) Thermodynamics of irreversible processes. Addison-Wesley, New York, Dover edition, New York, 1990
7. Maugin GA (1992) The thermomechanics of plasticity and fracture, C.U.P., U.K. (cf. Appendix 1)
8. Maugin GA (2013) Article “classical thermodynamics” in this ETS
9. Maugin GA (2013) Article “continuum thermodynamics” in this ETS

## Entropy: The Classical View

Janusz Badur and Marcin Lemański  
Energy Conversion Department,  
Institute of Fluid Flow Machinery, Polish  
Academy of Sciences, Gdańsk, Poland

## Overview

The thermodynamic interpretation of entropy concept, consistent with the classical thermodynamics, is presented and discussed in this entry. One can distinguish between two concepts of entropy promoted by famous theorists and scientists of the past times. Their efforts and researches have helped to create the entropy concept for both reversible and irreversible processes. In the first concept (reversible processes), the entropy plays the role of the state parameter and is responsible for the reversible part of the thermal phenomena. The keynote of this group is the thesis of Rankine, which say that “the entropy of the Universe is constant.” Besides Rankine, the researchers such as Carnot, Gibbs, Maxwell, Kestin, and Sieniutycz contributed to the development of this concept of entropy. The second concept of entropy (irreversible processes) was developed by researchers such as Fourier, Clausius, Zeuner, Okatov, Mach, Planck, Ostwald, and Smoluchowski. Ideological keynote of this group was the thesis of Clausius saying that “the entropy of Universe is a half-preserved, it cannot decrease or be constant, can only increase.” The details of these concepts of entropy, both Carnot and Rankine, as well as the concept of entropy created by Clausius are discussed here. Both definitions of entropy are presented in mathematical notation. The main attention is paid to the Clausius entropy, which immediately became inviolable paradigm



of continuum physics, but the line of reasoning of Carnot and Rankine had been forgotten. The semi-conservation law of Clausius entropy was also developed by researchers such as Planck, Duhem, Natanson, Onsager, and Eckart. Finally, Clifford Truesdell decided to define this law in the form of inequality and to name it as the “Clausius–Duhem inequality.”

### Three Concepts of Entropy

Entropy is an abstract concept, occurring in many disciplines and in everyday life. Three main sciences that use it are the thermomechanics (in the British Isles called thermodynamics), statistical physics, and computer science (information science). Therefore, there are at least three, little consistent with each other, definitions of entropy: thermodynamic, statistical, and informational [1, 2]. Although all of these entropies have the same physical dimensions – i.e.,  $(\text{J}/\text{kg}^\circ\text{K})$  – they are not related to each other, and, frankly speaking, they share only a common name.

Fortunately, all three sciences use different mathematical symbols for its determination. Historically speaking, the statistical entropy was intended to generalize the thermodynamic entropy to nonequilibrium states, while the information entropy was created to generalize the notion of statistical entropy on information nonmaterial objects. The consequences of these borrowings are three different concepts that are the foundation of three different disciplines.

It should be emphasized that simultaneously mixing and defining these three concepts, which takes place in textbooks and encyclopedias, is wrong from teaching point of view and harmfully contributes to the understanding of fundamental laws of physics. The fundamental laws of physics in the face of the enormous quantity of facts provided to us every day by advanced measuring tools should be rebuilt again and again in such a way that the concept of entropy found in them their adequate place. If we are to explain, justify, and understand the direction of the processes taking place on all scales of our observations that is not sufficient classical relationship

between entropy and the second law of thermodynamics. What is needed is a continuous change in our paradigm of thinking. However, there is no revision of our views without a clear statement of the reasons and goals which guided us in the past and which perhaps in a hidden manner guiding us today. Hence, it is believed that the history of the evolution of the concept of entropy is implicitly present in the whole process of teaching, application, and understanding. Therefore, the scientific foundations about entropy are presented here in a historical mode, because the main goal of that is to present the essence of this abstract concept to all readers of this encyclopedia. For instance, the readers should know that before Clausius introduced his concept of entropy, he studied the work of Rankine and his concept of entropy. Rankine’s action is not without significance in the further shaping of scientific concepts of entropy, because in the field of basic and fundamental concepts, human knowledge is accumulated and only later transformed into a new quality. This quality could be the concept of Rankine entropy.

Herein, the concept of entropy is confined only to its thermodynamic explanation. It is present with original point of view, which enables numerous attempts describing the problem and the associated second law of thermodynamics to divide into two main groups of reasoning, definition and practical use of this concept.

The first group – reversible process – which includes concepts of entropies of such scientist as follows: Carnot (1824), Rankine (1851), Reech (1853), Gibbs (1873), Thurston (1878), Maxwell (1878), Natanson (1890), Duhem (1901), Kestin (1971), Bejan (1990), and Sieniutycz (1999). These entropies played the role of the state parameter and were responsible for the reversible part of the thermal phenomena. The keynote of this group is the thesis of Rankine (1856) which say that “*the entropy of the Universe is constant*” [3]. Today’s technical thermodynamics and the thermodynamics of reversible processes just grow out of this group of reasoning (endoreversible thermodynamics) [4–6].

The second group – irreversible processes – starting with Fourier (1824), Clausius (1865), Zeuner (1868), Okatov (1855), Mach (1896),

Planck (1900), Ostwald (1896), and Smoluchowski (1914) was further developed, for instance, in the work of Onsager (1931), Eckart (1941), Prigogine (1947), Meisner (1954), Mushik (1960), Müller (1967), Lebon (1980), and Grmela (1999). Ideological keynote of this group was the thesis of Clausius (1865) saying that *“the entropy of Universe is a half-preserved, it cannot decrease or be constant, can only increase.”* There were many works belonged to this group that have attempted to estimate both the growth rate of entropy per 1 year and the limiting value of entropy causing the thermal death of the universe. Extended nonequilibrium thermodynamics (extended irreversible thermodynamics) [7] and nonequilibrium thermodynamics (thermodynamics of irreversible processes) [8, 9] stem from this line of reasoning, in which the primary task is to study irreversible phenomena and calculating the “entropy production.”

These two groups of reasoning are distinguished between each other by mathematical signs. The specific entropy and total entropy are denoted in the first group as  $\eta$  and  $H$ , respectively. In the second group, entropies are indicated as  $s$  and  $S$ , respectively.

## Idea of Carnot Entropy

Sadi Carnot was the first researcher, who set himself the task of creation a theory of heat engines based on the primary laws [10]. He was inspired by the Lagrange’s analytic mechanics, which was developed by his father – Lazare Carnot. However, Carnot did not accept Ampere’s thermal equations of motion, and he reached for a different pattern, i.e., Volta’s weightless electric fluid that in the solid state contains the conservative quantity called a charge. In analogy to this, Carnot proposed to describe the heat phenomenon by means of “the thermal charge” characterized by invariant scalar motion which is induced by both heating and cooling processes. Therefore, if the difference of voltage (temperature) determines the driving force of movement, the amount of thermal fluid

characterizes the stream carrying the charge per unit of time. That the driving force and the topological charge of heat motion is called “temperature” and “entropy” by Carnot, respectively. The working substance is a material carrier of thermal fluid. Hence, scientists often say: the gas entropy.

Carnot forms his theorems concerning thermal engines based on the law of conservation of entropy, which says that *after summing up all entropy changes that occur during the engine cycle due to heating and working processes, the entropy of the working body returns to the initial point.* This spoken law can be mathematically written as follows:

$$\oint \left( \frac{d}{dt} H \right) d\tau = \oint \left( \frac{d}{dt} \int \int \int_V \rho \eta dv \right) d\tau = 0. \quad (1)$$

Although, it refers to the conservation of the total entropy  $H$ , which is located in the working body (solid, fluid)  $B$  having a volume  $V$ , but it can be easily determined by the specific entropy  $\eta$  contained in a unit mass of the working fluid  $B$ . In this equation, the time  $\tau$  means the integration parameter. Hence, it differs from the local time  $\tau$  (Kestin 1966).

It is known that Carnot took into account only two processes of working fluid  $B$  in all five of his considered engines. The first process is the most essential to the concept of the ideal heat engine working without “unnecessary entropy losses.” It is based on specific and impossible to realize simultaneous processes of heating and working. It is important that these processes, specified by the mechanical energy flux  $\vec{\mathcal{F}}_{work}$  and thermal energy flux  $\vec{\mathcal{F}}_{heat}$ , took place on two disjoint surfaces limiting the volume  $V$  occupied by the agent  $B$ , i.e.,  $\partial V = A = A_{work} \cup A_{heat}$ . Ideality of the process lies in the fact that a reserve of agent internal energy during this process remains constant but the energy supplied as heat to the surface  $A_{heat}$  is instantaneously (elastically) converted to work as form of outgoing energy on the surface  $A_{work}$ . Therefore, it is a transformation with a constant internal energy of working fluid  $B$ . Presentation of this process is more complicated

from the standpoint of “thermal fluid.” Agent  $B$  touches the heat reservoir on its surface, so as result it has the same temperature which has a heat reservoir ( $\theta = \text{const}$ ), but the amount of agent entropy simultaneously increases. Weightless thermal fluid interacts with its carrier, i.e., working fluid in which it causes the changes in pressure and volume (or the stress and deformation – in the solid state). This allows on the induction of mechanical energy flux on the surface  $A_{\text{work}}$ , called “working” by Carnot (in French: *puissance motrice*). This “iso-energetic” transformation is named by Carnot as “drawing entropy” (heating) or “returning entropy” (cooling).

The amount of drawing entropy or on the other hand, its growth during the iso-energetic process taking place from time  $\tau_1$  to  $\tau_2$  is defined by Carnot by means of the first in the history, constitutive equations of thermoelasticity, who say about it as the “geometric formula” [10]:

$$d_{1,2}\eta = \eta_2 - \eta_1 = R \ln\left(\frac{v_2}{v_1}\right) \quad (2)$$

A unit of Carnot entropy is  $1.228 \text{ [kJ/(kg}^\circ\text{K)]}$ , but  $R = 0.3 = c_p - c_v$  is a constant elastic value discovered by him and always the same for all analyzed gases. In their calculations of ideal thermal cycles, Carnot uses the law of conservation of entropy (1) for the thermal cycle having only two iso-energetic transformations using the equation (2):

$$\oint (d\eta) d\tau = (\eta_2 - \eta_1) + (\eta_4 - \eta_3) = 0 \quad (3)$$

which can be interpreted in the following manner: *Drawing entropy during the process 1–2 is returned in the process 3–4.*

The entropy flux is another basic concept that Carnot verbally introduces. He stresses that the process of heating takes place at the interface of solid body (heater) and the working fluid  $B$ . The influx of thermal fluid and simultaneous thermal charge transfer happen even though both bodies have the same temperature. This charge is the entropy. The charge per unit area and per second

is called the entropy flux, and it is a vector indicated as  $\vec{h}$ , because the entropy itself is a scalar.

Mathematically speaking, we are interested in the influx that is only the component of the vector  $\vec{h}$  that is normal to the influx surface, i.e.,  $h_n = \vec{h} \cdot \vec{n}$ . Entropy flux cannot act in any quantities, because after passing the whole engine cycle, the entropy of working body returns to base level. Therefore, the total entropy flux, drawing and returning, in all processes have to be equal to zero:

$$\oint \left( \iint_{A_{\text{heat}}} \vec{h} \cdot \vec{n} dA \right) d\tau = 0 \quad (4)$$

The entropy flux is realized in Carnot engine only when the agent touches a heater surface at area  $A_{\text{hot}}$  or a cooler surface at area  $A_{\text{cold}}$ , then the whole area is equal to  $A_{\text{heat}} = A_{\text{hot}} \cup A_{\text{cold}}$ . Hence, (4) can be rewritten as follows:

$$\begin{aligned} \int_1^2 \left( \iint_{A_{\text{hot}}} \vec{h} \cdot \vec{n} dA \right) d\tau + \int_3^4 \left( \iint_{A_{\text{cold}}} \vec{h} \cdot \vec{n} dA \right) d\tau \\ = H_{1,2} + H_{3,4} = 0 \end{aligned} \quad (5)$$

and this equation can be interpreted in the following manner: *Drawing entropy flux in the upper heat source (hot) is entirely returned to the bottom heat source (cold).* The indexes 1, 2, 3, 4 mean starting and ending time point of interaction between agent and entropy source.

Carnot, speaking of the concept of entropy sources, several times recalls enigmatically about the inevitable losses of entropy, the incomplete reduction of entropy or entropy leaks, etc. using verbs relevant to irreversible processes. If the thermal fluid would have unknown origin internal sources of entropy, say  $\sigma_\eta$  they would result in a loss of entropy in one place and simultaneously a gain of entropy elsewhere. Nevertheless, if the entropy of agent  $B$  is to be invariant of engine cycle, the sources have to compensate each other, i.e.,

$$\oint \left( \iiint_V \rho \sigma_\eta dv \right) d\tau = 0 \quad (6)$$

In summary, (1), (4), and (6) describe the primary law of the engine cycle for which Carnot considers and proposes integrated laws. Hence, there are no statements about the local entropy balance in his work. It can be anticipated as a local law both in time and space that will be the equivalent of integral conservation laws of entropy (1), entropy flux (4), and entropy sources (6):

$$\iiint_V \left( \rho \frac{d}{dt} \eta = \operatorname{div} \vec{h} + \rho \sigma_n \right) dv \quad (7)$$

which is a combination of three integral terms of Carnot. There will be no exaggeration to say that Sadi Carnot is the author of the law of conservation of entropy, sometimes identified with the second law of thermodynamics. It was established before the law of conservation of energy, which is the first principle of thermodynamics.

Carnot also considers engine cycles on the basis of the another thermodynamic transformation, in which entropy fluxes are equal to zero, but the agent  $B$  still works using the accumulated internal energy decreasing simultaneously its potential. This second process is characterized by a constancy of entropy. Hence, this transformation is called by Carnot a constant entropy process. In its calculations for infinitesimal cycles, he used his second constitutive law expressing the specific volume as a function of pressure  $p$  and absolute temperature,  $\theta = c + 267$  [10]:

$$pv = R(c + 267) \quad (8)$$

where  $c$  is an empirical Celsius temperature.

This means that the two constitutive laws, i.e., (2) and (8) are only needed to calculate both the work cycle and heat cycle per mass unit of substance  $B$ . Nowadays, these laws are known as caloric and thermal equations of state. However, the Carnot cycle has to consist of two processes with constant entropy and two additional transformations with constant internal energy. In all of these four transformations, the mechanical energy fluxes occur on the area  $A_{work}$ .

Their sum leads to an integral quantity defined as the work cycle:

$$\mathcal{F}_{work}^{cycle} = \oint_{1 \cup 2 \cup 3 \cup 4} \left( \iint_{A_{work}} \vec{\mathcal{F}}_{work} \cdot \vec{n} dA \right) d\tau \quad (9)$$

Carnot's successors asked each other how to determine the work cycle. Finally, the work cycle was calculated based on the available thermal energy of fuel supplied by heater, as follows:

$$\begin{aligned} \mathcal{F}_{work}^{cycle} &= C \mathcal{F}_{heat}^{1,2} \\ \mathcal{F}_{heat}^{1,2} &= \int_1^2 \left( \iint_{A_{hot}} \vec{\mathcal{F}}_{heat} \cdot \vec{n} dA \right) d\tau \end{aligned} \quad (10)$$

where the main task is to find the proper expression for the Carnot function  $C$  in (10).

## Idea of Rankine Entropy

Carnot's laws of conservation of entropy, its flux and source, as well as his multiplicative constitutive equations (2) and (8) have not been accepted by successors. Therefore, a new concept of entropy, constructed by Rankine (1849), has been not referred to the Carnot cycle. Only in 1851, vaguely in the commentary to the Carnot cycle, Rankine gives a set of mathematical formulas used for his calculations with the apparent participation of entropy, which is called the thermodynamic function and is marked out as a letter  $\phi$  [11]. Rankine presents also the first time in the literature the visual diagram  $p - v$  of processes taking place in Carnot engine. Referring to the Stokes work (1851) concerning the heat flux  $\vec{\mathcal{F}}_{heat}$ , Rankine proposes to join the flux of thermal energy with the entropy flux by the following relationship:

$$\vec{\mathcal{F}}_{heat} = (\theta + \kappa) \vec{h} \quad (11)$$

This allowed him to rewrite the formula (5) as the formula expressed rather than flux of thermal energy or entropy flux [11]:

$$\int_1^2 \left( \iint_{A_{hot}} \frac{\vec{\mathcal{F}}_{heat} \cdot \vec{n}}{(\theta_{hot} + \kappa)} dA \right) d\tau + \int_3^4 \left( \iint_{A_{cold}} \frac{\vec{\mathcal{F}}_{heat} \cdot \vec{n}}{(\theta_{cold} + \kappa)} dA \right) d\tau = 0 \quad (12)$$

This equation talks nothing about equality of the heat collected in heater and devoted in the cooler. It is essentially a different conclusion than the one which concluded by Clapeyron (1834), Kelland (1937), Thompson (1849), Poggendorff (1843), Clausius (1850), Reech [12], and Zeuner [13]. In the above-mentioned formulas, there is Rankine absolute temperature  $\theta$  heightened by a constant temperature of the background  $\kappa$  – nowadays identified with the temperature vacuum of space.

The researchers regards to the problem of the relationship of thermal energy flux and entropy flux by dichotomous way [14]. For instance, when more general cases of working fluid are considered and when the reserve of internal energy depends not only on the entropy but entropy gradients, i.e., time or spatial, then Rankine formula (11) is not in force, and new formula of thermal energy flux  $\vec{\mathcal{F}}_{heat}^{inter}$  should be used. This new quantity is called “interstitial heating” [9]. The researchers belonging to the first group, i.e., reversible processes, use the following formula:  $\vec{\mathcal{F}}_{heat} = \theta \vec{h} + \vec{\mathcal{F}}_{heat}^{inter}$ , whereas authors representing the second group, i.e., irreversible processes and entropy of nonequilibrium (Müller 1971, [7]), employ the formula with an extra entropy flux defined as follows:  $\vec{h} = \frac{\vec{\mathcal{F}}_{heat}}{\theta} + \vec{k}$ . This means that both lines of approach to the problem of the definition of entropy differ not only in interpretation but in the mathematical formulation.

It should be emphasized that the concept of Rankine entropy in his pictorial presentation was not referred to Carnot’s “thermal charge” and was based on the idea of “vortex atom” in which the Rankine anticipates spinning electron carries circulating movement around the nucleus. Entropy was here a function of velocity vortex (spin), and the temperature was a function of the angle of the spin axis relative to the plane of the circulating movement. Using such a mental model can

explain what the internal energy is. Additionally, it can be shown that the conversion of thermal flux into the mechanical flux takes place at the level of “vortex atom.”

Reech [12] took over and developed the concept of Rankine entropy, proposing its designation by the letter, first as  $u$  and later as  $n$ . He proposed a systematization of the elastic constitutive equations – thermal:  $v = f(p, \theta)$  and caloric:  $\eta = f(p, \theta)$  [12], determining the specific volume and entropy as a function of the pressure and temperature and more importantly showed the relationship of these equations with the internal energy (so-called hyperelasticity) and the rate representation of these equations (hypoelasticity). In addition, he also correctly defined the free energy, enthalpy, and free enthalpy.

Gibbs (1873) put down entropy the same role of state parameter and marked it finally by the letter  $\eta$ . He finally made possible including of entropy balance in the overall energy balance writing the material increase in the internal energy through the parameters of the state [4]. At the same time, Gibbs develops Rankine’s geometric thermodynamics enriching it with the basic graphs and diagrams, because he wants to give thermodynamics a good geometric representation. He represents the surface of the internal energy as a function of volume and specific entropy and a temperature–entropy diagram for the Carnot cycle and also shows a geometric explanation of way to increase the efficiency of thermal cycle.

## Idea of Clausius Entropy

Conception of Clausius is the foundation of the second line of reasoning – assuming that the entropy is a certain invariant which measures human anthropocentric attitude to the surroundings. It is possible to observe and measure only irreversible phenomena occurring in it. The researchers of this group adopted from of everyday life many verbs denoting unidirectional natural phenomena: viscosity, resistance, friction, diffusion, dissolution, dispersion, mixing, etc.

Clausius had no great problems of interpretation – he already announced in the titles of his works that explores “the mechanical theory of heat,” which today is the view that the phenomenon of heat can be reduced to mechanical phenomenon, and these are described by a universal law of Newton. In the paper “On some extended form of the second law of thermodynamics,” Clausius (1854) acknowledges that the mechanical laws of heat motion have to be limited to a certain subclass of movements creating irreversible effects. Nevertheless, Clausius accepts Rankine’s equation (12) of entropy flux fading in engine cycle, writing it in the following form [15]:

$$\frac{Q_1}{T_1} + \frac{Q_2}{T_2} = 0 \quad \text{or} \quad \oint \frac{dQ}{T} d\tau = 0 \quad (13)$$

appropriate respectively to the Carnot cycle or any cycle. The entropy flux is called “compensated heat transformation” by Clausius (*kompensierte Verwandlung*). At this stage of consideration, it does not appear even the concept of entropy, although there is the notion of “uncompensated heat transformation”:  $N = \int \int \int_V \rho n_s dv$ . In 1862, when Clausius was working in parallel on the foundations of the kinetic theory of gases, he made an unsuccessful attempt to define entropy. The entropy was called “disgregation” and marked with the letter  $Z$ . Clausius rejects “disgregation” and introduces the concept of entropy until the next paper from 1865:

$$S = \int \int \int_V \rho s dv \quad (14)$$

Unfortunately, it comes here to write unfortunate and unintended mathematical notion, because the author’s intention was to deepen understanding of the abstract concept. In fact, Clausius contributed to the largest-ever study of ambiguity concerning a manner of definition of entropy [15]:

$$dS = \frac{dQ}{T} \quad (15)$$

This formula should be treated as a local in time but global in space (in the entire volume of the body) balance of Carnot entropy (7) restricted to the thermodynamic processes in which the uncompensated heat is equal to zero:  $N = 0$ .

Herein, saying such a radical statement one can cite earlier thesis of Clausius spoken as follows (1854): “*The sum of the compensated heat transformation of any thermal cycle is equal to the uncompensated heat transformation*,” which can be written as [15]

$$N + \oint \frac{dQ}{T} = 0 \quad (16)$$

Therefore, it is a prototype of semi-conservation law of entropy, but that does not appear explicitly in the entropy itself, because Clausius following the Carnot and Rankine, tacitly assumes that all entropy changes in the engine cycle are compensated:  $\oint dS d\tau = 0$ . Definition (15) made a lot of trouble to mathematicians. They developed a special formalism “differential forms” in which temperature played the role of “an integrating factor” (factor of proportionality, integrating factor, etc.) or any function dependent on temperature, which Müller (1970, [7]) called the “coldness.” Combining the growth of entropy, entropy fluxes, and uncompensated entropy source together, Clausius receives the semi-conservation law of entropy in the time interval  $\tau_0 - \tau$  (1865) [15]:

$$S - S_0 = \int_{\tau_0}^{\tau} \frac{dQ}{T} d\tau + N_{0-\tau} \quad (17)$$

In the sense of form, it is a law integral in both time and space. Nevertheless, in the sense of mathematical content, it is identical with the local conservation law of Carnot entropy. The only distinguishing element in this equation is a postulate independently spoken by Clausius, that “uncompensated heat transformation is always positive  $N > 0$ .” In the case of the Universe, modeled as a “perfect rarefied gas,” which instead of molecules has solar systems, entropy fluxes on its corners should be zero. Hence, it results from Equation (17) that the



entropy of the Universe continues to grow from some initial entropy  $S_0$ . Needless to say, that the last statement, terminating the famous work of Clausius, is still a source of new discussions, especially among the newly educated philosophers of nature.

## Clausius–Duhem Inequality

This above-mentioned semi-conservation law of Clausius entropy immediately became inviolable paradigm of continuum physics, but the line of reasoning of Carnot, Rankine, Reech, or Gibbs had been forgotten. Although, semi-conservation law of entropy, until the formation of the foundations of the kinetic theory of gases, was operated mainly for the development of the statistical approach introduced by Boltzmann, Hirn, Meyer, Stephen, Warburg, and others. It was used by a few researchers such as Planck (1899, [14]) and Duhem [16–18] on phenomenological basis. There was a need to define precisely this law only after the works of Natanson [8], Onsager (1931), Eckart [19] and others, because they gave the foundation for nonequilibrium thermodynamics (see, Sieniutycz [6]). In 1952, Truesdell decided to give it a form of inequality and to name the “inequality of Clausius–Duhem” [20]:

$$\frac{d}{dt}H > \iint_{A_{heat}} \frac{1}{\theta} \vec{\mathcal{F}}_{heat} \cdot \vec{n} dA + \iiint_V \rho \frac{r}{\theta} dv; \quad (18)$$

where  $H = \iiint_V \rho \eta dv$

This inequality can easily be written in the local form as follows:

$$\rho \frac{d}{dt} \eta > div \left( \frac{\vec{\mathcal{F}}_{heat}}{\theta} \right) + \rho \frac{r}{\theta} \quad (19)$$

Unfortunately, Truesdell – the founder of the analytical form of semi-conservation law of entropy – speaking by means of his pictorial language, saddled this inequality to some “the original sin.” He was the only one of the few

modern researchers who was aware that there are two entropy definitions in thermodynamics, i.e.,  $\eta$  and  $S$ . They are associated with the two approaches: reversible and irreversible, but Truesdell when speaking of the Clausius inequality, he did not use his original designation:  $S$  or  $s$ , which even today is clearly associated with nonequilibrium thermodynamics of Onsager. He probably had already called to pierce the soap bubble of the Onsager theory. Taking this into account, the removal of Clausius  $S$  from the formula and inserting competitive Gibbs marking  $\eta$  instead of it should be acclaimed in the science as a cardinal error. The next two errors of Truesdell, which contains the inequality (18), is that he uses thermal energy flux  $\vec{\mathcal{F}}_{heat}$  and sources of internal energy  $r$  in the entropy balance equation. Instead of it, he should use the entropy flux  $\vec{h}$  and uncompensated heat transformation  $n_s$ . Especially, the internal energy source, appearing *ex cathedra*, is an illegal extension of Clausius concept of heat to all other forms of energy.

Nowadays, Clausius–Duhem inequality (19) plays a special role in continuum thermodynamics, and it is the basis for determining the restrictions on the constitutive constants appearing in the describing equations. In practice, this equation is used in the manner outlined by Eckart [19] and Truesdell [20]. The first method was developed by Liu and Müller and is called “the procedure of Liu multipliers,” while the second one, based on the elimination of the internal energy source, was developed by Coleman and Noll (1963) and is called “Coleman–Noll procedure” [9]. There are also many papers showing the relationship of inequality (19) with the second law of thermodynamics [1, 5].

In summary, there are two distinct lines of reasoning in the phenomenological approach, which lead to the conservation or semi-conservation laws of entropy. The semi-conservation law of entropy has become a starting point for statistical and computer recognition of the problem [1]. Therefore, common understanding of entropy as a parameter measuring the degree of chaos is opposed to used by professionals the concept of Carnot entropy, reflecting the highest order of thermal motion.



## References

1. Falk G, Ruppel W (1976) *Energie und entropie*. Springer, Berlin
2. Fuchs FU (1996) *The dynamics of heat*. Springer, New York
3. Maxwell JC (1871) *Theory of heat*. Longmans Green and Co., London
4. Kestin J (1966) *A course of thermodynamics*, vol I. Blaisdell, Waltham/Toronto
5. Kestin J (1968) *A course of thermodynamics*, vol II. Blaisdell, Waltham/Toronto
6. Sieniutycz S (1994) *Conservation laws in variational thermo-hydrodynamics*. Kluwer Academic, Dordrecht
7. Muller I, Rugerri T (1993) *Extended thermodynamics*, vol 37, Springer tracts in natural philosophy. Springer, New York
8. Natanson W (1903) Inertia and coercion. *J Phys Chem* 7:118–135
9. Wilmański K (2008) *Continuum thermodynamics*. World Scientific, Hackensack
10. Carnot S (1824) *Reflexions sur la Puissance Motrice du feu el sur les Machines Propres a Developper cette Puissance*. Paris Bachelier, pp. 1–118 (1824) [rep. *Ann. Ecole Normale* (2) 1,393–457 (1872)]
11. Rankine WJ (1880) *Miscellaneous scientific papers*. Charles Griffin, London
12. Reech MF (1853) *Theorie generale des effects dynamique de la chaleur*. *J Math Pures Appl* 18:357–568
13. Zeuner G (1898) *Technische Thermodynamik*. A Felix, Berlin
14. Planck M (1879) *Über den zweiten Hauptsatz der Mechanischen Wärmetheorie*. Engelmann, München
15. Clausius R (1870) *Abhandlungen über der Mechanische Wärmetheorie Erste Abtheilung*. Dechsler, Branschweig
16. Duhem P (1901) *Reserches sur l'hydrodynamique*. *Ann Toulouse* 3:315–377, 379–431
17. Duhem P (1902) *Reserches sur l'hydrodynamique*. *Ann Toulouse* 4:101–169
18. Duhem P (1903) *Reserches sur l'hydrodynamique*. *Ann Toulouse* 5:5–61, 197–255, 353–404
19. Eckart C (1940) The thermodynamics of irreversible processes. *Phys Rev* 58:267–269
20. Truesdell C (1952) The mechanical foundation of elasticity and fluid dynamics. *J Ration Mech Anal* 1:125–300, errata (1953) 2:593–616

## Equation of Heat Conduction

► [Constitutive and Geometrical Equations for the Thermomechanical Analysis of Shells](#)

## Equation of Motion: Scalar Formalisms and Theory

M. Shimada and Kumar K. Tamma  
Department of Mechanical Engineering,  
University of Minnesota, Minneapolis,  
MN, USA

## Overview

The derivations of strong and weak forms of Cauchy's first equation of motion in the sense of the scalar formalisms, namely, from Hamilton's principle and from the principle of balance of total energy for an isothermal continuum body, are briefly summarized. In the scalar formalisms, unlike the vector formalism, we mainly deal with the scalar-valued functions, that is, the autonomous Lagrangian function and the autonomous total energy function of an isothermal continuum body, which is sometimes called the autonomous mechanical energy in the literature, and the autonomous Hamiltonian function, which is equivalent to the autonomous mechanical energy function. Both Hamilton's principle and the principle of balance of mechanical energy are consequences of Cauchy's first equation of motion. Once the Cauchy's first equation of motion in the Lagrangian and Hamiltonian mechanics is derived, the spatially discrete forms are readily obtained following the Galerkin finite element method.

## Hamilton's Principle and the Principle of Balance of Mechanical Energy

In this section, we derive the strong form of the initial boundary-value problem and its weak form for isothermal elastodynamical systems from Hamilton's principle and the principle balance of mechanical energy (in the Lagrangian and Hamiltonian mechanics frameworks).

### Hamilton's Principle

#### Lagrangian Mechanics Framework

Consider a continuum body in three-dimensional Euclidean space,  $\mathbb{R}^3$ , and define a smooth

configuration manifold  $\mathcal{C}$  for the admissible motion map  $\varphi(\mathbf{X}, t) : \mathcal{B} \times \mathbb{I} \rightarrow \mathcal{S}$ :

$$\mathcal{C} := \left\{ \varphi : \mathcal{B} \times \mathbb{I} \rightarrow \mathcal{S} \subset \mathbb{R}^3 \mid \varphi \in C^{2m}(\mathcal{B}), m \geq 1, \right. \\ \left. \varphi_{\mathbf{X}} \in C^2(\mathbb{I}), \det(\text{GRAD}\varphi) = |\mathbf{F}| > 0, \text{ and } \varphi|_{\partial\mathcal{B}_\varphi} = \bar{\varphi} \right\} \quad (1)$$

where  $\mathcal{B}$  denotes the reference configuration of the continuum body as an open, bounded, and simply connected set with a smooth boundary open set  $\partial\mathcal{B} = \partial\mathcal{B}_\sigma \cup \partial\mathcal{B}_\varphi$  with  $\partial\mathcal{B}_\sigma \cap \partial\mathcal{B}_\varphi = \emptyset$  in a topological space,  $\mathcal{S}$  denotes the current configuration, and  $\mathbb{I} = [t_0, t_N]$  with initial time  $t_0 = 0$  and final time  $t_N > t_0$  denotes the time interval;  $\mathbf{X} \in \mathcal{B}$  is a material point, that is, the position of a particle in  $\mathcal{B}$ ,  $\mathbf{F}(\mathbf{X}, t) = \text{GRAD} \varphi$  is the deformation gradient second-order tensor field, and  $\bar{\varphi}$  is the prescribed quantity in  $\partial\mathcal{B}_\varphi \times \mathbb{I}$ . Note that GRAD denotes the gradient operator of vector fields in  $\mathcal{B}$  with respect to the material point  $\mathbf{X} \in \mathcal{B}$ . The tangent bundle (infinite dimensional state space) associated with  $\mathcal{C}$  may be defined as

$$TC := \{(\varphi, \dot{\varphi}) : \mathcal{B} \times \mathbb{I} \rightarrow \mathbb{R}^3 \times \mathbb{R}^3 \mid \varphi \in \mathcal{C}, \\ \dot{\varphi} \in T_\varphi \mathcal{C}, \text{ and } \dot{\varphi}|_{\partial\mathcal{B}_\varphi} = 0\} \quad (2)$$

Define an autonomous Lagrangian  $\mathcal{L}(\varphi, \dot{\varphi}) : TC \rightarrow \mathbb{R}$  with dead loads as

$$\mathcal{L}(\varphi, \dot{\varphi}) := \int_{\mathcal{B}} \mathcal{L}(\varphi, \dot{\varphi}, \mathbf{F}) dV \\ + \int_{\partial\mathcal{B}_\sigma} \bar{\mathbf{T}}(\mathbf{X}, t, \hat{\mathbf{N}}) \cdot \varphi(\mathbf{X}, t) dA \quad (3)$$

where  $\bar{\mathbf{T}}(\mathbf{X}, t, \hat{\mathbf{N}})$  denotes the prescribed material traction vector field on  $\partial\mathcal{B}_\sigma$  at time  $t \in \mathbb{I}$ ,  $\hat{\mathbf{N}}(\mathbf{X}, t)$  denotes the outward unit normal vector field in the material description on  $\partial\mathcal{B}_\sigma$  at  $t \in \mathbb{I}$ , and  $\mathcal{L}(\varphi, \dot{\varphi}, \mathbf{F})$  denotes the Lagrangian density function given by

$$\mathcal{L}(\varphi, \dot{\varphi}, \mathbf{F}) := \frac{1}{2} \rho_0 \dot{\varphi}(\mathbf{X}, t) \cdot \dot{\varphi}(\mathbf{X}, t) \\ - \rho_0 \Psi(\mathbf{F}) + \rho_0 \mathbf{B} \cdot \varphi(\mathbf{X}, t) \quad (4)$$

where  $\Psi(\mathbf{F})$  denotes the Helmholtz free energy per unit mass in homogeneous materials as an elastic potential function in  $\mathcal{B}$ ,  $\rho_0(\mathbf{X}) \equiv \rho(\mathbf{X}, t_0)$  denotes the material density, and  $\mathbf{B}(\mathbf{X}, t)$  denotes the material body force vector field. Define the action map  $S : \Xi(\mathcal{C}) \rightarrow \mathbb{R}$  as

$$S[\varphi] := \int_{t_0}^{t_N} \mathcal{L}(\varphi, \dot{\varphi}) dt \quad (5)$$

defined in the smooth manifold

$$\Xi(\mathcal{C}) = \Xi(\mathbb{I}, \mathcal{C}) = \{\varphi : \mathcal{B} \times \mathbb{I} \rightarrow \mathcal{C} \mid \varphi \text{ is a } C^2 \text{ curve.}\} \quad (6)$$

Hamilton's principle reads

$$\delta S = \delta \int_{t_0}^{t_N} \mathcal{L}(\varphi, \dot{\varphi}) dt \\ = \delta \int_{t_0}^{t_N} \int_{\mathcal{B}} \mathcal{L}(\varphi, \dot{\varphi}, \mathbf{F}) dV dt \\ + \delta \int_{t_0}^{t_N} \int_{\partial\mathcal{B}_\sigma} \bar{\mathbf{T}} \cdot \varphi(\mathbf{X}, t) dA dt = 0 \quad (7)$$

with  $\delta\varphi(\mathbf{X}, t_0) = \delta\varphi(\mathbf{X}, t_N) = 0$

for holonomic systems with dead loads. The boundary conditions,  $\delta\varphi(\mathbf{X}, t_0) = \delta\varphi(\mathbf{X}, t_N) = 0$ , imply that the configurations at both  $t_0$  and  $t_N$  must be prescribed. Equation (7) yields

$$\begin{aligned}
\delta S &= \int_{t_0}^{t_N} \int_B \delta \mathcal{L}(\varphi, \dot{\varphi}, \mathbf{F}) dV dt \\
&\quad + \int_{t_0}^{t_N} \int_{\partial \mathcal{B}_\sigma} \bar{\mathbf{T}} \cdot \delta \varphi(\mathbf{X}, t) dA dt \\
&= \int_{t_0}^{t_N} \int_B \left[ \frac{\partial \mathcal{L}}{\partial \varphi} - \frac{d}{dt} \left( \frac{\partial \mathcal{L}}{\partial \dot{\varphi}} \right) - \left( \text{DIV} \frac{\partial \mathcal{L}}{\partial \mathbf{F}} \right) \right] \cdot \delta \varphi dV dt \\
&\quad + \int_{t_0}^{t_N} \int_B \text{DIV} \left( \delta \varphi \cdot \frac{\partial \mathcal{L}}{\partial \mathbf{F}} \right) dV dt \\
&\quad + \int_{t_0}^{t_N} \int_{\partial \mathcal{B}_\sigma} \bar{\mathbf{T}} \cdot \delta \varphi dA dt + \int_B \frac{\partial \mathcal{L}}{\partial \dot{\varphi}} \cdot \delta \varphi dV \Big|_{t_0}^{t_N} = 0
\end{aligned} \tag{8}$$

Using the Gauss theorem and the boundary conditions,  $\delta \varphi(\mathbf{X}, t_0) = \delta \varphi(\mathbf{X}, t_N) = 0$ ,

$$\begin{aligned}
\delta S &= \int_{t_0}^{t_N} \int_B \left[ \frac{\partial \mathcal{L}}{\partial \varphi} - \left( \text{DIV} \frac{\partial \mathcal{L}}{\partial \mathbf{F}} \right) - \frac{d}{dt} \left( \frac{\partial \mathcal{L}}{\partial \dot{\varphi}} \right) \right] \cdot \delta \varphi dV dt \\
&\quad + \int_{t_0}^{t_N} \int_{\partial \mathcal{B}_\sigma} \left[ \bar{\mathbf{T}} + \frac{\partial \mathcal{L}}{\partial \mathbf{F}} \cdot \hat{\mathbf{N}} \right] \cdot \delta \varphi dA dt = 0
\end{aligned} \tag{9}$$

Since  $\delta \varphi \in T_\varphi \Xi(\mathcal{C})$  is arbitrary, we obtain

$$\frac{d}{dt} \left( \frac{\partial \mathcal{L}}{\partial \dot{\varphi}} \right) - \frac{\partial \mathcal{L}}{\partial \varphi} = \text{DIV} \frac{\partial \mathcal{L}}{\partial \mathbf{F}} \quad \text{in } \mathcal{B} \times \mathbb{I} \tag{10}$$

$$\bar{\mathbf{T}} = - \frac{\partial \mathcal{L}}{\partial \mathbf{F}} \cdot \hat{\mathbf{N}} \quad \text{in } \partial \mathcal{B}_\sigma \times I \tag{11}$$

Note that, upon substituting the Lagrangian density function defined in (4), the right-hand side of (11) is as follows:

$$- \frac{\partial \mathcal{L}}{\partial \mathbf{F}} \cdot \hat{\mathbf{N}} = \rho_0 \frac{\partial \Psi(\mathbf{F})}{\partial \mathbf{F}} \cdot \hat{\mathbf{N}} = \frac{\partial W(\mathbf{F})}{\partial \mathbf{F}} \cdot \hat{\mathbf{N}} = \hat{\mathbf{P}}(\mathbf{F}) \cdot \hat{\mathbf{N}} \tag{12}$$

where  $W(\mathbf{F}) \in \mathbb{R}$  is the strain energy function and  $\hat{\mathbf{P}}(\mathbf{F})$  is the stress response function for the first Piola-Kirchhoff stress second-order tensor field  $\mathbf{P}(\mathbf{X}, t)$ . By substituting the Lagrangian density function defined in (4) into (10), Cauchy's first law of motion [1, 2] or simply Cauchy's equation of motion [3–6] is obtained as

$$\rho_0 \ddot{\varphi}(\mathbf{X}, t) = \text{DIV} \mathbf{P}(\mathbf{X}, t) + \rho_0 \mathbf{B}(\mathbf{X}, t) \tag{13}$$

in  $\mathcal{B} \times \mathbb{I}$ . Therefore, the strong form of the initial boundary-value problem for elastodynamical systems has been obtained from Hamilton's principle as follows: Find the motion map  $\varphi(\mathbf{X}, t) : \mathcal{B} \times \mathbb{I} \rightarrow \mathcal{S}$ , which is the dependent variable, from

$$\begin{aligned}
\frac{d}{dt} \left( \frac{\partial \mathcal{L}}{\partial \dot{\varphi}} \right) - \frac{\partial \mathcal{L}}{\partial \varphi} &= \text{DIV} \frac{\partial \mathcal{L}}{\partial \mathbf{F}} && \text{in } \mathcal{B} \times \mathbb{I} \\
\bar{\mathbf{T}}(\mathbf{X}, t, \hat{\mathbf{N}}) &= \mathbf{P}(\mathbf{X}, t) \cdot \hat{\mathbf{N}}(\mathbf{X}, t) && \text{in } \partial \mathcal{B}_\sigma \times \mathbb{I} \\
\varphi &= \bar{\varphi} && \text{in } \partial \mathcal{B}_\varphi \times \mathbb{I} \\
\varphi(\mathbf{X}, t_0) &= \varphi_0 = \mathbf{X} && \text{in } \mathcal{B} \\
\dot{\varphi}(\mathbf{X}, t_0) &= \dot{\varphi}_0 = \mathbf{V}_0 && \text{in } \mathcal{B}
\end{aligned} \tag{14}$$

where (14)<sub>4</sub> and (14)<sub>5</sub> are the initial conditions at time  $t_0$ .

**Weak Form** Note that we can obtain the following expression from (9):

$$\begin{aligned}
&\int_{t_0}^{t_N} \int_B \frac{d}{dt} \left( \frac{\partial \mathcal{L}}{\partial \dot{\varphi}} \right) \cdot \delta \varphi dV dt - \int_{t_0}^{t_N} \int_B \frac{\partial \mathcal{L}}{\partial \mathbf{F}} : \delta \mathbf{F} dV dt \\
&- \int_{t_0}^{t_N} \int_B \frac{\partial \mathcal{L}}{\partial \varphi} \cdot \delta \varphi dV dt - \int_{t_0}^{t_N} \int_{\partial \mathcal{B}_\sigma} \bar{\mathbf{T}} \cdot \delta \varphi dA dt = 0
\end{aligned} \tag{15}$$

Here, the variation of the deformation gradient tensor field is given as  $\delta \mathbf{F} = \text{GRAD } \delta \varphi$ . Assuming the integrand of the time integral in (15) is continuous in time, then we obtain the *Lagrangian version of the weak form* as follows due to the localization theorem in the time domain:

$$\begin{aligned}
&\int_B \frac{d}{dt} \left( \frac{\partial \mathcal{L}}{\partial \dot{\varphi}} \right) \cdot \delta \varphi dV - \int_B \frac{\partial \mathcal{L}}{\partial \mathbf{F}} : \delta \mathbf{F} dV \\
&- \int_B \frac{\partial \mathcal{L}}{\partial \varphi} \cdot \delta \varphi dV - \int_{\partial \mathcal{B}_\sigma} \bar{\mathbf{T}} \cdot \delta \varphi dA = 0 \\
\varphi(\mathbf{X}, t_0) &= \varphi_0 = \mathbf{X} \quad \text{in } \mathcal{B} \\
\dot{\varphi}(\mathbf{X}, t_0) &= \dot{\varphi}_0 = \mathbf{V}_0 \quad \text{in } \mathcal{B}
\end{aligned} \tag{16}$$

Note that (16)<sub>1</sub> yields the principle of virtual work in elastodynamical systems for dead load cases. Equation (16) can be used to derive the

semi-discrete equations of motion via the finite element method as shown in the next section.

**Remark 2.1**

1. *Representations with autonomous mechanical energy: An autonomous total energy,  $\mathcal{E}(\varphi, \dot{\varphi}) : TC \rightarrow \mathbb{R}$ , for isothermal elastodynamical systems, that is, autonomous mechanical energy, may be defined as*

$$\mathcal{E}(\varphi, \dot{\varphi}) := \int_B \mathcal{E}(\varphi, \dot{\varphi}, \mathbf{F}) dV - \int_{\partial B_\sigma} \bar{\mathbf{T}}(\mathbf{X}, t, \hat{\mathbf{N}}) \cdot \varphi(\mathbf{X}, t) dA \quad (17)$$

where the mechanical energy density function is given by

$$\mathcal{E}(\varphi, \dot{\varphi}, \mathbf{F}) := \frac{1}{2} \rho_0 \dot{\varphi}(\mathbf{X}, t) \cdot \dot{\varphi}(\mathbf{X}, t) + \rho_0 \Psi(\mathbf{F}) - \rho_0 \mathbf{B} \cdot \varphi(\mathbf{X}, t) \quad (18)$$

In terms of the autonomous mechanical energy, Hamilton's principle can be represented as

$$S[\varphi] := \int_{t_0}^{t_N} \left[ \int_B \rho_0 \dot{\varphi} \cdot \dot{\varphi} dV - \mathcal{E}(\varphi, \dot{\varphi}) \right] dt \quad (19)$$

and it leads to the strong form of the initial boundary-value problem which is equivalent to the system given in (14). That is,

$$\begin{aligned} \frac{d}{dt} \left( \frac{\partial \mathcal{E}}{\partial \dot{\varphi}} \right) + \frac{\partial \mathcal{E}}{\partial \varphi} &= \text{DIV} \frac{\partial \mathcal{E}}{\partial \mathbf{F}} && \text{in } \mathcal{B} \times \mathbb{I} \\ \bar{\mathbf{T}}(\mathbf{X}, t, \hat{\mathbf{N}}) &= \mathbf{P}(\mathbf{X}, t) \cdot \hat{\mathbf{N}}(\mathbf{X}, t) && \text{in } \partial \mathcal{B}_\sigma \times \mathbb{I} \\ + \varphi &= \bar{\varphi} && \text{in } \partial \mathcal{B}_\varphi \times \mathbb{I} \\ \varphi(\mathbf{X}, t_0) &= \varphi_0 = \mathbf{X} && \text{in } \mathcal{B} \\ \dot{\varphi}(\mathbf{X}, t_0) &= \dot{\varphi}_0 = \mathbf{V}_0 && \text{in } \mathcal{B} \end{aligned} \quad (20)$$

The autonomous mechanical energy version of the weak form yields

$$\begin{aligned} \int_B \frac{d}{dt} \left( \frac{\partial \mathcal{E}}{\partial \dot{\varphi}} \right) \cdot \delta \varphi dV + \int_B \frac{\partial \mathcal{E}}{\partial \varphi} : \delta \mathbf{F} dV \\ + \int_B \frac{\partial \mathcal{E}}{\partial \varphi} \cdot \delta \varphi dV + \int_{\partial B_\sigma} \bar{\mathbf{T}} \cdot \delta \varphi dA = 0 \\ \varphi(\mathbf{X}, t_0) = \varphi_0 = \mathbf{X} && \text{in } \mathcal{B} \\ \dot{\varphi}(\mathbf{X}, t_0) = \dot{\varphi}_0 = \mathbf{V}_0 && \text{in } \mathcal{B} \end{aligned} \quad (21)$$

**Hamiltonian Mechanics Framework**

The autonomous Hamiltonian for dead loads may be defined in the cotangent bundle (phase space),  $T_\varphi \mathcal{C}$ , associated with the configuration manifold  $\mathcal{C}$  as

$$\mathcal{H}(\phi, \varphi) = \int_B \mathcal{H}(\phi, \varphi, \mathbf{F}) dV - \int_{\partial B_\sigma} \bar{\mathbf{T}}(\mathbf{X}, t, \hat{\mathbf{N}}) \cdot \varphi(\mathbf{X}, t) dA \quad (22)$$

where the Hamiltonian density function is obtained via the Legendre transformation as

$$\begin{aligned} \mathcal{H}(\phi, \varphi, \mathbf{F}) &= \phi \cdot \dot{\varphi} - \mathcal{L}(\varphi, \dot{\varphi}, \mathbf{F}) \\ &= \frac{1}{2\rho_0} \phi(\mathbf{X}, t) \cdot \phi(\mathbf{X}, t) + \rho_0 \Psi(\mathbf{F}) \\ &\quad - \rho_0 \mathbf{B}(\mathbf{X}, t) \cdot \varphi(\mathbf{X}, t) \end{aligned} \quad (23)$$

where  $\phi(\mathbf{X}, t) = \rho_0 \dot{\varphi}(\mathbf{X}, t) : \mathcal{B} \times \mathbb{I} \rightarrow T_\varphi^* \mathcal{C}$  denotes the canonical momentum defined in the cotangent space, which is dual to the tangent space  $T_\varphi \mathcal{C}$ ,

$$T_\varphi^* \mathcal{C} := \{ \phi : \mathcal{B} \times \mathbb{I} \rightarrow \mathbb{R}^3 \} \quad (24)$$

The resulting action map in Hamiltonian mechanics may be defined as

$$S[\varphi, \phi] := \int_{t_0}^{t_N} \left[ \int_B \phi \cdot \dot{\varphi} dV - \mathcal{H}(\varphi, \dot{\varphi}) \right] dt \quad (25)$$

in terms of the primary variables  $\varphi \in \mathcal{C}$  and  $\phi$ . In Hamiltonian mechanics, the modified Hamilton's principle may read as

$$\begin{aligned}
\delta S &= \delta \int_{t_0}^{t_N} \left[ \int_B \phi \cdot \dot{\varphi} dV - \mathcal{H}(\varphi, \dot{\varphi}) \right] dt \\
&= \delta \int_{t_0}^{t_N} \int_B \phi \cdot \dot{\varphi} dV dt - \delta \int_{t_0}^{t_N} \int_B \mathcal{H}(\varphi, \phi, \mathbf{F}) dV dt \\
&\quad + \delta \int_{t_0}^{t_N} \int_{\partial B_\sigma} \bar{\mathbf{T}} \cdot \varphi(\mathbf{X}, t) dA dt = 0 \\
&\text{with } \delta\varphi(\mathbf{X}, t_0) = \delta\varphi(\mathbf{X}, t_N) = 0
\end{aligned} \tag{26}$$

which may lead to

$$\begin{aligned}
\delta S &= \int_{t_0}^{t_N} \int_B \left[ \left( \dot{\varphi} - \frac{\partial \mathcal{H}}{\partial \phi} \right) \cdot \delta\phi \right. \\
&\quad \left. - \left( \dot{\phi} + \frac{\partial \mathcal{H}}{\partial \varphi} - \text{DIV} \frac{\partial \mathcal{H}}{\partial \mathbf{F}} \right) \cdot \delta\varphi \right] dV dt \\
&\quad + \int_{t_0}^{t_N} \int_{\partial B_\sigma} \left( \bar{\mathbf{T}} - \frac{\partial \mathcal{H}}{\partial \mathbf{F}} \cdot \hat{\mathbf{N}} \right) \cdot \delta\varphi dA dt \\
&\quad + \left[ \int_B \phi \cdot \delta\varphi dV \right]_{t_0}^{t_N} = 0
\end{aligned} \tag{27}$$

Due to the boundary conditions,  $\delta\varphi(\mathbf{X}, t_0) = \delta\varphi(\mathbf{X}, t_N) = 0$ , the last term in (27) vanishes. Since  $\delta\varphi$  and  $\delta\phi$  are arbitrary, we readily obtain

$$\dot{\phi} = -\frac{\partial \mathcal{H}}{\partial \varphi} + \text{DIV} \frac{\partial \mathcal{H}}{\partial \mathbf{F}} \tag{28}$$

$$\dot{\varphi} = \frac{\partial \mathcal{H}}{\partial \phi} \tag{29}$$

in  $\mathcal{B} \times \mathbb{I}$ , with

$$\bar{\mathbf{T}} = \frac{\partial \mathcal{H}}{\partial \mathbf{F}} \cdot \hat{\mathbf{N}} = \rho_0 \frac{\partial \Psi(\mathbf{F})}{\partial \mathbf{F}} \cdot \hat{\mathbf{N}} = \frac{\partial W(\mathbf{F})}{\partial \mathbf{F}} \cdot \hat{\mathbf{N}} = \hat{\mathbf{P}}(\mathbf{F}) \cdot \hat{\mathbf{N}} \tag{30}$$

in  $\partial B_\sigma \times \mathbb{I}$ . Upon substitution of the Hamilton density function given in (23) into (28) and (29), the Cauchy's equations of motion in  $(\varphi, \phi)$  in the sense of the canonical equations, that is,

$$\dot{\phi}(\mathbf{X}, t) = \rho_0 \mathbf{B}(\mathbf{X}, t) + \text{DIV} \mathbf{P}(\mathbf{X}, t) \tag{31}$$

$$\dot{\varphi}(\mathbf{X}, t) = \rho_0^{-1}(\mathbf{X}) \phi(\mathbf{X}, t) \tag{32}$$

are readily obtained. Therefore, the strong form of the initial boundary-value problem for elastodynamical systems has been obtained from modified Hamilton's principle as follows: Find  $(\varphi, \phi)(\mathbf{X}, t) : \mathcal{B} \times \mathbb{I} \rightarrow T^*\mathcal{C}$  from

$$\begin{aligned}
\dot{\phi} &= -\frac{\partial \mathcal{H}}{\partial \varphi} + \text{DIV} \frac{\partial \mathcal{H}}{\partial \mathbf{F}} && \text{in } \mathcal{B} \times \mathbb{I} \\
\dot{\varphi} &= \frac{\partial \mathcal{H}}{\partial \phi} && \text{in } \mathcal{B} \times \mathbb{I} \\
\bar{\mathbf{T}}(\mathbf{X}, t, \hat{\mathbf{N}}) &= \mathbf{P}(\mathbf{X}, t) \cdot \hat{\mathbf{N}}(\mathbf{X}, t) && \text{in } \partial B_\sigma \times \mathbb{I} \\
\varphi &= \bar{\varphi} && \text{in } \partial B_\varphi \times \mathbb{I} \\
\varphi(\mathbf{X}, t_0) &= \varphi_0 = \mathbf{X} && \text{in } \mathcal{B} \\
\phi(\mathbf{X}, t_0) &= \phi_0 && \text{in } \mathcal{B}
\end{aligned} \tag{33}$$

*Weak form* From (27), we get

$$\begin{aligned}
&\int_{t_0}^{t_N} \int_B \dot{\phi} \cdot \delta\varphi dV dt + \int_{t_0}^{t_N} \int_B \frac{\partial \mathcal{H}}{\partial \mathbf{F}} : \delta\mathbf{F} dV dt \\
&+ \int_{t_0}^{t_N} \int_B \frac{\partial \mathcal{H}}{\partial \varphi} \cdot \delta\varphi dV dt - \int_{t_0}^{t_N} \int_{\partial B_\sigma} \bar{\mathbf{T}} \cdot \delta\varphi dA dt = 0 \\
&\int_{t_0}^{t_N} \int_B \dot{\varphi} \cdot \delta\phi dV dt - \int_{t_0}^{t_N} \int_{\partial B_\sigma} \frac{\partial \mathcal{H}}{\partial \varphi} \cdot \delta\phi dA dt = 0
\end{aligned} \tag{34}$$

Assuming the integrands of the time integral in (34) are continuous in time, then we obtain the *Hamiltonian version of the weak form* as follows due to the localization theorem in the time domain:

$$\begin{aligned}
&\int_B \dot{\phi} \cdot \delta\varphi dV + \int_B \frac{\partial \mathcal{H}}{\partial \mathbf{F}} : \delta\mathbf{F} dV \\
&+ \int_B \frac{\partial \mathcal{H}}{\partial \varphi} \cdot \delta\varphi dV - \int_{\partial B_\sigma} \bar{\mathbf{T}} \cdot \delta\varphi dA = 0 \\
&\int_B \dot{\varphi} \cdot \delta\phi dV - \int_{\partial B_\sigma} \frac{\partial \mathcal{H}}{\partial \varphi} \cdot \delta\phi dA = 0 \\
&\varphi(\mathbf{X}, t_0) = \varphi_0 = \mathbf{X} && \text{in } \mathcal{B} \\
&\phi(\mathbf{X}, t_0) = \phi_0 && \text{in } \mathcal{B}
\end{aligned} \tag{35}$$

Equation (35) can be employed to derive the semi-discrete canonical equations of motion via the finite element method as shown in the next section.

### Principle of Balance of Mechanical Energy

Alternatively, we show the development of the strong and weak forms of the equation(s) of motion from the principle of balance of mechanical energy in the sense of differential calculus (not variational calculus).

#### Total Energy Representation of Equation of Motion and Framework

Consider the autonomous mechanical energy and the associated mechanical energy density

function defined in (17) and (18), respectively. In isothermal elastodynamical conservative systems with dead loads, the *principle of balance of mechanical energy* (conservation of mechanical energy in this case) reads as

$$\begin{aligned} \frac{d}{dt} \mathcal{E}(\varphi, \dot{\varphi}) &= \frac{d}{dt} \int_B \mathcal{E}(\varphi, \dot{\varphi}, \mathbf{F}) dV \\ &\quad - \frac{d}{dt} \int_{\partial B_\sigma} \bar{\mathbf{T}} \cdot \varphi(\mathbf{X}, t) dA = 0 \end{aligned} \quad (36)$$

Equation (36) leads to

$$\begin{aligned} \frac{d}{dt} \mathcal{E}(\varphi, \dot{\varphi}) &= \int_B \left[ \frac{d}{dt} \left( \frac{\partial \mathcal{E}}{\partial \dot{\varphi}} \right) + \frac{\partial \mathcal{E}(\varphi, \dot{\varphi}, \mathbf{F})}{\partial \varphi} - \text{DIV} \frac{\partial \mathcal{E}}{\partial \mathbf{F}} \right] \cdot \dot{\varphi}(\mathbf{X}, t) dV \\ &\quad - \int_{\partial B_\sigma} \left( \bar{\mathbf{T}} - \frac{\partial \mathcal{E}}{\partial \mathbf{F}} \cdot \hat{\mathbf{N}} \right) \cdot \dot{\varphi}(\mathbf{X}, t) dA = 0 \end{aligned} \quad (37)$$

Since the material velocity vector field  $\dot{\varphi}(\mathbf{X}, t)$  is linearly independent in  $B$  and on  $\partial B_\sigma$ , we readily obtain the strong form of the initial boundary-value problem in terms of the mechanical energy density function as summarized in (20).

*Weak Form* Note that from (37), we can obtain the *theorem of power expended* for a conservative system as

$$\begin{aligned} \frac{d}{dt} \mathcal{E}(\varphi, \dot{\varphi}) &= \int_B \frac{d}{dt} \left( \frac{\partial \mathcal{E}}{\partial \dot{\varphi}} \right) \cdot \dot{\varphi} dV + \int_B \frac{\partial \mathcal{E}}{\partial \mathbf{F}} : \dot{\mathbf{F}} dV \\ &\quad + \int_B \frac{\partial \mathcal{E}}{\partial \varphi} \cdot \dot{\varphi} dV - \int_{\partial B_\sigma} \bar{\mathbf{T}} \cdot \dot{\varphi} dA = 0 \end{aligned} \quad (38)$$

Here, the total time derivative of the deformation gradient field is given as  $\dot{\mathbf{F}} = \text{GRAD} \dot{\varphi}$ . Equation (38) with the prescribed initial conditions forms the weak form in the differential calculus setting which is readily amenable to space discretization.

#### Remark 2.2

1. In terms of Lagrangian  $\mathcal{L}(\varphi, \dot{\varphi})$ , the mechanical energy, which is often called as the *Jacobi integral* in the literature, can be written as

$$\mathcal{E}(\varphi, \dot{\varphi}) = \frac{\partial \mathcal{L}}{\partial \dot{\varphi}} \cdot \dot{\varphi} - \mathcal{L} \quad (39)$$

and the strong form of the initial boundary-value problem summarized in (14) is obtained as the consequence of the principle of balance of mechanical energy, that is, (36). Therefore, the weak form yields

$$\begin{aligned} \int_B \frac{d}{dt} \left( \frac{\partial \mathcal{L}}{\partial \dot{\varphi}} \right) \cdot \dot{\varphi} dV - \int_B \frac{\partial \mathcal{L}}{\partial \mathbf{F}} : \dot{\mathbf{F}} dV \\ - \int_B \frac{\partial \mathcal{L}}{\partial \varphi} \cdot \dot{\varphi} dV - \int_{\partial B_\sigma} \bar{\mathbf{T}} \cdot \dot{\varphi} dA = 0 \end{aligned} \quad (40)$$

with the prescribed initial conditions.

### Hamiltonian Mechanics Framework

In Hamiltonian mechanics, the principle of balance of mechanical energy in isothermal elastodynamical conservative systems reads

$$\begin{aligned} \frac{d}{dt} \mathcal{H}(\varphi, \phi) &= \frac{d}{dt} \int_B \mathcal{H}(\varphi, \phi, \mathbf{F}) dV \\ &\quad - \frac{d}{dt} \int_{\partial B_\sigma} \bar{\mathbf{T}} \cdot \varphi(\mathbf{X}, t) dA = 0 \end{aligned} \quad (41)$$

which leads to

$$\begin{aligned} \frac{d}{dt} \mathcal{H}(\varphi, \phi) &= \int_B \left[ \left( \dot{\phi} + \frac{\partial \mathcal{H}}{\partial \varphi} - \text{DIV} \frac{\partial \mathcal{H}}{\partial \mathbf{F}} \right) \cdot \dot{\phi} \right. \\ &\quad \left. + \left( \frac{\partial \mathcal{H}}{\partial \phi} - \dot{\varphi} \right) \cdot \dot{\phi} \right] dV \\ &\quad - \int_{\partial B_\sigma} \left[ \bar{\mathbf{T}} - \frac{\partial \mathcal{H}}{\partial \mathbf{F}} \cdot \hat{\mathbf{N}} \right] \cdot \dot{\varphi} dA = 0 \end{aligned} \quad (42)$$

where the autonomous Hamiltonian and the Hamiltonian density function are defined in (22) and (23), respectively. Since both  $\dot{\phi}$  and  $\dot{\varphi}$  are *linearly independent*, we can readily obtain the strong form of the initial boundary-value problem for elastodynamical systems in terms of the autonomous Hamiltonian density function as summarized in (33). Note that the principle of balance of mechanical energy in Hamiltonian mechanics results in a two-field weighted residual form in  $(\varphi, \phi) \in T^*\mathcal{C}$ . Therefore, the strong form of the initial boundary-value problem for isothermal elastodynamical conservative systems can be obtained from the principle of balance of mechanical energy in the Hamiltonian mechanics framework and the differential calculus setting.

*Weak Form* From (42), we can also obtain the weak form in the sense of the space as

$$\begin{aligned} \int_B \dot{\phi} \cdot \dot{\varphi} dV + \int_B \frac{\partial \mathcal{H}}{\partial \mathbf{F}} : \dot{\mathbf{F}} dV + \int_B \frac{\partial \mathcal{H}}{\partial \varphi} \cdot \dot{\varphi} dV \\ - \int_{\partial B_\sigma} \bar{\mathbf{T}} \cdot \dot{\varphi} dA = 0 \\ \int_B \left( \dot{\varphi} - \frac{\partial \mathcal{H}}{\partial \phi} \right) \cdot \dot{\phi} dV = 0 \end{aligned} \quad (43)$$

with the prescribed initial conditions given in (35)<sub>3</sub> and (35)<sub>4</sub>.

### Spatial Discretizations by the Finite Element Method

#### Lagrangian and Total Energy Representations of Equation of Motion

Following the conventional Galerkin finite element method [7, 8], consider the admissible trial function  $\varphi^h$  represented by

$$\varphi(\mathbf{X}, t) \simeq \varphi^h(\mathbf{X}, t) = \mathbf{X} + \sum_{i=1}^{n_{\text{node}}} N_i(\mathbf{X}) \mathbf{q}^i(t) \quad (44)$$

where  $n_{\text{node}}$  denotes the number of nodes,  $N_i(\mathbf{X}) : \mathcal{B} \rightarrow \mathbb{R}$  denotes the prescribed shape functions which satisfy the completeness condition  $\sum_{i=1}^{n_{\text{node}}} N_i(\mathbf{X}) = 1$ , and  $\mathbf{q}^i(t) \in \mathbb{R}^3$  denotes the nodal displacement vector associated with the  $i$ th node at time  $t \in \mathbb{I}$ . For a set of nodal displacement vectors, we define the configuration manifold as

$$\mathcal{Q} = \{ \mathbf{q}(t) = (q^1(t), q^2(t), \dots, q^{n_{\text{dof}}}(t))^T : \mathbb{I} \rightarrow \mathbb{R}^{n_{\text{dof}}} \} \quad (45)$$

where  $n_{\text{dof}} = 3n_{\text{node}}$  denotes the number of degree of freedom. The trial function  $\varphi^h$  is of class  $C^{m-1}(\mathcal{B})$  over the entire domain, and it belongs to the subspace

$$\mathcal{C}^h = \left\{ \varphi^h(\mathbf{X}, t) : \mathcal{B} \times \mathbb{I} \rightarrow \mathbb{R}^3 \mid \varphi^h \in W_2^m(\mathcal{B}) \subset C^{m-1}(\mathcal{B}), \text{ in } \mathcal{B} \right\} \subset \mathcal{C} \quad (46)$$



From (44), the material velocity vector field may be approximated as

$$\begin{aligned} \mathbf{V}(\mathbf{X}, t) &\equiv \dot{\varphi}(\mathbf{X}, t) \simeq \dot{\varphi}^h(\mathbf{X}, t) \\ &= \sum_{i=1}^{n_{\text{node}}} \mathbf{N}_i(\mathbf{X}) \dot{\mathbf{q}}^i(t) \in T_{\varphi} \mathcal{C}^h \end{aligned} \quad (47)$$

where  $\dot{\mathbf{q}}(t) = (\dot{q}^1(t), \dot{q}^2(t), \dots, \dot{q}^{n_{\text{dof}}}(t))^T : \mathbb{I} \rightarrow T_{\mathbf{q}} \mathcal{Q}$  is a set of nodal velocity vector. Note that an arbitrary point  $(\varphi, \dot{\varphi})$  in the infinite dimensional tangent bundle  $T\mathcal{C}$  is projected onto  $(\varphi^h, \dot{\varphi}^h)$  in the finite dimensional tangent bundle  $TC^h \subset T\mathcal{C}$  by (44) and (47).

#### Discretization of the Weak Forms

Substituting (44) and (47) into the Lagrangian density function and mechanical energy density function, the Lagrangian and total energy versions of weak form given in (16) and (21) can be discretized in space as

$$\begin{aligned} &\int_B \frac{d}{dt} \left( \frac{\partial \mathcal{L}^h}{\partial \dot{\varphi}^h} \right) \cdot \delta \varphi^h dV - \int_B \frac{\partial \mathcal{L}^h}{\partial \mathbf{F}^h} : \delta \mathbf{F}^h dV \\ &- \int_B \frac{\partial \mathcal{L}^h}{\partial \varphi^h} \cdot \delta \varphi^h dV - \int_{\partial B_e} \bar{\mathbf{T}} \cdot \delta \varphi^h dA = 0 \end{aligned} \quad (48)$$

and

$$\begin{aligned} &\int_B \frac{d}{dt} \left( \frac{\partial \mathcal{E}^h}{\partial \dot{\varphi}^h} \right) \cdot \delta \varphi^h dV + \int_B \frac{\partial \mathcal{E}^h}{\partial \mathbf{F}^h} : \delta \mathbf{F}^h dV \\ &+ \int_B \frac{\partial \mathcal{E}^h}{\partial \varphi^h} \cdot \delta \varphi^h dV - \int_{\partial B_e} \bar{\mathbf{T}} \cdot \delta \varphi^h dA = 0 \end{aligned} \quad (49)$$

Respectively, with the prescribed initial conditions,  $\varphi(\mathbf{X}, t_0) = \varphi_0 = \mathbf{X}$  and  $\dot{\varphi}(\mathbf{X}, t_0) = \dot{\varphi}_0 = \mathbf{V}_0$ , where the space-discrete Lagrangian and mechanical energy density functions are given as

$$\begin{aligned} \mathcal{L}^h = \mathcal{L}(\varphi^h, \dot{\varphi}^h, \mathbf{F}^h) &= \frac{1}{2} \rho_0 \dot{\varphi}^h(\mathbf{X}, t) \cdot \dot{\varphi}^h(\mathbf{X}, t) \\ &- \rho_0 \Psi(\mathbf{F}^h) + \rho_0 \mathbf{B} \cdot \varphi^h(\mathbf{X}, t) \end{aligned} \quad (50)$$

$$\begin{aligned} \mathcal{E}^h = \mathcal{E}(\varphi^h, \dot{\varphi}^h, \mathbf{F}^h) &= \frac{1}{2} \rho_0 \dot{\varphi}^h(\mathbf{X}, t) \cdot \dot{\varphi}^h(\mathbf{X}, t) \\ &+ \rho_0 \Psi(\mathbf{F}^h) - \rho_0 \mathbf{B} \cdot \varphi^h(\mathbf{X}, t) \end{aligned} \quad (51)$$

respectively. After some tedious calculations, both (48) and (49) lead to

$$\sum_{i=1}^{n_{\text{node}}} \left[ \sum_{j=1}^{n_{\text{node}}} M_{ij} \ddot{\mathbf{q}}^j + \mathbf{F}_i^{\text{int}} - \mathbf{F}_i^{\text{ext}} \right] \cdot \delta \mathbf{q}^i = 0 \quad (52)$$

where  $M_{ij} = \int_B \rho_0 N_i N_j dV$  denotes the global symmetric mass matrix and  $\mathbf{F}_i^{\text{int}}$  and  $\mathbf{F}_i^{\text{ext}}$  denote the internal and external force vectors associated with the  $i$ th node at time  $t \in \mathbb{I}$  given by

$$\begin{aligned} \mathbf{F}_i^{\text{int}} &= \int_B \mathbf{P}^h \text{GRAD } N_i dV = \int_B \mathbf{F}^h \cdot \hat{\mathbf{S}}^h(\mathbf{F}^h) \text{GRAD } N_i dV \\ &= \sum_{j=1}^{n_{\text{node}}} \int_B \text{GRAD } N_i \cdot \hat{\mathbf{S}}(\mathbf{F}^h) \text{GRAD } N_j dV \mathbf{q}^j \end{aligned} \quad (53)$$

$$\mathbf{F}_i^{\text{ext}} = \int_B \rho_0 N_i \mathbf{B} dV + \int_{\partial B_e} N_i \bar{\mathbf{T}} dA \quad (54)$$

Note that  $\hat{\mathbf{S}}(\mathbf{F}^h)$  denotes the stress response function for the space-discrete symmetric second Piola-Kirchhoff stress tensor field, that is,  $\mathbf{S}^h(\mathbf{X}, t) = \hat{\mathbf{S}}(\mathbf{F}^h)$ , and the space-discrete deformation gradient tensor field is given as

$$\begin{aligned} \mathbf{F}^h(\mathbf{X}, t) &= \text{GRAD } \varphi^h(\mathbf{X}, t) \\ &= \mathbf{I} + \sum_{i=1}^{n_{\text{node}}} \mathbf{q}^i(t) \otimes \text{GRAD } N_i(\mathbf{X}) \end{aligned} \quad (55)$$

where  $\mathbf{I}$  denotes the identity second-order tensor. Since  $\delta \mathbf{q}$  is arbitrary, we obtain the initial-value problem for semi-discrete elastodynamical systems which yields

$$\begin{aligned} &\sum_{j=1}^{n_{\text{node}}} M_{ij} \ddot{\mathbf{q}}^j + \mathbf{F}_i^{\text{int}} = \mathbf{F}_i^{\text{ext}} \\ &\mathbf{q}(t_0) = \mathbf{q}_0 \quad \text{and} \quad \dot{\mathbf{q}}(t_0) = \dot{\mathbf{q}}_0 \end{aligned} \quad (56)$$

where  $\mathbf{q}_0 = (q^1(t_0), q^2(t_0), \dots, q^{n_{\text{dof}}}(t_0))^T$  and  $\dot{\mathbf{q}}_0 = (\dot{q}^1(t_0), \dot{q}^2(t_0), \dots, \dot{q}^{n_{\text{dof}}}(t_0))^T$  are the prescribed nodal displacement and velocity vectors at the initial time  $t_0$ .

### Remark 3.1

1. The total energy version of weak form with the mechanical energy representation given in (38) (in the differential calculus setting) can be discretized in space via (44) and (47) as

$$\int_B \frac{d}{dt} \left( \frac{\partial \mathcal{E}^h}{\partial \dot{\varphi}^h} \right) \cdot \dot{\varphi}^h dV + \int_B \frac{\partial \mathcal{E}^h}{\partial \mathbf{F}^h} : \dot{\mathbf{F}}^h dV + \int_B \frac{\partial \mathcal{E}^h}{\partial \varphi^h} \cdot \varphi^h dV - \int_{\partial B_\sigma} \bar{\mathbf{T}} \cdot \dot{\varphi}^h dA = 0 \quad (57)$$

Likewise, in terms of the Lagrangian (in the differential calculus setting),

$$\int_B \frac{d}{dt} \left( \frac{\partial \mathcal{L}^h}{\partial \dot{\varphi}^h} \right) \cdot \dot{\varphi}^h dV - \int_B \frac{\partial \mathcal{L}^h}{\partial \mathbf{F}^h} : \dot{\mathbf{F}}^h dV - \int_B \frac{\partial \mathcal{L}^h}{\partial \varphi^h} \cdot \varphi^h dV - \int_{\partial B_\sigma} \bar{\mathbf{T}} \cdot \dot{\varphi}^h dA = 0 \quad (58)$$

And both equations lead to

$$\sum_{i=1}^{n_{\text{node}}} \left[ \sum_{j=1}^{n_{\text{node}}} M_{ij} \ddot{\mathbf{q}}^j + \mathbf{F}_i^{\text{int}} - \mathbf{F}_i^{\text{ext}} \right] \cdot \dot{\mathbf{q}}^i = 0 \quad (59)$$

Since  $\dot{\mathbf{q}}$  is linearly independent, the initial-value problem for semi-discrete elastodynamical systems given in (17) is obtained.

### Hamiltonian Representation of Equation of Motion

In order to project an arbitrary point  $(\varphi, \phi)$  in the infinite dimensional cotangent bundle  $T^*\mathcal{C}$  onto  $(\varphi^h, \phi^h)$  in the finite dimensional tangent bundle  $T^*\mathcal{C}^h \subset T^*\mathcal{C}$ , employ

$$\begin{aligned} \varphi(\mathbf{X}, t) &\simeq \varphi^h(\mathbf{X}, t) = \mathbf{X} + \sum_{i=1}^{n_{\text{node}}} N_i(\mathbf{X}) \mathbf{q}^i(t) \\ \phi(\mathbf{X}, t) &\simeq \phi^h(\mathbf{X}, t) = \sum_{i=1}^{n_{\text{node}}} N_i(\mathbf{X}) \mathbf{p}_i(t) \end{aligned} \quad (60)$$

where  $\varphi^h$  and  $\phi^h$  denote the trial functions for the admissible configuration vector field and momentum vector field, respectively, and  $\mathbf{p}(t) = (p_1(t), p_2(t), \dots, p_{n_{\text{dof}}}(t)) : \mathbb{I} \rightarrow T_{\mathbf{q}}^*Q$  is a set of nodal canonical momentum vector.

### Discretization of the Weak Forms

Substituting (60)<sub>1</sub> and (60)<sub>2</sub> into the Hamiltonian density function, the Hamiltonian version of weak form given in (35) can be discretized in space as

$$\begin{aligned} \int_B \dot{\phi}^h \cdot \delta \varphi^h dV + \int_B \frac{\partial \mathcal{H}^h}{\partial \mathbf{F}^h} : \delta \mathbf{F}^h dV + \int_B \frac{\partial \mathcal{H}^h}{\partial \varphi^h} \cdot \delta \varphi^h dV - \int_{\partial B_\sigma} \bar{\mathbf{T}} \cdot \delta \varphi^h dA &= 0 \\ \int_B \dot{\varphi}^h \cdot \delta \phi^h dV - \int_{\partial B} \frac{\partial \mathcal{H}^h}{\partial \varphi^h} \cdot \delta \phi^h dV &= 0 \end{aligned} \quad (61)$$

with the prescribed initial conditions,  $\varphi(\mathbf{X}, t_0) = \varphi_0 = \mathbf{X}$  and  $\phi(\mathbf{X}, t_0) = \phi_0$ , where the space-discrete Hamiltonian density function is given as

$$\begin{aligned} \mathcal{H}^h &= \mathcal{H}(\phi^h, \varphi^h, \mathbf{F}^h) = \phi^h \cdot \dot{\varphi}^h - \mathcal{L}^h \\ &= \frac{1}{2\rho_0} \phi^h(\mathbf{X}, t) \cdot \phi^h(\mathbf{X}, t) + \rho_0 \Psi(\mathbf{F}^h) - \rho_0 \mathbf{B}(\mathbf{X}, t) \cdot \varphi^h(\mathbf{X}, t) \end{aligned} \quad (62)$$

From (61), we can show

$$\begin{aligned} \sum_{i=1}^{n_{\text{node}}} \left[ (\dot{\mathbf{p}}_i - \mathbf{F}_i^{\text{ext}} + \mathbf{F}_i^{\text{int}}) \cdot \delta \mathbf{q}^i - \left( \dot{\mathbf{q}}^i - \sum_{j=1}^{n_{\text{node}}} M_{ij}^{-1} \mathbf{p}_j \right) \cdot \delta \mathbf{p}_i \right] &= 0 \end{aligned} \quad (63)$$

and since both  $\delta \mathbf{q}$  and  $\delta \mathbf{p}$  are arbitrary, we obtain the initial-value problem for semi-discrete elastodynamical systems which reads

$$\begin{aligned} \dot{\mathbf{p}}_i &= \mathbf{F}_i^{\text{ext}} - \mathbf{F}_i^{\text{int}} \\ \dot{\mathbf{q}}^i &= \sum_{j=1}^{n_{\text{node}}} M_{ij}^{-1} \mathbf{p}_j \\ \mathbf{q}(t_0) &= \mathbf{q}_0 \quad \text{and} \quad \mathbf{p}(t_0) = \mathbf{p}_0 \end{aligned} \quad (64)$$

where  $\mathbf{q}_0 = (q^1(t_0), q^2(t_0), \dots, q^{n_{\text{dof}}}(t_0))^T$  and  $\mathbf{p}_0 = (p_1(t_0), p_2(t_0), \dots, p_{n_{\text{dof}}}(t_0))^T$  are the prescribed nodal displacement and canonical momentum vectors at the initial time  $t_0$ .

### Remark 3.2

1. The spatially discretized Hamiltonian version of weak form given in (43) (in the differential calculus setting)

$$\begin{aligned} \int_B \dot{\phi}^h \cdot \dot{\phi}^h dV + \int_B \frac{\partial \mathcal{H}^h}{\partial \mathbf{F}^h} : \dot{\mathbf{F}}^h dV \\ + \int_B \frac{\partial \mathcal{H}^h}{\partial \phi^h} \cdot \dot{\phi}^h dV - \int_{\partial B_\tau} \mathbf{T} \cdot \dot{\phi}^h dA = 0 \\ \int_B \left( \dot{\phi}^h - \frac{\partial \mathcal{H}^h}{\partial \phi} \right) \cdot \dot{\phi}^h dV = 0 \end{aligned} \quad (65)$$

also leads to

$$\sum_{i=1}^{n_{\text{node}}} \left[ (\dot{\mathbf{p}}_i - \mathbf{F}_i^{\text{ext}} + \mathbf{F}_i^{\text{int}}) \cdot \dot{\mathbf{q}}^i - \left( \dot{\mathbf{q}}^i - \sum_{j=1}^{n_{\text{node}}} M_{ij}^{-1} \mathbf{p}_j \right) \cdot \dot{\mathbf{p}}_i \right] = 0 \quad (66)$$

Since both  $\dot{\mathbf{q}}$  and  $\dot{\mathbf{p}}$  are linearly independent, we can obtain the initial-value problem for semi-discrete elastodynamical systems given in (64).

## Conclusion

A brief summary of the scalar formalisms of isothermal continuum elastodynamics and the spatial discretizations via the finite element method has been shown. The resultant spatially discrete (semi-discrete) equations of motion in the Lagrangian, total energy, and Hamiltonian representations are still continuous in time. The developments presented here also lead to the same representations as in the vector formalism [9, 10]. This is an alternative approach compared to traditional practices.

## References

1. Truesdell C, Toupin RA (1960) The classical field theories. In: Flugge S (ed) Handbuch der physik, vol III/1. Springer, Berlin

2. Truesdell C (1991) A first course in rational continuum mechanics, 2nd edn. Academic, Boston
3. Malvern LE (1969) Introduction to the mechanics of a continuous medium. Prentice-Hall, New Jersey
4. Marsden JE, Hughes TJR (1983) Mathematical foundations of elasticity. Prentice-Hall, Englewood Cliffs
5. Holzapfel GA (2000) Nonlinear solid mechanics: a continuum approach for engineering. Wiley, New York
6. Belytschko T, Liu WK, Moran B (2000) Nonlinear finite elements for continua and structures. Wiley, Chichester
7. Hughes TJR (1987) The finite element method, linear static and dynamic finite element analysis. Prentice-Hall, Englewood Cliffs
8. Reddy JN (2006) An introduction to the finite element method. McGraw-Hill, New York
9. Tamma KK, Har J, Zhou X, Shimada M, Hoitink A (2011) An overview and recent advances in vector and scalar formalisms: space/time discretizations in computational dynamics: a unified approach. Arch Comput Methods Eng. doi:10.1007/s11831-011-9060-y
10. Har J, Tamma KK (2012) Advanced computational dynamics of particles, materials and structures: a unified approach. Wiley, Chichester

## Equation of Motion: Vector Formalism and Theory

M. Shimada and Kumar K. Tamma  
Department of Mechanical Engineering,  
University of Minnesota, Minneapolis, MN, USA

## Overview

Here, we briefly summarize (1) the derivation of Cauchy's first equation of motion in the sense of the vector formalism, namely, from the principle of balance of total linear momentum for a continuum body, and (2) the derivation of its semi-discrete form following the Galerkin finite element method. Unlike the scalar formalisms, the vector formalism deals with the linear momentum vector field. The more detailed discussions on the vector and scalar formalisms to derive the equation of motion can be found in [1, 2].

## Cauchy's Equation of Motion in Elastodynamical Systems

Consider a continuum body in three-dimensional Euclidean space,  $\mathbb{R}^3$ . Let  $\mathcal{B}$  denote the reference configuration of the continuum body as an open, bounded, and simply connected set with a smooth boundary open set  $\partial\mathcal{B}$  in a topological space. The reference boundary is assumed to be  $\partial\mathcal{B}_\sigma \cup \partial\mathcal{B}_\varphi = \partial\mathcal{B}$  with  $\partial\mathcal{B}_\sigma \cap \partial\mathcal{B}_\varphi = \emptyset$ . The position of a particle in  $\mathcal{B}$  is sometimes called a material point, being denoted by  $\mathbf{X} \in \mathcal{B} \subset \mathbb{E}^3$ . The smooth motion of the body may be described  $\mathbf{x} = \varphi(\mathbf{X}, t) : \mathcal{B} \times \mathbb{I} \rightarrow \mathcal{S} \subset \mathbb{E}^3$  where  $\mathcal{S}$  denotes the current configuration and  $\mathbb{I} = [t_0, t_N]$  with initial time  $t_0 = 0$  and final time  $t_N > t_0$  denotes the time interval. A function  $\varphi(\mathbf{X}, t) \in \mathcal{S}$  is called the deformation map relative to  $\mathcal{B}$ , and it is assumed admissible. That is,  $\mathbf{x} = \varphi(\mathbf{X}, t) : \mathcal{B} \times \mathbb{I} \rightarrow \mathcal{S}$  is a one-to-one mapping and the deformation gradient second-order tensor field satisfies  $\det(\text{GRAD}\varphi) = |\mathbf{F}| > 0$  for all  $(\mathbf{X}, t) \in \mathcal{B} \times \mathbb{I}$ . In the sense of functional analysis,  $\varphi$  is a dependent variable and is of class  $C^{2m}(\mathcal{B})$  in space and of class  $C^2(\mathbb{I})$  in time. The smooth configuration manifold  $\mathcal{C}$  can be defined as

$$\mathcal{C} = \left\{ \begin{array}{l} \varphi : \mathcal{B} \times \mathbb{I} \rightarrow \mathcal{S} \subset \mathbb{R}^3 | \varphi \in C^{2m}(\mathcal{B}), m \geq 1 \\ \varphi_{\mathbf{X}} \in C^2(\mathbb{I}), \det(\text{GRAD}\varphi) = |\mathbf{F}| > 0, \text{ and } \varphi|_{\partial\mathcal{B}_\varphi} = \bar{\varphi} \end{array} \right\} \quad (1)$$

where  $\bar{\varphi}$  is the prescribed quantity on the prescribed displacement boundary  $\partial\mathcal{B}_\varphi$ . Note that GRAD denotes the gradient operator of vector fields in  $\mathcal{B}$  with respect to the material point  $\mathbf{X} \in \mathcal{B}$ .

## Principle of Balance of Linear Momentum

Strong Form of the Initial Boundary-Value Problem and Weak Form for Elastodynamical Systems

The principle of balance of linear momentum for a system in  $\mathcal{S}$  can be described as

$$\begin{aligned} & \frac{d}{dt} \int_{\mathcal{S}} \rho(\mathbf{x}, t) \mathbf{v}(\mathbf{x}, t) dV \\ &= \int_{\partial\mathcal{S}} \mathbf{t}(\mathbf{x}, t, \hat{\mathbf{n}}) dA + \int_{\mathcal{S}} \rho(\mathbf{x}, t) \mathbf{b}(\mathbf{x}, t) dV \end{aligned} \quad (2)$$

where  $\rho(\mathbf{x}, t) > 0$  and  $\mathbf{v}(\mathbf{x}, t)$  are, respectively, the spatial mass density scalar field and spatial velocity vector field at  $\mathbf{x} \in \mathcal{S}$  at time  $t \in \mathbb{I}$ ,  $\mathbf{t}(\mathbf{x}, t, \hat{\mathbf{n}})$  is the spatial traction vector field on  $\partial\mathcal{S}$  and  $\hat{\mathbf{n}}(\mathbf{x}, t)$  is the outward unit normal vector field, and  $\mathbf{b}(\mathbf{x}, t)$  is the spatial body force vector field per unit mass. Substituting  $\mathbf{x} = \varphi(\mathbf{X}, t)$ , the left-hand side of (2) yields

$$\begin{aligned} & \frac{d}{dt} \int_{\mathcal{S}} \rho(\mathbf{x}, t) \mathbf{v}(\mathbf{x}, t) dV \\ &= \frac{d}{dt} \int_{\mathcal{B}} \rho(\varphi(\mathbf{X}, t), t) \mathbf{v}(\varphi(\mathbf{X}, t), t) |\mathbf{F}| dV \\ &= \frac{d}{dt} \int_{\mathcal{B}} \rho_0(\mathbf{X}) \mathbf{V}(\mathbf{X}, t) dV \end{aligned} \quad (3)$$

where we have used the law of conservation of mass (continuity equation) in the Lagrangian form, i.e.,  $\rho(\varphi(\mathbf{X}, t), t) |\mathbf{F}| = \rho(\mathbf{X}, t_0) \equiv \rho_0(\mathbf{X})$ , and  $\mathbf{V}(\mathbf{X}, t) = \dot{\varphi}(\mathbf{X}, t)$  is the material velocity vector field. Recalling the Cauchy law,  $\mathbf{t}(\mathbf{x}, t, \hat{\mathbf{n}}) = \sigma(\mathbf{x}, t) \cdot \hat{\mathbf{n}}(\mathbf{x}, t)$  where  $\sigma(\mathbf{x}, t)$  is the Cauchy stress tensor field in the spatial description, the right-hand side of (2) yields

$$\begin{aligned} & \int_{\partial\mathcal{S}} \mathbf{t}(\mathbf{x}, t, \hat{\mathbf{n}}) dA + \int_{\mathcal{S}} \rho(\mathbf{x}, t) \mathbf{b}(\mathbf{x}, t) dV \\ &= \int_{\partial\mathcal{B}} |\mathbf{F}| \sigma(\varphi(\mathbf{X}, t), t) \cdot \mathbf{F}^{-T} \cdot \hat{\mathbf{n}}(\varphi(\mathbf{X}, t), t) dA \\ & \quad + \int_{\mathcal{B}} \rho(\varphi(\mathbf{X}, t), t) \mathbf{b}(\varphi(\mathbf{X}, t), t) dV \\ &= \int_{\partial\mathcal{B}} \mathbf{P}(\mathbf{X}, t) \cdot \hat{\mathbf{N}}(\mathbf{X}, t) dA + \int_{\mathcal{B}} \rho_0(\mathbf{X}) \mathbf{B}(\mathbf{X}, t) dV \end{aligned} \quad (4)$$

where we have used the Cauchy law via Nanson's formula, i.e., the first Piola-Kirchhoff stress tensor field is given as  $\mathbf{P}(\mathbf{X}, t) = |\mathbf{F}| \sigma(\mathbf{X}, t) \cdot \mathbf{F}^{-T}$  where  $\sigma(\mathbf{X}, t)$  is the Cauchy stress tensor field in the material description and  $\mathbf{B}(\mathbf{X}, t)$  is the material body force vector field per unit mass. Hence, the principle of balance of linear momentum in continuum-elastodynamics in the Lagrangian form is given as

$$\begin{aligned} \frac{d}{dt} \int_B \rho_0(\mathbf{X}) \dot{\varphi}(\mathbf{X}, t) dV &= \int_{\partial B} \mathbf{T}(\mathbf{X}, t, \hat{\mathbf{N}}) dA \\ &+ \int_B \rho_0(\mathbf{X}) \mathbf{B}(\mathbf{X}, t) dV \end{aligned} \quad (5)$$

where  $\mathbf{T}(\mathbf{X}, t, \hat{\mathbf{N}}) = \mathbf{P}(\mathbf{X}, t) \cdot \hat{\mathbf{N}}(\mathbf{X}, t)$  is the material traction vector field on  $\partial B$ . Invoking Reynolds transport theorem and the divergence theorem, (5) leads to

$$\int_B [\rho_0(\mathbf{X}) \ddot{\varphi} - \text{DIV } \mathbf{P}(\mathbf{X}, t) - \rho_0(\mathbf{X}) \mathbf{B}(\mathbf{X}, t)] dV = 0 \quad (6)$$

Thus, the principle of balance of linear momentum in Lagrangian form requires

$$\rho_0 \ddot{\varphi}(\mathbf{X}, t) = \text{DIV } \mathbf{P}(\mathbf{X}, t) + \rho_0 \mathbf{B}(\mathbf{X}, t) \quad (7)$$

for  $(\mathbf{X}, t) \in \mathcal{B} \times \mathbb{I}$ . Equation (7) is called Cauchy's first law of motion [3, 4] or simply Cauchy's equation of motion [5–8] and may be interpreted as the local form of balance of linear momentum. The strong form of the initial boundary-value problem for elastodynamical systems consists of (7), *Cauchy's fundamental theorem* [3, 4] (or simply *Cauchy's law* [5–8]) which is the prescribed traction boundary condition as the natural boundary condition, and the prescribed displacement boundary condition as the essential boundary condition, plus initial conditions as follows: Find the motion map  $\varphi(\mathbf{X}, t) : \mathcal{B} \times \mathbb{I} \rightarrow \mathcal{S}$ , which is the dependent variable, from

$$\begin{aligned} \rho_0 \ddot{\varphi}(\mathbf{X}, t) &= \text{DIV } \mathbf{P}(\mathbf{X}, t) + \rho_0 \mathbf{B}(\mathbf{X}, t) && \text{in } \mathcal{B} \times \mathbb{I} \\ \bar{\mathbf{T}}(\mathbf{X}, t, \hat{\mathbf{N}}) &= \mathbf{P}(\mathbf{X}, t) \cdot \hat{\mathbf{N}}(\mathbf{X}, t) && \text{in } \partial \mathcal{B}_\sigma \times \mathbb{I} \\ \varphi &= \bar{\varphi} && \text{in } \partial \mathcal{B}_\varphi \times \mathbb{I} \\ \varphi(\mathbf{X}, t_0) &= \varphi_0 = \mathbf{X} && \text{in } \mathcal{B} \\ \dot{\varphi}(\mathbf{X}, t_0) &= \dot{\varphi}_0 = \mathbf{V}_0 && \text{in } \mathcal{B} \end{aligned} \quad (8)$$

Note that  $\bar{\mathbf{T}}$ ,  $\bar{\varphi}$ , and  $\mathbf{V}_0$  are the prescribed vector fields in  $\partial \mathcal{B}_\sigma \times \mathbb{I}$ ,  $\partial \mathcal{B}_\varphi \times \mathbb{I}$ , and  $\mathcal{B}$ , respectively. From (8)<sub>1</sub>, the *Bubnov-Galerkin*

*weighted residual form* [9–13] can be established as

$$\int_B [\text{DIV } \mathbf{P}(\mathbf{X}, t) + \rho_0 \mathbf{B}(\mathbf{X}, t) - \rho_0 \ddot{\mathbf{u}}(\mathbf{X}, t)] \cdot \delta \mathbf{u}(\mathbf{X}, t) dV = 0 \quad (9)$$

where  $\mathbf{u}(\mathbf{X}, t) = \varphi(\mathbf{X}, t) - \mathbf{X}$  denotes the displacement vector field associated with  $\varphi(\mathbf{X}, t)$  and  $\delta \mathbf{u}(\mathbf{X}, t)$  denotes the virtual displacement vector field. Note that the material velocity and acceleration vector fields can be written as  $\dot{\varphi}(\mathbf{X}, t) = \dot{\mathbf{u}}(\mathbf{X}, t) \in T_\varphi \mathcal{C}$  and  $\ddot{\varphi}(\mathbf{X}, t) = \ddot{\mathbf{u}}(\mathbf{X}, t)$ , respectively. In  $\mathcal{B} \times \mathbb{I}$ , the variation of the deformation gradient tensor field is given as

$$\delta \mathbf{F} = \text{GRAD } \delta \mathbf{u} = \text{GRAD } \delta \varphi \quad (10)$$

due to  $\delta \mathbf{X} = 0$ . Note that the variation of the prescribed motion map in  $\partial \mathcal{B}_\varphi \times \mathbb{I}$  vanishes, i.e.,  $\delta \bar{\varphi} = 0$ . By invoking the product rule, we have

$$\begin{aligned} \text{DIV } \mathbf{P} \cdot \delta \mathbf{u} &= \text{DIV } (\delta \mathbf{u} \cdot \mathbf{P}) - \mathbf{P} : \\ \text{GRAD } \delta \mathbf{u} &= \text{DIV } (\delta \mathbf{u} \cdot \mathbf{P}) - \mathbf{P} : \delta \mathbf{F} \end{aligned} \quad (11)$$

Upon substitution of (11) into (9), one can obtain the following:

$$\begin{aligned} \int_B \rho_0 \ddot{\mathbf{u}} \cdot \delta \mathbf{u} dV + \int_B \mathbf{P} : \delta \mathbf{F} dV &= \int_B \rho_0 \mathbf{B} \cdot \delta \mathbf{u} dV \\ &+ \int_B \text{DIV } (\delta \mathbf{u} \cdot \mathbf{P}) dV \end{aligned} \quad (12)$$

Recalling the Gauss theorem, (12) yields the *principle of virtual work* for elastodynamical systems as

$$\begin{aligned} \int_B \rho_0 \ddot{\mathbf{u}} \cdot \delta \mathbf{u} dV + \int_B \mathbf{P} : \delta \mathbf{F} dV &= \\ \int_B \rho_0 \mathbf{B} \cdot \delta \mathbf{u} dV + \int_{\partial \mathcal{B}_\sigma} \bar{\mathbf{T}} \cdot \delta \mathbf{u} dA \end{aligned} \quad (13)$$

where we have used the natural and essential boundary conditions given in (8)<sub>2</sub>–(8)<sub>3</sub>. That is, (13) implicitly contains both natural and essential

boundary conditions as well as the governing equation. Of course, (13) can be also written as

$$\begin{aligned} & \int_B \rho_0 \ddot{\varphi} \cdot \delta \varphi \, dV + \int_B \mathbf{P} : \delta \mathbf{F} \, dV \\ &= \int_B \rho_0 \mathbf{B} \cdot \delta \varphi \, dV + \int_{\partial B_\sigma} \bar{\mathbf{T}} \cdot \delta \varphi \, dA \end{aligned} \quad (14)$$

Equations (13) or (14) is weaker than (9) in the sense of continuity requirements for the displacement-based finite element method. Therefore, the weak form for elastodynamical systems may consist of (13) and the initial conditions as follows:

$$\begin{aligned} & \int_B \rho_0 \ddot{\varphi} \cdot \delta \varphi \, dV + \int_B \mathbf{P} : \delta \mathbf{F} \, dV = \int_B \rho_0 \mathbf{B} \cdot \delta \varphi \, dV + \int_{\partial B_\sigma} \bar{\mathbf{T}} \cdot \delta \varphi \, dA \\ & \varphi(\mathbf{X}, t_0) = \varphi_0 = \mathbf{X} \quad \text{in } \mathcal{B} \\ & \dot{\varphi}(\mathbf{X}, t_0) = \dot{\varphi}_0 = \mathbf{V}_0 \quad \text{in } \mathcal{B} \end{aligned} \quad (15)$$

### Spatial Discretization by Finite Element Method

Following the conventional Galerkin finite element method [14, 15], consider the admissible trial function represented by

$$\tilde{\varphi}(\mathbf{X}, t) \simeq \tilde{\varphi}^h(\mathbf{X}, t) = \mathbf{X} + \sum_{i=1}^{n_{\text{node}}} N_i(\mathbf{X}) \mathbf{q}^i(t) \in \mathcal{C}^h \quad (16)$$

where  $n_{\text{node}}$  denotes the number of nodes,  $N_i(\mathbf{X}) : \mathcal{B} \rightarrow \mathbb{R}$  denotes the prescribed shape functions which satisfy the completeness condition  $\sum_{i=1}^{n_{\text{node}}} N_i(\mathbf{X}) = 1$ , and  $\mathbf{q}^i(t)$  denotes the nodal displacement vector associated with the  $i$ th node at time  $t \in \mathbb{I}$ . The trial function  $\tilde{\varphi}^h$  is of class  $\mathcal{C}^{m-1}(\mathcal{B})$  over the entire domain, and it belongs to the subspace

$$\mathcal{C}^h = \left\{ \begin{array}{l} \tilde{\varphi}^h(\mathbf{X}, t) : \mathcal{B} \times \mathbb{I} \rightarrow \mathbb{R}^3 \mid \tilde{\varphi}^h \in W_2^m(\mathcal{B}) \subset \mathcal{C}^{m-1}(\mathcal{B}), \text{ in } \mathcal{B} \\ \tilde{\varphi}^h = \bar{\varphi}, \text{ on } \partial \mathcal{B}_\varphi \end{array} \right\} \subset \mathcal{C} \quad (17)$$

Here, the configuration manifold for the nodal displacement vector may be defined as

$$\mathcal{Q} := \{\mathbf{q}(t) = (q^1(t), q^2(t), \dots, q^{n_{\text{dof}}}(t)) : \mathbb{I} \rightarrow \mathbb{R}^{n_{\text{dof}}}\} \quad (18)$$

where  $n_{\text{dof}} = 3n_{\text{node}}$  denotes the number of degree of freedom. Note that the variation of the admissible trial function  $\tilde{\varphi}^h(\mathbf{X}, t) : \mathcal{B} \times \mathbb{I} \rightarrow \mathcal{C}^h$  yields

$$\delta \tilde{\varphi}^h(\mathbf{X}, t) = \sum_{i=1}^{n_{\text{node}}} N_i(\mathbf{X}) \delta \mathbf{q}^i(t) \quad (19)$$

and the material velocity and acceleration vector fields are approximated as follows:

$$\begin{aligned} \tilde{\mathbf{V}}(\mathbf{X}, t) &\equiv \dot{\tilde{\varphi}}(\mathbf{X}, t) \simeq \dot{\tilde{\varphi}}^h(\mathbf{X}, t) = \sum_{i=1}^{n_{\text{node}}} \mathbf{N}_i(\mathbf{X}) \dot{\mathbf{q}}^i(t) \in T_\varphi \mathcal{C}^h \\ \tilde{\mathbf{A}}(\mathbf{X}, t) &\equiv \ddot{\tilde{\varphi}}(\mathbf{X}, t) \simeq \ddot{\tilde{\varphi}}^h(\mathbf{X}, t) = \sum_{i=1}^{n_{\text{node}}} \mathbf{N}_i(\mathbf{X}) \ddot{\mathbf{q}}^i(t) \end{aligned} \quad (20)$$

where  $\dot{\mathbf{q}}^i(t) \in T_{\mathbf{q}} \mathcal{Q}$  and  $\ddot{\mathbf{q}}^i(t)$  denote the nodal velocity and acceleration vectors associated with the  $i$ th node at time  $t \in \mathbb{I}$ , respectively. Substituting (16) and (20) into (13) yields

$$\sum_{i=1}^{n_{\text{node}}} \left[ \sum_{j=1}^{n_{\text{node}}} M_{ij} \ddot{\mathbf{q}}^j + \mathbf{F}_i^{\text{int}} - \mathbf{F}_i^{\text{ext}} \right] \cdot \delta \mathbf{q}^i = 0 \quad (21)$$

where the global symmetric mass matrix is defined as  $M_{ij} = \int_B \rho_0 N_i N_j dV$  and the internal and external force vectors associated with the  $i$ th node at time  $t \in \mathbb{I}$  are given as

$$\mathbf{F}_i^{\text{int}} = \int_B \mathbf{P}^h \text{GRAD } N_i dV \quad (22)$$

$$\mathbf{F}_i^{\text{ext}} = \int_B \rho_0 N_i \mathbf{B} dV + \int_{\partial B_\sigma} N_i \bar{\mathbf{T}} dA \quad (23)$$

According to Nanson's formula, the first Piola-Kirchhoff stress tensor field in space-discrete systems may be expressed as  $\mathbf{P}^h = \mathbf{F}^h \cdot \mathbf{S}^h$  where  $\mathbf{S}^h(\mathbf{X}, t)$  denotes the space-discrete second Piola-Kirchhoff stress second-order tensor field. Since the space-discrete deformation gradient tensor field can be written as

$$\mathbf{F}^h(\mathbf{X}, t) = \text{GRAD } \varphi^h(\mathbf{X}, t) = \mathbf{I} + \sum_{i=1}^{n_{\text{node}}} \mathbf{q}^i(t) \otimes \text{GRAD } N_i(\mathbf{X}) \quad (24)$$

$\mathbf{I}$  denotes the identity second-order tensor; the space-discrete symmetric second Piola-Kirchhoff stress tensor field is given as

$$\mathbf{S}^h(\mathbf{X}, t) = \hat{\mathbf{S}}(\mathbf{F}^h) \quad (25)$$

where  $\hat{\mathbf{S}}(\mathbf{F}^h)$  is the stress response function for  $\mathbf{S}(\mathbf{X}, t)$ . Hence, (22) can be also written as

$$\mathbf{F}_i^{\text{int}} = \int_B \mathbf{F}^h \cdot \hat{\mathbf{S}}^h(\mathbf{F}^h) \text{GRAD } N_i dV \quad (26)$$

From (26), we can also show the internal force vector as

$$\mathbf{F}_i^{\text{int}} = \sum_{j=1}^{n_{\text{node}}} \int_B \text{GRAD } N_i \cdot \hat{\mathbf{S}}(\mathbf{F}^h) \text{GRAD } N_j dV \mathbf{q}^j \quad (27)$$

Since the set  $\delta \mathbf{q} = (\delta q^1, \delta q^2, \dots, \delta q^{n_{\text{dof}}})^T$  is linearly independent, the terms enclosed in the

parenthesis in (21) can be regarded as individual coefficients [16–19]. Therefore, (21) stands for a linear combination of functions in the sense of functional analysis [20, 21]. Consequently, since  $\delta \mathbf{q}$  is arbitrary, we obtain

$$\sum_{j=1}^{n_{\text{node}}} M_{ij} \ddot{\mathbf{q}}^j + \mathbf{F}_i^{\text{int}} - \mathbf{F}_i^{\text{ext}} = 0 \quad (28)$$

Equation (28) is the semi-discrete second-order system of ordinary differential equations. The initial-value problem for semi-discrete elastodynamical systems consists of (28) and the initial conditions:

$$\begin{aligned} \sum_{j=1}^{n_{\text{node}}} M_{ij} \ddot{\mathbf{q}}^j + \mathbf{F}_i^{\text{int}} - \mathbf{F}_i^{\text{ext}} &= 0 \\ \mathbf{q}(t_0) &= \mathbf{q}_0 \\ \dot{\mathbf{q}}(t_0) &= \dot{\mathbf{q}}_0 \end{aligned} \quad (29)$$

where  $\mathbf{q}_0 = (q_0^1, q_0^2, \dots, q_0^{n_{\text{dof}}})^T$  and  $\dot{\mathbf{q}}_0 = (\dot{q}_0^1, \dot{q}_0^2, \dots, \dot{q}_0^{n_{\text{dof}}})^T$  are the prescribed nodal displacement and velocity vectors at the initial time  $t_0$ . These are finally integrated in time to find the dynamic response.

## Conclusions

The strong form of the initial boundary-value problem and its weak form for isothermal elastodynamical systems have been briefly shown from the principle of balance of linear momentum. Employing the Galerkin finite element method to the weak form which consists of the principle of virtual work and the prescribed initial conditions, the initial-value problem which consists of the semi-discrete ordinary equation and the prescribed initial conditions has been derived via the vector formalism.



## References

1. Tamma KK, Har J, Zhou X, Shimada M, Hoitink A (2011) An overview and recent advances in vector and scalar formalisms: space/time discretizations in computational dynamics: a unified approach. *Arch Comput Methods Eng*. doi:10.1007/s11831-011-9060-y
2. Har J, Tamma KK (2012) *Advanced computational dynamics of particles, materials and structures: a unified approach*. Wiley, Chichester
3. Truesdell C, Toupin RA (1960) The classical field theories. In: Flugge S (ed) *Handbuch der physik*, vol III/1. Springer, Berlin
4. Truesdell C (1991) *A first course in rational continuum mechanics*, 2nd edn. Academic, Boston
5. Malvern LE (1969) *Introduction to the mechanics of a continuous medium*. Prentice-Hall, New Jersey
6. Marsden JE, Hughes TJR (1983) *Mathematical foundations of elasticity*. Prentice-Hall, Englewood Cliffs
7. Holzapfel GA (2000) *Nonlinear solid mechanics: a continuum approach for engineering*. Wiley, New York
8. Belytschko T, Liu WK, Moran B (2000) *Nonlinear finite elements for continua and structures*. Wiley, Chichester
9. Bubnov IG (1913) Report on the works of Prof. Timoshenko which were awarded the Zhuranskii prize. In: *Symposium of the institute of communication engineers*, No. 81. All Union Special Planning Office
10. Galerkin BG (1915) Rods and plates. *Series in some problems of elastic equilibrium of rods and plates*. *Vestn Inzh Tech* 19:897–908
11. Crandall SH (1956) *Engineering analysis*. McGraw-Hill, New York
12. Mikhlin SG (1964) *Variational methods in mathematical physics*. Macmillan, New York
13. Finlayson BA (1972) *The method of weighted residuals and variational principles*. Academic, New York
14. Hughes TJR (1987) *The finite element method, linear static and dynamic finite element analysis*. Prentice-Hall, Englewood Cliffs
15. Reddy JN (2006) *An introduction to the finite element method*. McGraw-Hill, New York
16. Lanczos C (1970) *The variational principles of mechanics*. University of Toronto Press, Toronto
17. Greenwood DT (1977) *Classical dynamics*. Prentice-Hall, Reading
18. Goldstein H (2002) *Classical mechanics*. Addison Wesley, San Francisco
19. Ardenne MD (2005) *Analytical dynamics: theory and applications*. Kluwer/Plenum, New York
20. Rektorsky K (1980) *Variational methods in mathematics, science and engineering*, 2nd edn. D. Reidel, Dordrecht/Holland/Boston
21. Reddy JN (1986) *Applied functional analysis and variational methods in engineering*. McGraw-Hill, New York

## Equation of Phonon Radiative Transport: Formulation and Analysis by the Weighted Residual Method

V. M. Wheeler<sup>1</sup>, N. Shankar<sup>1,2,3</sup> and Kumar K. Tamma<sup>1</sup>

<sup>1</sup>Department of Mechanical Engineering, University of Minnesota, Minneapolis, MN, USA

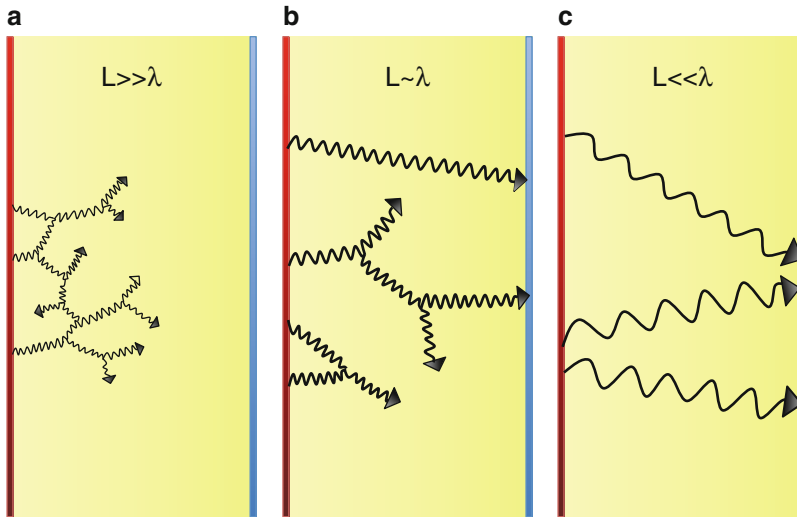
<sup>2</sup>Department of Mechanical Engineering, National Institute of Technology Karnataka, Surathkal Srinivasnagar, KA, India

<sup>3</sup>Mechanical Engineering and Engineering Mechanics, Michigan Technological University, Houghton, MI, USA

## Overview

Non-Fourier thermal transport in solids due to size effects was postulated as early as 1938 [1]. As the physical scales of engineering have shrunk in recent decades, the interest in these sub-continuum and low-dimensional processes has grown considerably. The heightened interest is due to the many potential applications, such as thermal management in field-effect transistors, and highly efficient thermoelectric materials [2]. A myriad of mathematical models has arisen in an attempt to explain thermal size effects. These models result from numerous approaches which include but are not limited to extended irreversible thermodynamics [3], coupling molecular dynamics to continuum models [4], and the Boltzmann transport equation (BTE) [5]. BTE-derived models have received considerable attention and have been demonstrated to be valid down to the scales of molecular dynamics [6]. Accurate and efficient solution methods must be applied to these models to facilitate nano- and microscale thermal engineering design. The current exposition focuses on the solution of one such model, the equation of phonon radiative transport (EPRT) [7].

EPRT is an integral partial differential equation whose integral term and convective term make the solution particularly challenging. The entry will proceed as follows: In section



**Equation of Phonon Radiative Transport: Formulation and Analysis by the Weighted Residual Method, Fig. 1** Size-dependent phonon transport regimes in a thin solid film. (a) The diffusive or Fourier regime: Heat carriers scatter repeatedly in traveling across the thin film creating the classical description of heat conduction associated with a temperature gradient. (b) The mesoscopic

regime: Since the thickness of the film is on the order of the mean free path of the heat carriers, some scatter and some do not, leading to partially ballistic and partially diffusive transport. (c) The ballistic or Casimir regime: All carriers travel in a ballistic manner across the film causing radiation-like transport

“Governing Equations and Boundary Conditions” we will review the important physics of the EPRT, its governing equation, and boundary conditions. Section “Discretization” gives the general solution formulation of EPRT using the discrete ordinates method and the weighted residual method. First we show that particular choices arising from this general framework result in the lattice Boltzmann method. We then give a more flexible and efficient alternative using Petrov-Galerkin finite elements in space and the GS4 family of algorithms in time. A numerical example is given in section “Numerical Example” and we conclude in section “Conclusion.”

## Governing Equations and Boundary Conditions

The key physical process that the EPRT is attempting to capture is ballistic transport of thermal carriers. In the case of EPRT, the carriers are limited to be phonons-quantas of energy due to

acoustic waves in a crystalline solid. In the classical view of heat conduction, phonons travel diffusively by scattering repeatedly as they propagate through a solid. These collisions happen so frequently that, in the presence of a temperature difference, the distribution of these energy-carrying particles can be assumed to be associated with a temperature gradient, i.e.,  $\frac{df}{dx} = \frac{df}{dT} \frac{dT}{dx}$ . However, this gradient approximation breaks down when the dimension of the physical system becomes so small that the average distance a phonon travels before it scatters,  $\lambda$ , is on the order of or less than the dimension of the system. This phenomenon is called ballistic transport. The different transport regimes due to this effect are shown in Fig. 1.

The EPRT does not make the gradient approximation and can capture ballistic transport physics. Its derivation is based upon the phonon-BTE which describes the out-of-equilibrium evolution of the phonon distribution function. For a location in space,  $\mathbf{r} = [x, y, z]$ , and energy carriers traveling with velocity,  $\mathbf{v}$ , the distribution,  $f$ ,

of phonons evolves over time according to the following:

$$\frac{\partial f}{\partial t} + \mathbf{v} \cdot \nabla f = \left( \frac{\partial f}{\partial t} \right)_{\text{collision}} \quad (1)$$

To get from (1) to the EPRT, we make these assumptions:

- Replace the collision term on the right-hand side of (1) with the relaxation time approximation

$$\left( \frac{\partial f}{\partial t} \right)_{\text{collision}} = \frac{f^0 - f}{\tau} \quad (2)$$

where  $f^0$  is the distribution function in thermal equilibrium and  $\tau$  is the relaxation time – the average time between phonon collisions.

- Consider the phonon propagation in a single direction,  $\hat{\mathbf{s}} = [s_x, s_y, s_z]$ , and assume the distribution function for each phonon polarization and frequency is a function of position, propagation direction, and time, i.e.,  $f = f_\omega(\mathbf{r}, \hat{\mathbf{s}}, t)$ .
- Impose that  $f^0$  ensures conservation of energy in the solution domain. This is achieved by

$$f^0 = \frac{1}{4\pi} \int_{4\pi} f d\Omega \quad (3)$$

where  $\Omega$  is the solid angle. Note that (3) results in energy conservation only at a particular frequency. This is a widely-used approximation in need of further consideration.

The result is the EPRT

$$\begin{aligned} \frac{\partial f}{\partial t} + \mathbf{v} \cdot \frac{\partial f}{\partial \mathbf{s}} &= \frac{\partial f}{\partial t} + s_x v \frac{\partial f}{\partial x} + s_y v \frac{\partial f}{\partial y} + s_z v \frac{\partial f}{\partial z} \\ &= \frac{1}{4\pi\tau} \int_{4\pi} f d\Omega - \frac{1}{\tau} f \end{aligned} \quad (4)$$

where  $v$  is the magnitude of phonon velocity which is assumed to be constant. The constant velocity assumption follows from the Debye approximation discussed shortly. Details of this derivation can be found in [7]. The solution to this equation, along with appropriate boundary and initial conditions, gives the distribution function

everywhere. Relevant heat transfer quantities, temperature and heat flux, can be deduced from  $f$ . Since the BTE describes the out-of-equilibrium distribution function, a true temperature (which is defined only in thermal equilibrium) cannot be assigned. However, what is generally referred to as the pseudo-temperature can be assigned and represents the temperature if the distribution were in an equilibrium state. The pseudo-temperature at any location in space and time can be calculated from the Planck distribution

$$\sum_p \int_{\omega} \int_{4\pi} f d\omega d\Omega = \int_{\omega} \frac{1}{e^{\frac{\hbar\omega}{k_B T}} - 1} d\omega \quad (5)$$

where  $\hbar$  is Planck's constant divided by  $2\pi$ ,  $k_B$  is Boltzmann's constant,  $T$  is the local temperature, and the summation is over phonon polarizations. The definition of heat flux is given by

$$\mathbf{q} = \sum_p \int_{\omega} \int_{4\pi} \mathbf{v} \hat{\mathbf{s}} \hbar \omega f D d\Omega d\omega \quad (6)$$

where  $D$  is the phonon density of states.

In order to evaluate (6), a relationship is needed between the frequency and phonon wave number,  $k$ , known as the dispersion relation. Both the density of states and velocity are dependent upon this relation. The most common approach is to use the Debye approximation which assumes all phonon branches of the dispersion relation are represented by a single straight line defined by  $\omega = vk$  such that the phonon dispersion relation is exactly analogous to the dispersion relation of electromagnetic waves in a vacuum. This is often referred to as the gray approximation.

In this work we will only consider a simple Dirichlet-type boundary condition where, at a surface, a distribution function is chosen for each phonon propagation direction

$$f(\mathbf{r}_b, \hat{\mathbf{s}}, t, \omega) = f_b \quad (7)$$

where  $\mathbf{r}_b$  is a location on the boundary. Despite the simplicity of this expression, one can impose either a desired boundary temperature (or pseudo-temperature) as well as a desired heat flux at the boundary by the careful selection of

$f_b$  at each point and direction such that (5) or (6) is satisfied.

In order to have a well-posed problem, we also need an initial condition given by

$$f(\mathbf{r}, \hat{\mathbf{s}}, 0, \omega) = f_{t=0} \quad (8)$$

## Discretization

We now present the general approach to the solution of (4) subject to (7) and (8). We first discretize the angular domain, then the spatial domain, and finally the temporal domain.

The angular domain is discretized by allowing phonons to propagate in a discrete number of directions (or ordinates) and approximating integration over solid angle with a numerical quadrature. This is known in the discrete ordinates method (DOM) or the  $S_N$  method in radiative heat transfer literature. As a result, we get  $\mathcal{N}$  coupled equations for  $\mathcal{N}$  ordinates,  $\hat{\mathbf{s}}_i$ . The subscript  $i$  will now be used to indicate a discrete phonon propagation direction

$$\begin{aligned} & \frac{\partial f_i}{\partial t} + s_{x,i} v \frac{\partial f_i}{\partial x} + s_{y,i} v \frac{\partial f_i}{\partial y} + s_{z,i} v \frac{\partial f_i}{\partial z} + \frac{1}{\tau} f_i \\ &= \frac{1}{4\pi\tau} \sum_{j=1}^{\mathcal{N}} \mathcal{W}_j f_j \quad i = 1, 2, 3, \dots, \mathcal{N} \end{aligned} \quad (9)$$

Equation (9) represents an approximation of the EPRT using  $\mathcal{N}$  coupled partial differential equations which are functions of only space and time. We are now able to apply standard methods to discretize in these domains. To examine these methods, we begin with a general starting point – the weighted residual method given by

$$\begin{aligned} & \int_{\Psi^e} \mathbb{W} \left( \frac{\partial f_i}{\partial t} + s_{x,i} v \frac{\partial f_i}{\partial x} + s_{y,i} v \frac{\partial f_i}{\partial y} + s_{z,i} v \frac{\partial f_i}{\partial z} \right. \\ & \left. + \frac{1}{\tau} f_i - \frac{1}{4\pi\tau} \sum_{j=1}^{\mathcal{N}} \mathcal{W}_j f_j \right) d\Psi = 0 \quad i = 1, 2, 3, \dots, \mathcal{N} \end{aligned} \quad (10)$$

where  $\mathbb{W}$  is a weighting function,  $\Psi$  is the solution domain, and  $\Psi^e$  is a subdomain or element in the finite-element sense.

## Lattice Boltzmann Method

One result that arises from the general discretization formulation, (10), is of particular interest. The lattice Boltzmann method (LBM) is an approach to solving the BTE that was originally formulated for small-scale fluid mechanics but has been recently applied to phonon transport [8]. We now show that it can be recovered from (10) by using a finite-element space-time collocation method. By defining the material derivative in a particular direction,  $\hat{\mathbf{s}}$ ,

$$\frac{d}{dt} = \frac{\partial}{\partial t} + v \frac{\partial}{\partial s} \quad (11)$$

where  $s$  is a distance along this direction, the problem is now effectively one-dimensional in space. Because of (11), a discretization in time must also lead to a discretization in space. We get a weighted residual statement of the form

$$\begin{aligned} & \int_{\Psi^e} \mathbb{W} \left( \frac{df_i}{dt} + \frac{1}{\tau} f_i - \frac{1}{4\pi\tau} \sum_{j=1}^{\mathcal{N}} \mathcal{W}_j f_j \right) d\Psi = 0 \\ & i = 1, 2, 3, \dots, \mathcal{N} \end{aligned} \quad (12)$$

From here we make the following choices for an arbitrary element extending from  $t$  to  $t + \Delta t$  in time and from  $\mathbf{r}$  to  $\mathbf{r} + v\Delta t\hat{\mathbf{s}}_i$  in space:

- Approximate the solution in each element with linear interpolation functions,  $f_i(\mathbf{r}, t) \approx N^e(t) f_i^e(\mathbf{r}(t), t)$  where  $N^e = \left[ 1 - \frac{t}{\Delta t} \quad \frac{t}{\Delta t} \right]$  and  $f_i^e = \begin{bmatrix} f_i(\mathbf{r}, t) \\ f_i(\mathbf{r} + v\Delta t\hat{\mathbf{s}}_i, t + \Delta t) \end{bmatrix}$ .
  - A weight function given by a Dirac delta function,  $\mathbb{W} = \delta(t)$
  - A numerical quadrature scheme where  $\sum_{j=1}^{\mathcal{N}} \mathcal{W}_j f_j = \frac{4\pi}{\mathcal{N}} \sum_{j=1}^{\mathcal{N}} f_j$
- Evaluating (12) with these choices gives

$$\begin{aligned}
\int_{\Psi^e} \delta(t) \left\{ \left[ -\frac{1}{\Delta t} \quad \frac{1}{\Delta t} \right] \begin{bmatrix} f_i(\mathbf{r}, t) \\ f_i(\mathbf{r} + v\Delta t \hat{\mathbf{s}}_i, t + \Delta t) \end{bmatrix} \right. \\
+ \frac{1}{\tau} \left[ 1 - \frac{t}{\Delta t} \quad \frac{t}{\Delta t} \right] \begin{bmatrix} f_i(\mathbf{r}, t) \\ f_i(\mathbf{r} + v\Delta t \hat{\mathbf{s}}_i, t + \Delta t) \end{bmatrix} \\
- \frac{1}{N\tau} \sum_{j=1}^N \left[ 1 - \frac{t}{\Delta t} \quad \frac{t}{\Delta t} \right] \\
\left. \begin{bmatrix} f_j(\mathbf{r}, t) \\ f_j(\mathbf{r} + v\Delta t \hat{\mathbf{s}}_i, t + \Delta t) \end{bmatrix} \right\} d\Psi = 0
\end{aligned} \quad (13)$$

resulting in the evolution equation of the LBM,

$$\begin{aligned}
f_i(\mathbf{r} + v\Delta t \hat{\mathbf{s}}_i, t + \Delta t) &= f_i(\mathbf{r}, t) - \frac{\Delta t}{\tau} f_i(\mathbf{r}, t) \\
&+ \frac{\Delta t}{\tau} \frac{1}{N} \\
&\times \sum_{j=1}^N f_j(\mathbf{r}, t) \quad (14)
\end{aligned}$$

From this derivation we have shown that the LBM is no more than a special case of the EPRT when solving by DOM and the method of weighted residuals. This is not surprising if one considers the roots of the phonon-LBM from the original LBM developed for fluid mechanics problems. In the fluids approach, the  $f^0$  term is formulated such that energy, momentum, and mass are conserved. In the phonon-LBM, only energy is assumed conserved because phonons are pseudo-particles and need not obey momentum or mass conservation. This is the same imposition made by Majumdar in deriving EPRT [7].

It is worth noting that although this method is simple, it is only first-order accurate [9] and, due to the coupling of space and time, becomes computationally infeasible in the Fourier limit [8]. Additionally, for 1D (thin film) studies, the approximation of the integral term is exceedingly coarse because only two propagation directions are allowed in the LBM framework. This has a dramatic effect on the transient development of the temperature profile. As more propagation directions are added in more spatial dimensions, the LBM should approach the same solution as EPRT. More flexible methods, with higher-order

accuracy and separate discretization of space and time, do not suffer from these restrictions. These methods are presented next.

### A Higher-Order Solution Approach

Again starting with (10), we show an alternative method to solving EPRT that is not coupled in time and space, which gives freedom to solve the model efficiently on a wider range of scales and exceeds first-order accuracy. To discretize in space, we use a Petrov-Galerkin method developed to handle strongly advective equations. For time integration we use the newly developed, implicit, second-order framework with selective controllable numerical dissipation known as GS4-1 [10].

#### Discretization in Space

Numerous well-known spatial discretization schemes can be obtained from the general weighted residual statement given in (10). An overview of such methods (including the finite-volume method, finite-differences method, discontinuous Galerkin method) and their relation to the weighted residual approach can be found in [11] and [12].

The Bubnov-Galerkin finite-element method is the most popular method which follows directly from the weighted residual approach. It has been shown, however, that the classical Bubnov-Galerkin finite-element method struggles to capture the physics of strongly advective terms and exhibits oscillatory numerical behavior. The Petrov-Galerkin finite-element method is the general name given to methods where the weighting function is not equal to the shape function that approximates a solution within an element. The streamline-upwind/Petrov-Galerkin (SUPG) is one such method designed to combat the difficulties encountered when using standard Bubnov-Galerkin finite elements to solve strongly advective equations. The EPRT falls under this heading, and we adopt the SUPG approach to the general solution. To formulate this method, we approximate the solution within some element with interpolation functions,  $N^e$ :

$$f_i(\mathbf{r}, t) \approx N^e(\mathbf{r})f_i^e(t) \quad (15)$$

where  $f_i^e(t)$  is the vector of nodal solutions of an element. For the SUPG method, the weight functions for all but the convective term are given by

$$\mathbb{W}_i = N^e \quad (16)$$

as in the standard Bubnov-Galerkin method.

For the convective term, we assign a weight function which has been modified to weight the element in the direction of phonon propagation more heavily than the element “downstream” at a particular node. Details on the derivation of SUPG and an argument that this treatment is consistent within a weighted residual framework are given in [13]. The convective weighting function for a particular element is given by

$$\begin{aligned} \mathbb{W}_i = N^e + \gamma \frac{\partial N^e}{\partial s} = N^e + \gamma_{s_x,i} \frac{\partial N^e}{\partial x} \\ + \gamma_{s_y,i} \frac{\partial N^e}{\partial y} + \gamma_{s_z,i} \frac{\partial N^e}{\partial z} \end{aligned} \quad (17)$$

where  $\gamma$  is a numerical parameter which decides the how strong the upwinding effect will be for a particular node. Substitution of (15), (16), and (17) into (10) results in a  $(\mathbb{N} \cdot \mathcal{N}) \times (\mathbb{N} \cdot \mathcal{N})$  system of ordinary differential equations in time of the form

$$\mathbf{M}\dot{\mathbf{f}} + \mathbf{K}\mathbf{f} = 0 \quad (18)$$

Where

$$\mathbf{M} = \sum_{e=1}^{\mathbb{N}} \mathbf{M}^e = \sum_{e=1}^{\mathbb{N}} \int_{\Psi^e} (N^{eT} N^e) d\Psi \quad (19)$$

$$\begin{aligned} \mathbf{K} = \sum_{e=1}^{\mathbb{N}} \mathbf{K}^e = \sum_{e=1}^{\mathbb{N}} \int_{\Psi^e} \left( v \left( N^e + \gamma \frac{\partial N^e}{\partial s} \right)^T \frac{\partial N^e}{\partial s} \right. \\ \left. + \frac{1}{\tau} N^{eT} N^e - \frac{1}{4\pi\tau} \sum_{j=1}^{\mathcal{N}} \mathcal{W}_j N^{eT} N^e \right) d\Psi \end{aligned} \quad (20)$$

and the superscript  $*$ <sup>T</sup> stands for the transpose operation. Choices for the discrete propagation directions of DOM have been investigated in the field of thermal radiative transfer. Recommended sets of ordinates, corresponding weighting functions, and a literature overview can be found in [14]. This completes the discretization of the spatial domain with an accuracy that exceeds first-order [13]. An example of the element matrices resulting from this formulation will be given in section “Numerical Example.”

#### Discretization in Time

Given our semi-discretized system, (18), we now repeat our weighted residuals approach to integrate in time:

$$\int_0^{\Delta t} \mathbb{W}(\mathbf{M}\dot{\mathbf{f}} + \mathbf{K}\mathbf{f}) dt = 0 \quad (21)$$

From this statement, using a general asymptotic expansion to approximate the variables,  $\mathbf{f}$  and  $\dot{\mathbf{f}}$ , Masuri et al. was able to design a family of numerical time integration schemes using the “Algorithms by Design” approach [10]. This family of algorithms, known as Generalized Single Step Single Solve for first-order systems (GS4-1), has an array of desirable attributes:

- Order-preserving with second-order time accuracy
- Implicit and unconditionally stable
- Controllable numerical dissipation and dispersion with selective features for both the primary variable and its time derivative

For our system, (18), the GS4-1 scheme is executed as follows: Given  $\mathbf{f}^n$  and  $\dot{\mathbf{f}}^n$ , one can find  $\mathbf{f}^{n+1}$  and  $\dot{\mathbf{f}}^{n+1}$  by first solving for  $\Delta\dot{\mathbf{f}}$  from

$$\begin{aligned} (\Lambda_6 W_1 \mathbf{C} + \Lambda_5 W_2 \Delta t \mathbf{K}) \Delta\dot{\mathbf{f}} \\ = -\mathbf{C}\dot{\mathbf{f}}^n - \mathbf{K}(\mathbf{f}^n + \Lambda_4 W_1 \Delta t \dot{\mathbf{f}}^n) \end{aligned} \quad (22)$$

followed by updating the variables as follows:

$$\mathbf{f}^{n+1} = \mathbf{f}^n + \lambda_4 \dot{\mathbf{f}}^n \Delta t + \lambda_5 \Delta\dot{\mathbf{f}} \Delta t \quad (23)$$

$$\dot{\mathbf{f}}^{n+1} = \dot{\mathbf{f}}^n + \Delta \dot{\mathbf{f}} \quad (24)$$

where

$$\begin{aligned} \Lambda_4 W_1 &= \frac{1}{1 + \rho_\infty} \\ \Lambda_5 W_2 &= \frac{1}{(1 + \rho_\infty)(1 + \rho_\infty^s)} \\ \Lambda_6 W_1 &= \frac{3 + \rho_\infty + \rho_\infty^s - \rho_\infty \rho_\infty^s}{2(1 + \rho_\infty)(1 + \rho_\infty^s)} \\ W_1 &= \frac{1}{1 + \rho_\infty}, \quad \lambda_4 = 1, \quad \lambda_5 = \frac{1}{1 + \rho_\infty^s} \end{aligned} \quad (25)$$

The constants,  $\lambda_m$ ,  $\Lambda_m$ , and  $W_m$  are coefficients to the aforementioned asymptotic expansions. The principle and spurious eigenvalues of the GS4-1 amplification matrix are given by  $\rho_\infty$  and  $\rho_\infty^s$ . These roots allow the user to define an algorithm for any choice of  $(\rho_\infty, \rho_\infty^s)$  such that  $0 \leq \rho_\infty^s \leq \rho_\infty \leq 1$ . The user can selectively control how much numerical dissipation is applied to  $\mathbf{f}$  and  $\dot{\mathbf{f}}$  by adjusting  $\rho_\infty$  and  $\rho_\infty^s$ , respectively, where 0 represents the most numerical dissipation and 1 represents the least. Strong numerical dissipation is important for the solution of strongly advective equations such as EPRT. Notable choices include  $(\rho_\infty, \rho_\infty^s) = (1, 1)$ , which recovers the well-known Crank-Nicolson method, and  $(\rho_\infty, \rho_\infty^s) = (0, 0)$ , which results in an L-stable algorithm. All algorithms in this framework with/without numerical dissipation are second-order accurate – a noteworthy feature of the GS4-1 framework.

## Numerical Example

We demonstrate the method given in the preceding sections with an illustrative example. We consider phonon propagation through a thin solid film of thickness,  $L$ . This is a standard

problem for the analysis of nanoscale thermal transport modeling. The problem we solve corresponds to a film initially at temperature,  $T = T_0$ , when suddenly the left boundary is raised to a higher temperature,  $T = T_b$ .

Before we proceed, we give a non-dimensionalization of the EPRT to give a solution that does not depend upon particular material parameters. Define  $\eta = \frac{x}{L}$ ,  $\xi = \frac{t}{\tau}$ , and  $K_n = \frac{L}{\ell}$  where  $K_n$  is the Knudsen number. We also assume a constant relaxation time so  $\nu = \frac{L}{\tau}$ . The resulting governing equation is

$$\frac{\partial f}{\partial \xi} + \mu K_n \frac{\partial f}{\partial \eta} + f = \frac{1}{2} \int_{-1}^1 f d\mu \quad (26)$$

where  $\mu = \cos \theta$  is the projection of the propagation direction onto the  $\eta$  direction. We have assumed that the distribution function is independent of the azimuthal direction resulting in a factor of  $2\pi$  in the integral term.

To apply the constant temperature boundary condition, we solve (5) for  $T(\eta = 0, \xi) = 300.1\text{K}$  and  $T(\eta = 0, \xi) = 300.0\text{K}$  under the Debye approximation, which results in a prescribed distribution function on each boundary,

$$f(\eta = 0, \xi) = f_1 \quad (27)$$

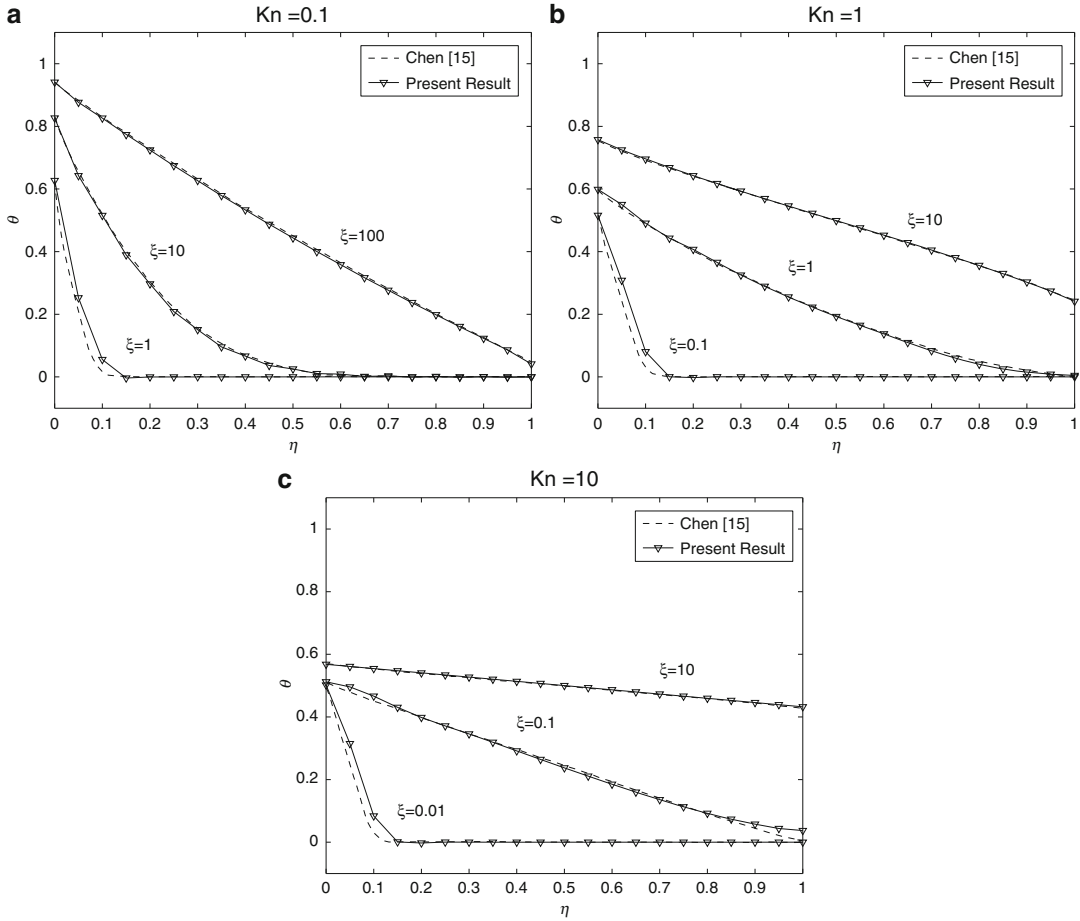
$$f(\eta = L, \xi) = f_0 \quad (28)$$

and an initial condition

$$f(\eta, \xi = 0) = f_0 \quad (29)$$

Note that these Dirichlet conditions on the distribution functions are only applied to the directions of propagation that go into the film. After the solution has been found, we can post-process the value of  $f$  at every point to recover a temperature distribution in the film again using (5). To non-dimensionalize our result, we introduce a nondimensional temperature,  $\theta = \frac{T - T_0}{T_1 - T_0}$ .





**Equation of Phonon Radiative Transport: Formulation and Analysis by the Weighted Residual Method, Fig. 2** Dimensionless temperature profiles for various Knudsen numbers and snapshots in time. All simulations were run using 20 elements and 20 timesteps. For

validation, all solutions are plotted along with results from [15]. Plots (a–c) correspond to the three space-dependent transport regimes given in Fig. 1. (a) Transport is mostly diffusive. (b) Thermal transport is partially diffusive and ballistic. (c) Transport is strongly ballistic

For clarity, we will now follow the spatial discretization process described in section “Discretization in Space” for our particular example. We choose linear shape functions for some element extending from  $\eta$  to  $\eta + \Delta\eta$ ,  $f_i \approx N^e(\eta)f_i^e(\eta, \xi)$ , where  $N^e = \left(1 - \frac{\eta}{\Delta\eta}, \frac{\eta}{\Delta\eta}\right)$  resulting in

$$\mathbf{M}^e = \int_0^{\Delta\eta} (N^{eT} N^e) d\eta = \frac{\Delta\eta}{6} \begin{pmatrix} 2 & 1 \\ 1 & 2 \end{pmatrix}_i \quad (30)$$

$$\begin{aligned} \mathbf{K}^e &= \int_0^{\Delta\eta} \left( K_n \mu_i \left( N^e + \gamma s_{\eta,i} \frac{\partial N^e}{\partial \eta} \right)^T \frac{\partial N^e}{\partial \eta} \right. \\ &\quad \left. + N^{eT} N^e - \frac{1}{2} \sum_{j=1}^N \mathcal{W}_j W_j N^{eT} N^e \right) d\eta \\ &= \frac{K_n \mu_i}{2} \begin{pmatrix} -1 + \gamma & 1 - \gamma \\ -1 - \gamma & 1 + \gamma \end{pmatrix}_i + \frac{\Delta\eta}{6} \begin{pmatrix} 2 & 1 \\ 1 & 2 \end{pmatrix}_i \\ &\quad - \sum_{j=1}^N \frac{\mathcal{W}_j}{12} \begin{pmatrix} 2 & 1 \\ 1 & 2 \end{pmatrix}_j \end{aligned} \quad (31)$$

where we are integrating over local coordinates. To approximate the integral term, we have chosen to use Gaussian quadrature which is a general numerical integration method for functions over a domain  $[-1, 1]$ . In total there are  $\mathcal{N} = 16$  propagation directions for phonons. With the element mass (30) and stiffness (31) matrices, we can now assemble the total  $(\mathbb{N} \cdot \mathcal{N}) \times (\mathbb{N} \cdot \mathcal{N})$  system. The final choice we need to make in the solution process is the particular algorithm from the GS4-1 time integration family.

Numerical results to this problem can be found in Fig. 2. The results are shown for scales that range from mostly diffusive to almost entirely ballistic behavior. Higher Knudsen numbers correspond to a more ballistic behavior as can be seen in comparing (a)–(c). One can see that a coarse mesh and large timestep can still produce very accurate results. It should be noted that the  $\xi = 10$  result in Fig. 2a using the lattice Boltzmann method with an equal number of elements would take 2,100 timesteps because of its space-time formulation. Our result is shown using just 20 timesteps. Similar results can be obtained for as little as 5 timesteps. Significant upwinding was only required in the strongly ballistic case where the upwinding parameter was set to  $\gamma = 1$ . This upwinding was still insufficient to control the numerical oscillations found in the solutions. To combat these oscillations, the GS4-1 parameters were chosen to provide the most numerical dissipation,  $(\rho_\infty, \rho_\infty^s) = (0, 0)$ , resulting in the accurate and smooth solutions found in Fig. 2a–c. Low Knudsen number simulations, such as in Fig. 2a, did not suffer from significant oscillatory behavior.

## Conclusion

We have presented a general solution method for the equation of phonon radiative transport in three dimensions by the discrete ordinates method and the weighted residual method. From this approach, we have shown that the recently developed phonon lattice Boltzmann method is a subcase of this formulation using space-time finite elements, linear shape functions, and

a weighting function given by the Dirac delta function. As an alternative we have proposed a finite-element method in space using a streamline-upwind/Petrov-Galerkin scheme. The resulting set of ordinary differential equations in time was solved using a second-order accurate family of schemes known as GS4-1. This particular solution method, also stemming from the weighted residual framework, is more efficiently able to model thermal transport on a larger range of spatial scales with higher-order accuracy.

## References

1. Casimir HBG (1938) Note on the conduction of heat in crystals. *Physica* 5:495–500
2. Cahill DG, Ford WK, Goodson KE, Mahan GD, Majumdar A, Maris HJ, Merlin R, Phillpot SR (2003) Nanoscale thermal transport. *J Appl Phys* 93:793
3. Alvarez FX, Jou D (2009) Memory and nonlocal effects in heat transport: from diffusive to ballistic regimes. *Appl Phys Lett* 90(8):083109
4. Crocombette JP, Gelebart L (2009) Multiscale modeling of the thermal conductivity of polycrystalline silicon carbide. *J Appl Phys* 106(8):083520
5. Anderson CVDR, Tamma KK (2006) Novel heat conduction model for bridging different space and time scales. *Phys Rev Lett* 96(18):184301
6. McGaughey AJH, Kaviany M (2004) Quantitative validation of the Boltzmann transport equation phonon thermal conductivity model under the single-mode relaxation time approximation. *Phys Rev B* 69(9):94303
7. Majumdar A (1993) Microscale heat conduction in dielectric thin films. *ASME T J Heat Trans* 115:7–16
8. Escobar RA, Amon CH et al (2008) Thin film phonon heat conduction by the dispersion lattice Boltzmann method. *J Heat Trans* 130:092402
9. He X, Luo LS (1997) Theory of the lattice Boltzmann method: from the Boltzmann equation to the lattice Boltzmann equation. *Phys Rev E* 56(6):6811
10. Masuri S, Sellier M, Zhou X, Tamma KK (2011) Design of order-preserving algorithms for transient first-order systems with controllable numerical dissipation. *Int J Numer Method Eng*. doi:10.1002/nme.3228
11. Reddy JN (1993) An introduction to the finite element method, vol 2. McGraw-Hill, New York
12. Li BQ (2006) Discontinuous finite elements in fluid dynamics and heat transfer. Springer, London
13. Brooks AN, Hughes TJR (1982) Streamline upwind/petrov-galerkin formulations for convection dominated flows with particular emphasis on the

incompressible navier–stokes equations. *Comput Meth Appl Mech Eng* 32:199–259

14. Modest MF (2003) Radiative heat transfer. Academic, New York
15. Chen G (2002) Ballistic-diffusive equations for transient heat conduction from nano to macroscales. *J Heat Trans* 124(2):320–328

---

## Equilibrium Path Method

- [Thermal Post-Buckling Paths of Square Plates](#)

---

## Equilibrium Theory

- [Basic Theorems in Thermoelastostatics of Bodies with Microtemperatures](#)

---

## Equivalent Single-Layer Approach

- [Refined and Advanced Governing Equations for the Thermomechanical Analysis of Shells](#)
- [Thermal Stress Analysis of Functionally Graded Material Plates](#)
- [Thermomechanical Bending in Functionally Graded Material Shells](#)

---

## Eshelby Tensors

- [Eshelby Tensors in Microcontinuum](#)

---

## Eshelby Tensors in Microcontinuum

Esin Inan<sup>1</sup> and Ahmet Kiris<sup>2</sup>

<sup>1</sup>Civil Engineering Department, Isik University, Istanbul, Turkey

<sup>2</sup>Mathematics Dept, Istanbul Technical University, Maslak, Istanbul, Turkey

---

## Synonyms

[Eshelby tensors](#); [Microstretch](#); [Microelongation](#)

## Overview

Some materials may show variety in elastic constants in some regions differing from other parts of the material even in the macroscale. In other words, materials may be inhomogeneous in nature or in production. Composites are good examples for such cases. The theoretical determination of the overall material properties for such inhomogeneous materials appears as an interesting problem from both practical and theoretical point of views. The classical homogenization techniques offer some methods to determine the overall material properties of inhomogeneous bodies to understand the overall behaviors of the bodies by the use of the properties of their constituents.

In the determination of overall material coefficients, usually the material is defined as the combination of two parts. One is “matrix material” which is considered as an elastic homogeneous material, and the other is the “inclusion” which is another elastic material and assumed embedded at arbitrary concentrations in such a way that the whole material appears as homogeneous one in average. In classical elasticity, the inclusion problem was first investigated by Eshelby [1] and he formulated a solution to establish the relations between the strains of matrix material and the inclusions in terms of some tensors which are usually known as Eshelby tensors. In his work, the term “inclusions” presents a subdomain of a homogeneous material which has been prescribed with certain distribution of eigenstrains [2] or stress-free strains.

In some cases, we cannot stay on the surface of the macrostructures, and we have to dive deeply into the microstructure. Damage phenomena may be a good example to this case. The damage, very simply, occurs when the atomic bonds break at the microstructural level like microvoids and microcracks [3]. These microscopic alterations effect the macroscopic thermodynamical material properties and appear as elastic softening, decreased conductivity, and similar. In order to take into account these deterioration processes in engineering design, a microscopic

modeling becomes necessary. The concept of microcontinuum like micromorphic theory proposed by Eringen and Şuhubi [4, 5] takes into account the microstructure of the material, while the theory itself still in the continuum formulation. Microcontinuum theories have great potential to characterize the general behavior of the material having complicated microstructures. However, the general micromorphic theory is very complicated even for the linear case. To overcome these difficulties, Eringen introduced first the micropolar elasticity [6], and then the microstretch elasticity [7]. Because of their well suitability to the nature of many materials, both theories were universally accepted.

The problem of the determination of overall material properties also exists for microstructural bodies. As it is mentioned above, the developed analytical methods in classical theory are usually based on Eshelby's fundamental solution. But it is more complicated in microstructural bodies, comparing to the similar problems in classical theory. Because, classical homogenization approach fails to predict the size dependence of the effective property [8], so the works done on the analysis on effective properties for microstructured material are few. The inclusion problem for micropolar medium was investigated by Cheng and He [9, 10] by following the idea of Eshelby and Green's function techniques. They found four Eshelby tensors for a spherical inclusion and showed that Eshelby tensors are not uniform inside the inclusion even for spherical case. Another work is given by Ma and Hu [11] for ellipsoidal inclusion in micropolar materials. Eshelby tensors for a spherical inclusion in microelongated and microstretch elastic fields are obtained for spherical inclusions by Kiris and Inan [12, 13] and Liu and Hu [14] and Ma and Hu [15].

The purpose of this entry is to give a general analysis on Eshelby tensors which has great importance in the problems of determination of overall material properties in microstretch elastic materials. For this purpose, this entry is arranged as follows: First a short summary is given for the determination of the classical Eshelby tensors. Then, some basic definitions are given for

microstructural bodies. Following these parts, a short summary of Mori-Tanaka Method [16] which is a well-known homogenization technique is given and then the general equations of microstretch body are summarized. Finally, the Eshelby tensors are obtained by following the basic method of Eshelby [1]. It is also shown that Eshelby tensors for microelongated, micropolar, and the classical cases may be derived from obtained results in microstretch theory as the limit cases [12, 13].

## Eshelby Tensors in Classical Case

The solution of inclusion problem given by Eshelby consists of three simple steps, namely, imaginary cutting, straining, and welding [1]. To show these steps and define the classical Eshelby tensor, we consider a linear isotropic elastic material. The constitutive equations and the strain-displacement relations are given as

$$\begin{aligned} t_{kl} &= \lambda e_{mm} \delta_{kl} + 2\mu e_{kl}, \quad e_{kl} \\ &= \frac{1}{2} (u_{k,l} + u_{l,k}) \end{aligned} \quad (1)$$

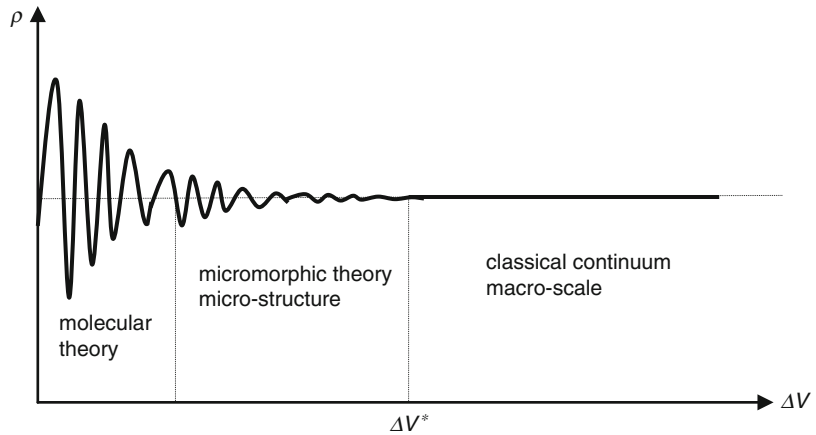
Here,  $t_{kl}$  and  $e_{kl}$  are stress and strain tensors, respectively.  $u_k$  is the component of the displacement vector,  $\lambda$  is Lamé constant, and  $\mu$  is the shear modulus. In the first step, inclusion is assumed removed and it is allowed to undergo a strain  $e_{kl}^T$  without changing its elastic constants [1]. Then, the corresponding stress,  $t_{kl}^T$ , will be

$$t_{kl}^T = \lambda e_{mm}^T \delta_{kl} + 2\mu e_{kl}^T \quad (2)$$

In other words,  $e_{kl}^T$  denotes the uniform transformation strain which the inclusion would undergo in the absence of the matrix. The problem here is to find the "constraint strain"  $e_{kl}^C$  in the inclusion when it transforms, while it is embedded in the matrix and the strain set up in the matrix. In the second step, we apply a surface traction  $-t_{kl}^T n_l$  to the inclusion [1]. This brings it back to the original shape and size. Here  $n_i$  is the outward normal. Then, it is put back into the matrix and reweld across the surface  $S$ . In the

### Eshelby Tensors in Microcontinuum,

**Fig. 1** Elementary volume element



last step, further distribution  $+t_{kl}^T n_l$  is applied over  $S$  to remove the effects of the traction applied in the second step. Now the body is free from the external forces but in a state of stress due to the transformation of the inclusion [1].

Then, the relation between the free strain of the inclusion  $e_{kl}^T$  and the strain  $e_{kl}^C$  of the matrix is written as

$$e_{kl}^C = S_{klmn} e_{mn}^T \quad (3)$$

Here  $S_{klmn}$  is called classical “Eshelby tensor.”

### Macro-Micro Continuum

A microelastic solid is defined by Eringen [4] as the one whose behaviors are affected by the local deformations of the material points of its volume element. Micromorphic theory takes into account these local effects without using molecular effect and uses the methods of statistical mechanics, so still stays at the continuum level.

The mathematical model of continuum mechanics assumes that mass is a continuous measure and a continuous density function  $\rho$  exists in the volume element  $\Delta V$ . When this volume element is less than a critical value  $\Delta V^*$ , this is not the case (Fig. 1). For this region,  $\Delta V < \Delta V^*$ , the deformations of the material contained in the volume, must be considered and included to the theory. In other words, a “macro-mass element”  $dM$  contains continuous mass distribution and it is the

average value of all masses in  $\Delta V$ . This is the basic idea and the starting point of micromorphic theory.

In general a micromorphic elastic solid possesses twelve degree of freedom; three translation degree of freedoms ( $u_i$ ;  $i = 1, 2, 3$ ) and nine degree of freedom of the microstructure ( $\phi_{kl}$ ;  $k, l = 1, 2, 3$ ) like rotation, shear, and dilatations. A microstretch solid has seven degree of freedoms; three for translation; three for rotation; and one for stretch. Micropolar media possess three rotations and three translations. In dilatational elasticity the microstructure has only one degree of freedom of dilatation in addition to the three classical translations degree of freedom.

### Eigenstrains and Eigenstresses

Any kind of nonelastic strain as thermal expansion, plastic strains, initial strains, misfit strains are called eigenstrain by Mura [2]. Eigenstress is also a generic name given to self-equilibrated internal stress caused by one or several of these eigenstrains in bodies which are free from any other external force and surface constraints. As it is known, the stress–strain relationship in a linear elastic body may be written as

$$\sigma^0 = C \epsilon^0 \quad (4)$$

Here  $\sigma$  denotes the stress tensor and  $\epsilon$  denotes the strain tensor in general. Equation (4) takes the

following form when the deformation field has some eigenstrains:

$$\boldsymbol{\sigma} = \mathbf{C}\boldsymbol{\varepsilon} = \mathbf{C}\boldsymbol{\varepsilon}^0 + \mathbf{C}\Delta\boldsymbol{\varepsilon} = \boldsymbol{\sigma}^0 + \Delta\boldsymbol{\sigma} \quad (5)$$

Here  $\boldsymbol{\sigma}$  is the total stress,  $\boldsymbol{\varepsilon}^0$ ,  $\boldsymbol{\sigma}^0$ ,  $\Delta\boldsymbol{\sigma}$ ,  $\Delta\boldsymbol{\varepsilon}$ ,  $\mathbf{C}$  are the elastic strain, elastic stress, eigenstress, eigenstrain, and the stiffness tensors, respectively.

## Mori-Tanaka Method

In the following part, we give the summary of Mori-Tanaka method which may be considered as the best method to find the overall moduli for the materials having inhomogeneities like composites and micromorphic materials. In this particular case, the material will be considered as unidirectionally aligned spherical inclusions or voids; other geometrical arrangements can be visualized in the similar way. The material is now subjected to a boundary traction which would give rise to a uniform stress  $\bar{\boldsymbol{\sigma}}$ . In the analysis, we also introduce an identical shaped comparison material including one single inclusion with the property of the matrix material and assume that it is subjected to the same boundary conditions. Then, the strain in the comparison material is uniform and given as

$$\bar{\boldsymbol{\sigma}} = \mathbf{C}_0\boldsymbol{\varepsilon}^0 \quad (6)$$

where  $\mathbf{C}_0$  is the stiffness or elastic moduli tensor of the matrix. Because of the presence of inclusions, the average stress and the strain in the matrix of the system are different from  $\bar{\boldsymbol{\sigma}}$  and  $\boldsymbol{\varepsilon}^0$ . Denoting these deviations by  $\tilde{\boldsymbol{\sigma}}$  and  $\tilde{\boldsymbol{\varepsilon}}$ , respectively, the average stresses in the matrix may be written as

$$\boldsymbol{\sigma}^{(0)} = \bar{\boldsymbol{\sigma}} + \tilde{\boldsymbol{\sigma}} = \mathbf{C}_0(\boldsymbol{\varepsilon}^0 + \tilde{\boldsymbol{\varepsilon}}) \quad (7)$$

and average strain and stress of the inclusion further differ from those of their surrounding matrix. Denoting these perturbed values by  $\boldsymbol{\sigma}^{pt}$  and  $\boldsymbol{\varepsilon}^{pt}$ , and using Eshelby's equivalence principle, we may write the average stress as

$$\begin{aligned} \boldsymbol{\sigma}^{(1)} &= \bar{\boldsymbol{\sigma}} + \tilde{\boldsymbol{\sigma}} + \boldsymbol{\sigma}^{pt} = \mathbf{C}_1(\boldsymbol{\varepsilon}^0 + \tilde{\boldsymbol{\varepsilon}} + \boldsymbol{\varepsilon}^{pt}) \\ &= \mathbf{C}_0(\boldsymbol{\varepsilon}^0 + \tilde{\boldsymbol{\varepsilon}} + \boldsymbol{\varepsilon}^{pt} - \boldsymbol{\varepsilon}^*) \end{aligned} \quad (8)$$

which  $\boldsymbol{\varepsilon}^*$  is the equivalent transformation strain, introduced into regions occupied by the inclusions, so that their elastic moduli  $\mathbf{C}_1$  can be replaced by  $\mathbf{C}_0$  to provide an identical  $\boldsymbol{\sigma}^{(1)}$ .

Here, the volume fractions of the matrix material and the inclusions will be denoted by  $c_0$  and  $c_1$ , respectively, with  $c_0 + c_1 = 1$ . Then the balance of the stress require that

$$\bar{\boldsymbol{\sigma}} = c_0\boldsymbol{\sigma}^{(0)} + c_1\boldsymbol{\sigma}^{(1)} \quad (9)$$

which leads to

$$\tilde{\boldsymbol{\sigma}} = -c_1\boldsymbol{\sigma}^{pt}, \quad \tilde{\boldsymbol{\varepsilon}} = c_1(\boldsymbol{\varepsilon}^{pt} - \boldsymbol{\varepsilon}^*) \quad (10)$$

In Mori-Tanaka method, the perturbed strain is defined as [16]

$$\boldsymbol{\varepsilon}^{pt} = \mathbf{S}\boldsymbol{\varepsilon}^* \quad (11)$$

where  $\mathbf{S}$  is the Eshelby's transformation tensor. The total strain of the inhomogeneous material is then obtained as

$$\bar{\boldsymbol{\varepsilon}} = \boldsymbol{\varepsilon}^0 + c_1\boldsymbol{\varepsilon}^* \quad (12)$$

After routine calculations, we find

$$[(\mathbf{C}_1 - \mathbf{C}_0)(c_1 + c_0\mathbf{S}) + \mathbf{C}_0]\boldsymbol{\varepsilon}^* = -(\mathbf{C}_1 - \mathbf{C}_0)\boldsymbol{\varepsilon}^0 \quad (13)$$

and by using the definition  $\bar{\boldsymbol{\sigma}} = \mathbf{C}\bar{\boldsymbol{\varepsilon}}$ , the effective moduli of the material,  $\mathbf{C}$  is found as

$$\begin{aligned} \mathbf{C} &= \mathbf{C}_0 \left\{ \mathbf{I} - c_1 [(\mathbf{C}_1 - \mathbf{C}_0)(c_1 + c_0\mathbf{S}) + \mathbf{C}_0]^{-1} \right. \\ &\quad \left. (\mathbf{C}_1 - \mathbf{C}_0) \right\}^{-1} \end{aligned} \quad (14)$$

where  $\mathbf{I}$  is fourth-rank identity tensor.

## Equations for Microstretch Medium

For microstretch theory, we write  $\phi_{kl}$  as the sum of its symmetric and antisymmetric parts as [13]

$$\phi_{kl} = \phi_{(kl)} + \phi_{[kl]} \quad (15)$$

where

$$\begin{aligned} \phi_{(kl)} &= \frac{1}{2}(\phi_{kl} + \phi_{lk}) = \theta \delta_{kl}, \\ \phi_{[kl]} &= \frac{1}{2}(\phi_{kl} - \phi_{lk}) = -e_{klm} \phi_m \end{aligned} \quad (16)$$

Here,  $\phi_k$  is defined as microrotation vector and  $\theta$  is the volumetric microstretch scalar. Then, the strain tensors take the following form:

$$\varepsilon_{kl} = u_{l,k} + e_{lkm} \phi_m, \quad \gamma_{kl} = \phi_{k,l}, \quad \gamma_k = 3 \theta_{,k} \quad (17)$$

The linearized constitutive equations for the microstretch medium are given by Eringen [7] as

$$\begin{aligned} t_{kl} &= A_{kl}^s \theta + A_{mkl}^s \theta_{,m} + A_{klmn} \varepsilon_{mn} + C_{klmn} \gamma_{mn} \\ m_{kl} &= B_{lk}^s \theta + B_{mlk}^s \theta_{,m} + C_{mnlk} \varepsilon_{mn} + B_{lkmn} \gamma_{mn} \\ m_k &= C_k^s \theta + C_{kl}^s \theta_{,l} + A_{klm}^s \varepsilon_{lm} + B_{klm}^s \gamma_{lm} \\ s - t &= C^s \theta + C_k^s \theta_{,k} + A_{kl}^s \varepsilon_{kl} + B_{kl}^s \gamma_{kl} \end{aligned} \quad (18)$$

where

$$\begin{aligned} A_{ij}^s &= \lambda_0 \delta_{ij}, \quad A_{kij}^s = 0 \\ A_{ijkl} &= \lambda \delta_{ij} \delta_{kl} + \left( \mu + \frac{\kappa}{2} \right) \delta_{ik} \delta_{jl} + \left( \mu - \frac{\kappa}{2} \right) \delta_{il} \delta_{jk} \\ B_{ij}^s &= 0, \quad B_{kij}^s = b_0 e_{kij} \\ B_{ijkl} &= \alpha \delta_{ij} \delta_{kl} + \beta \delta_{il} \delta_{jk} + \gamma \delta_{ik} \delta_{jl} \\ C^s &= \lambda_1, \quad C_i^s = 0, \quad C_{ij}^s = a_0 \delta_{ij}, \quad C_{ijkl} = 0 \end{aligned} \quad (19)$$

Here  $\lambda, \mu$  are Lamé constants,  $\alpha, \beta, \gamma$  and  $\kappa$  are new constitutive coefficients due to the

micropolar character of the medium,  $a_0, \lambda_0$  and  $\lambda_1$  are some new constitutive coefficients due to the microelongation and they are given as [7]

$$\begin{aligned} a_0 &= 6 \tau_1 + 6 \tau_2 + 9 \tau_3 + \tau_4 + 2 \tau_5 + \tau_6 + 3 \tau_7 \\ &\quad + 2 \tau_8 + \tau_9 + 3 \tau_{10} + \tau_{11}, \\ \lambda_0 &= 3 \nu + 2 \sigma, \quad \lambda_1 = 9 \tau + 6 \eta \end{aligned} \quad (20)$$

Then, seven field equations for linear isotropic microstretch medium are given as

$$\begin{aligned} \lambda_0 \theta_{,l} + \left( \lambda + \mu - \frac{\kappa}{2} \right) u_{k,lk} + \left( \mu + \frac{\kappa}{2} \right) u_{l,kk} \\ + \kappa e_{lkm} \phi_{m,k} + f_l = 0 \\ (\alpha + \beta) \phi_{k,lk} + \gamma \phi_{l,kk} + \kappa e_{lkm} u_{m,k} - 2 \kappa \phi_l + l_l = 0 \\ a_0 \theta_{,kk} - \lambda_1 \theta - \lambda_0 u_{k,k} + l = 0 \end{aligned} \quad (21)$$

To find the corresponding equations in the micropolar theory, that would be enough to write  $\theta = 0$  and take microstretch constants  $a_0, \lambda_0$  and  $\lambda_1$  as zero in (21).

## Eshelby Tensors for Microstretch Theory

To describe the deformations in an infinite microstretch material with inclusions, eigenstrains and microeigenstrains are defined as follows [2, 9]:

$$\begin{aligned} \varepsilon_{ij}^t &= \varepsilon_{ij}^* \Lambda(\Omega), \quad \gamma_{ij}^t = \gamma_{ij}^* \Lambda(\Omega), \quad \theta^t = \theta^* \Lambda(\Omega) \\ \Lambda(\Omega) &= \begin{cases} 1, & x \in \Omega, \\ 0, & x \in \mathbb{R}^3 - \Omega \end{cases} \end{aligned} \quad (22)$$

Here,  $\Omega$  is the subdomain of the infinite body occupied by the inclusion and the quantities with



superscript “\*” and “ $\hat{\cdot}$ ” denote the eigenstrains of the inclusion and general eigenstrains, respectively.

Now, we may obtain the final form of the field equations by considering the effects of the inclusion given in (22) as follows:

$$\begin{aligned} \lambda_0 \theta_{,i} + \left( \lambda + \mu - \frac{\kappa}{2} \right) u_{j,ij} + \left( \mu + \frac{\kappa}{2} \right) u_{i,jj} \\ + \kappa e_{ijk} \phi_{k,j} + f_i + f_i^t = 0 \\ (\alpha + \beta) \phi_{j,ij} + \gamma \phi_{i,jj} + \kappa e_{ijk} u_{k,j} - 2\kappa \phi_i \\ + l_i + l_i^t = 0 \\ a_0 \theta_{,ii} - \lambda_1 \theta - \lambda_0 u_{i,i} + l + l^t = 0 \end{aligned} \quad (23)$$

The terms that have the superscript “ $\hat{\cdot}$ ” in above equations are easily determined by the use of the balance equations. Thus, we write

$$\begin{aligned} f_i^t = -t_{ji,j}^t, \quad l_i^t = -m_{ji,j}^t - e_{ijk} t_{jk}^t \\ l^t = -m_{i,i}^t - t^t + s^t \\ t_{ij}^t = A_{ij}^s \theta^t + A_{ijkl}^s e_{kl}^t, \quad m_{ij}^t = B_{kji}^s \theta_{,k}^t + B_{jikl}^s \gamma_{kl}^t \\ m_i^t = C_{ij}^s \theta_j^t + B_{ijk}^s \gamma_{jk}^t, \quad s^t - t^t = C^s \theta^t + A_{ij}^s e_{ij}^t \end{aligned} \quad (24)$$

The unknown quantities  $\mathbf{u}$ ,  $\boldsymbol{\phi}$ , and  $\theta$  in (23) will be determined by the use of Green's functions. Here, the solution will be obtained in three steps and then the results will be combined by the use of reciprocity theorem. In the first step, we assume that only the body force  $\mathbf{f}$  is acting while the body moment  $\mathbf{l}$  and the body force density  $l$  are absent. Then, we write

$$\begin{aligned} \lambda_0 g_{n,i} + \left( \lambda + \mu - \frac{\kappa}{2} \right) \mathcal{G}_{jn,ij} + \left( \mu + \frac{\kappa}{2} \right) \mathcal{G}_{in,jj} \\ + \kappa e_{ijk} G_{kn,j} + \delta_{in} \delta(x - x') = 0 \\ (\alpha + \beta) G_{jn,ij} + \gamma G_{in,jj} + \kappa e_{ijk} \mathcal{G}_{kn,j} - 2\kappa G_{in} = 0, \\ a_0 g_{n,ii} - \lambda_1 g_n - \lambda_0 \mathcal{G}_{in,i} = 0 \end{aligned} \quad (25)$$

In the second step, we consider only the influences of body moment  $\mathbf{l}$ ,

$$\begin{aligned} \lambda_0 \hat{g}_{n,i} + \left( \lambda + \mu - \frac{\kappa}{2} \right) \hat{\mathcal{G}}_{jn,ij} + \left( \mu + \frac{\kappa}{2} \right) \hat{\mathcal{G}}_{in,jj} \\ + \kappa e_{ijk} \hat{G}_{kn,j} = 0 \\ (\alpha + \beta) \hat{G}_{jn,ij} + \gamma \hat{G}_{in,jj} + \kappa e_{ijk} \hat{\mathcal{G}}_{kn,j} - 2\kappa \hat{G}_{in} \\ + \delta_{in} \delta(x - x') = 0 \\ a_0 \hat{g}_{n,ii} - \lambda_1 \hat{g}_n - \lambda_0 \hat{\mathcal{G}}_{in,i} = 0 \end{aligned} \quad (26)$$

And, the last set of the equations due to the body force density  $l$  are

$$\begin{aligned} \lambda_0 \hat{\hat{g}}_{n,i} + \left( \lambda + \mu - \frac{\kappa}{2} \right) \hat{\hat{\mathcal{G}}}_{jn,ij} + \left( \mu + \frac{\kappa}{2} \right) \hat{\hat{\mathcal{G}}}_{in,jj} \\ + \kappa e_{ijk} \hat{\hat{G}}_{kn,j} = 0 \\ (\alpha + \beta) \hat{\hat{G}}_{jn,ij} + \gamma \hat{\hat{G}}_{in,jj} + \kappa e_{ijk} \hat{\hat{\mathcal{G}}}_{kn,j} - 2\kappa \hat{\hat{G}}_{in} = 0 \\ a_0 \hat{\hat{g}}_{n,ii} - \lambda_1 \hat{\hat{g}}_n - \lambda_0 \hat{\hat{\mathcal{G}}}_{in,i} + \delta_{in} I_i \delta(x - x') = 0 \end{aligned} \quad (27)$$

Here,  $\mathcal{G}_{in}$ ,  $\hat{\mathcal{G}}_{in}$ , and  $\hat{\hat{\mathcal{G}}}_{in}$  denote the Green's functions corresponding to  $u_i$ ,  $G_{in}$ ,  $\hat{G}_{in}$ , and  $\hat{\hat{G}}_{in}$  for  $\phi_i$ , and  $g_n$ ,  $\hat{g}_n$  and  $\hat{\hat{g}}_n$  for  $\theta$  due to the three different loading types mentioned above and  $I_i = -(1/4\pi)(1/r)_{,i}$ . The solutions of the system of (25–27) are given as follows. (Details may be found in Ref. [13]).

$$\begin{aligned} \mathcal{G}_{kn}(\mathbf{x} - \mathbf{x}') = \mathcal{G}_{kn}^C(\mathbf{x} - \mathbf{x}') + \mathcal{G}_{kn}^P(\mathbf{x} - \mathbf{x}') + \mathcal{G}_{kn}^E(\mathbf{x} - \mathbf{x}') \\ \hat{\mathcal{G}}_{kn}(\mathbf{x} - \mathbf{x}') = G_{kn}(\mathbf{x} - \mathbf{x}') = \frac{1}{8\pi\mu} e_{knl} \left( \frac{e^{-r/h_2} - 1}{r} \right)_{,l} \\ \hat{\hat{\mathcal{G}}}_{kn}(\mathbf{x} - \mathbf{x}') = \frac{\lambda_0 B_1}{4\pi B_0^2} \left[ \frac{1}{h_1^2} \frac{r_{,kn}}{2} + \left( \frac{1 - e^{-r/h_1}}{r} \right)_{,kn} \right] \\ \hat{G}_{kn}(\mathbf{x} - \mathbf{x}') = -\frac{1}{16\pi\mu} \left( \frac{e^{-r/h_2} - 1}{r} \right)_{,kn} \\ + \frac{1}{8\pi\kappa} \left( \frac{e^{-r/h_3} - e^{-r/h_2}}{r} \right)_{,kn} + \frac{2\mu + \kappa}{16\pi\mu\kappa h_2^2} \frac{e^{-r/h_2}}{r} \delta_{kn} \\ \hat{\hat{G}}_{kn}(\mathbf{x} - \mathbf{x}') = 0, \quad g_n(\mathbf{x} - \mathbf{x}') = -\frac{\lambda_0}{4\pi B_0} \left( \frac{1 - e^{-r/h_1}}{r} \right)_{,n} \\ \hat{g}_n(\mathbf{x} - \mathbf{x}') = 0, \quad \hat{\hat{g}}_n(\mathbf{x} - \mathbf{x}') = -\frac{\lambda + 2\mu}{4\pi B_0} \left( \frac{1 - e^{-r/h_1}}{r} \right)_{,n} \end{aligned} \quad (28)$$

Here,

$$\begin{aligned}\mathcal{G}_{kn}^C(\mathbf{x} - \mathbf{x}') &= \frac{1}{8\pi\mu} \left( 2 \frac{\delta_{kn}}{r} - \frac{\lambda + \mu}{\lambda + 2\mu} r_{,kn} \right) \\ \mathcal{G}_{kn}^P(\mathbf{x} - \mathbf{x}') &= \frac{B}{4\pi} \left[ h_2^2 \left( \frac{e^{-r/h_2} - 1}{r} \right)_{,kn} - \delta_{kn} \frac{e^{-r/h_2}}{r} \right] \\ \mathcal{G}_{kn}^E(\mathbf{x} - \mathbf{x}') &= \frac{a_0 \lambda_0^2}{4\pi B_0^2} \left[ \frac{1}{h_1^2} \frac{r_{,kn}}{2} + \left( \frac{1 - e^{-r/h_1}}{r} \right)_{,kn} \right]\end{aligned}\quad (29)$$

where  $B = \kappa/[\mu(2\mu + \kappa)]$  and the superscripts „C, P, E,“ are denoted the classical, micropolar, and microelongation quantities.

Now, to obtain the final solutions for  $u_k$ ,  $\phi_k$ , and  $\theta$ , we use the reciprocity theorem,

$$\begin{aligned}\int_V \left( \bar{F}_k u'_k - \bar{F}'_k u_k \right) dV + \int_V \left( \bar{C}_k \phi'_k - \bar{C}'_k \phi_k \right) dV \\ + \int_V \left( \bar{L} \theta' - \bar{L}' \theta \right) dV = 0\end{aligned}\quad (30)$$

Here,

$$\bar{F}_k = f'_k + f_k, \quad \bar{C}_k = l'_k + l_k, \quad \bar{L} = l' + l \quad (31)$$

And, we write

$$\begin{aligned}\{u'_k, \phi'_k, \theta', \bar{F}'_k, \bar{C}'_k, \bar{L}'\} \\ = \{G_{kn}, G_{kn}, g_n, \delta_{kn} \delta(\mathbf{x} - \mathbf{x}'), 0, 0\} \\ = \{\hat{G}_{kn}, \hat{G}_{kn}, \hat{g}_n = 0, 0, \delta_{kn} \delta(\mathbf{x} - \mathbf{x}'), 0\} \\ = \{\hat{\hat{G}}_{kn}, \hat{\hat{G}}_{kn} = 0, \hat{\hat{g}}_n = 0, 0, 0, \delta_{kn} I_k \delta(\mathbf{x} - \mathbf{x}')\}\end{aligned}\quad (32)$$

After same mathematical calculations, finally we may write

$$\begin{aligned}u_n(\mathbf{x}) &= u_n^C(\mathbf{x}) + I_{nij}(\mathbf{x}) \varepsilon_{ij}^* + J_{nij}(\mathbf{x}) \gamma_{ij}^* + K_n(\mathbf{x}) \theta^* \\ \phi_n(\mathbf{x}) &= \hat{I}_{nij}(\mathbf{x}) \varepsilon_{ij}^* + \hat{J}_{nij}(\mathbf{x}) \gamma_{ij}^* \\ \theta(\mathbf{x}) &= \hat{\hat{I}}_{ij}(\mathbf{x}) \varepsilon_{ij}^* + \hat{\hat{K}}(\mathbf{x}) \theta^*\end{aligned}\quad (33)$$

Here, we assumed that the asymmetric eigenstrain  $\varepsilon_{ij}^*$ , eigentorsion  $\gamma_{ij}^*$ , and the microeigenstrain  $\theta^*$  in the (22) are constants over the inclusion, and the coefficients of eigenstrain, eigentorsion, and microeigenstrain are

$$\begin{aligned}I_{nij}(\mathbf{x}) &= I_{nij}^P(\mathbf{x}) + I_{nij}^E(\mathbf{x}) \\ J_{nij}(\mathbf{x}) &= -\frac{1}{2\mu} [\gamma e_{nik} M_{1,jk}(\mathbf{x}) + \beta e_{njik} M_{1,ik}(\mathbf{x})] \\ &\quad + \frac{1}{2\mu} [\gamma e_{nik} M_{3,jk}(\mathbf{x}, h_2) + \beta e_{njik} M_{3,ik}(\mathbf{x}, h_2)] \\ K_n(\mathbf{x}) &= -2 \frac{\lambda_0 \lambda_1}{B_0} M_{1,n}(\mathbf{x}) \\ &\quad + \frac{a_0 \lambda_0 (2\lambda_0^2 - (\lambda + 2\mu)\lambda_1)}{B_0^2} M_{3,kkn}(\mathbf{x}, h_1) \\ &\quad + \frac{\lambda_1 \lambda_0}{B_0} M_{3,n}(\mathbf{x}, h_1) \\ \hat{I}_{ij}(\mathbf{x}) &= \frac{2\lambda_0(\lambda + \mu)}{B_0} \delta_{ij} + \frac{\lambda_0 \mu M_{2,ijn}(\mathbf{x})}{B_0 M_{1,n}(\mathbf{x})} \\ &\quad + \frac{2\lambda_0 B_1 \mu M_{1,ijn}(\mathbf{x})}{B_0^2 M_{1,n}(\mathbf{x})} \\ &\quad - \frac{\lambda \lambda_0 B_1}{B_0^2} \delta_{ij} \frac{M_{3,kkn}(\mathbf{x}, h_1)}{M_{1,n}(\mathbf{x})} \\ &\quad - \frac{2\lambda_0 B_1 \mu M_{3,ijn}(\mathbf{x}, h_1)}{B_0^2 M_{1,n}(\mathbf{x})} \\ &\quad - \frac{\lambda_0(\lambda + 2\mu)}{B_0} \delta_{ij} \frac{M_{3,n}(\mathbf{x}, h_1)}{M_{1,n}(\mathbf{x})}\end{aligned}\quad (34)$$

$$\begin{aligned}\hat{J}_{nij}(\mathbf{x}) &= -\frac{\gamma + \beta}{4\mu} M_{1,ijn}(\mathbf{x}) + \frac{2\mu + \kappa}{4\mu\kappa} [\alpha \delta_{ij} M_{3,kkn}(\mathbf{x}, h_2) \\ &\quad + (\gamma + \beta) M_{3,ijn}(\mathbf{x}, h_2)] \\ &\quad - \frac{1}{2\chi} [\alpha \delta_{ij} M_{3,kkn}(\mathbf{x}, h_3) + (\gamma + \beta) M_{3,ijn}(\mathbf{x}, h_3)] \\ &\quad - \frac{2\mu + \kappa}{4\mu\kappa h_2^2} [\alpha \delta_{ij} M_{3,n}(\mathbf{x}, h_2) + \gamma \delta_{in} M_{3,j}(\mathbf{x}, h_2) \\ &\quad + \beta \delta_{jn} M_{3,i}(\mathbf{x}, h_2)] \\ \hat{\hat{K}}(\mathbf{x}) &= \frac{\lambda_0^2 + (\lambda + 2\mu)\lambda_1}{B_0} \\ &\quad - \frac{B_1 [2\lambda_0^2 - (\lambda + 2\mu)\lambda_1]}{B_0^2} \frac{M_{3,kkn}(\mathbf{x}, h_1)}{M_{1,n}(\mathbf{x})} \\ &\quad - \frac{(\lambda + 2\mu)\lambda_1}{B_0} \frac{M_{3,n}(\mathbf{x}, h_1)}{M_{1,n}(\mathbf{x})}\end{aligned}$$

where

$$\begin{aligned}
 I_{nij}^C(\mathbf{x}) &= \frac{\lambda + \mu}{\lambda + 2\mu} M_{2,ijn}(\mathbf{x}) \\
 &\quad - \frac{\lambda}{\lambda + 2\mu} \delta_{ij} M_{1,n}(\mathbf{x}) \\
 &\quad - \delta_{in} M_{1,j}(\mathbf{x}) - \delta_{jn} M_{1,i}(\mathbf{x}) \\
 I_{nij}^P(\mathbf{x}) &= 2\mu B h_2^2 M_{1,ijn}(\mathbf{x}) \\
 &\quad + \frac{\kappa}{\mu} (\delta_{in} M_{1,j}(\mathbf{x}) - \delta_{jn} M_{1,i}(\mathbf{x})) \\
 &\quad - B h_2^2 (\lambda \delta_{ij} M_{3,kkn}(\mathbf{x}, h_2) + 2\mu M_{3,ijn}(\mathbf{x}, h_2)) \\
 &\quad + B \lambda \delta_{ij} M_{3,n}(\mathbf{x}, h_2) \\
 &\quad + \left[ B \left( \mu + \frac{\kappa}{2} \right) + \frac{\kappa}{2\mu} \right] \delta_{jn} M_{3,i}(\mathbf{x}, h_2) \\
 &\quad + \left[ B \left( \mu - \frac{\kappa}{2} \right) - \frac{\kappa}{2\mu} \right] \delta_{in} M_{3,j}(\mathbf{x}, h_2) \\
 I_{nij}^E(\mathbf{x}) &= -\frac{2(\lambda + \mu) \lambda_0^2}{(\lambda + 2\mu) B_0} \delta_{ij} M_{1,n}(\mathbf{x}) \\
 &\quad - \frac{\lambda_0^2}{(\lambda + 2\mu) B_0} \mu M_{2,ijn}(\mathbf{x}) \\
 &\quad + \frac{a_0 \lambda_0^2}{B_0^2} \lambda \delta_{ij} M_{3,kkn}(\mathbf{x}, h_1) \\
 &\quad + \frac{2a_0 \lambda_0^2}{B_0^2} \mu M_{3,ijn}(\mathbf{x}, h_1) \\
 &\quad - \frac{2a_0 \lambda_0^2}{B_0^2} \mu M_{1,ijn}(\mathbf{x}) + \frac{\lambda_0^2}{B_0} \delta_{ij} M_{3,n}(\mathbf{x}, h_1)
 \end{aligned} \quad (35)$$

here

$$M_{3,kkn}(\mathbf{x}, h) = \frac{1}{h^2} M_{3,n}(\mathbf{x}, h) \quad (36)$$

Now, we define the following potential functions:

$$\begin{aligned}
 M_1(\mathbf{x}) &= \frac{1}{4\pi} \int_{\Omega} \frac{1}{r} d\mathbf{x}', & M_2(\mathbf{x}) &= \frac{1}{4\pi} \int_{\Omega} r d\mathbf{x}', \\
 M_3(\mathbf{x}, h) &= \frac{1}{4\pi} \int_{\Omega} \frac{e^{-r/h}}{r} d\mathbf{x}'
 \end{aligned} \quad (37)$$

Eshelby tensor for an isotropic elastic body in classical elasticity are found by two integrals which are the same as the first two integrals of the (37) and they are given explicitly by Mura [2]. Therefore, the problem of determining Eshelby tensors for a microstretch solid is basically converted to the determination of third integral given by (37). The result for a spherical inclusion with radius  $a$  is given in Ref. [13] as

$$\begin{aligned}
 M_1(\mathbf{x}) &= \frac{1}{4\pi} \int_{\Omega} \frac{1}{r} d\mathbf{x}' \\
 &= \begin{cases} -\frac{1}{6}(x^2 - 3a^2), & \mathbf{x} \in \Omega, \\ \frac{a^3}{3x}, & \mathbf{x} \in \mathbb{R}^3 - \Omega, \end{cases} \\
 M_2(\mathbf{x}) &= \frac{1}{4\pi} \int_{\Omega} r d\mathbf{x}' \\
 &= \begin{cases} -\frac{1}{60}(x^4 - 10a^2x^2 - 15a^4), & \mathbf{x} \in \Omega, \\ \frac{a^3}{15}, \left(5x + \frac{a^2}{x}\right), & \mathbf{x} \in \mathbb{R}^3 - \Omega, \end{cases} \\
 M_3(\mathbf{x}, h) &= \frac{1}{4\pi} \int_{\Omega} \frac{e^{-r/h}}{r} d\mathbf{x}' \\
 &= \begin{cases} h^2 - h^2(h+a)e^{-a/h} \frac{\sinh x/h}{x}, & \mathbf{x} \in \Omega, \\ h^2 \left( a \cosh \frac{a}{h} - h \sinh \frac{a}{h} \right) \frac{e^{-x/h}}{x}, & \mathbf{x} \in \mathbb{R}^3 - \Omega \end{cases} \quad (38)
 \end{aligned}$$

Using the (17) and (33), we finally obtain strain, microtorsion, and microelongation in a microstretch material as

$$\begin{aligned}
 \varepsilon_{kl}(\mathbf{x}) &= K_{klj}(\mathbf{x}) \varepsilon_{ij}^* + L_{klj}(\mathbf{x}) \gamma_{ij}^* + M_{kl}(\mathbf{x}) \theta^* \\
 \gamma_{kl}(\mathbf{x}) &= \hat{K}_{klj}(\mathbf{x}) \varepsilon_{ij}^* + \hat{L}_{klj}(\mathbf{x}) \gamma_{ij}^* \\
 \theta(\mathbf{x}) &= \hat{K}_{ij}(\mathbf{x}) \varepsilon_{ij}^* + \hat{M}(\mathbf{x}) \theta^*
 \end{aligned} \quad (39)$$

Here,

$$\begin{aligned} K_{klij}(\mathbf{x}) &= I_{lij,k}^C(\mathbf{x}) + I_{lij,k}(\mathbf{x}) - e_{klm} \hat{I}_{mij}(\mathbf{x}) \\ L_{klij}(\mathbf{x}) &= J_{lij,k}(\mathbf{x}) - e_{klm} \hat{J}_{mij}(\mathbf{x}) \\ M_{kl}(\mathbf{x}) &= K_{l,k}(\mathbf{x}), \quad \hat{K}_{klij}(\mathbf{x}) = \hat{I}_{kij,l}(\mathbf{x}), \\ \hat{L}_{klij}(\mathbf{x}) &= \hat{J}_{kij,l}(\mathbf{x}), \quad \hat{K}_{ij}(\mathbf{x}) = \hat{I}_{ij}(\mathbf{x}) \\ \hat{M}(\mathbf{x}) &= \hat{K}(\mathbf{x}) \end{aligned} \quad (40)$$

These tensors are the modified version of the classical Eshelby tensors for microstretch materials including spherical inclusions. As it is expected, they are not homogeneous over the inclusion even for spherical case.

We may obtain the solutions due to the microelongation, the micropolar, and the classical theory as the limit cases of the microstretch theory by assuming the corresponding constitutive coefficients are zero. Thus, for the classical case, we may write

$$\begin{aligned} \phi_k &= \theta = 0, \\ \kappa &= \alpha = \beta = \gamma = a_0 = \lambda_0 = \lambda_1 = 0 \end{aligned} \quad (41)$$

and get only

$$K_{klij}(\mathbf{x}) = I_{lij,k}^C(\mathbf{x}) \quad (42)$$

In this case, all the other Eshelby tensors are zero. Eshelby tensor  $S_{ijkl}$  in classical theory of elasticity is defined as

$$\varepsilon_{ij} = S_{ijkl} \varepsilon_{kl}^* \quad (43)$$

To obtain this result as a limit case of the present problem, we may use (39)<sub>1</sub> and write

$$\frac{1}{2}(\varepsilon_{kl} + \varepsilon_{lk}) = \frac{1}{2} \left[ I_{lij,k}^C(\mathbf{x}) + I_{kij,l}^C(\mathbf{x}) \right] \frac{1}{2} (\varepsilon_{ij}^* + \varepsilon_{ji}^*) \quad (44)$$

$I_{lij,k}^C(\mathbf{x})$  is symmetric with respect to the indices  $i$  and  $j$ . On the other hand,  $\varepsilon_{kl}$  is a symmetric tensor in classical elasticity. Thus, the comparison of (43) and (44) gives

$$S_{klij} = \frac{1}{2} \left[ I_{lij,k}^C(\mathbf{x}) + I_{kij,l}^C(\mathbf{x}) \right] \quad (45)$$

For a spherical inclusion, (45) takes the following form:

$$S_{klij} = \frac{5\nu - 1}{15(1 - \nu)} \delta_{ij} \delta_{kl} + \frac{4 - 5\nu}{15(1 - \nu)} (\delta_{ik} \delta_{jl} + \delta_{il} \delta_{jk}) \quad (46)$$

This result is the well-known form of Eshelby tensor for a spherical inclusion in the classical theory of elasticity [2].

In the similar way, we neglect the terms due to micropolar effects in (39, 40) to arrive Eshelby tensors for microelongation. Then, we find

$$\begin{aligned} \varepsilon_{kl}(\mathbf{x}) &= K_{klij}(\mathbf{x}) \varepsilon_{ij}^* + L_{kl}(\mathbf{x}) \phi^* \\ \phi(\mathbf{x}) &= \hat{K}_{ij}(\mathbf{x}) \varepsilon_{ij}^* + \hat{L}(\mathbf{x}) \phi^* \end{aligned} \quad (47)$$

and

$$\begin{aligned} K_{klij}(\mathbf{x}) &= I_{lij,k}^C(\mathbf{x}) + I_{lji,k}(\mathbf{x}), \quad L_{kl}(\mathbf{x}) = J_{l,k}(\mathbf{x}), \\ \hat{K}_{ij}(\mathbf{x}) &= \hat{I}_{ji}(\mathbf{x}), \quad \hat{L}(\mathbf{x}) = \hat{J}(\mathbf{x}) \end{aligned} \quad (48)$$

finally obtain

$$\begin{aligned}
I_{nji}(\mathbf{x}) &= -\frac{2(\lambda + \mu) \lambda_0^2}{(\lambda + 2\mu) B_0} \delta_{ij} M_{1,n}(\mathbf{x}) \\
&\quad + \frac{\lambda_0^2}{B_0} \delta_{ij} M_{3,n}(\mathbf{x}, h_1) \\
&\quad - \frac{\lambda_0^2}{(\lambda + 2\mu) B_0} \mu M_{2,ijn}(\mathbf{x}) \\
&\quad - \frac{2 a_0 \lambda_0^2}{B_0^2} \mu M_{1,ijn}(\mathbf{x}) \\
&\quad + \frac{a_0 \lambda_0^2}{B_0^2} \lambda \delta_{ij} M_{3,kkn}(\mathbf{x}, h_1) \\
&\quad + \frac{2 a_0 \lambda_0^2}{B_0^2} \mu M_{3,ijn}(\mathbf{x}, h_1) \\
J_n(\mathbf{x}) &= -2 \frac{\lambda_0 \lambda_1}{B_0} M_{1,n}(\mathbf{x}) \\
&\quad + \frac{a_0 \lambda_0 [2\lambda_0^2 - \lambda_1(\lambda + 2\mu)]}{B_0^2} M_{3,kkn}(\mathbf{x}, h_1) \\
&\quad + \frac{\lambda_1 \lambda_0}{B_0} M_{3,n}(\mathbf{x}, h_1) \\
\hat{I}_{ji}(\mathbf{x}) &= 2 \frac{\lambda_0(\lambda + \mu)}{B_0} \delta_{ij} \\
&\quad + \left[ \frac{\lambda_0 \mu}{B_0} M_{2,ijn}(\mathbf{x}) + \frac{2 \lambda_0 B_1 \mu}{B_0^2} M_{1,ijn}(\mathbf{x}) \right. \\
&\quad - \frac{\lambda \lambda_0 B_1}{B_0^2} \delta_{ij} M_{3,kkn}(\mathbf{x}, h_1) \\
&\quad - \frac{2 \lambda_0 B_1 \mu}{B_0^2} M_{3,ijn}(\mathbf{x}, h_1) \\
&\quad \left. - \frac{\lambda_0 (\lambda + 2\mu)}{B_0} \delta_{ij} M_{3,n}(\mathbf{x}, h_1) \right] \frac{1}{M_{1,n}(\mathbf{x})} \\
\hat{J}(\mathbf{x}) &= \frac{\lambda_0^2 + \lambda_1 (\lambda + \mu)}{B_0} \\
&\quad - \left[ \frac{B_1 (2\lambda_0^2 - \lambda_1 (\lambda + 2\mu))}{B_0^2} M_{3,kkn}(\mathbf{x}, h_1) \right. \\
&\quad \left. + \frac{\lambda_1 (\lambda + 2\mu)}{B_0} M_{3,n}(\mathbf{x}, h_1) \right] \frac{1}{M_{1,n}(\mathbf{x})} \\
I_{nji}^C(\mathbf{x}) &= \frac{\lambda + \mu}{\lambda + 2\mu} M_{2,ijn}(\mathbf{x}) \\
&\quad - \frac{\lambda}{\lambda + 2\mu} \delta_{ij} M_{1,n}(\mathbf{x}) \\
&\quad - \delta_{in} M_{1,j}(\mathbf{x}) - \delta_{jn} M_{1,i}(\mathbf{x})
\end{aligned} \tag{49}$$

Details are given in Ref. [12].

The Eshelby tensors of micropolar theory may be obtained following the same way. Thus, we write

$$\begin{aligned}
\varepsilon_{mn}(\mathbf{x}) &= K_{mnji}(\mathbf{x}) \varepsilon_{ji}^* + L_{mnji}(\mathbf{x}) \gamma_{ji}^* \\
\gamma_{mn}(\mathbf{x}) &= \hat{K}_{mnji}(\mathbf{x}) \varepsilon_{ji}^* + \hat{L}_{mnji}(\mathbf{x}) \gamma_{ji}^*
\end{aligned} \tag{50}$$

and

$$\begin{aligned}
K_{mnji}(\mathbf{x}) &= I_{nji,m}^C(\mathbf{x}) + I_{nji,m}(\mathbf{x}) - e_{lmn} \hat{I}_{lji}(\mathbf{x}) \\
\hat{K}_{mnji}(\mathbf{x}) &= \hat{I}_{nji,m}(\mathbf{x}) \\
L_{mnji}(\mathbf{x}) &= J_{nji,m}(\mathbf{x}) - e_{lmn} \hat{J}_{lji}(\mathbf{x}) \\
\hat{L}_{mnji}(\mathbf{x}) &= \hat{J}_{nji,m}(\mathbf{x})
\end{aligned} \tag{51}$$

Then, we find

$$\begin{aligned}
I_{nji}(x) &= 2B\mu h_2^2 M_{1,ijn}(x) + \frac{\kappa}{\mu} [\delta_{jn} M_{1,i}(x) - \delta_{in} M_{1,j}(x)] \\
&\quad - Bh_2^2 [\lambda \delta_{ij} M_{3,kkn}(x, h_2) + 2\mu M_{3,ijn}(x, h_2)] \\
&\quad + B\lambda \delta_{ij} M_{3,n}(x, h_2) + [B(\mu + \frac{\kappa}{2}) \\
&\quad + \frac{\kappa}{2\mu}] \delta_{in} M_{3,j}(x, h_2) + [B(\mu - \frac{\kappa}{2}) \\
&\quad - \frac{\kappa}{2\mu}] \delta_{jn} M_{3,i}(x, h_2) \\
J_{nji}(x) &= -\frac{1}{2\mu} [\gamma e_{nik} M_{1,jk}(x) + \beta e_{nj k} M_{1,ik}(x)] \\
&\quad + \frac{1}{2\mu} [\gamma e_{nik} M_{3,jk}(x, h_2) + \beta e_{nj k} M_{3,ik}(x, h_2)] \\
\hat{I}_{nji}(x) &= \frac{1}{4\mu} [\kappa e_{ijk} M_{1,kn}(x) \\
&\quad - (2\mu + \kappa) e_{nik} M_{1,jk}(x) - (2\mu - \kappa) e_{nj k} M_{1,ik}(x)] \\
&\quad + \frac{1}{4\mu} [(2\mu + \kappa) e_{ijk} M_{3,kn}(x, h_2) \\
&\quad - (2\mu + \kappa) e_{nik} M_{3,jk}(x, h_2) \\
&\quad - (2\mu - \kappa) e_{nj k} M_{3,ik}(x, h_2)] \\
&\quad + \frac{1}{2} e_{ijk} M_{3,kn}(x, h_3) + \frac{2\mu + \kappa}{4\mu h_2^2} e_{ijn} M_3(x, h_2)
\end{aligned}$$

$$\begin{aligned}
\hat{J}_{nji}(x) = & -\frac{\gamma + \beta}{4\mu} M_{1,jn}(x) \\
& + \frac{2\mu + \kappa}{4\mu\kappa} [\alpha\delta_{ij}M_{3,kkn}(x, h_2) \\
& + (\gamma + \beta)M_{3,ijn}(x, h_2)] - \frac{1}{2\kappa} [\alpha\delta_{ij}M_{3,kkn}(x, h_3) \\
& + (\gamma + \beta)M_{3,ijn}(x, h_3)] \\
& - \frac{2\mu + \kappa}{4\mu\kappa h_2^2} [\alpha\delta_{ij}M_{3,jn}(x, h_2) + \\
& \gamma\delta_{in}M_{3,j}(x, h_2)] + \beta\delta_{jn}M_{3,i}(x, h_2)] \\
I_{nji}^C(x) = & \frac{\lambda + \mu}{\lambda + 2\mu} M_{2,jn}(x) \\
& - \frac{\lambda}{\lambda + 2\mu} \delta_{ij}M_{1,n}(x) - \delta_{in}M_{1,j}(x) \\
& - \delta_{jn}M_{1,i}(x)
\end{aligned} \tag{52}$$

Same results are also found by Cheng and He [10].

## Conclusion

In this work, we obtained the Eshelby tensors for isotropic homogeneous microstretch materials with a spherical inclusion. It is also shown that the solutions corresponding to the microelongation, the micropolar, and the classical cases are all the special cases of the microstretch theory. Using the obtained results, the Mori-Tanaka method may be extended to the microstretch medium which we still work on it and hopefully will give the details in a further work and determine the overall material moduli of damaged materials modeled as a microstretch continuum.

## References

1. Eshelby JD (1957) The determination of the elastic field of an ellipsoidal inclusion, and related problems. *Proceeding of Roy Soc A* 241:376–396
2. Mura T (1982) *Micromechanics of defects in solids*. Martinus Nijhoff, Netherlands
3. Markov KZ (1996) On the microstructural model of damage in solids. *Int J Eng Sci* 33:139–150

4. Eringen AC, Suhubi ES (1964) Nonlinear theory of simple microelastic solids-I. *Int J Eng Sci* 2:189–203
5. Suhubi ES, Eringen AC (1964) Nonlinear theory of simple microelastic solids-II. *Int J Eng Sci* 2:389–404
6. Eringen AC (1968) Theory of micropolar elasticity. In: Leibowitz H (ed) *Fracture and advanced treatise*. Academic, New York
7. Eringen AC (1999) *Microcontinuum field theories I. Foundations and solids*. Springer, New York
8. Cheng H, Hu GK, Zhuping H (2007) Effective moduli for micropolar composite with interface effects. *Int J Solids Struct* 44:8106–8118
9. Cheng ZQ, He LH (1995) Micropolar elastic fields due to spherical inclusion. *Int J Eng Sci* 33:389–397
10. Cheng ZQ, He LH (1997) Micropolar elastic fields due to circular cylindrical inclusion. *Int J Eng Sci* 35:659–668
11. Ma H, Hu G (2006) Eshelby tensors for an ellipsoidal inclusion in a micropolar material. *Int J Eng Sci* 44:595–605
12. Kiris A, Inan E (2005) Eshelby tensors for a spherical inclusion in microelongated elastic fields. *Int J Eng Sci* 43:49–58
13. Kiris A, Inan E (2006) Eshelby tensors for a spherical inclusion in microstretch elastic fields. *Int J Solids Struct* 43:4720–4738
14. Liu X, Hu GK (2004) Inclusion problem of microstretch medium. *Int J Eng Sci* 42:849–860
15. Ma H, Hu GK (2007) Eshelby tensors for an ellipsoidal inclusion in microstretch materials. *Int J Solids Struct* 44:3049–3061
16. Christensen RM (1990) A critical evaluation for a class of micromechanics models. *J Mech Phys Solids* 38:379–404

## Euler Beam Theory

► [Slender Beams, Thermal Buckling](#)

## Evolution of Micro-Cracks and Micro-Voids

► [Ductile Damage at Cryogenic Temperatures](#)

## Evolution of Micro-Damage, Damage in Structures

► [Cryogenic Condition, Damage In](#)

## Exact Solution for Classic Coupled Thermoelasticity in Cylindrical Coordinates

Mohsen Jabbari<sup>1</sup> and A. Moradi<sup>2</sup>

<sup>1</sup>Faculty of Engineering, Postgraduate School, South Tehran Branch, Islamic Azad University, Tehran, Iran

<sup>2</sup>Postgraduate School, Islamic Azad University, South Tehran Branch, Tehran, Iran

### Overview

In this entry, the classic coupled thermoelasticity model of hollow and solid cylinders under radial-symmetric loading condition ( $r, t$ ) is considered. A full analytical method is used, and an exact unique solution of the classic coupled equations is presented. The thermal and mechanical boundary conditions, the body force, and the heat source are considered in the most general forms, where no limiting assumption is used.

### Introduction

The coupled thermoelasticity of structural problems is frequently referred to in literature, where the assumption is used in the advanced engineering design problems for the structures under thermal shock loads. A thick circular cylindrical pressure vessel, as a structural member, may be subjected to mechanical and thermal shock loads. A pressure vessel under thermal shock at refineries and power plants, when the period of thermal shock is of the same order of magnitude as the period of lowest natural frequency of the vessel, may experience the stress wave fronts and thus should be analyzed through the coupled form of the energy and thermoelasticity equations. In this case, thermal stress and temperature wave fronts are produced and propagated through the structure. Engineering codes consider such a case as one of the loading conditions and put a limit on the magnitude of the resulting stresses by defining a proper allowable stress value [1].

The literature on the subject of coupled thermoelasticity for a bounded geometry with the given boundary conditions is extremely limited. The coupled thermoelasticity of an infinite space and a half-space is treated in literature, and exact solutions are available. For these cases, a few number of papers that present the closed form or analytical solution for the coupled thermoelasticity problems are available. Hetnarski [2] found the solution of coupled thermoelasticity in the form of a series of functions. Hetnarski and Ignaczak [3] presented a study of the one-dimensional thermoelastic waves produced by an instantaneous plane source of heat in homogeneous isotropic infinite and semi-infinite bodies of the Green–Lindsay type. The same authors presented an analysis of the laser-induced waves propagating in an absorbing thermoelastic semi-space of the Green–Lindsay type [4]. Georgiadis and Lykotrafitis [5] obtained a three-dimensional transient thermoelastic solution for the Rayleigh-type disturbances propagating on the surface of a half-space. Wagner [6] presented the fundamental matrix of a system of partial differential operators that governs the diffusion of heat and the strains in an elastic media. This method can be used to predict the temperature distribution and the strains by an instantaneous heat point source or by a suddenly applied delta force.

The mathematical treatment of such thermoelasticity problems by the analytical methods is rather complicated, and the numerical methods of solution are employed to analyze such problems. Milne et al. studied spherical elastic–plastic wave solutions [7]. These authors applied two closed-form radially symmetric elastic–plastic wave solutions corresponding to the spherical cavity loadings and compared the results with the numerical solutions constructed by a finite difference code. Berezovski et al. presented the numerical simulation of nonlinear elastic wave propagation in piecewise homogeneous media [8]. Also, Berezovski et al. presented the two-dimensional propagation of stress waves in functionally graded materials (FGMs) using a numerical method and by means of the composite wave-propagation algorithm [9]. They considered two distinct models of FGMs: first,



a multilayered metal-ceramic composite with averaged properties within the layers and, second, the randomly embedded ceramic particles in a metal matrix with prescribed volume fractions. Their analysis showed significant differences in the stress wave characteristics for the two distinct models, which can be used for optimizing the response of such structures to impact loading. Berezovski and Maugin simulated the wave front propagation in thermoelastic materials with phase transformation by means of the finite-volume numerical method [10]. These authors also simulated the thermoelastic wave propagation by means of a composite wave-propagation algorithm [11]. Engelbrecht et al. studied the nonlinear effects on the deformation waves in solids and dispersion [12]. In the mentioned work, the existence of solitary waves, the emergence of solitary wave trains, and the waves in piecewise nonlinear laminated materials are briefly discussed. Angel and Achenbach studied the effect of oblique incidence with an arbitrary angle on the reflection and transmission of elastic waves by a periodic array of cracks, and they studied the interaction of elastic waves with a planar array of periodically spaced cracks of equal lengths [13]. Mendelsohn et al. presented the two-dimensional scattering of incident surface waves and incident body waves by a surface-breaking crack [14]. Dempsey et al. computed the mode-III stress-intensity factor at the tip of the kinked crack for angles of incidence varying from normal to grazing incidence and for arbitrary subsonic crack tip speeds [15]. Achenbach derived explicit solutions for carrier waves supporting the surface waves and plate waves [16]. He reconsidered time-harmonic surface waves in a half-space and plate waves in a layer of a homogeneous transversely isotropic linearly elastic solid, where the  $x_1x_2$ -plane is the plane of transverse isotropy. Achenbach and Li studied the two-dimensional propagation of horizontally polarized transverse waves in a solid with a periodic distribution of cracks [17]. They used the theory of Floquet or Bloch waves, together with an appropriate Green's function and the condition of vanishing traction on the crack faces, which leads to a system of singular integral equations, which provides the basis for the

derivation of an exact dispersion equation. Roberts et al. investigated analytically and experimentally the reflection of elastic waves from a traction-free solid-air boundary of periodic saw-tooth profile [18]. Brind et al. studied the high-frequency scattering of elastic waves from the cylindrical cavities [19]. In their paper, the scattering of time-harmonic plane longitudinal elastic waves by smooth convex cylindrical cavities is investigated, and the exact solution for a circle is evaluated for wavelengths of the same order as the radius. Auld studied the acoustic fields and wave propagation in both isotropic and anisotropic solids [20]. He discussed the reflection and refraction at plane surfaces, composite media, waveguides, and resonators. Achenbach studied the wave propagation in elastic solids and presented an exposition of the basic concepts of mechanical wave propagation within a one-dimensional setting. He studied the formal aspects of elastodynamic theory in three dimensions and discussed the typical wave-propagation phenomena, such as radiation, reflection, refraction, propagation in waveguides, and diffraction [21].

In problems of coupled thermoelasticity, the majority of papers focus on the numerical methods of solution. Bagri and Eslami [22] studied the generalized coupled thermoelasticity of a functionally graded annular disk based on the Lord-Shulman model, where the Laplace transform is used to transform the governing equations into the Laplace domain. The Galerkin finite element method is employed to solve the system of ordinary differential equations in the space domain, where the actual physical quantities in the time domain are obtained using the numerical inversion of the Laplace transform. Lee and Yang [23] investigated an inverse problem of the coupled thermoelasticity of an infinite cylinder and estimated the time-varying heat flux of the cylinder at the outer boundary by the time history of the measured temperature on an interior point or distributed on the surface. Yang et al. [24] presented a technique to solve the inverse boundary value problems of coupled thermoelasticity in an infinitely long annular cylinder and computed the boundary time-varying heat flux by knowing

the strain history at any point of the cylinder. Subsequently, the distributions of temperature and thermal stresses in the cylinder at various times are determined. Eraslan and Orean [25] obtained the transient solution of the thermo-static-plastic deformation of internal heat-generating tubes by the thermomechanical coupling effect and temperature-dependent physical material parameters and used the partial differential solver PDECOL for this purpose. PDECOL is based on the method of lines and uses a finite element collocation procedure for the discretization of the spatial variable. Yang and Chu [26] analyzed the transient coupled thermoelasticity of an annular fin and neglected the effect of the inertia term in the equation of motion. They considered the mechanical coupling effect in heat conduction equation. Using the Laplace transform with respect to time, the governing equations became decoupled, and the approximate method (Fourier series technique) was used to achieve the inversion to the real time domain.

Bahtui and Eslami [27] studied the coupled thermoelastic response of a functionally graded circular cylindrical shell and used a Galerkin finite element formulation in the space domain and the Laplace transform in the time domain. Bakhshi et al. [28] studied the coupled thermoelasticity of a functionally graded disk and used the Laplace transform and the Galerkin finite element method to solve the governing equations. Hosseini-Tehrani and Eslami [29] used the boundary element method to develop the coupled thermoelasticity formulation of the thermal and mechanical shock problems in a two-dimensional finite domain. The formulation is based on the Laplace transfer technique in the time domain, where the solution is obtained using an appropriate numerical inversion technique. Tanigawa and Takeuti [30] developed a new technique for the coupled thermal stress problem of a hollow sphere under partial heating. The solution is obtained by a simultaneous determination of the stresses and temperature distribution by introducing a new harmonic function. They used the Laplace transform and Laplace inversion formulas with the theorem of residue. Bagri and Eslami [31] presented a solution for the

one-dimensional generalized thermoelasticity of a disk. They employed the Laplace transform and the Galerkin finite element method to solve the governing equations. Bagri et al. [32] proposed a unified formulation of the generalized coupled thermoelasticity and applied it to a layer of isotropic material, where the governing equations are solved by the Laplace transform and the numerical inverse of the Laplace transform. Cannarozzi and Ubertini [33] presented a mixed variational method for the linear coupled thermoelasticity, where a finite element model for the semi-discrete analysis is developed.

In this work, a full analytical method is proposed to obtain the response of the governing equations of the classical coupled thermoelasticity in cylindrical coordinates, where an exact solution is presented. The method of solution is based on the Fourier expansion and eigenfunction methods, which is a traditional and routine method in solving the partial differential equations. Since the coefficients of equations are not functions of the time variable ( $t$ ), an exponential form is considered for the general solution. For the particular solution, that is, the response to mechanical and thermal shocks, the eigenfunction method and Laplace transformation are used. This work [34] is the extension of the previous paper that presented an exact solution in the spherical coordinates [35].

## Governing Equations

A hollow cylinder with inner and outer radii  $r_i$  and  $r_o$  made of isotropic material subjected to the radial-symmetric mechanical and thermal shock loads is considered. The classical theory of coupled thermoelasticity for the wave propagation is considered.

If  $u$  is the displacement component in the radial direction, the strain–displacement relations for the radial-symmetric loading condition are

$$\begin{aligned}\varepsilon_{rr} &= u_{,r} \\ \varepsilon_{\theta\theta} &= \frac{u}{r}\end{aligned}\quad (1)$$

where  $(\cdot)$  denotes the partial derivative. The stress-strain relations for the plane strain condition are

$$\begin{aligned}\sigma_{rr} &= \frac{E_o}{(1+\nu)(1-2\nu)} [(1-\nu)\varepsilon_{rr} + \nu\varepsilon_{\theta\theta}] \\ &\quad - \frac{E\alpha_o}{(1-2\nu)} T(r, t) \\ \sigma_{\theta\theta} &= \frac{E_o}{(1+\nu)(1-2\nu)} [\nu\varepsilon_{rr} + (1-\nu)\varepsilon_{\theta\theta}] \\ &\quad - \frac{E\alpha_o}{(1-2\nu)} T(r, t)\end{aligned}\quad (2)$$

The equation of motion in the radial direct is

$$\sigma_{rr,r} + \frac{1}{r}(\sigma_{rr} - \sigma_{\theta\theta}) + X(r, t) = \rho_o \ddot{u} \quad (3)$$

Using relations (1)–(3), the Navier equation in terms of the displacement component is

$$\begin{aligned}u_{,rr} + \frac{1}{r}u_{,r} - \frac{1}{r^2}u - \alpha_o \frac{(1+\nu)}{(1-\nu)} T_{,r} \\ - \rho_o \frac{(1+\nu)(1-2\nu)}{(1-\nu)} \ddot{u} = -X(r, t)\end{aligned}\quad (4)$$

The coupled heat conduction equation for the radial-symmetric loading condition is [35, 36]

$$\begin{aligned}T_{,rr} + \frac{1}{r}T_{,r} - \frac{\rho_o c_o}{k_o} \dot{T} - \frac{E_o \alpha_o}{k_o(1-2\nu)} T_o \left( \dot{u}_{,r} + \frac{1}{r} \dot{u} \right) \\ = -R(r, t)\end{aligned}\quad (5)$$

where  $\alpha$ ,  $\rho$ ,  $E$ ,  $k$ ,  $c$ , and  $T_o$  denote the linear thermal coefficient, density, modulus of elasticity, thermal conduction coefficient, specific heat, and initial reference temperature, respectively. Here,  $F(r, t)$  and  $Q(r, t)$  are the body force and heat generation source, respectively. The mechanical and thermal boundary conditions are [35]

$$\begin{aligned}C_{11}u(ri, t) + C_{12}u_{,r}(ri, t) + C_{13}u_{,t}(ri, t) \\ + C_{14}u_{,tt}(ri, t) = f_1(t) \\ C_{21}u(ro, t) + C_{22}u_{,r}(ro, t) + C_{23}u_{,t}(ro, t) \\ + C_{24}u_{,tt}(ro, t) = f_2(t) \\ C_{31}T(ri, t) + C_{32}T_{,r}(ri, t) + C_{33}T_{,t}(ri, t) = f_3(t) \\ C_{41}T(ro, t) + C_{42}T_{,r}(ro, t) + C_{43}T_{,t}(ro, t) = f_4(t)\end{aligned}\quad (6)$$

where  $C_{ij}$  are the mechanical and thermal coefficients; by assigning different values for them, different types of mechanical and thermal boundary conditions may be obtained. These boundary conditions include the displacement, strain, stress, specified temperature, convection, and heat flux, and they are presented in [Appendixes 1](#) and [2](#). The initial boundary conditions are assumed in general form,

$$\begin{aligned}U(r, 0) &= f_5(r) \\ U_{,t}(r, 0) &= f_6(r) \\ T(r, 0) &= f_7(r)\end{aligned}\quad (7)$$

## Solution

Equations (4) and (5) are a system of nonhomogeneous partial differential equations with nonconstant coefficients functions of radial variable ( $t$ ) and with general and particular solutions.

### General Solution with Homogeneous Boundary Conditions

Since the coefficients of these equations are independent of time variable ( $t$ ), the exponential function form of the time variable may be assumed for the general solution as

$$\begin{aligned}u(r, t) &= [U(r)] e^{\lambda t} \\ T(r, t) &= [T(r)] e^{\lambda t}\end{aligned}\quad (8)$$

Substituting (8) into the homogeneous parts of (4) and (5) yields

$$\begin{aligned} u'' + \frac{1}{r}u' - \frac{1}{r^2}u + d_1T' + d_2\lambda^2u &= 0 \\ T'' + \frac{1}{r}T' + d_3\lambda T + d_4\lambda\left(u' + \frac{1}{r}u\right) &= 0 \end{aligned} \quad (9)$$

Equation (9) is a system of ordinary differential equations, where the prime symbol (') shows differentiation with respect to the radial variable ( $r$ ) and  $d_1$ – $d_4$  are constant parameters.

The first solutions of  $U_1$  and  $\theta_1$  are considered as

$$\begin{aligned} U_1(r) &= A_1J_1(\beta r) \\ \theta_1(r) &= B_1J_0(\beta r) \end{aligned} \quad (10)$$

Substituting (10) into (9) and using the formulas for derivatives of the Bessel function, such as  $dJ_0(\beta r)/dr = -\beta J_1(r)$  and  $dJ_n(\beta r)/dr = \beta J_{n-1}(\beta r) - n(J_n(\beta r)/r)$ , yield

$$\begin{aligned} \{(-\beta^2 + \lambda^2 d_2)A_1 - d_1\beta B_1\}J_1(\beta r) &= 0 \\ \{\lambda d_4\beta A_1 - (\beta^2 + \lambda d_3)B_1\}J_0(\beta r) &= 0 \end{aligned} \quad (11)$$

Equation (11) shows that  $U_1$  and  $\theta_1$  can be the solutions of (9) if and only if

$$\begin{bmatrix} (-\beta^2 + \lambda^2 d_2) & -d_1\beta \\ \lambda d_4\beta & (-\beta^2 + \lambda d_3) \end{bmatrix} \times \begin{Bmatrix} A_1 \\ B_1 \end{Bmatrix} = \begin{Bmatrix} 0 \\ 0 \end{Bmatrix} \quad (12)$$

The nontrivial solution of (12) is obtained by setting the determinant of this equation equal to zero as

$$(-\beta^2 + a\lambda\lambda_3)(-\beta^2 + \lambda^2 d_2) + d_1 d_4 \beta^2 \lambda = 0 \quad (13)$$

Equation (13) is the first characteristic equation. Thus, it is concluded that the first solutions for  $U_1$  and  $\beta_1$  satisfy the system of (9), and they are the first solutions of this system.

The second solution of the system of ordinary differential equations with nonconstant coefficients (9) must be considered as

$$\begin{aligned} U_2(r) &= [A_2J_1(\beta r) + A_3rJ_2(\beta r)] \\ \theta_2(r) &= [B_2J_0(\beta r) + B_3rJ_1(\beta r)] \end{aligned} \quad (14)$$

Substituting (14) into (9) yields

$$\begin{aligned} &\{(\beta^2 - \lambda^2 d_2)A_3 + d_1\beta B_3\}rJ_0(\beta r) \\ &+ \left\{(-\beta^2 + \lambda^2 d_2)A_2 + \lambda^2 d_2 \frac{2}{\beta}A_3 - d_1\beta B_2\right\}J_1(\beta r) = 0 \\ &\{A_2\lambda d_4\beta + (-\beta^2 + \lambda d_3)B_2 + 2\beta B_3\}J_0(\beta r) \\ &+ \{A_3\lambda d_4\beta(-\beta^2 + \lambda d_3)B_3\}rJ_1(\beta r) = 0 \end{aligned} \quad (15)$$

The expressions for  $U_2$  and  $\theta_2$  can be the solutions of (9) if and only if

$$\begin{bmatrix} (-\beta^2 + \lambda^2 d_2) & -d_1\beta \\ \lambda d_4\beta & (-\beta^2 + \lambda d_3) \end{bmatrix} \times \begin{Bmatrix} A_3 \\ B_3 \end{Bmatrix} = \begin{Bmatrix} 0 \\ 0 \end{Bmatrix} \quad (16)$$

$$\left\{(-\beta^2 + \lambda^2 d_2)A_2 + \lambda^2 d_2 \frac{2}{\beta}A_3 - d_1\beta B_2\right\} = 0 \quad (17)$$

$$\{\lambda d_4\beta A_2 + (-\beta^2 + \lambda d_3)B_2 + 2\beta B_3\} = 0 \quad (18)$$

The nontrivial solution of (16) is obtained by setting the determinant equal to zero as

$$(-\beta^2 + a\lambda\lambda_3)(-\beta^2 + \lambda^2 d_2) + d_1 d_4 \beta^2 \lambda = 0 \quad (19)$$

The characteristic (19) is the same as the characteristic (13). This equality is interesting as it prevents mathematical dilemma and complexity, and a single value for the eigenvalue  $\beta$  simultaneously satisfies both characteristic (13) and (19). Equations (17) and (18) give the relation between  $A_2, A_3, B_2$ , and  $B_3$ , and they play as the balancing ratios that help (14) to be the second solution of the system of (9). Equations (17) and (18) are two algebraic equations with six unknowns  $A_2, A_3, B_2, B_3, \lambda$ , and  $\beta$ . Since the number of unknowns is more than the equations, there

is no restriction to bring noncompatibility between (16)–(18). The complete general solutions for the solid cylinder are

$$\begin{aligned} u^g(r) &= A_1 J_1(\beta r) + A_2 [J_1(\beta r) + \zeta_1 r J_2(\beta r)] \\ \theta^g(r) &= A_1 \zeta_2 J_0(\beta r) + A_2 [\zeta_3 J_0(\beta r) + \zeta_4 r J_1(\beta r)] \end{aligned} \quad (20)$$

Those for the hollow cylinder are

$$\begin{aligned} u^g(r) &= A_1 J_1(\beta r) + A_2 [J_1(\beta r) + \zeta_1 r J_2(\beta r)] \\ &\quad + A_3 Y_1(\beta r) + A_4 [Y_1(\beta r) + \zeta_1 r Y_2(\beta r)] \\ \theta^g(r) &= A_1 \zeta_2 J_0(\beta r) + A_2 [\zeta_3 J_0(\beta r) + \zeta_4 r J_1(\beta r)] \\ &\quad + A_3 \zeta_2 Y_0(\beta r) + A_4 [\zeta_3 Y_0(\beta r) + \zeta_4 r Y_1(\beta r)] \end{aligned} \quad (21)$$

where  $\zeta_1 - \zeta_4$  are ratios obtained from (12), (17) and (18). Substituting  $Ug$  and  $\theta g$  in the homogeneous form of the boundary conditions (6), four linear algebraic equations are obtained as

$$\begin{bmatrix} \mu_{11} & \mu_{12} & \mu_{13} & \mu_{14} \\ \mu_{21} & \mu_{22} & \mu_{23} & \mu_{24} \\ \mu_{31} & \mu_{32} & \mu_{33} & \mu_{34} \\ \mu_{41} & \mu_{42} & \mu_{43} & \mu_{44} \end{bmatrix} \begin{Bmatrix} A_1 \\ A_2 \\ A_3 \\ A_4 \end{Bmatrix} = \begin{Bmatrix} 0 \\ 0 \\ 0 \\ 0 \end{Bmatrix} \quad (22)$$

where  $\mu_{ij}$  are the coefficients depending on  $\lambda$  and  $\beta$  are given in the appendix. Setting the determinant of the coefficients of (22) equal to zero, the second characteristic equation is obtained. Simultaneous solution of this equation and (13), results into infinite number of two eigenvalues  $\beta_n$  and  $\lambda_n$ . Therefore,  $U^g$  and  $\theta^g$  are rewritten as

$$\begin{aligned} u^g(r) &= A_1 [J_1(\beta n r) + [\zeta_5 J_1(\beta n r) + \zeta_6 r J_2(\beta n r)] \\ &\quad + \zeta_7 Y_1(\beta n r) + [\zeta_8 Y_1(\beta n r) + \zeta_9 r Y_2(\beta n r)]] \\ T^g(r) &= A_1 [\zeta_{10} J_0(\beta n r) + [\zeta_{11} J_0(\beta n r) + \zeta_{12} r J_1(\beta n r)] \\ &\quad + \zeta_{13} Y_0(\beta n r) + [\zeta_{14} Y_0(\beta n r) + \zeta_{15} r Y_1(\beta n r)]] \end{aligned} \quad (23)$$

where  $\zeta_5$  to  $\zeta_{15}$  are ratios presented in the appendix and are obtained from (22). Let us show the functions in the brackets of (23) by functions  $H_1$  and  $H_0$  as

$$\begin{aligned} H_1(\beta n r) &= J_1(\beta n r) + [\zeta_5 J_1(\beta n r) + \zeta_6 r J_2(\beta n r)] \\ &\quad + \zeta_7 Y_1(\beta n r) + [\zeta_8 Y_1(\beta n r) + \zeta_9 r Y_2(\beta n r)] \\ H_0(\beta n r) &= \zeta_{10} J_0(\beta n r) + [\zeta_{11} J_0(\beta n r) + \zeta_{12} r J_1(\beta n r)] \\ &\quad + \zeta_{13} Y_0(\beta n r) + [\zeta_{14} Y_0(\beta n r) + \zeta_{15} r Y_1(\beta n r)] \end{aligned} \quad (24)$$

According to Sturm-Liouville theories, these functions are orthogonal with respect to weight function  $p(r) = r$  as

$$\int_{r_i}^{r_o} H(\beta_n r) H(\beta_m r) r dr = \begin{cases} 0 & n \neq m \\ \|H(\beta_n r)\|^2 & n = m \end{cases} \quad (25)$$

where  $\|H(\beta_n r)\|$  is the norm the function  $H$  and equals

$$\|H(\beta_n r)\| = \left[ \int_{r_i}^{r_o} r H^2(\beta_n r) dr \right]^{\frac{1}{2}} \quad (26)$$

Due to the orthogonality of function  $H$ , every piece-wise continuous function, such as  $f(r)$ , can be expanded in terms of the function  $H$  (either for  $H_0$  or  $H_1$ ) and is called  $H$ -Fourier series as

$$f(r) = \sum_{n=1}^{\infty} e_n H(\beta_n r) \quad (27)$$

where  $e_n$  equals

$$e_n = \frac{I}{\|H(\beta_n r)\|^2} \int_{r_i}^{r_o} f(r) H(r) r dr \quad (28)$$

According to the numerical results, there are three groups for eigenvalues  $\lambda_n$ , where the first  $\lambda_{n1}$  are real and negative, and the second and third ones,  $\lambda_{n2}$ ,  $\lambda_{n3}$ , are conjugate complex with negative real part  $-\xi_n \omega_n$  and imaginary part  $\pm \omega_{dn}$ , where  $\omega_{dn}$  and  $\omega_n$  are damped and non-damped thermal-mechanical natural frequencies and  $\xi_n$  is damping ratio for  $n$ th natural mode. Equation (13) is an algebraic equation in polynomial form, and the determinant of (22) is an algebraic equation in the Bessel function form.

The exact analytical solution for this system of nonlinear algebraic equations is complicated, and the numerical method of solution is employed in this entry. Since the Bessel functions are periodic, the system has an infinite number of roots.

The numerical results of  $\beta_n$  and  $\lambda_n$  for 50 roots are presented in Sect. 4. Using (8), (23), and (24), the displacement and temperature distributions due to the general solution become By using (8), (10), (34), and (35) the displacement and temperature distribution due to general solution become

$$\begin{aligned} u^g(r, t) &= \sum_{n=1}^{\infty} \{a_n e^{-\lambda_n t} + e^{-\xi \omega n t} [b_n \cos \omega_{dn} t + c_n \sin \omega_{dn} t]\} H_1(\beta_n r) \\ T^g(r, t) &= \sum_{n=1}^{\infty} \{a_n e^{-\lambda_n t} + e^{-\xi \omega n t} [b_n \cos \omega_{dn} t + c_n \sin \omega_{dn} t]\} H_0(\beta_n r) \end{aligned} \quad (29)$$

Using the initial conditions (7) and with the help of (27)–(29), four unknown constants  $a_n$ ,  $b_n$ ,  $c_n$ , and  $\beta_n$  are obtained.

suitable to expand the body force  $F(r, t)$  and heat source  $Q(r, t)$  in  $H$ -Fourier expansion form as

### Particular Solution with Nonhomogeneous Boundary Conditions

The general solutions may be used as proper functions for guessing the particular solution adopted to the nonhomogeneous parts of (4) and (5) and nonhomogeneous boundary conditions (6) as

$$\begin{aligned} F(r, t) &= \sum_{n=1}^{\infty} F_n(t) H_1(\beta_n r) \\ Q(r, t) &= \sum_{n=1}^{\infty} Q_n(t) H_0(\beta_n r) \end{aligned} \quad (31)$$

where  $F_n(t)$  and  $Q_n(t)$  are

$$\begin{aligned} u^p(r, t) &= \sum_{n=1}^{\infty} \{[G_{1n}(t) J_1(\beta_n r) + G_{2n}(t) r J_2(\beta_n r)] + r^2 G_{5n}(t)\} \\ T^p(r, t) &= \sum_{n=1}^{\infty} \{[G_{3n}(t) J_0(\beta_n r) + G_{4n}(t) r J_1(\beta_n r)] + r^2 G_{6n}(t)\} \end{aligned} \quad (30)$$

$$\begin{aligned} F_n(t) &= \frac{1}{\|H_1(\beta_n r)\|^2} \int_{r_i}^{r_o} F(r, t) H_1(\beta_n r) r dr \\ Q_n(t) &= \frac{1}{\|H_0(\beta_n r)\|^2} \int_{r_i}^{r_o} Q(r, t) H_0(\beta_n r) r dr \end{aligned} \quad (32)$$

For the solid sphere, the second type of Bessel function  $Y$  is excluded. It is necessary and

Substituting (30) and (31) into the nonhomogeneous form of (4) and (5) yields

$$\begin{aligned} &\left\{ \begin{aligned} &-\beta_n^2 G_{1n}(t) + d_2 \ddot{G}_{1n}(t) + \frac{2}{\beta_n} d_2 \ddot{G}_{2n}(t) - d_1 \beta_n G_{3n}(t) + a n_1 C_0 G_{5n}(t) + a n_1 C_1 \frac{2}{\beta_n} G_{5n}(t) \\ &+ a n_2 C_0 G_{6n}(t) + a n_2 C_1 \frac{2}{\beta_n} G_{6n}(t) + a n_3 C_0 \ddot{G}_{5n}(t) + a n_3 C_1 \frac{2}{\beta_n} \ddot{G}_{5n}(t) + d_5 a n C_0 + \frac{2}{\beta_n} d_5 a n C_1 \end{aligned} \right\} r J_0(\beta_n r) \\ &+ \{ \beta_n^2 G_{2n}(t) - d_2 \ddot{G}_{2n}(t) + d_1 \beta_n G_{4n}(t) - a n_1 C_1 G_{5n}(t) - a n_3 C_1 \ddot{G}_{5n}(t) - a n_2 C_1 G_{6n}(t) - d_5 a n C_1 \} J_1(\beta_n r) = 0 \\ &\left\{ \begin{aligned} &d_4 \beta_n \dot{G}_{1n}(t) - \beta_n^2 G_{3n}(t) + d_3 \dot{G}_{3n}(t) + 2 \beta_n G_{4n}(t) + b n_2 E_0 \dot{G}_{5n}(t) + b n_5 E_0 \ddot{G}_{5n}(t) + b n_1 E_0 G_{6n}(t) \\ &+ b n_3 E_0 \dot{G}_{6n}(t) + d_6 b n E_0 \end{aligned} \right\} J_0(\beta_n r) \\ &+ \{ d_4 \beta_n \dot{G}_{2n}(t) - \beta_n^2 G_{4n}(t) + d_3 \dot{G}_{4n}(t) + b n_2 E_1 \dot{G}_{5n}(t) + b n_1 E_1 G_{6n}(t) + b n_3 E_1 \dot{G}_{6n}(t) + d_6 b n E_1 \} r J_1(\beta_n r) = 0 \end{aligned} \quad (33)$$

where  $d_7 - d_{18}$  and  $d_{37}$  and  $d_{38}$  are the coefficients of H-expansion and are given in the appendix. The

guessed functions (30) can satisfy the nonhomogeneous part of (4) and (5) if and only if

$$\begin{aligned} & \beta_n^2 G_{2n}(t) - d_2 \ddot{G}_{2n}(t) + d_1 \beta_n G_{4n}(t) - an_1 C_1 G_{5n}(t) - an_3 C_1 \ddot{G}_{5n}(t) - an_2 C_1 G_{6n}(t) - d_5 an C_1 = 0 \\ & - \beta_n^2 G_{1n}(t) + d_2 \ddot{G}_{1n}(t) + \frac{2}{\beta_n} d_2 \ddot{G}_{2n}(t) - d_1 \beta_n G_{3n}(t) + an_1 C_0 G_{5n}(t) + an_1 C_1 \frac{2}{\beta_n} G_{5n}(t) \\ & + an_2 C_0 G_{6n}(t) + an_2 C_1 \frac{2}{\beta_n} G_{6n}(t) + an_3 C_0 \ddot{G}_{5n}(t) + an_3 C_1 \frac{2}{\beta_n} \ddot{G}_{5n}(t) + d_5 an C_0 + \frac{2}{\beta_n} d_5 an C_1 = 0 \\ & d_4 \beta_n \dot{G}_{1n}(t) - \beta_n^2 G_{3n}(t) + d_3 \dot{G}_{3n}(t) + 2\beta_n G_{4n}(t) + bn_2 E_0 \dot{G}_{5n}(t) \\ & + bn_1 E_0 G_{6n}(t) + bn_3 E_0 \dot{G}_{6n}(t) + d_6 bn E_0 = 0 \\ & d_4 \beta_n \dot{G}_{2n}(t) - \beta_n^2 G_{4n}(t) + d_3 \dot{G}_{4n}(t) + bn_2 E_1 \dot{G}_{5n}(t) + bn_1 E_1 G_{6n}(t) + bn_3 E_1 \dot{G}_{6n}(t) + d_6 bn E_1 = 0 \end{aligned} \quad (34)$$

Taking the Laplace transform of (34) and using two boundary conditions of (6) (for solid

cylinder only second and forth boundary conditions are applicable) gives

$$\begin{bmatrix} -\beta_n^2 + d_2 s^2 & -\beta_n + d_2 \frac{6}{\beta_n} s^2 & -d_1 \beta_n & -d_1 & (d_7 + d_8 \frac{3}{\beta_n})(d_{12} + d_{13} s^2) & (d_7 + d_8 \frac{3}{\beta_n})d_{14} \\ 0 & \beta_n^2 - 2d_2 s^2 & 0 & d_1 \beta_n & -d_8 d_{12} - d_8 d_{13} s^2 & -d_8 d_{14} \\ d_4 \beta_n s & 0 & -\beta_n^2 + d_3 s & 2\beta_n & d_9 d_{15} s & d_9 d_{16} + d_9 d_{17} s \\ 0 & d_4 \beta_n s & 0 & -\beta_n^2 + d_3 s & d_{10} d_{15} s & d_{10} d_{16} + d_{10} d_{17} s \\ d_{19} & d_{20} & d_{21} & d_{22} & d_{23} & d_{24} \\ 0 & 0 & d_{25} & d_{26} & 0 & d_{27} \end{bmatrix} \times \begin{bmatrix} G_{1n}(s) \\ G_{2n}(s) \\ G_{3n}(s) \\ G_{4n}(s) \\ G_{5n}(s) \\ G_{6n}(s) \end{bmatrix} = \begin{bmatrix} -\left(d_7 d_{11} + d_8 d_{11} \frac{3}{\beta_n}\right) F_n(s) \\ d_8 d_{11} F_n(s) \\ -d_9 d_{18} Q_n(s) \\ -d_{10} d_{18} Q_n(s) \\ F_2(s) \\ F_4(s) \end{bmatrix} \quad (35)$$

Equation (35) is a system of algebraic equations and is solved for  $G_{1n}(s) - G_{6n}(s)$  by the Cramer methods in the Laplace domain, where by the inverse Laplace transform the functions are transformed into the real time domain. In the process of solution, it is necessary to consider the following points.

1. The initial conditions (7) are considered only for the general solutions (29). The initial

conditions of  $G_{1n}(t)$  to  $G_{6n}(t)$  for the particular solutions are considered equal to zero.

- Equation (35) is in polynomial form function of the Laplace parameter  $s$  (not the Bessel functions form of  $s$ ). Therefore, the exact inverse Laplace transform is possible and somehow simple.
- For the hollow cylinder, it is enough to include the second type of Bessel function  $Y(r)$  in sequence of particular solution as



$$\begin{aligned}
 u^p(r, t) &= \sum_{n=1}^{\infty} \{ [G_{1n}(t)J_1(\beta nr) + G_{2n}(t)rJ_2(\beta nr)] \\
 &\quad + [G_{3n}(t)Y_1(\beta nr) + G_{4n}(t)rY_2(\beta nr)] \\
 &\quad + r G_{5n}(t) + r^2 \{G_{6n}(t)\} \\
 T^p(r, t) &= \sum_{n=1}^{\infty} \{ [G_{7n}(t)J_0(\beta nr) + G_{8n}(t)rJ_1(\beta nr)] \\
 &\quad + [G_{9n}(t)Y_0(\beta nr) + G_{10n}(t)rY_1(\beta nr)] \\
 &\quad + r G_{11n}(t) + r^2 G_{12n}(t) \}
 \end{aligned}
 \tag{36}$$

By substituting (36) in (4) and (5), eight equations are obtained, where using the four boundary conditions (6), 12 functions  $G_{1n}(t) - G_{12n}(t)$  are obtained for the hollow cylinder.

## Results and Discussions

As an example, a solid sphere with radius  $r_o = 1\text{m}$  made of aluminum is considered. The material properties are shown in Table 1. Using the values of material properties given in Table 1, the first 50 roots of  $\lambda_n$  and  $\beta_n$  are calculated, as shown in Table 2.

The initial temperature  $T_o$  is considered to be  $293^\circ\text{K}$ . Now, an instantaneous hot outside surface temperature  $T(1, t) = 10^{-3}T_o\delta(t)$ , where  $\delta(t)$  is the unit Dirac function, is considered, and the outside radius of the cylinder is assumed to be fixed ( $u(1, t) = 0$ ). To draw the graphs, a nondimensional time  $\hat{t} = \frac{vt}{r_o}$  is considered, where  $v = \sqrt{E(1-\nu)/\rho(1+\nu)(1-2\nu)}$  is the dilatational-wave velocity. Figures 1 and 2 show the wave fronts of displacement and temperature.

As a second example, a mechanical shock wave of the form  $u(1, t) = 10^{-12}u_o\delta(t)$  is applied to the outside surface of the cylinder, where the surface is assumed to be at zero temperature ( $T(1, t) = 0$ ) and  $u_o = r_o\alpha T_o$  is an assumed initial displacement. Figures 3 and 4 show the wave fronts for the displacement and temperature distributions along the radial direction. The convergence of the solutions for these examples is achieved by consideration of 1,200 eigenvalues used for the  $H$ -Fourier expansion. More than

**Exact Solution for Classic Coupled Thermoelasticity in Cylindrical Coordinates, Table 1** Material properties of aluminum

$E = 70\text{ GPa}$
$\nu = 0.3$
$\alpha = 23 \times 10^{-6}\text{ 1/K}$
$\rho = 2707\text{ kg/m}^3$
$K = 204\text{ W/m K}$
$c = 903\text{ J/kg K}$

this number of eigenvalues result in increased round-off and truncation errors, which affect the quality of the graphs.

The convergence of solution is faster for displacement in comparison with the temperature. The small oscillations in Figs. 2 and 4 are due to the convergence of solutions.

Now, consider a periodic temperature shock at the outside surface in the form  $T(1, t) = T_o \sin \hat{t}$ , with  $u(1, t) = 0$ . Figures 5–8 show the penetration waves along the radius of the cylinder. The convergence of solution for this example is faster than the previous examples, where 500 eigenvalues are used for the  $H$ -Fourier expansion.

## Conclusion

In this entry, an analytical solution for the coupled thermoelasticity of thick cylinders under radial temperature or mechanical shock load is presented. The method is based on the eigenfunction Fourier expansion, which is a classical and traditional method of solution for the typical initial and boundary value problems. The strength of this method is its ability to reveal the fundamental mathematical and physical properties and the interpretations of the problem under study.

In the coupled thermoelastic problem of the radial-symmetric cylinder, the governing equations are a system of partial differential equations with two independent variables, the radius ( $r$ ) and the time ( $t$ ). The traditional procedure to solve this class of problems is to eliminate the time variable by using the Laplace transform.

Exact Solution for Classic Coupled Thermoelasticity in Cylindrical Coordinates, Table 2 The first 50 roots of  $\lambda_n$  and  $\beta_n$

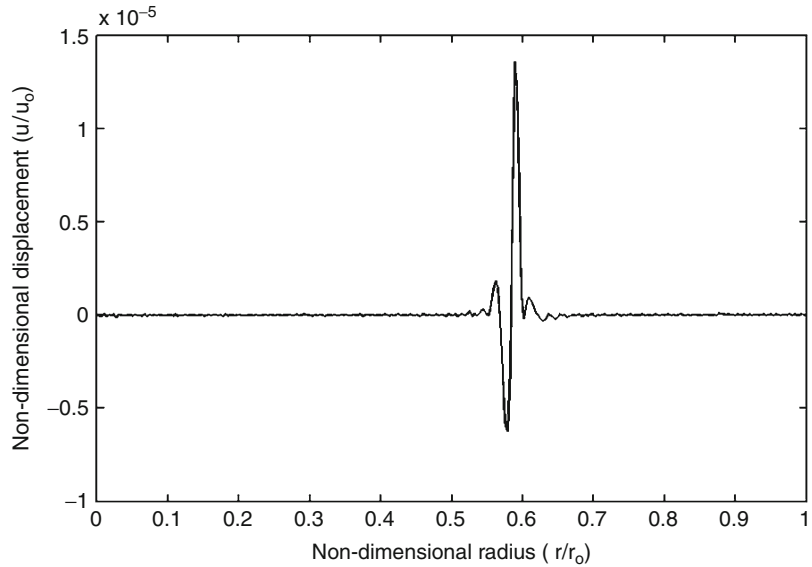
Root number	$\beta_n$	$\lambda_{n1}$	$\lambda_{n2}$	$\lambda_{n3}$
1	$9.88 \times 10^{-01}$	$-1.02 \times 10^{-05}$	$-49.2889 \times 10^{-009} + 5.7338 \times 10^{003};_1$	$-49.2889 \times 10^{-009} - 5.7338 \times 10^{003};_1$
2	$2.10 \times 10^{00}$	$-4.60 \times 10^{-05}$	$-223.0715 \times 10^{-009} + 12.1963 \times 10^{003};_1$	$-223.0715 \times 10^{-009} - 12.1963 \times 10^{003};_1$
3	$3.20 \times 10^{00}$	$-1.07 \times 10^{-04}$	$-517.7543 \times 10^{-009} + 18.5802 \times 10^{003};_1$	$-517.7543 \times 10^{-009} - 18.5802 \times 10^{003};_1$
4	$4.30 \times 10^{00}$	$-1.93 \times 10^{-04}$	$-934.9049 \times 10^{-009} + 24.9668 \times 10^{003};_1$	$-934.9049 \times 10^{-009} - 24.9668 \times 10^{003};_1$
5	$5.40 \times 10^{00}$	$-3.04 \times 10^{-04}$	$-1.4744 \times 10^{-006} + 31.3536 \times 10^{003};_1$	$-1.4744 \times 10^{-006} - 31.3536 \times 10^{003};_1$
6	$6.50 \times 10^{00}$	$-4.40 \times 10^{-04}$	$-2.1363 \times 10^{-006} + 37.7403 \times 10^{003};_1$	$-2.1363 \times 10^{-006} - 37.7403 \times 10^{003};_1$
7	$7.60 \times 10^{00}$	$-6.02 \times 10^{-04}$	$-2.9206 \times 10^{-006} + 44.1272 \times 10^{003};_1$	$-2.9206 \times 10^{-006} - 44.1272 \times 10^{003};_1$
8	$8.70 \times 10^{00}$	$-7.89 \times 10^{-04}$	$-3.8273 \times 10^{-006} + 50.5140 \times 10^{003};_1$	$-3.8273 \times 10^{-006} - 50.5140 \times 10^{003};_1$
9	$9.80 \times 10^{00}$	$-1.00 \times 10^{-03}$	$-4.8563 \times 10^{-006} + 56.9008 \times 10^{003};_1$	$-4.8563 \times 10^{-006} - 56.9008 \times 10^{003};_1$
10	$1.09 \times 10^{01}$	$-1.24 \times 10^{-03}$	$-6.0078 \times 10^{-006} + 63.2876 \times 10^{003};_1$	$-6.0078 \times 10^{-006} - 63.2876 \times 10^{003};_1$
11	$1.20 \times 10^{01}$	$-1.50 \times 10^{-03}$	$-7.2815 \times 10^{-006} + 69.6744 \times 10^{003};_1$	$-7.2815 \times 10^{-006} - 69.6744 \times 10^{003};_1$
12	$1.31 \times 10^{01}$	$-1.79 \times 10^{-03}$	$-8.6777 \times 10^{-006} + 76.0613 \times 10^{003};_1$	$-8.6777 \times 10^{-006} - 76.0613 \times 10^{003};_1$
13	$1.42 \times 10^{01}$	$-2.10 \times 10^{-03}$	$-10.1963 \times 10^{-006} + 82.4481 \times 10^{003};_1$	$-10.1963 \times 10^{-006} - 82.4481 \times 10^{003};_1$
14	$1.53 \times 10^{01}$	$-2.44 \times 10^{-03}$	$-11.8372 \times 10^{-006} + 88.8349 \times 10^{003};_1$	$-11.8372 \times 10^{-006} - 88.8349 \times 10^{003};_1$
15	$1.64 \times 10^{01}$	$-2.80 \times 10^{-03}$	$-13.6005 \times 10^{-006} + 95.2217 \times 10^{003};_1$	$-13.6005 \times 10^{-006} - 95.2217 \times 10^{003};_1$
16	$1.75 \times 10^{01}$	$-3.19 \times 10^{-03}$	$-15.4861 \times 10^{-006} + 101.6086 \times 10^{003};_1$	$-15.4861 \times 10^{-006} - 101.6086 \times 10^{003};_1$
17	$1.86 \times 10^{01}$	$-3.60 \times 10^{-03}$	$-17.4942 \times 10^{-006} + 107.9954 \times 10^{003};_1$	$-17.4942 \times 10^{-006} - 107.9954 \times 10^{003};_1$
18	$1.97 \times 10^{01}$	$-4.04 \times 10^{-03}$	$-19.6246 \times 10^{-006} + 114.3822 \times 10^{003};_1$	$-19.6246 \times 10^{-006} - 114.3822 \times 10^{003};_1$
19	$2.08 \times 10^{01}$	$-4.51 \times 10^{-03}$	$-21.8774 \times 10^{-006} + 120.7690 \times 10^{003};_1$	$-21.8774 \times 10^{-006} - 120.7690 \times 10^{003};_1$
20	$2.19 \times 10^{01}$	$-5.00 \times 10^{-03}$	$-24.2526 \times 10^{-006} + 127.1559 \times 10^{003};_1$	$-24.2526 \times 10^{-006} - 127.1559 \times 10^{003};_1$
21	$2.30 \times 10^{01}$	$-5.51 \times 10^{-03}$	$-26.7501 \times 10^{-006} + 133.5427 \times 10^{003};_1$	$-26.7501 \times 10^{-006} - 133.5427 \times 10^{003};_1$
22	$2.41 \times 10^{01}$	$-6.05 \times 10^{-03}$	$-29.3701 \times 10^{-006} + 139.9295 \times 10^{003};_1$	$-29.3701 \times 10^{-006} - 139.9295 \times 10^{003};_1$
23	$2.52 \times 10^{01}$	$-6.62 \times 10^{-03}$	$-32.1124 \times 10^{-006} + 146.3163 \times 10^{003};_1$	$-32.1124 \times 10^{-006} - 146.3163 \times 10^{003};_1$
24	$2.63 \times 10^{01}$	$-7.21 \times 10^{-03}$	$-34.9770 \times 10^{-006} + 152.7032 \times 10^{003};_1$	$-34.9770 \times 10^{-006} - 152.7032 \times 10^{003};_1$

25	$2.74 \times 10^{01}$	$-7.82 \times 10^{-03}$	$-37.9641 \times 10^{-06}$	$+159.0900 \times 10^{003};$	$-37.9641 \times 10^{-06}$	$-159.0900 \times 10^{003};$
26	$2.85 \times 10^{01}$	$-8.46 \times 10^{-03}$	$-41.0735 \times 10^{-06}$	$+165.4768 \times 10^{003};$	$-41.0735 \times 10^{-06}$	$-165.4768 \times 10^{003};$
27	$2.96 \times 10^{01}$	$-9.13 \times 10^{-03}$	$-44.3053 \times 10^{-06}$	$+171.8636 \times 10^{003};$	$-44.3053 \times 10^{-06}$	$-171.8636 \times 10^{003};$
28	$3.07 \times 10^{01}$	$-9.82 \times 10^{-03}$	$-47.6595 \times 10^{-06}$	$+178.2505 \times 10^{003};$	$-47.6595 \times 10^{-06}$	$-178.2505 \times 10^{003};$
29	$3.18 \times 10^{01}$	$-1.05 \times 10^{-02}$	$-51.1360 \times 10^{-06}$	$+184.6373 \times 10^{003};$	$-51.1360 \times 10^{-06}$	$-184.6373 \times 10^{003};$
30	$3.29 \times 10^{01}$	$-1.13 \times 10^{-02}$	$-54.7350 \times 10^{-06}$	$+191.0241 \times 10^{003};$	$-54.7350 \times 10^{-06}$	$-191.0241 \times 10^{003};$
31	$3.40 \times 10^{01}$	$-1.20 \times 10^{-02}$	$-58.4563 \times 10^{-06}$	$+197.4109 \times 10^{003};$	$-58.4563 \times 10^{-06}$	$-197.4109 \times 10^{003};$
32	$3.51 \times 10^{01}$	$-1.28 \times 10^{-02}$	$-62.3000 \times 10^{-06}$	$+203.7978 \times 10^{003};$	$-62.3000 \times 10^{-06}$	$-203.7978 \times 10^{003};$
33	$3.62 \times 10^{01}$	$-1.37 \times 10^{-02}$	$-66.2660 \times 10^{-06}$	$+210.1846 \times 10^{003};$	$-66.2660 \times 10^{-06}$	$-210.1846 \times 10^{003};$
34	$3.73 \times 10^{01}$	$-1.45 \times 10^{-02}$	$-70.3545 \times 10^{-06}$	$+216.5714 \times 10^{003};$	$-70.3545 \times 10^{-06}$	$-216.5714 \times 10^{003};$
35	$3.84 \times 10^{01}$	$-1.54 \times 10^{-02}$	$-74.5653 \times 10^{-06}$	$+222.9582 \times 10^{003};$	$-74.5653 \times 10^{-06}$	$-222.9582 \times 10^{003};$
36	$3.95 \times 10^{01}$	$-1.63 \times 10^{-02}$	$-78.8985 \times 10^{-06}$	$+229.3451 \times 10^{003};$	$-78.8985 \times 10^{-06}$	$-229.3451 \times 10^{003};$
37	$4.06 \times 10^{01}$	$-1.72 \times 10^{-02}$	$-83.3540 \times 10^{-06}$	$+235.7319 \times 10^{003};$	$-83.3540 \times 10^{-06}$	$-235.7319 \times 10^{003};$
38	$4.17 \times 10^{01}$	$-1.81 \times 10^{-02}$	$-87.9320 \times 10^{-06}$	$+242.1187 \times 10^{003};$	$-87.9320 \times 10^{-06}$	$-242.1187 \times 10^{003};$
39	$4.28 \times 10^{01}$	$-1.91 \times 10^{-02}$	$-92.6323 \times 10^{-06}$	$+248.5055 \times 10^{003};$	$-92.6323 \times 10^{-06}$	$-248.5055 \times 10^{003};$
40	$4.39 \times 10^{01}$	$-2.01 \times 10^{-02}$	$-97.4550 \times 10^{-06}$	$+254.8924 \times 10^{003};$	$-97.4550 \times 10^{-06}$	$-254.8924 \times 10^{003};$
41	$4.50 \times 10^{01}$	$-2.11 \times 10^{-02}$	$-102.4000 \times 10^{-06}$	$+261.2792 \times 10^{003};$	$-102.4000 \times 10^{-06}$	$-261.2792 \times 10^{003};$
42	$4.61 \times 10^{01}$	$-2.21 \times 10^{-02}$	$-107.4675 \times 10^{-06}$	$+267.6660 \times 10^{003};$	$-107.4675 \times 10^{-06}$	$-267.6660 \times 10^{003};$
43	$4.72 \times 10^{01}$	$-2.32 \times 10^{-02}$	$-112.6573 \times 10^{-06}$	$+274.0528 \times 10^{003};$	$-112.6573 \times 10^{-06}$	$-274.0528 \times 10^{003};$
44	$4.83 \times 10^{01}$	$-2.43 \times 10^{-02}$	$-117.9695 \times 10^{-06}$	$+280.4397 \times 10^{003};$	$-117.9695 \times 10^{-06}$	$-280.4397 \times 10^{003};$
45	$4.94 \times 10^{01}$	$-2.54 \times 10^{-02}$	$-123.4040 \times 10^{-06}$	$+286.8265 \times 10^{003};$	$-123.4040 \times 10^{-06}$	$-286.8265 \times 10^{003};$
46	$5.05 \times 10^{01}$	$-2.66 \times 10^{-02}$	$-128.9610 \times 10^{-06}$	$+293.2133 \times 10^{003};$	$-128.9610 \times 10^{-06}$	$-293.2133 \times 10^{003};$
47	$5.16 \times 10^{01}$	$-2.77 \times 10^{-02}$	$-134.6403 \times 10^{-06}$	$+299.6001 \times 10^{003};$	$-134.6403 \times 10^{-06}$	$-299.6001 \times 10^{003};$
48	$5.27 \times 10^{01}$	$-2.89 \times 10^{-02}$	$-140.4420 \times 10^{-06}$	$+305.9869 \times 10^{003};$	$-140.4420 \times 10^{-06}$	$-305.9869 \times 10^{003};$
49	$5.38 \times 10^{01}$	$-3.02 \times 10^{-02}$	$-146.3661 \times 10^{-06}$	$+312.3738 \times 10^{003};$	$-146.3661 \times 10^{-06}$	$-312.3738 \times 10^{003};$
50	$5.49 \times 10^{01}$	$-3.14 \times 10^{-02}$	$-152.4125 \times 10^{-06}$	$+318.7606 \times 10^{003};$	$-152.4125 \times 10^{-06}$	$-318.7606 \times 10^{003};$

### Exact Solution for Classic Coupled Thermoelasticity in Cylindrical Coordinates,

#### Fig. 1 Nondimensional displacement distribution

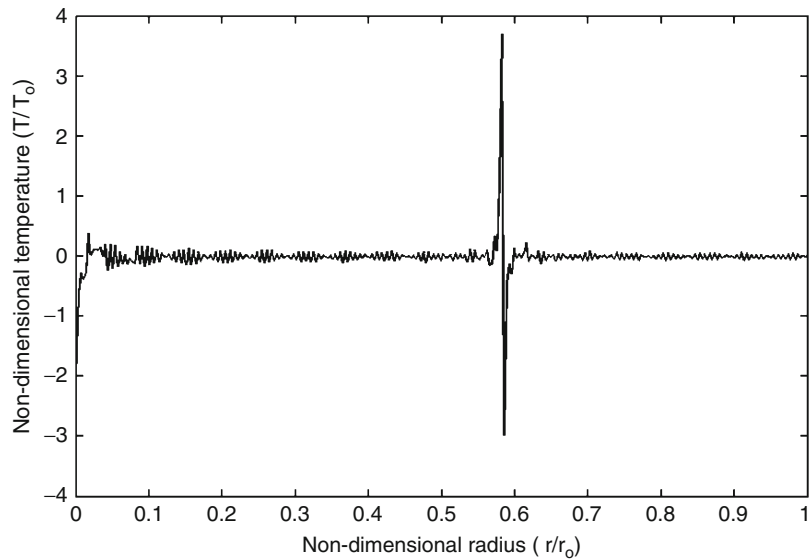
due to input  
 $T(1, t) = 10^{-3}T_0\delta(t)$  at  
 nondimensional time  
 $\hat{t} = 0.4$



### Exact Solution for Classic Coupled Thermoelasticity in Cylindrical Coordinates,

#### Fig. 2 Nondimensional temperature distribution

due to input  
 $T(1, t) = 10^{-3}T_0\delta(t)$  at  
 nondimensional time  
 $\hat{t} = 0.4$



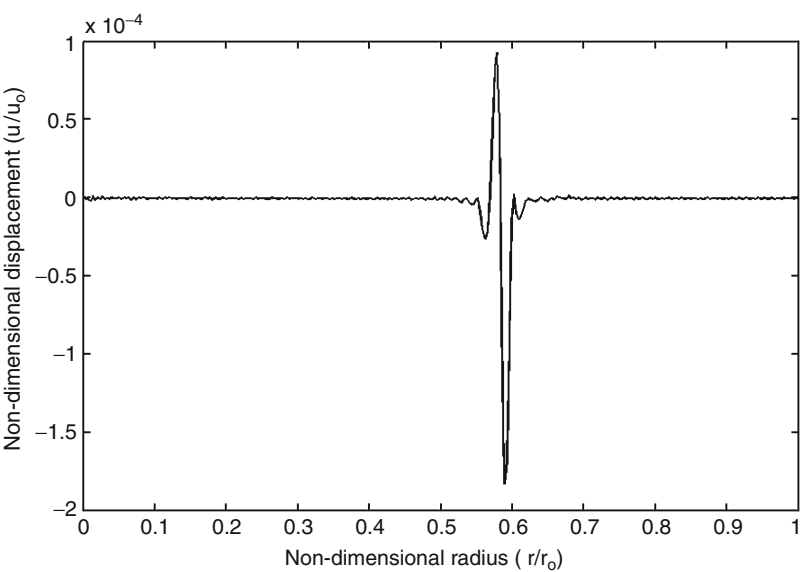
The resulting system is a set of ordinary differential equations in terms of the radius variable, which falls into the Bessel function family. This method of analysis brings the Laplace parameter ( $s$ ) in the argument of the Bessel functions, causing hardship or complications in carrying out the exact inverse of the Laplace transformation. As a result, the numerical inverse of the Laplace transformation is used

in the papers dealing with this type of problems in literature. In this entry, to prevent this problem, when the Laplace transform is applied to the particular solutions, it is postponed after eliminating the radius variable  $r$  by the  $H$ -Fourier expansion. Thus, the Laplace parameter ( $s$ ) appears in polynomial function forms, and hence the exact Laplace inversion transformations are possible.

Exact Solution for Classic Coupled

Thermoelasticity in Cylindrical Coordinates,

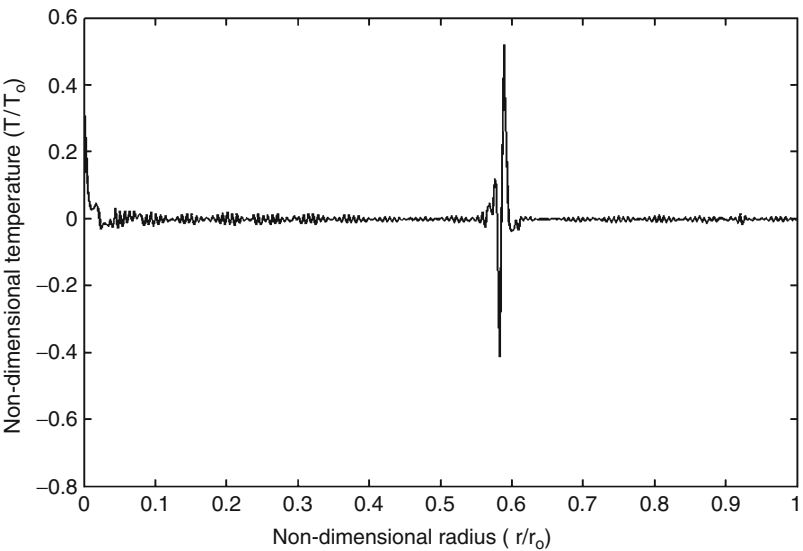
**Fig. 3** Nondimensional displacement distribution due to input  $u(1, t) = 10^{-12}u_0\delta(t)$  at nondimensional time  $\hat{t} = 0.4$



Exact Solution for Classic Coupled

Thermoelasticity in Cylindrical Coordinates,

**Fig. 4** Nondimensional temperature distribution due to input  $u(1, t) = 10^{-12}u_0\delta(t)$  at nondimensional time  $\hat{t} = 0.4$



The method described in this entry is an exact solution of the coupled thermoelasticity of thick cylinders with two given boundary conditions. The exact solutions found in literature for the coupled thermoelasticity problems are limited to the infinite spaces and half-spaces. The analytical method of solution presented in this entry is for a finite domain with specified and given boundary conditions. This is the novelty of the entry, where the solution of a popular structural component (a thick cylinder) with two specified boundary

conditions under the coupled thermoelastic assumption is given analytically and in terms of the series solution.

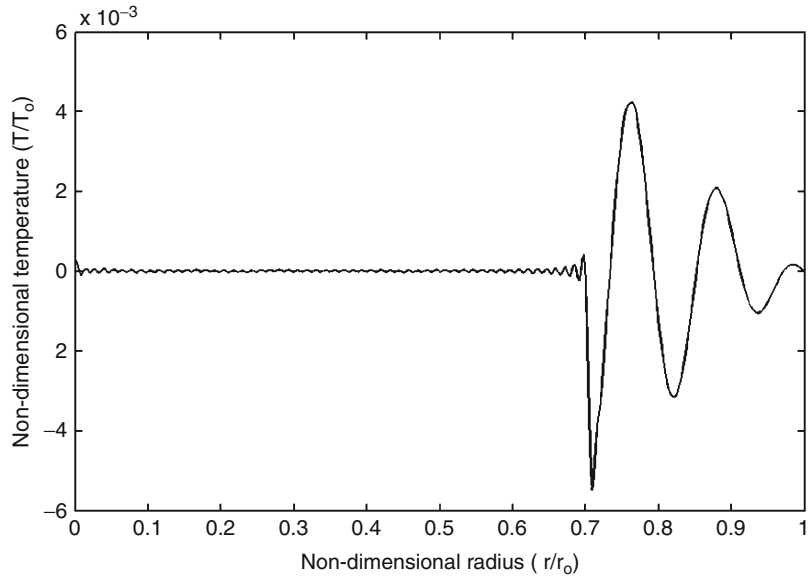
**Appendix 1 Mechanical Boundary Conditions**

For mechanical boundary conditions, four options are available: known radial displacement, known radial stress, and a combination of them.

### Exact Solution for Classic Coupled Thermoelasticity in Cylindrical Coordinates,

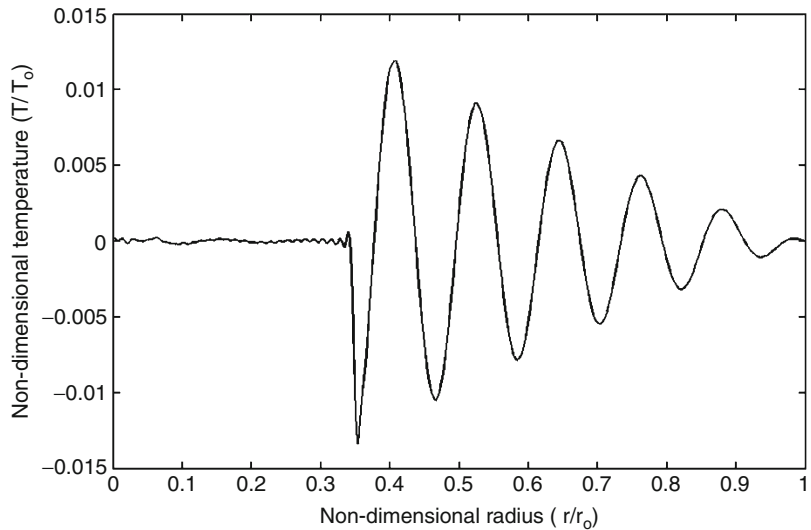
#### Fig. 5 Nondimensional temperature distribution due to input

$T(1, t) = T_0 \sin \hat{t}$  at nondimensional time  $\hat{t} = 0.3$



### Exact Solution for Classic Coupled Thermoelasticity in Cylindrical Coordinates,

#### Fig. 6 Nondimensional temperature distribution due to input $T(1, t) = T_0 \sin \hat{t}$ at nondimensional time $\hat{t} = 0.6$



1. Radial displacements at inner and outer surfaces are known as

$$u(r_i, t) = f_1(t)$$

$$u(r_o, t) = f_2(t)$$

In this case, we have  $C_{11} = 1$ ,  $C_{12} = 0$ ,  $C_{21} = 1$ , and  $C_{22} = 0$ .

For fixed surfaces, it is enough to consider  $f_1(t)$  and  $f_2(t)$  equal to zero.

2. When radial stress at inner and outer surfaces are known, by the help of (1) and (2), we can write

$$\sigma_{rr}(r_i, t) = \frac{E}{(1+\nu)(1-2\nu)} \left[ (1-\nu)u_{,r} + \nu \frac{1}{r_i} u \right]$$

$$- \frac{E\alpha}{(1-2\nu)} T(r_i, t) = f_1(t)$$

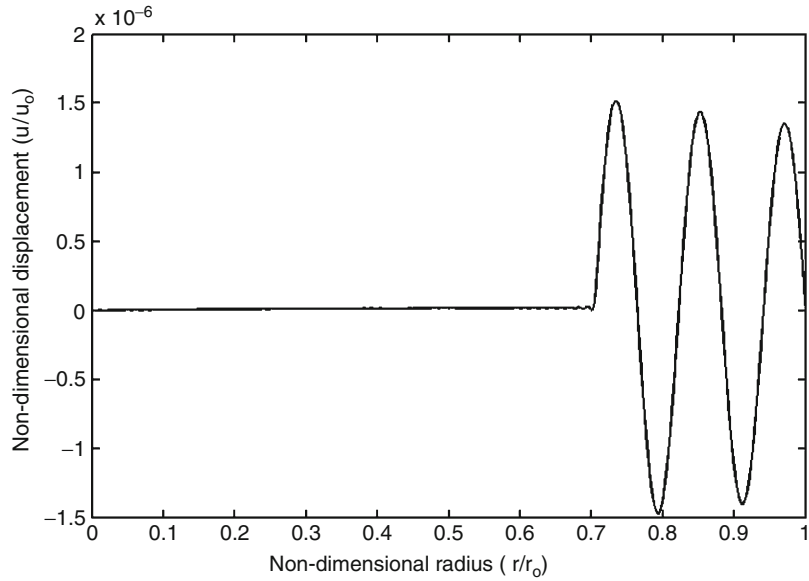
$$\sigma_{\theta\theta}(r_o, t) = \frac{E}{(1+\nu)(1-2\nu)} \left[ (1-\nu)u_{,r} + \nu \frac{1}{r_o} u \right]$$

$$- \frac{E\alpha}{(1-2\nu)} T(r_o, t) = f_2(t)$$

In this case, we have

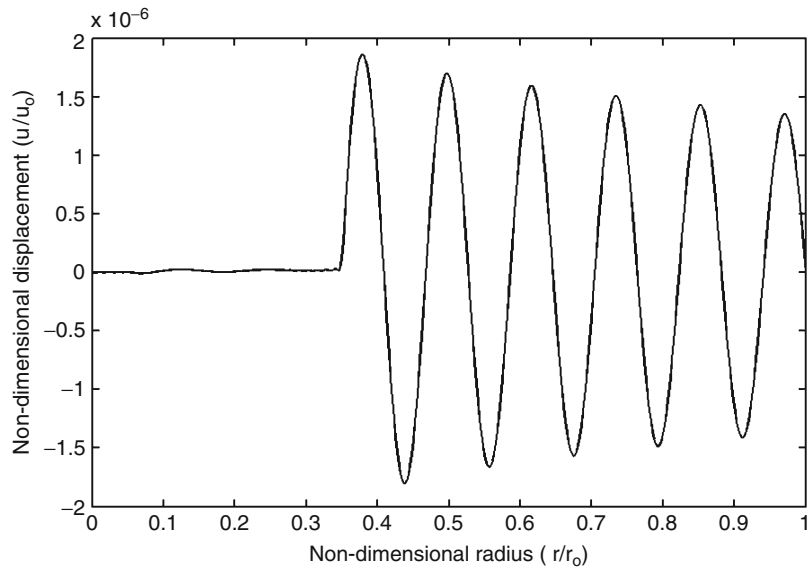
### Exact Solution for Classic Coupled Thermoelasticity in Cylindrical Coordinates,

**Fig. 7** Nondimensional displacement distribution due to input  $T(1, t) = T_o \sin \hat{t}$  at nondimensional time  $\hat{t} = 0.3$



### Exact Solution for Classic Coupled Thermoelasticity in Cylindrical Coordinates,

**Fig. 8** Nondimensional displacement distribution due to input  $T(1, t) = T_o \sin \hat{t}$  at nondimensional time  $\hat{t} = 0.6$



$$C_{11} = \frac{E}{(1+\nu)(1-2\nu)}, C_{11} = \frac{E(1-\nu)}{(1+\nu)(1-2\nu)}$$

$$C_{21} = \frac{E}{(1+\nu)(1-2\nu)}, C_{22} = \frac{E(1-\nu)}{(1+\nu)(1-2\nu)}$$

For traction free, it is enough to consider  $f_1(t)$  and  $f_2(t)$  equal to zero.

The third and fourth mechanical boundary conditions are the combination of above mentioned first and second boundary conditions.

## Appendix 2 Thermal Boundary Conditions

For thermal boundary conditions, six options are available: specified temperature, heat flux, and convection.

1. Temperatures at inner and outer surfaces are known as

$$T(r_i, t) = f_1(t)$$

$$T(r_o, t) = f_2(t)$$



In this case, we have  $C_{11} = 1$ ,  $C_{12} = 0$ ,  $C_{21} = 1$ , and  $C_{22} = 0$ .

- Heat fluxes at inner and outer surfaces are known as

$$\begin{aligned}T_{,r}(r_i, t) &= f_1(t) \\ T_{,r}(r_o, t) &= f_2(t)\end{aligned}$$

In this case, we have  $C_{31} = k$ ,  $C_{32} = 0$ ,  $C_{41} = k$ , and  $C_{42} = 0$ , where  $k$  is the thermal conduction coefficient.

For an insulated surface, it is enough to consider  $f_1(t)$  and  $f_2(t)$  equal to zero.

- Convections at inner and outer surfaces are known as

$$\begin{aligned}h_i T(r_i, t) + k T_{,r}(r_i, t) &= f_3(t) \\ h_o T(r_o, t) + k T_{,r}(r_o, t) &= f_4(t)\end{aligned}$$

In this case, we have  $C_{31} = h_i$ ,  $C_{32} = k$ ,  $C_{41} = h_o$ , and  $C_{42} = k$ , where  $h_i$  and  $h_o$  are the thermal convection coefficients at inner and outer surfaces of the cylinder, respectively. The fourth to sixth cases for thermal boundary conditions are combinations of the above-mentioned first to third boundary conditions.

## References

- ASME (2007) ASME boiler and pressure vessel code, section VIII, division 1. ASME, New York
- Hetnarski RB (1964) Solution of the coupled problem of thermoelasticity in the form of series of functions. *J Arch Mech Stosow* 12:919–941
- Hetnarski RB, Ignaczak J (1993) Generalized thermoelasticity: closed-form solutions. *J Therm Stresses* 16:473–498
- Hetnarski RB, Ignaczak J (1994) Generalized thermoelasticity: response of semi-space to a short laser pulse. *J Therm Stresses* 17:377–396
- Georgiadis HG, Lykotrafitis G (2005) Rayleigh waves generated by a thermal source: a three-dimensional transient thermoelasticity solution. *ASME J Appl Mech* 72:129–138
- Wagner P (1994) Fundamental matrix of the system of dynamic linear thermoelasticity. *J Therm Stresses* 17:549–565
- Milne PC, Morland LW, Yeung W (1988) Spherical elastic-plastic wave solutions. *J Mech Phys Solids* 36:15–28
- Berezovski A, Berezovski M, Engelbrecht J (2006) Numerical simulation of nonlinear elastic wave propagation in piecewise homogeneous media. *J Mater Sci Eng* 418:364–369
- Berezovski A, Engelbrecht J, Maugin GA (2003) Numerical simulation of two-dimensional wave propagation in functionally graded materials. *J Eur J Mech A Solids* 22:257–265
- Berezovski A, Maugin GA (2003) Simulation of wave and front propagation in thermoelastic materials with phase transformation. *J Comput Mater Sci* 28:478–485
- Berezovski A, Maugin GA (2001) Simulation of thermoelastic wave propagation by means of a composite wave-propagation algorithm. *J Comput Phys* 168:249–264
- Engelbrecht J, Berezovski A, Saluperea A (2007) Nonlinear deformation waves in solids and dispersion. *J Wave Motion* 44:493–500
- Angel YC, Achenbach JD (1985) Reflection and transmission of elastic waves by a periodic array of cracks: oblique incidence. *J Wave Motion* 7:375–397
- Mendelsohn DA, Achenbach JD, Keer LM (1980) Scattering of elastic waves by a surface-breaking crack. *J Wave Motion* 2:277–292
- Dempsey JP, Kuo MK, Achenbach JD (1982) Mode-III crack kinking under stress-wave loading. *J Wave Motion* 4:181–190
- Achenbach JD (1998) Explicit solutions for carrier waves supporting surface waves and plate waves. *J Wave Motion* 28:89–97
- Achenbach JD, Li ZL (1986) Propagation of horizontally polarized transverse waves in a solid with a periodic distribution of cracks. *J Wave Motion* 8:371–379
- Roberts R, Achenbach JD, Ko R, Adler L, Jungman A, Quentin G (1985) Reflection of a beam of elastic waves by a periodic surface profile. *J Wave Motion* 7:67–77
- Brind RJ, Achenbach JD, Gubernatis JE (1984) High-frequency scattering of elastic waves from cylindrical cavities. *J Wave Motion* 6:41–60
- Auld BA (1990) Acoustic fields and waves in solids. Krieger, Florida, 2 Sub edition
- Achenbach JD (1973) Wave propagation in elastic solids. North-Holland, Amsterdam
- Bagri A, Eslami MR (2008) Generalized coupled thermoelasticity of functionally graded annular disk considering the lord-shulman theory. *J Compos Struct* 83:168–179
- Lee HL, Yang YC (2001) Inverse problem of coupled thermoelasticity for prediction of heat flux and thermal stresses in an annular cylinder. *J Int Commun Heat Mass Tr* 28:661–670
- Yang YC, Chen UC, Chang WJ (2002) An inverse problem of coupled thermoelasticity in predicting heat flux and thermal stress by strain measurement. *J Therm Stresses* 25:265–281
- Eraslan AN, Oren Y (2002) Computation of transient thermal stresses in elastic-plastic tubes: effect of coupling and temperature-dependent physical properties. *J Therm Stresses* 25:559–572

26. Yang YC, Chu SS (2001) Transient coupled thermoelastic analysis of an annular Fin. *J Int Commun Heat Mass Tr* 28:1103–1114
27. Bahtui A, Eslami MR (2007) Coupled thermoelasticity of functionally graded cylindrical shells. *J Mech Res Commun* 34:1–18
28. Bakhshi M, Bagri A, Eslami MR (2006) Coupled thermoelasticity of functionally graded disk. *J Mech Adv Mater Struct* 13:214–225
29. Hosseini-Tehrani P, Eslami MR (2000) BEM analysis of thermal and mechanical shock in a two-dimensional finite domain considering coupled thermoelasticity. *J Eng Anal Bound Elem* 24:249–257
30. Tanigawa Y, Takeuti Y (1982) Coupled thermal stress problem in a hollow sphere under a partial heating. *J Int J Eng Sci* 20:41–48
31. Bagri A, Eslami MR (2004) Generalized coupled thermoelasticity of disks based on the lord-shulman model. *J Therm Stresses* 27:691–704
32. Bagri A, Taheri H, Eslami MR, Fariborz F (2006) Generalized coupled thermoelasticity of layer. *J Therm Stresses* 29:359–370
33. Cannarozzi AA, Ubertini F (2001) Mixed variational method for linear coupled thermoelastic analysis. *Int J Solids Struct* 38:717–739
34. Jabbari M, Dehbani H, Eslami MR (2011) An exact solution for classic coupled thermoelasticity in cylindrical coordinates. *J Pressure Vessel Technol* 133:051204–051210
35. Jabbari M, Dehbani H, Eslami MR (2010) An exact solution for classic coupled thermoelasticity in spherical coordinates. *ASME J Pressure Vessel Technol* 132:031201–031211
36. Hetnarski RB, Eslami MR (2009) *Thermal stresses-advanced theory and applications*. Springer, New York

## Exact Solution for Classic Coupled Thermoelasticity in Spherical Coordinates

Mohsen Jabbari<sup>1</sup> and H. Dehbani<sup>2</sup>

<sup>1</sup>Faculty of Engineering, Postgraduate School, South Tehran Branch, Islamic Azad University, Tehran, Iran

<sup>2</sup>Postgraduate School, South Tehran Branch, Islamic Azad University, Tehran, Iran

## Overview

In this entry, the classic coupled thermoelasticity model of hollow and solid spheres under

radial-symmetric loading condition  $(r, t)$  is considered. A full analytical method is used and an exact unique solution of the classic coupled equations is presented. The thermal and mechanical boundary conditions, the body force, and the heat source are considered in the most general forms, where no limiting assumption is used. This generality allows to simulate variety of applicable problems.

## Introduction

The classic and generalized theories of coupled thermoelasticity are enormously developed due to their many applications in the advanced structural design problems. Therefore, it is crucial to be able to obtain the deformation and temperature distributions in the structures under thermal shock loads. In the classical coupled problems of thermoelasticity, the first time rate of change of the first invariant of strain tensor appears in the first law of thermodynamics, causing coupling between the elastic and thermal fields. The mathematical treatment of coupled thermoelasticity problems by analytical methods is rather complicated. Only very basic problems of the coupled thermoelasticity theory, such as the problems of infinite and half spaces, are analytically treated in the literature and many works are reported using the numerical methods.

There are a limited number of papers that present the closed-form or analytical solution for the coupled thermoelasticity problems. Hetnarski [1] found the solution of coupled thermoelasticity in the form a series of functions. Hetnarski and Ignaczak presented a study of the one-dimensional thermoelastic waves produced by an instantaneous plane source of heat in homogeneous isotropic infinite and semi-infinite bodies of the Green-Lindsay type [2]. Also, these authors presented an analysis of the laser-induced waves propagating in an absorbing thermoelastic semi-space of the Green-Lindsay type [3]. Georgiadis and Lykotrakis obtained a three-dimensional transient thermoelastic solution for the Rayleigh-type disturbances propagating on the surface of a half-space [4]. Wagner [5] presented the fundamental matrix of a system of

partial differential operators that governs the diffusion of heat and strains in the elastic media. This method can be used to predict the temperature distribution and the strains by an instantaneous point heat source or by a suddenly applied delta force.

Majority of papers focus on the numerical methods of solution in the coupled problems. Bagri and Eslami [6] studied the generalized coupled thermoelasticity of functionally graded annular disk based on the Lord-Shulman model, where the Laplace transform is used to transform the governing equations into the Laplace domain. The Galerkin finite element method is employed to solve the system of ordinary differential equations in the space domain, where the actual physical quantities in the time domain are obtained using the numerical inversion of the Laplace transform. Lee and Yang [7] investigated an inverse problem of coupled thermoelasticity of an infinite cylinder and estimated the time-varying heat flux of the cylinder at the outer boundary by the time history of measured temperature on an interior point or distributed on the surface. Yang et al. [8] presented a technique to solve the inverse boundary value problems of coupled thermoelasticity in an infinitely long annular cylinder and computed the boundary time-varying heat flux by knowing the strain history at any point of the cylinder. Subsequently, the distributions of temperature and thermal stress in the cylinder at various times are determined. Eraslan and Orean [9] obtained the transient solution of the thermostatic-plastic deformation of internal heat-generating tubes by the thermomechanical coupling effect and temperature-dependent physical material parameters and used the partial differential solver PDECOL for this purpose. The PDECOL is based on the method of lines and uses a finite element collocation procedure for the discretization of the spatial variable. Yang and Chu [10] analyzed the transient coupled thermoelasticity of an annular fin and neglected the effect of inertia term in the equation of motion. They considered the mechanical coupling effect in heat conduction equation. Using the Laplace transform with respect to time, the

governing equations became decoupled and approximate method (Fourier series technique) is used to achieve the inversion to the real domain. Bahtui and Eslami [11] studied the coupled thermoelastic response of a functionally graded circular cylindrical shell and used a Galerkin finite element formulation in space domain and the Laplace transform in time domain. Bakhshi et al. [12] studied the coupled thermoelasticity of functionally graded disk and used the Laplace transform and Galerkin finite element method to solve the governing equations. Tehrani and Eslami [13] used the boundary element method to develop the coupled thermoelasticity formulation of the thermal and mechanical shock problem in a two-dimensional finite domain. The formulation is based on the Laplace transfer technique in time domain, where the solution is obtained using an appropriate numerical inversion technique. Tanigawa and Takeuti [14] developed a new technique for the coupled thermal stress problem of a hollow sphere under partial heating. The solution is obtained by simultaneous determination of the stresses and temperature distribution by introducing a new harmonic function. They used the Laplace transform and Laplace inversion formulas with the theorem of residue. Bagri and Eslami [15] presented a solution for one-dimensional generalized thermoelasticity of a disk. They employed the Laplace transform and Galerkin finite element method to solve the governing equations. Bagri et al. [16] proposed a unified formulation of the generalized coupled thermoelasticity and applied it to a layer of isotropic material, where the governing equations are solved by the Laplace transform and numerical inverse of the Laplace transform. Cannarozi and Ubertini [17] presented a mix variational method for the linear coupled thermoelasticity, where a finite element model for the semidiscrete analysis is developed.

In this work [18], a full analytical method is employed to obtain the response of a thick sphere under thermal and mechanical shock loads, where the solution is obtained under the classical coupled thermoelasticity assumption. The method of solution is based on the Fourier expansion and

eigenfunction methods, which is a traditional method to solve the partial differential equations. Since the coefficients of equations are not functions of the time variable ( $t$ ), an exponential form is considered for the general solution matched with the physical wave properties of the thermal and mechanical waves. For the particular solution, that is the response to mechanical and thermal shock loads, the eigenfunction method and Laplace transformation are used.

## Governing Equations

A hollow sphere with inner and outer radii  $r_i$  and  $r_o$ , respectively, made of isotropic material subjected to radial-symmetric mechanical and thermal shock loads is considered. The classic theory of coupled thermoelasticity for wave propagation is considered to allow coupling between the deformation and thermal energy fields and to describe the physical behavior of the elastic domain to mechanical and thermal shock loads. If  $u$  is the displacement component in the radial direction, the strain–displacement relations in the radial-symmetric condition are:

$$\begin{aligned}\varepsilon_{rr} &= u_{,r} \\ \varepsilon_{\theta\theta} &= \frac{u}{r}\end{aligned}\quad (1)$$

where  $(,)$  denotes partial derivative. The stress–strain relations for the plane strain condition are:

$$\begin{aligned}\sigma_{rr} &= \frac{E}{(1+\nu)(1-2\nu)}[(1-\nu)\varepsilon_{rr} + 2\nu\varepsilon_{\theta\theta}] \\ &\quad - \frac{E\alpha}{(1-2\nu)}T(r,t) \\ \sigma_{\theta\theta} &= \frac{E}{(1+\nu)(1-2\nu)}[\nu\varepsilon_{rr} + \varepsilon_{\theta\theta}] \\ &\quad - \frac{E\alpha}{(1-2\nu)}T(r,t)\end{aligned}\quad (2)$$

where  $\sigma_{ij}$  and  $\varepsilon_{ij}$  ( $i, j = r, \theta$ ) are the radial and hoop stresses and strains tensors, respectively,  $T(r, t)$  is the temperature distribution,  $\alpha$  is the coefficient of thermal expansion,  $E$  is the modulus of elasticity, and  $\nu$  is the Poisson's ratio.

The equation of motion in the radial direction is:

$$\sigma_{rr,r} + \frac{2}{r}(\sigma_{rr} - \sigma_{\theta\theta}) + F(r, t) = \rho \ddot{u} \quad (3)$$

where  $F(r, t)$  is the body force in the radial direction.

Using the relations (1)–(3), the Navier equation in term of the displacement components is obtained as:

$$\begin{aligned}u_{,rr} + \frac{2}{r}u_{,r} - \frac{2}{r^2}u - \alpha \frac{(1+\nu)}{(1-\nu)}T_{,r} \\ - \frac{\rho}{E} \frac{(1+\nu)(1-2\nu)}{(1-\nu)}\ddot{u} \\ = -\frac{1}{E} \frac{(1+\nu)(1-2\nu)}{(1-\nu)}F(r, t)\end{aligned}\quad (4)$$

The heat conduction equation for the radial-symmetric condition with the mechanical coupling term is:

$$\begin{aligned}T_{,rr} + \frac{2}{r}T_{,r} - \frac{\rho c}{k}\dot{T} - \frac{E\alpha T_o}{k(1-2\nu)}\left(\dot{u}_{,r} + \frac{2}{r}\dot{u}\right) \\ = -\frac{1}{k}Q(r, t)\end{aligned}\quad (5)$$

where  $\alpha, \rho, E, k, c$  and  $T_o$  are the linear thermal coefficient, the density, the modulus of elasticity, the thermal conduction coefficient, the specific heat, and the initial reference temperature, respectively. Here,  $F(r, t)$  and  $Q(r, t)$  are the body force and heat generation source, respectively. The mechanical and thermal boundary conditions are:

$$\begin{aligned}C_{11}u(r_i, t) + C_{12}u_r(r_i, t) + C_{13}T(r_i, t) &= f_1(t) \\ C_{21}u(r_o, t) + C_{22}u_r(r_o, t) + C_{23}T(r_o, t) &= f_2(t) \\ C_{31}T(r_i, t) + C_{32}T_{,r}(r_i, t) &= f_3(t) \\ C_{41}T(r_o, t) + C_{42}T_{,r}(r_o, t) &= f_4(t)\end{aligned}\quad (6)$$

where  $C_{ij}$  are the mechanical and thermal coefficients, which by assigning different values for

them, different types of mechanical and thermal boundary conditions may be obtained. These boundary conditions include the specified displacement, strain, stress, specified temperature, convection, and the specified heat flux. The initial boundary conditions are assumed in general form:

$$\begin{aligned} u(r, 0) &= f_5(r) \\ u_{,t}(r, 0) &= f_6(r) \\ T(r, 0) &= f_7(r) \end{aligned} \quad (7)$$

## Solution

Equations (4) and (5) are the system of nonhomogeneous partial differential equations with nonconstant coefficients (functions of radius variable  $r$  only) and have general and particular solutions.

### General Solution with Homogeneous Boundary Conditions

Since the coefficients of these equations are independent of time variable ( $t$ ), the exponential function form of time variable may be assumed for the general solution as:

$$\begin{aligned} u(r, t) &= [U^*(r)]e^{\lambda t} \\ T(r, t) &= [\theta^*(r)]e^{\lambda t} \end{aligned} \quad (8)$$

Substituting (8) into homogeneous parts of (4) and (5) yields:

$$\begin{aligned} U^{*''} + \frac{2}{r}U^{*'} - \frac{2}{r^2}U^* + d_1\theta^{*'} + d_2\lambda^2 U^* &= 0 \\ \theta^{*''} + \frac{2}{r}\theta^{*'} + d_3\lambda\theta^* + d_4\lambda\left(U^{*'} + \frac{2}{r}U^*\right) &= 0 \end{aligned} \quad (9)$$

Equations (9) are system of ordinary differential equations, where the prime symbol ( $'$ ) shows differentiation with respect to the radius variable ( $r$ ) and  $d_1$  to  $d_4$  are constant parameters given in the appendix.

### Change of Dependent Variables

To obtain a solution for (9), the dependent variables are changed as:

$$\begin{aligned} U^*(r) &= r^{-\frac{1}{2}}U(r) \\ \theta^*(r) &= r^{-\frac{1}{2}}\theta(r) \end{aligned} \quad (10)$$

Substituting (10) into (9) gives:

$$\begin{aligned} U'' + \frac{1}{r}U' - \frac{9}{4}\frac{1}{r^2}U - d_1\frac{1}{2}\frac{1}{r}\theta + d_1\theta' + d_2\lambda^2 U &= 0 \\ \theta'' + \frac{1}{r}\theta' - \frac{1}{4}\frac{1}{r^2}\theta + d_3\lambda\theta + d_4\lambda U' + d_4\lambda\frac{3}{2}\frac{1}{r}U &= 0 \end{aligned} \quad (11)$$

### Solution Justification

The first solution  $U_1$  and  $\theta_1$  is considered for solid sphere as:

$$\begin{aligned} U_1(r) &= A_1 J_{\frac{3}{2}}(\beta r) \\ \theta_1(r) &= B_1 J_{\frac{1}{2}}(\beta r) \end{aligned} \quad (12)$$

Substituting (12) into (11) and using the formulas for the derivatives of Bessel function, such as  $J'_n(\beta r) = \beta J_{n-1}(\beta r) - \frac{n}{r}J_n(\beta r)$ , yields:

$$\begin{aligned} \{(-\beta^2 + \lambda^2 d_2)A_1 - d_1\beta B_1\}J_{\frac{3}{2}}(\beta r) &= 0 \\ \{\lambda d_4\beta A_1 + (-\beta^2 + \lambda d_3)B_1\}J_{\frac{1}{2}}(\beta r) &= 0 \end{aligned} \quad (13)$$

Equations (13) show that  $U_1$  and  $\theta_1$  can be the solutions of (11), if and only if:

$$\begin{aligned} \begin{bmatrix} (-\beta^2 + \lambda^2 d_2) & -d_1\beta \\ \lambda d_4\beta & (-\beta^2 + \lambda d_3) \end{bmatrix} \begin{Bmatrix} A_1 \\ B_1 \end{Bmatrix} \\ = \begin{bmatrix} 0 \\ 0 \end{bmatrix} \end{aligned} \quad (14)$$

The nontrivial solution of (14) is obtained by setting the determinant of this equation equal to zero as:

$$(-\beta^2 + \lambda^2 d_2)(-\beta^2 + \lambda d_3) + d_1 d_4 \beta^2 \lambda = 0 \quad (15)$$

Equation (15) is the first characteristic equation. Thus, it is concluded that the first solutions for  $U_1$  and  $\theta_1$  satisfy the system of equations (11) and they are the first solutions of the system. Functions  $rJ_{\frac{3}{2}}(\beta r)$  and  $rJ_{\frac{5}{2}}(\beta r)$  are considered as the second solutions of  $U_2$  and  $\theta_2$ , respectively, as:

$$\begin{aligned} U_2(r) &= A_2 r J_{\frac{3}{2}}(\beta r) \\ \theta_2(r) &= B_2 r J_{\frac{3}{2}}(\beta r) \end{aligned} \quad (16)$$

Substituting (16) into (11) yields:

$$\begin{aligned} &\{(-\beta^2 + \lambda^2 d_2)A_2 - d_1 \beta B_2\} r J_{\frac{3}{2}}(\beta r) \\ &+ \left\{ \left( \frac{3}{\beta} \lambda^2 d_2 - \beta \right) A_2 - d_1 B_2 \right\} J_{\frac{5}{2}}(\beta r) = 0 \\ &2\beta B_2 J_{\frac{1}{2}}(\beta r) \\ &+ \{\lambda d_4 \beta A_2 + (-\beta^2 + \lambda d_3)B_2\} r J_{\frac{3}{2}}(\beta r) = 0 \end{aligned} \quad (17)$$

Equations (17) show that the second solution in form of (16) cannot satisfy the system of equations (11). Similar difficulty occurs in the following system of ordinary differential equations with constant coefficients:

$$\begin{cases} \frac{dx}{dt} = a_1 x + b_1 y \\ \frac{dy}{dt} = a_2 x + b_2 y \end{cases} \quad (18)$$

The general solution of system of equations (18) is in exponential form:

$$\begin{cases} x = A e^{mt} \\ y = B e^{mt} \end{cases} \quad (19)$$

Substituting (19) into the system (18) gives the characteristic equation as:

$$m^2 - (a_1 + b_2)m + (a_1 b_2 - a_2 b_1) = 0 \quad (20)$$

When the characteristic equation (20) has repeated roots  $m_{1,2} = m$  (For a case which

$[(a_1 + b_2)^2 - 4(a_1 b_2 - a_2 b_1)] = 0$ , then  $m_{1,2} = \frac{(a_1 + b_2)}{2}$ ) and the first solution for the repeated roots is considered as:

$$\begin{cases} x_2 = A_1 e^{mt} \\ y_2 = B_1 e^{mt} \end{cases} \quad (21)$$

The second solution for the repeated roots of the decoupled ordinary differential equation is considered as:

$$\begin{cases} x_2 = A_2 t e^{mt} \\ y_2 = B_2 t e^{mt} \end{cases} \quad (22)$$

Equations (22) do not satisfy the system of equations (18). As shown in Ref. [19] for the repeated roots, the second solution must be considered in the form of combination of repeated and non-repeated roots as:

$$\begin{cases} x_2 = (A_2 + A_3 t) e^{mt} \\ y_2 = (B_2 + B_3 t) e^{mt} \end{cases} \quad (23)$$

Substituting (23) into (18), the relation between the constants  $A_2$ ,  $A_3$ ,  $B_2$ , and  $B_3$  is obtained and establishes (23) to be the second solution of the system of equations (18). Thus, the complete unique solution of the system of equations (18) is:

$$\begin{cases} x = c_1 A_1 e^{mt} + c_2 (A_2 + A_3 t) e^{mt} \\ y = c_1 B_1 e^{mt} + c_2 (B_2 + B_3 t) e^{mt} \end{cases} \quad (24)$$

Similar to the system of ordinary differential equations with constant coefficients, the second solution of the system of ordinary differential equations with nonconstant coefficients (11) must be considered as the combination of solutions of the repeated and non-repeated roots as:

$$\begin{aligned} U_2(r) &= \left[ A_2 J_{\frac{3}{2}}(\beta r) + A_3 r J_{\frac{5}{2}}(\beta r) \right] \\ \theta_2(r) &= \left[ B_2 J_{\frac{3}{2}}(\beta r) + B_3 r J_{\frac{5}{2}}(\beta r) \right] \end{aligned} \quad (25)$$

Substituting (25) into (11) yields:

$$\begin{aligned} & \{(-\beta^2 + \lambda^2 d_2)A_3 - d_1 \beta B_3\} r J_{\frac{3}{2}}(\beta r) \\ & + \left\{(-\beta^2 + \lambda^2 d_2)A_2 + (\lambda^2 d_2 \frac{3}{\beta} - \beta)A_3 - d_1 \beta B_2 \right. \\ & \left. - d_1 B_3\right\} J_{\frac{3}{2}}(\beta r) = 0 \{ \lambda d_4 \beta A_2 + (-\beta^2 + \lambda d_3)B_2 \\ & + 2\beta B_3 \} J_{\frac{1}{2}}(\beta r) + \{ \lambda d_4 \beta A_3 + (-\beta^2 + \lambda d_3)B_3 \} \\ & r J_{\frac{3}{2}}(\beta r) = 0 \end{aligned} \quad (26)$$

The expressions for  $U_2$  and  $\theta_2$  can be the solutions of (11), if and only if

$$\begin{bmatrix} (-\beta^2 + \lambda^2 d_2) & -d_1 \beta \\ \lambda d_4 \beta & (-\beta^2 + \lambda d_3) \end{bmatrix} \begin{Bmatrix} A_3 \\ B_3 \end{Bmatrix} = \begin{Bmatrix} 0 \\ 0 \end{Bmatrix} \quad (27)$$

$$\begin{aligned} & (-\beta^2 + \lambda^2 d_2)A_2 + (\lambda^2 d_2 \frac{3}{\beta} - \beta)A_3 - d_1 \beta B_2 \\ & - d_1 B_3 = 0 \end{aligned} \quad (28)$$

$$\lambda d_4 \beta A_2 + (-\beta^2 + \lambda d_3)B_2 + 2\beta B_3 = 0 \quad (29)$$

The nontrivial solution of (27) is obtained by setting the determinant equal to zero as:

$$(-\beta^2 + \lambda^2 d_2)(-\beta^2 + \lambda d_3) + d_1 d_4 \beta^2 \lambda = 0 \quad (30)$$

The characteristic equation (30) is the same as the characteristic equation (15). This equality is interesting as it prevents mathematical dilemma and complexity and a single value for the eigenvalue  $\beta$  simultaneously satisfies both characteristic equations (15) and (30). Equations (28) and (29) give the relation between  $A_2$ ,  $A_3$ ,  $B_2$ , and  $\lambda_n$  and they play as the balancing ratios that help equations (25) to be the second solution of the system of equations (11).

The complete unique general solutions for the solid cylinder are:

$$\begin{aligned} u^s(r) &= A_1 J_{\frac{3}{2}}(\beta r) + A_2 \left[ J_{\frac{3}{2}}(\beta r) + \zeta_1 r J_{\frac{3}{2}}(\beta r) \right] \\ \theta^s(r) &= A_1 \zeta_2 J_{\frac{1}{2}}(\beta r) + A_2 \left[ \zeta_3 J_{\frac{1}{2}}(\beta r) + \zeta_4 r J_{\frac{3}{2}}(\beta r) \right] \end{aligned} \quad (31)$$

And the complete unique general solutions for the hollow sphere are:

$$\begin{aligned} U^g(r) &= A_1 J_{\frac{3}{2}}(\beta r) + A_2 \left[ J_{\frac{3}{2}}(\beta r) + \zeta_1 r J_{\frac{3}{2}}(\beta r) \right] \\ &+ A_3 Y_{\frac{3}{2}}(\beta r) + A_4 \left[ Y_{\frac{3}{2}}(\beta r) + \zeta_1 r Y_{\frac{3}{2}}(\beta r) \right] \\ \theta^g(r) &= A_1 \zeta_2 J_{\frac{1}{2}}(\beta r) + A_2 \left[ \zeta_3 J_{\frac{1}{2}}(\beta r) + \zeta_4 r J_{\frac{3}{2}}(\beta r) \right] \\ &+ A_3 \zeta_2 Y_{\frac{1}{2}}(\beta r) + A_4 \left[ \zeta_3 Y_{\frac{1}{2}}(\beta r) + \zeta_4 r Y_{\frac{3}{2}}(\beta r) \right] \end{aligned} \quad (32)$$

where  $\zeta_1$  to  $\zeta_4$  are the ratios obtained from (14), (27), (28), and (29) and are given in the appendix. Substituting  $U^g$  and  $\theta^g$  in the homogeneous form of the boundary conditions (6), the following four linear algebraic equations are obtained:

$$\begin{bmatrix} \mu_{11} & \mu_{12} & \mu_{13} & \mu_{14} \\ \mu_{21} & \mu_{22} & \mu_{23} & \mu_{24} \\ \mu_{31} & \mu_{32} & \mu_{33} & \mu_{34} \\ \mu_{41} & \mu_{42} & \mu_{43} & \mu_{44} \end{bmatrix} \begin{Bmatrix} A_1 \\ A_2 \\ A_3 \\ A_4 \end{Bmatrix} = \begin{Bmatrix} 0 \\ 0 \\ 0 \\ 0 \end{Bmatrix} \quad (33)$$

where  $\mu_{ij}$  are the coefficients depending on  $\lambda$  and  $\beta$  are given in the appendix. Setting the determinant of the coefficients of (33) equal to zero, the second characteristic equation is obtained. Simultaneous solution of this equation and (15) results into infinite number of two eigenvalues  $\beta_n$  and  $\lambda_n$ . Therefore,  $U^g$  and  $\theta^g$  are rewritten as:

$$\begin{aligned} U^g(r) &= A_1 \left[ J_{\frac{3}{2}}(\beta_n r) + \left[ \zeta_5 J_{\frac{3}{2}}(\beta_n r) + \zeta_6 r J_{\frac{3}{2}}(\beta_n r) \right] \right. \\ &\quad \left. + \zeta_7 Y_{\frac{3}{2}}(\beta_n r) + \left[ \zeta_8 Y_{\frac{3}{2}}(\beta_n r) + \zeta_9 r Y_{\frac{3}{2}}(\beta_n r) \right] \right] \\ \theta^g(r) &= A_1 \left[ \zeta_{10} J_{\frac{1}{2}}(\beta_n r) + \left[ \zeta_{11} J_{\frac{1}{2}}(\beta_n r) + \zeta_{12} r J_{\frac{3}{2}}(\beta_n r) \right] \right. \\ &\quad \left. + \zeta_{13} Y_{\frac{1}{2}}(\beta_n r) + \left[ \zeta_{14} Y_{\frac{1}{2}}(\beta_n r) + \zeta_{15} r Y_{\frac{3}{2}}(\beta_n r) \right] \right] \end{aligned} \quad (34)$$

where  $\zeta_5$  to  $\zeta_{15}$  are ratios presented in the appendix and are obtained from (33). Let us show the functions in the brackets of (34) by functions  $H_1$  and  $H_0$  as:



$$\begin{aligned}
 H_1(\beta_n r) &= J_{\frac{3}{2}}(\beta_n r) + \left[ \zeta_5 J_{\frac{3}{2}}(\beta_n r) + \zeta_6 r J_{\frac{5}{2}}(\beta_n r) \right] \\
 &\quad + \zeta_7 Y_{\frac{3}{2}}(\beta_n r) + \left[ \zeta_8 Y_{\frac{3}{2}}(\beta_n r) + \zeta_9 r Y_{\frac{5}{2}}(\beta_n r) \right] \\
 H_0(\beta_n r) &= \zeta_{10} J_{\frac{1}{2}}(\beta_n r) + \left[ \zeta_{11} J_{\frac{1}{2}}(\beta_n r) + \zeta_{12} r J_{\frac{3}{2}}(\beta_n r) \right] \\
 &\quad + \zeta_{13} Y_{\frac{1}{2}}(\beta_n r) + \left[ \zeta_{14} Y_{\frac{1}{2}}(\beta_n r) + \zeta_{15} r Y_{\frac{3}{2}}(\beta_n r) \right]
 \end{aligned} \quad (35)$$

According to Sturm-Liouville theories, these functions are orthogonal with respect to weight function  $p(r) = r$  as:

$$\int_{r_i}^{r_o} H(\beta_n r) H(\beta_m r) r dr = \begin{cases} 0 & n \neq m \\ \|H(\beta_n r)\|^2 & n = m \end{cases} \quad (36)$$

where  $\|H(\beta_n r)\|$  is the norm the function  $H$  and equals:

$$\|H(\beta_n r)\| = \left[ \int_{r_i}^{r_o} r H^2(\beta_n r) dr \right]^{\frac{1}{2}} \quad (37)$$

Due to the orthogonality of function  $H$ , every piece-wise continuous function, such as  $f(r)$ , can be expanded in terms of the function  $H$  (either for  $H_0$  or  $H_1$ ), and is called H-Fourier series as:

$$f(r) = \sum_{n=1}^{\infty} e_n H(\beta_n r) \quad (38)$$

where  $e_n$  equals:

$$e_n = \frac{1}{\|H(\beta_n r)\|^2} \int_{r_i}^{r_o} f(r) H(r) r dr \quad (39)$$

There are three groups for eigenvalues  $\lambda_n$ , where the first  $\lambda_{n1}$  are real and negative, and the second and third ones,  $\lambda_{n2}$ ,  $\lambda_{n3}$ , are conjugate complex with negative real part  $-\xi_n \omega_n$  and imaginary part  $\pm \omega_{dn}$ , where  $\omega_{dn}$  and  $\omega_n$  are damped and non-damped thermal-mechanical natural frequencies and  $\xi_n$  is damping ratio for  $n^{\text{th}}$  natural mode. By using (8), (10), (34), and (35) the displacement and temperature distribution due to general solution become:

$$\begin{aligned}
 u^g(r, t) &= r^{-\frac{1}{2}} \sum_{n=1}^{\infty} \{ a_n e^{\lambda_{n1} t} \\
 &\quad + e^{-\xi_n \omega_n t} [b_n \cos \omega_{dn} t + c_n \sin \omega_{dn} t] H_1(\beta_n r) \} \\
 T^g(r, t) &= r^{-\frac{1}{2}} \sum_{n=1}^{\infty} \{ a_n e^{\lambda_{n1} t} \\
 &\quad + e^{-\xi_n \omega_n t} [b_n \cos \omega_{dn} t + c_n \sin \omega_{dn} t] H_0(\beta_n r) \}
 \end{aligned} \quad (40)$$

Using the initial conditions (7) and with the help of (38), (39), and (40), three unknown constants  $a_n$ ,  $b_n$ , and  $c_n$  are obtained.

### Particular Solution with Nonhomogeneous Boundary Conditions

The general solutions may be used as proper functions for guessing the particular solution adopted to the nonhomogeneous parts of (4) and (5) and nonhomogeneous boundary conditions (6) as:

$$\begin{aligned}
 u^p(r, t) &= r^{-\frac{1}{2}} \sum_{n=1}^{\infty} \left\{ \left[ G_{1n}(t) J_{\frac{3}{2}}(\beta_n r) + G_{2n}(t) r J_{\frac{5}{2}}(\beta_n r) \right] \right. \\
 &\quad \left. + r^2 G_{5n}(t) \right\} \\
 T^p(r, t) &= r^{-\frac{1}{2}} \sum_{n=1}^{\infty} \left\{ \left[ G_{3n}(t) J_{\frac{1}{2}}(\beta_n r) + G_{4n}(t) r J_{\frac{3}{2}}(\beta_n r) \right] \right. \\
 &\quad \left. + r^2 G_{6n}(t) \right\}
 \end{aligned} \quad (41)$$

For the solid sphere, the second type of Bessel function  $Y$  is excluded. It is necessary and suitable to expand the  $r^{\frac{1}{2}} F(r, t)$  and  $r^{\frac{1}{2}} Q(r, t)$  in H-Fourier expansion form as:

$$\begin{aligned}
 r^{\frac{1}{2}} F(r, t) &= \sum_{n=1}^{\infty} F_n(t) H_1(\beta_n r) \\
 r^{\frac{1}{2}} Q(r, t) &= \sum_{n=1}^{\infty} Q_n(t) H_0(\beta_n r)
 \end{aligned} \quad (42)$$

where  $F_n(t)$  and  $Q_n(t)$  are:

$$\begin{aligned}
 F_n(t) &= \frac{1}{\|H_1(\beta_n r)\|^2} \int_{r_i}^{r_o} F(r, t) H_1(\beta_n r) r^{\frac{3}{2}} dr \\
 Q_n(t) &= \frac{1}{\|H_0(\beta_n r)\|^2} \int_{r_i}^{r_o} Q(r, t) H_0(\beta_n r) r^{\frac{3}{2}} dr
 \end{aligned} \quad (43)$$

Substituting equations (41) and (42) into the nonhomogeneous form of equations (4) and (5) yields:

$$\begin{aligned}
 & \left\{ -\beta_n^2 G_{1n}(t) + d_2 \ddot{G}_{1n}(t) - \beta_n G_{2n}(t) \right. \\
 & + d_2 \frac{6}{\beta_n} \ddot{G}_{2n}(t) - d_1 \beta_n G_{3n}(t) - d_1 G_{4n}(t) \\
 & + \left( d_7 d_{12} + d_8 d_{12} \frac{3}{\beta_n} \right) G_{5n}(t) \\
 & + \left( d_7 d_{13} + d_8 d_{13} \frac{3}{\beta_n} \right) \ddot{G}_{5n}(t) + \left( d_7 d_{14} + d_8 d_{14} \frac{3}{\beta_n} \right) \\
 & G_{6n}(t) + \left( d_7 d_{11} + d_8 d_{11} \frac{3}{\beta_n} \right) F_n(t) \left. \right\} J_{\frac{3}{2}}(\beta_n r) \\
 & + \{ \beta_n^2 G_{2n}(t) - 2d_2 \ddot{G}_{2n}(t) + d_1 \beta_n G_{4n}(t) \\
 & - d_8 d_{12} G_{5n}(t) - d_8 d_{13} \ddot{G}_{5n}(t) - d_8 d_{14} G_{6n}(t) \\
 & - d_8 d_{11} F(t) \} r J_{\frac{1}{2}}(\beta_n r) = 0 \\
 & \left\{ d_4 \beta_n \dot{G}_{1n}(t) - \beta_n^2 G_{3n}(t) + d_3 \dot{G}_{3n}(t) + 2\beta_n G_{4n}(t) \right. \\
 & + d_9 d_{15} \dot{G}_{5n}(t) + d_9 d_{16} G_{6n}(t) \\
 & + d_9 d_{17} \dot{G}_{6n}(t) + d_9 d_{18} Q_n(t) \left. \right\} J_{\frac{1}{2}}(\beta_n r) + \\
 & + \left\{ d_4 \beta_n \dot{G}_{2n}(t) - \beta_n^2 G_{4n}(t) + d_3 \dot{G}_{4n}(t) + d_{10} d_{15} \dot{G}_{5n}(t) \right. \\
 & + d_{10} d_{16} G_{6n}(t) + d_{10} d_{17} \dot{G}_{6n}(t) \\
 & + d_{10} d_{18} Q_n(t) \left. \right\} r J_{\frac{3}{2}}(\beta_n r) = 0
 \end{aligned} \quad (44)$$

where  $d_7$  to  $d_{18}$  are the coefficients of H-expansion and are given in the appendix. The guessed functions (41) can satisfy the nonhomogeneous part of (4) and (5) if and only if:

$$\begin{aligned}
 & -\beta_n^2 G_{1n}(t) + d_2 \ddot{G}_{1n}(t) - \beta_n G_{2n}(t) + d_2 \frac{6}{\beta_n} \ddot{G}_{2n}(t) \\
 & - d_1 \beta_n G_{3n}(t) - d_1 G_{4n}(t) + \left( d_7 d_{12} + d_8 d_{12} \frac{3}{\beta_n} \right) G_{5n}(t) \\
 & + \left( d_7 d_{13} + d_8 d_{13} \frac{3}{\beta_n} \right) \ddot{G}_{5n}(t) + \left( d_7 d_{14} + d_8 d_{14} \frac{3}{\beta_n} \right) G_{6n}(t) \\
 & + \left( d_7 d_{11} + d_8 d_{11} \frac{3}{\beta_n} \right) F_n(t) = 0 \\
 & \beta_n^2 G_{2n}(t) - 2d_2 \ddot{G}_{2n}(t) + d_1 \beta_n G_{4n}(t) - d_8 d_{12} G_{5n}(t) \\
 & - d_8 d_{13} \ddot{G}_{5n}(t) - d_8 d_{14} G_{6n}(t) - d_8 d_{11} F(t) = 0 \\
 & d_4 \beta_n \dot{G}_{1n}(t) - \beta_n^2 G_{3n}(t) + d_3 \dot{G}_{3n}(t) + 2\beta_n G_{4n}(t) \\
 & + d_9 d_{15} \dot{G}_{5n}(t) + d_9 d_{16} G_{6n}(t) + d_9 d_{17} \dot{G}_{6n}(t) + d_9 d_{18} Q_n(t) = 0 \\
 & d_4 \beta_n \dot{G}_{2n}(t) - \beta_n^2 G_{4n}(t) + d_3 \dot{G}_{4n}(t) + d_{10} d_{15} \dot{G}_{5n}(t) \\
 & + d_{10} d_{16} G_{6n}(t) + d_{10} d_{17} \dot{G}_{6n}(t) + d_{10} d_{18} Q_n(t) = 0
 \end{aligned} \quad (45)$$

Taking the Laplace transform of (45) and using two boundary conditions of (6) (for solid cylinder only second and forth boundary conditions are applicable) gives:

$$\begin{bmatrix}
 -\beta_n^2 + d_2 s^2 & -\beta_n + d_2 \frac{6}{\beta_n} s^2 & -d_1 \beta_n & -d_1 & (d_7 + d_8 \frac{3}{\beta_n})(d_{12} + d_{13} s^2) & (d_7 + d_8 \frac{3}{\beta_n}) d_{14} \\
 0 & \beta_n^2 - 2d_2 s^2 & 0 & d_1 \beta_n & -d_8 d_{12} - d_8 d_{13} s^2 & -d_8 d_{14} \\
 d_4 \beta_n s & 0 & -\beta_n^2 + d_3 s & 2\beta_n & d_9 d_{15} s & d_9 d_{16} + d_9 d_{17} s \\
 0 & d_4 \beta_n s & 0 & -\beta_n^2 + d_3 s & d_{10} d_{15} s & d_{10} d_{16} + d_{10} d_{17} s \\
 d_{19} & d_{20} & d_{21} & d_{22} & d_{23} & d_{24} \\
 0 & 0 & d_{25} & d_{26} & 0 & d_{27}
 \end{bmatrix}
 \times
 \begin{bmatrix}
 G_{1n}(s) \\
 G_{2n}(s) \\
 G_{3n}(s) \\
 G_{4n}(s) \\
 G_{5n}(s) \\
 G_{6n}(s)
 \end{bmatrix}
 =
 \begin{bmatrix}
 -(d_7 d_{11} + d_8 d_{11} \frac{3}{\beta_n}) F_n(s) \\
 d_8 d_{11} F_n(s) \\
 -d_9 d_{18} Q_n(s) \\
 -d_{10} d_{18} Q_n(s) \\
 F_2(s) \\
 F_4(s)
 \end{bmatrix} \quad (46)$$

Equations (46) are a system of algebraic equations and are solved by Cramer's methods in the Laplace domain, where by the inverse Laplace transform the functions are transformed into the real time domain. Here,  $G_{1n}(t)$  to  $G_{6n}(t)$  are calculated. In this process, it is necessary to consider the following points:

1. The initial conditions (7) are considered only for the general solutions (40) and the initial conditions of  $G_{1n}(t)$  to  $G_{6n}(t)$  for the particular solutions are considered equal to zero.
2. Equations (46) are in polynomial form function of the Laplace parameter  $s$  (not the Bessel functions form of  $s$ ). Therefore, the exact inverse Laplace transform is possible and somehow simple.
3. For the hollow sphere, it is enough to include the second type of Bessel function  $Y(r)$  in sequence of particular solution as:

$$\begin{aligned}
 u^p(r, t) &= r^{-\frac{1}{2}} \sum_{n=1}^{\infty} \left\{ \left[ G_{1n}(t) J_{\frac{3}{2}}(\beta n r) + G_{2n}(t) r J_{\frac{3}{2}}(\beta n r) \right] \right. \\
 &\quad + \left[ G_{3n}(t) Y_{\frac{3}{2}}(\beta n r) + G_{4n}(t) r Y_{\frac{3}{2}}(\beta n r) \right] \\
 &\quad \left. + r G_{5n}(t) + r^2 G_{6n}(t) \right\} \\
 T^p(r, t) &= r^{-\frac{1}{2}} \sum_{n=1}^{\infty} \left\{ \left[ G_{7n}(t) J_{\frac{3}{2}}(\beta n r) + G_{8n}(t) r J_{\frac{3}{2}}(\beta n r) \right] \right. \\
 &\quad + \left[ G_{9n}(t) Y_{\frac{3}{2}}(\beta n r) + G_{10n}(t) r Y_{\frac{3}{2}}(\beta n r) \right] \\
 &\quad \left. + r G_{11n}(t) + r^2 G_{12n}(t) \right\}
 \end{aligned} \quad (47)$$

By substituting (47) in (4) and (5), eight equations are obtained, where using the four boundary conditions (6), twelve functions  $G_{1n}(t)$  to  $G_{6n}(t)$  are obtained for the hollow sphere.

## Results and Discussions

As an example, a solid sphere with radius 1 (m) made of aluminum is considered. The material properties are:

### Material properties of Aluminum

$E = 70$  (GPa)

$\nu = 0.3$

$\alpha = 23 \times 10^{-6}$  (1/K)

$\rho = 2,707$  (kg/m<sup>3</sup>)

$K = 204$  (W/m K)

$c = 903$  (J/kg K)

The initial temperature  $T_o$  is considered to be 293°K. Now, an instantaneous hot spot  $T(1, t) = 10^{-3} \delta(t)$ , where  $\delta(t)$  is unit Dirac function, is considered and the outside radius of the sphere is assumed to be fixed ( $u(1, t) = 0$ ). Figures 1 and 2 show the wave fronts for the displacement and temperature distribution at locations.

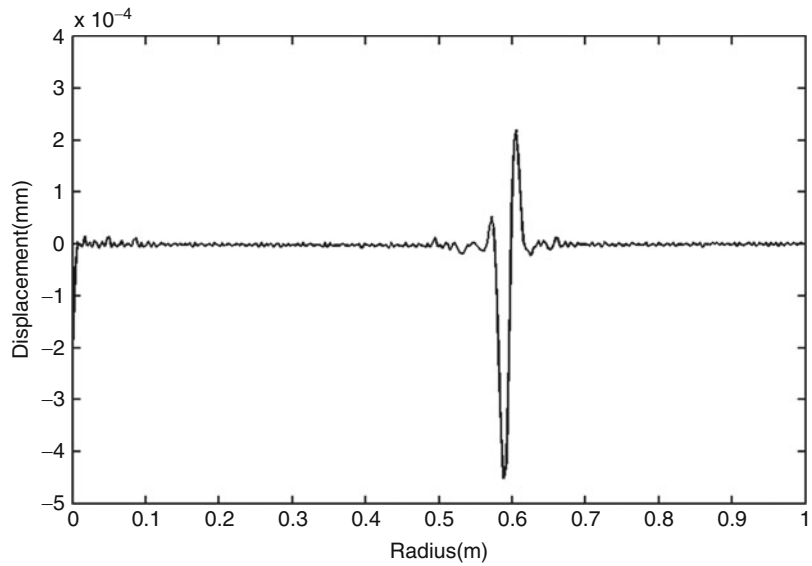
For the second example, a mechanical shock wave is applied to the outside surface of the sphere given as  $u(1, t) = 10^{-12} \delta(t)$ , and the surface is assumed to be at zero temperature ( $T(1, t) = 0$ ). Figures 3 and 4 show the wave fronts for the displacement and temperature distributions at the location. The convergence of the solutions for these examples is achieved by consideration of 1,200 eigenvalues used for the H-Fourier expansion. More than this number for eigenvalues, the increased roundoff and truncation errors affect the quality of the graphs.

The convergence of solution is better for displacement in comparison with the temperature. The small oscillations in Figs. 2 and 4 are due to the convergence of solutions. To verify the solution, an example is chosen from reference [20], where the finite element method is employed for the analysis. In this case, a hollow thick sphere is considered. The pressure at inner surface of the sphere is assumed to be traction free ( $\sigma_{rr}(r_i, t) = 0$ ) with thermal shock ( $T(r_i, t) = 1 + (t^2 - t - 1)e^{-t}$ ), and the outer surface of the sphere is fixed ( $u(r_o, t) = 0$ ) and insulated ( $T_{,r}(r_o, t) = 0$ ). To plot the graphs of this example, the dimensionless variables  $\bar{T} = \frac{T - T_o}{T_o}$ ,  $\bar{u} = \frac{(1-\nu)}{(1+\nu)\rho} \frac{\rho c c_1 u}{k \alpha T_o}$ ,  $\bar{r} = \frac{\rho c c_1 r}{k}$ ,  $\bar{t} = \frac{\rho c c_1^2 t}{k}$ , and  $c_1 = \sqrt{\frac{(1-\nu)E}{(1+\nu)(1-2\nu)\rho}}$  are considered. Figures 5 and 6 show the temperature and displacement

### Exact Solution for Classic Coupled

### Thermoelasticity in Spherical Coordinates,

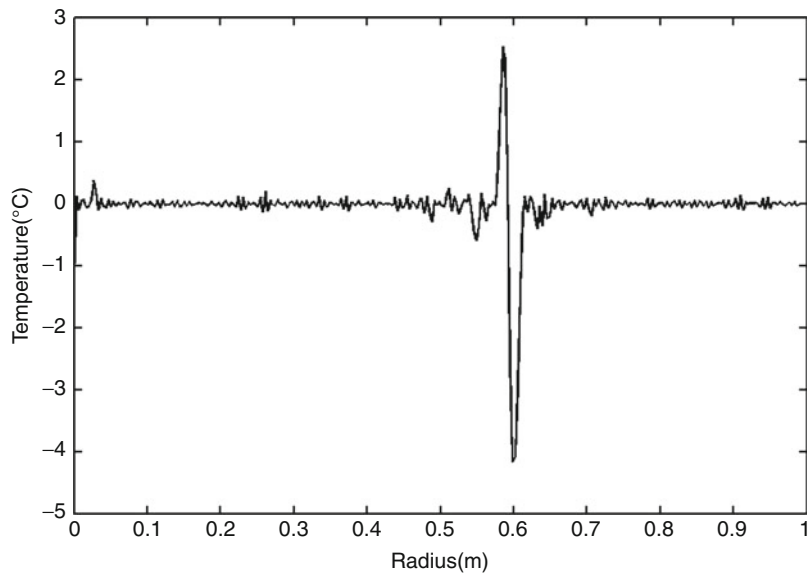
**Fig. 1** Displacement distribution due to input  $T(1, t) = 10^{-3}\delta(t)$  at  $7 \times 10^{-5}$  s



### Exact Solution for Classic Coupled

### Thermoelasticity in Spherical Coordinates,

**Fig. 2** Temperature distribution due to  $T(1, t) = 10^{-3}\delta(t)$  at  $7 \times 10^{-5}$  s



distributions, where the comparison is well justified between the exact and finite element solutions.

## Conclusion

In this entry, an analytical solution for the classic coupled thermoelasticity of thick sphere under radial temperature is presented. The method is

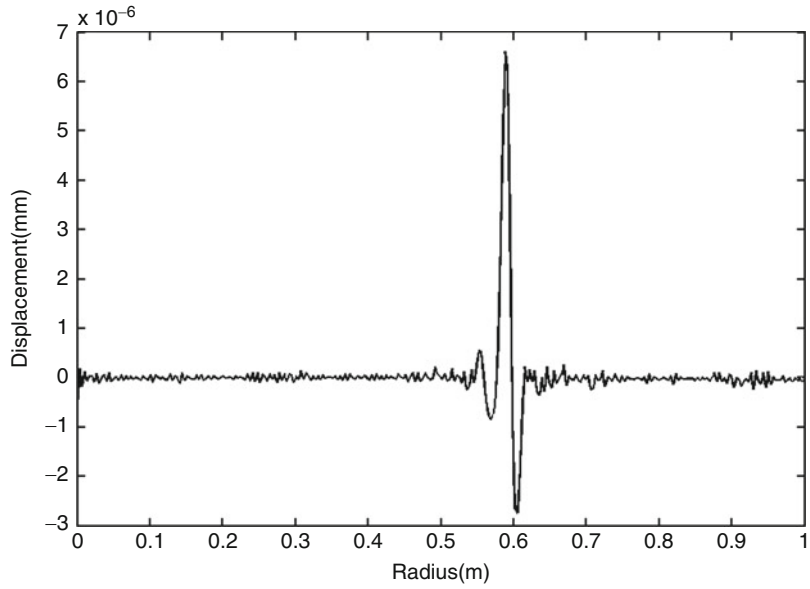
based on the eigenfunctions Fourier expansion, which is a classical and traditional method of solution for the typical initial and boundary value problems. The noncompetitive strength of this method is its ability to reveal the fundamental mathematical and physical properties and interpretations of the problem under studying.

In the coupled thermoelastic problem of radial-symmetric sphere, the governing equations are a system of partial differential equations with two independent variables, radius ( $r$ ) and time ( $t$ ).

**Exact Solution for Classic Coupled**

**Thermoelasticity in Spherical Coordinates,**

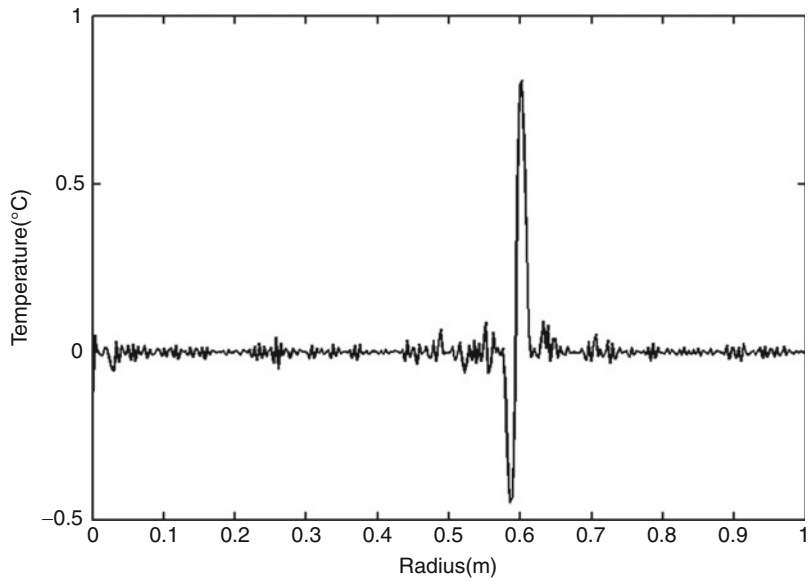
**Fig. 3** Displacement distribution due to input  $u(1, t) = 10^{-12}\delta(t)$  at  $7 \times 10^{-5}$  s



**Exact Solution for Classic Coupled**

**Thermoelasticity in Spherical Coordinates,**

**Fig. 4** Displacement distribution due to  $u(1, t) = 10^{-12}\delta(t)$  at  $7 \times 10^{-5}$  s



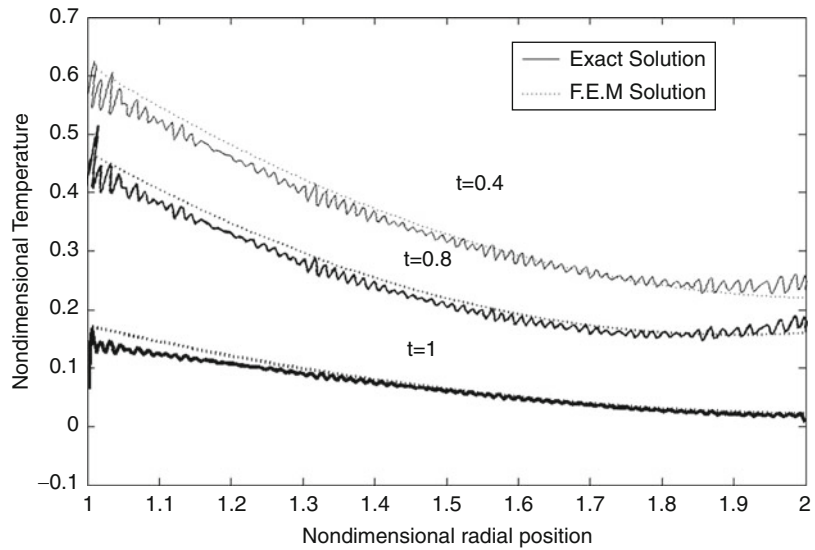
The traditional procedure to solve this class of problems is to eliminate the time variable by using the Laplace transform.

The resulting system is a set of ordinary differential equations in terms of the radius variable, which falls in the Bessel functions family. This method of analysis brings the Laplace parameter ( $s$ ) in the argument of the Bessel functions, causing hardship or impossibility in

carrying out the exact inverse of the Laplace transformation. As a result, the numerical inverse of the Laplace transformation is used in the papers dealing with this type of problems in literature. In this entry, to prevent this problem, when the Laplace transform is applied to the particular solutions, it is postponed after eliminating the radius variable, using the H-Fourier expansion. Thus, the Laplace parameter ( $s$ ) appears in polynomial function

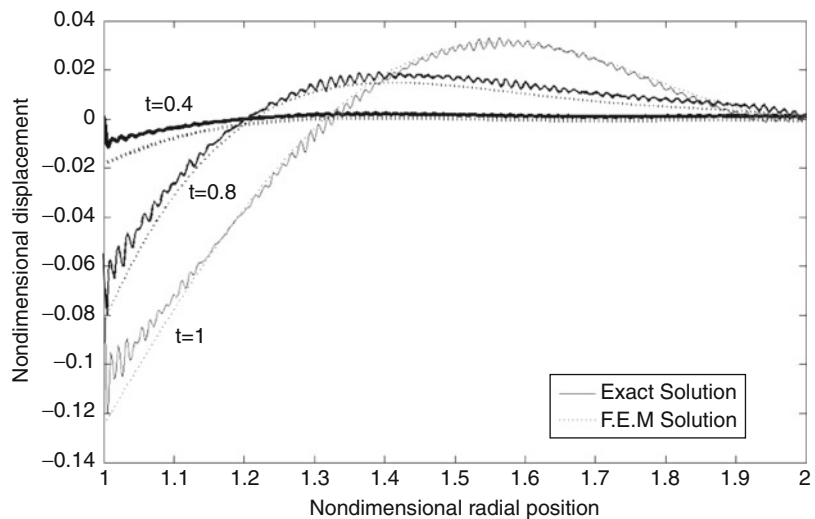
### Exact Solution for Classic Coupled Thermoelasticity in Spherical Coordinates,

#### Fig. 5 Temperature distribution at different values of the time



### Exact Solution for Classic Coupled Thermoelasticity in Spherical Coordinates,

#### Fig. 6 Displacement distribution at different values of the time



forms and hence, the exact Laplace inversion transformations are possible.

Another point is that in the partial differential equations, the number of eigenvalues is equal to the number of variables. For example, in transient one-dimensional problems in cylindrical coordinate,  $\lambda_n$  and  $\beta_n$  are eigenvalues for time  $t$  and radius  $r$  variables, respectively. In the decoupled case, this relation is implicit such as  $\lambda_n = e\beta_n$ , but in the coupled case, this relation is explicit as two characteristic equations, such as

(15) and determinant of (33). From the mathematical point of view, this difference is the fundamental distinctiveness between the coupled and decoupled problems.

Finally, it seems that the convergence might be the question of this method of solution. This problem raise from truncation and roundoff errors in the numerical procedure for calculation of the eigenvalues and Fourier expansions. This problem can be reduced by using more digits for calculations but cannot be completely erased.

## References

1. Hetnarski RB (1964) Solution of the coupled problem of thermoelasticity in the form of series of functions. *J Arch Mech Stos* 16:919–941
2. Hetnarski RB, Ignaczak J (1993) Generalized thermoelasticity: closed-form solutions. *J Therm Stress* 16:473–498
3. Hetnarski RB, Ignaczak J (1994) Generalized thermoelasticity: response of semi-space to a short laser pulse. *J Therm Stress* 17:377–396
4. Georgiadis HG, Lykotrafitis G (2005) Rayleigh waves generated by a thermal source: a three-dimensional transient thermoelasticity solution. *J Appl Mech* 72:129–138
5. Wagner P (1994) Fundamental matrix of the system of dynamic linear thermoelasticity. *J Therm Stress* 17:549–565
6. Bagri A, Eslami MR (2008) Generalized thermoelasticity of functionally graded annular disk considering the lord-shulman theory. *J Compos Struct* 83:168–179
7. Lee HL, Yang YC (2001) Inverse problem of coupled thermoelasticity for prediction of heat flux and thermal stress in annular cylinder. *J Int Commun Heat Mass Trans* 28:661–670
8. Yang YC, Chen UC, Chang WJ (2002) An inverse problem of coupled thermoelasticity in predicting heat flux and thermal stress by strain measurement. *J Therm Stress* 25:265–281
9. Eraslan AN, Oren Y (2002) Computation of transient thermal stresses in elastic–plastic tubes: effect of coupling and temperature-dependent physical properties. *J Therm Stress* 25:559–572
10. Yang YC, Chu SS (2001) Transient coupled thermoelastic analysis of an annular fin. *J Int Commun Heat Mass Trans* 28:1103–1114
11. Bahtui A, Eslami MR (2007) Coupled thermoelasticity of functionally graded cylindrical shells. *J Mech Res Commun* 34:1–18
12. Bakhshi M, Bagri A, Eslami MR (2006) Coupled thermoelasticity of functionally graded disk. *Mech Adv Mater Struct* 13:214–225
13. Hosseini-Tehrani P, Eslami MR (2000) BEM analysis of thermal and mechanical shock in a two-dimensional finite domain considering coupled thermoelasticity. *J Eng Anal* 24:249–257
14. Tanigawa Y, Takeuti Y (1982) Coupled thermal stress problem in a hollow sphere under a partial heating. *J Eng Sci* 20:41–48
15. Bagri A, Eslami MR (2004) Generalized coupled thermoelasticity of disks based on the Lord-Shulman model. *J Therm Stress* 27:691–704
16. Bagri A, Taheri H, Eslami MR, Fariborz F (2006) Generalized coupled thermoelasticity of layer. *J Therm Stress* 29:359–370
17. Cannarozzi AA, Ubertini F (2001) Mixed variational method for linear coupled thermoelastic analysis. *J Int J Solid Struct* 38:717–739
18. Jabbari M, Dehbani H, Eslami MR (2010) An exact solution for classic coupled thermoelasticity in spherical coordinates. *ASME J Pressure Vessel Technol* 132:031201
19. Simmons GF (1972) Differential equations with applications and historical notes. McGraw-Hill, New York
20. Hetnarski RB, Eslami MR (2009) Thermal stresses – advanced theory and applications. Springer, Berlin

## Exact Solution for Classic Coupled Thermoporoelasticity in Axisymmetric Cylinder

Mohsen Jabbari<sup>1</sup> and H. Dehbani<sup>2</sup>

<sup>1</sup>Faculty of Engineering, Postgraduate School, South Tehran Branch, Islamic Azad University, Tehran, Iran

<sup>2</sup>Postgraduate School, South Tehran Branch, Islamic Azad University, Tehran, Iran

## Overview

In this entry, the classic coupled porothermoelasticity model of hollow and solid cylinders under radial-symmetric loading condition  $(r, z, t)$  is considered. A full analytical method is used and an exact unique solution of the classic coupled equations is presented.

The thermal and pressure boundary conditions, the body force, the heat source, and the injected volume rate per unit volume of a distribute water source are considered in the most general forms and no limiting assumption is used. This generality allows simulation of various applicable problems.

## Introduction

Coupled thermal and poro-mechanical processes play an important role in a number of problems of interest in the geomechanics such as stability of boreholes and permeability enhancement in geothermal reservoirs or high temperature petroleum bearing formations. A thermoporoelastic approach combines the theory of heat conduction with poroelastic constitutive equations and



coupling the temperature field with the stresses and pore pressure.

There are a limited number of papers that present the closed-form or analytical solution for the coupled porothermoelasticity problems. Bai [1] investigated the response of saturated porous media subjected to local thermal loading on the surface of semi-infinite space. He used the numerical integral methods for calculating the unsteady temperature, pore pressure, and displacement fields. This author also studied the fluctuation responses of saturated porous media subjected to cyclic thermal loading [2]. In the mentioned paper, an analytical solution was deduced proposed by using the Laplace transform and the Gauss-Legendre method and Laplace transform inversion. Droujinine [3] investigated dispersion and attenuation of body waves in a wide range of materials representing realistic rock structures. He used the time-domain asymptotic ray theory to a new generalized coordinate-free wave equation with an arbitrary tensor relaxation function. Bai and Li [4] found a solution for cylindrical cavity in saturated thermoporoelastic medium by using Laplace transform and numerical Laplace transform inversion.

The number of papers that present the closed form or analytical solution for the coupled thermoelasticity problems is also limited. Hetnarski [5] found the solution of the coupled thermoelasticity in the form of a series of functions. Hetnarski and Ignaczak presented a study of the one-dimensional thermoelastic waves produced by an instantaneous plane source of heat in homogeneous isotropic infinite and semi-infinite bodies of the Green-Lindsay type [6]. Also, these authors presented an analysis for laser-induced waves propagating in an absorbing thermoelastic semi-space of the Green-Lindsay type [7]. Georgiadis and Lykotraftitis obtained a three-dimensional transient thermoelastic solution for Rayleigh-type disturbances propagating on the surface of a half-space [8]. Wagner [9] presented the fundamental matrix of a system of partial differential operators that governs the diffusion of heat and the strains in elastic media.

This method can be used to predict the temperature distribution and the strains by an instantaneous point heat, point source of heat, or by a suddenly applied delta force.

In this entry [10], a full analytical method is used to obtain the response of the governing equations and an exact solution is presented. The method of solution is based on the Fourier's expansion and eigenfunction methods, which are traditional and routine methods in solving the partial differential equations. Since the coefficients of equations are not functions of the time variable ( $t$ ), an exponential form is considered for the general solution matched with the physical wave properties of thermal and mechanical waves. For the particular solution, that is the response to mechanical and thermal shocks, the eigenfunction method and Laplace transformation is used. This work is following the previous work which presented for radially symmetric cylindrical coordinates [11].

## Governing Equations

A short hollow cylinder with inner and outer radius  $r_i$  and  $r_o$ , respectively, and length  $l$  made of isotropic material subjected to radial-symmetric mechanical, thermal, and pressure shocks is considered.

The classic theory of porothermoelasticity for wave propagation is considered to allow coupling between deformation, thermal energy, and pressure fields and to describe the physical behavior of the elastic domain to mechanical, thermal, and pressure shock loads.

Navier equation in terms of the displacement components is obtained as [4]

$$\left\{ \begin{aligned} &u_{,rr} + \frac{1}{r}u_{,r} - \frac{1}{r^2}u + \frac{1}{2}\left(\frac{1-2\nu}{1-\nu}\right)u_{,zz} \\ &+ \frac{1}{2}\frac{1}{(1-\nu)}w_{,rz} - \frac{(1+\nu)}{(1-\nu)}\alpha T_{,r} \\ &- \alpha\frac{(1+\nu)(1-2\nu)}{(1-\nu)^2E}p_{,r} - \beta\frac{(1+\nu)(1-2\nu)}{(1-\nu)^2E}T_{,r} \\ &- \rho\frac{(1+\nu)(1-2\nu)}{(1-\nu)^2E}\ddot{u} = -\frac{(1+\nu)(1-2\nu)}{(1-\nu)^2E}F(r, z, t) \end{aligned} \right\} \quad (1)$$

$$\left\{ \begin{aligned} &w_{,rr} + \frac{1}{r}w_{,r} + 2\frac{(1-\nu)}{(1-2\nu)}w_{,zz} + \frac{1}{(1-2\nu)}u_{,zr} \\ &+ \frac{1}{(1-2\nu)}\frac{1}{r}u_{,z} - 2\frac{(1+\nu)}{(1-2\nu)}\alpha T_{,z} \\ &- 2\alpha\frac{(1+\nu)}{(1-\nu)E}p_{,z} - 2\beta\frac{(1+\nu)}{(1-\nu)E}T_{,z} \\ &- 2\rho\frac{(1+\nu)}{(1-\nu)E}\ddot{w} = -2\frac{(1+\nu)}{(1-\nu)E}R(r, z, t) \end{aligned} \right. \quad (2)$$

Heat conduction equation in radial-symmetric direction with the mechanical coupling term is

$$\begin{aligned} T_{,rr} + \frac{1}{r}T_{,r} + T_{,zz} - Z\frac{T_o}{K}\dot{T} + Y\frac{T_o}{K}\dot{p} \\ - \beta\frac{T_o}{K}(\dot{u}_{,r} + \frac{1}{r}\dot{u} + \dot{w}_{,z}) = -\frac{1}{K}Q(r, z, t) \end{aligned} \quad (3)$$

According to Darcy's law and continuity condition of seepage, the equation of mass conservation can be written as

$$\begin{aligned} p_{,rr} + \frac{1}{r}p_{,r} + p_{,zz} - \alpha_p\frac{\gamma_w}{k}\dot{p} + Y\frac{\gamma_w}{k}\dot{T} \\ - \alpha\frac{\gamma_w}{k}(\dot{u}_{,r} + \frac{1}{r}\dot{u} + \dot{w}_{,z}) = -\frac{\gamma_w}{k}W(r, z, t) \end{aligned} \quad (4)$$

where (.) denotes partial derivative,  $u$  is the displacement component in the radial direction,  $p$  is the pore pressure,  $\rho$  is bulk mass density,  $\alpha = 1 - \frac{C_s}{C}$  is the Biot's coefficient,  $C_s = 3(1 - 2\nu_s)E_s$  is the coefficient of volumetric compression of the solid grains, with  $E_s$  and  $\nu_s$  being the elastic modulus and Poisson's ratio of solid grains and  $C = 3(1 - 2\nu)E$  is the coefficient of volumetric compression of solid skeleton, with  $E$  and  $\nu$  being the elastic modulus and Poisson's ratio of solid skeleton,  $T_o$  is initial reference temperature,  $\beta = \frac{3\alpha_s}{C}$  is the thermal expansion factor,  $\alpha_s$  is the coefficient of linear thermal expansion of solid grains,  $Y = 3(n\alpha_w + (\alpha - n)\alpha_s)$  and  $\alpha_p = n(C_w - C_s) + \alpha C_s$  are coupling parameters,

$\alpha_w$  and  $C_w$  are the coefficients of linear thermal expansion and volumetric compression of pure water,  $n$  is the porosity,  $k$  is the hydraulic conductivity,  $\gamma_w$  is the unit of pore water and  $Z = \frac{((1-n)\rho_s C_s + n\rho_w C_w)}{T_o} - 3\beta\alpha_s$  is coupling parameter,  $\rho_w$  and  $\rho_s$  are the densities of pore water and solid grains and  $c_w$  and  $c_s$  are the heat capacities of pore water and solid grains and  $K$  is the coefficient of heat conductivity. Here,  $F(r, t)$ ,  $R(z, t)$ ,  $Q(r, t)$ , and  $W(r, t)$  are the body forces, heat generation source, and the injected volume rate per unit volume of a distribute water source, respectively. The mechanical, thermal, and pressure boundary conditions for inner and outer surface of cylinder are

$$\begin{aligned} &C_{11}u(r_i, z, t) + C_{12}u_{,r}(r_i, z, t) + C_{13}T(r_i, z, t) \\ &\quad + C_{14}p(r_i, z, t) = f_1(t) \\ &C_{21}u(r_o, z, t) + C_{22}u_{,r}(r_o, z, t) + C_{23}T(r_o, z, t) \\ &\quad + C_{24}p(r_o, z, t) = f_2(t) \\ &C_{31}w(r_i, z, t) + C_{32}w_{,r}(r_i, z, t) + C_{33}T(r_i, z, t) \\ &\quad + C_{34}p(r_i, z, t) = f_3(t) \\ &C_{41}w(r_o, z, t) + C_{42}w_{,r}(r_o, z, t) + C_{43}T(r_o, z, t) \\ &\quad + C_{44}p(r_o, z, t) = f_4(t) \\ &C_{51}T(r_i, z, t) + C_{52}T_{,r}(r_i, z, t) = f_5(t) \\ &C_{61}T(r_o, z, t) + C_{62}T_{,r}(r_o, z, t) = f_6(t) \\ &C_{71}p(r_i, z, t) = f_7(t) \\ &C_{81}p(r_o, z, t) = f_8(t) \end{aligned} \quad (5)$$

where  $C_{ij}$  are the mechanical, thermal, and pressure coefficients, and which by assigning different values for them, different types of mechanical, thermal, and pressure boundary conditions may be obtained. These boundary conditions include the displacement, strain, stress, specified temperature, convection, pressure, and heat flux condition.

The boundary conditions at the ends of cylinder are considered in simply support as [12]

$$\begin{aligned}
 u(r, 0, t) &= 0 \\
 u(r, l, t) &= 0 \\
 w_z(r, 0, t) &= 0 \\
 w_z(r, l, 0) &= 0 \\
 T(r, 0, t) &= 0 \\
 T(r, l, t) &= 0 \\
 p(r, 0, t) &= 0 \\
 p(r, l, t) &= 0
 \end{aligned} \tag{6}$$

with nonconstant coefficients (functions of the radius variable  $r$  only) has general and particular solutions.

### General Solution with Homogeneous Boundary Conditions

A form of solution can be suitable for (1)–(4) and the boundary conditions (6) may be assumed for the general solution as

The initial boundary conditions are assumed in the following general form

$$\begin{aligned}
 u(r, z, 0) &= f_9(r) \\
 u_t(r, z, 0) &= f_{10}(r) \\
 w(r, z, 0) &= f_{11}(r) \\
 w_t(r, z, 0) &= f_{12}(r) \\
 T(r, z, 0) &= f_{13}(r) \\
 p(r, z, 0) &= f_{14}(r)
 \end{aligned} \tag{7}$$

$$\begin{aligned}
 u(r, t) &= \sum_{n=1}^{\infty} U(r) e^{\lambda t} \sin(\zeta_n z) \\
 w(r, t) &= \sum_{n=1}^{\infty} W(r) e^{\lambda t} \cos(\zeta_n z) \\
 T(r, t) &= \sum_{n=1}^{\infty} \theta(r) e^{\lambda t} \sin(\zeta_n z) \\
 p(r, t) &= \sum_{n=1}^{\infty} P(r) e^{\lambda t} \sin(\zeta_n z)
 \end{aligned} \tag{8}$$

### Solution

Equations (1)–(4) constitute a system of nonhomogeneous partial differential equations

where  $\zeta_n$  is  $\frac{n\pi}{l}$ . Substituting (8) into homogeneous parts of (1)–(4) yields

$$\begin{aligned}
 U'' + \frac{1}{r} U' - \frac{1}{r^2} U + d_1 \zeta_n^2 U + d_2 \zeta_n W' + d_3 P' + d_4 \theta' + d_5 \lambda^2 U &= 0 \\
 W'' + \frac{1}{r} W' + d_6 \zeta_n^2 W + d_7 \zeta_n U' + d_8 \zeta_n \frac{1}{r} U + d_9 \zeta_n P + d_{10} \zeta_n \theta + d_{11} \lambda^2 W &= 0 \\
 \theta'' + \frac{1}{r} \theta' - \zeta_n^2 \theta + d_{12} \lambda \theta + d_{13} \lambda P + d_{14} \lambda (U' + \frac{1}{r} U - W \zeta_n) &= 0 \\
 P'' + \frac{1}{r} P' - \zeta_n^2 P + d_{15} \lambda P + d_{16} \lambda \theta + d_{17} \lambda (U' + \frac{1}{r} U - W \zeta_n) &= 0
 \end{aligned} \tag{9}$$

The first solutions of  $U_1$ ,  $W_1$ ,  $\theta_1$ , and  $P_1$  are considered as

$$\begin{aligned} U_1(r) &= A_1 J_1(\beta r) \\ W_1(r) &= B_1 J_0(\beta r) \\ \theta_1(r) &= C_1 J_0(\beta r) \\ P_1(r) &= D_1 J_0(\beta r) \end{aligned} \quad (10)$$

Substituting (10) into (19) yields

$$\begin{aligned} &\left\{ \begin{aligned} &(-\beta^2 + d_1 \zeta_n^2 + d_5 \lambda^2) A_1 - d_2 \zeta_n \beta B_1 \\ &- d_4 \beta C_1 - d_3 \beta D_1 \end{aligned} \right\} J_0(\beta r) = 0 \\ &\left\{ \begin{aligned} &- d_7 \zeta_n \beta A_1 + (\beta^2 - d_6 \zeta_n^2 - d_{11} \lambda^2) B_1 \\ &- d_{10} \zeta_n C_1 - d_9 \zeta_n D_1 \end{aligned} \right\} J_1(\beta r) = 0 \\ &\left\{ \begin{aligned} &- d_{14} \lambda \beta A_1 + \zeta_n d_{14} \lambda B_1 + (\beta^2 + \zeta_n^2 - d_{12} \lambda) C_1 \\ &- d_{13} \lambda D_1 \end{aligned} \right\} J_1(\beta r) = 0 \\ &\left\{ \begin{aligned} &- d_{17} \lambda \beta A_1 + d_{17} \zeta_n \lambda B_1 + d_{16} \lambda C_1 \\ &+ (\beta^2 + \zeta_n^2 - d_{15} \lambda) D_1 \end{aligned} \right\} J_1(\beta r) = 0 \end{aligned} \quad (11)$$

Equations (11) show that  $U_1$ ,  $W_1$ ,  $\theta_1$ , and  $P_1$  can be the solutions of (9), if and only if

$$\begin{bmatrix} (-\beta^2 + d_1 \zeta_n^2 + d_5 \lambda^2) & -d_2 \zeta_n \beta & -d_4 \beta & -d_3 \beta \\ -d_7 \zeta_n \beta & (\beta^2 - d_6 \zeta_n^2 - d_{11} \lambda^2) & -d_{10} \zeta_n & -d_9 \zeta_n \\ -d_{14} \lambda \beta & d_{14} \lambda \zeta_n & (\beta^2 - d_6 \zeta_n^2 - d_{11} \lambda) & -d_{13} \lambda \\ -d_{17} \lambda \beta & +d_{17} \lambda \zeta_n & -d_{16} \lambda & (\beta^2 - d_6 \zeta_n^2 - d_{11} \lambda) \end{bmatrix} \times \begin{Bmatrix} A_1 \\ B_1 \\ C_1 \\ D_1 \end{Bmatrix} = \begin{bmatrix} 0 \\ 0 \\ 0 \\ 0 \end{bmatrix} \quad (12)$$

The nontrivial solution of (12) is obtained by equating the determinant of this equation to zero and brings the first characteristic equation.

The second solutions of  $U_2$ ,  $W_2$ ,  $\theta_2$ , and  $P_2$  are considered as

$$\begin{aligned} U_2(r) &= [A_2 J_1(\beta r) + A_3 r J_2(\beta r)] \\ W_2(r) &= [B_2 J_0(\beta r) + B_3 r J_1(\beta r)] \\ \theta_2(r) &= [C_2 J_0(\beta r) + C_3 r J_1(\beta r)] \\ P_2(r) &= [D_2 J_0(\beta r) + D_3 r J_1(\beta r)] \end{aligned} \quad (13)$$

The expressions for  $U_2$ ,  $W_2$ ,  $\theta_2$ , and  $P_2$  can be the solutions of (9), if and only if

$$\begin{bmatrix} \begin{pmatrix} -\beta^2 + d_1\zeta_n^2 \\ +d_5\lambda^2 \end{pmatrix} & -d_2\zeta_n\beta & -d_4\beta & -d_3\beta \\ -d_7\zeta_n\beta & \begin{pmatrix} \beta^2 - d_6\zeta_n^2 \\ -d_{11}\lambda^2 \end{pmatrix} & -d_{10}\zeta_n & -d_9\zeta_n \\ -d_{14}\lambda\beta & d_{14}\lambda\zeta_n & \begin{pmatrix} \beta^2 - d_6\zeta_n^2 \\ -d_{11}\lambda \end{pmatrix} & -d_{13}\lambda \\ -d_{17}\lambda\beta & +d_{17}\lambda\zeta_n & -d_{16}\lambda & \begin{pmatrix} \beta^2 - d_6\zeta_n^2 \\ -d_{11}\lambda \end{pmatrix} \end{bmatrix} \times \begin{Bmatrix} A_3 \\ B_3 \\ C_3 \\ D_3 \end{Bmatrix} = \begin{bmatrix} 0 \\ 0 \\ 0 \\ 0 \end{bmatrix} \quad (14)$$

$$\begin{aligned} (d_5\lambda^2 - \beta^2 + d_1\zeta_n^2)A_2 + (d_5\lambda^2 + d_1\zeta_n^2)\frac{2}{\beta}A_3 \\ - d_2\zeta_n\beta B_2 - d_4\beta C_2 - d_3D_2\beta = 0 \end{aligned} \quad (15)$$

The nontrivial solution of (14) is obtained by equating the determinant of coefficients matrix of this equation to zero as second characteristic equation and it is completely similar to the first characteristic equation.

$$\begin{aligned} d_7\zeta_n\beta A_2 + (-\beta^2 + d_{11}\lambda^2 + d_6\zeta_n^2)B_2 + 2\beta B_3 \\ + d_{10}\zeta_n C_2 + d_9\zeta_n D_2 = 0 \end{aligned} \quad (16)$$

$$U_3(r) = [A_4J_1(\beta r) + A_5rJ_2(\beta r) + A_6r^2J_3(\beta r)]$$

$$W_3(r) = [B_4J_0(\beta r) + B_5rJ_1(\beta r) + B_6r^2J_2(\beta r)]$$

$$\theta_3(r) = [C_4J_0(\beta r) + C_5rJ_1(\beta r) + C_6r^2J_2(\beta r)]$$

$$P_3(r) = [D_4J_0(\beta r) + D_5rJ_1(\beta r) + D_6r^2J_2(\beta r)]$$

$$\begin{aligned} -C_2\beta^2 + 2\beta C_3 - \zeta_n^2 C_2 + d_{12}\lambda C_2 + d_{13}\lambda D_2 \\ - \zeta_n d_{14}\lambda B_2 + d_{14}\lambda A_2\beta = 0 \end{aligned} \quad (17)$$

Equations (15)–(18) give the relations between  $A_2, B_2, B_3, C_2, C_3, D_2$  and  $D_3$ . They play as the balancing ratios that make (13) to be the second solution of the system of (9).

$$\begin{aligned} d_{17}\lambda\beta A_2 - d_{17}\lambda\zeta_n B_2 + d_{16}\lambda C_2 \\ + (-\zeta_n^2 - \beta^2 + d_{15}\lambda)D_2 + 2\beta D_3 = 0 \end{aligned} \quad (18)$$

The third solution of the system of the ordinary differential equations with nonconstant coefficients (9) must be considered as

$$\begin{bmatrix}
 \begin{pmatrix} -\beta^2 + d_1 \zeta_n^2 \\ + d_5 \lambda^2 \end{pmatrix} & -d_2 \zeta_n \beta & -d_4 \beta & -d_3 \beta \\
 -d_7 \zeta_n \beta & \begin{pmatrix} \beta^2 - d_6 \zeta_n^2 \\ -d_{11} \lambda^2 \end{pmatrix} & -d_{10} \zeta_n & -d_9 \zeta_n \\
 -d_{14} \lambda \beta & d_{14} \lambda \zeta_n & \begin{pmatrix} \beta^2 - d_6 \zeta_n^2 \\ -d_{11} \lambda \end{pmatrix} & -d_{13} \lambda \\
 -d_{17} \lambda \beta & +d_{17} \lambda \zeta_n & -d_{16} \lambda & \begin{pmatrix} \beta^2 - d_6 \zeta_n^2 \\ -d_{11} \lambda \end{pmatrix}
 \end{bmatrix} \times \begin{Bmatrix} A_6 \\ B_6 \\ C_6 \\ D_6 \end{Bmatrix} = \begin{bmatrix} 0 \\ 0 \\ 0 \\ 0 \end{bmatrix} \quad (20)$$

$$\begin{aligned}
 (d_5 \lambda^2 - \beta^2 + d_1 \zeta_n^2) A_4 + (d_5 \lambda^2 + d_1 \zeta_n^2) \frac{2}{\beta} A_5 & \quad d_7 \zeta_n \beta A_4 + (-\beta^2 + d_{11} \lambda^2 + d_6 \zeta_n^2) B_4 \\
 + (d_5 \lambda^2 + d_1 \zeta_n^2) \frac{8}{\beta^2} A_6 - d_2 \zeta_n \beta B_4 & \quad + 2\beta B_5 + d_{10} \zeta_n C_4 + d_9 \zeta_n D_4 = 0 \\
 -d_4 \beta C_4 - d_3 \beta D_4 = 0 & \quad (21)
 \end{aligned}$$

$$\begin{aligned}
 (-d_5 \lambda^2 + \beta^2 - d_1 \zeta_n^2) A_5 - (d_5 \lambda^2 + d_1 \zeta_n^2) \frac{4}{\beta} A_6 & \\
 + d_2 \zeta_n \beta B_5 + d_4 \beta C_5 + d_3 \beta D_5 = 0 & \quad (22)
 \end{aligned}$$

$$\left\{ \begin{aligned}
 & + d_7 \zeta_n A_5 \beta + 2d_7 \zeta_n A_6 + (-\beta^2 + d_6 \zeta_n^2 + d_{11} \lambda^2) B_5 \\
 & + \left( 2\beta + d_6 \zeta_n^2 \frac{2}{\beta} + d_{11} \lambda^2 \frac{2}{\beta} \right) B_6 \\
 & + d_{10} \zeta_n C_5 + d_{10} \zeta_n C_6 \frac{2}{\beta} + d_9 \zeta_n D_5 + d_9 \zeta_n D_6 \frac{2}{\beta}
 \end{aligned} \right\} = 0 \quad (24)$$

$$-\beta^2 C_4 + 2\beta C_5 - \zeta_n^2 C_4 + d_{12}\lambda C_4 + d_{13}\lambda D_4 - \zeta_n d_{14}\lambda B_4 + d_{14}\lambda \beta A_4 = 0 \quad (25)$$

$$\left\{ \begin{array}{l} + d_{14}\lambda \beta A_5 + 2d_{14}\lambda A_6 - \zeta_n d_{14}\lambda B_5 - \frac{2}{\beta} \zeta_n d_{14}\lambda B_6 \\ + (-\beta^2 - \zeta_n^2 + d_{12}\lambda) C_5 \\ + \left( \beta - \zeta_n^2 \frac{2}{\beta} + \beta + d_{12}\lambda \frac{2}{\beta} \right) C_6 \\ + d_{13}\lambda D_5 + d_{13}\lambda \frac{2}{\beta} D_6 \end{array} \right\} = 0 \quad (26)$$

$$\left\{ \begin{array}{l} + d_{17}\lambda A_5 \beta + 2d_{17}\lambda A_6 - d_{17}\zeta_n \lambda B_5 - d_{17}\zeta_n \lambda B_6 \frac{2}{\beta} \\ + d_{16}\lambda C_5 + d_{16}\lambda C_6 \\ + \frac{2}{\beta} (-\beta^2 + d_{15}\lambda - \zeta_n^2) D_5 \\ + \left( d_{15}\lambda \frac{2}{\beta} + 2\beta - \zeta_n^2 \frac{2}{\beta} \right) D_6 \end{array} \right\} = 0 \quad (28)$$

The expressions for  $U_3$ ,  $W_3$ ,  $\theta_3$ , and  $P_3$  can be solutions of (9), if and only if

$$d_{17}\lambda \beta A_4 - d_{17}\lambda \zeta_n B_4 + d_{16}\lambda C_4 + (-\zeta_n^2 - \beta^2 + d_{15}\lambda) D_4 + 2\beta D_5 = 0 \quad (27)$$

$$\begin{aligned} U_4(r) &= [A_7 J_1(\beta r) + A_8 r J_2(\beta r) + A_9 r^2 J_3(\beta r) + A_{10} r^3 J_4(\beta r)] \\ W_4(r) &= [B_7 J_0(\beta r) + B_8 r J_1(\beta r) + B_9 r^2 J_2(\beta r) + B_{10} r^3 J_3(\beta r)] \\ \theta_4(r) &= [C_7 J_0(\beta r) + C_8 r J_1(\beta r) + C_9 r^2 J_2(\beta r) + C_{10} r^3 J_3(\beta r)] \\ P_4(r) &= [D_7 J_0(\beta r) + D_8 r J_1(\beta r) + D_9 r^2 J_2(\beta r) + D_{10} r^3 J_3(\beta r)] \end{aligned} \quad (29)$$

The nontrivial solution of (20) is obtained by equating the determinant to zero of this equation and brings the third characteristic equation and it is as same as first and second characteristic equations.

Equations (21)–(28) give the relation between  $A_4, A_5, B_4, B_5, B_6, C_4, C_5, C_6, D_4, D_5$ , and  $D_6$ .

They play as the balancing ratios that help (19) to be the third solution of the system of (9).

The fourth solutions of  $U_1, W_1, \theta_1$ , and  $P_1$  are considered as

$$\left[ \begin{array}{cccc} (-\beta^2 + d_{11}\zeta_n^2 + d_5\lambda^2) & -d_2\zeta_n\beta & -d_4\beta & -d_3\beta \\ -d_7\zeta_n\beta & \begin{pmatrix} \beta^2 - d_6\zeta_n^2 \\ -d_{11}\lambda^2 \end{pmatrix} & -d_{10}\zeta_n & -d_9\zeta_n \\ -d_{14}\lambda\beta & d_{14}\lambda\zeta_n & \begin{pmatrix} \beta^2 \\ -d_6\zeta_n^2 \\ -d_{11}\lambda \end{pmatrix} & -d_{13}\lambda \\ -d_{17}\lambda\beta & +d_{17}\lambda\zeta_n & -d_{16}\lambda & \begin{pmatrix} \beta^2 \\ -d_6\zeta_n^2 \\ -d_{11}\lambda \end{pmatrix} \end{array} \right] \times \left\{ \begin{array}{c} A_{10} \\ B_{10} \\ C_{10} \\ D_{10} \end{array} \right\} = \left[ \begin{array}{c} 0 \\ 0 \\ 0 \\ 0 \end{array} \right] \quad (30)$$



The expressions for  $U_4$ ,  $W_4$ ,  $\theta_4$ , and  $P_4$  can be solutions of (9), if and only if

$$\left\{ \begin{array}{l} (d_5\lambda^2 - \beta^2 + d_1\zeta_n^2)A_7 + (d_5\lambda^2 + d_1\zeta_n^2)\frac{2}{\beta}A_8 \\ + (d_5\lambda^2 + d_1\zeta_n^2)\frac{8}{\beta^2}A_9 \\ + (d_5\lambda^2 + d_1\zeta_n^2)\frac{48}{\beta^3}A_{10} \\ - d_2\zeta_n B_7\beta - d_4C_7\beta - d_3D_7\beta \end{array} \right\} = 0 \quad (31)$$

$$\left\{ \begin{array}{l} (-d_5\lambda^2 + \beta^2 - d_1\zeta_n^2)A_8 - (d_5\lambda^2 + d_1\zeta_n^2)\frac{4}{\beta}A_9 \\ - (d_5\lambda^2 + d_1\zeta_n^2)\frac{24}{\beta^2}A_{10} \\ + d_2\zeta_n B_8\beta + d_4C_8\beta + d_3D_8\beta \end{array} \right\} = 0 \quad (32)$$

$$\left\{ \begin{array}{l} + (-d_5\lambda^2 + \beta^2 - d_1\zeta_n^2)A_9 + \left(-d_5\lambda^2\frac{8}{\beta} + 2\beta - d_1\zeta_n^2\frac{8}{\beta}\right)A_{10} \\ + d_2\zeta_n\beta B_9 + 2d_2\zeta_n B_{10} + d_4C_9\beta + 2d_4C_{10} \\ + d_3\beta D_9 + 2d_3D_{10} \end{array} \right\} = 0 \quad (33)$$

$$\left\{ \begin{array}{l} d_7\zeta_n\beta A_7 + (-\beta^2 + d_{11}\lambda^2 + d_6\zeta_n^2)B_7 + 2\beta B_8 - B_{10}r^2\beta \\ + d_{10}\zeta_n C_7 + d_9\zeta_n D_7 \end{array} \right\} = 0 \quad (34)$$

$$\left\{ \begin{array}{l} + d_7\zeta_n A_8\beta + 2d_7\zeta_n A_9 + \frac{8}{\beta}d_7\zeta_n A_{10} + (-\beta^2 + d_6\zeta_n^2 + d_{11}\lambda^2)B_8 \\ + \left(2\beta + d_6\zeta_n^2\frac{2}{\beta} + d_{11}\lambda^2\frac{2}{\beta}\right)B_9 \\ + \left(4 + d_6\zeta_n^2\frac{8}{\beta^2} + d_{11}\lambda^2\frac{8}{\beta^2}\right)B_{10} + d_{10}\zeta_n C_8 + d_{10}\zeta_n C_9\frac{2}{\beta} \\ + d_{10}\zeta_n C_{10}\frac{8}{\beta^2} \\ + d_9\zeta_n D_8 + d_9\zeta_n D_9\frac{2}{\beta} + d_9\zeta_n D_{10}\frac{8}{\beta^2} \end{array} \right\} = 0 \quad (35)$$

$$\left\{ \begin{array}{l} -d_7\zeta_n\beta A_9 + (-5d_7\zeta_n + d_8\zeta_n)A_{10} + (B_9\beta^2 - d_{11}\lambda^2 B_9 - d_6\zeta_n^2)B_9 \\ - \left(\beta + d_{11}\lambda^2\frac{4}{\beta} + d_6\zeta_n^2\frac{4}{\beta}\right)B_{10} \\ - d_{10}\zeta_n\left\{C_9 + C_{10}\frac{4}{\beta}\right\} - d_9\zeta_n\left\{D_9 + D_{10}\frac{4}{\beta}\right\} \end{array} \right\} = 0 \quad (36)$$

$$\{-C_7\beta^2 + 2C_8\beta - \zeta_n^2 C_7 + d_{12}\lambda C_7 + d_{13}\lambda D_7 - \zeta_n d_{14}\lambda B_7 + d_{14}\lambda A_7\beta\} = 0 \quad (37)$$

$$\left\{ \begin{array}{l} + d_{14}\lambda A_8\beta + 2d_{14}\lambda A_9 + d_{14}\lambda \frac{8}{\beta} A_{10} - B_8\zeta_n d_{14}\lambda - B_9\frac{2}{\beta}\zeta_n d_{14}\lambda - B_{10}\frac{8}{\beta^2}\zeta_n d_{14}\lambda \\ + (-\beta^2 - \zeta_n^2 + d_{12}\lambda)C_8 \\ + \left(\beta - \zeta_n^2\frac{2}{\beta} + \beta + d_{12}\lambda\frac{2}{\beta}\right)C_9 + \left(4 - \zeta_n^2\frac{8}{\beta^2} + d_{12}\lambda\frac{8}{\beta^2}\right)C_{10} + d_{13}\lambda D_8 \\ + d_{13}\lambda\frac{2}{\beta}D_9 + d_{13}\lambda\frac{8}{\beta^2}D_{10} \end{array} \right\} = 0 \quad (38)$$

$$\left\{ \begin{array}{l} - d_{14}\lambda\beta A_9 - 4d_{14}\lambda A_{10} + \zeta_n d_{14}\lambda B_9 + \zeta_n d_{14}\lambda B_{10}\frac{4}{\beta} \\ (\beta^2 + \zeta_n^2 - d_{12}\lambda)C_9 - \left(2\beta + d_{12}\lambda\frac{4}{\beta} + \zeta_n^2\frac{4}{\beta}\right)C_{10} - d_{13}\lambda D_9 - d_{13}\lambda D_{10}\frac{4}{\beta} \end{array} \right\} = 0 \quad (39)$$

$$\{d_{17}\lambda\beta A_7 - d_{17}\lambda\zeta_n B_7 + d_{16}\lambda C_7 + (-\zeta_n^2 - \beta^2 + d_{15}\lambda)D_7 + 2\beta D_8\} = 0 \quad (40)$$

$$\left\{ \begin{array}{l} + d_{17}\lambda A_8\beta + 2d_{17}\lambda A_9 + d_{17}\lambda \frac{8}{\beta} A_{10} - d_{17}\zeta_n\lambda B_8 - d_{17}\zeta_n\lambda B_9\frac{2}{\beta} - d_{17}\zeta_n\lambda B_{10}\frac{8}{\beta^2} \\ + d_{16}\lambda C_8 + d_{16}\lambda C_9\frac{2}{\beta} + d_{16}\lambda C_{10}\frac{8}{\beta^2} \\ (-\beta^2 + d_{15}\lambda - \zeta_n^2)D_8 + \left(d_{15}\lambda\frac{2}{\beta} + 2\beta - \zeta_n^2\frac{2}{\beta}\right)D_9 + \left(4 + d_{15}\lambda\frac{8}{\beta^2} - \zeta_n^2\frac{8}{\beta^2}\right)D_{10} \end{array} \right\} = 0 \quad (41)$$

$$\left\{ \begin{array}{l} - 4d_{17}\lambda A_{10} - d_{17}\lambda A_9\beta + d_{17}\zeta_n\lambda B_9 + d_{17}\zeta_n\lambda B_{10}\frac{4}{\beta} - d_{16}\lambda C_9 - d_{16}\lambda C_{10}\frac{4}{\beta} \\ + \left(-\beta J_0(\beta r) + \zeta_n^2\frac{4}{\beta} - \beta - d_{15}\lambda\frac{4}{\beta}\right)D_{10} + (\zeta_n^2 + \beta^2 - d_{15}\lambda)D_9 \end{array} \right\} = 0 \quad (42)$$

The nontrivial solution of (30) is obtained by equating the determinant of coefficients matrix of this equation to zero as fourth characteristic equation and it is completely similar to the first, second, and third characteristic equations.

This equality is interesting as it prevents mathematical dilemma and complexity and a single value for the eigenvalue  $\beta$  simultaneously

satisfies three characteristic equations. Equations (31)–(42) gives the relation between  $A_7, A_8, A_9, B_7, B_8, B_9, B_{10}, C_7, C_8, C_9, C_{10}, D_7, D_8, D_9$ , and  $D_{10}$  and they play as the balancing ratios that help (29) to be the third solution of the system of (9).

Therefore, the complete general solutions for the solid cylinder are

$$\begin{aligned}
U^g(r) &= A_1 J_1(\beta r) + A_3 [\zeta_1 J_1(\beta r) + r J_2(\beta r)] \\
&\quad + A_6 [\zeta_2 J_1(\beta r) + \zeta_3 r J_2(\beta r) + r^2 J_3(\beta r)] \\
&\quad + A_{10} [\zeta_4 J_1(\beta r) + \zeta_5 r J_2(\beta r) + \zeta_6 r^2 J_3(\beta r) + r^3 J_4(\beta r)] \\
W^g(r) &= A_1 \zeta_7 J_0(\beta r) + A_3 [\zeta_8 J_0(\beta r) + \zeta_9 r J_1(\beta r)] \\
&\quad + A_6 [\zeta_{10} J_0(\beta r) + \zeta_{11} r J_1(\beta r) + \zeta_{12} r^2 J_2(\beta r)] \\
&\quad + A_{10} [\zeta_{13} J_0(\beta r) + \zeta_{14} r J_1(\beta r) + \zeta_{15} r^2 J_2(\beta r) + \zeta_{16} r^3 J_3(\beta r)] \\
\theta^g(r) &= A_1 \zeta_{17} J_0(\beta r) + A_3 [\zeta_{18} J_0(\beta r) + \zeta_{19} r J_1(\beta r)] \\
&\quad + A_6 [\zeta_{20} J_0(\beta r) + \zeta_{21} r J_1(\beta r) + \zeta_{22} r^2 J_2(\beta r)] \\
&\quad + A_{10} \left[ \begin{aligned} &\zeta_{23} J_0(\beta r) + \zeta_{24} r J_1(\beta r) + \zeta_{25} r^2 J_2(\beta r) \\ &+ \zeta_{26} r^3 J_3(\beta r) \end{aligned} \right] \\
P^g(r) &= A_1 \zeta_{27} J_0(\beta r) + A_3 [\zeta_{28} J_0(\beta r) + \zeta_{29} r J_1(\beta r)] \\
&\quad + A_6 [\zeta_{30} J_0(\beta r) + \zeta_{31} r J_1(\beta r) + \zeta_{32} r^2 J_2(\beta r)] \\
&\quad + A_{10} \left[ \begin{aligned} &\zeta_{33} J_0(\beta r) + \zeta_{34} r J_1(\beta r) + \zeta_{35} r^2 J_2(\beta r) \\ &+ \zeta_{36} r^3 J_3(\beta r) \end{aligned} \right]
\end{aligned} \tag{43}$$

where  $\zeta_1$  to  $\zeta_{36}$  are ratios obtained from (31) to (42), (21) to (28), (15) to (18), and (12). Substituting  $U^g$ ,  $W^g$ ,  $\theta^g$ , and  $P^g$  in the homogeneous form of the boundary conditions (5), three linear algebraic equations are obtained. They are the coefficients depending on  $\lambda$  and  $\beta$ .

Setting the determinant of the coefficients equal to zero, the fifth characteristic equation is obtained. Simultaneous solution of this equation and (15), results into infinite number of two eigenvalues  $\beta_n$  and  $\lambda_n$ . Therefore,  $U^g$ ,  $W^g$ ,  $\theta^g$ , and  $P^g$  are rewritten as

$$\begin{aligned}
U^g(r) &= A_1 \left[ \begin{aligned} &J_1(\beta r) + \zeta_{37} [\zeta_1 J_1(\beta r) + r J_2(\beta r)] \\ &+ \zeta_{38} [\zeta_2 J_1(\beta r) + \zeta_3 r J_2(\beta r) + r^2 J_3(\beta r)] \\ &+ \zeta_{39} [\zeta_4 J_1(\beta r) + \zeta_5 r J_2(\beta r) + \zeta_6 r^2 J_3(\beta r) + r^3 J_4(\beta r)] \end{aligned} \right] \\
W^g(r) &= A_1 \left[ \begin{aligned} &\zeta_7 J_0(\beta r) + \zeta_{37} [\zeta_8 J_0(\beta r) + \zeta_9 r J_1(\beta r)] \\ &+ \zeta_{38} [\zeta_{10} J_0(\beta r) + \zeta_{11} r J_1(\beta r) + \zeta_{12} r^2 J_2(\beta r)] \\ &+ \zeta_{39} \left[ \begin{aligned} &\zeta_{13} J_0(\beta r) + \zeta_{14} r J_1(\beta r) + \zeta_{15} r^2 J_2(\beta r) \\ &+ \zeta_{16} r^3 J_3(\beta r) \end{aligned} \right] \end{aligned} \right] \\
\theta^g(r) &= A_1 \left[ \begin{aligned} &\zeta_{17} J_0(\beta r) + \zeta_{37} [\zeta_{18} J_0(\beta r) + \zeta_{19} r J_1(\beta r)] \\ &+ \zeta_{38} [\zeta_{20} J_0(\beta r) + \zeta_{21} r J_1(\beta r) + \zeta_{22} r^2 J_2(\beta r)] \\ &+ \zeta_{39} \left[ \begin{aligned} &\zeta_{23} J_0(\beta r) + \zeta_{24} r J_1(\beta r) + \zeta_{25} r^2 J_2(\beta r) \\ &+ \zeta_{26} r^3 J_3(\beta r) \end{aligned} \right] \end{aligned} \right] \\
P^g(r) &= A_1 \left[ \begin{aligned} &\zeta_{27} J_0(\beta r) + \zeta_{37} [\zeta_{28} J_0(\beta r) + \zeta_{29} r J_1(\beta r)] \\ &+ \zeta_{38} [\zeta_{30} J_0(\beta r) + \zeta_{31} r J_1(\beta r) + \zeta_{32} r^2 J_2(\beta r)] \\ &+ \zeta_{39} \left[ \begin{aligned} &\zeta_{33} J_0(\beta r) + \zeta_{34} r J_1(\beta r) + \zeta_{35} r^2 J_2(\beta r) \\ &+ \zeta_{36} r^3 J_3(\beta r) \end{aligned} \right] \end{aligned} \right]
\end{aligned} \tag{44}$$

where  $\zeta_{37}$  to  $\zeta_{39}$  are constant parameters. brackets of (44) by functions  $H_0, H_1, H_2$ , and Let us show the functions in the  $H_3$  as

$$\begin{aligned}
 H_0(r) &= \begin{bmatrix} J_1(\beta r) + \zeta_{37}[\zeta_{11}J_1(\beta r) + rJ_2(\beta r)] \\ + \zeta_{38}[\zeta_{21}J_1(\beta r) + \zeta_{31}rJ_2(\beta r) + r^2J_3(\beta r)] \\ + \zeta_{39}[\zeta_{41}J_1(\beta r) + \zeta_{51}rJ_2(\beta r) + \zeta_{61}r^2J_3(\beta r) + r^3J_4(\beta r)] \end{bmatrix} \\
 H_1(r) &= \begin{bmatrix} \zeta_7J_0(\beta r) + \zeta_{37}[\zeta_8J_0(\beta r) + \zeta_9rJ_1(\beta r)] \\ + \zeta_{38}[\zeta_{10}J_0(\beta r) + \zeta_{11}rJ_1(\beta r) + \zeta_{12}r^2J_2(\beta r)] \\ + \zeta_{39} \begin{bmatrix} \zeta_{13}J_0(\beta r) + \zeta_{14}rJ_1(\beta r) + \zeta_{15}r^2J_2(\beta r) \\ + \zeta_{16}r^3J_3(\beta r) \end{bmatrix} \end{bmatrix} \\
 H_2(r) &= \begin{bmatrix} \zeta_{17}J_0(\beta r) + \zeta_{37}[\zeta_{18}J_0(\beta r) + \zeta_{19}rJ_1(\beta r)] \\ + \zeta_{38}[\zeta_{20}J_0(\beta r) + \zeta_{21}rJ_1(\beta r) + \zeta_{22}r^2J_2(\beta r)] \\ + \zeta_{39} \begin{bmatrix} \zeta_{23}J_0(\beta r) + \zeta_{24}rJ_1(\beta r) + \zeta_{25}r^2J_2(\beta r) \\ + \zeta_{26}r^3J_3(\beta r) \end{bmatrix} \end{bmatrix} \\
 H_3(r) &= \begin{bmatrix} \zeta_{27}J_0(\beta r) + \zeta_{37}[\zeta_{28}J_0(\beta r) + \zeta_{29}rJ_1(\beta r)] \\ + \zeta_{38}[\zeta_{30}J_0(\beta r) + \zeta_{31}rJ_1(\beta r) + \zeta_{32}r^2J_2(\beta r)] \\ + \zeta_{39} \begin{bmatrix} \zeta_{33}J_0(\beta r) + \zeta_{34}rJ_1(\beta r) + \zeta_{35}r^2J_2(\beta r) \\ + \zeta_{36}r^3J_3(\beta r) \end{bmatrix} \end{bmatrix}
 \end{aligned} \quad (45)$$

According to the Sturm-Liouville theorem,  $H_0$  or  $H_1$  or  $H_2$  or  $H_3$ ) and is called the H-Fourier series as these functions are orthogonal with respect to the weight function  $p(r) = r$  such as

$$\int_{r_i}^{r_o} H(\beta_n r) H(\beta_m r) r dr = \begin{cases} 0 & n \neq m \\ \|H(\beta_n r)\|^2 & n = m \end{cases} \quad f(r) = \sum_{n=1}^{\infty} e_n H(\beta_n r) \quad (46)$$

where  $e_n$  equals

where  $\|H(\beta_n r)\|$  is norm of the  $H$  function and equals

$$\|H(\beta_n r)\| = \left[ \int_{r_i}^{r_o} r H^2(\beta_n r) dr \right]^{\frac{1}{2}} \quad e_n = \frac{1}{\|H(\beta_n r)\|^2} \int_{r_i}^{r_o} f(r) H(r) r dr \quad (47) \quad (49)$$

Due to the orthogonality of function  $H$ , every piece-wise continuous function, such as  $f(r)$ , can be expanded in terms of the function  $H$  (either

Using (8), (44), and (45) the displacement and temperature distributions due to the general solution become

$$\begin{aligned}
 u^g(r, t, z) &= \sum_{n=1}^{\infty} \sum_{m=1}^{\infty} \left\{ \sum_{K=1}^6 a_{nmk} e^{\lambda_{nmk} t} \right\} H_0(\beta_{nm} r) \sin(\zeta_n z) \\
 w^g(r, t, z) &= \sum_{n=1}^{\infty} \sum_{m=1}^{\infty} \left\{ \sum_{K=1}^6 B_{nmk} a_{nmk} e^{\lambda_{nmk} t} \right\} H_1(\beta_{nm} r) \cos(\zeta_n z) \\
 T^g(r, t, z) &= \sum_{n=1}^{\infty} \sum_{m=1}^{\infty} \left\{ \sum_{K=1}^6 N_{nmk} a_{nmk} e^{\lambda_{nmk} t} \right\} H_2(\beta_{nm} r) \sin(\zeta_n z) \\
 p^g(r, t, z) &= \sum_{n=1}^{\infty} \sum_{m=1}^{\infty} \left\{ \sum_{K=1}^6 M_{nmk} a_{nmk} e^{\lambda_{nmk} t} \right\} H_3(\beta_{nm} r) \sin(\zeta_n z)
 \end{aligned} \quad (50)$$

where  $B_{mn}$ ,  $N_{mn}$ , and  $M_{nm}$  are ratios obtained by substituting (1)–(4). Using the initial conditions (7) and with the help of (47)–(49) and (45) and (50), six unknown constants are obtained.

### Particular Solution with Nonhomogeneous Boundary Conditions

The general solutions may be used as proper functions for guessing the particular solution adopted to the nonhomogeneous parts of the (1)–(4) and the nonhomogeneous boundary conditions (5) as

$$\begin{aligned} u^p(r, t) &= \sum_{n=1}^{\infty} \sum_{m=1}^{\infty} \left\{ \begin{aligned} & \left[ G_1(t)J_1(\beta\beta_{nm}r) + G_2(t)rJ_2(\beta\beta_{nm}r) \right. \\ & \left. + G_3(t)r^2J_3(\beta\beta_{nm}r) + G_4(t)r^3J_4(\beta\beta_{nm}r) \right. \\ & \left. + r^2G_5(t) \right] \end{aligned} \right\} \sin(\zeta_n z) \\ w^p(r, t) &= \sum_{n=1}^{\infty} \sum_{m=1}^{\infty} \left\{ \begin{aligned} & \left[ G_6(t)J_0(\beta\beta_{nm}r) + G_7(t)rJ_1(\beta\beta_{nm}r) \right. \\ & \left. + G_8(t)r^2J_3(\beta\beta_{nm}r) + G_9(t)r^3J_4(\beta\beta_{nm}r) \right. \\ & \left. + r^2G_{10}(t) \right] \end{aligned} \right\} \cos(\zeta_n z) \\ T^p(r, t) &= \sum_{n=1}^{\infty} \sum_{m=1}^{\infty} \left\{ \begin{aligned} & \left[ G_{11}(t)J_0(\beta\beta_{nm}r) + G_{12}(t)rJ_1(\beta\beta_{nm}r) \right. \\ & \left. + G_{13}(t)r^2J_3(\beta\beta_{nm}r) + G_{14}(t)r^3J_4(\beta\beta_{nm}r) \right. \\ & \left. + r^2G_{15}(t) \right] \end{aligned} \right\} \sin(\zeta_n z) \\ p^p(r, t) &= \sum_{n=1}^{\infty} \sum_{m=1}^{\infty} \left\{ \begin{aligned} & \left[ G_{16}(t)J_0(\beta\beta_{nm}r) + G_{17}(t)rJ_1(\beta\beta_{nm}r) \right. \\ & \left. + G_{18}(t)r^2J_3(\beta\beta_{nm}r) + G_{19}(t)r^3J_4(\beta\beta_{nm}r) \right. \\ & \left. + r^2G_{20}(t) \right] \end{aligned} \right\} \sin(\zeta_n z) \end{aligned} \quad (51)$$

It is necessary and suitable to expand the body force  $F(r, t)$ ,  $R(z, t)$ , heat source  $Q(r, t)$ , and porosity function  $W(r, t)$  in H-Fourier expansion form as

$$\begin{aligned} F(r, t) &= \sum_{n=1}^{\infty} \sum_{m=1}^{\infty} F_{nm}(t)H_0(\beta_{nm}r) \sin(\zeta_n z) \\ R(z, t) &= \sum_{n=1}^{\infty} \sum_{m=1}^{\infty} R_{nm}(t)H_1(\beta_{nm}r) \cos(\zeta_n z) \\ Q(r, t) &= \sum_{n=1}^{\infty} \sum_{m=1}^{\infty} Q_{nm}(t)H_2(\beta_{nm}r) \sin(\zeta_n z) \\ P(r, t) &= \sum_{n=1}^{\infty} \sum_{m=1}^{\infty} P_{nm}(t)H_3(\beta_{nm}r) \sin(\zeta_n z) \end{aligned} \quad (52)$$

where  $F_n(t)$ ,  $R_n(t)$ ,  $Q_n(t)$ , and  $P_n(t)$  are

$$\begin{aligned} F_n(t) &= \frac{2}{\|H_0(\beta_n r)\|^2 l} \int_0^l \int_{r_i}^{r_o} F(r, t) H_0(\beta_n r) r \sin(\zeta_n z) dr dz \\ R_n(t) &= \frac{2}{\|H_1(\beta_n r)\|^2 l} \int_0^l \int_{r_i}^{r_o} Q(r, t) H_1(\beta_n r) r \cos(\zeta_n z) dr dz \\ Q_n(t) &= \frac{2}{\|H_2(\beta_n r)\|^2 l} \int_0^l \int_{r_i}^{r_o} Q(r, t) H_2(\beta_n r) r \sin(\zeta_n z) dr dz \\ P_n(t) &= \frac{2}{\|H_3(\beta_n r)\|^2 l} \int_0^l \int_{r_i}^{r_o} P(r, t) H_3(\beta_n r) r \sin(\zeta_n z) dr dz \end{aligned} \quad (53)$$

Substituting (51) and (53) into nonhomogeneous form of (1) into (4) yield

$$\begin{aligned}
& \left\{ \begin{aligned} & - \left\{ G_1(t) \beta_{nm}^2 + G_2(t) \beta_{nm} + 4G_3(t) + \frac{24}{\beta_{nm}} G_4(t) \right\} \\ & + \left\{ G_2(t) \beta_{nm} + 3G_3(t) + \frac{16}{\beta_{nm}} G_4(t) \right\} \\ & + \left\{ G_4(t) \frac{8}{\beta_{nm}} + G_3(t) \right\} - d_1 \zeta_n^2 \left\{ \begin{aligned} & G_1(t) + \frac{2}{\beta_{nm}} G_2(t) \\ & + \frac{8}{\beta_{nm}^2} G_3(t) + \frac{48}{\beta_{nm}^3} G_4(t) \end{aligned} \right\} \\ & + d_2 \zeta_n G_6(t) \beta_{nm} - d_3 G_{16}(t) \beta_{nm} - d_4 G_{11}(t) \beta_{nm} \\ & + d_5 \left\{ \ddot{G}_1(t) + \frac{2}{\beta} \ddot{G}_2(t) + \frac{8}{\beta^2} \ddot{G}_3(t) + \frac{48}{\beta^3} \ddot{G}_4(t) \right\} \\ & \left\{ \begin{aligned} & \mu_1 G_5(t) + \mu_2 G_5(t) + \mu_3 G_{10}(t) + \mu_4 G_{20}(t) \\ & + \mu_5 G_{15}(t) + \mu_6 \ddot{G}_5(t) + d_{18} F_{nm}(t) \end{aligned} \right\} \\ & \times \left\{ \chi_0 + \frac{2}{\beta} \chi_1 + \frac{8}{\beta^2} \chi_2 + \frac{48}{\beta^3} \chi_3 \right\} \end{aligned} \right\} = 0 \\
& + \left\{ \begin{aligned} & \left\{ G_2(t) \beta_{nm}^2 + G_3(t) \beta_{nm} + 6G_4(t) \right\} + \left\{ -5G_4(t) - G_3(t) \beta_{nm} \right\} \\ & + G_4(t) + d_4 G_{12}(t) \beta_{nm} \\ & + d_1 \zeta_n^2 \left\{ G_2(t) + \frac{4}{\beta_{nm}} G_3(t) + \frac{24}{\beta_{nm}^2} A_{10} \right\} - d_2 \zeta_n G_7(t) \beta_{nm} \\ & + d_3 G_{17}(t) \beta_{nm} - d_5 \left\{ \ddot{G}_2(t) + \frac{4}{\beta} \ddot{G}_3(t) + \frac{24}{\beta^2} \ddot{G}_4(t) \right\} \\ & - \left\{ \begin{aligned} & \mu_1 G_5(t) + \mu_2 G_5(t) + \mu_3 G_{10}(t) \\ & + \mu_4 G_{20}(t) + \mu_5 G_{15}(t) \\ & + \mu_6 \ddot{G}_5(t) + d_{18} F_{nm}(t) \end{aligned} \right\} \times \left\{ \chi_1 + \frac{4}{\beta} \chi_2 + \frac{24}{\beta^2} \chi_3 \right\} r J_0(\beta r) \end{aligned} \right\} = 0 \quad (54a) \\
& + \left\{ \begin{aligned} & \left\{ 3G_4(t) \beta_{nm} + G_3(t) \beta_{nm}^2 \right\} - G_4(t) \beta_{nm} \\ & + d_1 \zeta_n^2 \left\{ G_4(t) \frac{8}{\beta_{nm}} + G_3(t) \right\} - d_2 \zeta_n \{ G_8(t) \beta_{nm} + 2G_9(t) \} \\ & + d_3 \{ G_{18}(t) \beta_{nm} + 2G_{19}(t) \} + d_4 \{ G_{13}(t) \beta_{nm} + 2G_{14}(t) \} \\ & - d_5 \left\{ \ddot{G}_4(t) \frac{8}{\beta} + \ddot{G}_3(t) \right\} - \left\{ \begin{aligned} & \mu_1 G_5(t) + \mu_2 G_5(t) + \mu_3 G_{10}(t) \\ & + \mu_4 G_{20}(t) + \mu_5 G_{15}(t) \\ & + \mu_6 \ddot{G}_5(t) + d_{18} F_{nm}(t) \end{aligned} \right\} \times \left\{ \chi_3 \frac{8}{\beta} + \chi_2 \right\} \end{aligned} \right\} = 0 \\
& \left\{ \begin{aligned} & - G_4(t) \beta_{nm}^2 - d_1 \zeta_n^2 G_4(t) + d_2 \zeta_n G_9(t) \beta_{nm} \\ & - d_3 G_{19}(t) \beta_{nm} - d_4 G_{14}(t) \beta_{nm} + \ddot{G}_4(t) \\ & \left\{ \begin{aligned} & \mu_1 G_5(t) + \mu_2 G_5(t) + \mu_3 G_{10}(t) + \mu_4 G_{20}(t) \\ & + \mu_5 G_{15}(t) + \mu_6 \ddot{G}_5(t) + d_{18} F_{nm}(t) \end{aligned} \right\} \end{aligned} \right\} r^3 J_0(\beta r) = 0
\end{aligned}$$

$$\begin{aligned}
& \left\{ \begin{aligned} & \{-G_6(t)\beta^2 + G_7(t)\beta\} + G_7(t)\beta - d_6\zeta_n^2 G_6(t) \\ & + d_7\zeta_n \left\{ G_1(t)\beta + G_2(t) + \frac{4}{\beta} G_3(t) + \frac{24}{\beta^2} G_4(t) \right\} J_0(\beta r) \\ & - d_8\zeta_n \left\{ G_2(t) + \frac{4}{\beta} G_3(t) + \frac{24}{\beta^2} G_4(t) \right\} + d_9\zeta_n G_{16}(t) \\ & + d_{10}\zeta_n G_{11}(t) + d_{11}\ddot{G}_6(t) \\ & + \left\{ \begin{aligned} & \mu_7 G_{10}(t) + \mu_8 G_{10}(t) + \mu_9 G_{10}(t) + \mu_{10} G_{10}(t) \\ & + \mu_{11} G_{20}(t) + \mu_{12} G_{15}(t) + \mu_{13} \ddot{G}_{10}(t) + d_{19} R_{nm}(t) \end{aligned} \right\} \chi_4 \end{aligned} \right\} = 0 \\
& + \left\{ \begin{aligned} & \{-G_7(t)\beta^2 + G_8(t)\beta + 2G_9(t)\} + \{G_8(t)\beta + 2G_9(t)\} \\ & - d_6\zeta_n^2 \left\{ G_7(t) + G_8(t) \frac{2}{\beta} + G_9(t) \frac{8}{\beta^2} \right\} \\ & + d_7\zeta_n \left\{ G_2(t)\beta + 3G_3(t) + \frac{16}{\beta} G_4(t) \right\} - d_8\zeta_n \left\{ G_4(t) \frac{8}{\beta} + G_3(t) \right\} \\ & + d_9\zeta_n \left\{ G_{17}(t) + G_{18}(t) \frac{2}{\beta} + G_{19}(t) \frac{8}{\beta^2} \right\} \\ & + d_{10}\zeta_n \left\{ G_{12}(t) + G_{13}(t) \frac{2}{\beta} + G_{14}(t) \frac{8}{\beta^2} \right\} \\ & + d_{11} \left\{ \ddot{G}_7(t) + \ddot{G}_8(t) \frac{2}{\beta} + \ddot{G}_9(t) \frac{8}{\beta^2} \right\} \\ & + \left\{ \begin{aligned} & \mu_7 G_{10}(t) + \mu_8 G_{10}(t) + \mu_9 G_{10}(t) + \mu_{10} G_{10}(t) + \mu_{11} G_{20}(t) \\ & + \mu_{12} G_{15}(t) + \mu_{13} \ddot{G}_{10}(t) + d_{19} R_{nm}(t) \end{aligned} \right\} \\ & \times \left\{ \chi_5 + \chi_6 \frac{2}{\beta} + \chi_7 \frac{8}{\beta^2} \right\} \end{aligned} \right\} = 0 \\
& + \left\{ \begin{aligned} & \{G_8(t)\beta^2 - G_9(t)\beta\} - G_9(t)\beta + d_6\zeta_n^2 \left\{ G_8(t) + G_9(t) \frac{4}{\beta} \right\} \\ & + d_7\zeta_n \{-5G_4(t) - G_3(t)\beta\} \\ & + d_8\zeta_n A_{10} - d_9\zeta_n \left\{ G_{18}(t) + G_{19}(t) \frac{4}{\beta} \right\} \\ & - d_{10}\zeta_n \left\{ G_{13}(t) + G_{14}(t) \frac{4}{\beta} \right\} - d_{11} \left\{ \ddot{G}_8(t) + \ddot{G}_9(t) \frac{4}{\beta} \right\} \\ & - \left\{ \begin{aligned} & \mu_7 G_{10}(t) + \mu_8 G_{10}(t) + \mu_9 G_{10}(t) + \mu_{10} G_{10}(t) + \mu_{11} G_{20}(t) \\ & + \mu_{12} G_{15}(t) + \mu_{13} \ddot{G}_{10}(t) + d_{19} R_{nm}(t) \end{aligned} \right\} \\ & \times \left\{ \chi_6 + \chi_7 \frac{4}{\beta} \right\} \end{aligned} \right\} = 0 \\
& + \left\{ \begin{aligned} & G_9(t)\beta^2 + d_6\zeta_n^2 G_9(t) - d_7\zeta_n G_4(t)\beta \\ & - d_9\zeta_n G_{19}(t) - d_{10}\zeta_n G_{14}(t) - d_{11}\ddot{G}_9(t) \\ & + \left\{ \begin{aligned} & \mu_7 G_{10}(t) + \mu_8 G_{10}(t) + \mu_9 G_{10}(t) + \mu_{10} G_{10}(t) \\ & + \mu_{11} G_{20}(t) + \mu_{12} G_{15}(t) + \mu_{13} \ddot{G}_{10}(t) + d_{19} R_{nm}(t) \end{aligned} \right\} \chi_7 \end{aligned} \right\} = 0
\end{aligned} \tag{54b}$$



$$\begin{aligned}
& \left\{ \begin{aligned} & \left\{ -G_{11}(t)\beta_{nm}^2 + G_{12}(t)\beta_{nm} \right\} + G_{12}(t)\beta_{nm} \\ & - \zeta_n^2 G_{11}(t) + d_{12}\dot{G}_{11}(t) + d_{13}\dot{G}_{16}(t) \\ & + d_{14} \left\{ \dot{G}_1(t)\beta_{nm} + \dot{G}_2(t) + \frac{4}{\beta_{nm}}\dot{G}_3(t) + \frac{24}{\beta_{nm}^2}\dot{G}_4(t) \right\} \\ & - d_{14} \left\{ \dot{G}_2(t) + \frac{4}{\beta_{nm}}\dot{G}_3(t) + \frac{24}{\beta_{nm}^2}\dot{G}_4(t) \right\} - d_{14}\zeta_n\dot{G}_6(t) \\ & \left\{ \mu_{14}G_{15}(t) + \mu_{15}G_{15}(t) + \mu_{16}\dot{G}_{15}(t) + \mu_{17}\dot{G}_{20}(t) \right\} \chi_8 \\ & + \mu_{18}\dot{G}_5(t) + \mu_{19}\dot{G}_{10}(t) + d_{20}Q_{nm}(t) \end{aligned} \right\} \chi_8 \Bigg\} = 0 \\
& + \left\{ \begin{aligned} & \left\{ -G_{12}(t)\beta_{nm}^2 + G_{13}(t)\beta_{nm} + 2G_{14}(t) \right\} \\ & + \left\{ G_{13}(t)\beta_{nm} + 2G_{14}(t) \right\} \\ & - \zeta_n^2 \left\{ G_{12}(t) + G_{13}(t)\frac{2}{\beta_{nm}} + G_{14}(t)\frac{8}{\beta_{nm}^2} \right\} \\ & + d_{12} \left\{ \dot{G}_{12}(t) + \dot{G}_{13}(t)\frac{2}{\beta_{nm}} + \dot{G}_{14}(t)\frac{8}{\beta_{nm}^2} \right\} \\ & + d_{13} \left\{ \dot{G}_{17}(t) + \dot{G}_{18}(t)\frac{2}{\beta_{nm}} + \dot{G}_{19}(t)\frac{8}{\beta_{nm}^2} \right\} \\ & + d_{14} \left\{ \dot{G}_2(t)\beta_{nm} + 3\dot{G}_3(t) + \frac{16}{\beta_{nm}}\dot{G}_4(t) \right\} \\ & - d_{14} \left\{ \dot{G}_4(t)\frac{8}{\beta_{nm}} + \dot{G}_3(t) \right\} \\ & - d_{14}\zeta_n \left\{ \dot{G}_7(t) + \dot{G}_8(t)\frac{2}{\beta_{nm}} + \dot{G}_9(t)\frac{8}{\beta_{nm}^2} \right\} \\ & \left\{ \mu_{14}G_{15}(t) + \mu_{15}G_{15}(t) + \mu_{16}\dot{G}_{15}(t) + \mu_{17}\dot{G}_{20}(t) + \mu_{18}\dot{G}_5(t) \right\} \\ & + \mu_{19}\dot{G}_{10}(t) + d_{20}Q_{nm}(t) \\ & \times \left\{ \chi_9 + \chi_{10}\frac{2}{\beta} + \chi_{11}\frac{8}{\beta^2} \right\} \end{aligned} \right\} = 0 \tag{54c} \\
& + \left\{ \begin{aligned} & \left\{ G_{13}(t)\beta_{nm}^2 - G_{14}(t)\beta_{nm} \right\} - G_{14}(t)\beta_{nm} + \zeta_n^2 \left\{ G_{13}(t) + G_{14}(t)\frac{4}{\beta_{nm}} \right\} \\ & - d_{12} \left\{ \dot{G}_{13}(t) + \dot{G}_{14}(t)\frac{4}{\beta_{nm}} \right\} \\ & - d_{13} \left\{ \dot{G}_{18}(t) + \dot{G}_{19}(t)\frac{4}{\beta_{nm}} \right\} + d_{14} \left\{ -5\dot{G}_4(t) - \dot{G}_3(t)\beta_{nm} \right\} \\ & + d_{14}\dot{G}_4(t) + d_{14}\zeta_n \left\{ \dot{G}_8(t) + \dot{G}_9(t)\frac{4}{\beta_{nm}} \right\} \\ & - \left\{ \mu_{14}G_{15}(t) + \mu_{15}G_{15}(t) + \mu_{16}\dot{G}_{15}(t) + \mu_{17}\dot{G}_{20}(t) + \mu_{18}\dot{G}_5(t) \right\} \\ & + \mu_{19}\dot{G}_{10}(t) + d_{20}Q_{nm}(t) \\ & \times \left\{ \chi_{10} + \chi_{11}\frac{4}{\beta} \right\} \end{aligned} \right\} = 0 \\
& + \left\{ \begin{aligned} & G_{14}(t)\beta^2 + \zeta_n^2 G_{14}(t) - d_{12}\dot{G}_{14}(t) - d_{13}\dot{G}_{19}(t) \\ & - d_{14}\dot{G}_4(t)\beta_{nm} + d_{14}\zeta_n\dot{G}_9(t) \\ & - \chi_{11} \left\{ \mu_{14}G_{15}(t) + \mu_{15}G_{15}(t) + \mu_{16}\dot{G}_{15}(t) + \mu_{17}\dot{G}_{20}(t) \right\} \\ & + \mu_{18}\dot{G}_5(t) + \mu_{19}\dot{G}_{10}(t) + d_{20}Q_{nm}(t) \end{aligned} \right\} = 0
\end{aligned}$$

$$\begin{aligned}
 & \left\{ \begin{aligned} & \left\{ -G_{16}(t)\beta_{nm}^2 + G_{17}(t)\beta_{nm} \right\} + G_{17}(t)\beta_{nm} - \zeta_n^2 G_{16}(t) \\ & + d_{15}\dot{G}_{16}(t) + d_{16}\dot{G}_{11}(t) \\ & d_{17} \left\{ \dot{G}_1(t)\beta_{nm} + \dot{G}_2(t) + \frac{4}{\beta_{nm}}\dot{G}_3(t) + \frac{24}{\beta_{nm}^2}\dot{G}_4(t) \right\} \\ & - d_{17} \left\{ \dot{G}_2(t) + \frac{4}{\beta_{nm}}\dot{G}_3(t) + \frac{24}{\beta_{nm}^2}\dot{G}_4(t) \right\} - \zeta_n d_{17}\dot{G}_6(t) \\ & \chi_{12} \left\{ \begin{aligned} & \mu_{20}G_{20}(t) + \mu_{21}G_{20}(t) + \mu_{22}\dot{G}_{20}(t) + \mu_{23}\dot{G}_{15} \\ & + \mu_{24}\dot{G}_5 + \mu_{25}\dot{G}_{10} + d_{21}P_{nm}(t) \end{aligned} \right\} \end{aligned} \right\} = 0 \\
 & + \left\{ \begin{aligned} & \left\{ -G_{17}(t)\beta_{nm}^2 + G_{18}(t)\beta_{nm} + 2G_{19}(t) \right\} + \left\{ G_{18}(t)\beta_{nm} + 2G_{19}(t) \right\} \\ & - \zeta_n^2 \left\{ G_{17}(t) + G_{18}(t)\frac{2}{\beta_{nm}} + G_{19}(t)\frac{8}{\beta_{nm}^2} \right\} \\ & + d_{15} \left\{ \dot{G}_{17}(t) + \dot{G}_{18}(t)\frac{2}{\beta_{nm}} + \dot{G}_{19}(t)\frac{8}{\beta_{nm}^2} \right\} \\ & + d_{16} \left\{ \dot{G}_{12}(t) + \dot{G}_{13}(t)\frac{2}{\beta_{nm}} + \dot{G}_{14}(t)\frac{8}{\beta_{nm}^2} \right\} \\ & + d_{17} \left\{ \dot{G}_2(t)\beta_{nm} + 3\dot{G}_3(t) + \frac{16}{\beta_{nm}}\dot{G}_4(t) \right\} \\ & - d_{17} \left\{ \dot{G}_4(t)\frac{8}{\beta_{nm}} + \dot{G}_3(t) \right\} \\ & - \zeta_n d_{17} \left\{ \dot{G}_7(t) + \dot{G}_8(t)\frac{2}{\beta_{nm}} + \dot{G}_9(t)\frac{8}{\beta_{nm}^2} \right\} \\ & \left\{ \chi_{13} + \chi_{14}\frac{2}{\beta} + \chi_{15}\frac{8}{\beta^2} \right\} \left\{ \begin{aligned} & \mu_{20}G_{20}(t) + \mu_{21}G_{20}(t) \\ & + \mu_{22}\dot{G}_{20}(t) + \mu_{23}\dot{G}_{15} + \mu_{24}\dot{G}_5 \\ & + \mu_{25}\dot{G}_{10} + d_{21}P_{nm}(t) \end{aligned} \right\} \end{aligned} \right\} = 0 \quad (54d) \\
 & + \left\{ \begin{aligned} & \left\{ G_{18}(t)\beta_{nm}^2 - G_{19}(t)\beta_{nm} \right\} - G_{19}(t)\beta_{nm} \\ & + \zeta_n^2 \left\{ G_{18}(t) + G_{19}(t)\frac{4}{\beta_{nm}} \right\} - d_{15} \left\{ \dot{G}_{18}(t) + \dot{G}_{19}(t)\frac{4}{\beta_{nm}} \right\} \\ & - d_{16} \left\{ \dot{G}_{13}(t) + \dot{G}_{14}(t)\frac{4}{\beta_{nm}} \right\} + d_{17} \left\{ -5\dot{G}_4(t) - \dot{G}_3(t)\beta_{nm} \right\} \\ & + d_{17}\dot{G}_4(t) + \zeta_n d_{17} \left\{ \dot{G}_8(t) + \dot{G}_9(t)\frac{4}{\beta_{nm}} \right\} \\ & - \left\{ \chi_{14} + \chi_{15}\frac{4}{\beta} \right\} \left\{ \begin{aligned} & \mu_{20}G_{20}(t) + \mu_{21}G_{20}(t) + \mu_{22}\dot{G}_{20}(t) \\ & + \mu_{23}\dot{G}_{15} + \mu_{24}\dot{G}_5 + \mu_{25}\dot{G}_{10} + d_{21}P_{nm}(t) \end{aligned} \right\} \end{aligned} \right\} = 0 \\
 & + \left\{ \begin{aligned} & G_{19}(t)\beta^2 + \zeta_n^2 G_{19}(t) - d_{15}\dot{G}_{19}(t) - d_{16}\dot{G}_{14}(t) \\ & - d_{17}\dot{G}_4(t)\beta + \zeta_n d_{17}\dot{G}_9(t) \\ & - \chi_{15} \left\{ \begin{aligned} & \mu_{20}G_{20}(t) + \mu_{21}G_{20}(t) + \mu_{22}\dot{G}_{20}(t) + \mu_{23}\dot{G}_{15} \\ & + \mu_{24}\dot{G}_5 + \mu_{25}\dot{G}_{10} + d_{21}P_{nm}(t) \end{aligned} \right\} \end{aligned} \right\} = 0
 \end{aligned}$$

**Exact Solution for Classic Coupled Thermoporoelasticity in Axisymmetric Cylinder, Table 1** Material parameters

Parameters	Value	Unit	Parameters	Value	Unit
$n$	0.4	—	$\alpha_s$	$1.5 \times 10^{-5}$	$1/^\circ\text{C}$
$E$	$6 \times 10^5$	Pa	$\alpha_w$	$2 \times 10^{-4}$	$1/^\circ\text{C}$
$\nu$	0.3	—	$c_s$	0.8	$\text{J/g}^\circ\text{C}$
$T_o$	293	$^\circ\text{K}$	$c_w$	4.2	$\text{J/g}^\circ\text{C}$
$K_s$	$2 \times 10^{10}$	Pa	$\rho_s$	$2.6 \times 10^6$	$\text{g/m}^3$
$K_w$	$5 \times 10^9$	Pa	$\rho_w$	$1 \times 10^6$	$\text{g/m}^3$
$K$	0.5	$\text{W/m}^\circ\text{C}$	$\alpha$	1	—

where  $d_{10}$  to  $d_{27}$  are the coefficients of the H-expansion and constant parameters. By taking Laplace transform of (54a) and using four boundary conditions of (5) (for solid cylinder only second, forth, sixth, and eighth boundary conditions are applicable), a system of algebraic equations is obtained and solved by Carmer's methods in the Laplace domain, where by the inverse Laplace transform the functions are transformed into the real time domain and finally  $G_1(t)$  to  $G_{20}(t)$  are calculated

In this process it is necessary to consider the following points

1. The initial conditions (7) are considered only for the general solutions and the, initial conditions of  $G_1(t)$  to  $G_{20}(t)$  for the particular solutions are considered equal to zero.
2. Laplace transform of (54a) is in terms of polynomial function form of the Laplace parameter  $s$  (not the Bessel functions form of  $s$ ). Therefore, the exact inverse Laplace transform is possible and somehow simple.

## Results and Discussions

As an example, a solid cylinder with  $r_i = 0$ ,  $r_o = 1$  m and  $L = \pi$  m is considered. The material properties are (Table 1)

The initial temperature  $T_o$  is considered to be  $293^\circ\text{K}$ . Now, an instantaneous hot spot

$T(1, z, t) = 10^{-3}T_o\delta(t) \sin(z)$ , where  $\delta(t)$  is unit Dirac function, is considered and the outside

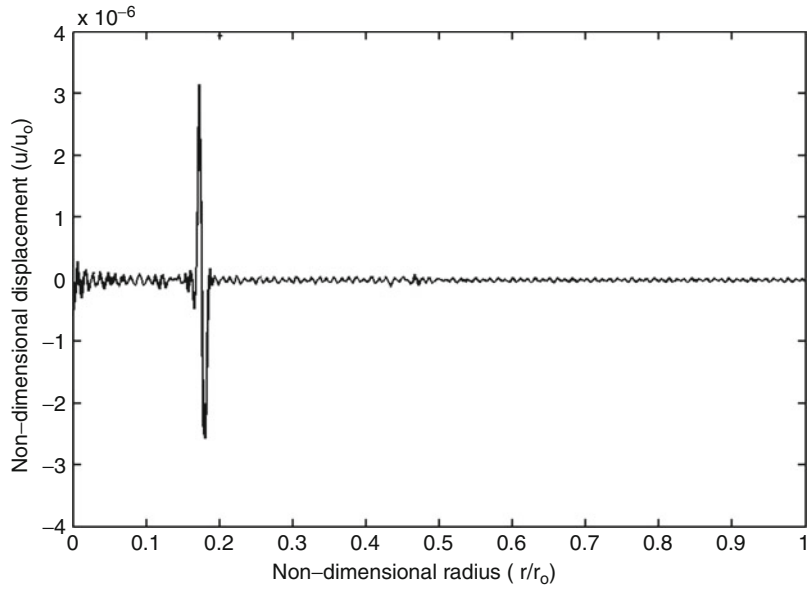
radius of the cylinder is assumed to be fixed ( $u(1, z, t) = 0$ ). For drawing the graphs a nondimensional time  $\hat{t} = \frac{vt}{r_o}$  is considered where  $v = \sqrt{\frac{E(1-\nu)}{\rho(1+\nu)(1-2\nu)}}$  is dilatational wave velocity. Figures 1–4 show wave front for displacement, temperature, and pressure. For the second example, mechanical shock wave is applied to the outside surface of the cylinder given as  $u(1, z, t) = 10^{-12}u_o\delta(t) \sin(z)$ , and the surface is assumed to be at zero temperature ( $T(1, z, t) = 0$ ). Figures 5–8 show the wave fronts for the displacement and temperature distributions. The convergence of the solutions for these examples is achieved by consideration of 1,200 eigenvalues used for the H-Fourier expansion. More than this number for eigenvalues, the increased round-off and truncation errors effect the quality of the graphs. The convergence of solution is better for displacement in comparison with the temperature and pressure.

## Conclusion

In this entry, analytical solution for the coupled porothermoelasticity of thick cylinders under radial temperature is presented. The method is based on the eigenfunctions Fourier expansion, which is a classical and traditional method of solution of the typical initial and boundary value problems. The noncompetitive strength of this method is its ability to reveal the fundamental

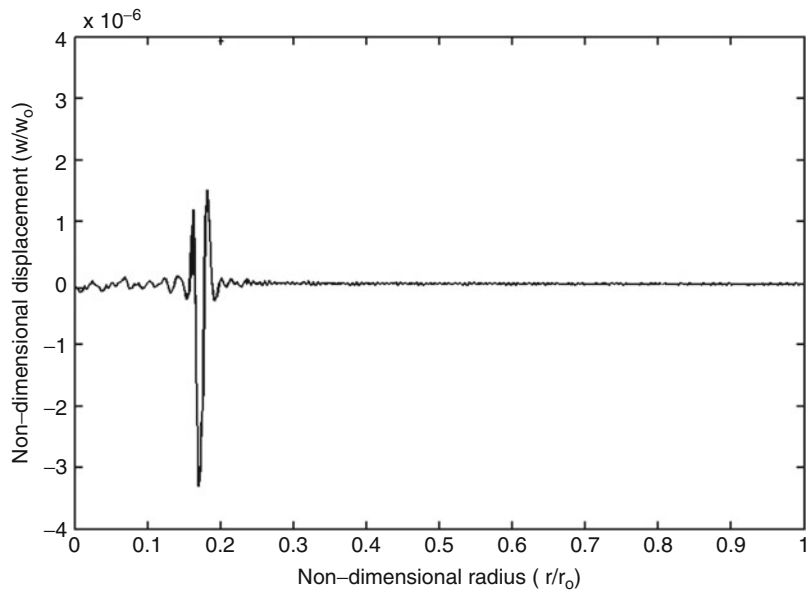
**Exact Solution for Classic Coupled Thermoporoelasticity in Axisymmetric Cylinder,**

**Fig. 1** Non-dimensional displacement  $u(1, z, t) = 10^{-12}u_0\delta(t) \sin(z)$  at non-dimensional time  $\hat{t} = 0.8$



**Exact Solution for Classic Coupled Thermoporoelasticity in Axisymmetric Cylinder,**

**Fig. 2** Non-dimensional displacement  $u(1, z, t) = 10^{-12}u_0\delta(t) \sin(z)$  at non-dimensional time  $\hat{t} = 0.8$

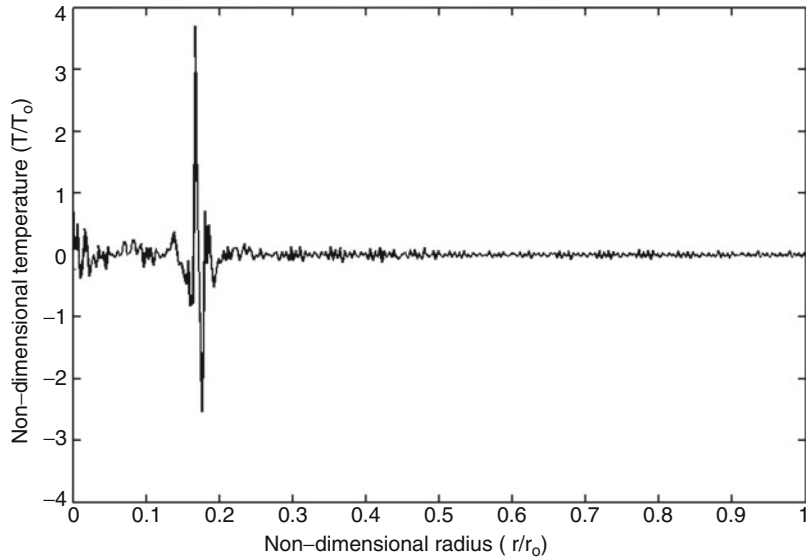


mathematical and physical properties and interpretations of the problem under studying. In the coupled porothermoelastic problem of radial-symmetric cylinder, the governing equations are

a system of partial differential equations with two independent variables, radius ( $r$ ) and time ( $t$ ). The traditional procedure to solve this class of problems is to eliminate the time variable by using the

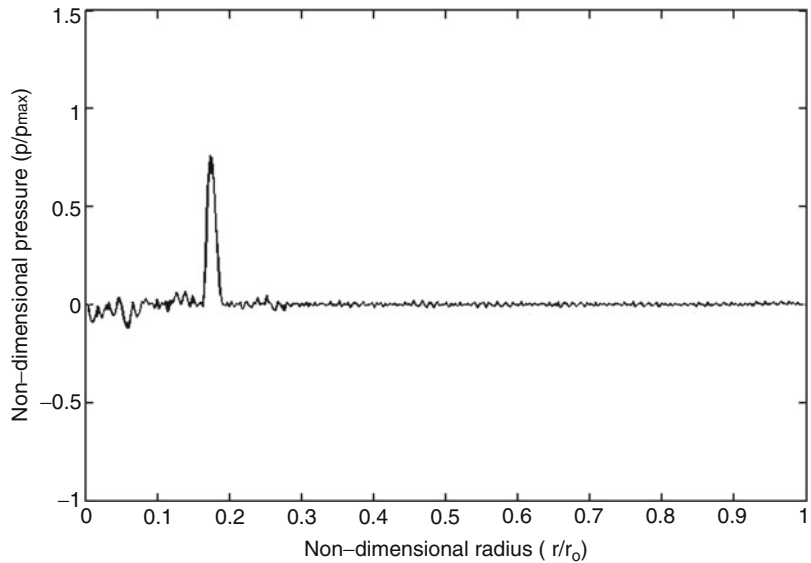
**Exact Solution for  
Classic Coupled  
Thermoporoelasticity in  
Axisymmetric Cylinder,**

**Fig. 3** Non-dimensional  
temperature  $u(1, z,$   
 $t) = 10^{-12}u_0\delta(t) \sin(z)$  at  
non-dimensional time  
 $\hat{t} = 0.8$



**Exact Solution for  
Classic Coupled  
Thermoporoelasticity in  
Axisymmetric Cylinder,**

**Fig. 4** Non-dimensional  
pressure  $u(1, z,$   
 $t) = 10^{-12}u_0\delta(t) \sin(z)$  at  
non-dimensional time  
 $\hat{t} = 0.8$

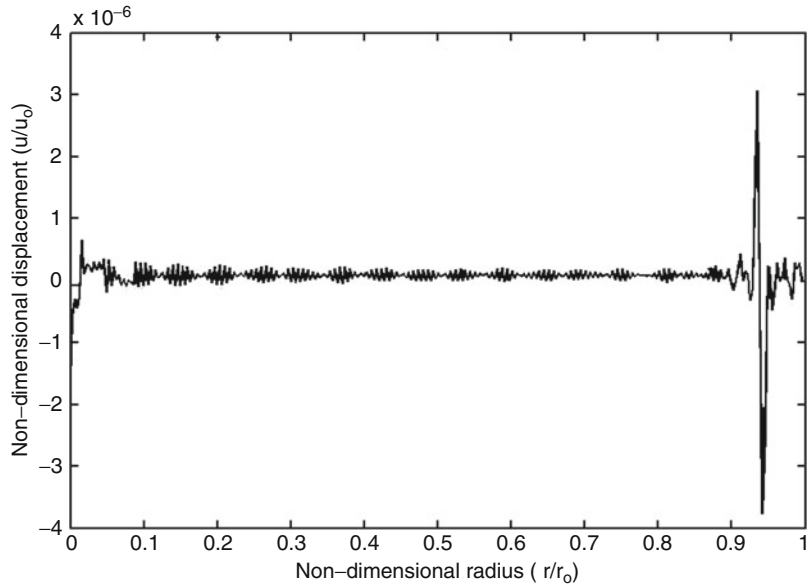


Laplace transform. The resulting system is a set of ordinary differential equations in terms of the radius variable, which falls in the Bessel functions family. This method of analysis brings the

Laplace parameter ( $s$ ) in the argument of the Bessel functions, causing hardship or impossibility in carrying out the exact inverse of the Laplace transformation. As a result, the numerical inverse

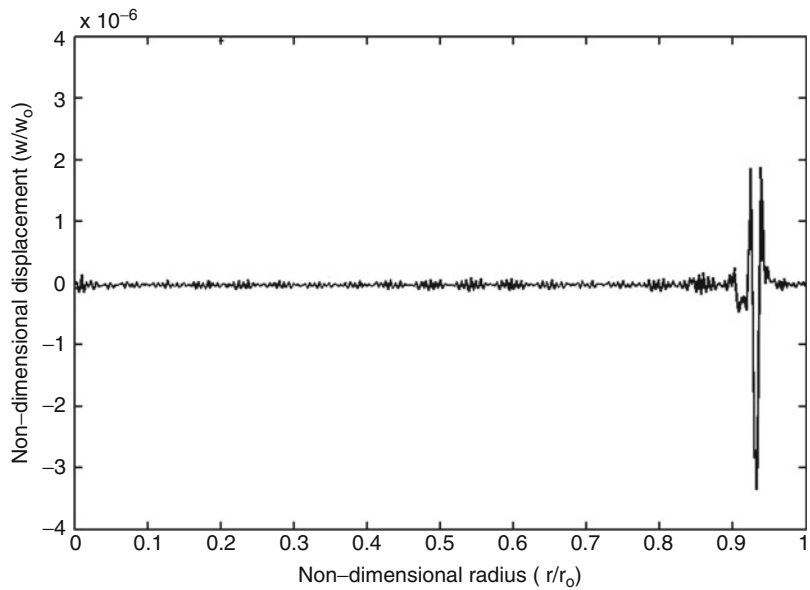
**Exact Solution for  
Classic Coupled  
Thermoporoelasticity in  
Axisymmetric Cylinder,**

**Fig. 5** Non-dimensional  
displacement  
 $T(1, z, t) = 10^{-3}T_0\delta(t) \sin(z)$   
at non-dimensional time  
 $\hat{t} = 0.1$



**Exact Solution for  
Classic Coupled  
Thermoporoelasticity in  
Axisymmetric Cylinder,**

**Fig. 6** Non-dimensional  
displacement  
 $T(1, z, t) = 10^{-3}T_0\delta(t) \sin(z)$   
at non-dimensional time  
 $\hat{t} = 0.1$

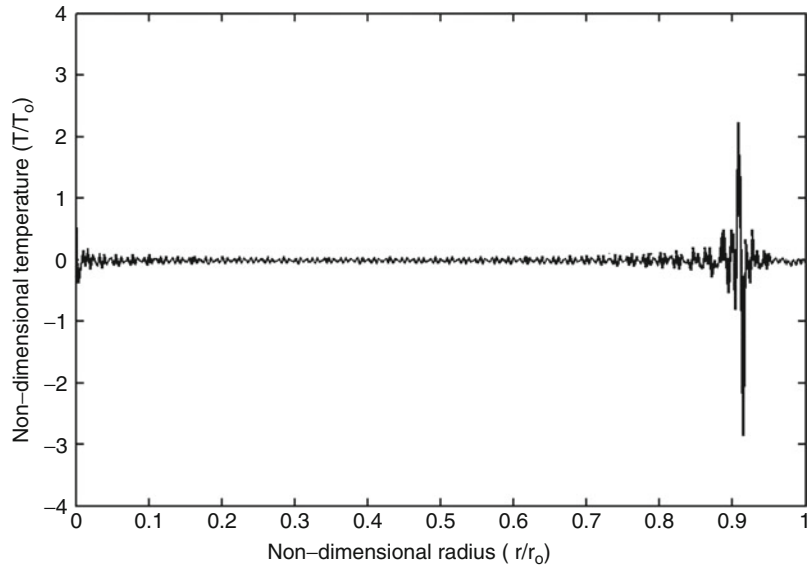


of the Laplace transformation is used in the papers dealing with this type of problems in literature. In this entry, to prevent this problem, when the Laplace transform is applied to the particular solutions, it is postponed after

eliminating the radius variable  $r$  by H-Fourier expansion. Thus, the Laplace parameter ( $s$ ) appears in polynomial function forms and hence the exact Laplace inversion transformation is possible.

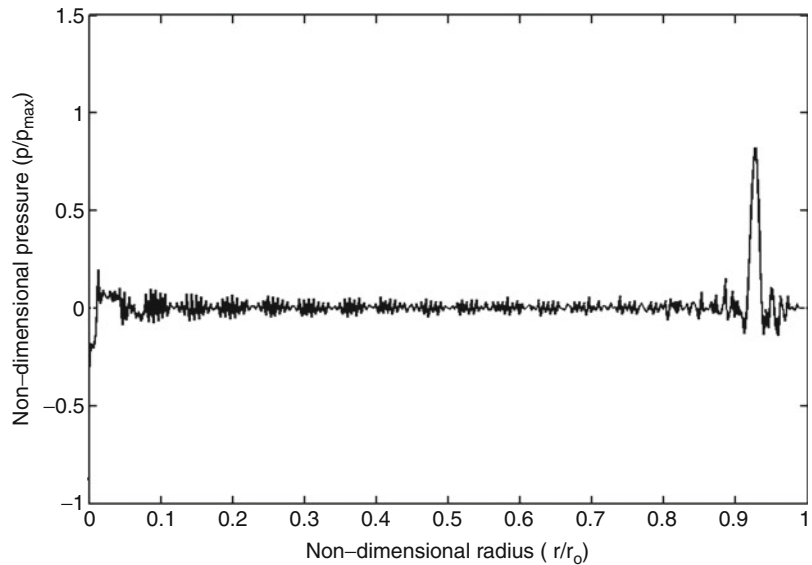
**Exact Solution for  
Classic Coupled  
Thermoporoelasticity in  
Axisymmetric Cylinder,  
Fig. 7**

Non-dimensional  
temperature  
 $T(1, z, t) = 10^{-3}T_0\delta(t) \sin(z)$   
at non-dimensional time  
 $\hat{t} = 0.1$



**Exact Solution for  
Classic Coupled  
Thermoporoelasticity in  
Axisymmetric Cylinder,  
Fig. 8**

Non-dimensional  
pressure  
 $T(1, z, t) = 10^{-3}T_0\delta(t) \sin(z)$   
at non-dimensional time  
 $\hat{t} = 0.1$



## References

1. Bai B (2006) Response of saturated porous media subjected to local thermal loading on the surface of semi-infinite space. *J Acta Mech Sinica* 22:54–61
2. Bai B (2006) Fluctuation responses of saturated porous media subjected to cyclic thermal loading. *J Comput Geotech* 33:396–403
3. Droujinine A (2006) Generalized an elastic asymptotic Ray theory. *J Wave Motion* 43:357–367
4. Bai B, Li T (2009) Solution for cylindrical cavity in saturated thermoporoelastic medium. *J Acta Mech Sinica* 22:85–92
5. Hetnarski RB (1964) Solution of the coupled problem of thermoelasticity in the form of series of functions. *J Arch Mech Stos* 16:919–941
6. Hetnarski RB, Ignaczak J (1993) Generalized thermoelasticity: closed-form solutions. *J Therm Stresses* 16:473–498
7. Hetnarski RB, Ignaczak J (1994) Generalized thermoelasticity: response of semi-space to a shortlaser pulse. *J Therm Stresses* 17:377–396
8. Georgiadis HG, Lykotrafitis G (2005) Rayleigh waves generated by a thermal source: a three dimensional transient thermoelasticity solution. *J Appl Mech* 72:129–138

9. Wagner P (1994) Fundamental matrix of the system of dynamic linear thermoelasticity. *J Therm stresses* 17:549–565
10. Jabbari M, Dehbani H (2010) An exact solution for classic coupled thermoporoelasticity in axisymmetric cylinder. *J Solid Mech* 2:129–143
11. Jabbari M, Dehbani H (2009) An exact solution for classic coupled thermoporoelasticity in cylindrical coordinates. *J Solid mech arak* 1:343–357
12. Jabbari M, Mohazzab AH, Bahtui A, Eslami MR (2007) Analytical solution for three-dimensional stresses in a short length FGM hollow. *ZAMM J Appl Math Mech* 87:413–429

## Exact Solution for Classic Coupled Thermoporoelasticity in Cylindrical Coordinates

Mohsen Jabbari<sup>1</sup> and H. Dehbani<sup>2</sup>

<sup>1</sup>Faculty of Engineering, Postgraduate School, South Tehran Branch, Islamic Azad University, Tehran, Iran

<sup>2</sup>Postgraduate School, South Tehran Branch, Islamic Azad University, Tehran, Iran

### Overview

In this entry, the classic coupled porothermoelasticity model of hollow and solid cylinders under radial-symmetric loading condition ( $r$ ,  $t$ ) is considered. A full analytical method is used and an exact unique solution of the classic coupled equations is presented.

The thermal and pressure boundary conditions, the body force, the heat source, and the injected volume rate per unit volume of a distribute water source are considered in the most general forms and no limiting assumption is used. This generality allows simulation of various applicable problems.

### Introduction

Coupled thermal and poro-mechanical processes play an important role in a number of problems of interest in the geomechanics such as stability of boreholes and permeability enhancement in geothermal reservoirs or high temperature petroleum

bearing formation. A thermoporoelastic approach combines the theory of heat conduction with poroelastic constitutive equations and coupling the temperature field with the stresses and pore pressure.

There are a limited number of papers that present the closed form or analytical solution for the coupled porothermoelasticity problems. Bai [1] investigated the response of saturated porous media subjected to local thermal loading on the surface of semi-infinite space. He used the numerical integral methods for calculating the unsteady temperature, pore pressure, and displacement fields. This author also studied the fluctuation responses of saturated porous media subjected to cyclic thermal loading [2]. In the mentioned paper, an analytical solution was deduced proposed by using the Laplace transform and the Gauss-Legendre method and Laplace transform inversion. Droujinine [3] investigated dispersion and attenuation of body waves in a wide range of materials representing realistic rock structures. He used the time-domain asymptotic ray theory to a new generalized coordinate-free wave equation with an arbitrary tensor relaxation function. Bai and Li [4] found a solution for cylindrical cavity in saturated thermoporoelastic medium by using Laplace transform and numerical Laplace transform inversion.

The number of papers that present the closed form or analytical solution for the coupled thermoelasticity problems are also limited. Hetnarski [5] found the solution of the coupled thermoelasticity in the form of a series of functions. Hetnarski and Ignaczak presented a study of the one-dimensional thermoelastic waves produced by an instantaneous plane source of heat in homogeneous isotropic infinite and semi-infinite bodies of the Green-Lindsay [6]. Also, these authors presented an analysis for laser-induced waves propagating in an absorbing thermoelastic semi-space of the Green-Lindsay [7]. Georgiadis and Lykotrafitis obtained a three-dimensional transient thermoelastic solution for Rayleigh-type disturbances propagating on the surface of a half-space [8]. Wagner [9] presented the fundamental matrix of a system of partial differential operators that governs the diffusion of heat and the strains in elastic media. This method can be used



to predict the temperature distribution and the strains by an instantaneous point heat, point source of heat, or by a suddenly applied delta force.

In this entry [10], a full analytical method is used to obtain the response of the governing equations and an exact solution is presented. The method of solution is based on the Fourier's expansion and eigenfunction methods, which are traditional and routine methods in solving the partial differential equations. Since the coefficients of equations are not functions of the time variable ( $t$ ), an exponential form is considered for the general solution matched with the physical wave properties of thermal and mechanical waves. For the particular solution, that is the response to mechanical and thermal shocks, the eigenfunction method and Laplace transformation is used.

## Governing Equations

A hollow cylinder with inner and outer radius  $r_i$  and  $r_o$ , respectively, made of isotropic material subjected to radial-symmetric mechanical, thermal, and pressure shocks is considered.

The classic theory of porothermoelasticity for wave propagation is considered to allow coupling between deformation, thermal energy, and pressure fields and to describe the physical behavior of the elastic domain to mechanical, thermal, and pressure shock loads.

Navier equation in terms of the displacement components is obtained as [4]

$$u_{,rr} + \frac{1}{r}u_{,r} - \frac{1}{r^2}u - \alpha \frac{(1+\nu)(1-2\nu)}{(1-\nu)E}p_{,r} - \beta \frac{(1+\nu)(1-2\nu)}{(1-\nu)E}T_{,r} - \rho \frac{(1+\nu)(1-2\nu)}{(1-\nu)E}\ddot{u} = -\frac{(1+\nu)(1-2\nu)}{(1-\nu)E}F(r,t) \quad (1)$$

Heat conduction equation in radial-symmetric direction with the mechanical coupling term is

$$T_{,rr} + \frac{1}{r}T_{,r} - Z\frac{T_o}{K}\dot{T} + Y\frac{T_o}{K}\dot{p} - \beta\frac{T_o}{K}(\dot{u}_{,r} + \frac{1}{r}\dot{u}) = -\frac{1}{K}Q(r,t) \quad (2)$$

According to Darcy's law and continuity condition of seepage, the equation of mass conservation can be written as

$$p_{,rr} + \frac{1}{r}p_{,r} - \alpha_p\frac{\gamma_w}{k}\dot{p} - Y\frac{\gamma_w}{k}\dot{T} - \alpha\frac{\gamma_w}{k}(\dot{u}_{,r} + \frac{1}{r}\dot{u}) = -\frac{\gamma_w}{k}W(r,t) \quad (3)$$

where  $(\cdot)$  denotes partial derivative,  $u$  is the displacement component in the radial direction,  $p$  is

the pore pressure,  $\rho$  is bulk mass density,  $\alpha = 1 - \frac{C_s}{C}$  is the Biot's coefficient,  $C_s = 3(1-2\nu_s)E_s$  is the coefficient of volumetric compression of the solid grains, with  $E_s$  and  $\nu_s$  being the elastic modulus and Poisson's ratio of solid grains and  $C = 3(1-2\nu)E$  is the coefficient of volumetric compression of solid skeleton, with  $E$  and  $\nu$  being the elastic modulus and Poisson's ratio of solid skeleton,  $T_o$  is initial reference temperature,  $\beta = \frac{3\alpha_s}{C}$  is the thermal expansion factor,  $\alpha_s$  is the coefficient of linear thermal expansion of solid grains,  $Y = 3(n\alpha_w + (\alpha - n)\alpha_s)$  and  $\alpha_p = n(C_w - C_s) + \alpha C_s$  are coupling parameters,  $\alpha_w$  and  $C_w$  are the coefficients of linear thermal expansion and volumetric compression of pure water,  $n$  is the porosity,  $k$  is the hydraulic conductivity,  $\gamma_w$  is the unit of pore water and  $Z = \frac{((1-n)\rho_s c_s + n\rho_w c_w)}{T_o} - 3\beta\alpha_s$  is coupling

parameter,  $\rho_w$  and  $\rho_s$  are the densities of pore water and solid grains and  $c_w$  and  $c_s$  are the heat capacities of pore water and solid grains and  $K$  is the coefficient of heat conductivity. Here,  $F(r, t)$ ,  $Q(r, t)$ , and  $W(r, t)$  are the body force, heat generation source, and the injected volume rate per unit volume of a distribute water source, respectively. The mechanical, thermal, and pressure boundary conditions are

$$\begin{aligned} C_{11}u(r_i, t) + C_{12}u_r(r_i, t) + C_{13}T(r_i, t) \\ + C_{14}p(r_i, t) = f_1(t) \\ C_{21}u(r_o, t) + C_{22}u_r(r_o, t) + C_{23}T(r_o, t) \\ + C_{24}p(r_o, t) = f_2(t) \\ C_{31}T(r_i, t) + C_{32}T_r(r_i, t) = f_3(t) \\ C_{41}T(r_o, t) + C_{42}T_r(r_o, t) = f_4(t) \\ C_{51}p(r_i, t) = f_5(t) \\ C_{61}p(r_o, t) = f_6(t) \end{aligned} \quad (4)$$

where  $C_{ij}$  are the mechanical, thermal, and pressure coefficients, and which by assigning different values for them, different types of mechanical, thermal, and pressure boundary conditions may be obtained. These boundary conditions include the displacement, strain, stress, specified temperature, convection, pressure, and heat flux condition. The initial boundary conditions are assumed in the following general form

$$\begin{aligned} u(r, 0) = f_7(r) \\ u_t(r, 0) = f_8(r) \\ T(r, 0) = f_9(r) \\ p(r, 0) = f_{10}(r) \end{aligned} \quad (5)$$

## Solution

Equations (1) to (3) are the system of non-homogeneous partial differential equations with nonconstant coefficients (functions of the

radius variable  $r$  have only general and particular solutions).

## General Solution with Homogeneous Boundary Conditions

Since the coefficients of (1)–(3) are independent of the time variable ( $t$ ), an exponential function form in terms of the time variable may be assumed for the general solution as

$$\begin{aligned} u(r, t) &= [U(r)]e^{\lambda t} \\ T(r, t) &= [\theta(r)]e^{\lambda t} \\ p(r, t) &= [P(r)]e^{\lambda t} \end{aligned} \quad (6)$$

Substituting (6) into homogeneous parts of (1)–(3), yields

$$\begin{aligned} U'' + \frac{1}{r}U' - \frac{1}{r^2}U + d_1P' + d_2\theta' + d_3\lambda^2U &= 0 \\ \theta'' + \frac{1}{r}\theta' + d_4\lambda\theta + d_5\lambda P + d_6\lambda\left(U' + \frac{1}{r}U\right) &= 0 \\ P'' + \frac{1}{r}P' + d_7\lambda P + d_8\lambda\theta + d_9\lambda\left(U' + \frac{1}{r}U\right) &= 0 \end{aligned} \quad (7)$$

Equation (7) constitute a system of ordinary differential equations, where the prime symbol (') indicates differentiation with respect to the radius variable ( $r$ ) and  $d_1$  to  $d_9$  are constant parameters given in the appendix.

The first solutions of  $U_1$ ,  $\theta_1$ , and  $P_1$  are considered as

$$\begin{aligned} U_1(r) &= A_1J_1(\beta r) \\ \theta_1(r) &= B_1J_0(\beta r) \\ P_1(r) &= C_1J_0(\beta r) \end{aligned} \quad (8)$$

Substituting (8) into (7) yields

$$\begin{aligned} \{(-\beta^2 + \lambda^2 d_3)A_1 - d_2\beta B_1 - d_1\beta C_1\}J_1(\beta r) &= 0 \\ \{\lambda d_6\beta A_1 + \lambda d_4B_1 + (-\beta^2 + \lambda d_5)C_1\}J_0(\beta r) &= 0 \\ \{\lambda d_9\beta A_1 + (-\beta^2 + \lambda d_7)B_1 + \lambda d_8C_1\}J_0(\beta r) &= 0 \end{aligned} \quad (9)$$

Equations (9) shows that  $U_1$ ,  $\theta_1$ , and  $P_1$  can be the solutions of (7), if and only if

$$\begin{bmatrix} -\beta^2 + \lambda^2 d_3 & -d_2 \beta & -d_1 \beta \\ \lambda d_6 \beta & \lambda d_4 & -\beta^2 + \lambda d_5 \\ \lambda d_9 \beta & -\beta^2 + \lambda d_7 & \lambda d_8 \end{bmatrix} \begin{Bmatrix} A_1 \\ B_1 \\ C_1 \end{Bmatrix} = \begin{Bmatrix} 0 \\ 0 \\ 0 \end{Bmatrix} \quad (10)$$

The nontrivial solution of (10) is obtained by equating the determinant of this equation to zero as

$$\begin{aligned} & -\beta^2 \lambda^2 d_4 d_7 + \beta^6 - \beta^4 \lambda d_7 - \beta^4 \lambda d_5 \\ & + \beta^2 \lambda^2 d_5 d_7 + \lambda^4 d_3 d_4 d_7 - \lambda^2 d_3 \beta^4 \\ & + \lambda^3 d_3 \beta^2 d_7 + \lambda^3 d_3 d_5 \beta^2 - \lambda^4 d_3 d_5 d_7 \\ & + \lambda^2 d_6 \beta^2 d_2 d_7 + \lambda d_6 \beta^4 d_1 \\ & - \lambda^2 d_6 \beta^2 d_1 d_7 + \lambda d_9 \beta^4 d_2 \\ & - \lambda^2 d_9 \beta^2 d_2 d_5 + \lambda^2 d_9 \beta^2 d_1 d_4 = 0 \end{aligned} \quad (11)$$

Equation (11) is the first characteristic equation. Thus, it is concluded that  $U_1$ ,  $\theta_1$ , and  $P_1$  satisfy the system of (7) and they are the first solution of the system.

The second solutions of  $U_2$ ,  $\theta_2$ , and  $P_2$  are considered as

$$\begin{aligned} U_2(r) &= [A_2 J_1(\beta r) + A_3 r J_2(\beta r)] \\ \theta_2(r) &= [B_2 J_0(\beta r) + B_3 r J_1(\beta r)] \\ P_2(r) &= [C_2 J_0(\beta r) + C_3 r J_1(\beta r)] \end{aligned} \quad (12)$$

Substituting (12) to (7) yields

$$\begin{aligned} & \{(-\beta^2 + \lambda^2 d_3)A_3 - d_2 \beta B_3 - d_1 \beta C_3\} r J_0(\beta r) \\ & + \{(\beta^2 - d_3 \lambda^2)A_2 - \frac{2}{\beta} d_3 \lambda^2 A_3 \\ & + d_2 \beta B_2 + d_1 \beta C_2\} J_1(\beta r) = 0 \\ & \{\lambda d_6 \beta A_3 + \lambda d_4 B_3 + (-\beta^2 + \lambda d_5)C_3\} r J_1(\beta r) \\ & + \{d_6 \lambda \beta A_2 + d_4 \lambda B_2 + (-\beta^2 + d_5 \lambda)C_2 \\ & + 2\beta C_3\} J_0(\beta r) = 0 \\ & \{\lambda d_9 \beta A_3 + (-\beta^2 + \lambda d_7)B_3 \\ & + \lambda d_8 C_3\} r J_1(\beta r) \\ & + \{d_9 \lambda \beta A_2 + (-\beta^2 + d_7 \lambda)B_2 \\ & + d_8 \lambda C_2 + 2\beta B_3\} J_0(\beta r) = 0 \end{aligned} \quad (13)$$

The expressions for  $U_2$ ,  $\theta_2$ , and  $P_2$  can be the solutions of (7), if and only if

$$\begin{bmatrix} -\beta^2 + \lambda^2 d_3 & -d_2 \beta & -d_1 \beta \\ \lambda d_6 \beta & \lambda d_4 & -\beta^2 + \lambda d_5 \\ \lambda d_9 \beta & -\beta^2 + \lambda d_7 & \lambda d_8 \end{bmatrix} \begin{Bmatrix} A_3 \\ B_3 \\ C_3 \end{Bmatrix} = \begin{Bmatrix} 0 \\ 0 \\ 0 \end{Bmatrix} \quad (14)$$

$$(\beta^2 - d_3 \lambda^2)A_2 - \frac{2}{\beta} d_3 \lambda^2 A_3 + d_2 \beta B_2 + d_1 \beta C_2 = 0 \quad (15)$$

$$d_6 \lambda \beta A_2 + d_4 \lambda B_2 + (-\beta^2 + d_5 \lambda)C_2 + 2\beta C_3 = 0 \quad (16)$$

$$d_9 \lambda \beta A_2 + (-\beta^2 + d_7 \lambda)B_2 + d_8 \lambda C_2 + 2\beta B_3 = 0 \quad (17)$$

The nontrivial solution of (14) is obtained by equating the determinant to zero as

$$\begin{aligned} & -\beta^2 \lambda^2 d_4 d_7 + \beta^6 - \beta^4 \lambda d_7 - \beta^4 \lambda d_5 + \beta^2 \lambda^2 d_5 d_7 \\ & + \lambda^4 d_3 d_4 d_7 - \lambda^2 d_3 \beta^4 + \lambda^3 d_3 \beta^2 d_7 + \lambda^3 d_3 d_5 \beta^2 \\ & - \lambda^4 d_3 d_5 d_7 + \lambda^2 d_6 \beta^2 d_2 d_7 + \lambda d_6 \beta^4 d_1 - \lambda^2 d_6 \beta^2 d_1 d_7 \\ & + \lambda d_9 \beta^4 d_2 - \lambda^2 d_9 \beta^2 d_2 d_5 + \lambda^2 d_9 \beta^2 d_1 d_4 = 0 \end{aligned} \quad (18)$$

Equations (15)–(17) give the relations between  $A_2, A_3, B_2, B_3, C_2$ , and  $C_3$ . They play as the balancing ratios that make (12) to be the second solution of the system of (7).

The third solution of the system of the ordinary differential equations with nonconstant coefficients (7) must be considered as

$$\begin{aligned} U_3(r) &= [A_4 J_1(\beta r) + A_5 r J_2(\beta r) + A_6 r^2 J_3(\beta r)] \\ \theta_3(r) &= [B_4 J_0(\beta r) + B_5 r J_1(\beta r) + B_6 r^2 J_2(\beta r)] \\ P_3(r) &= [C_4 J_0(\beta r) + C_5 r J_1(\beta r) + C_6 r^2 J_2(\beta r)] \end{aligned} \quad (19)$$

Substituting (19) into (7) yields

$$\begin{aligned} &\{(-\lambda^2 d_3 + \beta^2)A_6 + d_2 \beta B_6 + d_1 \beta C_6\} r^2 J_1(\beta r) \\ &+ \{(\beta^2 - d_3 \lambda^2)A_5 + d_2 \beta B_5 \\ &+ d_1 \beta C_5 - \frac{4}{\beta} d_3 \lambda^2 A_6\} r J_0(\beta r) = 0 \\ &+ \{(d_3 \lambda^2 - \beta^2)A_4 - d_1 \beta C_4 - d_2 \beta B_4 \\ &+ \frac{2}{\beta} d_3 \lambda^2 A_5 + \frac{8}{\beta^2} d_3 \lambda^2 A_6\} J_1(\beta r) = 0 \\ &\{-\lambda d_6 \beta A_6 - \lambda d_4 B_6 + (\beta^2 - \lambda d_5)C_6\} r^2 J_0(\beta r) \\ &+ \{d_6 \lambda \beta A_4 + d_4 \lambda B_4 + (-\beta^2 + d_5 \lambda)C_4 + 2\beta C_5\} J_0(\beta r) \\ &+ \{d_6 \lambda \beta A_5 + d_4 \lambda B_5 + (-\beta^2 + d_5 \lambda)C_5 + 2d_6 \lambda A_6 \\ &+ \frac{2}{\beta} d_4 \lambda B_6 + (2\beta + \frac{2}{\beta} d_5 \lambda)C_6\} r J_1(\beta r) = 0 \\ &\{-\lambda d_9 \beta A_6 + (\beta^2 - \lambda d_7)B_6 - \lambda d_8 C_6\} r^2 J_0(\beta r) \\ &+ \{d_9 \lambda \beta A_4 + (-\beta^2 + d_7 \lambda)B_4 + d_8 \lambda C_4 + 2\beta B_5\} J_0(\beta r) \\ &+ \{\beta d_9 \lambda A_5 + (-\beta^2 + d_7 \lambda)B_5 + d_8 \lambda C_5 + 2d_9 \lambda A_6 \\ &+ (2\beta + \frac{2}{\beta} d_7 \lambda)B_6 + \frac{2}{\beta} d_8 \lambda C_6\} r J_1(\beta r) = 0 \end{aligned} \quad (20)$$

The expressions for  $U_3$ ,  $\theta_3$ , and  $P_3$  can be solutions of (7), if and only if

$$\begin{bmatrix} -\beta^2 + \lambda^2 d_3 & -d_2 \beta & -d_1 \beta \\ \lambda d_6 \beta & \lambda d_4 & -\beta^2 + \lambda d_5 \\ \lambda d_9 \beta & -\beta^2 + \lambda d_7 & \lambda d_8 \end{bmatrix} \begin{Bmatrix} A_6 \\ B_6 \\ C_6 \end{Bmatrix} = \begin{Bmatrix} 0 \\ 0 \\ 0 \end{Bmatrix} \quad (21)$$

$$\begin{aligned} &(\beta^2 - d_3 \lambda^2)A_5 + d_2 \beta B_5 + d_1 \beta C_5 - \frac{4}{\beta} d_3 \lambda^2 A_6 = 0 \\ &(d_3 \lambda^2 - \beta^2)A_4 - d_1 \beta C_4 - d_2 \beta B_4 \\ &+ \frac{2}{\beta} d_3 \lambda^2 A_5 + \frac{8}{\beta^2} d_3 \lambda^2 A_6 = 0 \\ &d_6 \lambda \beta A_4 + d_4 \lambda B_4 + (-\beta^2 + d_5 \lambda)C_4 + 2\beta C_5 = 0 \\ &d_6 \lambda \beta A_5 + d_4 \lambda B_5 + (-\beta^2 + d_5 \lambda)C_5 + 2d_6 \lambda A_6 \\ &+ \frac{2}{\beta} d_4 \lambda B_6 + (2\beta + \frac{2}{\beta} d_5 \lambda)C_6 = 0 \\ &d_9 \lambda \beta A_4 + (-\beta^2 + d_7 \lambda)B_4 + d_8 \lambda C_4 + 2\beta B_5 = 0 \\ &\beta d_9 \lambda A_5 + (-\beta^2 + d_7 \lambda)B_5 + d_8 \lambda C_5 + 2d_9 \lambda A_6 \\ &+ (2\beta + \frac{2}{\beta} d_7 \lambda)B_6 + \frac{2}{\beta} d_8 \lambda C_6 = 0 \end{aligned} \quad (22)$$

The nontrivial solution of (21) is obtained by equating the determinant of this equation to zero as

$$\begin{aligned} &-\beta^2 \lambda^2 d_4 d_7 + \beta^6 - \beta^4 \lambda d_7 - \beta^4 \lambda d_5 + \beta^2 \lambda^2 d_5 d_7 \\ &+ \lambda^4 d_3 d_4 d_7 - \lambda^2 d_3 \beta^4 + \lambda^3 d_3 \beta^2 d_7 + \lambda^3 d_3 d_5 \beta^2 \\ &- \lambda^4 d_3 d_5 d_7 + \lambda^2 d_6 \beta^2 d_2 d_7 \\ &+ \lambda d_6 \beta^4 d_1 - \lambda^2 d_6 \beta^2 d_1 d_7 \\ &+ \lambda d_9 \beta^4 d_2 - \lambda^2 d_9 \beta^2 d_2 d_5 + \lambda^2 d_9 \beta^2 d_1 d_4 = 0 \end{aligned} \quad (23)$$

The characteristic (23) is the same as the (11) and (18).

This equality is interesting as it prevents mathematical dilemma and complexity and a single value for the eigenvalue  $\beta$  simultaneously satisfies three characteristic (11), (18), and (23). (22) give the relation between  $A_4, A_5, A_6, B_4, B_5, B_6, C_4, C_5$ , and  $C_6$ . They play as the balancing ratios that help (19) to be the third solution of the system of (7). Therefore, the complete general solutions for the solid cylinder are

$$\begin{aligned}
U^g(r) &= A_1 J_1(\beta r) + A_3 [\zeta_1 J_1(\beta r) + r J_2(\beta r)] \\
&+ A_6 [\zeta_2 J_1(\beta r) + \zeta_3 r J_2(\beta r) + r^2 J_3(\beta r)] \\
\theta^g(r) &= A_1 \zeta_4 J_0(\beta r) + A_3 [\zeta_5 J_0(\beta r) + \zeta_6 r J_1(\beta r)] \\
&+ A_6 [\zeta_7 J_0(\beta r) + \zeta_8 r J_1(\beta r) + \zeta_9 r^2 J_2(\beta r)] \\
P^g(r) &= A_1 \zeta_{10} J_0(\beta r) + A_3 [\zeta_{11} J_0(\beta r) + \zeta_{12} r J_1(\beta r)] \\
&+ A_6 [\zeta_{13} J_0(\beta r) + \zeta_{14} r J_1(\beta r) + \zeta_{15} r^2 J_2(\beta r)]
\end{aligned} \quad (24)$$

and for hollow cylinder are

$$\begin{aligned}
U^g(r) &= A_1 J_1(\beta r) + A_3 [\zeta_1 J_1(\beta r) + r J_2(\beta r)] \\
&+ A_6 [\zeta_2 J_1(\beta r) + \zeta_3 r J_2(\beta r) + r^2 J_3(\beta r)] \\
&+ \hat{A}_1 Y_1(\beta r) + \hat{A}_3 [\zeta_1 Y_1(\beta r) + r Y_2(\beta r)] \\
&+ \hat{A}_6 [\zeta_2 Y_1(\beta r) + \zeta_3 r Y_2(\beta r) + r^2 Y_3(\beta r)] \\
\theta^g(r) &= A_1 \zeta_4 J_0(\beta r) + A_3 [\zeta_5 J_0(\beta r) + \zeta_6 r J_1(\beta r)] \\
&+ A_6 [\zeta_7 J_0(\beta r) + \zeta_8 r J_1(\beta r) + \zeta_9 r^2 J_2(\beta r)] \\
&+ \hat{A}_1 \zeta_4 Y_0(\beta r) + \hat{A}_3 [\zeta_5 Y_0(\beta r) + \zeta_6 r Y_1(\beta r)] \\
&+ \hat{A}_6 [\zeta_7 Y_0(\beta r) + \zeta_8 r Y_1(\beta r) + \zeta_9 r^2 Y_2(\beta r)] \\
P^g(r) &= A_1 \zeta_{10} J_0(\beta r) + A_3 [\zeta_{11} J_0(\beta r) + \zeta_{12} r J_1(\beta r)] \\
&+ A_6 [\zeta_{13} J_0(\beta r) + \zeta_{14} r J_1(\beta r) + \zeta_{15} r^2 J_2(\beta r)] \\
&+ \hat{A}_1 \zeta_{10} Y_0(\beta r) + \hat{A}_3 [\zeta_{11} Y_0(\beta r) + \zeta_{12} r Y_1(\beta r)] \\
&+ \hat{A}_6 [\zeta_{13} Y_0(\beta r) + \zeta_{14} r Y_1(\beta r) + \zeta_{15} r^2 Y_2(\beta r)]
\end{aligned} \quad (25)$$

where  $\zeta_1$  to  $\zeta_{15}$  are ratios obtained from (21) to (22), (14) to (17), and (10) and are given in the appendix. Substituting  $U^g$ ,  $\theta^g$ , and  $P^g$  in the homogeneous form of the boundary conditions (4), three linear algebraic equations are obtained. They are the coefficients depending on  $\lambda$  and  $\beta$ . Setting the determinant of the coefficients equal to zero, the second characteristic equation is obtained. Simultaneous solution of this equation and (11), results into infinite number of two eigenvalues  $\beta_n$  and  $\lambda_n$ . Therefore,  $U^g$ ,  $\theta^g$ , and  $P^g$  are rewritten as

$$\begin{aligned}
U^g(r) &= A_1 [J_1(\beta r) + \zeta_{16} [\zeta_1 J_1(\beta r) + r J_2(\beta r)] \\
&+ \zeta_{17} [\zeta_2 J_1(\beta r) + \zeta_3 r J_2(\beta r) + r^2 J_3(\beta r)]] \\
\theta^g(r) &= A_1 [\zeta_4 J_0(\beta r) + \zeta_{16} [\zeta_5 J_0(\beta r) + \zeta_6 r J_1(\beta r)] \\
&+ \zeta_{17} [\zeta_7 J_0(\beta r) + \zeta_8 r J_1(\beta r) + \zeta_9 r^2 J_2(\beta r)]] \\
P^g(r) &= A_1 [\zeta_{10} J_0(\beta r) + \zeta_{16} [\zeta_{11} J_0(\beta r) + \zeta_{12} r J_1(\beta r)] \\
&+ \zeta_{17} [\zeta_{13} J_0(\beta r) + \zeta_{14} r J_1(\beta r) + \zeta_{15} r^2 J_2(\beta r)]]
\end{aligned} \quad (26)$$

where  $\zeta_{16}$  and  $\zeta_{17}$  are presented in the appendix. Let us show the functions in the brackets of (26) by functions  $H_0$ ,  $H_1$ , and  $H_2$  as

$$\begin{aligned}
H_0 &= J_1(\beta r) + \zeta_{16} [\zeta_1 J_1(\beta r) + r J_2(\beta r)] \\
&+ \zeta_{17} [\zeta_2 J_1(\beta r) + \zeta_3 r J_2(\beta r) + r^2 J_3(\beta r)] \\
H_1 &= \zeta_4 J_0(\beta r) + \zeta_{16} [\zeta_5 J_0(\beta r) + \zeta_6 r J_1(\beta r)] \\
&+ \zeta_{17} [\zeta_7 J_0(\beta r) + \zeta_8 r J_1(\beta r) + \zeta_9 r^2 J_2(\beta r)] \\
H_2 &= \zeta_{10} J_0(\beta r) + \zeta_{16} [\zeta_{11} J_0(\beta r) + \zeta_{12} r J_1(\beta r)] \\
&+ \zeta_{17} [\zeta_{13} J_0(\beta r) + \zeta_{14} r J_1(\beta r) + \zeta_{15} r^2 J_2(\beta r)]
\end{aligned} \quad (27)$$

According to the Sturm-Liouville theorem, these functions are orthogonal with respect to the weight function  $p(r) = r$  such as

$$\int_{r_1}^{r_0} H(\beta_n r) H(\beta_m r) r dr = \begin{cases} 0 & n \neq m \\ \|H(\beta_n r)\|^2 & n = m \end{cases} \quad (28)$$

where  $\|H(\beta_n r)\|$  is norm of the  $H$  function and equals

$$\|H(\beta_n r)\| = \left[ \int_{r_1}^{r_0} r H^2(\beta_n r) dr \right]^{\frac{1}{2}} \quad (29)$$

Due to the orthogonality of function  $H$ , every piecewise continuous function, such as  $f(r)$ , can be expanded in terms of the function  $H$  (either  $H_0$  or  $H_1$  or  $H_2$ ), and is called the H-Fourier series as

$$f(r) = \sum_{n=1}^{\infty} e_n H(\beta_n r) \quad (30)$$

where  $e_n$  equals

$$e_n = \frac{1}{\|H(\beta_n r)\|^2} \int_{r_i}^{r_o} f(r) H(r) r \, dr \quad (31)$$

Using eqs. (6), (26), and (27) the displacement and temperature distributions due to the general solution become

$$\begin{aligned} u^g(r, t) &= \sum_{n=1}^{\infty} \left\{ \sum_{m=1}^4 a_{nm} e^{\lambda_{nm} t} \right\} H_0(\beta_n r) \\ T^g(r, t) &= \sum_{n=1}^{\infty} \left\{ \sum_{m=1}^4 N_{nm} a_{nm} e^{\lambda_{nm} t} \right\} H_1(\beta_n r) \\ p^g(r, t) &= \sum_{n=1}^{\infty} \left\{ \sum_{m=1}^4 M_{nm} a_{nm} e^{\lambda_{nm} t} \right\} H_2(\beta_n r) \end{aligned} \quad (32)$$

where  $N_{nm}$  and  $M_{nm}$  are ratios obtained by substituting (32) to (1)–(3). Using the initial conditions (5) and with the help of (29), (30), and (31), four unknown constants are obtained.

### Particular Solution with Nonhomogeneous Boundary Conditions

The general solutions may be used as proper functions for guessing the particular solution adopted to the nonhomogeneous parts of the (1)–(3) and the nonhomogeneous boundary conditions (4) as

$$\begin{aligned} u^p(r, t) &= \sum_{n=1}^{\infty} \left\{ \left[ G_{1n}(t) J_1(\beta_n r) + G_{2n}(t) r J_2(\beta_n r) + G_{3n}(t) r^2 J_3(\beta_n r) \right] + r^2 G_{4n}(t) \right\} \\ T^p(r, t) &= \sum_{n=1}^{\infty} \left\{ \left[ G_{5n}(t) J_0(\beta_n r) + G_{6n}(t) r J_1(\beta_n r) + G_{7n}(t) r^2 J_2(\beta_n r) \right] + r^2 G_{8n}(t) \right\} \\ p^p(r, t) &= \sum_{n=1}^{\infty} \left\{ \left[ G_{9n}(t) J_0(\beta_n r) + G_{10n}(t) r J_1(\beta_n r) + G_{11n}(t) r^2 J_2(\beta_n r) \right] + r^2 G_{12n}(t) \right\} \end{aligned} \quad (33)$$

For the solid cylinder, the second type of Bessel function  $Y$  is excluded. It is necessary and suitable to expand the body force  $F(r, t)$ , heat source  $Q(r, t)$ , and porosity function  $W(r, t)$  in H-Fourier expansion form as

$$\begin{aligned} F(r, t) &= \sum_{n=1}^{\infty} F_n(t) H_0(\beta_n r) \\ Q(r, t) &= \sum_{n=1}^{\infty} Q_n(t) H_1(\beta_n r) \\ P(r, t) &= \sum_{n=1}^{\infty} P_n(t) H_2(\beta_n r) \end{aligned} \quad (34)$$

where  $F_n(t)$ ,  $Q_n(t)$ , and  $P_n(t)$  are

$$\begin{aligned} F_n(t) &= \frac{1}{\|H_0(\beta_n r)\|^2} \int_{r_i}^{r_o} F(r, t) H_0(\beta_n r) r \, dr \\ Q_n(t) &= \frac{1}{\|H_1(\beta_n r)\|^2} \int_{r_i}^{r_o} Q(r, t) H_1(\beta_n r) r \, dr \\ P_n(t) &= \frac{1}{\|H_2(\beta_n r)\|^2} \int_{r_i}^{r_o} P(r, t) H_2(\beta_n r) r \, dr \end{aligned} \quad (35)$$

Substituting (33) and (34) into non-homogeneous form of (1) into (3) yields

$$\begin{aligned}
& G_2(t)\beta^2 - \ddot{G}_2(t)d_3 - 4\ddot{G}_3(t)\frac{1}{\beta}d_3 - d_{13}G_4(t)C_1 \\
& - 4d_{13}G_4(t)C_2\frac{1}{\beta} - d_{16}\ddot{G}_4(t)C_1 - 4d_{16}\ddot{G}_4(t)C_2\frac{1}{\beta} \\
& + G_6(t)d_2\beta - d_{15}G_8(t)C_1 \\
& - 4d_{15}G_8(t)C_2\frac{1}{\beta} + G_{10}(t)d_1\beta - d_{14}G_{12}(t)C_1 \\
& - 16d_{14}G_{12}(t)C_2\frac{1}{\beta} - d_{25}d_{10}FC_1 - 4d_{25}d_{10}FC_2\frac{1}{\beta} = 0
\end{aligned}$$

$$\begin{aligned}
& - G_1(t)\beta^2 + \ddot{G}_1(t)d_3 + 2\ddot{G}_2(t)\frac{1}{\beta}d_3 \\
& + 8\ddot{G}_3(t)\frac{1}{\beta^2}d_3d_{13}G_4(t)C_0 \\
& + 2d_{13}G_4(t)C_1\frac{1}{\beta} + 8d_{13}G_4(t)C_2\frac{1}{\beta^2} + d_{16}\ddot{G}_4(t)C_0 \\
& + 2d_{16}\ddot{G}_4(t)C_1\frac{1}{\beta} + 8d_{16}\ddot{G}_4(t)C_2\frac{1}{\beta^2} \\
& - G_5(t)\beta d_2 + d_{15}G_8(t)C_0 \\
& + 2d_{15}G_8(t)C_1\frac{1}{\beta} + 8d_{15}G_8(t)C_2\frac{1}{\beta^2} - G_9(t)\beta d_1 \\
& + d_{14}G_{12}(t)C_0 + 2d_{14}G_{12}(t)C_1\frac{1}{\beta} \\
& + 8d_{14}G_{12}(t)C_2\frac{1}{\beta^2} + d_{25}d_{10}FC_0 \\
& + 2d_{25}d_{10}FC_1\frac{1}{\beta} + 8d_{25}d_{10}FC_2\frac{1}{\beta^2} = 0
\end{aligned}$$

$$\begin{aligned}
& G_3(t)\beta^2 - \ddot{G}_3(t)d_3 - d_{13}G_4(t)C_2 \\
& - d_{16}\ddot{G}_4(t)C_2 + G_7(t)\beta d_2 \\
& - d_{15}G_8(t)C_2 + G_{11}(t)\beta d_1 \\
& - d_{14}G_{12}(t)C_2 - d_{25}d_{10}FC_2 = 0
\end{aligned}$$

$$\begin{aligned}
& d_6\beta\dot{G}_1(t) + d_{18}E_0\dot{G}_4(t) - \beta^2G_5(t) + d_4\dot{G}_5(t) \\
& + 2\beta G_6(t) + d_{17}E_0G_8(t) + d_{19}E_0\dot{G}_8(t) \\
& + d_5\dot{G}_9(t) + d_{20}E_0\dot{G}_{12}(t) + d_{26}d_{11}E_0Q_n(t) = 0
\end{aligned}$$

$$\begin{aligned}
& - d_6\beta\dot{G}_3(t) - E_2d_{18}\dot{G}_4(t) + \beta^2G_7(t) - d_4\dot{G}_7(t) \\
& - d_{17}E_2G_8(t) - d_{19}E_2\dot{G}_8(t) - d_5\dot{G}_{11}(t) \\
& - d_{20}E_2\dot{G}_{12}(t) - d_{26}E_2Q_n(t) = 0
\end{aligned}$$

$$\begin{aligned}
& d_6\beta\dot{G}_2(t) + 2d_6\dot{G}_3(t) + \left(d_{18}E_1 + \frac{2}{\beta}d_{14}E_2\right)\dot{G}_4(t) \\
& - \beta^2G_6(t) + d_4\dot{G}_6(t) + 2\beta G_7(t) + \frac{2}{\beta}d_4\dot{G}_7(t) \\
& + \left(d_{17}E_1 + \frac{2}{\beta}d_{17}E_2\right)G_8(t) + \left(d_{19}E_1 + \frac{2}{\beta}E_2d_{19}\right)\dot{G}_8(t) \\
& + \dot{G}_{10}(t)d_5 + \frac{2}{\beta}\dot{G}_{11}(t)d_5 + \left(d_{20}E_1 + \frac{2}{\beta}d_{20}E_2\right)\dot{G}_{12}(t) \\
& + \left(d_{26}E_1 + \frac{2}{\beta}d_{26}E_2\right)Q_n(t) = 0
\end{aligned}$$

$$\begin{aligned}
& d_9\beta\dot{G}_1(t) + d_{22}D_0\dot{G}_4(t) + d_7\dot{G}_5(t) + d_{23}D_0\dot{G}_8(t) \\
& - \beta^2G_9(t) + d_8\dot{G}_9(t) + 2G_{10}(t)\beta + d_{21}G_{12}(s)D_0 \\
& + d_{24}\dot{G}_{12}(t) + d_{27}d_{12}D_0W_n(t) = 0 \\
& - d_9\beta\dot{G}_3(t) - d_{22}D_2\dot{G}_4(t) - d_7\dot{G}_7(t) - d_{23}D_2\dot{G}_8(t) \\
& + \beta^2G_{11}(t) - d_8\dot{G}_{11}(t) - d_{21}D_2G_{12}(t) \\
& - d_{24}\dot{G}_{12}(t)D_2 - d_{27}d_{12}E_2W_n(t) = 0
\end{aligned}$$

$$\begin{aligned}
& d_9\dot{G}_2(t)\beta + d_92\dot{G}_3(t) + \left(d_{22}D_1 + \frac{2}{\beta}d_{22}D_2\right)\dot{G}_4(t) \\
& + d_7\dot{G}_6(t) + \frac{2}{\beta^2}d_7\dot{G}_7(t) + \left(d_{23}D_1 + \frac{2}{\beta}d_{23}D_2\right)\dot{G}_8(t) \\
& - \beta^2G_{10}(t) + d_8\dot{G}_{10}(t) + 2\beta G_{11}(t) + \frac{2}{\beta}d_8\dot{G}_{11}(t) \\
& + \left(d_{21}D_1 + \frac{2}{\beta}d_{21}D_2\right)G_{12}(t) \\
& + \left(d_{24}D_1 + \frac{2}{\beta}d_{24}D_2\right)\dot{G}_{12}(t) = 0
\end{aligned}$$

(36)

where  $d_{10}$  to  $d_{27}$  are the coefficients of the H-expansion and constant parameters presented in the appendix. By taking Laplace transform of (36) and using three boundary conditions of (4) (for solid cylinder only second, fourth, and sixth boundary conditions are applicable), a system of algebraic equations is obtained and solved by Cramer's methods in the Laplace domain, where by the inverse Laplace transform the functions are transformed into the real time domain and finally  $G_{1n}(t)$  to  $G_{12n}(t)$  are calculated.

In this process, it is necessary to consider the following points

**Exact Solution for Classic Coupled Thermoporoelasticity in Cylindrical Coordinates, Table 1** Material parameters

Parameters	Value	Unit	Parameters	Value	Unit
$n$	0.4	—	$\alpha_{\zeta}$	$1.5 \times 10^{-5}$	$1/^{\circ}C$
$E$	$6 \times 10^5$	Pa	$\alpha_{\mu}$	$2 \times 10^{-4}$	$1/^{\circ}C$
$\nu$	0.3	—	$c_z$	0.8	$J/g.^{\circ}C$
$T_w$	293	$^{\circ}K$	$c_w$	4.2	$J/g.^{\circ}C$
$K_{\delta}$	$2 \times 10^{10}$	Pa	$\rho_{\zeta}$	$2.6 \times 10^6$	$g/m^3$
$K_{\mu}$	$5 \times 10^9$	Pa	$\rho_{\mu}$	$1 \times 10^6$	$g/m^3$
$K$	0.5	$W/m.^{\circ}C$	$\alpha$	1	—

1. The initial conditions (5) are considered only for the general solutions and the, initial conditions of  $G_{1n}(t)$  to  $G_{12n}(t)$  for the particular solutions are considered equal to zero.
2. Laplace transform of (36) is in terms of polynomial function form of the Laplace parameter  $s$  (not the Bessel functions form of  $s$ ). Therefore, the exact inverse Laplace transform is possible and somehow simple.
3. For the hollow cylinder it is enough to include the second type of Bessel function  $Y(r)$  in a sequence of the particular solution as By substituting (37) in (1)–(3), 18 equations are obtained, where using the six boundary conditions (4) 24 functions  $G_{1n}(t)$  to  $G_{24n}(t)$  are obtained for the hollow cylinder.

$$\begin{aligned}
 u^p(r, t) &= \sum_{n=1}^{\infty} \left\{ \left[ G_{1n}(t)J_1(\beta nr) + G_{2n}(t)rJ_2(\beta nr) + G_{3n}(t)r^2J_3(\beta nr) \right] \right. \\
 &\quad \left. + [G_{4n}(t)Y_1(\beta nr) + G_{5n}(t)rY_2(\beta nr) + G_{6n}(t)r^2Y_3(\beta nr)] + rG_{7n}(t) + r^2G_{8n}(t) \right\} \\
 T^p(r, t) &= \sum_{n=1}^{\infty} \left\{ \left[ G_{9n}(t)J_0(\beta nr) + G_{10n}(t)rJ_1(\beta nr) + G_{11n}(t)r^2J_2(\beta nr) \right] \right. \\
 &\quad \left. + [G_{12n}(t)Y_0(\beta nr) + G_{13n}(t)rY_1(\beta nr) + G_{14n}(t)r^2Y_2(\beta nr)] + rG_{15n}(t) + r^2G_{16n}(t) \right\} \\
 p^p(r, t) &= \sum_{n=1}^{\infty} \left\{ \left[ G_{17n}(t)J_0(\beta nr) + G_{18n}(t)rJ_1(\beta nr) + G_{19n}(t)r^2J_2(\beta nr) \right] \right. \\
 &\quad \left. + [G_{20n}(t)Y_0(\beta nr) + G_{21n}(t)rY_1(\beta nr) + G_{22n}(t)r^2Y_2(\beta nr)] + rG_{23n}(t) + r^2G_{24n}(t) \right\}
 \end{aligned} \tag{37}$$

## Results and Discussions

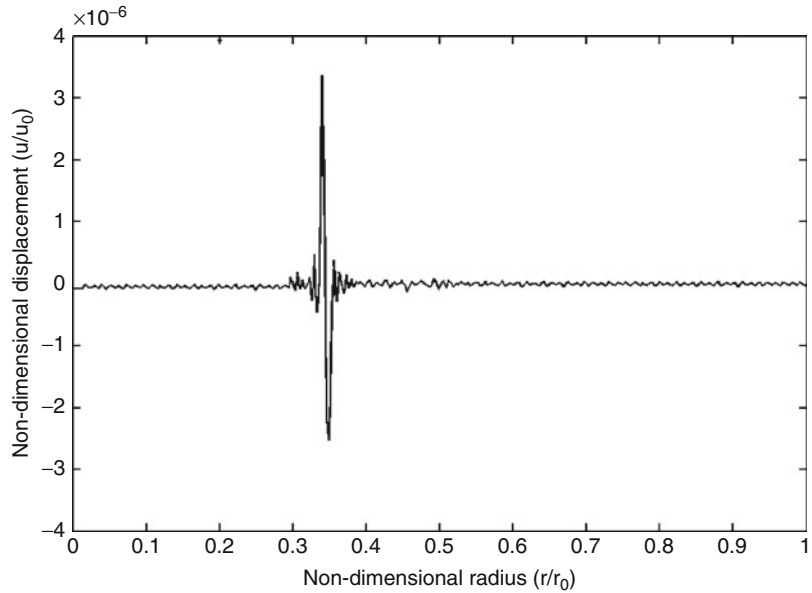
As an example, a solid cylinder with  $r_i = 0$ ,  $r_o = 1$  m is considered. The material properties are listed in Table 1. The initial temperature  $T_o$  is considered to be  $293^{\circ}K$ . Now, an instantaneous

hot spot  $T(1, t) = 10^{-3}T_o\delta(t)$ , where  $\delta(t)$  is unit dirac function, is considered and the outside radius of the cylinder is assumed to be fixed ( $u(1, t) = 0$ ). For plotting the graphs a nondimensional time  $\hat{t} = \frac{vt}{r_o}$  is considered where  $v = \sqrt{\frac{E(1-\nu)}{\rho(1+\nu)(1-2\nu)}}$  is the dilatational wave



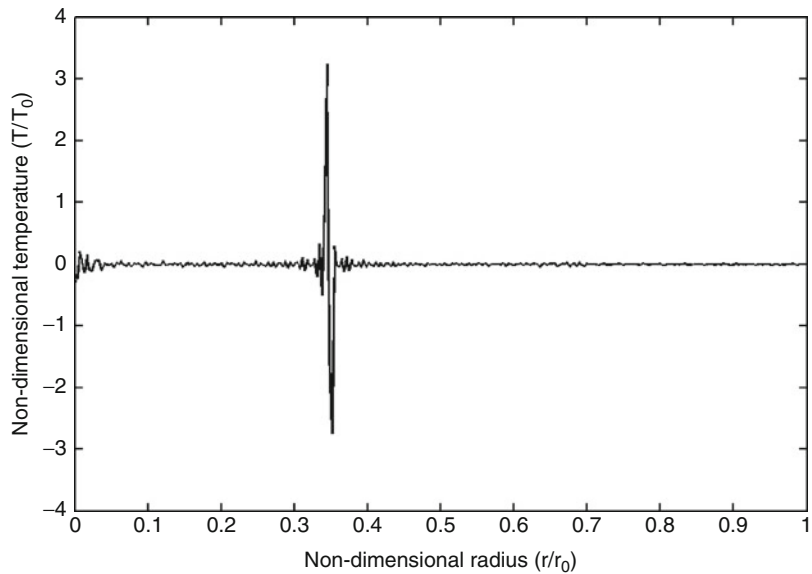
**Exact Solution for  
Classic Coupled  
Thermoporoelasticity in  
Cylindrical Coordinates,**

**Fig. 1** Nondimensional  
displacement distribution  
due to input  
 $u(1, t) = 10^{-12}u_0\delta(t)$  at  
nondimensional time  
 $\hat{t} = 0.3$



**Exact Solution for  
Classic Coupled  
Thermoporoelasticity in  
Cylindrical Coordinates,**

**Fig. 2** Nondimensional  
temperature distribution  
due to input  
 $T(1, t) = 10^{-3}T_0\delta(t)$  at  
nondimensional time  
 $\hat{t} = 0.3$

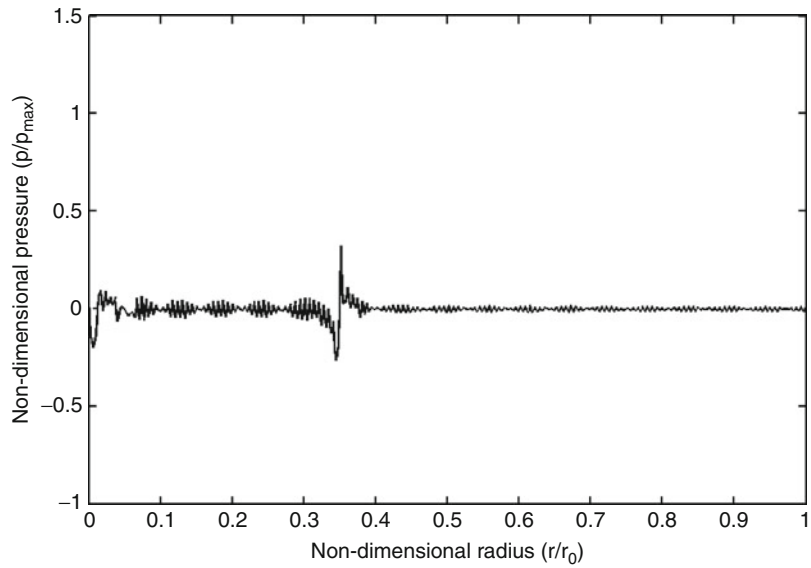


velocity. [Figures 1–3](#) show the wave front for the displacement, temperature, and pressure. As a second example, mechanical shock wave is applied to the outside surface of the cylinder given as  $u(1, t) = 10^{-12}u_0\delta(t)$ , and the surface is assumed to be at zero temperature ( $T(1, t) = 0$ ). [Figures 4–6](#) show the wave fronts for the displacement and temperature distributions. The convergence of the solutions for these examples is achieved by

consideration of 1,200 eigenvalues used for the H-Fourier expansion. Choosing more than this number for eigenvalues, the increase in round-off and truncation errors can affect the quality of the graphs. The convergence of the solution is better for the displacement result in comparison with the temperature. The small oscillations in [Figs. 3](#) and [5](#) are due to the convergence errors of solutions.

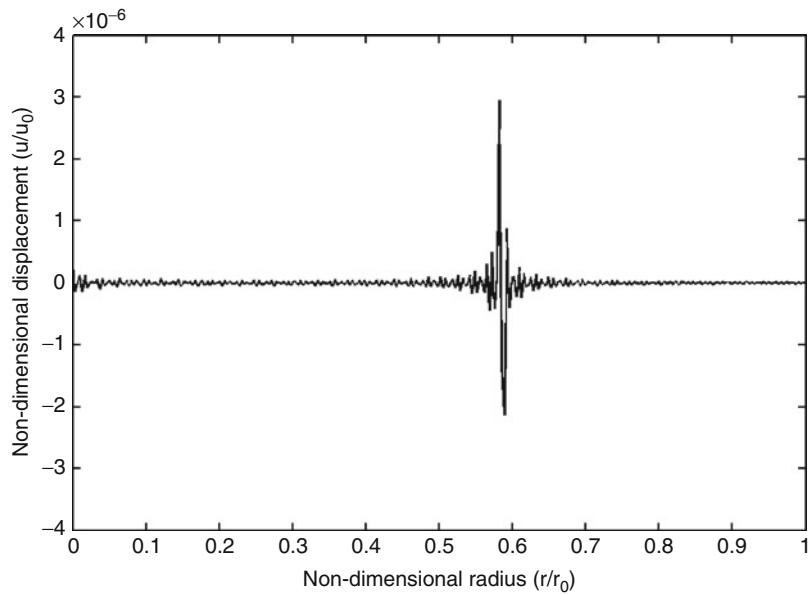
**Exact Solution for Classic Coupled Thermoporoelasticity in Cylindrical Coordinates,**

**Fig. 3** Nondimensional pressure distribution due to input  $p(1, t) = 10^{-3}p_0\delta(t)$  at nondimensional time  $\hat{t} = 0.3$



**Exact Solution for Classic Coupled Thermoporoelasticity in Cylindrical Coordinates,**

**Fig. 4** Nondimensional displacement distribution due to input  $u(1, t) = 10^{-12}u_0\delta(t)$  at nondimensional time  $\hat{t} = 0.6$



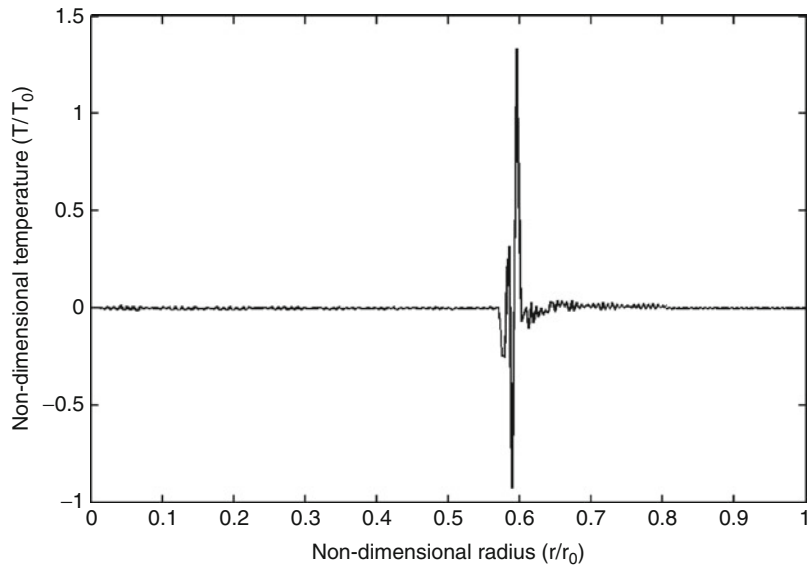
**Conclusion**

In this entry, an analytical solution for the coupled thermoporoelasticity of thick cylinders under radial temperature is presented. The method is based on the eigenfunctions Fourier expansion, which is a classical and traditional method of solution of the typical initial and boundary value problems. The noncompetitive

strength of this method is its ability to reveal the fundamental mathematical and physical properties and interpretations of the problem under studying. In the coupled thermoporoelastic problem of radial-symmetric cylinder, the governing equations constitute a system of partial differential equations with two independent variables, radius ( $r$ ) and time ( $t$ ). The traditional procedure to solve this class of problems is to eliminate the

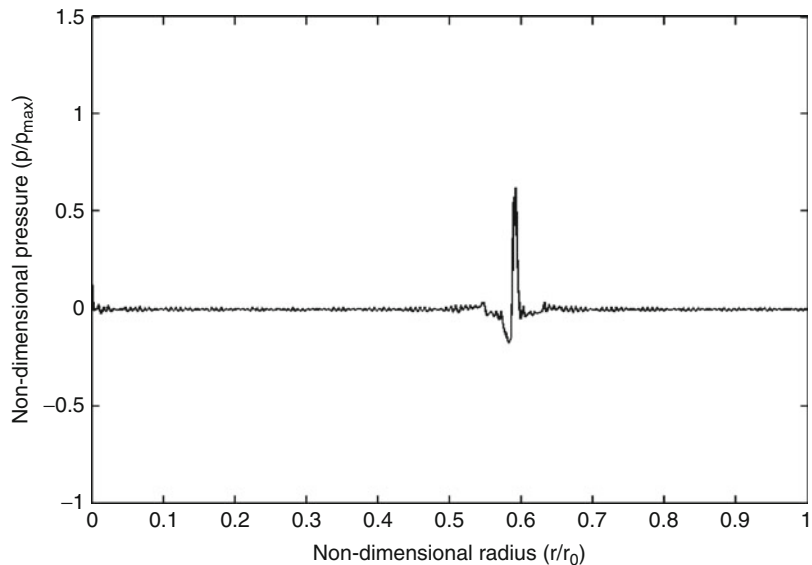
**Exact Solution for  
Classic Coupled  
Thermoporoelasticity in  
Cylindrical Coordinates,  
Fig. 5**

Nondimensional  
temperature distribution  
due to input  
 $T(1, t) = 10^{-3}T_0\delta(t)$  at  
nondimensional time  
 $\hat{t} = 0.6$



**Exact Solution for  
Classic Coupled  
Thermoporoelasticity in  
Cylindrical Coordinates,  
Fig. 6**

Nondimensional  
pressure distribution due to  
input  $p(1, t) = 10^{-3}p_0\delta(t)$   
at nondimensional time



time variable by using the Laplace transform. The resulting system is a set of ordinary differential equations in terms of the radius variable, whose solution falls in the Bessel functions family. This method of the analysis brings the Laplace parameter ( $s$ ) in the argument of the Bessel functions, causing hardship or difficulties in carrying out the exact inverse of the Laplace transformation. As a result, the numerical inversion of the Laplace

transformation is used in the papers dealing with this type of problems in literature. In this entry, to prevent this problem, when the Laplace transform is applied to the particular solutions, it is postponed after eliminating the radius variable  $r$  by H-Fourier expansion. Thus, the Laplace parameter ( $s$ ) appears in polynomial function forms and hence the exact Laplace inversion transformation is possible.

## References

1. Bai B (2006) Response of saturated porous media subjected to local thermal loading on the surface of semi-infinite space. *J Acta Mech Sinica* 22:54–61
2. Bai B (2006) Fluctuation responses of saturated porous media subjected to cyclic thermal loading. *J Comput Geotech* 33:396–403
3. Droujinine A (2006) Generalized anelastic asymptotic Ray theory. *J Wave Motion* 43:357–367
4. Bai B, Li T (2009) Solution for cylindrical cavity in saturated thermoporoelastic medium. *J Acta Mech Sinica* 22:85–92
5. Hetnarski RB (1964) Solution of the coupled problem of thermoelasticity in the form of series of functions. *J Arch Mech Stos* 16:919–941
6. Hetnarski RB, Ignaczak J (1993) Generalized thermoelasticity: closed-form solutions. *J Therm Stresses* 16:473–498
7. Hetnarski RB, Ignaczak J (1994) Generalized thermoelasticity: response of semi-space to a shortlaser pulse. *J Therm Stresses* 17:377–396
8. Georgiadis HG, Lykotrafitis G (2005) Rayleigh waves generated by a thermal source: a three-dimensional transient thermoelasticity solution. *J Appl Mech* 72:129–138
9. Wagner P (1994) Fundamental matrix of the system of dynamic linear thermoelasticity. *J Therm stresses* 17:549–565
10. Jabbari M, Dehbani H (2009) An exact solution for classic coupled thermoporoelasticity in cylindrical coordinates. *J Solid mech arak* 1:343–357

## Exact Solution for Lord-Shulman Generalized Coupled Thermoporoelasticity in Cylindrical Coordinates

Mohsen Jabbari<sup>1</sup> and H. Dehbani<sup>2</sup>

<sup>1</sup>Faculty of Engineering, Postgraduate School, South Tehran Branch, Islamic Azad University, Tehran, Iran

<sup>2</sup>Postgraduate School, South Tehran Branch, Islamic Azad University, Tehran, Iran

## Overview

In this entry, the generalized coupled thermoporoelasticity model of hollow and solid cylinders under radial-symmetric loading condition ( $r, t$ ) is

considered. A full analytical method is used and an exact unique solution of the generalized coupled equations is presented. The thermal, mechanical, and pressure boundary conditions, the body force, the heat source, and the injected volume rate per unit volume of a distribute water source are considered in the most general forms and where no limiting assumption is used. This generality allows the simulation of varieties of applicable problems.

## Introduction

The classical theory of thermoelasticity is based on the conventional heat conduction equation. The conventional heat conduction theory assumes that the thermal disturbances propagate at infinite speeds. This prediction is unrealistic from a physical point of view, particularly in simulations like those involving very short transient duration, sudden high heat flux situations, and/or very low temperatures near the absolute zero [1]. Thus, some modified dynamic thermoelastic models are proposed to analyze the problems with the second sound effects, such as the Lord-Shulman (LS) [2], the Green-Lindsay [3], and the Green-Naghdi [4] theories. These nonclassical theories are referred to as the generalized thermoelasticity theories with finite thermal wave speed, or thermoelasticity with the second sound effect. For the generalized thermoporoelasticity problems, coupled thermal and poromechanical processes play an important role in a number of problems of interest in the geomechanics such as stability of boreholes and permeability enhancement in geothermal reservoirs. A thermoporoelastic approach combines the theory of heat conduction with poroelastic constitutive equations and coupling the temperature field with the stresses and pore pressure.

There are a limited number of papers that present the closed-form or analytical solution for the coupled porothermoelasticity problems. H.M. Youssef [5] derived the governing equations, which describe the behavior of thermoelastic porous medium in the context of the theory of generalized thermoelasticity with

one relaxation time (Lord-Shulman). Bai [6] investigated the response of saturated porous media subjected to local thermal loading on the surface of semi-infinite space. He used the numerical integral methods for calculating the unsteady temperature, pore pressure, and displacement fields. This author also studied the fluctuation responses of saturated porous media subjected to cyclic thermal loading [7]. In the mentioned paper, an analytical solution was deduced proposed by using the Laplace transform and the Gauss-Legendre method and Laplace transform inversion. Droujinine [8] investigated dispersion and attenuation of body waves in a wide range of materials representing realistic rock structures. He used the time-domain asymptotic ray theory to a new generalized coordinate-free wave equation with an arbitrary tensor relaxation function. Bai and Li [9] found a solution for cylindrical cavity in saturated thermoporoelastic medium by using Laplace transform and numerical Laplace transform inversion.

The number of papers that present the closed-form or analytical solution for the coupled thermoelasticity problems is also limited. Hetnarski [10] found the solution of the coupled thermoelasticity in the form of a series of functions. Hetnarski and Ignaczak presented a study of the one-dimensional thermoelastic waves produced by an instantaneous plane source of heat in homogeneous isotropic infinite and semi-infinite bodies of the Green-Lindsay type [11]. Also, these authors presented an analysis for laser-induced waves propagating in an absorbing thermoelastic semi-space of the Green-Lindsay theory [12]. Georgiadis and Lyktraftis obtained a three-dimensional transient thermoelastic solution for Rayleigh-type disturbances propagating on the surface of a half-space [13]. Wagner [14] presented the fundamental matrix of a system of partial differential operators that governs the diffusion of heat and the strains in elastic media. This method can be used to predict the temperature distribution and the strains by an instantaneous point heat, point source of heat, or by a suddenly applied delta force.

In the present [15] a full analytical method is used to obtain the response of the governing

equations, an exact solution is presented. The method of solution is based on the Fourier's expansion and eigenfunction methods, which are traditional and routine methods in solving the partial differential equations. Since the coefficients of equations are not functions of the time variable ( $t$ ), an exponential form is considered for the general solution matched with the physical wave properties of thermal and mechanical waves. For the particular solution, that is the response to mechanical and thermal shocks, the eigenfunction method and Laplace transformation is used. This work is following the previous works for coupled problems [16–19].

## Governing Equations

A hollow cylinder with inner and outer radii  $r_i$  and  $r_o$ , respectively, made of isotropic material subjected to radial-symmetric mechanical, thermal, and pressure shocks, is considered. The generalized coupled thermoelastic equations of the cylinder, with plane stress assumption, based in LS theory is obtained from [1] as:

$$\begin{aligned} u_{,rr} + \frac{1}{r}u_{,r} - \frac{1}{r^2}u - \alpha \frac{(1+\nu)(1-2\nu)}{(1-\nu)E}p_{,r} \\ - \beta \frac{(1+\nu)(1-2\nu)}{(1-\nu)E}T_{,r} - \rho \frac{(1+\nu)(1-2\nu)}{(1-\nu)E}\ddot{u} \\ = -\frac{(1+\nu)(1-2\nu)}{(1-\nu)E}F(r,t) \end{aligned} \quad (1)$$

Heat conduction equation in radial-symmetric direction with the mechanical and pressure coupling term is:

$$\begin{aligned} T_{,rr} + \frac{1}{r}T_{,r} - Z\frac{T_o}{K}(\dot{T} + t_o\ddot{T}) + Y\frac{T_o}{K}\dot{p} \\ - \beta\frac{T_o}{K}\left(t_o\left(\ddot{u}_{,r} + \frac{1}{r}\ddot{u}\right) + \dot{u}_{,r} + \frac{1}{r}\dot{u}\right) = -\frac{1}{K}Q(r,t) \end{aligned} \quad (2)$$

According to Darcy's law and continuity condition of seepage, the equation of mass conservation can be written as:

$$p_{,rr} + \frac{1}{r}p_{,r} - \alpha_p \frac{\gamma_w}{k} \dot{p} - Y \frac{\gamma_w}{k} \dot{T} - \alpha \frac{\gamma_w}{k} \left( \dot{u}_{,r} + \frac{1}{r} \dot{u} \right) = - \frac{\gamma_w}{k} W(r, t) \quad (3)$$

where  $(,)$  denotes partial derivative,  $u$  is the displacement component in the radial direction,  $p$  the pore pressure,  $\rho$  bulk mass density,  $\alpha = 1 - \frac{C_s}{C}$  the Biot's coefficient,  $C_s = 3(1 - 2\nu_s)E_s$  the coefficient of volumetric compression of solid grains, with  $E_s$  and  $\nu_s$  being the elastic modulus and Poisson's ratio of solid grains and  $C = 3(1 - 2\nu)E$  is the coefficient of volumetric compression of solid skeleton, with  $E$  and  $\nu$  being the elastic modulus and Poisson's ratio of solid skeleton,  $T_o$  initial reference temperature,  $\beta = \frac{3\alpha_s}{C}$  the thermal expansion factor,  $\alpha_s$  is the coefficient of linear thermal expansion of solid grains,  $Y = 3(n\alpha_w + (\alpha - n)\alpha_s)$  and  $\alpha_p = n(C_w - C_s) + \alpha C_s$  are coupling parameters,  $\alpha_w$  and  $C_w$  are the coefficients of linear thermal expansion and volumetric compression of pure water,  $n$  is the porosity,  $k$  is the hydraulic conductivity,  $\gamma_w$  is the unit of pore water and  $Z = \frac{((1-n)\rho_s c_s + n\rho_w c_w)}{T_o} - 3\beta\alpha_s$  is coupling parameter,  $\rho_w$  and  $\rho_s$  are the densities of pore water and solid grains and  $c_w$  and  $c_s$  are the heat capacities of pore water and solid grains and  $K$  is the coefficient of heat conductivity.  $t_0$  is relaxation time. Here,  $F(r, t)$ ,  $Q(r, t)$ , and  $W(r, t)$  are the body force, heat generation source, and the injected volume rate per unit volume of a distribute water source, respectively. The mechanical, thermal, and pressure boundary conditions are:

$$\begin{aligned} C_{11}u(r_i, t) + C_{12}u_{,r}(r_i, t) + C_{13}T(r_i, t) + C_{14}p(r_i, t) &= f_1(t) \\ C_{21}u(r_o, t) + C_{22}u_{,r}(r_o, t) + C_{23}T(r_o, t) + C_{24}p(r_o, t) &= f_2(t) \\ C_{31}T(r_i, t) + C_{32}T_{,r}(r_i, t) &= f_3(t) \\ C_{41}T(r_o, t) + C_{42}T_{,r}(r_o, t) &= f_4(t) \\ C_{51}p(r_i, t) &= f_5(t) \\ C_{61}p(r_o, t) &= f_6(t) \end{aligned} \quad (4)$$

where  $C_{ij}$  are the mechanical, thermal, and pressure coefficients, which by assigning different values for them different types of mechanical, thermal, and pressure boundary conditions may

be obtained. These boundary conditions include the displacement, strain, stress, specified temperature, convection, pressure, and heat flux. The initial boundary conditions are assumed in general form:

$$\begin{aligned} u(r, 0) &= f_7(r) \\ u_{,r}(r, 0) &= f_8(r) \\ T(r, 0) &= f_9(r) \\ T_{,r}(r, 0) &= f_{10}(r) \\ p(r, 0) &= f_{11}(r) \end{aligned} \quad (5)$$

## Solution

Equations (1)–(3) are the system of nonhomogeneous partial differential equations with nonconstant coefficients (functions of radius variable  $r$  only) has general and particular solutions.

### General Solution with Homogeneous Boundary Conditions

Since the coefficients of these equations are independent of time variable  $(t)$ , the exponential function form of time variable may be assumed for the general solution as:

$$\begin{aligned} u(r, t) &= [U(r)]e^{\lambda t} \\ T(r, t) &= [\theta(r)]e^{\lambda t} \\ p(r, t) &= [P(r)]e^{\lambda t} \end{aligned} \quad (6)$$

Substituting (6) into homogeneous parts of (1)–(3) yields:

$$\begin{aligned} U'' + \frac{1}{r}U' - \frac{1}{r^2}U + d_1P' + d_2\theta' + d_3\lambda^2U &= 0 \\ \theta'' + \frac{1}{r}\theta' + d_4(\lambda + t_o\lambda^2)\theta + d_5\lambda P \\ &+ d_6(\lambda + t_o\lambda^2)\left(U' + \frac{1}{r}U\right) = 0 \\ P'' + \frac{1}{r}P' + d_7\lambda P + d_8\lambda\theta + d_9\lambda\left(U' + \frac{1}{r}U\right) &= 0 \end{aligned} \quad (7)$$

Equation (7) are system of ordinary differential equations, where the prime symbol (') shows differentiation with respect to the radius variable ( $r$ ) and  $d_1$  to  $d_9$  are constant parameters given in the appendix.

The first solutions of  $U_1$ ,  $\theta_1$ , and  $P_1$  are considered as:

$$\begin{aligned} U_1(r) &= A_1 J_1(\beta r) \\ \theta_1(r) &= B_1 J_0(\beta r) \\ P_1(r) &= C_1 J_0(\beta r) \end{aligned} \quad (8)$$

Substituting (8) into (7) yields:

$$\begin{aligned} \{(-\beta^2 + \lambda^2 d_3)A_1 - d_2 \beta B_1 - d_1 \beta C_1\} J_1(\beta r) &= 0 \\ \{(\lambda + t_o \lambda^2) d_6 \beta A_1 + (\lambda + t_o \lambda^2) d_4 B_1 \\ + (-\beta^2 + \lambda d_5) C_1\} J_0(\beta r) &= 0 \\ \{\lambda d_9 \beta A_1 + (-\beta^2 + \lambda d_7) B_1 + \lambda d_8 C_1\} J_0(\beta r) &= 0 \end{aligned} \quad (9)$$

Equation (9) show that  $U_1$ ,  $\theta_1$  and  $P_1$  can be the solutions of (7), if and only if:

$$\begin{bmatrix} -\beta^2 + \lambda^2 d_3 & -d_2 \beta & -d_1 \beta \\ (\lambda + t_o \lambda^2) d_6 \beta & (\lambda + t_o \lambda^2) d_4 & -\beta^2 + \lambda d_5 \\ \lambda d_9 \beta & -\beta^2 + \lambda d_7 & \lambda d_8 \end{bmatrix} \begin{Bmatrix} A_1 \\ B_1 \\ C_1 \end{Bmatrix} = \begin{Bmatrix} 0 \\ 0 \\ 0 \end{Bmatrix} \quad (10)$$

The nontrivial solution of (10) is obtained by equating the determinant of this equation to zero as:

$$\begin{aligned} -\beta^2 \lambda (\lambda + t_o \lambda^2) d_4 d_7 + \beta^6 - \beta^4 \lambda d_7 - \beta^4 \lambda d_5 \\ + \beta^2 \lambda^2 d_5 d_7 + \lambda^3 (\lambda + t_o \lambda^2) d_3 d_4 d_7 - \lambda^2 d_3 \beta^4 \\ + \lambda^3 d_3 \beta^2 d_7 + \lambda^3 d_3 d_5 \beta^2 - \lambda^4 d_3 d_5 d_7 \\ + \lambda (\lambda + t_o \lambda^2) d_6 \beta^2 d_2 d_7 + (\lambda + t_o \lambda^2) d_6 \beta^4 d_1 \\ - \lambda (\lambda + t_o \lambda^2) d_6 \beta^2 d_1 d_7 + \lambda d_9 \beta^4 d_2 \\ - \lambda^2 d_9 \beta^2 d_2 d_5 + \lambda^2 d_9 \beta^2 d_1 d_4 = 0 \end{aligned} \quad (11)$$

Equation (11) is the first characteristic equation. Thus, it is concluded that  $U_1$ ,  $\theta_1$ , and  $P_1$  satisfy the system of (7) and they are the first solution of the system.

The second solutions of  $U_2$ ,  $\theta_2$  and  $P_2$  are considered as:

$$\begin{aligned} U_2(r) &= [A_2 J_1(\beta r) + A_3 r J_2(\beta r)] \\ \theta_2(r) &= [B_2 J_0(\beta r) + B_3 r J_1(\beta r)] \\ P_2(r) &= [C_2 J_0(\beta r) + C_3 r J_1(\beta r)] \end{aligned} \quad (12)$$

Substituting (12) into (7) yields:

$$\begin{aligned} \{(-\beta^2 + \lambda^2 d_3)A_3 - d_2 \beta B_3 - d_1 \beta C_3\} r J_0(\beta r) \\ + \{(\beta^2 - d_3 \lambda^2)A_2 - \frac{2}{\beta} d_3 \lambda^2 A_3 + d_2 \beta B_2 \\ + d_1 \beta C_2\} J_1(\beta r) = 0 \\ \{(\lambda + t_o \lambda^2) d_6 \beta A_3 + (\lambda + t_o \lambda^2) d_4 B_3 \\ + (-\beta^2 + \lambda d_5) C_3\} r J_1(\beta r) \\ + \{d_6 (\lambda + t_o \lambda^2) \beta A_2 + d_4 (\lambda + t_o \lambda^2) B_2 \\ + (-\beta^2 + d_5 \lambda) C_2 + 2 \beta C_3\} J_0(\beta r) = 0 \\ \{\lambda d_9 \beta A_3 + (-\beta^2 + \lambda d_7) B_3 + \lambda d_8 C_3\} r J_1(\beta r) \\ + \{d_9 \lambda \beta A_2 + (-\beta^2 + d_7 \lambda) B_2 \\ + d_8 \lambda C_2 + 2 \beta B_3\} J_0(\beta r) = 0 \end{aligned} \quad (13)$$

The expressions for  $U_2$ ,  $\theta_2$ , and  $P_2$  can be the solutions of (7), if and only if:

$$\begin{bmatrix} -\beta^2 + \lambda^2 d_3 & -d_2 \beta & -d_1 \beta \\ (\lambda + t_o \lambda^2) d_6 \beta & (\lambda + t_o \lambda^2) d_4 & -\beta^2 + \lambda d_5 \\ \lambda d_9 \beta & -\beta^2 + \lambda d_7 & \lambda d_8 \end{bmatrix} \begin{Bmatrix} A_3 \\ B_3 \\ C_3 \end{Bmatrix} = \begin{Bmatrix} 0 \\ 0 \\ 0 \end{Bmatrix} \quad (14)$$

$$(\beta^2 - d_3\lambda^2)A_2 - \frac{2}{\beta}d_3\lambda^2A_3 + d_2\beta B_2 + d_1\beta C_2 = 0 \quad (15)$$

$$d_6(\lambda + t_o\lambda^2)\beta A_2 + d_4(\lambda + t_o\lambda^2)B_2 + (-\beta^2 + d_5\lambda)C_2 + 2\beta C_3 = 0 \quad (16)$$

$$d_9\lambda\beta A_2 + (-\beta^2 + d_7\lambda)B_2 + d_8\lambda C_2 + 2\beta B_3 = 0 \quad (17)$$

The nontrivial solution of (14) is obtained by equating the determinant to zero as:

$$\begin{aligned} & -\beta^2\lambda(\lambda + t_o\lambda^2)d_4d_7 + \beta^6 - \beta^4\lambda d_7 - \beta^4\lambda d_5 \\ & + \beta^2\lambda^2d_5d_7 + \lambda^3(\lambda + t_o\lambda^2)d_3d_4d_7 - \lambda^2d_3\beta^4 \\ & + \lambda^3d_3\beta^2d_7 + \lambda^3d_3d_5\beta^2 - \lambda^4d_3d_5d_7 \\ & + \lambda(\lambda + t_o\lambda^2)d_6\beta^2d_2d_7 + (\lambda + t_o\lambda^2)d_6\beta^4d_1 \\ & - \lambda(\lambda + t_o\lambda^2)d_6\beta^2d_1d_7 + \lambda d_9\beta^4d_2 \\ & - \lambda^2d_9\beta^2d_2d_5 + \lambda^2d_9\beta^2d_1d_4 = 0 \end{aligned} \quad (18)$$

Equations (15)–(17) give the relation between  $A_2, A_3, B_2, B_3, C_2$  and  $C_3$ , and they play as the balancing ratios that help (12) to be the second solution of the system of (7).

The third solution of the system of ordinary differential equations with nonconstant coefficients (7) must be considered as:

$$\begin{aligned} U_3(r) &= [A_4J_1(\beta r) + A_5rJ_2(\beta r) + A_6r^2J_3(\beta r)] \\ \theta_3(r) &= [B_4J_0(\beta r) + B_5rJ_1(\beta r) + B_6r^2J_2(\beta r)] \\ P_3(r) &= [C_4J_0(\beta r) + C_5rJ_1(\beta r) + C_6r^2J_2(\beta r)] \end{aligned} \quad (19)$$

Substituting (19) into (7) yields:

$$\begin{aligned} & \{(-\lambda^2d_3 + \beta^2)A_6 + d_2\beta B_6 + d_1\beta C_6\}r^2J_1(\beta r) \\ & + \{(\beta^2 - d_3\lambda^2)A_5 + d_2\beta B_5 + d_1\beta C_5 \\ & - \frac{4}{\beta}d_3\lambda^2A_6\}rJ_0(\beta r) = 0 \\ & + \{(d_3\lambda^2 - \beta^2)A_4 - d_1\beta C_4 - d_2\beta B_4 + \frac{2}{\beta}d_3\lambda^2A_5 \\ & + \frac{8}{\beta^2}d_3\lambda^2A_6\}J_1(\beta r) = 0 \\ & \{-(\lambda + t_o\lambda^2)d_6\beta A_6 - (\lambda + t_o\lambda^2)d_4B_6 \\ & + (\beta^2 - \lambda d_5)C_6\}r^2J_0(\beta r) + \{d_6(\lambda + t_o\lambda^2)\beta A_4 \\ & + d_4(\lambda + t_o\lambda^2)B_4 + (-\beta^2 + d_5\lambda)C_4 + 2\beta C_5\}J_0(\beta r) \\ & + \{d_6(\lambda + t_o\lambda^2)\beta A_5 + d_4(\lambda + t_o\lambda^2)B_5 \\ & + (-\beta^2 + d_5\lambda)C_5 + 2d_6(\lambda + t_o\lambda^2)A_6 \\ & + \frac{2}{\beta}d_4(\lambda + t_o\lambda^2)B_6 + \left(2\beta + \frac{2}{\beta}d_5\lambda\right) \\ & C_6\}rJ_1(\beta r) = 0 \\ & \{-\lambda d_9\beta A_6 + (\beta^2 - \lambda d_7)B_6 - \lambda d_8C_6\}r^2J_0(\beta r) \\ & + \{d_9\lambda\beta A_4 + (-\beta^2 + d_7\lambda)B_4 \\ & + d_8\lambda C_4 + 2\beta B_5\}J_0(\beta r) \\ & + \{\beta d_9\lambda A_5 + (-\beta^2 + d_7\lambda)B_5 + d_8\lambda C_5 + 2d_9\lambda A_6 \\ & + \left(2\beta + \frac{2}{\beta}d_7\lambda\right)B_6 + \frac{2}{\beta}d_8\lambda C_6\}rJ_1(\beta r) = 0 \end{aligned} \quad (20)$$

The expressions for  $U_3$ ,  $\theta_3$ , and  $P_3$  can be the solutions of (7), if and only if :

$$\begin{bmatrix} -\beta^2 + \lambda^2d_3 & -d_2\beta & -d_1\beta \\ (\lambda + t_o\lambda^2)d_6\beta & (\lambda + t_o\lambda^2)d_4 & -\beta^2 + \lambda d_5 \\ \lambda d_9\beta & -\beta^2 + \lambda d_7 & \lambda d_8 \end{bmatrix} \begin{Bmatrix} A_6 \\ B_6 \\ C_6 \end{Bmatrix} = \begin{Bmatrix} 0 \\ 0 \\ 0 \end{Bmatrix} \quad (21)$$

$$(\beta^2 - d_3\lambda^2)A_5 + d_2\beta B_5 + d_1\beta C_5 - \frac{4}{\beta}d_3\lambda^2A_6 = 0 \quad (22)$$

$$\begin{aligned} & (d_3\lambda^2 - \beta^2)A_4 - d_1\beta C_4 - d_2\beta B_4 \\ & + \frac{2}{\beta}d_3\lambda^2A_5 + \frac{8}{\beta^2}d_3\lambda^2A_6 = 0 \end{aligned} \quad (23)$$



$$d_6(\lambda + t_o\lambda^2)\beta A_4 + d_4(\lambda + t_o\lambda^2)B_4 + (-\beta^2 + d_5\lambda)C_4 + 2\beta C_5 = 0 \quad (24)$$

$$d_6(\lambda + t_o\lambda^2)\beta A_5 + d_4(\lambda + t_o\lambda^2)B_5 + (-\beta^2 + d_5\lambda)C_5 + 2d_6(\lambda + t_o\lambda^2)A_6 + \frac{2}{\beta}d_4(\lambda + t_o\lambda^2)B_6 + \left(2\beta + \frac{2}{\beta}d_5\lambda\right)C_6 = 0 \quad (25)$$

$$d_9\lambda\beta A_4 + (-\beta^2 + d_7\lambda)B_4 + d_8\lambda C_4 + 2\beta B_5 = 0 \quad (26)$$

$$\beta d_9\lambda A_5 + (-\beta^2 + d_7\lambda)B_5 + d_8\lambda C_5 + 2d_9\lambda A_6 + \left(2\beta + \frac{2}{\beta}d_7\lambda\right)B_6 + \frac{2}{\beta}d_8\lambda C_6 = 0 \quad (27)$$

The nontrivial solution of (21) is obtained by equating the determinant of this equation to zero as:

$$\begin{aligned} & -\beta^2\lambda(\lambda + t_o\lambda^2)d_4d_7 + \beta^6 - \beta^4\lambda d_7 - \beta^4\lambda d_5 \\ & + \beta^2\lambda^2d_5d_7 + \lambda^3(\lambda + t_o\lambda^2)d_3d_4d_7 - \lambda^2d_3\beta^4 \\ & + \lambda^3d_3\beta^2d_7 + \lambda^3d_3d_5\beta^2 - \lambda^4d_3d_5d_7 \\ & + \lambda(\lambda + t_o\lambda^2)d_6\beta^2d_2d_7 + (\lambda + t_o\lambda^2)d_6\beta^4d_1 \\ & - \lambda(\lambda + t_o\lambda^2)d_6\beta^2d_1d_7 + \lambda d_9\beta^4d_2 \\ & - \lambda^2d_9\beta^2d_2d_5 + \lambda^2d_9\beta^2d_1d_4 = 0 \end{aligned} \quad (28)$$

The characteristic equation (28) is the same as the characteristic equations (11) and (18). This equality is interesting as it prevents mathematical dilemma and complexity and a single value for the eigenvalue  $\beta$  simultaneously satisfies three characteristic equations (11), (18), and (28). Equations (22)–(27) give the relation between  $A_4, A_5, A_6, B_4, B_5, B_6, C_4, C_5$  and  $C_6$ . These relations play as the balancing ratios that help (19) to be the third solution of the system of (7).

The complete general solutions for the hollow cylinder are:

$$\begin{aligned} U^g(r) &= A_1J_1(\beta r) + A_3[\zeta_1J_1(\beta r) + rJ_2(\beta r)] \\ &+ A_6[\zeta_2J_1(\beta r) + \zeta_3rJ_2(\beta r) + r^2J_3(\beta r)] \\ \theta^g(r) &= A_1\zeta_4J_0(\beta r) + A_3[\zeta_5J_0(\beta r) + \zeta_6rJ_1(\beta r)] \\ &+ A_6[\zeta_7J_0(\beta r) + \zeta_8rJ_1(\beta r) + \zeta_9r^2J_2(\beta r)] \\ P^g(r) &= A_1\zeta_{10}J_0(\beta r) + A_3[\zeta_{11}J_0(\beta r) + \zeta_{12}rJ_1(\beta r)] \\ &+ A_6[\zeta_{13}J_0(\beta r) + \zeta_{14}rJ_1(\beta r) + \zeta_{15}r^2J_2(\beta r)] \end{aligned} \quad (29)$$

Here  $\zeta_1$  to  $\zeta_{15}$  are ratios obtained from (21)–(27), (14)–(17), and (10) are given in the appendix. Substituting  $U^g$ ,  $\theta^g$ , and  $P^g$  in the homogeneous form of the boundary conditions (4), three linear algebraic equations are obtained. They have the coefficients depending on  $\lambda$  and  $\beta$ . Setting the determinant of the coefficients equal to zero, the second characteristic equation is obtained. Simultaneous solution of this equation and (11) results into infinite number of two eigenvalues  $\beta_n$  and  $\lambda_n$ . Therefore  $U^g$ ,  $\theta^g$ , and  $P^g$  are rewritten as:

$$\begin{aligned} U^g(r) &= A_1[J_1(\beta r) + \zeta_{16}[\zeta_1J_1(\beta r) + rJ_2(\beta r)] \\ &+ \zeta_{17}[\zeta_2J_1(\beta r) + \zeta_3rJ_2(\beta r) + r^2J_3(\beta r)]] \\ \theta^g(r) &= A_1[\zeta_4J_0(\beta r) + \zeta_{16}[\zeta_5J_0(\beta r) + \zeta_6rJ_1(\beta r)] \\ &+ \zeta_{17}[\zeta_7J_0(\beta r) + \zeta_8rJ_1(\beta r) + \zeta_9r^2J_2(\beta r)]] \\ P^g(r) &= A_1[\zeta_{10}J_0(\beta r) + \zeta_{16}[\zeta_{11}J_0(\beta r) + \zeta_{12}rJ_1(\beta r)] \\ &+ \zeta_{17}[\zeta_{13}J_0(\beta r) + \zeta_{14}rJ_1(\beta r) + \zeta_{15}r^2J_2(\beta r)]] \end{aligned} \quad (31)$$

where  $\zeta_{16}$  and  $\zeta_{17}$  are presented in the appendix. Let us show the functions in the brackets of (31) by functions  $H_0, H_1$  and  $H_2$  as:

$$\begin{aligned} H_0 &= J_1(\beta r) + \zeta_{16}[\zeta_1J_1(\beta r) + rJ_2(\beta r)] \\ &+ \zeta_{17}[\zeta_2J_1(\beta r) + \zeta_3rJ_2(\beta r) + r^2J_3(\beta r)] \\ H_1 &= \zeta_4J_0(\beta r) + \zeta_{16}[\zeta_5J_0(\beta r) + \zeta_6rJ_1(\beta r)] \\ &+ \zeta_{17}[\zeta_7J_0(\beta r) + \zeta_8rJ_1(\beta r) + \zeta_9r^2J_2(\beta r)] \\ H_2 &= \zeta_{10}J_0(\beta r) + \zeta_{16}[\zeta_{11}J_0(\beta r) + \zeta_{12}rJ_1(\beta r)] \\ &+ \zeta_{17}[\zeta_{13}J_0(\beta r) + \zeta_{14}rJ_1(\beta r) + \zeta_{15}r^2J_2(\beta r)] \end{aligned} \quad (32)$$

According to the Sturm-Liouville theories, these functions are orthogonal with respect to the weight function  $p(r) = r$  as:

$$\int_{r_i}^{r_o} H(\beta_n r) H(\beta_m r) r dr = \begin{cases} 0 & n \neq m \\ \|H(\beta_n r)\|^2 & n = m \end{cases} \quad (33)$$

where  $\|H(\beta_n r)\|$  is norm of  $H$  function and equals:

$$\|H(\beta_n r)\| = \left[ \int_{r_i}^{r_o} r H^2(\beta_n r) dr \right]^{\frac{1}{2}} \quad (34)$$

Due to the orthogonality of function  $H$ , every piece-wise continuous function, such as  $f(r)$ , can be expanded in terms of the function  $H$  (either for  $H_0$  or  $H_1$  or  $H_2$ ), and is called the H-Fourier series as:

$$f(r) = \sum_{n=1}^{\infty} e_n H(\beta_n r) \quad (35)$$

where  $e_n \psi$  equals:

$$e_n = \frac{1}{\|H(\beta_n r)\|^2} \int_{r_i}^{r_o} f(r) H(r) r dr \quad (36)$$

Using (6), (31), and (32), the displacement and temperature distributions due to the general solution become:

$$\begin{aligned} u^g(r, t) &= \sum_{n=1}^{\infty} \left\{ \sum_{m=1}^4 a_{nm} e^{\lambda_{nm} t} \right\} H_0(\beta_n r) \\ T^g(r, t) &= \sum_{n=1}^{\infty} \left\{ \sum_{m=1}^4 N_{nm} a_{nm} e^{\lambda_{nm} t} \right\} H_1(\beta_n r) \\ p^g(r, t) &= \sum_{n=1}^{\infty} \left\{ \sum_{m=1}^4 M_{nm} a_{nm} e^{\lambda_{nm} t} \right\} H_2(\beta_n r) \end{aligned} \quad (37)$$

where  $N_{mn}$  and  $M_{mn}$  are ratios obtained by substituting (37) to (1)–(3). Using the initial conditions (5) and with the help of (34), (35) and (36), four unknown constants are obtained.

### Particular Solution with Nonhomogeneous Boundary Conditions

The general solutions may be used as proper functions for guessing the particular solution adopted to the nonhomogeneous parts of the (1)–(3) and nonhomogeneous boundary conditions (4) as:

$$\begin{aligned} u^p(r, t) &= \sum_{n=1}^{\infty} \left\{ \left[ G_{1n}(t) J_1(\beta_n r) + G_{2n}(t) r J_2(\beta_n r) \right] \right. \\ &\quad \left. + G_{3n}(t) r^2 J_3(\beta_n r) + r^2 G_{4n}(t) \right\} \\ T^p(r, t) &= \sum_{n=1}^{\infty} \left\{ \left[ G_{5n}(t) J_0(\beta_n r) + G_{6n}(t) r J_1(\beta_n r) \right] \right. \\ &\quad \left. + G_{7n}(t) r^2 J_2(\beta_n r) + r^2 G_{8n}(t) \right\} \\ p^p(r, t) &= \sum_{n=1}^{\infty} \left\{ \left[ G_{9n}(t) J_0(\beta_n r) + G_{10n}(t) r J_1(\beta_n r) \right] \right. \\ &\quad \left. + G_{11n}(t) r^2 J_2(\beta_n r) + r^2 G_{12n}(t) \right\} \end{aligned} \quad (38)$$

For the solid cylinder, the second type of Bessel function  $Y$  is excluded. It is necessary and suitable to expand the body force  $F(r, t)$ , heat source  $Q(r, t)$ , and poro function  $W(r, t)$  in H-Fourier expansion form as:

$$\begin{aligned} F(r, t) &= \sum_{n=1}^{\infty} F_n(t) H_0(\beta_n r) \\ Q(r, t) &= \sum_{n=1}^{\infty} Q_n(t) H_1(\beta_n r) \\ P(r, t) &= \sum_{n=1}^{\infty} P_n(t) H_2(\beta_n r) \end{aligned} \quad (39)$$

where  $F_n(t)$ ,  $Q_n(t)$ , and  $P_n(t)$  are:

$$F_n(t) = \frac{1}{\|H_0(\beta_n r)\|^2} \int_{r_i}^{r_o} F(r, t) H_0(\beta_n r) r dr$$

$$Q_n(t) = \frac{1}{\|H_1(\beta_n r)\|^2} \int_{r_i}^{r_o} Q(r, t) H_1(\beta_n r) r dr \quad (40)$$

$$P_n(t) = \frac{1}{\|H_2(\beta_n r)\|^2} \int_{r_i}^{r_o} P(r, t) H_2(\beta_n r) r dr$$

Substituting (38) and (40) into nonhomogeneous form of equations (1)–(3) yields:

$$G_2(t)\beta^2 - \ddot{G}_2(t)d_3 - 4\ddot{G}_3(t)\frac{1}{\beta}d_3 - d_{13}G_4(t)C_1 - 4d_{13}G_4(t)C_2\frac{1}{\beta} - d_{16}\ddot{G}_4(t)C_1 - 4d_{16}\ddot{G}_4(t)C_2\frac{1}{\beta} + G_6(t)d_2\beta - d_{15}G_8(t)C_1 - 4d_{15}G_8(t)C_2\frac{1}{\beta} + G_{10}(t)d_1\beta - d_{14}G_{12}(t)C_1 - 16d_{14}G_{12}(t)C_2\frac{1}{\beta} - d_{25}d_{10}FC_1 - 4d_{25}d_{10}FC_2\frac{1}{\beta} = 0 \quad (41a)$$

$$-G_1(t)\beta^2 + \ddot{G}_1(t)d_3 + 2\ddot{G}_2(t)\frac{1}{\beta}d_3 + 8\ddot{G}_3(t)\frac{1}{\beta^2}d_3d_{13}G_4(t)C_0 + 2d_{13}G_4(t)C_1\frac{1}{\beta} + 8d_{13}G_4(t)C_2\frac{1}{\beta^2} + d_{16}\ddot{G}_4(t)C_0 + 2d_{16}\ddot{G}_4(t)C_1\frac{1}{\beta} + 8d_{16}\ddot{G}_4(t)C_2\frac{1}{\beta^2} - G_5(t)\beta d_2 + d_{15}G_8(t)C_0 + 2d_{15}G_8(t)C_1\frac{1}{\beta} + 8d_{15}G_8(t)C_2\frac{1}{\beta^2} - G_9(t)\beta d_1 + d_{14}G_{12}(t)C_0 + 2d_{14}G_{12}(t)C_1\frac{1}{\beta} + 8d_{14}G_{12}(t)C_2\frac{1}{\beta^2} + d_{25}d_{10}FC_0 + 2d_{25}d_{10}FC_1\frac{1}{\beta} + 8d_{25}d_{10}FC_2\frac{1}{\beta^2} = 0 \quad (41b)$$

$$G_3(t)\beta^2 - \ddot{G}_3(t)d_3 - d_{13}G_4(t)C_2 - d_{16}\ddot{G}_4(t)C_2 + G_7(t)\beta d_2 - d_{15}G_8(t)C_2 + G_{11}(t)\beta d_1 - d_{14}G_{12}(t)C_2 - d_{25}d_{10}FC_2 = 0 \quad (41c)$$

$$d_6\beta\{\dot{G}_1(t) + t_o\ddot{G}_1(t)\} + d_{18}E_0\dot{G}_4(t) - \beta^2G_5(t) + d_4\{\dot{G}_5(t) + t_o\ddot{G}_5(t)\} + 2\beta G_6(t) + d_{17}E_0G_8(t) + d_{19}E_0\dot{G}_8(t) + d_5\dot{G}_9(t) + d_{20}E_0\dot{G}_{12}(t) + d_{26}d_{11}E_0Q_n(t) = 0 \quad (41d)$$

$$-d_6\beta\{\dot{G}_3(t) + t_o\ddot{G}_3(t)\} - E_2d_{18}\dot{G}_4(t) + \beta^2G_7(t) - d_4\{\dot{G}_7(t) + t_o\ddot{G}_7(t)\} - d_{17}E_2G_8(t) - d_{19}E_2\dot{G}_8(t) - d_5\dot{G}_{11}(t) - d_{20}E_2\dot{G}_{12}(t) - d_{26}E_2Q_n(t) = 0 \quad (41e)$$

$$d_6\beta\{\dot{G}_2(t) + t_o\ddot{G}_2(t)\} + 2d_6\{\dot{G}_3(t) + t_o\ddot{G}_3(t)\} + \left(d_{18}E_1 + \frac{2}{\beta}d_{14}E_2\right)\dot{G}_4(t) - \beta^2G_6(t) + d_4\{\dot{G}_6(t) + t_o\ddot{G}_6(t)\} + 2\beta G_7(t) + \frac{2}{\beta}d_4\{\dot{G}_7(t) + t_o\ddot{G}_7(t)\} + \left(d_{17}E_1 + \frac{2}{\beta}d_{17}E_2\right)G_8(t) + \left(d_{19}E_1 + \frac{2}{\beta}E_2d_{19}\right)\dot{G}_8(t) + \dot{G}_{10}(t)d_5 + \frac{2}{\beta}\dot{G}_{11}(t)d_5 + \left(d_{20}E_1 + \frac{2}{\beta}d_{20}E_2\right)\dot{G}_{12}(t) + \left(d_{26}E_1 + \frac{2}{\beta}d_{26}E_2\right)Q_n(t) = 0 \quad (41f)$$

$$d_9\beta\dot{G}_1(t) + d_{22}D_0\dot{G}_4(t) + d_7\dot{G}_5(t) + d_{23}D_0\dot{G}_8(t) - \beta^2G_9(t) + d_8\dot{G}_9(t) + 2G_{10}(t)\beta + d_{21}G_{12}(s)D_0 + d_{24}\dot{G}_{12}(t) + d_{27}d_{12}D_0W_n(t) = 0 \quad (41g)$$

$$-d_9\beta\dot{G}_3(t) - d_{22}D_2\dot{G}_4(t) - d_7\dot{G}_7(t) - d_{23}D_2\dot{G}_8(t) + \beta^2G_{11}(t) - d_8\dot{G}_{11}(t) - d_{21}D_2G_{12}(t) - d_{24}\dot{G}_{12}(t)D_2 - d_{27}d_{12}E_2W_n(t) = 0 \quad (41h)$$

$$d_9\dot{G}_2(t)\beta + d_92\dot{G}_3(t) + \left(d_{22}D_1 + \frac{2}{\beta}d_{22}D_2\right)\dot{G}_4(t) + d_7\dot{G}_6(t) + \frac{2}{\beta^2}d_7\dot{G}_7(t) + \left(d_{23}D_1 + \frac{2}{\beta}d_{23}D_2\right)\dot{G}_8(t) - \beta^2G_{10}(t) + d_8\dot{G}_{10}(t) + 2\beta G_{11}(t) + \frac{2}{\beta}d_8\dot{G}_{11}(t) + \left(d_{21}D_1 + \frac{2}{\beta}d_{21}D_2\right)G_{12}(t) + \left(d_{24}D_1 + \frac{2}{\beta}d_{24}D_2\right)\dot{G}_{12}(t) = 0 \quad (41i)$$

where  $d_{10}$  to  $d_{27}$  are the coefficients of H-expansion and constant parameters presented

in the appendix. By taking the Laplace transform of (41a) and using three boundary conditions of (4) (for solid cylinder only second, fourth, and sixth boundary conditions are applicable), a system of algebraic equations is obtained and solved by the Cramer's methods in the Laplace domain, whereby the inverse Laplace transform the functions are transformed into the real time domain and finally  $G_{1n}(t)$  to  $G_{12n}(t)$  are calculated. In this process, it is necessary to consider the following points:

1. The initial conditions (5) are considered only for the general solutions and the initial conditions of  $G_{1n}(t)$  to  $G_{12n}(t)$  for the particular solutions are considered equal to zero.
2. Laplace transform of (41a) is in polynomial function form of the Laplace parameter  $s$  (not the Bessel functions form of  $s$ ). Therefore, the exact inverse Laplace transform is possible and somehow simple.
3. For the hollow cylinder, it is enough to include the second type of Bessel function  $Y(r)$  in sequence of particular solution as:

$$\begin{aligned}
 u^p(r,t) &= \sum_{n=1}^{\infty} \left\{ \left[ G_{1n}(t)J_1(\beta_n r) + G_{2n}(t)rJ_2(\beta_n r) \right] \right. \\
 &\quad \left. + \left[ G_{4n}(t)Y_1(\beta_n r) + G_{5n}(t)rY_2(\beta_n r) \right] \right. \\
 &\quad \left. + \left[ G_{6n}(t)r^2Y_3(\beta_n r) \right] \right. \\
 &\quad \left. + rG_{7n}(t) + r^2G_{8n}(t) \right\} \\
 T^p(r,t) &= \sum_{n=1}^{\infty} \left\{ \left[ G_{9n}(t)J_0(\beta_n r) + G_{10n}(t)rJ_1(\beta_n r) \right] \right. \\
 &\quad \left. + \left[ G_{11n}(t)r^2J_2(\beta_n r) \right] \right. \\
 &\quad \left. + \left[ G_{12n}(t)Y_0(\beta_n r) + G_{13n}(t)rY_1(\beta_n r) \right] \right. \\
 &\quad \left. + \left[ G_{14n}(t)r^2Y_2(\beta_n r) \right] \right. \\
 &\quad \left. + rG_{15n}(t) + r^2G_{16n}(t) \right\} \\
 p^p(r,t) &= \sum_{n=1}^{\infty} \left\{ \left[ G_{17n}(t)J_0(\beta_n r) + G_{18n}(t)rJ_1(\beta_n r) \right] \right. \\
 &\quad \left. + \left[ G_{19n}(t)r^2J_2(\beta_n r) \right] \right. \\
 &\quad \left. + \left[ G_{20n}(t)Y_0(\beta_n r) + G_{21n}(t)rY_1(\beta_n r) \right] \right. \\
 &\quad \left. + \left[ G_{22n}(t)r^2Y_2(\beta_n r) \right] \right. \\
 &\quad \left. + rG_{23n}(t) + r^2G_{24n}(t) \right\}
 \end{aligned} \tag{42}$$

By substituting (41a) in (1)–(3), 18 equations are obtained, where using the six boundary conditions (4) 24 functions  $G_{1n}(t)$  to  $G_{24n}(t)$  are obtained for the hollow cylinder.

## Results and Discussions

As an example, a solid cylinder with  $r_i = 0$ ,  $r_o = 1$  m is considered. The material properties are listed in Table 1.

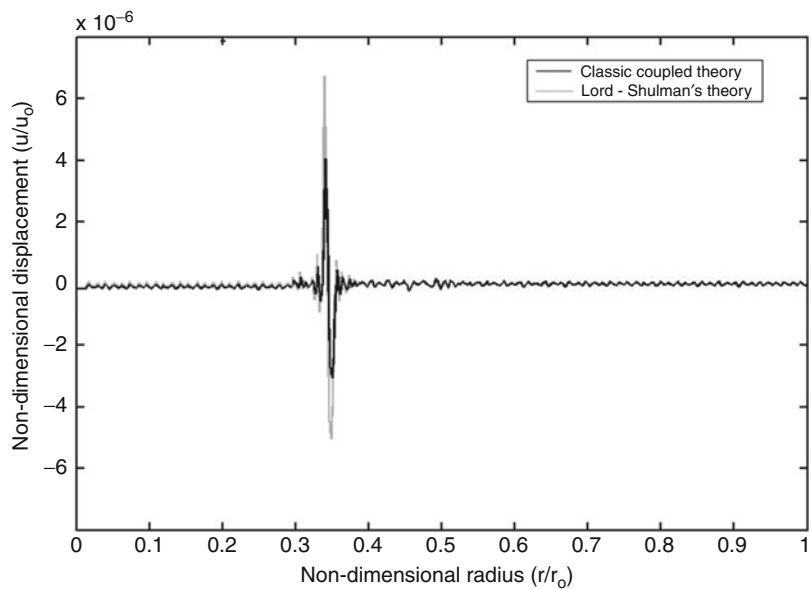
To give a clear explanation, numerical results have been considered and the radial distributions of displacement, temperature, and pressure for two cases (Classic coupled theory and Lord-Shulman's theory) computed. An instantaneous hot spot  $T(1,t) = 10^{-3}T_o\delta(t)$ , where  $\delta(t)$  is unit dirac function, is considered and the outside radius of the cylinder is assumed to be fixed ( $u(1,t) = 0$ ). For plotting the graphs a nondimensional time  $\hat{t} = \frac{vt}{r_o}$  is considered

where  $v = \sqrt{\frac{E(1-\nu)}{\rho(1+\nu)(1-2\nu)}}$  is the dilatational wave velocity. Figures 1–3 show the wave front for the displacement, temperature, and pressure (Classic coupled theory and Lord-Shulman's theory). As a second example, mechanical shock wave is applied to the outside surface of the cylinder given as  $u(1,t) = 10^{-12}u_o\delta(t)$ , and the surface is assumed to be at zero temperature ( $T(1,t) = 0$ ). Figures 4–6 show the wave fronts for the displacement and temperature distributions versus the nondimensional radius (Classic coupled theory and Lord-Shulman's theory). The convergence of the solutions for these examples is achieved by consideration of 1,200 eigenvalues used for the H-Fourier expansion. Choosing more than this number for eigenvalues, the increase in round-off and truncation errors can affect the quality of the graphs. The convergence of the solution is better for the displacement result in comparison with the temperature. The small oscillations in Figs. 3 and 5 are due to the convergence errors of solutions.

**Exact Solution for Lord-Shulman Generalized Coupled Thermoporoelasticity in Cylindrical Coordinates, Table 1** Material parameters

Material parameters					
Parameters	Value	Unit	Parameters	Value	Unit
$t_o$	$1 \times 10^{-5}$	—	$\alpha_s$	$1.5 \times 10^{-5}$	$1/^\circ\text{C}$
$E$	$6 \times 10^5$	Pa	$\alpha_w$	$2 \times 10^{-4}$	$1/^\circ\text{C}$
$\nu$	0.3	—	$c_s$	0.8	$\text{J/g}\cdot^\circ\text{C}$
$T_o$	293	$^\circ\text{K}$	$c_w$	4.2	$\text{J/g}\cdot^\circ\text{C}$
$K_s$	$2 \times 10^{10}$	Pa	$\rho_s$	$2.6 \times 10^6$	$\text{g/m}^3$
$K_w$	$5 \times 10^9$	Pa	$\rho_w$	$1 \times 10^6$	$\text{g/m}^3$
$K$	$5 \times 10^9$	$\text{W/m}\cdot^\circ\text{C}$	$\alpha$	1	—

**Exact Solution for Lord-Shulman Generalized Coupled Thermoporoelasticity in Cylindrical Coordinates, Fig. 1** Nondimensional displacement distribution due to input  $T(1, t) = 10^{-3}T_0\delta(t)$  at nondimensional time  $\hat{t} = 0.65$



## Conclusion

In this entry, an analytical solution for the generalized coupled thermoporoelasticity of thick cylinders under radial temperature is presented. Figures 1–6 show relaxation time effect on variation of displacement, temperature, and pressure.

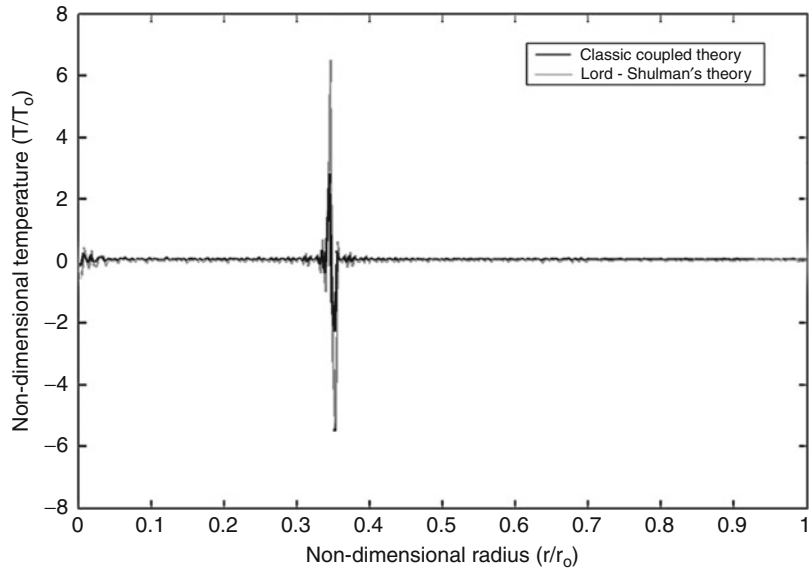
It is observed that the peak value of Lord-Shulman's theory for displacement, temperature, and pressure increases. The method is based on

the eigenfunctions Fourier expansion, which is a classical and traditional method of solution of the typical initial and boundary value problems. The noncompetitive strength of this method is its ability to reveal the fundamental mathematical and physical properties and interpretations of the problem under studying. In the generalized coupled thermoporoelastic problem of radial-symmetric cylinder, the governing equations constitute a system of partial differential

**Exact Solution for Lord-Shulman Generalized Coupled**

**Thermoporoelasticity in Cylindrical Coordinates,**

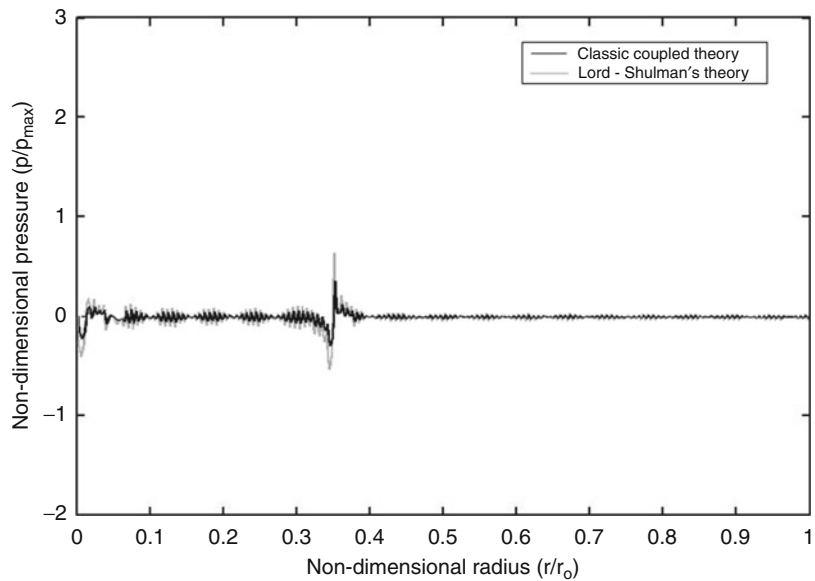
**Fig. 2** Nondimensional temperature distribution due to input  $T(1, t) = 10^{-3}T_0\delta(t)$  at nondimensional time  $\hat{t} = 0.65$



**Exact Solution for Lord-Shulman Generalized Coupled**

**Thermoporoelasticity in Cylindrical Coordinates,**

**Fig. 3** Nondimensional pressure distribution due to input  $T(1, t) = 10^{-3}T_0\delta(t)$  at nondimensional time  $\hat{t} = 0.65$



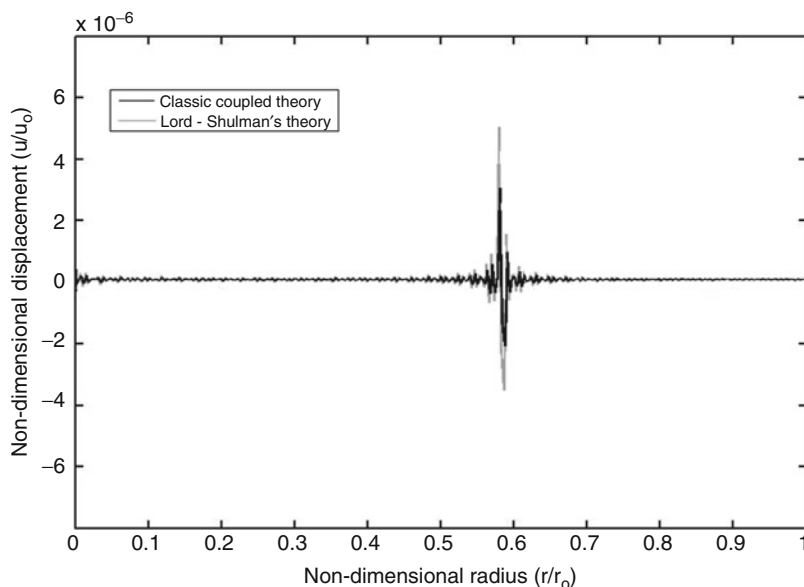
equations with two independent variables, radius ( $r$ ) and time ( $t$ ). The traditional procedure to solve this class of problems is to eliminate the time variable by using the Laplace transform. The resulting system is a set of ordinary differential equations in terms of the radius variable, whose

solution falls in the Bessel functions family. This method of the analysis brings the Laplace parameter ( $s$ ) in the argument of the Bessel functions, causing hardship or difficulties in carrying out the exact inverse of the Laplace transformation. As a result, the numerical inversion of

### Exact Solution for Lord-Shulman Generalized Coupled Thermoporoelasticity in Cylindrical Coordinates,

#### Fig. 4 Nondimensional displacement distribution due to input

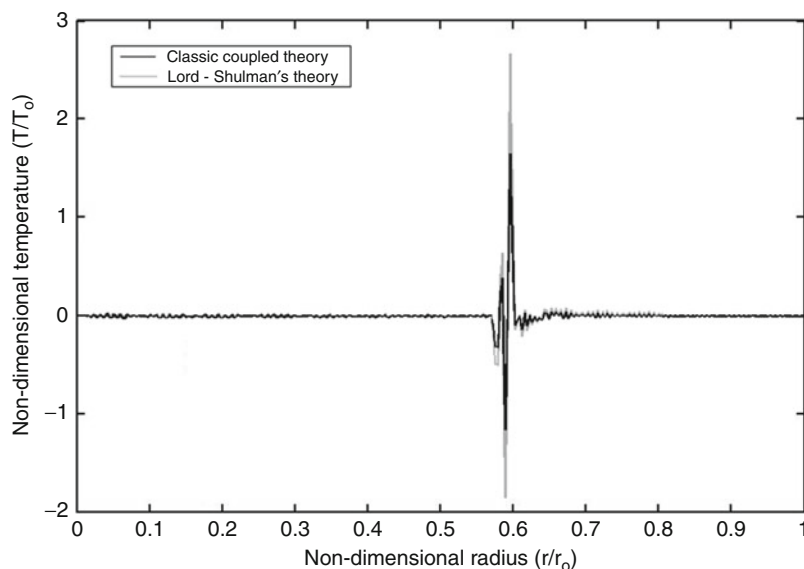
$u(1, t) = 10^{-12} u_0 \delta(t)$   
at nondimensional time  $\hat{t} = 0.4$



### Exact Solution for Lord-Shulman Generalized Coupled Thermoporoelasticity in Cylindrical Coordinates,

#### Fig. 5 Nondimensional temperature distribution due to input

$u(1, t) = 10^{-12} u_0 \delta(t)$   
at nondimensional time  $\hat{t} = 0.4$

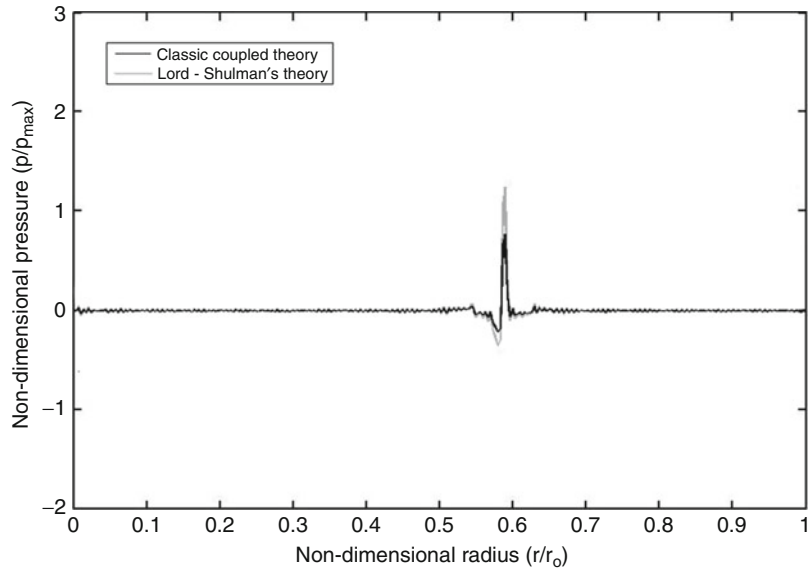


the Laplace transformation is used in the papers dealing with this type of problems in literature. In the present paper, to prevent this problem, when the Laplace transform is applied to the particular solutions, it is postponed after

eliminating the radius variable  $r$  by H-Fourier expansion. Thus, the Laplace parameter ( $s$ ) appears in polynomial function forms and hence the exact Laplace inversion transformation is possible.

### Exact Solution for Lord-Shulman Generalized Coupled Thermoporoelasticity in Cylindrical Coordinates,

**Fig. 6** Nondimensional pressure distribution due to input  $u(1, t) = 10^{-12} u_0 \delta(t)$  at nondimensional time  $\hat{t} = 0.4$



## References

1. Hetnarski RB, Eslami MR (2009) Thermal stresses – advanced theory and applications. Springer, New York
2. Lord HW, Shulman Y (1967) A generalized dynamical theory of thermoelasticity. *J Mech Phys Solid* 15:299–309
3. Green AE, Lindsay KA (1972) Thermoelasticity. *J Elast* 2:1–7
4. Green AE, Naghdi PM (1972) Thermoelasticity without energy dissipation. *J Elast* 2:1–7
5. Youssef HM (2006) Theory of generalized porothermoelasticity. *J Rock Mech Min* 44:222–227
6. Bai B (2006) Response of saturated porous media subjected to local thermal loading on the surface of semi-infinite space. *Acta Mech Sinica* 22:54–61
7. Bai B (2006) Fluctuation responses of saturated porous media subjected to cyclic thermal loading. *Comput Geotech* 33:396–403
8. Droujinine A (2006) Generalized an elastic asymptotic Ray theory. *Wave Motion* 43:357–367
9. Bai B, Li T (2009) Solution for cylindrical cavity in saturated thermoporoelastic medium. *J Acta Mech Sinica* 22:85–92
10. Hetnarski RB (1964) Solution of the coupled problem of thermoelasticity in the form of series of functions. *J Arch Mech Stos* 16:919–941
11. Hetnarski RB, Ignaczak J (1993) Generalized thermoelasticity: closed-form solutions. *J Therm Stress* 16:473–498
12. Hetnarski RB, Ignaczak J (1994) Generalized thermoelasticity: response of semi-space to a shortlaser pulse. *J Therm Stress* 17:377–396
13. Georgiadis HG, Lykotrafitis G (2005) Rayleigh waves generated by a thermal source: a three dimensional transient thermoelasticity solution. *J Appl Mech* 72:129–138
14. Wagner P (1994) Fundamental matrix of the system of dynamic linear thermoelasticity. *J Therm stress* 17:549–565
15. Jabbari M, Dehbani H (2011) An exact solution for Lord-Shulman generalized coupled thermoporoelasticity in cylindrical coordinates. In: Ninth international congress on thermal stress, Budapest
16. Jabbari M, Dehbani H, Eslami MR (2009) An exact solution for classic coupled thermoelasticity in spherical coordinates. *J Pres Ves ASME Trans* 132:031201–031211
17. Jabbari M, Dehbani H (2009) An exact solution for classic coupled thermoporoelasticity in cylindrical coordinates. *J Solid Mech* 1:343–357
18. Jabbari M, Dehbani H, Eslami MR (2011) An exact solution for classic coupled thermoelasticity in cylindrical coordinates. *J Pres Ves Technol ASME* 133:05120401–05120410
19. Jabbari M, Dehbani H, Eslami MR (2011) An exact solution for classic coupled thermoelasticity in cylindrical coordinates. *ASME J Pres Ves Technol* 133:051204–051210



## Exact Solution for Lord-Shulman Generalized Coupled Thermoporoelasticity in Spherical Coordinates

Mohsen Jabbari<sup>1</sup> and H. Dehbani<sup>2</sup>

<sup>1</sup>Faculty of Engineering, Postgraduate School, South Tehran Branch, Islamic Azad University, Tehran, Iran

<sup>2</sup>Postgraduate School, South Tehran Branch, Islamic Azad University, Tehran, Iran

### Overview

In this entry, the generalized coupled thermoporoelasticity model of hollow and solid spheres under radial-symmetric loading condition ( $r, t$ ) is considered. A full analytical method is used and an exact unique solution of the generalized coupled equations is presented.

The thermal, mechanical, and pressure boundary conditions, the body force, the heat source, and the injected volume rate per unit volume of a distribute water source are considered in the most general forms and where no limiting assumption is used. This generality allows the simulation of varieties of applicable problems.

### Introduction

The classical theory of thermoelasticity is based on the conventional heat conduction equation. The conventional heat conduction theory assumes that the thermal disturbances propagate at infinite speeds. This prediction is unrealistic from a physical point of view, particularly in simulations like those involving very short transient duration, sudden high heat flux situations, and/or for very low temperatures near the absolute zero [1]. Thus, some modified dynamic thermoelastic models are proposed to analyze the problems with the second sound effects, such as the Lord-Shulman (LS) [2], the Green-Lindsay [3], and the Green-Naghdi [4] theories.

These nonclassical theories are referred to as the generalized thermoelasticity theories with finite thermal wave speed, or thermoelasticity with the second sound effect. For the generalized thermoporoelasticity problems, coupled thermal and poromechanical processes play an important role in a number of problems of interest in the geomechanics such as stability of boreholes and permeability enhancement in geothermal reservoirs.

A thermoporoelastic approach combines the theory of heat conduction with poroelastic constitutive equations and coupling the temperature field with the stresses and pore pressure.

There are a limited numbers of papers that present the closed-form or analytical solution for the coupled porothermoelasticity problems. H.M. Youssef [5] derived the governing equations, which describe the behavior of thermoelastic porous medium in the context of the theory of generalized thermoelasticity with one relaxation time (Lord-Shulman). Bai [6] investigated the response of saturated porous media subjected to local thermal loading on the surface of semi-infinite space. He used the numerical integral methods for calculating the unsteady temperature, pore pressure, and displacement fields. This author also studied the fluctuation responses of saturated porous media subjected to cyclic thermal loading [7]. In the mentioned paper, an analytical solution was deduced proposed by using the Laplace transform and the Gauss-Legendre method and Laplace transform inversion. Droujinine [8] investigated dispersion and attenuation of body waves in a wide range of materials representing realistic rock structures. He used the time-domain asymptotic ray theory to a new generalized coordinate-free wave equation with an arbitrary tensor relaxation function. Bai and Li [9] found a solution for cylindrical cavity in saturated thermoporoelastic medium by using Laplace transform and numerical Laplace transform inversion.

The number of papers that present the closed-form or analytical solution for the coupled thermoelasticity problems is also limited. Hetnarski [10] found the solution of the coupled thermoelasticity in the form of a series of

functions. Hetnarski and Ignaczak presented a study of the one-dimensional thermoelastic waves produced by an instantaneous plane source of heat in homogeneous isotropic infinite and semi-infinite bodies of the Green-Lindsay type [11]. Also, these authors presented an analysis for laser-induced waves propagating in an absorbing thermoelastic semi-space of the Green-Lindsay theory [12]. Georgiadis and Lykotrafitis obtained a three-dimensional transient thermoelastic solution for Rayleigh-type disturbances propagating on the surface of a half-space [13]. Wagner [14] presented the fundamental matrix of a system of partial differential operators that governs the diffusion of heat and the strains in elastic media. This method can be used to predict the temperature distribution and the strains by an instantaneous point heat, point source of heat, or by a suddenly applied delat force.

In the present [15] a full analytical method is used to obtain the response of the governing equations, an exact solution is presented. The method of solution is based on the Fourier's expansion and eigenfunction methods, which are traditional and routine methods in solving the partial differential equations. Since the coefficients of equations are not functions of the time variable ( $t$ ), an exponential form is considered for the general solution matched with the physical wave properties of thermal and mechanical waves. For the particular solution, that is the response to mechanical and thermal shocks, the eigenfunction method and Laplace transformation is used. This work is following the previous works for coupled problems [16–19].

## Governing Equations

A hollow sphere with inner and outer radii,  $r_i$  and  $r_o$ , respectively, made of isotropic material subjected to radial-symmetric mechanical, thermal, and pressure shocks, is considered.

The generalized coupled thermoelastic equations of the sphere, with plane stress assumption, based in LS theory is obtained from [1] as:

$$\begin{aligned} u_{,rr} + \frac{2}{r}u_{,r} - \frac{2}{r^2}u - \alpha \frac{(1+\nu)(1-2\nu)}{(1-\nu)E}p_{,r} \\ - \beta \frac{(1+\nu)(1-2\nu)}{(1-\nu)E}T_{,r} - \rho \frac{(1+\nu)(1-2\nu)}{(1-\nu)E} \\ \ddot{u} = - \frac{(1+\nu)(1-2\nu)}{(1-\nu)E}F(r, t) \end{aligned} \quad (1)$$

Heat conduction equation in radial-symmetric direction with the mechanical and pressure coupling term is:

$$\begin{aligned} T_{,rr} + \frac{2}{r}T_{,r} - Z\frac{T_o}{K}(\dot{T} + t_0\ddot{T}) + Y\frac{T_o}{K}\dot{p} \\ - \beta\frac{T_o}{K}\left(t_0\left(\ddot{u}_{,r} + \frac{2}{r}\ddot{u}\right) + \dot{u}_{,r} + \frac{2}{r}\dot{u}\right) \\ = -\frac{1}{K}Q(r, t) \end{aligned} \quad (2)$$

According to Darcy's law and continuity condition of seepage, the equation of mass conservation can be written as:

$$\begin{aligned} p_{,rr} + \frac{2}{r}p_{,r} - \alpha_p\frac{\gamma_w}{k}\dot{p} - Y\frac{\gamma_w}{k}\dot{T} \\ - \alpha\frac{\gamma_w}{k}\left(\dot{u}_{,r} + \frac{2}{r}\dot{u}\right) = -\frac{\gamma_w}{k}W(r, t) \end{aligned} \quad (3)$$

where  $(\cdot)$  denotes partial derivative,  $u$  is the displacement component in the radial direction,  $p$  is the pore pressure,  $\rho$  is bulk mass density,  $\alpha = 1 - \frac{C_s}{C}$  is the Biot's coefficient,  $t_0$  is relaxation time,  $C_s = 3(1 - 2\nu_s)E_s$  is the coefficient of volumetric compression of the solid grains, with  $E_s$  and  $\nu_s$  being the elastic modulus and Poisson's ratio of solid grains and  $C = 3(1 - 2\nu)E$  is the coefficient of volumetric compression of solid skeleton, with  $E$  and  $\nu$  being the elastic modulus and Poisson's ratio of solid skeleton,  $T_o$  is initial reference temperature,  $\beta = \frac{3\alpha_s}{C}$  is the thermal expansion factor,  $\alpha_s$  is the coefficient of linear thermal expansion of solid grains,  $Y = 3(n\alpha_w + (\alpha - n)\alpha_s)$  and  $\alpha_p = n(C_w - C_s) + \alpha C_s$  are coupling parameters,  $\alpha_w$  and  $C_w$  are the coefficients of linear thermal expansion and volumetric compression of pure water,

$n$  is the porosity,  $k$  is the hydraulic conductivity,  $\gamma_w$  is the unit of pore water and  $Z = \frac{(1-n)\rho_s c_s + n\rho_w c_w}{T_0} - 3\beta\alpha_s$  is coupling parameter,  $\rho_w$  and  $\rho_s$  are the densities of pore water and solid grains and  $c_w$  and  $c_s$  are the heat capacities of pore water and solid grains and  $K$  is the coefficient of heat conductivity. Here,  $F(r, \psi t)$ ,  $Q(r, \psi t)$ , and  $W(r, \psi t)$  are the body force, heat generation, and the injected volume rate per unit volume of a distribute water source, respectively. The mechanical, thermal, and pressure boundary conditions are:

$$\begin{aligned} C_{11}u(r_i, t) + C_{12}u_r(r_i, t) + C_{13}T(r_i, t) + C_{14}p(r_i, t) &= f_1(t) \\ C_{21}u(r_o, t) + C_{22}u_r(r_o, t) + C_{23}T(r_o, t) + C_{24}p(r_o, t) &= f_2(t) \\ C_{31}T(r_i, t) + C_{32}T_r(r_i, t) &= f_3(t) \\ C_{41}T(r_o, t) + C_{42}T_r(r_o, t) &= f_4(t) \\ C_{51}p(r_i, t) &= f_5(t) \\ C_{61}p(r_o, t) &= f_6(t) \end{aligned} \quad (4)$$

where  $C_{ij}$  are the mechanical, thermal, and pressure coefficients, and by assigning different values for them, different types of mechanical, thermal, and pressure boundary conditions may be obtained. These boundary conditions include the displacement, strain, stress (for the first and second boundary conditions), specified temperature, convection, heat flux condition (for the third and forth boundary conditions), and pressure (for the fifth and sixth boundary conditions).  $f_1(r)$  to  $f_6(r)$  are arbitrary functions which show mechanical, thermal, and pressure shocks, respectively. The initial boundary conditions are assumed in the following general form:

$$\begin{aligned} u(r, 0) &= f_7(r) \\ u_t(r, 0) &= f_8(r) \\ T(r, 0) &= f_9(r) \\ T_t(r, 0) &= f_{10}(r) \\ p(r, 0) &= f_{11}(r) \end{aligned} \quad (5)$$

where  $f_7(r)$  to  $f_{10}(r)$  are arbitrary functions which show initial distributions of displacement, temperature, and pressure, respectively.

## Solution

Equations (1)–(3) are the system of nonhomogeneous partial differential equations with nonconstant coefficients (functions of radius variable  $r$  only) has general and particular solutions.

### General Solution with Homogeneous Boundary Conditions

Since the coefficients of these equations are independent of time variable ( $t$ ), the exponential function form of time variable may be assumed for the general solution as:

$$\begin{aligned} u(r, t) &= [U^*(r)]e^{\lambda t} \\ T(r, t) &= [\theta^*(r)]e^{\lambda t} \\ p(r, t) &= [P^*(r)]e^{\lambda t} \end{aligned} \quad (6)$$

Substituting (6) into homogeneous parts of (1)–(3) yields:

$$\begin{aligned} U^{*''} + \frac{2}{r}U^{*'} - \frac{2}{r^2}U^* + d_1P^{*'} + d_2\theta^{*'} \\ + d_3\lambda^2 U^* &= 0 \\ \theta^{*''} + \frac{2}{r}\theta^{*'} + d_4(\lambda + t_0\lambda^2)\theta^* + d_5\lambda P^* \\ + d_6(\lambda + t_0\lambda^2)\left(U^{*'} + \frac{2}{r}U^*\right) &= 0 \\ P^{*''} + \frac{2}{r}P^{*'} + d_7\lambda P^* + d_8\lambda\theta^* \\ + d_9\lambda\left(U^{*'} + \frac{2}{r}U^*\right) &= 0 \end{aligned} \quad (7)$$

Equation (7) are system of ordinary differential equations, where the prime symbol ( $'$ ) shows differentiation with respect to the radius variable ( $r$ ) and  $d_1$  to  $d_9$  are constant parameters given in the appendix.

### Change in Dependent Variables

To obtain a solution for (7), the dependent variables are changed as:

$$\begin{aligned} U^*(r) &= r^{-\frac{1}{2}}U(r) \\ \theta^*(r) &= r^{-\frac{1}{2}}\theta(r) \\ P^*(r) &= r^{-\frac{1}{2}}P(r) \end{aligned} \quad (8)$$

Substituting (8) into (7) gives:

$$\begin{aligned}
 U'' + \frac{1}{r}U' - \frac{9}{4}\frac{1}{r^2}U + d_3\lambda^2U - d_2\frac{1}{2}\frac{1}{r}\theta \\
 + d_2\theta' - d_1\frac{1}{2}\frac{1}{r}P + d_1P' = 0 \\
 \theta'' + \frac{1}{r}\theta' - \frac{1}{4}\frac{1}{r^2}\theta + d_4(\lambda + t_o\lambda^2)\theta \\
 + d_6(\lambda + t_o\lambda^2)\frac{3}{2}\frac{1}{r}U + d_6(\lambda + t_o\lambda^2)U' + d_5\lambda P = 0 \\
 P'' + \frac{1}{r}P' - \frac{1}{4}\frac{1}{r^2}P + d_7\lambda P + d_8\lambda\theta \\
 + d_9\lambda\frac{3}{2}\frac{1}{r}U + d_9\lambda U' = 0
 \end{aligned} \quad (9)$$

### Solution

The first solutions of  $U_1$ ,  $\theta_1$  and  $P_1$  are considered as:

$$\begin{aligned}
 U_1(r) &= A_1 J_{\frac{3}{2}}(\beta r) \\
 \theta_1(r) &= B_1 J_{\frac{1}{2}}(\beta r) \\
 P_1(r) &= C_1 J_{\frac{1}{2}}(\beta r)
 \end{aligned} \quad (10)$$

Substituting (10) into (9) yields:

$$\begin{aligned}
 \{(-\beta^2 + \lambda^2 d_3)A_1 - d_2\beta B_1 - d_1\beta C_1\}J_{\frac{3}{2}}(\beta r) &= 0 \\
 \{(\lambda + t_o\lambda^2)d_6\beta A_1 + (-\beta^2 + (\lambda + t_o\lambda^2)d_4)B_1 \\
 + \lambda d_5 C_1\}J_{\frac{1}{2}}(\beta r) &= 0 \\
 \{\lambda d_9\beta A_1 + \lambda d_8 B_1 + (-\beta^2 + \lambda d_7)C_1\}J_{\frac{1}{2}}(\beta r) &= 0
 \end{aligned} \quad (11)$$

Equation (11) shows that  $U_1$ ,  $\theta_1$ , and  $P_1$  can be the solutions of (9), if and only if:

$$\begin{bmatrix}
 -\beta^2 + \lambda^2 d_3 & -d_2\beta & -d_1\beta \\
 (\lambda + t_o\lambda^2)d_6\beta - \beta^2 + (\lambda + t_o\lambda^2)d_4 & \lambda d_5 & \\
 \lambda d_9\beta & \lambda d_8 & -\beta^2 + \lambda d_7
 \end{bmatrix}
 \begin{Bmatrix}
 A_1 \\
 B_1 \\
 C_1
 \end{Bmatrix}
 =
 \begin{Bmatrix}
 0 \\
 0 \\
 0
 \end{Bmatrix} \quad (12)$$

The nontrivial solution of (12) is obtained by equating the determinant of this equation to zero as:

$$\begin{aligned}
 d_3 d_4 d_7 (\lambda + t_o\lambda^2) \lambda^3 - d_3 d_5 d_8 \lambda^4 - \beta^2 d_3 d_4 (\lambda + t_o\lambda^2) \lambda^2 \\
 - \beta^2 d_3 d_7 \lambda^3 - \beta^2 d_4 d_7 (\lambda + t_o\lambda^2) \lambda + \beta^2 d_5 d_8 \lambda^2 \\
 + \beta^2 d_1 d_4 d_9 (\lambda + t_o\lambda^2) \lambda - \beta^2 d_1 d_6 d_8 (\lambda + t_o\lambda^2) \lambda \\
 + \beta^2 d_2 d_6 d_7 (\lambda + t_o\lambda^2) \lambda - \beta^2 d_2 d_5 d_9 \lambda^2 + \beta^4 d_3 \lambda^2 \\
 + \beta^4 d_4 (\lambda + t_o\lambda^2) + \beta^4 d_7 \lambda - \beta^4 d_2 d_6 (\lambda + t_o\lambda^2) \\
 - \beta^4 d_1 d_9 \lambda - \beta^6 = 0
 \end{aligned} \quad (13)$$

Equation (13) is the first characteristic equation. Thus, it is concluded that  $U_1$ ,  $\theta_1$ , and  $P_1$  satisfy the system of (9) and they are the first solution of the system.

The second solutions of  $U_2$ ,  $\theta_2$ , and  $P_2$  are considered as:

$$\begin{aligned}
 U_2(r) &= [A_2 J_{\frac{3}{2}}(\beta r) + A_3 r J_{\frac{3}{2}}(\beta r)] \\
 \theta_2(r) &= [B_2 J_{\frac{1}{2}}(\beta r) + B_3 r J_{\frac{1}{2}}(\beta r)] \\
 P_2(r) &= [C_2 J_{\frac{1}{2}}(\beta r) + C_3 r J_{\frac{1}{2}}(\beta r)]
 \end{aligned} \quad (14)$$

Substituting (14) into (9) yields:

$$\begin{aligned}
 \{(\beta^2 - d_3\lambda^2)A_3 + C_3 d_1\beta + B_3 d_2\beta\}r J_{\frac{1}{2}}(\beta r) \\
 + \left\{ -A_3\beta + A_2 d_3\lambda^2 - A_2\beta^2 - C_3 d_1 - B_3 d_2 - B_2 d_2\beta - C_2 d_1\beta + A_3 d_3\lambda^2 \frac{3}{\beta} \right\} J_{\frac{3}{2}}(\beta r) &= 0 \\
 \{-B_2\beta^2 + 2B_3\beta + B_2 d_4(\lambda + t_o\lambda^2) + A_2 d_6\beta(\lambda + t_o\lambda^2) + C_2 d_5\lambda\}J_{\frac{1}{2}}(\beta r) \\
 + \{A_3 d_6\beta(\lambda + t_o\lambda^2) + (-\beta^2 + d_4(\lambda + t_o\lambda^2))B_3 + C_3 d_5\lambda\}r J_{\frac{3}{2}}(\beta r) &= 0 \\
 \{2C_3\beta + C_2 d_7\lambda + B_2 d_8\lambda + A_2 d_9\lambda\beta - C_2\beta^2\}J_{\frac{1}{2}}(\beta r) \\
 + \{A_3 d_9\lambda\beta + B_3 d_8\lambda + (-\beta^2 + d_7\lambda)C_3\}r J_{\frac{3}{2}}(\beta r) &= 0
 \end{aligned} \quad (15)$$

The expressions for  $U_2$ ,  $\theta_2$ , and  $P_2$  can be the solutions of (9), if and only if:

$$\begin{bmatrix} -\beta^2 + \lambda^2 d_3 & -d_2 \beta & -d_1 \beta \\ (\lambda + t_o \lambda^2) d_6 \beta & -\beta^2 + (\lambda + t_o \lambda^2) d_4 & \lambda d_5 \\ \lambda d_9 \beta & \lambda d_8 & -\beta^2 + \lambda d_7 \end{bmatrix}$$

$$\begin{Bmatrix} A_3 \\ B_3 \\ C_3 \end{Bmatrix} = \begin{Bmatrix} 0 \\ 0 \\ 0 \end{Bmatrix} \quad (16)$$

$$(d_3 \lambda^2 - \beta^2) A_2 + \left( d_3 \lambda^2 \frac{3}{\beta} - \beta \right) A_3 - d_2 \beta B_2 - d_2 B_3 - d_1 \beta C_2 - d_1 C_3 = 0 \quad (17)$$

$$d_6 (\lambda + t_o \lambda^2) \beta A_2 + (-\beta^2 + d_4 (\lambda + t_o \lambda^2)) B_2 + 2\beta B_3 + d_5 \lambda C_2 = 0 \quad (18)$$

$$d_9 \lambda \beta A_2 + d_8 \lambda B_2 + (d_7 \lambda - \beta^2) C_2 + 2\beta C_3 = 0 \quad (19)$$

The nontrivial solution of (16) is obtained by equating the determinant to zero as:

$$\begin{aligned} & d_3 d_4 d_7 (\lambda + t_o \lambda^2) \lambda^3 - d_3 d_5 d_8 \lambda^4 - \beta^2 d_3 d_4 (\lambda + t_o \lambda^2) \lambda^2 \\ & - \beta^2 d_3 d_7 \lambda^3 - \beta^2 d_4 d_7 (\lambda + t_o \lambda^2) \lambda + \beta^2 d_5 d_8 \lambda^2 \\ & + \beta^2 d_1 d_4 d_9 (\lambda + t_o \lambda^2) \lambda - \beta^2 d_1 d_6 d_8 (\lambda + t_o \lambda^2) \lambda \\ & + \beta^2 d_2 d_6 d_7 (\lambda + t_o \lambda^2) \lambda - \beta^2 d_2 d_5 d_9 \lambda^2 + \beta^4 d_3 \lambda^2 \\ & + \beta^4 d_4 (\lambda + t_o \lambda^2) + \beta^4 d_7 \lambda - \beta^4 d_2 d_6 (\lambda + t_o \lambda^2) \\ & - \beta^4 d_1 d_9 \lambda - \beta^6 = 0 \end{aligned} \quad (20)$$

Equations (17)–(19) give the relations between  $A_2, A_3, B_2, B_3, C_2$  and  $C_3$  and they play as the balancing ratios that make (14) to be the second solution of the system of (9).

The third solution of the system of the ordinary differential equations with nonconstant coefficients (9) must be considered as:

$$\begin{aligned} U_3(r) &= [A_4 J_{\frac{3}{2}}(\beta r) + A_5 r J_{\frac{3}{2}}(\beta r) + A_6 r^2 J_{\frac{3}{2}}(\beta r)] \\ \theta_3(r) &= [B_4 J_{\frac{3}{2}}(\beta r) + B_5 r J_{\frac{3}{2}}(\beta r) + B_6 r^2 J_{\frac{3}{2}}(\beta r)] \\ P_3(r) &= [C_4 J_{\frac{3}{2}}(\beta r) + C_5 r J_{\frac{3}{2}}(\beta r) + C_6 r^2 J_{\frac{3}{2}}(\beta r)] \end{aligned} \quad (21)$$

Substituting (21) into (9) yields:

$$\begin{aligned} & \left\{ \begin{aligned} & (-\beta^2 + d_3 \lambda^2) A_4 + \left( -\beta + d_3 \lambda^2 \frac{3}{\beta} \right) A_5 + \left( -3 + d_3 \lambda^2 \frac{15}{\beta^2} \right) A_6 \\ & - B_4 d_2 \beta - d_2 B_5 - 3 d_2 \frac{1}{\beta} B_6 - C_4 \beta d_1 - \frac{3}{2} C_5 d_1 - C_6 \frac{3}{\beta} d_1 \end{aligned} \right\} J_{\frac{3}{2}}(\beta r) = 0 \\ & \{ (\beta^2 - d_3 \lambda^2) A_6 + C_6 \beta d_1 + B_6 d_2 \beta \} r^2 J_{\frac{3}{2}}(\beta r) = 0 \\ & \left\{ \begin{aligned} & (\beta^2 - d_3 \lambda^2) A_5 + \left( \beta - \frac{5}{\beta} d_3 \lambda^2 \right) A_6 + B_5 d_2 \beta + d_2 B_6 + C_5 \beta d_1 \\ & + C_6 \frac{3}{2} d_1 - \frac{1}{2} C_6 d_1 \end{aligned} \right\} r J_{\frac{3}{2}}(\beta r) = 0 \\ & \{ d_6 (\lambda + t_o \lambda^2) \beta A_4 + (-\beta^2 + d_4 (\lambda + t_o \lambda^2)) B_4 + 2\beta B_5 + d_5 \lambda C_4 \} J_{\frac{3}{2}}(\beta r) = 0 \\ & \{ -d_6 (\lambda + t_o \lambda^2) \beta A_6 + (\beta^2 - d_4 (\lambda + t_o \lambda^2)) B_6 - d_5 \lambda C_6 \} r^2 J_{\frac{3}{2}}(\beta r) = 0 \\ & \left\{ \begin{aligned} & d_6 (\lambda + t_o \lambda^2) \beta A_5 + 3 d_6 (\lambda + t_o \lambda^2) A_6 + (d_4 (\lambda + t_o \lambda^2) - \beta^2) B_5 \\ & + \left( d_4 \frac{3}{\beta} (\lambda + t_o \lambda^2) + \beta \right) B_6 + d_5 \lambda C_5 + d_5 \frac{3}{\beta} \lambda C_6 \end{aligned} \right\} r J_{\frac{3}{2}}(\beta r) = 0(2) \\ & \{ +d_9 \lambda A_4 \beta + d_8 \lambda B_4 + (-\beta^2 + d_7 \lambda) C_4 + 2 C_5 \beta \} J_{\frac{3}{2}}(\beta r) = 0 \\ & \{ (-d_7 \lambda + \beta^2) C_6 - d_8 \lambda B_6 - d_9 \lambda A_6 \beta \} r^2 J_{\frac{3}{2}}(\beta r) = 0 \\ & \left\{ \begin{aligned} & (-\beta^2 + d_7 \lambda) C_5 + \left( \beta + d_7 \lambda \frac{3}{\beta} \right) C_6 + d_8 \lambda B_5 \\ & + d_8 \frac{3}{\beta} \lambda B_6 + d_9 \lambda \beta A_5 + 3 d_9 \lambda A_6 \end{aligned} \right\} r J_{\frac{3}{2}}(\beta r) = 0 \end{aligned} \quad (22)$$

The expressions for  $U_3$ ,  $\theta_3$  and  $P_3$  can be solutions of (9), if and only if:

$$\begin{bmatrix} -\beta^2 + \lambda^2 d_3 & -d_2 \beta & -d_1 \beta \\ (\lambda + t_o \lambda^2) d_6 \beta & -\beta^2 + (\lambda + t_o \lambda^2) d_4 & \lambda d_5 \\ \lambda d_9 \beta & \lambda d_8 & -\beta^2 + \lambda d_7 \end{bmatrix} \begin{Bmatrix} A_6 \\ B_6 \\ C_6 \end{Bmatrix} = \begin{Bmatrix} 0 \\ 0 \\ 0 \end{Bmatrix} \quad (23)$$

$$\begin{aligned} & (-\beta^2 + d_3 \lambda^2) A_4 + \left( -\beta + d_3 \lambda^2 \frac{3}{\beta} \right) A_5 \\ & + \left( -3 + d_3 \lambda^2 \frac{15}{\beta^2} \right) A_6 - B_4 d_2 \beta - d_2 B_5 \\ & - 3 d_2 \frac{1}{\beta} B_6 - C_4 \beta d_1 - \frac{3}{2} C_5 d_1 - C_6 \frac{3}{\beta} d_1 = 0 \end{aligned} \quad (24)$$

$$\begin{aligned} & (\beta^2 - d_3 \lambda^2) A_5 + \left( \beta - \frac{5}{\beta} d_3 \lambda^2 \right) A_6 + B_5 d_2 \beta + d_2 B_6 \\ & + C_5 \beta d_1 + C_6 \frac{3}{2} d_1 - \frac{1}{2} C_6 d_1 = 0 \end{aligned} \quad (25)$$

$$\begin{aligned} & d_6 (\lambda + t_o \lambda^2) \beta A_4 + (-\beta^2 + d_4 (\lambda + t_o \lambda^2)) B_4 \\ & + 2 \beta B_5 + d_5 \lambda C_4 = 0 \end{aligned} \quad (26)$$

$$\begin{aligned} & d_6 (\lambda + t_o \lambda^2) \beta A_5 + 3 d_6 (\lambda + t_o \lambda^2) A_6 \\ & + (d_4 (\lambda + t_o \lambda^2) - \beta^2) B_5 + \left( d_4 \frac{3}{\beta} (\lambda + t_o \lambda^2) + \beta \right) B_6 \\ & + d_5 \lambda C_5 + d_5 \frac{3}{\beta} C_6 = 0 \end{aligned} \quad (27)$$

$$d_9 \lambda A_4 \beta + d_8 \lambda B_4 + (-\beta^2 + d_7 \lambda) C_4 + 2 C_5 \beta = 0 \quad (28)$$

$$\begin{aligned} & (-\beta^2 + d_7 \lambda) C_5 + \left( \beta + d_7 \lambda \frac{3}{\beta} \right) C_6 + d_8 \lambda B_5 \\ & + d_8 \frac{3}{\beta} \lambda B_6 + d_9 \lambda \beta A_5 + 3 d_9 \lambda A_6 = 0 \end{aligned} \quad (29)$$

The nontrivial solution of (23) is obtained by equating the determinant of this equation to zero as:

$$\begin{aligned} & d_3 d_4 d_7 (\lambda + t_o \lambda^2) \lambda^3 - d_3 d_5 d_8 \lambda^4 - \beta^2 d_3 d_4 (\lambda + t_o \lambda^2) \lambda^2 \\ & - \beta^2 d_3 d_7 \lambda^3 - \beta^2 d_4 d_7 (\lambda + t_o \lambda^2) \lambda + \beta^2 d_5 d_8 \lambda^2 \\ & + \beta^2 d_1 d_4 d_9 (\lambda + t_o \lambda^2) \lambda - \beta^2 d_1 d_6 d_8 (\lambda + t_o \lambda^2) \lambda \\ & + \beta^2 d_2 d_6 d_7 (\lambda + t_o \lambda^2) \lambda - \beta^2 d_2 d_5 d_9 \lambda^2 + \beta^4 d_3 \lambda^2 \\ & + \beta^4 d_4 (\lambda + t_o \lambda^2) + \beta^4 d_7 \lambda - \beta^4 d_2 d_6 (\lambda + t_o \lambda^2) \\ & - \beta^4 d_1 d_9 \lambda - \beta^6 = 0 \end{aligned} \quad (30)$$

The characteristic equation (30) is the same as the characteristic equations (13) and (20).

This equality is interesting as it prevents mathematical dilemma and complexity, and a single value for the eigenvalue  $\beta$  simultaneously satisfies three characteristic equations (13), (20), and (30). Equations (24)–(29) give the relations between  $A_4, A_5, A_6, B_4, B_5, B_6, C_4, C_5$  and  $C_6$ . These relations play as the balancing ratios that help (21) to be the third solution of the system of (9).

The complete general solutions for the solid sphere are:

$$\begin{aligned} U^s(r) &= A_1 J_{\frac{3}{2}}(\beta r) + A_3 [\zeta_1 J_{\frac{3}{2}}(\beta r) + r J_{\frac{5}{2}}(\beta r)] \\ &+ A_6 [\zeta_2 J_{\frac{3}{2}}(\beta r) + \zeta_3 r J_{\frac{5}{2}}(\beta r) + r^2 J_{\frac{7}{2}}(\beta r)] \\ \theta^s(r) &= A_1 \zeta_4 J_{\frac{3}{2}}(\beta r) + A_3 [\zeta_5 J_{\frac{3}{2}}(\beta r) + \zeta_6 r J_{\frac{5}{2}}(\beta r)] \\ &+ A_6 [\zeta_7 J_{\frac{3}{2}}(\beta r) + \zeta_8 r J_{\frac{5}{2}}(\beta r) + \zeta_9 r^2 J_{\frac{7}{2}}(\beta r)] \\ P^s(r) &= A_1 \zeta_{10} J_{\frac{3}{2}}(\beta r) + A_3 [\zeta_{11} J_{\frac{3}{2}}(\beta r) + \zeta_{12} r J_{\frac{5}{2}}(\beta r)] \\ &+ A_6 [\zeta_{13} J_{\frac{3}{2}}(\beta r) + \zeta_{14} r J_{\frac{5}{2}}(\beta r) + \zeta_{15} r^2 J_{\frac{7}{2}}(\beta r)] \end{aligned} \quad (31)$$

and for hollow sphere are:

$$\begin{aligned}
U^g(r) &= A_1 J_{\frac{3}{2}}(\beta r) + A_3 [\zeta_1 J_{\frac{3}{2}}(\beta r) + r J_{\frac{3}{2}}(\beta r)] \\
&\quad + A_6 [\zeta_2 J_{\frac{3}{2}}(\beta r) + \zeta_3 r J_{\frac{3}{2}}(\beta r) + r^2 J_{\frac{3}{2}}(\beta r)] \\
&\quad + \hat{A}_1 Y_{\frac{3}{2}}(\beta r) + \hat{A}_3 [\zeta_1 Y_{\frac{3}{2}}(\beta r) + r Y_{\frac{3}{2}}(\beta r)] \\
&\quad + \hat{A}_6 [\zeta_2 Y_{\frac{3}{2}}(\beta r) + \zeta_3 r Y_{\frac{3}{2}}(\beta r) + r^2 Y_{\frac{3}{2}}(\beta r)] \\
\theta^g(r) &= A_1 \zeta_4 J_{\frac{3}{2}}(\beta r) + A_3 [\zeta_5 J_{\frac{3}{2}}(\beta r) + \zeta_6 r J_{\frac{3}{2}}(\beta r)] \\
&\quad + A_6 [\zeta_7 J_{\frac{3}{2}}(\beta r) + \zeta_8 r J_{\frac{3}{2}}(\beta r) + \zeta_9 r^2 J_{\frac{3}{2}}(\beta r)] \\
&\quad + \hat{A}_1 \zeta_4 Y_{\frac{3}{2}}(\beta r) + \hat{A}_3 [\zeta_5 Y_{\frac{3}{2}}(\beta r) + \zeta_6 r Y_{\frac{3}{2}}(\beta r)] \\
&\quad + \hat{A}_6 [\zeta_7 Y_{\frac{3}{2}}(\beta r) + \zeta_8 r Y_{\frac{3}{2}}(\beta r) + \zeta_9 r^2 Y_{\frac{3}{2}}(\beta r)] \\
P^g(r) &= A_1 \zeta_{10} J_{\frac{3}{2}}(\beta r) + A_3 [\zeta_{11} J_{\frac{3}{2}}(\beta r) + \zeta_{12} r J_{\frac{3}{2}}(\beta r)] \\
&\quad + A_6 [\zeta_{13} J_{\frac{3}{2}}(\beta r) + \zeta_{14} r J_{\frac{3}{2}}(\beta r) + \zeta_{15} r^2 J_{\frac{3}{2}}(\beta r)] \\
&\quad + \hat{A}_1 \zeta_{10} Y_{\frac{3}{2}}(\beta r) + \hat{A}_3 [\zeta_{11} Y_{\frac{3}{2}}(\beta r) + \zeta_{12} r Y_{\frac{3}{2}}(\beta r)] \\
&\quad + \hat{A}_6 [\zeta_{13} Y_{\frac{3}{2}}(\beta r) + \zeta_{14} r Y_{\frac{3}{2}}(\beta r) + \zeta_{15} r^2 Y_{\frac{3}{2}}(\beta r)]
\end{aligned} \tag{32}$$

where  $\zeta_1$  to  $\zeta_{15}$  are ratios obtained from (23)–(29), (16)–(19), and (12) and are given in the appendix. Substituting  $U^g$ ,  $\theta^g$ , and  $P^g$  in the homogeneous form of the boundary conditions (4), three linear algebraic equations are obtained. They are the coefficients depending on  $\lambda$  and  $\beta$ . Setting the determinant of the coefficients equal to zero, the second characteristic equation is obtained. Simultaneous solution of this equation and (11) results into infinite number of two eigenvalues  $\beta_n$  and  $\lambda_n$ . Therefore,  $U^g$ ,  $\theta^g$ , and  $P^g$  for solid sphere are rewritten as:

$$\begin{aligned}
U^g(r) &= A_1 \left[ J_{\frac{3}{2}}(\beta r) + \zeta_{16} [\zeta_1 J_{\frac{3}{2}}(\beta r) + r J_{\frac{3}{2}}(\beta r)] \right. \\
&\quad \left. + \zeta_{17} [\zeta_2 J_{\frac{3}{2}}(\beta r) + \zeta_3 r J_{\frac{3}{2}}(\beta r) + r^2 J_{\frac{3}{2}}(\beta r)] \right] \\
\theta^g(r) &= A_1 \left[ \zeta_4 J_{\frac{3}{2}}(\beta r) + \zeta_{16} [\zeta_5 J_{\frac{3}{2}}(\beta r) + \zeta_6 r J_{\frac{3}{2}}(\beta r)] \right. \\
&\quad \left. + \zeta_{17} [\zeta_7 J_{\frac{3}{2}}(\beta r) + \zeta_8 r J_{\frac{3}{2}}(\beta r) + \zeta_9 r^2 J_{\frac{3}{2}}(\beta r)] \right] \\
P^g(r) &= A_1 \left[ \zeta_{10} J_{\frac{3}{2}}(\beta r) + \zeta_{16} [\zeta_{11} J_{\frac{3}{2}}(\beta r) + \zeta_{12} r J_{\frac{3}{2}}(\beta r)] \right. \\
&\quad \left. + \zeta_{17} [\zeta_{13} J_{\frac{3}{2}}(\beta r) + \zeta_{14} r J_{\frac{3}{2}}(\beta r) + \zeta_{15} r^2 J_{\frac{3}{2}}(\beta r)] \right]
\end{aligned} \tag{33}$$

where  $\zeta_{16}$  and  $\zeta_{17}$  are presented in the appendix. Let us show the functions in the brackets of (33) by functions  $H_0$ ,  $H_1$  and  $H_2$  as:

$$\begin{aligned}
H_0 &= J_{\frac{3}{2}}(\beta r) + \zeta_{16} [\zeta_1 J_{\frac{3}{2}}(\beta r) + r J_{\frac{3}{2}}(\beta r)] \\
&\quad + \zeta_{17} [\zeta_2 J_{\frac{3}{2}}(\beta r) + \zeta_3 r J_{\frac{3}{2}}(\beta r) + r^2 J_{\frac{3}{2}}(\beta r)] \\
H_1 &= \zeta_4 J_{\frac{3}{2}}(\beta r) + \zeta_{16} [\zeta_5 J_{\frac{3}{2}}(\beta r) + \zeta_6 r J_{\frac{3}{2}}(\beta r)] \\
&\quad + \zeta_{17} [\zeta_7 J_{\frac{3}{2}}(\beta r) + \zeta_8 r J_{\frac{3}{2}}(\beta r) + \zeta_9 r^2 J_{\frac{3}{2}}(\beta r)] \\
H_2 &= \zeta_{10} J_{\frac{3}{2}}(\beta r) + \zeta_{16} [\zeta_{11} J_{\frac{3}{2}}(\beta r) + \zeta_{12} r J_{\frac{3}{2}}(\beta r)] \\
&\quad + \zeta_{17} [\zeta_{13} J_{\frac{3}{2}}(\beta r) + \zeta_{14} r J_{\frac{3}{2}}(\beta r) + \zeta_{15} r^2 J_{\frac{3}{2}}(\beta r)]
\end{aligned} \tag{34}$$

According to the Sturm-Liouville theorem, these functions are orthogonal with respect to the weight function  $p(r) = r$  such as:

$$\int_{r_i}^{r_o} H(\beta_n r) H(\beta_m r) r dr = \begin{cases} 0 & n \neq m \\ \|H(\beta_n r)\|^2 & n = m \end{cases} \tag{35}$$

where  $\|H(\beta_n r)\|$  is norm of the  $H$  function and equals:

$$\|H(\beta_n r)\| = \left[ \int_{r_i}^{r_o} r H^2(\beta_n r) dr \right]^{\frac{1}{2}} \tag{36}$$

Due to the orthogonality of function  $H$ , every piece-wise continuous function, such as  $f(r)$ , can be expanded in terms of the function  $H$  (either  $H_0$ ,  $H_1$  or  $H_2$ ), and is called the H-Fourier series as:

$$f(r) = \sum_{n=1}^{\infty} e_n H(\beta_n r) \tag{37}$$

where  $e_n$  equals:

$$e_n = \frac{1}{\|H(\beta_n r)\|^2} \int_{r_i}^{r_o} f(r) H(r) r dr \tag{38}$$

Using (6), (33), and (34), the displacement and temperature distributions due to the general solution become:

$$\begin{aligned} u^g(r,t) &= \sum_{n=1}^{\infty} \left\{ \sum_{m=1}^4 a_{nm} e^{\lambda_{nm} t} \right\} H_0(\beta_n r) \\ T^g(r,t) &= \sum_{n=1}^{\infty} \left\{ \sum_{m=1}^4 N_{nm} a_{nm} e^{\lambda_{nm} t} \right\} H_1(\beta_n r) \\ p^g(r,t) &= \sum_{n=1}^{\infty} \left\{ \sum_{m=1}^4 M_{nm} a_{nm} e^{\lambda_{nm} t} \right\} H_2(\beta_n r) \end{aligned} \quad (39)$$

where  $N_{nm}$  and  $M_{nm}$  are ratios obtained by substituting (39) into (1)–(3). Using the initial conditions (5) and with the help of (36), (37), and (38), four unknown constants are obtained.

### Particular Solution with Nonhomogeneous Boundary Conditions

The general solutions may be used as proper functions for guessing the particular solution adopted to the nonhomogeneous parts of the (1)–(3) and the nonhomogeneous boundary conditions (4) as:

$$\begin{aligned} u^p(r,t) &= \sum_{n=1}^{\infty} \left\{ \left[ G_{1n}(t) J_{\frac{3}{2}}(\beta_n r) + G_{2n}(t) r J_{\frac{5}{2}}(\beta_n r) + G_{3n}(t) r^2 J_{\frac{7}{2}}(\beta_n r) \right] + r^2 G_{4n}(t) \right\} \\ T^p(r,t) &= \sum_{n=1}^{\infty} \left\{ \left[ G_{5n}(t) J_{\frac{1}{2}}(\beta_n r) + G_{6n}(t) r J_{\frac{3}{2}}(\beta_n r) + G_{7n}(t) r^2 J_{\frac{5}{2}}(\beta_n r) \right] + r^2 G_{8n}(t) \right\} \\ p^p(r,t) &= \sum_{n=1}^{\infty} \left\{ \left[ G_{9n}(t) J_{\frac{1}{2}}(\beta_n r) + G_{10n}(t) r J_{\frac{3}{2}}(\beta_n r) + G_{11n}(t) r^2 J_{\frac{5}{2}}(\beta_n r) \right] + r^2 G_{12n}(t) \right\} \end{aligned} \quad (40)$$

For the solid sphere, the second type of Bessel function  $Y$  is excluded. It is necessary and suitable to expand the body force  $F(r, t)$ , heat source  $Q(r, t)$ , and porosity function  $W(r, t)$  in H-Fourier expansion form as:

$$\begin{aligned} F(r,t) &= \sum_{n=1}^{\infty} F_n(t) H_0(\beta_n r) \\ Q(r,t) &= \sum_{n=1}^{\infty} Q_n(t) H_1(\beta_n r) \\ P(r,t) &= \sum_{n=1}^{\infty} P_n(t) H_2(\beta_n r) \end{aligned} \quad (41)$$

where  $F_n(t)$ ,  $Q_n(t)$ , and  $P_n(t)$  are:

$$\begin{aligned} F_n(t) &= \frac{1}{\|H_0(\beta_n r)\|^2} \int_{r_i}^{r_o} F(r,t) H_0(\beta_n r) r dr \\ Q_n(t) &= \frac{1}{\|H_1(\beta_n r)\|^2} \int_{r_i}^{r_o} Q(r,t) H_1(\beta_n r) r dr \\ P_n(t) &= \frac{1}{\|H_2(\beta_n r)\|^2} \int_{r_i}^{r_o} P(r,t) H_2(\beta_n r) r dr \end{aligned} \quad (42)$$

Substituting (40) and (41) into nonhomogeneous form of (1)–(3) yields:



$$\left\{ \begin{aligned} & -G_1(t)\beta^2 + d_3\ddot{G}_1(t) - G_2(t)\beta + d_3\ddot{G}_2(t)\frac{3}{\beta} - 3G_3(t) \\ & + d_3\ddot{G}_3(t)\frac{15}{\beta^2} + \left\{ C_0 + C_1\frac{3}{\beta} + C_2\frac{15}{\beta^2} \right\} d_{16}G_4(t) \\ & + \left\{ C_0 + C_1\frac{3}{\beta} + C_2\frac{15}{\beta^2} \right\} d_{19}\ddot{G}_4(t) - G_5(t)d_2\beta \\ & - d_2G_6(t) - 3d_2G_7(t)\frac{1}{\beta} + \left\{ C_0 + C_1\frac{3}{\beta} + C_2\frac{15}{\beta^2} \right\} \\ & d_{17}G_8(t) - d_1G_9(t)\beta - d_1G_{10}(t) - 3d_1G_{11}(t)\frac{1}{\beta} + \\ & \left\{ C_0 + C_1\frac{3}{\beta} + C_2\frac{15}{\beta^2} \right\} d_{18}G_{12}(t) - \left\{ C_0 + C_1\frac{3}{\beta} + C_2\frac{15}{\beta^2} \right\} \\ & d_{10}d_{13}F_n(t) \end{aligned} \right\} = 0 \quad (43a)$$

$$\left\{ \begin{aligned} & G_3(t)\beta^2 - d_3\ddot{G}_3(t) - d_{16}C_2G_4(t) - d_{19}C_2\ddot{G}_4(t) + G_7(t)d_2\beta \\ & - d_{17}C_2G_8(t) - d_{18}C_2G_{12}(t) + d_1G_{11}(t)\beta + d_{10}d_{13}C_2F_n(t) \end{aligned} \right\} = 0 \quad (43b)$$

$$\left\{ \begin{aligned} & G_2(t)\beta^2 - d_3\ddot{G}_2(t) + G_3(t)\beta - d_3\ddot{G}_3(t)\frac{5}{\beta} \\ & + \left\{ -C_1 - C_2\frac{5}{\beta} \right\} d_{16}G_4(t) \\ & + \left\{ -C_1 - C_2\frac{5}{\beta} \right\} d_{19}\ddot{G}_4(t) + d_2G_6(t)\beta + d_2G_7(t) \\ & - \left\{ C_1 + C_2\frac{5}{\beta} \right\} d_{17}G_8(t) + d_1G_{10}(t)\beta + d_1G_{11}(t) \\ & - \left\{ C_1 + C_2\frac{5}{\beta} \right\} d_{18}G_{12}(t) + \left\{ C_1F_n(t) + C_2\frac{5}{\beta} \right\} d_{10}d_{13}F_n(t) \end{aligned} \right\} = 0 \quad (43c)$$

$$\left\{ \begin{aligned} & + d_6\{\dot{G}_1(t) + t_o\ddot{G}_1(t)\}\beta + d_{21}E_0\dot{G}_4(t) - G_5(t)\beta^2 \\ & + d_4\{\dot{G}_5(t) + t_o\ddot{G}_5(t)\} + 2G_6(t)\beta + d_{20}E_0G_8(t) \\ & + d_{22}E_0\dot{G}_8(t) + d_5\dot{G}_9(t)d_{23}E_0\dot{G}_{12}(t) - d_{11}d_{14}E_0Q_n(t) \end{aligned} \right\} = 0 \quad (43d)$$

$$\left\{ \begin{aligned} & -d_6\{\dot{G}_3(t) + t_o\ddot{G}_3(t)\}\beta - d_{21}E_2\dot{G}_4(t) + G_7(t)\beta^2 \\ & - d_4\{\dot{G}_7(t) + t_o\ddot{G}_7(t)\} - d_{20}E_2G_8(t) - d_{22}E_2\dot{G}_8(t) - d_5\dot{G}_{11}(t) \\ & - d_{23}E_2\dot{G}_{12}(t) + d_{11}d_{14}E_2Q_n(t) \end{aligned} \right\} = 0 \quad (43e)$$

$$\left\{ \begin{aligned} & d_6 \{ \dot{G}_2(t) + t_0 \ddot{G}_2(t) \} \beta + 3d_6 \dot{G}_3(t) + \left\{ E_1 + E_2 \frac{3}{\beta} \right\} d_{21} \dot{G}_4(t) \\ & - G_6(t) \beta^2 + d_4 \{ \dot{G}_6(t) + t_0 \ddot{G}_6(t) \} + G_7(t) \beta \\ & + d_4 \{ \dot{G}_7(t) + t_0 \ddot{G}_7(t) \} \frac{3}{\beta} + \left\{ E_1 + E_2 \frac{3}{\beta} \right\} d_{20} G_8(t) \\ & + \left\{ E_1 + E_2 \frac{3}{\beta} \right\} d_{22} \dot{G}_8(t) + d_5 \dot{G}_{10}(t) + d_5 \dot{G}_{11}(t) \frac{3}{\beta} \\ & + \left\{ E_1 + E_2 \frac{3}{\beta} \right\} d_{23} \dot{G}_{12}(t) - \left\{ E_1 + E_2 \frac{3}{\beta} \right\} d_{11} d_{14} Q_n(t) \end{aligned} \right\} = 0 \quad (43f)$$

$$\left\{ \begin{aligned} & + \dot{G}_1(t) d_9 \beta + D_0 d_{25} \dot{G}_4(t) + d_8 \dot{G}_5(t) - G_9(t) \beta^2 \\ & + d_7 \dot{G}_9(t) + D_0 d_{26} \dot{G}_8(t) + 2G_{10}(t) \beta + D_0 d_{24} G_{12}(t) \\ & + D_0 d_{27} \dot{G}_{12}(t) - d_{12} d_{15} D_0 W_n(t) \end{aligned} \right\} = 0 \quad (43g)$$

$$\left\{ \begin{aligned} & G_{11}(t) \beta^2 - d_7 \dot{G}_{11}(t) - d_8 \dot{G}_7(t) - d_9 \dot{G}_3(t) \beta \\ & - D_2 r^2 d_{25} \dot{G}_4(t) - D_2 d_{26} \dot{G}_8(t) - D_2 d_{24} G_{12}(t) \\ & - D_2 d_{27} \dot{G}_{12}(t) + d_{12} d_{15} D_2 W_n(t) \end{aligned} \right\} = 0 \quad (43h)$$

$$\left\{ \begin{aligned} & + \dot{G}_2(t) \beta d_9 + 3\dot{G}_3(t) d_9 + \left\{ D_1 + D_2 \frac{3}{\beta} \right\} d_{25} \dot{G}_4(t) + d_8 \dot{G}_6(t) \\ & + d_8 \dot{G}_7(t) \frac{3}{\beta} \left\{ D_1 \dot{G}_8(t) + D_2 \frac{3}{\beta} \right\} \dot{G}_8(t) d_{26} - G_{10}(t) \beta^2 \\ & + d_7 \dot{G}_{10}(t) + G_{11}(t) \beta + d_7 \dot{G}_{11}(t) \frac{3}{\beta} + \left\{ D_1 + D_2 \frac{3}{\beta} \right\} d_{27} \dot{G}_{12}(t) \\ & + \left\{ D_1 + D_2 \frac{3}{\beta} \right\} d_{24} G_{12}(t) - \left\{ + D_1 + D_2 \frac{3}{\beta} \right\} d_{12} d_{15} W_n(t) \end{aligned} \right\} = 0 \quad (43i)$$

where  $d_{10}$  to  $d_{27}$  are the coefficients of the H-expansion and constant parameters presented in the appendix. By taking Laplace transform of (43a) and using three boundary conditions of (4) (for solid sphere only second, fourth, and sixth boundary conditions are applicable), a system of algebraic equations is obtained and solved by Cramer's methods in the Laplace domain, where by the inverse Laplace

transform the functions are transformed into the real time domain and finally  $G_{1n}(t)$  to  $G_{12n}(t)$  are calculated.

In this process, it is necessary to consider the following points:

1. The initial conditions (5) are considered only for the general solutions and the initial conditions of  $G_{1n}(t)$  to  $G_{12n}(t)$  for the particular solutions are considered equal to zero.

2. Laplace transform of (43a) is in terms of polynomial function form of the Laplace parameter  $s$  (not the Bessel functions form of  $s$ ). Therefore, the exact inverse Laplace transform is possible and somehow simple.
3. For the hollow sphere, it is enough to include the second type of Bessel function  $Y(r)$  in a sequence of the particular solution as:

$$\begin{aligned}
 u^p(r, t) &= \sum_{n=1}^{\infty} \left\{ \left[ G_{1n}(t)J_{\frac{3}{2}}(\beta nr) + G_{2n}(t)rJ_{\frac{5}{2}}(\beta nr) + G_{3n}(t)r^2J_{\frac{7}{2}}(\beta nr) \right] \right. \\
 &\quad \left. + \left[ G_{4n}(t)Y_{\frac{3}{2}}(\beta nr) + G_{5n}(t)rY_{\frac{5}{2}}(\beta nr) + G_{6n}(t)r^2Y_{\frac{7}{2}}(\beta nr) \right] + rG_{7n}(t) + r^2G_{8n}(t) \right\} \\
 T^p(r, t) &= \sum_{n=1}^{\infty} \left\{ \left[ G_{9n}(t)J_{\frac{1}{2}}(\beta nr) + G_{10n}(t)rJ_{\frac{3}{2}}(\beta nr) + G_{11n}(t)r^2J_{\frac{5}{2}}(\beta nr) \right] \right. \\
 &\quad \left. + \left[ G_{12n}(t)Y_{\frac{1}{2}}(\beta nr) + G_{13n}(t)rY_{\frac{3}{2}}(\beta nr) + G_{14n}(t)r^2Y_{\frac{5}{2}}(\beta nr) \right] + rG_{15n}(t) + r^2G_{16n}(t) \right\} \\
 p^p(r, t) &= \sum_{n=1}^{\infty} \left\{ \left[ G_{17n}(t)J_{\frac{1}{2}}(\beta nr) + G_{18n}(t)rJ_{\frac{3}{2}}(\beta nr) + G_{19n}(t)r^2J_{\frac{5}{2}}(\beta nr) \right] \right. \\
 &\quad \left. + \left[ G_{20n}(t)Y_{\frac{1}{2}}(\beta nr) + G_{21n}(t)rY_{\frac{3}{2}}(\beta nr) + G_{23n}(t)r^2J_{\frac{5}{2}}(\beta nr) \right] + r^2G_{24n}(t) \right\}
 \end{aligned} \tag{44}$$

By substituting (44) in (1)–(3), 18 are obtained, where using the six boundary conditions (4) 24 functions  $G_{1n}(t)$  to  $G_{24n}(t)$  are obtained for the hollow sphere.

## Results and Discussions

As an example, a solid sphere with  $r_i = 0$ ,  $r_o = 1$  m is considered. The material properties are listed in Table 1.

To give clear explanation, numerical results have been considered and the radial distributions of displacement, temperature, and pressure for two cases (Classic coupled theory and Lord-Shulman's theory) computed. An instantaneous hot spot  $T(1, t) = 10^{-3}T_o\delta(t)$ , where  $\delta(t)$  is unit dirac function, is considered and the outside radius of the sphere is assumed to be fixed

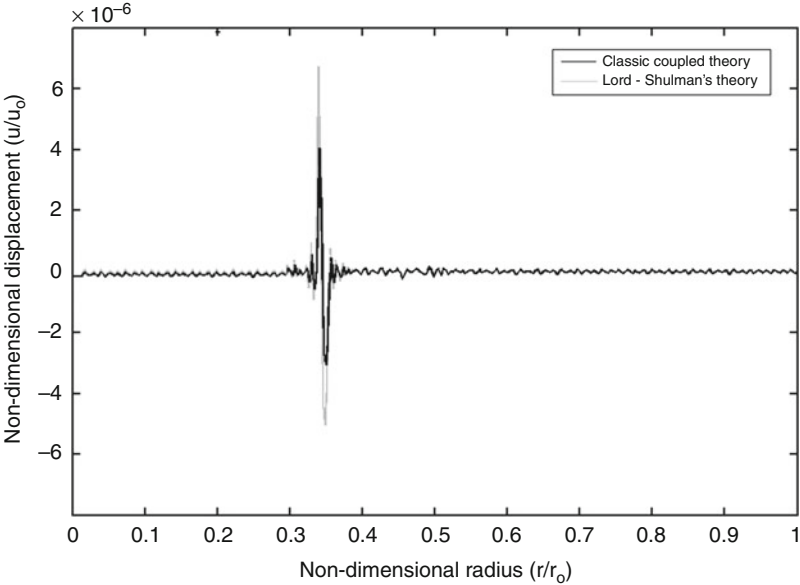
( $u(1, t) = 0$ ). For plotting the graphs, a nondimensional time  $\hat{t} = \frac{vt}{r_o}$  is considered where  $v = \sqrt{\frac{E(1-\nu)}{\rho(1+\nu)(1-2\nu)}}$  is the dilatational wave velocity. Figures 1–3 show the wave-front for the displacement, temperature, and pressure (Classic coupled theory and Lord-Shulman's theory). As a second example, mechanical shock wave is applied to the outside surface of the sphere given as  $u(1, t) = 10^{-12}u_o\delta(t)$ , and the surface is assumed to be at zero temperature ( $T(1, t) = 0$ ). Figures 4–6 show the wave fronts for the displacement and temperature distributions versus the nondimensional radius (Classic coupled theory and Lord-Shulman's theory). The convergence of the solutions for these examples is achieved by consideration of 1,200 eigenvalues used for the H-Fourier expansion. Choosing more than this number for eigenvalues, the increase in

**Exact Solution for Lord-Shulman Generalized Coupled Thermoporoelasticity in Spherical Coordinates, Table 1** Material parameters

Unit	Value	Parameters	Unit	Value	Parameters
$t_o$	$1 \times 10^{-5}$	—	$\alpha_s$	$1.5 \times 10^{-5}$	$1/^{\circ}\text{C}$
E	$6 \times 10^5$	Pa	$\alpha_w$	$2 \times 10^{-4}$	$1/^{\circ}\text{C}$
$\nu$	0.3	—	$c_s$	0.8	$\text{J/g} \cdot ^{\circ}\text{C}$
$T_o$	293	$^{\circ}\text{K}$	$c_w$	4.2	$\text{J/g} \cdot ^{\circ}\text{C}$
$K_s$	$2 \times 10^{10}$	Pa	$\rho_s$	$2.6 \times 10^6$	$\text{g/m}^3$
$K_w$	$5 \times 10^9$	Pa	$\rho_w$	$1 \times 10^6$	$\text{g/m}^3$
$K$	$5 \times 10^9$	$\text{W/m} \cdot ^{\circ}\text{C}$	$\alpha$	1	—

E

**Exact Solution for Lord-Shulman Generalized Coupled Thermoporoelasticity in Spherical Coordinates, Fig. 1** Nondimensional displacement distribution due to input  $T(1, t) = 10^{-3}T_0\delta(t)$  at nondimensional time  $t = 0.65$



round-off and truncation errors can affect the quality of the graphs. The convergence of the solution is better for the displacement result in comparison with the temperature. The small oscillations in Figs. 3 and 5 are due to the convergence errors of solutions.

Conclusion

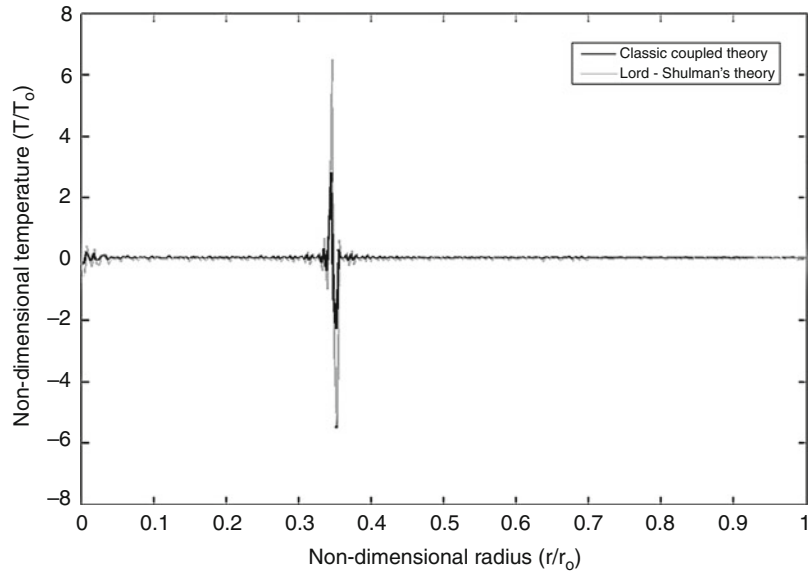
In this entry, an analytical solution for the generalized coupled thermoporoelasticity of thick

spheres under radial temperature is presented. Figures 1–6 show relaxation time effect on variation of displacement, temperature, and pressure.

It is observed that the peak value of Lord-Shulman’s theory for displacement, temperature, and pressure increases. The method is based on the eigenfunctions Fourier expansion, which is a classical and traditional method of solution of the typical initial and boundary value problems. The noncompetitive strength of this method is its ability to reveal the fundamental mathematical

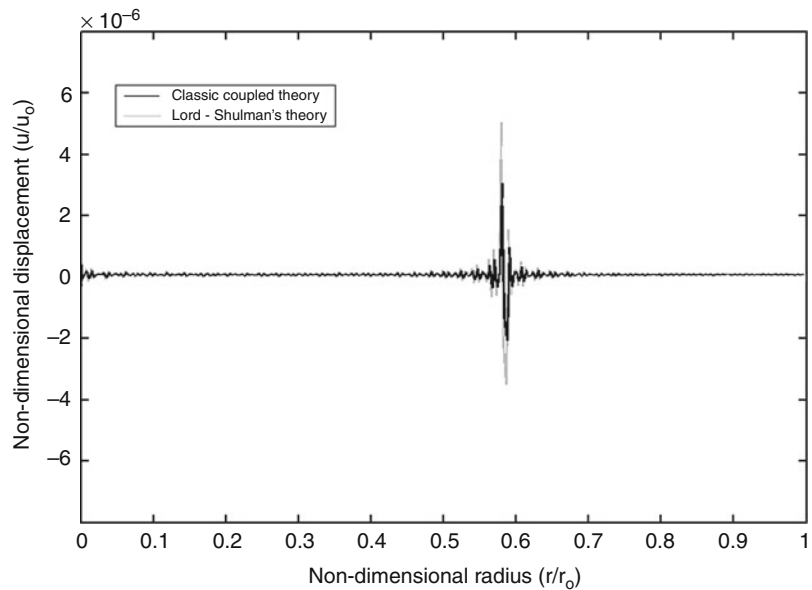
### Exact Solution for Lord-Shulman Generalized Coupled Thermoporoelasticity in Spherical Coordinates,

**Fig. 2** Nondimensional temperature distribution due to input  $T(1, t) = 10^{-3}T_0\delta(t)$  at nondimensional time  $t = 0.65$



### Exact Solution for Lord-Shulman Generalized Coupled Thermoporoelasticity in Spherical Coordinates,

**Fig. 3** Nondimensional pressure distribution due to input  $T(1, t) = 10^{-3}T_0\delta(t)$  at nondimensional time  $t = 0.65$

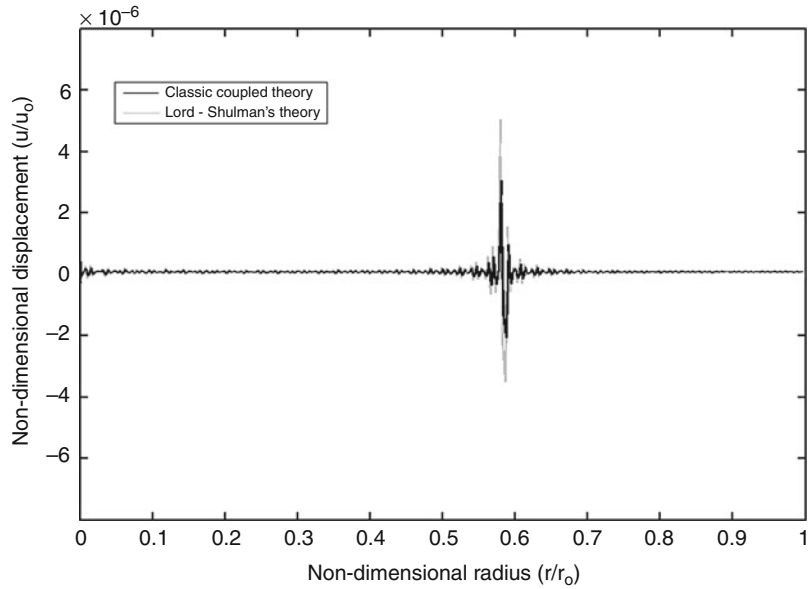


and physical properties and interpretations of the problem under studying. In the coupled thermoporoelastic problem of radial-symmetric sphere, the governing equations constitute a system of partial differential equations with two independent variables, radius ( $r$ ) and time

( $t$ ). The traditional procedure to solve this class of problems is to eliminate the time variable by using the Laplace transform. The resulting system is a set of ordinary differential equations in terms of the radius variable, whose solution falls in the Bessel functions family. This method of the

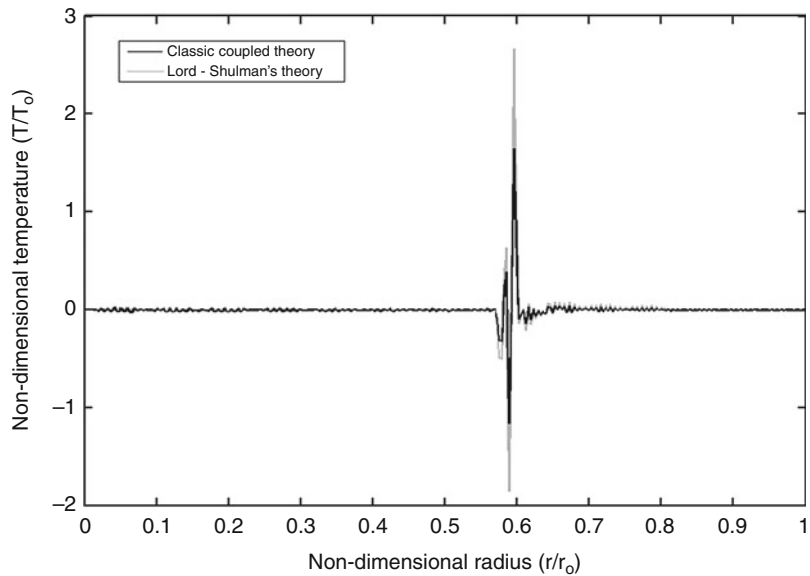
**Exact Solution for Lord-Shulman Generalized Coupled Thermoporoelasticity in Spherical Coordinates,**

**Fig. 4** Nondimensional displacement distribution due to input  $u(1, t) = 10^{-12}u_0\delta(t)$  at nondimensional time  $t = 0.4$



**Exact Solution for Lord-Shulman Generalized Coupled Thermoporoelasticity in Spherical Coordinates,**

**Fig. 5** Nondimensional temperature distribution due to input  $u(1, t) = 10^{-12}u_0\delta(t)$  at nondimensional time  $t = 0.4$

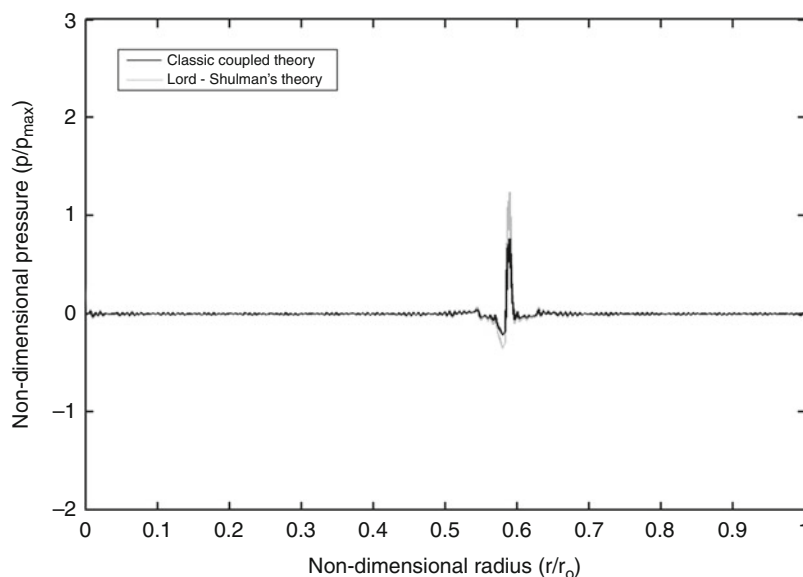


analysis brings the Laplace parameter ( $s$ ) in the argument of the Bessel functions, causing hardship or difficulties in carrying out the exact inverse of the Laplace transformation. As a result, the numerical inversion of the Laplace transformation is used in the papers dealing with this type of problems in literature. In this entry, to

prevent this problem, when the Laplace transform is applied to the particular solutions, it is postponed after eliminating the radius variable  $r$  by H-Fourier Expansion. Thus, the Laplace parameter ( $s$ ) appears in polynomial function forms, and hence, the exact Laplace inversion transformation is possible.

### Exact Solution for Lord-Shulman Generalized Coupled Thermoporoelasticity in Spherical Coordinates,

**Fig. 6** Nondimensional pressure distribution due to input  $u(1, t) = 10^{-12} u_0 \delta(t)$  at nondimensional time  $t = 0.4$



## References

1. Hetnarski RB, Eslami MR (2009) Thermal stresses – advanced theory and applications. Springer, New York
2. Lord HW, Shulman Y (1967) A generalized dynamical theory of thermoelasticity. *J Mech Phys Solid* 15:299–309
3. Green AE, Lindsay KA (1972) Thermoelasticity. *J Elast* 2:1–7
4. Green AE, Naghdi PM (1972) Thermoelasticity without energy dissipation. *J Elast* 2:1–7
5. Youssef HM (2006) Theory of generalized porothermoelasticity. *J Rock Mech Min* 44:222–227
6. Bai B (2006) Response of saturated porous media subjected to local thermal loading on the surface of semi-infinite space. *Acta Mech Sinica* 22:54–61
7. Bai B (2006) Fluctuation responses of saturated porous media subjected to cyclic thermal loading. *Comput Geotech* 33:396–403
8. Droujinine A (2006) Generalized an elastic asymptotic ray theory. *Wave Motion* 43:357–367
9. Bai B, Li T (2009) Solution for cylindrical cavity in saturated thermoporoelastic medium. *J Acta Mech Sinica* 22:85–92
10. Hetnarski RB (1964) Solution of the coupled problem of thermoelasticity in the form of series of functions. *J Arch Mech Stos* 16:919–941
11. Hetnarski RB, Ignaczak J (1993) Generalized thermoelasticity: closed-form solutions. *J Therm Stress* 16:473–498
12. Hetnarski RB, Ignaczak J (1994) Generalized thermoelasticity: response of semi-space to a shortlaser pulse. *J Therm Stress* 17:377–396
13. Georgiadis HG, Lykotrafitis G (2005) Rayleigh waves generated by a thermal source: a three dimensional transient thermoelasticity solution. *J Appl Mech* 72:129–138
14. Wagner P (1994) Fundamental matrix of the system of dynamic linear thermoelasticity. *J Ther Stress* 17:549–565
15. Jabbari M, Dehbani H (2011) An exact solution for Lord-Shulman generalized coupled thermoporoelasticity in cylindrical coordinates. In: Ninth international conference on thermal stress, Budapest
16. Jabbari M, Dehbani H, Eslami MR (2009) An exact solution for classic coupled thermoelasticity in spherical coordinates. *J Press Vessel ASME Trans* 132:031201–031211
17. Jabbari M, Dehbani H (2009) An exact solution for classic coupled thermoporoelasticity in cylindrical coordinates. *J Solid Mech* 1:343–357
18. Jabbari M, Dehbani H, Eslami MR (2009) An exact solution for classic coupled thermoelasticity in cylindrical coordinates, *J Press Vessel ASME Trans* October 2011, 133:05120401–05120410 Transactions of the ASME
19. Jabbari M, Dehbani H, Eslami MR (2011) An exact solution for classic coupled thermoelasticity in cylindrical coordinates. *ASME J Press Vessel Technol* 133:051204–051210

## Exact Solution for Quasi-Static Porothermoelasticity in Spherical Coordinates

Mohsen Jabbari<sup>1</sup> and H. Dehbani<sup>2</sup>

<sup>1</sup>Faculty of Engineering, Postgraduate School, South Tehran Branch, Islamic Azad University, Tehran, Iran

<sup>2</sup>Postgraduate School, South Tehran Branch, Islamic Azad University, Tehran, Iran

### Overview

In this entry, the quasi-static porothermoelasticity model of a hollow and solid sphere under radial-symmetric loading condition ( $r$ ,  $t$ ) is considered. A full analytical method is used and an exact unique solution of the quasi-static equations is presented. The thermal, mechanical, and pressure boundary conditions, the body force, the heat source, and the injected volume rate per unit volume of a distribute water source are considered in the most general forms where no limiting assumption is used. This generality allows the simulation of a variety of applicable problems.

### Introduction

Quasi-static thermal and poromechanical processes play an important role in a number of problems of interest in geomechanics such as stability of boreholes and permeability enhancement in geothermal reservoirs or high temperature petroleum bearing formations. A porothermoelastic approach combines the theory of heat conduction with poroelastic constitutive equations coupling the temperature field with the stresses and pore pressure. There are a limited number of papers that present the closed-form or analytical solution for the quasi-static porothermoelasticity problems. Bai [1] investigated the response of saturated porous media subjected to local thermal loading on the surface of semi-infinite space. He used the

numerical integral methods for calculating the unsteady temperature, pore pressure, and displacement fields. This author also studied the fluctuation responses of saturated porous media subjected to cyclic thermal loading [2]. In the mentioned paper, an analytical solution was deduced by using the Laplace transform and the Gauss-Legendre method of Laplace transform inversion. Droujinine [3] investigated dispersion and attenuation of body waves in a wide range of materials representing realistic rock structures. He used the time-domain asymptotic ray theory to a new generalized coordinate-free wave equation with an arbitrary tensor relaxation function. Bai and Li [4] found solution for cylindrical cavity in saturated thermoporoelastic medium by using Laplace transform and numerical Laplace transform inversion. Also the number of papers that present the closed-form or analytical solutions for the quasi-static thermoelasticity problems is limited. Hetnarski [5] found the solution of quasi-static thermoelasticity in the form a series of functions. Hetnarski and Ignaczak presented a study of the one-dimensional thermoelastic waves produced by an instantaneous plane source of heat in homogeneous isotropic infinite and semi-infinite bodies of the Green-Lindsay type [6]. Also, these authors presented an analysis of laser-induced waves propagating in an absorbing thermoelastic semi-space of the Green-Lindsay type [7]. Georgiadis and Lykotrafitis obtained a three-dimensional transient thermoelastic solution for Rayleigh-type disturbances propagating on the surface of a half-space [8]. Wagner [9] presented the fundamental matrix of a system of partial differential operators that governs the diffusion of heat and the strains in elastic media. This method can be used to predict the temperature distribution and the strains by an instantaneous point heat, point source of heat, or by a suddenly applied delta force. Smith and Booker presented [10] a direct method (Green's functions) for porothermoelasticity in the Laplace transform domain. The boundary element techniques have been successfully applied to many geological engineering the boundary element method (BEM) or the boundary integral equation



formulation also has proven effective for the poroelastic and thermoelastic problems. Koshelev and Ghassemi [11] suggested a stationary boundary element method for thermo- and poroelasticity based on the complex variable hypersingular boundary integral equation. Zhou and Ghassemi [12] developed a finite element method to implement the fully coupled chemo-porothermoelastic linear and nonlinear problems.

In this work [13], a full analytical method is used to obtain the response of the governing equations, where an exact solution is presented. The method of solution is based on the Fourier expansion and eigenfunction methods, which is a traditional and routine method in solving the partial differential equations. Since the coefficients of equations are not functions of the time variable ( $t$ ), an exponential form is considered for the general solution matched with the physical wave properties of thermal, mechanical, and pressure waves. For the particular solution, that is the response to mechanical and thermal shocks, the eigenfunction method and Laplace transformation is used.

## Governing Equations

A hollow cylinder with inner and outer radii  $r_i$  and  $r_o$ , respectively, made of isotropic material subjected to radial-symmetric mechanical, thermal, and pressure shocks, is considered. The theory of porothermoelasticity for wave propagation is considered to allow coupling between deformation, thermal energy, and pressure fields and to describe the physical behavior of the elastic domain to mechanical, thermal, and pressure shock loads. Navier equation in term of the displacement components is obtained as [4]:

$$\begin{aligned} u_{,rr} + \frac{2}{r}u_{,r} - \frac{2}{r^2}u - \alpha \frac{(1+\nu)(1-2\nu)}{(1-\nu)E}p_{,r} \\ - \beta \frac{(1+\nu)(1-2\nu)}{(1-\nu)E}T_{,r} - \rho \frac{(1+\nu)(1-2\nu)}{(1-\nu)E}\ddot{u} \\ = - \frac{(1+\nu)(1-2\nu)}{(1-\nu)E}F(r, t) \end{aligned} \quad (1)$$

Heat conduction equation in radial-symmetric direction with the mechanical coupling term is:

$$\begin{aligned} T_{,rr} + \frac{2}{r}T_{,r} - Z \frac{T_o}{K}\dot{T} + Y \frac{T_o}{K}\dot{p} - \beta \frac{T_o}{K}(\dot{u}_{,r} + \frac{2}{r}\dot{u}) \\ = - \frac{1}{K}Q(r, t) \end{aligned} \quad (2)$$

According to Darcy's law and continuity condition of seepage, the equation of mass conservation can be written as:

$$\begin{aligned} p_{,rr} + \frac{2}{r}p_{,r} - \alpha_p \frac{\gamma_w}{k}\dot{p} - Y \frac{\gamma_w}{k}\dot{T} - \alpha \frac{\gamma_w}{k}(\dot{u}_{,r} + \frac{2}{r}\dot{u}) \\ = - \frac{\gamma_w}{k}W(r, t) \end{aligned} \quad (3)$$

where  $(\cdot)$  denotes partial derivative,  $u$  is the displacement component in the radial direction,  $p$  the pore pressure, and  $\alpha = 1 - C_s/C$  is Biot's coefficient,  $C_s = 3(1 - 2\nu_s)E_s$  is the coefficient of volumetric compression of solid grains, with  $E_s$  and  $\nu_s$  being the elastic modulus and Poisson's ratio of solid grains and  $C = 3(1 - 2\nu)E$  is the coefficient of volumetric compression of solid skeleton, with  $E$  and  $\nu$  being the elastic modulus and Poisson's ratio of solid skeleton,  $T_o$  is the initial reference temperature,  $\beta = 3\alpha_s/C$  the thermal expansion factor,  $\alpha_s$  is the coefficient of linear thermal expansion of solid grains,  $Y = 3(n\alpha_w + (\alpha - n)\alpha_s)$  and  $\alpha_p = n(C_w - C_s) + \alpha C_s$  are coupling parameters,  $\alpha_w$  and  $C_w$  are the coefficients of linear thermal expansion and volumetric compression of pure water,  $n$  is the porosity,  $k$  is the hydraulic conductivity,  $\gamma_w$  is the unit of pore water and  $Z = ((1 - n)\rho_s c_s + n\rho_w c_w)/T_o - 3\beta\alpha_s$  is coupling parameter,  $\rho_w$  and  $\rho_s$  are the densities of pore water and solid grains,  $c_w$  and  $c_s$  are the heat capacities of pore water and solid grains and  $K$  is the coefficient of heat conductivity. Here,  $F(r, t)$ ,  $Q(r, t)$ , and  $W(r, t)$  are the body force, heat generation source, and the injected volume rate per unit volume of a distribute water source, respectively. The mechanical, thermal, and pressure boundary conditions are:

$$\begin{aligned}
C_{11}u(r_i, t) + C_{12}u_{,r}(r_i, t) + C_{13}T(r_i, t) \\
+ C_{14}p(r_i, t) = f_1(t) \\
C_{21}u(r_o, t) + C_{22}u_{,r}(r_o, t) + C_{23}T(r_o, t) \\
+ C_{24}p(r_o, t) = f_2(t) \\
C_{31}T(r_i, t) + C_{32}T_{,r}(r_i, t) = f_3(t) \\
C_{41}T(r_o, t) + C_{42}T_{,r}(r_o, t) = f_4(t) \\
C_{51}p(r_i, t) = f_5(t) \\
C_{61}p(r_o, t) = f_6(t)
\end{aligned} \quad (4)$$

where  $C_{ij}$  are the mechanical, thermal, and pressure coefficients, which by assigning different values for them different types of mechanical, thermal, and pressure boundary conditions may be obtained. These boundary conditions include the displacement, strain, stress, specified temperature, convection, pressure, and heat flux. The initial boundary conditions are assumed in general form:

$$\begin{aligned}
u(r, 0) &= f_7(r) \\
u_{,t}(r, 0) &= f_8(r) \\
T(r, 0) &= f_9(r) \\
p(r, 0) &= f_{10}(r)
\end{aligned} \quad (5)$$

## Solution

Equations (1) to (3) are the system of nonhomogeneous partial differential equations with nonconstant coefficients (functions of radius variable  $r$  only) has general and particular solutions.

### General Solution with Homogeneous Boundary Conditions

Since the coefficients of these equations are independent of time variable ( $t$ ), the exponential function form of time variable may be assumed for the general solution as:

$$\begin{aligned}
u(r, t) &= [U(r)]e^{\lambda t} \\
T(r, t) &= [\theta(r)]e^{\lambda t} \\
p(r, t) &= [P(r)]e^{\lambda t}
\end{aligned} \quad (6)$$

Substituting (6) into homogeneous parts of (1–3) yields:

$$\begin{aligned}
U'' + \frac{1}{r}U' - \frac{1}{r^2}U + d_1P' + d_2\theta' &= 0 \\
\theta'' + \frac{1}{r}\theta' + d_4\lambda\theta + d_5\lambda P + d_6\lambda(U' + \frac{1}{r}U) &= 0 \\
P'' + \frac{1}{r}P' + d_7\lambda P + d_8\lambda\theta + d_9\lambda(U' + \frac{1}{r}U) &= 0
\end{aligned} \quad (7)$$

Equations (7) are a system of ordinary differential equations, where the prime symbol (') shows differentiation with respect to the radius variable  $r$  and  $d_1$  to  $d_9$  are constant parameters given in the appendix.

### Change in Dependent Variables

To obtain a solution for (7), the dependent variables are changed as:

$$\begin{aligned}
U^*(r) &= r^{-\frac{1}{2}}U(r) \\
\theta^*(r) &= r^{-\frac{1}{2}}\theta(r) \\
P^*(r) &= r^{-\frac{1}{2}}P(r)
\end{aligned} \quad (8)$$

Substituting (8) into (7) gives:

$$\begin{aligned}
U'' + \frac{1}{r}U' - \frac{9}{4}\frac{1}{r^2}U + d_3\lambda^2U - d_2\frac{1}{2}\frac{1}{r}\theta \\
+ d_2\theta' - d_1\frac{1}{2}\frac{1}{r}P + d_1P' = 0 \\
\theta'' + \frac{1}{r}\theta' - \frac{1}{4}\frac{1}{r^2}\theta + d_4\lambda\theta + d\lambda\frac{3}{2}\frac{1}{r}U \\
+ d_6\lambda U' + d_5\lambda P = 0 \\
P'' + \frac{1}{r}P' - \frac{1}{4}\frac{1}{r^2}P + d_7\lambda P + d_8\lambda\theta + d_9\lambda\frac{3}{2}\frac{1}{r}U \\
+ d_9\lambda U' = 0
\end{aligned} \quad (9)$$

**Solution**

The first solutions of  $U_1$ ,  $\theta_1$  and  $P_1$  are considered as:

$$\begin{aligned} U_1(r) &= A_1 J_{\frac{3}{2}}(\beta r) \\ \theta_1(r) &= B_1 J_{\frac{1}{2}}(\beta r) \\ P_1(r) &= C_1 J_{\frac{1}{2}}(\beta r) \end{aligned} \quad (10)$$

Substituting (10) into (9) yields:

$$\begin{aligned} \{(-\beta^2 + \lambda^2 d_3)A_1 - d_2\beta B_1 - d_1\beta C_1\} J_{\frac{3}{2}}(\beta r) &= 0 \\ \{\lambda d_6\beta A_1 + (-\beta^2 + \lambda d_4)B_1 + \lambda d_5 C_1\} J_{\frac{1}{2}}(\beta r) &= 0 \\ \{\lambda d_9\beta A_1 + \lambda d_8 B_1 + (-\beta^2 + \lambda d_7)C_1\} J_{\frac{1}{2}}(\beta r) &= 0 \end{aligned} \quad (11)$$

Equations (11) show that  $U_1$ ,  $\theta_1$  and  $P_1$  can be the solutions of (9), if and only if:

$$\begin{bmatrix} -\beta^2 + \lambda^2 d_3 & -d_2\beta & -d_1\beta \\ \lambda d_6\beta & -\beta^2 + \lambda d_4 & \lambda d_5 \\ \lambda d_9\beta & \lambda d_8 & -\beta^2 + \lambda d_7 \end{bmatrix} \begin{Bmatrix} A_1 \\ B_1 \\ C_1 \end{Bmatrix} = \begin{Bmatrix} 0 \\ 0 \\ 0 \end{Bmatrix} \quad (12)$$

The nontrivial solution of (12) is obtained by equating the determinant of this equation to zero as:

$$\begin{aligned} d_3 d_4 d_7 \lambda^4 - d_3 d_5 d_8 \lambda^4 - \beta^2 d_3 d_4 \lambda^3 - \beta^2 d_3 d_7 \lambda^3 \\ - \beta^2 d_4 d_7 \lambda^2 + \beta^2 d_5 d_8 \lambda^2 + \beta^2 d_1 d_4 d_9 \lambda^2 \\ - \beta^2 d_1 d_6 d_8 \lambda^2 + \beta^2 d_2 d_6 d_7 \lambda^2 - \beta^2 d_2 d_5 d_9 \lambda^2 \\ + \beta^4 d_3 \lambda^2 + \beta^4 d_4 \lambda + \beta^4 d_7 \lambda - \beta^4 d_2 d_6 \lambda \\ - \beta^4 d_1 d_9 \lambda - \beta^6 = 0 \end{aligned} \quad (13)$$

Equation (13) is the first characteristic equation. Thus, it is concluded that  $U_1$ ,  $\theta_1$  and  $P_1$  satisfy the system of equations (9) and they are the first solution of the system.

The second solutions of  $U_2$ ,  $\theta_2$  and  $P_2$  are considered as:

$$\begin{aligned} U_2(r) &= [A_2 J_{\frac{3}{2}}(\beta r) + A_3 r J_{\frac{3}{2}}(\beta r)] \\ \theta_2(r) &= [B_2 J_{\frac{1}{2}}(\beta r) + B_3 r J_{\frac{1}{2}}(\beta r)] \\ P_2(r) &= [C_2 J_{\frac{1}{2}}(\beta r) + C_3 r J_{\frac{1}{2}}(\beta r)] \end{aligned} \quad (14)$$

Substituting (14) into (9) yields:

$$\begin{aligned} \{(\beta^2 - d_3 \lambda^2)A_3 + C_3 d_1 \beta + B_3 d_2 \beta\} r J_{\frac{3}{2}}(\beta r) \\ + \left\{ \begin{aligned} &-A_3 \beta + A_2 d_3 \lambda^2 - A_2 \beta^2 - C_3 d_1 - B_3 d_2 \\ &-B_2 d_2 \beta - C_2 d_1 \beta + A_3 d_3 \lambda^2 \frac{3}{\beta} \end{aligned} \right\} \\ J_{\frac{3}{2}}(\beta r) = 0 \\ \{-B_2 \beta^2 + 2B_3 \beta + B_2 d_4 \lambda + A_2 d_6 \beta \lambda + C_2 d_5 \lambda\} \\ J_{\frac{1}{2}}(\beta r) + \{A_3 d_6 \beta \lambda + (-\beta^2 + d_4 \lambda)B_3 + C_3 d_5 \lambda\} \\ r J_{\frac{1}{2}}(\beta r) = 0 \\ \{2C_3 \beta + C_2 d_7 \lambda + B_2 d_8 \lambda + A_2 d_9 \lambda \beta - C_2 \beta^2\} \\ J_{\frac{1}{2}}(\beta r) + \{+A_3 d_9 \lambda \beta + B_3 d_8 \lambda + (-\beta^2 + d_7 \lambda)C_3\} \\ r J_{\frac{1}{2}}(\beta r) = 0 \end{aligned} \quad (15)$$

The expressions for  $U_2$ ,  $\theta_2$  and  $P_2$  can be the solutions of (9), if and only if:

$$\begin{bmatrix} -\beta^2 + \lambda^2 d_3 & -d_2\beta & -d_1\beta \\ \lambda d_6\beta & -\beta^2 + \lambda d_4 & \lambda d_5 \\ \lambda d_9\beta & \lambda d_8 & -\beta^2 + \lambda d_7 \end{bmatrix} \begin{Bmatrix} A_3 \\ B_3 \\ C_3 \end{Bmatrix} = \begin{Bmatrix} 0 \\ 0 \\ 0 \end{Bmatrix} \quad (16)$$

$$\begin{aligned} (d_3 \lambda^2 - \beta^2)A_2 + \left(d_3 \lambda^2 \frac{3}{\beta} - \beta\right)A_3 - d_2 \beta B_2 \\ - d_2 B_3 - d_1 \beta C_2 - d_1 C_3 = 0 \end{aligned} \quad (17)$$

$$d_6 \lambda \beta A_2 + (-\beta^2 + d_4 \lambda)B_2 + 2\beta B_3 + d_5 \lambda C_2 = 0 \quad (18)$$

$$d_9\lambda\beta A_2 + d_8\lambda B_2 + (d_7\lambda - \beta^2)C_2 + 2\beta C_3 = 0 \quad (19)$$

The nontrivial solution of (16) is obtained by equating the determinant to zero as:

$$\begin{aligned} & d_3d_4d_7\lambda^4 - d_3d_5d_8\lambda^4 - \beta^2d_3d_4\lambda^3 - \beta^2d_3d_7\lambda^3 \\ & - \beta^2d_4d_7\lambda^2 + \beta^2d_5d_8\lambda^2 + \beta^2d_1d_4d_9\lambda^2 - \beta^2d_1d_6d_8\lambda^2 \\ & + \beta^2d_2d_6d_7\lambda^2 - \beta^2d_2d_5d_9\lambda^2 + \beta^4d_3\lambda^2 + \beta^4d_4\lambda \\ & + \beta^4d_7\lambda - \beta^4d_2d_6\lambda - \beta^4d_1d_9\lambda - \beta^6 = 0 \end{aligned} \quad (20)$$

Equations (17) to (19) give the relations between  $A_2, A_3, B_2, B_3, C_2$  and  $C_3$  and they play as the balancing ratios that make (14) to be the second solution of the system of equations (9). The third solution of the system of the ordinary differential equations with nonconstant coefficients (9) must be considered as:

$$\begin{aligned} U_3(r) &= [A_4J_{\frac{3}{2}}(\beta r) + A_5rJ_{\frac{3}{2}}(\beta r) + A_6r^2J_{\frac{3}{2}}(\beta r)] \\ \theta_3(r) &= [B_4J_{\frac{3}{2}}(\beta r) + B_5rJ_{\frac{3}{2}}(\beta r) + B_6r^2J_{\frac{3}{2}}(\beta r)] \\ P_3(r) &= [C_4J_{\frac{3}{2}}(\beta r) + C_5rJ_{\frac{3}{2}}(\beta r) + C_6r^2J_{\frac{3}{2}}(\beta r)] \end{aligned} \quad (21)$$

Substituting (21) into (9) yields:

$$\begin{aligned} & \left\{ \begin{aligned} & (-\beta^2 + d_3\lambda^2)A_4 + \left(-\beta + d_3\lambda^2\frac{3}{\beta}\right)A_5 \\ & + \left(-3 + d_3\lambda^2\frac{15}{\beta^2}\right)A_6 \\ & - B_4d_2\beta - d_2B_5 - 3d_2\frac{1}{\beta}B_6 - C_4\beta d_1 - \frac{3}{2}C_5d_1 - C_6\frac{3}{\beta}d_1 \end{aligned} \right\} J_{\frac{3}{2}}(\beta r) = 0 \\ & \{(\beta^2 - d_3\lambda^2)A_6 + C_6\beta d_1 + B_6d_2\beta\} r^2 J_{\frac{3}{2}}(\beta r) = 0 \\ & \left\{ \begin{aligned} & (\beta^2 - d_3\lambda^2)A_5 + \left(\beta - \frac{5}{\beta}d_3\lambda^2\right)A_6 + B_5d_2\beta + d_2B_6 \\ & + C_5\beta d_1 + C_6\frac{3}{2}d_1 - \frac{1}{2}C_6d_1 \end{aligned} \right\} rJ_{\frac{3}{2}}(\beta r) = 0 \\ & \{d_6\lambda\beta A_4 + (-\beta^2 + d_4\lambda)B_4 + 2\beta B_5 + d_5\lambda C_4\} J_{\frac{1}{2}}(\beta r) = 0 \\ & \{-d_6\lambda\beta A_6 + (\beta^2 - d_4\lambda)B_6 - d_5\lambda C_6\} r^2 J_{\frac{1}{2}}(\beta r) = 0 \\ & \left\{ \begin{aligned} & d_6\lambda\beta A_5 + 3d_6\lambda A_6 + (d_4\lambda - \beta^2)B_5 + \left(d_4\frac{3}{\beta}\lambda + \beta\right)B_6 \\ & + d_5\lambda C_5 + d_5\frac{3}{\beta}\lambda C_6 \end{aligned} \right\} rJ_{\frac{3}{2}}(\beta r) = 0 \\ & \{+d_9\lambda A_4\beta + d_8\lambda B_4 + (-\beta^2 + d_7\lambda)C_4 + 2C_5\beta\} J_{\frac{1}{2}}(\beta r) = 0 \\ & \{(-d_7\lambda + \beta^2)C_6 - d_8\lambda B_6 - d_9\lambda A_6\beta\} r^2 J_{\frac{1}{2}}(\beta r) = 0 \\ & \left\{ \begin{aligned} & (-\beta^2 + d_7\lambda)C_5 + \left(\beta + d_7\lambda\frac{3}{\beta}\right)C_6 + d_8\lambda B_5 + d_8\frac{3}{\beta}\lambda B_6 \\ & + d_9\lambda\beta A_5 + 3d_9\lambda A_6 \end{aligned} \right\} rJ_{\frac{3}{2}}(\beta r) = 0 \end{aligned} \quad (22)$$

The expressions for  $U_3$ ,  $\theta_3$  and  $P_3$  can be solutions of (9), if and only if:

$$\begin{bmatrix} -\beta^2 + \lambda^2 d_3 & -d_2 \beta & -d_1 \beta \\ \lambda d_6 \beta & -\beta^2 + \lambda d_4 & \lambda d_5 \\ \lambda d_9 \beta & \lambda d_8 & -\beta^2 + \lambda d_7 \end{bmatrix} \begin{Bmatrix} A_6 \\ B_6 \\ C_6 \end{Bmatrix} = \begin{Bmatrix} 0 \\ 0 \\ 0 \end{Bmatrix} \quad (23)$$

$$\begin{aligned} & (-\beta^2 + d_3 \lambda^2) A_4 + \left( -\beta + d_3 \lambda^2 \frac{3}{\beta} \right) A_5 \\ & + \left( -3 + d_3 \lambda^2 \frac{15}{\beta^2} \right) A_6 - B_4 d_2 \beta - d_2 B_5 \\ & - 3 d_2 \frac{1}{\beta} B_6 - C_4 \beta d_1 - \frac{3}{2} C_5 d_1 - C_6 \frac{3}{\beta} d_1 = 0 \end{aligned} \quad (24)$$

$$\begin{aligned} & (\beta^2 - d_3 \lambda^2) A_5 + \left( \beta - \frac{5}{\beta} d_3 \lambda^2 \right) A_6 + B_5 d_2 \beta \\ & + d_2 B_6 + C_5 \beta d_1 + C_6 \frac{3}{2} d_1 - \frac{1}{2} C_6 d_1 = 0 \end{aligned} \quad (25)$$

$$d_6 \lambda \beta A_4 + (-\beta^2 + d_4 \lambda) B_4 + 2 \beta B_5 + d_5 \lambda C_4 = 0 \quad (26)$$

$$\begin{aligned} & d_6 \lambda \beta A_5 + 3 d_6 \lambda A_6 + (d_4 \lambda - \beta^2) B_5 \\ & + \left( d_4 \frac{3}{\beta} \lambda + \beta \right) B_6 + d_5 \lambda C_5 + d_5 \frac{3}{\beta} \lambda C_6 = 0 \end{aligned} \quad (27)$$

$$d_9 \lambda A_4 \beta + d_8 \lambda B_4 + (-\beta^2 + d_7 \lambda) C_4 + 2 C_5 \beta = 0 \quad (28)$$

$$\begin{aligned} & (-\beta^2 + d_7 \lambda) C_5 + \left( \beta + d_7 \lambda \frac{3}{\beta} \right) C_6 + d_8 \lambda B_5 \\ & + d_8 \frac{3}{\beta} \lambda B_6 + d_9 \lambda \beta A_5 + 3 d_9 \lambda A_6 = 0 \end{aligned} \quad (29)$$

The nontrivial solution of (23) is obtained by equating the determinant of this equation to zero as:

$$\begin{aligned} & d_3 d_4 d_7 \lambda^4 - d_3 d_5 d_8 \lambda^4 - \beta^2 d_3 d_4 \lambda^3 - \beta^2 d_3 d_7 \lambda^3 \\ & - \beta^2 d_4 d_7 \lambda^2 + \beta^2 d_5 d_8 \lambda^2 + \beta^2 d_1 d_4 d_9 \lambda^2 \\ & - \beta^2 d_1 d_6 d_8 \lambda^2 + \beta^2 d_2 d_6 d_7 \lambda^2 - \beta^2 d_2 d_5 d_9 \lambda^2 \\ & + \beta^4 d_3 \lambda^2 + \beta^4 d_4 \lambda + \beta^4 d_7 \lambda - \beta^4 d_2 d_6 \lambda \\ & - \beta^4 d_1 d_9 \lambda - \beta^6 = 0 \end{aligned} \quad (30)$$

The characteristic equation (30) is the same as the characteristic equations (13) and (20).

This equality is interesting as it prevents mathematical dilemma and complexity and a single value for the eigenvalue  $\beta$  simultaneously satisfies three characteristic equations (13), (20), and (30). Equations (24) to (29) give the relations between  $A_4, A_5, A_6, B_4, B_5, B_6, C_4, C_5$  and  $C_6$ . These relations play as the balancing ratios that help (21) to be the third solution of the system of equations (9). The complete general solutions for the solid sphere are:

$$\begin{aligned} U^g(r) &= A_1 J_{\frac{3}{2}}(\beta r) + A_3 [\zeta_1 J_{\frac{3}{2}}(\beta r) + r J_{\frac{5}{2}}(\beta r)] \\ &\quad + A_6 [\zeta_2 J_{\frac{3}{2}}(\beta r) + \zeta_3 r J_{\frac{3}{2}}(\beta r) + r^2 J_{\frac{5}{2}}(\beta r)] \\ \theta^g(r) &= A_1 \zeta_4 J_{\frac{1}{2}}(\beta r) + A_3 [\zeta_5 J_{\frac{1}{2}}(\beta r) + \zeta_6 r J_{\frac{3}{2}}(\beta r)] \\ &\quad + A_6 [\zeta_7 J_{\frac{1}{2}}(\beta r) + \zeta_8 r J_{\frac{3}{2}}(\beta r) + \zeta_9 r^2 J_{\frac{5}{2}}(\beta r)] \\ P^g(r) &= A_1 \zeta_{10} J_{\frac{1}{2}}(\beta r) + A_3 [\zeta_{11} J_{\frac{1}{2}}(\beta r) + \zeta_{12} r J_{\frac{3}{2}}(\beta r)] \\ &\quad + A_6 [\zeta_{13} J_{\frac{1}{2}}(\beta r) + \zeta_{14} r J_{\frac{3}{2}}(\beta r) + \zeta_{15} r^2 J_{\frac{5}{2}}(\beta r)] \end{aligned} \quad (31)$$

and for hollow sphere are:

$$\begin{aligned}
 U^g(r) &= A_1 J_{\frac{3}{2}}(\beta r) + A_3 [\zeta_1 J_{\frac{3}{2}}(\beta r) + r J_{\frac{5}{2}}(\beta r)] \\
 &\quad + A_6 [\zeta_2 J_{\frac{3}{2}}(\beta r) + \zeta_3 r J_{\frac{3}{2}}(\beta r) + r^2 J_{\frac{7}{2}}(\beta r)] \\
 &\quad + \hat{A}_1 Y_{\frac{3}{2}}(\beta r) + \hat{A}_3 [\zeta_1 Y_{\frac{3}{2}}(\beta r) + r Y_{\frac{5}{2}}(\beta r)] \\
 &\quad + \hat{A}_6 [\zeta_2 Y_{\frac{3}{2}}(\beta r) + \zeta_3 r Y_{\frac{3}{2}}(\beta r) + r^2 Y_{\frac{7}{2}}(\beta r)] \\
 \theta^g(r) &= A_1 \zeta_4 J_{\frac{1}{2}}(\beta r) + A_3 [\zeta_5 J_{\frac{1}{2}}(\beta r) + \zeta_6 r J_{\frac{3}{2}}(\beta r)] \\
 &\quad + A_6 [\zeta_7 J_{\frac{1}{2}}(\beta r) + \zeta_8 r J_{\frac{3}{2}}(\beta r) + \zeta_9 r^2 J_{\frac{5}{2}}(\beta r)] \\
 &\quad + \hat{A}_1 \zeta_4 Y_{\frac{1}{2}}(\beta r) + \hat{A}_3 [\zeta_5 Y_{\frac{1}{2}}(\beta r) + \zeta_6 r Y_{\frac{3}{2}}(\beta r)] \\
 &\quad + \hat{A}_6 [\zeta_7 Y_{\frac{1}{2}}(\beta r) + \zeta_8 r Y_{\frac{3}{2}}(\beta r) + \zeta_9 r^2 Y_{\frac{5}{2}}(\beta r)] \\
 P^g(r) &= A_1 \zeta_{10} J_{\frac{1}{2}}(\beta r) + A_3 [\zeta_{11} J_{\frac{1}{2}}(\beta r) + \zeta_{12} r J_{\frac{3}{2}}(\beta r)] \\
 &\quad + A_6 [\zeta_{13} J_{\frac{1}{2}}(\beta r) + \zeta_{14} r J_{\frac{3}{2}}(\beta r) + \zeta_{15} r^2 J_{\frac{5}{2}}(\beta r)] \\
 &\quad + \hat{A}_1 \zeta_{10} Y_{\frac{1}{2}}(\beta r) + \hat{A}_3 [\zeta_{11} Y_{\frac{1}{2}}(\beta r) + \zeta_{12} r Y_{\frac{3}{2}}(\beta r)] \\
 &\quad + \hat{A}_6 [\zeta_{13} Y_{\frac{1}{2}}(\beta r) + \zeta_{14} r Y_{\frac{3}{2}}(\beta r) + \zeta_{15} r^2 Y_{\frac{5}{2}}(\beta r)]
 \end{aligned} \tag{32}$$

where  $\zeta_1$  to  $\zeta_{15}$  are ratios obtained from (23–29), (16–19), and (12) and are given in the appendix. Substituting  $U^g$ ,  $\theta^g$  and  $P^g$  in the homogeneous form of the boundary conditions (4), three linear algebraic equations are obtained. They are the coefficients depending on  $\lambda$  and  $\beta$ . Setting the determinant of the coefficients equal to zero, the second characteristic equation is obtained. Simultaneous solution of this equation and (11) results into infinite number of two eigenvalues  $\beta_n$  and  $\lambda_n$ . Therefore,  $U^g$ ,  $\theta^g$  and  $P^g$  for solid sphere are rewritten as:

$$\begin{aligned}
 U^g(r) &= A_1 \left[ J_{\frac{3}{2}}(\beta r) + \zeta_{16} [\zeta_1 J_{\frac{3}{2}}(\beta r) + r J_{\frac{5}{2}}(\beta r)] \right. \\
 &\quad \left. + \zeta_{17} [\zeta_2 J_{\frac{3}{2}}(\beta r) + \zeta_3 r J_{\frac{3}{2}}(\beta r) + r^2 J_{\frac{7}{2}}(\beta r)] \right] \\
 \theta^g(r) &= A_1 \left[ \zeta_4 J_{\frac{1}{2}}(\beta r) + \zeta_{16} [\zeta_5 J_{\frac{1}{2}}(\beta r) + \zeta_6 r J_{\frac{3}{2}}(\beta r)] \right. \\
 &\quad \left. + \zeta_{17} [\zeta_7 J_{\frac{1}{2}}(\beta r) + \zeta_8 r J_{\frac{3}{2}}(\beta r) + \zeta_9 r^2 J_{\frac{5}{2}}(\beta r)] \right] \\
 P^g(r) &= A_1 \left[ \zeta_{10} J_{\frac{1}{2}}(\beta r) + \zeta_{16} [\zeta_{11} J_{\frac{1}{2}}(\beta r) + \zeta_{12} r J_{\frac{3}{2}}(\beta r)] \right. \\
 &\quad \left. + \zeta_{17} [\zeta_{13} J_{\frac{1}{2}}(\beta r) + \zeta_{14} r J_{\frac{3}{2}}(\beta r) + \zeta_{15} r^2 J_{\frac{5}{2}}(\beta r)] \right]
 \end{aligned} \tag{33}$$

where  $\zeta_{16}$  and  $\zeta_{17}$  are presented in the appendix. Let us show the functions in the brackets of (33) by functions  $H_0$ ,  $H_1$  and  $H_2$  as:

$$\begin{aligned}
 H_0 &= J_{\frac{3}{2}}(\beta r) + \zeta_{16} [\zeta_1 J_{\frac{3}{2}}(\beta r) + r J_{\frac{5}{2}}(\beta r)] \\
 &\quad + \zeta_{17} [\zeta_2 J_{\frac{3}{2}}(\beta r) + \zeta_3 r J_{\frac{3}{2}}(\beta r) + r^2 J_{\frac{7}{2}}(\beta r)] \\
 H_1 &= \zeta_4 J_{\frac{1}{2}}(\beta r) + \zeta_{16} [\zeta_5 J_{\frac{1}{2}}(\beta r) + \zeta_6 r J_{\frac{3}{2}}(\beta r)] \\
 &\quad + \zeta_{17} [\zeta_7 J_{\frac{1}{2}}(\beta r) + \zeta_8 r J_{\frac{3}{2}}(\beta r) + \zeta_9 r^2 J_{\frac{5}{2}}(\beta r)] \\
 H_2 &= \zeta_{10} J_{\frac{1}{2}}(\beta r) + \zeta_{16} [\zeta_{11} J_{\frac{1}{2}}(\beta r) + \zeta_{12} r J_{\frac{3}{2}}(\beta r)] \\
 &\quad + \zeta_{17} [\zeta_{13} J_{\frac{1}{2}}(\beta r) + \zeta_{14} r J_{\frac{3}{2}}(\beta r) + \zeta_{15} r^2 J_{\frac{5}{2}}(\beta r)]
 \end{aligned} \tag{34}$$

According to the Sturm-Liouville theorem, these functions are orthogonal with respect to the weight function  $p(r) = r$  such as:

$$\int_{r_1}^{r_0} H(\beta_n r) H(\beta_m r) r dr = \begin{cases} 0 \\ \|H(\beta_n r)\|^2 \end{cases} \tag{35}$$

where  $\|H(\beta_n r)\|$  is norm of the  $H$  function and equals:

$$\|H(\beta_n r)\| = \left[ \int_{r_1}^{r_0} r H^2(\beta_n r) dr \right]^{\frac{1}{2}} \tag{36}$$

Due to the orthogonality of function  $H$ , every piece-wise continuous function, such as  $f(r)$ , can be expanded in terms of the function  $H$  (either  $H_0, H_1$  or  $H_2$ ), and is called the  $H$ -Fourier series as:

$$f(r) = \sum_{n=1}^{\infty} e_n H(\beta_n r) \quad (37)$$

where  $e_n$  equals:

$$e_n = \frac{1}{\|H(\beta_n r)\|^2} \int_{r_i}^{r_o} f(r) H(r) r dr \quad (38)$$

Using (6), (33), and (34), the displacement and temperature distributions due to the general solution become:

$$\begin{aligned} u^g(r, t) &= \sum_{n=1}^{\infty} \left\{ \sum_{m=1}^4 a_{nm} e^{\lambda_{nm} t} \right\} H_0(\beta_n r) \\ T^g(r, t) &= \sum_{n=1}^{\infty} \left\{ \sum_{m=1}^4 N_{nm} a_{nm} e^{\lambda_{nm} t} \right\} H_1(\beta_n r) \quad (39) \\ p^g(r, t) &= \sum_{n=1}^{\infty} \left\{ \sum_{m=1}^4 M_{nm} a_{nm} e^{\lambda_{nm} t} \right\} H_2(\beta_n r) \end{aligned}$$

where  $N_{nm}$  and  $M_{nm}$  are ratios obtained by substituting (39) to (1–3). Using the initial conditions (5) and with the help of (36), (37), and (38), four unknown constants are obtained.

### Particular Solution with Nonhomogeneous Boundary Conditions

The general solutions may be used as proper functions for guessing the particular solution adopted to the nonhomogeneous parts of the (1–3) and the nonhomogeneous boundary conditions (4) as:

$$\begin{aligned} u^p(r, t) &= \sum_{n=1}^{\infty} \left\{ \left[ G_{1n}(t) J_{\frac{3}{2}}(\beta_n r) + G_{2n}(t) r J_{\frac{5}{2}}(\beta_n r) + G_{3n}(t) r^2 J_{\frac{7}{2}}(\beta_n r) \right] + r^2 G_{4n}(t) \right\} \\ T^p(r, t) &= \sum_{n=1}^{\infty} \left\{ \left[ G_{5n}(t) J_{\frac{1}{2}}(\beta_n r) + G_{6n}(t) r J_{\frac{3}{2}}(\beta_n r) + G_{7n}(t) r^2 J_{\frac{5}{2}}(\beta_n r) \right] + r^2 G_{8n}(t) \right\} \quad (40) \\ p^p(r, t) &= \sum_{n=1}^{\infty} \left\{ \left[ G_{9n}(t) J_{\frac{3}{2}}(\beta_n r) + G_{10n}(t) r J_{\frac{5}{2}}(\beta_n r) + G_{11n}(t) r^2 J_{\frac{7}{2}}(\beta_n r) \right] + r^2 G_{12n}(t) \right\} \end{aligned}$$

For the solid sphere, the second type of Bessel function  $Y$  is excluded. It is necessary and suitable to expand the body force  $F(r, t)$ , heat source  $Q(r, t)$ , and porosity function  $W(r, t)$  in  $H$ -Fourier expansion form as:

$$\begin{aligned} F(r, t) &= \sum_{n=1}^{\infty} F_n(t) H_0(\beta_n r) \\ Q(r, t) &= \sum_{n=1}^{\infty} Q_n(t) H_1(\beta_n r) \quad (41) \\ P(r, t) &= \sum_{n=1}^{\infty} P_n(t) H_2(\beta_n r) \end{aligned}$$

where  $F_n(t)$ ,  $Q_n(t)$ , and  $P_n(t)$  are:

$$\begin{aligned} F_n(t) &= \frac{1}{\|H_0(\beta_n r)\|^2} \int_{r_i}^{r_o} F(r, t) H_0(\beta_n r) r dr \\ Q_n(t) &= \frac{1}{\|H_1(\beta_n r)\|^2} \int_{r_i}^{r_o} Q(r, t) H_1(\beta_n r) r dr \quad (42) \\ P_n(t) &= \frac{1}{\|H_2(\beta_n r)\|^2} \int_{r_i}^{r_o} P(r, t) H_2(\beta_n r) r dr \end{aligned}$$

Substituting (40) and (41) into nonhomogeneous form of equations (1) into (3) yields:

$$\begin{cases} -d_6\dot{G}_3(t)\beta - d_{21}E_2\dot{G}_4(t) + G_7(t)\beta^2 \\ -d_4\dot{G}_7(t) - d_{20}E_2G_8(t) - d_{22}E_2\dot{G}_8(t) \\ -d_5\dot{G}_{11}(t) - d_{23}E_2\dot{G}_{12}(t) + d_{11}d_{14}E_2Q_n(t) \end{cases} = 0 \quad (43e)$$

$$\begin{cases} -G_1(t)\beta^2 + d_3\ddot{G}_1(t) - G_2(t)\beta + d_3\ddot{G}_2(t)\frac{3}{\beta} - 3G_3(t) \\ + d_3\ddot{G}_3(t)\frac{15}{\beta^2} + \left\{C_0 + C_1\frac{3}{\beta} + C_2\frac{15}{\beta^2}\right\}d_{16}G_4(t) \\ + \left\{C_0 + C_1\frac{3}{\beta} + C_2\frac{15}{\beta^2}\right\}d_{19}\ddot{G}_4(t) \\ - G_5(t)d_2\beta - d_2G_6(t) - 3d_2G_7(t)\frac{1}{\beta} \\ + \left\{C_0 + C_1\frac{3}{\beta} + C_2\frac{15}{\beta^2}\right\}d_{17}G_8(t) \\ - d_1G_9(t)\beta - d_1G_{10}(t) - 3d_1G_{11}(t)\frac{1}{\beta} \\ + \left\{C_0 + C_1\frac{3}{\beta} + C_2\frac{15}{\beta^2}\right\}d_{18}G_{12}(t) \\ - \left\{C_0 + C_1\frac{3}{\beta} + C_2\frac{15}{\beta^2}\right\}d_{10}d_{13}F_n(t) \end{cases} = 0 \quad (43a)$$

$$\begin{cases} d_6\dot{G}_2(t)\beta + 3d_6\dot{G}_3(t) + \left\{E_1 + E_2\frac{3}{\beta}\right\}d_{21}\dot{G}_4(t) \\ - G_6(t)\beta^2 + d_4\dot{G}_6(t) + G_7(t)\beta + d_4\dot{G}_7(t)\frac{3}{\beta} \\ + \left\{E_1 + E_2\frac{3}{\beta}\right\}d_{20}G_8(t) + \left\{E_1 + E_2\frac{3}{\beta}\right\}d_{22}\dot{G}_8(t) \\ + d_5\dot{G}_{10}(t) + d_5\dot{G}_{11}(t)\frac{3}{\beta} \\ + \left\{E_1 + E_2\frac{3}{\beta}\right\}d_{23}\dot{G}_{12}(t) - \left\{E_1 + E_2\frac{3}{\beta}\right\} \\ d_{11}d_{14}Q_n(t) \end{cases} = 0 \quad (43f)$$

$$\begin{cases} + \dot{G}_1(t)d_9\beta + D_0d_{25}\dot{G}_4(t) + d_8\dot{G}_5(t) - G_9(t)\beta^2 \\ + d_7\dot{G}_9(t) + D_0d_{26}\dot{G}_8(t) + 2G_{10}(t)\beta \\ + D_0d_{24}G_{12}(t) + D_0d_{27}\dot{G}_{12}(t) - d_{12}d_{15}D_0W_n(t) \end{cases} = 0 \quad (43g)$$

$$\begin{cases} G_3(t)\beta^2 - d_3\ddot{G}_3(t) - d_{16}C_2G_4(t) - d_{19}C_2\ddot{G}_4(t) \\ + G_7(t)d_2\beta - d_{17}C_2G_8(t) - d_{18}C_2G_{12}(t) \\ + d_1G_{11}(t)\beta + d_{10}d_{13}C_2F_n(t) \end{cases} = 0 \quad (43b)$$

$$\begin{cases} G_{11}(t)\beta^2 - d_7\dot{G}_{11}(t) - d_8\dot{G}_7(t) - d_9\dot{G}_3(t)\beta \\ - D_2r^2d_{25}\dot{G}_4(t) - D_2d_{26}\dot{G}_8(t) - D_2d_{24}G_{12}(t) \\ - D_2d_{27}\dot{G}_{12}(t) + d_{12}d_{15}D_2W_n(t) \end{cases} = 0 \quad (43h)$$

$$\begin{cases} G_2(t)\beta^2 - d_3\ddot{G}_2(t) + G_3(t)\beta - d_3\ddot{G}_3(t)\frac{5}{\beta} \\ + \left\{-C_1 - C_2\frac{5}{\beta}\right\}d_{16}G_4(t) + \left\{-C_1 - C_2\frac{5}{\beta}\right\} \\ d_{19}\ddot{G}_4(t) + d_2G_6(t)\beta + d_2G_7(t) - \left\{C_1 + C_2\frac{5}{\beta}\right\} \\ d_{17}G_8(t) + d_1G_{10}(t)\beta + d_1G_{11}(t) - \left\{C_1 + C_2\frac{5}{\beta}\right\} \\ d_{18}G_{12}(t) + \left\{C_1F_n(t) + C_2\frac{5}{\beta}\right\}d_{10}d_{13}F_n(t) \end{cases} = 0 \quad (43c)$$

$$\begin{cases} + \dot{G}_2(t)\beta d_9 + 3\dot{G}_3(t)d_9 + \left\{D_1 + D_2\frac{3}{\beta}\right\} \\ d_{25}\dot{G}_4(t) + d_8\dot{G}_6(t) + d_8\dot{G}_7(t)\frac{3}{\beta} \left\{D_1\dot{G}_8(t) + D_2\frac{3}{\beta}\right\} \\ \dot{G}_8(t)d_{26} - G_{10}(t)\beta^2 + d_7\dot{G}_{10}(t) + G_{11}(t)\beta \\ + d_7\dot{G}_{11}(t)\frac{3}{\beta} + \left\{D_1 + D_2\frac{3}{\beta}\right\}d_{27}\dot{G}_{12}(t) \\ + \left\{D_1 + D_2\frac{3}{\beta}\right\}d_{24}G_{12}(t) - \left\{D_1 + D_2\frac{3}{\beta}\right\} \\ d_{12}d_{15}W_n(t) \end{cases} = 0 \quad (43i)$$

$$\begin{cases} + d_6\dot{G}_1(t)\beta + d_{21}E_0\dot{G}_4(t) - G_5(t)\beta^2 \\ + d_4\dot{G}_5(t) + 2G_6(t)\beta + d_{20}E_0G_8(t) \\ + d_{22}E_0\dot{G}_8(t) + d_5\dot{G}_9(t)d_{23}E_0\dot{G}_{12}(t) \\ - d_{11}d_{14}E_0Q_n(t) \end{cases} = 0 \quad (43d)$$

where  $d_{10}$  to  $d_{27}$  are the coefficients of the H-expansion and constant parameters presented in the appendix. By taking Laplace transform of (43) and using three boundary conditions of (4) (for solid sphere only second, fourth, and sixth boundary conditions are applicable),



a system of algebraic equations is obtained and solved by Cramer's methods in the Laplace domain, where by the inverse Laplace transform the functions are transformed into the real time domain and finally  $G_{1n}(t)$  to  $G_{12n}(t)$  are calculated.

In this process, it is necessary to consider the following points:

1. The initial conditions (5) are considered only for the general solutions and the initial conditions of  $G_{1n}(t)$  to  $G_{12n}(t)$  for the particular solutions are considered equal to zero.
2. Laplace transform of (43) is in terms of polynomial function form of the Laplace parameter  $s$  (not the Bessel functions form of  $s$ ). Therefore, the exact inverse Laplace transform is possible and somehow simple.
3. For the hollow sphere, it is enough to include the second type of Bessel function  $Y(r)$  in a sequence of the particular solution as:

$$\begin{aligned}
 u^p(r, t) &= \sum_{n=1}^{\infty} \left\{ \left[ G_{1n}(t) J_{\frac{3}{2}}(\beta n r) + G_{2n}(t) r J_{\frac{5}{2}}(\beta n r) \right. \right. \\
 &\quad \left. \left. + G_{3n}(t) r^2 J_{\frac{7}{2}}(\beta n r) \right] + \left[ G_{4n}(t) Y_{\frac{3}{2}}(\beta n r) \right. \right. \\
 &\quad \left. \left. + G_{5n}(t) r Y_{\frac{5}{2}}(\beta n r) + G_{6n}(t) r^2 Y_{\frac{7}{2}}(\beta n r) \right] \right. \\
 &\quad \left. + r G_{7n}(t) + r^2 G_{8n}(t) \right\} \\
 T^p(r, t) &= \sum_{n=1}^{\infty} \left\{ \left[ G_{9n}(t) J_{\frac{3}{2}}(\beta n r) + G_{10n}(t) r J_{\frac{5}{2}}(\beta n r) \right. \right. \\
 &\quad \left. \left. + G_{11n}(t) r^2 J_{\frac{7}{2}}(\beta n r) \right] \left[ G_{12n}(t) Y_{\frac{3}{2}}(\beta n r) \right. \right. \\
 &\quad \left. \left. + G_{13n}(t) r Y_{\frac{5}{2}}(\beta n r) + G_{14n}(t) r^2 Y_{\frac{7}{2}}(\beta n r) \right] \right. \\
 &\quad \left. + r G_{15n}(t) + r^2 G_{16n}(t) \right\} \\
 p^p(r, t) &= \sum_{n=1}^{\infty} \left\{ \left[ G_{17n}(t) J_{\frac{3}{2}}(\beta n r) + G_{18n}(t) r J_{\frac{5}{2}}(\beta n r) \right. \right. \\
 &\quad \left. \left. + G_{19n}(t) r^2 J_{\frac{7}{2}}(\beta n r) \right] + \left[ G_{20n}(t) J_{\frac{1}{2}}(\beta n r) \right. \right. \\
 &\quad \left. \left. + G_{21n}(t) r J_{\frac{3}{2}}(\beta n r) + G_{23n}(t) r^2 J_{\frac{5}{2}}(\beta n r) \right] \right. \\
 &\quad \left. + r^2 G_{24n}(t) \right\}
 \end{aligned} \tag{44}$$

**Exact Solution for Quasi-Static Porothermoelasticity in Spherical Coordinates, Table 1** Material parameters

Material Parameters					
Unit	Value	Parameter	Unit	Value	Parameter
n	0.4	—	$\alpha_s$	$10^{-5} \times 1.5$	$1/^\circ\text{C}$
E	$105 \times 6$	Pa	$\alpha_w$	$10^{-4} \times 2$	$1/^\circ\text{C}$
v	0.3	—	$c_s$	0.8	$\text{J/g}^\circ\text{C}$
$T_0$	293		$c_w$	4.2	$\text{J/g}^\circ\text{C}$
$K_s$	$1010 \times 2$	Pa	$\rho_s$	$106 \times 2.6$	$\text{g/m}^3$
$K_w$	$109 \times 5$	Pa	$\rho_w$	$106 \times 1$	$\text{g/m}^3$
K	0.3	$\text{w/m}^\circ\text{C}$	$\alpha$	1	—

By substituting (44) in (1–3), eighteen equations are obtained, where using the six boundary conditions (4) twenty four functions  $G_{1n}(t)$  to  $G_{24n}(t)$  are obtained for the hollow sphere.

## Results and Discussions

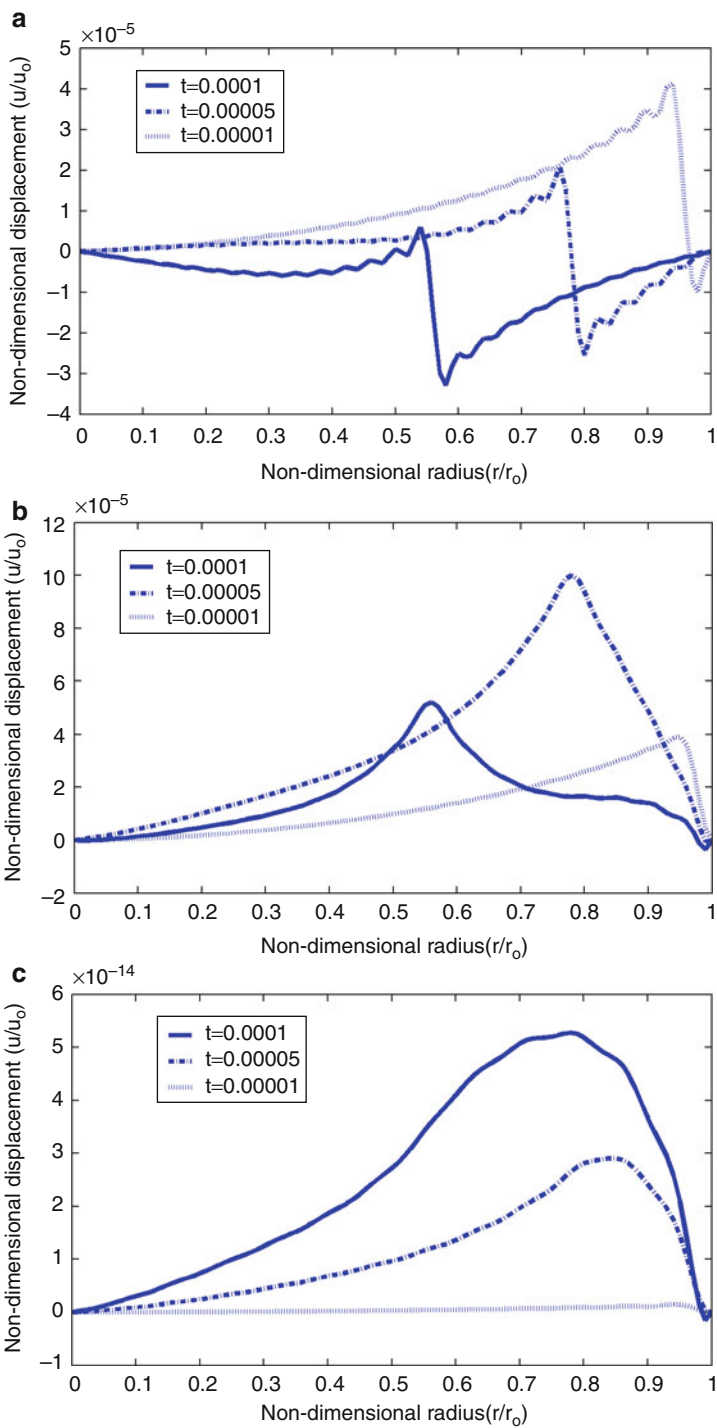
In this section, the responses of a solid cylinder with radius 1 m under different thermal boundary are considered. The results obtained from the present formulation for a solid cylinder are shown for several cases. These include investigating the wave propagation in solid cylinder on variation of the temperature, displacement. The initial temperature  $T_0$  is considered to be  $293^\circ\text{K}$ . The material properties are:

For the first example, an instantaneous hot spot  $T(1, t) = 10^{-3} T_0 \delta(t)$ , where  $\delta(t)$  is a unit Dirac function, is considered and the outside radius of the cylinder is assumed to be fixed ( $u(1, t) = 0$  and  $p(1, t) = 0$ ). Figures 1a to 3a show the wave fronts for the displacement, temperature, and pressure at three times (0.0001, 0.00005, 0.00001 s).

For the second example, a Heaviside function is applied to the outside surface of the cylinder given as  $T(1, t) = 10^{-3} H(t)$ , and the surface is assumed to be at zero temperature ( $u(1, t) = 0$  and  $p(1, t) = 0$ ). Figures 1b to 3b show variations for the displacement, temperature, and pressure at three times (0.0001, 0.00005, 0.00001 s).

**Exact Solution for  
Quasi-Static  
Porothermoelasticity  
in Spherical  
Coordinates, Fig. 1**

- (a) Nondimensional displacement distribution due to input  $T(1,t) = 10^{-3}T_0\delta(t)$ ,
- (b) nondimensional displacement distribution due to input  $T(1,t) = 10^{-3}H(t)$ ,
- (c) nondimensional displacement distribution due to input  $T(1,t) = \sin(10^{-3}t)$



For the third example, a sinosial function is applied to the outside surface of the cylinder given as  $T(1,t) = \sin(10^{-3}t)$ , and the surface is assumed to be at zero temperature

( $u(1,t) = 0$  and  $p(1,t) = 0$ ). Figures 1c to 3c show variations for the displacement, temperature, and pressure at three times (0.0001, 0.00005, 0.00001 s).

**Exact Solution for  
Quasi-Static  
Porothermoelasticity  
in Spherical  
Coordinates, Fig. 2**

(a) Nondimensional temperature distribution due to input

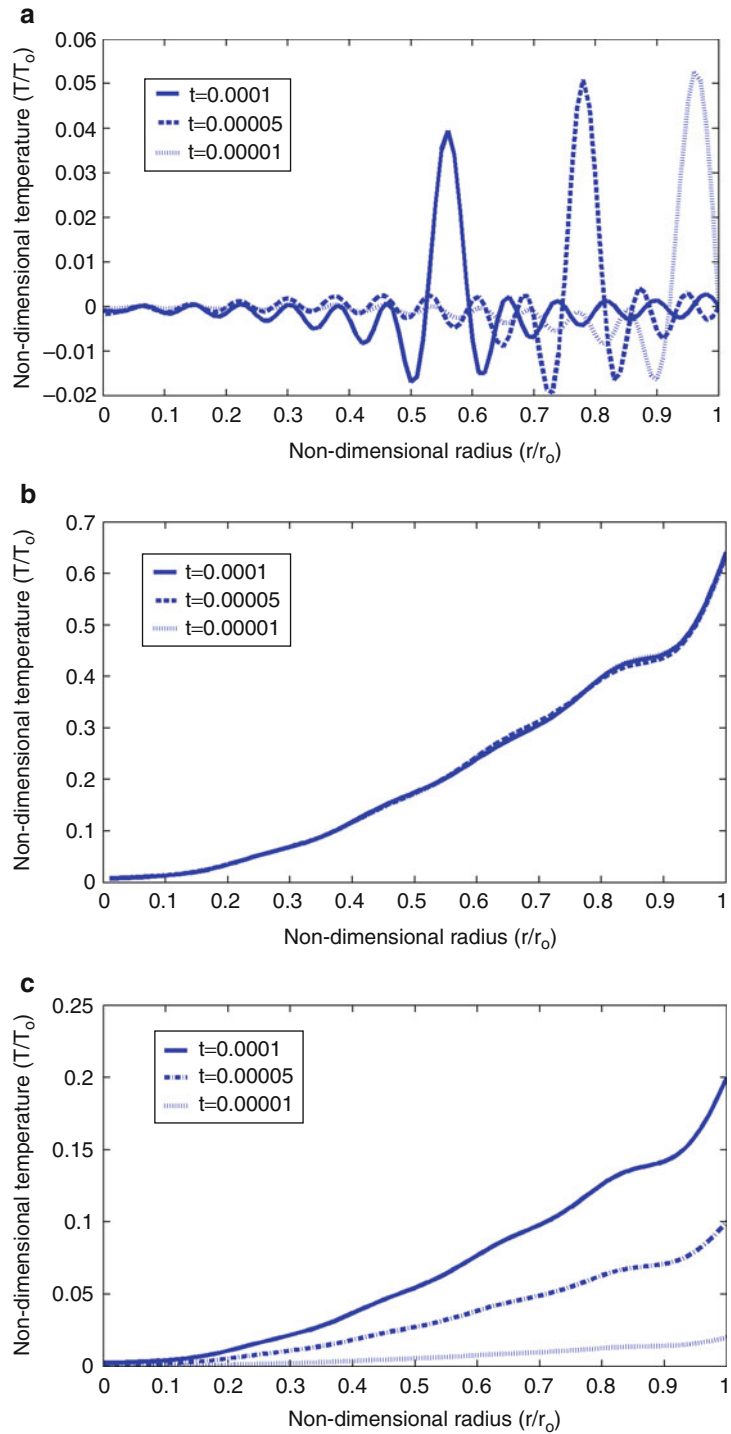
$$T(1, t) = 10^{-3} T_0 \delta(t),$$

(b) nondimensional temperature distribution due to input

$$T(1, t) = 10^{-3} H(t),$$

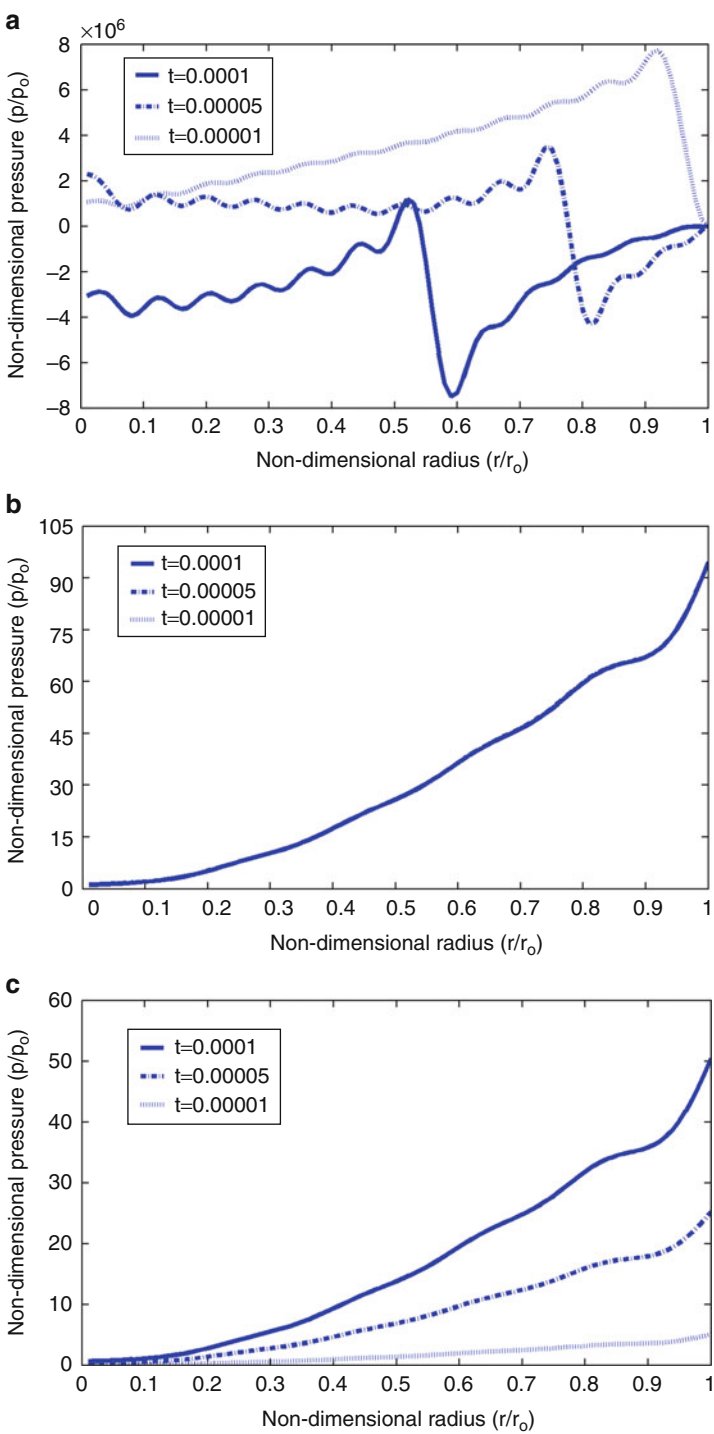
(c) nondimensional temperature distribution due to input

$$T(1, t) = \sin(10^{-3} t)$$



**Exact Solution for  
Quasi-Static  
Porothermoelasticity  
in Spherical  
Coordinates, Fig. 3**

(a) Nondimensional pressure distribution due to input  $T(1,t) = 10^{-3}T_0\delta(t)$ ,  
(b) nondimensional pressure distribution due to input  $T(1,t) = 10^{-3}H(t)$ ,  
(c) nondimensional pressure distribution due to input  $T(1,t) = \sin(10^{-3}t)$



## Conclusion

In this entry, analytical solution for the quasi-static porothermoelasticity of thick cylinders under radial temperature is presented. The method is based on the eigenfunctions Fourier expansion, which is a classical and traditional method of solution of the typical initial and boundary value problems. The noncompetitive strength of this method is its ability to reveal the fundamental mathematical and physical properties and interpretations of the problem under studying. In the quasi-static porothermoelastic problem of radial-symmetric cylinder, the governing equations are a system of partial differential equations with two independent variables, radius ( $r$ ) and time ( $t$ ). The traditional procedure to solve this class of problems is to eliminate the time variable by using the Laplace transform. The resulting system is a set of ordinary differential equations in terms of the radius variable, which falls in the Bessel functions family. This method of analysis brings the Laplace parameter ( $s$ ) in the argument of the Bessel functions, causing hardship or impossibility in carrying out the exact inverse of the Laplace transformation. As a result, the numerical inverse of the Laplace transformation is used in the papers dealing with this type of problems in literature. In this entry, to prevent this problem, when the Laplace transform is applied to the particular solutions, it is postponed after eliminating the radius variable  $r$  by H-Fourier Expansion. Thus, the Laplace parameter ( $s$ ) appears in polynomial function forms, and hence, the exact Laplace inversion transformation is possible.

## References

1. Bai B (2006) Response of saturated porous media subjected to local thermal loading on the surface of semi-infinite space. *J Acta Mech Sinica* 22:54–61
2. Bai B (2006) Fluctuation responses of saturated porous media subjected to cyclic thermal loading. *J Comput Geotech* 33:396–403
3. Droujinine A (2006) Generalized anelastic asymptotic ray theory. *J Wave Motion* 43:357–367
4. Bai B, Li T (2009) Solution for cylindrical cavity in saturated thermoporoelastic medium. *J Acta Mech Sinica* 22:85–92
5. Hetnarski RB (1964) Solution of the coupled problem of thermoelasticity in the form of series of functions. *J Arch Mech Stos* 16:919–941
6. Hetnarski RB, Ignaczak J (1993) Generalized thermoelasticity: closed-form solutions. *J Therm Stresses* 16:473–498
7. Hetnarski RB, Ignaczak J (1994) Generalized thermoelasticity: response of semi-space to a shortlaser pulse. *J Therm Stresses* 17:377–396
8. Georgiadis HG, Lykotrafitis G (2005) Rayleigh waves generated by a thermal source: a three-dimensional transient thermoelasticity solution. *J Appl Mech* 72:129–138
9. Wagner P (1994) Fundamental matrix of the system of dynamic linear thermoelasticity. *J Therm stresses* 17:549–565
10. Jabbari M, Dehbani H (2009) An exact solution for classic coupled thermoporoelasticity in cylindrical coordinates. *J Solid Mech Arak* 1:343–357
11. Kosheleva V, Ghassemi A (2004) Complex variable BEM for thermo- and poroelasticity. *J Eng Anal Bound Elem* 28:825–832
12. Zhou X, Ghassemi A (2009) Finite element analysis of coupled chemo-poro-thermo-mechanical effects around a wellbore in swelling shale. *Int J Rock Mech Min* 46:769–778
13. Jabbari M, Dehbani H (2012) An exact solution for quasi-static poro-thermoelasticity in spherical coordinates. *I J Mech Eng T ISME, I Soc Mech Eng* 12:86–108
14. Smith DW, Booker JR (1993) Green's Functions for a fully coupled thermoporoelastic material. *J Numer Anal Met Geo mech* 17:139–63

## Exact Solution of Inverse Heat Conduction Problems

Jan Taler

Institute of Thermal Power Engineering, Faculty of Mechanical Engineering, Cracow University of Technology, Cracow, Poland

## Overview

In inverse problems, boundary conditions are determined on the basis of temperature measurements taken at the selected internal points in

a body. Temperature, heat flux, or heat transfer coefficient can be determined at a boundary [1–11]. If the heat transfer coefficient is to be determined, the fluid temperature is measured as well. The thermophysical properties of the body,  $k$ ,  $c$ , and  $\rho$ , are also known.

Inverse heat transfer problems also include optimization problems in the field of heating or cooling of construction elements [11–15]. In terms of the optimization problems, boundary conditions should change in time so that temperature at selected internal points or thermal stresses at a boundary point or a point that lies inside the element would change as the given time transient prescribes. In terms of thermal stresses, one has to determine the allowed temperature transients of a medium (while heat transfer coefficient is known at the surface of a construction element) that thermal stresses would not exceed the allowable stresses at selected points.

Because of the rapid temperature changes of the fluid taking place during start-up and shut-down of a power plant, high thermal stresses occur in thick-walled elements of installations. Analytical, exact solutions for temperature and thermal stresses were developed for linear and sudden time changes of ambient temperature [16–18], but the knowledge of the time-independent heat transfer coefficient is required. In the simplified method for calculating one-dimensional thermal stresses [11, 19–21], based on the quasi steady state, the knowledge of the heat transfer coefficient at the inner surface of the component is not necessary. However, the quasi steady state approach assumes that the rate of fluid temperature changes is constant over a long time period. Such conditions are rarely encountered in the engineering practice.

The objective of the developed method is fast and simple evaluation of the temperature and thermal stresses under assumption of arbitrary changing ambient temperature and time-dependent heat transfer coefficient. In practice, however, it is not possible to calculate the heat transfer coefficient exactly enough knowing mass

flow rate, pressure, and temperature. Solving the inverse heat conduction problem for the temperature distribution makes it possible to calculate the thermal stresses with higher accuracy [2, 22]. In [22] the Beck method of solving, the inverse problem was used. In this method unique mathematical solution of the transient temperature distribution requires the knowledge of the initial temperature in each point of the body. Therefore, practical application of this method to the real-time thermal stresses monitoring is highly limited.

The highest stresses caused by temperature differences and fluid pressure take place at the body inner surface. The thermal stresses at the inner surface of the body are proportional to the difference between the inner surface temperature and the mean integral temperature. This difference will be evaluated usually by measuring the temperature at two or three locations of various depths in the wall, first of them being placed possibly close to the inner surface, second in the wall middle, and third close to the outer surface. Because the distance from the inner surface to the first measuring point cannot be smaller than 3.5 mm due to the mechanical stresses, real temperature changes of the inner surface can be significantly different from the measured changes. Furthermore, the point of temperature equivalent to the mean temperature does not lie in the wall middle, in the quasi steady, and in the transient cases; its location alters in the transient case. In [4–8] the methods allowing to calculate the temperature difference  $\Delta T = T_m(t) - T(r_{in}, t)$  from the time-temperature changes measured on the outer surface were developed. The methods presented in [4–8] have two advantageous features:

- Only one temperature sensor is needed.
- The component wall does not need to be drilled for mounting the temperature sensor.

In the following, analytical solutions of the inverse heat conduction problems will be analyzed. The methods for determining the transient temperature distribution over the wall thickness when input data, that is, the thermocouples

responses, are known only at one or at several interior locations will be discussed.

### Derivation of Formulas for Temperature Distribution and Heat Flux in a Simple-Shape Bodies on the Basis of a Measured Temperature Transient in a Single Point

Derive formulas for temperature distribution and heat flux in a plate, cylinder, and sphere with constant thermophysical properties:  $k$ ,  $c$ , and  $\rho$ . Temperature transient  $f(t_i)$ ,  $i = 1, 2, 3, \dots, N$  on an insulated plate surface or inside a cylinder or a sphere is known from the measurements taken. Number  $N$  is the number of measurement points ( $t_i, f_i$ ). Known temperature transient at discrete points is approximated by function  $y(t)$ , which one can differentiate a finite number of times.

Temperature distribution is defined by the heat conduction equation

$$\frac{1}{r^m} \frac{\partial}{\partial r} \left( r^m \frac{\partial T}{\partial r} \right) = \frac{1}{\kappa} \frac{\partial T}{\partial t} \quad (1)$$

and conditions

$$T|_{r=0} = y(t) \quad (2)$$

$$\left. \frac{\partial T}{\partial r} \right|_{r=0} = 0 \quad (3)$$

where  $m = 0$  for the plate,  $m = 1$  for the cylinder, and  $m = 2$  for the sphere.

In contrast to simple heat conduction problems, conditions (2) and (3) are prescribed in an inverse problem on the same boundary  $r = 0$ . Temperature  $T_s(t)$  and heat flux  $q_s(t)$  are determined at the boundary  $r = L$  or  $r = r_z$ . The unknown temperature distribution has the following form [1, 11]:

$$T(r, t) = \sum_{n=0}^{\infty} h_n(r) \frac{d^n y}{dt^n} \quad (4)$$

By substituting formula (4) into (1), one obtains

$$\frac{1}{r^m} \frac{d}{dr} \left( r^m \frac{dh_0}{dr} \right) = 0 \quad \text{dla } n = 0 \quad (5)$$

and

$$\frac{1}{r^m} \frac{d}{dr} \left( r^m \frac{dh_n}{dr} \right) = \frac{1}{\kappa} h_{n-1} \quad \text{dla } n = 1, 2, 3 \dots \quad (6)$$

By substituting expression (4) into conditions (2) and (3), one obtains

$$h_0(0) = 1, \quad h_n(0) = 0, \quad n = 1, 2, 3 \dots \quad (7)$$

and

$$\left. \frac{dh_n}{dr} \right|_{r=0} = 0, \quad n = 0, 1, 2, 3 \dots \quad (8)$$

The solutions of (5) and (6) with conditions (7) and (8) will be discussed for the plate, cylinder, and sphere below.

#### Plate

The solution of (5) and (6) with conditions (7) and (8) has the following form for  $m = 0$ :

$$h_n(r) = \frac{1}{(2n)!} \frac{r^{2n}}{\kappa^n}, \quad n = 0, 1 \dots \quad (9)$$

By substituting dependence (9) into (4), a formula for the plate temperature distribution is obtained:

$$T(r, t) = y(t) + \sum_{n=1}^{\infty} \frac{1}{(2n)!} \left( \frac{r^2}{\kappa} \right)^n \frac{d^n y}{dt^n} \quad (10)$$

Heat flux is determined from the Fourier law:

$$q(r) = k \frac{\partial T}{\partial r} = c \rho r \sum_{n=1}^{\infty} \frac{1}{(2n-1)!} \left( \frac{r^2}{\kappa} \right)^{n-1} \frac{d^n y}{dt^n} \quad (11)$$

By substituting  $r = L$ , the formula for the heat flux at the surface of the plate is obtained:



$$\begin{aligned}
 q_s &= q(r)|_{r=L} \\
 &= c\rho L \sum_{n=1}^{\infty} \frac{1}{(2n-1)!} \left(\frac{L^2}{\kappa}\right)^{n-1} \frac{d^n y}{dt^n} \\
 &= k \sum_{n=1}^{\infty} \frac{L^{2n-1}}{(2n-1)!} \frac{1}{\kappa^n} \frac{d^n y}{dt^n} \quad (12)
 \end{aligned}$$

### Cylinder

The solution of (5) and (6) has the following form for the sphere and cylinder:

$$h_n(r) = \frac{r^{2n}}{2^n(n!)(m+1)(m+3)\dots(m+2n-1)\kappa^n} \quad (13)$$

By substituting formula (13) into (4), one obtains for the cylinder ( $m = 1$ ):

$$T(r, t) = y(t) + \sum_{n=1}^{\infty} \frac{r^{2n}}{2^{2n}(n!)^2\kappa^n} \frac{d^n y}{dt^n} \quad (14)$$

The heat flux is determined from the Fourier law:

$$q(r, t) = k \frac{\partial T}{\partial r} = k \sum_{n=1}^{\infty} \frac{n r^{2n-1}}{2^{2n-1}(n!)^2\kappa^n} \frac{d^n y}{dt^n} \quad (15)$$

The heat flux at the cylinder surface  $q_s(t)$  is obtained by substituting  $r = r_o$  into expression (15).

### Sphere

Since for the sphere  $m = 2$ , then the expression for temperature distribution is obtained by substituting expression (13) into (4)

$$T(r, t) = y(t) + \sum_{n=1}^{\infty} \frac{r^{2n}}{(2n+1)!\kappa^n} \frac{d^n y}{dt^n} \quad (16)$$

The heat flux  $q(r, t)$  is determined from the Fourier law:

$$q(r, t) = k \frac{\partial T}{\partial r} = k \sum_{n=1}^{\infty} \frac{2n r^{2n-1}}{(2n+1)!\kappa^n} \frac{d^n y}{dt^n} \quad (17)$$

The heat flux on the sphere surface  $q_s(t)$  is obtained by substituting  $r = r_o$  into expression (17).

The solutions for the temperature distribution  $T(r, t)$  and heat flux  $q(r, t)$  presented above are very sensitive to the slightest temperature measurement random errors in  $f(t)$ . This is the result of temperature and heat flux extrapolation, measured or known (e.g., from symmetry condition of temperature field) at a point that lies inside the body in the direction of the body surface.

In terms of the direct problems, fast changes in heat flux or temperature, which occur at the body surface, are quickly suppressed inside it when boundary conditions are known.

In the case of inverse problems, small measurement errors are magnified even dozens of times, causing large oscillations in the determined heat flux or surface temperature.

Additional information regarding the inverse problems can be found in papers [1–11, 23].

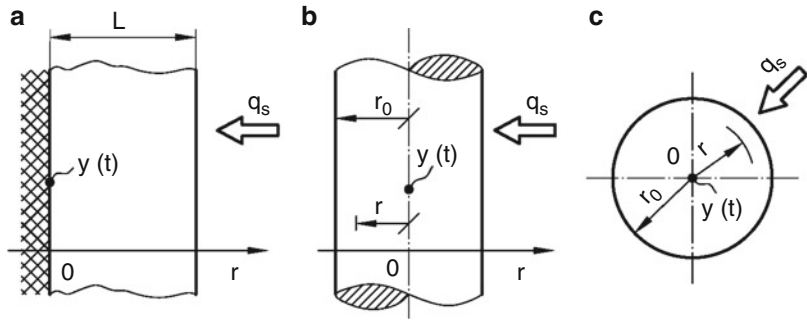
### Monitoring of Transient Thermal Stress in Thick-Walled Components

A new analytical method for determining transient temperature and thermal stress distributions in thick-walled components of steam boilers when the temperature measurements in time are taken with a thermocouple positioned at the outer surface. The solution is assumed to be in the form of the power series in which the measured temperature and its time derivatives are multiplied by known spatial functions. Since the problem considered is ill posed and the results are very sensitive to the inaccurate experimental measurements, the thermocouple readings are smoothed using an eleven-point digital filter. The presented solution of the inverse problem does not require a specification of the initial temperature distribution, so it is very appropriate for on-line thermal stress monitoring. The method may be used to determine transient temperature and thermal stress distributions in slabs, hollow cylinders, and spheres. The present method incorporates the advantages of simplicity and accuracy inherent to analytical closed form



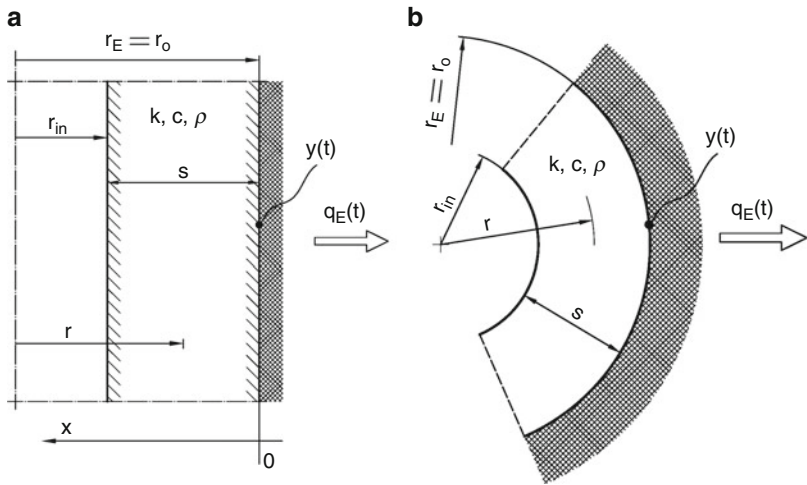
### Exact Solution of Inverse Heat Conduction Problems,

**Fig. 1** Schematic of the inverse transient heat conduction problem in bodies of simple shape; (a) slab, (b) cylinder, and (c) sphere



### Exact Solution of Inverse Heat Conduction Problems, Fig. 2

Inverse heat conduction problem for plane (a) and cylindrical or spherical (b) wall



solutions. Numerical results are presented as verification of the presented technique.

### Mathematical Formulation

A transient temperature distribution over the thickness of the plane (Fig. 2a) and cylindrical or spherical wall (Fig. 2b) will be determined based on the known histories of temperature  $y(t)$  and heat flux  $q_E(t)$  at the outer surface  $r = r_o$ .

The inverse problem is governed by the heat conduction equation

$$\frac{1}{r^m} \frac{\partial}{\partial r} \left( r^m \frac{\partial T}{\partial r} \right) = \frac{1}{\kappa} \frac{\partial T}{\partial t} \quad (18)$$

which is subject to the boundary conditions at  $r = r_E$

$$T|_{r=r_E} = y(t) \quad (19)$$

$$-k \frac{\partial T}{\partial r} \bigg|_{r=r_E} = q_E(t) \quad (20)$$

where  $m = 0$  for plane wall,  $m = 1$  for cylindrical wall, and  $m = 2$  for spherical wall.

The general solution of the inverse problem (18)–(20) has the following form [1]:

$$T(r, t) = \sum_{n=0}^{\infty} h_n(r) \frac{d^n y}{dt^n} - \frac{1}{k} \sum_{n=0}^{\infty} g_n(r) \frac{d^n q_E}{dt^n} \quad (21)$$

Substituting the solution (21) into (18) gives two ordinary differential equations for  $h_n(r)$

$$\frac{1}{r^m} \frac{d}{dr} \left( r^m \frac{dh_n}{dr} \right) = 0 \quad (22)$$

$$\frac{1}{r^m} \frac{d}{dr} \left( r^m \frac{dh_n}{dr} \right) = \frac{1}{\kappa} h_{n-1}, \quad n = 1, 2, 3, \dots \quad (23)$$

and  $g_n(r)$

$$\frac{1}{r^m} \frac{d}{dr} \left( r^m \frac{dg_0}{dr} \right) = 0 \quad (24)$$

$$\frac{1}{r^m} \frac{d}{dr} \left( r^m \frac{dg_n}{dr} \right) = \frac{1}{\kappa} g_{n-1}, \quad n = 1, 2, 3, \dots \quad (25)$$

Applying the boundary conditions (19) and (20), we see that the functions  $h_n(r)$  and  $g_n(r)$  should satisfy the conditions:

$$h_0(r_E) = 1, \quad h_n(r_E) = 0, \quad n = 1, 2, 3, \dots, \quad (26)$$

$$\left. \frac{dh_n}{dr} \right|_{r=r_E} = 0, \quad n = 0, 1, 2, \dots, \quad (27)$$

and

$$g_n(r_E) = 0, \quad n = 0, 1, 2, 3, \dots, \quad (28)$$

$$\left. \frac{dg_0}{dr} \right|_{r=r_E} = 1, \quad \left. \frac{dg_n}{dr} \right|_{r=r_E} = 0, \quad n = 1, 2, 3, \dots \quad (29)$$

The ordinary (22)–(25) which are subject to the boundary conditions (26)–(29) will be solved sequentially. First, (22) and (24) are solved for  $n = 0$ , then (23) and (25) for  $n = 1, 2, 3, \dots$

Introducing the dimensionless variables: the radius,  $R = r/r_E$  and the Fourier number,  $Fo = \alpha t/r_E^2$ , the solution (21) can be written in the form:

$$T(R, Fo) = y(Fo) + \sum_{n=0}^{\infty} H_n(R) \frac{d^n y}{dFo^n} - \frac{r_E}{k} \left[ q_E G_0(R) + \sum_{n=0}^{\infty} G_n(R) \frac{d^n q_E}{dFo^n} \right] \quad (30)$$

The general forms of the solutions  $H_n(R)$  and  $G_n(R)$  for the plane, cylindrical, and spherical walls are [5, 6]:

#### Plane wall

$$H_n(R) = \frac{(1-R)^{2n}}{(2n)!}, \quad n = 1, 2, \dots \quad (31)$$

$$G_n(R) = \frac{(1-R)^{2n+1}}{(2n+1)!}, \quad n = 0, 1, 2, \dots \quad (32)$$

where  $R = r/r_E$ ,  $r = r_E - x$  (Fig. 2a)

#### Spherical wall

$$H_n(R) = \left( 1 + \frac{2n}{R} \right) \frac{(R-1)^{2n}}{(2n+1)!}, \quad n = 1, 2, \dots \quad (33)$$

$$G_0(R) = 1 - \frac{1}{R}, \quad G_n(R) = \frac{1}{(2n+1)!} \frac{1}{R} (R-1)^{2n+1}, \quad n = 1, 2, \dots \quad (34)$$

#### Cylindrical wall

There is no a general solution for the hollow cylinder. The first five terms in the series in the solution (30) are as follows [8, 9]:

$$\begin{aligned} H_1(R) &= \frac{1}{4} (R^2 - 1 - 2 \ln R) \\ H_2(R) &= \frac{1}{64} (4R^2 + R^4 - 4 \ln R - 8R^2 \ln R - 5) \\ H_3(R) &= \frac{1}{2304} (R^6 + 18R^4 - 9R^2 - 10 \\ &\quad - 6 \ln R - 36R^2 \ln R - 18R^4 \ln R) \\ H_4(R) &= \frac{1}{442368} [3R^8 + 128R^6 + 108R^4 - 192R^2 - 47 \\ &\quad - 24(4R^6 + 18R^4 + 12R^2 + 1) \ln R] \\ H_5(R) &= \frac{1}{88473600} [6R^{10} + 475R^8 + 1400R^6 - 600R^4 \\ &\quad - 1150R^2 - 131 - 60(5R^8 + 40R^6 + 60R^4 \\ &\quad + 20R^2 + 1) \ln R] \end{aligned} \quad (35)$$

and

$$\begin{aligned}
 G_0(R) &= \ln R \\
 G_1(R) &= \frac{1}{4} [1 - R^2 + (R^2 + 1) \ln R] \\
 G_2(R) &= \frac{1}{256} [6 - 6R^4 + (4R^4 + 16R^2 + 4) \ln R] \\
 G_3(R) &= \frac{1}{13824} [11 + 27R^2 - 27R^4 - 11R^6 \\
 &\quad + (6R^6 + 54R^4 + 54R^2 + 6) \ln R] \\
 G_4(R) &= \frac{1}{1769472} [25 + 160R^2 - 160R^6 - 25R^8 \\
 &\quad + (12R^8 + 192R^6 + 432R^4 + 192R^2 + 12) \ln R] \\
 G_5(R) &= \frac{1}{884736000} [500 + 1625R^2 + 2000R^4 \\
 &\quad - 2000R^6 - 1625R^8 - 137R^{10} \\
 &\quad + (60R^{10} + 1500R^8 + 6000R^6 \\
 &\quad + 6000R^4 + 1500R^2 + 60) \ln R]
 \end{aligned} \quad (36)$$

If the series in the expression (30) is truncated after the first five terms, fast transient processes can be analyzed.

### Thermal Stresses in Plane, Cylindrical, and Spherical Walls

The largest thermal stresses in thick-walled pressure components occur at the heated inner surface.

The circumferential  $\sigma_\varphi$ , axial  $\sigma_a$ , and radial stresses  $\sigma_r$  at the inner surface of the cylindrical or spherical wall and at the heated surface of the plate are given by

$$\begin{aligned}
 \sigma_a &= \sigma_\varphi = \frac{E\alpha}{1-\nu} [T_m( Fo ) - T(\omega, Fo)] \\
 \sigma_r &= 0
 \end{aligned} \quad (37)$$

The formula (37) was derived under assumption that the plate and cylinder can freely elongate, but not bend. Equation (37) can be used for stress calculations in plates and hollow cylinders in cross-sections which are sufficiently distant from ends, so that their impact on the stress distribution can be neglected. In the following, the symbol  $\sigma_a$  will be used for denoting thermal stresses at the heated component surface.

The mean integral temperature over the wall thickness  $T_m( Fo )$  is defined as

$$T_m( Fo ) = \frac{1}{V} \int_V T dV = \frac{m+1}{1-\omega^{m+1}} \int_\omega^1 R^m T(R, Fo) dR \quad (38)$$

where

$m = 0$  for plane wall,

$m = 1$  for cylindrical wall,

and

$m = 2$  for spherical wall.

Assuming that  $q_E(t) = 0$ ,  $r_E = r_o$ , and substituting (30) into (38) gives the formulas for the mean temperature over the wall thickness of:

### Plane wall

$$T_m( Fo ) = y( Fo ) + \sum_{n=1}^{\infty} \frac{(1-\omega)^{2n}}{(2n+1)!} \frac{d^n y}{dFo^n} \quad (39)$$

### Cylindrical wall

$$\begin{aligned}
 T_m( Fo ) &= y( Fo ) + \left[ \frac{1+\omega^2}{8} + \frac{\omega^2 \ln \omega}{2(1-\omega^2)} \right] \frac{dy}{dFo} \\
 &+ \left\{ \frac{3\omega^2}{64} + \frac{1}{192} [(1+\omega^2)^2 - \omega^2] + \frac{\omega^2(1+\omega^2) \ln \omega}{16(1-\omega^2)} \right\} \frac{d^2 y}{dFo^2} \\
 &+ \frac{1}{1152} \left\{ \frac{(1+\omega^2)(1+\omega^4)}{8} + \frac{7}{2} [(1+\omega^2)^2 - \omega^2] - \frac{7}{2} \right. \\
 &\quad \left. + \frac{3(1+3\omega^2+\omega^4)\omega^2 \ln \omega}{1-\omega^2} \right\} \frac{d^3 y}{dFo^3} \\
 &+ \frac{1}{442368} \left[ \frac{1}{5} (3\omega^8 + 178\omega^6 \right. \\
 &\quad \left. + 478\omega^4 + 178\omega^2 + 3) \right. \\
 &\quad \left. + \frac{24\omega^2 \ln \omega}{1-\omega^2} (\omega^6 + 6\omega^4 + 6\omega^2 + 1) \right] \frac{d^4 y}{dFo^4} \\
 &+ \frac{1}{88473600} \left[ \omega^{10} + 102\omega^8 + 527\omega^6 + 527\omega^4 \right. \\
 &\quad \left. + 102\omega^2 + 1 + \frac{60\omega^2 \ln \omega}{1-\omega^2} \right. \\
 &\quad \left. (\omega^8 + 10\omega^6 + 20\omega^4 + 10\omega^2 + 1) \right] \frac{d^5 y}{dFo^5}
 \end{aligned} \quad (40)$$

**Spherical wall**

$$T_m(For) = y(For) + \frac{3}{1 + \omega + \omega^2} \sum_{n=1}^{\infty} \frac{(1 - \omega)^{2n}}{(2n + 1)!} \frac{\omega^2 + (2n + 1)\omega + 1}{2n + 3} \frac{d^n y}{dFor^n} \quad (41)$$

where  $\omega = r_{in}/r_o$ , and  $For = \kappa t/r_o^2$ .

The formulas for the thermal stresses at the inner surface of the component  $R_{in} = \omega = r_{in}/r_o$  with the insulated outer surface ( $q_E = 0$ ) are obtained from (37):

**Plane wall**

$$\sigma_a = -\frac{E\alpha}{1 - \nu} \sum_{n=1}^{\infty} \frac{2n}{(2n + 1)!} (1 - \omega)^{2n} \frac{d^n y}{dFor^n} \quad (42)$$

**Cylindrical wall**

$$\begin{aligned} \sigma_a = & \frac{E\alpha}{1 - \nu} \left\{ \frac{1}{8} \left( 3 - \omega^2 + \frac{4 \ln \omega}{1 - \omega^2} \right) \frac{dy}{dFor} \right. \\ & + \frac{1}{32} \left[ \frac{1}{3} (8 - \omega^2 - \omega^4) \right. \\ & + \left. \frac{2 \ln \omega}{1 - \omega^2} (1 + 2\omega^2 - \omega^4) \right] \frac{d^2 y}{dFor^2} \\ & + \frac{1}{2304} \left[ \frac{1}{4} (41 + 65\omega^2 - 43\omega^4 - 3\omega^6) \right. \\ & + \left. \frac{6 \ln \omega}{1 - \omega^2} (1 + 6\omega^2 - 2\omega^6) \right] \frac{d^3 y}{dFor^3} \\ & + \frac{1}{442368} \left[ \frac{1}{5} (238 + 1138\omega^2 - 62\omega^4 \right. \\ & - 462\omega^6 - 12\omega^8) + \frac{24 \ln \omega}{1 - \omega^2} \\ & + \frac{1}{88473600} \left[ 132 + 1252\omega^2 + 1127\omega^4 \right. \\ & - 873\omega^6 - 373\omega^8 - 5\omega^{10} \\ & + \left. \frac{60 \ln \omega}{1 - \omega^2} (1 + 20\omega^2 + 50\omega^4 - 25\omega^8 - 4\omega^{10}) \right] \left. \right] \frac{d^5 y}{dFor^5} \end{aligned} \quad (43)$$

**Spherical wall**

$$\begin{aligned} \sigma_a = & \frac{E\alpha}{1 - \nu} \sum_{n=1}^{\infty} \frac{(1 - \omega)^{2n}}{(2n + 1)!} \\ & \left[ \frac{3[\omega^2 + (2n + 1)\omega + 1]}{(2n + 3)(1 + \omega + \omega^2)} - \left( 1 + \frac{2n}{\omega} \right) \right] \\ \frac{d^n y}{dFor^n} = & \frac{E\alpha}{1 - \nu} \sum_{n=1}^{\infty} \frac{(1 - \omega)^{2n}}{(2n + 1)!} \\ & \left\{ \frac{3}{1 + \omega + \omega^2} \cdot \left[ \omega + \frac{(1 - \omega)^2}{2n + 3} \right] \right. \\ & \left. - \left( 1 + \frac{2n}{\omega} \right) \right\} \frac{d^n y}{dFor^n} \end{aligned} \quad (44)$$

The series (42)–(44) converge very fast. In order to obtain satisfactory accuracy, only the first three or four terms can be taken into account.

**Quasi Steady State**

Steady-state temperature and stress distributions form in the wall after heating or cooling the component with a constant fluid temperature rate. After a sufficient long time period,  $t \geq 0.5 s^2/\kappa$ , the temperature difference over the wall thickness is time invariable and depends only on the temperature rate  $v_T = dy/dt$ . When quasi steady state occurs, the wall temperature changes also with the same constant rate  $v_T$ , that is,

$$v_T = \frac{dy}{dt}, \text{ and } \frac{d^2 y}{dFor^2} = \frac{d^3 y}{dFor^3} = \dots = 0 \quad (45)$$

The formulas (42)–(44) can be substantially simplified for the quasi steady state. Substituting (45) into the expressions (42)–(44), we have:

**Plane wall**

$$\sigma_a = -\frac{1}{3} \frac{E\alpha}{1 - \nu} \frac{v_T s^2}{\kappa} \quad (46)$$

### Cylindrical wall

$$\begin{aligned}\sigma_a &= \frac{E\alpha}{1-\nu} \frac{v_T r_o^2}{\kappa} \frac{1}{8} \left( 3 - \omega^2 + \frac{4 \ln \omega}{1 - \omega^2} \right) \\ &= \frac{E\alpha}{1-\nu} \frac{v_T s^2}{\kappa} \frac{1}{8} \frac{(u^2 - 1)(3u^2 - 1) - 4u^4 \ln u}{(u - 1)^2 (u^2 - 1)}\end{aligned}\quad (47)$$

### Spherical Wall

$$\begin{aligned}\sigma_a &= \frac{E\alpha}{1-\nu} \frac{v_T r_o^2}{\kappa} \frac{(1 - \omega)^2}{6} \left[ \frac{3(\omega^2 + 3\omega + 1)}{5(\omega^2 + \omega + 1)} - \frac{2}{\omega} - 1 \right] \\ &= -\frac{E\alpha}{1-\nu} \frac{v_T s^2}{\kappa} \frac{5u^6 - 9u^5 + 5u^3 - 1}{15(u - 1)^2 (u^3 - 1)} \\ &= -\frac{E\alpha}{1-\nu} \frac{v_T s^2}{\kappa} \frac{5u^3 + 6u^2 + 3u + 1}{15(u^2 + u + 1)}\end{aligned}\quad (48)$$

where  $s = r_o - r_{in}$ ,  $\omega = r_{in}/r_o$ , and  $u = 1/\omega = r_o/r_{in}$ .

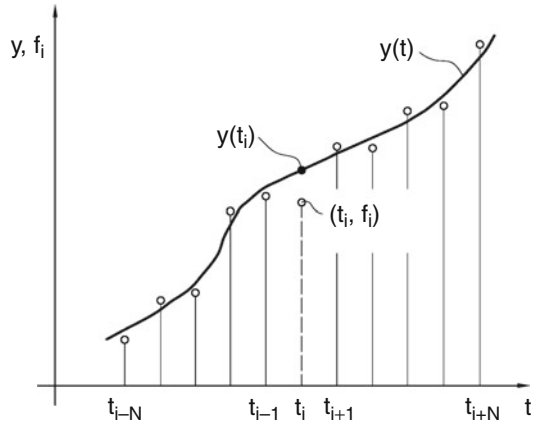
The derived formulas are used in [19, 23] and in boiler standards TRD 301 [20] and European Norm EN 12952-3 [21] for the evaluation of the thermal stresses in thick-walled pressure components.

### Smoothing of the Experimental Data

The inverse procedure for the determination of the thermal stresses is very sensitive to random measurement errors. Since measured temperatures are always burdened with random errors, it is desirable that all measurement data should be smoothed prior differentiation with respect to time [11, 23]. After approximation of the discrete data points by an appropriate function, the measured temperature transients can be differentiated to find derivatives  $d^n y/dt^n$  of different orders.

A simple way of the data approximation, which is also useful in on-line monitoring of thermal stresses, is to approximate  $(2N+1)$  subsequent data points by a polynomial of the third degree with respect to time. The successive measurement data  $(t_i, f(t_i))$  are approximated by the third-degree polynomial.

The value of the function  $y(t)$  and its derivatives  $dy^n/dt^n$ ,  $n = 1, 2, \dots$  are calculated only in the middle point  $N+1$  of the time interval  $2N\Delta t$ .



**Exact Solution of Inverse Heat Conduction Problems, Fig. 3** Smoothing of measured temperature using  $(2N+1)$  – point digital filter

The coefficients  $a_1, a_2, \dots, a_m$  of the polynomial

$$\begin{aligned}y(t) &= a_0 + a_1 t + a_2 t^2 + a_3 t^3 + \dots + a_m t^m, \\ m &< (2N + 1)\end{aligned}\quad (49)$$

are determined using the method of least squares. Minimizing the sum

$$\sum_{i=-N}^N [f(t_i) - y(t_i)]^2 = \min \quad (50)$$

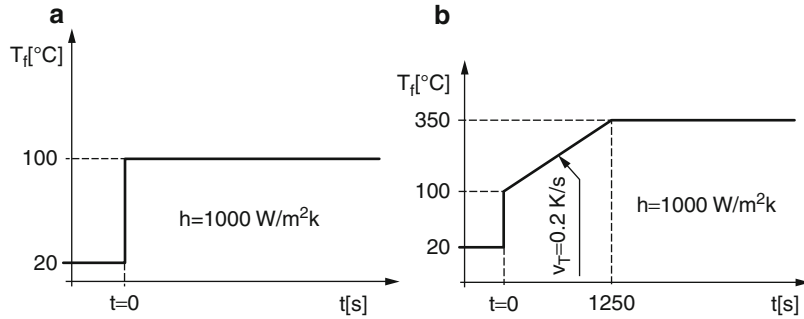
gives the coefficients  $a_1, a_2, \dots, a_m$ .

If the temperature values  $f_i$  are measured at the time points  $t_i$  with the constant time step  $\Delta t = t_{i+1} - t_i$  then the coefficients of the polynomial can be expressed as functions of measured values  $f_i$ . Assuming that the polynomial coefficients are determined based on eleven consecutive data points ( $N = 5$ ) (Fig. 3), the smoothed values of the measured temperature and its derivatives:  $y_i \frac{dy_i}{dt}$ ,  $\frac{d^2 y_i}{dt^2}$ ,  $\frac{d^3 y_i}{dt^3}$  are given by

$$\begin{aligned}y_i &= \frac{1}{429} (-36f_{i-5} + 9f_{i-4} + 44f_{i-3} + 69f_{i-2} + 84f_{i-1} \\ &\quad + 89f_i + 84f_{i+1} + 69f_{i+2} + 44f_{i+3} + 9f_{i+4} - 36f_{i+5})\end{aligned}\quad (51)$$

**Exact Solution of Inverse Heat Conduction Problems, Fig. 4**

Fluid temperature changes, (a) stepwise temperature increase and (b) fluid temperature variation in the ramp form



$$\left. \frac{dy}{dt} \right|_{t=t_i} = \frac{1}{5148 \Delta t} (300f_{i-5} - 294f_{i-4} - 532f_{i-3} - 503f_{i-2} - 296f_{i-1} + 296f_{i+1} + 503f_{i+2} + 532f_{i+3} + 294f_{i+4} - 300f_{i+5}) \quad (52)$$

$$\left. \frac{d^2y}{dt^2} \right|_{t=t_i} = \frac{5}{143 (\Delta t)^2} \left( f_{i-5} + \frac{2}{5}f_{i-4} - \frac{1}{15}f_{i-3} - \frac{2}{5}f_{i-2} - \frac{3}{5}f_{i-1} - \frac{2}{3}f_i - \frac{3}{5}f_{i+1} - \frac{2}{5}f_{i+2} - \frac{1}{15}f_{i+3} + \frac{2}{5}f_{i+4} + f_{i+5} \right) \quad (53)$$

$$\left. \frac{d^3y}{dt^3} \right|_{t=t_i} = \frac{5}{143 (\Delta t)^3} \left( -f_{i-5} + \frac{1}{5}f_{i-4} + \frac{11}{15}f_{i-3} + \frac{23}{30}f_{i-2} + \frac{7}{15}f_{i-1} - \frac{7}{15}f_{i+1} - \frac{23}{30}f_{i+2} - \frac{11}{15}f_{i+3} - \frac{1}{5}f_{i+4} + f_{i+5} \right) \quad (54)$$

Introducing the Fourier number  $Fo$  defined as  $Fo = \kappa t / r_E^2$  we can express the  $n$ th time derivative as

$$\frac{d^n y}{dt^n} = \frac{d^n y}{dFo^n} \cdot \frac{d^n Fo}{dt^n} = \left( \frac{\kappa}{r_E} \right)^n \frac{d^n y}{dFo^n}, \quad n = 1, 2, \dots \quad (55)$$

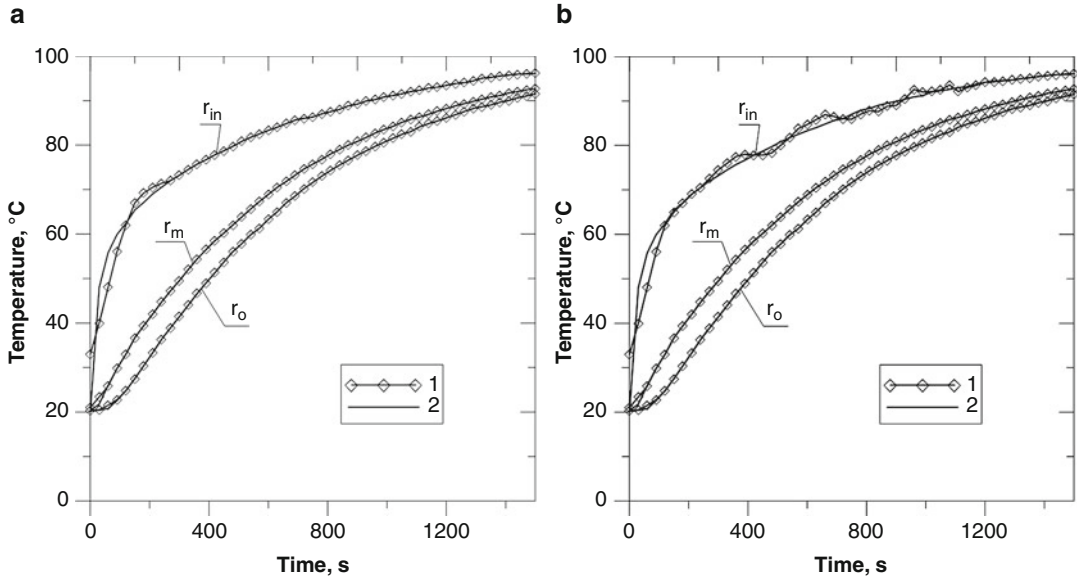
The formulas (51)–(54) are simple and accurate and can be used for reducing random

inaccuracies which are inherent in measured temperature histories.

**Example 1.** The first example presents thermal stresses evaluation using the developed method in the cylinder with  $2r_o = 1.8$  m diameter and  $s = 0.09$  m wall thickness made from 15 NiCuMoNb5 steel. The cylinder initial temperature is 20 °C. The method was tested for the sudden fluid temperature increase when the fluid temperature  $T_f$  raises stepwise from the initial temperature  $T_o = 20$ – $100$  °C (Fig. 4a) and for the ramp-wise fluid temperature change. The hollow cylinder has the initial temperature of 20 °C. The temperature of the medium increases rapidly from 20 °C to 100 °C and raises constantly with the rate of  $v_T = dT_f/dt = 0.2$  K/s (Fig. 4b).

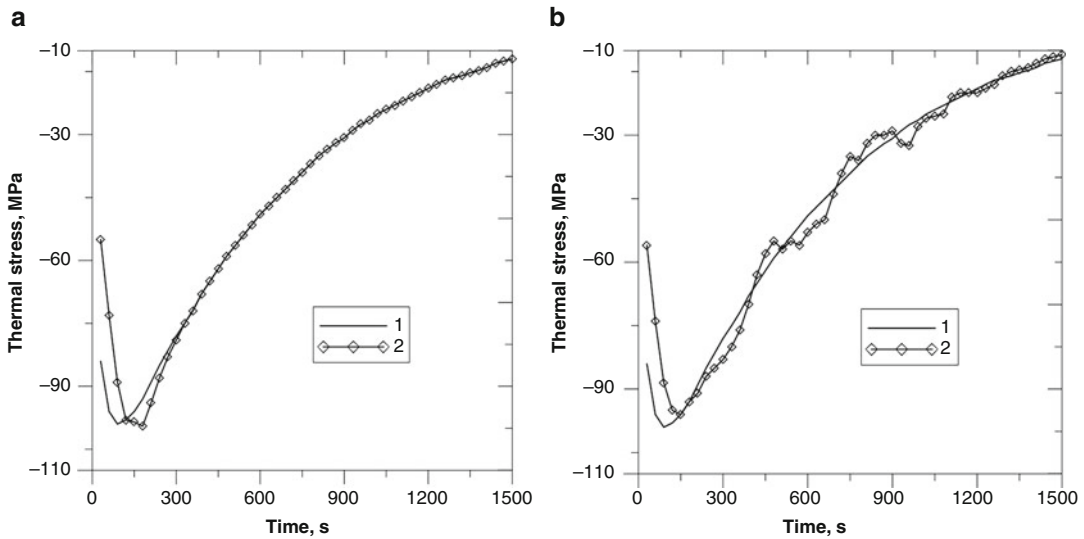
The heat transfer coefficient is  $h = 1,000$  W/(m<sup>2</sup>·K). Other data are  $\kappa = 1.2 \cdot 10^{-5}$  m<sup>2</sup>/s,  $E\alpha/(1-\nu) = 3.7857$  MPa/K, and  $\Delta t = 30$  s. The input temperatures for the inverse problem are first calculated from the direct problem. Then, they are disturbed by random measuring errors and used in the developed method instead of the measured data. Normally distributed random numbers from the range  $\pm 1$  K simulate the influence of the measuring errors. They were added to each calculated temperature every  $\Delta t$  seconds. The temperature changes at the cylinder outer surface are approximated by the polynomial of the 3rd degree. The results are shown in Figs. 5 and 6.

Errors are larger only at the beginning of heating. These inaccuracies occur because the polynomial of the 3rd degree ( $m = 3$ ) cannot approximate the rapid temperature changes in the beginning of heating process. The random temperature measurement errors lead to the



**Exact Solution of Inverse Heat Conduction Problems, Fig. 5** Temperature at the inner and outer surfaces and at the middle of the cylinder wall after the fluid

temperature is stepwise raised, (a) exact measurement data and (b) measured temperature is burdened with random errors



**Exact Solution of Inverse Heat Conduction Problems, Fig. 6** Thermal stresses at the inner surface of the cylinder after the fluid temperature is stepwise raised,

(a) exact measurement data and (b) measured temperature is burdened with random errors

oscillations of temperature and thermal stresses at the cylinder inner surface. It can be seen, however, that for longer time the discrepancy from the direct solution is much smaller. It is also

apparent that the accuracy of temperature changes calculations is better when compared with the accuracy of thermal stresses calculations.

The next test of the presented method deals with a spherical valve wall. The following data are known:

- Outer diameter  $d_o = 2r_o = 0.4829$  m
- Wall thickness  $s = 0.0619$  m
- Material X20CrMoV121
- Heat transfer coefficient  $h = 1000$  W/(m<sup>2</sup>·K)
- Thermal diffusivity  $\kappa = 4.8483 \cdot 10^{-6}$  m<sup>2</sup>/s
- Material constant  $E\alpha/(1-\nu) = 3.47$  MPa/K

The fluid temperature changes ramp-wise (Fig. 4b).

First, the wall temperature at the outer surface temperature  $r = r_o$  was calculated and disturbed by normally distributed random errors from the range of  $\pm 1$ K. These temperatures simulate the measured values to be used by the developed method. Like for the previous tests,  $\Delta t = 30$ s.

The presented method gives highly accurate results. The calculated temperatures obtained from the solution of the direct problem  $T(r_{in}, t)$  and  $T(r_m, t)$  are compared in Fig. 7 with the results obtained from the solution of the inverse problem for the same locations:  $r_{in}$  and  $r_o$ .

Figure 8 depicts the changes of the thermal stresses at the inner surface of the sphere.

If the temperature measured at the outer sphere surface is errorless, then the stresses at the inner surfaces are reconstructed with high accuracy (Figs. 8a and b). In the beginning of the heating process, the differences between the inverse and direct solutions are larger. The presented method gives also satisfactory results if the measured temperature is burdened with random errors. Although the assumed temperature errors are relatively large, the time changes of the thermal stresses are evaluated with good accuracy (Fig. 8c).

In order to improve the accuracy of the solution, the degree of the approximating polynomial on which the digital filter is based can be increased, but it will also increase the sensitivity of the solution to the random measuring errors (Fig. 8d).

## Overdetermined Inverse Heat Conduction Problem

The measured data should be smoothed in order to avoid the inverse solution being influenced by

random measurement errors. To improve the accuracy and the stability of the inverse problem solutions, the inner and mean integral temperatures can be determined based on the temperature measurements at two or more points.

Thermal stresses in pressure components of steam boilers are calculated based on the measured temperature difference at two points located close to the inner surface and in the middle of the wall (Fig. 9). Existing temperature difference measuring points with two or three thermocouples can be used for these calculations. The developed method uses the time-temperature changes obtained from one, two, or more measuring points. It is known that accuracy of the inverse solution increases with the number of measuring points. The proposed method of solving the overdetermined inverse problems lends itself to evaluation of the thermal stresses in plates, hollow cylinders, and hollow spheres. When the temperature on the outer surface is only measured, the problem reduces to the method described in the foregoing.

The presented technique uses the time-temperature changes obtained from one, two, or more measuring points. The calculations of the transient one-dimensional temperature distribution in the component wall are based on the Fourier's heat conduction (18).

Additionally, the perfect insulation of the component outer surface is assumed

$$\left[ k \frac{\partial T}{\partial r} \right]_{r=r_o} = 0 \quad (56)$$

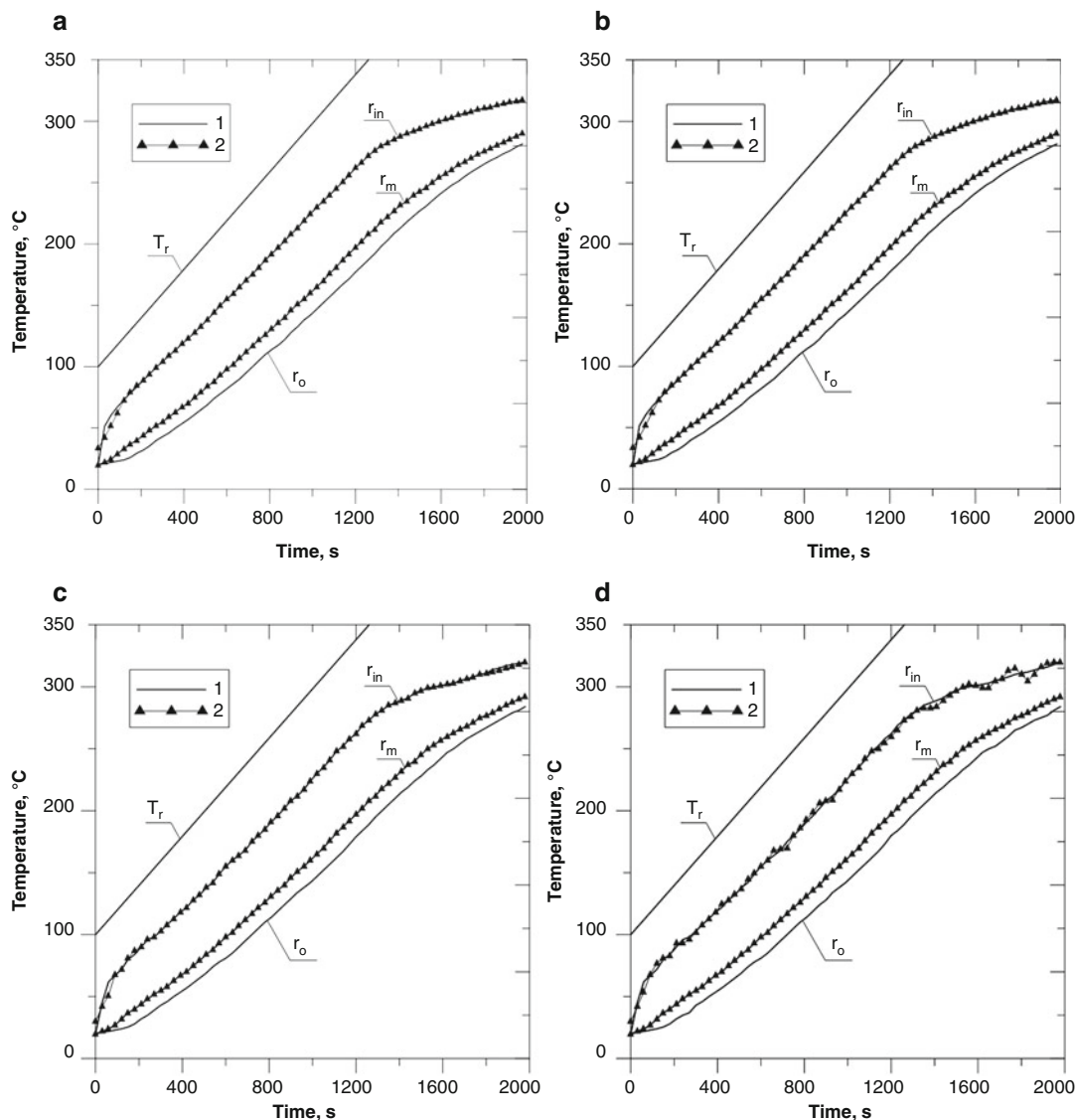
The boundary condition for the inner surface is unknown. The searched temperature distribution  $T(r, t)$  should match the measured temperature changes  $f_i(t)$  in  $M$  measuring points

$$T(r, t)|_{r=r_i} \cong f_i(t), \quad i = 1, \dots, M \quad (57)$$

The locations of the measuring points are shown in Fig. 10.

The fluid temperature  $T_f(t)$  is also needed for evaluating the heat transfer coefficient on the component inner surface. Evaluating the changes



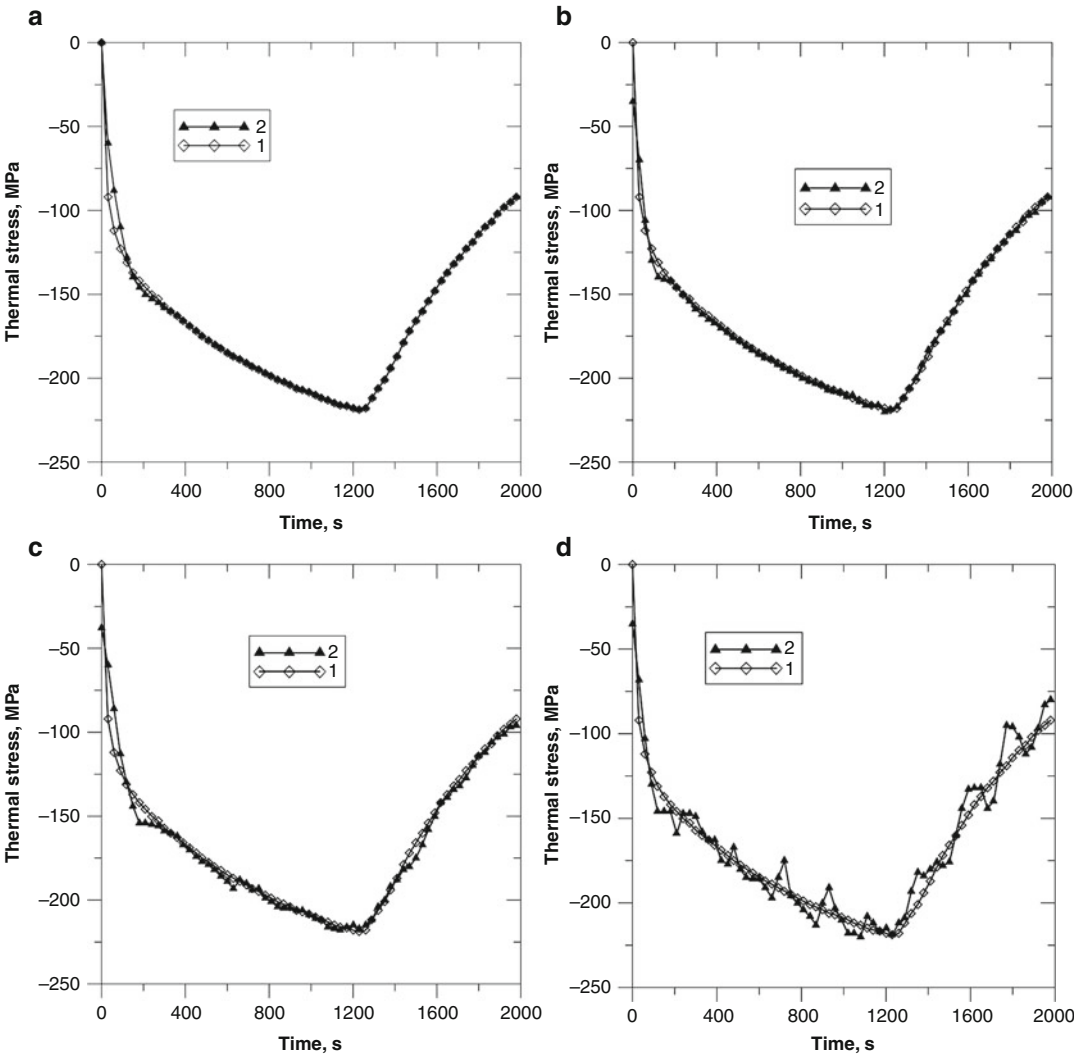


**Exact Solution of Inverse Heat Conduction Problems, Fig. 7** Fluid temperature and temperatures inside the spherical component; (1) numerical solution of the direct problem, (2) inverse solution, (a) errorless measured temperature smoothed with 11-point digital filter based on the polynomial of the third order, (b) errorless measured temperature smoothed with 11-point digital

filter based on the polynomial of the fourth order, (c) measured temperature disturbed by random errors smoothed with 11-point digital filter based on the polynomial of the third order, and (d) measured temperature disturbed by random errors smoothed with 11-point digital filter based on the polynomial of the fourth order

of the heat transfer coefficient is important for operating control of thermal conditions of turbines rotating parts. Because the direct measurements in the rotating turbine shafts cannot be safely performed, the characteristic temperatures and stresses have to be calculated.

The temperature sensor is placed in the region of temperature conditions similar to the monitored part of the rotor. Based on the temperature measurements in several points at various depths in turbine housing and measured steam temperature, the heat transfer coefficient and thermal



**Exact Solution of Inverse Heat Conduction Problems, Fig. 8** Thermal stresses on the inner surface of the sphere. (1) — numerical solution of the direct problem, (2) ▲ ▲ ▲ ▲ inverse solution, (a) errorless measured temperature smoothed with 11-point digital filter based on the polynomial of the third order, (b) errorless measured temperature smoothed with 11-point digital

filter based on the polynomial of the fourth order, (c) measured temperature disturbed by random errors smoothed with 11-point digital filter based on the polynomial of the third order, and (d) measured temperature disturbed by random errors smoothed with 11-point digital filter based on the polynomial of the fourth order

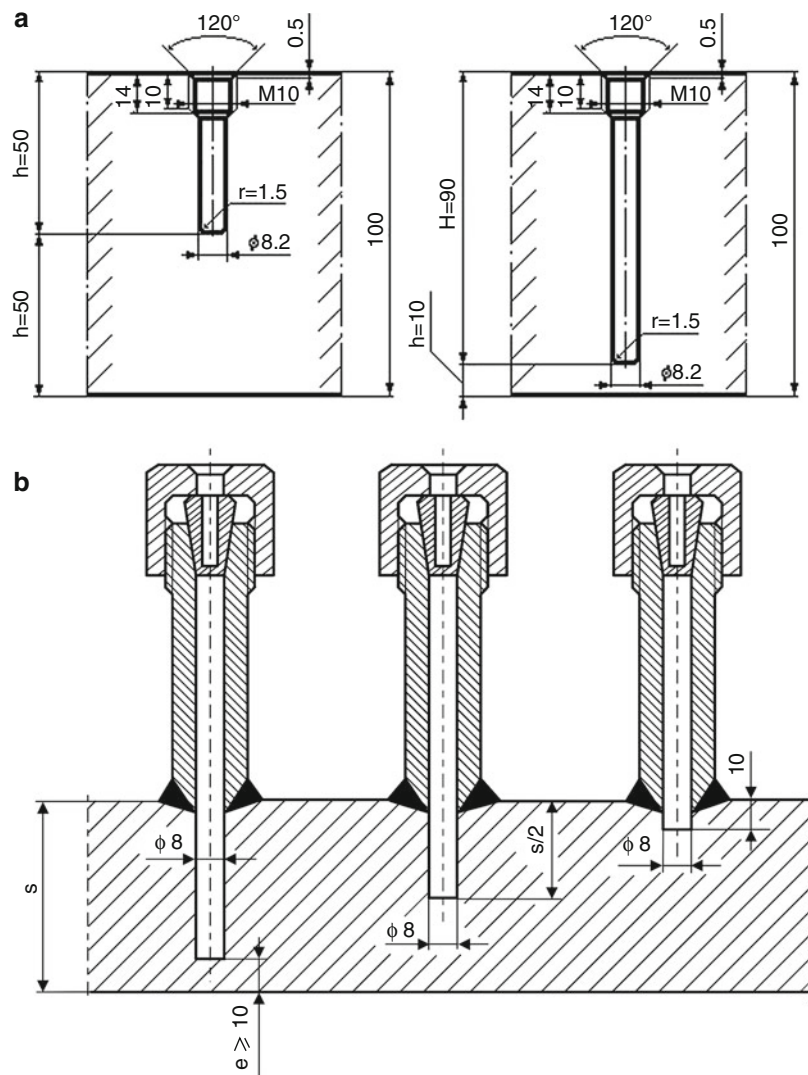
stresses in the turbine rotor are calculated by computer. This method is more exact than calculating the heat transfer coefficient from such quantities like steam pressure, temperature, and number of rotor revolutions per minute.

**Solving the Overdetermined Inverse Heat Conduction Problem**

The time changes of the temperature at the outer surface are approximated by the polynomial of the  $p$ th degree (Fig. 11).

### Exact Solution of Inverse Heat Conduction Problems,

**Fig. 9** Measurement of temperature in thick-walled components of steam boilers for thermal stress monitoring; (a) measurement of temperature difference (two temperature sensors) and (b) measurement of temperature and temperature difference with 3 temperature sensors



In the coordinate system with the axis passing through  $Fo_n$ , the approximating polynomial  $y(Fo)$  passes through  $(2N + 1) \geq p$  data points

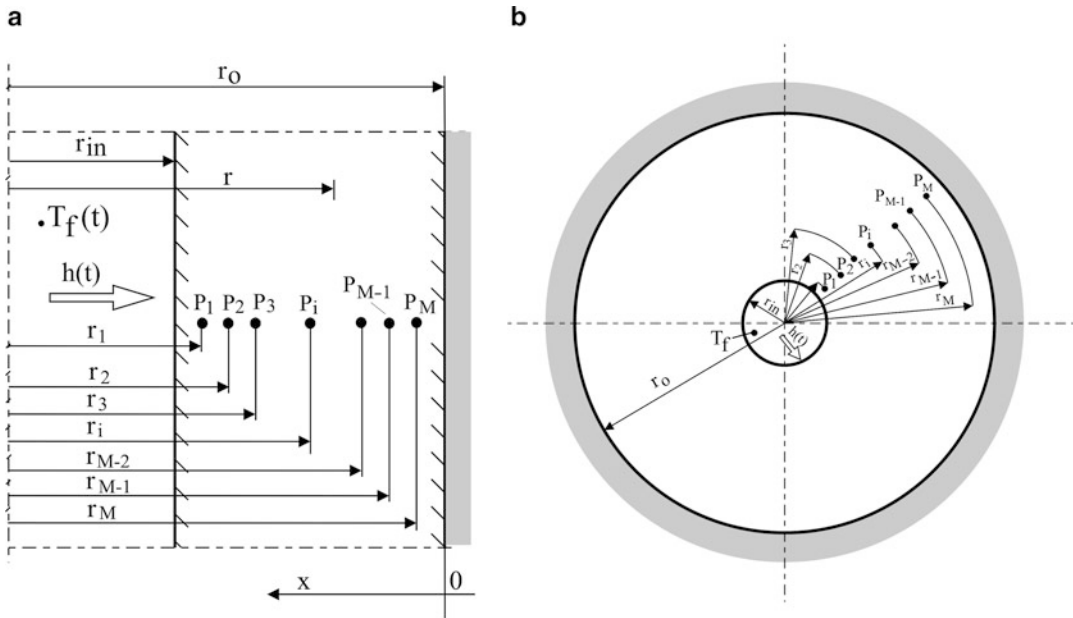
$$\begin{aligned} y(Fo) = T(1, Fo) = & a_0 + a_1(Fo - Fo_n) \\ & + a_2(Fo - Fo_n)^2 + a_3(Fo - Fo_n)^3 \\ & + a_4(Fo - Fo_n)^4 + \dots, \\ & + a_p(Fo - Fo_n)^p = \sum_{i=0}^p a_i(Fo - Fo_n)^i \end{aligned} \quad (58)$$

where  $Fo = \kappa t / r_o^2$ .

Therefore the temperature distribution takes the form

$$\begin{aligned} T(R, Fo) = & a_0\varphi_0 + a_1\varphi_1 + a_2\varphi_2 + \dots, \\ = & a_p\varphi_p = \sum_{i=0}^p a_i\varphi_i \end{aligned} \quad (59)$$

Functions  $\varphi_i(R, Fo)$  can be calculated in the following way:



**Exact Solution of Inverse Heat Conduction Problems, Fig. 10** Position of temperature sensors; (a) plane and cylindrical wall and (b) spherical wall

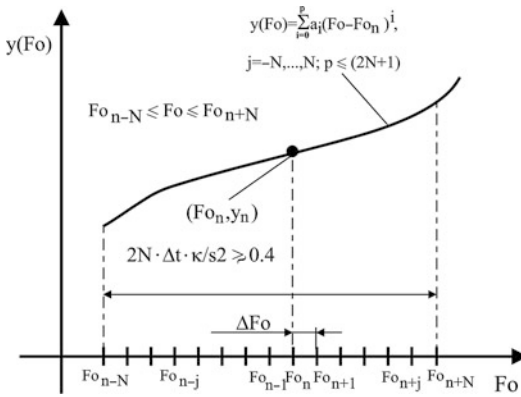
$$\begin{aligned} \varphi_i &= (Fo - Fo_n)^i + i(Fo - Fo_n)^{i-1}H_1(R) \\ &+ i(i-1)(Fo - Fo_n)^{i-2}H_2(R) + \dots + \\ i &= 0, 1, \dots, p \\ &+ i(i-1) \dots 3(Fo - Fo_n)^2H_{i-2}(R) \\ &+ i!(Fo - Fo_n)H_{i-1}(R) + i!H_i(R) \end{aligned} \quad (60)$$

The polynomial of the third degree is sufficient for local approximation of the temperature changes at the outer surface in the time interval  $(Fo_n - N \cdot \Delta Fo) \leq Fo \leq (Fo_n + N \cdot \Delta Fo)$  with good accuracy. Furthermore, the coefficients  $a_i$ ,  $i = 0, 1, \dots, p$  can be calculated from the normal equations without difficulties as long as the degree of the polynomial is smaller than 5. For the polynomials of higher degrees, the polynomial coefficients can be noticeably influenced by the round-off errors. The following expressions for the functions  $\varphi_i(R, Fo)$  for the polynomial of the 5th degree can be calculated from Eq. (60)

$$\begin{aligned} \varphi_0 &= 1, \\ \varphi_1 &= (Fo - Fo_n) + H_1(R) \\ \varphi_2 &= (Fo - Fo_n)^2 + 2(Fo - Fo_n)H_1(R) + 2H_2(R) \\ \varphi_3 &= (Fo - Fo_n)^3 + 3(Fo - Fo_n)^2H_1(R) \\ &+ 6(Fo - Fo_n)H_2(R) + 6H_3(R) \\ \varphi_4 &= (Fo - Fo_n)^4 + 4(Fo - Fo_n)^3H_1(R) \\ &+ 12(Fo - Fo_n)^2H_2(R) \\ &+ 24(Fo - Fo_n)H_3(R) + 24H_4(R), \\ \varphi_5 &= (Fo - Fo_n)^5 + 5(Fo - Fo_n)^4H_1(R) \\ &+ 20(Fo - Fo_n)^3H_2(R) \\ &+ 60(Fo - Fo_n)^2H_3(R) \\ &+ 120(Fo - Fo_n)H_4(R) + 120H_5(R) \end{aligned}$$

(61)

The values of the polynomial (58) and derivatives  $d^k y / dFo^k$  will be used for calculating the temperature and the thermal stresses only for time point  $Fo = Fo_n$ . The derivatives in this case become



**Exact Solution of Inverse Heat Conduction Problems, Fig. 11** Temperature  $y(Fo)$  at outer surface of the component. Smoothed values of the polynomial and its derivatives are calculated only at center point  $Fo_n$

$$\left. \frac{d^k y}{dFo^k} \right|_{Fo=Fo_n} = k! a_k \quad k = 0, 1, 2, \dots, p \quad (62)$$

For the polynomial of the 5th degree simple expressions for the smoothed values of the derivatives are obtained:

$$\begin{aligned} y(Fo_n) &= a_0; \quad y'(Fo_n) = a_1; \quad y''(Fo_n) = 2a_2; \\ y'''(Fo_n) &= 6a_3; \quad y^{IV}(Fo_n) = 24a_4; \quad y^V(Fo_n) = 120a_5 \end{aligned} \quad (63)$$

The coefficients  $a_i$  needed for calculating the wall temperature are obtained using the least squares method. For known time interval,  $2N \cdot \Delta t \geq 0.4 s^2/\kappa$  the wall temperature in  $M$  measuring points  $r_i$  (Fig. 11) will be measured densely one after other, for example, every  $\Delta t = 0.04 s^2/\kappa$ . It is assumed that the measuring errors are connected only with temperature measurements  $f_{i,j}$ . The abscissas  $r_i$  and  $t_j$  are assumed to be exact (Fig. 12).

The polynomial coefficients should be evaluated so that the sum of the discrepancies between the values of the polynomial  $T(R_i, Fo_j)$  and measured values  $f(R_i, Fo_j)$  is minimal:

$$S = \sum_{i=1}^M \sum_{j=-N}^N [T(R_i, Fo_{n+j}) - f(R_i, Fo_{n+j})]^2 = \min \quad (64)$$

Necessary and in this case sufficient condition of existence of this minimum is vanishing of the partial derivatives of the function  $S$  with respect to coefficient  $a_k$

$$\frac{\partial S}{\partial a_k} (a_0, a_1, \dots, a_p) = 0, \quad k = 0, 1, \dots, p \quad (65)$$

From the above equation follows:

$$\begin{aligned} \frac{\partial S}{\partial a_k} &= 2 \sum_{i=1}^M \sum_{j=-N}^N \varphi_k(R_i, Fo_{n+j}) [a_0 \varphi_0(R_i, Fo_{n+j}) \\ &\quad + a_1 \varphi_1(R_i, Fo_{n+j}) + \dots + \\ &\quad + a_p \varphi_p(R_i, Fo_{n+j}) - f(R_i, Fo_{n+j})] = 0 \end{aligned} \quad (66)$$

$$k = 0, 1, \dots, p$$

After transformations and placing  $f(R_i, Fo_{n+j})$  on the right side, the normal equations are obtained:

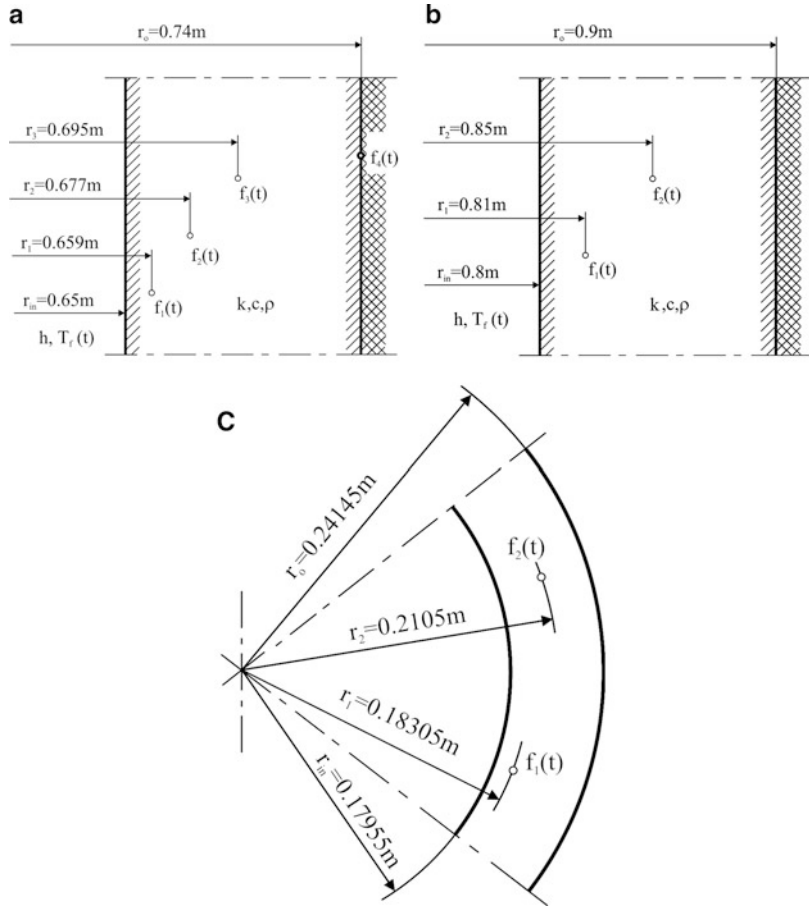
$$\begin{bmatrix} \sum \sum \varphi_0 \varphi_0 & \sum \sum \varphi_0 \varphi_1 & \dots & \sum \sum \varphi_0 \varphi_p \\ \sum \sum \varphi_1 \varphi_0 & \sum \sum \varphi_1 \varphi_1 & \dots & \sum \sum \varphi_1 \varphi_p \\ \dots & \dots & \dots & \dots \\ \sum \sum \varphi_p \varphi_0 & \sum \sum \varphi_p \varphi_1 & \dots & \sum \sum \varphi_p \varphi_p \end{bmatrix} \begin{bmatrix} a_0 \\ a_1 \\ a_2 \\ \vdots \\ a_p \end{bmatrix} = \begin{bmatrix} \sum \sum \varphi_0 f(R_i, Fo_{n+j}) \\ \sum \sum \varphi_1 f(R_i, Fo_{n+j}) \\ \sum \sum \varphi_2 f(R_i, Fo_{n+j}) \\ \dots \\ \sum \sum \varphi_p f(R_i, Fo_{n+j}) \end{bmatrix} \quad (67)$$

where  $\varphi_k = \varphi_k(R_i, Fo_{n+j})$ ,  $k = 0, \dots, p$ , and  $\sum \sum \varphi_0 \varphi_0 = M(2N + 1)$ . The sums are calculated for  $i = 1$  to  $M$  in space and for  $j = -N$  to  $N$  in time,

that is,  $\sum \sum = \sum_{i=1}^M \sum_{j=-N}^N$ . In the calculations the number  $2N$  and the length of the measuring time step  $\Delta Fo$  are constant; also the sensor locations

### Exact Solution of Inverse Heat Conduction Problems,

**Fig. 12** Coordinates of temperature sensors in the component; (a) four sensors in a drum wall, (b) two sensors in a drum wall, and (c) two sensors in a spherical component



remain the same, so the matrix of coefficients on the left side of the Equation system (67) is the same for all the time points. It makes the calculations of the polynomial coefficients  $a_k$ ,  $k = 0, 1, \dots, p$  much faster because the matrix has to be inverted only once.

### Transient Thermal Stresses in Plates, Hollow Cylinders, and Hollow Spheres

The expressions for circumferential, axial, and radial stresses at the inner surface of the component insulated at the outer surface are given by (37). The wall temperature difference  $\Delta T = T_m(fo) - T(\omega, fo)$  is evaluated in most cases by measuring the metal temperature at the center of the wall tube and at the location close to the wall inner surface. This leads to the

inaccuracies mentioned in the foregoing and requires much effort to place the sensors at the inside of the pressure component. Therefore, the theoretical calculations of the thermal stresses from the (37) seem to be more efficient. Substituting (30) and (31) into (37) and transforming yields for the plate

$$\sigma_a(\omega, fo) = -\frac{E\alpha}{1-\nu} \sum_{k=1}^{\infty} \frac{2k}{(2k+1)!} (1-\omega)^{2k} \frac{d^k y}{dfo^k} \quad (68)$$

Taking (62) into consideration, (68) gives for  $fo = fo_n$

$$\sigma_a(\omega, fo_n) = -\frac{E\alpha}{1-\nu} \sum_{k=1}^p \frac{2k^2(k-1)!}{(2k+1)!} a_k (1-\omega)^{2k} \quad (69)$$

The thermal stresses in the spherical components can be calculated from (37) using (33)

$$\sigma(\omega, Fo) = \frac{E\alpha}{1-\nu} \sum_{k=1}^{\infty} \frac{(1-\omega)^{2k}}{(2k+1)!} \left[ \frac{3[\omega^2 + (2k+1)\omega + 1]}{(2k+3)(\omega^2 + \omega + 1)} - \left(1 + \frac{2k}{\omega}\right) \right] \frac{d^k y}{dFo^n} \quad (70)$$

and for time point  $Fo = Fo_n$ ,

$$\sigma(\omega, Fo_n) = \frac{E\alpha}{1-\nu} \sum_{k=1}^p \frac{k! a_k (1-\omega)^{2k}}{(2k+1)!} \left[ \frac{3[\omega^2 + (2k+1)\omega + 1]}{(2k+3)(\omega^2 + \omega + 1)} - \left(1 + \frac{2k}{\omega}\right) \right] \quad (71)$$

The equations for calculating the thermal stresses in the hollow cylinder are built similarly to the equations for the plate and hollow sphere:

$$\sigma_a(\omega, Fo) = \frac{E\alpha}{1-\nu} \sum_{k=1}^5 W_k(\omega) \frac{d^k y}{dFo^k} \quad (72)$$

and

$$\sigma_a(\omega, Fo_n) = \frac{E\alpha}{1-\nu} \sum_{k=1}^5 k! a_k W_k(\omega) \quad (73)$$

Functions  $W_k(\omega)$  introduced in (72) and (73) for abbreviation are:

$$\begin{aligned} W_1(\omega) &= \frac{1}{8} \left( 3 - \omega^2 + \frac{4 \ln \omega}{1 - \omega^2} \right) \\ W_2(\omega) &= \frac{1}{32} \left[ \frac{1}{3} (8 - \omega^2 - \omega^4) + \frac{2 \ln \omega}{1 - \omega^2} (1 + 2\omega^2 - \omega^4) \right] \\ W_3(\omega) &= \frac{1}{2304} \left[ \frac{1}{4} (41 + 65\omega^2 - 43\omega^4 - 3\omega^6) + \frac{6 \ln \omega}{1 - \omega^2} (1 + 6\omega^2 - 2\omega^6) \right] \end{aligned} \quad (74)$$

$$\begin{aligned} W_4(\omega) &= \frac{1}{442368} \left[ \frac{1}{5} (238 + 1138\omega^2 - 62\omega^4 - 462\omega^6 - 12\omega^8) + \frac{24 \ln \omega}{1 - \omega^2} (1 + 12\omega^2 + 12\omega^4 - 8\omega^6 - 3\omega^8) \right] \\ W_5(\omega) &= \frac{1}{88473600} \left[ 132 + 1252\omega^2 + 1127\omega^4 - 873\omega^6 - 373\omega^8 - 5\omega^{10} + \frac{60 \ln \omega}{1 - \omega^2} \times (1 + 20\omega^2 + 50\omega^4 - 25\omega^8 - 4\omega^{10}) \right] \end{aligned}$$

The calculations of the temperature and thermal stress distributions in the presented way does not require much effort and can be performed in on-line mode. The presented method was successfully applied in the monitoring system for thermal stresses and remnant life evaluation of the thick-walled components of steam generators.

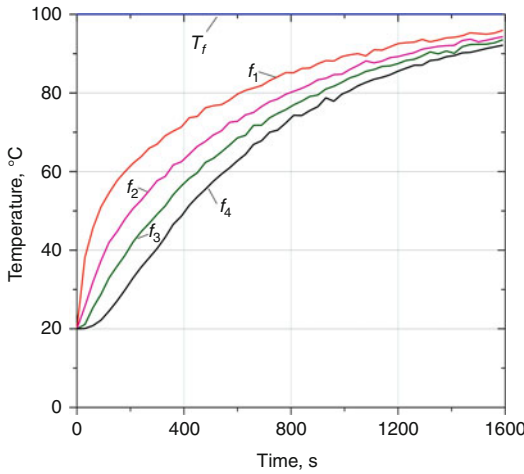
## Examples

The first example presents thermal stresses evaluation using the developed method in the cylinder with 1.48 m diameter and 0.09 m wall thickness made from 15 NiCuMoNb5 steel (Fig. 12a).

The cylinder initial temperature is 20 °C. Fluid temperature raises rapidly from 20 °C to 100 °C. The value of the heat transfer coefficient  $h = 1,000 \text{ W/(m}^2 \cdot \text{K)}$  is assumed. Other data are  $\kappa = k/(c \cdot \rho) = 1.1 \cdot 10^{-5} \text{ m}^2/\text{s}$ ,  $E\alpha/(1-\nu) = 3.69 \text{ MPa/K}$ ,  $\Delta t = 30 \text{ s}$ , and  $N = 5$ .

The input temperatures for the inverse problem are first calculated from the direct problem (Fig. 13). Then, they are disturbed by random measuring errors and used in the developed method instead of the measured data. Normally distributed random numbers from the range  $\pm 1 \text{ K}$  simulate the influence of the measuring errors. They were added to each calculated temperature every  $\Delta t$  seconds. The temperature changes on the cylinder outer surface are approximated by the polynomial of the 3rd degree. The calculations are carried out for four temperature measuring points ( $M = 4$ ), as well as for one ( $M = 1$ ) temperature sensor on the insulated outer cylinder surface. The results are shown in Figs. 14 and 15.





**Exact Solution of Inverse Heat Conduction Problems, Fig. 13** Fluid temperature and temperatures inside the cylindrical wall; position of the thermocouples is shown in Fig. 12a

Errors are larger only at the beginning of heating. These differences occur because the polynomial of the 3rd degree ( $p = 3$ ) cannot approximate the rapid temperature changes in the beginning of heating process. The random temperature measurement errors lead to the oscillations of temperature and thermal stresses on the cylinder inner surface. It can be seen, however, that for four measuring points the discrepancy from the direct solution is much smaller. It is also apparent that the accuracy of temperature changes calculations is better when compared with the accuracy of thermal stresses calculations.

The second example compares the thermal stresses  $\sigma'_a$  calculated by using the measured temperature difference

$$\sigma'_a = \frac{E\alpha}{1-\nu} (f_2 - f_1) \quad (75)$$

and thermal stresses  $\sigma_a$  evaluated using the developed method. The symbols  $f_2$  and  $f_1$  stand for the measured wall temperatures at the wall center and at the location close to the inner component surface.

In the standard thermal stresses calculations using (75), it is assumed that both temperatures  $f_1$

and  $f_2$  are measured exactly. The ramp-heated drum of  $d_o = 2r_o = 1.8$  m diameter and wall thickness  $s = r_o - r_{in} = 0.1$  m made from 15NiCuMoNb5 is considered. The initial temperature profile at  $t = 0$  is assumed to be constant  $T_0 = 20$  °C over the wall thickness. The material constants are  $\kappa = 1.2 \cdot 10^{-5}$  m<sup>2</sup>/s,  $E\alpha/(1-\nu) = 3.786$  MPa/K, and they are not temperature-dependent.

The temperature measurements were performed in the wall middle and near the drum inner surface, using the sensor placed in the hole drilled up to 10 mm from the inner surface (Fig. 12b). The two temperatures  $f_1$  and  $f_2$  shown in Fig. 16 are calculated from the direct problem for the assumed fluid temperature changes  $T_f(Fo)$  and heat transfer coefficient  $h = 1,000$  W/(m<sup>2</sup>·K).

The calculated temperatures are disturbed by the random measuring error of range  $\pm 1$ K. The calculated values are used as measured temperature changes in further calculations.

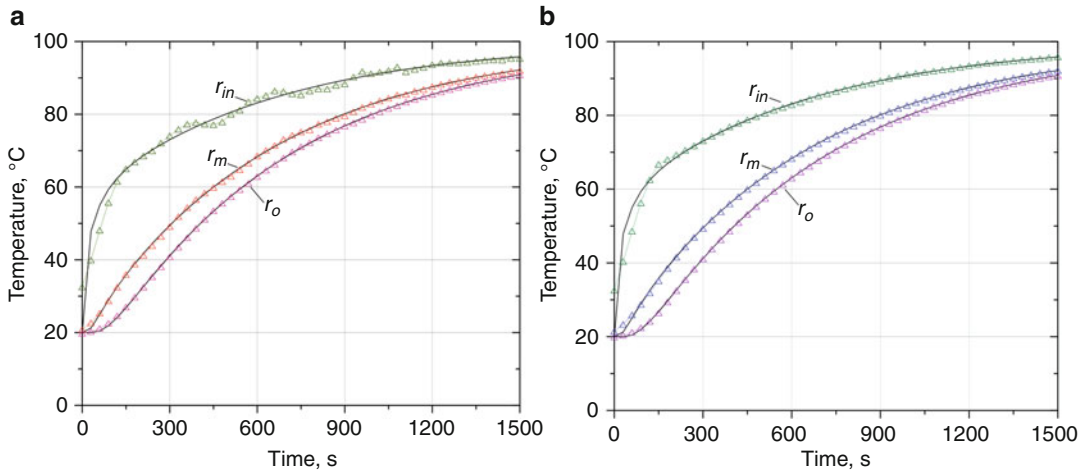
The time step is set to  $\Delta t = 30$  s. As the results of the calculations, the temperatures  $T(r_{in}, t)$  and  $T_m(t)$  are shown in Fig. 17.

It can be seen that the measured temperatures  $f_1$  and  $f_2$  are significantly different from the inner and middle temperature. Large errors also occur by evaluating the thermal stresses using the (75), while the presented method gives highly accurate results. Although the temperature errors are relatively large, the time changes of the thermal stresses are evaluated with good accuracy (Fig. 18).

The next test of the presented method deals with spherical bodies. The analyzed sphere has the initial temperature of 20 °C. The temperature of the heated medium raises rapidly from 20 °C to 100 °C and additionally raises constantly with the rate of  $v_T = dT_f/dt = 0.2$  K/s. Figure 12c shows the location of the thermocouples. The following data are known:

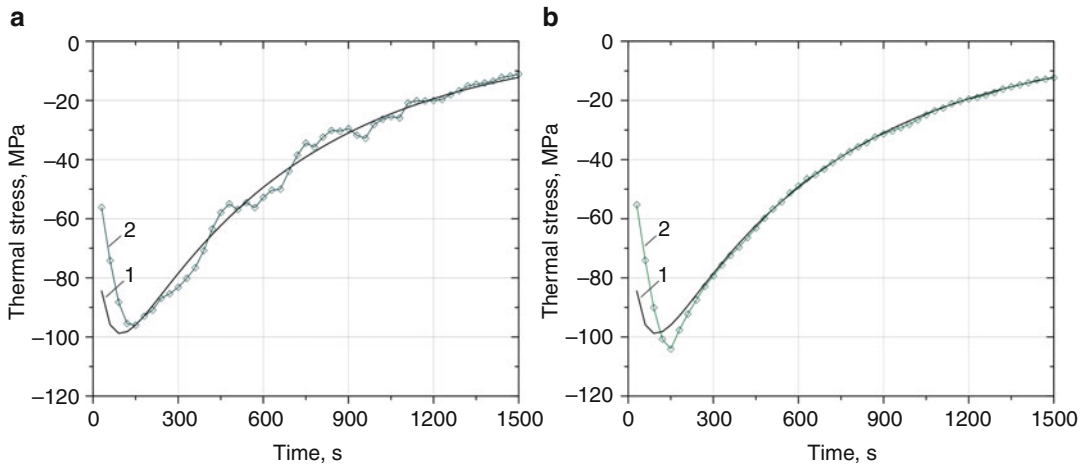
- Outer diameter  $d_o = 2r_o = 0.4829$  m
- Wall thickness  $s = 0.0619$  m
- Material X20CrMoV121
- Heat transfer coefficient  $h = 1,000$  W/(m<sup>2</sup>·K)
- Thermal diffusivity  $\kappa = 4.8483 \cdot 10^{-6}$  m<sup>2</sup>/s
- Material constant  $E\alpha/(1-\nu) = 3.47$  MPa/K





**Exact Solution of Inverse Heat Conduction Problems, Fig. 14** Temperatures at the inner and outer surfaces and at the wall center of the drum after the fluid

temperature is suddenly raised. (a)  $M = 1$ ; (b)  $M = 4$   
 ——— numerical solution of the direct problem;  
 $\Delta\Delta\Delta\Delta$  – inverse solution



**Exact Solution of Inverse Heat Conduction Problems, Fig. 15** Thermal stresses at the inner and outer surfaces and at the wall center of the drum after the fluid

temperature is suddenly raised; (a)  $M = 1$ ; (b)  $M = 4$ , (1)  
 ——— numerical solution of the direct problem; (2)  
 $\diamond$  – inverse solution

First, the temperature at the points  $r_1$  and  $r_2$  will be calculated and disturbed by random errors from the range of  $\pm 1\text{K}$ . These temperatures simulate the measured values to be used by the developed method. Like for the previous tests,  $\Delta t = 30\text{s}$  and  $p = 3$ .

The calculated temperatures  $T(r_{in}, t)$ ,  $T(r_m, t)$  and results obtained from the inverse problem solution for the same locations are compared in Fig. 19. Figure 20 depicts the changes of the

thermal stresses on the inner surface of the sphere.

In the beginning of the heating process, the differences between the inverse and direct solutions are larger. In order to improve the accuracy of the solution, the degree of the approximating polynomial can be increased, but it would also increase the sensitivity of the solution to the random measuring errors.

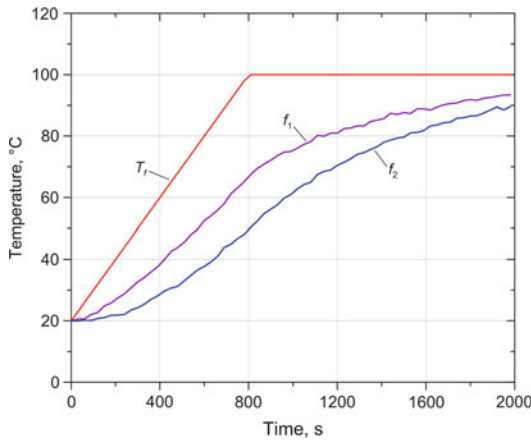
There was a possibility of verifying the developed calculation method during the cold start of the Benson steam generator. The objective of this test was to provide the proof that the presented method can be practically applied by showing the compatibility between the theoretical model and the real object. The measurements, locations of the thermocouples, and

material properties of the spherical element are the same as in the above example. The measured time changes of temperature in locations  $r_1 = 0.18305$  m and  $r_2 = 0.2105$  m (Fig. 12c) are shown in Fig. 21.

It can be seen from Fig. 21 that the thermal stresses based on the inverse solution differ from the thermal stresses obtained by using (75). The presented method allows to recognize fast time changes more exactly.

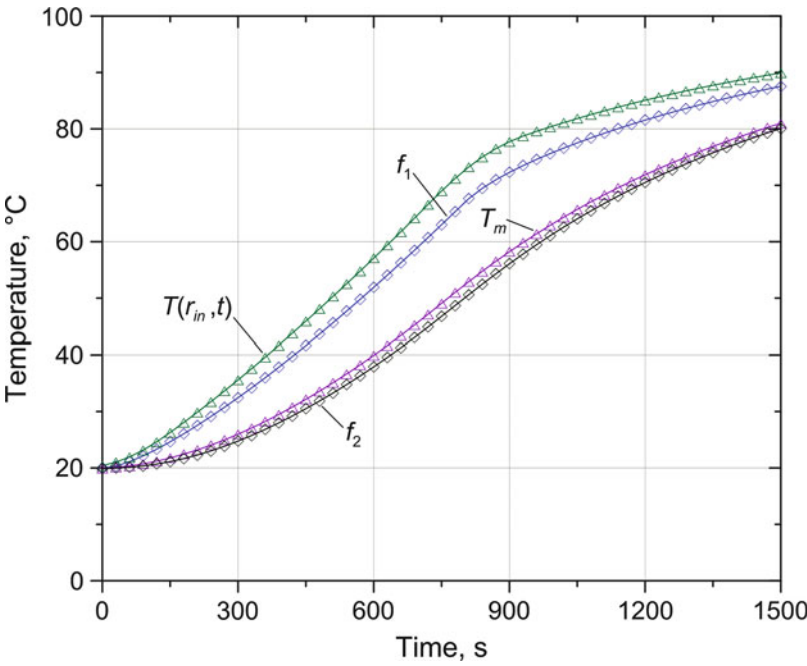
During fast temperature changes, the calculated temperature difference  $\Delta T = T_m(t) - T(r_1, t)$  differ from the measured temperature difference  $\Delta T' = f_2 - f_1$  (Fig. 22).

It should be noted that heavy thermocouple pockets can cause large dynamic errors when  $\Delta T'$  is measured. Furthermore, the temperature field inside the element is affected by mounting the temperature sensors. Another disturbing factor is bad thermal contact between the thermocouple and the thermocouple pocket. Also heat conduction through the thermometer housing increases measuring errors. Generally, thin thermocouples should be used to influence the temperature distribution and component geometry as little as possible.



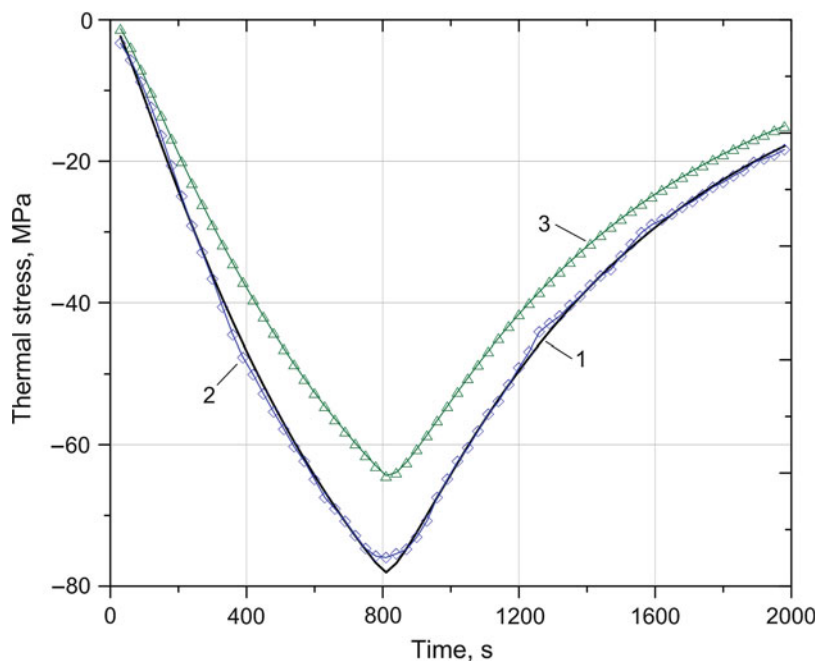
**Exact Solution of Inverse Heat Conduction Problems, Fig. 16** Fluid and measured drum wall temperatures; location of thermocouples is shown in Fig. 12b

**Exact Solution of Inverse Heat Conduction Problems, Fig. 17** Calculated temperatures of the drum wall; position of the thermocouples is shown in Fig. 12b;  $f_1$  and  $f_2$  – numerical solution of the direct problem at the locations  $r_1$  and  $r_2$ , respectively;  $T(r_{in}, t)$  and  $T_m$  – inner surface and mean temperature, respectively, obtained from the inverse solution



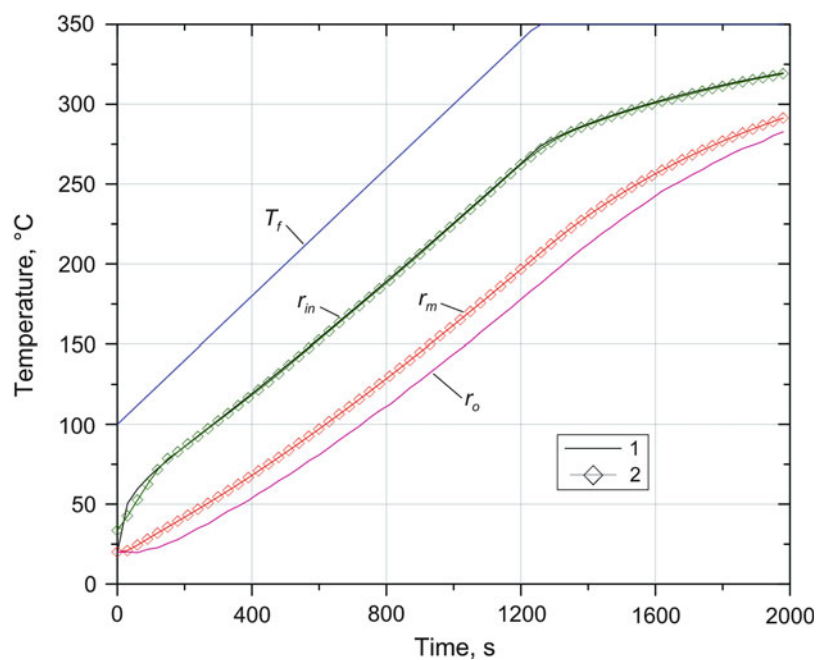
### Exact Solution of Inverse Heat Conduction Problems,

**Fig. 18** Thermal stresses at the inner surface of the drum; (1) numerical solution of the direct problem (given comparative value), (2) inverse solution, and (3) conventional measurement with two thermocouples



### Exact Solution of Inverse Heat Conduction Problems, Fig. 19

Fluid temperature and temperatures inside the spherical component shown in Fig. 12c; ———— – numerical solution of the direct problem, ◇◇◇◇◇◇ – inverse solution



## Conclusions

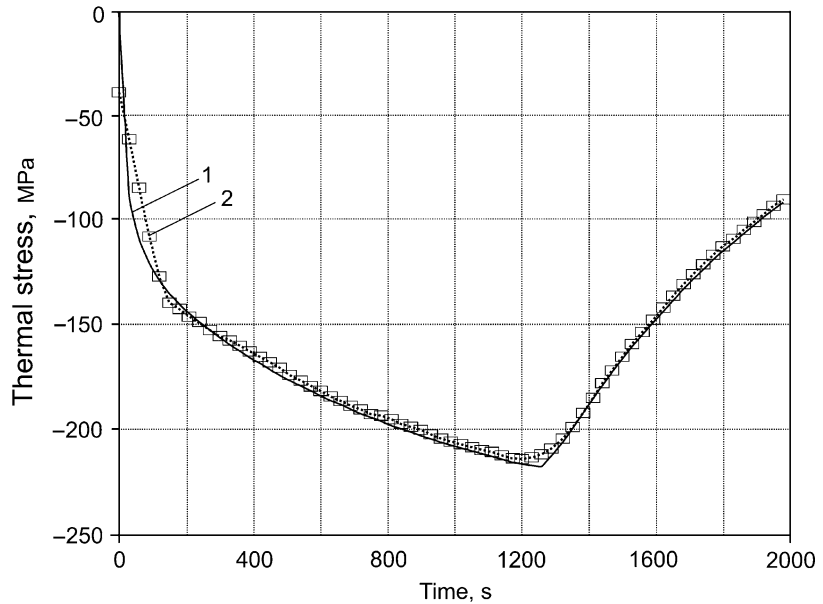
The analytical methods for solving the inverse heat conduction problems are presented. The transient temperature distribution and thermal

stresses are calculated using the temperature measurements in one or more locations inside the body.

The methods apply to the plates, hollow cylinders, and hollow spheres, most common among

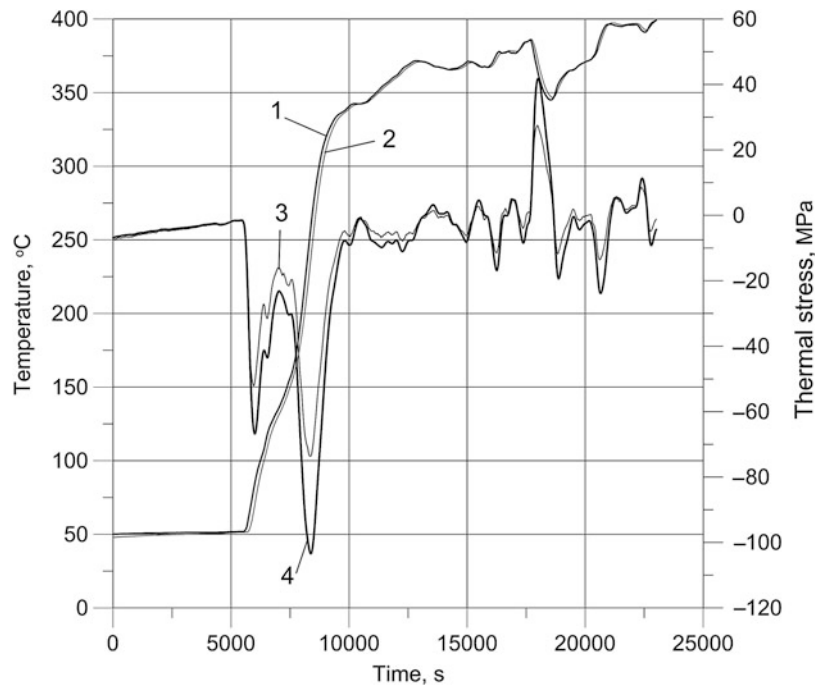
### Exact Solution of Inverse Heat Conduction Problems,

**Fig. 20** Thermal stresses at the inner surface of the spherical component; position of the temperature sensors is shown in Fig. 12c; (1) numerical solution of the direct problem and (2) inverse solution



### Exact Solution of Inverse Heat Conduction Problems,

**Fig. 21** Warm-up of the spherical component during the cold start-up of the Benson steam boilers; (1) wall temperature close to the inner surface (3.5 mm from the inner surface), (2) temperature at the wall center, (3) thermal stress  $\sigma'_a$  calculated by the conventional method  $[\sigma'_a = E\alpha(f_2 - f_1)/(1 - \nu)]$ , and (4) thermal stress  $\sigma_a$  at the inner surface – inverse solution



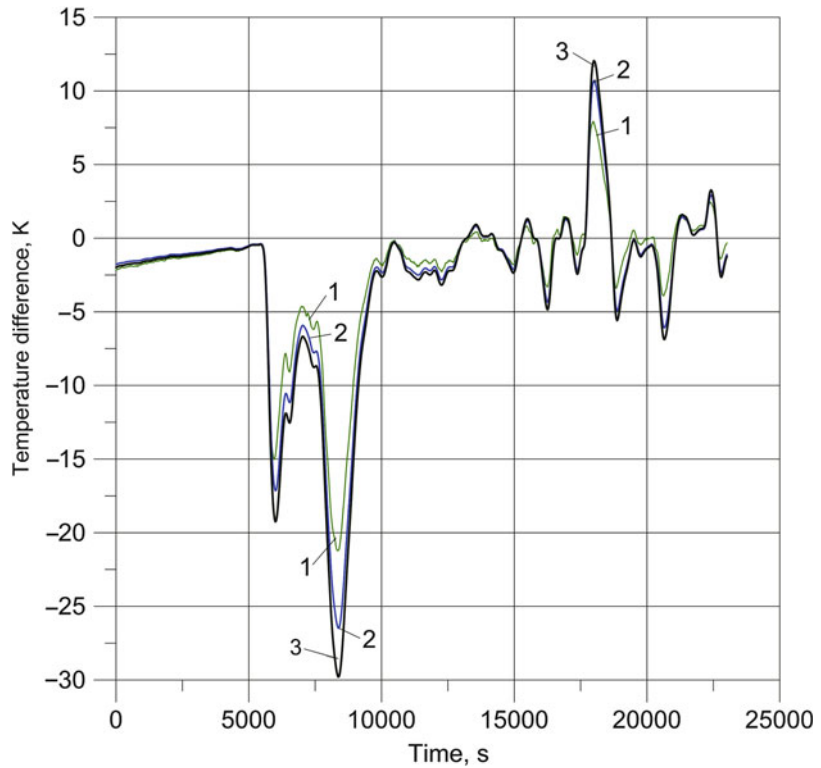
the pressure components in power installations. The body temperature can be measured only on its outer surface. The conventional wall temperature measurements using two temperature sensors in the wall middle and close to the inner

surface can also be used as the input temperatures.

The usage of the new methods was explained in several test examples. The results obtained by using the presented methods are also compared

### Exact Solution of Inverse Heat Conduction Problems,

**Fig. 22** Temperature difference in the spherical component during the cold start-up of the Benson steam boiler; (1) conventional measurement  $[\Delta T'(t) = f_2(t) - f_1(t)]$ , (2) inverse solution  $[\Delta T(t) = T(r_2, t) - T(r_1, t)]$ , and (3) temperature difference  $\Delta T(t) = T_m(t) - T(r_{in}, t)$  used in correct equation for thermal stresses



with the measured time-temperature changes acquired during the cold start of the spherical element with equipped wall temperature sensors.

### References

- Burggraf OR (1964) An exact solution of the inverse problem in heat conduction theory and applications. *Trans ASME J Heat Transf* 86:373–382
- Beck JV, Blackwell B, St. Clair CR (1985) *Inverse heat conduction Ill-posed problems*. Wiley-Interscience, New York
- Brockel D (1985) Prozeßführungsrechner für Kraftwerksdampferzeuger. *VGB Kraftwerkstechnik* 65:510–515
- Speitkamp L (1988) Bestimmung von Temperaturdifferenzen in dicken Druckbehälterwänden aus der zeitlichen Folge von Temperaturmeßwerten an der isolierten Wandaußenseite. *VGB Kraftwerkstechnik* 68:182–189
- Leithner R, Steege F, Pich R, Erlmann K, Chi TN (1990) Vergleich verschiedener Verfahren zur Bestimmung der Temperaturdifferenz in dickwandigen Bauteilen für die Lebensdauerberechnung. *VGB Kraftwerkstechnik* 70:446–457
- Taler J (1996) A semi-numerical method for solving inverse heat conduction problems. *Heat and Mass Transfer* 31:105–111
- Taler J, Lehne F (1996) Bestimmung von Wärmespannungen in dickwandigen Bauteilen mittels einer Temperaturmeßstelle. *Brennstoff-Wärme-Kraft* 48:57–60
- Taler J (1997) Überwachung von instationären Wärmespannungen in dickwandigen Bauteilen. *Forschung im Ingenieurwesen* 63:127–135
- Taler J (1997) Analytical solution of the over-determined inverse heat conduction problem with an application to monitoring thermal stresses. *Heat Mass Trans* 33:209–218
- Taler J, Zima W (1999) Solution of inverse heat conduction problems using control volume approach. *Int J Heat Mass Trans* 42:1123–1140
- Taler J, Duda P (2006) *Solving direct and inverse heat conduction problems*. Springer, Berlin
- Taler J, Zborowski M (1998) Solution of the inverse problems in heat transfer and thermal stress analysis. *J Therm Stresses* 21:563–579
- Taler J, Dzierwa P (2007) Proposition of new rules for determining allowable medium temperature rates during heating and cooling of thick-walled steam boiler components. *Archiv Thermodyn* 37:91–108
- Taler J, Dzierwa P, Taler D (2009) Optimum heating of pressure components of large steam boilers. *Forschung im Ingenieurwesen* 73:183–192

15. Taler J, Dzierwa P (2011) A new method for optimum heating of steam boiler pressure components. *Int J Energy Res* 35:897–908
16. Albrecht W (1966) Stationäre Wärmespannungen in Hohlzylindern. *Konstruktion* 18:224–231
17. Elizarov DP (1971) Thermal shock in steam lines of thermal power stations. *Teploenergetika* 18:78–82
18. Strong BR, Slagis GC (1981) TRANS2A: An unconditionally stable code for thermal transient stress analysis in piping. *Trans ASME J Pressure Vessel Technol* 103:50–58
19. Pich R (1979) Wärmespannungen in druckführenden Bauteilen und deren meßtechnische Überwachung. *VGB Kraftwerkstechnik* 59:510–517
20. TRD 301 (2001) Zylinderschalen unter innerem Überdruck. Technische Regeln für Dampfkessel (TRD), Köln – Berlin, Heymanns Beuth
21. EN 12952–3 (2002) Water-tube boilers and auxiliary installations – Part 3: design and calculation for pressure parts, European Committee for Standardization, Brussels
22. Baba K, Ochi M (1994) Monitoring of transient temperature distribution in piping. *Trans ASME J Pressure Vessel Technol* 116:419–422
23. Taler J (1995) Theory and practice of identification of heat transfer processes. Ossolineum, Wrocław/Warszawa/Kraków (in Polish)

## Existence

### ► Well-Posed Problems

## Existence and Uniqueness for Thermoelastic Contact

Lars-Erik Andersson  
Department of Mathematics, Linköping  
University, Linköping, Sweden

### Overview

In mechanical systems such as brakes and clutches, frictional heating causes thermal expansion which affects the geometry of the contacting bodies. As may be expected, the influence of resistance to heat flow across the sliding interface governs the behavior of the system to a great extent. Here we will formulate some theorems

concerning existence and uniqueness of steady-state solutions for such systems. The criteria established depend upon the nature of the relation between thermal resistance and contact pressure.

## A Thermoelastic Body in Frictional Contact with an Obstacle

In the first subsection below, some basic notation and definitions are introduced.

Then, in the next subsection, we give a brief account of the classical *steady-state heat conduction problem* where we have a body which is subject to time-independent interior and surface heat sources, has prescribed temperature and heat flow at some parts of its boundary, and exchanges heat with some adjacent body having a prescribed temperature.

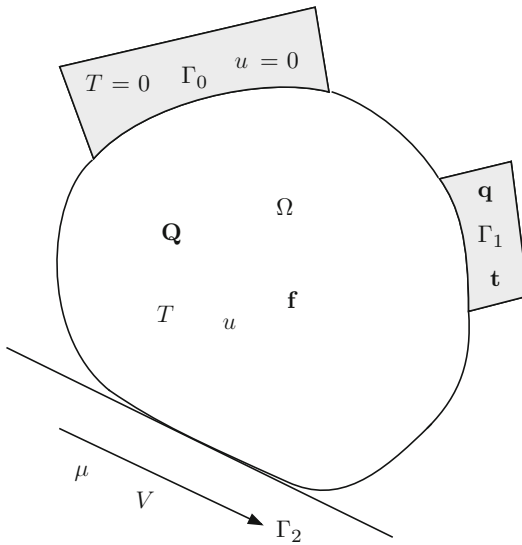
In the third subsection, we describe the classical *mechanical equilibrium problem*, that is, we consider an elastic body which may come into contact with a rigid obstacle, and we give the equations and variational formulations governing the equilibrium, without taking into account friction or heating.

In the fourth section, we consider the *coupled problem* when we have frictional heating at the part  $\Gamma_2$  of the boundary and want to solve for both the temperature and the displacements taking into account the thermoelastic coupling between stresses and temperature.

Finally, in the last section, we will indicate how to perform a more detailed analysis for a one-dimensional elastic system, in which case explicit solution formulas are available.

## Notation and Definitions

We will consider an elastic body subject to external forces and heating, including heating caused by sliding friction against an obstacle; see Fig. 1. We assume that the body occupies a bounded region  $\Omega \subset \mathbb{R}^3$  and that it is fixed along some part  $\Gamma_0 \subset \partial\Omega$ , where we also have a fixed temperature  $T = 0$ . In the interior of  $\Omega$ , the body is subject to a volume force field  $f(x)$  and a volume



**Existence and Uniqueness for Thermoelastic Contact, Fig. 1** Elastic system in thermoelastic contact with a moving obstacle

heat source field  $Q(x)$ . At some part  $\Gamma_1 \subset \partial\Omega$ , the body is subject to prescribed traction forces  $t(x)$  and a prescribed inward heat flow  $q(x)$ . At  $\Gamma_2 \subset \partial\Omega$ , the body can come into contact with an obstacle, having an initial gap equal to zero if there are no loads or heat sources. We also assume that the obstacle has the prescribed temperature  $T_0(x)$  along  $\Gamma_2$  and that we have a heat transfer resistance  $R = 1/k$  between  $\Omega$  and the obstacle.

By  $L^2(\Omega)$ , we denote the class of functions  $f : \Omega \rightarrow \mathbb{R}^3$  (or  $f : \Omega \rightarrow \mathbb{R}$ ) such that  $\|f\|_{L^2(\Omega)} := (\int_{\Omega} |f(x)|^2 dx)^{1/2} < \infty$ . By  $L^2(\partial\Omega)$ , we denote the class of functions  $f : \partial\Omega \rightarrow \mathbb{R}^3$  (or  $f : \partial\Omega \rightarrow \mathbb{R}$ ) such that  $\|f\|_{L^2(\partial\Omega)} := (\int_{\partial\Omega} |f(x)|^2 dS)^{1/2} < \infty$ . Here  $dS$  denotes the surface element on  $\partial\Omega$ . We will also need the Sobolev space  $H^1(\Omega)$  and its so-called trace space  $H^{1/2}(\partial\Omega)$  where  $H^1(\Omega)$  is defined as the set of all functions  $f : \Omega \rightarrow \mathbb{R}^3$  (or  $f : \Omega \rightarrow \mathbb{R}$ ) such that

$$\|f\|_{H^1(\Omega)} := \left( \int_{\Omega} (|f(x)|^2 + |\nabla f(x)|^2) dx \right)^{1/2} < \infty$$

$H^{1/2}(\partial\Omega)$  is defined as the set of all restrictions  $f|_{\partial\Omega}$  to the boundary of functions  $f \in H^1(\Omega)$ .

Further, by  $L^\infty(\Omega)$  and  $L^\infty(\partial\Omega)$ , respectively, we denote the class functions defined on  $\Omega$  and  $\partial\Omega$ , respectively, which are bounded, having norms  $\|f\|_\infty = \sup_x |f(x)|$ . For properties of the spaces  $L^2$ ,  $L^\infty$ ,  $H^1(\Omega)$ , and  $H^{\pm 1/2}(\partial\Omega)$ , see, for example, [3].

We assume that  $\Omega$  has a Lipschitz boundary. This means that locally the boundary may be represented by an equation

$$x_3 = g(x_1, x_2)$$

where  $g : \mathbb{R}^2 \rightarrow \mathbb{R}$  is Lipschitz continuous, that is, for some constant  $L$   $|g(x) - g(y)| \leq L|x - y|$ , for all  $x, y \in \mathbb{R}^2$ . We note that if  $g$  is continuously differentiable, then it is Lipschitz continuous. We further assume that  $\Gamma_i, i = 0, 1, 2$  are relatively open subsets of the boundary, with mutually disjoint closures. We also introduce the following convex subsets of the Sobolev space  $H^1(\Omega)$ :

$$K_1 = \left\{ u \in H^1(\Omega) : u|_{\Gamma_0} = 0, u_N|_{\Gamma_2} \leq 0 \right\}$$

$$V_2 = \left\{ T \in H^1(\Omega) : T|_{\Gamma_0} = 0 \right\}$$

Here  $u_N = u_i n_i$  denotes the outer normal component of  $u$  at the boundary, and  $n_i$  the outer unit normal to  $\partial\Omega$ .

We will use the equations of linearized elasticity and linear heat conduction. For the temperature, we use the notation  $T$  and for the displacement field  $u$ .

### Temperature Equilibrium Without Frictional Heat Exchange

The steady-state (time-independent) temperature distribution  $T(x)$  is given by the following equations and boundary conditions (where we use the summation convention):

$$\frac{\partial}{\partial x_i} \left( K_{ij} \frac{\partial T}{\partial x_j} \right) = -Q \text{ in } \Omega \text{ (prescribed)} \quad (1)$$

$$T = 0 \text{ on } \Gamma_0$$



$$\begin{aligned}
 K_{ij} \frac{\partial T}{\partial x_j} n_i &= q \text{ on } \Gamma_1 \text{ (prescribed)} \\
 -K_{ij} \frac{\partial T}{\partial x_j} n_i &= k(T - T_0) \text{ on } \Gamma_2 \text{ (prescribed)}
 \end{aligned} \tag{2}$$

If we assume that  $T$  is sufficiently regular, we can multiply (1) by  $\varphi$  and integrate by parts. Then these classical partial differential equations take the following variational form.

Find  $T(x)$ , with  $T = T_0$  on  $\Gamma_0$ , such that

$$\begin{aligned}
 &\int_{\Omega} K_{ij} \frac{\partial T}{\partial x_j} \frac{\partial \varphi}{\partial x_i} dx + \int_{\Gamma_2} k(T - T_0) \varphi dS \\
 &= \int_{\Omega} Q \varphi dx + \int_{\partial \Gamma_1} q \varphi dS
 \end{aligned}$$

for all functions  $\varphi$  (sufficiently regular) with  $\varphi = 0$  on  $\Gamma_0$ . Introducing the bilinear form  $a_2$  and the linear functional  $L_2$  given by

$$\begin{aligned}
 a_2(T, \varphi) &= \int_{\Omega} K_{ij} \frac{\partial T}{\partial x_j} \frac{\partial \varphi}{\partial x_i} dx + \int_{\Gamma_2} kT \varphi dS \\
 \langle L_2, \varphi \rangle &= \int_{\Omega} Q \varphi dx + \int_{\partial \Gamma_1} q \varphi dS + \\
 &\quad + \int_{\Gamma_2} kT_0 \varphi dS
 \end{aligned}$$

we have to find  $T$  with  $T = T_0$  on  $\Gamma_0$ , such that

$$a_2(T, \varphi) = \langle L_2, \varphi \rangle \tag{3}$$

for all  $\varphi$  sufficiently regular. This variational formulation is the basis for a rigorous proof of existence and uniqueness of a solution and a finite element discretization for finding an approximation of this solution. It is well known that the problem (3) is equivalent to finding a minimizer  $T$  of the quadratic energy functional

$$\frac{1}{2} a_2(T, T) - \langle L_2, T \rangle \tag{4}$$

The appropriate functional setting for these variational problems is to require that

$Q \in L^2(\Omega)$ ,  $q \in H^{-1/2}(\Omega)$ ,  $T, T_0, \varphi \in V_2$ ,  $k \geq 0$ ,  $q \in H^{-1/2}(\partial\Omega)$ ,  $K_{ij} \in L^\infty(\Omega)$ , and the matrix  $K_{ij}$  is symmetric and uniformly positive definite, that is, that for some constant  $\alpha > 0$ ,  $\sum_{ij} K_{ij} \xi_j \xi_i \geq \alpha \sum \xi_i^2$ , for all real vectors  $\xi_i$ . Under these assumptions, it is straightforward to prove that there exists a unique solution  $T \in V_2$  satisfying (3) for all  $\varphi \in V_2$  or, equivalently, minimizing the quadratic functional in (4).

### Equilibrium for an Elastic Body Constrained by a Rigid Obstacle

We now consider the case when the elastic body is not subject to any heat sources or any frictional heating, only that it is in (frictionless) contact with the obstacle along  $\Gamma_2 \subset \Omega$ .

We then have the following equations and boundary conditions for the displacement field  $u$ :

$$\frac{\partial \sigma_{ij}}{\partial x_j} = -f_i \tag{5}$$

where

$$\sigma_{ij}(u) = E_{ijkl} \frac{\partial u_k}{\partial x_l}, \text{ in } \Omega \tag{6}$$

$$u_i = 0 \text{ on } \Gamma_0 \tag{7}$$

$$\sigma_{ij} n_j = t_i \text{ on } \Gamma_1 \tag{8}$$

$$\begin{aligned}
 u_N &\leq 0, p \leq 0, u_N p = 0, \text{ where} \\
 u_N &= u_i n_i, \text{ and } p n_i = -\sigma_{ij} n_j \text{ on } \Gamma_2
 \end{aligned} \tag{9}$$

The first equation is  $\frac{\partial}{\partial x_j} (E_{ijkl} \frac{\partial u_k}{\partial x_l}) = -f_i$ , and if we multiply with  $u_i - v_i$  and integrate by parts, we get

$$\begin{aligned}
 &\int_{\Omega} E_{ijkl} \frac{\partial u_k}{\partial x_l} \left( \frac{\partial v_i}{\partial x_j} - \frac{\partial u_i}{\partial x_j} \right) dx \\
 &- \int_{\partial \Omega} E_{ijkl} \frac{\partial u_k}{\partial x_l} n_j (v_i - u_i) dS = \int_{\Omega} f_i (v_i - u_i) dx
 \end{aligned}$$



If we assume that we have enough regularity, we see that finding  $u$  satisfying the conditions (6)–(9) is equivalent to finding  $u$  such that  $u = 0$  on  $\Gamma_0$ ,  $u_i n_i = u_N \leq 0$  on  $\Gamma_2$ , and

$$a_1(u, v - u) \geq \langle L_1, v - u \rangle \quad (10)$$

for all  $v$  such that  $v = 0$  on  $\Gamma_0$  and  $v_i n_i = v_N \leq 0$  on  $\Gamma_2$ . Here  $a_1$  and  $L_1$  are defined by

$$a_1(u, v) = \int_{\Omega} E_{ijkl} \frac{\partial u_k}{\partial x_l} \frac{\partial v_i}{\partial x_j} dx$$

$$\langle L_1, u \rangle = \int_{\Omega} f_i u_i dx + \int_{\Gamma_1} t_i u_i dS$$

We also note that we get the same conditions if we minimize the energy functional  $\frac{1}{2}a_1(u, u) - \langle L_1, u \rangle$  over all  $u$  such that  $u_i n_i = u_N \leq 0$  on  $\Gamma_2$ .

In order to give a rigorous analysis, we require that  $f \in L^2(\Omega)$  and  $u, v \in H^1(\Omega)$ . Further  $\Omega$  should have a Lipschitz-continuous boundary, the sets  $\Gamma_i$ ,  $i = 1, 2, 3$  should be relatively open subsets of  $\partial\Omega$  with mutually disjoint closures. For the elasticity, we further assume that  $E_{ijkl} \in L^\infty(\Omega)$  and that, for some constant  $\alpha > 0$ ,

$$E_{ijkl} \xi_{ij} \xi_{kl} \geq \alpha \sum_{ij} \xi_{ij}^2$$

for all  $\{\xi_{ij} \in \mathbb{R}\}_{1 \leq i, j \leq 3}$ .

Under these assumptions, it is straightforward to show that the variational problem given by (10) has a unique solution. A finite element discretization of (10) gives a numerical algorithm for approximating this solution.

## The Coupled Problem with Frictional Heating

We now consider the situation when the contact obstacle (for instance, a planar or cylindrical surface) moves with a constant tangential velocity  $V$  relative to the region  $\Omega$ . Then the friction forces at the contact surface will generate an inward heat flow which we assume to be proportional to  $\mu V p$  where  $\mu$  is the coefficient of friction and  $p$  the

normal pressure. This generated heat makes us replace the equality (7) above by

$$-K_{ij} \frac{\partial T}{\partial x_j} n_i = k(p)(T - T_0) - \mu V p \quad \text{on } \Gamma_2$$

where the conductivity matrix  $\{K_{ij}\}$  is symmetric and positive definite and the heat transfer coefficient  $k = k(p) \geq 0$  is assumed to be some nonincreasing function of the normal pressure  $p = -\sigma_{ij} n_i n_j$ . Further taking into account thermoelastic effects, we replace the expression for  $\sigma_{ij}$  in (6) by

$$\sigma_{ij}(u) = E_{ijkl} \frac{\partial u_k}{\partial x_l} - s_{ij} T$$

where the matrix  $\{s_{ij}\}$  is symmetric and positive semi-definite.

We then have the following conditions:

$$\frac{\partial \sigma_{ij}}{\partial x_j} = -f_i, \quad \text{where } \sigma_{ij}(u) = E_{ijkl} \frac{\partial u_k}{\partial x_l} - s_{ij} T, \quad \text{in } \Omega \quad (11)$$

$$u = 0, T = 0 \quad \text{on } \Gamma_0 \quad (12)$$

$$\sigma_{ij} n_j = t_i \quad \text{and} \quad K_{ij} \frac{\partial T}{\partial x_j} n_i = q \quad \text{on } \Gamma_1 \quad (13)$$

$$u_N \leq 0, p \leq 0, u_N p = 0, \quad \text{where} \quad (14)$$

$$u_N = u_i n_i, \quad \text{and} \quad p n_i = -\sigma_{ij} n_j \quad \text{on } \Gamma_2$$

$$-K_{ij} \frac{\partial T}{\partial x_j} n_i = k(p)(T - T_0) - \mu V p \quad \text{on } \Gamma_2 \quad (15)$$

In order to simplify, we have here, by (14), formulated the problem so that the tangential friction forces at the sliding surface  $\Gamma_2$  become zero, an approximation which obviously contradicts the assumption that the friction forces produce heating. However, such an approximation is well established in contact mechanics, sometimes referred to as the Goodman approximation [4].

Arguing as in the previous cases, we now obtain the following variational formulation of the coupled problem.

Find  $u \in K_1$  and  $T \in V_2$  such that, for all  $v \in K_1$  and  $\varphi \in V_2$ :

$$a_1(u, v - u) - \int_{\Omega} T s_{ij} \frac{\partial(v_i - u_i)}{\partial x_j} dx \geq \langle L_1, v - u \rangle \quad (16)$$

$$a_2(T, \varphi) + \int_{\Omega} [k(p)(T - T_0) - \mu V p] \varphi dS = \langle L_2, \varphi \rangle \quad (17)$$

In [1], one has in addition replaced the normal pressure  $p \in H^{-1/2}(\partial\Omega)$  by a regularized function  $p^* \in L^2(\partial\Omega)$  given by some linear mapping

$$H^{-1/2}(\partial\Omega) \ni p \mapsto p^* \in L^2(\partial\Omega)$$

The analysis there may, however, be generalized to the general case with  $0 \leq p \in H^{-1/2}(\partial\Omega)$ .

In order to solve the coupled problem in (16, 17), it is natural to use an iterative approach. For a given function  $T$ , we may solve the problem (16) for  $u$ . Then with this solution  $u$ , we solve (17) for  $T$ , and then we go back to (16) and solve for  $u$ , etc. If the process converges, it gives us the solution.

One may now prove the following results:

**Theorem 1.** *If  $k(p) = 0$  for  $p \leq 0$ ; if, with some  $m > 0$ ,  $mp \leq k(p)$ ; and if  $k$  is continuous, then the problem has at least one solution  $(u, T)$ . Moreover, for this solution, we have*

$$\|T\|_{H^1(\Omega)} \leq C(V \|\mu\|_{1/2, \partial\Omega}, 1/m)$$

where  $C(\cdot, \cdot)$  is an increasing function of both arguments.

The growth condition imposed on the heat transfer coefficient  $k$  is therefore sufficient to guarantee that the generated frictional heat can flow into the obstacle instead to remain in the elastic body, where it might cause the temperature to increase to infinity, ruling out the existing of a steady state.

If we do not impose any growth condition on  $k$  but instead restrict the magnitude of  $\mu V$ , we have the following:

**Theorem 2.** *If  $k(p) = 0$  for  $p \leq 0$ , if  $k(p) \geq 0$  for  $p \geq 0$ , if  $k$  is continuous, and if  $V \|\mu\|_{L^\infty(\partial\Omega)}$  is small enough, then the problem has at least one solution  $(u, T)$ .*

In order to obtain a result of uniqueness, we need to assume that  $k$  is Lipschitz continuous, that is that for some constant  $L$  we have  $|k(p_1) - k(p_2)| \leq L|p_1 - p_2|$  for all  $p_1, p_2$ , and impose some constraint on  $L, V$ , and  $\mu$ .

**Theorem 3.** *The solutions proven to exist in the previous theorems are unique if  $k$  is Lipschitz continuous with Lipschitz constant  $L$ , and if  $L, V$  and  $\|\mu\|_{L^\infty}$  or  $\|\mu\|_{L^2}$  are small enough.*

The proofs of these theorems are rather technical. Details may be found in [1].

## The Frictional Heating Problem for a One-Dimensional Elastic System

The results above are easily specialized to one space dimension. We will discuss the following example where explicit expressions for the temperature and displacement field are available.

We consider a thermoelastic rod  $AB$  of length  $L$  that is built into a rigid wall at  $x = 0$  and makes unilateral contact with a second rigid wall at  $x = L$ ; see Fig. 2. The wall at  $B$  is assumed to be moving at speed  $V$  perpendicular to the rod. We assume that the temperature at the wall to the right of  $x = L$  is  $T_B$ , that at  $A$  we have  $T(0) = T_A$ , and that there are no other forces or heat sources than those caused by the frictional heating. Then we have the following conditions, where  $E > 0$ ,  $K > 0$ ,  $k(p) \geq 0$ , and  $s \geq 0$ , corresponding to the equations and inequalities (11)–(15) for the three-dimensional case:

$$\frac{d\sigma}{dx} = 0 \text{ on } (0, L) \quad (18)$$

$$\sigma = E \left( \frac{du}{dx} - sT \right) \text{ on } (0, L) \quad (19)$$

$$\frac{d^2T}{dx^2} = 0 \text{ on } (0, L) \quad (20)$$

$$u(0) = 0, T(0) = T_A \quad (21)$$

$$-\sigma = p \geq 0, \hat{E}u(L) \leq 0, pu(L) = 0 \quad (22)$$

$$-K \frac{dT}{dx}(L) = k(p)(T(L) - T_B) - \mu V p \quad (23)$$

By (18) and (19), we get

$$\sigma(x) = \sigma(L) = -p = E(u'(x) - sT(x)) \text{ for } x \in (0, L),$$

and by (20),

$$T(x) = T_A + \frac{x}{L}(T(L) - T_A)$$

Then, integrating  $u'(x) = sT(x) - p/E$ , we have

$$u(x) = s \frac{x^2}{2L}(T(L) - T_A) + sxT_A - px/E$$

and taking  $x = L$ ,

$$u(L) = \frac{sL}{2}T(L) + \frac{sL}{2}T_A - pL/E \quad (24)$$

Further, since  $T'(x) = (T(L) - T_A)/L$ , we have by (23)

$$-K \frac{T(L) - T_A}{L} = k(p)(T(L) - T_B) - \mu V p$$

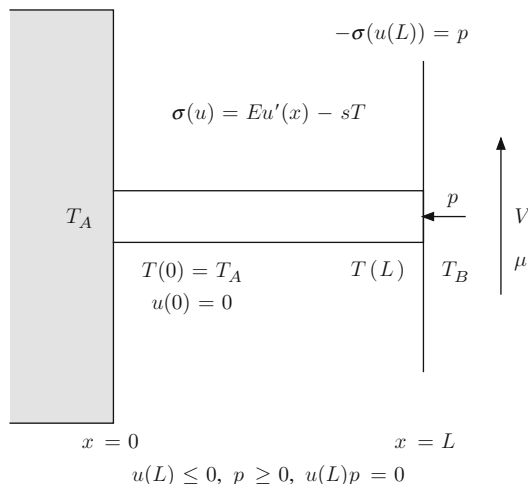
that is,

$$T(L) = \frac{k(p)T_B + KT_A/L + \mu V p}{k(p) + K/L}$$

Then, inserting into (24),

$$u(L) = \frac{sL}{2} \frac{k(p)T_B + KT_A/L + \mu V p}{k(p) + K/L} + sLT_A/2 - pL/E := F(p)$$

We note that  $F(0) = sLT_A$ .



**Existence and Uniqueness for Thermoelastic Contact, Fig. 2** An elastic rod in thermoelastic contact with a moving obstacle

By (23), we now get the following necessary and sufficient condition for the existence of a steady-state solution:

$$p \geq 0, \quad F(p) \leq 0, \quad pF(p) = 0$$

We conclude the following:

If  $F(0) = sLT_A \leq 0$ , then a solution exists with  $p = 0$  and  $T(x) = T_A \leq 0$ ,  $u(x) = sxT_A$ .

If  $T_A > 0$ , so that  $F(0) > 0$ , then the steady states are given by the positive zeros of  $F$ , if any. Now assume that  $k$  is a nondecreasing function of  $p$  with  $\lim_{p \rightarrow \infty} k(p) = k_c$ . Since  $F(p)$  is of the form

$$F(p) = p \left( -L/E + \frac{\mu V s L/2}{k(p) + K/L} \right) + \frac{sL}{2} \times \left( \frac{k(p)T_B + KT_A/L}{k(p) + K/L} + T_A \right) \quad (25)$$

we see that  $\lim_{p \rightarrow \infty} F(p) = -\infty$  if

$$L/E > \frac{\mu V s L/2}{k_c + K/L} \quad (26)$$

that is, that there exists at least one solution provided that

$$\mu V < \frac{2L(k_c + K/L)}{sEL}$$

More details can be found in [2] and [1]:

$$p = \frac{\frac{E_S}{2} \left( T_A \frac{2+Lk(p)/K}{1+Lk(p)/K} + \frac{k(p)T_B}{1+Lk(p)/K} \right)}{1 - \frac{\mu V s L E}{2K(1+Lk(p)/K)}} \quad (27)$$

It follows that if  $\|k'\|_\infty$  and  $\mu V$  are small enough, then the solution of (27) is unique and close to  $p = EsT_A$ . This is in agreement with the general results given in Theorem 3.

## References

1. Andersson L-E, Klarbring A, Barber JR, Ciavarella M (2005) On the existence and uniqueness of steady state solutions in thermoelastic contact with frictional heating. *Proc R Soc A Math Phys Eng Sci* 461(2057):1261–1282
2. Ciavarella M, Johansson L, Afferrante L, Klarbring A, Barber JR (2003) Interaction of thermal contact resistance and frictional heating in thermoelastic instability. *Int J Solids Struct* 40:5583–5597
3. Evans LC (2002) Partial differential equations, vol 19, Graduate studies in mathematics. American Mathematical Society, Providence
4. Johnson KL (1985) Contact mechanics. Cambridge University Press, Cambridge

## Existence and Uniqueness: Solutions of Thermoelastodynamics

Maria Grazia Naso

Università degli Studi di Brescia, Brescia, Italy

## Synonyms

Well-posedness in thermoelasticity

## Overview

We are concerned with a linear one-dimensional thermoelastic system where the hyperbolic elastic system is joined with the parabolic heat

equation. In order to study the well posedness of the associated initial boundary value problem, a basic procedure is analyzed by means of semigroup techniques. For a detailed study in more general cases, some references are given at the end of this section.

## A Simple Model in Thermoelasticity

### The One-Dimensional Linear Thermoelastic System

For  $T > 0$ , we consider the following one-dimensional linear thermoelastic system

$$u_{tt} - \alpha u_{xx} + \gamma \theta_x = 0 \quad \text{in } (0, \ell) \times (0, T) \quad (1)$$

$$\theta_t - k \theta_{xx} + \gamma u_{xt} = 0 \quad \text{in } (0, \ell) \times (0, T) \quad (2)$$

supplemented with initial conditions

$$u(x, 0) = u_0(x), \quad u_t(x, 0) = u_1(x) \quad \text{in } (0, \ell) \quad (3)$$

$$\theta(x, 0) = \theta_0(x) \quad \text{in } (0, \ell) \quad (4)$$

and boundary conditions

$$u(0, t) = 0, \quad u(\ell, t) = 0 \quad \text{in } (0, T) \quad (5)$$

$$\theta(0, t) = 0, \quad \theta(\ell, t) = 0 \quad \text{in } (0, T) \quad (6)$$

in the unknown variables  $u = u(x, t) : (0, \ell) \times (0, T) \rightarrow \mathbb{R}$  and  $\theta = \theta(x, t) : (0, \ell) \times (0, T) \rightarrow \mathbb{R}$ . With regard to the physical meaning of the variables in play,  $u$  represents the longitudinal deflection of a bar of length  $\ell$  with unit reference density, while  $\theta$  actually arises from the temperature variation with respect to a reference value. Constants  $\alpha, k \in \mathbb{R}^+$  and  $\gamma \in \mathbb{R} \setminus \{0\}$  depend on the material properties. Here and in what follows, the subscripts  $x$  and  $t$  indicate partial derivatives.

For a detailed derivation of the modeling under consideration, we refer, e.g., to [2, 4].

Solutions in appropriate Hilbert spaces will be found by means of semigroup theory.

Without loss of generality, throughout this section we choose  $\alpha = 1$ .

Notation

Putting  $\Omega = (0, \ell)$ , let us introduce the space

$$\mathcal{H} = H_0^1(\Omega) \times L^2(\Omega) \times L^2(\Omega)$$

with norm

$$\|(u, u_t, \theta)\|_{\mathcal{H}} = \left( \|u_x\|^2 + \|u_t\|^2 + \|\theta\|^2 \right)^{1/2}$$

where

$$\|\varphi\| = \left[ \int_0^\ell |\varphi(x)|^2 dx \right]^{1/2}$$

is the  $L^2$  norm in  $\Omega$ . Furthermore, we denote by  $\langle \cdot, \cdot \rangle_{\mathcal{H}}$  and  $\langle \cdot, \cdot \rangle$  the inner products in  $\mathcal{H}$  and  $L^2$ , respectively.

Formulation of the Problem

Setting  $v = u_t$ ,  $z = (u, v, \theta)^T$ , and  $z_0 = (u_0, u_1, \theta_0)^T \in \mathcal{H}$ , system (1)–(2) can be rewritten as an evolution system in  $\mathcal{H}$  of the form

$$z_t(t) = Az(t), \quad t > 0 \quad (7)$$

$$z(0) = z_0 \quad (8)$$

The operator  $A : \mathcal{D}(A) \subseteq \mathcal{H} \rightarrow \mathcal{H}$  is defined as

$$A = \begin{bmatrix} 0 & I & 0 \\ (\cdot)_{xx} & 0 & -\gamma(\cdot)_x \\ 0 & -\gamma(\cdot)_x & k(\cdot)_{xx} \end{bmatrix}$$

with domain

$$\begin{aligned} \mathcal{D}(A) = & [H^2(\Omega) \cap H_0^1(\Omega)] \times H_0^1(\Omega) \\ & \times [H^2(\Omega) \cap H_0^1(\Omega)] \end{aligned}$$

We can observe that  $A$  is a densely defined operator from  $\mathcal{D}(A)$  to  $\mathcal{H}$ .

Useful Results in the Theory of Semigroups

We conclude this introductory part with some basic facts about semigroups of operators. For a detailed exposition of the subject, the reader is referred to, e.g., [9].

**Theorem 1 (Lumer-Phillips).** *Let  $A$  be a linear operator with dense domain  $\mathcal{D}(A)$  in a Hilbert space  $\mathcal{H}$ . If  $A$  is dissipative (i.e.,  $\operatorname{Re} \langle Az, z \rangle_{\mathcal{H}} \leq 0$  for every  $z \in \mathcal{D}(A)$ ) and  $\operatorname{Range} (\lambda_0 I - A) = \mathcal{H}$  for some  $\lambda_0 > 0$ , then  $A$  is the infinitesimal generator of a  $C_0$ -semigroup of contractions (i.e., a  $C_0$ -semigroup  $S(t) = e^{tA}$  such that  $\|S(t)\|_{\mathcal{L}(\mathcal{H})} \leq 1$  for every  $t \geq 0$ ).*

Denoting by  $\rho(A)$  the resolvent set of  $A$ , here we will apply the following corollary of Lumer-Phillips theorem.

**Corollary 1.** *Let  $A$  be a linear operator with dense domain  $\mathcal{D}(A)$  in a Hilbert space  $\mathcal{H}$ . If  $A$  is dissipative and  $0 \in \rho(A)$ , then  $A$  is the infinitesimal generator of a  $C_0$ -semigroup of contractions.*

**Remark 1.** Abstract Cauchy problems and strongly continuous semigroups are connected. In particular, given  $z_0 \in \mathcal{D}(A)$ , if operator  $A$  generates a strongly continuous semigroup  $S(t) = e^{tA}$ , then (see, e.g., [9], Chap. 4)

$$z(t) = S(t)z_0 \in C([0, +\infty), \mathcal{D}(A)) \cap C^1([0, +\infty), \mathcal{H})$$

and system (7)–(8) holds in  $\mathcal{H}$  and for every  $t > 0$ .

Well Posedness

To study the well posedness of system (1)–(6), we now analyze if the assumptions of Corollary 1 are satisfied.

- $A$  is a dissipative operator.

In fact, integrating by parts and considering boundary conditions (5)–(6), for any  $z \in \mathcal{D}(A)$ , we find

$$\langle Az, z \rangle_{\mathcal{H}} = \left\langle \begin{bmatrix} v \\ u_{xx} - \gamma \theta_x \\ -\gamma v_x + k \theta_{xx} \end{bmatrix}, \begin{bmatrix} u \\ v \\ \theta \end{bmatrix} \right\rangle_{\mathcal{H}}$$

$$\begin{aligned}
&= \langle v_x, u_x \rangle + \langle u_{xx}, v \rangle - \gamma \langle \theta_x, v \rangle - \gamma \langle v_x, \theta \rangle \\
&\quad + k \langle \theta_{xx}, \theta \rangle \\
&= -k \|\theta_x\|^2 \leq 0
\end{aligned}$$

- $0 \in \rho(A)$

Indeed, let  $F = (f_1, f_2, f_3)^T \in \mathcal{H}$  and consider equation

$$Az = F \quad (9)$$

or in components

$$v = f_1 \quad (10)$$

$$u_{xx} - \gamma \theta_x = f_2 \quad (11)$$

$$-\gamma v_x + k \theta_{xx} = f_3 \quad (12)$$

Substituting (10) into (12), we obtain

$$k \theta_{xx} = f_3 + \gamma f_{1x} \quad (13)$$

where term  $f_3 + \gamma f_{1x}$  belongs to  $L^2(\Omega)$ . Therefore, Lax-Milgram theorem provides (see, e.g., [1], Chap. IX.5) the existence and uniqueness of a solution  $\theta \in H^2(\Omega) \cap H_0^1(\Omega)$  for problem (13). Substituting  $\theta$ , solution of (13), into (11), we have

$$u_{xx} = \gamma \theta_x + f_2 \quad (14)$$

where  $\gamma \theta_x + f_2 \in L^2(\Omega)$ . Hence, by Lax-Milgram theorem (see, e.g., [1], Chap. IX.5), analogously there exists a unique solution  $u \in H^2(\Omega) \cap H_0^1(\Omega)$  for (14).

By Corollary 1, operator  $A$  is the infinitesimal generator of a  $C_0$ -semigroup  $S(t) = e^{tA}$  of contractions on  $\mathcal{H}$ . Then system (1)–(6) has a unique solution given by  $z(t) = S(t)z_0$ .

Moreover, let us analyze equation

$$(I - A)z = F$$

where  $F = (f_1, f_2, f_3)^T \in \mathcal{H}$ . We consider

$$\langle (I - A)z, z \rangle_{\mathcal{H}} = \langle F, z \rangle_{\mathcal{H}}$$

or equivalently,

$$\begin{aligned}
&\|u_x\|^2 - \langle v_x, u_x \rangle + \|v\|^2 - \langle u_{xx}, v \rangle + \gamma \langle \theta_x, v \rangle \\
&\quad + \|\theta\|^2 + \gamma \langle v_x, \theta \rangle - k \langle \theta_{xx}, \theta \rangle \\
&= \langle f_{1x}, u_x \rangle + \langle f_2, v \rangle + \langle f_3, \theta \rangle
\end{aligned}$$

Integrating by parts and by boundary conditions (5)–(6) and applying Young inequality (i.e.,  $ab \leq (\delta/2)a^2 + (2\delta)^{-1}b^2$ ,  $\forall a, b \in \mathbb{R}$ , and  $\delta \in \mathbb{R}^+$ ), we have

$$\begin{aligned}
&\|u_x\|^2 + \|v\|^2 + \|\theta\|^2 + k\|\theta_x\|^2 = \langle f_{1x}, u_x \rangle \\
&\quad + \langle f_2, v \rangle + \langle f_3, \theta \rangle \\
&\leq \frac{1}{2} \left( \|f_{1x}\|^2 + \|u_x\|^2 + \|f_2\|^2 + \|v\|^2 + \|f_3\|^2 + \|\theta\|^2 \right)
\end{aligned}$$

Then there exists a positive constant  $C$  independent of  $z$  such that

$$\|z\|_{\mathcal{H}} \leq C\|F\|_{\mathcal{H}}$$

$$\|\theta_x\| \leq C\|F\|_{\mathcal{H}}$$

We can resume the analysis above on the well posedness of problem (1)–(6) into the following theorem.

**Theorem 2 (Existence and Uniqueness).** *Let  $u_0 \in H^2(\Omega) \cap H_0^1(\Omega)$ ,  $u_1 \in H_0^1(\Omega)$ ,  $\theta_0 \in H^2(\Omega) \cap H_0^1(\Omega)$  and compatible with boundary conditions (5)–(6) for  $t = 0$ . Then, there exists a unique couple  $(u, \theta)$  such that*

$$\begin{aligned}
&u \in C(0, T; H^2(\Omega) \cap H_0^1(\Omega)) \cap C^1(0, T; H_0^1(\Omega)) \\
&\quad \cap C^2(0, T; L^2(\Omega)) \\
&\theta \in C(0, T; H^2(\Omega) \cap H_0^1(\Omega)) \cap C^1(0, T; H_0^1(\Omega))
\end{aligned}$$

fulfilling (1)–(6).

**Remark 2.** For a more complete treatment of linear well posedness

- in bounded domains see, e.g., [3, 4, 11];
- for  $\Omega \equiv \mathbb{R}^n$  or arbitrary unbounded domains, see, e.g., [7, 8, 10].

**Remark 3.** As far as nonlinear thermoelastic systems are concerned, global well-posedness results for smooth or weak solutions and blow-up results, in one or more space dimensions, are discussed in, e.g., [5, 6, 12].

The list of references is quite long but does not claim to be exhaustive (cf. [6] for further references on different topics).

In particular, the references under further reading section may be useful for those interested in learning more about the existence and the uniqueness of the solutions for thermoelastic systems.

## References

- Brezis H (1983) *Analyse fonctionnelle. Collection mathématiques appliquées pour la maîtrise. [Collection of applied mathematics for the master's degree]*, Masson, Paris, théorie et applications. [Theory and applications]
- Carlson DE (1972) Linear thermoelasticity. In: Truesdell C (ed) *Handbuch der physik*, vol VIA/2. Springer, Berlin, pp 297–345
- Dafermos C (1976) Contraction semigroups and trend to equilibrium in continuum mechanics. In: Germain P, Nayroles B (eds) *Applications of methods of functional analysis to problems in mechanics, lecture notes in mathematics*, vol 503. Springer, Berlin/Heidelberg, pp 295–306
- Dafermos CM (1968) On the existence and the asymptotic stability of solutions to the equations of linear thermoelasticity. *Arch Ration Mech Anal* 29:241–271
- Hsiao L, Jiang S (2004) Nonlinear hyperbolic-parabolic coupled systems. In: Dafermos CM, Feireisl E (eds) *Evolutionary equations. Vol. I, Handb. Differ. Equ., North-Holland, Amsterdam*, pp 287–384
- Jiang S, Racke R (2000) *Evolution equations in thermoelasticity*, Chapman & Hall/CRC monographs and surveys in pure and applied mathematics, vol 112. Chapman & Hall/CRC, Boca Raton
- Leis R (1980) *Außenraumaufgaben in der linearen elastizitätstheorie. Math Method Appl Sci* 2(4):379–396
- Leis R (1986) *Initial-boundary value problems in mathematical physics*. B. G. Teubner, Stuttgart
- Pazy A (1983) *Semigroups of linear operators and applications to partial differential equations, applied mathematical sciences*, vol 44. Springer, New York
- Racke R (1987) On the time-asymptotic behaviour of solutions in thermoelasticity. *Proc Roy Soc Edinburgh Sect A* 107(3–4):289–298
- Racke R (2009) Thermoelasticity. In: Dafermos CM, Pokorný M (eds) *Handbook of differential equations: evolutionary equations. Vol. V, Handb. Differ. Equ., Elsevier/North-Holland, Amsterdam*, pp 315–420
- Slemrod M (1981) Global existence, uniqueness, and asymptotic stability of classical smooth solutions in one-dimensional nonlinear thermoelasticity. *Arch Ration Mech Anal* 76(2):97–133

## Further Reading

- Bonfanti G, Muñoz Rivera JE, Naso MG (2008) Global existence and exponential stability for a contact problem between two thermoelastic beams. *J Math Anal Appl* 345(1):186–202
- Bonfanti G, Fabrizio M, Muñoz Rivera JE, Naso MG (2010) On the energy decay for a thermoelastic contact problem involving heat transfer. *J Therm Stresses* 33(11):1049–1065
- Chiriță S, Ciarletta M (2010) Spatial behavior for some non-standard problems in linear thermoelasticity without energy dissipation. *J Math Anal Appl* 367(1):58–68
- Ciarletta M (2002) On the uniqueness and continuous dependence of solutions in dynamical thermoelasticity backward in time. *J Therm Stresses* 25(10):969–984
- Ciarletta M, Scalia A (1994) Theory of thermoelastic dielectrics with voids. *J Therm Stresses* 17(4):529–548
- Ciarletta M, Scalia A, Svanadze M (2007) Fundamental solution in the theory of micropolar thermoelasticity for materials with voids. *J Therm Stresses* 30(3):213–229
- Ciarletta M, Svanadze M, Buonanno L (2009) Plane waves and vibrations in the theory of micropolar thermoelasticity for materials with voids. *Eur J Mech A Solids* 28(4):897–903
- Henry DB, Perissinotto A Jr, Lopes O (1993) On the essential spectrum of a semigroup of thermoelasticity. *Nonlinear Anal* 21(1):65–75
- Jiang S (1992) Global solutions of the Neumann problem in one-dimensional nonlinear thermoelasticity. *Nonlinear Anal* 19(2):107–121
- Kawashima S, Shibata Y (1995) On the Neumann problem of one-dimensional nonlinear thermoelasticity with time-independent external forces. *Czechoslovak Math J* 45(120/1):39–67
- Muñoz Rivera JE, Qin Y (2002) Global existence and exponential stability in one-dimensional nonlinear thermoelasticity with thermal memory. *Nonlinear Anal* 51(1):11–32, Ser. A: Theory Methods
- Racke R (1986) Eigenfunction expansions in thermoelasticity. *J Math Anal Appl* 120(2):596–609
- Racke R (1988) Initial boundary value problems in one-dimensional nonlinear thermoelasticity. *Math Meth Appl Sci* 10(5):517–529
- Racke R, Shibata Y (1991) Global smooth solutions and asymptotic stability in one-dimensional nonlinear thermoelasticity. *Arch Ration Mech Anal* 116(1):1–34
- Racke R, Shibata Y, Zheng S (1993) Global solvability and exponential stability in one-dimensional nonlinear thermoelasticity. *Quart Appl Math* 51(4):751–763



## Existence of Minimizers in Nonlinear Elastostatics of Micromorphic Solids

Patrizio Neff

Faculty of Mathematics, University  
Duisburg–Essen, Essen, Germany

### Synonyms

Micromorphic; Microstructure; Polar materials;  
Solid mechanics; Structured continua;  
Variational methods

### Overview

We consider the mathematical analysis of geometrically exact generalized continua of micromorphic type. The two-field minimization problem (for the macrodeformation field and the affine microdeformation field) is investigated in a variational form, namely, in the quasistatic, conservative load case. Two existence theorems in Sobolev spaces are given for the resulting nonlinear boundary value problems. These results comprise existence results for the microincompressible case and the Cosserat micropolar case. The mathematical analysis employs the direct methods of the calculus of variations and an extended Korn's inequality.

### Introduction

This contribution addresses the mathematical analysis of geometrically exact generalized continua of micromorphic type. General continuum models involving independent rotations have been introduced by the Cosserat brothers [5] at the beginning of the last century. Since then, the Cosserat concept has been generalized in various directions; for an overview of these so-called microcontinuum theories, we refer to [3, 4, 7, 8, 19, 20]. The micromorphic model includes in a natural way size effects, i.e., small samples behave comparatively stiffer than large samples.

These effects have recently received much attention in conjunction with nano-devices. From a computational point of view, theories with size effect are increasingly used to regularize non-well-posed situations, e.g., shear banding in elastoplasticity without hardening. It has already been shown that infinitesimal elastoplasticity augmented with purely elastic Cosserat effects indeed leads to a well-posed problem, for both the quasistatic and dynamic case [26, 27].

The mathematical analysis of general micromorphic solids restricted to the infinitesimal, linear elastic models is presented already, e.g., in [6, 9, 10] for linear micropolar models and in [11–13] for linear microstretch or micromorphic models. New developments regarding the weakest possible curvature contribution and invariance questions related to the infinitesimal model can be found in [14, 15, 30–33]. A connection of micromorphic models to gradient plasticity has been given in [35, 36].

The major difficulty of the mathematical treatment in the finite-strain case is related to the geometrically exact (fully frame indifferent) formulation of the theory and the appearance of nonlinear manifolds necessary for the description of the microstructure. In addition, coercivity turns out to be a delicate problem related to the possible fracture of the material. For related work on existence theorems in the case where coercivity is postulated from the beginning as a constitutive assumption, we refer the reader to [18, 39, 40].

This entry is organized as follows: first, we shortly review the basic concepts of the geometrically exact elastic micromorphic theories in a variational context, i.e., we formulate the quasistatic conservative load case as a two-field minimization problem. Then, the existence proof is presented. Since the two-field variational problem is only conditionally coercive, we need to introduce a modification for the applied loads in order to ensure first that the functional to be minimized is bounded below and second that the curvature contribution can be controlled. This modification of the loads, herein called principle of bounded external work, expresses nothing but the physical fact that by arbitrarily



moving the solid in a force field, only a finite amount of work can be gained. Such a condition is, however, unnecessary in classical finite elasticity. With this preparation, existence of minimizers in Sobolev spaces is then established using the direct methods of the calculus of variations and an extended inequality of Korn type.

The application of this micromorphic model and some constitutive issues are discussed in [22, 24, 29]. The corresponding finite element implementation is treated, e.g., in [16, 17].

## The Finite-Strain Elastic Micromorphic Model

### Useful Notations

Let  $\Omega \subset \mathbb{R}^3$  be a bounded domain with Lipschitz boundary  $\partial\Omega$  and let  $\Gamma$  be a smooth subset of  $\partial\Omega$  with nonvanishing two-dimensional Hausdorff measure. For  $a, b \in \mathbb{R}^3$ , we let  $\langle a, b \rangle_{\mathbb{R}^3}$  denote the scalar product on  $\mathbb{R}^3$  with associated vector norm  $\|a\|_{\mathbb{R}^3}^2 = \langle a, a \rangle_{\mathbb{R}^3}$ . We denote by  $\mathbb{M}^{3 \times 3}$  the set of real  $3 \times 3$  second-order tensors, written with capital letters, and by  $\mathfrak{T}(3)$  the set of all third-order tensors. The standard Euclidean scalar product on  $\mathbb{M}^{3 \times 3}$  is given by  $\langle X, Y \rangle_{\mathbb{M}^{3 \times 3}} = \text{tr}[XY^T]$ , and thus, the Frobenius tensor norm is  $\|X\|^2 = \langle X, X \rangle_{\mathbb{M}^{3 \times 3}}$ . In the following we omit the index  $\mathbb{R}^3$ ,  $\mathbb{M}^{3 \times 3}$ . The identity tensor on  $\mathbb{M}^{3 \times 3}$  will be denoted by  $\mathbf{1}$ , so that  $\text{tr}[X] = \langle X, \mathbf{1} \rangle$ . We let  $\text{Sym}$  and  $\text{PSym}$  denote the symmetric and positive-definite symmetric tensors, respectively. We adopt the usual abbreviations of Lie-group theory, i.e.,  $\text{GL}(3, \mathbb{R}) := \{X \in \mathbb{M}^{3 \times 3} \mid \det[X] \neq 0\}$  the general linear group,  $\text{SL}(3, \mathbb{R}) := \{X \in \text{GL}(3, \mathbb{R}) \mid \det[X] = 1\}$ ,  $\text{O}(3) := \{X \in \text{GL}(3, \mathbb{R}) \mid X^T X = \mathbf{1}\}$ , and  $\text{SO}(3, \mathbb{R}) := \{X \in \text{GL}(3, \mathbb{R}) \mid X^T X = \mathbf{1}, \det[X] = 1\}$  with corresponding Lie algebras  $\mathfrak{so}(3) := \{X \in \mathbb{M}^{3 \times 3} \mid X^T = -X\}$  of skew symmetric tensors and  $\mathfrak{s}(3) := \{X \in \mathbb{M}^{3 \times 3} \mid \text{tr}[X] = 0\}$  of traceless tensors. We set  $\text{sym}(X) = \frac{1}{2}(X^T + X)$  and  $\text{skew}(X) = \frac{1}{2}(X - X^T)$  such that  $X = \text{sym}(X) + \text{skew}(X)$ . We write the classical polar decomposition in the form

$F = R U = \text{polar}(F) U$  with  $R = \text{polar}(F)$  the orthogonal part of  $F$  and  $U$  the positive-definite Biot stretch tensor. For a second-order tensor  $X$ , we define the third-order tensor  $\mathfrak{h} = D_x X(x) = (\nabla(X(x) \cdot e_1), \nabla(X(x) \cdot e_2), \nabla(X(x) \cdot e_3)) = (\mathfrak{h}^1, \mathfrak{h}^2, \mathfrak{h}^3) \in \mathbb{M}^{3 \times 3} \times \mathbb{M}^{3 \times 3} \times \mathbb{M}^{3 \times 3}$ . For third-order tensors  $\mathfrak{h} \in \mathfrak{T}(3)$ , we set  $\|\mathfrak{h}\|^2 = \sum_{i=1}^3 \|\mathfrak{h}^i\|^2$  together with  $\text{sym}(\mathfrak{h}) := (\text{sym}\mathfrak{h}^1, \text{sym}\mathfrak{h}^2, \text{sym}\mathfrak{h}^3)$  and  $\text{tr}[\mathfrak{h}] := (\text{tr}[\mathfrak{h}^1], \text{tr}[\mathfrak{h}^2], \text{tr}[\mathfrak{h}^3]) \in \mathbb{R}^3$ . Moreover, for any second-order tensor  $X$ , we define  $X \cdot \mathfrak{h} := (X\mathfrak{h}^1, X\mathfrak{h}^2, X\mathfrak{h}^3)$  and  $\mathfrak{h} \cdot X$  correspondingly. In general we work in the context of nonlinear, finite elasticity. For the total deformation  $\varphi \in C^1(\overline{\Omega}, \mathbb{R}^3)$ , we have the deformation gradient  $F = \nabla\varphi \in C(\overline{\Omega}, \mathbb{M}^{3 \times 3})$  and we use  $\nabla$  in general only for column vectors in  $\mathbb{R}^3$ . We employ the standard notation of Sobolev spaces, i.e.,  $L^2(\Omega)$ ,  $H^{1,2}(\Omega)$ ,  $H_o^{1,2}(\Omega)$ , which we use indifferently for scalar-valued functions as well as for vector-valued and tensor-valued functions. Moreover, we set  $\|X\|_\infty = \sup_{x \in \Omega} \|X(x)\|$ . We use capital letters to denote possibly large positive constants, e.g.,  $C^+$ ,  $K$ , and lowercase letters to denote possibly small positive constants, e.g.,  $c^+$ ,  $d^+$ .

### Basic Equations

We now present the finite-strain micromorphic approach in a strictly Lagrangian description. We first introduce an independent kinematical field of microdeformations  $P \in \text{GL}^+(3, \mathbb{R})$  together with its right polar decomposition

$$\begin{aligned} P &= \bar{R}_p \cdot U_p = \text{polar}(P) \cdot U_p = \bar{R}_p e^{\frac{\bar{\sigma}_p}{3}} \bar{U}_p, \det[P] = e^{\bar{\sigma}_p}, \\ \bar{U}_p &= \frac{U_p}{\det[U_p]^{1/3}} \in \text{SL}(3, \mathbb{R}), \\ \bar{P} &= \frac{P}{\det[P]^{1/3}} \in \text{SL}(3, \mathbb{R}) \end{aligned} \quad (1)$$

with  $\bar{R}_p \in \text{SO}(3, \mathbb{R})$  and  $\bar{U}_p \in \text{PSym}(3, \mathbb{R}) \cap \text{SL}(3, \mathbb{R})$ . The microdeformations  $P$  are meant to describe the substructure of the material which can rotate, stretch, shear, and shrink. We refer to  $\bar{R}_p$  as microrotations. Following Eringen [7, p. 13], we distinguish the general micromorphic case,  $P \in \text{GL}^+(3, \mathbb{R}) = \mathbb{R}^+ \cdot \text{SL}(3, \mathbb{R})$  with

9 additional degrees of freedom (DOF); the micro-incompressible micromorphic case,  $P \in \text{SL}(3, \mathbb{R})$  with 8 DOF; the microstretch case,  $P \in \mathbb{R}^+ \cdot \text{SO}(3, \mathbb{R})$  with 4 DOF; and the micropolar case,  $P \in \text{SO}(3, \mathbb{R})$  with only 3 additional DOF. The theory with voids is included if  $P \in \mathbb{R}^+ \cdot \mathbf{1}$  with one DOF.

The micromorphic theory we deal with can formally be obtained by introducing the multiplicative decomposition of the macroscopic deformation gradient  $F$  into independent microdeformation  $P$  and the micromorphic, nonsymmetric right stretch tensor  $\bar{U}$  (first Cosserat deformation tensor, the relative distortion) with

$$F = P \cdot \bar{U}, \quad \bar{U} = P^{-1}F, \quad \bar{U} \in \text{GL}^+(3, \mathbb{R}) \quad (2)$$

leading altogether to a micro-compressible, micromorphic formulation.

In the quasistatic case, the micromorphic theory is derived from a two-field variational principle by postulating the following “Euclidean action” [5, p. 156]  $I$  for the finite macroscopic deformation  $\varphi : [0, T] \times \bar{\Omega} \mapsto \mathbb{R}^3$  and the independent microdeformation  $P : [0, T] \times \bar{\Omega} \mapsto \text{GL}^+(3, \mathbb{R})$ :

$$\begin{aligned} I(\varphi, P) = & \int_{\Omega} W(F, P, D_x P) - \Pi_f(\varphi) - \Pi_M(P) \, dV \\ & - \int_{\Gamma_S} \Pi_N(\varphi) \, dS \\ & - \int_{\Gamma_C} \Pi_{M_c}(P) \, dS \mapsto \min \text{ w.r.t. } (\varphi, P), \\ P|_{\Gamma} = P_d, \quad \varphi|_{\Gamma} = g_d(t) \end{aligned} \quad (3)$$

The elastically stored energy density  $W$  depends on the macroscopic deformation gradient  $F = \nabla \varphi$  as usual but in addition on the microdeformation  $P$  together with their first-order space derivatives, represented through the third-order tensor  $D_x P$ . Here  $\Omega \subset \mathbb{R}^3$  is a domain with boundary  $\partial\Omega$  and  $\Gamma \subset \partial\Omega$  is that part of the boundary, where Dirichlet conditions  $g_d, P_d$  for displacements and microdeformations,

respectively, can be prescribed, while  $\Gamma_S \subset \partial\Omega$  is a part of the boundary, where traction boundary conditions in the form of the potential of applied surface forces  $\Pi_N$  are given with  $\Gamma \cap \Gamma_S = \emptyset$ . The potential of external applied volume force is  $\Pi_f$  and  $\Pi_M$  takes on the role of the potential of applied external volume couples. In addition,  $\Gamma_C \subset \partial\Omega$  is the part of the boundary, where the potential of applied surface couples  $\Pi_{M_c}$  is applied with  $\Gamma \cap \Gamma_C = \emptyset$ . On the free boundary  $\partial\Omega \setminus \{\Gamma \cup \Gamma_S \cup \Gamma_C\}$ , corresponding natural boundary conditions for  $\varphi$  and  $P$  apply, which are obtained automatically in the variational process.

Variation of the action  $I$  with respect to  $\varphi$  yields the traditional equation for balance of linear momentum, and variation of  $I$  with respect to  $P$  yields the additional balance of moment of momentum [see 29]. The standard conclusion from frame-indifference (invariance of the free energy under superposed rigid body motions) is as follows: for all

$$\begin{aligned} \forall Q \in \text{SO}(3, \mathbb{R}) \Rightarrow W(F, P, D_x P) \\ = W(QF, QP, D_x[QP]) \\ = W(QF, QP, QD_x P) \end{aligned}$$

and this leads to the reduced representation of the energy (specify  $Q = \bar{R}_p^T$ ):

$$\begin{aligned} W(F, \bar{P}, D_x P) &= W(\bar{R}_p^T F, \bar{R}_p^T P, \bar{R}_p^T D_x P) \\ &= W(U_p \bar{U}, U_p, \bar{R}_p^T D_x P) \quad (4) \\ &= W^\sharp(\bar{U}, U_p, \mathfrak{K}_p, \nabla \bar{\alpha}_p) \end{aligned}$$

where for  $\bar{P} = \bar{R}_p \bar{U}_p \in \text{SL}(3, \mathbb{R})$  we set

$$\begin{aligned} \mathfrak{K}_p &:= \bar{R}_p^T D_x \bar{P} \\ &= \left( \bar{R}_p^T \nabla(\bar{P} \cdot e_1), \bar{R}_p^T \nabla(\bar{P} \cdot e_2), \bar{R}_p^T \nabla(\bar{P} \cdot e_3) \right) \\ &\in \mathbb{M}^{3 \times 3} \times \mathbb{M}^{3 \times 3} \times \mathbb{M}^{3 \times 3} \end{aligned} \quad (5)$$

For a geometrically exact (macroscopically isotropic) theory, we assume in the following an additive split of the total free-energy density

into micromorphic relative local stretch (macroscopic), stretch of the substructure itself (microscopic), and micromorphic curvature part according to

$$W^\# = \underbrace{W_{\text{mp}}(\bar{U})}_{\text{relative macroscopic energy}} + \underbrace{W_{\text{foam}}(\bar{U}_p, \bar{\alpha}_p)}_{\text{microscopic local energy}} + \underbrace{W_{\text{curv}}(K_p, \nabla \bar{\alpha}_p)}_{\text{microscopic interaction energy}} \quad (6)$$

since a possible coupling between  $\bar{U}$  and  $\mathfrak{K}_p$  for centrosymmetric bodies can be ruled out [37, p. 14].

### The Elastic Macroscopic Micromorphic Strain Energy Density

For a macroscopic theory which is relevant mainly for small elastic strain, we require that  $W_{\text{mp}}(\bar{U})$  is a nonnegative isotropic quadratic form (leading to a physically linear problem). This covers already many cases of physical interest. For the local energy contribution elastically stored in the substructure, we assume the nonlinear expression

$$\begin{aligned} W_{\text{foam}}(U_p) &= \underbrace{\mu^m \left\| \frac{U_p}{\det[U_p]^{(1/3)}} - \mathbf{1} \right\|^2}_{\text{isochoric substructure energy}} \\ &\quad + \underbrace{\frac{\lambda^m}{4} \left( (\det[U_p] - 1)^2 + \left( \frac{1}{\det[U_p]} - 1 \right)^2 \right)}_{\text{volumetric energy}} \\ &= \mu^m \|\bar{U}_p - \mathbf{1}\|^2 \\ &\quad + \frac{\lambda^m}{4} \left( (e^{\bar{\alpha}_p} - 1)^2 + (e^{-\bar{\alpha}_p} - 1)^2 \right) \\ &=: W_{\text{foam}}(\bar{U}_p, \bar{\alpha}_p) \end{aligned} \quad (7)$$

avoiding self-interpenetration in a variational setting, since  $W_{\text{foam}} \rightarrow \infty$  as  $\det[P] = \det[U_p] \rightarrow 0$  if  $\lambda^m > 0$ .

The most general isotropic quadratic form of  $W_{\text{mp}}$  is

$$W_{\text{mp}}(\bar{U}) = \mu_e \|\text{sym}(\bar{U} - \mathbf{1})\|^2 + \mu_c \|\text{skew}(\bar{U} - \mathbf{1})\|^2 + \frac{\lambda_e}{2} \text{tr}[\text{sym}(\bar{U} - \mathbf{1})]^2 \quad (8)$$

with material constants  $\mu_e, \mu_c, \lambda_e$  such that  $\mu_e, 3\lambda_e + 2\mu_e, \mu_c \geq 0$  from non-negativity of (8) [see 7].

The coefficients  $\mu_e, \lambda_e$  are effective elastic constants which in general do not coincide with the classical Lamé constants. The so-called Cosserat couple modulus  $\mu_c$  (rotational couple modulus) remains for the moment unspecified, but we note that  $\mu_c = 0$  is physically possible, even in the micropolar case, since the micromorphic reaction stress  $D_{\bar{U}} W_{\text{mp}}(\bar{U}) \cdot \bar{U}^T$  is not symmetric in general, i.e., the problem does not decouple [28]. By formal similarity with the classical formulation, we may call  $\mu^m, \lambda^m$  the microscopic Lamé moduli of the affine substructure.

### The Nonlinear Elastic Curvature Energy Density

The curvature energy is responsible for the size-dependent resistance of the substructure against local twisting and inhomogeneous volume change. Thus, inhomogeneous microstructural rearrangements are penalized. For the curvature term, to be specific, we assume

$$\begin{aligned} W_{\text{curv}}(\mathfrak{K}_p, \nabla \bar{\alpha}_p) &= \mu \frac{L_c^{1+p}}{12} \left( 1 + \alpha_4 L_c^q \|\mathfrak{K}_p\|^q \right) \\ &\quad \times \left( \alpha_5 \|\text{sym} \mathfrak{K}_p\|^2 + \alpha_6 \|\text{skew} \mathfrak{K}_p\|^2 + \alpha_7 \text{tr}[\mathfrak{K}_p]^2 \right)^{\frac{1+p}{2}} \\ &\quad + \mu \frac{L_c^{1+p}}{12} \left( \alpha_8 \|\nabla \bar{\alpha}_p\|^{1+p} + \alpha_8 L_c \|\nabla \bar{\alpha}_p\|^{2+p} \right) \end{aligned} \quad (9)$$

where  $L_c > 0$  is setting an internal length scale with units of length. It is to be noted that we have decoupled the curvature coming from inhomogeneous volume changes and from pure twisting. The values  $\alpha_4 \geq 0, p > 0$  and  $q \geq 0$  are additional material constants. We mean  $\text{tr}[\mathfrak{K}_p]^2 = \|\text{tr}[\mathfrak{K}_p]\|^2$  by abuse of notation.

In the finite-strain regime,  $W_{\text{curv}}$  should preferably be coercive in the sense that we impose pointwise

$$\exists c^+ > 0 \exists r > 1 : \forall \mathfrak{K}_p \in \mathfrak{T}(3) \forall \xi \in \mathbb{R}^3 : \\ W_{\text{curv}}(\mathfrak{K}_p, \xi) \geq c^+ \|(\mathfrak{K}_p, \xi)\|^r$$

(10)

or less demanding

$$\exists r > 1 : \frac{W_{\text{curv}}(\mathfrak{K}_p, \xi)}{\|(\mathfrak{K}_p, \xi)^r\|} \rightarrow \infty \text{ as } \|(\mathfrak{K}_p, \xi)\| \rightarrow \infty$$

(11)

which implies necessarily  $\alpha_6, \alpha_8 > 0$  in (9). Observe that our formulation of the micromorphic curvature tensor is mathematically convenient in the sense that  $\|\mathfrak{K}_p\| = \|\bar{R}_p^T D_x \bar{P}\| = \|D_x \bar{P}\|$  provides pointwise control of all first derivatives of  $\bar{P}$  independent of the values of  $\bar{P}$  itself.

Note that the presented formulation includes a finite-strain Cosserat micropolar model as a special case, if we set  $\bar{P} = \bar{R} \in \text{SO}(3, \mathbb{R})$ . In the Cosserat case, an alternative curvature tensor based on  $\bar{R}^T \text{Curl} \bar{R}$  suggests itself [34].

Altogether, we have the following correspondence of limit problems:

$$\begin{aligned} \lambda^m \rightarrow \infty &\Rightarrow \text{micro-incompressible} \\ &\text{model :} \\ &\text{manifold } \text{SL}(3, \mathbb{R}) \\ \mu^m \rightarrow \infty &\Rightarrow \text{microstretch model :} \\ &\text{manifold } \mathbb{R}^+ \cdot \text{SO}(3, \mathbb{R}) \\ \mu^m, \lambda^m \rightarrow \infty &\Rightarrow \text{micropolar model :} \\ &\text{manifold } \text{SO}(3, \mathbb{R}) \\ \mu^m, \lambda^m, \mu_c \rightarrow \infty &\Rightarrow \text{higher (second) gradient} \\ &\text{continua of Mindlin-type} \end{aligned}$$

(12)

## Analysis of the Mathematical Problem

### The Micromorphic Problem in Variational Form

Let us gather the obtained three-field problem posed in a variational form. The task is to

find a triple  $(\varphi, \bar{P}, \bar{\alpha}_p) : \Omega \subset \mathbb{R}^3 \mapsto \mathbb{R}^3 \times \text{SL}(3, \mathbb{R}) \times \mathbb{R}$  of macroscopic deformation  $\varphi$  and independent microdeformation  $P = e^{\frac{\bar{\alpha}_p}{3}} \bar{P}$ , minimizing the energy functional  $I$  with

$$\begin{aligned} I(\varphi, \bar{P}, \bar{\alpha}_p) = & \int_{\Omega} [W_{\text{mp}}(P^{-1} \nabla \varphi) + W_{\text{foam}}(\bar{U}_p, \bar{\alpha}_p) \\ & + W_{\text{curv}}(\bar{R}_p^T D_x \bar{P}, \nabla \bar{\alpha}_p) - \Pi_f(\varphi) \\ & - \Pi_M(P)] dV - \int_{\Gamma_S} \Pi_N(\varphi) dS \\ & - \int_{\Gamma_C} \Pi_{M_c}(P) dS \mapsto \min. \text{ w.r.t. } (\varphi, \bar{P}, \bar{\alpha}_p) \end{aligned}$$

(13)

under the constraints

$$\begin{aligned} \bar{U}_p &= \bar{R}_p^T \bar{P}, \quad \bar{R}_p = \text{polar}(\bar{P}) \\ \bar{U} &= P^{-1} \nabla \varphi, \quad P = e^{\frac{\bar{\alpha}_p}{3}} \bar{P} \end{aligned}$$

(14)

and the Dirichlet boundary conditions

$$\begin{aligned} \varphi|_r &= g_d, \quad \bar{R}_p|_r = \bar{R}_{p_d}, \quad \bar{U}_p|_r = \bar{U}_{p_d} \Rightarrow \\ \bar{P}|_r &= \bar{R}_{p_d} \bar{U}_{p_d}, \quad \bar{\alpha}_p|_r = \bar{\alpha}_{p_d} \end{aligned}$$

(15)

Here, the constitutive assumptions on the densities are taken to be

$$\begin{aligned} W_{\text{mp}}(\bar{U}) &= \mu_c \|\text{sym}(\bar{U} - \mathbf{1})\|^2 \\ &+ \mu_c \|\text{skew}(\bar{U})\|^2 + \frac{\lambda_e}{2} \text{tr}[\text{sym}(\bar{U} - \mathbf{1})]^2 \\ W_{\text{foam}}(\bar{U}_p, \bar{\alpha}_p) &= \mu^m \|\bar{U}_p - \mathbf{1}\|^2 \\ &+ \frac{\lambda_c^m}{4} \left( (e^{\bar{\alpha}_p} - 1)^2 + (e^{-\bar{\alpha}_p} - 1)^2 \right) \\ W_{\text{curv}}(\mathfrak{K}_p, \nabla \bar{\alpha}_p) &= \mu \frac{L_c^{1+p}}{12} (1 + \alpha_4 L_c^q \|\mathfrak{K}_p\|^q) \\ &\times \left( \alpha_5 \|\text{sym} \mathfrak{K}_p\|^2 + \alpha_6 \|\text{skew} \mathfrak{K}_p\|^2 + \alpha_7 \text{tr}[\mathfrak{K}_p]^2 \right)^{\frac{1+p}{2}} \\ &+ \mu \frac{L_c^{1+p}}{12} \left( \alpha_8 \|\nabla \bar{\alpha}_p\|^{1+p} + \alpha_8 L_c \|\nabla \bar{\alpha}_p\|^{2+p} \right) \\ \mathfrak{K}_p &= \bar{R}_p^T D_x \bar{P} = \left( \bar{R}_p^T \nabla(\bar{P} \cdot e_1), \bar{R}_p^T \nabla(\bar{P} \cdot e_2), \bar{R}_p^T \nabla(\bar{P} \cdot e_3) \right) \end{aligned}$$

(16)

It is assumed that  $\mu_e, \lambda_e > 0$ ,  $\mu_c \geq 0$ , and  $\mu^m, \lambda^m, L_c > 0$ . The parameters  $\alpha_i$ ,  $i = 1, \dots, 8$  are dimensionless weighting factors. If not stated otherwise, we assume that  $\alpha_5 > 0, \alpha_6 > 0, \alpha_8 > 0, \alpha_7 \geq 0$ .

Traditionally, in the conservative dead load case, one would have

$$\begin{aligned} \Pi_f(\varphi) &= \langle f, \varphi \rangle, & \Pi_M(P) &= \langle M, P \rangle \\ \Pi_N(\varphi) &= \langle N, \varphi \rangle, & \Pi_{M_c}(P) &= \langle M_c, P \rangle \end{aligned} \quad (17)$$

for the potentials of applied loads with given functions  $f \in L^2(\Omega, \mathbb{R}^3)$ ,  $M \in L^2(\Omega, \mathbb{M}^{3 \times 3})$ ,  $N \in L^2(\Gamma_S, \mathbb{R}^3)$ ,  $M_c \in L^2(\Gamma_C, \mathbb{M}^{3 \times 3})$ .

For the treatment of our model, we need to assume, however, that the external potentials, describing the configuration dependent applied loads, are continuous with respect to the topology of  $L^1(\Omega)$ ,  $L^1(\Gamma_S)$ ,  $L^1(\Gamma_C)$ , respectively, and satisfy in addition the crucial condition

$$\begin{aligned} \exists C^+ > 0 \quad \forall \varphi \in L^1(\Omega, \mathbb{R}^3), \\ P \in L^1(\Omega, GL^+(3, \mathbb{R})) : \\ \int_{\Omega} \Pi_f(\varphi) - \Pi_M(P) \, dV, \\ \int_{\Gamma_S} \Pi_N(\varphi) \, dS, \\ \int_{\Gamma_C} \Pi_{M_c}(P) \, dS \leq C^+ \end{aligned} \quad (18)$$

While continuity is satisfied, e.g., for the dead load case  $\Pi_f(\varphi) = \langle f, \varphi \rangle$  and  $f \in L^\infty(\Omega)$ , the second condition (18) restricts attention to “bounded external work.” If we want to describe a situation corresponding to the classical dead load case, we could take

$$\Pi_f(\varphi) = \frac{1}{1 + [\|\varphi(x)\| - K^+]_+} \langle f(x), \varphi(x) \rangle \quad (19)$$

for some large positive constant  $K^+$  and  $[\cdot]_+$  the positive part of a scalar argument. It suffices now that  $f \in L^1(\Omega)$ , then  $\int_{\Omega} \Pi_f(\varphi) \, dV \leq C^+$ , independent of  $\varphi \in L^1(\Omega)$ .

The new condition (18) can be rephrased as saying that only a finite amount of work can be performed against the external loads, regardless of the magnitude of translation and microdeformation. This is certainly true for any real field of applied loads [23]. The mathematical consequence is that when considering infimizing sequences without this assumption, it could happen that the curvature contribution is not controlled while the total energy remains bounded.

### The Coercivity Inequality

We distinguish three different situations:

Case 1:  $\mu_c > 0$ ,  $\alpha_4 \geq 0$ ,  $p \geq 1$ ,  $q \geq 0$ . Elastic macro-stability, local first-order micromorphic. Fracture excluded

Case 2:  $\mu_c = 0$ ,  $\alpha_4 > 0$ ,  $p \geq 1$ ,  $q > 1$ . Elastic pre-stability, nonlocal second-order micromorphic, macroscopic specimens, in a sense close to classical elasticity, zero Cosserat couple modulus. Fracture excluded for bounded external work

Case 3:  $\mu_c = 0$ ,  $\alpha_4 = 0$ ,  $0 < p \leq 1$ ,  $q = 0$ . Elastic pre-stability, nonlocal second-order micromorphic theory, macroscopic specimens, in a sense close to classical elasticity, zero Cosserat couple modulus. Since possibly  $\varphi \notin W^{1,1}(\Omega, \mathbb{R}^3)$ , due to lack of elastic coercivity, including fracture in multiaxial situations.

We refer to  $0 < p < 1$ ,  $q \geq 0$  as the subcritical case, to  $p = 1$ ,  $q \geq 0$  as the critical case, and to  $p \geq 1$ ,  $q > 1$  as the supercritical case. We will treat the first two cases mathematically.

The decisive analytical tool underlying the treatment of case 2 (supercritical,  $\mu_c = 0$ ) is the following inequality establishing coercivity:

**Theorem 1. (Extended Korn’s First Inequality).** *Let  $\Omega \subset \mathbb{R}^3$  be a bounded Lipschitz domain and let  $\Gamma \subset \partial\Omega$  be a smooth part of the boundary with nonvanishing 2-dimensional Hausdorff measure. Define  $H_o^{1,2}(\Omega, \Gamma) := \{\phi \in H^{1,2}(\Omega) \mid \phi|_{\Gamma} = 0\}$  and let  $F_p, F_p^{-1} \in C^0(\overline{\Omega}, GL(3, \mathbb{R}))$ . Then*

$$\begin{aligned} \exists c^+ > 0 \forall \phi \in H_o^{1,2}(\Omega, \Gamma) : \\ \left\| \nabla \phi F_p^{-1}(x) + F_p^{-T}(x) \nabla \phi^T \right\|_{L^2(\Omega)}^2 \\ \geq c^+ \|\phi\|_{H^{1,2}(\Omega)}^2 \end{aligned}$$

**Proof.** The proof of this version of Korn's inequality is presented in [38], which is improving on a similar result of the present author [21] where the possible validity of the inequality has been first observed.

### Existence Results for the Geometrically Exact Elastic Micromorphic Model

The following results have first been obtained in [23].

**Theorem 2. (Existence for Elastic Micromorphic Model: Case 1).** *Let  $\Omega \subset \mathbb{R}^3$  be a bounded Lipschitz domain and assume for the boundary data  $g_d \in H^1(\Omega, \mathbb{R}^3)$  and  $P_d \in W^{1,1+p}(\Omega, GL^+(3, \mathbb{R}))$ . Moreover, let the applied external potentials satisfy (18). Then (13) with material constants conforming to case 1 and  $p > 1$  admits at least one minimizing solution triple  $(\varphi, \bar{P}, \bar{\alpha}_p) \in H^1(\Omega, \mathbb{R}^3) \times W^{1,1+p}(\Omega, SL(3, \mathbb{R})) \times W^{1,2+p}(\Omega, \mathbb{R})$ .*

**Proof.** The proof is based on the direct methods of the calculus of variations. The influence of the external potentials is gathered in writing  $\Pi(\varphi, P)$ . With the prescription of  $(g_d, P_d)$  as data of the problem, it is clear that  $I < \infty$  for exactly this pair of functions after decomposing  $P_d$  in its rotational, isochoric stretch and volumetric stretch. Since (18) is assumed, it is also clear that  $I$  is bounded below for all  $\varphi \in L^2(\Omega, \mathbb{R}^3)$  and  $P \in L^2(\Omega, GL^+(3, \mathbb{R}))$ .

We may therefore choose infimizing “sequences of triples”

$$\begin{aligned} (\varphi^k, \bar{P}^k, \bar{\alpha}_p^k) \in H^1(\Omega, \mathbb{R}^3) \times W^{1,1+p}(\Omega, SL(3, \mathbb{R})) \\ \times W^{1,2+p}(\Omega, \mathbb{R}) \end{aligned} \quad (20)$$

such that

$$\lim_{k \rightarrow \infty} I(\varphi^k, \bar{P}^k, \bar{\alpha}_p^k) = \inf \{ I(\varphi, \bar{P}, \bar{\alpha}_p) \mid \varphi \in L^1(\Omega, \mathbb{R}^3), \bar{P} \in L^1(\Omega, SL(3, \mathbb{R})), \bar{\alpha}_p \in L^1(\Omega, \mathbb{R}) \} \quad (21)$$

The total curvature contribution  $W_{\text{curv}}$  along this sequence is bounded independent of the number  $k$  again on account of (18).

Observe now that the micromorphic curvature term  $\mathfrak{K}_p$  controls  $\bar{P} \in W^{1,1+p}(\Omega, SL(3, \mathbb{R}))$ , in view of  $\|\mathfrak{K}_p\| = \|\bar{R}_p^T D_x \bar{P}\| = \|D_x \bar{P}\|$  pointwise, the assumption that  $\alpha_5, \alpha_6 > 0$  and the application of Poincaré's inequality with the Dirichlet conditions on  $\bar{P}$ . Moreover, since  $\alpha_8 > 0$  we obtain boundedness of  $\bar{\alpha}_p^k \in W^{1,2+p}(\Omega, \mathbb{R})$ , again independent of  $k \in \mathbb{N}$ . This result remains true already without specification of Dirichlet boundary conditions for  $\bar{\alpha}_p$  since the term  $e^{\bar{\alpha}_p}$  estimates any  $L^q$ -norm of  $\bar{\alpha}_p$ . For  $p > 1$  Sobolev's embedding shows that we can choose a subsequence, not relabeled, such that strongly

$$\bar{\alpha}_p^k \rightarrow \widehat{\alpha}_p \in C^0(\Omega, \mathbb{R}), \quad k \rightarrow \infty \quad (22)$$

Now we may extract a subsequence again denoted by  $\bar{P}^k$  converging strongly in  $L^{1+p}(\Omega)$  to an element  $\hat{P} \in W^{1,1+p}(\Omega, \mathbb{M}^{3 \times 3})$  since  $p > 0$  by assumption. Moreover, a further subsequence can be found, such that the curvature tensor  $\mathfrak{K}_{p,k}$  converges weakly to some  $\widehat{\mathfrak{K}}_p$  in  $L^{1+p}(\Omega)$ . For  $1 < (1+p) < 3$ , the embedding

$$W^{1,1+p}(\Omega) \subset L^{\frac{3(1+p)}{3-(1+p)-\delta}}(\Omega), \quad \delta \geq 0 \quad (23)$$

for three space dimensions is compact for  $\delta > 0$  and shows that the subsequence  $\bar{P}^k$  can be chosen such that it converges indeed strongly in the topology of  $L^{6-\delta}(\Omega)$ , since we have moreover  $p \geq 1$ , which implies immediately that  $\hat{P} \in W^{1,1+p}(\Omega, SL(3, \mathbb{R}))$ . If  $1+p \geq 3$ , we can use better embeddings to have the same conclusion.

Because  $\mu_c > 0$ , we have the simple algebraic estimate

$$\begin{aligned}
 W_{\text{mp}}(P^{-1,k}F^k) &\geq \mu_c \|P^{-1,k}F^k - \mathbf{1}\|^2 \\
 &= \mu_c \left( \|P^{-1,k}F^k\|^2 - 2\langle P^{-1,k}F^k, \mathbf{1} \rangle + 3 \right) \\
 &\geq \mu_c \left( \|\bar{U}_k\|^2 - 2\sqrt{3}\|\bar{U}_k\| + 3 \right)
 \end{aligned} \quad (24)$$

implying the boundedness of the micromorphic stretch  $\bar{U}_k = P^{-1,k}F^k$  in  $L^2(\Omega)$ . Moreover, by Hölder's inequality, we obtain

$$\begin{aligned}
 \|F^k\|_{s,\Omega} &= \|P^k P^{-1,k}F^k\|_{s,\Omega} \\
 &\leq \|P^k\|_{r_1,\Omega} \|P^{-1,k}F^k\|_{r_2,\Omega} \\
 &= \|e^{\frac{\bar{\alpha}_p^k}{3}} \bar{P}^k\|_{r_1,\Omega} \|P^{-1,k}F^k\|_{r_2,\Omega} \\
 &\leq \sup_{x \in \Omega} e^{\frac{\bar{\alpha}_p^k(x)}{3}} \|\bar{P}^k\|_{r_1,\Omega} \|P^{-1,k}F^k\|_{r_2,\Omega}, \\
 \frac{1}{s} &= \frac{1}{r_1} + \frac{1}{r_2}
 \end{aligned} \quad (25)$$

Since  $\bar{P}^k$  is bounded in  $L^6(\Omega)$  (see (23)) and  $P^{-1,k}F^k$  is bounded in  $L^2(\Omega)$  and  $\bar{\alpha}_p^k$  is strongly converging in  $C^0(\Omega, \mathbb{R})$  (22), we may choose  $r_1 = 6, r_2 = 2$  to obtain boundedness of  $F^k = \nabla \varphi_k$  in  $L^s(\Omega)$ ,  $s = \frac{3}{2}$ . Using the Dirichlet boundary conditions for  $\varphi_k$  and the generalized Poincaré inequality, we get

$$\|\varphi_k\|_{W^{1,s}(\Omega, \mathbb{R}^3)} \leq \text{Const} \quad (26)$$

By the boundedness of  $\varphi^k$  in  $W^{1,s}(\Omega, \mathbb{R}^3)$  we may extract a subsequence, not relabeled, such that  $\varphi^k \rightharpoonup \hat{\varphi} \in W^{1,s}(\Omega, \mathbb{R}^3)$ . Furthermore, we may always obtain a subsequence of  $(\varphi^k, P^k)$  such that  $\bar{U}_k = P^{-1,k}F^k$  converges weakly in  $L^2(\Omega)$  to some element  $\hat{U}$  on account of the boundedness of the stretch energy and  $\mu_c > 0$ .

We have already shown that for  $p \geq 1$ , the sequence  $\bar{P}^k$  converges indeed strongly in  $L^r(\Omega)$  to an element  $\hat{P} \in W^{1,1+p}(\Omega, \text{SL}(3, \mathbb{R}))$ . Therefore,

$$\begin{aligned}
 \bar{P}^{-1,k} &= \frac{1}{\det[\bar{P}^k]} \text{Adj} \bar{P}^k \rightarrow \frac{1}{\det[\hat{P}]} \text{Adj} \hat{P} \\
 &= \hat{P}^{-1} \text{ in } L^{\frac{r}{2}}(\Omega, \text{SL}(3, \mathbb{R})), \\
 r &= \frac{3(1+p)}{(3-(1+p))} - \delta, \quad \text{if } 1 < (1+p) < 3
 \end{aligned} \quad (27)$$

and we obtain for  $p > 1$  that  $\bar{P}^{-1,k} \rightarrow \hat{P}^{-1}$  strongly in  $L^{3+\tilde{\delta}}(\Omega, \text{SL}(3, \mathbb{R}))$ ,  $\tilde{\delta} > 0$ . Moreover,

$$P^{-1,k} = e^{-\frac{\bar{\alpha}_p^k}{3}} \bar{P}^{-1,k} \rightarrow \hat{P}^{-1} = e^{-\frac{\hat{\alpha}_p}{3}} \hat{P}^{-1,k} \quad (28)$$

on account of the strong convergence of  $\bar{\alpha}_p^k$ . Thus,  $\bar{P}^{-1,k}F^k$  converges certainly weakly to  $\hat{P}^{-1}F$  in  $L^1(\Omega)$  on account of Hölder's inequality (sharp). The weak limit in  $L^1(\Omega)$  must coincide with the weak limit of  $\bar{U}_k$  in  $L^2(\Omega)$ . Hence, the identity  $\hat{U} = \hat{P}^{-1} \nabla \hat{\varphi}$  holds.

Since the mapping  $\text{polar} : GL^+(3, \mathbb{R}) \mapsto \text{SO}(3, \mathbb{R})$  is a bounded continuous function on invertible matrices with positive determinant, it generates a nonlinear superposition operator

$$\text{polar}(\cdot) : L^r(\Omega, GL^+(3, \mathbb{R})) \mapsto L^r(\Omega, \text{SO}(3, \mathbb{R})) \quad (29)$$

which, moreover, is continuous [1, p. 101, Th. 3.7]. Thus,  $\bar{R}_k = \text{polar}(\bar{P}_k) \rightarrow \hat{R} = \text{polar}(\hat{P})$  strongly in  $L^r(\Omega)$ , and a similar argument as for the sequence  $\bar{U}_k$  shows that

$$\mathfrak{K}_{p,k} \rightharpoonup \widehat{\mathfrak{K}}_p = \text{polar}(\hat{P})^T D_x \hat{P} \quad (30)$$

in  $L^{1+p}(\Omega)$ , weakly. Again on account of  $\bar{P}^k \rightarrow \hat{P}$  in  $L^r(\Omega, \text{SL}(3, \mathbb{R}))$ , we infer now

$$\begin{aligned}
 \bar{U}_p^k &= \sqrt{\bar{P}^{k,T} \bar{P}^k} \rightarrow \sqrt{\hat{P}^T \hat{P}} = \hat{U}_p \\
 &\text{in } L^r(\Omega, \text{SL}(3, \mathbb{R}))
 \end{aligned} \quad (31)$$



because the map  $\mathbb{M}^{3 \times 3} \mapsto \text{PSym}(3)$ ,  $X \mapsto \sqrt{X^T X}$  is continuous and has linear growth.

Since the total energy is convex in the extended set of variables  $(\bar{U}, \bar{U}_p, \bar{\mathfrak{R}}_p, \nabla \bar{\alpha}_p)$  and continuous w.r.t.  $\bar{\alpha}_p$ , and the external potential  $\Pi$  is continuous w.r.t. strong convergence in  $L^1(\Omega)$  on account of (18), we get

$$\begin{aligned} I(\hat{\varphi}, \hat{P}, \hat{\alpha}_p) &= \int_{\Omega} W_{\text{mp}}(\hat{U}) + W_{\text{foam}}(\hat{U}_p, \hat{\alpha}_p) \\ &\quad + W_{\text{curv}}(\hat{\mathfrak{R}}_p, \nabla \hat{\alpha}_p) \, dV - \Pi(\hat{\varphi}, \hat{P}) \\ &\leq \liminf_{k \rightarrow \infty} \int_{\Omega} W_{\text{mp}}(\bar{U}_k) + W_{\text{foam}}(\bar{U}_p^k) \\ &\quad + W_{\text{curv}}(\bar{\mathfrak{R}}_{p,k}, \nabla \bar{\alpha}_p^k) \, dV - \Pi(\varphi_k, P_k) \\ &= \lim_{k \rightarrow \infty} I(\varphi^k, \bar{P}^k, \bar{\alpha}_p^k) \\ &= \inf \{ I(\varphi, \bar{P}, \bar{\alpha}_p) \mid \varphi \in L^1(\Omega, \mathbb{R}^3), \\ &\quad \bar{P} \in L^1(\Omega, \text{SL}(3, \mathbb{R})), \bar{\alpha}_p \in L^1(\Omega, \mathbb{R}) \} \end{aligned} \quad (32)$$

which implies that the limit triple  $(\hat{\varphi}, \hat{P}, \hat{\alpha}_p)$  is a minimizer. Note that the limit

microdeformations  $P = e^{\frac{\bar{\alpha}_p}{3}} \bar{R}_p \bar{U}_p$  may fail to be continuous, if  $p \leq 2$  (nonexistence or limit case of Sobolev embedding). Moreover, uniqueness cannot be ascertained, since  $\text{SL}(3, \mathbb{R})$  is a nonlinear manifold (and the considered problem is indeed highly nonlinear), such that convex combinations in  $\text{SL}(3, \mathbb{R})$  may leave  $\text{SL}(3, \mathbb{R})$ . Since the functional  $I$  is differentiable, the minimizing pair is a stationary point and therefore a solution of the corresponding field equations. Note again that the limit microdeformations may fail to be continuously distributed in space. That under these unfavorable circumstances a minimizing solution may nevertheless be found is entirely due to  $\mu_c > 0$  and  $p > 1$ . The proof simplifies considerably in the geometrically exact Cosserat micropolar case  $\bar{P} \in \text{SO}(3, \mathbb{R})$ , in which case  $p \geq 1$  is already sufficient, c.f. [39].

We continue with the supercritical case which is more appropriate for macroscopic situations and closer to classical elasticity [23].

**Theorem 3. (Existence for Elastic Micromorphic Model: Case 2).** *Let  $\Omega \subset \mathbb{R}^3$*

*be a bounded Lipschitz domain and assume for the boundary data  $g_d \in H^1(\Omega, \mathbb{R}^3)$  and  $P_d \in W^{1,1+p+q}(\Omega, \text{SL}(3, \mathbb{R}))$ . Moreover, let the applied external potentials satisfy (18). Then (13) with material constants conforming to case 2 admits at least one minimizing solution triple  $(\varphi, \bar{P}, \bar{\alpha}_p) \in H^1(\Omega, \mathbb{R}^3) \times W^{1,1+p+q}(\Omega, \text{SL}(3, \mathbb{R})) \times W^{1,2+p}(\Omega, \mathbb{R})$ .*

**Proof.** We repeat the arguments of case 1. However, the boundedness of infimizing sequences is not immediately clear. Boundedness of the microdeformations  $\bar{P}^k$  holds true in the space  $W^{1,1+p+q}(\Omega, \text{SL}(3, \mathbb{R}))$  with  $1+p+q > N = 3$ ; hence, we may extract a subsequence, not relabeled, such that  $\bar{P}^k$  converges strongly to  $\hat{P} \in C^0(\bar{\Omega}, \text{SL}(3, \mathbb{R}))$  in the topology of  $C^0(\bar{\Omega}, \text{SL}(3, \mathbb{R}))$  on account of the Sobolev-embedding theorem. Since

$P^{-1,k} = e^{-\frac{\bar{\alpha}_p^k}{3}} \bar{P}^{-1,k}$ , we obtain as well that

$$P^{-1,k} \rightarrow \hat{P}^{-1} \in C^0(\bar{\Omega}, \text{GL}^+(3, \mathbb{R})) \quad (33)$$

on account of strong convergence of  $\bar{\alpha}_p^k$ .

Along such strongly convergent sequence of microdeformations, the sequence of deformations  $\varphi^k$  is also bounded in  $H^1(\Omega, \mathbb{R}^3)$ . However, this is not due to a basically simple estimate as in case 1, but only true after integration over the domain: at face value, we only control certain mixed symmetric expressions in the deformation gradient. Let us define  $u_k \in H^{1,2}(\Omega, \mathbb{R}^3)$  by  $\varphi^k = g_d + (\varphi^k - g_d) = g_d + u_k$ . We then prove the inequality [23]

$$\begin{aligned} \infty &> I(g_d, \bar{P}_d, \bar{\alpha}_{p,d}) > \int_{\Omega} W_{\text{mp}}(\bar{U}_k) + W_{\text{foam}}(\bar{U}_p^k, \bar{\alpha}_p^k) \\ &\quad + W_{\text{curv}}(\bar{\mathfrak{R}}_{p,k}, \nabla \bar{\alpha}_p^k) \, dV - \Pi(\varphi_k, P^k) \\ &\geq \left( \frac{\mu_c}{8} c_K - C_2 \left\| \hat{P}^{-1} - P^{-1,k} \right\|_{\infty} \right) \|u_k\|_{H^{1,2}(\Omega)}^2 - C \end{aligned} \quad (34)$$

where we applied the extended Korn's inequality Theorem 1 yielding the positive constant  $c_K$  for the continuous microdeformation  $\hat{P}^{-1}$ .



Since  $\|\hat{P}^{-1} - P^{-1,k}\|_{\infty} \rightarrow 0$  for  $k \rightarrow \infty$  due to (33), we are able to conclude the boundedness of  $u_k$  in  $H^1(\Omega)$ . Hence,  $\varphi_k$  is bounded in  $H^1(\Omega)$ . Now we obtain that  $\bar{U}_k \rightharpoonup \bar{U} = \hat{P}^{-1} \nabla \hat{\varphi}$  by construction with the notations as in case 1. The remainder proceeds as in case 1. This finishes the argument. The limit microdeformations  $\hat{P}$  are indeed found to be continuous.

We mention that both existence results can be easily adapted to cover the micromorphic micro-incompressible case  $\bar{\alpha}_p \equiv 1$ .

## Conclusions

The presented variational micromorphic problem fits neatly into the framework of the direct methods of the calculus of variations. The coercivity part for the deformation is, however, nontrivial, and for the (uncommon) value of the Cosserat couple modulus  $\mu_c = 0$ , additional difficulties arise which can only be circumvented by the use of the generalized Korn's first inequality. In both cases 1 and 2, more realistic assumptions on the applied external loads  $\Pi$  are necessary to establish a lower bound for the energy  $I$  and a control of the curvature independent of the magnitude of deformation.

Altogether, the quasistatic finite micromorphic theory is established on firm mathematical grounds. With the same methods, the geometrically exact microstretch case (restricted manifold  $\mathbb{R}^+ \cdot \text{SO}(3, \mathbb{R})$ ) can also be treated.

An extension of the method to other choices of strain and curvature measures is possible. A related method has been employed for the treatment of nonlinear Cosserat shell models in [25]. Thermal stress problems for Cosserat shells have been investigated in [2]. The open case (case 3) allows for discontinuous macroscopic deformations and might therefore be a model problem allowing to describe fracture. The presented variational framework is ideally suited for subsequent numerical treatment by the finite element method.

## References

1. Appell J, Zabrejko P (1990) Nonlinear superposition operators, vol 95, Cambridge tracts in mathematics. Cambridge University Press, Cambridge
2. Bîrsan M (2009) Thermal stresses in cylindrical Cosserat elastic shells. *Eur J Mech A/Solid* 28:94–101
3. Capriz G (1989) Continua with microstructure. Springer, Heidelberg
4. Chen Y, Lee JD (2003) Connecting molecular dynamics to micromorphic theory. I: Instantaneous and averaged mechanical variables. II: Balance laws. *Physica A* 322:359–376, 376–392
5. Cosserat E, Cosserat F (1909) Théorie des corps déformables. (trans: Hermann A et Fils, Paris, Theory of deformable bodies, NASA TT F-11 561, 1968)
6. Duvaut G (1970) Élasticité linéaire avec couples de contraintes: théorèmes d'existence. *J Mec Paris* 9:325–333
7. Eringen AC (1999) Microcontinuum field theories. Springer, Heidelberg
8. Gurtin ME, Podio-Guidugli P (1992) On the formulation of mechanical balance laws for structured continua. *Z Angew Math Phys* 43:181–190
9. Hlavacek I, Hlavacek M (1969) On the existence and uniqueness of solutions and some variational principles in linear theories of elasticity with couple-stresses. I: Cosserat continuum. II: Mindlin's elasticity with micro-structure and the first strain gradient. *J Appl Mat* 14:387–426
10. Ieşan D (1971) Existence theorems in micropolar elastostatics. *Int J Eng Sci* 9:59–78
11. Ieşan D (2002) On the micromorphic thermoelasticity. *Int J Eng Sci* 40:549–568
12. Ieşan D, Pompei A (1995) On the equilibrium theory of microstretch elastic solids. *Int J Eng Sci* 33:399–410
13. Ieşan D, Quintanilla R (1994) Existence and continuous dependence results in the theory of microstretch elastic bodies. *Int J Eng Sci* 32:991–1001
14. Jeong J, Neff P (2010) Existence, uniqueness and stability in linear Cosserat elasticity for weakest curvature conditions. *Math Mech Solid* 15:78–95
15. Jeong J, Ramezani H, Münch I, Neff P (2009) A numerical study for linear isotropic Cosserat elasticity with conformally invariant curvature. *ZAMM* 89:552–569
16. Klawonn A, Neff P, Rheinbach O, Vanis S (2010) Solving geometrically exact micromorphic elasticity with a staggered algorithm. *GAMM-Mitteilungen* 33:57–72
17. Klawonn A, Neff P, Rheinbach O, Vanis S (2011) FETI-DP domain decomposition methods for elasticity with structural changes:  $P$ -elasticity. *ESAIM: Math Mod Num Anal* 45:563–602
18. Mariano PM, Modica G (2009) Ground states in complex bodies. *ESAIM: Control, Optim Calc Var* 15:377–402

19. Mariano PM, Stazi FL (2005) Computational aspects of the mechanics of complex materials. *Arch Comput Meth Eng* 12:392–478
20. Maugin GA (1998) On the structure of the theory of polar elasticity. *Philos Trans R Soc Lond A* 356:1367–1395
21. Neff P (2002) On Korn's first inequality with nonconstant coefficients. *Proc R Soc Edinb* 132A:221–243
22. Neff P (2005) On material constants for micromorphic continua. In: Wang Y, Hutter K (eds) *Trends in applications of mathematics to mechanics*. STAMM Proceedings (Seeheim 2004), Shaker Verlag, Aachen, pp 337–348
23. Neff P (2006) Existence of minimizers for a finite-strain micromorphic elastic solid. *Proc R Soc Edinb* 136A:997–1012
24. Neff P (2006) The Cosserat couple modulus for continuous solids is zero viz the linearized Cauchy-stress tensor is symmetric. *ZAMM* 86:892–912
25. Neff P (2007) A geometrically exact planar Cosserat shell-model with microstructure: existence of minimizers for zero Cosserat couple modulus. *Math Models Methods Appl Sci* 17:363–392
26. Neff P, Chelminski K (2005) Infinitesimal elastic-plastic Cosserat micropolar theory: modelling and global existence in the rate independent case. *Proc R Soc Edinb* 135A:1017–1039
27. Neff P, Chelminski K (2007) Well-posedness of dynamic Cosserat plasticity. *Appl Math Optim* 56:19–35
28. Neff P, Fischle A, Münch I (2008) Symmetric Cauchy-stresses do not imply symmetric Biot-strains in weak formulations of isotropic hyperelasticity with rotational degrees of freedom. *Acta Mech* 197:19–30
29. Neff P, Forest S (2007) A geometrically exact micromorphic model for elastic metallic foams accounting for affine microstructure: modelling, existence of minimizers, identification of moduli and computational results. *J Elast* 87:239–276
30. Neff P, Jeong J (2009) A new paradigm: the linear isotropic Cosserat model with conformally invariant curvature energy. *ZAMM* 89:107–122
31. Neff P, Jeong J, Fischle A (2010) Stable identification of linear isotropic Cosserat parameters: bounded stiffness in bending and torsion implies conformal invariance of curvature. *Acta Mech* 211:237–249
32. Neff P, Jeong J, Münch I, Ramezani H (2009) Mean field modeling of isotropic random Cauchy elasticity versus microstretch elasticity. *ZAMP* 3:479–497
33. Neff P, Jeong J, Ramezani H (2009) Subgrid interaction and micro-randomness – novel invariance requirements in infinitesimal gradient elasticity. *Int J Solid Struct* 46:4261–4276
34. Neff P, Münch I (2008) Curl bounds grad on  $SO_{(3)}$ . *ESAIM: Control, Optim Calc Var* 14:148–159
35. Neff P, Pauly D, Witsch KJ (2011) A canonical extension of Korn's first inequality to  $H(\text{Curl})$  motivated by gradient plasticity with plastic spin. *C R Acad Sci Paris, Ser I*, doi:10.1016/j.crma.2011.10.003
36. Neff P, Pauly D, Witsch KJ (2012) Maxwell meets Korn: a new coercive inequality for tensor fields in  $\mathbb{R}^{N \times N}$  with square integrable exterior derivative. *Math Meth Appl Sci* 35:65–71
37. Nowacki W (1986) *Theory of asymmetric elasticity*. Pergamon Press, Oxford
38. Pompe W (2003) Korn's first inequality with variable coefficients and its generalizations. *Comment Math Univ Carolinae* 44:57–70
39. Tambaca J, Velicic I (2010) Existence theorem for nonlinear micropolar elasticity. *ESAIM: Control, Optim Calc Var* 16:92–110
40. Tambaca J, Velicic I (2010) Semicontinuity theorem in the micropolar elasticity. *ESAIM: Control, Optim Calc Var* 16:337–355

## Existence Theorems

► [Large Existence of Solutions in Thermoelasticity Theory of Steady Vibrations](#)

## Experimental Analysis of Hot Spotting in Sliding Systems

P. Dufrénoy<sup>1</sup> and Dieter Weichert<sup>2</sup>

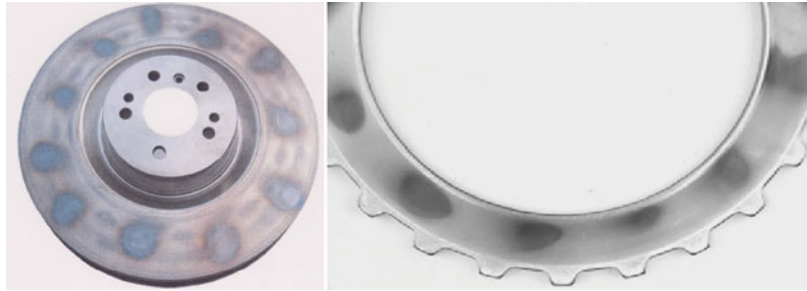
<sup>1</sup>Laboratoire de Mécanique de Lille, Université de Lille Nord, Lille, France

<sup>2</sup>Institute for General Mechanics, RWTH Aachen University, Aachen, Germany

## Overview

Systems including components with relative sliding, like clutches, brakes, hot forming tools, induce heating due to conversion of mechanical to thermal energy. The corresponding heating is a major design parameter as it influences the tribological and mechanical performances (wear of the materials, friction performances, risks of cracks, vibrations, etc.). Various types of thermal localizations may appear, usually named as hot spots, which could lead to very high local temperatures. The difficulty of understanding and modeling all of these phenomena still remains

**Experimental Analysis of Hot Spotting in Sliding Systems, Fig. 1** Dark marks of material phase transformation on hot spots for disk brake and clutch [1, 2]



due to the complex interactions of thermal, mechanical, and tribological effects. Experimental investigation is still nowadays a major instrument for detecting and understanding the physical effects.

In this entry, we propose to consider a spectacular example of frictional system leading to various types of hot spotting: the disk braking system. It is proposed to illustrate various experimental results of thermal measurements. The difficulty of obtaining accurate temperature measurements during friction, at the surface, is firstly described. Then the various types of hot spots that could be observed on this system are illustrated. It is also shown that hot spotting has to be considered as a transient phenomenon with variations in space and time. This result is of major importance in the understanding of the coupling with the mechanical and tribological aspects. Finally, some influencing parameters on hot spotting are illustrated.

## Introduction

A major problem in the design of frictional organs like brakes and clutches is to understand the complex thermomechanical effects occurring in these elements due to conversion of mechanical to thermal energy. Their amounts can be, for instance, in high speed train brakes, very high leading locally even to temperatures close to fusion. May be more important, the gradients of temperature can be very large, leading to high stresses and strains which can induce important inelastic effects. All this has to be considered in

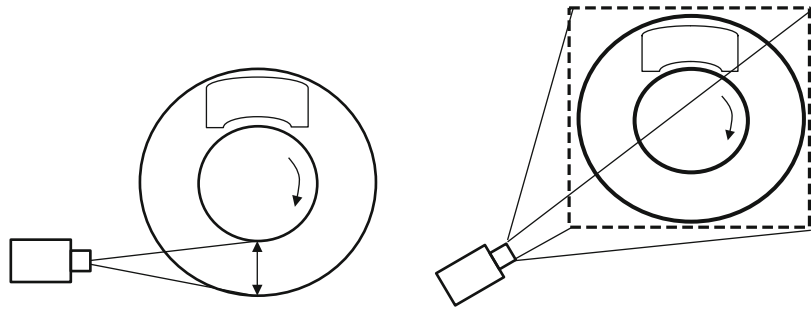
a framework of transient processes, depending upon geometry, material properties, loading history, and boundary conditions.

Although modeling of such processes has had a tremendous progress over the last decades, we are far away of anticipating all important effects by numerical simulation and experimental investigation remains a major instrument for detecting and understanding physical effects.

Here, in particular, the phenomenon of so-called hot spots is analyzed: Due to inhomogeneous contact conditions, thermal dissipation in frictional elements is not always uniform. This leads to more or less regularly distributed areas with elevated temperature, called “hot spots.” They consequently correspond to various thermal gradients on the rubbing surface. In case of high energy dissipation and because of the effective reduced heat flux areas, high local temperatures occur, leading to unacceptable friction performances such as *fading*, *cracking*, or undesirable low frequency vibrations called “hot judder.” *Fading* is due to friction material transformation at high temperature degrading tribological properties. *Cracking* is early failure of the disk, corresponding to thermal low cycle fatigue induced by a cycling of tensile and compressive stresses with plastic strain variations due to repeated heating and cooling [1–3]. *Judder* is a low frequency vibration due to the nonuniform disk distortion linked with the nonuniform temperature [4]. Figure 1 shows hot spots on a braking disk and clutch. Dark marks correspond to metallurgical transformations on hot spots when the material is heated above the austenitic phase level followed by a rapid cooling. We observe the

### Experimental Analysis of Hot Spotting in Sliding Systems,

**Fig. 2** Illustration of radiative measurements at the surface of a rotating object (brake disk): scanning mode (one detector) or snap-shot mode (full frame of detectors)



periodic distribution of hot spots which indicates the interaction between structural, geometrical, and local thermal effects.

Measuring thermal localizations during friction is still a challenge. As the contact is closed, measurements at the friction surface are not directly possible.

In this entry, we propose first to consider the difficulty of thermal measurements at the contact surface. Then, examples of measurements on brake disks illustrate the various types of hot spots that can be observed. Some improved analyses are finally discussed considering the evolution of hot spotting and some influencing parameters on their appearance.

### Thermal Measurements in Frictional Contact

Experimental observations of hot spots have been reported in many practical applications, particularly in automotive, railway, and aircraft brakes [3–5]. Anderson and Knapp first proposed a classification of hot spots in automotive brake systems [3]. From experimental investigations on the rubbing surface of railway brake disks on a testing bench, Dufrénoy et al. have given a similar classification which takes into account the specific difference between automotive and railway brakes [4]. These classifications are based on thermal measurements which are usually done by infrared thermography. The principle of this noncontact thermal measurement technique is to measure the radiative heat flux of a surface with photoelectric detectors.

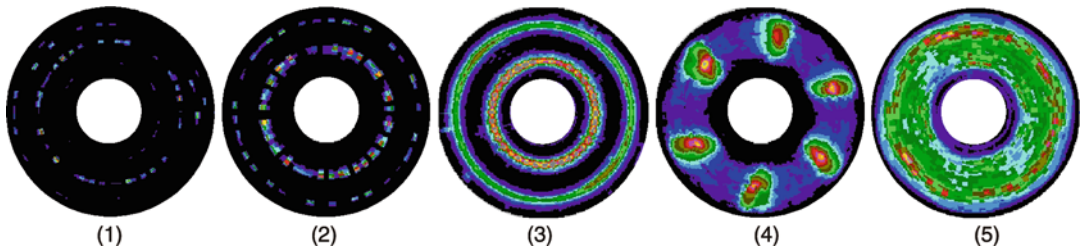
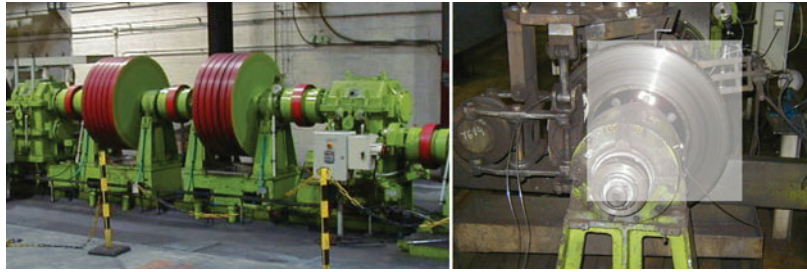
Two means may be used: one detector scanning a straight line radially (scanning mode) or a focal plane area of multiple detectors (snap-shot mode). These detectors measure the number of photons radiated by the observed surface. Thanks to the Boltzmann relation, this radiative flux is related with the temperature with the following relation:

$$q = \sigma S \varepsilon T^4$$

with  $q$  the radiative heat flux,  $\sigma$  the Stefan-Boltzmann constant,  $S$  the surface of radiation (here the disk friction surface),  $\varepsilon$  the emissivity of the surface ( $0 \leq \varepsilon \leq 1$ ), and  $T$  the absolute temperature of the surface. Once the infrared camera is calibrated, assuming a black body ( $\varepsilon \approx 1$ ) media, the relation between the radiative heat flux and the temperature can be established (Fig. 2).

More precise quantitative measurements require knowing the real emissivity of the surface which is a major problem as it varies with the surface topography which changes with friction. Usually, the emissivity is assumed to be uniform and constant which is not sufficient for quantitative temperature measurement. Recent developments are focused on this issue of dual unknowns, temperature and emissivity, trying to measure these two parameters simultaneously. Such investigations use the bicolor principle of two measurements with two infrared sensors or cameras set on two close wavelengths. Assuming that the emissivity is the same on the two wavelengths, the two unknown data  $T$  and  $\varepsilon$  may be obtained simultaneously. First results applied on

**Experimental Analysis of Hot Spotting in Sliding Systems, Fig. 3** Example of experimental apparatus for braking disk thermal analysis for railway applications. The clear windows correspond to the measuring windows of an IR camera in snap-shot mode [7]



**Experimental Analysis of Hot Spotting in Sliding Systems, Fig. 4** Classification of hot spotting in railway disks illustrated by thermographs [4]

brake disks and using a point-shaped specific bicolor pyrometer are discussed in [6]. It shows that the emissivity may reach high values, close to 1, outside the contact area and decreases significantly during friction. This improved measurement illustrates the difficulty of infrared measurements, which generally consider a uniform and constant emissivity that underestimate the real temperatures. However, if looking only at the thermal localizations, the temperature distribution assuming an emissivity equal to 1 is generally used for qualitative indications of thermal gradients. Other types of thermal measurements can be done with classical thermocouples inserted in the materials, but they give only local temperatures and not at the surface. As the contact is closed, direct measurements are not possible and surface temperatures are generally extrapolated from two measurements: at the surface, outside the contact, by infrared thermograph and/or in depth by inserted thermocouples.

### Hot Spot Observation and Classification

An example of experimental apparatus for the analysis of brake disks is shown in Fig. 3 [7].

A typical rotating test bench is used. The energy to dissipate is provided to the brake disk by mechanical inertia and electric engine. In addition to classical rotation speed and torque measurements, an infrared camera is located in front of the disk. Apart from surface disk measurements, thermocouples can be inserted in the disk and in the friction pad, giving local information of temperature in the materials. In the present case, the disk is made of 28CrMoV5-08 steel manufactured by a forging process. The inner and outer diameters are respectively 380 and 640 mm with a thickness of 45 mm without internal ventilation (full disk). Friction pads are made of sintered material of organic resin-bounded composite respectively for high and limited energy applications.

Figure 4 shows the various types of hot spots that can be observed when measuring temperatures in scanning mode (one IR detector scanning along the radius of the disk at high speed during rotation). Thermographs are carried out on a line under a fixed angular position of the disk. Acquisition of the angular velocity is done simultaneously from the testing bench. The conversion of the data to polar coordinates reconstitutes an image of the disk for each revolution.



**Experimental Analysis of Hot Spotting in Sliding Systems, Table 1** Railway disk hot spots classification [4]

Type	Width (mm)	Temperature	Duration
1. Asperity	<1	1,200 °C peak	<1 ms
2. Gradients on hot bands or focal hot spots	5–20	650–1,000 °C	0.5–10 s
3. Hot bands	5–50	800 °C	>10 s
4. Macroscopic hot spots	40–110	1,100 °C peak	>10 s
5. Regional hot spots	80–200	20–300 °C	>10 s

These experimental results illustrate the classification proposed in Table 1 [4].

- Asperity type corresponds to rapid temperature rising briefly on very small areas of the rubbing surface. They result from discrete asperity contacts.
- Gradients on hot bands correspond to small contact sites which appear along a single rubbing path.
- Hot bands appear as reduced contact friction areas of the pad in the radial direction. It is seen on the disk as narrow rings of high temperatures in the direction of sliding. They can move along the radial direction during braking, according to the evolution of the bearing surface.
- Macroscopic hot spots (MHSs) are large thermal gradients regularly distributed on the disk surface. They are fixed on the disk and appear as a kind of buckling pattern of the disk. This phenomenon reduces drastically the contact surface area with high local temperatures.
- Regional hot spots are low thermal gradients on the whole surface of the disk, due to inhomogeneous cooling. Such distributions appear at the end of braking due to thermal diffusion.

This classification slightly differs from the automotive one proposed by Anderson and Knapp [1]. This is due to the differences in disk size, geometry, energy dissipation, and braking duration. As noticed by Anderson and Knapp, some metallurgic transformations may occur, especially martensite formation at hot spot site.

Martensite is due to high temperature above the austenitic phase level followed by a rapid cooling and may produce severe local strains due to the associated increase of specific volume. Cracks at the periphery of hot spot sites may initiate during cooling after the martensite formation.

The most critical hot spots correspond to type 2, 3, and 4. Type 1 corresponds to short times and type 5 to a conventional heat diffusion that should normally appear when hot spotting is reduced.

It is now well known that “hot bands” (type 3) are linked to reduced contact area of the pad depending on pad design, thermal dilatations, and also wear of the friction material. Some models have been developed in the literature that shows good agreement with experiments when introducing these phenomena [8–10]. “Macroscopic hot spots” (type 4) correspond to a global distortion of the disk with a waviness shape, as it will be showed further. Some authors have shown that this waviness deformation is progressive when the disk is submitted to high energy dissipation [11]. “Gradients on hot band” or “focal hot spots” (type 2) are supposed to be associated to frictionally excited thermoelastic instabilities (TEIs) [12].

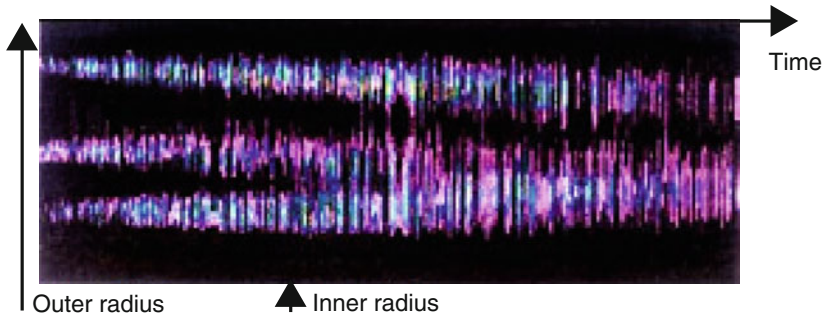
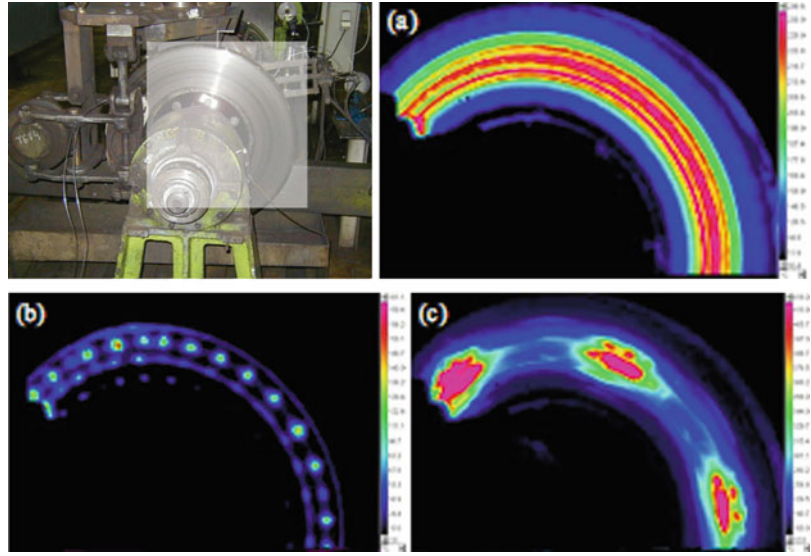
The exact conditions of appearance of these localizations are still debated. It is not discussed here and readers could refer to the proposed references, but it shows the great importance of getting experimental data of thermal heating.

## Hot Spots Development: A Transient Process

Hot spots development has to be seen as a progressive phenomenon linked to the rise of temperature that influences the thermomechanical deformations. It is linked to the geometry of the brake and to the amount of dissipated energy and corresponds to a sequential logic. In order to study this logic, some works have been done focusing on the hot spots development when increasing the dissipated energy [1, 7]. An example of detailed analyses has been done on a non-ventilated disk brake used for the TGV high speed train [7]. For low energy dissipation, hot

### Experimental Analysis of Hot Spotting in Sliding Systems,

**Fig. 5** Illustration of the “classic” sequence of hot spots formation (thermograms are obtained by a focal plane IR camera in snap-shot mode)



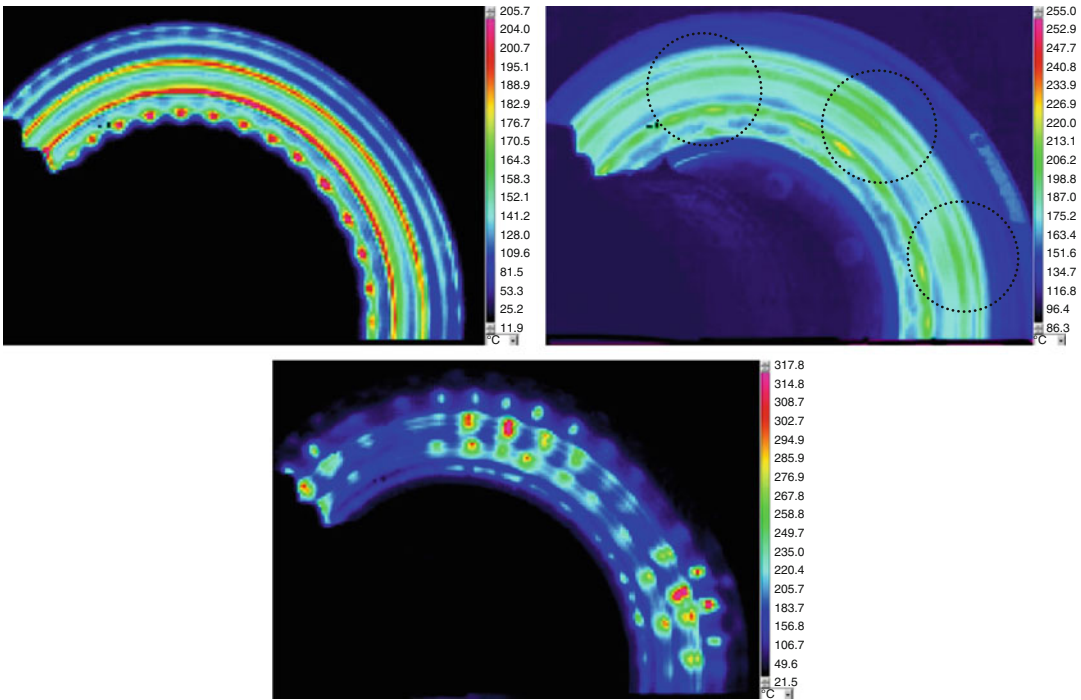
**Experimental Analysis of Hot Spotting in Sliding Systems, Fig. 6** Illustration of hot band radial migration (IR measurement in scanning mode along the radius of the disk) [13]

spotting is generally limited to “hot banding.” If the energy increases, hot spot development may differ for various tested coupled disk pads. However, among all observed scripts, one of them is more frequently observed, qualified as “classic,” appearing for high energetic braking. After the hot band formation on the surface of the disk (Fig. 5a), which is relatively uniform in the angular direction and is able to move along the radius of the disk, small thermal gradients on hot bands can appear. Their angular disposition is very regular and fixed on the disk. They correspond to “gradients on hot bands” or “focal hot spots” (Fig. 5b). Next, if energy is high, “macroscopic hot spots” (MHSs) appear on the surface, also very regularly distributed (Fig. 5c). They are

fixed on the disk and are qualified as “stationary.” An important point is that the MHS generally remains on the disk as far as they are formed. It corresponds to an out-of-plane pattern which becomes persistent due to plastic flow of the material.

Some variations of the classical MHS evolution script may be observed. It illustrates the difficulty of determining the thermal loading as it varies with time and is never perfectly stationary on the surface.

- Radial displacement of hot bands is often observed. It can be illustrated when following the radial thermal distribution as shown in Fig. 6 [13]. The measurements are recording in scanning mode along the radius of the disk



**Experimental Analysis of Hot Spotting in Sliding Systems, Fig. 7** Three example of simultaneous combination of hot spots

and are presented along the braking duration. The figure shows that the hot bands migrate along the braking with possible merging.

- “Focal hot spots” and “hot bands” may appear simultaneously on the disk (Fig. 7 on the left).
- “Macroscopic hot spots” occurrence does not occult systematically the other hot spots. So, MHS may be observed with “hot bands” (Fig. 7 in the middle), for low energy braking while MHS already existed; “gradients on hot bands” may also be simultaneously observed with MHS (Fig. 7 on the right). In this case, “gradients on hot bands” existed before the appearance of the MHS.

### Macroscopic Hot Spots

*Waviness shape:* MHSs have to be considered in detail, as they are considered as the most damaging for the disk. They occur generally for high braking power and high velocity but also for lighter braking applications. Practically, a

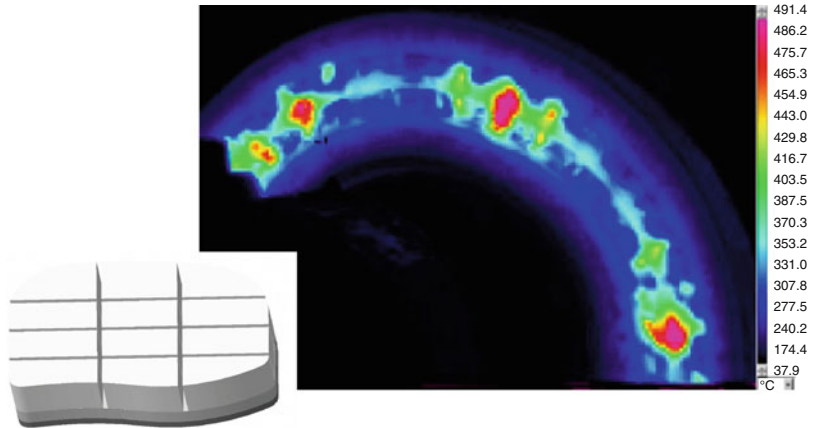
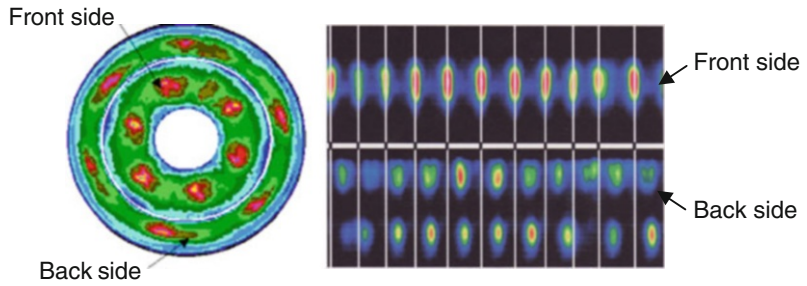
reduced number of MHS per side is commonly observed. Various analyses, with simultaneous measurements on both faces of the disk, have shown that they are located alternatively on both sides of the disk (Fig. 8). This asymmetrical distribution indicates a waviness deformation pattern of the whole disk. Complementary analyses have shown that this pattern is generally definitively marked, due to plastic deformation, and hard to remove. However, successive measurements show that hot spots migrate in the angular direction. It is probably due to the dissymmetry of the contact with friction leading to a nonsymmetric heating of hot spot which is higher at the leading edge of the pad. Due to this asymmetric contact, plastic flow occurs modifying slowly the shape of the waviness deformation. This analysis is consistent with the direction of rotation of the MHS migration which is opposite to the direction of rotation of the disk.

*Number of hot spots:* The number of hot spots in the case of MHS is generally associated to the ratio of the disk mean perimeter to the pad contact



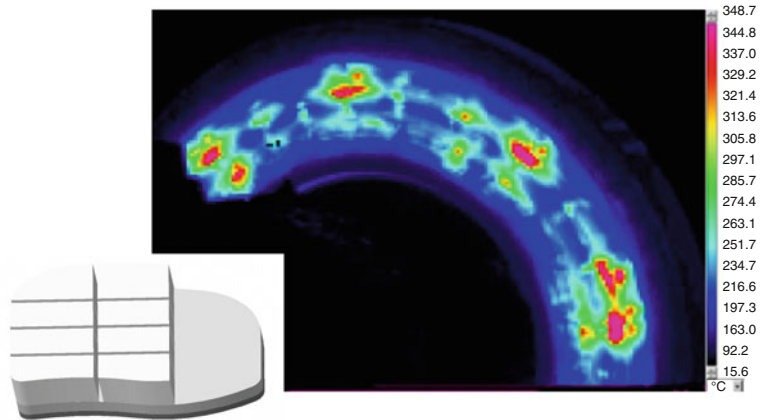
### Experimental Analysis of Hot Spotting in Sliding Systems,

**Fig. 8** Simultaneous thermographs of the two sides of the disk for railway [4] and automotive [1] applications



### Experimental Analysis of Hot Spotting in Sliding Systems,

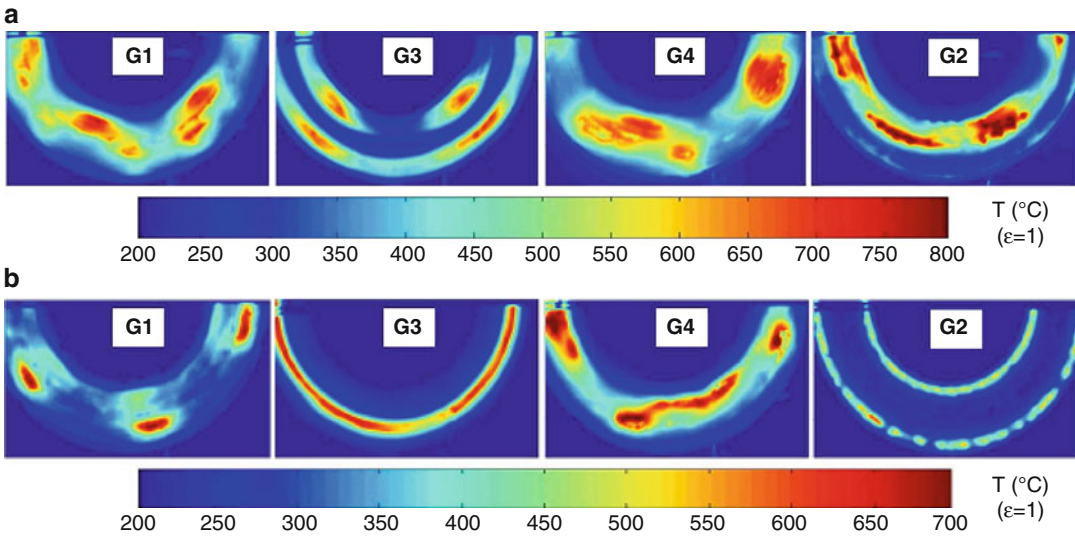
**Fig. 9** Thermographs of the disc surface for two pad lengths (covering 66 and 44 degrees on the disc) consistent with the number of hot spots (6 and 9 respectively), considering the anular ratio with the 360 degree perimeter of the disc [7]



length, as illustrated in Fig. 9 [7]. But, in some analyses, this correspondence is not strictly respected. However, one should consider the effective contact length that could be significantly reduced compared to the apparent one, due to thermal dilatations, nonuniform contact pressure, etc. It may lead to a higher number of hot spots than the strict ratio between the

mean perimeter of the disk and the apparent contact length.

*Influence of friction pad:* As previously described, MHS corresponds to the last stage of disk deformation, when the dissipated energy is high. Consequently, their appearance is linked to the rigidity of the disk, to its geometry, and to the fastening device.



**Experimental Analysis of Hot Spotting in Sliding Systems, Fig. 10** IR thermographs of separated railway TGV brake disks equipped with different pads, at the time of maximal temperature for a Stop-Braking (a) from 300

to 0 km.h<sup>-1</sup> with a dissipated energy of 13.9 MJ (b) for a Stop-Braking from 270 to 0 km.h<sup>-1</sup> with a dissipated energy of 11.2 MJ

Following this reasoning, the pad type should normally have less influence. Such result is illustrated in Fig. 10a showing IR thermographs for four separated disks equipped with different pads G1 to G4 (the pads differ in terms of rigidity) and for a high energy braking. For each pad type MHS occurs, with less or more variations in terms of shape and gradient.

Figure 10b shows similar observations but for another braking with lower energy and lower deceleration. It shows that even if the disk is already deformed by previous braking with a waviness shape, the MHS could be less or more intense giving various thermal gradient types. It shows that for such braking, the pad may significantly influence the thermal loading. As this loading is strongly linked with the thermomechanical solicitation (thermal stresses), it may influence the risk of damage.

## Conclusion

Frictional organs with high energy dissipation as brakes or clutches may induce nonuniform heated

areas usually called hot spots. Hot spotting has a major influence on the wear of materials, on friction performances, and also on the risk of vibrations and damage.

It has been shown that the evolution of the various types of hot spots that occur in brake disks is highly complex. Some classifications of these thermal gradients have been proposed illustrating this complexity. A main result is that hot spotting has to be considered as a transient phenomenon with variations of the heating surface and possible evolutions of hot spots types during time. It has been shown that a kind of logic exists in the mechanisms of hot spot appearance and evolution. This logic is consistent with the corresponding physical phenomena assumed to be involved in the thermal localizations. Indeed, even if several aspects of the origin of hot spots are still badly known, all of these observations are consistent with the assumed explanations of the three main types: “hot banding,” “focal hot spots,” and “macroscopic hot spots.”

Considering the evolution of these thermal gradients should improve the understanding of the associated consequences (wear, damage,

vibrations, etc.). In this way, the corresponding material modifications, metallurgical transformations for the disk, and physicochemical modification for the pad have also to be investigated and remain a future scientific challenge. In this way, quantitative data of temperatures are required and remain a difficulty due to the closed contact, the sliding velocity, and the evolution of the surfaces during friction. Some recent developments, using a bicolor technique and briefly presented here, show that quantitative measurements are possible.

The braking application is a wonderful example of hot spotting but such phenomena may also be seen in other applications. A lot of parameters have been identified influencing the appearance and hot spot type, which could be extended for other applications, taking into account their specificities.

## References

1. Sardá A, Haag M, Winner H, Semsch M (2008) Experimental investigation of hot spots and thermal judder. SAE Technical Paper 2008-01-2544. doi:10.4271/2008-01-2544
2. Yi Y, Barber JR, Zagrodzki P (2000) Eigenvalue solution of thermoelastic instability problems using Fourier reduction. Proc R Soc Lond Ser A A456:2799–2821
3. Anderson AE, Knapp RA (1990) Hot spotting in automotive friction systems. Wear 135:319–337
4. Dufrénoy P, Panier S, Weichert D (1998) A study on hot spotting in railway disc brakes. In: Proceedings of the European braking conference, 9–10 Dec 1998. GRRT, Lille, pp 245–257
5. Audebert N, Barber JR, Zagrodzki P (1998) Buckling of automatic transmission clutch plates due to thermoelastic/plastic residual stresses. J Therm Stress 21:309–326
6. Kasem H, Thevenet J, Boidin X, Siroux M, Dufrénoy P, Desmet B, Desplanques Y (2010) An emissivity-corrected method for the accurate radiometric measurement of transient surface temperatures during braking. Tribol Int 43:1823–1830
7. Panier S, Dufrénoy P, Weichert D (2004) An experimental investigation of hot spots in railway disc brakes. Wear 256(7–8):764–773
8. Kennedy FE, Ling FF (1974) A thermal, thermoelastic and wear simulation of a high-energy sliding contact problem. Trans ASME J Lubrication Tech 96:497–507
9. Day AJ, Newcomb TP (1995) The dissipation of frictional energy from the interface of an annular disc brake. Proc Inst Mech Eng 198:201–209
10. Dufrénoy P, Weichert D (1995) Prediction of railway disc brake temperatures taking into account the bearing surface variations into account. Proc Inst Mech Eng Pt F 209:67–76
11. Panier S, Dufrénoy P, Brunel J-F, Weichert D (2005) Progressive waviness distortion: a new approach of hot spotting in disc brakes. J Therm Stress 28(1):47–62
12. Lee K, Barber JR (1994) An experimental investigation of frictionally-excited instability in automotive disk brakes under a drag brake application. J Tribol 116:409–414
13. Dufrénoy P (2004) An hybrid 2D/3D model of the thermomechanical behaviour of a disc braking system. Proc Inst Mech Eng Pt F 218:17–30

---

## Experimental Determination of Material Time-Dependent Properties

Igor Emri, Joamin Gonzalez-Gutierrez,  
Marina Gergesova, Barbara V. Zupančič and  
Ivan Saprunov

Center for Experimental Mechanics, Faculty of  
Mechanical Engineering, University of  
Ljubljana, Ljubljana, Slovenia

## Overview

Many important materials, such as natural and synthetic polymers, can be considered as time-dependent materials, since their properties change with time and thus their functionality and applicability can change considerably after a certain period of time. The time dependency of materials is an inherent property of their structure, which further depends on the initial kinetics and applied thermomechanical boundary conditions. Therefore, material structure depends on its thermal properties, which are generally measured through differential scanning calorimetry. The mechanical properties of time-dependent materials depend on the mode of loading (static or dynamic) and the type of deformation (shear or bulk). All together, there are 21 material functions that describe the time-dependent behavior of materials, seven (7) of them are determined by static and fourteen (14) by dynamic methods of measurements. Material functions determined in

shear represent changes of specimen geometry, whereas the bulk material functions represent changes of its volume. Bulk material functions change with time very little, while the shear material functions show very distinctive time dependence. Time-dependent properties are experimentally determined in a segmental form at different temperatures and/or pressures, which can be then combined into master curves that provide a more complete description of the material behavior over a prolonged period of time. There are several methods of preparing master curves, such as the closed-form shifting algorithm.

This entry provides a brief overview on experimental approaches commonly used to determine the thermal and the time-dependent mechanical properties in shear and bulk of materials along with the numerical procedures for obtaining the unique master curve of the selected material function. Characterization of the frequency-dependent properties requires utilization of other experimental methods and/or approaches, which due to the space limitation are not discussed here.

## Introduction

It is a well-established fact that macroscopic properties of any material generally depend on its morphology. This can be vividly demonstrated by the example of *polymorphism phenomenon* – the ability of a substance to form structures with the same chemical composition, but different arrangements of atoms/molecules. Formation of a particular polymorph with its specific properties depends on the boundary (loading) conditions applied. This is particularly important when dealing with time-dependent materials such as polymers. The final structure of a solid polymer will depend on the material *morphological properties* that are affected either by *initial kinetics* and/or the thermomechanical boundary conditions to which it is exposed during the technological process. The material initial kinetics include molecular characteristics such as *topology of molecules* and *molecular mass distribution*,

while thermomechanical boundary conditions include temperature, pressure, and mechanical loading (or their combined effect) to which a time-dependent material is exposed during a technological process.

Regarding the importance of morphological characteristics that govern the macroscopic mechanical behavior of *time-dependent materials*, the beginning of this entry introduces the reader with the basics of the *differential scanning calorimetry (DSC)* as one of the methods that enable study of morphology through analysis of phase transitions related to topological arrangement of molecules.

The macroscopic mechanical behavior of many important materials, such as polymers, is characterized by their time-dependent mechanical properties. In practice, this means that the functionality and applicability of time-dependent materials can change considerably after a certain period of time. This may lead to the appearance of defects and loss of product functionality. It is therefore important to understand material functions that describe time dependence of their properties.

In the case of time-dependent materials, the linear stress-strain relations known from elasto- and plastomechanics are replaced by *convolution (Stieltjes) integrals*, whereas material constants (moduli) with *time-dependent material functions*. The form of material functions depends on the mode of loading, i.e., static (or time-dependent) and dynamic (or frequency-dependent).

There are two fundamental modes of deformation, *bulk deformation* (relating to the changes in size) and *shear deformation* (relating to the changes in shape), that must be considered to be independent of one another [1]. Since uniaxial deformation combines both change in size and shape, it cannot be considered fundamental. In respect to this, in the following sections of this entry, we are discussing theoretical background as well as experimental approaches for characterization of time-dependent properties regarding only fundamental deformational modes, i.e., shear and bulk.

In addition, this entry presents a numerical procedure for treatment of the measured data in

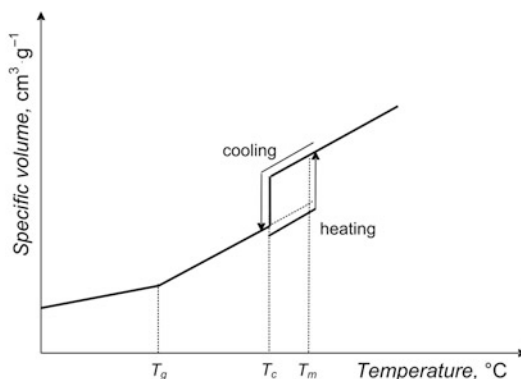
order to overcome the time limitation of the real experiment and to obtain long-term information on a given time-dependent property.

However, this entry does not discuss behavior of the time-dependent materials under dynamic mode of loading, which would yield frequency-dependent material characteristics. Frequency dependence can be either characterized by properly selected experimental techniques or by applying mathematical relations for interconversion between material functions [1].

## Thermal Properties

### Theoretical Background

The manner in which polymers react to thermal loading can be studied by *thermal analysis*. When polymers are melted, the melt is totally disordered, and during their solidification, three phases can be observed: the totally disordered phase or *amorphous phase*, partially ordered or *semicrystalline phase*, and the ordered or *crystalline phase*. In other words, if polymeric materials are exposed to thermal loads, they could undergo several *phase transitions*, depending on the magnitude and direction of load (heating or cooling). These transitions can be seen as changes in *specific volume* (Fig. 1) and include the *glass transition*, *crystallization*, and *melting*, all of which are linked to a temperature ( $T_g$ , *glass transition temperature*;  $T_c$ , *crystallization temperature*;  $T_m$ , *melting temperature*) or range of temperatures where particular transition takes place. Many theories for modeling the effect of thermodynamic parameters, such as temperature (or pressure), on the time-dependent behavior of polymers are based on the *free-volume* concept. This concept assumes that the change in properties depends on the distribution of inter- and intramolecular space (holes) in the material, often called *free volume*. In this way, the free volume represents the unoccupied intermolecular space available for molecular motion, while so-called *occupied volume* represents volume occupied by the molecules of the material.



**Experimental Determination of Material Time-Dependent Properties, Fig. 1** Phase transitions for a semicrystalline material

### Experimental Methodology

There exists several thermo-analytical techniques which include differential thermal analysis (DTA), thermogravimetric analysis (TGA), dynamic mechanical analysis (DMA), and dielectric thermal analysis (DEA), but in general, differential scanning calorimetry – DSC – is the most widely used technique for the determination of phase transitions [2].

DSC is a thermo-analytical technique in which the difference in heat flow rate between the sample and a reference sample is monitored against time while both samples are exposed to the same temperature program [3]. More precisely, it is a technique for determining the quantity of heat that is either absorbed or released by a substance undergoing a physical or a chemical change.

Heat absorption or release during any transition alters the *substance total energy*, which at constant pressure is characterized in terms of enthalpy,  $H$ . For practical applications, the change of enthalpy between two states,  $\delta H$ , is of interest:

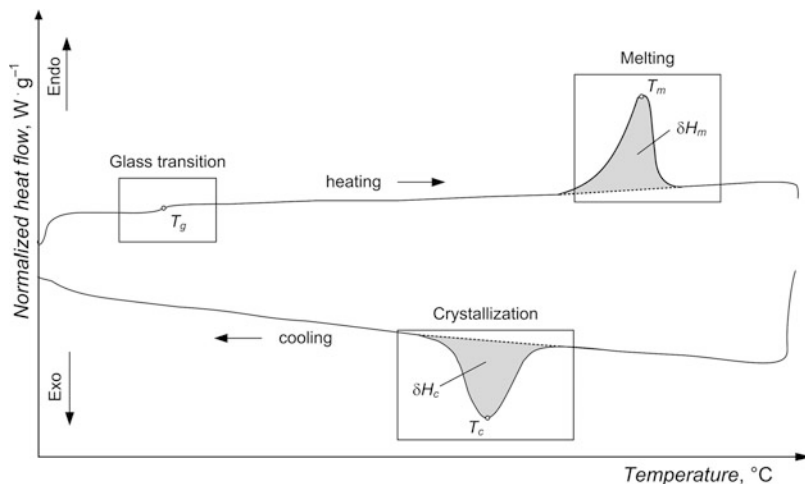
$$\delta H = \int c_p \cdot dT \quad (1)$$

where  $c_p$  is *specific heat capacity* and  $T$  is temperature.

Processes that increase enthalpy are said to be *endothermic* (glass transition, melting,



**Experimental Determination of Material Time-Dependent Properties, Fig. 2** Schematics of DSC curve of the heat flow as a function of temperature



evaporation), while those that lower it are called *exothermic* (crystallization, decomposition).

Direct measurements of  $c_p$ , involved in (1), are rather hard to perform; furthermore, elaborate equipment is needed. For this reason, an alternative approach for determination of  $\delta H$  is used. From the *first law of thermodynamics*, it can be explained that at constant pressure, the change in enthalpy of a system undergoing a transition is exactly equal to the heat absorbed or released. Therefore,  $c_p$  can be calculated by knowing the *heat flow*,  $\dot{Q}$ , *heating/cooling rate*,  $v_T$ , and sample mass,  $m$ , using the following equation:

$$c_p = \frac{\dot{Q}}{m \cdot v_T} \quad (2)$$

This ratio clearly shows that the heating (or cooling) rate,  $v_T$ , and the sample mass,  $m$ , are important factors that have a significant influence on the experimental results. Besides this, (2) also shows that the heat flow is proportional to the heat capacity. As a consequence, the glass transition temperature,  $T_g$ , can be determined directly from the former one by observing the change in slope of the heat flow against time or temperature curve (see “glass transition” region in Fig. 2). By increasing the temperature above  $T_g$  of partially crystalline materials, such as polymers, it is observed that crystals begin to fall apart and

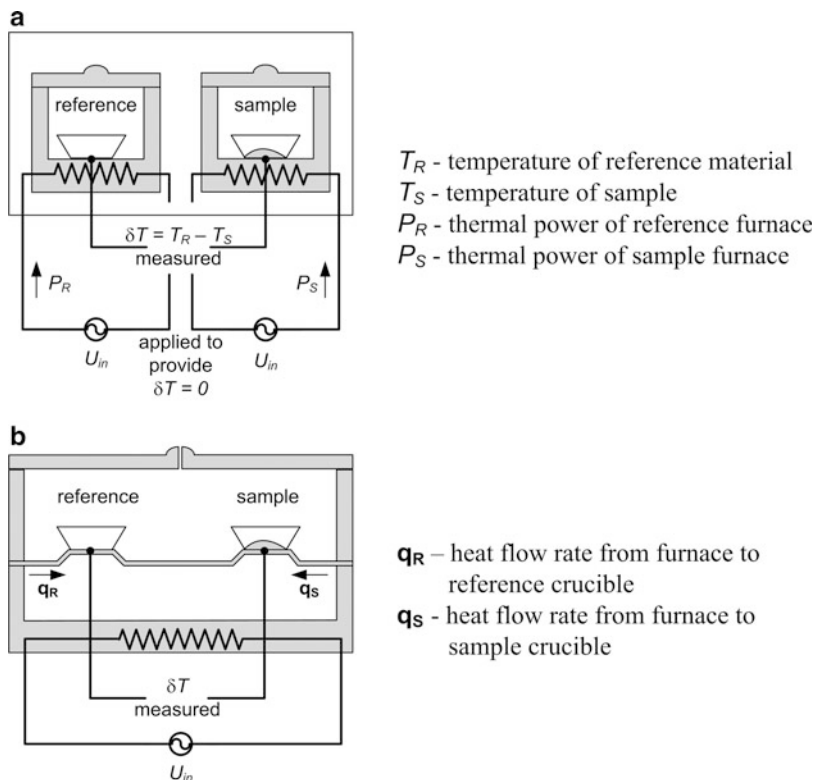
chains come out of their ordered arrangement in what it is called melting. This endothermic transition is represented by a peak in the heat flow, where the top of the peak is considered as the melting temperature,  $T_m$ , and from the area below such peak, the latent heat,  $\delta H_m$ , can be estimated (see “melting” region in Fig. 2). A similar approach is also valid for the crystallization, in this case considered as exothermic transition (see “crystallization” region in Fig. 2).

There exist several types of DSC apparatuses, and depending on their operating principles, most of them fall into one of the following categories: *power compensation* or *heat flux*.

The test chamber of a power-compensation DSC apparatus consists of two small, separate furnaces that are controlled independently by a defined primary heating program. Each of them contains their own temperature sensor and a heater (Fig. 3a). The furnaces are thermally decoupled. In one furnace, a pan with the sample is placed, in another, a pan with the reference sample. Generally, an empty pan identical to the one with the sample is used as a reference. A control circuit supplies the same heating power to both furnaces in order to change their mean temperature according to the preset temperature-time program. In the case of ideal thermal symmetry, the temperature of both furnaces is the same. When a sample reaction (exothermic or endothermic) occurs, the symmetry is

### Experimental Determination of Material Time-Dependent Properties,

**Fig. 3** (a) Principal scheme of a power-compensation DSC and (b) principal scheme of a heat-flux DSC



disturbed, which results in a temperature difference,  $\delta T$ , between the furnaces. This temperature difference is at the same time the measured signal and the input signal of a second proportional control circuit, which tries to compensate it by applying an additional heating power either to the sample or to the reference. When power is applied to the reference, it is “+” and when to the specimen is “-.” Ideally,  $\delta T = 0$  should be provided all the time. The difference in applied thermal power,  $\delta P$ , is equal to the change in heat flow,  $\delta \dot{Q}$ .

In a heat-flux DSC, the signal is derived from the temperature difference established when the sample and reference are heated in the same furnace. A defined exchange of the heat to be measured with the environment takes place via a well-defined heat conduction path with a given thermal resistance [4]. The temperature difference between sample and reference is measured with thermocouples arranged back to back (Fig. 3b). As with the power-compensation DSC, the sample and a reference material are

placed in individual crucibles [5]. When heat is applied by the furnace, it flows to the samples through a solid of known resistance. If the arrangement is symmetrical, the same heat flows into the sample and reference; thus, the change in temperature is equal to zero,  $\delta T = 0$ . If the equilibrium is disturbed by a phase transition of the sample, a differential signal is generated that is proportion between the heat flow rates to the sample and reference. The measured heat flux is linearly related to the measured  $\delta T$  by a calibration constant [4].

The procedure of DSC measurement is standardized. The experiments can be performed and the obtained results reported according to several standards in order to estimate transition temperatures, transition enthalpies, and specific heat capacity. In addition and according to several standards, DSC measurements can be used to determine purity of substances, oxidation induction parameters, reaction-curve temperatures, degree of conversion, enthalpy of reaction, and crystallization kinetics [6–8].

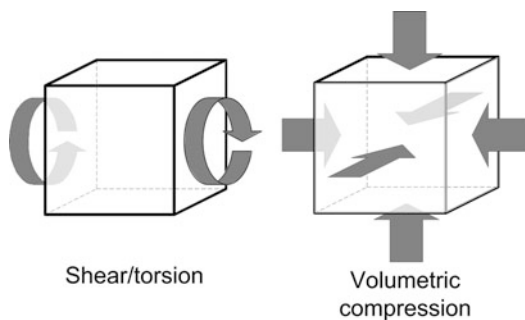
The rate of cooling and heating can affect not only the thermal properties of materials and products but also other physical properties such as mechanical and optical properties. This is a well-known fact, and it is exploited in many industrial processes to obtain products with different functionalities using the same starting material. Many of these practical processes utilize much faster cooling and heating rates than the typically used laboratory rates in conventional DSC apparatuses, e.g., 20 °C/min. For this reason, new DSC devices have been developed; examples of these devices include high-performance DSC with operating scanning rates up to 750 °C/min, rapid-scanning DSC with rates up to 2,000 °C/min, and flash DSC with cooling rates up to 10,000 °C/min and heating rates up to 40,000 °C/min. These newer devices work on the principle of power compensation or heat flux, depending on the manufacturer; however, the way these principles are implemented is slightly different. For example, flash DSC relies on a calorimetry chips based on MEMS (micro-electromechanical systems) sensor technology. In order to achieve such high scanning rates, fast DSC apparatuses require the use of smaller samples; from the typical milligram level for standard DSC, they go down to the microgram or even nanogram level [9].

## Time-Dependent Mechanical Properties

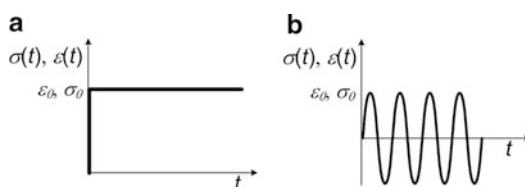
### Theoretical Background

The properties of polymeric materials can significantly change with time. This can influence on their long-term durability. In practice, this means that functionality and, consequently, applicability of polymeric products can change considerably after certain period of time, defects appear, and the products can become permanently useless. These time-dependent changes in the materials' mechanical properties under constant thermomechanical loading conditions are caused by the viscoelastic nature of polymers.

Experimentally, one seeks to characterize material properties by performing simple laboratory tests. Two fundamental tests are (a) tests on



**Experimental Determination of Material Time-Dependent Properties, Fig. 4** Spatial orientation of loading



**Experimental Determination of Material Time-Dependent Properties, Fig. 5** Standard types of loading: (a) step loading and (b) harmonic loading

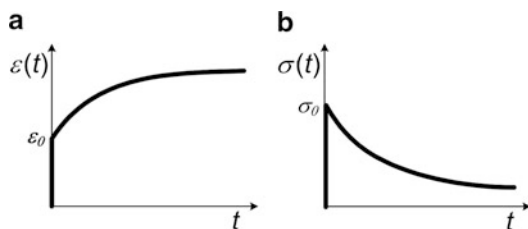
torsion (shear deformation) and (b) volumetric compression (bulk deformation) (Fig. 4).

In such experiments when a stress or a strain is impressed upon a body, molecular *rearrangements* take place inside the material by which it responds to the imposed excitation. In any real material, these rearrangements necessarily require a *finite time*. When the time of changes is comparable to the time scale of the experiment, the material is considered to be *viscoelastic* [1].

Since the viscoelastic behavior of polymers is time dependent, it will differ according to the form of excitation chosen to obtain the response. There are two forms of excitations: *static* and *dynamic*. The step excitation (Fig. 5a), as a representative of static group, and harmonic (sinusoidal steady state) excitation (Fig. 5b) from dynamic group are referred to as *standard excitations*.

Viscoelastic responses naturally fall into two groups according to whether they arise from a strain or a stress excitation (*relaxation* or





**Experimental Determination of Material Time-Dependent Properties, Fig. 6** (a) Creep behavior and (b) relaxation behavior

creep behavior, consequently). The typical response on the step loading is given in Fig. 6.

As a consequence from the above, the viscoelastic behavior can be described by *time-dependent response functions* which are typically consist of time-dependent part, the viscoelastic (or material) function, and time-independent part, the viscoelastic (material) constant. There exist 21 response functions which differ by type (shear, tension, bulk, Poisson's ratio) of loading, mode (stress or strain) of loading, and domain (time or frequency) [10]. All these functions are given in Table 1.

Phenomenologically, it is known that within each set of time-dependent material properties in respect to the certain type of loading (shear, bulk (volumetric), or uniaxial), all material functions are mathematically equivalent. This means that if a material function is known within the whole time range ( $-\infty < \log t < \infty$ ), it contains complete information on static/dynamic creep as well as on static/dynamic relaxation for particular type of loading. Based on this, it is possible to interconvert one material function to another regarding the same loading type by applying their interrelation through mathematical expressions.

Since this entry concerns mostly the time dependence, but not the frequency-dependent properties, it is necessary to mention that characterization of the latter requires utilization of different experimental techniques. Alternatively, frequency-dependent properties may be obtained from the time-dependent ones by using mathematical relations for interconversion between material functions [1].

### Effect of Temperature and Pressure on Time-Dependent Properties

In order to obtain complete information on time-dependent (viscoelastic) properties of a polymeric material, it is necessary to perform experiments in a wide range of time scale that can extend over several years. Since this is not acceptable from the practical and economical point, measurements are usually performed within a certain experimental time interval, the so-called *experimental window* at different environmental conditions (temperatures and/or pressures). For practical reasons, experimental window is typically limited to  $10^4$ s, which is approximately 3h. However, these intervals do not cover the entire set of material's viscoelastic properties. Therefore, a method of extrapolation which allows moving from one excitation time to another was developed. Such extrapolation is based on the principle of equivalency of time and temperature and is called *time-temperature superposition principle* (TTSP) [1, 11]. If the polymer of interest obeys TTSP, i.e., it is *thermorheologically simple*, then the viscoelastic properties measured at different temperatures,  $T_i$ ;  $i = 1, 2, \dots, N$ , and constant pressure,  $p_0$ , over a fixed period of time have similar shape within the superimposing interval and can be exactly superimposed by shifting the curves horizontally along the time axis with respect to a certain *reference temperature*,  $T_r$ . Figure 7a shows  $t$ - $T$  superposition on the example of shear creep compliance. In effect, by changing temperature, one is able to rescale time. The curve created by superposition is called a *master curve*, while the amount of shifting along the horizontal axis for each curve is called a *shift factor*,  $a_T$ .

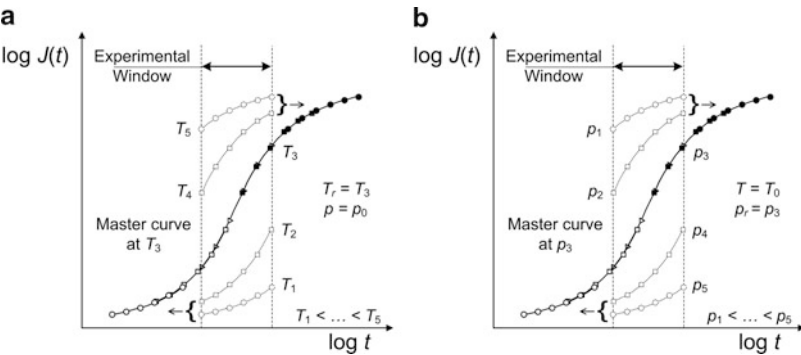
TTSP asserts that the obtained master curve after shifting is identical to the response that would be found at longer times at the reference temperature, if one would be able to do the experiment. Thus, one effectively has a measure of the complete material behavior by applying TTSP to isotherms measured within experimentally accessible time windows.

However, one should pay attention that TTSP may be applied only if material was in equilibrium state at each tested temperature.

Experimental Determination of Material Time-Dependent Properties, Table 1 Viscoelastic material functions

			Type of loading			
	Mode of loading		Shear	Bulk	Uniaxial extension	Poisson's ratio
Static	Relaxation		$G(t)$	$K(t)$	$E(t)$	$\nu(t)$
	Creep		$J(t)$	$B(t)$	$D(t)$	
Dynamic	Relaxation	In phase	$G'(\omega)$	$K'(\omega)$	$E'(\omega)$	$\nu'(\omega)$
		Out of phase	$G''(\omega)$	$K''(\omega)$	$E''(\omega)$	$\nu''(\omega)$
	Creep	In phase	$J'(\omega)$	$B'(\omega)$	$D'(\omega)$	
		Out of phase	$J''(\omega)$	$B''(\omega)$	$D''(\omega)$	

Experimental Determination of Material Time-Dependent Properties, Fig. 7 Schematics: (a) time-temperature superposition of  $J(t)$  (b) time-pressure superposition of  $J(t)$



Material can be brought to equilibrium sufficiently close only well above the glass transition temperature, i.e.,  $T > T_g + 50\text{ }^{\circ}\text{C}$  [12].

The effect of pressure on the relaxation and retardation behavior of polymers is analogous to the effect of temperature taking into account that high temperature corresponds to low pressure and vice versa [13, 14]. As for temperature, when all response times are equally affected by a change in pressure, the material is called *piezorheologically simple*, i.e., it permits *time-pressure superposition*, i.e., the shifting of isobaric segments in a similar manner as shifting of isotherms measured at constant temperature,  $T_0$ , by taking in consideration certain *reference pressure*,  $p_r$ . Figure 7b shows  $t$ - $P$  superposition on the example of shear creep compliance.

Determination and Modeling of Shift Factors

It is clear from above remarks that shift factor is one of the key parameters in application of TTSP. The shift factor is not only a mathematical quantity, but it is also physically defined as the ratio between any specific *response time* at

a temperature of interest,  $T$ , to its value at selected *reference temperature*,  $T_r$ ,

$$\frac{\lambda(T)}{\lambda(T_r)} = a_{T_r}(T) = a_T \tag{3}$$

Since for most amorphous polymers the retardation (or relaxation) times have the same temperature dependence [12], the value  $a_T$  will stay the same for all response times at a given reference conditions. It follows then that the data taken isothermally at different constant temperatures and plotted against  $\log t$  can be translated along the logarithmic time axis to form a smooth master curve, valid at  $T_r$ , if within the overlapping area (Fig. 8a), the condition

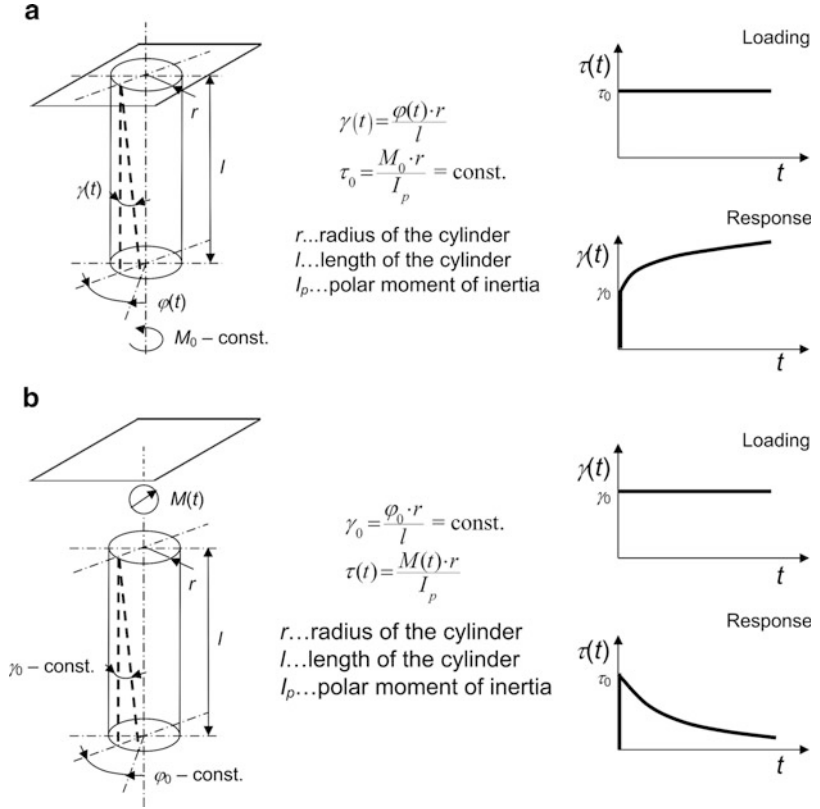
$$J(t, T) = J(t/a_T, T_r) \tag{4}$$

is fulfilled.

The ratio in (3) is commonly abbreviated as  $a_T$ , but in fact, it is a function of temperature, which form is different for each reference temperature [15]. These temperature dependences

### Experimental Determination of Material Time-Dependent Properties,

**Fig. 8** (a) Schematics of the shear creep experiment and (b) shear relaxation experiment



are generally modeled by the well-known WLF equation, named after its originators, Williams, Landel, and Ferry [16]:

$$\log a_T = \frac{-c_1^r \cdot (T - T_r)}{c_2^r + T - T_r} \quad (5)$$

where  $c_1^r$  and  $c_2^r$  are material constants at the reference temperature,  $T_r$ . The WLF equation is typically used to describe behavior of polymers above the glass transition temperature,  $T_g$ . Below  $T_g$  another model, called Arrhenius equation, is commonly applied [17]:

$$\log a_T = C_a \left( \frac{1}{T} - \frac{1}{T_r} \right) \quad (6)$$

Here  $C_a$  is the material constant depending on the activation energy,  $\Delta H_a$ , and ideal gas constant,  $R$ , i.e.,  $C_a = \Delta H_a / R$ .

The appropriate model which describes combined effect of temperature and pressure on mechanical properties of materials is the FMT (Filler-Moonan-Tschoegl) model [18, 19] which comprises the WLF equation as a special case [14, 16]. The equation reads

$$\log a_{T,p} = - \frac{c_1^{rr} \cdot [T - T_r - \theta(p)]}{c_2^{rr}(p) + T - T_r - \theta(p)} \quad (7)$$

where  $T$  and  $p$  are the (absolute) temperature and pressure, respectively, and  $\theta(p)$  is a function of pressure, related to the free-volume change and the thermal expansion. It is equal to zero,  $\theta(p) = 0$ , when  $p = p_r$ .  $c_1^{rr}$  and  $c_2^{rr}$  are material constants that refer to the reference temperature and reference pressure [15].

## Shear Creep and Shear Relaxation Measurements

### Theoretical Background

When the step loading is applied as stress of the constant magnitude, one can observe the *creep* of the material, whereas, when the step loading is applied as strain of constant magnitude, the *relaxation* process in the material can be observed. In this respect, shear creep compliance and shear relaxation modulus are in practice, the most commonly experimentally measured properties characterizing the time-dependent behavior of materials. Figure 8a, b schematically presents creep and relaxation processes via shear loading and corresponding response of the material. However, creep and relaxation can also occur by other means of deformation, e.g., harmonic excitation with constant stress or strain amplitude, as mentioned previously.

When the loading conditions are given as a step function of constant shear stress,  $\tau_0$ , the time-dependent *shear creep compliance*,  $J(t)$ , can be expressed as follows:

$$J(t) = \frac{\gamma(t)}{\tau_0} \quad (8)$$

where  $t$  represents time and  $\gamma(t)$  the shear strain response as function of time.

When the loading conditions are given as a step function of constant shear strain,  $\gamma_0$ , the time-dependent *shear relaxation modulus* of material,  $G(t)$ , takes the form of

$$G(t) = \frac{\tau(t)}{\gamma_0} \quad (9)$$

where  $\tau(t)$  is the shear-stress time-dependent response.

Rate of creep or relaxation process has exponentially decreasing mode in dependence of time; that is why it is more convenient to represent time-dependent properties in logarithmic scales (i.e.,  $\log J(t)$  vs.  $\log t$  or, equivalently, in  $\log G(t)$  vs.  $\log t$ ). At  $t = 0$ , the creep

compliance is equal  $J(t = 0) = J_g$ , where  $J_g$  represents the *glassy compliance*, whereas at  $t \rightarrow \infty$ ,  $J(t \rightarrow \infty) = J_e$ , where  $J_e$  is the *equilibrium compliance*. The equilibrium compliance is absent if the material is capable of steady state flow. In analogous way,  $G_g$  and  $G_e$  are the *glassy* and the *equilibrium modulus*, respectively.

### Experimental Methodology

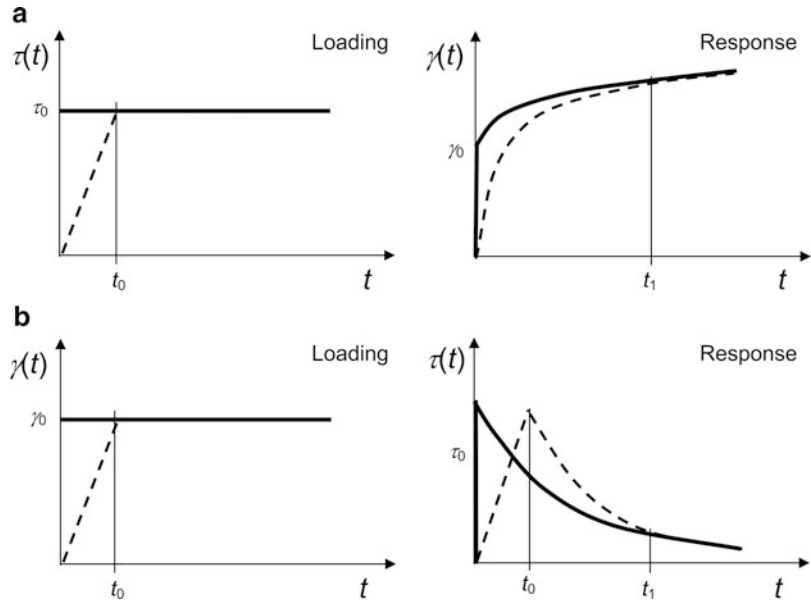
In reality, it is not possible to achieve step loading conditions, but only to get close to it via *ramp loading* of certain rate by which the loading magnitude  $\tau_0$  or  $\gamma_0$  is achieved in time  $t_0$ . As a consequence, one can obtain the results of measurements that can be further on processed, only after certain time  $t_1$ , when the material response to the real ramp loading approximates the assumed material response under step loading conditions close enough. The commonly applied criterion determines that  $t_1$  should be at least 10 times of time  $t_0$ . However, to assure results with higher accuracy, this may not be sufficient. Figure 9a, b is schematically showing step and ramp loading and corresponding time-dependent responses in creep and relaxation.

As previously mentioned, from practical reasons, characterization of time-dependent properties is usually done through measurements in segmental form within the so-called experimental window (EW) and further use of time-temperature superposition principle (TTSP). The beginning of the EW is usually determined with  $t_1$ , which results from the limitation of the ramp loading.

Measurements of creep and/or relaxation usually consist of several steps. Initial phase is specimen conditioning (annealing) at the elevated temperature in order to erase residual stress-strain state in the material, which is followed by the slow cooling of the sample to the first temperature level at which the segment measurement is performed. This phase yields one measured segment as a part of the creep compliance or relaxation modulus master curve. After the loading phase, the specimen is unloaded, and the temperature is increased to the next temperature level.

### Experimental Determination of Material Time-Dependent Properties,

**Fig. 9** (a) Material creep response to the shear-stress step (solid line) and ramp (dashed line) loading, and (b) material relaxation response to the shear strain step (solid line) and ramp (dashed line) loading



Recovery of the material takes place during unloading phase that should be at least as long as the loading period. After recovery process and increase of the temperature to the next temperature level, the specimen is again loaded, and the procedure of exchanging the phases of loading, unloading, and temperature conditioning is repeated over the entire temperature range determined for complete measurement. The methodology for generating master curves from the measured segments is described at the end of this entry.

## Bulk Measurements

### Theoretical Background

Time-dependent materials, such as polymers, are frequently subjected to rapid temperature and/or pressure changes during their exploitation. Understanding how the volume of the polymer responds in these circumstances is important in several engineering applications and manufacturing processes. As previously mentioned, changes in volume (size), associated with the bulk deformation mode, can be characterized as material bulk properties, i.e., as *bulk relaxation modulus*,  $K$ , and/or *bulk creep compliance*,  $B$ , that

may depend on time, frequency, temperature, pressure, and/or other factors (e.g., humidity).

The bulk creep compliance,  $B(t)$ , is determined from the time-dependent *relative volumetric contraction* in response to an instantly applied hydrostatic pressure drop (or increase),  $\delta p$ , while the temperature is maintained constant. It is obtained from the expression [12]:

$$B(t) = -\frac{\delta v(t)}{v_0 \cdot \delta p}, \quad (10)$$

where  $\delta v(t)$  is the specimen volume change at time  $t$ , while  $v_0$  is its initial volume before deformational process occurs.

On the other hand, bulk relaxation modulus,  $K(t)$ , determines how much of hydrostatic pressure is generated in the material after instant change of its volume,  $\delta v_0$ :

$$K(t) = -v_0 \cdot \frac{p(t)}{\delta v_0} \quad (11)$$

where  $p(t)$  stands for measured pressure inside the material (internal stress state) as a function of time [12]. It is known, that for any material that is in equilibrium at a given temperature and pressure,  $B(t)$  becomes the *thermodynamic*

compressibility,  $\beta = (\frac{1}{v}) \cdot (\frac{\partial v}{\partial p})$  at a given temperature, while  $K(t)$  becomes the corresponding equilibrium bulk modulus [12].

In the case of the bulk creep compliance, it is important to emphasize that pressure,  $p$ , acts as environmental boundary condition, while pressure change,  $\delta p$ , as a loading condition. Therefore,  $B(t)$  in (10) may be presented as a functional of pressure, pressure change, temperature, and time, i.e.,

$$B(p, \delta p, T, t) = B_g(p, \delta p, T) + \delta B(p, \delta p, T, t) \quad (12)$$

where  $\delta B(p, \delta p, T, t=0)=0$  and  $\delta B(p, \delta p, T, t=\infty)=B_e(p, \delta p, T)-B_g(p, \delta p, T)$ .  $B_g$  and  $B_e$  are pressure and temperature-dependent glassy and equilibrium bulk creep compliances [20].

The equilibrium bulk compliance  $B_e$  (as well as equilibrium bulk modulus,  $K_e$ ) may be attributed to compression of the occupied volume, as well as to a collapse of the free volume. Glassy compliance,  $B_g$ , is attributed to compression of the occupied volume only.

### Experimental Methodology

In practice, it is hard to measure bulk relaxation modulus of a material directly and precisely. Such experiments would require as an excitation a known *volumetric compression* and measurements of the internal stress state (11), which is in practice extremely difficult. In analogy to the shear-stress relaxation experiment, bulk relaxation measurement requires sudden compression of the sample to a smaller volume, and the pressure required to hold it at constant volume is recorded as function of time. Apparatus for this purpose has been described by Matsuoka and Maxwell [21]. Measurements of this kind require techniques of high-pressure physics; in particular, freedom from voids and gas bubbles is naturally very important.

On the other hand, measurement of the corresponding bulk creep compliance is more feasible, since it requires rapid hydrostatic pressure change to be applied to the sample, and measurements of the specimen time-dependent

volume change (10). In analogy to the shear creep experiment, the bulk creep measurement requires maintaining constant pressure, while decrease of volume is followed in time. An apparatus for very precise measurements at moderate pressures has been described by Goldbach and Rehage [22]. In their case, the volume change is measured by motion of mercury in a capillary (*mercury confinement dilatometry*). Another device, suitable for high pressures, has been used by Mandelkern and by Findley [23, 24], who measured volumetric deformation by utilizing strain gauges.

Recently, in comparison to mentioned approaches, a measuring system was developed at the Center for Experimental Mechanics, University of Ljubljana, Slovenia [10]. It enables characterization of bulk creep response based on *displacement dilatometry* principle with high degree of precision within certain pressure and temperature range. Dilatometry measurements are performed by monitoring the volume change of the specimen which results from the imposed changes of pressure and/or temperature by measuring the change in specimen length with the aid of a built-in linear variable differential transformer (LVDT).

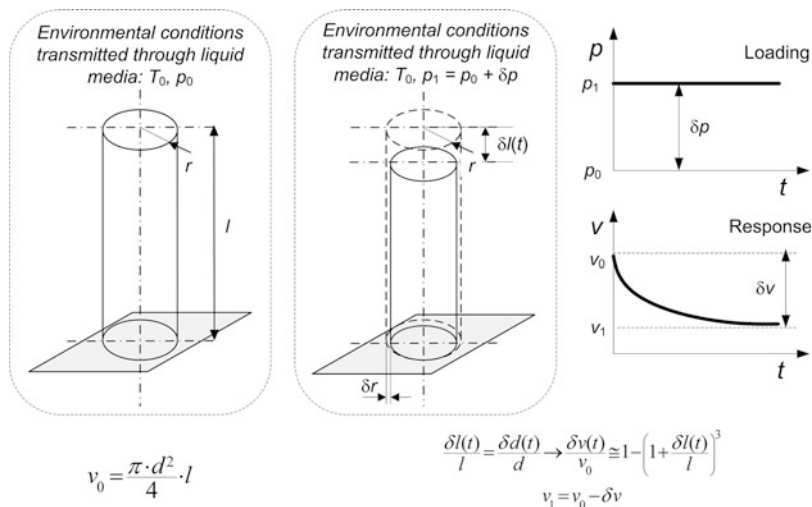
Figure 10 schematically represents displacement dilatometry measuring principle for cylindrical sample. Its volume change can be expressed in terms of its length,  $l$ , assuming isotropic volume reduction, according to which we consider that  $\delta l/l = \delta d/d$ , where  $d = 2r$  is the diameter and  $r$  is the radius of the circular cross section of the cylinder in Fig. 10. The volume estimate can be considered accurate if the change in volume is small and the material is isotropic.

Displacement dilatometry has an accuracy advantage over the mercury confinement dilatometry [22] inasmuch as it allows an easily automated measurement process for tracking transient volume changes over extended periods of time. However, for soft materials, an important limitation arises (usually at higher temperatures) when the specimen starts to creep under its own weight.

We have to note that bulk measurements face the same issues as experiments in shear. As it was



**Experimental Determination of Material Time-Dependent Properties, Fig. 10** Schematics of displacement dilatometry principle



previously mentioned in the section “[Shear Creep and Shear Relaxation Measurements](#),” it is not possible to achieve step loading conditions in reality. The commonly applied criterion that determines starting time of useful data acquisition is set to 10 times of “ramp” loading time,  $t_0$ . When the pressure is a loading parameter, the “ramp” loading time can significantly increase due to the long-term pressure stabilization caused by compressibility of gas bubbles inside the liquid media supplying pressure, compaction (or expansion) of pressure-vessel parts, where the sample is placed, and pressure changes due to temperature variations. As a consequence, one can obtain results of the bulk measurements that can be further on processed only after certain time  $t_1$ , which is relatively long (from 10 to 100s). To overcome this problem, real-time control systems for pressure-level adjustment have to be used.

Similarly as measurements in shear, the measurements of bulk properties are also performed in segmental form, utilizing time-temperature-pressure superposition principle, as explained in section “[Time-Dependent Mechanical Properties](#)” (“[Effect of Temperature and Pressure on Time-Dependent Properties](#)”). Procedure for constructing the bulk property master curve from individual segments according to the

time-temperature and/or time-pressure superposition principle is discussed in the following section.

## Methods for Constructing Master Curves

When constructing a master curve, the shift factors are usually defined “by hand,” i.e., the isothermal segments of the response function are manually translated to a previously selected reference segment along the logarithmic time scale until they overlap. Commonly this is done with a spreadsheet for graphical display of the curves. The major drawback of the hand shifting is the lack of any rules how the procedure should be implemented. Mostly it is done intuitively relying on one’s own experience. Along with the “hand shifting,” there exist several numerical procedures for calculating the shift factors. Most of them are based on the least-square method, though there are few other approaches. Usually these methods require, as a preliminary step, smoothing of the experimentally obtained isotherms. This brings in additional divergence in the obtained results since the approximating procedure by itself is not universal. The form of smoothing functions suggested in the literature varies from a simple linear fitting to multiparameter complex expressions [25].

The shifting procedure is therefore one of the weakest points in the utilization of the time-temperature(-pressure) superposition principle.

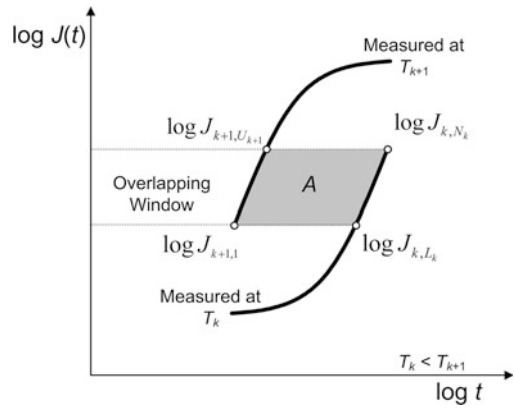
Recently, the new methodology for automated construction of the master curves, called the *closed-form shifting (CFS) algorithm*, was developed by Gergesova et al. [25]. The proposed method works with the unprocessed (raw) data segments. Since it is based on a closed-form solution for the shift factors, it constructs a unique master curve and, therefore, completely removes previously mentioned ambiguities of other shifting methods.

The proposed mathematical formulation of the CFS procedure is based on equilibrium thermodynamics and takes into account that viscoelastic functions measured at two different temperature and/or pressure boundary conditions represent behavior of the material at two different thermodynamic states, which differ in the corresponding Gibbs free energy,  $G$ . The latter represents the portion of the total system energy that is available for useful work or, in other words, the mechanical energy absorbed per unit volume of viscoelastic material in the deformation from the initial time,  $t_0$ , up to the current time,  $t$ .

The rate at which mechanical energy is absorbed at a given boundary conditions  $(T_k, p_k)$  is equal to the *stress power* ( $\sigma$ ), i.e., the rate at which work is performed [26]. The stress power at time  $t$  is

$$\frac{dG(t, T_k, p_k)}{dt} = \sigma(t, T_k, p_k) \frac{d\varepsilon(t)}{dt} \quad (13)$$

The absorbed mechanical energy causes material inherent structural (molecular) rearrangements during the relaxation or creep experiment. Thus, any two segments of the material function, measured at the reference state  $(T_k, p_k)$ , and any other selected state  $(T_{k+1}, p_{k+1})$  that needs to be superimposed (shifted) into a master curve should have the same stress power at all points of the superimposing interval. This criterion may be expressed as



**Experimental Determination of Material Time-Dependent Properties, Fig. 11** Schematics of the CFS shifting procedure

$$\frac{dG(t, T_{k+1}, p_{k+1})}{d \log t} = \frac{dG(t/a_k, T_k, p_k)}{d \log t} \quad (14)$$

The condition in (14) is fulfilled when overlapping area,  $A$ , between two isotherms is equal to zero (Fig. 11).

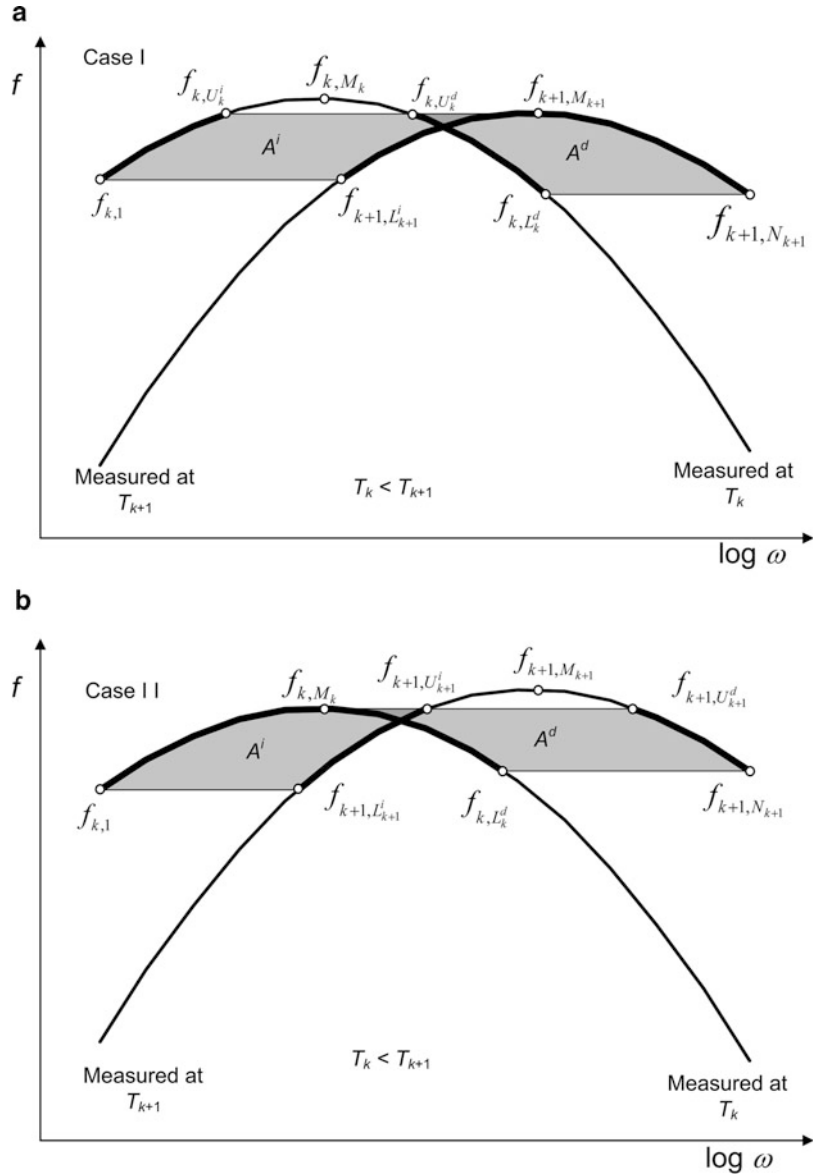
The creep (Fig. 11) and relaxation data in time domain may be modeled with monotonically increasing and decreasing functions, correspondingly. However, data in frequency domain (dynamic data) can appear as non-monotonic functions of logarithmic frequency, e.g., loss moduli and compliances (Table 1) or the ratio between loss and storage material functions referred to as  $\tan \delta(\omega)$ . In this case, the condition in (14) is fulfilled when the total overlapping area, consisting of increasing overlapping area,  $A^i$ , and decreasing overlapping area,  $A^d$ , is equal to zero (Fig. 12).

Based on these considerations, the CFS algorithm, applicable for any type of material functions in time and frequency domain, was derived. Thus, for two non-monotonic segments measured at two adjacent temperatures  $T_k$  and  $T_{k+1}$ , and given with  $N_k$  and  $N_{k+1}$  discrete datum points, respectively,

$$\Theta = \{ \log \omega_{j,n} = \log \omega_n(T_j), f_{j,n} = f(\omega_n, T_j); j = k, k+1, n = 1, 2, \dots, N_j \},$$



**Experimental Determination of Material Time-Dependent Properties, Fig. 12** Schematics of the CFS shifting procedure for non-monotonic functions



the closed-form solution for shift factor will be

$$\log a_{k+1} = \frac{\left( \sum_{n=L_{k+1}^i}^{S-1} F_{k+1,n} - \sum_{n=1}^{R-1} F_{k,n} \right)_i}{(f_{k,1} - Y)_i - (Y - f_{k+1,N_{k+1}})_d}, \quad (15)$$

$$- \frac{\left( \sum_{n=C}^{N_{k+1}-1} F_{k+1,n} - \sum_{n=P}^{L_k^d-1} F_{k,n} \right)_d}{(f_{k,1} - Y)_i - (Y - f_{k+1,N_{k+1}})_d}$$

where

$f_{j,n}$  denotes the non-monotonic function, e.g.,  $\log J''$  or  $\tan \delta = J''/J'$ .

$$F_{j,n} = \frac{\log \omega_{j,n} + \log \omega_{j,n+1}}{2} \cdot (f_{j,n+1} - f_{j,n}),$$

$$j = \kappa, \kappa + 1 \quad (16)$$

$$Y = \min\{f_{\kappa,M_\kappa}, f_{\kappa+1,M_{\kappa+1}}\} \quad (17)$$

**Experimental Determination of Material Time-Dependent Properties, Table 2** Coefficients for the generalized equation

Case \ Variable	$S$	$R$	$C$	$P$
I	$M_{\kappa+1}$	$U_{\kappa}^i$	$M_{\kappa+1}$	$U_{\kappa}^d$
II	$U_{\kappa+1}^i$	$M_{\kappa}$	$U_{\kappa+1}^d$	$M_{\kappa}$

and variables  $S, R, C$ , and  $P$  can take different values depending on the shifting case as shown in Table 2. As can be seen in Fig. 12, case I and case II differ in that which segment has the highest value. The subscripts or superscripts “ $i$ ” and “ $d$ ” indicate the increasing or decreasing part respectively, from which the term is coming.

When applying (15) for shifting of monotonically decreasing functions, the terms with subscript “ $i$ ” become zero, and (15) reduces to the following form:

$$\log a_{\kappa+1} = \frac{\sum_{n=U_{\kappa+1}^d}^{N_{\kappa+1}-1} F_{\kappa+1,n} - \sum_{n=C}^{L_{\kappa}^d-1} F_{\kappa,n}}{Y - f_{\kappa+1,N_{\kappa+1}}} \quad (18)$$

and in the case of monotonically increasing functions, the terms with subscript “ $d$ ” vanish, and (15) becomes

$$\log a_{\kappa+1} = \frac{\sum_{n=L_{\kappa+1}^i}^{N_{\kappa+1}-1} F_{\kappa+1,n} - \sum_{n=1}^{U_{\kappa}^i-1} F_{\kappa,n}}{f_{\kappa,1} - Y} \quad (19)$$

Therefore, CFS methodology may be used for all material functions measured in time and frequency domain. It can be also applied for materials which require vertical shifting of storage and loss data. Calculated in such a way, vertical shift factors allow estimation of a thermal expansion coefficient, which is difficult to obtain experimentally for certain materials.

## References

1. Tschoegl NW (1989) The phenomenological theory of linear viscoelastic behavior. Springer, Berlin
2. Menczel JD, Judovits L, Prime RB, Bair HE, Reading M, Swier S (2009) Differential scanning calorimetry (DSC). In: Menczel JD, Prime RB (eds) Thermal analysis of polymers: fundamentals and applications. Wiley, Hoboken, pp 7–240
3. Haines PJ, Reading M, Wilburn FW (1998) Differential thermal analysis and differential scanning calorimetry. In: Gallagher PK, Brown ME, Kemp RB (eds) Handbook of thermal analysis and calorimetry: principles and practice. Elsevier Science BV, Amsterdam, pp 279–287
4. Höhne G, Hemminger W, Flammersheim HJ (2003) Types of differential scanning calorimeters and modes of operation. Differential scanning calorimetry. Springer, Berlin, pp 9–30
5. Laye PG (2002) Differential thermal analysis and differential scanning calorimetry. In: Haines PJ (ed) Principles of thermal analysis and calorimetry. The Royal Society of Chemistry, Cambridge, UK, pp 55–93
6. ASTM D3418 -08 Standard Test Method for Transition Temperatures and Enthalpies of Fusion and Crystallization of Polymers by Differential Scanning Calorimetry. Book of standards Vol. 08.02. ASTM E793-06 Standard Test Method for Enthalpies of Fusion and Crystallization by Differential Scanning Calorimetry. Book of Standards Vol. 14.02. ASTM E928-08 Standard Test Method for Determination of Purity by Differential Scanning Calorimetry. Book of Standards Vol. 14.02. ASTM E1269-11 Standard Test Method for Determining Specific Heat capacity by Differential Scanning Calorimetry. Book of Standards Vol. 14.02. ASTM E1356-08 Standard Test Method for Assignment of the Glass Transition Temperature by Differential Scanning Calorimetry. Book of Standards Vol. 14.02
7. DIN EN 12614 (2005-01) Products and systems for the protection and repair of concrete structures – Test methods – Determination of glass transition temperature of polymers. DIN 51005 (2005-08) Thermal analysis (TA) – Terms. DIN 53765 (1994-03) Testing of plastics and elastomers; thermal analysis; DSC-method.
8. ISO 11357-1: 2009 Plastics - Differential scanning calorimetry (DSC) – Part 1: General principles. ISO 11357-2: 1999 Plastics – Differential scanning calorimetry (DSC) – Part 2: Determination of glass transition temperature. ISO 11357-3: 2011 Plastics – Differential scanning calorimetry (DSC) – Part 3: Determination of temperature and enthalpy of melting and crystallization. ISO 11357-4: 2005 Plastics – Differential scanning calorimetry (DSC) – Part 4: Determination of specific heat capacity. ISO 11357-5: 1999 Plastics – Differential scanning calorimetry (DSC) – Part 5: Determination of characteristic reaction-curve temperatures and times, enthalpy of reaction and degree of conversion.

- ISO 11357-6: 2008 Plastics – Differential scanning calorimetry (DSC) – Part 6: Determination of oxidation induction time (isothermal OIT) and oxidation induction temperature (dynamic OIT). ISO 11357-7: 2002 Plastics – Differential scanning calorimetry (DSC) – Part 7: Determination of crystallization kinetics.
9. Mathot V, Pyda M, Pijpers T, Vanden Poel G, van de Kerkhof E, van Herwaarden S, van Herwaarden F, Leenaers A (2011) The flash DSC 1, a power compensation twin-type, chip-based fast scanning calorimeter (FSC): first findings on polymers. *Thermochimica Acta* 522:36–45
  10. Knauss WG, Emri I, Lu H (2008) Mechanics of polymers: viscoelasticity. In: William N (ed) *Handbook of experimental solid mechanics*. Springer, New York, pp 49–95
  11. Aklonis JJ, MacKnight WJ (1983) *Introduction to polymer viscoelasticity*, 2nd edn. Wiley, New York
  12. Ferry JD (1980) *Viscoelastic properties of polymers*, 3rd edn. Wiley, New York
  13. Kralj A, Prodan T, Emri I (2001) An apparatus for measuring the effect of pressure on the time-dependent properties of polymers. *J Rheol* 45(4):929–943
  14. Tschoegl NW, Knauss WG, Emri I (2002) The effect of temperature and pressure on the mechanical properties of thermo- and/or piezorheologically simple polymeric materials in thermodynamic equilibrium – a critical review. *Mech Time-Depend Mater* 6(1):53–99
  15. Emri I (1997) Use of polymers and polymer based composites in structural mechanics. In: Roorda J, Srivastava NK (eds) *Trends in structural mechanics*. Kluwer, Dordrecht, pp 75–93
  16. Williams ML, Landel RF, Ferry JD (1955) The temperature dependence of relaxation mechanisms in amorphous polymers and other glass forming liquids. *J Amer Chem Soc* 77:3701–3707
  17. Arrhenius S (1916) The viscosity of pure liquids. *Meddelanden Från K. Vetenskapsakademiens Nobelinstitut* 3:1–40
  18. Fillers RW, Tschoegl NW (1997) The effect of pressure on the mechanical properties of polymers. *Trans Soc Rheol* 21:51–100
  19. Moonan WK, Tschoegl NW (1985) The effect of pressure on the mechanical properties of polymers IV. Measurements in torsion. *J Polym Sci Polym Phys Ed* 23:623–651
  20. McKinney JE, Belcher HV (1963) Dynamic compressibility of poly(vinyl acetate) and its relation to free volume. *J Res Natl Bur Stand A* 67:43
  21. Matsuoka S, Maxwell B (1958) Response of linear high polymers to hydrostatic pressure. *J Polym Sci* 32:131
  22. Goldbach G, Rehage G (1967) Untersuchungen Über die Lineare Volumennachwirkung bei Amorphen Hochpolymeren. *J Polym Sci* 16(4):2289–2298
  23. Martin GM, Mandelkern L (1967) Effect of hydrostatic pressures on the crystallization kinetics of natural rubber. *J Appl Phys* 34:2312
  24. Findley WN, Reed RM, Stern P (1967) Hydrostatic creep of solid plastics. *J Appl Mech* 34:895
  25. Gergesova M, Zupančič B, Saprunov I, Emri I (2011) The closed form t-T-P shifting (CFS) methodology. *J Rheol* 55:1–17
  26. Mainardi F (2010) *Fractional calculus and waves in linear viscoelasticity: an introduction to mathematical models*. Imperial College Press, London

---

## Experimental Stress-Measuring Techniques

► [Residual Stresses in Thin Films Evaluated by Different Experimental Techniques](#)

---

## Explicit Finite-Difference Method for Solving Transient Heat Conduction Problems

Piotr Wais

Institute of Thermal Power Engineering, Faculty of Mechanical Engineering, Cracow University of Technology, Cracow, Poland

### Overview

In many applications, the temperatures are varying with time, and the understanding of the time history of the temperature change is required to be known. In general, the temperature field depends on time and on geometrical coordinates (body position).

In the Cartesian coordinate system, the coordinate surfaces are planes perpendicular to the respective axis, and the coordinates are  $x$ ,  $y$ , and  $z$  for directions and  $t$  for variation with time. The temperature variation can be expressed as a function  $T(x, y, z, t)$ , and the transient heat conduction problems are described by the heat equation:

$$\frac{\partial}{\partial x} \left( k \frac{\partial T}{\partial x} \right) + \frac{\partial}{\partial y} \left( k \frac{\partial T}{\partial y} \right) + \frac{\partial}{\partial z} \left( k \frac{\partial T}{\partial z} \right) + q_v = \rho c_p \frac{\partial T}{\partial t} \quad (1)$$

where

$k$  – thermal conductivity

$q_v$  – rate of energy generation per unit volume

$c_p$  – specific heat at constant pressure,

$\rho$  – mass density

Second-order partial differential equation for heat conduction problem is a parabolic one. The spatial and temporal derivatives in heat conduction equation show that the temperature varies in both space and time.

Introducing thermal diffusivity, defined as  $\kappa = \frac{k}{\rho c_p}$ , and if thermal conductivity  $k$  is constant, (1) can be written as

$$\frac{\partial^2 T}{\partial x^2} + \frac{\partial^2 T}{\partial y^2} + \frac{\partial^2 T}{\partial z^2} + \frac{q}{k} = \frac{1}{\kappa} \frac{\partial T}{\partial t} \quad (2)$$

In two-dimensional system, with constant thermal conductivity and without energy generation, (2) reduces to

$$\frac{\partial^2 T}{\partial x^2} + \frac{\partial^2 T}{\partial y^2} = \frac{1}{\kappa} \frac{\partial T}{\partial t} \quad (3)$$

If the heat transfer is one dimensional, the governing differential equation (3) for heat conduction with constant thermal conductivity and without energy generation reduces to

$$\frac{\partial^2 T}{\partial x^2} = \frac{1}{\kappa} \frac{\partial T}{\partial t} \quad (4)$$

From above equations (1), (2), (3), or (4), it is possible to calculate the temperature distribution that is one of the main tasks in transient heat conduction problems.

The solution of a transient heat conduction task can be found [1]:

- Analytically, by a closed solution of the heat conduction equation, fulfilling all the boundary conditions
- Numerically, by numerical solution of the differential equation with boundary conditions
- Experimentally, by an experimental method in analogy process (electrical conduction is described by the same form of partial differential equation, and the results can be transferred)

Analytical solutions to transient problems are restricted to simple geometries and boundary conditions. In many cases, the geometry or boundary excludes the use of analytical techniques, and numerical solution of conduction problems is the most used analysis approach. The numerical solution of a transient heat conduction problem is also important when the temperature-dependent material properties are considered [2]. Two general techniques are applied for the numerical solution of initial boundary value problems:

- Finite-difference method
- Finite element concepts

## Model Discretization

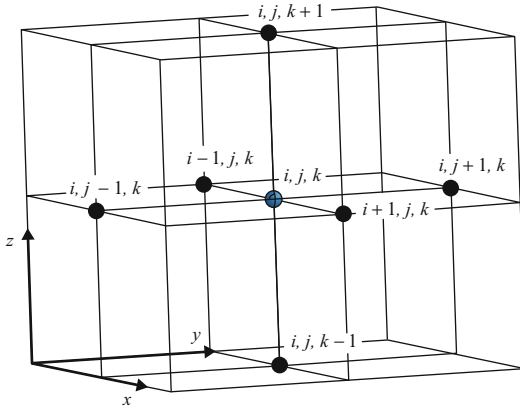
The principle of all methods for the numerical solution of partial difference method is to obtain discrete numerical values which approximate the exact solution. There are different methods for the numerical approximation. One of the oldest is the finite-difference method [3].

There are different methods to write a finite-difference solution for a differential equation:

- The discrete finite-difference grid, using the continuous physical domain as a function of nodal temperatures (applied in this entry)
- The finite-difference approximation, using the partial derivatives in the partial differential equation (see Implicit Finite-Difference Method for Solving Transient Heat Conduction Problems).

In order to define the nodes, a system of orthogonal coordinate surfaces is superimposed. To discretize the spatiotemporal continuum, space steps  $\Delta x > 0$ ,  $\Delta y > 0$ , and  $\Delta z > 0$  and a time step  $\Delta t > 0$  are introduced. An internal node is defined by the intersection of three coordinate surfaces. The variables  $(x, y, z, t)$  are independent.

A grid is established along the strip  $x_0 \leq x \leq x_n$ ,  $y_0 \leq y \leq y_n$ ,  $z_0 \leq z \leq z_n$ , and  $t \geq t_0$ , with mesh size  $\Delta x$  in the  $x$  direction,  $\Delta y$  in the  $y$  direction,  $\Delta z$  in the  $z$  direction, and  $\Delta t$  in the  $t$  direction.



**Explicit Finite-Difference Method for Solving Transient Heat Conduction Problems, Fig. 1** Internal node  $i, j, k$  and grid structure in three-dimensional heat conduction

Time increment  $\Delta t$  may be calculated after splitting the total time on the  $s$  intervals  $\Delta t = \frac{t}{s}$  and where

$$t_p = t_0 + p \Delta t \quad \text{with } p = 0, 1, 2, \dots \quad (5)$$

Also

$$x_i = x_0 + i \Delta x \quad \text{with } i = 0, 1, 2, \dots \quad (6)$$

$$y_j = y_0 + j \Delta y \quad \text{with } j = 0, 1, 2, \dots \quad (7)$$

$$z_k = z_0 + k \Delta z \quad \text{with } k = 0, 1, 2, \dots \quad (8)$$

The approximate value of temperature  $T(x_i, y_j, z_k, t_p)$  at grid point  $i, j, k, p$  is indicated by  $T_{i,j,k}^p = T(x_i, y_j, z_k, t_p)$ . The superscript designates the time increment.

An internal node is defined by the intersection of three coordinate surfaces, as shown in Fig. 1:

Heat may flow from the internal node to each adjacent node along paths that are parallel to each axis and to each of its six neighboring nodes:

$$\begin{aligned} & i, j-1, k \\ & i, j+1, k \\ & i, j, k-1 \\ & i, j, k+1 \\ & i-1, j, k \\ & i+1, j, k \end{aligned}$$

If the analysis is limited to the two-dimensional system, then a two-dimensional body is divided into increments, as shown in Fig. 2:

In the two-dimensional system, heat can flow from the internal node to four neighboring points. Each node represents a certain region, and its temperature is a measure of the average temperature of the region. In 2D coordinate system, the temperature of the node  $i, j$  is viewed as the average temperature of the surrounding nodal points:

$$T_{i,j} = \frac{1}{4}(T_{i,j-1} + T_{i,j+1} + T_{i-1,j} + T_{i+1,j}) \quad (9)$$

Generally, for the grid point shown in Fig. 2, the distances  $\Delta x$  and  $\Delta y$  cannot be equal. Sometimes, the use of nonuniform grid spacing enables deploying computing power effectively because there is no need to use a fine grid in regions where the variable  $T$  changes rather slowly with  $x$  or  $y$ .

For one-dimensional system, the grid can be presented, as in Fig. 3, in which the coordinates of the grid point  $i, p$  are  $x_i, t_p$ :

The selection of the nodal points (mesh generation) depends on the geometry and desired accuracy. The numerical accuracy of the calculations depends strongly on the number of designed nodal points. Accurate solution can be obtained for a fine mesh (large number of points).

## Difference Form of Heat Conduction Equation

To develop a difference equation in two-dimensional unsteady conduction problems, a discrete time step  $\Delta t$  and discrete spatial steps  $\Delta x$  and  $\Delta y$  are defined.

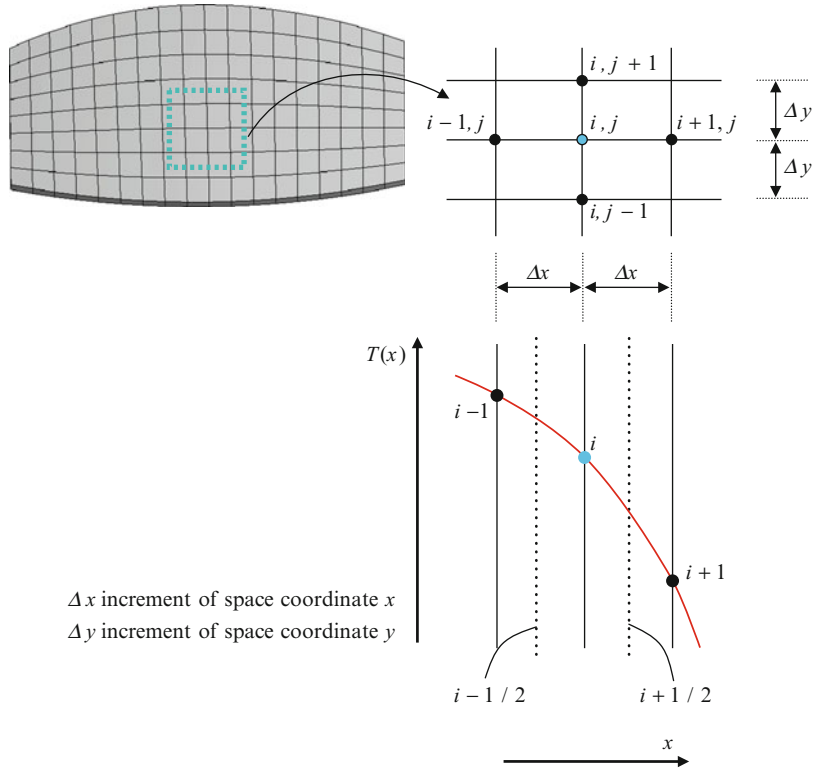
Nodal temperatures now depend on three indices,  $i, j$ , and  $p$ , which correspond to the spatial and time dependencies, respectively:  $T_{i,j}^p = T(x_i, y_j, t_p)$ .

The temperature gradients may be expressed as a function of nodal temperatures, see Fig. 2:

$$\left. \frac{\partial T}{\partial x} \right|_{i+1/2,j} \approx \frac{T_{i+1,j} - T_{i,j}}{\Delta x} \quad (10)$$

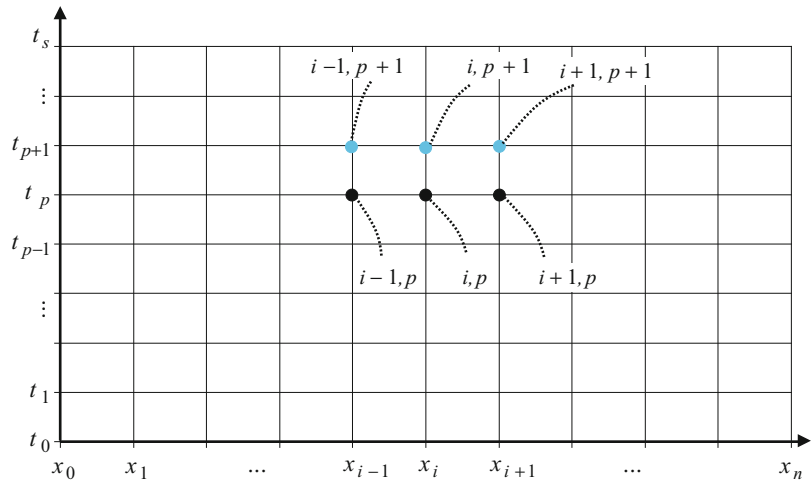
### Explicit Finite-Difference Method for Solving Transient Heat Conduction Problems,

**Fig. 2** 2D nodal network with internal node  $i, j$  and temperature distribution in direction  $x$



### Explicit Finite-Difference Method for Solving Transient Heat Conduction Problems,

**Fig. 3** Discretization for heat conduction equation in one-dimensional heat conduction



$$\frac{\partial T}{\partial x} \Big|_{i-1/2,j} \approx \frac{T_{i,j} - T_{i-1,j}}{\Delta x} \quad (11)$$

From above (10), (11), and (12), the second derivate can be expressed as

and the second derivate:

$$\frac{\partial^2 T}{\partial x^2} \Big|_{i,j} \approx \frac{\frac{\partial T}{\partial x} \Big|_{i+1/2,j} - \frac{\partial T}{\partial x} \Big|_{i-1/2,j}}{\Delta x} \quad (12)$$

$$\frac{\partial^2 T}{\partial x^2} \Big|_{i,j} \approx \frac{T_{i+1,j} + T_{i-1,j} - 2 \cdot T_{i,j}}{(\Delta x)^2} \quad (13)$$

In analogy,

$$\frac{\partial^2 T}{\partial y^2} \Big|_{i,j} \approx \frac{\frac{\partial T}{\partial y} \Big|_{i,j+1/2} - \frac{\partial T}{\partial y} \Big|_{i,j-1/2}}{\Delta y} \quad (14)$$

and

$$\frac{\partial^2 T}{\partial y^2} \Big|_{i,j} \approx \frac{T_{i,j+1} + T_{i,j-1} - 2 \cdot T_{i,j}}{(\Delta y)^2} \quad (15)$$

The heat conduction process is a transient one and must be discretized additionally in time. The time derivative is approximated by

$$\frac{\partial T}{\partial t} \Big|_{i,j} \approx \frac{T_{i,j}^{p+1} - T_{i,j}^p}{\Delta t} \quad (16)$$

The superscript  $p + 1$  describes the temperature value after a time increment  $\Delta t$  from the time point  $p$ .

Calculations must be performed at successive times separated by the interval  $\Delta t$ , and the temperature determination depends on discrete points in space and in time. The specific time, at which the temperatures are evaluated, influences on the finite-difference solution. The temperatures can be evaluated [2]:

- At the previous time ( $p$ )
- At the new time ( $p + 1$ )

In two-dimensional system with constant thermal conductivity and without energy generation, equation  $\frac{\partial^2 T}{\partial x^2} + \frac{\partial^2 T}{\partial y^2} = \frac{1}{\kappa} \frac{\partial T}{\partial t}$  reduces to

(a) At the previous time ( $p$ ),

$$\begin{aligned} & \frac{T_{i+1,j}^p + T_{i-1,j}^p - 2 \cdot T_{i,j}^p}{(\Delta x)^2} \\ & + \frac{T_{i,j+1}^p + T_{i,j-1}^p - 2 \cdot T_{i,j}^p}{(\Delta y)^2} \\ & = \frac{1}{\kappa} \frac{T_{i,j}^{p+1} - T_{i,j}^p}{\Delta t} \end{aligned} \quad (17)$$

(b) At the new time ( $p + 1$ ),

$$\begin{aligned} & \frac{T_{i+1,j}^{p+1} + T_{i-1,j}^{p+1} - 2 \cdot T_{i,j}^{p+1}}{(\Delta x)^2} \\ & + \frac{T_{i,j+1}^{p+1} + T_{i,j-1}^{p+1} - 2 \cdot T_{i,j}^{p+1}}{(\Delta y)^2} \\ & = \frac{1}{\kappa} \frac{T_{i,j}^{p+1} - T_{i,j}^p}{\Delta t} \end{aligned} \quad (18)$$

Having the grid specified, the finite-difference solutions of differential equations are obtained by discretizing the continuous solution domain. The exact derivatives in the differential equation are replaced by finite-difference approximations. Such approximations are called finite-difference equations.

The solution could be found, and the explicit method can be used based on the information from the defined boundary and initial conditions. Those conditions should also be discretized.

## Discretization of the Boundary Condition

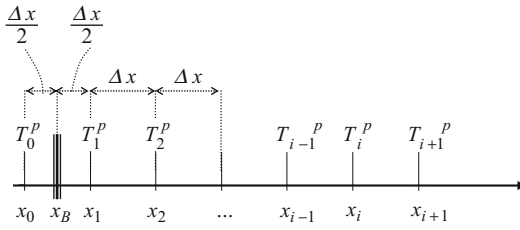
In one-dimensional system, (4) can be solved if the two boundary conditions in  $x$ , direction in the region  $x_0 \leq x \leq x_n$ , and one initial condition for times  $t \geq t_0$  are known. The boundary conditions are defined mainly as boundary temperatures or as a known heat flux at the body boundary. The initial condition is specified as the initial temperature distribution for each node:  $T(x)$  for  $t = t_0$ .

## Boundary Temperatures in One-Dimensional Coordinate System

If the temperatures at boundaries  $x_0$  and  $x_n$  are given, then the grid division should be chosen in such a way that the boundary coincides with a grid line  $x_i = \text{const}$ . The left-hand boundary is then  $x_{B1} = x_0$  with the right-hand boundary  $x_{B2} = x_{n+1} = x_0 + (n + 1) \Delta x$ . The given temperatures  $T(x_{B1}, t_p)$  and  $T(x_{B2}, t_p)$  are used as the temperature value  $T_0^p$  or  $T_{n+1}^p$  in (17).

## Boundary Heat Flux in One-Dimensional Coordinate System

With a given heat flux  $q(t)$ , the condition  $-k \frac{\partial T}{\partial n} \Big|_{x=x_B} = q(t)$  has to be satisfied at the boundary. The derivative must be formed in the outward normal direction, and the heat flux  $q$  is positive if it flows in this direction. The grid is established in such a way that the boundary lies between two grid lines [1]. Boundary condition is shown in Fig. 4.



**Explicit Finite-Difference Method for Solving Transient Heat Conduction Problems, Fig. 4** Boundary condition introduced by means of temperature outside the body (left-hand boundary condition)

The local derivative  $-k \frac{\partial T}{\partial n} |_{x=x_B}$  is replaced by the central difference quotient:

$$\frac{\partial T}{\partial x} \Big|_{\frac{\Delta x}{2}} = \frac{T_1^p - T_0^p}{\Delta x} + O(\Delta x^2) \quad (19)$$

Then the equation  $-k \frac{\partial T}{\partial n} |_{x=x_B} = q(t)$  can be written as

$$\frac{T_1^p - T_0^p}{\Delta x} = \frac{q(t)}{k} \quad (20)$$

and

$$T_0^p = T_1^p - \frac{\Delta x}{k} q(t) \quad (21)$$

Calculating  $T_0^p$  from (17) for  $i = 1$ ,

$$T_1^{p+1} = Fo (T_2^p + T_0^p) + (1 - 2 \cdot Fo) T_1^p \quad (22)$$

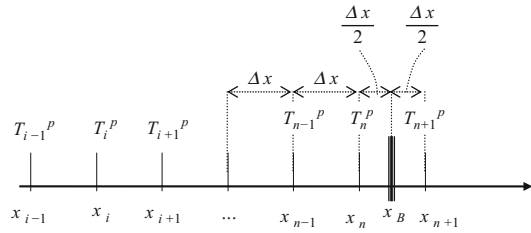
$$T_0^p = \frac{T_1^{p+1} - (1 - 2 \cdot Fo) T_1^p}{Fo} - T_2^p \quad (23)$$

where  $Fo$  is a Fourier number of the difference method and

$$Fo = \frac{\kappa \Delta t}{(\Delta x)^2}$$

Comparing (21) and (23), the  $T_1^{p+1}$  can be calculated:

$$T_1^p - \frac{\Delta x}{k} q(t) = \frac{T_1^{p+1} - (1 - 2 \cdot Fo) T_1^p}{Fo} - T_2^p \quad (24)$$



**Explicit Finite-Difference Method for Solving Transient Heat Conduction Problems, Fig. 5** Boundary condition introduced by means of temperature outside the body (right-hand boundary condition)

$$T_1^{p+1} = Fo T_1^p + (1 - 2 \cdot Fo) T_1^p + Fo T_2^p - Fo \frac{\Delta x}{k} q(t) \quad (25)$$

$$T_1^{p+1} = (1 - Fo) T_1^p + Fo T_2^p - Fo \frac{\Delta x}{k} q(t) \quad (26)$$

Equation (26) is the left-hand boundary condition.

The right-hand boundary condition is designed in Fig. 5.

The temperature  $T_{n+1}^p$  is calculated from the difference equation and from the boundary condition. The right-hand boundary condition is expressed as

$$T_n^{p+1} = Fo T_{n-1}^p + (1 - Fo) T_n^p + Fo \frac{\Delta x}{k} q(t) \quad (27)$$

If the heat is transferred at the boundary to a fluid at temperature  $T_f$  where the heat transfer coefficient  $h$  is given, then the heat transfer condition is

$$-k \frac{\partial T}{\partial n} |_{x=x_B} = h (T - T_f) \quad (28)$$

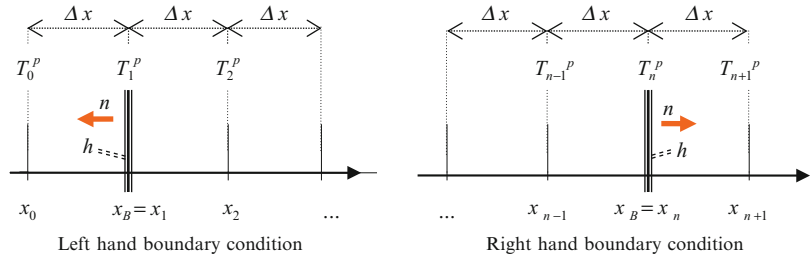
For the discretization, it is most convenient if the boundary coincides with a grid line, see Fig. 6:

The temperatures  $T_0^p$  and  $T_{n+1}^p$  which are in conjunction to the boundary condition can be eliminated from the difference equations.



### Explicit Finite-Difference Method for Solving Transient Heat Conduction Problems,

**Fig. 6** Heat transfer condition with heat transfer coefficient



At the left-hand boundary, the outward normal to the surface points in the negative  $x$  direction, then

$$\frac{\partial T}{\partial x} \Big|_{x=x_B=x_1} = \frac{h}{k} (T_1^p - T_f^p) \quad (29)$$

and

$$\begin{aligned} \frac{\partial T}{\partial x} \Big|_{x_1} &= \frac{T_2^p - T_0^p}{2 \cdot \Delta x} + O(\Delta x^2) \\ &= \frac{h}{k} (T_1^p - T_f^p) \end{aligned} \quad (30)$$

$$T_0^p = T_2^p - 2 \cdot \Delta x \frac{h}{k} (T_1^p - T_f^p) \quad (31)$$

If  $Bi = \frac{h \Delta x}{k}$ , Biot number of the finite-difference method, then

$$T_0^p = T_2^p - 2 \cdot Bi (T_1^p - T_f^p) \quad (32)$$

Using (32) and (17) for  $i = 1$ , (17) for  $i = 1$  gives (23), the temperature  $T_0^p$  can be eliminated, and the boundary condition:

$$\begin{aligned} T_1^{p+1} &= [1 - 2 \cdot Fo (1 + Bi)] T_1^p \\ &\quad + 2 \cdot Fo T_2^p + 2Fo \cdot Bi T_f^p \end{aligned} \quad (33)$$

At the right boundary, the boundary condition:

$$-\frac{\partial T}{\partial x} \Big|_{x=x_B=x_n} = -\frac{h}{k} (T_n^p - T_f^p) \quad (34)$$

Replacing with the central difference quotient:

$$\begin{aligned} -\frac{\partial T}{\partial x} \Big|_{x_n} &= -\frac{T_{n+1}^p - T_{n-1}^p}{2 \cdot \Delta x} + O(\Delta x^2) \\ &= \frac{h}{k} (T_n^p - T_f^p) \end{aligned} \quad (35)$$

$$T_{n+1}^p = T_{n-1}^p - 2 \cdot \Delta x \frac{h}{k} (T_n^p - T_f^p) \quad (36)$$

$$T_{n+1}^p = T_{n-1}^p - 2 \cdot Bi (T_n^p - T_f^p) \quad (37)$$

From (37) and (17) for  $i = n$  gives

$$T_n^{p+1} = Fo (T_{n+1}^p + T_{n-1}^p) + (1 - 2 \cdot Fo) T_n^p \quad (38)$$

the boundary conditions

$$\begin{aligned} T_n^{p+1} &= Fo \cdot [T_{n-1}^p - 2 \cdot Bi (T_n^p - T_f^p)] \\ &\quad + (1 - 2 \cdot Fo) T_n^p + Fo \cdot T_{n+1}^p \end{aligned} \quad (39)$$

and

$$\begin{aligned} T_n^{p+1} &= 2 \cdot Fo T_{n-1}^p + [1 - 2 \cdot Fo (1 + Bi)] T_n^p \\ &\quad + 2Fo \cdot Bi T_f^p \end{aligned} \quad (40)$$

To guarantee the stability, the coefficients in (33) or (40) must be positive:

$$1 - 2 \cdot Fo (1 + Bi) \geq 0 \quad (41)$$

It leads to the condition

$$Fo \leq \frac{1}{2 \cdot (1 + Bi)} \quad (42)$$

Having chosen the step  $\Delta x$ , the time step  $\Delta t$  can be calculated from (42).

## Explicit Finite-Difference Method

Equation (17) is developed on the basis of forward-difference method to the time derivative.

For a mesh, in which  $\Delta x = \text{const}$ ,  $\Delta y = \text{const}$ , and  $\Delta x = \Delta y$ , (17) can be written as

$$\begin{aligned} & T_{i+1,j}^p + T_{i-1,j}^p - 2 \cdot T_{i,j}^p + T_{i,j+1}^p \\ & + T_{i,j-1}^p - 2 \cdot T_{i,j}^p \\ & = \frac{(\Delta x)^2}{\kappa} \frac{T_{i,j}^{p+1} - T_{i,j}^p}{\Delta t} \end{aligned} \quad (43)$$

Introducing Fourier number of the difference method,

$$Fo = \frac{\kappa \Delta t}{(\Delta x)^2} \quad (44)$$

The explicit form of the finite-difference equation for an interior node  $i, j$  in 2D coordinate system reduces to

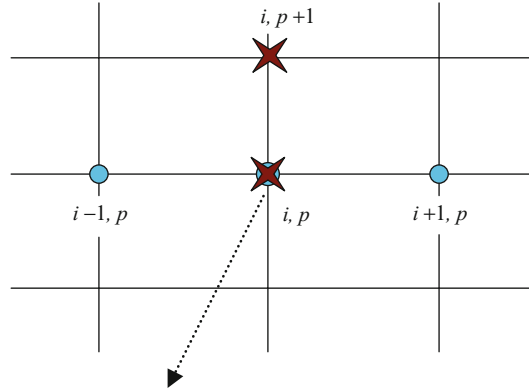
$$\begin{aligned} T_{i,j}^{p+1} = Fo \cdot (T_{i+1,j}^p + T_{i-1,j}^p - 4 \cdot T_{i,j}^p \\ + T_{i,j+1}^p + T_{i,j-1}^p) + T_{i,j}^p \end{aligned} \quad (45)$$

or



$$\begin{aligned} T_{i,j}^{p+1} = Fo \cdot (T_{i+1,j}^p + T_{i-1,j}^p + T_{i,j+1}^p \\ + T_{i,j-1}^p) + (1 - 4 \cdot Fo) T_{i,j}^p \end{aligned} \quad (46)$$

The temperature of the node at point  $i, j, p+1$  (at time level  $p+1$ ) depends only on the solution at the surrounding nodal temperatures at time level  $p$ . The expressions are called explicit methods because it is possible to specify the nodal temperatures  $T_{i,j}^{p+1}$  at each point explicitly in terms of the previous known nodal temperatures  $T_{i-1,j}^p$ ,  $T_{i,j}^p$ ,  $T_{i+1,j}^p$ ,  $T_{i,j-1}^p$ , and  $T_{i,j+1}^p$  at the neighboring points at time level  $p$ . It means that the temperature distribution at the new time can be determined if the complete temperature distribution at time  $t_p$  is known. The calculation proceeds directly from one time increment to the next until the temperature distribution is calculated at the desired final state.

For one-dimensional system at the previous time  $p$ , the differential equation  $\frac{\partial^2 T}{\partial x^2} = \frac{1}{\kappa} \frac{\partial T}{\partial t}$  reduces to



common point for time and space difference

 point involved in time difference  
 point involved in space difference

**Explicit Finite-Difference Method for Solving Transient Heat Conduction Problems, Fig. 7** Grid points for explicit form

$$\begin{aligned} & \frac{T_{i+1}^p + T_{i-1}^p - 2 \cdot T_i^p}{(\Delta x)^2} \\ & = \frac{1}{\kappa} \frac{T_i^{p+1} - T_i^p}{\Delta t} \end{aligned} \quad (47)$$

and

$$T_i^{p+1} = Fo \cdot (T_{i+1}^p + T_{i-1}^p) + (1 - 2 \cdot Fo) T_i^p \quad (48)$$

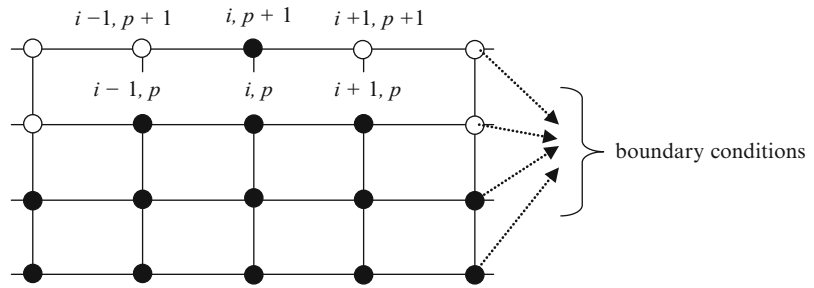
Equation (48) has only a single unknown  $T_i^{p+1}$  and allows calculating explicitly the temperatures  $T_i^{p+1}$  of the next time level  $t_{p+1} = t_p + \Delta t$  from three known temperatures of the time level  $t = t_p$ :  $(T_{i+1}^p, T_i^p, T_{i-1}^p)$ . Equation (48) can be written for all the interior nodes and enables to compute values at each node for a future time, based on the present values at the node and its neighbors. The temperature distribution as a function of position at an initial time should be defined. For  $p = 0$  (that gives  $t = t_0$ ), all the temperatures  $T_i^0$  are known from the initial temperature profile.

Computational grid points for the explicit method are shown in Fig. 7:

Each finite-difference equation involves only one unknown, and the resulting equations at time level  $p+1$  are solved independently to provide

### Explicit Finite-Difference Method for Solving Transient Heat Conduction Problems,

**Fig. 8** Effect of the boundary conditions for the explicit formulation



the values of the unknowns. To solve (48) numerically, two loops are needed (one inside another). If the temperatures of internal nodes are known at  $t = 0$  (or  $p = 0$ ) from prescribed initial conditions, then the calculations begin for  $p = 1$  and interior node temperatures are calculated. Knowing the temperatures for  $p = 1$ , the next steps are repeated for the next time step and so forth. The explicit equation is often called the forward-difference equation [4].

An explicit formula provides a procedure to obtain the solution at each point, knowing the proceeding points and boundary values, but can have problems related to stability. In addition, the information that has a bearing on the solution is excluded [5]. The black nodes, illustrated in Fig. 8, have an influence on  $i, p$ , whereas the white nodes which really affect  $i, p$  are rejected.

The information at the boundaries at the same time level  $p + 1$  does not enter the computation process to find the unknowns at  $p + 1$ . The knowledge of values in white points is not required, and an explicit finite-difference formula provides the situation in which the value can be calculated if the boundary conditions are not specified at each point.

It is necessary to remember that solving the problem numerically, the small initial and rounding errors can become larger as the calculation proceeds, which can even lead to false results. The discretization error goes to zero with a reduction in the mesh size  $\Delta x$  and the time step  $\Delta t$ . A reduction in the mesh size increases the number of grid points and therefore the accuracy of the approximation, although a reduction also increases the computation demands. Applying a finite-difference method, a compromise between accuracy and computation time is made. Because the

temperature determination is also of the time variable nature, the stability of the solution using presented explicit method should be examined.

### Accuracy and Stability Condition of the Finite-Difference Method

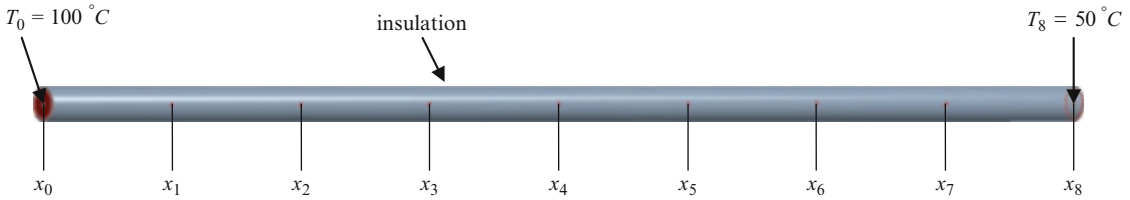
The solution of the explicit equation should be stable, convergent, and without numerically induced oscillations. Stability means that errors at any stage of the computation do not grow with the solution of the finite-difference equation. Convergence means that as  $\Delta x$  and  $\Delta t$  approach zero, the results of the finite-difference method approach the true solution of the partial differential equation. To prevent the situation in which oscillations appear, a limitation on the size of the time step  $\Delta t$  should be maintained below a certain limit. The limit depends on  $\Delta x$  and other parameters that form a stability criterion. A general condition for stability of explicit difference formulae in two-dimensional system is the requirement that no coefficient in (46) is negative, which means the coefficient  $(1 - 4 \cdot Fo)$  is greater than or equal to zero. In one-dimensional system, that requirement is applied to (48) for coefficient  $(1 - 2 \cdot Fo)$ . Otherwise, the oscillations in the solution occur.

This means that the stability criterion for a two-dimensional node is

$$(1 - 4 \cdot Fo) \geq 0 \quad (49)$$

that gives

$$Fo \leq \frac{1}{4} \quad (50)$$



**Explicit Finite-Difference Method for Solving Transient Heat Conduction Problems, Fig. 9** A long thin rod

For a one-dimensional interior node is

$$(1 - 2 \cdot Fo) \geq 0 \quad (51)$$

and

$$Fo \leq \frac{1}{2} \quad (52)$$

Above equations indicate that difference equations are only conditionally stable. They are stable for certain step or mesh size for which the Fourier number satisfies the condition for two-dimensional heat conduction

$$Fo = \frac{\kappa \Delta t}{(\Delta x)^2} \leq \frac{1}{4} \quad (53)$$

and for one-dimensional heat conduction

$$Fo = \frac{\kappa \Delta t}{(\Delta x)^2} \leq \frac{1}{2} \quad (54)$$

To eliminate the oscillations, the time steps are sufficiently small, which requires more computation time. Also to increase solution accuracy by using smaller values of  $\Delta x$ , the smaller time steps should be used according to (53) or (54). That also increases the computation time. In practice, the time step  $\Delta t$  will be set to a value somewhat smaller than that prescribed by (53) or (54) [6].

For a given value of space increment  $\Delta x$  and given value of  $\kappa$ , the upper limit of time interval  $\Delta t$  should be calculated from (53) or (54) to make the process accurate and compatible with stability requirements. The solution proceeds more rapidly for larger values of  $\Delta x$  or  $\Delta t$ . On the other hand, the smaller the value of these increments in the independent variables, the

more accuracy will be obtained. But the small distance increments cannot be used for greater accuracy in combination with large time increments to speed the solution because the finite-difference equation limits the values of  $\Delta t$  which may be used once  $\Delta x$  is chosen. For example, if  $\Delta x$  is halved to improve the approximation, then the time step in one-dimensional system must be quartered to maintain convergence and stability. A compromise between the accuracy and computational requirements must be defined because increasing the number of nodes or decreasing the time interval, the calculation time increases.

**Example.** A long thin rod of 16 cm has the temperature of 10 °C. The rod is made of aluminum alloy and has material thermal conductivity  $k = 170 \frac{\text{W}}{\text{m}\cdot\text{K}}$ , specific heat  $c_p = 880 \frac{\text{J}}{\text{kg}\cdot\text{K}}$ , and density  $\rho = 2780 \frac{\text{kg}}{\text{m}^3}$ . The rod surface is isolated except at its ends. Suddenly, the rod ends are set at different fix temperatures of 100 °C and 50 °C.

- Determine how the temperature changes through the rod at various time using the explicit method.
- Show what happens when  $Fo > \frac{1}{2}$ .
- Calculate the temperature changes when  $Fo = \frac{1}{2}$ .

**Solution**

Because the rod is thin and isolated, the heat is distributed evenly over its cross section without lateral heat flow.

The space increment  $\Delta x$  is chosen to be  $\Delta x = 2 \text{ cm}$  (Fig. 9).

Then, from Fourier number  $Fo = \frac{\kappa \Delta t}{(\Delta x)^2} \leq \frac{1}{2}$ , the time step  $\Delta t$  is calculated. The thermal diffusivity is found from equation  $\kappa = \frac{k}{\rho c_p}$ :

$$\kappa = \frac{k}{\rho c_p} = \frac{170}{2780 \cdot 880} \frac{m^2}{s} = 0.0000695 \frac{m^2}{s}$$

Answer (A)

For  $Fo = 0.1$ :

$$\Delta t = \frac{Fo (\Delta x)^2}{\kappa} = \frac{0.1 \cdot 0.02^2}{0.0000695} s = 0.5756 s$$

Using the equation  $T_i^{p+1} = Fo \cdot (T_{i+1}^p + T_{i-1}^p) + (1 - 2 \cdot Fo) T_i^p$ , the temperature can be calculated.

At  $x_1 = 0.02 m$  and  $t_1 = 0.5756 s$ , the temperatures are  $T_0^0 = 100^\circ C$ ,  $T_1^0 = 10^\circ C$ , and  $T_2^0 = 10^\circ C$ ; then

$$T_1^1 = [0.1 \cdot (10 + 100) + (1 - 2 \cdot 0.1) \cdot 10]^\circ C = 19.0^\circ C$$

At the other nodes:

$$x_2 = 0.04 m$$

$$T_2^1 = [0.1 \cdot (10 + 10) + (1 - 2 \cdot 0.1) \cdot 10]^\circ C = 10.0^\circ C$$

$$x_3 = 0.06 m$$

$$T_3^1 = [0.1 \cdot (10 + 10) + (1 - 2 \cdot 0.1) \cdot 10]^\circ C = 10.0^\circ C$$

$$x_4 = 0.08 m$$

$$T_4^1 = [0.1 \cdot (10 + 10) + (1 - 2 \cdot 0.1) \cdot 10]^\circ C = 10.0^\circ C$$

$$x_5 = 0.10 m$$

$$T_5^1 = [0.1 \cdot (10 + 10) + (1 - 2 \cdot 0.1) \cdot 10]^\circ C = 10.0^\circ C$$

$$x_6 = 0.12 m$$

$$T_6^1 = [0.1 \cdot (10 + 10) + (1 - 2 \cdot 0.1) \cdot 10]^\circ C = 10.0^\circ C$$

$$x_7 = 0.14 m$$

$$T_7^1 = [0.1 \cdot (50 + 10) + (1 - 2 \cdot 0.1) \cdot 10]^\circ C = 14.0^\circ C$$

At  $t_2 = 2 \Delta t = 2 \cdot 0.5756 s = 1.1512 s$ :

$$T_1^2 = [0.1 \cdot (10 + 100) + (1 - 2 \cdot 0.1) \cdot 19]^\circ C = 26.2^\circ C$$

$$T_2^2 = [0.1 \cdot (10 + 19) + (1 - 2 \cdot 0.1) \cdot 10]^\circ C = 10.9^\circ C$$

$$T_3^2 = [0.1 \cdot (10 + 10) + (1 - 2 \cdot 0.1) \cdot 10]^\circ C = 10.0^\circ C$$

$$T_4^2 = [0.1 \cdot (10 + 10) + (1 - 2 \cdot 0.1) \cdot 10]^\circ C = 10.0^\circ C$$

$$T_5^2 = [0.1 \cdot (10 + 10) + (1 - 2 \cdot 0.1) \cdot 10]^\circ C = 10.0^\circ C$$

$$T_6^2 = [0.1 \cdot (14 + 10) + (1 - 2 \cdot 0.1) \cdot 10]^\circ C = 10.4^\circ C$$

$$T_7^2 = [0.1 \cdot (50 + 10) + (1 - 2 \cdot 0.1) \cdot 14]^\circ C = 17.2^\circ C$$

The grid used for calculation and the values of temperature with initial and boundary conditions are given in [Fig. 10](#):

The computation continues and the results are presented in [Table 1](#) and in [Fig. 11](#):

Answer (B)

For  $Fo = 1$ :

$$\Delta t = \frac{Fo (\Delta x)^2}{\kappa} = \frac{1 \cdot 0.02^2}{0.0000695} s = 5.755 s$$

Using the equation  $T_i^{p+1} = Fo \cdot (T_{i+1}^p + T_{i-1}^p) + (1 - 2 \cdot Fo) T_i^p$ , the temperature can be calculated in the similar way.

At  $x_1 = 0.02 m$  and  $t_1 = 5.755 s$ :

$$T_1^1 = [1 \cdot (10 + 100) + (1 - 2 \cdot 1) \cdot 10]^\circ C = 100.0^\circ C$$

At  $x_2 = 0.04 m$  and  $t_1 = 5.755 s$ :

$$T_2^1 = [1 \cdot (10 + 10) + (1 - 2 \cdot 1) \cdot 10]^\circ C = 10.0^\circ C$$

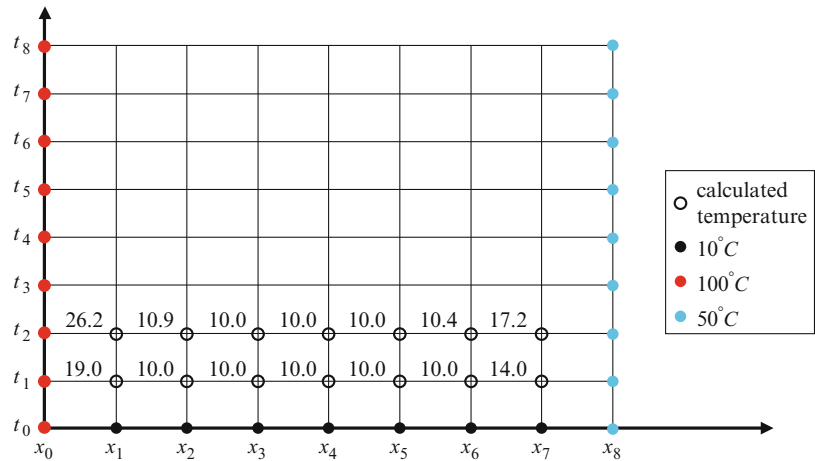
At  $x_3 = 0.06 m$  and  $t_1 = 5.755 s$ :

$$T_3^1 = [1 \cdot (10 + 10) + (1 - 2 \cdot 1) \cdot 10]^\circ C = 10.0^\circ C$$

At  $x_4 = 0.08 m$  and  $t_1 = 5.755 s$ :

$$T_4^1 = [1 \cdot (10 + 10) + (1 - 2 \cdot 1) \cdot 10]^\circ C = 10.0^\circ C$$

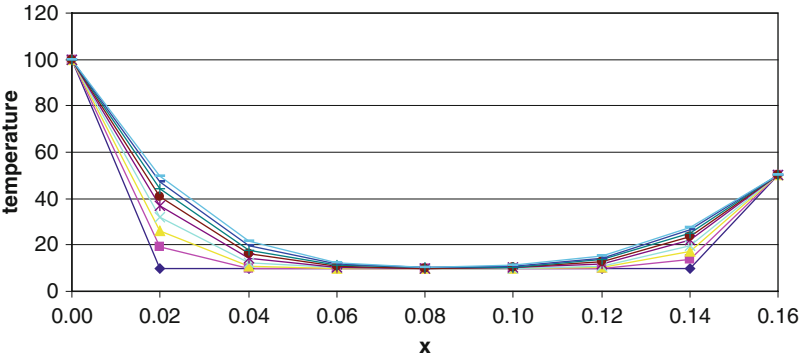
**Explicit Finite-Difference Method for Solving Transient Heat Conduction Problems, Fig. 10** Grid for given example with temperature values at  $t_1 = 0.5756\text{ s}$  and  $t_2 = 1.1512\text{ s}$  (explicit method)



**Explicit Finite-Difference Method for Solving Transient Heat Conduction Problems, Table 1** Temperature value in a long thin rod at different nodes for  $Fo = 0.1$  (explicit method)

		Temperature in nodes								
Time		$T_0$	$T_1$	$T_2$	$T_3$	$T_4$	$T_5$	$T_6$	$T_7$	$T_8$
$t = 0$	$p = 0$	100	10.0	10.0	10.0	10.0	10.0	10.0	10.0	50
$t = 0.5756$	$p = 1$	100	19.0	10.0	10.0	10.0	10.0	10.0	14.0	50
$t = 1.1512$	$p = 2$	100	26.2	10.9	10.0	10.0	10.0	10.4	17.2	50
$t = 1.7268$	$p = 3$	100	32.1	12.3	10.1	10.0	10.0	11.0	19.8	50
$t = 2.3024$	$p = 4$	100	36.9	14.1	10.3	10.0	10.1	11.8	21.9	50
$t = 2.8780$	$p = 5$	100	40.9	16.0	10.7	10.1	10.3	12.7	23.7	50
$t = 3.4536$	$p = 6$	100	44.3	17.9	11.1	10.1	10.5	13.5	25.3	50
$t = 4.0292$	$p = 7$	100	47.3	19.9	11.7	10.3	10.8	14.4	26.6	50
$t = 4.6048$	$p = 8$	100	49.8	21.8	12.4	10.5	11.1	15.3	27.7	50

**Explicit Finite-Difference Method for Solving Transient Heat Conduction Problems, Fig. 11** Temperature distribution at time in a long thin rod for  $Fo = 0.1$  (explicit method)



**Explicit Finite-Difference Method for Solving Transient Heat Conduction Problems, Table 2** Temperature value in a long thin rod at different nodes for  $Fo = 1$  (explicit method)

		Temperature in nodes								
Time		$T_0$	$T_1$	$T_2$	$T_3$	$T_4$	$T_5$	$T_6$	$T_7$	$T_8$
$t = 0$	$p = 0$	100	10	10	10	10	10	10	10	50
$t = 5.755$	$p = 1$	100	100	10	10	10	10	10	50	50
$t = 11.510$	$p = 2$	100	10	100	10	10	10	50	10	50
$t = 17.265$	$p = 3$	100	190	-80	100	10	50	-30	90	50
$t = 23.020$	$p = 4$	100	-170	370	-170	140	-70	170	-70	50
$t = 28.775$	$p = 5$	100	640	-710	680	-380	380	-310	290	50
$t = 34.530$	$p = 6$	100	-1,250	2,030	-1,770	1,440	-1,070	980	-550	50
$t = 40.285$	$p = 7$	100	3,380	-5,050	5,240	-4,280	3,490	-2,600	1,580	50
$t = 46.040$	$p = 8$	100	-8,330	13,670	-14,570	13,010	-10,370	7,670	-4,130	50

At  $x_5 = 0.10m$  and  $t_1 = 5.755s$ :

$$T_5^1 = [1 \cdot (10 + 10) + (1 - 2 \cdot 1) \cdot 10]^\circ\text{C} = 10.0^\circ\text{C}$$

At  $x_6 = 0.12m$  and  $t_1 = 5.755s$ :

$$T_6^1 = [1 \cdot (10 + 10) + (1 - 2 \cdot 1) \cdot 10]^\circ\text{C} = 10.0^\circ\text{C}$$

At  $x_7 = 0.14m$  and  $t_1 = 5.755s$ :

$$T_7^1 = [1 \cdot (50 + 10) + (1 - 2 \cdot 1) \cdot 10]^\circ\text{C} = 50.0^\circ\text{C}$$

At  $t_2 = 2\Delta t = 2 \cdot 5.755s = 11.510s$ :

$$T_1^2 = [1 \cdot (10 + 100) + (1 - 2 \cdot 1) \cdot 100]^\circ\text{C} = 10.0^\circ\text{C}$$

$$T_2^2 = [1 \cdot (10 + 100) + (1 - 2 \cdot 1) \cdot 10]^\circ\text{C} = 100.0^\circ\text{C}$$

$$T_3^2 = [1 \cdot (10 + 10) + (1 - 2 \cdot 1) \cdot 10]^\circ\text{C} = 10.0^\circ\text{C}$$

$$T_4^2 = [1 \cdot (10 + 10) + (1 - 2 \cdot 1) \cdot 10]^\circ\text{C} = 10.0^\circ\text{C}$$

$$T_5^2 = [1 \cdot (10 + 10) + (1 - 2 \cdot 1) \cdot 10]^\circ\text{C} = 10.0^\circ\text{C}$$

$$T_6^2 = [1 \cdot (50 + 10) + (1 - 2 \cdot 1) \cdot 10]^\circ\text{C} = 50.0^\circ\text{C}$$

$$T_7^2 = [1 \cdot (50 + 10) + (1 - 2 \cdot 1) \cdot 50]^\circ\text{C} = 10.0^\circ\text{C}$$

At  $t_3 = 3\Delta t = 3 \cdot 5.755s = 17.265s$ :

$$T_1^3 = [1 \cdot (100 + 100) + (1 - 2 \cdot 1) \cdot 10]^\circ\text{C} = 190.0^\circ\text{C}$$

$$T_2^3 = [1 \cdot (10 + 10) + (1 - 2 \cdot 1) \cdot 100]^\circ\text{C} = -80.0^\circ\text{C}$$

$$T_3^3 = [1 \cdot (10 + 100) + (1 - 2 \cdot 1) \cdot 10]^\circ\text{C} = 100.0^\circ\text{C}$$

$$T_4^3 = [1 \cdot (10 + 10) + (1 - 2 \cdot 1) \cdot 10]^\circ\text{C} = 10.0^\circ\text{C}$$

$$T_5^3 = [1 \cdot (50 + 10) + (1 - 2 \cdot 1) \cdot 10]^\circ\text{C} = 50.0^\circ\text{C}$$

$$T_6^3 = [1 \cdot (10 + 10) + (1 - 2 \cdot 1) \cdot 50]^\circ\text{C} = -30.0^\circ\text{C}$$

$$T_7^3 = [1 \cdot (50 + 50) + (1 - 2 \cdot 1) \cdot 10]^\circ\text{C} = 90.0^\circ\text{C}$$

At  $t_4 = 4\Delta t = 4 \cdot 5.755s = 23.020s$ :

$$T_1^4 = [1 \cdot (-80 + 100) + (1 - 2 \cdot 1) \cdot 190]^\circ\text{C} \\ = -170.0^\circ\text{C}$$

$$T_2^4 = [1 \cdot (100 + 190) + (1 - 2 \cdot 1) \cdot (-80)]^\circ\text{C} \\ = 370.0^\circ\text{C}$$

$$T_3^4 = [1 \cdot (10 - 80) + (1 - 2 \cdot 1) \cdot 100]^\circ\text{C} \\ = -170.0^\circ\text{C}$$

$$T_4^4 = [1 \cdot (50 + 100) + (1 - 2 \cdot 1) \cdot 10]^\circ\text{C} \\ = 140.0^\circ\text{C}$$

$$T_5^4 = [1 \cdot (-30 + 10) + (1 - 2 \cdot 1) \cdot 50]^\circ\text{C} \\ = -70.0^\circ\text{C}$$

$$T_6^4 = [1 \cdot (90 + 50) + (1 - 2 \cdot 1) \cdot (-30)]^\circ\text{C} \\ = 170.0^\circ\text{C}$$

$$T_7^4 = [1 \cdot (50 - 30) + (1 - 2 \cdot 1) \cdot 90]^\circ\text{C} \\ = -70.0^\circ\text{C}$$

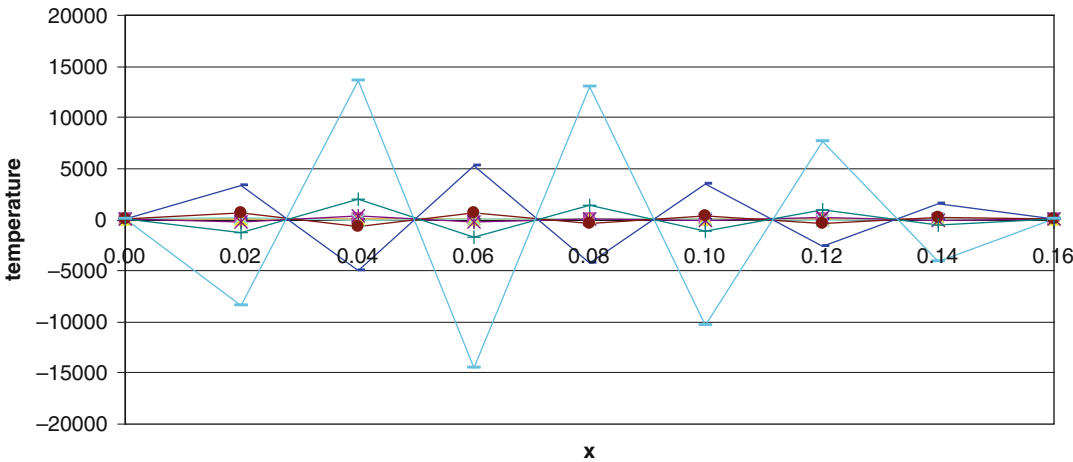
Calculations carry on and the outcomes are shown in [Table 2](#) and in [Fig. 12](#):

Answer (C)

For  $Fo = \frac{1}{2}$ :

$$\Delta t = \frac{Fo(\Delta x)^2}{\kappa} = \frac{\frac{1}{2} \cdot 0.02^2}{0.0000695} s = 2.878 s$$

Using the equation  $T_i^{p+1} = Fo \cdot (T_{i+1}^p + T_{i-1}^p) + (1 - 2 \cdot Fo) T_i^p$ , the temperature can be calculated in the similar way.



**Explicit Finite-Difference Method for Solving Transient Heat Conduction Problems, Fig. 12** Temperature distribution at time in a long thin rod for  $Fo = 1$

(explicit method). The oscillations are observed, which increase progressively

**Explicit Finite-Difference Method for Solving Transient Heat Conduction Problems, Table 3** Temperature value in a long thin rod at different nodes for  $Fo = \frac{1}{2}$  (explicit method)

		Temperature in nodes								
Time		$T_0$	$T_1$	$T_2$	$T_3$	$T_4$	$T_5$	$T_6$	$T_7$	$T_8$
t = 0	p = 0	100	10.0	10.0	10.0	10.0	10.0	10.0	10.0	50
t = 2.878	p = 1	100	55.0	10.0	10.0	10.0	10.0	10.0	30.0	50
t = 5.756	p = 2	100	55.0	32.5	10.0	10.0	10.0	20.0	30.0	50
t = 8.634	p = 3	100	66.3	32.5	21.3	10.0	15.0	20.0	35.0	50
t = 11.512	p = 4	100	66.3	43.8	21.3	18.1	15.0	25.0	35.0	50
t = 14.390	p = 5	100	71.9	43.8	30.9	18.1	21.6	25.0	37.5	50
t = 17.268	p = 6	100	71.9	51.4	30.9	26.3	21.6	29.5	37.5	50
t = 20.146	p = 7	100	75.7	51.4	38.8	26.3	27.9	29.5	39.8	50
t = 23.024	p = 8	100	75.7	57.3	38.8	33.4	27.9	33.8	39.8	50

At  $t_1 = 2.878s$ :

$$\begin{aligned} T_1^1 &= [0.5 \cdot (10 + 100) + (1 - 2 \cdot 0.5) \cdot 10]^\circ\text{C} = 55.0^\circ\text{C} \\ T_2^1 &= [0.5 \cdot (10 + 10) + (1 - 2 \cdot 0.5) \cdot 10]^\circ\text{C} = 10.0^\circ\text{C} \\ T_3^1 &= [0.5 \cdot (10 + 10) + (1 - 2 \cdot 0.5) \cdot 10]^\circ\text{C} = 10.0^\circ\text{C} \\ T_4^1 &= [0.5 \cdot (10 + 10) + (1 - 2 \cdot 0.5) \cdot 10]^\circ\text{C} = 10.0^\circ\text{C} \\ T_5^1 &= [0.5 \cdot (10 + 10) + (1 - 2 \cdot 0.5) \cdot 10]^\circ\text{C} = 10.0^\circ\text{C} \\ T_6^1 &= [0.5 \cdot (10 + 10) + (1 - 2 \cdot 0.5) \cdot 10]^\circ\text{C} = 10.0^\circ\text{C} \\ T_7^1 &= [0.5 \cdot (50 + 10) + (1 - 2 \cdot 0.5) \cdot 10]^\circ\text{C} = 30.0^\circ\text{C} \end{aligned}$$

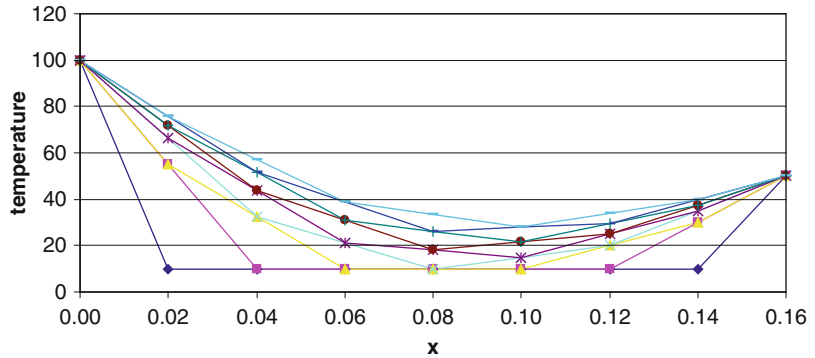
At  $t_2 = 2\Delta t = 2 \cdot 2.878s = 5.756s$ :

$$\begin{aligned} T_1^2 &= [0.5 \cdot (10 + 100) + (1 - 2 \cdot 0.5) \cdot 55]^\circ\text{C} = 55.0^\circ\text{C} \\ T_2^2 &= [0.5 \cdot (10 + 55) + (1 - 2 \cdot 0.5) \cdot 10]^\circ\text{C} = 32.5^\circ\text{C} \\ T_3^2 &= [0.5 \cdot (10 + 10) + (1 - 2 \cdot 0.5) \cdot 10]^\circ\text{C} = 10.0^\circ\text{C} \\ T_4^2 &= [0.5 \cdot (10 + 10) + (1 - 2 \cdot 0.5) \cdot 10]^\circ\text{C} = 10.0^\circ\text{C} \\ T_5^2 &= [0.5 \cdot (10 + 10) + (1 - 2 \cdot 0.5) \cdot 10]^\circ\text{C} = 10.0^\circ\text{C} \\ T_6^2 &= [0.5 \cdot (30 + 10) + (1 - 2 \cdot 0.5) \cdot 10]^\circ\text{C} = 20.0^\circ\text{C} \\ T_7^2 &= [0.5 \cdot (50 + 10) + (1 - 2 \cdot 0.5) \cdot 30]^\circ\text{C} = 30.0^\circ\text{C} \end{aligned}$$



### Explicit Finite-Difference Method for Solving Transient Heat Conduction Problems,

**Fig. 13** Temperature distribution at time in a long thin rod for  $Fo = \frac{1}{2}$  (explicit method). No oscillations



Calculations continue and the outcomes are shown in Table 3 and in Fig. 13.

### References

1. Baehr HD, Stephan K (2006) Heat and mass transfer. Springer, Heidelberg. ISBN 978-3-540-29526-6
2. Incropera FP, Dewitt DP, Bergman TL, Lavine AS (2006) Fundamentals of heat and mass transfer. Wiley, New York. ISBN 978-0-471-45728-2
3. Allaire G (2007) Numerical analysis and optimization: an introduction to mathematical modeling and numerical simulation. Oxford University Press, Oxford. ISBN 978-0-19-920521-9
4. Ames WF (1977) Numerical methods for partial differential equations. Academic, New York. ISBN 0-12-056760-1
5. Chapra SC, Canale RP (2006) Numerical methods for engineers. McGraw-Hill, Singapore. ISBN 007-124429-8
6. Kreith F, Manglik RM, Bohn MS (2011) Principles of heat transfer. Cengage Learning, Stanford. ISBN 978-0-495-66770-4

## Explicit Time Integrators and Designs for First-/Second-Order Linear Transient Systems

M. Shimada and Kumar K. Tamma  
Department of Mechanical Engineering,  
University of Minnesota, Minneapolis, MN, USA

### Overview

We first develop the predictor-corrector explicit GS4 designs of algorithms (*PCE-GS4-2 algorithms*) from the U0- and V0-family-based implicit GS4 designs of algorithms (*I-GS4-2*

*algorithms*) [1–3] in second-order systems in time. We can also adapt (*i* Integration Framework) the V0-family-based PCE-GS4-2 algorithms to obtain the PCE-GS4 algorithms in first-order systems in time (*PCE-GS4-1 algorithm*), following the similar procedures used for the adapting from the V0-family-based I-GS4-2 algorithm designs to the implicit GS4 algorithm designs in first-order systems (I-GS4-1 algorithms).

Alternatively, we also show the general explicit GS-4 algorithm designs (*E-GS4-2 algorithms*) developed for the second-order system which additionally contain the algorithm designs over and beyond the PCE-GS4-2 algorithms. The underlying reason is we relax the conditions of unconditional stability and invoke conditional stability for all explicit GS4 general structure of algorithms. The algorithmic parameters of the PCE-GS4-2 algorithms are directly employed from the I-GS4-2 algorithms, i.e., they are defined in terms of the principal and spurious roots at the high-frequency range; however, E-GS4-2 algorithm designs have been developed in terms of the principal and spurious root at the bifurcation limit.

## Linear Explicit Generalized Single-Step Single-Solve Algorithms for Second- and First-Order Systems

### Linear Predictor-Corrector Explicit Generalized Single-Step Single-Solve Algorithms

From the U0-family and V0-family I-GS4-2 algorithms, we introduce the *PCE-GS4-2 algorithms*. By making the I-GS4-2 algorithms to be

explicit, the general structure of the PCE-GS4-2 algorithms may be designed to take the following form. If the algorithmic velocity  $\hat{\mathbf{v}}$  in the balance equation does not include any information at the next time step, we call it an explicit treatment of the physical damping. Likewise, if the algorithmic velocity includes information at the next time step, we call it an implicit treatment of the physical damping.

**Algorithm 1. PCE-GS4-2 Algorithm Designs for Linear Elastodynamics**

**Predictor:**

$$\begin{aligned}\hat{\mathbf{q}} &= \mathbf{q}_n + \lambda_1 \dot{\mathbf{q}}_n \Delta t + (\lambda_2 - \lambda_3 \eta) \ddot{\mathbf{q}}_n \Delta t^2 \\ \hat{\mathbf{v}} &= \dot{\mathbf{q}}_n + (\lambda_4 - \lambda_5) \ddot{\mathbf{q}}_n \Delta t\end{aligned}$$

**Balance equation:**

$$\mathbf{M}\tilde{\mathbf{a}} + \mathbf{C}\bar{\mathbf{v}} + \mathbf{K}\bar{\mathbf{q}} = \tilde{\mathbf{f}}$$

where

$$\begin{aligned}\bar{\mathbf{q}} &= \mathbf{q}_n + \frac{W_3 \Lambda_3}{\lambda_3} (\hat{\mathbf{q}} - \mathbf{q}_n) + \left( W_1 \Lambda_1 - \frac{\lambda_1}{\lambda_3} W_3 \Lambda_3 \right) \\ &\quad \times \dot{\mathbf{q}}_n \Delta t + \left( W_2 \Lambda_2 - \frac{\lambda_2}{\lambda_3} W_3 \Lambda_3 \right) \ddot{\mathbf{q}}_n \Delta t^2 \\ \bar{\mathbf{v}} &= \dot{\mathbf{q}}_n + \frac{W_2 \Lambda_5}{\lambda_5} (\hat{\mathbf{v}} - \dot{\mathbf{q}}_n) + \left( W_1 \Lambda_4 - \frac{\lambda_4}{\lambda_5} W_2 \Lambda_5 \right) \\ &\quad \times \ddot{\mathbf{q}}_n \Delta t \\ \tilde{\mathbf{a}} &= \ddot{\mathbf{q}}_n + W_1 \Lambda_6 (\ddot{\mathbf{q}}_{n+1} - \ddot{\mathbf{q}}_n) \\ \tilde{\mathbf{f}} &= \mathbf{f}_n + W_1 (\mathbf{f}_{n+1} - \mathbf{f}_n) \text{ or } \mathbf{f}(t_{n+W_1})\end{aligned}$$

**Corrector:**

$$\begin{aligned}\mathbf{q}_{n+1} &= \hat{\mathbf{q}} + \lambda_3 \eta \ddot{\mathbf{q}}_{n+1} \Delta t^2 \\ \dot{\mathbf{q}}_{n+1} &= \hat{\mathbf{v}} + \lambda_5 \ddot{\mathbf{q}}_{n+1} \Delta t\end{aligned}$$

**Initial conditions:**

$$\begin{aligned}\mathbf{q}(t_0) &= \mathbf{q}_0 \\ \dot{\mathbf{q}}(t_0) &= \dot{\mathbf{q}}_0\end{aligned}$$

**Remark 1. (Algorithm 1)**

1. Algorithm 1 is the predictor-corrector explicit (PCE) forms of the U0-family and V0-family

I-GS4-2 algorithms, i.e., U0-family and V0-family of I-GS4-2 algorithms, respectively, with the explicit treatment of the physical damping. The algorithmic parameters for Algorithm 1 are directly employed from the U0-family and V0-family I-GS4-2 algorithms to obtain the U0-family-based PCE-GS4-2 and the V0-family-based PCE-GS4-2 algorithms, respectively.

2. If we simply take

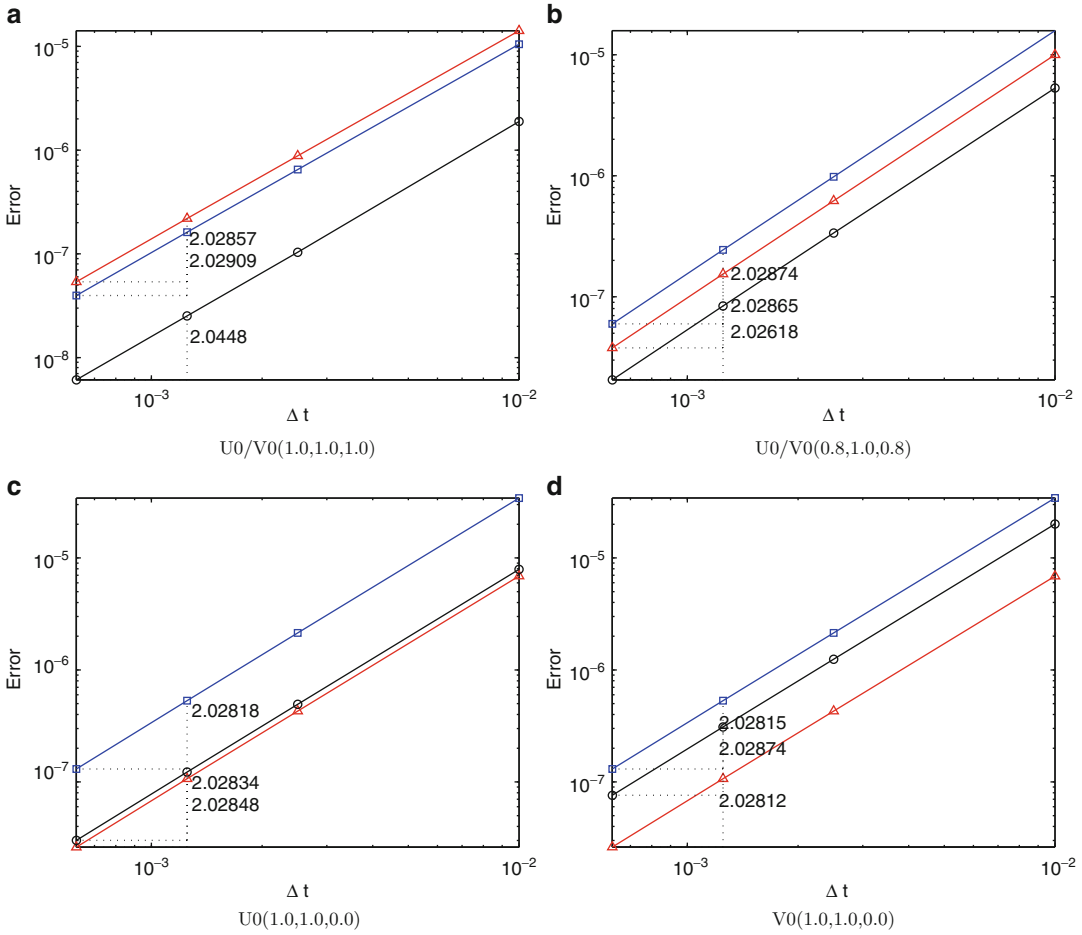
$$\begin{aligned}W_2 \Lambda_5 &= \frac{3 + \rho_\infty^{\min} + \rho_\infty^{\max} - \rho_\infty^{\min} \rho_\infty^{\max}}{2(1 + \rho_\infty^{\min})(1 + \rho_\infty^{\max})(1 + \rho_\infty^s)} \text{ in} \\ &\quad \text{the U0-family based PCE-GS4} \\ W_2 \Lambda_5 &= \frac{2}{(1 + \rho_\infty^{\min})(1 + \rho_\infty^{\max})(1 + \rho_\infty^s)} \text{ in} \\ &\quad \text{the V0-family based PCE-GS4}\end{aligned}\quad (1)$$

all members in Algorithm 1 are conditionally stable and cannot achieve second-order time accuracy. To maintain the order of time accuracy, we must impose  $\Lambda_5 = 0$ . In this case,  $\bar{\mathbf{v}}$  reduces to

$$\bar{\mathbf{v}} = \dot{\mathbf{q}}_n + W_1 \Lambda_4 \ddot{\mathbf{q}}_n \Delta t \quad (2)$$

If we treat the physical damping implicitly,  $\Lambda_5 = 0$  is not required in order to obtain the second-order time accuracy of the algorithms. That is, we can directly employ the algorithmic parameters from U0-family and V0-family I-GS4-2 algorithms for this case. See Figs. 1 and 2 for the time accuracy and stability plots of the selected algorithms within Algorithm 1.

3. When selecting  $(\rho_\infty^{\min}, \rho_\infty^{\max}, \rho_\infty^s) = (1, 1, 1)$   $\eta = 1$ , in both U0- and V0-family-based designs of Algorithm 1, we obtain an unconditionally unstable algorithm.
4. Angular momentum is exactly conserved within a time step when we select  $(\rho_\infty^{\min}, \rho_\infty^{\max}, \rho_\infty^s) = (1, 1, 0)$   $\eta = 0$ , in the V0-family-based designs of Algorithm 1.
5. Stability features tend to be improved when we selecting  $\eta = 0$ . The central difference method [4] is recovered by



**Explicit Time Integrators and Designs for First-/Second-Order Linear Transient Systems, Fig. 1** Time accuracy plots of selected algorithms within Algorithm 1

$(\rho_{\infty}^{\min}, \rho_{\infty}^{\max}, \rho_{\infty}^s) = (1, 1, 0)$  and  $\eta = 0$  in the  $U0$  family-based family of algorithms. Algorithms obtained by  $(\rho_{\infty}^{\min}, \rho_{\infty}^{\max}, \rho_{\infty}^s) = (1, 1, \rho_{\infty}^s)$ ,  $(\rho_{\infty}^{\min}, \rho_{\infty}^{\max}, \rho_{\infty}^s) = (\rho_{\infty}^{\min}, 1, 0)$ , and  $(\rho_{\infty}^{\min}, \rho_{\infty}^{\max}, \rho_{\infty}^s) = (0, 0, 0)$  have no numerical dissipation.

#### Adapting PCE-GS4-2 to PCE-GS4-1: PCE-GS4 Algorithms in the First-Order System

Following the adaptation shown below, which we term as *i* Integration (Isochronous Integration Framework), we readily obtain the PCE-GS4 algorithm designs and framework for the first-order system (PCE-GS4-1 algorithm) from  $V0$ -family-based PCE-GS4-2 algorithm designs. **For matrices:** ( $V0$ -family-based PCE-GS4-2  $\rightarrow$  PCE-GS4-1)

$$\mathbf{M} \rightarrow \mathbf{M}, \quad \mathbf{C} \rightarrow \mathbf{K}, \quad \text{and} \quad \mathbf{K} \rightarrow 0 \quad (3)$$

**For  $\mathbf{f}$ :** ( $V0$ -family-based PCE-GS4-2  $\rightarrow$  PCE-GS4-1)

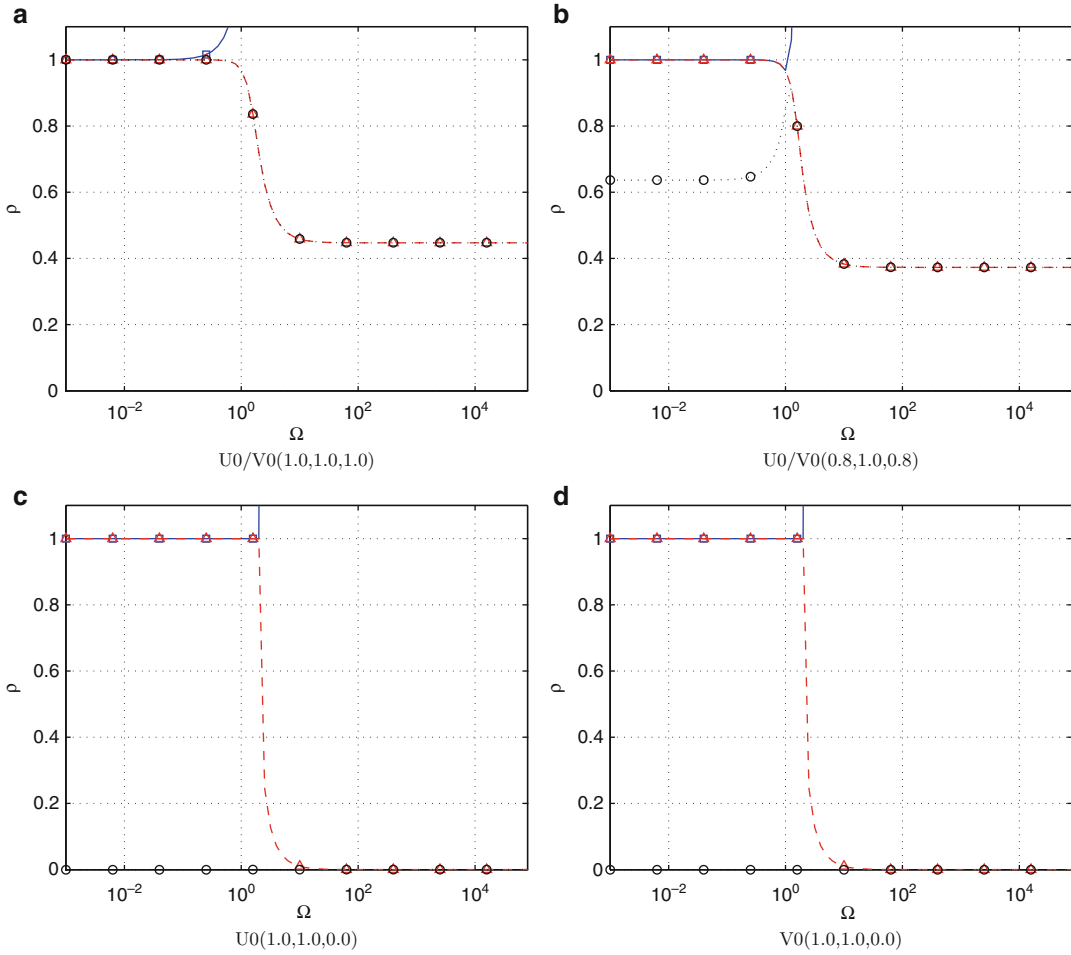
$$\mathbf{f} \rightarrow \mathbf{f} \quad (4)$$

**For variables:** ( $V0$ -family-based PCE-GS4-2  $\rightarrow$  PCE-GS4-1)

$$\ddot{\mathbf{q}} \rightarrow \dot{\mathbf{q}} \quad \text{and} \quad \dot{\mathbf{q}} \rightarrow \mathbf{q} \quad (5)$$

and neglect  $\mathbf{q}$  in the  $V0$ -family-based PCE-GS4-2, i.e., treat as a dummy variable.

**For algorithmic parameters:** ( $V0$ -family-based PCE-GS4-2  $\rightarrow$  PCE-GS4-1)



**Explicit Time Integrators and Designs for First-/Second-Order Linear Transient Systems, Fig. 2** Stability plots of selected algorithms within Algorithm 1 with  $\eta = 1$

$$\rho_{\infty}^{\max} \rightarrow 1, \quad \rho_{\infty}^{\min} \rightarrow \rho_{\infty} \quad \text{and} \quad \rho_{\infty}^s \rightarrow \rho_{\infty}^s \quad (6) \quad \text{Balance equation:}$$

where  $\rho_{\infty}$  and  $\rho_{\infty}^s$  are the principal root or spectral radius and spurious root at the high-frequency range, respectively, in I-GS4-1, and they satisfy

$$0 \leq \rho_{\infty}^s \leq \rho_{\infty} \leq 1 \quad (7)$$

**Algorithm 2. PCE-GS4-1 Algorithm Designs for Linear First-Order Systems**

**Predictor:**

$$\hat{\mathbf{q}} = \mathbf{q}_n + (\lambda_4 - \lambda_5) \dot{\mathbf{q}}_n \Delta t$$

$$\mathbf{M}\tilde{\mathbf{v}} + \mathbf{K}\bar{\mathbf{q}} = \tilde{\mathbf{f}}$$

where

$$\begin{aligned} \bar{\mathbf{q}} &= \mathbf{q}_n + \frac{W_2 \Lambda_5}{\lambda_5} (\hat{\mathbf{q}} - \mathbf{q}_n) + \left( W_1 \Lambda_4 - \frac{\lambda_4}{\lambda_5} W_2 \Lambda_5 \right) \\ &\quad \times \dot{\mathbf{q}}_n \Delta t \\ \tilde{\mathbf{v}} &= \dot{\mathbf{q}}_n + W_1 \Lambda_6 (\dot{\mathbf{q}}_{n+1} - \dot{\mathbf{q}}_n) \\ \tilde{\mathbf{f}} &= \mathbf{f}_n + W_1 (\mathbf{f}_{n+1} - \mathbf{f}_n) \quad \text{or} \quad \mathbf{f}(t_{n+W_1}) \end{aligned}$$

**Corrector:**

$$\mathbf{q}_{n+1} = \hat{\mathbf{q}} + \lambda_5 \dot{\mathbf{q}}_{n+1} \Delta t$$

**Initial conditions:**

$$\mathbf{q}(t_0) = \mathbf{q}_0$$

**Remark 2. (Algorithm 2)**

1. Algorithm 2 is the predictor-corrector explicit (PCE) form of the implicit GS4 algorithm designs in first-order systems (I-GS4-1 algorithms). Employing the algorithmic parameters of I-GS4-1 algorithms, Algorithm 2 can be reduced to

**Predictor:**

$$\hat{\mathbf{q}} = \mathbf{q}_n + \frac{\rho_\infty^s}{1 + \rho_\infty^s} \dot{\mathbf{q}}_n \Delta t$$

**Balance equation:**

$$\mathbf{M}\tilde{\mathbf{v}} + \mathbf{K}\bar{\mathbf{q}} = \tilde{\mathbf{f}}$$

where

$$\begin{aligned}\bar{\mathbf{q}} &= \mathbf{q}_n + W_1(\hat{\mathbf{q}} - \mathbf{q}_n) \\ \tilde{\mathbf{v}} &= \dot{\mathbf{q}}_n + W_1\Lambda_6(\dot{\mathbf{q}}_{n+1} - \dot{\mathbf{q}}_n) \\ \tilde{\mathbf{f}} &= \mathbf{f}_n + W_1(\mathbf{f}_{n+1} - \mathbf{f}_n) \text{ or } \mathbf{f}(t_{n+W_1})\end{aligned}$$

**Corrector:**

$$\mathbf{q}_{n+1} = \hat{\mathbf{q}} + \frac{1}{1 + \rho_\infty^s} \dot{\mathbf{q}}_{n+1} \Delta t$$

where  $W_1 = 1/(1 + \rho_\infty)$ .

2. Regardless of the choices of  $(\rho_\infty, \rho_\infty^s)$  with

$$0 \leq \rho_\infty^s \leq \rho_\infty \leq 1 \quad (8)$$

we obtain second-order time accurate, conditionally stable algorithms.

### Linear General Explicit Generalized Single-Step Single-Solve Algorithms and Designs

Here, we introduce the general explicit GS4 algorithm designs (*E-GS4-2 algorithms*) developed for linear elastodynamics. When designing E-GS4-2 algorithms, we relax the conditions of the unconditional stability zero-order configuration or velocity overshoot which has been imposed in the design of I-GS4-2 algorithms. The general structure of the E-GS4 algorithm designs takes the following form:

**Algorithm 3. Single-Field Form E-GS4-2 Algorithm Designs for Linear Dynamical Systems Integrator:**

$$W_1\Lambda_6\mathbf{M}\Delta\mathbf{a} = \tilde{\mathbf{f}} - \mathbf{K}\tilde{\mathbf{q}} - \mathbf{C}\tilde{\mathbf{v}} - \mathbf{M}\ddot{\mathbf{q}}_n$$

where

$$\begin{aligned}\tilde{\mathbf{q}} &= \mathbf{q}_n + W_1\Lambda_1 \dot{\mathbf{q}}_n \Delta t + (W_2\Lambda_2 - W_3\Lambda_3) \ddot{\mathbf{q}}_n \Delta t^2 \\ \tilde{\mathbf{v}} &= \dot{\mathbf{q}}_n + (W_1\Lambda_4 - W_2\Lambda_5) \ddot{\mathbf{q}}_n \Delta t \\ \tilde{\mathbf{f}} &= \mathbf{f}_n + W_1(\mathbf{f}_{n+1} - \mathbf{f}_n) \text{ or } \mathbf{f}(t_{n+W_1})\end{aligned}$$

**Updates:**

$$\begin{aligned}\mathbf{q}_{n+1} &= \mathbf{q}_n + \lambda_1 \dot{\mathbf{q}}_n \Delta t + \lambda_2 \ddot{\mathbf{q}}_n \Delta t^2 + \lambda_3 \eta \Delta \mathbf{a} \Delta t^2 \\ \dot{\mathbf{q}}_{n+1} &= \dot{\mathbf{q}}_n + \lambda_4 \ddot{\mathbf{q}}_n \Delta t + \lambda_5 \Delta \mathbf{a} \Delta t \\ \ddot{\mathbf{q}}_{n+1} &= \ddot{\mathbf{q}}_n + \Delta \mathbf{a}\end{aligned}$$

**Initial conditions:**

$$\begin{aligned}\mathbf{q}(t_0) &= \mathbf{q}_0 \\ \dot{\mathbf{q}}(t_0) &= \dot{\mathbf{q}}_0\end{aligned}$$

**Algorithmic parameters:**

$$\begin{aligned}W_1\Lambda_6 &= \frac{2 + \rho_b^s - \rho_b^s \rho_b}{(1 + \rho_b)(1 + \rho_b^s)} \\ W_1\Lambda_1 + \lambda_5 &= \frac{5 + 3\rho_b^s + \rho_b - \rho_b^s \rho_b}{2(1 + \rho_b)(1 + \rho_b^s)} \\ W_2\Lambda_2 - W_3\Lambda_3 + \lambda_3\eta_3 &= \frac{\rho_b^s \rho_b - \rho_b^s - 2}{2\Lambda_6^2(1 + \rho_b^s)^2(1 + \rho_b)^2} \\ &\quad [2(\rho_b^s \rho_b - \rho_b^s - 2) \\ &\quad - \Lambda_6(\rho_b^s \rho_b - 3\rho_b^s - \rho_b - 5)] \\ &\quad - \frac{5 + 3\rho_b + \rho_b^s(1 - \rho_b)(4 + \rho_b^s + 2\rho_b)}{(\rho_b^s \rho_b - \rho_b^s - 2)(1 + \rho_b^s)(1 + \rho_b)^2} \\ \lambda_1 &= \lambda_4 = 1 \\ \lambda_2 &= \frac{1}{2} \\ W_2\Lambda_5 &= W_1(\Lambda_4 - \Lambda_1)\end{aligned}$$

**Remark 3. (Algorithm 3)**

1. All explicit schemes in Algorithm 3 are second-order time accurate regardless of any choices of  $(\rho_b, \rho_b^s)$ , where  $\rho_b$  and  $\rho_b^s$  are the principal root and spurious root at the bifurcation limit, respectively. At the bifurcation limit, the maximum and minimum principal roots have the same real value, i.e.,  $\rho_b^{\max} = \rho_b^{\min} = \rho_b \in \mathbb{R}_+$  with

$$0 \leq \rho_b^s \leq \rho_b \leq 1 \quad (9)$$

2. The bifurcation limit,  $\Omega_b \geq 0$ , is given as

$$\Omega_b = \sqrt{(1 + \rho_b)[2 + \rho_b^s(1 - \rho_b)]} \quad (10)$$

When selecting  $\rho_b = 1$  and  $\rho_b^s \in [0, 1]$ , we have

$$\Omega_b = \Omega_s = 2 \quad (11)$$

When selecting  $\rho_b^s = \rho_b$ , we have

$$\begin{aligned} \Omega_b &= \sqrt{(1 + \rho_b)(2 + \rho_b - \rho_b^2)} \in [\sqrt{2}, 2] \\ \Omega_s &= 2\sqrt{\frac{-3(2 - \rho_b)(1 + \rho_b)^3}{-10 + \rho_b(\rho_b^3 - \rho_b^2 + \rho_b - 15)}} \in [2\sqrt{\frac{3}{5}}, 2] \end{aligned} \quad (12)$$

Note that  $\Omega_b$  and  $\Omega_s$  take minimum values at  $\rho_b = 0$  when  $\rho_b^s = \rho_b$ ; see Fig. 3.

3. When we treat the physical damping implicitly, the last condition in the algorithmic parameters, i.e.,

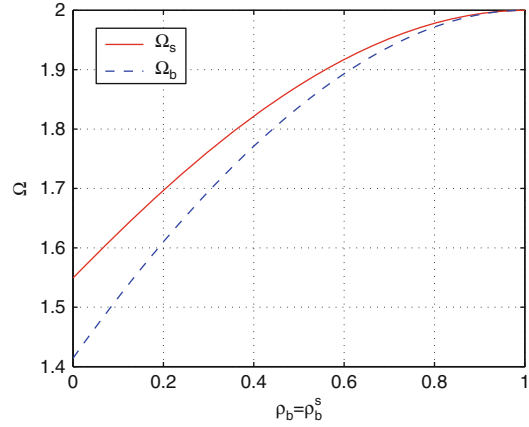
$$W_2\Lambda_5 = W_1(\Lambda_4 - \Lambda_1) \quad (13)$$

is replaced with

$$\Lambda_1 = \Lambda_4 = 1 \quad (14)$$

to achieve the second-order time accuracy of the algorithm. The bifurcation and stability limits are still given by (10),

4. Substituting the predictors,  $\hat{\mathbf{q}}$  and  $\hat{\mathbf{v}}$ , into  $\bar{\mathbf{q}}$  and  $\bar{\mathbf{v}}$  in the balance equation in Algorithm 1, respectively, yields  $\bar{\mathbf{q}} = \tilde{\mathbf{q}}$  and  $\bar{\mathbf{v}} = \tilde{\mathbf{v}}$ .



**Explicit Time Integrators and Designs for First-/Second-Order Linear Transient Systems, Fig. 3** Stability and bifurcation limits when  $\rho_b^s = \rho_b \in [0, 1]$

Therefore, the general structures of Algorithm 1 and Algorithm 3 are actually the same; only the algorithmic parameters used are different.

5. When selecting E-GS4-2  $(\rho_b, \rho_b^s) = (1, 0)$  with  $\lambda_3 = 1/2$ ,  $\lambda_5 = 0$ , and  $W_2\Lambda_5 = 1/2$  with the implicit treatment of the physical damping, we recover the **central difference method** ( $\Omega_s = \Omega_b = 2$ ) which belongs to the Newmark family of algorithms [4]. Note that it is equivalent to the **velocity verlet algorithm** ( $\Omega_s = \Omega_b = 2$ ) [5], which is widely used in molecular dynamics simulation, in non-dissipative systems.
6. When selecting  $\rho_b = \rho_b^s \in [0, 1]$ , we recover the **explicit generalized- $\alpha$  algorithm** [6].
7. Algorithms by design in the two-field form  $(\mathbf{q}, \mathbf{v}) \in TQ$  yields the only second-order time accurate scheme which is the **explicit velocity-based scheme** [7–9] which takes the form

$$\begin{aligned} \mathbf{M} \frac{\mathbf{v}_{n+1} - \mathbf{v}_n}{\Delta t} + \mathbf{C} \tilde{\mathbf{v}} + \mathbf{K} \mathbf{q} &= \tilde{\mathbf{f}} \\ \mathbf{q} &= \mathbf{q}_n + \frac{\Delta t}{2} \mathbf{v}_n \\ \tilde{\mathbf{v}} &= \frac{\mathbf{v}_{n+1} + \mathbf{v}_n}{2} = \frac{\mathbf{q}_{n+1} - \mathbf{q}_n}{\Delta t} \\ \tilde{\mathbf{f}} &= \mathbf{f}(t_{n+1/2}) \end{aligned} \quad (15)$$

Details of algorithms by design in the two-field form are not discussed here.

## Conclusion

A brief summary of the explicit versions of the GS4 algorithms and designs has been shown via the implicit counterparts. All explicit time integration schemes are second-order time accurate, and various common schemes are also included within the present frameworks. An *i* Integration Framework (Isochronous Integration Framework) is also described which employs the same framework for integrating both second- and first-order transient systems.

## References

1. Zhou X, Tamma KK (2006) Algorithms by design with illustrations to solid and structural mechanics/dynamics. *Int J Numer Meth Eng* 66:1738–1790
2. Tamma KK, Har J, Zhou X, Shimada M, Hoitink A (2011) An overview and recent advances in vector and scalar formalisms: space/time discretizations in computational dynamics: a unified approach. *Arch Comput Meth Eng*. doi:10.1007/s11831-011-9060-y
3. Har J, Tamma KK (2012) Advanced computational dynamics of particles, materials and structures: a unified approach. Wiley, Chichester
4. Newmark NM (1959) A method of computation for structural dynamics. *J Am Soc Civil Eng* 1:67–94
5. Swope WC, Anderson HC, Berens PH, Wilson KR (1882) A computer simulation method for the calculation of equilibrium constants for the formation of physical clusters of molecules: application to small water clusters. *J Chem Phys* 76:648
6. Hulbert GM, Chung J (1996) Explicit time integration algorithms for structural dynamics with optimal numerical dissipation. *Comput Meth Appl Mech Eng* 137:175
7. Tamma KK, Namburu RR (1988) A new finite element based Lax-Wendroff/Taylor-Galerkin methodology for computational dynamics. *Comput Meth Appl Mech Eng* 71:137–150
8. Tamma KK, Namburu RR (1990) Applicability and evaluation of an implicit self-starting unconditionally stable methodology for dynamics of structures. *Comput Struct* 34:835–842
9. Tamma KK, Namburu RR (1997) Computational approaches with applications to non-classical and classical thermomechanical problems. *Appl Mech Rev* 50:514

## Extended Displacement Discontinuity Boundary Integral Equation Method for Analysis of Cracks in Smart Materials

CuiYing Fan<sup>1</sup>, MingHao Zhao<sup>1</sup> and Ernian Pan<sup>1,2</sup>

<sup>1</sup>Henan Key Engineering Laboratory for Anti-fatigue Manufacturing Technology and the School of Mechanical Engineering, Zhengzhou University, Zhengzhou, People's Republic of China

<sup>2</sup>Department of Civil Engineering, Computer Modeling and Simulation Group, University of Akron, Akron, OH, USA

## Overview

Fractures greatly affect the integrity and reliability of structures, and crack analysis is one of the main tasks in fracture mechanics. The singularity of stresses near a crack tip and the geometric identity of the two surfaces of a crack have challenged all theoretical and numerical methods.

In 1976, Crouch proposed the displacement discontinuity method (DDM) [1], which is also called the displacement discontinuity boundary integral equation method (DDBIEM). In the DDM, the basic characteristic of a crack, namely, the displacement discontinuity, is automatically contained. In the last 35 years, this method has been studied intensively and extensively in dealing with fracture problems in two- and three-dimensional elastic media.

Along with the increasing usage of smart materials, e.g., the piezoelectric materials and the magnetoelectroelastic (MEE) materials, in various branches of the engineering field, fracture mechanics of these new materials is attracting more and more attention. As one of the key advances, the DDM has been extended to the study of cracks in piezoelectric and MEE media [2–4]. In the extended DDM for the piezoelectric material, the extended displacement discontinuity (DD) includes the elastic displacement discontinuities and the electric potential discontinuity; and for the MEE material, the extended DD includes further the magnetic potential discontinuity.



## Extended Displacement Discontinuities

In the absence of body force, electric charge, and electric current, the coupled constitutive equations for a three-dimensional (3D) MEE medium can be expressed in terms of the elastic displacement components  $u_i$  ( $u_1 = u$ ,  $u_2 = v$  and  $u_3 = w$ ), the electric potential  $\varphi$  and the magnetic potential  $\psi$

$$\sigma_{ij} = c_{ijkl}(u_{k,l} + u_{l,k})/2 + e_{kij}\varphi_{,k} + f_{kij}\psi_{,k} \quad (1a)$$

$$D_i = e_{ikl}(u_{k,l} + u_{l,k})/2 - \varepsilon_{ik}\varphi_{,k} - g_{ik}\psi_{,k} \quad (1b)$$

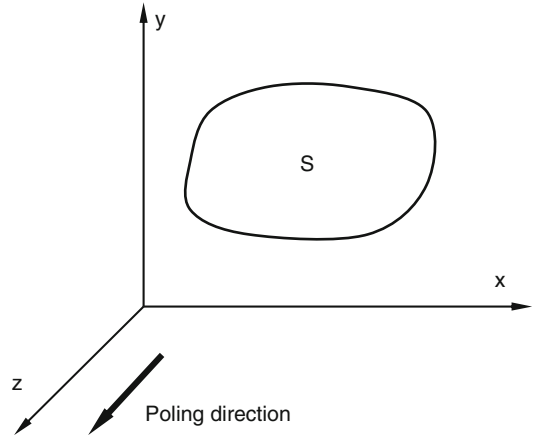
$$B_i = f_{ikl}(u_{k,l} + u_{l,k})/2 - g_{ik}\varphi_{,k} - \mu_{ik}\psi_{,k} \quad (1c)$$

where  $\sigma_{ij}$ ,  $D_i$ , and  $B_i$  denote the stress, electric displacement, and magnetic induction components, respectively,  $c_{ijkl}$ ,  $e_{ijk}$ ,  $f_{ijk}$ ,  $\varepsilon_{ij}$ ,  $g_{ij}$  and  $\mu_{ij}$  are, respectively, the elastic, piezoelectric, piezomagnetic, dielectric permittivity, electromagnetic, and magnetic permeability coefficients. A subscript comma denotes the partial differentiation with respect to the coordinate. It is noted that by letting  $f_{ijk} = 0$ ,  $g_{ij} = 0$  and  $\mu_{ij} = 0$ , the constitutive equation in (1) is reduced to that for a piezoelectric material, and by further setting  $e_{ijk} = 0$  and  $\varepsilon_{ij} = 0$ , (1) is reduced to the constitutive equation for a purely elastic material.

In the following analyses, we assume that the smart material with cracks is transversely isotropic. As an example, let us consider an arbitrarily shaped planar crack  $S$  on the  $oxy$  plane, which coincides with the plane of isotropy of an infinite smart medium as shown in Fig. 1. The poling direction is along the  $z$ -axis. The front and back faces of the crack  $S$  are denoted by  $S^+$  and  $S^-$ , respectively. Across the crack faces, the displacement discontinuities  $\|u_i\|$  ( $i = 1, 2, 3$ ), the electric potential discontinuity  $\|\varphi\|$ , and the magnetic potential discontinuity  $\|\psi\|$  are denoted by

$$\begin{aligned} \|u_i\| &= u_i(S^+) - u_i(S^-) \\ \|\varphi\| &= \varphi(S^+) - \varphi(S^-) \\ \|\psi\| &= \psi(S^+) - \psi(S^-) \end{aligned} \quad (2)$$

which are called the extended displacement discontinuities.



**Extended Displacement Discontinuity Boundary Integral Equation Method for Analysis of Cracks in Smart Materials, Fig. 1** A crack of arbitrary shape in the isotropic  $oxy$  plane of an infinite medium

## Boundary Integral Equation Method for Homogeneous Materials

We consider the general case where the applied extended tractions on the crack faces satisfy

$$\begin{aligned} p_i|_{S^+} &= -p_i|_{S^-}, \quad \omega|_{S^+} = -\omega|_{S^-}, \quad \gamma|_{S^+} = -\gamma|_{S^-}, \\ i &= 1, 2, 3 \quad \text{or } x, y, z \end{aligned} \quad (3)$$

Based on the Green's functions of the unit extended point force [5] and the Somigliana identity, the extended displacement discontinuity boundary integral equations are derived

$$\begin{aligned} \int_{S^+} \{ [L_{11}(1 - 3\cos^2\theta) + L_{12}(1 - 3\sin^2\theta)] \|u\| \\ + L_{13} \cos\theta \sin\theta \|v\| \} \frac{1}{r^3} dS(\xi, \eta) = -p_x(x, y) \end{aligned} \quad (4)$$

$$\begin{aligned} \int_{S^+} \{ L_{13} \cos\theta \sin\theta \|u\| + [L_{12}(1 - 3\cos^2\theta) \\ + L_{11}(1 - 3\sin^2\theta)] \|v\| \} \frac{1}{r^3} dS(\xi, \eta) = -p_y(x, y) \end{aligned} \quad (5)$$

$$\begin{aligned} \int_{S^+} [L_{31}\|w\| + L_{32}\|\varphi\| + L_{33}\|\psi\|] \frac{1}{r^3} dS(\xi, \eta) \\ = -p_z(x, y) \end{aligned} \quad (6)$$



$$\int_{S^+} [L_{41}||w|| + L_{42}||\varphi|| + L_{43}||\psi||] \frac{1}{r^3} dS(\xi, \eta) = -\omega(x, y) \quad (7)$$

$$\int_{S^+} [L_{51}||w|| + L_{52}||\varphi|| + L_{53}||\psi||] \frac{1}{r^3} dS(\xi, \eta) = -\gamma(x, y) \quad (8)$$

where

$$r^2 = (\xi - x)^2 + (\eta - y)^2, \quad \cos \theta = (\xi - x)/r, \quad \sin \theta = (\eta - y)/r \quad (9)$$

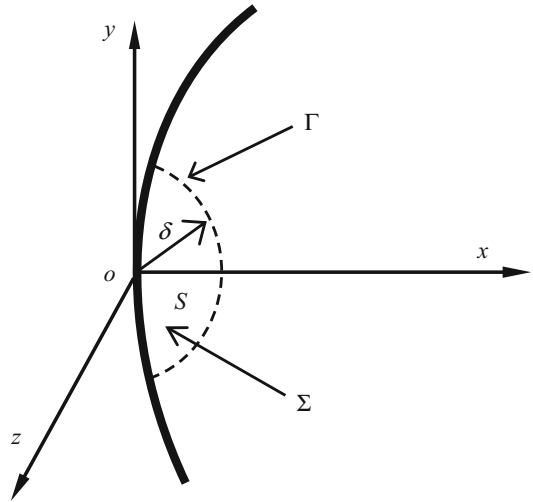
and  $L_{ij}$  are the material related constants given in Zhao et al. [4] for MEE media, in Zhao et al. [2] for piezoelectric media, and in Zhao et al. [6] for elastic media.

In (4)–(8), the kernel functions have the singularity of  $O(1/r^3)$ , and hence the integral equations are hyper-singular. The displacement discontinuities  $||u||$  and  $||v||$  on the crack faces are coupled through (4) and (5), while the displacement discontinuity  $||w||$ , the electric potential discontinuity  $||\varphi||$ , and the magnetic potential discontinuity  $||\psi||$  are coupled through (6)–(8).

## Singular Index

The singular behavior of the fields near the crack tip and the corresponding field intensity factors are the keys in fracture mechanics. Based on the extended displacement discontinuity boundary integral equations (4)–(8), the field singularity index and intensity factor in terms of the extended displacement discontinuity can be derived.

We choose an arbitrary but smooth point  $o$  on the crack front  $\Gamma$  to analyze the singular behavior (Fig. 2). We assume that the Cartesian coordinate system  $oxyz$  is located such that the  $y$ -axis and  $x$ -axis are tangential and normal to  $\Gamma$ , respectively, while the  $z$ -axis is normal to the crack plane  $S$ . The infinitesimal  $\delta$  denotes the radius of a circle  $\Sigma$  centered at point  $o$  contained in  $S$ .



**Extended Displacement Discontinuity Boundary Integral Equation Method for Analysis of Cracks in Smart Materials, Fig. 2** The local coordinate system

Now, we assume that the extended displacement discontinuities at the neighborhood of point  $o$  are given by

$$\begin{aligned} ||u|| &= A_x(o)x^{\alpha_x}, & ||v|| &= A_y(o)x^{\alpha_y}, & ||w|| &= A_z(o)x^{\alpha_z}, \\ ||\varphi|| &= A_\varphi(o)x^{\alpha_\varphi}, & ||\psi|| &= A_\psi(o)x^{\alpha_\psi} \end{aligned} \quad (10)$$

where the coefficients  $A_x, A_y, A_z, A_\varphi$ , and  $A_\psi$  depend on the location of the point  $o$ , and  $\alpha_x, \alpha_y, \alpha_z, \alpha_\varphi$ , and  $\alpha_\psi$  are the singular indices of the extended displacements with their values between (0,1).

Substituting (10) into (4)–(8), letting  $\varepsilon$  be sufficiently small and taking the limit  $x \rightarrow 0$ , and further making use of the finite-part integral theory, we obtain the conditions for the existence of a nontrivial solution

$$\cot \pi \alpha_x = \cot \pi \alpha_y = \cot \pi \alpha_z = \cot \pi \alpha_\varphi = \cot \pi \alpha_\psi = 0 \quad (11)$$

Finally, one obtains the singular indexes

$$\alpha_x = \alpha_y = \alpha_z = \alpha_\varphi = \alpha_\psi = \frac{1}{2} \quad (12)$$

This result reveals that the extended displacements near the crack tip have the classical singularity  $r^{\frac{1}{2}}$  as in the fracture mechanics of conventional elastic materials.

## Intensity Factor

Substituting (12) into (10), and using (4)–(8) and the constitutive equation (1), the extended stresses at points  $(-\rho, y, 0)$  ( $\rho > 0$ ) near point  $o$  are expressed as

$$\begin{aligned}\sigma_{zx} &= -L_{11}A_x(o)\pi/\sqrt{\rho} \\ \sigma_{zy} &= -L_{12}A_y(o)\pi/\sqrt{\rho} \\ \sigma_{zz} &= [L_{31}A_z(o) + L_{32}A_\varphi(o) + L_{33}A_\psi(o)]\pi/\sqrt{\rho} \\ D_z &= [L_{41}A_z(o) + L_{42}A_\varphi(o) + L_{43}A_\psi(o)]\pi/\sqrt{\rho} \\ B_z &= [L_{51}A_z(o) + L_{52}A_\varphi(o) + L_{53}A_\psi(o)]\pi/\sqrt{\rho}\end{aligned}\quad (13)$$

Defining the intensity factors

$$\begin{aligned}K_I^F &= \lim_{\rho \rightarrow 0} \sqrt{2\pi\rho} \sigma_{zz}(-\rho, y, 0) \\ K_I^D &= \lim_{\rho \rightarrow 0} \sqrt{2\pi\rho} D_z(-\rho, y, 0) \\ K_I^B &= \lim_{\rho \rightarrow 0} \sqrt{2\pi\rho} B_z(-\rho, y, 0) \\ K_{II}^F &= \lim_{\rho \rightarrow 0} \sqrt{2\pi\rho} \sigma_{zx}(-\rho, y, 0) \\ K_{III}^F &= \lim_{\rho \rightarrow 0} \sqrt{2\pi\rho} \sigma_{zy}(-\rho, y, 0)\end{aligned}\quad (14)$$

and inserting (13) into (14), and considering (10), the intensity factors can be expressed in terms of the extended displacement discontinuities

$$\begin{aligned}K_I^F &= \sqrt{2\pi} \lim_{x \rightarrow 0} [L_{31}||w|| + L_{32}||\varphi|| + L_{33}||\psi||]/\sqrt{x} \\ K_I^D &= \sqrt{2\pi} \lim_{x \rightarrow 0} [L_{41}||w|| + L_{42}||\varphi|| + L_{43}||\psi||]/\sqrt{x} \\ K_I^B &= \sqrt{2\pi} \lim_{x \rightarrow 0} [L_{51}||w|| + L_{52}||\varphi|| + L_{53}||\psi||]/\sqrt{x} \\ K_{II}^F &= -\sqrt{2\pi} \lim_{x \rightarrow 0} L_{11}||u||/\sqrt{x} \\ K_{III}^F &= -\sqrt{2\pi} \lim_{x \rightarrow 0} L_{12}||v||/\sqrt{x}\end{aligned}\quad (15)$$

Equation (15) demonstrates that once the extended displacement discontinuities are calculated, the intensity factor can be obtained by (15). This conclusion is held for any shape and dimension of the planar crack and for general distribution of the mechanical-electric-magnetic loading. The cracks may be multiple coplanar cracks, and the loading may be point loading.

The singularity of stresses near a crack tip and the intensity factor of a crack in piezoelectric media were given in Zhao et al. [2].

## Boundary Integral Equation Method for Two-Phase Materials

Using the same method as given in the previous section, the boundary integral-differential equations of an interface crack in a two-phase MEE material can be further derived [7]

$$\begin{aligned}\int_{s^+} \{ [K_{11}\cos^2\theta + K_{12}\sin^2\theta] ||u|| \\ + (K_{11} - K_{12}) \sin\theta \cos\theta ||v|| \} \frac{1}{r^3} dS \\ + 2\pi K_{41} \frac{\partial ||w||}{\partial x} + 2\pi K_{42} \frac{\partial ||\varphi||}{\partial x} \\ + 2\pi K_{43} \frac{\partial ||\psi||}{\partial x} = -p_x\end{aligned}\quad (16a)$$

$$\begin{aligned}\int_{s^+} (K_{11} - K_{12}) \sin\theta \cos\theta ||u|| \\ + [K_{11}\sin^2\theta + K_{12}\cos^2\theta] ||v|| \} \frac{1}{r^3} dS \\ + 2\pi K_{41} \frac{\partial ||w||}{\partial y} + 2\pi K_{42} \frac{\partial ||\varphi||}{\partial y} \\ + 2\pi K_{43} \frac{\partial ||\psi||}{\partial y} = -p_y\end{aligned}\quad (16b)$$

$$\begin{aligned}\int_{s^+} [K_{z1}||w|| + K_{z2}||\varphi|| + K_{z3}||\psi||] \frac{1}{r^3} dS \\ + 2\pi K_1 \left( \frac{\partial ||u||}{\partial x} + \frac{\partial ||v||}{\partial y} \right) = -p_z\end{aligned}\quad (16c)$$

$$\int_{s^+} [K_{z12}\|w\| + K_{z22}\|\varphi\| + K_{z32}\|\psi\|] \frac{1}{r^3} dS + 2\pi K_2 \left( \frac{\partial\|u\|}{\partial x} + \frac{\partial\|v\|}{\partial y} \right) = -\omega \quad (16d)$$

$$\int_{s^+} [K_{z13}\|w\| + K_{z23}\|\varphi\| + K_{z33}\|\psi\|] \frac{1}{r^3} dS + 2\pi K_3 \left( \frac{\partial\|u\|}{\partial x} + \frac{\partial\|v\|}{\partial y} \right) = -\gamma \quad (16e)$$

where the coefficients  $K_s$  with different subscript “s” are material constants given in Zhao et al. [7] for MEE media and in Zhao et al. [8, 9] for piezoelectric media. Note that the kernels in (16) have the singularity order  $O(r^{-3})$ , and hence the integral-differential equations are hyper-singular. It should be pointed out that the boundary integral-differential equations are applicable to multiple coplanar interface cracks.

When the bimaterial becomes homogeneous, one has

$$K_{41} = K_{42} = K_{43} = K_1 = K_2 = K_3 = 0 \quad (17)$$

and the differential terms in (16) disappear. Therefore, the boundary integral-differential equations are reduced to the hyper-singular boundary integral equations in (4–8).

## Solutions of the Boundary Integral Equation for Two-Phase Materials

Making use of (16c–16e), one obtains

$$(K_{z1} - C_3 K_{z12}) \int_{s^+} [\|w\| + C_1 \|\varphi\| + C_2 \|\psi\|] \frac{1}{r^3} dS = -p_z + C_3 \omega \quad (18)$$

where  $C_i$  are constants related to the material property given by Zhao et al. [7]. Equation (18) is analogous to the boundary integral equation for the displacement discontinuity in the normal direction of the crack in an elastic medium [10]. Thus, the solution of the combined extended

displacement discontinuity  $\|w\| + C_1 \|\varphi\| + C_2 \|\psi\|$  can be directly obtained from the corresponding elastic solution.

The extended stress near the crack tip in the crack plane can be expressed in the following form:

$$\sigma_{zz} - C_3 D_z = (K_{z1} - C_3 K_{z12}) \times \int_{s^+} [\|w\| + C_1 \|\varphi\| + C_2 \|\psi\|] \frac{1}{r^3} dS \quad (19)$$

Therefore, the Mode I extended intensity factor in a MEE bimaterial can be defined as

$$K_{I1} = \lim_{r \rightarrow 0} \sqrt{2\pi r} (\sigma_{zz} - C_3 D_z) = \pi \sqrt{2\pi} (K_{z1} - C_3 K_{z12}) \lim_{\rho \rightarrow 0} \frac{\|w\| + C_1 \|\varphi\| + C_2 \|\psi\|}{\sqrt{\rho}} \quad (20)$$

Similarly, the other extended stress and the corresponding intensity factor near the crack tip in the crack plane can be written as

$$\sigma_{zz} - C_6 B_z = (K_{z1} - C_6 K_{z13}) \int_{s^+} [\|w\| + C_4 \|\varphi\| + C_5 \|\psi\|] \frac{1}{r^3} dS \quad (21)$$

$$K_{I2} = \lim_{r \rightarrow 0} \sqrt{2\pi r} (\sigma_{zz} - C_6 B_z) = \pi \sqrt{2\pi} (K_{z1} - C_6 K_{z13}) \lim_{\rho \rightarrow 0} \frac{\|w\| + C_4 \|\varphi\| + C_5 \|\psi\|}{\sqrt{\rho}} \quad (22)$$

## Solutions of the Boundary Integral-Differential Equations for Two-Phase Materials

Combining (16c)–(16e) with (16a) and (16b) gives

$$\int_{s^+} \left\{ \left[ \frac{L K_{12}}{K_{41}} \frac{1}{r^3} + \frac{L(K_{11} - K_{12})}{K_{41}} \frac{(x - \xi)^2}{r^5} \right] \|u\| + \frac{L(K_{11} - K_{12})}{K_{41}} \frac{(x - \xi)(y - \eta)}{r^5} \|v\| \right\} dS + 2\pi \frac{\partial\|w^*\|}{\partial x} = -\frac{L p_x}{K_{41}} \quad (23a)$$

$$\int_{s^+} \left\{ \frac{L(K_{11} - K_{12})}{K_{41}} \frac{(x - \xi)(y - \eta)}{r^5} \|u\| + \left[ \frac{LK_{12}}{K_{41}} + \frac{L(K_{11} - K_{12})}{K_{41}} \frac{(y - \eta)^2}{r^5} \right] \|v\| \right\} dS + 2\pi \frac{\partial \|w^*\|}{\partial y} = -\frac{Lp_y}{K_{41}} \quad (23b)$$

$$\frac{(K_{z1} + C_7K_{z12} + C_8K_{z13})}{L(K_1 + C_7K_2 + C_8K_3)} \int_{s^+} \|w^*\| \frac{1}{r^3} dS + 2\pi \left( \frac{\partial \|u\|}{\partial x} + \frac{\partial \|v\|}{\partial y} \right) = -\frac{p_z + C_7\omega + C_8\gamma}{K_1 + C_7K_2 + C_8K_3} \quad (23c)$$

where  $L$  and  $\|w^*\|$  are given by

$$L = \sqrt{-\frac{3K_{41}(K_{z1} + C_7K_{z12} + C_8K_{z13})}{(2K_{11} + K_{12})(K_1 + C_7K_2 + C_8K_3)}}, \quad \|w^*\| = L(\|w\| + C_9\|\varphi\| + C_{10}\|\psi\|) \quad (23d)$$

Equation (23) is similar to the boundary integral-differential equations for interface crack problem in a 3D isotropic elastic bimaterial system given by Tang et al. [11].

We assume that the displacement discontinuities near the crack tip are

$$\begin{aligned} \|u\| &= A_x(o)x^{\alpha_x} \\ \|v\| &= A_y(o)x^{\alpha_y} \\ \|w^*\| &= A_z(o)x^{\alpha_z} \end{aligned} \quad (24)$$

where  $A_y(o)$  is an arbitrary real constant,  $A_x(o)$  and  $A_z(o)$  are complex constants, and  $\alpha_i$  are the singularity indexes [11]. Inserting (24) into (23), and using the integrals given in Zhao et al. [7], we can obtain

$$\alpha_y = \frac{1}{2}, \quad \alpha_x = \alpha_z = \frac{1}{2} \pm i\varepsilon \quad (25)$$

where  $\varepsilon$  is a constant related to the bimaterial property. Equation (25) shows that the displacement discontinuity  $\|v\|$  has the classical

singularity index  $1/2$ , while  $\|u\|$  or  $\|w^*(\xi, \eta)\|$  has the oscillating singularity index  $1/2 \pm i\varepsilon$  as in the purely elastic bimaterial system case.

The stresses, electric displacement, and magnetic induction at point  $(-r, 0, 0)$  near the crack tip outside of the crack are obtained based on the fundamental solution of the extended displacement discontinuities

$$\int_{-\infty}^{\infty} \int_0^{\infty} \left[ \frac{L(K_{11} - K_{12})}{K_{41}} \times \frac{(x+r)^2}{R^5} + \frac{LK_{12}}{K_{41}} \frac{1}{R^3} \right] \|u\| d\xi d\eta = \frac{L}{K_{41}} \sigma_{zy} \quad (26a)$$

$$\int_{-\infty}^{\infty} \int_0^{\infty} \left[ \frac{L(K_{11} - K_{12})}{K_{41}} \frac{y^2}{R^5} + \frac{LK_{12}}{K_{41}} \frac{1}{R^3} \right] \|v\| d\xi d\eta = \frac{L}{K_{41}} \sigma_{zy} \quad (26b)$$

$$\begin{aligned} &\frac{(K_{z1} + C_7K_{z12} + C_8K_{z13})}{L(K_1 + C_7K_2 + C_8K_3)} \int_{-\infty}^{\infty} \int_0^{\infty} \frac{\|w^*\|}{R^3} d\xi d\eta \\ &- \frac{L}{K_{41}} C_{12}(\sigma_{zz} + C_7D_z + C_8B_z) \end{aligned} \quad (26c)$$

$$\text{where } R = \sqrt{(x+r)^2 + y^2}$$

The new intensity factors for an interface crack in a MEE bimaterial are defined as

$$\begin{aligned} K_{I3} &= \lim_{r \rightarrow 0} \sqrt{2\pi r} r^{-i\varepsilon} C_{12}(\sigma_{zz}(-r, 0, 0) \\ &\quad + C_7D_z(-r, 0, 0) + C_8B_z(-r, 0, 0)) \\ K_{II} &= \lim_{r \rightarrow 0} \sqrt{2\pi r} r^{-i\varepsilon} \sigma_{zx}(-r, 0, 0) \\ K_{III} &= \lim_{r \rightarrow 0} \sqrt{2\pi r} \sigma_{zy}(-r, 0, 0) \end{aligned} \quad (27)$$

Finally, the corresponding intensity factors can be expressed in terms of the extended displacement discontinuities

$$\begin{aligned} K_{I3} + iK_{II} &= \sqrt{2\pi} \frac{2\pi K_{41}(1 + 2i\varepsilon)e^{\pi\varepsilon}}{(\eta_2 - 1)} \\ &\quad \times \lim_{r \rightarrow 0} \left[ \frac{(\|w\| + C_9\|\varphi\| + C_{10}\|\psi\|) - i\|u\|/L}{r^{1/2+i\varepsilon}} \right] \\ K_{III} &= \sqrt{\frac{\pi}{2}} \frac{2\pi\eta_1 K_{41}}{(\eta_2 - 1)L} \lim_{r \rightarrow 0} \frac{\|v\|}{\sqrt{r}} \end{aligned} \quad (28)$$

## Concluding Remarks

The displacement discontinuity method for fracture mechanics in elastic media has been extended to the piezoelectric and MEE media. By using the analogy between the hyper-singular boundary integral/integral-differential equations of elastic media and those of MEE media, the singularity of stresses near a crack tip is studied, and the extended intensity factors are expressed by the extended displacement discontinuities. This result holds for the arbitrarily shaped planar crack and interface crack of any geometric size under the general distribution of the mechanical-electric-magnetic loading. Furthermore, the multiple coplanar cracks and point loading cases can be analyzed.

Fracture of piezoelectric or MEE materials is complex, and thus, various nonlinear models, such as the strip polarization saturation model [12], the strip dielectric breakdown model [13, 14] for piezoelectric media, strip electric-magnetic breakdown model [15], strip electric-magnetic polarization saturation model [16] for MEE media, were proposed to understand the fracture behaviors. However, the extended intensity factors are still the fundamental parameters in these nonlinear models and are important in the corresponding fracture criteria.

**Acknowledgments** The work was supported by the National Natural Science Foundation of China (No. 11102186, No.11072221, No. 11272290), and the Construction Project of Key Laboratory in Henan Colleges.

## References

1. Crouch SL (1976) Solution of plane elasticity problems by the displacement discontinuity method. *Int J Meth Eng* 10:301–343
2. Zhao MH, Shen YP, Liu YJ, Liu GN (1997) Isolated crack in three-dimensional piezoelectric solid: part II—stress intensity factors for circular crack. *Theor Appl Fract Mech* 26:141–149
3. Zhang T-Y, Zhao MH, Tong P (2002) Fracture of piezoelectric ceramics. *Adv Appl Mech* 38:147–289
4. Zhao MH, Fan CY, Yang F, Liu T (2007) Analysis method of planar cracks of arbitrary shape in the isotropic plane of a three-dimensional transversely isotropic magnetoelastoelectric medium. *Int J Solids Struct* 44:4505–4523

5. Ding HJ, Jiang AM, Hou PF, Chen WQ (2005) Green's functions for two-phase transversely isotropic magnetoelastoelectric media. *Eng Anal Bound Elem* 29:551–561
6. Zhao MH, Liu YJ, Cheng CJ (1994) Boundary integral equation and boundary element method for three-dimensional fracture mechanics. *Eng Anal Bound Elem* 13:333–338
7. Zhao MH, Li N, Fan CY, Xu GT (2008) Analysis method of planar interface cracks of arbitrary shape in three-dimensional transversely isotropic magnetoelastoelectric Bimaterials. *Int J Solids Struct* 45:1804–1824
8. Zhao MH, Fang PZ, Shen YP (2004) Boundary integral-differential equations and boundary element method for interfacial cracks in three-dimensional piezoelectric media. *Eng Anal Bound Elem* 28:753–762
9. Zhao MH, Li N, Fan CY (2008) Solution method of interface cracks in three-dimensional transversely isotropic piezoelectric bimaterials. *Eng Anal Bound Elem* 32:545–555
10. Ioakimidis NI (1982) A natural approach to the introduction of finite-part integrals to crack problems of three-dimensional elasticity. *Eng Fract Mech* 16:669–673
11. Tang RJ, Chen MC, Yue JC (1998) Theoretical analysis of three-dimensional interface crack. *Sci China (Ser A)* 28:177–182
12. Gao HJ, Zhang TY, Tong P (1997) Local and global energy release rates for an electrically yielded crack in a piezoelectric ceramic. *J Mech Phys Solids* 45:491–510
13. Zhang T-Y, Zhao MH, Cao CF (2005) The strip dielectric breakdown model. *Int J Fract* 132:311–327
14. Fan CY, Zhao MH, Zhou YH (2009) Numerical solution of polarization saturation/dielectric breakdown model in 2D finite piezoelectric media. *J Mech Phys Solids* 57:1527–1544
15. Zhao MH, Fan CY (2008) Strip electric-magnetic breakdown model in magnetoelastoelectric medium. *J Mech Phys Solids* 56:3441–3458
16. Fan CY, Zhao MH (2011) Nonlinear fracture of 2D magnetoelastoelectric media: analytical and numerical solutions. *Int J Solids Struct* 48:2373–2382

---

## Extended Surfaces (Fins and Pins)

Piotr Wais

Institute of Thermal Power Engineering, Faculty of Mechanical Engineering, Cracow University of Technology, Cracow, Poland

## Overview

Heat transfer from a system can be increased by extending the surface area through the addition of

fins. Fins are used when the convective heat transfer coefficient  $h_c$  is low, as is often the case for gases such as air, particularly under natural-convection conditions [1]. Common examples are the cooling fins on electronics components, on the cylinders of air-cooled motorcycles and lawnmowers, and on cooling electric power transformers.

Because there must be a temperature gradient along the fin to conduct the heat, the added area is not as efficient as the original surface area. The thermal conductivity of the fin material has a strong effect on the temperature distribution along the fin and therefore influences the degree to which the heat transfer rate is enhanced. Ideally, the fin material should have a large thermal conductivity to minimize temperature variations from its base to its tip. In the limit of infinite thermal conductivity, the entire fin would be at the temperature of the base surface, thereby providing the maximum possible heat transfer enhancement [2].

Fins can be of different configurations [2]:

- Straight fin, extended surface that is attached to a plane wall
  - Uniform cross-sectional area
  - Cross-sectional area that varies with the distance from the wall
- Annular fin, circumferentially attached to a cylinder, its cross-section varies with radius from the wall of the cylinder
- Pin fin or spine, extended surface of circular cross section
  - Uniform cross-sectional area
  - Cross-sectional area that varies with the distance from the wall

In any application, selection of a particular fin configuration may depend on space, weight, manufacturing, and cost considerations, as well as on the extent to which the fins reduce the surface convection coefficient and increase the pressure drop associated with flow over the fins. The heat transfer rate associated with a fin is often the primary interest of engineers.

## Heat Transfer from Fins and Fin Efficiency

To evaluate the efficiency of fin  $\eta_f$ , it is necessary to analyze heat flow in a fin and to determine the

temperature variation along the fin. Because fins are thin in one direction, it can be assumed that the temperature variation in the direction of the thickness is negligible. This key assumption allows the conduction along the fin to be treated as if it were one-dimensional, which simplifies the analysis.

To analyze the heat transfer problem, a set of assumptions is introduced so that the resulting theoretical models are simple enough for the analysis. These basic assumptions are proposed by Murray (1938) and Gardner (1945) and are called Murray-Gardner assumptions [3]:

- The heat flow in the fin and its temperatures remain constant with time.
- The fin material is homogeneous, its thermal conductivity is the same in all directions, and it remains constant.
- The convective heat transfer on the faces of the fin is constant and uniform over the entire surface of the fin.
- The temperature of the medium surrounding the fin is uniform.
- The fin thickness is small, compared with its height and length, so that temperature gradient across the fin thickness and heat transfer from the edges of the fin may be neglected.
- The temperature at the base of the fin is uniform.
- There is no contact resistance where the base of the fin joins the prime surface.
- There are no heat sources within the fin itself.
- The heat transferred through the tip of the fin is negligible compared with the heat leaving its lateral surface.
- Heat transfer to or from the fin is proportional to the temperature excess between the fin and the surrounding medium.
- Radiation heat transfer from and to the fin is neglected.

In general, the study of the extended surface heat transfer compromises the movement of the heat within the fin by conduction and the process of the heat exchange between the fin and the surroundings by convection.

## Straight Fin Analysis

Straight fin is any extended surface that is attached to a plane wall [2]. It may be of uniform cross-sectional area, or its cross-sectional area may vary with the distance  $x$  from the wall. The fin of variable thickness is shown in Fig. 1.

Both the conduction through the fin cross section and the convection over the fin surface area take place in and around the fin. When the fin temperature is lower than the base (primary surface) temperature  $T_0$ , the heat is transferred from the fin to the surroundings [4].

The fin height is  $l$ , width is  $w$ , and variable thickness  $\delta(x)$ . Its perimeter for surface convection depends on coordinate  $x$  and is  $P(x) = 2[w + \delta(x)]$ . Its cross-sectional area for heat conduction at any cross section is  $A(x) = \delta(x) \cdot w$ .

The temperature distribution can be calculated taking into consideration an energy balance on a typical element between  $x$  and  $x + dx$ , shown in Fig. 2.

The energy balance:

$$\dot{Q}_x - \dot{Q}_{x+dx} - d\dot{Q}_{CONV} = 0 \quad (1)$$

where

$$\dot{Q}_x = -k_f A_{k,x} \frac{dT}{dx} \quad (2)$$

$$\dot{Q}_{x+dx} = -k_f \left( A_{k,x} \frac{dT}{dx} + \frac{d}{dx} \left( A_{k,x} \frac{dT}{dx} \right) dx \right) \quad (3)$$

$$d\dot{Q}_{CONV} = hA_f (T - T_S) = hP dx (T - T_S) \quad (4)$$

where

$k_f$  – fin thermal conductivity

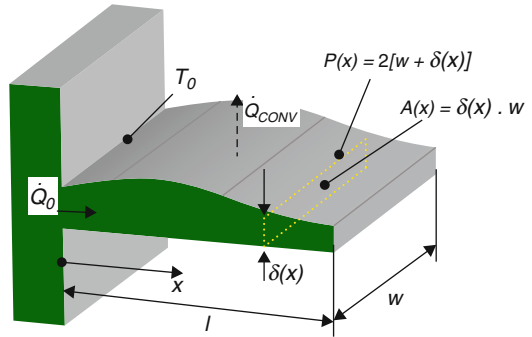
$h$  – heat transfer coefficient

$T_S$  – surrounding temperature

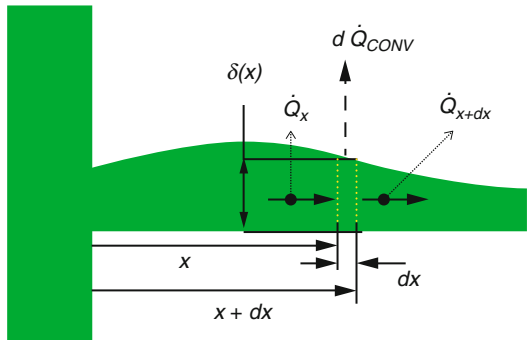
$A_f$  – fin surface area

$A_{k,x}$  – cross-sectional area as a function of  $k$  and  $x$

$P$  – perimeter (function of  $x$ )



**Extended Surfaces (Fins and Pins), Fig. 1** Straight fin of variable cross section



**Extended Surfaces (Fins and Pins), Fig. 2** Energy balance on a typical element

Then

$$k_f \frac{d}{dx} \left( A_{k,x} \frac{dT}{dx} \right) dx = hP dx (T - T_S) \quad (5)$$

and

$$\frac{d^2T}{dx^2} + \frac{1}{A_{k,x}} \frac{dA_{k,x}}{dx} \frac{dT}{dx} - \frac{hP}{k_f A_{k,x}} (T - T_S) = 0 \quad (6)$$

or

$$\frac{d^2T}{dx^2} + \frac{d(\ln A_{k,x})}{dx} \frac{dT}{dx} - m^2 (T - T_S) = 0 \quad (7)$$

where

$$m^2 = \frac{hP}{k_f A_{k,x}} \quad (8)$$

Both  $P$  and  $A_{k,x}$  are the function of  $x$  or a variable cross section.

To simplify the equation, the new dependent variable is introduced:

$$\theta(x) = T(x) - T_s \quad (9)$$

where  $\theta$  – temperature difference between a point on a fin surface and the surroundings, °C.

Because the ambient (surrounding) temperature is assumed to be constant, then:

$$\frac{d\theta}{dx} = \frac{dT}{dx} \quad (10)$$

and

$$\frac{d^2\theta}{dx^2} + \frac{d(\ln A_{k,x})}{dx} \frac{d\theta}{dx} - m^2\theta = 0 \quad (11)$$

or from (6):

$$\frac{d^2\theta}{dx^2} + \frac{1}{A_{k,x}} \frac{dA_{k,x}}{dx} \frac{d\theta}{dx} - \frac{hP}{k_f A_{k,x}} \theta = 0 \quad (12)$$

This second-order, linear, homogeneous ordinary differential equation with nonconstant coefficients is valid for any thin fins of variable cross section. Once the boundary conditions and the fin geometry are specified, its solution will provide the temperature distribution and subsequently, the heat transfer rate through the fin [4].

## Longitudinal Fins

### Longitudinal Fin of Rectangular Profile

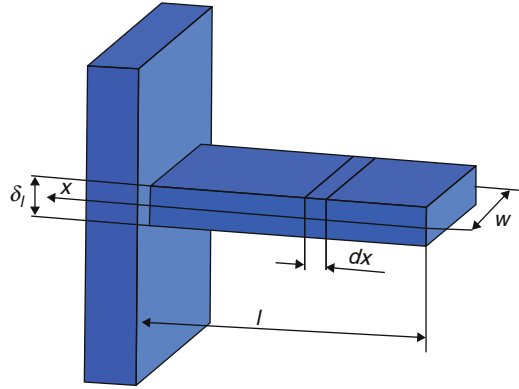
The profile function that describes rectangular profile can be written as (Fig. 3):

$$f(x) = \frac{\delta_l}{2} \quad (13)$$

where  $\delta(l) = \delta_l$ .

Cross-sectional area:

$$A_x = \delta_l \cdot w \quad (14)$$



**Extended Surfaces (Fins and Pins),**  
**Fig. 3** Longitudinal fin of rectangular profile

and its derivation:

$$\frac{dA_x}{dx} = 0 \quad (15)$$

Perimeter:

$$P = 2 \cdot \delta_l + 2 \cdot w \quad (16)$$

When the fin thickness is small in comparison to its length,  $\delta_l \ll w$  then

$$P = 2 \cdot w \quad (17)$$

The governing differential equation becomes:

$$\frac{d^2\theta}{dx^2} + 0 - \frac{h \cdot 2w}{k_f \delta w} \theta = 0 \quad (18)$$

$$\frac{d^2\theta}{dx^2} - m^2\theta = 0 \quad (19)$$

Above function is an ordinary second-order differential equation with constant coefficients. Its general solution is of the form:

$$\theta(x) = C_1 e^{mx} + C_2 e^{-mx} \quad (20)$$

To evaluate the constants  $C_1$  and  $C_2$ , it is necessary to specify appropriate boundary conditions. When the convective heat loss from the tip fin is negligible, (or the tip is insulated) then:



$$\frac{d\theta}{dx}\bigg|_{x=0} = 0 \quad (21)$$

The second boundary condition is the fin temperature at the base:

$$\theta(l) = T_l - T_S = \theta_l \quad (22)$$

From (20), (21), and (22):

$$\frac{d(C_1 e^{mx} + C_2 e^{-mx})}{dx}\bigg|_{x=0} = 0 \quad (23)$$

$$\theta_l = C_1 e^{ml} + C_2 e^{-ml} \quad (24)$$

Solving above equations, the value of  $C_1$  and  $C_2$  are:

$$C_1 = \frac{\theta_l}{e^{ml} + e^{-ml}} \quad (25)$$

$$C_2 = \frac{\theta_l}{e^{ml} + e^{-ml}} \quad (26)$$

And (20) can be written as:

$$\begin{aligned} \theta &= \theta_l \left( \left( \frac{e^{mx}}{e^{ml} + e^{-ml}} \right) + \left( \frac{e^{-mx}}{e^{ml} + e^{-ml}} \right) \right) \\ &= \theta_l \left( \frac{e^{mx} + e^{-mx}}{e^{ml} + e^{-ml}} \right) \end{aligned} \quad (27)$$

Introducing hyperbolic functions:

$$\sinh x = \frac{e^x - e^{-x}}{2} \quad \text{and} \quad \cosh x = \frac{e^x + e^{-x}}{2} \quad (28)$$

we receive the temperature distribution:

$$\frac{\theta}{\theta_l} = \frac{\cosh mx}{\cosh ml} \quad (29)$$

Because the orientation of the coordinate  $x$  is opposed to the direction of the heat flow in the fin, the heat flow through the base of the fin  $\dot{Q}_f$  is obtained from:

$$\dot{Q}_f = kA_f \frac{d\theta}{dx}\bigg|_{x=l} \quad (30)$$

The fin cross-sectional area is equal to  $A_f = \delta_l \cdot w$  so the fin heat transfer rate after derivation at  $x = l$  is:

$$\dot{Q}_f = mk \delta_l w \theta_l \tanh hl \quad (31)$$

The ideal heat flow:

$$\dot{Q}_{id} = h(2wl) \theta_l \quad (32)$$

The efficiency can be written as:

$$\eta = \frac{\dot{Q}_f}{\dot{Q}_{id}} = \frac{mk \delta_l w \theta_l \tanh hl}{2hl w \theta_l} \quad (33)$$

$$\eta = \frac{\tanh hl}{hl} \quad (34)$$

### Longitudinal Fin of Triangular Profile

Longitudinal fin of triangular profile is shown in Fig. 4.

The profile function becomes:

$$f(x) = \frac{\delta_l}{2} \frac{1}{l} x \quad (35)$$

the cross-sectional area  $A_x$ , as a function of  $x$ :

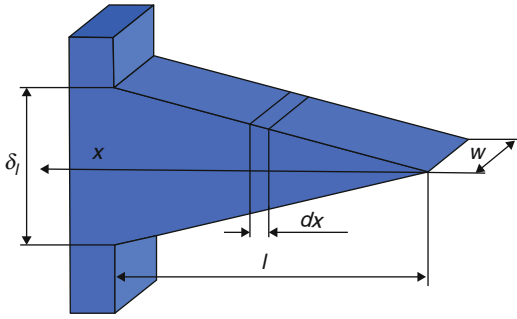
$$A_x = 2 \frac{\delta_l}{2} \frac{1}{l} x \cdot w \quad (36)$$

and perimeter  $P$ :

$$P = 4 \left( \frac{\delta_l}{2} \frac{1}{l} x \right) + 2 \cdot w \quad (37)$$

When the fin thickness is small in comparison to its length  $l \gg 2 \cdot \frac{\delta_l}{2} \frac{1}{l} x$ , then

$$P = 2 \cdot w \quad (38)$$



**Extended Surfaces (Fins and Pins),**  
**Fig. 4** Longitudinal fin of triangular profile

Calculating  $\frac{dA_x}{dx} = \frac{\delta_l}{l} \cdot w$  and substituting into (12), the governing differential equation for the temperature excess  $\theta$  becomes

$$\frac{d^2\theta}{dx^2} + \frac{1}{\frac{\delta_l}{l} x \cdot w} \frac{\delta_l}{l} w \frac{d\theta}{dx} - \frac{h \cdot 2 \cdot w}{k_f \frac{\delta_l}{l} x \cdot w} \theta = 0 \quad (39)$$

and

$$x \frac{d^2\theta}{dx^2} + \frac{d\theta}{dx} - \frac{2h}{k_f \delta_l} l \theta = 0 \quad (40)$$

$$\text{introducing } m^2 = \frac{2h}{k_f \delta_l} \quad (41)$$

$$x \frac{d^2\theta}{dx^2} + \frac{d\theta}{dx} - m^2 l \theta = 0 \quad (42)$$

Equation (42) is an ordinary second-order differential equation with variable coefficients. Its general solution is [3]:

$$\theta(x) = C_1 I_0(2m\sqrt{lx}) + C_2 K_0(2m\sqrt{lx}) \quad (43)$$

To have a finite temperature excess at the fin tip where  $x = 0$  (see Fig. 4), the constant  $C_2$  must be 0. This leaves

$$\theta(x) = C_1 I_0(2m\sqrt{lx}) \quad (44)$$

Because the temperature at the fin base is  $\theta = \theta(l) = \theta_l$ , then

$$\theta_l = C_1 I_0(2m\sqrt{ll}) \quad (45)$$

$$C_1 = \frac{\theta_l}{I_0(2ml)} \quad (46)$$

Then, the particular solution:

$$\theta(x) = \frac{\theta_l}{I_0(2ml)} I_0(2m\sqrt{lx}) \quad (47)$$

The heat dissipated by the fin is equal to the heat flow through the base of the fin:

$$\dot{Q}_l = k_f A_l \frac{dT}{dx} \Big|_{x=l} \quad (48)$$

$$\dot{Q}_l = \frac{2hw\theta_l I_1(2ml)}{ml I_0(2ml)} \quad (49)$$

The fin efficiency is the ratio of the actual heat flow given by (49) to the ideal heat flow  $\dot{Q}_{id} = 2hlw\theta_l$

$$\eta = \frac{2hw\theta_l I_1(2ml)}{ml I_0(2ml) 2hlw\theta_l} = \frac{I_1(2ml)}{(ml) I_0(2ml)} \quad (50)$$

### Longitudinal Fin of Concave Parabolic Profile

For concave parabolic profile, the fin profile can be described by the function:

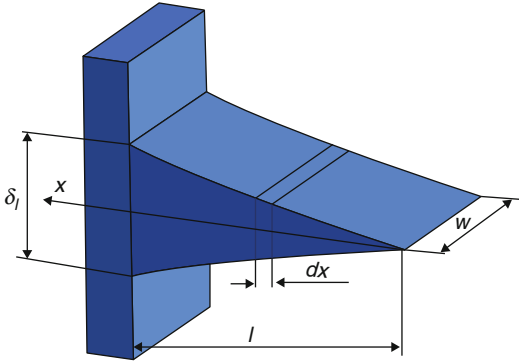
$$f(x) = \frac{\delta_l}{2} \left(\frac{x}{l}\right)^2 \quad (51)$$

Cross-sectional area:

$$A_x = \delta \cdot w = 2 \frac{\delta_l}{2} \left(\frac{x}{l}\right)^2 \cdot w \quad (52)$$

Perimeter:

$$P = 2\delta + 2 \cdot w = 4 \left(\frac{\delta_l}{2} \left(\frac{x}{l}\right)^2\right) + 2 \cdot w \quad (53)$$



**Extended Surfaces (Fins and Pins),**  
**Fig. 5** Longitudinal fin of concave parabolic profile

When the fin thickness is small in comparison to its length, then (Fig. 5)

$$P = 2 \cdot w \quad (54)$$

Calculating  $\frac{dA_x}{dx} = 2 \frac{\delta_l}{l^2} \cdot w \cdot x$  and substituting into (12), the governing differential equation for the temperature excess  $\theta$  becomes:

$$\frac{d^2\theta}{dx^2} + \frac{1}{\delta_l \left(\frac{x}{l}\right)^2 \cdot w} 2 \frac{\delta_l}{l^2} \cdot w \cdot x \frac{d\theta}{dx} - \frac{h2 \cdot w}{k_f \delta_l \left(\frac{x}{l}\right)^2 \cdot w} \theta = 0 \quad (55)$$

and

$$x^2 \frac{d^2\theta}{dx^2} + 2x \frac{d\theta}{dx} - \frac{2h w}{k_f \delta_l \cdot w} l^2 \theta = 0 \quad (56) \quad \text{where}$$

introducing  $m^2 = \frac{2h}{k_f \delta_l}$  then

$$x^2 \frac{d^2\theta}{dx^2} + 2x \frac{d\theta}{dx} - m^2 l^2 \theta = 0 \quad (57)$$

Equation (57) is an ordinary second-order differential equation with variable coefficients. It is known as an Euler equation and its general solution is obtained by making the transformation  $v = \ln x$ :

$$\frac{d\theta}{dx} = \frac{d\theta}{dv} \frac{dv}{dx} = \frac{1}{x} \frac{d\theta}{dv} \quad (58)$$

$$\begin{aligned} \frac{d^2\theta}{dx^2} &= \frac{d\theta}{dv} \frac{dv}{dx} = \frac{d}{dx} \left( \frac{1}{x} \frac{d\theta}{dv} \right) \\ &= -\frac{1}{x^2} \frac{d\theta}{dv} + \frac{1}{x} \frac{d}{dx} \left( \frac{d\theta}{dv} \right) \end{aligned} \quad (59)$$

After simplification

$$\frac{d^2\theta}{dx^2} = -\frac{1}{x^2} \frac{d\theta}{dv} + \frac{1}{x^2} \frac{d^2\theta}{dv^2} \quad (60)$$

Then governing differential equation:

$$x^2 \left( -\frac{1}{x^2} \frac{d\theta}{dv} + \frac{1}{x^2} \frac{d^2\theta}{dv^2} \right) + 2x \frac{1}{x} \frac{d\theta}{dv} - m^2 l^2 \theta = 0 \quad (61)$$

$$\frac{d^2\theta}{dv^2} - \frac{d\theta}{dv} + 2 \frac{d\theta}{dv} - m^2 l^2 \theta = 0 \quad (62)$$

$$\frac{d^2\theta}{dv^2} + \frac{d\theta}{dv} - m^2 l^2 \theta = 0 \quad (63)$$

Its general solution is:

$$\theta = C_1 e^{\alpha v} + C_2 e^{\beta v} \quad (64)$$

Because  $v = \ln x$ , then  $x = e^v$  and

$$\theta = C_1 x^\alpha + C_2 x^\beta \quad (64)$$

where

$$\alpha, \beta = -\frac{1}{2} \pm \frac{1}{2} (1 + 4m^2 l^2)^{\frac{1}{2}} \quad (65)$$

Then

$$\theta(x) = C_1 x^\alpha + C_2 x^\beta \quad (66)$$

It can be observed that at  $x = 0$ , the temperature excess will be unbounded unless  $C_2 = 0$ . Therefore,

$$\theta(x) = C_1 x^\alpha \quad (67)$$

From consideration of the temperature excess at the fin base where  $x = l$ , the particular solution is obtained:

$$\theta(x) = \theta_l \left(\frac{x}{l}\right)^\alpha \quad (68)$$

The heat flow through the base of the fin is obtained from Fourier's law, where  $x = l$  and  $A_l = \delta_l \cdot w$ :

$$\dot{Q}_f = k_f A_l \frac{dT}{dx} \Big|_{x=l} \quad (69)$$

$$\dot{Q}_f = k_f A_l \frac{d\theta}{dx} \Big|_{x=l} \quad (70)$$

$$\dot{Q}_f = k_f \delta_l \cdot \theta_l w \frac{\alpha}{l} \quad (71)$$

$$\dot{Q}_f = k_f \delta_l \cdot \theta_l w \frac{1}{2l} (-1 + (1 + 4m^2 l^2)^{\frac{1}{2}}) \quad (72)$$

Ideal heat flow and efficiency:

$$\dot{Q}_{id} = 2 h l w \theta_l \quad (73)$$

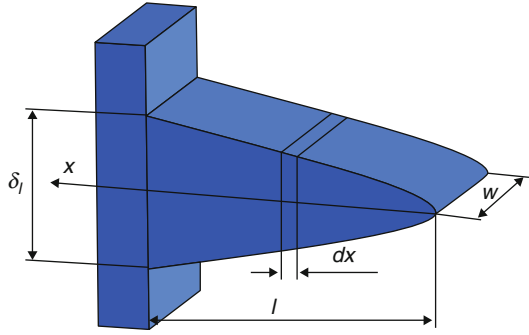
$$\eta = \frac{k_f \delta_l \cdot \theta_l w \frac{1}{2l} (-1 + (1 + 4m^2 l^2)^{\frac{1}{2}})}{2 h l w \theta_l} \quad (74)$$

$$\eta = \frac{k_f \delta_l \cdot \theta_l w \left(-1 + \sqrt{1 + (2m l)^2}\right)}{2l \cdot 2 h l w \theta_l} \quad (75)$$

$$\eta = \frac{-1 + \sqrt{1 + (2m l)^2}}{2 (m l)^2} \quad (76)$$

And finally:

$$\eta = \frac{2}{1 + \sqrt{1 + (2m l)^2}} \quad (77)$$



**Extended Surfaces (Fins and Pins),**  
**Fig. 6** Longitudinal fin of convex parabolic profile

### Longitudinal Fin of Convex Parabolic Profile

For the longitudinal fin of convex parabolic profile, the fin profile can be expressed by function (Fig. 6):

$$f(x) = \frac{\delta_l}{2} \left(\frac{x}{l}\right)^{\frac{1}{2}} \quad (78)$$

Cross-sectional area:

$$A_x = \delta \cdot w = 2 \frac{\delta_l}{2} \left(\frac{x}{l}\right)^{\frac{1}{2}} \cdot w \quad (79)$$

Perimeter:

$$P = 2\delta + 2 \cdot w = 4 \left(\frac{\delta_l}{2} \left(\frac{x}{l}\right)^{\frac{1}{2}}\right) + 2 \cdot w \quad (80)$$

When the fin thickness is small in comparison to its length, then

$$P = 2 \cdot w \quad (81)$$

Calculating  $\frac{dA_x}{dx} = \frac{1}{2} \frac{\delta_l}{\sqrt{l}} \cdot w \cdot \frac{1}{\sqrt{x}}$  and substituting into (12), the governing differential equation for the temperature excess  $\theta$  becomes:

$$\frac{d^2\theta}{dx^2} + \frac{1}{\delta_l \left(\frac{x}{l}\right)^{\frac{1}{2}} \cdot w} \frac{1}{2} \frac{\delta_l}{\sqrt{l}} \cdot w \cdot \frac{1}{\sqrt{x}} \frac{d\theta}{dx} - \frac{h2 \cdot w}{k_f \delta_l \left(\frac{x}{l}\right)^{\frac{1}{2}} \cdot w} \theta = 0 \quad (82)$$

$$\sqrt{x} \frac{d^2\theta}{dx^2} + \frac{1}{2} \frac{1}{\sqrt{x}} \frac{d\theta}{dx} - m^2 \sqrt{l} \theta = 0 \quad (83)$$

The general solution for temperature excess:

$$\theta(x) = x^{\frac{1}{4}} \left[ C_1 I_{1/3} \left( \frac{4}{3} m l^{1/4} x^{3/4} \right) + C_2 I_{-1/3} \left( \frac{4}{3} m l^{1/4} x^{3/4} \right) \right] \quad (84)$$

Evaluation of constants leads to particular solution [3]:

$$\theta(x) = \theta_l \left( \frac{x}{l} \right)^{\frac{1}{4}} \frac{I_{-1/3} \left( \frac{4}{3} m l^{1/4} x^{3/4} \right)}{I_{-1/3} \left( \frac{4}{3} m l \right)} \quad (85)$$

The heat flow through the base of the fin:

$$\dot{Q}_f = k_f \delta_l w m \cdot \theta_l \frac{I_{2/3} \left( \frac{4}{3} m l \right)}{I_{-1/3} \left( \frac{4}{3} m l \right)} \quad (86)$$

The fin efficiency:

$$\eta = \frac{\dot{Q}_f}{\dot{Q}_{id}} = \frac{k_f \delta_l w m \cdot \theta_l \frac{I_{2/3} \left( \frac{4}{3} m l \right)}{I_{-1/3} \left( \frac{4}{3} m l \right)}}{2 h l w \theta_l} \quad (87)$$

$$\eta = \frac{k_f \delta_l m I_{2/3} \left( \frac{4}{3} m l \right)}{2 h l I_{-1/3} \left( \frac{4}{3} m l \right)} = \frac{m I_{2/3} \left( \frac{4}{3} m l \right)}{m^2 l I_{-1/3} \left( \frac{4}{3} m l \right)} \quad (88)$$

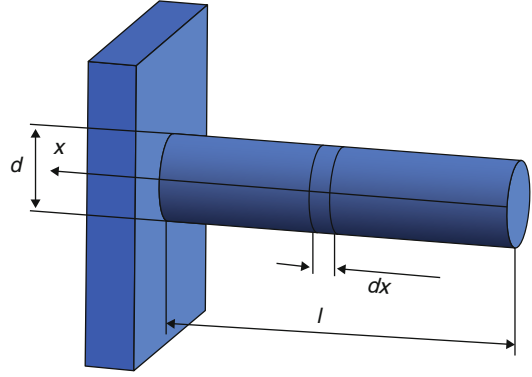
$$\eta = \frac{I_{2/3} \left( \frac{4}{3} m l \right)}{m l I_{-1/3} \left( \frac{4}{3} m l \right)} \quad (89)$$

## Spines

### Cylindrical Spines

For cylindrical spine, the profile function can be written as follows (Fig. 7):

$$f(x) = \frac{d}{2} \quad (90)$$



**Extended Surfaces (Fins and Pins), Fig. 7** Cylindrical spine

Cross-sectional area:

$$A_x = \frac{\pi d^2}{4} \quad (91)$$

and its derivation:

$$\frac{dA_x}{dx} = 0 \quad (92)$$

Perimeter:

$$P = \pi d \quad (93)$$

The governing differential equation for the temperature excess  $\theta$  becomes:

$$\frac{d^2\theta}{dx^2} + 0 - \frac{h\pi d}{k_f \frac{\pi d^2}{4}} \theta = 0 \quad (94)$$

$$\frac{d^2\theta}{dx^2} + 0 - \frac{4h}{k_f d} \theta = 0 \quad (95)$$

introducing  $m^2 = \frac{4h}{k_f d}$ , we obtain:

$$\frac{d^2\theta}{dx^2} - m^2 \theta = 0 \quad (96)$$

Equation (96) is identical in form to (19). The general solution, the boundary conditions, the particular solution, the heat flow through the fin base, and the fin efficiency all have the same

form as those for the longitudinal fin of rectangular profile. It must be noted that the spine diameter is used instead of the fin thickness, and the performance factor  $m^2 = \frac{4h}{k_f d}$  instead of  $m^2 = \frac{2h}{k_f \delta}$ .

So, the temperature excess:

$$\frac{\theta}{\theta_l} = \frac{\cos h m x}{\cos h m l} \quad (97)$$

The heat flow through the spine base (equals to dissipated heat by spine):

$$\dot{Q}_f = k A_f \left. \frac{d\theta}{dx} \right|_{x=l} \quad (98)$$

$$A_f = \frac{\pi d^2}{4} \quad (99)$$

$$\dot{Q}_f = m k \frac{\pi d^2}{4} \theta_l \tan h m l \quad (100)$$

$$\dot{Q}_f = \frac{\pi}{4} m k d^2 \theta_l \tan h m l \quad (101)$$

The fin efficiency:

$$\eta = \frac{\tan h m l}{m l} \quad (102)$$

### Rectangular Spines

The profile function that describes rectangular spine is (Fig. 8):

$$f(x) = \delta_l \quad (103)$$

Cross-sectional area:

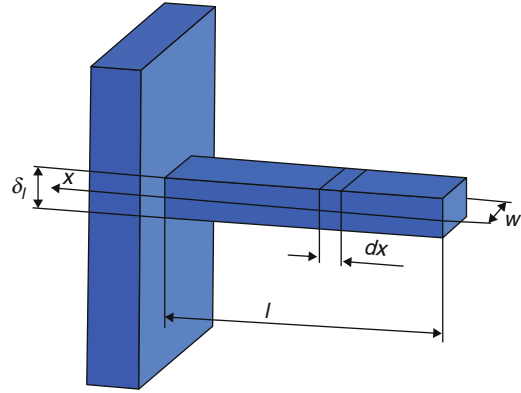
$$A_x = \delta_l \delta_w \quad (104)$$

and its derivation:

$$\frac{dA_x}{dx} = 0 \quad (105)$$

Perimeter:

$$P = 2 \delta_l + 2 w \quad (106)$$



**Extended Surfaces (Fins and Pins), Fig. 8** Rectangular spine

The differential equation:

$$\frac{d^2 \theta}{dx^2} + 0 - \frac{h 2 (\delta_l + w)}{k_f 2 \delta_l \cdot w} \theta = 0 \quad (107)$$

Introducing  $m^2 = \frac{h 2 (\delta_l + w)}{k_f 2 \delta_l \cdot w}$  the differential equation for temperature excess:

$$\frac{d^2 \theta}{dx^2} - m^2 \theta = 0 \quad (108)$$

Equation (108) is identical with (19) and the temperature excess:

$$\frac{\theta}{\theta_l} = \frac{\cos h m x}{\cos h m l} \quad (109)$$

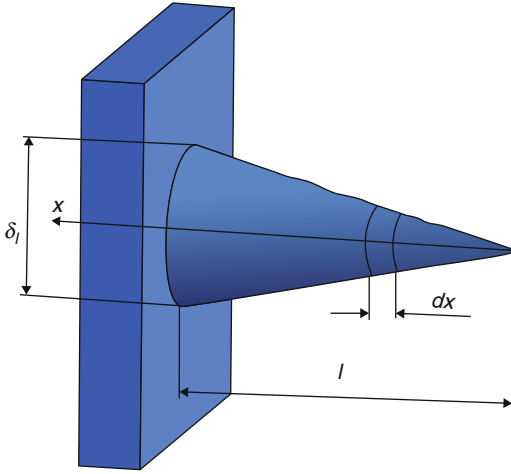
The heat flow through the base:

$$\dot{Q}_f = k A_f \left. \frac{d\theta}{dx} \right|_{x=l} \quad (110)$$

$$\dot{Q}_f = m k \delta_l w \theta_l \tan h m l \quad (111)$$

The fin efficiency:

$$\eta = \frac{\tan h m l}{m l} \quad (112)$$



**Extended Surfaces (Fins and Pins), Fig. 9** Conical spine

### Conical Spines

The profile function for conical spines is defined by equation (Fig. 9):

$$f(x) = \frac{\delta_l}{2} \frac{1}{l} x \quad (113)$$

the cross-sectional area  $A_x$  as a function of  $x$

$$A_x = \pi \left( \frac{\delta_l}{2} \frac{1}{l} x \right)^2 \quad (114)$$

then

$$\frac{dA_x}{dx} = 2\pi \left( \frac{\delta_l}{2} \frac{1}{l} \right)^2 x \quad (115)$$

and perimeter  $P$ :

$$P = 2\pi \left( \frac{\delta_l}{2} \frac{1}{l} x \right) \quad (116)$$

The governing differential equation for the temperature excess  $\theta$  becomes:

$$\frac{d^2\theta}{dx^2} + \frac{1}{\pi \left( \frac{\delta_l}{2} \frac{1}{l} x \right)^2} 2\pi \left( \frac{\delta_l}{2} \frac{1}{l} \right)^2 x \frac{d\theta}{dx} - \frac{h2\pi \left( \frac{\delta_l}{2} \frac{1}{l} x \right)}{k_f \pi \left( \frac{\delta_l}{2} \frac{1}{l} x \right)^2} \theta = 0 \quad (117)$$

$$\frac{d^2\theta}{dx^2} + 2 \frac{1}{x} \frac{d\theta}{dx} - \frac{h2}{k_f \left( \frac{\delta_l}{2} \frac{1}{l} x \right)} \theta = 0 \quad (118)$$

$$x^2 \frac{d^2\theta}{dx^2} + 2x \frac{d\theta}{dx} - x \frac{h2}{k_f \delta_l \left( \frac{1}{2} \frac{1}{l} \right)} \theta = 0 \quad (119)$$

Because  $m^2 = \frac{2h}{k_f \delta_l}$ , then

$$x^2 \frac{d^2\theta}{dx^2} + 2x \frac{d\theta}{dx} - xm^2 2l \theta = 0 \quad (120)$$

Introducing  $M^2 = m^2 2l$ , the differential equation is:

$$x^2 \frac{d^2\theta}{dx^2} + 2x \frac{d\theta}{dx} - M^2 x \theta = 0 \quad (121)$$

The general solution of (121):

$$\theta(x) = x^{-\frac{1}{2}} [C_1 I_1(2M\sqrt{x}) + C_2 K_1(2M\sqrt{x})] \quad (122)$$

Constants  $C_1$  and  $C_2$  are evaluated from the boundary conditions:  $\theta(l) = \theta_l$  and  $\frac{d\theta}{dx}|_{x=0} = 0$ . But in order to have finite temperature excess at  $x = 0$ ,  $C_2$  must be equal zero. Then,  $C_1$  needs to be calculated at  $x = l$ :

$$\theta_l = l^{-\frac{1}{2}} [C_1 I_1(2M\sqrt{l})] \quad (123)$$

$$C_1 = \frac{\theta_l}{l^{-\frac{1}{2}} [I_1(2M\sqrt{l})]} \quad (124)$$

The particular solution for the temperature excess:

$$\theta(x) = x^{-\frac{1}{2}} \left[ \frac{\theta_l}{l^{-\frac{1}{2}} [I_1(2M\sqrt{l})]} I_1(2M\sqrt{x}) \right] \quad (125)$$

$$\frac{\theta}{\theta_l} = \frac{l^{\frac{1}{2}}}{x^{\frac{1}{2}}} \frac{I_1(2M\sqrt{x})}{I_1(2M\sqrt{l})} \quad (126)$$

$$\frac{\theta}{\theta_l} = \left(\frac{l}{x}\right)^{1/2} \frac{I_1(2M\sqrt{x})}{I_1(2M\sqrt{l})} \quad (127)$$

The heat flow through the base:

$$\dot{Q}_f = k A_f \left. \frac{d\theta}{dx} \right|_{x=l} \quad (128)$$

Introducing the transformation of variable and calculating  $\frac{d\theta}{dx}$ , the heat flow [3]:

$$\dot{Q}_f = \frac{\pi k_f \delta_l^2 \theta_l M}{4\sqrt{l}} \frac{I_2(2M\sqrt{l})}{I_1(2M\sqrt{l})} \quad (129)$$

The surface area of conical spine:

$$S = \pi \frac{\delta_l}{2} \sqrt{\left(\frac{\delta_l}{2}\right)^2 + l^2} \quad (130)$$

Because  $l \gg \frac{\delta_l}{2}$ , then  $S = \pi \frac{\delta_l}{2} l$

The ideal heat flow is obtained from the surface  $S$  and equals:

$$\dot{Q}_{id} = h \pi \frac{\delta_l}{2} l \theta_l \quad (131)$$

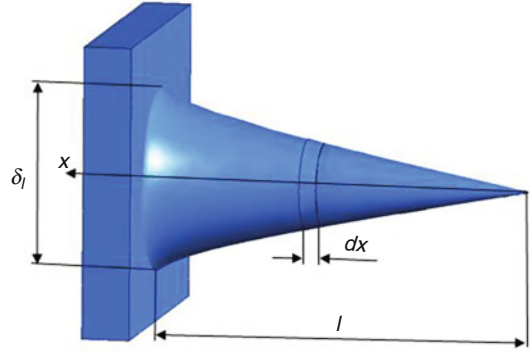
The conical spine efficiency:

$$\eta = \frac{\dot{Q}_f}{\dot{Q}_{id}} = \frac{\frac{\pi k_f \delta_l^2 \theta_l M}{4\sqrt{l}} \frac{I_2(2M\sqrt{l})}{I_1(2M\sqrt{l})}}{h \pi \frac{\delta_l}{2} l \theta_l} \quad (132)$$

$$\eta = \frac{k_f \delta_l M \frac{I_2(2M\sqrt{l})}{I_1(2M\sqrt{l})}}{2\sqrt{l} h l} \quad (133)$$

$$\eta = \frac{k_f \delta_l \sqrt{m^2 2 l} \frac{I_2(2\sqrt{m^2 2 l} \sqrt{l})}{I_1(2\sqrt{m^2 2 l} \sqrt{l})}}{2\sqrt{l} h l} \quad (134)$$

$$\eta = \frac{k_f \delta_l \sqrt{2} m \frac{I_2(2m l \sqrt{2})}{I_1(2m l \sqrt{2})}}{2 h l} \quad (135)$$



**Extended Surfaces (Fins and Pins), Fig. 10** Spine of concave parabolic profile

$$\eta = \frac{\sqrt{2} \frac{I_2(2m l \sqrt{2})}{I_1(2m l \sqrt{2})}}{m l} \quad (136)$$

$$\eta = \frac{\sqrt{2}}{m l} \frac{I_2(\sqrt{2} 2m l)}{I_1(\sqrt{2} 2m l)} \quad (137)$$

### Spine of Concave Parabolic Profile

The profile function for conical spines is defined by equation (Fig. 10):

$$f(x) = \frac{\delta_l}{2} \left(\frac{x}{l}\right)^2 \quad (138)$$

The cross-sectional area  $A_x$  as a function of  $x$

$$A_x = \pi \left(\frac{\delta_l}{2} \left(\frac{x}{l}\right)^2\right)^2 \quad (139)$$

then

$$\frac{dA_x}{dx} = 4 \pi \left(\left(\frac{\delta_l}{2}\right)^2 \left(\frac{1}{l}\right)^4\right) x^3 \quad (140)$$

and perimeter  $P$ :

$$P = 2 \pi \left(\frac{\delta_l}{2} \left(\frac{x}{l}\right)^2\right) \quad (141)$$

The governing differential equation for the temperature excess  $\theta$  becomes:



$$\frac{d^2 \theta}{dx^2} + \frac{1}{\pi \left( \frac{\delta_l}{2} \left( \frac{x}{l} \right)^2 \right)^2} 4 \pi \left( \left( \frac{\delta_l}{2} \right)^2 \left( \frac{1}{l} \right)^4 \right) x^3 \frac{d \theta}{dx} - \frac{h 2 \pi \left( \frac{\delta_l}{2} \left( \frac{x}{l} \right)^2 \right)}{k_f \pi \left( \frac{\delta_l}{2} \left( \frac{x}{l} \right)^2 \right)^2} \theta = 0 \quad (142)$$

$$\frac{d^2 \theta}{dx^2} + \frac{4}{x} \frac{d \theta}{dx} - \frac{h 2}{k_f \frac{\delta_l}{2} \left( \frac{x}{l} \right)^2} \theta = 0 \quad (143)$$

Because  $m^2 = \frac{2h}{k_f \delta_l}$ , then

$$\frac{d^2 \theta}{dx^2} + \frac{4}{x} \frac{d \theta}{dx} - \frac{2 m^2 l^2}{x^2} \theta = 0 \quad (144)$$

Introducing  $M = \sqrt{2} ml$ :

$$x^4 \frac{d^2 \theta}{dx^2} + 4 x^3 \frac{d \theta}{dx} - M^2 x^2 \theta = 0 \quad (145)$$

Equation (145) is an Euler equation. In analogy to the longitudinal fin of concave parabolic profile, a particular solution is obtained:

$$\theta(x) = \theta_l \left( \frac{x}{l} \right)^\alpha \quad (146)$$

where

$$\alpha = -\frac{3}{2} + \frac{1}{2} (9 + 4 M^2)^{1/2} \quad (147)$$

The heat flow through the fin base:

$$\dot{Q}_f = k_f \frac{\pi \delta_l^2}{4} \frac{d \theta}{dx} \Big|_{x=l} \quad (148)$$

and

$$\dot{Q}_f = k_f \frac{\pi \delta_l^2}{4} \frac{\alpha}{l} \theta_l \quad (149)$$

$$\dot{Q}_f = k_f \frac{\pi \delta_l^2}{4} \frac{1}{l} \left( -\frac{3}{2} + \frac{1}{2} (9 + 4 M^2)^{1/2} \right) \theta_l \quad (150)$$

$$\dot{Q}_f = k_f \frac{\pi \delta_l^2}{8 l} \left( -3 + (9 + 4 M^2)^{1/2} \right) \theta_l \quad (151)$$

The spine surface area:

$$S = \frac{1}{3} \pi \delta_l l \quad (160)$$

The ideal heat flow is obtained from the surface  $S$  and equals:

$$\dot{Q}_{id} = h \frac{1}{3} \pi \delta_l l \theta_l \quad (161)$$

The spine efficiency:

$$\eta = \frac{\dot{Q}_f}{\dot{Q}_{id}} = \frac{k_f \frac{\pi \delta_l^2}{8 l} \left( -3 + (9 + 4 M^2)^{1/2} \right) \theta_l}{h \frac{1}{3} \pi \delta_l l \theta_l} \quad (162)$$

$$\eta = \frac{3 k_f \delta_l \left( -3 + (9 + 4 M^2)^{1/2} \right)}{8 h l^2} \quad (163)$$

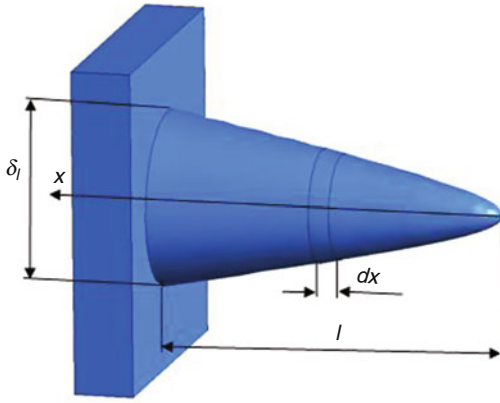
$$\eta = \frac{3 \left( -3 + (9 + 4 \cdot 2 m^2 l^2)^{1/2} \right)}{4 m^2 l^2} \quad (164)$$

$$\eta = \frac{3 \left( -3 + (9 + 8 m^2 l^2)^{1/2} \right)}{4 m^2 l^2} \quad (165)$$

$$\eta = \frac{3 \left( -3 + (9 + 8 m^2 l^2)^{1/2} \right) \left( 3 + (9 + 8 m^2 l^2)^{1/2} \right)}{4 m^2 l^2 \left( 3 + (9 + 8 m^2 l^2)^{1/2} \right)} \quad (166)$$

$$\eta = \frac{3 \left( -9 + (9 + 8 m^2 l^2) \right)}{4 m^2 l^2 \left( 3 + (9 + 8 m^2 l^2)^{1/2} \right)} \quad (167)$$

$$\eta = \frac{24 m^2 l^2}{4 m^2 l^2 \left( 3 + 3 \left( 1 + \frac{8}{9} m^2 l^2 \right)^{1/2} \right)} \quad (168)$$



**Extended Surfaces (Fins and Pins), Fig. 11** Spine of convex parabolic profile

Finally,

$$\eta = \frac{2}{\left(1 + \left(1 + \frac{8}{9} m^2 l^2\right)^{1/2}\right)} \quad (169)$$

### Spine of Convex Parabolic Profile

The general fin profile is expressed by the function (Fig. 11):

$$f(x) = \frac{\delta_l}{2} \left(\frac{x}{l}\right)^{1/2} \quad (170)$$

The cross-sectional area  $A_x$  as a function of  $x$

$$A_x = \pi \left(\frac{\delta_l}{2} \left(\frac{x}{l}\right)^{1/2}\right)^2 = \pi \left(\frac{\delta_l}{2}\right)^2 \frac{x}{l} \quad (171)$$

then

$$\frac{dA_x}{dx} = \pi \left(\frac{\delta_l}{2}\right)^2 \frac{1}{l} \quad (172)$$

and perimeter  $P$ :

$$P = 2\pi \left(\frac{\delta_l}{2} \left(\frac{x}{l}\right)^{1/2}\right) \quad (173)$$

The governing differential equation for the temperature excess  $\theta$ :

$$\frac{d^2 \theta}{dx^2} + \frac{1}{\pi \left(\frac{\delta_l}{2}\right)^2 \frac{x}{l}} \pi \left(\frac{\delta_l}{2}\right)^2 \frac{1}{l} \frac{d\theta}{dx} - \frac{h 2\pi \left(\frac{\delta_l}{2} \left(\frac{x}{l}\right)^{1/2}\right)}{k_f \pi \left(\frac{\delta_l}{2}\right)^2 \frac{x}{l}} \theta = 0 \quad (174)$$

$$\frac{d^2 \theta}{dx^2} + \frac{1}{x} \frac{d\theta}{dx} - \frac{h 2}{k_f \left(\frac{\delta_l}{2}\right)^2 \left(\frac{x}{l}\right)^{1/2}} \theta = 0 \quad (175)$$

$$x \frac{d^2 \theta}{dx^2} + \frac{d\theta}{dx} - \frac{4 h l^{1/2} x^{1/2}}{k_f \delta_l} \theta = 0 \quad (176)$$

Because  $m^2 = \frac{2h}{k_f \delta_l}$ , then

$$x \frac{d^2 \theta}{dx^2} + \frac{d\theta}{dx} - 2 m^2 l^{1/2} x^{1/2} \theta = 0 \quad (177)$$

If  $M^2 = 2m^2 l^{1/2}$ , then

$$x \frac{d^2 \theta}{dx^2} + \frac{d\theta}{dx} - M^2 \sqrt{x} \theta = 0 \quad (178)$$

The general solution of (178):

$$\theta(x) = C_1 I_0 \left(\frac{4}{3} M x^{3/4}\right) + C_2 K_0 \left(\frac{4}{3} M x^{3/4}\right) \quad (179)$$

Because  $K_0(0)$  is unbounded, in order to maintain a finite temperature excess at  $x = 0$ ,  $C_2$  must be zero [3].

$C_1$  needs to be calculated using the boundary condition at  $x = l$ :

$$\theta_l = C_1 I_0 \left(\frac{4}{3} M l^{3/4}\right) \quad (180)$$

$$C_1 = \frac{\theta_l}{I_0 \left(\frac{4}{3} M l^{3/4}\right)} \quad (181)$$

The particular solution for the temperature excess:

$$\theta = \frac{\theta_l}{I_0 \left(\frac{4}{3} M l^{3/4}\right)} I_0 \left(\frac{4}{3} M x^{3/4}\right) \quad (182)$$

$$\frac{\theta}{\theta_l} = \frac{I_0 \left( \frac{4}{3} M x^{3/4} \right)}{I_0 \left( \frac{4}{3} M l^{3/4} \right)} \quad (183)$$

The heat flow through the fin base  $\dot{Q}_f = k A_f \frac{d\theta}{dx}|_{x=l}$  is equal [3]:

$$\dot{Q}_f = \frac{\sqrt{2}}{4} k_f \pi \delta_l^2 \theta_l m \frac{I_1 \left( \frac{4}{3} \sqrt{2} m l \right)}{I_0 \left( \frac{4}{3} \sqrt{2} m l \right)} \quad (184)$$

The surface area of convex parabolic spine:

$$S = \frac{2}{3} \pi \delta_l l \quad (185)$$

The ideal heat flow that is obtained from the surface  $S$ :

$$\dot{Q}_{id} = h \frac{2}{3} \pi \delta_l l \theta_l \quad (186)$$

The spine efficiency:

$$\eta = \frac{\dot{Q}_f}{\dot{Q}_{id}} = \frac{\frac{\sqrt{2}}{4} k_f \pi \delta_l^2 \theta_l m \frac{I_1 \left( \frac{4}{3} \sqrt{2} m l \right)}{I_0 \left( \frac{4}{3} \sqrt{2} m l \right)}}{h \frac{2}{3} \pi \delta_l l \theta_l} \quad (187)$$

$$\eta = \frac{3\sqrt{2}}{4} \frac{k_f \delta_l}{2 h} \frac{m}{l} \frac{I_1 \left( \frac{4}{3} \sqrt{2} m l \right)}{I_0 \left( \frac{4}{3} \sqrt{2} m l \right)} \quad (188)$$

$$\eta = \frac{3\sqrt{2}}{4} \frac{1}{m l} \frac{I_1 \left( \frac{4}{3} \sqrt{2} m l \right)}{I_0 \left( \frac{4}{3} \sqrt{2} m l \right)} \quad (189)$$

## References

1. Mills AF (1995) Heat and mass transfer. Richard D. Irwin, Chicago. ISBN 0-256-11443-9
2. Incropera FP, Dewitt DP, Bergman TL, Lavine AS (2006) Fundamentals of heat and mass transfer. Wiley, New York. ISBN 978-0-471-45728-2
3. Kraus A, Aziz A, Welty J (2001) Extended surface heat transfer. Wiley, New York. ISBN 0-471-39550-1
4. Shah RK, Sekulic DP (2003) Fundamentals of heat exchanger design. Wiley, New York. ISBN 0-471-32171-0

## Extension

► [Saint-Venant's Problem for Cosserat Elastic Shells](#)

## External Force and Displacement Boundary Value Problems

Norio Hasebe

Department of Civil Engineering, Nagoya Institute of Technology, Showa-ku, Nagoya, Japan

## Synonyms

[Point heat source](#); [Thermal stress](#); [Uniform heat flux](#)

## Overview

The theory of thermoelasticity, as a classical problem in the field of solid mechanics, has been developed for a long time since the nineteenth century. The thermal stress problem still remains attracting research interest due to some new engineering applications such as in the very large-scale integration (VLSI) systems, new materials, nuclear engineering, and the field of aeronautics in recent years. Heating or nonuniform temperature fields make failures or reduce the service life of materials and structures. The investigations of the related problems have brought a considerable number of research works, both theoretical and experimental, treating various aspects of thermal stresses encountered in practice.

The following problems are solved: uniform heat flux problems for external force and displacement boundary value and heat point source problems for respective boundary values.

Revised version of: Hasebe N, Wang X (2005) Complex Variable Method for Thermal Stress Problem. Journal of Thermal Stresses Vol 28-6: 595–648, reprinted by permission of © Taylor & Francis Group, LLC (<http://tandfonline.com>)

## Scientific Fundamentals

### Rational Mapping Function

Although the thermoelastic problem of an infinite plane containing a hole is considered in this entry, the rational mapping function for an arbitrary shape is stated here. The rational mapping function is expressed by the sum of fractional expressions.

The shapes of two-dimensional elastic bodies can be classified into three cases:

A finite region mapped into a unit circle

$$z = \omega(\zeta) = \sum_{k=1}^N \frac{E_k}{\zeta_k - \zeta} + E_c \quad (\zeta \leq 1) \quad (1)$$

or

$$z = \omega(\zeta) = E_0 \zeta + \sum_{K=1}^N \frac{E_k}{\zeta_k - \zeta} + E_c \quad (\zeta \leq 1) \quad (2)$$

In the case of mapping a finite region, it is convenient to map the region into a unit circle to understand the corresponding points on the physical and mapping regions. This mapping function was used for analyzing a strip with cracks [1–3]. A circular region is mapped into a unit circle when using  $E_0 \neq 0, E_k = 0 (k = 1, 2, 3, \dots, n)$  in (2).

A semi-infinite region mapped into a unit circle:

$$z = \omega(\zeta) = \frac{E_0}{1 - \zeta} + \sum_{k=1}^N \frac{E_k}{\zeta_k - \zeta} + E_c \quad (\zeta \leq 1) \quad (3)$$

This mapping function is used for a semi-infinite region with a notch or a mound. The infinite point on the physical plane corresponds to  $\zeta = 1$  on the unit circle. A flat half plane is mapped into a unit circle when the coefficients  $E_0 \neq 0, E_k = 0 (k = 1, 2, 3, \dots, n)$  are used in (3). This mapping function was used in the analysis of a semi-infinite plane with a notch or a crack [4–6].

An infinite region with a hole mapped onto the exterior of a unit circle:

$$z = \omega(\zeta) = E_0 \zeta + \sum_{k=1}^N \frac{E_k}{\zeta_k - \zeta} + E_c \quad (\zeta \geq 1) \quad (4)$$

$$z = \omega(\zeta) = E_0 \zeta + \sum_{k=1}^N \frac{E_k}{\zeta_k - \zeta} + \frac{E_{N+1}}{\zeta} + E_c \quad (\zeta \geq 1) \quad (5)$$

The infinite point in the physical plane corresponds to the infinite point in the mapped plane. It is convenient to determine the corresponding points by mapping an infinite region with a hole onto the exterior of a unit circle. The mapping functions of the coefficients  $E_0 \neq 0, E_k = 0 (k = 1, 2, 3, \dots, n)$  in (4) and  $E_0 \neq 0, E_{N+1} \neq 0, E_k = 0 (k = 1, 2, 3, \dots, n)$  in (5) are ones of the infinite region outside a circular hole and an elliptical hole, respectively, onto the exterior of a unit circle. Equation 5 is a special case of (4). This mapping function was used in the analysis of an infinite plane containing cracks or holes [7–9]. Since problems of an infinite region with a hole are stated in this entry, the fabrication of this kind of rational mapping function is shown by simple examples.

**Example 1.** The mapping of the exterior of the cracked elliptical hole in the  $z$ -plane (Fig. 1a) onto the exterior of a unit circle in the  $\zeta$ -plane is considered [9].

Parameters  $e$ ,  $a$ , and  $b$  denote the length of edge crack, the half axes of the elliptical hole in the  $x$ , and  $y$  directions, respectively. The shape parameters  $e_1 = e/a$  and  $\lambda = b/a$  are used in the analysis in which  $\lambda = 1$  represents a circular hole, while  $\lambda \neq 1$  represents an elliptical hole.

From Fig. 1a, b, we have the mapping

$$z = \zeta_1 + \lambda \sqrt{\zeta_1^2 - 1} \quad (6)$$

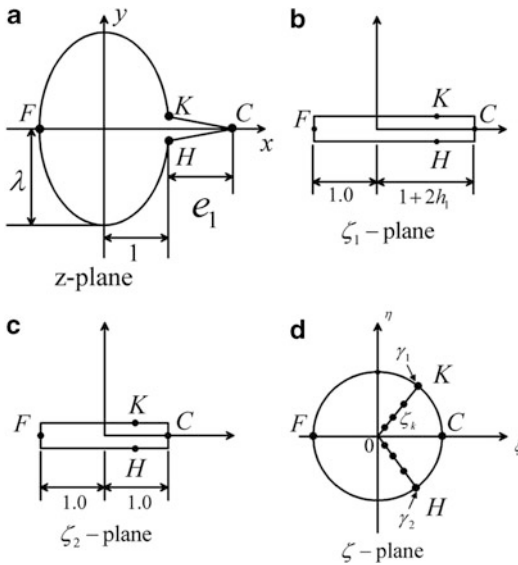
Through coordinate translation and scaling, we obtain

$$\zeta_1 = (1 + h_1)\zeta_2 + h_1 \quad (7)$$

where

$$h_1 = \frac{e_1^2}{4(1 + e_1)} (\lambda = 1)$$

$$h_1 = \frac{2(e_1 + \lambda^2) - 2\lambda\sqrt{\lambda^2 + 2e_1 + e_1^2}}{4(1 - \lambda^2)} (\lambda \neq 1) \quad (8)$$



**External Force and Displacement Boundary Value Problems, Fig. 1** Mapping function for an elliptical hole with an edge crack

Mapping the slit onto the unit circle, we have

$$\zeta_2 = \frac{1}{2} \left( \zeta + \frac{1}{\zeta} \right) \quad (9)$$

The mapping function is obtained by combination of the procedure (6–9) as

$$z = \omega(\zeta) = \frac{1+h_1}{2} \left( \zeta + \frac{1}{\zeta} \right) + h_1 + \lambda \frac{1+h_1}{2} (\zeta+1) \left( 1 - \frac{\gamma_1}{\zeta} \right)^{0.5} \left( 1 - \frac{\gamma_2}{\zeta} \right)^{0.5} \quad (10)$$

where

$$\left. \begin{matrix} \gamma_1 \\ \gamma_2 \end{matrix} \right\} = \frac{1-h_1}{1+h_1} \pm i \frac{2\sqrt{h_1}}{1+h_1} \quad (11)$$

The irrational terms in (10) are replaced by the rational ones expressed by the sum of fractional expressions as

$$\left( 1 - \frac{\gamma_1}{\zeta} \right)^{0.5} = 1 + \sum_{j=1}^{12} \left( \frac{-A_j}{1 - \gamma_1 \alpha_j / \zeta} + A_j \right) \quad (12)$$

The expressions for  $\gamma_2$  can be obtained by merely changing  $\gamma_1$  with  $\gamma_2$  in the above equation. The determination of coefficients  $A_j, \alpha_j$  can be referred to Appendix or Refs. [1, 6]. Substituting (12) and the expression for  $\gamma_2$  into (10) and making some arrangement, the general form of (5) is obtained. In this case, we chose  $N = 24$ .

### Basic Equations in the Mapped Plane

The basic equations for the temperature and thermoelastic field analysis are given here when a mapping function  $z = \omega(\zeta)$  is introduced [10–12].

### Temperature Field

The complex temperature function becomes

$$\Omega_0(z) = \Omega_0[\omega(\zeta)] \equiv \Omega(\zeta) \quad (13)$$

The temperature  $T(x, y)$  and the heat flux components  $q_x, q_y$  are then

$$T(x, y) = [\Omega(\zeta) + \overline{\Omega(\zeta)}] / 2 \quad (14)$$

$$q_x - iq_y = -k \Omega'(\zeta) / \omega'(\zeta) \quad (15)$$

where  $k$  signifies the heat conductivity. The heat flux components in the curvilinear coordinates generated by the mapping function are

$$q_r + iq_\theta = \frac{\overline{\zeta \omega'(\zeta)}}{|\zeta \omega'(\zeta)|} (q_x + iq_y) \quad (16)$$

The heat flux along a line between two points can be given by [10]

$$\Omega(\zeta) - \overline{\Omega(\zeta)} = -\frac{2i}{k} \int q_n(s) ds + \text{const.} \quad (17)$$

When considering the boundary point  $\zeta = \sigma$ , the boundary conditions for temperature and heat flux are as follows:

for temperature boundary condition,

$$\Omega(\sigma) + \overline{\Omega(\sigma)} = 2T(x, y) \equiv 2T(\sigma, \bar{\sigma}) \quad (18)$$

for heat flux boundary condition,

$$\Omega(\sigma) - \overline{\Omega(\sigma)} = -\frac{2i}{k} \int q_n(s) ds + const \quad (19)$$

Equations 18 and 19 are mathematically identical when they are used for determination of function  $\Omega(\zeta)$ . When the right-hand sides in (18) and (19) are zero, they can be combined into a single equation as

$$\Omega(\sigma) - \Gamma \overline{\Omega(\sigma)} = const \quad (20)$$

where  $\Gamma = 1$  for the adiabatic condition and  $\Gamma = -1$  for the isothermal condition.

### Thermal Stress Field

Introducing the mapping function, the complex stress functions become

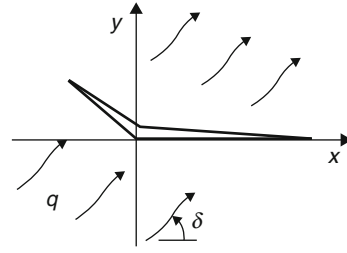
$$\begin{aligned} \varphi(z) &= \varphi[\omega(\zeta)] \equiv \phi(\zeta) \\ \chi'(z) &= \chi'[\omega(\zeta)] \equiv \psi(\zeta) \end{aligned} \quad (21)$$

The stress components and the displacements can be expressed as [10, 13]

$$\begin{aligned} \sigma_x + \sigma_y &= 4\text{Re} \left[ \frac{\phi'(\zeta)}{\omega'(\zeta)} \right] \\ \sigma_y - \sigma_x + 2i\tau_{xy} &= 2 \left[ \frac{\overline{\omega(\zeta)}}{\omega'(\zeta)} \left\{ \frac{\phi'(\zeta)}{\omega'(\zeta)} \right\}' + \frac{\psi'(\zeta)}{\omega'(\zeta)} \right] \\ u + iv &= \frac{1}{2G} \left[ \kappa \phi(\zeta) - \frac{\omega(\zeta)}{\omega'(\zeta)} \overline{\phi'(\zeta)} - \overline{\psi(\zeta)} \right] \\ &\quad + \alpha' \int \Omega(\zeta) \omega'(\zeta) d\zeta \end{aligned} \quad (22)$$

And the components of stress and displacements in the curvilinear coordinates  $(r, \theta)$  expressed by the mapping function are [13]

$$\begin{aligned} \sigma_r + \sigma_\theta &= \sigma_x + \sigma_y \\ \sigma_\theta - \sigma_r + 2i\tau_{r\theta} &= \frac{\zeta^2 \omega'(\zeta)}{|\zeta|^2 \overline{\omega'(\zeta)}} (\sigma_y - \sigma_x + 2i\tau_{xy}) \\ u_r + iv_\theta &= \frac{\overline{\zeta \omega'(\zeta)}}{|\zeta \omega'(\zeta)|} (u + iv) \end{aligned} \quad (23)$$



**External Force and Displacement Boundary Value Problems, Fig. 2** Kinked crack under uniform heat flux

Since the principle of superposition is applicable, without loss of generality, the external forces or displacements on the boundary may be let zero for the thermoelastic problem. The stress and displacement boundary conditions are, respectively,

$$\begin{aligned} \varphi(\sigma) + \frac{\omega(\sigma)}{\omega'(\sigma)} \overline{\varphi'(\sigma)} + \overline{\psi(\sigma)} &= 0 \\ \kappa \varphi(\sigma) - \frac{\omega(\sigma)}{\omega'(\sigma)} \overline{\varphi'(\sigma)} - \overline{\psi(\sigma)} &= -2G\alpha' \int \Omega(\sigma) \omega'(\sigma) d\sigma \end{aligned} \quad (24)$$

where  $\sigma$  represents  $\zeta$  on the boundary.

### External Force Boundary Value Problem

An infinite plane containing a hole under uniform heat flux or point heat sources is analyzed in this entry. The mapping function (4) is used. Without loss of generality, the hole boundary can be treated as traction free.

### Uniform Heat Flux Problem

The temperature function for the adiabatic boundary condition under is given heat flux by (see Fig. 2) [10, 11]

$$\Omega(\zeta) = -\frac{q}{k} \left( e^{-i\delta} E_0 \zeta + \frac{E_0}{\zeta} e^{i\delta} \right) + const \quad (25)$$

The external force boundary condition is expressed by the first equation in (24).

Substituting (25) into the third equation in (22) and carrying out the integration, the logarithmic

function appears. This term is of a multiple value that does not return to the starting value when moving round the hole, i.e., it causes the dislocation in the displacement. Since a displacement must be single-valued, a stress function that may cancel this dislocation is considered as follows [14, 15]:

$$\begin{aligned}\phi_1(\zeta) &= A \log \zeta \\ \psi_1(\zeta) &= B \log \zeta\end{aligned}\quad (26)$$

Substituting the above equation into the first of (24), the resultant force must return to the starting value when moving round the hole. Furthermore, substituting these equations into the second equation in (24), the displacement must return to the starting value when moving round the hole. From these single-valuedness conditions, the following equation is obtained:

$$\begin{aligned}B &= \bar{A} \\ A &= \frac{\alpha_0 q G R}{2k} E_0 \left( e^{-i\delta} \sum_{k=1}^N E_k + e^{i\delta} \bar{E}_0 \right) \\ R &= \frac{1+\nu}{1-\nu} \quad \text{Plane strain state} \\ R &= 1+\nu \quad \text{Plane stress state}\end{aligned}\quad (27)$$

Regarding (26), the stress functions to be determined can be expressed as follows:

$$\begin{aligned}\phi(\zeta) &= \phi_1(\zeta) + \phi_2(\zeta) \\ \psi(\zeta) &= \psi_1(\zeta) + \psi_2(\zeta)\end{aligned}\quad (28)$$

Substituting the above equation into the first equation in (24), multiplying by  $d\sigma/[2\pi i(\sigma - \zeta)]$ , and carrying out the Cauchy integration, we have

$$\phi_2(\zeta) + \sum_{k=1}^N \frac{\bar{A}_k B_k}{\zeta_k' - \zeta} = -\bar{A} \sum_{k=1}^N \frac{\zeta_k B_k}{\zeta_k' - \zeta} \quad (29)$$

where  $B_k \equiv E_k / \omega'(\zeta_k')$  and  $A_k \equiv \phi_2'(\zeta_k')$ ,  $\zeta_k' \equiv 1/\bar{\zeta}_k$ . Assuming  $\zeta = \zeta_j'$  ( $j = 1, 2, 3, \dots, N$ ) in the derivative of (29), a system of algebraic equations  $A_j = \phi_2'(\zeta_j')$  regarding the real and imaginary parts of the unknowns  $A_k$  can be obtained, and

then  $A_k$  are decided. Function  $\psi(\zeta)$  can be obtained from the following procedures: taking the conjugate form of the external force boundary condition, 1st equation in (24), multiplying by  $d\sigma/[2\pi i(\sigma - \zeta)]$ , and carrying out the Cauchy integration, the 2nd equation in (28) is finally obtained as

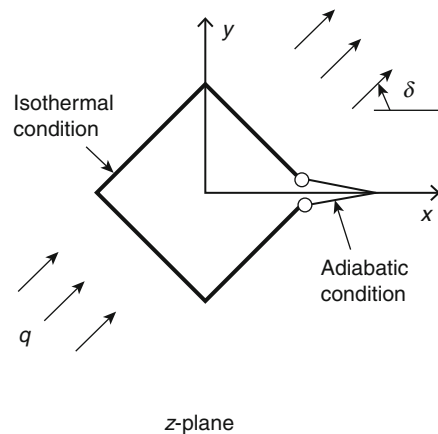
$$\begin{aligned}\psi(\zeta) &= \bar{A} \log \zeta - A \frac{\bar{\omega}(1/\zeta)}{\omega'(\zeta)} \frac{1}{\zeta} - A \sum_{k=1}^N \frac{\bar{B}_k \zeta_k'}{\zeta_k' - \zeta} \\ &\quad - \frac{\bar{\omega}(1/\zeta)}{\omega'(\zeta)} \phi_2'(\zeta) - \sum_{k=1}^N \frac{\bar{B}_k A_k \zeta_k'^2}{\zeta_k' - \zeta} + const\end{aligned}\quad (30)$$

However, it can be directly obtained from analytical continuation on the traction-free boundary on which no external force is applied [13].

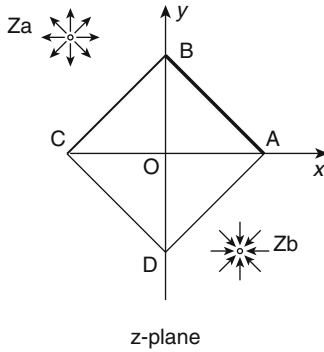
$$\psi(\zeta) = -\overline{\phi(1/\bar{\zeta})} - \overline{\frac{\omega(1/\bar{\zeta})}{\omega'(\zeta)}} \phi'(\zeta) \quad (31)$$

### Uniform Heat Flux with Mixed Heat Boundary Condition

The stress function for the mixed heat boundary condition under uniform heat flux can be derived by the same way in the above section (see Fig. 3) [14]. However, the coefficient  $A$  in (27) is given by the following equation:



**External Force and Displacement Boundary Value Problems, Fig. 3** Mixed heat conduction boundary



**External Force and Displacement Boundary Value Problems, Fig. 4** Heat and sink sources in an infinite plane with a hole

$$A = \frac{\alpha_0 q G R E_0}{2k} \left( e^{-i\delta} \sum_{k=1}^N E_k - \frac{e^{i\delta} \bar{E}_0 (\alpha + \beta)}{2\chi(0)} - \frac{1}{8} e^{-i\delta} E_0 (\alpha - \beta)^2 \right) \quad (32)$$

where  $\alpha, \beta, \chi(0)$  are given in [14]

$$\chi(\zeta) = (\zeta - \alpha)^{0.5} (\zeta - \beta)^{0.5} \quad (33)$$

### Heat Source and Heat Sink at Arbitrary Positions

Consider a heat source and a heat sink at  $\zeta_a, \zeta_b$  in the mapped plane, respectively (see Fig. 4) [15, 16]. The temperature function is given by

$$\Omega(\zeta) = -\frac{M}{2\pi k} \left\{ \log \left( \frac{\zeta - \zeta_a}{\zeta - \zeta_b} \right) + \Gamma \log \left( \frac{\zeta - \zeta'_a}{\zeta - \zeta'_b} \right) \right\} + const \quad (34)$$

The stress functions to be determined are expressed by (28).

The terms for a heat source in an infinite plane and the terms to remove the thermal dislocation in the displacement are considered as follows:

$$\begin{aligned} \phi_1(\zeta) &= \frac{\alpha_0 M G R}{4\pi k} [\{\omega(\zeta) - \omega(\zeta_a)\} \log(\zeta - \zeta_a) \\ &\quad - \{\omega(\zeta) - \omega(\zeta_b)\} \log(\zeta - \zeta_b)] + A \log \zeta \\ \psi_1(\zeta) &= -\frac{\alpha_0 M G R}{4\pi k} [\overline{\omega(\zeta_a)} \log(\zeta - \zeta_a) \\ &\quad - \overline{\omega(\zeta_b)} \log(\zeta - \zeta_b)] + B \log \zeta \end{aligned} \quad (35)$$

The coefficients  $A$  and  $B$  of the function  $\log$  are determined from the condition that the stresses in the external force boundary condition should be single-valued when moving round the hole,

$$B = \bar{A} \quad (36)$$

Further, substituting (35) into the third equation of (22),  $A$  is obtained from the condition that the displacement is single-valued when moving round the hole,

$$A = \frac{\alpha_0 M G R}{4\pi k} \left\{ -\Gamma E_0 (\zeta'_a - \zeta'_b) + \sum_{k=1}^N \frac{E_k}{\zeta_k - \zeta_a} - \sum_{k=1}^N \frac{E_k}{\zeta_k - \zeta_b} \right\} \quad (37)$$

Substituting (28) into the external force boundary condition, multiplying by  $d\sigma/[2\pi i(\sigma - \zeta)]$ , and carrying out the Cauchy integration, we have

$$\begin{aligned} \phi_2(\zeta) &= -\frac{\alpha_0 M G R}{4\pi k} \left[ \left\{ \omega(\zeta) - \omega(\zeta_a) \right\} \log \left( \frac{1}{\zeta} - \zeta_a \right) \right. \\ &\quad - \left. \left\{ \omega(\zeta) - \omega(\zeta_b) \right\} \log \left( \frac{1}{\zeta} - \zeta_b \right) \right. \\ &\quad - E_0 \zeta \log \left( \frac{\zeta_a}{\zeta_b} \right) + \sum_{k=1}^N \frac{E_k}{\zeta_k - \zeta} \log \left( \frac{\zeta_k - \zeta_a}{\zeta_k - \zeta_b} \right) \\ &\quad + \sum_{j=1}^N \frac{B_j}{\zeta_j - \zeta} \sum_{k=1}^N \left\{ \frac{\bar{E}_k}{(\zeta_k - \zeta'_j)(\zeta_k - \zeta_a)} \right. \\ &\quad - \left. \frac{\bar{E}_k}{(\zeta_k - \zeta'_j)(\zeta_k - \zeta_b)} \right\} \left. \right] \\ &\quad - \sum_{k=1}^N \frac{(\bar{A}_k + \bar{A} \zeta_k) B_k}{\zeta_k - \zeta} + const \end{aligned} \quad (38)$$



where  $A_k \equiv \phi'_2(\zeta'_k)$ ,  $\zeta'_k \equiv 1/\bar{\zeta}_k$ . The real and the imaginary parts of the unknown constants  $A_k$  are determined from a system of algebraic linear equations obtained by assuming  $\zeta = \zeta'_j$  ( $j=1, 2, 3, \dots, N$ ) in the derivative  $A_j = \phi'_2(\zeta'_j)$ . The final stress function  $\phi(\zeta)$  is expressed by the first equation in (27), while function  $\psi(\zeta)$  can be directly obtained from analytical continuation by (31).

From the stress function  $\phi(\zeta)$ , we can see that the point of the heat source will not be a singular point when the heat source is located on the boundary, i.e., the stresses on the traction-free boundary will not become infinite due to no displacement restraint [16, 17].

### Heat Source at an Arbitrary Position and Heat Sink at Infinity

Consider a heat source located at  $\zeta_a$  in the mapped plane [16, 17]. The temperature function is given by

$$\Omega(\zeta) = -\frac{M}{2\pi k} \left\{ \log(\zeta - \zeta_a) + \Gamma \log\left(\frac{\zeta - \zeta'_a}{\zeta}\right) \right\} + \text{const} \quad (39)$$

The stress functions to be determined are expressed by (28), in which  $\phi_1(\zeta)$ ,  $\psi_1(\zeta)$  are expressed as follows:

$$\begin{aligned} \phi_1(\zeta) &= \frac{\alpha_0 MGR}{4\pi k} \{ \omega(\zeta) - \omega(\zeta_a) \} \{ \log(\zeta - \zeta_a) - 1 \} \\ &\quad + A \log \zeta \\ \psi_1(\zeta) &= -\frac{\alpha_0 MGR}{4\pi k} \overline{\omega(\zeta_a)} \log(\zeta - \zeta_a) + B \log \zeta \end{aligned} \quad (40)$$

The coefficients  $A$  and  $B$  are

$$\begin{aligned} A &= \frac{\alpha_0 MGR}{4\pi k} \left\{ -\Gamma E_0 \zeta'_a + \sum_{k=1}^N \frac{E_k}{\zeta_k - \zeta_a} \right\} \\ B &= \bar{A} \end{aligned} \quad (41)$$

Using the same procedure as before, we obtained

$$\begin{aligned} \phi_2(\zeta) &= -\frac{\alpha_0 MGR}{4\pi k} \left[ \{ \omega(\zeta) - \omega(\zeta_a) \} \log\left(\frac{1}{\zeta} - \bar{\zeta}_a\right) \right. \\ &\quad - E_0 \zeta \log(-\bar{\zeta}_a) - 2 \sum_{k=1}^N \frac{E_k}{\zeta_k - \zeta} \\ &\quad + \sum_{k=1}^N \frac{E_k}{\zeta_k - \zeta} \log(\zeta_k - \zeta_a) \\ &\quad + \sum_{j=1}^N \frac{B_j}{\zeta_j - \zeta} \left\{ \bar{E}_0 + \sum_{k=1}^N \frac{\bar{E}_k}{(\zeta_k - \zeta'_j)(\bar{\zeta}_k - \bar{\zeta}_a)} \right\} \\ &\quad \left. - \sum_{k=1}^N \frac{(\bar{A}_k + \bar{A} \zeta'_k) B_k}{\zeta_k - \zeta} + \text{const} \right] \end{aligned} \quad (42)$$

where the real and imaginary parts of constants  $A_k$  can be determined from the relations  $A_k \equiv \phi'_2(\zeta'_k)$ ,  $\zeta'_k \equiv 1/\bar{\zeta}_k$ . Finally, the stress function  $\phi(\zeta)$  is expressed by the first equation in (28). Function  $\psi(\zeta)$  can be obtained from analytical continuation by (31).

The stress functions (40) and (42) for a point heat source and sink at  $\zeta_a, \zeta_b$ , respectively, are also obtainable by the superposition of the function with an intensity of heat  $M$  and sink  $(-M)$  at  $\zeta_a$  and  $\zeta_b$ , respectively, using (40) and (41).

### Heat Source at Arbitrary Position and Heat Sink at Infinity for Elliptical Hole

The mapping function that maps the exterior of an elliptical hole onto the exterior of a unit circle can be expressed as a special case of (4) as

$$z = \omega(\zeta) = E_0 \zeta + \frac{E_1}{\zeta}, \quad E_0 = \frac{a+b}{2}, \quad E_1 = \frac{a-b}{2} \quad (43)$$

$a$  and  $b$  are the half axes of the ellipse, respectively, at the  $x$  and  $y$  directions [16]. Using this mapping function and the method previously stated, the stress function  $\phi(\zeta)$  can be obtained as

$$\begin{aligned} \phi(\zeta) = A \log \zeta + \frac{\alpha_0 MGR}{4\pi k} & \left[ \{\omega(\zeta) - \omega(\zeta_a)\} \{\log(\zeta - \zeta_a) - 1\} \right. \\ & \left. - \{\omega(\zeta) - \omega(\zeta_a)\} \log\left(\frac{1}{\zeta} - \bar{\zeta}_a\right) + E_0 \zeta \log(-\bar{\zeta}_a) - \frac{E_1}{\zeta} \log(-\zeta_a) + \frac{E_1}{\zeta} \right] \end{aligned} \quad (44)$$

where

$$A = \frac{\alpha_0 MGR}{4\pi k} \left\{ -\Gamma E_0 \zeta'_a + \frac{E_1}{\zeta_a} \right\} \quad (45)$$

The solutions for a point heat source and heat sink at respective arbitrary positions can be obtained by the superposition stated in previous section ([Scientific Fundamentals](#)). Function  $\psi(\zeta)$  can be obtained from analytical continuation by (31).

### Displacement Boundary Value Problem

Consider an infinite plane with the displacement restraint boundary under uniform heat flux or point heat sources. For simplicity, the zero-displacement boundary condition is used since the principle of superposition is applicable. Such a boundary condition corresponds to the models of a rigid reinforced ring around a hole or a rigid inclusion in the elastic plate. It is assumed that the heat flux does not flow in or out through the boundary in either of the cases. The rigid inclusion is assumed fixed in the plane without rigid body rotation. The relative displacement between the inclusion and the point heat source is not restrained. The solutions for the inclusion with a rigid body rotation and with zero relative displacement between the inclusion and the heat source have been considered in [18].

### Uniform Heat Flux Problem

The mapping function is expressed by the general formula (4) [19]. The temperature function for the adiabatic boundary condition is given by (25). The displacement boundary condition is expressed by the 2nd equation in (24).

The stress functions to be determined are expressed by (28), in which  $\phi_1(\zeta)$ ,  $\psi_1(\zeta)$  can be

obtained from (26) and (27). Substituting (28) into the second equation of the displacement boundary condition (24), multiplying it by  $d\sigma/[2\pi i(\sigma - \zeta)]$ , and carrying out the Cauchy integration, we obtain

$$\begin{aligned} \kappa \varphi_2(\zeta) = \bar{A} \sum_{k=1}^N \frac{\zeta_k B_k}{\zeta_k - \zeta} - \sum_{k=1}^N \frac{\bar{A}_k B_k}{\zeta_k - \zeta} + \frac{2G\alpha' q}{k} F(\zeta) \\ F(\zeta) = E_0 e^{-i\delta} \left( -\sum_{k=1}^N E_k \log \frac{\zeta}{\zeta_k - \zeta} + \sum_{k=1}^N \frac{E_k \zeta_k}{\zeta_k - \zeta} \right) \\ + \bar{E}_0 e^{i\delta} \left( \sum_{k=1}^N \frac{E_k}{\zeta_k^2} \log \frac{\zeta}{\zeta_k - \zeta} + \sum_{k=1}^N \frac{E_k}{\zeta_k} \frac{1}{\zeta_k - \zeta} \right) \end{aligned} \quad (46)$$

where  $B_k \equiv E_k / \omega'(\zeta'_k)$  and  $A_k \equiv \phi'_2(\zeta'_k)$ ,  $\zeta'_k \equiv 1/\bar{\zeta}_k$ . The unknown constants  $A_k$  are determined as follows: using the  $A_j = \phi'_2(\zeta'_j)$ , ( $j = 1, 2, 3, \dots, N$ ), and (46), the real and the imaginary parts of  $A_j$ ,  $\bar{A}_j$  are determined by solving the resulting  $2N$  linear algebraic equations. Function  $\psi(\zeta)$  can be obtained from the following procedures: taking the conjugate form of the displacement boundary condition (24), multiplying it by  $d\sigma/[2\pi i(\sigma - \zeta)]$ , and carrying out the Cauchy integration, the final function  $\psi(\zeta)$  is obtained as

$$\begin{aligned} \psi(\zeta) = \bar{A} \log \zeta - \frac{\overline{\omega(1/\bar{\zeta})}}{\omega'(\zeta)} \varphi'(\zeta) - \sum_{k=1}^N \frac{A_k \bar{B}_k \zeta_k'^2}{\zeta'_k - \zeta} \\ - A \sum_{k=1}^N \frac{\zeta'_k \bar{B}_k}{\zeta'_k - \zeta} - \frac{\alpha' G q E_0^2 e^{i\delta}}{k} \frac{1}{\zeta^2} \end{aligned} \quad (47)$$

However, it can be directly obtained from the analytical continuation on the zero-displacement boundary condition as

$$\psi(\zeta) = \kappa \phi\left(\frac{1}{\bar{\zeta}}\right) - \frac{\omega(1/\bar{\zeta})}{\omega'(\zeta)} \phi'(\zeta) + 2G\alpha' \left[ \int_{\bar{\zeta}=1/\zeta} \overline{\Omega(\zeta)} \omega'(\zeta) d\bar{\zeta} \right] \quad (48)$$

### Heat Source at an Arbitrary Position and Heat Sink at Infinity

Consider a heat source located at  $\zeta_a$  in the mapped plane [18]. The temperature function is given by (39). The stress functions to be determined are expressed by (28), in which

$\phi_1(\zeta)$ ,  $\psi_1(\zeta)$  have the same forms as those in (40) and (41). Substituting the stress functions (28) into the displacement boundary condition, multiplying it by  $d\sigma/[2\pi i(\sigma - \zeta)]$ , and carrying out the Cauchy integration along the unit circle, we have

$$\begin{aligned} \phi_2(\zeta) = & \frac{1}{\kappa} \sum_{k=1}^N \frac{(\bar{A}\zeta_k + \bar{A}_k)B_k}{\zeta_k - \zeta} + \frac{\alpha_0 MGR}{4\pi k} \sum_{k=1}^N \frac{E_k}{\zeta_k - \zeta} + \frac{1}{\kappa} \frac{\alpha_0 MGR}{4\pi k} \left[ \sum_{k=1}^N \frac{E_k}{\zeta_k - \zeta} \log(\zeta_k - \zeta_a) \right. \\ & + \{ \omega(\zeta) - \omega(\zeta_a) \} \log\left(\frac{1}{\zeta} - \bar{\zeta}_a\right) - E_0 \zeta \log(-\bar{\zeta}_a) - \sum_{k=1}^N \frac{E_k}{\zeta_k - \zeta} \\ & + \sum_{j=1}^N \frac{B_j}{\zeta_j - \zeta} \left\{ \bar{E}_0 + \sum_{k=1}^N \frac{\bar{E}_k}{(\zeta_k - \bar{\zeta}'_j)(\zeta_k - \bar{\zeta}_a)} \right\} \left. \right] - \frac{1}{\kappa} \frac{1}{2\pi i} \int \frac{F(\sigma)}{\sigma - \zeta} d\sigma \\ \frac{1}{2\pi i} \int \frac{F(\sigma)}{\sigma - \zeta} d\sigma = & \frac{\alpha MGR}{4\pi k} (1 + \kappa) \left[ \Gamma E_0 \left\{ \zeta \log\left(\frac{\zeta}{\zeta - \zeta'_a}\right) - \zeta'_a \log\left(\frac{\zeta}{\zeta - \zeta'_a}\right) \right\} \right. \\ & + \Gamma \sum_{k=1}^n \frac{E_k}{\zeta_k - \zeta} \log\left(\frac{\zeta}{\zeta - \zeta'_a}\right) - \Gamma \sum_{k=1}^n \frac{E_k}{\zeta_k} \log\left(\frac{\zeta}{\zeta - \zeta_k}\right) + \sum_{k=1}^n \frac{E_k}{\zeta_k - \zeta_a} \log\left(\frac{\zeta}{\zeta - \zeta_k}\right) \\ & \left. + \Gamma \sum_{k=1}^n \frac{E_k}{\zeta_k - \zeta'_a} \log\left(\frac{\zeta - \zeta'_a}{\zeta - \zeta_k}\right) \right] - C \frac{\alpha MGR}{4\pi k} (1 + \kappa) \sum_{k=1}^n \frac{E_k}{\zeta_k - \zeta} \end{aligned} \quad (49)$$

where  $B_k \equiv E_k / \overline{\omega'(\zeta'_k)}$  and  $A_k \equiv \phi'_2(\zeta'_k)$ ,  $\zeta'_k \equiv 1/\bar{\zeta}_k$ . Solving a system of  $2N$  algebraic equations  $A_j = \phi'_2(\zeta'_j)$  ( $j=1, 2, 3, \dots, N$ ), the real and the imaginary parts of the unknown constants  $A_j, \bar{A}_j$  can be determined. Finally, function  $\phi(\zeta)$  can be obtained from (28). Similar to the preceding section, function  $\psi(\zeta)$  can be obtained from the analytical continuation over the zero-displacement boundary by (48).

locating at  $\zeta_b$ . Also similar to the preceding section, function  $\psi(\zeta)$  can be given by (48).

### Appendix: Rational Mapping Function in Example 1

Equation 12 can be expressed in the following form and further expanded to a power series [1, 6, 12]:

### Heat Source and Heat Sink at Respective Arbitrary Positions

The solution can be obtained by the superposition of the stress functions in the preceding section (Overview) with the original forms and the stress functions for a heat source of intensity  $(-M)$

$$\begin{aligned} (1 - \zeta)^\alpha &= \sum_{k=0}^{\infty} \frac{\alpha(\alpha-1) \dots (\alpha-k+1)}{k!} (-1)^k \zeta^k \\ &= 1 - a_1 \zeta - a_2 \zeta^2 - a_3 \zeta^3 + \dots \end{aligned} \quad (50)$$

This term represents the shape with a projection where coefficient  $\alpha$  ( $0 < \alpha < 1$ ) is determined by the angle of the projection.

Consider the following fractional expression and the expansion of the power series corresponding to (50):

$$1 + \sum_{j=1}^n \left[ \frac{-A_j}{1 - \alpha_j \zeta} + A_j \right] = 1 - \sum_{j=1}^n (A_j \alpha_j \zeta + A_j \alpha_j^2 \zeta^2 + A_j \alpha_j^3 \zeta^3 + \dots) \quad (51)$$

where  $|\alpha_j| < 1$ . The signs in front of  $A_j$  is determined from the condition that the signs of the coefficients in (50) and (51) are identical. The  $2n$  unknowns  $A_j$ ,  $\alpha_j$  are determined by approximately equating the corresponding coefficients of the terms with the same power in the series of (52) and (53), respectively,

$$\sum_{j=1}^n A_j \alpha_j^k = a_k \quad (52)$$

The selection of  $2n$  numbers of  $a_k$  depends on the convergence of the expanded power series, which is treated separately for the cases of rapidly and slowly convergent terms. Here, considering the slow convergence of the series in (50), the monotonous decrease of its coefficients and the convenience of the numerical calculation  $a_k$  are selected up to high order of power for  $\zeta$  in the following way:

1 <sup>st</sup> block	$a_1, a_2, a_3, a_4, a_5, a_6, a_7, a_8$
2 <sup>nd</sup> block	$a_{2M}, a_{3M}, a_{4M}, a_{5M}$
3 <sup>rd</sup> block	$a_{2M^2}, a_{3M^2}, a_{4M^2}, a_{5M^2}$
4 <sup>th</sup> block	$a_{2M^3}, a_{3M^3}, a_{4M^3}, a_{5M^3}$
5 <sup>th</sup> block	$a_{2M^4}, a_{3M^4}, a_{4M^4}, a_{5M^4}$
6 <sup>th</sup> block	$a_{2M^5}, a_{3M^5}, a_{4M^5}, a_{5M^5}$

(53)

28 of  $a_k$  (in this case) was selected in six blocks of which the particular terms are defined by M. Equation 54 is solved by the iteration. In this case, the number of the fractional expressions

is  $n = 14$ . The number of blocks may be increased or decreased due to the convergence of the series in (52). The value of  $M$  is related to the interval of  $a_k$ .  $M = 8$  or its vicinity 7 or 9 is selected due to our experience for the good agreement between (50) and (51) and the good convergence of the numerical iteration. That more numbers of  $a_k$  are adopted in the 1st block than others is to make the coefficients of low power agree well.

The nonlinear equations (52) are solved by the numerical iteration because it cannot be solved analytically in the following way: chiefly,  $A_1, \alpha_1$  and  $A_2, \alpha_2$  of  $A_j, \alpha_j$  are determined from the 6th block and  $A_3, \alpha_3, A_4, \alpha_4$  from the 5th block and so forth. The calculation is started from the 6th block. All initial values of  $A_j, \alpha_j$  except  $A_1, \alpha_1$  and  $A_2, \alpha_2$  which will be determined from the 6th block can be treated as zero in the first iterative calculation. By subtracting the influence of  $A_3, \alpha_3, A_4, \alpha_4$  in the 5th block, i.e.,  $A_3 \alpha_3^{2M^5} + A_4 \alpha_4^{2M^5}$ ,  $A_3 \alpha_3^{3M^5} + A_4 \alpha_4^{3M^5}$ ,  $A_3 \alpha_3^{4M^5} + A_4 \alpha_4^{4M^5}$ , and  $A_3 \alpha_3^{5M^5} + A_4 \alpha_4^{5M^5}$  from the 4 numbers of  $a_{2M^5}, a_{3M^5}, a_{4M^5}, a_{5M^5}$  in the 6th block,  $A_1, \alpha_1$  and  $A_2, \alpha_2$  can be obtained by solving the following equations expressed in terms of  $a'_{2M^5}, a'_{3M^5}, a'_{4M^5}, a'_{5M^5}$ :

$$\begin{aligned} A_1 \alpha_1^{2M^5} + A_2 \alpha_2^{2M^5} &= a_{2M^5} - (A_3 \alpha_3^{2M^5} + A_4 \alpha_4^{2M^5}) \equiv a'_{2M^5} \\ A_1 \alpha_1^{3M^5} + A_2 \alpha_2^{3M^5} &= a_{3M^5} - (A_3 \alpha_3^{3M^5} + A_4 \alpha_4^{3M^5}) \equiv a'_{3M^5} \\ A_1 \alpha_1^{4M^5} + A_2 \alpha_2^{4M^5} &= a_{4M^5} - (A_3 \alpha_3^{4M^5} + A_4 \alpha_4^{4M^5}) \equiv a'_{4M^5} \\ A_1 \alpha_1^{5M^5} + A_2 \alpha_2^{5M^5} &= a_{5M^5} - (A_3 \alpha_3^{5M^5} + A_4 \alpha_4^{5M^5}) \equiv a'_{5M^5} \end{aligned} \quad (54)$$

$\alpha_1^{M^5}, \alpha_2^{M^5}$  are obtained by solving the linear equations in two variables and a square equation. After that,  $A_1, A_2$  are obtained from the 1st two equations in (54). Next, consider the 5th block to determine  $A_3, \alpha_3, A_4, \alpha_4$ . By subtracting the effect of  $A_5, \alpha_5, A_6, \alpha_6$  and  $A_1, \alpha_1, A_2, \alpha_2$  in the 4th and 6th block, respectively, which corresponds to  $a_{2M^4}$  et al., from the 4 numbers of  $a_{2M^4}$  et al. in the 5th block,  $A_3, \alpha_3^{M^4}, A_4, \alpha_4^{M^4}$  can be obtained by solving four equations similar equation (52) to the 6th block. In case of treating the 4th block, the effect of the 3rd, 5th, and 6th blocks needs to be

considered. The influence of the blocks in lower order on the blocks in higher order is small because  $|\alpha_j| < 1$ . For example, the values of  $\alpha_9^{M^5}$  and  $\alpha_{10}^{M^5}$  obtained from the 2nd block or the values of  $\alpha_{11}^{M^5}, \alpha_{12}^{M^5}, \alpha_{13}^{M^5}, \alpha_{14}^{M^5}$  from the 1st block have almost no effect on the blocks in high order in case  $M = 8$ . The 1st block, having 8 elements, may be determined by solving the linear equations in 4 variables and an equation of 4th power. Thus, after solving the 1st block, return to the 6th block and do the same iterative procedure till the variation becomes small enough. Finally, we have the values of  $A_j, \alpha_j$ , which should satisfy the condition  $|\alpha_j| < 1$ .

From the above statement, we know the number of elements in each block in (53) does not have to be 4. If it is 6, in order to determine the fractional expressions in each block, the linear equations in 3 variables instead of 2 and a cube equation instead of the square one must be solved. And it does not matter to use 4 elements in the 1st block in (53). The selection depends on the needed accuracy, the interval of  $a_j$ , and the value of  $M$ . The term of (53) must present in the mapping function in case that there is a projection in the configuration to be analyzed. The index  $\alpha$  depends on the angle of the projection. Accordingly, e.g.,  $\alpha = 0.5$  when the angle of the projection is  $90^\circ$ . It is not necessary to compute the values of  $A_j, \alpha_j$  every time in the analysis once they have been obtained for the particular angles.

## References

- Hasebe N, Horiuchi Y (1978) Stress analysis for a strip with semi-elliptical notches of crack on both sides by means of rational mapping function. *Ingenieur Archiv* 47:169–179
- Hasebe N, Miura M (1981) Cracks initiating at the end of an embedded strip. *Trans Jpn Soc Mech Eng* 47A(423):1129–1136 (in Japanese)
- Hasebe N, Matsuura S, Kondo N (1984) Stress analysis of a strip with a step and a crack. *Eng Fracture Mech* 20:447–462
- Hasebe N (1971) Stress analyses of a semi-infinite plate with a triangular notch or mound. *Trans of Jpn Soc Civ Eng* 194:29–40 (in Japanese)
- Hasebe N, Iida J (1978) A crack originating from a triangular notch on a rim of a semi-infinite plate. *Eng Fracture Mech* 10:773–782
- Hasebe N, Inohara S (1980) Stress analysis of a semi-infinite plate with an oblique edge crack. *Ingenieur Archiv* 49:51–62
- Hasebe N, Ueda M (1980) Crack originating from a corner of a square hole. *Eng Fracture Mech* 13:913–928
- Hasebe N, Keer LM, Nemat-Nasser S (1984) Stress analysis of a kinked crack initiating from a rigid line inclusion I. formulation. *Mech Mater* 3:131–145
- Hasebe N, Chen YZ (1996) Stress intensity solutions for the interaction between a hole edge crack and a line crack. *Int J Fracture* 77:351–366
- Hasebe N, Tamai K, Nakamura T (1986) Analysis of a kinked crack under uniform heat flow. *ASCE. J Eng Mech* 112:31–42
- Hasebe N, Tomida A, Nakamura T (1988) Thermal stresses of a cracked circular hole due to uniform heat flux. *J Therm Stresses* 11:381–391
- Hasebe N, Wang X (2005) Complex variable method for thermal stress problem. *J Therm Stresses* 28(6–7):595–648
- Muskhelishvili NI (1963) Some basic problems of mathematical theory of elasticity, 4th edn. Noordhoff, The Netherlands
- Florence AL, Goodier JN (1959) Thermal stress at spherical cavities and circular holes in uniform heat flow. *ASME. J Appl Mech* 26:293–294
- Florence AL, Goodier JN (1960) Thermal stresses due to disturbance of uniform heat flow by an insulated ovaloid hole. *ASME. J Appl Mech* 27:635–639
- Yoshikawa K, Hasebe N (1999) Heat source in infinite plane with elliptic rigid inclusion and hole. *ASCE. J Eng Mech* 125:684–691
- Yoshikawa K, Hasebe N (1999) Green's function for a heat source in an infinite region with an arbitrary shaped hole. *ASME. J Appl Mech* 66:204–210
- Yoshikawa K, Hasebe N (1999) Green's function of the displacement boundary value problem for a heat source in an infinite plane with an arbitrary shaped rigid inclusion. *Arch Appl Mech* 69:227–239
- Hasebe N, Tomida A, Nakamura T (1989) Solution of displacement boundary value problem under uniform heat flux. *J Therm Stresses* 12:71–81